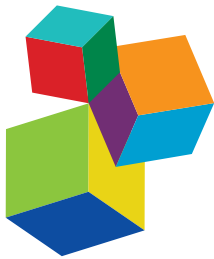


RECENT ADVANCES IN UNDERSTANDING THE BASIC MECHANISMS OF ATRIAL FIBRILLATION USING NOVEL COMPUTATIONAL APPROACHES

EDITED BY: Jichao Zhao, Oleg Aslanidi, Paweł Kuklik, Geoffrey Lee, Gary Tse,
Steven Alexander Niederer and Edward Joseph Vigmond

PUBLISHED IN: *Frontiers in Physiology*



Frontiers Copyright Statement

© Copyright 2007-2019 Frontiers Media SA. All rights reserved.

All content included on this site, such as text, graphics, logos, button icons, images, video/audio clips, downloads, data compilations and software, is the property of or is licensed to Frontiers Media SA ("Frontiers") or its licensees and/or subcontractors. The copyright in the text of individual articles is the property of their respective authors, subject to a license granted to Frontiers.

The compilation of articles constituting this e-book, wherever published, as well as the compilation of all other content on this site, is the exclusive property of Frontiers. For the conditions for downloading and copying of e-books from Frontiers' website, please see the Terms for Website Use. If purchasing Frontiers e-books from other websites or sources, the conditions of the website concerned apply.

Images and graphics not forming part of user-contributed materials may not be downloaded or copied without permission.

Individual articles may be downloaded and reproduced in accordance with the principles of the CC-BY licence subject to any copyright or other notices. They may not be re-sold as an e-book.

As author or other contributor you grant a CC-BY licence to others to reproduce your articles, including any graphics and third-party materials supplied by you, in accordance with the Conditions for Website Use and subject to any copyright notices which you include in connection with your articles and materials.

All copyright, and all rights therein, are protected by national and international copyright laws.

The above represents a summary only. For the full conditions see the Conditions for Authors and the Conditions for Website Use.

ISSN 1664-8714
ISBN 978-2-88963-184-1
DOI 10.3389/978-2-88963-184-1

About Frontiers

Frontiers is more than just an open-access publisher of scholarly articles: it is a pioneering approach to the world of academia, radically improving the way scholarly research is managed. The grand vision of Frontiers is a world where all people have an equal opportunity to seek, share and generate knowledge. Frontiers provides immediate and permanent online open access to all its publications, but this alone is not enough to realize our grand goals.

Frontiers Journal Series

The Frontiers Journal Series is a multi-tier and interdisciplinary set of open-access, online journals, promising a paradigm shift from the current review, selection and dissemination processes in academic publishing. All Frontiers journals are driven by researchers for researchers; therefore, they constitute a service to the scholarly community. At the same time, the Frontiers Journal Series operates on a revolutionary invention, the tiered publishing system, initially addressing specific communities of scholars, and gradually climbing up to broader public understanding, thus serving the interests of the lay society, too.

Dedication to Quality

Each Frontiers article is a landmark of the highest quality, thanks to genuinely collaborative interactions between authors and review editors, who include some of the world's best academicians. Research must be certified by peers before entering a stream of knowledge that may eventually reach the public - and shape society; therefore, Frontiers only applies the most rigorous and unbiased reviews.

Frontiers revolutionizes research publishing by freely delivering the most outstanding research, evaluated with no bias from both the academic and social point of view. By applying the most advanced information technologies, Frontiers is catapulting scholarly publishing into a new generation.

What are Frontiers Research Topics?

Frontiers Research Topics are very popular trademarks of the Frontiers Journals Series: they are collections of at least ten articles, all centered on a particular subject. With their unique mix of varied contributions from Original Research to Review Articles, Frontiers Research Topics unify the most influential researchers, the latest key findings and historical advances in a hot research area! Find out more on how to host your own Frontiers Research Topic or contribute to one as an author by contacting the Frontiers Editorial Office: researchtopics@frontiersin.org

RECENT ADVANCES IN UNDERSTANDING THE BASIC MECHANISMS OF ATRIAL FIBRILLATION USING NOVEL COMPUTATIONAL APPROACHES

Topic Editors:

Jichao Zhao, The University of Auckland, New Zealand

Oleg Aslanidi, King's College London, United Kingdom

Pawel Kuklik, Klinik für Kardiologie, Asklepios Klinik St. Georg, Germany

Geoffrey Lee, Royal Melbourne Hospital, Australia

Gary Tse, Xiamen University Affiliated Cardiovascular Hospital, China

Steven Alexander Niederer, King's College London, United Kingdom

Edward Joseph Vigmond, Université de Bordeaux, France

Citation: Zhao, J., Aslanidi, O., Kuklik, P., Lee, G., Tse, G., Niederer, S. A., Vigmond, E. J., eds. (2019). Recent Advances in Understanding the Basic Mechanisms of Atrial Fibrillation Using Novel Computational Approaches. Lausanne: Frontiers Media.
doi: 10.3389/978-2-88963-184-1

Table of Contents

- 06 Editorial: Recent Advances in Understanding the Basic Mechanisms of Atrial Fibrillation Using Novel Computational Approaches**
Jichao Zhao, Oleg Aslanidi, Pawel Kuklik, Geoffrey Lee, Gary Tse, Steven Niederer and Edward J. Vigmond
- 11 Atrial Fibrillation Recurrence and Peri-Procedural Complication Rates in nMARQ vs. Conventional Ablation Techniques: A Systematic Review and Meta-Analysis**
Ka H. C. Li, Mei Dong, Mengqi Gong, George Bazoukis, Ishan Lakhani, Yan Y. Ting, Sunny H. Wong, Guangping Li, William K. K. Wu, Vassiliou S. Vassiliou, Martin C. S. Wong, Konstantinos Letsas, Yimei Du, Victoria Laxton, Bryan P. Yan, Yat S. Chan, Yunlong Xia, Tong Liu, Gary Tse and International Health Informatics Study (IHIS) Network
- 19 A Machine Learning Aided Systematic Review and Meta-Analysis of the Relative Risk of Atrial Fibrillation in Patients With Diabetes Mellitus**
Zhaohan Xiong, Tong Liu, Gary Tse, Mengqi Gong, Patrick A. Gladding, Bruce H. Smaill, Martin K. Stiles, Anne M. Gillis and Jichao Zhao
- 31 Noninvasive Assessment of Atrial Fibrillation Complexity in Relation to Ablation Characteristics and Outcome**
Marianna Meo, Thomas Pambrun, Nicolas Derval, Carole Dumas-Pomier, Stéphane Puyo, Josselin Duchâteau, Pierre Jaïs, Mélèze Hocini, Michel Haïssaguerre and Rémi Dubois
- 50 Information Theory and Atrial Fibrillation (AF): A Review**
Dhani Dharmapranji, Lukah Dykes, Andrew D. McGavigan, Pawel Kuklik, Kenneth Pope and Anand N. Ganesan
- 69 A Heart for Diversity: Simulating Variability in Cardiac Arrhythmia Research**
Haibo Ni, Stefano Morotti and Eleonora Grandi
- 88 Atrial Rotor Dynamics Under Complex Fractional Order Diffusion**
Juan P. Ugarte, Catalina Tobón, António M. Lopes and J. A. Tenreiro Machado
- 102 Stationary Atrial Fibrillation Properties in the Goat do not Entail Stable or Recurrent Conduction Patterns**
Arne van Hunnik, Stef Zeemering, Piotr Podziemski, Jorik Simons, Giulia Gatta, Laura Hannink, Bart Maesen, Marion Kuiper, Sander Verheule and Ulrich Schotten
- 118 Dispersion of Recovery and Vulnerability to Re-entry in a Model of Human Atrial Tissue With Simulated Diffuse and Focal Patterns of Fibrosis**
Richard H. Clayton
- 134 The Subcellular Distribution of Ryanodine Receptors and L-Type Ca^{2+} Channels Modulates Ca^{2+} -Transient Properties and Spontaneous Ca^{2+} -Release Events in Atrial Cardiomyocytes**
Henry Sutanto, Bart van Sloun, Patrick Schönleitner, Marc A. M. J. van Zandvoort, Gudrun Antoons and Jordi Heijman

- 152 Morphological Substrates for Atrial Arrhythmogenesis in a Heart With Atrioventricular Septal Defect**
Robert S. Stephenson, Jack Rowley-Nobel, Caroline B. Jones, Rafael Guerrero, Tristan Lowe, Jichao Zhao, Henggui Zhang and Jonathan C. Jarvis
- 164 The Fibrotic Substrate in Persistent Atrial Fibrillation Patients: Comparison Between Predictions From Computational Modeling and Measurements From Focal Impulse and Rotor Mapping**
Patrick M. Boyle, Joe B. Hakim, Sohail Zahid, William H. Franceschi, Michael J. Murphy, Adityo Prakosa, Konstantinos N. Aronis, Tarek Zghaib, Muhammed Balouch, Esra G. Ipek, Jonathan Chrispin, Ronald D. Berger, Hiroshi Ashikaga, Joseph E. Marine, Hugh Calkins, Saman Nazarian, David D. Spragg and Natalia A. Trayanova
- 176 Automatic Detection of Atrial Fibrillation Based on Continuous Wavelet Transform and 2D Convolutional Neural Networks**
Runnan He, Kuanquan Wang, Na Zhao, Yang Liu, Yongfeng Yuan, Qince Li and Henggui Zhang
- 187 Loss of Side-to-Side Connections Affects the Relative Contributions of the Sodium and Calcium Current to Transverse Propagation Between Strands of Atrial Myocytes**
Jichao Zhao, Ulrich Schotten, Bruce Smaill and Sander Verheule
- 197 Computational Modeling of Electrophysiology and Pharmacotherapy of Atrial Fibrillation: Recent Advances and Future Challenges**
Márcia R. S. S. Vagos, Ilsebeth G. M. van Herck, Joakim Sundnes, Hermenegild J. Arevalo, Andrew G. Edwards and Jussi T. Koivumäki
- 226 Characterizing Electrogram Signal Fidelity and the Effects of Signal Contamination on Mapping Human Persistent Atrial Fibrillation**
David Vidmar, Mahmood I. Alhusseini, Sanjiv M. Narayan and Wouter-Jan Rappel
- 237 Description of the Human Atrial Action Potential Derived From a Single, Congruent Data Source: Novel Computational Models for Integrated Experimental-Numerical Study of Atrial Arrhythmia Mechanisms**
Michael A. Colman, Priyanka Saxena, Sarah Kettlewell and Antony J. Workman
- 254 Wavelength and Fibrosis Affect Phase Singularity Locations During Atrial Fibrillation**
Mirabeau Saha, Caroline H. Roney, Jason D. Bayer, Marianna Meo, Hubert Cochet, Remi Dubois and Edward J. Vigmond
- 266 Targeting the Substrate in Ablation of Persistent Atrial Fibrillation: Recent Lessons and Future Directions**
Martin K. Stiles, Prashanthan Sanders and Dennis H. Lau
- 277 A Computational Framework to Benchmark Basket Catheter Guided Ablation in Atrial Fibrillation**
Martino Alessandrini, Maddalena Valinoti, Laura Unger, Tobias Oesterlein, Olaf Dössel, Cristiana Corsi, Axel Loewe and Stefano Severi
- 290 Image-Based Computational Evaluation of the Effects of Atrial Wall Thickness and Fibrosis on Re-entrant Drivers for Atrial Fibrillation**
Aditi Roy, Marta Varela and Oleg Aslanidi

- 306 Myocyte Remodeling Due to Fibro-Fatty Infiltrations Influences Arrhythmogenicity**
Tim De Coster, Piet Claus, Gunnar Seemann, Rik Willems, Karin R. Sipido and Alexander V. Panfilov
- 319 Commentary: Atrial Rotor Dynamics Under Complex Fractional Order Diffusion**
Alfonso Bueno-Orovio
- 322 Atrial Fibrillation Mechanisms and Implications for Catheter Ablation**
Ghassen Cheniti, Konstantinos Vlachos, Thomas Pambrun, Darren Hooks, Antonio Frontera, Masateru Takigawa, Felix Bourier, Takeshi Kitamura, Anna Lam, Claire Martin, Carole Dumas-Pommier, Stephane Puyo, Xavier Pillois, Josselin Duchateau, Nicolas Klotz, Arnaud Denis, Nicolas Derval, Pierre Jais, Hubert Cochet, Meleze Hocini, Michel Haissaguerre and Frederic Sacher
- 346 Modeling Left Atrial Flow, Energy, Blood Heating Distribution in Response to Catheter Ablation Therapy**
Desmond Dillon-Murphy, David Marlevi, Bram Ruijsink, Ahmed Qureshi, Henry Chubb, Eric Kerfoot, Mark O'Neill, David Nordsletten, Oleg Aslanidi and Adelaide de Vecchi
- 359 Clinical Implications of Unmasking Dormant Conduction After Circumferential Pulmonary Vein Isolation in Atrial Fibrillation Using Adenosine: A Systematic Review and Meta-Analysis**
Cheng Chen, Daobo Li, Jeffery Ho, Tong Liu, Xintao Li, Zhao Wang, Yajuan Lin, Fuquan Zou, Gary Tse and Yunlong Xia
- 374 The Association Between Diabetes Mellitus and Atrial Fibrillation: Clinical and Mechanistic Insights**
Loryn J. Bohne, Dustin Johnson, Robert A. Rose, Stephen B. Wilton and Anne M. Gillis
- 386 Understanding the Beat-to-Beat Variations of P-Waves Morphologies in AF Patients During Sinus Rhythm: A Scoping Review of the Atrial Simulation Studies**
Dimitrios Filos, Dimitrios Tachmatzidis, Nicos Maglaveras, Vassilios Vassilikos and Ioanna Chouvarda



Editorial: Recent Advances in Understanding the Basic Mechanisms of Atrial Fibrillation Using Novel Computational Approaches

Jichao Zhao ^{1*}, Oleg Aslanidi², Paweł Kuklik³, Geoffrey Lee^{4,5}, Gary Tse^{6,7}, Steven Niederer² and Edward J. Vigmond^{8,9}

¹ Auckland Bioengineering Institute, University of Auckland, Auckland, New Zealand, ² School of Biomedical Engineering and Imaging Sciences, King's College London, London, United Kingdom, ³ Department of Cardiology, University Heart Center Hamburg, Hamburg, Germany, ⁴ Royal Melbourne Hospital, Melbourne, VIC, Australia, ⁵ Department of Cardiology, University of Melbourne, Melbourne, VIC, Australia, ⁶ Department of Medicine and Therapeutics, Faculty of Medicine, Chinese University of Hong Kong, Hong Kong, China, ⁷ Faculty of Medicine, Li Ka Shing Institute of Health Sciences, Chinese University of Hong Kong, Hong Kong, China, ⁸ IMB, UMR 5251, University of Bordeaux, Pessac, France, ⁹ IHU Liryc, Electrophysiology and Heart Modeling Institute, Fondation Bordeaux University, Pessac, France

Keywords: atrial fibrillation, cardiac electrophysiology, computer simulation, computational modeling, arrhythmia mechanisms

OPEN ACCESS

Edited and reviewed by:

Raimond L. Winslow,
Johns Hopkins University,
United States

*Correspondence:

Jichao Zhao
j.zhao@auckland.ac.nz

Specialty section:

This article was submitted to
Computational Physiology and
Medicine,
a section of the journal
Frontiers in Physiology

Received: 06 June 2019

Accepted: 02 August 2019

Published: 20 August 2019

Citation:

Zhao J, Aslanidi O, Kuklik P, Lee G, Tse G, Niederer S and Vigmond EJ (2019) Editorial: Recent Advances in Understanding the Basic Mechanisms of Atrial Fibrillation Using Novel Computational Approaches. *Front. Physiol.* 10:1065. doi: 10.3389/fphys.2019.01065

Editorial on the Research Topic

Recent Advances in Understanding the Basic Mechanisms of Atrial Fibrillation Using Novel Computational Approaches

WHERE WE ARE AT REGARDING ATRIAL FIBRILLATION

Atrial fibrillation (AF) is the most common sustained heart rhythm disturbance, associated with substantial morbidity and mortality (Andrade et al., 2014). The current prevalence of AF is ~2% of the general population worldwide and is projected to more than double in the following decades, becoming a global epidemic due to the aging population and the increasing incidence of heart failure and other comorbidities such as hypertension and diabetes (Colilla et al., 2013; Krijthe et al., 2013). Current clinical treatment for AF is suboptimal. Ablation treatment for persistent and permanent AF and AF with concurrent cardiac diseases is disappointing with long term success rates being <30% for single ablation procedures (Brooks et al., 2010; Nishida and Nattel, 2014). Furthermore, anti-arrhythmic drugs (AADs) often lose their efficacy and have side effects (Woods and Ogin, 2014). The poor clinical outcomes are primarily due to a lack of basic understanding of the AF mechanism and quantitative tools to optimize treatment strategies in a clinical setting (Haissaguerre et al., 2007; Hansen et al., 2015).

Novel computational approaches and techniques are playing an important role in our understanding and treatment of AF. Multi-scale computer models of the human atria have been used to investigate the important role of fibrosis in AF and consistently demonstrated that AF is perpetuated by the re-entrant circuits persisting in the fibrotic boundary zones (Bayer et al., 2016; Morgan et al., 2016; Vigmond et al., 2016; Zahid et al., 2016; Zhao et al., 2017). Moreover, models have been applied to propose efficient ablation (Bayer et al., 2016) and AAD (Varela et al., 2016) treatments for AF. To improve patients outcomes, novel computational analysis-aided

ablation strategies have also been proposed. Narayan et al. have identified stable AF re-entrant drivers in patients using phase singularity analysis and atrial cellular restitution properties and demonstrated that it was possible to reverse AF in 80.3% of patients by directly targeting these regions in their Focal Impulse and Rotor Modulation (FIRM) trial (Narayan et al., 2014). In addition to the FIRM trial study, Haissaguerre et al. studied 103 patients with persistent AF using a non-invasive ECG imaging (ECGI) approach (Haissaguerre et al., 2014) and concluded that AF is sustained by localized spatially stable drivers where targeted ablation led to 85% of patients being freed from AF at 12 months post ablation. These high success rates are yet to be confirmed in a multi-center randomized clinical trial and the recent REAFFIRM clinical trial presented during a late-breaking session at Heart Rhythm 2019, however, failed to provide evidence of the superiority of the FIRM approach over pulmonary vein isolation. Meanwhile, machine learning is proving to be a promising tool for helping us to understand AF. For example, deep convolutional neural networks have been used to classify AF from single-lead ECGs (Hannun et al., 2019) and to reconstruct 3D left atrial chambers from gadolinium-enhanced MRIs (Xiong et al., 2019) with superior performance.

The aim of this Research Topic was to collect a series of reviews and original research articles presenting recent advances toward a better understanding and treatment of AF through the development or use of: (1) structure-detailed computer modeling; (2) biophysics-based atrial cellular modeling; (3) signal processing and clinical mapping; and (4) meta-analysis and clinical studies. A total of 27 accepted articles were published under this Research Topic. Here in this editorial, we will summarize the new knowledge and approaches generated, and discuss how these can contribute to an improved understanding of AF mechanisms and clinical treatment, as well as how they may shape future research directions.

CRITICAL INSIGHTS LEARNED FROM STRUCTURE-DETAILED COMPUTER MODELING

Improvements in clinical imaging and mapping allow detailed characterization of atrial anatomy, structure and electrophysiology. Computer models of atrial electrical activation provide a powerful computational framework for understanding the structure-function relationship that underlies atrial re-entrant arrhythmias. Atrial structure, including wall thickness, fibrosis, and myofiber orientation, have been suggested to dictate the locations of AF re-entrant drivers in explanted human heart studies (Bishop et al., 2015; Zhao et al., 2015, 2017). Of all atrial structures, fibrosis, the hallmark of structural remodeling, has been investigated extensively in this Research Topic. Clayton studied the effect of the spatial scale (size) of simulated fibrosis on electrical propagations by smoothly varying the diffusion coefficient in 2D atrial tissue models. His study concludes that the spatial scale of fibrosis has important effects on both dispersion of recovery and vulnerability to re-entry. The Aslanidi group evaluated the effects of both atrial wall thickness and

fibrosis on AF re-entrant drivers using two sets of computer models, a simple model of an atrial tissue slab with a step change in wall thickness and a synthetic fibrosis patch, and a set of 3D patient-specific computer models based on MRI (Roy et al.). In the slab model, they observed that an AF re-entrant driver drifted toward and along the regions with changes/gradients in wall thickness. Furthermore, they discovered that additional patchy fibrosis would pull the AF re-entrant driver toward it, and that the locations of AF re-entrant drivers were determined by both fibrosis and wall thickness gradients. On the other hand, results from the patient-specific computer models suggested that the interaction between wall thickness and fibrosis plays a very important role in the right atrium due to extensive trabecular structure, whilst fibrosis performs a more decisive role in the left atrium due to a comparably smaller trabecular structure and more extensive fibrotic remodeling (Roy et al.). In another study conducted by Stephenson et al. using micro-CT imaging and anatomically accurate computer modeling, morphological substrates for atrial arrhythmogenesis were discovered in archived human hearts with atrioventricular septal defect. To directly link computer modeling to clinical treatment, Boyle et al. have carried out a multi-modal assessment of the arrhythmogenic propensity of the fibrotic substrate in patients with persistent AF by comparing locations of AF driver regions found in patient-specific computer simulations to those detected by the clinical FIRM approach. They discovered that computer modeling successfully detected most AF driver regions that were identified and ablated using the FIRM approach.

The interaction and impact of atrial structural and electrical remodeling on electrical propagation were also investigated in this Research Topic. The Vigmond group have studied the effects of fibrosis and wavelength on the locations of AF re-entrant drivers using bi-layer atrial models (Saha et al.). They observed that AF re-entrant drivers became more unstable with decreasing wavelength and that driver locations were largely influenced by the degree and distribution of fibrosis as well as the choice of implementation approach. Zhao et al. modeled the loss of lateral connections in atrial myocytes due to fibrotic remodeling and investigated the relative contributions of the sodium and L-type calcium currents to transverse propagation using a simple computer model of two parallel atrial myocyte strands. They discovered that although transverse propagation depends on both sodium and calcium currents, their relative contribution and sensitivity to channel blockage depends on the distribution of transverse connections. Fibrosis is important but structural remodeling involves many factors. Recent experiments suggest that adipocytes lead to a 69–87% increase in action potential duration in neighboring cells as well as an increase in resting membrane potential by 2.5 to 5.5 mV (De Coster et al.). The Panfilov group investigated the electrical interaction of fat and normal myocytes using multi-scale computer models and concluded that adipose remodeling may induce spiral wave dynamics to a complex arrhythmia (De Coster et al.).

Besides, Bueno-Orovio and Ugarte et al. developed a novel approach to model cardiac structural heterogeneity by using a fractional diffusion for the description of cardiac conduction. Their studies remind us that the current cardiac

modeling approach itself is not perfect and needs improvement. Dillon-Murphy et al. presented a novel patient-specific modeling workflow for characterizing the thermal-fluid dynamics in the human atria. This is a potentially useful tool for evaluating ablation treatment and minimizing stroke risks.

BIOPHYSICS-BASED ATRIAL CELLULAR MODELING

The vast majority of patients with AF are treated pharmacologically. However, AADs are often ineffective in ~40% of AF patients (Wyse et al., 2002). Cardiac cellular models were widely used to improve our understanding of electrical remodeling and to facilitate AAD design and development. In this Research Topic, Sutanto et al. presented a novel integrative approach by combining an experimental animal study, confocal imaging and computer modeling to study the effects of the subcellular distribution of ryanodine receptors (RyR2) and L-type Ca^{2+} channels on Ca^{2+} transient properties and spontaneous Ca^{2+} release events (SCaEs) in atrial cardiomyocytes. They discovered that SCAEs preferentially arise from regions of high local RyR2 expression and the propagation of Ca^{2+} waves is modulated by the distance between RyR2 bands. On the other hand, incorporation of axial tubules in various amounts and locations reduce Ca^{2+} -transient time to peak; and selective hyperphosphorylation of RyR2 around axial tubules increases the number of spontaneous waves (Sutanto et al.). These novel findings significantly enhance our understanding of the atrial structure-function relationship at the subcellular level. In another modeling study, Colman et al. developed a human atrial cell model derived from a single congruent data source which offers a unique approach for directly relating the model to the experiment.

There are also two important review articles devoted to the modeling of atrial cellular electrophysiology and pharmacotherapy. The Grandi group review recent advances in statistical and computational techniques, i.e., population-based and sample-specific modeling, simulating physiological variability when building cellular computer models of cardiac electrophysiology in both physiological and diseased conditions (Ni et al.); The Koivumäki group detail the unique aspects of AF pathophysiology, modeling approaches for drug testing and how heterogeneity and variability can be incorporated into AF-specific models (Vagos et al.).

INSIGHTS ON SIGNAL PROCESSING AND CLINICAL MAPPING

Ineffective signal processing and atrial mapping approaches impede our understanding of AF mechanisms and the identification of effective targets for treatment. To determine accurate intracardiac maps, the Rappel group investigated AF re-entrant drivers using phase maps from patients with persistent AF in the presence of various signal contamination (Vidmar et al.). They conclude that domains of low fidelity electrograms can be produced at rotational cores which are most sensitive

to far-field activation. By contrast, based on atrial electrograms collected using ECGI from patients with persistent AF, Meo et al. have utilized a new approach to measure AF complexity, a non-dipolar component index, and have correlated this with ablation outcomes and AF pathophysiology. Finally, the Zhang group developed a new 2D convolutional neural network for automatic detection of AF using the MIT-BIH ECG database with superior performance (He et al.).

Animal models and computer simulations are often utilized to validate atrial mapping and signal processing. The Schotten group mapped 12 goats with persistent AF for 3–4 weeks using a 249-electrode array and analyzed the AF episodes collected from the left atrial free wall to quantify its degree of spatiotemporal stationarity (van Hunnik et al.). They discovered that AF properties were stationary; however, they argue that this could not be attributed to stable recurrent conduction patterns. Instead, they postulate that the structural properties of the atria may explain the very variable conduction patterns underlying stationary AF properties. A 64-channel basket mapping catheter was used in the FIRM trials and widely used now in clinics for patients with AF; however, it remains uncertain how reliable this clinical mapping tool is. Alessandrini et al. have developed a computer modeling framework to evaluate basket catheter guided AF ablation. They discovered that a stable re-entrant driver needs a high-density mapping catheter (<3 mm) and a low distance to the atrial surface (<10 mm) for accurate mapping. Finally, the Ganeshan group review information theory, such as Shannon entropy, and its application to AF mapping, in the hopes of better pinpointing effective targets (Dharmapranji et al.).

META-ANALYSIS AND CLINICAL STUDIES

In this Research Topic, there are four original meta-analysis articles. Through a pooled analysis of a total of 17 studies including 5,169 participants, Chen et al. found that the adenosine test and elimination of dormant conduction provoked by adenosine may not improve the long-term success rate in AF patients that undergo circumferential pulmonary vein isolation. Their study raises a serious question about the clinical usage of adenosine to unmask dormant conduction of pulmonary veins as potential reconnection sites. The Tse group has systematically compared AF recurrence rates and complication rates between a novel ablation approach (circular irrigated radiofrequency ablation) and conventional ablation techniques based on 161 original publications (Li et al.). They found that the performance between the two is comparable though circular irrigated radiofrequency ablation has a higher mortality. Filos et al. conducted a scoping review by mapping existing literature in the field of atrial models and their associations with AF to synthesize the vast knowledge toward the mechanism between AF-related P-wave morphologies and atrial computer models. The final meta-analysis study was aided by a novel machine learning approach (Xiong et al.). The growth in medical research publications is accelerating across the board; therefore, there is an urgent need to develop an intelligent automated approach, such as machine learning, to facilitate the identification and

selection of relevant articles for meta-analysis. The Zhao group developed a novel machine learning approach to assist in the screening of potentially relevant articles for large-scale meta-analyses and systematic review (Xiong et al.). Their approach led to a 87% reduction in the number of publications needed for manual screening. More importantly, their study demonstrates that diabetes mellitus is a strong, independent risk factor for AF, particularly for women.

It is always important to link or interpret computational approaches and their results back to clinical settings. There are three clinical review papers devoted to this area. Stiles et al. reviewed computational approaches for detecting AF substrates, ranging from complex fractionated atrial electrograms (CFAEs), dominant frequency, ECGI, FIRM, and fibrosis-guided ablation to risk factor modification. Clearly, some of these approaches did not work that well, as demonstrated by recent high-profile clinical studies (Verma et al., 2015), due to our lack of understanding of AF mechanisms. Cheniti et al. focus on reviewing the AF mechanisms that are further obscured and complicated by intermingled multilevel atrial remodeling, various concurrent conditions such as genetic factors (PITX2), obesity/metabolic syndrome, and the limitations of each mapping/imaging/ablation methodology. Bohne et al. systematically review the structural, electrical, and autonomic remodeling underlying elevated AF in diabetes mellitus conditions. Further studies are required to investigate the inter-relationship among obesity, diabetes mellitus, and metabolic syndrome, as well as the role of insulin resistance in AF.

CONCLUSIONS AND FUTURE DIRECTIONS

The articles collected under this Research Topic advance our understanding of atrial structural and electrical remodeling, presenting recent progress on the development of computational

modeling, signal processing, atrial mapping, and machine learning approaches, as well as how the gap between basic and clinical studies is being bridged. There is a growing body of evidence supporting a more integrative approach by combining new and established computational and experimental/clinical approaches to improve our understanding and treatment of AF. More importantly, computer modeling of AF will need to be truly multiscale, going from subcellular genetic changes to tissue-level fibrosis to organ-scale geometry and electrical connectivity. AF is a complex disease; therefore, future work should extend the current paradigm to investigate upstream mechanisms and therapy, such as the genetic factors (PITX2) and concurrent clinical conditions (metabolic syndrome). Finally, in the world of meta-data and wearable technology, more effective computational approaches, such as machine learning and large physiological and clinical datasets will need to be used to aid traditional approaches toward further advancements in this exciting research area. Together, these methods will no doubt be an important part of global efforts to tackle this most common, yet elusive, cardiac disease.

AUTHOR CONTRIBUTIONS

JZ wrote the draft. The remaining authors provided comments and edits. All authors approved the final version of this article.

FUNDING

Sources of support are the National Institutes of Health grants (HL115580 and HL135109 to JZ); the Health Research Council of New Zealand (16/385 to JZ); the British Heart Foundation (PG/15/8/31130 to OA); the French Government as part of the Investments of the Future program managed by the National Research Agency (ANR) (Grant reference ANR-10-IAHU-04 to EV).

REFERENCES

- Andrade, J., Khairy, P., Dobrev, D., and Nattel, S. (2014). The clinical profile and pathophysiology of atrial fibrillation relationships among clinical features, epidemiology, and mechanisms. *Circ. Res.* 114, 1453–1468. doi: 10.1161/CIRCRESAHA.114.303211
- Bayer, J. D., Roney, C. H., Pashaei, A., Jaïs, P., and Vigmond, E. J. (2016). Novel radiofrequency ablation strategies for terminating atrial fibrillation in the left atrium: a simulation study. *Front. Physiol.* 7:108. doi: 10.3389/fphys.2016.00108
- Bishop, M., Rajani, R., Plank, G., Gaddum, N., Carr-White, G., Wright, M., et al. (2015). Three-dimensional atrial wall thickness maps to inform catheter ablation procedures for atrial fibrillation. *Europace* 18, 376–383. doi: 10.1093/europace/euv073
- Brooks, A. G., Stiles, M. K., Laborderie, J., Lau, D. H., Kuklik, P., Shipp, N. J., et al. (2010). Outcomes of long-standing persistent atrial fibrillation ablation: a systematic review. *Heart Rhythm* 7, 835–846. doi: 10.1016/j.hrthm.2010.01.017
- Colilla, S., Crow, A., Petkun, W., Singer, D. E., Simon, T., and Liu, X. (2013). Estimates of current and future incidence and prevalence of atrial fibrillation in the US adult population. *Am. J. Cardiol.* 112, 1142–1147. doi: 10.1016/j.amjcard.2013.05.063
- Haissaguerre, M., Hocini, M., Denis, A., Shah, A. J., Komatsu, Y., Yamashita, S., et al. (2014). Driver domains in persistent atrial fibrillation. *Circulation* 130, 530–538. doi: 10.1161/CIRCULATIONAHA.113.05421
- Haissaguerre, M., Lim, K.-T., Jacquemet, V., Rotter, M., Dang, L., Hocini, M., et al. (2007). Atrial fibrillatory cycle length: computer simulation and potential clinical importance. *Europace* 9, vi64–vi70. doi: 10.1093/europace/eum208
- Hannun, A. Y., Rajpurkar, P., Haghpanahi, M., Tison, G. H., Bourn, C., Turakhia, M. P., et al. (2019). Cardiologist-level arrhythmia detection and classification in ambulatory electrocardiograms using a deep neural network. *Nat. Med.* 25, 65–69. doi: 10.1038/s41591-018-0268-3
- Hansen, B. J., Zhao, J., Csepe, T. A., Moore, B. T., Li, N., Jayne, L. A., et al. (2015). Atrial fibrillation driven by micro-anatomic intramural re-entry revealed by simultaneous sub-epicardial and sub-endocardial optical mapping in explanted human hearts. *Eur. Heart J.* 36, 2390–2401. doi: 10.1093/eurheartj/ehv233
- Krijthe, B. P., Kunst, A., Benjamin, E. J., Lip, G. Y., Franco, O. H., Hofman, A., et al. (2013). Projections on the number of individuals with atrial fibrillation in the European Union, from 2000 to 2060. *Eur. Heart J.* 34, 2746–2751. doi: 10.1093/eurheartj/eht280
- Morgan, R., Colman, M. A., Chubb, H., Seemann, G., and Aslanidi, O. V. (2016). Slow conduction in the border zones of patchy fibrosis stabilizes the drivers for atrial fibrillation: insights from multi-scale human atrial modeling. *Front. Physiol.* 7:474. doi: 10.3389/fphys.2016.00474

- Narayan, S., Baykaner, T., Clopton, P., Schricker, A., Lalani, G., Krummen, D., et al. (2014). Ablation of rotor and focal sources reduces late recurrence of atrial fibrillation compared with trigger ablation alone: extended follow-up of the CONFIRM trial (Conventional Ablation for Atrial Fibrillation With or Without Focal Impulse and Rotor Modulation). *J. Am. Coll. Cardiol.* 63, 1761–1768. doi: 10.1016/j.jacc.2014.02.543
- Nishida, K., and Nattel, S. (2014). Atrial fibrillation compendium historical context and detailed translational perspective on an important clinical problem. *Circ. Res.* 114, 1447–1452. doi: 10.1161/CIRCRESAHA.114.303466
- Varela, M., Colman, M. A., Hancox, J. C., and Aslanidi, O. V. (2016). Atrial heterogeneity generates re-entrant substrate during atrial fibrillation and anti-arrhythmic drug action: mechanistic insights from canine atrial models. *PLoS Comput. Biol.* 12:e1005245. doi: 10.1371/journal.pcbi.1005245
- Verma, A., Jiang, C.-Y., Betts, T. R., Chen, J., Deisenhofer, I., Mantovan, R., et al. (2015). Approaches to catheter ablation for persistent atrial fibrillation. *N. Eng. J. Med.* 372, 1812–1822. doi: 10.1056/NEJMoa1408288
- Vigmond, E., Pashaei, A., Amraoui, S., Cochet, H., and Hassaguerre, M. (2016). Percolation as a mechanism to explain atrial fractionated electrograms and reentry in a fibrosis model based on imaging data. *Heart Rhythm* 13, 1536–1543. doi: 10.1016/j.hrthm.2016.03.019
- Woods, C. E., and Olgin, J. (2014). Atrial fibrillation therapy now and in the future: drugs, biologicals, and ablation. *Circ. Res.* 114, 1532–1546. doi: 10.1161/CIRCRESAHA.114.302362
- Wyse, D. G., Waldo, A. L., DiMarco, J. P., Domanski, M. J., Rosenberg, Y., Schron, E. B., et al. (2002). A comparison of rate control and rhythm control in patients with atrial fibrillation. *N. Eng. J. Med.* 347, 1825–1833. doi: 10.1056/NEJMoa021328
- Xiong, Z., Fedorov, V. V., Fu, X., Cheng, E., Macleod, R., and Zhao, J. (2019). Fully automatic left atrium segmentation from late gadolinium-enhanced magnetic resonance imaging using a dual fully convolutional neural network. *IEEE Trans. Med. Imaging* 38, 515–524. doi: 10.1109/TMI.2018.2866845
- Zahid, S., Cochet, H., Boyle, P. M., Schwarz, E. L., Whyte, K. N., Vigmond, E. J., et al. (2016). Patient-derived models link re-entrant driver localization in atrial fibrillation to fibrosis spatial pattern. *Cardiovasc. Res.* 110, 443–454. doi: 10.1093/cvr/cvw073
- Zhao, J., Hansen, B. J., Csepe, T. A., Lim, P., Wang, Y., Williams, M., et al. (2015). Integration of high-resolution optical mapping and 3-dimensional micro-computed tomographic imaging to resolve the structural basis of atrial conduction in the human heart. *Circul. Arrhythmia Electrophysiol.* 8, 1514–1517. doi: 10.1161/CIRCEP.115.03064
- Zhao, J., Hansen, B. J., Wang, Y., Csepe, T. A., Sul, L. V., Tang, A., et al. (2017). Three-dimensional integrated functional, structural, and computational mapping to define the structural “fingerprints” of heart-specific atrial fibrillation drivers in human heart *ex vivo*. *J. Am. Heart Assoc.* 6:e005922. doi: 10.1161/JAHA.117.005922

Conflict of Interest Statement: The authors declare that the research was conducted in the absence of any commercial or financial relationships that could be construed as a potential conflict of interest.

Copyright © 2019 Zhao, Aslanidi, Kuklik, Lee, Tse, Niederer and Vigmond. This is an open-access article distributed under the terms of the Creative Commons Attribution License (CC BY). The use, distribution or reproduction in other forums is permitted, provided the original author(s) and the copyright owner(s) are credited and that the original publication in this journal is cited, in accordance with accepted academic practice. No use, distribution or reproduction is permitted which does not comply with these terms.



Atrial Fibrillation Recurrence and Peri-Procedural Complication Rates in nMARQ vs. Conventional Ablation Techniques: A Systematic Review and Meta-Analysis

OPEN ACCESS

Edited by:

Gabriele Giacomo Schiattarella,
University of Naples Federico II, Italy

Reviewed by:

Celestino Sardu,
Università degli Studi della Campania
"Luigi Vanvitelli" Naples, Italy

Douglas L. Jones,
University of Western Ontario, Canada

*Correspondence:

Tong Liu
liutongdoc@126.com
Gary Tse
tseg@cuhk.edu.hk

[†]Co-first authors.

Specialty section:

This article was submitted to
Clinical and Translational Physiology,
a section of the journal
Frontiers in Physiology

Received: 27 November 2017

Accepted: 27 April 2018

Published: 22 May 2018

Citation:

Li KHC, Dong M, Gong M, Bazoukis G, Lakhani I, Ting YY, Wong SH, Li G, Wu WKK, Vassiliou VS, Wong MCS, Letsas K, Du Y, Laxton V, Yan BP, Chan YS, Xia Y, Liu T, Tse G and International Health Informatics Study (IHIS) Network (2018) Atrial Fibrillation Recurrence and Peri-Procedural Complication Rates in nMARQ vs. Conventional Ablation Techniques: A Systematic Review and Meta-Analysis. *Front. Physiol.* 9:544. doi: 10.3389/fphys.2018.00544

Ka H. C. Li^{1,2,3†}, Mei Dong^{4†}, Mengqi Gong⁵, George Bazoukis⁶, Ishan Lakhani^{2,3}, Yan Y. Ting^{2,3}, Sunny H. Wong^{2,3}, Guangping Li⁷, William K. K. Wu⁸, Vassilios S. Vassiliou⁹, Martin C. S. Wong¹⁰, Konstantinos Letsas⁵, Yimei Du¹¹, Victoria Laxton¹², Bryan P. Yan¹, Yat S. Chan¹, Yunlong Xia¹², Tong Liu^{2*}, Gary Tse^{2,3*} and International Health Informatics Study (IHIS) Network

¹ Faculty of Medicine, Newcastle University, Newcastle upon Tyne, United Kingdom, ² Department of Medicine and Therapeutics, Faculty of Medicine, Chinese University of Hong Kong, Hong Kong, China, ³ Li Ka Shing Institute of Health Sciences, Faculty of Medicine, Chinese University of Hong Kong, Hong Kong, China, ⁴ Department of Cardiology, The Affiliated Yantai Yuhuangding Hospital of Qingdao University, Yantai City, China, ⁵ Tianjin Key Laboratory of Ionic-Molecular Function of Cardiovascular Disease, Department of Cardiology, Tianjin Institute of Cardiology, Second Hospital of Tianjin Medical University, Tianjin, China, ⁶ Laboratory of Cardiac Electrophysiology, Second Department of Cardiology, Evangelismos General Hospital of Athens, Athens, Greece, ⁷ Key Laboratory of Cardiovascular Remodeling and Function Research, Chinese Ministry of Education and Chinese Ministry of Health, Department of Cardiology, Shandong University Qilu Hospital, Jinan, China, ⁸ Department of Anaesthesia and Intensive Care, State Key Laboratory of Digestive Disease, LKS Institute of Health Sciences, The Chinese University of Hong Kong, Hong Kong, China, ⁹ Norwich Medical School, University of East Anglia, Norwich, United Kingdom, ¹⁰ The Jockey Club School of Public Health and Primary Care, Faculty of Medicine, The Chinese University of Hong Kong, Hong Kong, China, ¹¹ Research Center of Ion Channelopathy, Institute of Cardiology, Union Hospital, Tongji Medical College, Huazhong University of Science and Technology, Wuhan, China, ¹² Department of Cardiology, First Affiliated Hospital of Dalian Medical University, Dalian, China

Background and Objectives: Atrial fibrillation is a common abnormal cardiac rhythm caused by disorganized electrical impulses. AF which is refractory to antiarrhythmic management is often treated with catheter ablation. Recently a novel ablation system (nMARQ) was introduced for PV isolation. However, there has not been a systematic review of its efficacy or safety compared to traditional ablation techniques. Therefore, we conducted this meta-analysis on the nMARQ ablation system.

Methods: PubMed and EMBASE were searched up until 1st of September 2017 for articles on nMARQ. A total of 136 studies were found, and after screening, 12 studies were included in this meta-analysis.

Results: Our meta-analysis shows that the use of nMARQ was associated with higher odds of AF non-recurrence ($n = 1123$, odds ratio = 6.79, 95% confidence interval 4.01–11.50; $P < 0.05$; I^2 took a value of 83%). Moreover, the recurrence rate of AF using nMARQ was not significantly different from that of traditional ablation procedures ($n = 158$ vs. 196; $OR = 0.97$, 95% confidence interval: 0.59–1.61). No significant difference in complication rates was observed between these groups (RR: 0.86; 95% CI: 0.37–1.99; $P > 0.05$). There were four reported mortalities in the nMARQ group compared to none in the conventional ablation group (relative risk: 1.58; 95% CI: 0.09–29.24; $P > 0.05$).

Conclusions: AF recurrence rates are comparable between nMARQ and conventional ablation techniques. Although general complication rates are similar for both groups, the higher mortality with nMARQ suggests that conventional techniques should be used for resistant AF until improved safety profiles of nMARQ can be demonstrated.

Keywords: nMARQ, nMARQTM, ablation, atrial fibrillation, recurrence

INTRODUCTION

Atrial fibrillation (AF) is the most common arrhythmia encountered in clinical practice. It can have both re-entrant and triggered mechanisms (Tse et al., 2016), the latter exemplified by impulses originating from the roots of the pulmonary veins (Hu et al., 2015). One of the major concerns associated with AF is an increased risk of thrombo-embolic events (stroke or systemic embolism). Anticoagulation therapies are therefore recommended in all patients with AF who are at moderate-to-high risk of stroke (Singer et al., 2008; Camm et al., 2010), which include the presence of co-morbidities such as type 2 diabetes mellitus (Marfella et al., 2013; Steinberg et al., 2015). As well as the increased risk of thrombo-embolic events, AF also remains a major aetiological factor of heart failure and increased hospitalization rates. As such, establishing an effective monitoring system for early AF detection along with an effective approach to treating AF is essential (Sardu et al., 2016).

Numerous studies have demonstrated the superiority of interventions over pharmacological approaches for the maintenance of sinus rhythm in patients with both paroxysmal and persistent AF. Considering that the pulmonary vein (PV) can produce rapid focal activation that contributes to AF persistence, disruption of the electrical connection between the left atrium and the left and right PVs by circumferential PV isolation may prevent occurrence of the arrhythmia (Calkins et al., 2012b; Camm et al., 2012). Apart from the irrigated single-tip, point-by-point delivery technique, innovative technologies such as single-shot devices, balloon technology, and circumferential multipolar ablation catheters have been introduced over the last decade as alternatives for ablation procedures. These new ablation tools have allowed for safer and more efficient isolation by applying different forms of energy to create linear lesions at the peri-PV ostia region (Deneke et al., 2011; Schade et al., 2012; Packer et al., 2013).

Recently, circular irrigated radiofrequency ablation using the novel ablation system, nMARQ, (Biosense Webster, Diamond Bar, CA, USA) has been introduced for circumferential PV isolation. Several studies have compared nMARQ with conventional ablation tools. However, the definite efficacy of this new system has not been clearly elucidated due to differing results from the studies and there has not been a systematic evaluation to date. In this study, we therefore conducted a systematic review and meta-analysis to examine AF recurrence as well as peri-procedural complications between the nMARQ ablation system and traditional ablation techniques.

Pathophysiology of AF

Currently, a combination of triggered and re-entrant mechanisms involving not only the atrium itself but structures such as ganglionated plexi and the pulmonary veins have been proposed to underlie the generation and maintenance of AF (Calkins et al., 2012a). Autonomic modulation is thought to be an important mediator of arrhythmogenesis (Marrouche et al., 2014; Rizzo et al., 2015). Recently, Yang Felix et al. proposed a common pathophysiological pathway that can cause the development and progression of AF associated with inflammatory and fibrotic changes (Yang et al., 2017). This was supported by Cochet et al. who described the difference in atrial fibrosis distribution between patients with and without AF (Cochet et al., 2015).

METHODS

Search Strategy, Inclusion, and Exclusion Criteria

The meta-analysis was performed according to the Preferred Reporting Items for Systematic Reviews and Meta-Analyses statement (Moher et al., 2009). PubMed and EMBASE were searched for studies that investigated AF recurrence rates using nMARQ and/or conventional ablation techniques. The following terms were used: “nMARQ” and “nMARQTM.” The search period was from the beginning of the databases through to 1st September 2017 with no language restrictions. The following inclusion criteria were applied: (i) the design was a case-control, prospective or retrospective cohort study in humans, (ii) AF recurrence and complication rates were reported for nMARQ with or without comparison to conventional ablation techniques. Included studies also adhered to the follow-up recommendations post-ablation from the 2016 ESC guidelines for the management of atrial fibrillation developed in collaboration with EACTS. These suggest that “patients should be seen at least once by a rhythm specialist in the first 12 months after ablation” (Kirchhof et al., 2016).

The quality assessment of these studies included in our meta-analysis was performed using the Newcastle–Ottawa Quality Assessment Scale (NOS). The point score system evaluated the categories of study participant selection, comparability of the results, and quality of the outcomes. The following characteristics were assessed: (a) representativeness of the exposed cohort; (b) selection of the non-exposed cohort; (c) ascertainment of exposure; (d) demonstration that outcome of interest was not present at the start of study; (e) comparability of cohorts on the basis of the design or analysis; (f) assessment of outcomes; (g)

follow-up period sufficiently long for outcomes to occur; and (h) adequacy of follow-up of cohorts. This scale varied from zero to nine stars, which indicated that studies were graded as poor quality if they met <5 criteria, fair if they met 5 to 7 criteria, and good if they met >8 criteria. The details of the NOS quality assessment are shown in Supplementary Table 1.

Data Extraction and Statistical Analysis

Data from the studies were entered in a pre-specified spreadsheet in Microsoft Excel. All publications identified were assessed for compliance with the inclusion criteria. In this meta-analysis the extracted data elements consisted of: (i) publication details: surname name of first author, publication year; (ii) study design; (iii) follow-up duration; (iv) the quality score; and (v) the characteristics of the population including sample size, gender, age. Two reviewers (CL and MD) independently reviewed each included study and disagreements were resolved by adjudication with input from a third reviewer (TL). Research findings from abstracts are frequently significantly different from the final publication and have not undergone the same degree of rigorous peer review process as normally required for journal articles. For these reasons only full-text publications were included in this meta-analysis.

Heterogeneity across studies was determined using Cochran's Q -value and the I^2 statistic from the standard chi-square test. Cochran's Q -value is the weighted sum of squared differences between individual study effects and the pooled effect across studies. The I^2 statistic from the standard chi-square test describes the percentage of variability in the effect estimates resulting from heterogeneity. $I^2 > 50\%$ was considered to reflect significant statistical heterogeneity. The random-effects model using the inverse variance heterogeneity method was used with $I^2 > 50\%$. To locate the origin of the heterogeneity, subgroup analyses based on different disease conditions and different endpoints were performed. Sensitivity analysis excluding one study at a time was also performed. Funnel plots showing standard errors or precision against the logarithms of the odds ratio were constructed. The Begg and Mazumdar rank correlation test and Egger's test were used to assess for possible publication bias.

RESULTS

Efficacy of the nMARQ Ablation Technique

A flow diagram detailing the above search strategy with inclusion and exclusion criteria is shown in **Figure 1**. A total of 31 publications were found and further assessment demonstrated that 13 met the inclusion criteria. The Kiss et al. (2014) study was excluded due to AF recurrence not being reported as an endpoint. Therefore, a total of 12 studies were included in this meta-analysis (Scaglione et al., 2014; Zellerhoff et al., 2014; Dello Russo et al., 2015; Farkash et al., 2015; Mahida et al., 2015; Burri et al., 2016; Laish-Farkash et al., 2016; Lauschke et al., 2016; Rodriguez-Entem et al., 2016; Rosso et al., 2016; Vurma et al., 2016; Wakili et al., 2016). Of these, six reported efficacy of the novel nMARQ ablation system without any comparison. Four studies compared it to other ablation techniques such as

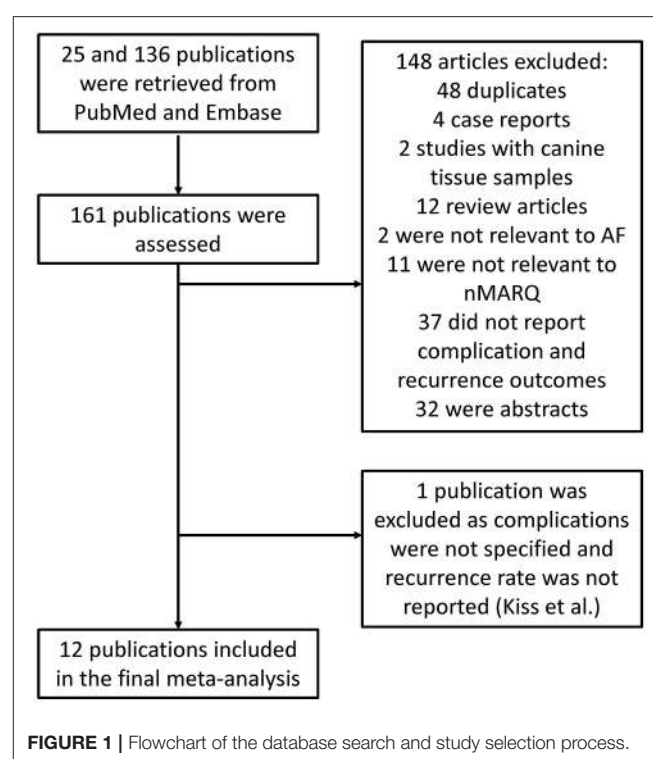


FIGURE 1 | Flowchart of the database search and study selection process.

single-catheter ablation catheterisation (SAC) (Lauschke et al., 2016; Wakili et al., 2016), "Smart Touch" radiofrequency (Rosso et al., 2016) and pulmonary vein ablation catheterisation (Laish-Farkash et al., 2016) which uses two circular multi-electrode catheters. Two studies divided the nMARQ sample into either different technical approaches (Dello Russo et al., 2015) or into the efficacy of nMARQ in paroxysmal and persistent AF (Vurma et al., 2016). The baseline characteristics of these studies are listed in **Table 1**. Three were retrospective studies and nine were prospective studies. The mean follow-up duration was 9.3 months based on 11 out of 12 studies as one study did not provide information regarding this.

Efficacy of the nMARQ Ablation Technique Compared to Conventional Ablation Techniques

The conventional ablation techniques include (i) "point-by-point" radiofrequency using a single irrigated tip ablation catheter and (ii) pulmonary vein ablation catheter, which uses two circular multi-electrode catheters. Three studies compared nMARQ with single-tip ablation catheter and one with the two circular multi-electrode catheters. A total of 158 patients were treated with nMARQ compared to 196 patients undergoing conventional ablation procedures (**Table 2**). The mean age for the conventional ablation group was 61.5 ± 10.5 years and 61.2% of the subjects were male. The mean total procedure time was 103.8 ± 32.4 min and the mean total fluoroscopy time was 27.9 ± 12.4 min. Our meta-analysis shows that the recurrence rate of AF using nMARQ was not significantly different from that

TABLE 1 | Baseline characteristics of the included studies.

	Sample no. (n)	Mean age (years \pm SD)	Males n(%)	Paroxysmal AF n(%)	Mean LVEF (% \pm SD)	Mean Follow-up (Months)	Total procedure time (min \pm SD)	Fluoroscopy time (min \pm SD)	Cum. Radiofrequency time (min \pm SD)	Acute success rate n(%)	Periprocedural complications n(%)
Burri et al., 2016	50	58 \pm 10	37(74)	50(100)	55 \pm 5	15	100 \pm 25	22 \pm 8	13.3 \pm 2.2	—	—
Dello Russo et al., 2015	37	53.5 \pm 10	28(75.5)	31(83.8)	61 \pm 3.5	3	nMARQ with ICE	23.1 \pm 9	—	—	2
Laish-Farkash et al., 2016	82	63 \pm 10.6	55(67)	62(76)	>5	83 \pm 23	nMARQ with ICE + TC tech	27.7 \pm 5	78(95)	8	—
Lauschke et al., 2016	11	59.6 \pm 8	8(72.7)	6(54.5)	53 \pm 15	10.6	111.8 \pm 34.9	30 \pm 8.5	—	—	1
Manida et al., 2015	374	60 \pm 10	264(70.6)	263(70.3)	60 \pm 8	12	160 \pm 42	205 \pm 8.9	243(65)	2	243(65)
Rodriguez-Entem et al., 2016	35	57.3 \pm 8.6	28(80)	35(100)	62.6 \pm 5.8	16.8	79.5 \pm 39.3	31.6 \pm 8.2	33(94.2)	1	33(94.2)
Rosso et al., 2016	36	58 \pm 10	27(75)	23(64)	>5	20.3	101 \pm 26.4	25.9 \pm 9.5	28(78)	0	28(78)
Scaglione et al., 2014	25	57 \pm 13	19(76)	25(100)	61 \pm 6	6	131 \pm 49	1.8 \pm 2	24(96)	3	24(96)
Vurman et al., 2016	327	Paroxysmal	131(40.1)	>5	Paroxysmal	6	Paroxysmal	14.9 \pm 3.7	Paroxysmal	—	17
Wakili et al., 2016	29	63 \pm 10	62.4 \pm 10	Persistent	68.6 \pm 22.5	18.9 \pm 6.4	Persistent	14.8 \pm 6.6	Persistent	—	—
Zellerhoff et al., 2014	39	64.8 \pm 8.2	64.3 \pm 11.1	16(55)	57.5 \pm 11	13.3	75 \pm 22.7	16.8 \pm 6.3	22.1 \pm 6.1	—	—
Farkash et al., 2015 (group 1)	37	60 \pm 10	31(79)	39(100)	61.5 \pm 12.1	5	132 \pm 37	31 \pm 12	21 \pm 9	—	4
Farkash et al., 2015 (group 2)	41	64 \pm 10.5	23(62)	32(86.5)	>5	86 \pm 29	22.2 \pm 6.5	10 \pm 4.6	37(95)	1	37(95)
		62.5 \pm 11	29(71)	27(66)	>5	12	78 \pm 19	30 \pm 9	10.3 \pm 3.6	36(97)	7
						12	85.5 \pm 18.5	29.5 \pm 8.7	12 \pm 4	40(97.5)	1

TABLE 2 | Efficacy of the nMARQ ablation technique compared to other techniques.

	Sample no. (n)	Mean age (years \pm SD)	Males n(%)	Paroxysmal AF n(%)	Mean LVEF (% \pm SD)	Mean Follow-up (Months)	Total procedure time (min \pm SD)	Fluoroscopy time (min \pm SD)	Cum. Radiofrequency time (min \pm SD)	Acute success rate n(%)	Periprocedural complications n(%)
Wakili et al., 2016	29	64.3 \pm 11.1	16(55)	29(100)	63.4 \pm 7.1	13.3	109 \pm 30	23 \pm 10	35 \pm 12	—	1
Rosso et al., 2016	50	62 \pm 8	32(64)	34(68)	—	19.7	105 \pm 16.6	24 \pm 6	41(82)	0	0
Laish-Farkash et al., 2016	93	61 \pm 10	56(60)	81(87)	>5	94 \pm 27	33 \pm 13	—	90(97)	5	5
Lauschke et al., 2016	24	59.2 \pm 12.3	16(66.6)	20(83.3)	59 \pm 8	13.6	132.7 \pm 48.2	22.4 \pm 9.4	18.6 \pm 13.9	—	0

of traditional ablation procedures ($OR = 0.97$, 95% confidence interval: 0.59–1.61; **Figure 2**).

Peri-Procedural Complications

All studies included in the analysis provided data on perioperative complications. A total of 47 peri-procedural complications (4.19%) occurred in the nMARQ group ($n = 1123$) while complications were observed in 6 patients (3.06%) in the conventional ablation group ($n = 196$). The following complications occurred following the use of nMARQ: groin hematomas ($n = 17$), transient ST-segment elevation ($n = 8$), access site injury ($n = 8$), death ($n = 4$), pericardial tamponade ($n = 4$), pericardial effusion ($n = 3$), phrenic nerve palsy ($n = 1$), oesophageal lesion ($n = 1$), charring injury ($n = 1$). Regarding the complications with the conventional ablation techniques the following occurred: transient ST-segment elevation ($n = 3$), access site injuries ($n = 2$), groin haematoma ($n = 1$). In terms of peri-procedural mortality, four were reported in the nMARQ group from the Mahida et al. and Vurma et al. studies (Mahida et al., 2015; Vurma et al., 2016). Three deaths were attributed to procedure-induced esophageal-pericardial fistulae. The remaining death was due to sepsis (Mahida et al., 2015). By contrast, there was zero mortality in the conventional ablation group.

Additionally, when head-to-head analysis was conducted, the conventional ablation group was associated with lower odds of periprocedural complications (Odds ratio: 2.59; 95% CI: 0.98–6.80; $P = 0.05$). In the head-to-head analysis, the nMARQ group had 1 phrenic nerve palsy, 1 oesophageal lesion, 1 groin haematoma, 1 charring injury, 1 pericardial tamponade, 1 pericardial effusion, 3 transient ST-elevations and 4 access site injuries. In the conventional ablation group there was only 1 haematoma, 3 transient ST-elevations, and 2 access site injuries.

DISCUSSION

This systematic review and meta-analysis evaluated the efficacy of the nMARQ catheter against conventional ablation approaches. Since the main objective of ablation is to treat drug-resistant AF, this study defined AF recurrence as the end-point. All studies adhered to the post-ablation follow-up 2016 ESC guidelines for the management of AF developed in collaboration with EACTS. Physical examinations, evaluation of symptoms, 12-lead ECG recordings, transthoracic echocardiography and Holter ECG recordings (ranging between 1 and 7 days) were included in follow-up monitoring. According to multiple studies included in this meta-analysis AF recurrence is assumed as any atrial tachyarrhythmia lasting at least 30 s on an ECG loop recorder or ECG, regardless if it is organized into flutter or not.

The main findings are that (i) the use of the nMARQ catheter is a useful technique in resolving treatment resistant AF accompanied by low rates of recurrences; ii) when cross-analyzed with conventional techniques, nMARQ is equally as effective as conventional ablation procedures; iii) overall periprocedural complication risk was greater with the use of nMARQ compared to conventional techniques, iv) when mortality was analyzed as a

separate end-point higher mortality was observed in the nMARQ group but this did not achieve statistical significance.

Procedural Parameters

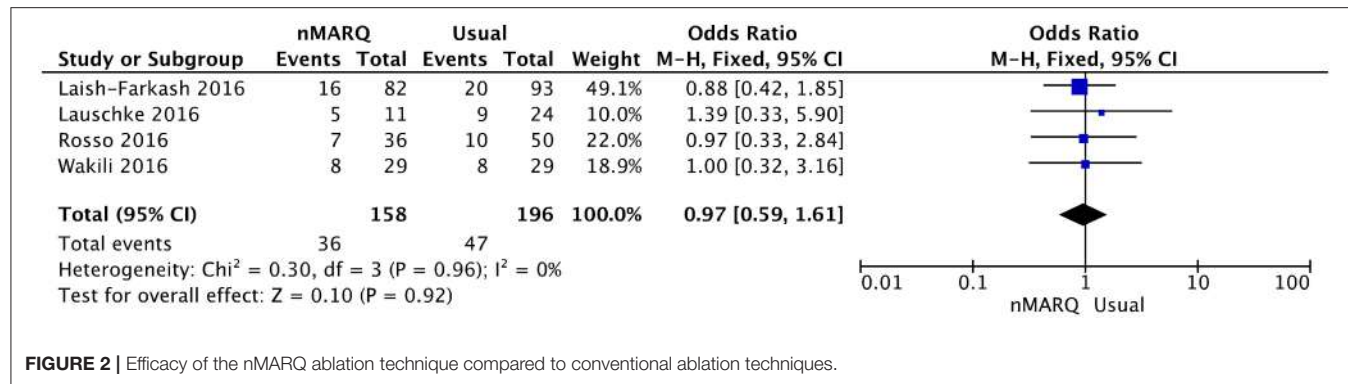
The mean total procedure time (94.6 ± 18.7 vs. 103.8 ± 32.4) and fluoroscopy time (22.1 ± 8.8 vs. 27.9 ± 12.4) were significantly shorter for nMARQ compared to conventional approaches. This difference is due to the variability in the transseptal and procedural approach. Some studies used a dual trans-septal access approach while others used a single-access approach without using a circular mapping catheter (CMC) to confirm pulmonary vein isolation. Studies that used PV mapping were found to have a longer fluoroscopy time of 31–35 min compared to the 20–24 min fluoroscopy time in studies without PV mapping (Wakili et al., 2016). Another possible difference in the procedure and fluoroscopy time is the “learning curve.” In Wakili et al. there was no observable trend in procedural parameters with time. However, in Rosso et al. a significant learning curve was observed with decreasing fluoroscopy and procedural times (Wakili et al., 2016). Burning time was shorter for nMARQ compared to PVAC. The longer total burning time was attributed to the availability of 3D mapping used with nMARQ and not with PVAC. Additionally, nMARQ ablation can be stopped at any point after PV signals are no longer detected after 1 min (Wakili et al., 2016). In terms of left ventricular ejection fraction (LVEF), the values were similar between the nMARQ group (60.4 ± 10.3) and the “Usual” group, which were only reported specifically by Wakili et al. and Lauschke et al. as 63.4 ± 7.1 and 59 ± 8 respectively.

Advantages of nMARQ Over Conventional Ablation Techniques

The availability of 3D mapping with nMARQ confers many advantages over conventional ablation techniques. It allows visualization of catheter position in relation to the PV ostia, guides voltage mapping of the atrium and adds location points of the phrenic nerve route. Moreover, fluoroscopy time can be reduced by using CARTO-MERGE technology. Lines of ablations outside PV ostium can also be added. According to the same study higher atrial arrhythmia incidence was observed for PVAC when compared to nMARQ patients (95 vs. 36.5%, $P = 0.0001$). The origin of the arrhythmogenic activity with PVAC system can be due to the presence of a guide wire stimulating the PV ostia or the different energy used with unipolar electrodes in nMARQ compared to bipolar electrodes in PVAC (Wakili et al., 2016).

Concerns With Success in Achieving Pulmonary Vein Isolation and Peri-Procedural Complications in nMARQ vs. Conventional Ablation Procedures

Confirming ablation success is impulsive for accurately predicting AF recurrence. This is because an incomplete PVI will more likely give rise to a post-procedural AF. The use of the novel circulation ablation catheter, nMARQ, has raised concerns with regard to its ability to successfully achieve successful PVI (von Bary et al., 2011; Wakili et al., 2016). However, Scaglione



et al. and Rosso et al. have adequately addressed this issue (Rosso et al., 2014; Scaglione et al., 2014). Rosso et al. suggested that the nMARQ catheter is associated with poor signal concordance after radiofrequency (RF) application. Their group used a dual transseptal approach instead of the single approach from the start of the procedure, thereby potentially facilitating a successful ablation of residual PV conduction by simultaneous PV mapping with the CMC. The nMARQ most commonly missed persistent atrial PV conduction which was observed in 30% of the examined PVs using a CMC. Similarly, in Scaglione et al., 22% of PVs were found to be persisting post-procedure even though the nMARQ catheter suggested complete PVI. These findings are in keeping with the many studies on nMARQ alone that have all indicated >98% of PVIs are successful (Scaglione et al., 2014; Zellerhoff et al., 2014; Mahida et al., 2015; Burri et al., 2016; Rodriguez-Entem et al., 2016). This is an important aspect to address as it will determine if nMARQ could effectively substitute existing approaches or if supplementary post-RF conduction is required to confirm ablation success (Wakili et al., 2016). Indeed, Lauschke et al. confirmed that complete PV re-isolation is possible with nMARQ (Lauschke et al., 2016). The difficulty in sufficiently isolating the left-inferior pulmonary vein (LIPV) was shown by Wakili et al. as greater RF energy is required but it is also associated with oesophageal injury (Wakili et al., 2016). Another possible complication includes phrenic nerve palsy, which was reported in only one case and occurred despite prophylactic phrenic nerve stimulation (Arroja and Zimmermann, 2015).

In terms of oesophageal complications following ablation, Halbfass et al. recently conducted a retrospective study into their incidences in nMARQ vs. conventional ablation. A total 150 endoscopically detected oesophageal lesions were detected. Of these 26 occurred in 149 patients undergoing nMARQ (17.4%) and 124 occurred in 683 patients undergoing ablation using single-tip catheters (18.2%). Of the 150 endoscopically detected oesophageal lesions detected 98 were erosion injuries and 52 were ulcers of which 5 (9.6%) progressed to perforation (Halbfass et al., 2017).

Periprocedural Mortality in nMARQ vs. Conventional Ablation Techniques

The published studies on nMARQ have demonstrated non-statistically significant higher mortality rates when compared to

conventional ablation techniques (Mahida et al., 2015; Vurma et al., 2016). Of the four deaths that occurred in the nMARQ group, three were due to atrio-oesophageal fistulation and the one due to sepsis. The only multi-center study was halted immediately after the two fatalities were observed (Vurma et al., 2016). Since then it has been recognized that lower power settings were associated with less oesophageal damage (Dekker, 2016). It is possible that deaths could be prevented with lower power settings and greater operator experience. The overall mortality in the nMARQ group was 4.4% compared to 0% in the conventional group. This may be due to different sample sizes in the respective groups (1121 vs. 196). However, a multi-center survey showed that mortality was 0.1% in a sample size of 32,569 patients. This incidence remains much lower than that reported in our meta-analytical study for the nMARQ group (Cappato et al., 2009). Further studies on the efficacy of nMARQ have been stopped due to concerns of increased mortality with its use.

LIMITATIONS

Several limitations of this study should be noted. Firstly, a high degree of heterogeneity was found in our meta-analysis, which may suggest that inconsistency of evidence and therefore our results must be interpreted with caution. This high degree of heterogeneity may be due to differences in the baseline population characteristics between the groups, such as age. Other potential contributing factors include the difference in the proportion of patients with paroxysmal and persistent AF and procedural times in each study. Secondly, cumulative analysis for parameters such as mean LVEF was not calculated due to the lack of information provided by the respective studies. There is also no data with regard to the inflammatory pathways and epigenetic modifications that were reported in the included studies and these can have an influence on therapeutic ablation response (Sardu et al., 2015, 2017).

CONCLUSION

AF recurrence rates are comparable between nMARQ and conventional ablation techniques. Although general complication rates are similar for both groups, the higher

mortality with nMARQ suggests that conventional techniques should be used for resistant AF until improved safety profiles of nMARQ can be demonstrated.

AUTHOR CONTRIBUTION

KL and MD: data extraction and analysis, drafted manuscript; MG: data interpretation, quality analysis; TL: supervision of study, data interpretation, critical revision of manuscript; GT: supervision of study, data analysis, creation of figures, drafted and critical revision of manuscript. All other authors data interpretation, critical revision of manuscript.

REFERENCES

- Arroja, J. D., and Zimmermann, M. (2015). Phrenic nerve lesion: a potential complication of the nMARQ ablation technique. *Int. J. Cardiol.* 180, 91–92. doi: 10.1016/j.ijcard.2014.11.160
- Burri, H., Park, C. I., Poku, N., Giraudet, P., Stettler, C., and Zimmermann, M. (2016). Pulmonary vein isolation for paroxysmal atrial fibrillation using a circular multipolar ablation catheter: safety and efficacy using low-power settings. *J. Cardiovasc. Electrophysiol.* 27, 170–174. doi: 10.1111/jce.12853
- Calkins, H., Kuck, K. H., Cappato, R., Brugada, J., Camm, A. J., Chen, S. A., et al. (2012a). 2012 HRS/EHRA/ECAS expert consensus statement on catheter and surgical ablation of atrial fibrillation: recommendations for patient selection, procedural techniques, patient management and follow-up, definitions, endpoints, and research trial design. *Europace* 14, 528–606. doi: 10.1093/europace/eus027
- Calkins, H., Kuck, K. H., Cappato, R., Brugada, J., Camm, A. J., Chen, S. A., et al. (2012b). 2012 HRS/EHRA/ECAS expert consensus statement on catheter and surgical ablation of atrial fibrillation: recommendations for patient selection, procedural techniques, patient management and follow-up, definitions, endpoints, and research trial design: a report of the Heart Rhythm Society (HRS) Task Force on Catheter and Surgical Ablation of Atrial Fibrillation. Developed in partnership with the European Heart Rhythm Association (EHRA), a registered branch of the European Society of Cardiology (ESC) and the European Cardiac Arrhythmia Society (ECAS); and in collaboration with the American College of Cardiology (ACC), American Heart Association (AHA), the Asia Pacific Heart Rhythm Society (APHRS), and the Society of Thoracic Surgeons (STS). Endorsed by the governing bodies of the American College of Cardiology Foundation, the American Heart Association, the European Cardiac Arrhythmia Society, the European Heart Rhythm Association, the Society of Thoracic Surgeons, the Asia Pacific Heart Rhythm Society, and the Heart Rhythm Society. *Heart Rhythm* 9, 632 e621–696 e621. doi: 10.1016/j.hrthm.2011.12.016
- Camm, A. J., Kirchhof, P., Lip, G. Y., Schotten, U., Savelieva, I., Ernst, S., et al. (2010). Guidelines for the management of atrial fibrillation: the Task Force for the Management of Atrial Fibrillation of the European Society of Cardiology (ESC). *Eur. Heart J.* 31, 2369–2429. doi: 10.1093/eurheartj/ehq278
- Camm, A. J., Lip, G. Y., De Caterina, R., Savelieva, I., Atar, D., Hohnloser, S. H., et al. (2012). 2012 focused update of the ESC Guidelines for the management of atrial fibrillation: an update of the 2010 ESC Guidelines for the management of atrial fibrillation—developed with the special contribution of the European Heart Rhythm Association. *Europace* 14, 1385–1413. doi: 10.1093/europace/eus305
- Cappato, R., Calkins, H., Chen, S. A., Davies, W., Iesaka, Y., Kalman, J., et al. (2009). Prevalence and causes of fatal outcome in catheter ablation of atrial fibrillation. *J. Am. Coll. Cardiol.* 53, 1798–1803. doi: 10.1016/j.jacc.2009.02.022
- Cochet, H., Mouries, A., Nivat, H., Sacher, F., Derval, N., Denis, A., et al. (2015). Age, atrial fibrillation, and structural heart disease are the main determinants of left atrial fibrosis detected by delayed-enhanced magnetic resonance imaging in a general cardiology population. *J. Cardiovasc. Electrophysiol.* 26, 484–492. doi: 10.1111/jce.12651
- Dekker, L. R. (2016). Last call on nMARQ™ safety. *EP Europace* 18, 1119–1120. doi: 10.1093/europace/euw134
- Dello Russo, A., Fassini, G., Casella, M., Di Monaco, A., Riva, S., Romano, V., et al. (2015). Usefulness of intracardiac echocardiography during pulmonary vein isolation with the novel multipolar irrigated ablation catheter (nMARQ). *J. Interv. Card. Electrophysiol* 44, 39–45. doi: 10.1007/s10840-015-0026-0
- Deneke, T., Mugge, A., Balta, O., Horlitz, M., Grewe, P. H., and Shin, D. I. (2011). Treatment of persistent atrial fibrillation using phased radiofrequency ablation technology. *Expert Rev. Cardiovasc. Ther.* 9, 1041–1049. doi: 10.1586/erc.11.110
- Farkash, A. L., Katz, A., Cohen, O., Fishman, E., Yosefy, C., and Khalameizer, V. (2015). Safety and feasibility of contrast injection during pulmonary vein isolation with the nMARQ multi-electrode catheter. *J. Atr. Fibrillat.* 8:1324. doi: 10.4022/jafib.1324
- Halbfass, P., Pavlov, B., Muller, P., Nentwich, K., Sonne, K., Barth, S., et al. (2017). Progression from esophageal thermal asymptomatic lesion to perforation complicating atrial fibrillation ablation: a single-center registry. *Circ. Arrhythm. Electrophysiol.* 10:e005233. doi: 10.1161/CIRCEP.117.005233
- Hu, Y. F., Chen, Y. J., Lin, Y. J., and Chen, S. A. (2015). Inflammation and the pathogenesis of atrial fibrillation. *Nat. Rev. Cardiol.* 12, 230–243. doi: 10.1038/nrccardio.2015.2
- Kirchhof, P., Benussi, S., Kotecha, D., Ahlsson, A., Atar, D., Casadei, B., et al. (2016). 2016 ESC Guidelines for the management of atrial fibrillation developed in collaboration with EACTS. *Eur. Heart J.* 37, 2893–2962. doi: 10.1093/eurheartj/ehw210
- Kiss, A., Nagy-Baló, E., Sándorfi, G., Edes, I., and Csanádi, Z. (2014). Cerebral microembolization during atrial fibrillation ablation: comparison of different single-shot ablation techniques. *Int. J. Cardiol.* 174, 276–281. doi: 10.1016/j.ijcard.2014.03.175
- Laish-Farkash, A., Khalameizer, V., Fishman, E., Cohen, O., Yosefy, C., Cohen, I., et al. (2016). Safety, efficacy, and clinical applicability of pulmonary vein isolation with circular multi-electrode ablation systems: PVAC(R) vs. nMARQ for atrial fibrillation ablation. *Europace* 18, 807–814. doi: 10.1093/europace/euv258
- Lauschke, J., Schneider, R., Wissmann, J., Tischer, T., and Bansch, D. (2016). Single-catheter approach to pulmonary vein reisolation in selected patients: data from a prospective registry. *Herz* 41, 625–629. doi: 10.1007/s00059-016-4402-z
- Mahida, S., Hooks, D. A., Nentwich, K., Ng, G. A., Grimaldi, M., Shin, D. I., et al. (2015). nMARQ ablation for atrial fibrillation: results from a multicenter study. *J. Cardiovasc. Electrophysiol.* 26, 724–729. doi: 10.1111/jce.12698
- Marfella, R., Sasso, F. C., Siniscalchi, M., Cirillo, M., Paolosso, P., Sardu, C., et al. (2013). Brief episodes of silent atrial fibrillation predict clinical vascular brain disease in type 2 diabetic patients. *J. Am. Coll. Cardiol.* 62, 525–530. doi: 10.1016/j.jacc.2013.02.091
- Marrouche, N. F., Wilber, D., Hindricks, G., Jais, P., Akoum, N., Marchlinski, F., et al. (2014). Association of atrial tissue fibrosis identified by delayed enhancement MRI and atrial fibrillation catheter ablation: the DECAAF study. *JAMA* 311, 498–506. doi: 10.1001/jama.2014.3
- Moher, D., Liberati, A., Tetzlaff, J., and Altman, D. G. (2009). Preferred reporting items for systematic reviews and meta-analyses: the PRISMA statement. *BMJ* 339:b2535. doi: 10.1136/bmj.b2535

ACKNOWLEDGMENTS

GT and SW are supported by Clinical Assistant Professorships from the Croucher Foundation of Hong Kong. This work was supported by grants (81570298 to TL) from the National Natural Science Foundation of China.

SUPPLEMENTARY MATERIAL

The Supplementary Material for this article can be found online at: <https://www.frontiersin.org/articles/10.3389/fphys.2018.00544/full#supplementary-material>

- Packer, D. L., Kowal, R. C., Wheelan, K. R., Irwin, J. M., Champagne, J., Guerra, P. G., et al. (2013). Cryoballoon ablation of pulmonary veins for paroxysmal atrial fibrillation: first results of the North American Arctic Front (STOP AF) pivotal trial. *J. Am. Coll. Cardiol.* 61, 1713–1723. doi: 10.1016/j.jacc.2012.11.064
- Rizzo, M. R., Sasso, F. C., Marfella, R., Siniscalchi, M., Paolisso, P., Carbonara, O., et al. (2015). Autonomic dysfunction is associated with brief episodes of atrial fibrillation in type 2 diabetes. *J. Diabetes Complicat.* 29, 88–92. doi: 10.1016/j.jdiacomp.2014.09.002
- Rodriguez-Entem, F., Exposito, V., Rodriguez-Manero, M., Gonzalez-Enriquez, S., Fernandez-Lopez, X. A., Garcia-Seara, J., et al. (2016). Initial experience and treatment of atrial fibrillation using a novel irrigated multielectrode catheter: results from a prospective two-center study. *J. Arrhythm.* 32, 95–101. doi: 10.1016/j.joa.2015.09.011
- Rosso, R., Chorin, E., Levi, Y., Rogowski, O., and Viskin, S. (2016). Radiofrequency ablation of atrial fibrillation: nonrandomized comparison of circular versus point-by-point “smart” ablation for achieving circumferential pulmonary vein isolation and curing arrhythmic symptoms. *J. Cardiovasc. Electrophysiol.* doi: 10.1111/jce.13058. [Epub ahead of print].
- Rosso, R., Halkin, A., Michowitz, Y., Belhassen, B., Glick, A., and Viskin, S. (2014). Radiofrequency ablation of paroxysmal atrial fibrillation with the new irrigated multipolar nMARQ ablation catheter: verification of intracardiac signals with a second circular mapping catheter. *Heart Rhythm* 11, 559–565. doi: 10.1016/j.hrthm.2013.12.029
- Sardu, C., Santamaria, M., Paolisso, G., and Marfella, R. (2015). microRNA expression changes after atrial fibrillation catheter ablation. *Pharmacogenomics* 16, 1863–1877. doi: 10.2217/pgs.15.117
- Sardu, C., Santamaria, M., Rizzo, M. R., Barbieri, M., di Marino, M., Paolisso, G., et al. (2016). Telemonitoring in heart failure patients treated by cardiac resynchronization therapy with defibrillator (CRT-D): the TELECART Study. *Int. J. Clin. Pract.* 70, 569–576. doi: 10.1111/ijcp.12823
- Sardu, C., Santulli, G., Santamaria, M., Barbieri, M., Sacra, C., Paolisso, P., et al. (2017). Effects of alpha lipoic acid on multiple cytokines and biomarkers and recurrence of atrial fibrillation within 1 year of catheter ablation. *Am. J. Cardiol.* 119, 1382–1386. doi: 10.1016/j.amjcard.2017.01.040
- Scaglione, M., Caponi, D., Anselmino, M., Di Clemente, F., Blandino, A., Ferraris, F., et al. (2014). Pulmonary vein isolation with a new multipolar irrigated radiofrequency ablation catheter (nMARQTM): feasibility, acute and short-term efficacy, safety, and impact on postablation silent cerebral ischemia. *J. Cardiovasc. Electrophysiol.* 25, 1299–1305. doi: 10.1111/jce.12500
- Schade, A., Krug, J., Szollosi, A. G., El Tarahony, M., and Deneke, T. (2012). Pulmonary vein isolation with a novel endoscopic ablation system using laser energy. *Expert Rev. Cardiovasc. Ther.* 10, 995–1000. doi: 10.1586/erc.12.86
- Singer, D. E., Albers, G. W., Dalen, J. E., Fang, M. C., Go, A. S., Halperin, J. L., et al. (2008). Antithrombotic therapy in atrial fibrillation: american college of chest physicians evidence-based clinical practice guidelines (8th Edition). *Chest* 133, 546s–592s. doi: 10.1378/chest.08-0678
- Steinberg, B. A., Hellkamp, A. S., Lokhnygina, Y., Patel, M. R., Breithardt, G., Hankey, G. J., et al. (2015). Higher risk of death and stroke in patients with persistent vs. paroxysmal atrial fibrillation: results from the ROCKET-AF Trial. *Eur. Heart J.* 36, 288–296. doi: 10.1093/eurheartj/ehu359
- Tse, G., Lai, E. T., Lee, A. P., Yan, B. P., and Wong, S. H. (2016). Electrophysiological mechanisms of gastrointestinal arrhythmogenesis: lessons from the heart. *Front. Physiol.* 7:230. doi: 10.3389/fphys.2016.00230
- von Bary, C., Fredersdorf-Hahn, S., Heinicke, N., Jungbauer, C., Schmid, P., Rieger, G. A., et al. (2011). Comparison of PV signal quality using a novel circular mapping and ablation catheter versus a standard circular mapping catheter. *J. Interv. Card. Electrophysiol.* 31, 131–139. doi: 10.1007/s10840-011-9546-4
- Vurma, M., Dang, L., Brunner-La Rocca, H. P., Sutsch, G., Attenhofer-Jost, C. H., Duru, F., et al. (2016). Safety and efficacy of the nMARQ catheter for paroxysmal and persistent atrial fibrillation. *Europace* 18, 1164–1169. doi: 10.1093/europace/euw048
- Wakili, R., Siebermair, J., Fichtner, S., Sinner, M. F., Klocker, E., Olesch, L., et al. (2016). One-year clinical outcome after ablation with a novel multipolar irrigated ablation catheter for treatment of atrial fibrillation: potential implications for clinical use. *Europace* 18, 1170–1178. doi: 10.1093/europace/euv349
- Yang, F., Tiano, J., Mittal, S., Turakhia, M., Jacobowitz, I., and Greenberg, Y. (2017). Towards a mechanistic understanding and treatment of a progressive disease: atrial fibrillation. *J. Atr. Fibrillat.* 10:1627. doi: 10.4022/jafib.1627
- Zellerhoff, S., Daly, M., Lim, H. S., Denis, A., Komatsu, Y., Jesel, L., et al. (2014). Pulmonary vein isolation using a circular, open irrigated mapping and ablation catheter (nMARQ): a report on feasibility and efficacy. *Europace* 16, 1296–1303. doi: 10.1093/europace/euu133

Conflict of Interest Statement: The authors declare that the research was conducted in the absence of any commercial or financial relationships that could be construed as a potential conflict of interest.

Copyright © 2018 Li, Dong, Gong, Bazoukis, Lakhani, Ting, Wong, Li, Wu, Vassiliou, Wong, Letsas, Du, Laxton, Yan, Chan, Xia, Liu, Tse and International Health Informatics Study (IHIS) Network. This is an open-access article distributed under the terms of the Creative Commons Attribution License (CC BY). The use, distribution or reproduction in other forums is permitted, provided the original author(s) and the copyright owner are credited and that the original publication in this journal is cited, in accordance with accepted academic practice. No use, distribution or reproduction is permitted which does not comply with these terms.



A Machine Learning Aided Systematic Review and Meta-Analysis of the Relative Risk of Atrial Fibrillation in Patients With Diabetes Mellitus

Zhaohan Xiong¹, Tong Liu^{2,3}, Gary Tse⁴, Mengqi Gong^{2,3}, Patrick A. Gladding⁵, Bruce H. Smaill¹, Martin K. Stiles⁶, Anne M. Gillis⁷ and Jichao Zhao^{1*}

¹ Auckland Bioengineering Institute, The University of Auckland, Auckland, New Zealand, ² Department of Cardiology, Second Hospital of Tianjin Medical University, Tianjin, China, ³ Key Laboratory of Ionic-Molecular Function of Cardiovascular Disease, Tianjin Institute of Cardiology, Tianjin, China, ⁴ Department of Medicine and Therapeutics, Li Ka Shing Institute of Health Sciences, The Chinese University of Hong Kong, Shatin, Hong Kong, ⁵ Department of Cardiology, Waitemata District Health Board, Auckland, New Zealand, ⁶ Waikato Hospital, Hamilton, New Zealand, ⁷ Department of Cardiac Sciences, Libin Cardiovascular Institute of Alberta, University of Calgary, Calgary, AB, Canada

OPEN ACCESS

Edited by:

Alexander Pantilov,
Ghent University, Belgium

Reviewed by:

Sanjay Ram Kharche,
University of Western Ontario, Canada
Mohammad Hasan Imam,
American International
University-Bangladesh, Bangladesh

*Correspondence:

Jichao Zhao
j.zhao@auckland.ac.nz

Specialty section:

This article was submitted to
Computational Physiology and
Medicine,
a section of the journal
Frontiers in Physiology

Received: 19 March 2018

Accepted: 13 June 2018

Published: 03 July 2018

Citation:

Xiong Z, Liu T, Tse G, Gong M, Gladding PA, Smaill BH, Stiles MK, Gillis AM and Zhao J (2018) A Machine Learning Aided Systematic Review and Meta-Analysis of the Relative Risk of Atrial Fibrillation in Patients With Diabetes Mellitus. *Front. Physiol.* 9:835. doi: 10.3389/fphys.2018.00835

Background: Meta-analysis is a widely used tool in which weighted information from multiple similar studies is aggregated to increase statistical power. However, the exponential growth of publications in key areas of medical science has rendered manual identification of relevant studies increasingly time-consuming. The aim of this work was to develop a machine learning technique capable of robust automatic study selection for meta-analysis. We have validated this approach with an up-to-date meta-analysis to investigate the association between diabetes mellitus (DM) and new-onset atrial fibrillation (AF).

Methods: The PubMed online database was searched from 1960 to September 2017 where 4,177 publications that mentioned both DM and AF were identified. Relevant studies were selected as follows. First, publications were clustered based on common text features using an unsupervised K-means algorithm. Clusters that best matched the selected set of potentially relevant studies (a “training” set of 139 articles) were then identified by using maximum entropy classification. The 139 articles selected automatically on this basis were screened manually to identify potentially relevant studies. To determine the validity of the automated process, a parallel set of studies was also assembled by manually screening all initially searched publications. Finally, detailed manual selection was performed on the full texts of the studies in both sets using standard criteria. Quality assessment, meta-regression random-effects models, sensitivity analysis and publication bias assessment were then conducted.

Results: Machine learning-assisted screening identified the same 29 studies for meta-analysis as those identified by using manual screening alone. Machine learning enabled more robust and efficient study selection, reducing the number of studies needed for manual screening from 4,177 to 556 articles. A pooled analysis using the most

conservative estimates indicated that patients with DM had ~49% greater risk of developing AF compared with individuals without DM. After adjusting for three additional risk factors i.e., hypertension, obesity and heart disease, the relative risk was 23%. Using multivariate adjusted models, the risk for developing AF in patients with DM was similar for all DM subtypes. Women with DM were 24% more likely to develop AF than men with DM. The risk for new-onset AF in patients with DM has also increased over the years.

Conclusions: We have developed a novel machine learning method to identify publications suitable for inclusion in meta-analysis. This approach has the capacity to provide for a more efficient and more objective study selection process for future such studies. We have used it to demonstrate that DM is a strong, independent risk factor for AF, particularly for women.

Keywords: atrial fibrillation, diabetes mellitus, meta-analysis, machine learning, risk factor

INTRODUCTION

Meta-analysis is a powerful epidemiological tool that is increasingly used in all fields of scientific research. It seeks to amplify statistical power by aggregating weighted information from multiple similar studies (Moher et al., 2009). This approach is driven by the view that common trends, masked by potential error in individual scientific investigations, will be revealed if sufficient numbers of conceptually similar studies are combined and different sources of error are appropriately accounted for. The exponential growth of publications in key areas of medical science offers important new opportunities to extend the scope of meta-analyses, however, it has also rendered conventional manual identification of relevant studies increasingly time-consuming. Furthermore, the selection of studies for meta-analysis must be based on objective criteria and bias that is introduced from manual selection can affect results.

Atrial fibrillation (AF) is the most commonly sustained arrhythmia that is associated with substantial morbidity and mortality (Colilla et al., 2013). In the developed world, one in five strokes in people aged over 60 years is associated with AF (Colilla et al., 2013; Krijthe et al., 2013). The overall prevalence of AF is currently ~2% of the general population worldwide and is projected to more than double in the next four decades due to the aging population and the increasing incidence of other concurrent diseases (Colilla et al., 2013; Krijthe et al., 2013). Risk factors of AF include age, hypertension, obesity, valvular heart disease, heart failure and obstructive sleep apnea (Movahed et al., 2005). The relationship between AF and diabetes mellitus (DM) is complex since both diseases are associated with confounders, such as hypertension, obesity and vascular disease (Schoen et al., 2012). Some (Krahn et al., 1995; Kannel et al., 1998; Movahed et al., 2005; Aksnes et al., 2008; Huxley et al., 2011) but not all epidemiological studies (Frost et al., 2005; Fontes et al., 2012; Huxley et al., 2012; Johnson et al., 2014) have suggested that DM represents an independent risk factor for AF. However, these studies have been limited by their diverse research designs and lack of a sufficient number of enrolled patients. Individually, no study has established overwhelming evidence of the association.

The causality of the relationship between DM and AF was initially investigated by a small-scale meta-analysis (Huxley et al., 2011) that included only six prospective cohort studies and four case-control studies with significant heterogeneity selected from 482 publications searched in 2010. Over the past 8 years, more than 2,000 additional publications have reported the association between DM and AF. These additional data samples enhance the statistical power of meta-analyses to determine the association between DM and AF, but they also amplify the burden of selection at the same time. The aims of this study were therefore to develop a novel machine learning technique to provide a more efficient and robust study selection method for meta-analysis, and to perform an up-to-date meta-analysis to determine the association between DM and new-onset AF.

MATERIALS AND METHODS

Data Sources and Searches

We conducted this study in accordance with Preferred Reporting Items for Systematic Review and Meta-Analysis (PRISMA) guidelines (Moher et al., 2009) (refer to the PRISMA 2009 Flow Diagram in Figure S1). A strategic search was conducted on the PubMed online database of publications from 1960 to 1 September 2017. The search included any studies that contained the keywords “diabetes”/“diabetic” and “atrial fibrillation” in any field without language restriction. This identified a wide range of research studies that involved both DM and AF.

Study Selection Criteria

Study selection was limited to cohort studies, randomized trials and case-control studies in adult populations (participants aged >18 years old) where an association between DM and AF was reported. Patients with established comorbidities such as cardiac disease, hypertension and obesity/body mass index (BMI) were included so that the potential influence of these conditions on AF could be evaluated and the adjusted risk ratios were calculated. To reduce publication bias, previous review and meta-analysis papers were excluded. Furthermore, where multiple findings were reported from the same or overlapping patient datasets, the most contemporary study was used.

Machine Learning Assisted Study Selection and Validation

Conventionally, study selection is a two-stage process. During the first stage, titles and abstracts of all articles returned from the initial strategic search are manually screened to decide whether they potentially meet the study selection criteria. Full texts of the subset of studies identified are then reviewed in detail and those that meet the criteria are selected. Decisions are made by two experts at both stages. Any conflict was referred to a third expert and resolved by discussion and consensus. A novel machine learning approach was developed to automate the first-stage screening process and to facilitate the process of study selection. This was implemented in *R*, an open-source environment for data mining, text processing, machine learning and statistical analysis (R Core Team, 2013). The approach used is outlined schematically in **Figures 1, 2**, where a more detailed description is provided in the Supplementary Methods.

Articles returned by the PubMed search were grouped into clusters with common attributes (**Figure 1**). A well-established feature detection method was used to assign weighting factors based on the frequency of occurrence of words and word combinations in the PubMed texts (including titles and abstracts). An unsupervised K-means clustering algorithm was utilized to group publications with similar content (based on these weightings) and sort them into a limited number of clusters. This was done by iteratively removing the smallest cluster of publications and re-clustering the remainder until the number of remaining publications was <250. The residual studies were then grouped as a remainder cluster.

A subset of articles from the initial search was extracted as a training set for machine learning-assisted screening. First, articles most likely to be relevant were identified by searching for the keywords “diabetes”/“diabetic” and “atrial fibrillation” in the title. Titles and abstracts of these articles were then screened manually and labeled as potentially meeting or not meeting the selection criteria. Supervised machine learning (maximum entropy classification) was used to fit a predictive model to the labeled training set and this was applied across all clusters to identify clusters of articles that best matched this selection (**Figure 2**). Titles and abstracts of the articles in these clusters were then screened manually to select relevant studies for further study. Finally, full texts of the studies identified were reviewed and selections were made according to the stated criteria, removing any duplicate studies in the process.

To validate our machine learning assisted screening approach, study selection using this approach was compared to the results of conventional manual selection (see **Figure 1**). Identical manual screening and selection procedures were used in both study arms. The Newcastle-Ottawa or modified Jadad Scale was used to evaluate the quality of the included studies.

Data Synthesis and Analysis

Baseline demographics collected from individual studies included the nature of the study (cohort/case-control/randomized), year of subject’s enrolment, country

of the study, number of subjects, AF subtypes, DM subtypes, sex, age, year of follow up and comorbidities. Quantitative estimates of the association between DM and AF were also extracted from the original publications together with their respective confidence intervals (CIs). These included either hazard ratios (HR) for cohort/randomized studies or odds ratio (OR) for retrospective case-control studies. Age-and/or-gender/none adjusted (minimal adjusted) estimates were extracted from individual studies as well as other multivariate adjusted estimates when provided. Relative risk (RR) was estimated using the DerSimonian and Laird random-effects model across different studies and subgroups such as men vs. women.

The most conservative estimates provided in individual studies were used in the meta-analysis to take advantage of all included studies. Multivariate adjusted estimates were applied wherever possible using a subset of these studies by utilizing the studies with age, sex, and additional multiple adjustments for various reported risk factors. Furthermore, risk estimates for AF were adjusted separately for hypertension, obesity and various heart diseases in addition to other adjustments.

Sensitivity Analysis and Publication Bias

The effects on RR of CIs, publication year, year of the study, age, mean follow-up years and number of adjusted factors were investigated using polynomial regression analysis with Pearson’s correlation. Throughout this study, statistical significance was assessed using the 2-tailed *T*-test. Publication bias was assessed using the Egger regression test and is presented as a funnel plot.

RESULTS

Validation of Machine Learning-Assisted Study Selection

The initial PubMed search yielded a total of 4,177 publications and these were automatically sorted into 14 groups using unsupervised clustering. The training dataset consisted of 139 articles of which 26 were labeled as potentially relevant and 113 not relevant (**Figure 1**). Using machine learning, it was found that one cluster (#5) had substantially greater similarity to the 26 studies identified as potentially relevant in the training set than all others (**Figure 2B**, Figure S2). Manual screening of the titles and abstracts of the 416 articles in this cluster resulted in 38 being selected as potentially relevant compared to the 45 selected following direct manual screening of all 4,177 articles. Manual review of the full articles in both cases yielded the same 29 final selections (Details of these studies are provided in Tables S1, S2).

The 29 articles selected for meta-analysis (Tables S1, S2) had a study population of 8,037,756. Further details of the 9 studies that were excluded following machine learning assisted screening are given in Table S3. Scores for the quality assessment (Newcastle-Ottawa quality assessment scale (NOS)/modified Jadad score) ranged from 5 to 9 for the cohort/randomized/case-control

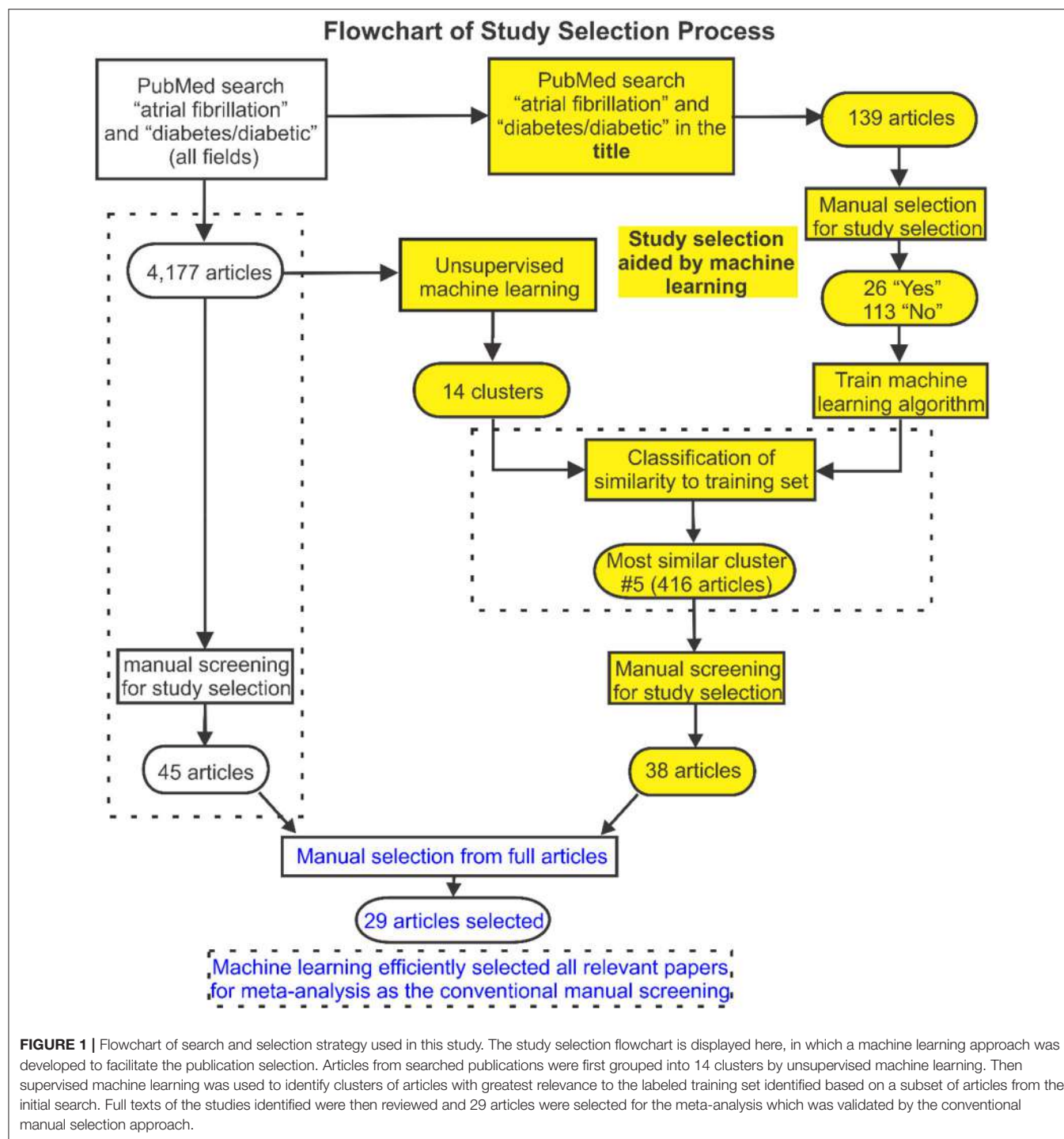


FIGURE 1 | Flowchart of search and selection strategy used in this study. The study selection flowchart is displayed here, in which a machine learning approach was developed to facilitate the publication selection. Articles from searched publications were first grouped into 14 clusters by unsupervised machine learning. Then supervised machine learning was used to identify clusters of articles with greatest relevance to the labeled training set identified based on a subset of articles from the initial search. Full texts of the studies identified were then reviewed and 29 articles were selected for the meta-analysis which was validated by the conventional manual selection approach.

studies (9 representing the highest quality). The overall average score was 7.4 (Tables S4, S5).

Risk Estimates of New-Onset AF in Patients With DM Baseline Estimates

Analysis of the combined cohort, randomized and case-control studies identified that patients with DM had \sim 49%

greater risk of developing AF (RR 1.49, 95% CI 1.24–1.79) compared to individuals without DM (Figure 3). The forest plot shows a significantly lower risk in the cohort/randomized studies (RR 1.28, 95% CI 1.22–1.35) compared to the eight case control studies (OR 1.97, 95% CI 1.53–2.55, $p < 0.01$). Funnel plot assessment (Figure S3A) provided evidence for no publication bias ($p = 0.87$, $z = 0.16$).

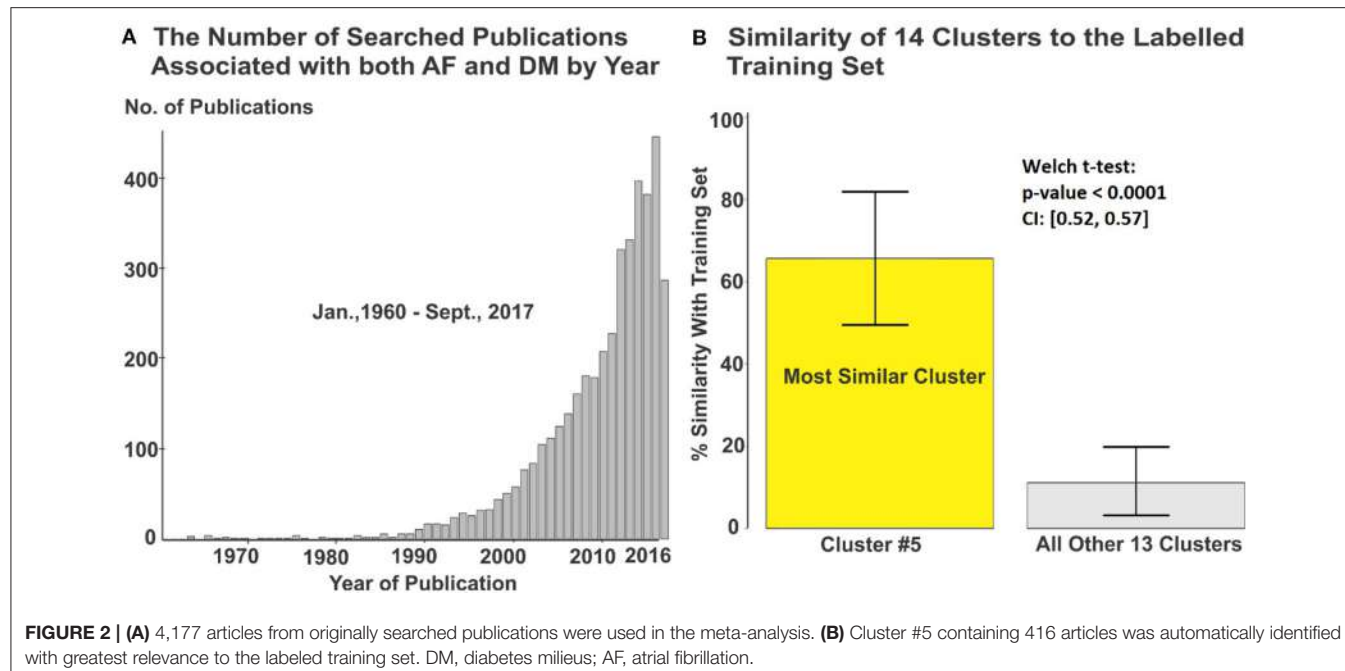


FIGURE 2 | (A) 4,177 articles from originally searched publications were used in the meta-analysis. **(B)** Cluster #5 containing 416 articles was automatically identified with greatest relevance to the labeled training set. DM, diabetes milieus; AF, atrial fibrillation.

Estimates Adjusted for Confounding Risks

Nine studies were adjusted for risk estimates based only on age-and/or-gender/none, while 20 included adjustments for multiple risk factors including different combinations of hypertension, BMI, height, smoking, blood pressure, alcohol consumption, various cardiac diseases and race (Figure S4). The levels of adjustment used in different publications influenced the calculated RRs. For studies with minimal adjustments (only age-and/or-gender/none), the summary estimate of risk of AF was significantly higher (RR 2.28, 95% CI 1.95–2.67), compared with studies that included adjustments for additional risk factors (RR 1.25, 95% CI 1.12–1.41).

Hypertension, cardiac disease, and obesity are known risk factors for AF (Movahed et al., 2005). Analysis of the studies that reported risk of AF after adjusting for at least one of the three common risk factors yielded lower RRs (1.20, 95% CI 1.15–1.26; 1.27, 95% CI 1.11–1.45; 1.22, 95% CI 1.09–1.38) (Figures 4A–C). Nine publications with reduced study heterogeneity of 82.8% (I^2 statistic) included adjustments for all the three factors and the estimated overall risk of AF in patients with DM was lower (RR 1.23, 95% CI 1.03–1.46) (Figure 4D).

Impact of Study Demographics on AF Incidence

Impact of Major Demographical Components

The effects on RR of the width of the CIs (number of enrolled patients), publication year, study location, year of patient enrollment, AF subtype, DM subtype, sex, age and mean follow-up year were also investigated. Continental location (Figure S3B) had no significant impact on RRs ($p = 0.8$), and mean follow-up duration displayed a minor impact (Figure S3C). Furthermore, we observed an inverse relationship

between the number of adjusted risk factors and estimated RRs, as well as between the CI widths and RRs. Removing the study with the largest population (Pallisgaard et al., 2016) (narrowest CI) or the paper with relative higher/lower risk estimate led to negligible changes in the overall risk estimates. Polynomial regression analysis yielded a positive linear correlation between age and the RR (Pearson's correlation: $R^2 = 0.32$, $p = 0.049$).

Impact of AF and DM Subtypes

There were only 4 studies exploring the linkage between DM and a specific AF subtype, compared with 27 studies reporting the relationship between DM and AF (all subtypes). Our results with multivariate adjustment for confounders found no significant difference ($p = 0.5$) between the risks of the different AF subtypes (RR 1.4, 95% CI 1.0–1.8; RR 1.3, 95% CI 1.0–1.8; RR 1.3, 95% CI 1.0–1.9 for paroxysmal/persistent/permanent AF, respectively) in patients with DM, compared with all subtypes of AF (RR 1.3, 95% CI 1.1–1.5). Similarly, using the multivariate risk model, no significant difference in the AF risk estimate ($p = 0.4$) was observed in the studies grouped by undefined DM subtypes ($N = 6,543,691$), DM type 2 ($N = 1,012,628$), and DM type 1 ($N = 216,238$) (Dahlqvist et al., 2017) (Figure 5). The estimated RRs were 1.2 (95% CI 1.2–1.3), 1.3 (95% CI 1.0–1.7) and 1.3 (95% CI 1.0–1.7) for the three subgroups, respectively (Figures S5, S6).

Impact of Gender and Enrolment Date

Our results with multivariate adjustment for confounders show a higher risk of AF in women (RR 1.38, 95% CI 1.19–1.60) compared to men (RR 1.11, 95% CI 1.01–1.22, $p < 0.001$) (Figure 6). Analysis of the median year of patient enrolment in the 23 studies from the past 35 years

RR Estimates Using the Most Conservative Risks Provided by Included Individual Studies

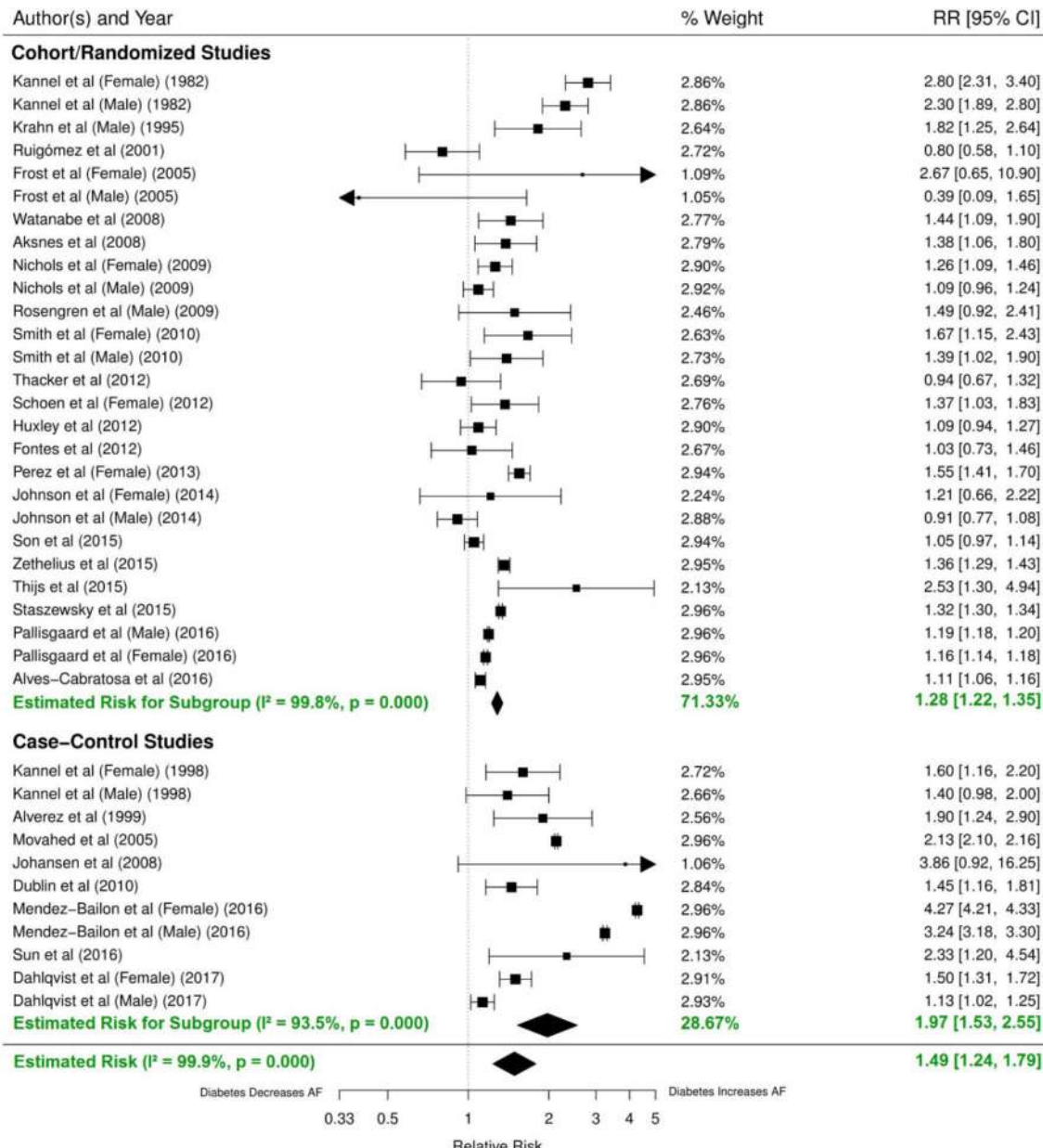


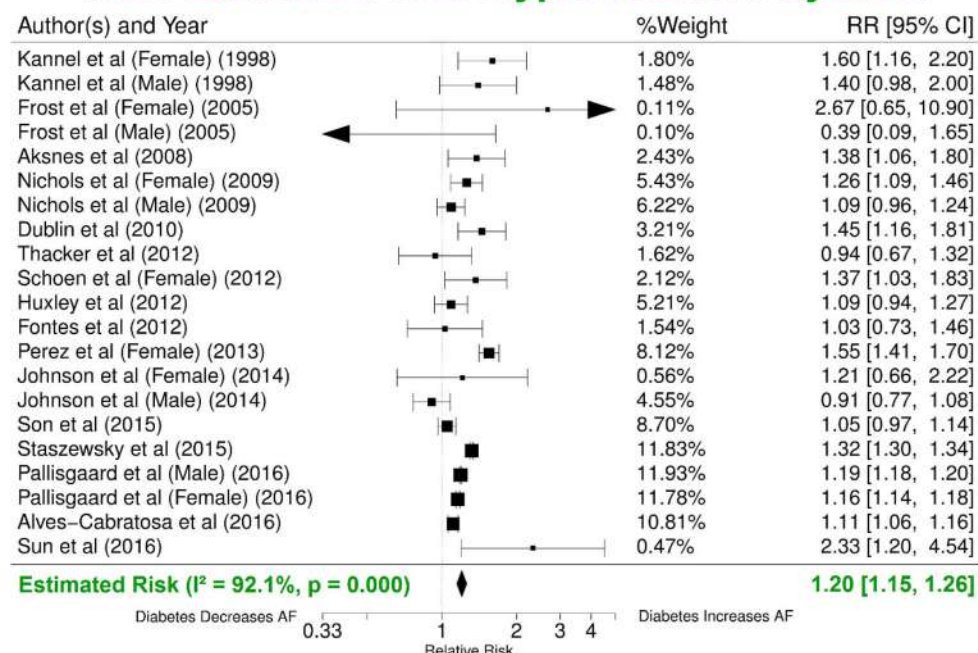
FIGURE 3 | Estimated risks of AF in patients with DM using the most conservative risk estimates provided in the individual studies. Subgroup summaries for cohort/randomized and case-control studies are in bold at the bottom of each subgroup. DM, diabetes milieus; AF, atrial fibrillation; RR, relative risk; CI, confidence interval.

identified an increasing risk of AF over time in patients with DM using the most conservative adjustment (Figure 7). The RR estimated for the most recent studies (2001–2016) was significantly higher than for the studies prior to 2001 (RR 1.62, 95% CI 1.18–2.23 vs. RR 1.30 95%, CI 1.05–1.61, $p < 0.05$).

DISCUSSION

This systematic review and meta-analysis systematically analyzed 29 studies with a total of 8,037,756 participants from three continents, selected from 4,177 articles returned from an initial strategic search. To our knowledge, this is the largest study of

A Risk Estimated with Hypertension Adjusted



B Risk Estimated with Heart Diseases Adjusted

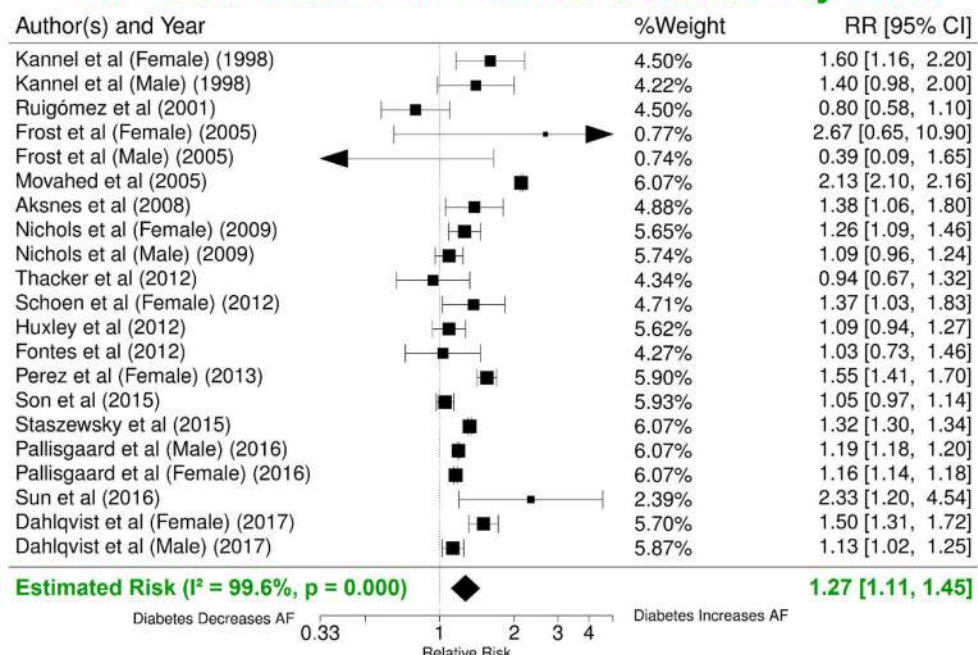
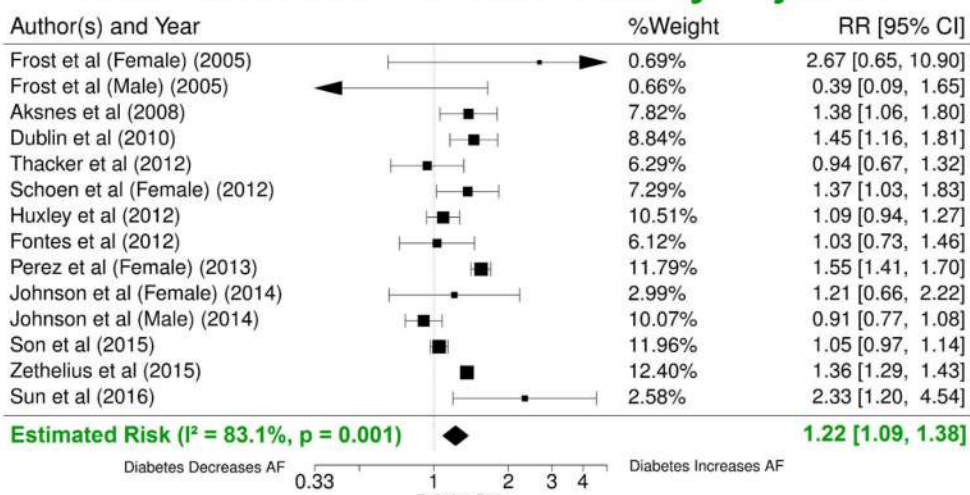


FIGURE 4 | Continued.

c Risk Estimated with BMI/Obesity Adjusted



d Hypertension, BMI & Heart Diseases Adjusted

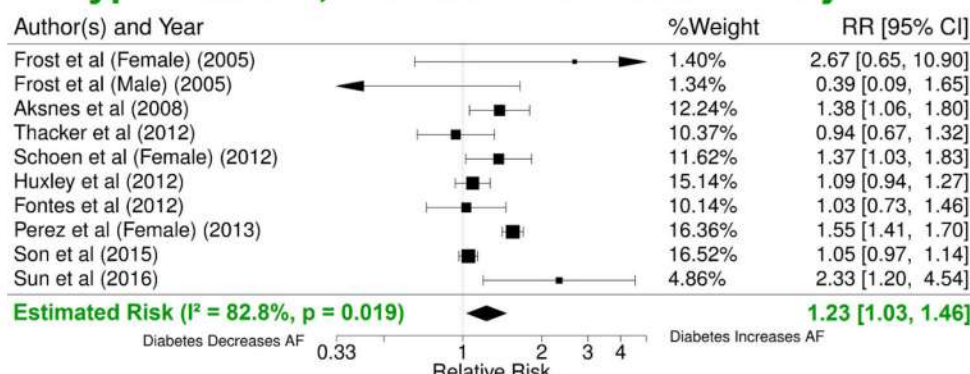


FIGURE 4 | Risk estimates with different additional risk factor adjustments. **(A)** Forest plot of risk values adjusted for hypertension in addition to age-and/or-sex/none and other included risk factors. **(B)** RR estimate adjusted for BMI in addition to age-and/or-sex/none and other included risk factors. **(C)** RR estimate adjusted for various heart conditions in addition to age-and/or-sex/none and other included risk factors. **(D)** Summary estimate for RRs after adjusting for hypertension, BMI and various heart conditions in addition to age-and/or-sex/none and other included risk factors. BMI, body mass index; DM, diabetes milieus; AF, atrial fibrillation; RR, relative risk; CI, confidence interval.

this kind to explore the association between AF and DM, and the first to employ a machine learning approach to facilitate study selection.

Benefits and Validation of Machine Learning Approach for Study Selection

From our literature research, the total number of publications related to the association investigated here has increased more than 4-fold over the last 10 years. The growth in medical research publications is accelerating across the board and we expect that it will no longer be feasible in the near future to maintain current manual study selection methods for large-scale meta-analyses and systematic review. Therefore, there is an urgent need to develop an intelligent automated approach, such as machine learning, to facilitate identification and selection of relevant articles for this purpose.

In this study, we have used machine learning to assist the screening of potentially relevant articles for large-scale meta-analyses and systematic review. To the best of our knowledge, we are the first to employ such an approach to facilitate study selection. With our approach, the burden of manual screening is reduced from all the articles returned by the initial online strategic search to those in the training set and in the principal cluster(s) identified by supervised machine learning. In this study, the number of publications for which manual screening was needed reduced from 4,177 to 555 using machine learning assisted screening, i.e., an 87% reduction. The iterative clustering approach (unsupervised machine learning) utilized vastly improved the similarity of the articles in individual clusters. Subsequent use of supervised machine learning (maximum entropy classification) with a representative training data subset enabled us to screen articles more rapidly than conventional manual procedures.

Automated methods of meta-analyses have been proposed in previous studies; however, few have automated the most labour intensive initial study screening stage. A study by Michelson

(2014) proposed a method in which numerical features from different articles were first extracted into a matrix, and the matrices from of different articles were then grouped using a clustering algorithm to sort studies with similar content into the same group. The initial features were extracted by creating a program which carefully defined sets of rules based on patterns in the wording of the articles. Although this study also used an automated method, it differs significantly from our study. Manually setting decision criteria for extracting specific features about each article is time consuming, and does not generalize well to new data with different formats; while on the other hand, our proposed methods extracted generalized features not dependent on any individual study. Previous studies have also proposed automated methods of text mining to aid the initial screening stage of meta-analyses (Ananiadou et al., 2009; Kim et al., 2011; Thomas et al., 2011; Cohen et al., 2012; García Adeva et al., 2013) as we did in our systematic review. However, for their proposed supervised machine learning, a manually selected initial training set will still be required to automate the remaining literature search (Ananiadou et al., 2009; Cohen et al., 2012; García Adeva et al., 2013). Furthermore, their studies were not validated in a large scale meta-analysis. Our study utilizes an ensemble of methodologies including text mining, clustering and supervised machine learning to efficiently extract the relevant

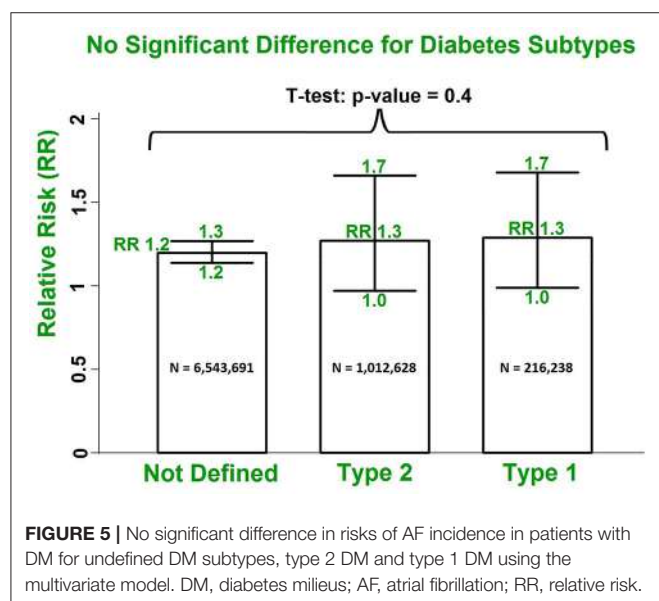
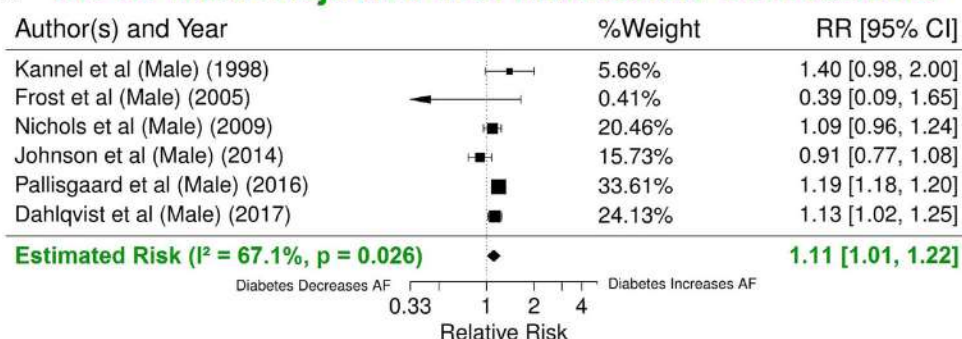


FIGURE 5 | No significant difference in risks of AF incidence in patients with DM for undefined DM subtypes, type 2 DM and type 1 DM using the multivariate model. DM, diabetes milieus; AF, atrial fibrillation; RR, relative risk.

A RR for Males Adjusted with Multivariate Confounders



B RR for Females Adjusted with Multivariate Confounders

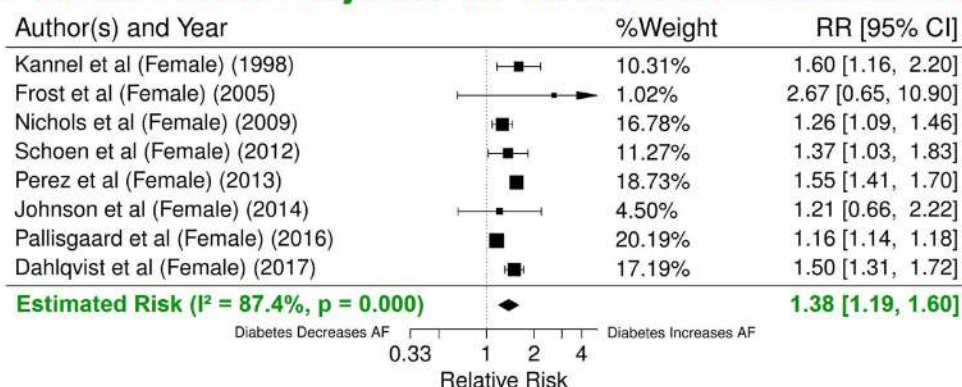


FIGURE 6 | Significant difference in the risk of AF incidence between men and women with DM using the multivariate model. Summary estimate for publications that reported risk values for men (A) and for women (B). DM, diabetes milieus; AF, atrial fibrillation; RR, relative risk; CI, confidence interval.

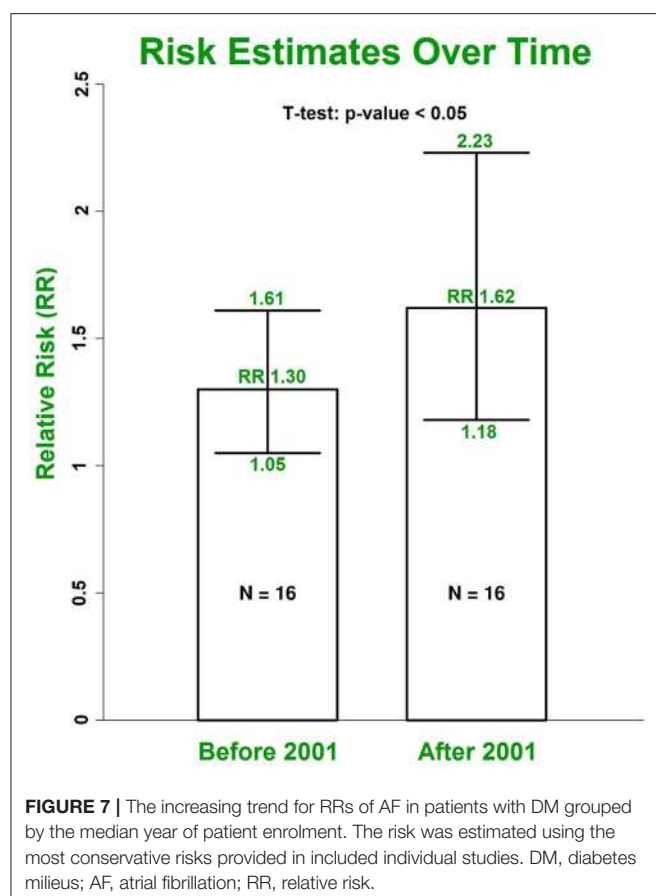


FIGURE 7 | The increasing trend for RRs of AF in patients with DM grouped by the median year of patient enrolment. The risk was estimated using the most conservative risks provided in included individual studies. DM, diabetes mellitus; AF, atrial fibrillation; RR, relative risk.

literature, and was verified as the literature extracted from our algorithm was the same as the literature identified through manual search. Furthermore, our results were also validated by comparing the risk estimates produced from the meta-analysis which was consistent with prior clinical studies.

A further benefit of machine learning-assisted selection of studies for meta-analysis is that identical screening can be applied and consistent results will be obtained if the meta-analysis is recapitulated with additional articles, minimizing the introduction of time-related bias. Machine learning-assisted screening therefore has the capacity to provide more efficient and more objective study selection for future meta-analyses. We expect that the novel automated approaches demonstrated will be extended and refined in the future.

Impact of Comorbidities on Risk Estimate

AF is associated with several well-established risk factors including age, hypertension, BMI and various cardiovascular diseases. The RRs assessed for these established risk factors have varied between studies and over time. Recent data from the Framingham Heart Study indicate that mean systolic blood pressures and evidence of left ventricular hypertrophy have declined, likely as a consequence of improved therapy for hypertension. In contrast, increasing BMI and DM have

contributed to increased risk of AF in the population (Schnabel et al., 2015; Lau et al., 2017).

For reliable estimation of the independent risk of AF due to DM, it is necessary to adjust for these established risk factors of AF. In our study, patients with DM have an overall adjusted RR of 1.49 (95% CI 1.24–1.79) for AF incidence using the most conservative adjustments provided in each individual study. After adjusting for three common risk factors (hypertension/blood pressure, BMI and various cardiovascular conditions) in addition to age, gender and possible others, the estimated risk for AF is 1.23 (95% CI 1.03–1.46). Our results are consistent with others, e.g., Dublin et al. estimated the RR for AF is 1.40 (95% CI 1.15–1.71) after adjusting for confounders including hypertension and BMI (Alves-Cabrataosa et al., 2016) and the previous 2010 meta-analysis by Huxley et al. (2011) reported that patients with DM had a multivariate-adjusted RR 1.24 (95% CI 1.06–1.44) of new-onset AF than individuals without DM.

The association among DM, obesity and AF is complex, and reported results vary. For example, obesity was demonstrated to be more significantly associated with new-onset AF in Spanish hypertensive patients compared with DM (RR 1.41, 95% CI 1.22–1.64 vs. RR 1.11, 95% CI 1.06–1.16) (Alves-Cabrataosa et al., 2016). Interestingly enough, another recent study indicated that DM is an independent risk factor for AF, but not hypertension and obesity in 11,956 subjects from rural Chinese areas (Sun et al., 2015).

Trends of AF Incidence in Patients With DM

AF subtype was not analyzed in most of the studies. Only one study reported an association between cumulative exposure to DM and new-onset AF with all three AF subtypes (Dublin et al., 2010) and 6 studies reported the association between DM and one AF subtype. For the first time, our study has indicated that the risk estimate is not significantly different for any AF subtype. Since few studies have specifically addressed AF subtype and DM, future studies are warranted.

Patients with type 2 DM were exclusively enrolled in 7 out of the 29 selected studies, and there was only one study on the risk estimate of AF in patients with type 1 DM. Twenty-one studies did not explicitly define DM subtypes in their studies. Our study found no significant risk difference among these sub-groups. Interestingly enough, the study on type 1 DM by Dahlqvist et al. (2017) reported a similar gender difference in AF risk. Furthermore, they also observed the tendency of higher AF risk in younger people with DM.

AF incidence and prevalence are lower in women than in men. Sex hormones and delayed onset of cardiovascular disease in women are likely to contribute to these differences. However, the absolute number of women with AF exceeds that of men because women live longer (Perez et al., 2013; Gillis, 2017). Furthermore, women with AF are more likely to develop stroke than men with AF (Dublin et al., 2010; Sun et al., 2015). Our analysis confirms the increased risk of AF in women with DM compared to men, even though the average age between the two (54.16 ± 11.79 vs. 54.88 ± 12.87 year old) is the same. After adjusting for multiple comorbidities, the risk estimates are reduced but the

gender difference for AF risk have become more pronounced (an increase from 17 to 24%).

The prevalence of AF in the general population is projected to more than double in the next few decades, becoming a global epidemic (Krijthe et al., 2013). On the other hand, DM is a common chronic disease and an increasing public health problem worldwide (Schnabel et al., 2015). Our study indicates that the trend of AF incidence in patients with DM is also increasing over time. The RR estimated for studies from 2001 to 2016 is significantly higher than the risk estimate for an equivalent number of studies from 1982 to 2001 (Figure 7). This potentially explains the reason why our overall risk estimate is higher than the estimated risk in the previous 2010 meta-analysis by Huxley et al. (2011). The increased AF incidence in diabetic patients may reflect enhanced awareness of this association and increased screening for AF. The trend also likely reflects the growing epidemic of obesity particularly in the developed world and the associated risk of developing metabolic syndrome.

Nevertheless, there are some important findings that are yet to be confirmed, such as the impact of median follow-up and age from new-onset DM on AF risk estimate. Some individual studies have suggested that the first 4–5 years after new-onset DM is the most vulnerable period for developing AF (Aksnes et al., 2008; Dublin et al., 2010; Pallisgaard et al., 2016); while some studies reported that AF incidence in patients with DM is most pronounced in young patients (Pallisgaard et al., 2016; Dahlqvist et al., 2017). However, most individual studies and our meta-analysis could not provide strong evidence to confirm these findings.

Clinical Significance

The recent review paper by Lau and his colleagues has proposed a promising integrated care model that incorporates risk factor management, including DM, as the fourth pillar of AF care alone with rate control, rhythm control and anticoagulation therapy (Lau et al., 2017). The benefits of lifestyle and risk factor modifications in atrial remodeling, disease progression and recurrence were clearly demonstrated in their previous studies (Pathak et al., 2014). The enriched knowledge with regard to DM and AF generated from our study will provide additional evidence to support and define a comprehensive lifestyle and optimal risk factor management for AF as an upstream therapy, as well as for stroke and mortality prevention (Lau et al., 2017).

REFERENCES

- Aksnes, T. A., Schmieder, R. E., Kjeldsen, S. E., Ghani, S., Hua, T. A., and Julius, S. (2008). Impact of new-onset diabetes mellitus on development of atrial fibrillation and heart failure in high-risk hypertension (from the VALUE Trial). *Am. J. Cardiol.* 101, 634–638. doi: 10.1016/j.amjcard.2007.10.025
- Alves-Cabrato, L., Garcia-Gil, M., Comas-Cuff, M., Martí, R., Ponjoan, A., Parramon, D., et al. (2016). Diabetes and new-onset atrial fibrillation in a hypertensive population. *Ann. Med.* 48, 119–127. doi: 10.3109/07853890.2016.1144930

Study Limitations

Our study has several limitations. The utility of a promising machine learning approach for publication selection is demonstrated in this study for the first time. However, future development and validation is needed for this approach to achieve its full capacity. The studies included in this meta-analysis are heterogeneous and include differences in patient demographics and marked variation in follow-up duration, though it is substantially reduced in subgroup studies. Furthermore, not all studies were adjusted for the multiple risk factors known to influence AF incidence. In addition, the efficacy of glycemic control on AF risk has not been assessed. Finally, the AF risk estimate for patients with DM in this study only demonstrates the possible causal association between DM and AF, the exact underlying mechanism remains elusive due to the complex nature of concurrent diseases and the limitations of current population-based clinical studies.

CONCLUSIONS

We have demonstrated the utility of machine learning for meta-analyses. Our study has indicated that the AF risk estimates in patients with DM may be underestimated and has reinforced the view that DM is an independent risk factor for AF even after adjusting for other known concurrent risk factors.

AUTHOR CONTRIBUTIONS

ZX and JZ conceived and designed the experiments; ZX, TL, GT, MG, MS, AG, and JZ data curation; PG, BS, MS, AG, and JZ investigation; ZX, TL, GT, and MG data analysis; All authors draft, reviewing and editing of the manuscript.

FUNDING

This study was supported by The Health Research Council of New Zealand (JZ).

SUPPLEMENTARY MATERIAL

The Supplementary Material for this article can be found online at: <https://www.frontiersin.org/articles/10.3389/fphys.2018.00835/full#supplementary-material>

Ananiadou, S., Rea, B., Okazaki, N., Procter, R., and Thomas, J. (2009). Supporting systematic reviews using text mining. *Soc. Sci. Comp. Rev.* 27, 509–523. doi: 10.1177/0894439309332293

Cohen, A. M., Ambert, K., and McDonagh, M. (2012). Studying the potential impact of automated document classification on scheduling a systematic review update. *BMC Med. Inform. Decis. Mak.* 12:33. doi: 10.1186/1472-6947-12-33

Colilla, S., Crow, A., Petkun, W., Singer, D. E., Simon, T., and Liu, X. (2013). Estimates of current and future incidence and prevalence of atrial fibrillation in the US adult population. *Am. J. Cardiol.* 112, 1142–1147. doi: 10.1016/j.amjcard.2013.05.063

- Dahlqvist, S., Rosengren, A., Gudbjörnsdóttir, S., Pivodic, A., Wedel, H., Kosiborod, M., et al. (2017). Risk of atrial fibrillation in people with type 1 diabetes compared with matched controls from the general population: a prospective case-control study. *Lancet Diabetes Endocrinol.* 5, 799–807. doi: 10.1016/S2213-8587(17)30262-0
- Dublin, S., Glazer, N. L., Smith, N. L., Psaty, B. M., Lumley, T., Wiggins, K. L., et al. (2010). Diabetes mellitus, glycemic control, and risk of atrial fibrillation. *J. Gen. Intern. Med.* 25, 853–858. doi: 10.1007/s11606-010-1340-y
- Fontes, J. D., Lyass, A., Massaro, J. M., Rienstra, M., Dallmeier, D., Schnabel, R. B., et al. (2012). Insulin resistance and atrial fibrillation (from the Framingham Heart Study). *Am. J. Cardiol.* 109, 87–90. doi: 10.1016/j.amjcard.2011.08.008
- Frost, L., Hune, L. J., and Vestergaard, P. (2005). Overweight and obesity as risk factors for atrial fibrillation or flutter: the danish diet, cancer, and health study. *Am. J. Med.* 118, 489–495. doi: 10.1016/j.amjmed.2005.01.031
- García Adeva, J. J., Pikatza Atxa, J. M., Ubeda Carrillo, M., and Ansuategi Zengotitabengoa, E. (2013). Automatic text classification to support systematic reviews in medicine. *Exp. Syst. Appl.* 41, 1498–1508. doi: 10.1016/j.eswa.2013.08.047
- Gillis, A. M. (2017). Atrial fibrillation and ventricular arrhythmias: Sex differences in electrophysiology, epidemiology, clinical presentation, and clinical outcomes. *Circulation* 135, 593–608. doi: 10.1161/CIRCULATIONAHA.116.025312
- Huxley, R. R., Alonso, A., Lopez, F. L., Filion, K. B., Agarwal, S. K., Loehr, L. R., et al. (2012). Type 2 diabetes, glucose homeostasis and incident atrial fibrillation: the atherosclerosis risk in communities study. *Heart* 98, 133–138. doi: 10.1136/heartjnl-2011-300503
- Huxley, R. R., Filion, K. B., Konety, S., and Alonso, A. (2011). Meta-analysis of cohort and case-control studies of type 2 diabetes mellitus and risk of atrial fibrillation. *Am. J. Cardiol.* 108, 56–62. doi: 10.1016/j.amjcard.2011.03.004
- Johnson, L. S., Juhlin, T., Engström, G., and Nilsson, P. M. (2014). Low fasting plasma insulin is associated with atrial fibrillation in men from a cohort study - the Malmö preventive project. *BMC Cardiovasc. Disord.* 14:107. doi: 10.1186/1471-2261-14-107
- Kannel, W. B., Wolf, P. A., Benjamin, E. J., and Levy, D. (1998). Prevalence, incidence, prognosis, and predisposing conditions for atrial fibrillation: population-based estimates. *Am. J. Cardiol.* 82, 2N–9N. doi: 10.1016/S0002-9149(98)00583-9
- Kim, S. N., Martinez, D., Cavedon, L., and Yencken, L. (2011). Automatic classification of sentences to support evidence based medicine. *BMC Bioinform.* 12:S5. doi: 10.1186/1471-2105-12-S2-S5
- Krahn, A. D., Manfreda, J., Tate, R. B., Mathewson, F. A., and Cuddy, T. E. (1995). The natural history of atrial fibrillation: incidence, risk factors, and prognosis in the Manitoba Follow-Up Study. *Am. J. Med.* 98, 476–484. doi: 10.1016/S0002-9343(99)80348-9
- Krijthe, B. P., Kunst, A., Benjamin, E. J., Lip, G. Y., Franco, O. H., Hofman, A., et al. (2013). Projections on the number of individuals with atrial fibrillation in the European Union, from 2000 to 2060. *Euro. Heart J.* 34, 2746–2751. doi: 10.1093/eurheartj/eht280
- Lau, D. H., Nattel, S., Kalman, J. M., and Sanders, P. (2017). Modifiable risk factors and atrial fibrillation. *Circulation* 136, 583–596. doi: 10.1161/CIRCULATIONAHA.116.023163
- Michelson, M. (2014). "Automating meta-analyses of randomized clinical trials: a first look," in *2014 AAAI Fall Symposium Series*. Arlington, VA.
- Moher, D., Liberati, A., Tetzlaff, J., Altman, D. G., and Group, P. (2009). Preferred reporting items for systematic reviews and meta-analyses: the PRISMA statement. *PLoS Med.* 6:e1000097. doi: 10.1371/journal.pmed.1000097
- Movahed, M.-R., Hashemzadeh, M., and Jamal, M. M. (2005). Diabetes mellitus is a strong, independent risk for atrial fibrillation and flutter in addition to other cardiovascular disease. *Int. J. Cardiol.* 105, 315–318. doi: 10.1016/j.ijcard.2005.02.050
- Pallisaard, J. L., Schjerning, A.-M., Lindhardt, T. B., Procida, K., Hansen, M. L., Torp-Pedersen, C., et al. (2016). Risk of atrial fibrillation in diabetes mellitus: a nationwide cohort study. *Eur. J. Prev. Cardiol.* 23, 621–627. doi: 10.1177/2047487315599892
- Pathak, R. K., Middeldorp, M. E., Lau, D. H., Mehta, A. B., Mahajan, R., Twomey, D., et al. (2014). Aggressive risk factor reduction study for atrial fibrillation and implications for the outcome of ablation: the ARREST-AF cohort study. *J. Am. Coll. Cardiol.* 64, 2222–2231. doi: 10.1016/j.jacc.2014.09.028
- Perez, M. V., Wang, P. J., Larson, J. C., Soliman, E. Z., Limacher, M., Rodriguez, B., et al. (2013). Risk factors for atrial fibrillation and their population burden in postmenopausal women: the women's health initiative observational study. *Heart* 99, 1173–1178. doi: 10.1136/heartjnl-2013-303798
- R Core Team (2013). *A Language and Environment for Statistical Computing*. Vienna: R Core Team.
- Schnabel, R. B., Yin, X., Gona, P., Larson, M. G., Beiser, A. S., McManus, D. D., et al. (2015). 50 year trends in atrial fibrillation prevalence, incidence, risk factors, and mortality in the Framingham Heart Study: a cohort study. *Lancet* 386, 154–162. doi: 10.1016/S0140-6736(14)61774-8
- Schoen, T., Pradhan, A. D., Albert, C. M., and Conen, D. (2012). Type 2 diabetes mellitus and risk of incident atrial fibrillation in women. *J. Am. College Cardiol.* 60, 1421–1428. doi: 10.1016/j.jacc.2012.06.030
- Sun, G.-Z., Guo, L., Wang, X.-Z., Song, H.-J., Li, Z., Wang, J., et al. (2015). Prevalence of atrial fibrillation and its risk factors in rural China: a cross-sectional study. *Int. J. Cardiol.* 182, 13–17. doi: 10.1016/j.ijcard.2014.12.063
- Thomas, J., McNaught, J., and Ananiadou, S. (2011). Applications of text mining within systematic reviews. *Res. Synth. Meth.* 2, 1–14. doi: 10.1002/jrsm.27

Conflict of Interest Statement: The authors declare that the research was conducted in the absence of any commercial or financial relationships that could be construed as a potential conflict of interest.

Copyright © 2018 Xiong, Liu, Tse, Gong, Gladding, Smaill, Stiles, Gillis and Zhao. This is an open-access article distributed under the terms of the Creative Commons Attribution License (CC BY). The use, distribution or reproduction in other forums is permitted, provided the original author(s) and the copyright owner(s) are credited and that the original publication in this journal is cited, in accordance with accepted academic practice. No use, distribution or reproduction is permitted which does not comply with these terms.



Noninvasive Assessment of Atrial Fibrillation Complexity in Relation to Ablation Characteristics and Outcome

Marianna Meo^{1,2,3*}, Thomas Pambrun^{1,4}, Nicolas Derval^{1,4}, Carole Dumas-Pomier⁵, Stéphane Puyo^{1,4}, Josselin Duchâteau^{1,2,3,4}, Pierre Jaïs^{1,2,3,4}, Mélèze Hocini^{1,2,3,4}, Michel Haïssaguerre^{1,2,3,4} and Rémi Dubois^{1,2,3}

¹ Institute of Electrophysiology and Heart Modeling (IHU Liryc), Foundation Bordeaux University, Pessac-Bordeaux, France

² University of Bordeaux, CRCTB, U1045, Bordeaux, France, ³ INSERM, CRCTB, U1045, Bordeaux, France, ⁴ Bordeaux University Hospital Centre Hospitalier Universitaire, Electrophysiology and Ablation Unit, Pessac, France,

⁵ Cardiointeract, Medtronic, Minneapolis, MN, United States

OPEN ACCESS

Edited by:

Pawel Kuklik,
Universitätsklinikum
Hamburg-Eppendorf, Germany

Reviewed by:

Jordi Heijman,
Maastricht University, Netherlands
Junaid Zaman,
Imperial College London,
United Kingdom

*Correspondence:

Marianna Meo
marianna.meo@ihu-liryc.fr

Specialty section:

This article was submitted to
Computational Physiology and
Medicine,
a section of the journal
Frontiers in Physiology

Received: 29 March 2018

Accepted: 25 June 2018

Published: 17 July 2018

Citation:

Meo M, Pambrun T, Derval N,
Dumas-Pomier C, Puyo S,
Duchâteau J, Jaïs P, Hocini M,
Haïssaguerre M and Dubois R (2018)
Noninvasive Assessment of Atrial
Fibrillation Complexity in Relation to
Ablation Characteristics and
Outcome. *Front. Physiol.* 9:929.
doi: 10.3389/fphys.2018.00929

Background: The use of surface recordings to assess atrial fibrillation (AF) complexity is still limited in clinical practice. We propose a noninvasive tool to quantify AF complexity from body surface potential maps (BSPMs) that could be used to choose patients who are eligible for AF ablation and assess therapy impact.

Methods: BSPMs (mean duration: 7 ± 4 s) were recorded with a 252-lead vest in 97 persistent AF patients (80 male, 64 ± 11 years, duration 9.6 ± 10.4 months) before undergoing catheter ablation. Baseline cycle length (CL) was measured in the left atrial appendage. The procedural endpoint was AF termination. The ablation strategy impact was defined in terms of number of regions ablated, radiofrequency delivery time to achieve AF termination, and acute outcome. The atrial fibrillatory wave signal extracted from BSPMs was divided in 0.5-s consecutive segments, each projected on a 3D subspace determined through principal component analysis (PCA) in the current frame. We introduced the nondipolar component index (NDI) that quantifies the fraction of energy retained after subtracting an equivalent PCA dipolar approximation of heart electrical activity. AF complexity was assessed by the NDI averaged over the entire recording and compared to ablation strategy.

Results: AF terminated in 77 patients (79%), whose baseline AF CL was 177 ± 40 ms, whereas it was 157 ± 26 ms in patients with unsuccessful ablation outcome ($p = 0.0586$). Mean radiofrequency emission duration was 35 ± 21 min; 4 \pm 2 regions were targeted. Long-lasting AF patients (≥ 12 months) exhibited higher complexity, with higher NDI values (≥ 12 months: 0.12 ± 0.04 vs. < 12 months: 0.09 ± 0.03 , $p < 0.01$) and short CLs (< 160 ms: 0.12 ± 0.03 vs. between 160 and 180 ms: 0.10 ± 0.03 vs. > 180 ms: 0.09 ± 0.03 , $p < 0.01$). More organized AF as measured by lower NDI was associated with successful ablation outcome (termination: 0.10 ± 0.03 vs. no termination:

0.12 ± 0.04 , $p < 0.01$), shorter procedures (<30 min: 0.09 ± 0.04 vs. ≥ 30 min: 0.11 ± 0.03 , $p < 0.001$) and fewer ablation targets (<4 : 0.09 ± 0.03 vs. ≥ 4 : 0.11 ± 0.04 , $p < 0.01$).

Conclusions: AF complexity can be noninvasively quantified by PCA in BSPMs and correlates with ablation outcome and AF pathophysiology.

Keywords: atrial fibrillation, catheter ablation, body surface potential maps, principal component analysis, atrial fibrillation complexity

INTRODUCTION

Atrial fibrillation (AF) is the most common cardiac arrhythmia, and it is associated with an increased risk of stroke, heart failure, and mortality (Kirchhof et al., 2016). Despite the apparently random and uncoordinated electrical wavefronts propagating through the atria (Moe, 1962), several studies have confirmed the presence of intrinsic organization of atrial activations during AF, whose triggering and maintenance may be explained by some underlying, deterministic mechanisms (Schricker et al., 2014), involving multiple atrial wavelets and re-entrant sources (Allessie et al., 1977; Konings et al., 1994; Pandit and Jalife, 2013; Haissaguerre et al., 2014). Complexity of the atrial substrate is strictly correlated with the evolutionary nature of AF, and it tends to increase in more severe, persistent forms of this disease (Wijffels et al., 1995). Despite the increasing use of catheter ablation (CA) to treat persistent and chronic AF patients, its results are not satisfactory yet and extremely disparate due to the variety of ablation approaches currently adopted (Verma et al., 2015).

Even though AF electrophysiological complexity can be assessed using invasive direct contact mapping, there is an increasing interest in noninvasive methodologies as well, due to the immediate availability of cardiac body surface potentials in clinical daily practice (Lankveld et al., 2014) and their proven ability to predict the outcome of AF cardioversion or ablation and help identify positive responders to therapy. Most of the complexity ECG measures investigated so far have been determined both in the frequency [e.g., dominant frequency, DF (Bollmann et al., 2003)] and the time domain [fibrillatory wave amplitude (Nault et al., 2009; Cheng et al., 2013), sample entropy (Alcaraz et al., 2011), AF cycle length (CL, Matsuo et al., 2009)]. Correlation between several markers of complexity from standard electrocardiogram (ECG) and invasive measures of AF complexity from high density epicardial mapping has been systematically investigated in Bonizzi et al. (2014). Spectral measures of spatiotemporal organization computed from surface

ECG were able to discriminate between persistent and long-standing AF (Uldry et al., 2012). Atrial complexity indices from ECG could also predict sinus rhythm (SR) maintenance in patients undergoing electrical cardioversion, either alone (Lankveld et al., 2016a) or in combination with other clinical parameters (Zeemering et al., 2017). An optimal set of ECG descriptors of AF complexity has also been determined in Lankveld et al. (2016b), and it was shown to be predictive of CA outcome.

The main limitation of the aforementioned methods is that most of them were applied to single or pairs of ECG leads [typically V_1 , exhibiting the highest atrial-to-ventricular amplitude ratio (Petrutiu et al., 2006), or the precordial leads], thus the spatial diversity of multilead recordings was not fully exploited. Furthermore, frequency domain measures of AF complexity may be inaccurate if they are assessed in short ECG recordings or if QRST cancellation is not properly performed. This background justifies the interest in exploiting the spatial diversity of multilead recordings to assess the complexity of the AF wavefront propagation.

A multilead characterization of AF spatiotemporal organization in body surface potential maps (BSPMs) has been proposed in Bonizzi et al. (2010), where it was quantified as a function of the error of signal estimation by principal component analysis (PCA). Despite the relevance of these results and the proven superiority of this methodology over standard single-lead analysis, its ability to guide AF therapy and its applicability to a real clinical scenario were not verified in that study. In Di Marco et al. (2012), AF spatial complexity was defined in terms of the residual cumulative variance of the three dominant PCA sources and correlated with its spectral variability overs BSPM electrodes. However, body surface cardiac activity characterization has not been correlated with the properties of the underlying atrial substrate nor correlated with AF treatment strategy. Multilead measures of atrial signal amplitude (Meo et al., 2013a) and spatiotemporal variability (Meo et al., 2013b) obtained by PCA proved to be predictive of CA outcome. Nevertheless, the lack of comparison with intracardiac recordings hampered their validation as indices of AF complexity.

This study takes a step from this research and puts forward a noninvasive PCA-based approach for the quantification of AF spatiotemporal complexity. Additionally, in Meo et al. (2017) some PCA-derived parameters were developed to predict changes in body surface complexity during ventricular fibrillation episodes. In this study, a similar methodology is proposed

Abbreviations: AAD, antiarrhythmic drugs; AF, atrial fibrillation; ANOVA, one-way analysis of variance; AUC, area under curve; BSPM, body surface potential map; CA, catheter ablation; CL, cycle length; DCC, electrical cardioversion; DF, dominant frequency; ECG, electrocardiogram; EGM, electrogram; LA, left atrium; LAA, left atrial appendage; LR, logistic regression; NA, not applicable; NDI, nondipolar component index; NMSE, normalized mean square error; NRI, net reclassification improvement; ns, not significant; PCA, principal component analysis; RA, right atrium; ROC, receiver operating characteristic; std, standard deviation.

to quantify the spatiotemporal organization of AF waveform propagation pattern as measured on body surface potentials. The approach proposed not only provides some insights about AF chronification reflecting the severity of the alterations of the atrial substrate, but it also predicts CA outcome and correlates with procedural characteristics.

METHODS

Study Population

A group of 97 persistent AF patients was enrolled in this study. Their baseline characteristics are reported in **Table 1**.

This study was carried out in accordance with the recommendations of the protocol CARRY, ID-RCB: 2015-A00401-48, Comité de Protection des Personnes Sud-Ouest et Outre Mer III. The protocol was approved by the Comité de Protection des Personnes Sud-Ouest et Outre Mer III. All subjects gave written informed consent in accordance with the Declaration of Helsinki.

BSPM Acquisition and Preprocessing

BSPMs were recorded with a 252-lead vest (CardioInsight, Medtronic, MN) in AF patients before undergoing CA at a sampling frequency of 1 kHz. Mean duration of the signals was 7 ± 4 s. TQ intervals were segmented from BSPMs with long ventricular pauses (≥ 1 s), either spontaneous or induced

by diltiazem. Since the outcome of the data decomposition techniques applied in this study was not affected by the specific temporal location of each signal sample, TQ intervals could be concatenated and mean-centered to form the atrial activity signal. Baseline wandering was removed using the median estimation method (Sörnmo and Laguna, 2005). Atrial fibrillatory wave (f-wave) signals were arranged as a $L \times N$ matrix $Y = [y(1) \dots y(N)] \in \mathbb{R}^{L \times N}$, where $L = 252$ is the number of BSPM leads, and N the number of samples. Electrodes with excessive noise level were discarded after signal visual inspection, thus in certain cases less than L electrodes were retained. A representative f-wave signal is reported in **Figure 1**.

Electrophysiological Atrial Mapping

Intracardiac electrograms (EGMs) were continuously recorded through a computer-based digital amplifier/recorder system (Labsystem Pro, Bard Electrophysiology). Baseline CL was measured in the left atrial appendage (LAA), and monitored during the procedure to assess local CA impact. For AF electrophysiological study, we used a 20-pole steerable mapping catheter with a five-branched star design (1-mm electrodes separated by 4-mm interelectrode spacing) spanning a surface with a diameter of 3.5 cm (PentaRay, Biosense-Webster). A steerable decapolar catheter (5-mm interelectrode spacing, Xtrem, Sorin Medical, Montrouge, France) was also positioned in the coronary sinus.

CA Protocol

For the sake of the ablation strategy analysis, the computed tomography-reconstructed atrial anatomy was divided into 7 regions (**Figure 2**).

The ablation was sequentially performed in the LA in the decreasing order of arrhythmogenic activity as estimated through noninvasive phase mapping (Haissaguerre et al., 2014) until AF terminated. Briefly, the acquisition system described in section Electrophysiological Atrial Mapping enabled the estimation of unipolar epicardial EGMs from body surface signals. Color-coded phase maps were derived from EGM phase signals by plotting the instantaneous phase values on personalized 3D atrial geometry, which was previously reconstructed through CT scan in each patient. Surrogates of the depolarization and repolarization wavefronts were computed from the isophasic values, equal to $\pi/2$ and $-\pi/2$, respectively. CA targets were identified in correspondence to phase singularity points, around which phase spanned the entire range between the two aforementioned values, as they identify AF reentrant sources (Jalife, 2003). The AF waveform sequences detected were accumulated in a single spatiotemporal density map, displaying the distribution of active driver zones and passive conduction areas. AF drivers were classified as focal, when centrifugal activation originated from a point or an area, or reentrant, when at least 1 complete wave rotation around a center on phase progression could be tracked. Right atrium (RA) was also inspected and targeted if AF could not terminate after LA ablation. An irrigated-tip quadripolar catheter with a distal 3.5-mm tip and three 1-mm proximal electrodes with

TABLE 1 | Study population characteristics.

	<i>n</i> = 97
Sex, male, <i>n</i> (%)	80 (82)
Age, mean \pm std, years	64 \pm 11
Hypertension, <i>n</i> (%)	42 (42)
Diabetes mellitus, <i>n</i> (%)	10 (17)
Emolic events, <i>n</i> (%)	8 (8)
Structural heart disease, <i>n</i> (%)	61 (62)
Ischemic, <i>n</i> (%)	10 (10)
Valvular, <i>n</i> (%)	6 (6)
Hypertrophic, <i>n</i> (%)	8 (8)
Dilated, <i>n</i> (%)	35 (36)
Other, <i>n</i> (%)	2 (2)
Left ventricular ejection fraction, mean \pm std, %	52 \pm 13
LA diameter, parasternal long axis, mm	48 \pm 7
LA Area, mm ²	26 \pm 6
Patients presenting in AF, AF duration, months	9.6 \pm 10.2
< 12 months	74 (76)
≥ 12 months	23 (24)
Patient presenting in SR, <i>n</i> (%)	48 (49)
Patients with more than 1 DCC, <i>n</i> (%)	54 (56)
Number of AADs before CA, mean \pm std	2 \pm 1
Patients on amiodarone before CA, <i>n</i> (%)	40 (41)

Baseline characteristics of the AF population; std, standard deviation; DCC, electrical cardioversion; AAD, antiarrhythmic drugs.

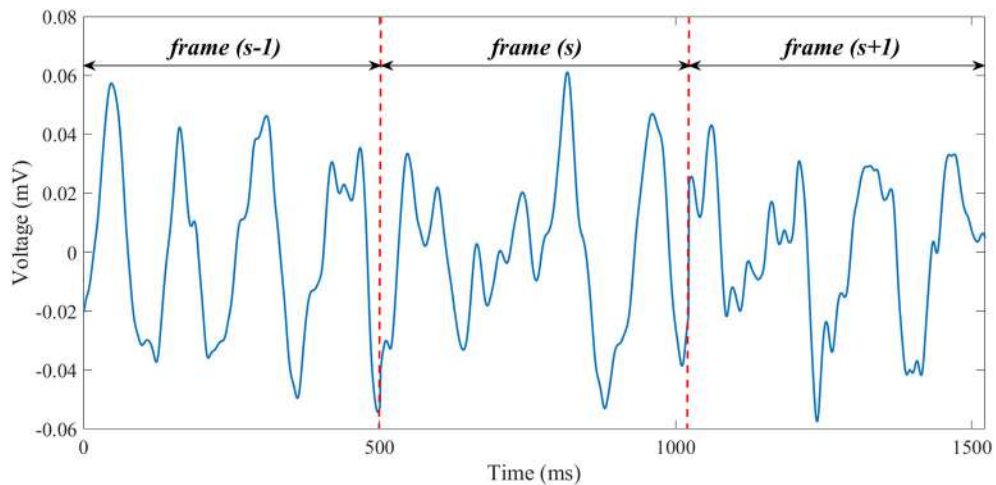


FIGURE 1 | A representative example of f-wave signal extracted from a BSPM recording in an AF patient (lead 1). Concatenated, preprocessed TQ intervals are separated by dashed, red, vertical lines.

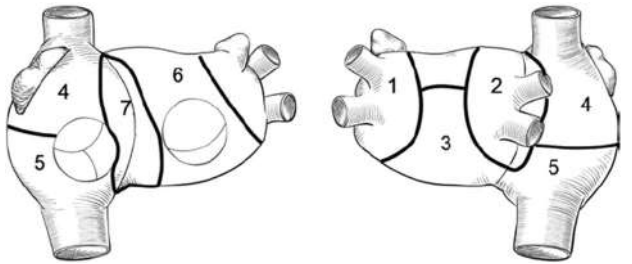


FIGURE 2 | Biatrial schematic representation: 1, left pulmonary veins and LAA; 2, right pulmonary veins and posterior interatrial groove; 3, inferior and posterior left atrium; 4, upper half of right atrium and appendage; 5, lower half of right atrium; 6, anterior left atrium and roof; 7, anterior interatrial groove.

interelectrode distance of 2, 5, and 2 mm (Thermocool, Biosense-Webster) was used for AF ablation. The procedural endpoint was AF termination, i.e., conversion of AF either to SR or to intermediate atrial tachycardia (AT). AF CL was determined simultaneously in the RA with the mapping catheter and in the LAA with the ablation catheter, before and after ablation of each region, by automatically averaging 30 consecutive cycles (Bard Electrophysiology). If AF termination could not be achieved by CA, electrical cardioversion was performed.

Theoretical Basis of PCA

We investigated whether we could measure AF complexity as a function of the ability of PCA to compress the input BSPM signal into a few components while retaining the maximum amount of information as measured by variance. To this end, BSPMs were divided in $N_s = 500$ -ms segments, and in each frame (s) singular value decomposition of the input data $Y^{(s)}$ was performed as in Bonizzi et al. (2010); Meo et al. (2013a,b, 2017):

$$Y^{(s)} = USV^T$$

Where U and V represent the left and right singular vectors of $Y^{(s)}$ respectively, and the diagonal matrix S contains the singular values σ_l , $l = 1, \dots, L$, each associated with the principal components (PCs) $X^{(s)}$, which are mutually uncorrelated and linked with the BSPM observations through the linear relation:

$$Y^{(s)} = M^{(s)}X^{(s)}$$

Where $M^{(s)} = US/\sqrt{N_s}$ represents the PCA transfer matrix. PCs are computed and ordered so that the first few retain most of the variance present in the input signals.

Measuring AF Spatiotemporal Complexity

In line with (Bonizzi et al., 2010; Di Marco et al., 2012), we used the distance between the input BSPM signal and its rank-3 PCA approximation to measure AF organization. Since heart electrical activity on surface recordings can be well approximated by an electric dipole (Holt et al., 1969) and most of the body surface potential energy can be adequately characterized by the first 3 PCs (Lux et al., 1981), we hypothesized that organized atrial activity could be accurately retained by a 3D subspace as spanned by the first 3 columns of the PCA mixing matrix $M_3^{(s)}$. By contrast, more complex and unpredictable patterns will require a higher number of PCs to be described with sufficient accuracy, therefore the subspace chosen will yield a higher PCA reconstruction error. We introduced the nondipolar component index (NDI) to quantify the residual amount of energy which was retained by the PCA eigenvalues $\sigma_l, l = 4, \dots, L$, outside the projection subspace spanned by the columns $M_3^{(s)}$:

$$NDI = 1 - \frac{\sum_{l=1}^3 \sigma_l}{\sum_{l=1}^L \sigma_l}.$$

The global NDI parameter was determined as the average of all the values computed in each frame and served as a marker of AF complexity, with higher values denoting more disorganized and

irregular signal waveforms. To increase statistical confidence, we required a minimum BSPM duration of 1 s so as to compute the NDI as the average of at least 2 values in the examined recording.

Comparison With Patient's Clinical Characteristics

From previous studies (Rostock et al., 2011; Scherr et al., 2015) it is known that some clinical parameters are predictive of favorable CA outcomes, such as a shorter AF duration and smaller LA size. As a consequence, the proposed signal processing methodology has been compared to the maximum continuous AF duration and LA area measured with transesophageal echocardiography.

Comparison With Other Descriptors of AF Complexity on Surface Recordings

Our multilead approach has been compared with some traditional single-lead markers of AF organization from surface recordings. To this end, NDI was also computed on a subset of BSPM electrodes at the locations of standard ECG leads and denoted NDI_{ECG} , in order to verify whether this ensemble of electrodes could equally allow for a thorough characterization of AF spatiotemporal organization. As in Meo et al. (2013a), leads III and augmented leads aV_R , aV_L , and aV_F were not included as they are linearly dependent on the other frontal leads. In order to verify whether any additional information could be derived from posterior BSPM leads, alternative ECG lead placement configurations were also tested. Accordingly, we assessed NDI in the optimized atrial cardiogram (OACG) system proposed in Ihara et al. (2007); van Oosterom et al. (2007), including five of the standard ECG leads (I, II, III, V_1 , and V_4), three electrodes on the chest (V_1S , above V_1 ; V_2RS , at the right of V_1S ; V_{LC} , below the left clavicle), and a posterior one (V_1P , at the same level as V_1), for a total of nine electrodes. NDI computation was also performed in the extended ECG described in Petrucci et al. (2009), consisting of 15 leads, i.e., the standard 12 ECG leads and three posterior leads V_7 , V_8 , and V_9 , which are placed below the left scapula, at the same level as V_6 , and are considered to better reflect LA activity than conventional precordial leads.

In keeping with (Nault et al., 2009; Cheng et al., 2013), f-wave amplitude A_{V1} was computed in V_1 using a custom algorithm described in Meo et al. (2013a) and based on the interpolation of atrial signal local extrema through polynomial envelopes. In the same ECG lead AF CL was also considered as in Matsuo et al. (2009). Local maxima above a voltage threshold equal to 0.01 mV were automatically detected based on derivative sign change and a global marker CL_{V1} was obtained by averaging all CLs longer than 90 ms, so as to reject the influence of spurious local extrema.

Some multilead methods were also investigated and compared to our approach. As in Bonizzi et al. (2010), the normalized mean square error (NMSE) between the input BSPM signal and its rank-3 PCA reconstruction was determined in V_1 and denoted $NMSE_3$; the same tuning parameters suggested in that study were set. A multilead extension of this parameter introduced in Meo et al. (2013b) was also considered, and AF complexity was quantified as a weighted mean on NMSE values determined in multiple electrodes in the original signal and

denoted $WNMSE_{BSPM}$. Finally, a multilead characterization of f-wave amplitude as illustrated in Meo et al. (2013a) was also applied to our AF database, and a median descriptor of atrial amplitude of the rank-1 PCA estimation extracted from the input ECG was computed (A_{BSPM}). All the BSPM-derived parameters of AF organization were also computed in the other ECG configuration previously described, thus yielding $WNMSE_{ECG}$ and A_{ECG} for the 12-lead ECG counterpart of $WNMSE_{BSPM}$ and A_{BSPM} , $WNMSE_{OACG}$ and A_{OACG} in the OACG system, and $WNMSE_{ECG15}$ and A_{ECG15} in the extended 15-lead ECG, respectively.

Evaluation of the Clinical Value of AF Complexity Markers

Body surface AF complexity was linked to the NDI and compared to patient's pathophysiology, meant in terms of characteristics of the underlying atrial substrate and severity of disease. Accordingly, we investigated whether rapid AF activities as measured on the baseline CL would reflect on the surface and correlate with NDI, as intracardiac AF CL is regarded as a surrogate of local refractory periods (Kim et al., 1996) and shortens with maintenance of the arrhythmia. Additionally, the relation between the proposed noninvasive index and continuous AF duration was examined. Longer AF duration was proven to be associated with a higher number of atrial AF driving sources, both focal and rotational (Lim et al., 2017), and a more complex substrate, i.e., a higher number of activation wavefronts and breakthrough waves, electrical dissociation, slower conduction and higher fractionation (De Groot et al., 2010; Lau et al., 2017). Accordingly, we hypothesized that higher NDI should be observed in long-lasting AF patients (≥ 12 months, 23 patients) rather than in persistent forms (< 12 months, 74 patients).

Our PCA-based feature was also compared to the ablation strategy. We assumed that more severe AF forms will be more difficult to be treated, as not only the number of driving sources will be higher, but they will also appear in a higher number of sites (Haissaguerre et al., 2014; Lim et al., 2017). Therefore, we expected that CA procedures will be longer (> 30 min) in terms of the amount of radiofrequency energy emission required for tissue cauterization and a higher number of atrial regions (≥ 4) will have to be targeted to accomplish CA successfully. Moreover, acute AF termination is considered less likely to be achieved.

The same analysis was led for the markers of AF organization reported in section Comparison With Other Descriptors of AF Complexity on Surface Recordings.

Statistical Analysis and Classification Performance Assessment

All continuous variables were expressed as mean \pm standard deviation. Parameters' distribution was checked using a Lilliefors test. For normally distributed data, intergroup differences were verified by an unpaired Student's *t*-test with Welch's correction for unequal group variances and sizes. Otherwise, a Wilcoxon's rank sum test was applied. For multivariate comparisons, one-way analysis of variance (ANOVA) was applied to normally distributed data, otherwise a Kruskall-Wallis test was used.

Statistical tests were considered significant if their *p*-value was below 0.05.

We reported the area under the curve (AUC) output by the receiver operating characteristic (ROC) analysis as an index of univariate prediction performance for all AF complexity parameters. Additionally, the rates of correct detections per group were expressed in terms of the sensitivity and the specificity (i.e., the fraction of true positive and true negative cases correctly identified, respectively) associated with the optimal cutoff. Accordingly, CA procedures performed in long-lasting AF patients, with longer ablation time and a higher number of atrial targets were associated with higher AF complexity and therefore referred to as positive cases, whereas persistent AF forms and less extensive ablations (in terms of radiofrequency energy emission duration and number of regions) were regarded as negative cases.

Finally, we verified whether the evaluation of AF ablation impact (in terms of procedure outcome, duration and number of targets) based on patient's clinical data only could benefit from the integration of information about AF complexity as quantified by the aforementioned indices. Accordingly, a subset of data was used for training, whereas the other samples formed the validation set. To evaluate the ability of the multivariate features to predict ablation outcome and the number of ablated atrial sites, features from 77 patients were included in the training, whereas the remaining ones were used for validation. By contrast, since AF ablation duration had been measured only for successful procedures, smaller datasets were considered accordingly (62 training samples and 15 validation samples). Only markers of AF complexity highlighting statistically significant intergroup differences (*p*-value ≤ 0.05) were investigated. Patient's clinical data included: age, AF duration, LA area, LVEF. As in Lankveld et al. (2016b); Zeemering et al. (2017), multivariate prediction models combining clinical data (F_{CLIN}) and each of the retained signal complexity parameters ($F_{CLIN+SIG}$) were built by logistic regression (LR); 15-fold cross validation was performed in order to get an unbiased evaluation of a model fit on the training dataset. The output model was then applied to the validation set to determine the LR probability estimates and assign them to the related category. Prediction performance in the training and validation phase was assessed by ROC analysis as for the univariate parameters. Training and validation of classification models were first performed on multivariate features depending on patient's clinical information only (F_{CLIN}). The same procedure was applied again to multivariate classifiers obtained by integrating clinical data with the parameter of signal complexity under exam ($F_{CLIN+SIG}$). Classification models based on clinical data only were trained, tested and re-evaluated each time a signal complexity feature was examined, so as to specifically investigate the effect of the presence/absence of each measure of AF complexity and ensure a consistent comparison between classification scores always on the same datasets, especially in case of missing data. The predictive accuracy of AF duration was tested using the same methodology as well and compared with the clinical set of variables F_{CLIN} (including patient's age, LA area and LVEF). The improvement in classification accuracy provided by the integration of the

signal-derived parameter was evaluated in terms of the net reclassification index (NRI), which is defined as the sum of the net percentages of correctly reclassified samples in the categories of interest (Pencina et al., 2008). Null NRI values denote the absence of improvement in the classification by adding a new variable. The null hypothesis NRI=0 was verified by a *z*-test and considered statistically significant if *p*-value was <0.05 .

RESULTS

Electrophysiological Mapping and Ablation

Baseline AF CL was 178 ± 55 ms. It was shorter than 160 ms in 33 patients, between 160 and 180 ms in 15 patients, and longer than 180 ms in the remaining ones. LA area was 26 ± 6 cm². Out of 97 patients, 17 of them underwent a redo ablation (17%). AF induction was performed in 48 patients (49%) prior to CA. AF converted to SR in 27 patients, to AT in 50 patients (global AF termination rate: 79%). Intracardiac AF CL was 177 ± 40 ms in AF-free patients, whereas it was 157 ± 26 ms for failed procedures (*p* = 0.0586). Mean ablation duration was 35 ± 21 min (<30 min in 38 out of 97 patients) and 4 ± 2 regions (between 1 and 3 sites in 36 AF patients) were targeted by CA. BSPM recordings acquired in 3 subjects were discarded from our analysis as their duration was below our requirements.

Assessment of AF Complexity in Body Surface Potentials

Results related to the analysis of the relation between the BSPM indices of AF organization and intracardiac AF CL are shown in Figure 3.

A significantly inverse correlation between the NDI and the CL measured in the LAA was demonstrated, with high complexity values observed in very advanced AF forms (AF CL < 160 ms) and progressively decreasing in less severe cases. Similar results could be retrieved in the alternative OACG lead configuration. A significantly direct correlation with intracardiac CL was remarked for CLv1 instead, i.e., higher body surface complexity as quantified by high NDI values reflected faster activations of the atrial substrate. Higher values of the multilead index of AF complexity WNMSE_{OACG} were also associated with more rapid intracardiac AF CL.

Statistical analysis outcome for the signal features assessed in persistent and long-lasting AF cases is shown in Figure 4.

LA surface did not highlight significant differences between the two groups of patients (persistent AF: 27 ± 6 cm²; long-lasting AF: 25 ± 7 cm², *p* = 0.38). NDI computed from BSPMs was the only one parameter highlighting significantly higher signal disorganization in more advanced AF forms, which were more accurately discriminated by the parameter according to the ROC analysis, as shown in Table 2.

The impact of AF complexity on the procedural time was quantified in Table 3.

Significantly low NDI values characterized shorter CA procedures, whereas higher complexity was measured by the

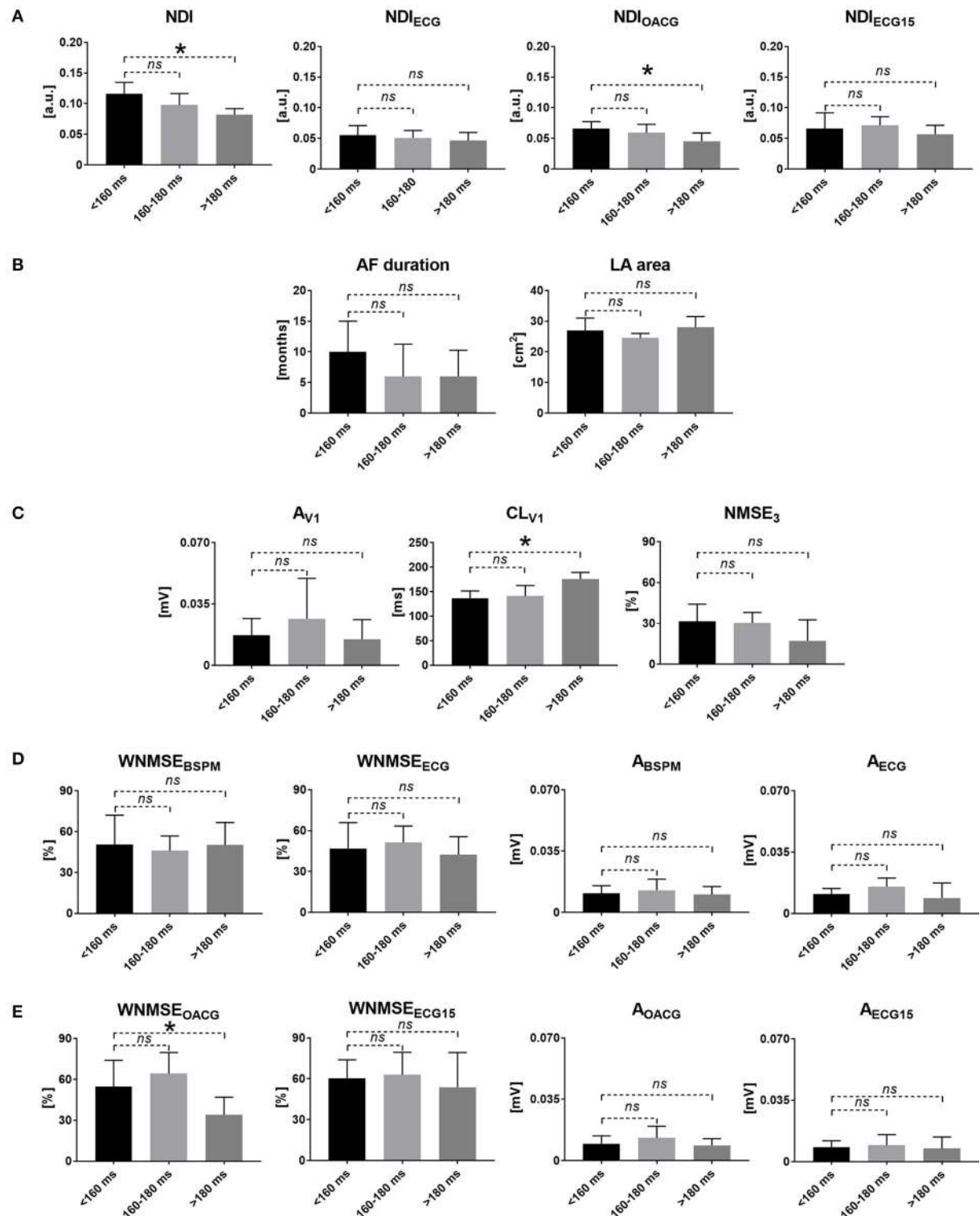
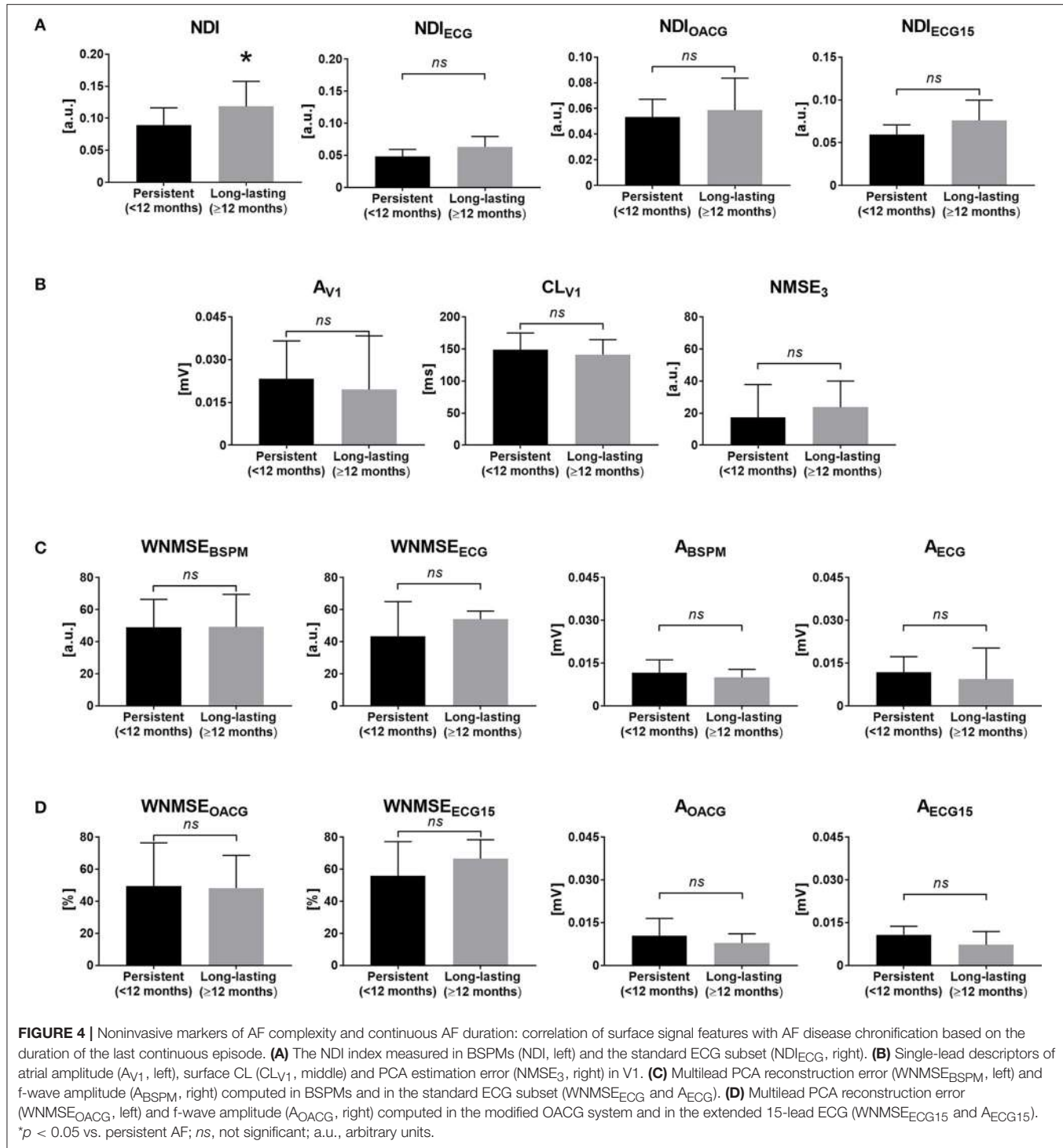


FIGURE 3 | Noninvasive markers of AF complexity and AF CL: correlation of surface signal features with AF disease chronification based on atrial AF CL. **(A)** The NDI index measured in BSPMs (NDI, left) and the standard ECG subset (NDI_{ECG}, right). **(B)** Clinical measures of cardiac activity: AF duration (left) and LA area (right). **(C)** Single-lead descriptors of atrial amplitude (Av₁, left), surface CL (CL_{V1}, middle) and PCA estimation error (NMSE₃, right) in V1. **(D)** Multilead PCA reconstruction error (WNMSE_{BSPM}, left) and f-wave amplitude (A_{BSPM}, right) computed in BSPMs and in the standard ECG subset (WNMSE_{ECG} and A_{ECG}). **(E)** Multilead PCA reconstruction error (WNMSE_{OACG}, left) and f-wave amplitude (A_{OACG}, right) computed in the modified OACG system and in the extended 15-lead ECG (WNMSE_{ECG15} and A_{ECG15}). **p* < 0.05 vs. <160 ms; ns, not significant; a.u., arbitrary units.



index in longer ablations. Similarly, NDI_{ECG15} put more disorganized signal waveforms from the modified 15-lead ECG in relation to longer procedural time. Finally, the multilead assessment of f-wave amplitude in the same ECG lead system underlined statistically significant differences between the groups examined, even if it unexpectedly correlated lower amplitude values with shorter CA. Among all multilead descriptors of AF

complexity, NDI assessed in BSPMs was the only one exhibiting a high predictive power as well, as confirmed by the ROC analysis in Table 4.

By contrast, NDI_{ECG15} was characterized by low predictive accuracy as proven by the ROC analysis. Long-lasting AF patients also underwent significantly longer CA procedures, although the predictive value of AF duration was quite low. Surface CL

TABLE 2 | ROC analysis of the AF complexity features and AF duration.

	AUC [%]	Sensitivity [%]	Specificity [%]
NDI [a.u]	70	55	79
LA area [cm ²]	59	36	79
A _{V1} [mV]	52	55	60
CL _{V1} [ms]	60	45	82
NMSE ₃ [%]	51	55	60
WNMSE _{BSPM} [%]	58	86	42
A _{BSPM} [mV]	59	91	30
NDI _{ECG} [a.u]	63	58	84
WNMSE _{ECG} [%]	58	55	68
A _{ECG} [mV]	54	58	64
NDI _{OACG} [a.u]	59	37	90
WNMSE _{OACG} [%]	57	47	69
A _{OACG} [mV]	58	79	48
NDI _{ECG15} [a.u]	65	63	76
WNMSE _{ECG15} [%]	56	95	24
A _{ECG15} [mV]	61	42	85

Assessment of the ability of the AF organization markers to discriminate between persistent and long-lasting AF patients. Sensitivity and specificity indicate the rate of correct detections in the long-lasting and persistent AF patients' groups, respectively. Results for the parameters with the highest classification performance (AUC \geq 70%) are highlighted in boldface. AUC, area under curve; a.u., arbitrary units.

CL_{V1} was also significantly shorter in patients requiring longer CA procedures, and ROC analysis yielded predictive results as well. Unexpectedly, the multilead marker of f-wave amplitude A_{ECG} was significantly higher in patients undergoing longer CA procedures. The same results were output by A_{ECG15} in the extended 15-lead ECG set. However, in both cases the ROC analysis underlined low predictive performance, due to the inability to correctly identify long CA procedures based on AF complexity content.

In Table 5 we illustrated the relation between AF complexity and CA effectiveness, expressed in terms of the number of atrial regions to be ablated to achieve the procedural endpoint.

Also in this case, CA procedures requiring a lower number of targets to terminate AF characterized more organized waveforms, quantified by significantly lower NDI and higher CL_{V1} values. Nevertheless, both indices were characterized by low predictive accuracy, as confirmed by the ROC analysis in Table 6. Longer AF duration was also predictive of a more extensive ablation.

Finally, in Figure 5 the ability of the BSPM indices to assess short-term CA outcome was examined. Low NDI values were predictive of procedural AF termination, whereas AF forms which were less likely to be successfully converted to other rhythms by CA presented higher disorganization, quantified by higher NDI.

CA outcome prediction performance was assessed by ROC analysis in Table 7.

It yielded AUC = 69%, sensitivity = 70%, specificity = 67% for NDI. Moreover, patients with longer AF episodes were significantly less likely to experience procedural success. AF termination by CA was also predicted by significantly higher f-wave amplitude, quantified by higher A_{BSPM} values, but with a poor ROC analysis outcome. The multilead BSPM descriptors

TABLE 3 | Noninvasive markers of AF complexity and ablation time.

	Ablation time (\leq 30 min)	Ablation time ($>$ 30 min)	p-value
NDI [a.u]	0.086 \pm 0.036	0.107 \pm 0.032	0.0009
AF duration [months]	5.9 \pm 6.0	9.2 \pm 8.7	0.030
LA area [cm ²]	26 \pm 6	26 \pm 7	0.65
A _{V1} [mV]	0.022 \pm 0.015	0.032 \pm 0.023	0.063
CL _{V1} [ms]	168 \pm 34	145 \pm 32	0.002
NMSE ₃ [%]	23.4 \pm 17.7	25.2 \pm 19.4	0.71
WNMSE _{BSPM} [%]	42.4 \pm 26.0	53.8 \pm 26.3	0.064
A _{BSPM} [mV]	0.013 \pm 0.006	0.012 \pm 0.005	0.81
NDI _{ECG} [a.u]	0.047 \pm 0.016	0.055 \pm 0.023	0.26
WNMSE _{ECG} [%]	42.4 \pm 25.3	46.8 \pm 24.0	0.49
A _{ECG} [mV]	0.010 \pm 0.006	0.015 \pm 0.008	0.017
NDI _{OACG} [a.u]	0.051 \pm 0.022	0.060 \pm 0.025	0.15
WNMSE _{OACG} [%]	49.6 \pm 27.6	48.0 \pm 25.5	0.72
A _{OACG} [mV]	0.010 \pm 0.0006	0.013 \pm 0.007	0.11
NDI _{ECG15} [a.u]	0.058 \pm 0.019	0.071 \pm 0.029	0.043
WNMSE _{ECG15} [%]	55.6 \pm 25.0	55.3 \pm 26.6	0.80
A _{ECG15} [mV]	0.009 \pm 0.004	0.013 \pm 0.007	0.025

Correlation of body surface signal features with the duration of radiofrequency emission duration to achieve procedural AF termination; p values in boldface are statistically significant; a.u., arbitrary units.

of AF organization were also computed in the modified configurations of the standard 12-lead ECG, and the statistical analysis results were shown together with the aforementioned parameters. Nevertheless, overall those parameters did not yield significant results ($p > 0.05$).

We also evaluated the classification accuracy of each of the examined AF complexity markers in combination with AF patients' clinical information.

In Table 8 the ability of multivariate classifiers to distinguish between short and long CA procedures was reported.

Clinical indices alone could not effectively discriminate ablation interventions based on their duration. Adding an AF complexity marker considerably improved the classification accuracy in the validation set in terms of AUC more clearly than in the training set for the univariate AF CL CL_{V1} and the multivariate descriptors of amplitude assessed in the full set of BSPM electrodes (A_{BSPM}) and in the 15-lead ECG subset (A_{ECG15}). Similar findings were made for the NDI assessed in the same lead configuration (NDI_{ECG15}), but these results could not be reproduced on the original BSPM lead configuration. However, the degree of improvement of classification performance as assessed by the NRI was not statistically significant for any of these multivariate features.

In Table 9 the ability of the multivariate classifiers to characterize more extensive ablation interventions in terms of the number of procedural targets was investigated.

Classification accuracy based on clinical data was improved by the introduction of the NDI marker in the validation set (AUC=86%, sensitivity=86%, specificity=83%). Similarly, CA

TABLE 4 | ROC analysis of the AF complexity features and ablation time.

	AUC [%]	Sensitivity [%]	Specificity [%]
NDI [a.u]	72	71	78
AF duration [months]	64	28	97
LA area [cm ²]	53	51	66
A _{V1} [mV]	64	61	73
CL _{V1} [ms]	73	74	70
NMSE ₃ [%]	53	35	83
WNMSE _{BSPM} [%]	63	79	47
A _{BSPM} [mV]	52	44	71
NDI _{ECG} [a.u]	59	63	61
WNMSE _{ECG} [%]	56	48	70
A _{ECG} [mV]	68	57	79
NDI _{OACG} [a.u]	61	43	82
WNMSE _{OACG} [%]	53	90	29
A _{OACG} [mV]	61	37	89
NDI _{ECG15} [a.u]	65	70	61
WNMSE _{ECG15} [%]	52	23	93
A _{ECG15} [mV]	67	47	86

Assessment of the ability of the AF organization descriptors to distinguish between short and long AF ablation procedures. Sensitivity and specificity indicate the percentage of interventions correctly identified by the signal features based on the duration of radiofrequency emission duration to AF termination, i.e., longer/shorter than 30 min, respectively. Results for the parameters with the highest classification performance (AUC \geq 70%) are highlighted in boldface. AUC, area under curve; a.u., arbitrary units.

procedures could be better discriminated based on the number of ablated atrial regions by adding CL_{V1}. By contrast, no benefits were provided by information about AF duration. Overall, none of these changes was statistically significant according to NRI analysis.

Finally, in Table 10 the classification performance of multidimensional predictors of CA outcome was shown.

As in the previous case, prediction accuracy in the validation phase was higher when NDI was also included into the classification model (AUC=70%, sensitivity=100%, specificity=50%). Similar remarks could be made for the single-lead CL CL_{V1}. Information provided by AF duration to the classification model was poor instead, both in the training and the validation phase. However, also in this case changes in the classification scores as measured by the NRI were not statistically significant.

DISCUSSION

In this study we proposed a noninvasive PCA-based approach to evaluate AF complexity in BSPMs, which can be accurately characterized even in very short recordings (<10s in our database). The algorithm overcomes limitations of QRST cancelation, which may be affected by R peak misalignment or sudden changes in signal voltage, thus minimizing the influence of residual ventricular far field. Indeed, since PCA assumptions rely on signal second-order statistics at zero time lag, i.e., the coherence between consecutive samples is neglected, the use

TABLE 5 | Noninvasive markers of AF complexity and number of CA targets.

	Number of CA targets (<4)	Number of CA targets (\geq4)	p-value
NDI [a.u]	0.086 \pm 0.030	0.111 \pm 0.037	0.002
AF duration [months]	4.6 \pm 3.4	12.6 \pm 13.1	<0.0001
LA area [cm ²]	27 \pm 6	26 \pm 6	0.56
A _{V1} [mV]	0.024 \pm 0.016	0.030 \pm 0.024	0.27
CL _{V1} [ms]	167 \pm 35	147 \pm 29	0.007
NMSE ₃ [%]	21.8 \pm 18.0	24.4 \pm 18.5	0.54
WNMSE _{BSPM} [%]	43.3 \pm 27.6	52.8 \pm 24.7	0.065
A _{BSPM} [mV]	0.012 \pm 0.006	0.011 \pm 0.005	0.32
NDI _{ECG} [a.u]	0.048 \pm 0.019	0.055 \pm 0.022	0.18
WNMSE _{ECG} [%]	39.1 \pm 24.9	46 \pm 59, 23.4	0.49
A _{ECG} [mV]	0.011 \pm 0.006	0.013 \pm 0.008	0.26
NDI _{OACG} [a.u]	0.054 \pm 0.027	0.059 \pm 0.022	0.18
WNMSE _{OACG} [%]	46.9 \pm 29.1	50.8 \pm 24.1	0.62
A _{OACG} [mV]	0.012 \pm 0.006	0.0012 \pm 0.007	0.71
NDI _{ECG15} [a.u]	0.059 \pm 0.021	0.071 \pm 0.029	0.11
WNMSE _{ECG15} [%]	51.7 \pm 26.2	57.4 \pm 22.9	0.75
A _{ECG15} [mV]	0.010 \pm 0.005	0.011 \pm 0.006	0.63

Correlation of BSPM features with the number of atrial sites ablated to achieve procedural AF termination; p values in boldface are statistically significant; a.u., arbitrary units.

of temporally consecutive samples is not necessary (Bonizzi et al., 2010). Furthermore, it does not require any a priori selection of specific electrodes, as it automatically condenses the most relevant signal information into a few components based on its energy content. In addition, apart from the duration of the signal to be processed, no further tuning parameters need to be set, thus making this tool easier to be implemented and integrated to AF complexity analysis than other indices from the state of the art, e.g., sample entropy (Alcaraz et al., 2011). Our methodology provided relevant insights into the characteristics of AF disease and substrate and correlated with CA strategy.

Surface AF Complexity and Characteristics of AF Disease and Substrate

The proposed methodology can quantify AF organization in surface recordings and correlate it to the underlying electrophysiological substrate.

A decreasing trend of NDI as a function of AF CL was observed, and more rapid local activities in the atria reflected on higher complexity on body surface.

Similar evidence was found for CL_{V1}, thus proving a direct correlation between the invasive measure of the atrial fibrillatory rate and the surface electrical activity, which was previously demonstrated in (Matsuo et al., 2009) as well.

By contrast, no significant correlation between continuous AF duration and body surface complexity. Indeed, this clinical parameter may not reliably reflect the properties of the underlying atrial substrate, as it is often difficult to determine, unless continuous long-term ECG monitoring is performed (Ciccone et al., 2017). However, this approach would not be

TABLE 6 | ROC analysis of the AF complexity features and number of CA targets.

	AUC [%]	Sensitivity [%]	Specificity [%]
NDI [a.u]	69	67	71
AF duration [months]	75	64	75
LA area [cm ²]	54	67	45
AV ₁ [mV]	58	54	64
CL _{V1} [ms]	68	85	39
NMSE ₃ [%]	54	35	82
WNMSE _{BSPM} [%]	61	88	38
A _{BSPM} [mV]	56	23	92
NDI _{ECG} [a.u]	59	37	92
WNMSE _{ECG} [%]	59	69	50
A _{ECG} [mV]	58	80	38
NDI _{OACG} [a.u]	59	47	77
WNMSE _{OACG} [%]	53	82	35
A _{OACG} [mV]	53	86	31
NDI _{ECG15} [a.u]	61	37	88
WNMSE _{ECG15} [%]	56	74	42
A _{ECG15} [mV]	53	92	19

Assessment of the ability of the AF organization descriptors to identify extensive ablation procedures in terms of the number of atrial sites targeted to achieve AF termination. Sensitivity and specificity indicate the percentage of procedures correctly classified by the signal features based on the number of ablation targets, i.e., more/less than 4 sites, respectively. Results for the parameters with the highest classification performance (AUC \geq 70%) are highlighted in boldface. AUC, area under curve; a.u., arbitrary units.

helpful in asymptomatic AF patients (Ahmad and Kirchhof, 2013), whose diagnosis is still challenging. Paradoxically, current guidelines increasingly tend not to distinguish between the prognostic implications of paroxysmal vs. long-standing AF (Calkins et al., 2012). Some studies demonstrated that patients with similar clinical characteristics (including AF history) may present very different substrates (Kottkamp, 2013) and even some paroxysmal AF forms may be due to sources other than those in the pulmonary veins (Sanchez-Quintana et al., 2012). Nevertheless, the relation between number of AF driving sources and disease duration has been shown elsewhere (Lim et al., 2017), thus making it harder to reach a consensus about the role of AF duration as a marker of complexity.

Higher complexity was measured by higher NDI in patients with longer AF episode duration, which may result from a longer electrical remodeling of the atrial substrate, due to disease progression (Lau et al., 2017) and the onset of multiple sources located even outside the pulmonary vein areas (Lim et al., 2017). The strength of this correlation was also supported by the ROC analysis, confirming the ability of the proposed index to assess atrial activity rate based on body surface signal complexity.

Surprisingly, longer AF duration and larger LA area did not show any evident correlation with faster AF CLs, in contrast with evidence reported in Ammar et al. (2014). However, the same study claims that variations in intracardiac CL depend both on other patient's clinical characteristics, including age and other comorbidities, and external factors, such as pharmacological interventions, thus this finding should be investigated in a broader context.

Body surface measures of f-wave amplitude could not significantly reflect the properties of the AF wavefront propagation in terms of CL. Moreover, all amplitude features did not exhibit any significant correlation with AF duration. While some studies have discovered a correlation between atrial amplitude and AF duration and echocardiographic characteristics (Yamamoto et al., 2005), in Nault et al. (2009) and other more recent studies that finding was impossible to reproduce, thus confirming the divergence between results reported in literature.

Indices of complexity based on PCA reconstruction error (i.e., NMSE₃ and WNMSE_{BSPM}) could not effectively quantify the degree of AF chronification. In contrast with our intuition, higher PCA projection errors did not significantly reflect faster intracardiac AF activation. Additionally, the accuracy of PCA estimation was not significantly lower in long-lasting AF patients. This may be partially explained by the use of the setting proposed in the related reference studies, which may be not suitable for our signal database. Furthermore, those parameters rather aimed to quantify the degree of stationarity and repetitiveness of atrial components across the electrodes, which may not be sufficiently evident in short recordings as those examined in our study.

Surface AF Complexity and CA Strategy

Our PCA-derived parameter could also quantify the impact of AF complexity on the CA therapy strategy. Indeed, higher complexity was underlined by NDI in surface recordings in patients undergoing shorter ablation procedures, and the univariate ROC analysis corroborated the ability of the index to accurately distinguish between interventions of different duration based on the signal complexity information. Furthermore, a lower number of atrial targets and higher procedural success probability were associated with more complex AF waveforms, despite the weaker predictive performance. By contrast, more disorganized AF forms were less likely to be successfully converted to other rhythms by CA, and they generally required longer interventions and a more extensive cauterization of atrial tissue.

Continuous AF duration proved to be a significant univariate predictor of CA outcome, and long-lasting cases overall required a more extensive ablation, in line with previous research (Scherr et al., 2009; Rostock et al., 2011). Despite this performance, it is essential to keep in mind some of the aforementioned limitations of AF duration, e.g., the potentially inaccurate evaluation of its value in certain patients, or the lack of correlation with the atrial substrate, which may lead to an erroneous evaluation of the ablation strategy, thus corroborating the added descriptive value from cardiac signal processing parameters. Conversely, LA surface did not show any relevant correlation with CA strategy and effectiveness. This finding may appear in contrast with current literature (Zhuang et al., 2012; Scherr et al., 2015). Nevertheless, as pointed out in Hoit (2014), despite current recommendations for LA size assessment, clinical studies report a wide variety of 1-dimensional linear and 2D area measurements, which may lead to contrasting results

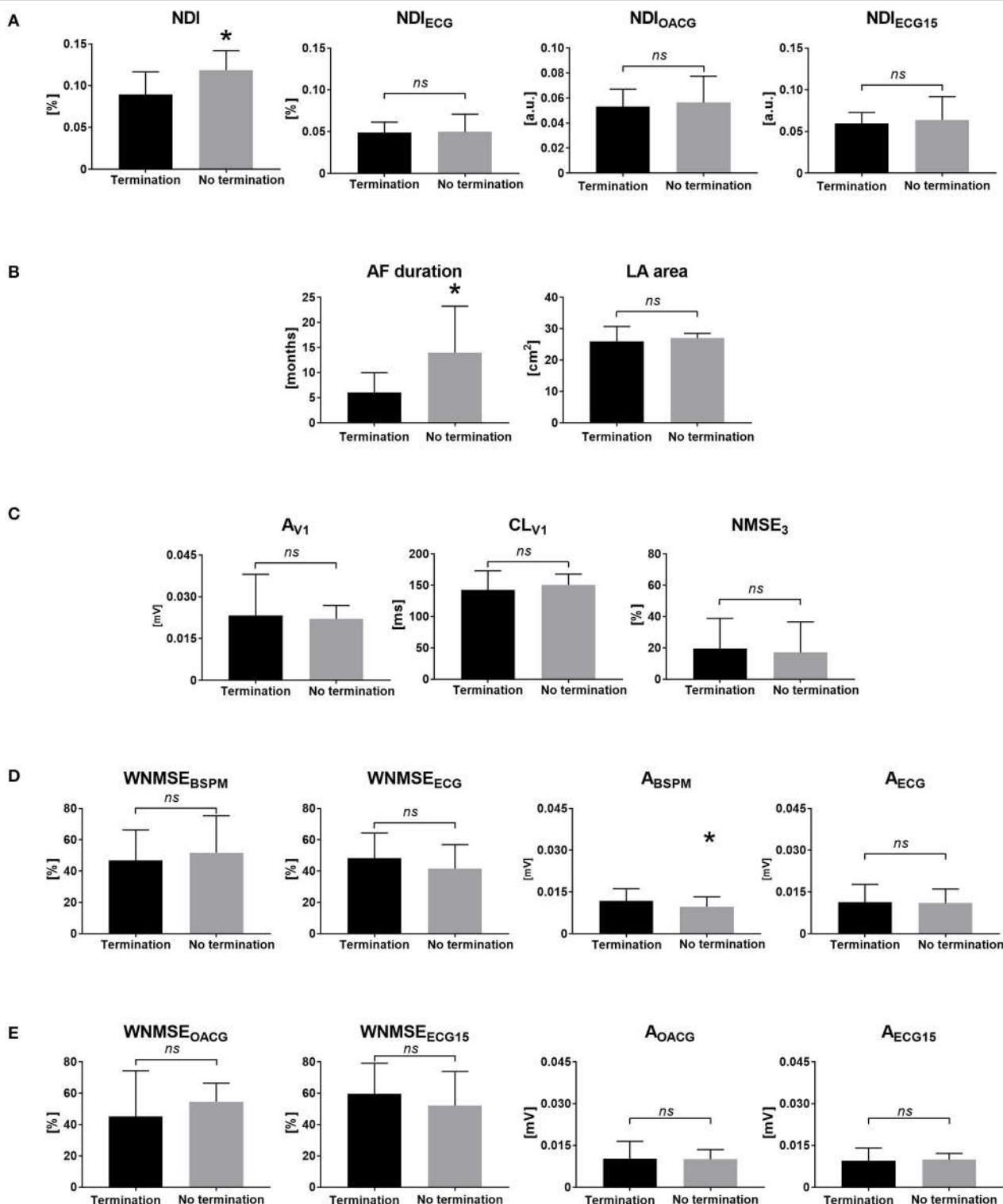


FIGURE 5 | Noninvasive markers of AF complexity and CA outcome: correlation of BSPM features with the acute CA outcome. **(A)** The NDI index measured in BSPMs (NDI, left) and the standard ECG subset (NDI_{ECG}, right). **(B)** Clinical measures of cardiac activity: AF duration (left) and LA area (right). **(C)** Single-lead descriptors of atrial amplitude (A_{V1}, left), surface CL (CL_{V1}, middle) and PCA estimation error (NMSE₃, right) in V1. **(D)** Multilead PCA reconstruction error (WNMSE_{BSPM}, left) and f-wave amplitude (A_{BSPM}, right) computed in BSPMs and in the standard ECG subset (WNMSE_{ECG} and A_{ECG}). **(E)** Multilead PCA reconstruction error (WNMSE_{OACG}, left) and f-wave amplitude (A_{OACG}, right) computed in the modified OACG system and in the extended 15-lead ECG (WNMSE_{ECG15} and A_{ECG15}). * p < 0.05 vs. AF termination; ns, not significant; a.u., arbitrary units.

TABLE 7 | ROC analysis of the AF complexity features and CA outcome.

	AUC [%]	Sensitivity [%]	Specificity [%]
NDI [a.u]	69	70	67
AF duration [months]	70	55	87
LA area [cm ²]	51	65	53
A _{V1} [mV]	51	84	33
CL _{V1} [ms]	52	37	75
NMSE ₃ [%]	56	32	85
WNMSE _{BSPM} [%]	57	95	26
A _{BSPM} [mV]	67	85	40
NDI _{ECG} [a.u]	56	37	81
WNMSE _{ECG} [%]	53	63	49
A _{ECG} [mV]	51	84	33
NDI _{OACG} [a.u]	57	37	88
WNMSE _{OACG} [%]	52	63	52
A _{OACG} [mV]	50	98	24
NDI _{ECG15} [a.u]	58	47	85
WNMSE _{ECG15} [%]	51	95	26
A _{ECG15} [mV]	54	84	33

Assessment of the ability of the AF organization descriptors to predict AF termination by CA. Sensitivity and specificity indicate the rate of detection of successful and failed ablation procedures, respectively. Results for the parameters with the highest classification performance (AUC \geq 70%) are highlighted in boldface. AUC, area under curve; a.u., arbitrary units.

and a make it harder to understand the clinical value of this parameter.

Preprocedural CL measured in lead V₁ (CL_{V1}) also appeared longer in ablations characterized by a lower number of candidate atrial sites for CA and with lower amount of radiofrequency energy emission. In keeping with (Matsuo et al., 2009), this finding suggests that CA results are not caused by operator bias, but by an increased complexity of AF substrate, and it is corroborated by ROC analysis as well. However, the index was not predictive of acute AF termination by CA, in contrast with results presented in Matsuo et al. (2009).

Acute CA outcome was significantly predicted by the multilead amplitude feature A_{BSPM}, which is consistent with results described in Meo et al. (2013a), despite the weak predictive performance. By contrast, its single-lead counterpart A_{V1} did not significantly discriminate between successful and failing CA procedures, which is in contradiction with evidence shown in Nault et al. (2009). However, as pointed out in the same study, f-wave amplitude measure is highly dependent on ECG acquisition modalities and it is sensitive to external artifacts, thus results reported by clinical studies are quite disparate and difficult to interpret.

Multilead PCA-based descriptors of AF organization NMSE₃ and WNMSE_{BSPM} could not significantly quantify the impact of atrial substrate complexity on AF ablation characteristics. As explained in section Surface AF Complexity and Characteristics of AF Disease and Substrate, a potential explanation of their weak predictive performance can be the impossibility to assess the spatiotemporal variability of the atrial signal pattern in very short signals. Nevertheless, this remark should be verified by additional experiments.

Benefits From the Spatial Variability of Multilead Recordings

All the multilead PCA-based descriptors of AF complexity obtained in BSPMs were also computed in an equivalent set of electrodes of the standard 12-lead ECG, thus yielding NDI_{ECG}, WNMSE_{ECG} and A_{ECG}, and the same statistical analysis was performed. Similarly, alternative body surface lead configurations were tested, i.e., the OACG system developed in Ihara et al. (2007); van Oosterom et al. (2007) and the extended 15-lead ECG system examined in Petrucci et al. (2009), with the AF complexity markers denoted as NDI_{OACG}, WNMSE_{OACG} and A_{OACG} and NDI_{ECG15}, WNMSE_{ECG15}, A_{ECG15}, respectively.

No index from 12-led ECG did significantly correlate neither with atrial substrate properties during AF nor with CA procedure characteristics and outcome. This may be due to the inability of standard ECG to sufficiently capture the spatial variability of AF pattern waveform, which can be instead more accurately characterized in larger sets of electrodes. Indeed, slight improvements in this characterization were observed in the OACG system, thus confirming the benefits of the analysis of the cardiac electrical activity in additional leads.

The relation between body surface complexity as measured by WNMSE_{OACG} and intracardiac AF CL in the OACG subset was also significant, but not strictly decreasing as for the aforementioned measures of AF organization, thus further investigation should be performed in the assessment of this quantitative relation. These results underlined the added value of the posterior OACG lead, which is assumed to better characterize LA activity, due to its proximity to lead M of Frank's vector lead system (Ihara et al., 2007). However, a more strategic and effective ECG lead placement configuration should be investigated in more detail in order to increase the predictive power of the related AF organization measures.

BSPM capability of providing a more comprehensive view of surface cardiac electrical activity has been previously demonstrated for ventricular electrical disorders (Robinson et al., 2009), and advances in diagnosis and therapy of supraventricular arrhythmias have been obtained as well, thanks to the more reliable identification of arrhythmogenic sources driving and sustaining the pathological rhythm (SippensGroenewegen et al., 2004; Haissaguerre et al., 2013; Yamashita et al., 2015), thus corroborating the clinical value of BSPM analysis.

Concerning the CA strategy, the NDI determined from the extended 15-lead ECG proposed in Petrucci et al. (2009) correlated higher body surface complexity with prolonged ablation procedures, thus demonstrating that relevant insights into AF therapy can be better provided by additional leads reflecting the underlying LA activity on body surface (i.e., V₇, V₈, and V₉) rather than conventional precordial leads, in particular V₁, which is closer to RA (Holm et al., 1998).

The multilead index of f-wave amplitude A_{ECG} associated higher values with longer procedures, despite the poor outcome of the predictive accuracy analysis. Similar results were reported for the same parameter computed from the extended 15-lead ECG. This finding may appear in contrast with our clinical intuition, which correlates higher atrial amplitude with a more homogeneous and organized waveform of tissue depolarization.

TABLE 8 | Multivariate classification performance based on ablation duration and NRII assessment.

	<i>F_{CLIN}</i>						<i>F_{CLIN+SIG}</i>					
	Training			Validation			Training			Validation		
	AUC [%]	Sensitivity [%]	Specificity [%]	AUC [%]	Sensitivity [%]	Specificity [%]	AUC [%]	Sensitivity [%]	Specificity [%]	AUC [%]	Sensitivity [%]	Specificity [%]
NDI [a.u.]	56	42	65	29	100	14	62	45	65	65	80	57
AF duration [months]	41	32	52	49	40	86	53	39	68	29	100	14
CL v1 [ms]	59	42	71	29	100	14	61	42	71	85	100	60
ABSPM [mV]	54	35	65	29	100	14	54	35	65	85	100	80
NDIECG15 [a.u.]	57	19	66	43	100	29	63	46	55	85	100	60
AECG15 [mV]	57	35	71	29	100	14	61	39	71	70	100	60
											60	-0.04
												0.89

ROC analysis of the multivariate classifiers obtained by using clinical data only (*F_{CLIN}*) and by integrating an AF complexity descriptor (*F_{CLIN+SIG}*) in the training and validation sets based on procedural duration. Training and validation of classification models were first performed on multivariate features depending on patient's clinical information only (*F_{CLIN}*). The same procedure was applied again to multivariate classifiers obtained by integrating clinical data with the parameter of signal complexity under exam (*F_{CLIN+SIG}*). Classification models based on *F_{CLIN}* were trained, tested and re-evaluated each time a signal complexity feature was examined. The variable *F_{CLIN+SIG}* including AF duration was compared to *F_{CLIN}*. * Differences in classification accuracy were quantified by the NRI. Results for the parameters with the highest classification performance ($AUC \geq 70\%$) are highlighted in boldface; AUC, area under curve; a.u., arbitrary units.

TABLE 9 | Multivariate classification performance based on the number of ablation targets and NRII assessment.

	<i>F_{CLIN}</i>						<i>F_{CLIN+SIG}</i>					
	Training			Validation			Training			Validation		
	AUC [%]	Sensitivity [%]	Specificity [%]	AUC [%]	Sensitivity [%]	Specificity [%]	AUC [%]	Sensitivity [%]	Specificity [%]	AUC [%]	Sensitivity [%]	Specificity [%]
NDI [a.u.]	72	79	53	64	50	86	79	47	79	86	86	83
AF duration [months]	53	96	7	40	100	17	75	82	52	71	50	0.17
CLv1 [ms]	74	80	52	52	71	50	77	86	41	71	57	100
											-0.04	0.81

ROC analysis of the multivariate classifiers obtained by using clinical data only (*F_{CLIN}*) and by integrating an AF complexity descriptor (*F_{CLIN+SIG}*) in the training and validation sets based on the number of atrial sites targeted by ablation. Training and validation of classification models were first performed on multivariate features depending on patient's clinical information only (*F_{CLIN}*). The same procedure was applied again to multivariate classifiers obtained by integrating clinical data with the parameter of signal complexity under exam (*F_{CLIN+SIG}*). Classification models based on *F_{CLIN}* were trained, tested and re-evaluated each time a signal complexity feature was examined. The variable *F_{CLIN+SIG}* including AF duration was compared to *F_{CLIN}*. * Differences in classification accuracy were quantified by the NRI. Results for the parameters with the highest classification performance ($AUC \geq 70\%$) are highlighted in boldface; a.u., arbitrary units.

TABLE 10 | Multivariate ablation outcome classification performance and NRI assessment.

	F_{CLIN}						$F_{CLIN+SIG}$							
	Training			Validation			Training			Validation				
	AUC [%]	Sensitivity [%]	Specificity [%]	AUC [%]	Sensitivity [%]	Specificity [%]	AUC [%]	Sensitivity [%]	Specificity [%]	AUC [%]	Sensitivity [%]	Specificity [%]	NRI [a.u.]	p-value
NDI [a.u.]	58	19	97	67	67	90	60	25	92	70	100	50	0	N.A.
AF duration [months]	19	0	100	43	33	100	56	98	19	67	67	90	0	N.A.
ABSPM [mV]	59	15	97	67	67	90	66	15	97	79	67	100	0.25	0.32

ROC analysis of the multivariate predictors of ablation outcome obtained by using clinical data only (F_{CLIN}) and by integrating an AF complexity descriptor ($F_{CLIN+SIG}$) in the training and validation sets. Training and validation of classification models were first performed on multivariate features depending on patients' clinical information only (F_{CLIN}). The same procedure was applied again to multivariate classifiers obtained by integrating clinical data with the parameter of signal complexity under exam ($F_{CLIN+SIG}$). Classification models based on F_{CLIN} were trained, tested and re-evaluated each time a signal complexity feature was examined. The variable $F_{CLIN+SIG}$ including AF duration was compared to F_{CLIN} . Differences in classification accuracy were quantified by the NRI. Results for the parameters with the highest classification performance ($AUC \geq 70\%$) are highlighted in boldface; AUC, area under curve; a.u., arbitrary units; N.A., not applicable.

However, similar evidence was also found in Zeemering et al. (2017), pointing out that higher f-wave amplitude may predict AF recurrence after pharmacological cardioversion. Due to the difficult interpretability of the physiological background, such aspects deserve more detailed investigation.

Assessment of AF Ablation Impact in a Multivariate Framework

The ability of clinical parameters alone to predict CA effectiveness and predict larger CA interventions (in terms of procedural time and targets) was overall limited, in line with previous research (Lankveld et al., 2016b; Zeemering et al., 2017). As pointed out in those studies, information about patient's clinical background may be incomplete or imprecise. Parameters such as AF duration may be difficult to evaluate in some patients due to the asymptomatic or slightly symptomatic nature of some AF episodes (Lankveld et al., 2016b), thus justifying the need for the introduction of more objective, quantitative indices which can be noninvasively quantified from body surface cardiac signals. Moreover, while clinical parameters from patient's history can give an overview of AF disease severity before CA, they cannot offer any additional information during the procedure itself, e.g., between two consecutive sets of lesions, or before/after pulmonary vein isolation (unpublished data). By contrast, BSPMs can be acquired at any moment of the intervention, thus enabling a more flexible and dynamic re-evaluation of body surface AF organization and a providing a more precise indication of CA intermediate effect on arrhythmia complexity.

Characterization of protracted CA procedures was improved by the introduction of multilead f-wave amplitude, thus corroborating its ability to reflect the degree of heterogeneity of the AF wavefront propagation through the underlying atrial substrate (De Groot et al., 2010). Similarly, single-lead surface CL in V_1 also contributed to increase classification accuracy, thus confirming that the degree of complexity of endocardial atrial activation during AF can be reflected on body surface potentials (Matsuo et al., 2009) and may require longer CA interventions to organize the arrhythmia. NDI assessed in the extended 15-lead ECG, but not in the entire BSPM lead set, equally helped improving the classification performance of clinical parameters, suggesting that in this framework the correlation between body surface AF organization and the duration of the CA procedure may come from specific anatomical locations only.

CA interventions requiring a higher number of lesions were also more accurately described in a multidimensional classification framework when NDI was integrated with patient's clinical characteristics, as confirmed by the ROC analysis. This result may be explained by the presence of a higher number of AF driving sources, located in multiple atrial locations (Lim et al., 2017), thus requiring the operator to target a higher number of atrial regions to terminate AF. Similar evidence was reported for the AF CL in V_1 , hinting at a relation between AF firing rate and the extent of its spatial distribution over atrial tissue.

CA outcome prediction was improved by combining clinical data with NDI, thus linking body surface AF organization as estimated by our marker with ablation therapy effectiveness. The

results obtained were comparable with those reported in previous studies (Lankveld et al., 2016b; Zeemering et al., 2017) and underlined the relevance of body surface complexity as a marker of ablation therapy impact. Also f-wave amplitude contributed to increase multidimensional classification accuracy, as proved elsewhere (Lankveld et al., 2016b; Zeemering et al., 2017).

Surprisingly, even though we observed some improvements in classification performance as quantified by ROC analysis and we obtained results similar to those shown in other studies, the changes observed when combining clinical and signal features overall were not statistically significant according to the NRI analysis. No benefit was provided by the integration of information related to body surface AF organization, regardless of the descriptor chosen. This issue may originate from multiple factors. First, it may be due to the choice of the classification model, which may be not appropriate for our dataset, therefore other classifiers should be investigated in future works. Secondly, the accuracy of some multidimensional predictors may have been limited by the reduced number of training observations in relation to the classifier's dimension, in particular when dealing with the analysis of CA duration or with missing feature values, which could have led to biased estimates. Furthermore, the absence of improvements in classification accuracy (at least with regard to the NRI analysis) may be explained by an inappropriate selection of AF organization markers. In Zeemering et al. (2017), indices of f-wave amplitude and DF estimated in specific ECG leads were automatically selected via elastic net regularization and combined with patient's weight and right atrial volume. These results suggest that: (1) more than one signal feature may be required to better characterize the descriptive power of AF complexity; (2) contributions from specific BSPM leads (or subsets of leads) may be more relevant to the classification model than those provided by other electrodes. On the other hand, these models may have included parameters whose physiological interpretation may be less clear. For instance, in Lankveld et al. (2016b), simultaneous analysis of AF duration and single-lead f-wave amplitude (in V_6) was predictive of CA outcome. However, lead V_1 usually exhibits the maximum ratio of atrial to ventricular amplitude (Petrutiu et al., 2006), therefore those findings are more difficult to justify and apply to a real clinical scenario. Finally, the NRI metric itself may not be suitable for the comparison between two classification models, especially if they do not fit the training datasets accurately (Pepe et al., 2015). Furthermore, since the assessment of NRI significance proposed by Pencina et al. (2008) has never been systematically validated (Kerr et al., 2014), further metrics should be investigated to validate NRI results.

Limitations and Perspectives

The diversity of the criteria used for AF complexity definition and clinical CA protocols and endpoints made the comparison between parameters from current literature more challenging. While a more systematic overview of classical descriptors of AF spatiotemporal organization has been attempted (Bonizzi et al., 2014; Lankveld et al., 2014), the integration of such contributions to clinical practice is still an open issue, and the predictive accuracy of most of the univariate indices examined needs to be improved.

To this end, we tested whether our understanding of AF characteristics and therapy management could benefit from combining patient's clinical characteristics and signal complexity features. However, as pointed out in section Assessment of AF Ablation Impact in a Multivariate Framework, the evaluation of multidimensional classifiers may be limited by several factors, including the limited number of observations, the choice of the classification model and the complexity indices, and the metrics used for model comparison. Even though our study offers some relevant insights into AF multidimensional analysis, several aspects should be investigated with more attention in future works, in particular the type of signal features and the BSPM leads to be selected, potentially through automatic algorithms, as well as the introduction of information coming from other imaging systems, such as fibrosis distribution assessed by magnetic resonance (Jadidi et al., 2013).

The correlation between the examined indices of AF pathophysiology and impact of the CA strategy and AF duration could not be significantly quantified by a pairwise Pearson's linear analysis neither in our study nor by other groups (Ammar et al., 2014). This limitation also justifies the choice to discriminate between persistent and long-lasting AF patients according to the definition provided in Calkins et al. (2012) and regard AF duration as a dichotomous variable rather than continuous, since none of the descriptors of AF organization linearly correlated with this clinical parameter.

Secondly, frequency measures of AF organization were not explored in our comparative analysis, due to the impossibility to retrieve the original BSPMs from the acquisition system, as TQ interval segmentation is performed at the moment of the ablation procedure. To this end, we examined the AF CL in lead V_1 , which was demonstrated to correlate with the intracardiac atrial fibrillatory rate in Matsuo et al. (2009). While in that study this measure was manually assessed in standard ECG, in our work we introduced an algorithm for the automatic computation of the rate of atrial signal local extrema, which may be sensitive to the presence of artifacts and spurious peaks if proper settings as those described in section Comparison With Other Descriptors of AF Complexity on Surface Recordings are not applied.

Some BSPM electrodes may present artifacts due to patient's breathing or mechanical motion. As a consequence, all signals have been visually inspected and electrodes with too high levels of noise were discarded.

The assumption that more complex AF forms require the operator to target a higher number of atrial sites is supported by previous clinical studies claiming that in advanced AF forms the density of driving sources over atrial tissue tends to be higher, thus covering more sites (Lim et al., 2017). However, this should be confirmed by phase mapping analysis as well.

The ability of the AF complexity parameters to predict long-term CA outcome has not been investigated due to the unavailability of such information for some patients at the moment of the study, and it therefore represents an open perspective of this research.

Furthermore, it may be clinically relevant to assess changes in complexity in BSPMs within the CA procedure and between intermediate steps (for instance, after pulmonary vein isolation),

so as to understand whether modifications of atrial substrate by CA immediately reflect on surface electrical activity.

Future research also includes the investigation of the relation between body surface complexity and AF termination sites. This task may present some challenges, in particular in relation to the identification of the most suitable electrodes to be associated with the atrial regions of interest.

Finally, the application of our noninvasive methodology to other types of AF therapy (e.g., electrical cardioversion) may help improve their management.

CONCLUSIONS

This research put forward a tool for the quantification of AF organization by PCA of multilead BSPMs. Our analysis underlined a significant correlation of such noninvasive information with AF chronification and CA practice. This methodology can provide relevant insights into AF substrate characterization from the body surface ablation therapy.

AUTHOR CONTRIBUTIONS

All authors have made substantial contributions to this study. MM designed the study, implemented the signal processing

algorithms, analyzed, and interpreted the results, and drafted the manuscript. TP, ND, and JD performed CA procedures and contributed to the interpretation of the clinical data. CD-P and SP acquired and segmented atrial activity signals from BSPM recordings. PJ, MéH, and MiH supervised clinical data acquisition and helped assessing signal processing algorithm performance. RD helped conceive the study, provided feedback about the implementation of the methods and the interpretation of the results, and revised the manuscript.

FUNDING

This study received financial support from the French Government as part of the Investments of the Future program managed by the National Research Agency (ANR), Grant reference ANR-10-IAHU-04.

ACKNOWLEDGMENTS

The research presented in this manuscript extends a study submitted to Heart Rhythm Society Congress 2018. Some methodological aspects have been also applied to ventricular fibrillation analysis and presented at Computing in Cardiology 2017 conference (Meo et al., 2017).

REFERENCES

- Ahmad, Y., and Kirchhof, P. (2013). Gone fishing (for silent atrial fibrillation). *Circulation* 127, 870–872. doi: 10.1161/CIRCULATIONAHA.112.000985
- Alcaraz, R., Hornero, F., and Rieta, J. J. (2011). Noninvasive time and frequency predictors of long-standing atrial fibrillation early recurrence after electrical cardioversion. *PACE - Pacing Clin. Electrophysiol.* 34, 1241–1250. doi: 10.1111/j.1540-8159.2011.03125.x
- Allessie, M. A., Bonke, F. I., and Schopman, F. J. (1977). Circus movement in rabbit atrial muscle as a mechanism of tachycardia. III. the “leading circle” concept: a new model of circus movement in cardiac tissue without the involvement of an anatomical obstacle. *Circul. Res.* 41, 9–18.
- Ammar, S., Hessling, G., Paulik, M., Reents, T., Dillier, R., Buiatti, A., et al. (2014). Impact of baseline atrial fibrillation cycle length on acute and long-term outcome of persistent atrial fibrillation ablation. *J. Intervent. Cardiac Electrophysiol.* 41, 253–259. doi: 10.1007/s10840-014-9927-6
- Bollmann, A., Husser, D., Stridh, M., Soernmo, L., Majic, M., Klein, H. U., et al. (2003). Frequency measures obtained from the surface electrocardiogram in atrial fibrillation research and clinical decision-making. *J. Cardiovasc. Electrophysiol.* 14(Suppl. 10), S154–S161. doi: 10.1046/j.1540.8167.90305.x
- Bonizzi, P., Guillem Mde, L., Climent, A. M., Millet, J., Zarzoso, V., Castells, F., et al. (2010). Noninvasive assessment of the complexity and stationarity of the atrial waveform patterns during atrial fibrillation. *IEEE Trans. Biomed. Eng.* 57, 2147–2157. doi: 10.1109/TBME.2010.2052619
- Bonizzi, P., Zeemering, S., Karel, J. M., Di Marco, L. Y., Uldry, L., Van Zaen, J., et al. (2014). Systematic comparison of non-invasive measures for the assessment of atrial fibrillation complexity: a step forward towards standardization of atrial fibrillation electrogram analysis. *Europace* 17, 318–325. doi: 10.1093/europace/euu202
- Calkins, H., Kuck, K. H., Cappato, R., Brugada, J., Camm, A. J., Chen, S. A., et al. (2012). 2012 HRS/EHRA/ECAS expert consensus statement on catheter and surgical ablation of atrial fibrillation: recommendations for patient selection, procedural techniques, patient management and follow-up, definitions, endpoints, and research trial design. *J. Int. Cardiac Electrophysiol.* 33, 171–257. doi: 10.1007/s10840-012-9672-7
- Cheng, Z., Deng, H., Cheng, K., Chen, T., Gao, P., Yu, M., et al. (2013). The amplitude of fibrillatory waves on leads aVF and V1 predicting the recurrence of persistent atrial fibrillation patients who underwent catheter ablation. *Ann. Noninvasive Electrocardiol.* 18, 352–358. doi: 10.1111/anec.12041
- Ciccone, G., Giacopelli, D., and Pappone, C. (2017). The role of implantable cardiac monitors in atrial fibrillation management. *J. Atr. Fibrillation.* 10:1590. doi: 10.4022/jafib.1590
- de Groot, N. M., Houben, R. P., Smeets, J. L., Boersma, E., Schottem, U., Schalij, M. J., et al. (2010). Electropathological substrate of longstanding persistent atrial fibrillation in patients with structural heart disease: epicardial breakthrough. *Circulation* 122, 1674–1682. doi: 10.1161/CIRCULATIONAHA.109.910901
- Di Marco, L. Y., Bourke, J. P., and Langley, P. (2012). Spatial complexity and spectral distribution variability of atrial activity in surface ECG recordings of atrial fibrillation. *Med. Biol. Eng. Comput.* 50, 439–446. doi: 10.1007/s11517-012-0878-8
- Haissaguerre, M., Hocini, M., Denis, A., Shah, A. J., Komatsu, Y., Yamashita, S., et al. (2014). Driver domains in persistent atrial fibrillation. *Circulation* 130, 530–538. doi: 10.1161/CIRCULATIONAHA.113.005421
- Haissaguerre, M., Hocini, M., Shah, A. J., Derval, N., Sacher, F., Jais, P., et al. (2013). Noninvasive panoramic mapping of human atrial fibrillation mechanisms: a feasibility report. *J. Cardiovasc. Electrophysiol.* 24, 711–717. doi: 10.1111/jce.12075
- Hoit, B. D. (2014). Left atrial size and function: role in prognosis. *J. Am. Coll. Cardiol.* 63, 493–505. doi: 10.1016/j.jacc.2013.10.055
- Holm, M., Pehrson, S., Ingemansson, M., Sörnmo, L., Johansson, R., Sandhall, L., et al. (1998). Non-invasive assessment of the atrial cycle length during atrial fibrillation in man: introducing, validating and illustrating a new ECG method. *Cardiovasc. Res.* 38, 69–81. doi: 10.1016/S0008-6363(97)00289-7
- Holt, J. H., Barnard, A. C., Lynn, M. S., and Svendsen, P. (1969). A study of the human heart as a multiple dipole electrical source in normal adult male subjects. *Circulation* 40, 687–696. doi: 10.1161/01.CIR.40.5.687
- Ihara, Z., van Oosterom, A., Jacquemet, V., and Hoekema, R. (2007). Adaptation of the standard 12-lead electrocardiogram system dedicated to the analysis of atrial fibrillation. *J. Electrocardiol.* 40:68.e1–8. doi: 10.1016/j.jelectrocard.2006.04.006

- Jadidi, A. S., Cochet, H., Shah, A. J., Kim, S. J., Duncan, E., Miyazaki, S., et al. (2013). Inverse relationship between fractionated electrograms and atrial fibrosis in persistent atrial fibrillation: combined magnetic resonance imaging and high-density mapping. *J. Am. Coll. Cardiol.* 62, 802–812. doi: 10.1016/j.jacc.2013.03.081
- Jalife, J. (2003). Rotors and spiral waves in atrial fibrillation. *J. Cardiovasc. Electrophysiol.* 14, 776–780. doi: 10.1046/j.1540-8167.2003.03136.x
- Kerr, K. F., Wang, Z., Janes, H., McClelland, R. L., Psaty, B. M., and Pepe, M. S. (2014). Net reclassification indices for evaluating risk prediction instruments. *Epidemiology* 25, 114–21. doi: 10.1097/EDE.0000000000000018
- Kim, K. B., Rodefeld, M. D., Schuessler, R. B., Cox, J. L., and Boineau, J. P. (1996). Relationship between local atrial fibrillation interval and refractory period in the isolated canine atrium. *Circulation* 94, 2961–2967. doi: 10.1161/01.CIR.94.11.2961
- Kirchhof, P., Benussi, S., Kotecha, D., Ahlsson, A., Atar, D., Casadei, B., et al. (2016). 2016 ESC Guidelines for the management of atrial fibrillation developed in collaboration with EACTS. *Europace* 18, 1609–1678. doi: 10.1093/europace/euw295
- Konings, K. T., Kirchhof, C. J., Smeets, J. R., Wellens, H. J., Penn, O. C., and Allessie, M. A. (1994). High-density mapping of electrically induced atrial fibrillation in humans. *Circulation* 89, 1665–1680. doi: 10.1161/01.CIR.89.4.1665
- Kottkamp, H. (2013). Human atrial fibrillation substrate: towards a specific fibrotic atrial cardiomyopathy. *Eur. Heart J.* 34, 2731–2738. doi: 10.1093/eurheartj/eht194
- Lankveld, T. A., Zeemering, S., Crijns, H. J., and Schotten, U. (2014). The ECG as a tool to determine atrial fibrillation complexity. *Heart* 100, 1077–1084. doi: 10.1136/heartjnl-2013-305149
- Lankveld, T., de Vos, C. B., Limantoro, I., Zeemering, S., Dudink, E., Crijns, H. J., et al. (2016a). Systematic analysis of ECG predictors of sinus rhythm maintenance after electrical cardioversion for persistent atrial fibrillation. *Heart Rhythm* 13, 1020–1027. doi: 10.1016/j.hrthm.2016.01.004
- Lankveld, T., Zeemering, S., Scherr, D., Kuklik, P., Hoffmann, B. A., Willems, S., et al. (2016b). Atrial fibrillation complexity parameters derived from surface ECGs predict procedural outcome and long-term follow-up of stepwise catheter ablation for atrial fibrillation. *Circ. Arrhythm. Electrophysiol.* 9:e003354. doi: 10.1161/CIRCEP.115.003354
- Lau, D. H., Linz, D., Schotten, U., Mahajan, R., Sanders, P., and Kalman, J. M. (2017). Pathophysiology of paroxysmal and persistent atrial fibrillation: rotors, foci and fibrosis. *Heart Lung and Circulation*. Australian and New Zealand Society of Cardiac and Thoracic Surgeons (ANZSCTS) and the Cardiac Society of Australia and New Zealand (CSANZ). 26, 887–893. doi: 10.1016/j.hlc.2017.05.119
- Lim, H. S., Hocini, M., Dubois, R., Denis, A., Derval, N., Zellerhoff, S., et al. (2017). Complexity and distribution of drivers in relation to duration of persistent atrial fibrillation. *J. Am. Coll. Cardiol.* 69, 1257–1269. doi: 10.1016/j.jacc.2017.01.014
- Lux, R. L., Evans, A. K., Burgess, M. J., Wyatt, R. F., Abildskov, J. A. (1981). Redundancy reduction for improved display and analysis of body surface potential maps. *Circ. Res.* 49:186–196. doi: 10.1161/01.RES.49.1.186
- Matsu, S., Lellouche, N., Wright, M., Bevilacqua, M., Knecht, S., Nault, I., et al. (2009). Clinical predictors of termination and clinical outcome of catheter ablation for persistent atrial fibrillation. *J. Am. Coll. Cardiol.* 54, 788–795. doi: 10.1016/j.jacc.2009.01.081
- Meo, M., Potse, M., Puyo, S., Bear, L., Hocini, M., Haissaguerre, M., et al. (2017). Non-invasive assessment of spatiotemporal organization of ventricular fibrillation through principal component analysis. *Comput. Cardiol.* 44, 1–4. doi: 10.22489/CinC.2017.101-051
- Meo, M., Zarzoso, V., Meste, O., Latcu, D. G., and Saoudi, N. (2013a). Spatial variability of the 12-lead surface ECG as a tool for noninvasive prediction of catheter ablation outcome in persistent atrial fibrillation. *IEEE Trans. Biomed. Eng.* 60, 20–27. doi: 10.1109/TBME.2012.2220639
- Meo, M., Zarzoso, V., Meste, O., Latcu, D. G., and Saoudi, N. (2013b). Catheter ablation outcome prediction in persistent atrial fibrillation using weighted principal component analysis. *Biomed. Signal Process. Control* 8, 958–968. doi: 10.1016/j.bspc.2013.02.002
- Moe, G. K. (1962). On the multiple wavelet hypothesis of atrial fibrillation. *Arch. Int. Pharmacodyn. Ther.* 140, 83–188.
- Nault, I., Lellouche, N., Matsuo, S., Knecht, S., Wright, M., Lim, K. T., et al. (2009). Clinical value of fibrillatory wave amplitude on surface ECG in patients with persistent atrial fibrillation. *J. Intervent. Cardiac Electrophysiol.* 26, 11–19. doi: 10.1007/s10840-009-9398-3
- Pandit, S. V., and Jalife, J. (2013). Rotors and the dynamics of cardiac fibrillation. *Circ. Res.* 112, 849–862. doi: 10.1161/CIRCRESAHA.111.300158
- Pencina, M. J., D'Agostino, R. B., D'Agostino, R. B., and Vasan, R. S. (2008). Evaluating the added predictive ability of a new marker: from area under the ROC curve to reclassification and beyond. *Stat. Med.* 27, 157–172. doi: 10.1002/sim.2929
- Petrutiu, S., Ng, J., Nijm, G. M., Al-Angari, H., Swiryn, S., and Sahakian, A. V. (2006). Atrial fibrillation and waveform characterization: a time domain perspective in the surface ECG. *IEEE Eng. Med. Biol. Mag.* 24–30. doi: 10.1109/EMB.M.2006.250505
- Pepe, M. S., Fan, J., Feng, Z., Gerds, T., and Hilden, J. (2015). The net reclassification index (NRI): a misleading measure of prediction improvement even with independent test data sets. *Stat. Biosci.* 7, 282–295. doi: 10.1007/s12561-014-9118-0
- Petrutiu, S., Sahakian, A. V., Fisher, W., and Swiryn, S. (2009). Manifestation of left atrial events and interatrial frequency gradients in the surface electrocardiogram during atrial fibrillation: contributions from posterior leads. *J. Cardiovasc. Electrophysiol.* 20, 1231–1236. doi: 10.1111/j.1540-8167.2009.01523.x
- Robinson, M. R., and Curzen, N. (2009). Electrocardiographic body surface mapping: potential tool for the detection of transient myocardial ischemia in the 21st century? *Delta* 14, 201–210. doi: 10.1111/j.1542-474X.2009.00284.x
- Rostock, T., Salukhe, T. V., Steven, D., Drewitz, I., Hoffmann, B. A., Bock, K., et al. (2011). Long-term single- and multiple-procedure outcome and predictors of success after catheter ablation for persistent atrial fibrillation. *Heart Rhythm* 8, 1391–1397. doi: 10.1016/j.hrthm.2011.04.012
- Sánchez-Quintana, D., López-Mínguez J. R., Pizarro, G., Murillo, M., and Cabrera, J. A. (2012). Triggers and anatomical substrates in the genesis and perpetuation of atrial fibrillation. *Curr. Cardiol. Rev.* 8, 310–326. doi: 10.2174/157340312803760721
- Scherr, D., Dalal, D., Cheema, A., Nazarian, S., Almasry, I., Bilchick, K., et al. (2009). Long- and short-term temporal stability of complex fractionated atrial electrograms in human left atrium during atrial fibrillation. *J. Cardiovasc. Electrophysiol.* 20, 13–21. doi: 10.1111/j.1540-8167.2008.01278.x
- Scherr, D., Khairy, P., Miyazaki, S., Aurillac-Lavignolle, V., Pascale, P., Wilton, S. B., et al. (2015). Five-year outcome of catheter ablation of persistent atrial fibrillation using termination of atrial fibrillation as a procedural endpoint. *Circ. Arrhythm. Electrophysiol.* 8, 18–24. doi: 10.1161/CIRCEP.114.001943
- Schricker, A. A., Lalani, G. G., Krummen, D. E., Rappel, W. J., and Narayan, S. M. (2014). Human atrial fibrillation initiates via organized rather than disorganized mechanisms. *Circ. Arrhythm. Electrophysiol.* 7, 816–824. doi: 10.1161/CIRCEP.113.001289
- SippensGroenewegen, A., Natale, A., Marrouche, N. F., Bash, D., and Cheng, J. (2004). Potential role of body surface ECG mapping for localization of atrial fibrillation trigger sites. *J. Electrocardiol.* 37, 47–52. doi: 10.1016/j.jelectrocard.2004.08.017
- Sörnmo, L., and Laguna, P. (2005). *Chapter 7 - ECG Signal Processing in Bioelectrical Signal Processing in Cardiac and Neurological Applications*. Burlington, MA: Elsevier Academic Press, 453–566.
- Uldry, L., Van Zaen, J., Prudat, Y., Kappenberg, L., and Vesin, J. M. (2012). Measures of spatiotemporal organization differentiate persistent from long-standing atrial fibrillation. *Europace* 14, 1125–1131. doi: 10.1093/europace/eur436
- van Oosterom, A., Ihara, Z., Jacquemet, V., and Hoekema, R. (2007). Vectorcardiographic lead systems for the characterization of atrial fibrillation. *J. Electrocardiol.* 40, 1–11. doi: 10.1016/j.jelectrocard.2006.08.002
- Verma, A., Jiang, C. Y., Betts, T. R., Chen, J., Deisenhofer, I., Mantovan, R., et al. (2015). Approaches to catheter ablation for persistent atrial fibrillation. *New Engl. J. Med.* 372, 1812–1822. doi: 10.1056/NEJMoa1408288
- Wijffels, M. C., Kirchhof, C. J., Dorland, R., and Allessie, M. A. (1995). Atrial fibrillation begets atrial fibrillation: a study in awake chronically instrumented goats. *Circulation* 92, 1954–1968. doi: 10.1161/01.CIR.92.7.1954

- Yamamoto, S., Suwa, M., Ito, T., Murakami, S., Umeda, T., Tokaji, Y., et al. (2005). Comparison of frequency of thromboembolic events and echocardiographic findings in patients with chronic nonvalvular atrial fibrillation and coarse versus fine electrocardiographic fibrillatory waves. *Am. J. Cardiol.* 96, 408–411. doi: 10.1016/j.amjcard.2005.03.087
- Yamashita, S., Shah, A. J., Mahida, S., Sellal, J. M., Berte, B., Hooks, D., et al. (2015). Body surface mapping to guide atrial fibrillation ablation. *Arrhythm. Electrophysiol. Rev.* 4, 172–176. doi: 10.15420/aer.2015.4.3.172
- Zeemering, S., Lankveld, T. A. R., Bonizzi, P., Limantoro, I., Bekkers, S. C. A. M., Crijns, H. J. G. M., et al. (2017). The electrocardiogram as a predictor of successful pharmacological cardioversion and progression of atrial fibrillation. *EP Europace* 20, e96–e104. doi: 10.1093/europace/eux234.
- Zhuang, J., Wang, Y., Tang, K., Li, X., Peng, W., Liang, C., et al. (2012). Association between left atrial size and atrial fibrillation recurrence

after single circumferential pulmonary vein isolation: a systematic review and meta-analysis of observational studies. *Europace* 14, 638–645. doi: 10.1093/europace/eur364

Conflict of Interest Statement: The authors declare that the research was conducted in the absence of any commercial or financial relationships that could be construed as a potential conflict of interest.

Copyright © 2018 Meo, Pambrun, Derval, Dumas-Pomier, Puyo, Duchâteau, Jaïs, Hocini, Haissaguerre and Dubois. This is an open-access article distributed under the terms of the Creative Commons Attribution License (CC BY). The use, distribution or reproduction in other forums is permitted, provided the original author(s) and the copyright owner(s) are credited and that the original publication in this journal is cited, in accordance with accepted academic practice. No use, distribution or reproduction is permitted which does not comply with these terms.



Information Theory and Atrial Fibrillation (AF): A Review

Dhani Dharmapranji¹, Lukah Dykes², Andrew D. McGavigan^{1,2}, Paweł Kuklik³, Kenneth Pope⁴ and Anand N. Ganesan^{1,2*}

¹ College of Medicine and Public Health, Flinders University of South Australia, Adelaide, SA, Australia, ² Department of Cardiovascular Medicine, Flinders Medical Centre, Adelaide, SA, Australia, ³ Department of Cardiology, University Medical Centre, Hamburg, Germany, ⁴ College of Science and Engineering, Flinders University of South Australia, Adelaide, SA, Australia

OPEN ACCESS

Edited by:

Ahsan H. Khandoker,
Khalifa University,
United Arab Emirates

Reviewed by:

Luca Faes,
Università degli Studi di Palermo, Italy
Richard Gray,
State Food and Drug Administration,
China

*Correspondence:

Anand N. Ganesan
anand.ganesan@flinders.edu.au

Specialty section:

This article was submitted to
Computational Physiology and
Medicine,
a section of the journal
Frontiers in Physiology

Received: 31 March 2018

Accepted: 29 June 2018

Published: 18 July 2018

Citation:

Dharmapranji D, Dykes L, McGavigan AD, Kuklik P, Pope K and Ganesan AN (2018) Information Theory and Atrial Fibrillation (AF): A Review. *Front. Physiol.* 9:957. doi: 10.3389/fphys.2018.00957

Atrial Fibrillation (AF) is the most common cardiac rhythm disorder seen in hospitals and in general practice, accounting for up to a third of arrhythmia related hospitalizations. Unfortunately, AF treatment is in practice complicated by the lack of understanding of the fundamental mechanisms underlying the arrhythmia, which makes detection of effective ablation targets particularly difficult. Various approaches to AF mapping have been explored in the hopes of better pinpointing these effective targets, such as Dominant Frequency (DF) analysis, complex fractionated electrograms (CFAE) and unipolar reconstruction (FIRM), but many of these methods have produced conflicting results or require further investigation. Exploration of AF using information theoretic-based approaches may have the potential to provide new insights into the complex system dynamics of AF, whilst also providing the benefit of being less reliant on empirically derived definitions in comparison to alternate mapping approaches. This work provides an overview of information theory and reviews its applications in AF analysis, with particular focus on AF mapping. The works discussed in this review demonstrate how understanding AF from a signal property perspective can provide new insights into the arrhythmic phenomena, which may have valuable clinical implications for AF mapping and ablation in the future.

Keywords: information theory, atrial fibrillation, entropy, AF mapping, catheter ablation

INTRODUCTION

Catheter ablation is a potentially curative treatment for atrial fibrillation (AF) that has been gaining interest within the last few decades. It uses percutaneously induced catheters to apply focal burns to specific areas of heart muscle in order to cease or modify the AF (Baumert et al., 2016). This method was first popularized following the breakthrough investigation published by Haissaguerre et al. (1998), which reported successful termination of up to 90% of paroxysmal AF (PAF) cases using catheter ablation on ectopic triggers located at the pulmonary veins. Although pulmonary vein isolation (PVI) is recognized as a landmark development for the treatment of paroxysmal AF, the extending application of ablative therapies for the highly varied persistent AF populace has seen relatively lower rates of success

(Verma et al., 2015). Consequently, the optimal approach to ablation in this population is currently the subject of ongoing debate, as effective ablation targets remain unknown (Verma et al., 2015).

To help determine potentially effective targets, AF mapping is employed. The aim of AF mapping is to locate triggers and substrates that lead to AF termination, which in turn can be used as targets in clinical ablation procedures (Baumert et al., 2016). Unfortunately, the highly complex wave dynamics of AF have thus far been responsible for the difficulties in understanding what these effective targets may be, as the mechanisms underlying AF are arguably one of the most challenging problems in cardiology. As a result, a number of mapping approaches have been explored, including complex fractionated electrograms (CFAE) (Nademanee et al., 2004; Nademanee and Oketani, 2009; Hayward et al., 2011; Li et al., 2011), dominant frequency (DF) by Fast Fourier transform (Skanes et al., 1998; Sanders et al., 2006) and unipolar electrogram reconstruction (FIRM) (Narayan et al., 2012). Unfortunately, these approaches have either lead to conflicting outcomes (Nademanee et al., 2004; Narayan et al., 2012) or are still undergoing investigation (Dawes et al., 1992). In light of this, it is clear that exploration of new mapping methods are both warranted and necessary to understanding the mechanisms of AF and potentially improving the efficacy of catheter ablation.

Information theoretic-based approaches may be an appealing new avenue in AF mapping, as they have (i) a strong theoretical foundation in mathematics and (ii) use quantitative definitions rooted in intrinsic signal properties, instead of arbitrary, empirically derived definitions. In addition, although information theoretic approaches are seldom used in the field of cardiology, such techniques are already prevalent and widely accepted in other disciplines such as engineering, neurobiology, computer science, physics, quantum computing, linguistics, and cryptography (Verdu, 1998).

The objective of this review is to provide an overview of information theory in atrial fibrillation (AF). We begin by introducing the concept of information theory, and follow by discussing the use of information theoretic-based measures of entropy in three common areas of AF research: (i) AF detection, (ii) AF prediction and characterization, and (iii) AF mapping. Within the context of AF detection, studies successfully implementing entropy measures to distinguish between normal sinus patterns and AF are presented. Specifically, such studies develop AF detection algorithms based on detecting variations in the RR interval, or changes in the ECG morphology. Following this, the application of entropy for AF prediction and characterization is also described, outlining the use of entropy-based measures to understand the dynamical properties associated with the onset and termination of AF, as well as paroxysmal and persistent AF. Finally, we detail the current studies that employ information theoretic measures for AF mapping with respect to rotor identification, quantifying AF synchronization, and studying information flow within the atria. To conclude, we discuss the potential gaps in AF research that information theory may be able to address both now, and in the future.

INFORMATION THEORY

What Is Information Theory?

Information theory is a branch of mathematics that incorporates probability theory and statistics (Ephremides, 2009). Modern information theory was established after the publication of Claude E. Shannon's seminal original paper (Shannon, 1948), which earned him the title of pioneer and founding father of information theory. Shannon's work introduced, for the first time, a number of key ideas that shaped the field of information theory, including the concept of digitizing information into binary digits known as "bits," the formal architecture of communication systems, and source coding, which deals with the efficiency of data representation (Shannon, 1948). In short, the scope of information theory focuses on the transmission, processing, storage, and receiving of messages (Aftab et al., 2001; Lombardi et al., 2016). Although information theory was initially developed for use in communication systems, principally concerning itself with the transmission of telecommunication signals, it is now commonly used in a number of fields such as computer science, engineering, neuroscience and linguistics (Verdu, 1998; Xiong et al., 2017).

What Is Information and How Can It Be Measured?

As Shannon argued, the semantic aspects of communication can be thought of as irrelevant to the engineering problem (Shannon, 1948). Consequently, the term "information" in reference to information theory does not refer to the meaning of a message as one might assume intuitively, but instead how much can be learnt from that message (Lombardi et al., 2016). To conceptualize this further, take for example the scenario in which someone is asked to guess a number from 1 to 10, whilst obtaining help from a friend through clues. With respect to information theory, the clue itself does not matter, but the amount of information that can be inferred from the clue does. As such, if they are told that the number is >11 , then this clue is deemed uninformative. On the other hand, if they are told that the number is even, then this fact is considered much more informative, though revealing that the number is odd would also be equally as informative, as these both reduce the possible selections to 5. In this respect, information can be thought of as **how much** is learnt, rather than **what** is learnt (Shannon, 1948).

Relating to this concept is the information theoretic measure known as "entropy." As information can alternatively be thought of as the amount of uncertainty that is eliminated or resolved, measuring this uncertainty will intuitively quantify information. Conceptually speaking, entropy utilizes this principle to measure information content, with greater uncertainty in turn generating higher entropy (Shannon, 1948; Cover and Thomas, 1991; Gray, 2011). As entropy increases with uncertainty, it will be maximal for completely random systems (Shannon, 1948; Costa et al., 2002b). Such metrics have potentially useful clinical implications, particularly with respect to diagnostic tools using biological signals and understanding the underlying dynamic properties of physiological systems (Costa et al., 2005).

Although there are several ways that information can be measured outside of entropy, it is one of the most prevalently used classical measures of information theory, particularly in the context of AF. With this in mind, entropy-based approaches to quantifying information will be the focus of this review, and an overview of the various entropy algorithms commonly used to analyze AF will be described in the following.

SHANNON ENTROPY

Named after Claude E. Shannon himself, Shannon entropy is the classical measure of information theory and measures the *Shannon information content* of a random variable (Shannon, 1948; Xiong et al., 2017). It was first introduced by Shannon to describe the relationships between information, noise and power in a digital communication stream (Aftab et al., 2001), quantifying the amount of storage required to store a signal (in bits) (Vajapeyam, 2014). Now, it is also commonly used as a measure of information content across many fields (Aftab et al., 2001). Shannon entropy (ShEn) can be defined as:

$$ShEn = - \sum_{i=1}^M p(i) \log_2 p(i) \quad (1)$$

where M is the number of discrete values the variable can take, and $p(i)$ the probability density function of the variable x assuming the i^{th} value. Note that Shannon entropy is given in the unit bits (Shannon, 1948).

An intuitive example of how information is quantified using ShEn is the simple coin toss. A fair coin with a head and tail will result in maximum entropy, as the outcome cannot be predicted. As a result, the probability of choosing the correct outcome is $\frac{1}{2}$, as there are two possible outcomes that may occur with equal probability. Each coin toss will deliver one bit of information, as (Shannon, 1948):

$$ShEn = - \sum_{i=1}^2 \left(\frac{1}{2}\right) \log_2 \left(\frac{1}{2}\right) = 1 \text{ bit} \quad (2)$$

Conversely, a double-headed coin will result in an entropy of zero, as the probability of the outcome is $1/1$. Hence there is no uncertainty, and no information is gained from the outcome of the coin toss (Shannon, 1948):

$$ShEn = - \sum_{i=1}^1 (1) \log_2 (1) = 0 \text{ bits} \quad (3)$$

In AF analysis, ShEn is often used to measure the information content of an ECG or EGM. Typically, this is achieved by constructing the amplitude distribution or histogram of the signal (Shannon, 1948; Ganesan et al., 2012, 2014; Baumert et al., 2016). Specifically, a voltage histogram can be acquired by binning signal samples according to its amplitude. Following this, the relative probability density function $p(i)$ is obtained by dividing the sum of counts in each amplitude bin by the total number of counts. In effect, ECG or EGM with regular

morphologies (i.e., signals that only possess a few states) will yield a narrow amplitude distribution (Ganesan et al., 2012). Conversely, complex morphologies containing a number of dissimilar deflections, such signals in AF, will lead to more varying amplitudes and in turn a broader amplitude distribution (Figure 1) (Ganesan et al., 2012). In effect, as ShEn is taken a sum of the probabilities, broader amplitude distributions will result in higher ShEn (Ganesan et al., 2012, 2014).

The ShEn equation defined in (1) can be classified as a “static” measure, as it does not consider any temporal information when describing the observed probability distribution. In other words, it measures information content by quantifying the amount of information contained only in the present value of the time series (Xiong et al., 2017).

APPROXIMATE ENTROPY

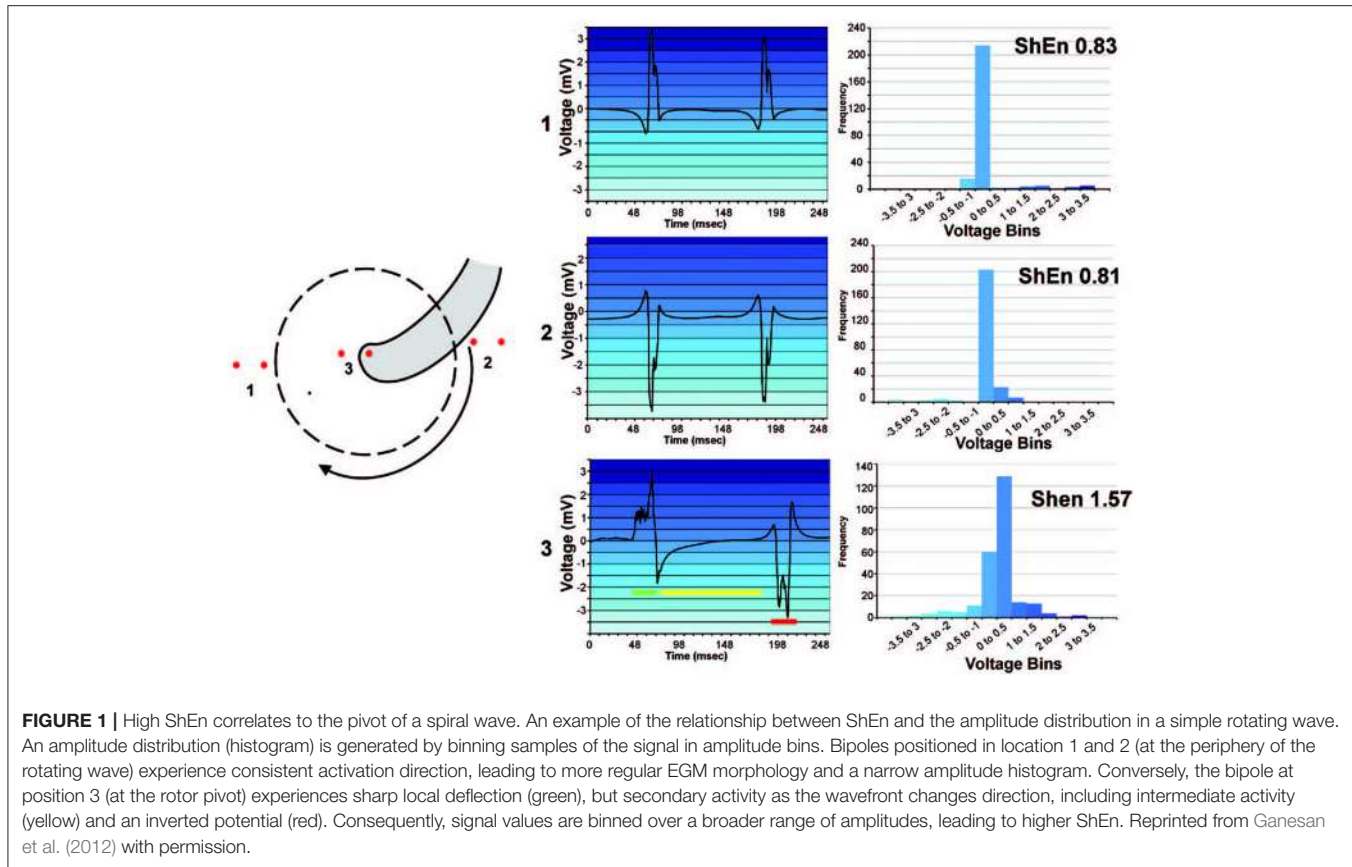
In contrast to the “static” measure of ShEn described in (1), “dynamic” measures of entropy are those that study the information content of a process representing the activity of a system that is changing over time. An example of such a dynamic measure of entropy is conditional entropy (Xiong et al., 2017).

Conditional entropy, also referred to as the Kolmogorov-Sinai entropy (Eckmann and Ruelle, 1985), is defined as the average rate of creation of new information. Generally speaking, the current state of an observed process is partly determined by its past, but also conveys some amount of new information that can't be inferred from the past. Conditional entropy measures this residual information to quantify the rate of creation of new information (Xiong et al., 2017). In mathematical notation, this can be given by:

$$C(X) = H(X_n | X_n^-) = H(X_n^-, X_n) - H(X_n^-) = -\mathbb{E} [\log p(x_n | x_1, \dots, x_{n-1})] \quad (4)$$

where $p(x_n | x_1, \dots, x_{n-1})$ is the conditional probability that X assumes the value x_n at time n , given that previous values are taken at x_1, \dots, x_{n-1} (Xiong et al., 2017). In effect, if the process is fully predictable, the system will not create new information and hence the conditional entropy is equal to zero. Contrastingly, a fully random process produces information at the maximum rate and will yield maximum conditional entropy. If the process is stationary, the system will produce information at a constant rate, and therefore the conditional entropy will not change over time (Xiong et al., 2017).

A number of entropy estimates and measures have been developed to quantify conditional entropy. One specific example, which is commonly used to study physiological signals, is Approximate Entropy (ApEn). ApEn is a regularity metric that was originally developed for physiological signals such as heart rate (Ganesan et al., 2014). As accurate entropy calculation using regularity statistics is often found unfeasible in real-life applications due to the influence of system noise and the large amounts of data required, Pincus developed ApEn to manage these limitations (Pincus et al., 1991; Ganesan et al.,



2014). It can be noted that the approximate entropy family of statistics has been widely implemented in clinical cardiovascular studies (Pincus et al., 1991, 1993; Dawes et al., 1992; Fleisher et al., 1993, 1997; Goldberger et al., 1994; Ryan et al., 1994; Mäkkilä et al., 1996, 1998; Tulppo et al., 1996; Ho et al., 1997; Lipsitz et al., 1997; Hogue et al., 1998; Nelson et al., 1998; Palazzolo et al., 1998; Schuckers, 1998; Korpelainen et al., 1999).

Specifically, ApEn quantifies the amount of regularity in a signal by measuring the logarithmic likelihood that runs of patterns similar to one another will remain similar when incrementally compared (Richman and Moorman, 2000; Baumert et al., 2016). The prevalence of repetitive patterns in a signal is identified by forming a sequence of vectors using the time series data, and measuring the difference between them (Baumert et al., 2016). If the relative difference between any pair of corresponding measurements is less than the length of the pattern, the pattern is deemed similar (Pincus, 1991). In mathematical notation, this can be expressed using the equation:

$$ApEn(S_N, m, r) = \ln \frac{Cm(r)}{Cm + 1(r)} \quad (5)$$

where m is the pattern length, r is the similarity criterion or threshold, and $Cm(r)$ the prevalence of patterns of length m in the sequence S_N (Pincus, 1991). ApEn is quantified in bits.

Conceptualizing ApEn further, take for example two time series, t_1 and t_2 :

$$t_1 = (1, 2, 1, 2, 1, 2, 1, 2, 1, 2 \dots)$$

$$t_2 = (1, 2, 1, 1, 1, 2, 1, 2, 2, 1 \dots)$$

As t_1 follows a very regular pattern alternating between 1 and 2 s, knowing that a term is valued at 1 will consequently allow the next value to be predicted, which in this case is always 2. Thus, t_1 possesses high predictability and low conditional entropy. Conversely, t_2 demonstrates a much more random pattern and hence will possess greater conditional entropy. Translating this to the cardiac space, a signal in normal sinus rhythm will exhibit periodicity and relatively uniform complexes, thus ApEn will detect the presence of similar patterns and identify this regularity (Figure 2). On the other hand, signals with complex morphologies will exhibit less regular patterns, hence yield higher ApEn (Pincus, 1991).

Computationally speaking, as opposed to the binning method used in ShEn algorithms, a kernel estimator is often used when calculating ApEn. Specifically, the kernel estimator is a model free approach of constructing a probability distribution of a variable, which centers kernel functions at each outcome of the variable and uses the estimated probabilities to compute appropriate entropy estimates (Xiong et al., 2017). The distance of each point in the time series to the reference point is

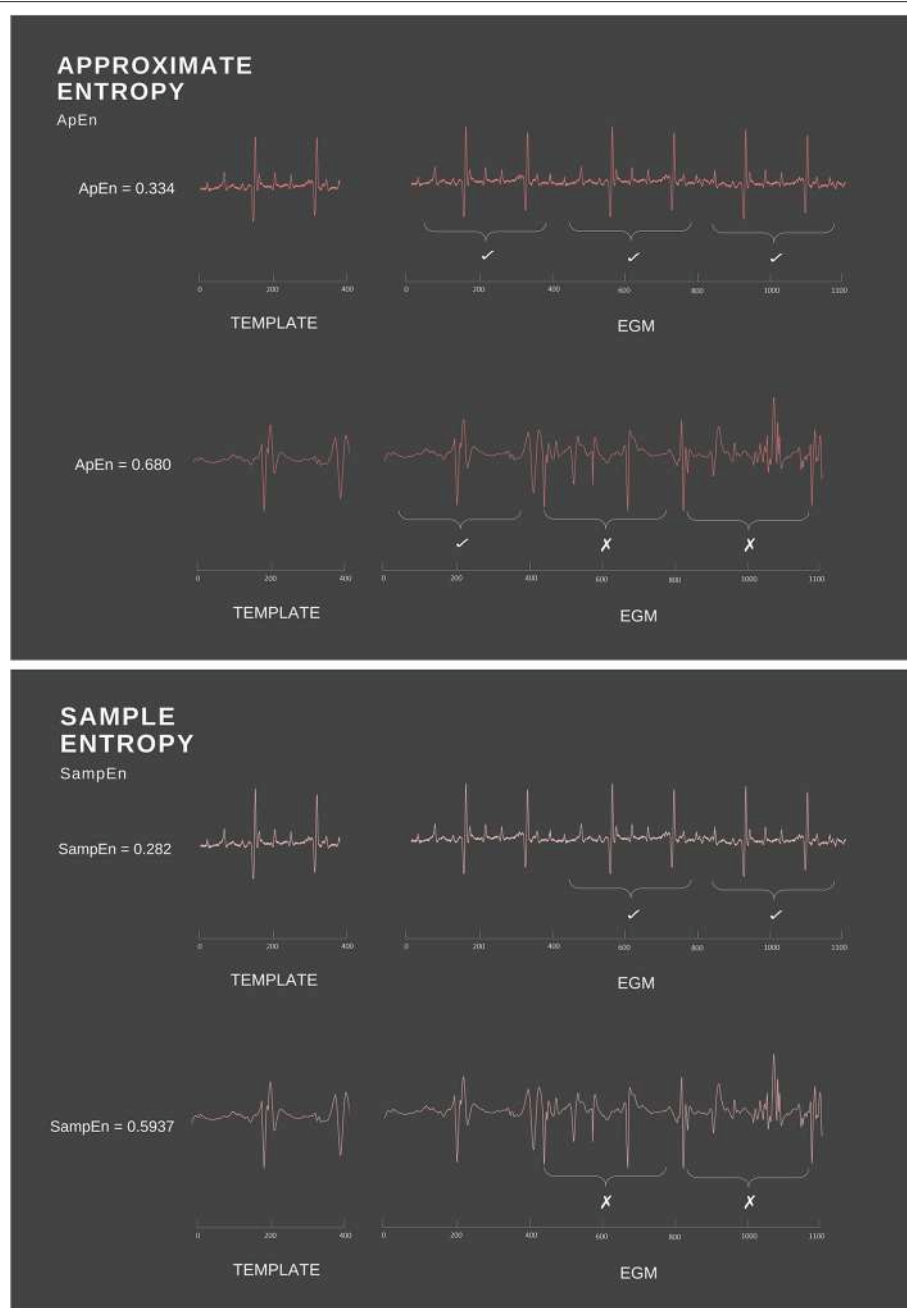


FIGURE 2 | Simple example of ApEn and SampEn calculation. ApEn and SampEn examine the presence of repetitive patterns by measuring the difference between the template vector and the rest of the time series data. As ApEn will compare a vector to itself, the regularity of the overall signal is increased. In comparison, SampEn excludes self matches, thus avoiding biased regularity.

weighted depending on the kernel function, and commonly, a Heaviside kernel function is used. The Heaviside kernel sets a threshold r as the weight for each point, which is equal to the width of the Heaviside kernel function and determines the precision of the density estimation (Xiong et al., 2017). A small r obtains a more detailed estimate, but requires more data points to ensure accuracy, whilst a larger r yields

coarse probability estimates as too many points neighboring the reference will be included. With this in mind, r is typically set to a fraction of the data variance in practical applications, e.g., a function of the standard deviation of the dataset, to remove the dependence of entropy on the amplitude of the observed process (Xiong et al., 2017). Other estimators, such as linear and nearest neighbor estimators, are also available but

are not as widely utilized in ApEn computation (Xiong et al., 2017).

Another important computational consideration is the length of the compared runs or window length m . The window length m allows the ApEn algorithm to search through the sequence S_N and measure the likelihood or prevalence, $C_m(r)$, that runs of patterns similar for m observations remain close on the next incremental observation (Yentes et al., 2013). Although there is no established consensus for ApEn parameter selection, it is typically suggested that an $m = 2$ be used for clinical data. Though such a value is frequently used in literature and allows comparison of study results to other published findings, it is important to acknowledge that ApEn estimates depend strongly on the combination choice of m , r and the epoch length N . Hence, thoughtful consideration with respect to what m represents in a biological sense is necessary for each individual dataset (Yentes et al., 2013).

SAMPLE ENTROPY

Another estimate of conditional entropy is sample entropy (SampEn). SampEn is a modified rendition of ApEn that works in much the same fashion (Richman and Moorman, 2000; Richman et al., 2004). Computationally, however, SampEn differs in two primary ways: (i) it is not length dependent and (ii) it does not include self-comparison of the template vector (Richman and Moorman, 2000). In ApEn calculations, the template vector (the vector being matched to) is compared to all others in the time signal, including itself. As a consequence, the probability of the vector $C_m(r)$ will never equal zero (Richman and Moorman, 2000). As a result of this, the overall ApEn is lowered, since a self-match will create the appearance of increased regularity (Richman et al., 2004). By foregoing comparisons between a vector and itself (Figure 2), Richman et al. were able to create the SampEn family of statistics with an ability to avoid this biased regularity (Richman and Moorman, 2000). SampEn is derived from previous approaches established by Grassberger and Procaccia (1983), Ben-Mizrahi et al. (1984), Grassberger (1988) and Grassberger et al. (1991), and uses the natural logarithm of the conditional probability that two vectors that are similar at m points will remain similar at an incremental point (Richman and Moorman, 2000). Specifically, SampEn can be defined mathematically as:

$$\text{SampEn} = -\log \frac{\sum A_i}{\sum B_i} = -\log \frac{A}{B} \quad (6)$$

where A_i is the number of matches of length $m + 1$ with the i^{th} template, B_i the number of matches of length m with the i^{th} template and SampEn the entropy measured in bits (Richman et al., 2004).

Like ApEn, SampEn is also commonly computed using kernel estimators. Computationally, estimation of SampEn using kernel estimation is achieved using the conditional entropy Equation (7), which is implemented with the Heaviside kernel function and uses the maximum norm to compute distances

(Xiong et al., 2017):

$$C(X) = H(X_n | X_n^m) = -\ln \frac{\langle p(x_n, x_n^m) \rangle}{p(x_n^m)} \quad (7)$$

Where $p(x_n^m)$ is used to estimate the joint probability distributions $p(x_{n-1}, \dots, x_{n-m})$ and $p(x_n, x_n^m)$ in the m -dimensional and $(m+1)$ -dimensional spaces spanned by X_n^m and (X_n, X_n^m) . Note that $\langle \cdot \rangle$ represents the averaging across patterns, and K represents the Heaviside kernel function:

$$K = \Theta(\|x_n - x_i\|) = \begin{cases} 1, & \|x_n - x_i\| \leq r \\ 0, & \|x_n - x_i\| > r \end{cases} \quad (8)$$

and $p(x_n)$ the kernel estimate of the probability distribution:

$$p(x_n) = \frac{1}{N} \sum_{i=1}^N K(\|x_n - x_i\|) \quad (9)$$

where $\| \cdot \|$ is the maximum norm. Consequently, this kernel estimate of conditional entropy reduces the bias seen in ApEn (Xiong et al., 2017).

In studies, SampEn demonstrated greater robustness over a broad range of conditions, which potentially makes it a more useful algorithm in studies analyzing physiological data (Richman and Moorman, 2000). SampEn also showed greater performance with short datasets, showing less dependency on the data length in comparison to ApEn estimates (Yentes et al., 2013). Like ApEn however, SampEn is also sensitive to parameter choice, though showed greater relative consistency over a broad range of possible combination values for r , m , and N (Costa et al., 2005). Despite this, care should still be taken when choosing SampEn parameters.

MULTISCALE ENTROPY

As discussed, ApEn and SampEn approaches evaluate the appearance of repetitive patterns to compute the regularity of a signal and calculate entropy. One potential limitation of these methods, however, is that increased entropy may not always translate to increased dynamical complexity (Costa et al., 2002b). As Costa et al. argue, entropy-based measures such as the Kolmogorov complexity and entropy rate, grow monotonically with randomness (Costa et al., 2005). Consequently, such measures will yield high entropies for uncorrelated random signals such as white noise, which possess low predictability but are not structurally “complex.” A randomized time series will also yield higher entropy than the original signal, despite the fact that the process of creating surrogate data destroys correlations and degrades the information content of the time series (Costa et al., 2002b). With this in mind, Costa et al. aimed to develop a quantitative measure of dynamical complexity with three basic hypotheses in mind: (i) that the complexity of a biological system reflects its ability to function and adapt in an evolving environment; (ii) biological systems operate between multiple spatial and temporal scales, thus possessing multiscaled complexity; and

(iii) a number of disease states that reduce the adaptive capacity of the individual seemingly degrades the information carried by output variables (Costa et al., 2005). As such, Costa et al. introduce a multiscaled entropy (MSE) approach that quantifies entropy over a range of time scales (Humeau-Heurtier, 2015).

Using MSE, measurements have the ability to reflect that both completely ordered and completely random signals are not truly complex, and identifies that correlated random signals are more complex than uncorrelated random signals (Costa et al., 2002a, 2005; Costa and Healey, 2003). The inclusion of measurements from a variety of temporal scales also includes two major advantages: (i) the ability to assess complexity at longer and shorter time scales and (ii) quantification of the overall system complexity, which is equal to the sum of entropy values over all temporal scales (Busa and van Emmerik, 2016).

Computationally, MSE implements the SampEn algorithm to assess complexity. The primary motive for using SampEn as opposed to ApEn is its greater consistency over a broad range of r , m , and N values, as well as its reduced dependency on the time series length (Costa et al., 2005). In comparison to the multiscaled complexity approach introduced by Zhang et al. for physical systems (Zhang, 1991), which is based on ShEn, the use of SampEn also allows MSE to become better suited to physiologic time series. The use of Shannon's definition of entropy in Zhang's method requires a large amount of virtually noiseless data in order to accurately map to a discrete symbolic sequence, which introduces limitations when applied to free-running physiologic signals (Costa et al., 2005).

In recognizing these considerations, Costa bases MSE on a modification of Zhang's and Pincus' approaches. Specifically, MSE comprises of two steps: (i) "coarse-graining" of the time series, which derives the representations of a system's dynamics at varying temporal scales (a form of resampling) and (ii) application of SampEn on each of the coarse-grained time series (Costa et al., 2005). Specifically, construction of a coarse-grained time series involves averaging a successively increasing number of data points using non-overlapping windows. Mathematically, each element of the coarse-grained signal is computed using:

$$y_j^{(\tau)} = 1/\tau \sum_{i=(j-1)\tau+1}^{j\tau} x_i \quad (10)$$

where τ represents the scale factor and $1 \leq j \leq N/\tau$ (Costa et al., 2002a). In effect, the length of each coarse grained data will equal the length of the original time series divided by the scaling factor τ (Wu et al., 2013).

Following this, SampEn is used to calculate an entropy estimate for each coarse-grained time series plotted as a function of the scaling factor τ . This step is referred to as the multiscale entropy analysis. In traditional uses of SampEn, data from certain pathologic time series that may be chaotic/unpredictable but arise from less physiologically complex systems and mechanisms, such as data from episodes of atrial fibrillation, will result in higher SampEn. This is because such SampEn estimates are

based on a single scale and hence will not account for features related to structure and organization on other scales (Costa et al., 2005). The MSE results published by Costa et al. support this, showing that at a single scale, the entropy assigned to the time series of atrial fibrillation and congestive heart failure patients is higher than those of healthy patients. Contrastingly, when analyzed at multiple scales, the time series of healthy subjects are assigned with highest entropy, reflecting that healthy cardiac dynamics are the most physiologically complex (Costa et al., 2005). Whilst these results contradict those obtained using traditional ShEn, SampEn, and ApEn algorithms, they more accurately reflect the physiological complexity of the underlying system.

It is important to note that although Costa's MSE algorithm is widely used in multiple fields, this approach still suffers from limitations. First, spurious MSE oscillations are introduced due to the inefficient process of eliminating fast temporal scales, and the original coarse graining procedure also artificially reduces MSE (Valencia et al., 2009). To rectify these issues, Valencia et al. develop a refined multiscale entropy approach (RMSE) (Valencia et al., 2009). The RSME approach utilizes a low-pass Butterworth filter instead of an FIR filter to eliminate fast temporal scales, which ensures a more accurate elimination of components above the specified cut-off frequency. In addition, RMSE uses a refined coarse graining procedure that implements a continuously updating r , defined as a percentage of the standard deviation of the filtered series. In effect, this compensates for the decrease in variance related to the filtering procedure for removal of the fast temporal scales (Valencia et al., 2009).

Though RSME overcomes spurious MSE oscillations and biased reduction of MSE estimates, it is difficult to reliably compute over short time series. In response, Faes et al. introduce the linear MSE (LMSE) method (Faes et al., 2017), which utilizes linear state-space models to provide a multiscale parametric representation of an autoregressive process observed at multiple time scales. LMSE exploits the state-space parameters to quantify the complexity of the process. Results show that in comparison to both RSME and MSE, application of LMSE to short cardiovascular data provides a better description of the physiological mechanisms producing biological oscillations at different temporal scales (Faes et al., 2017).

Another limitation of MSE is that the statistical reliability of SampEn for a coarse-grained time series is reduced as the time scale factor τ increases. This is because for an N point time series, the length of the coarse-gained series at scale factor τ is N/τ . Consequently, the larger the scaling factor, the shorter the coarse-grained series and hence, the variance of the estimated entropy will increase as the scaling factor increases. To overcome this, Wu et al. developed the concept of a composite multiscale entropy (CSME) to reduce the variance of estimated entropy values at large scales (Wu et al., 2013). Specifically, CSME achieves this by calculating the sample entropy of all coarse-gained time series and finding the mean of the τ entropy values, rather than only the first coarse-grained time series as proposed by Costa (Wu et al., 2013).

WAVELET ENTROPY

While the aforementioned algorithms all compute entropy in the time domain, entropy estimates can also be calculated in the frequency space. Broadly speaking, computing entropy in the frequency domain consists of transforming the time series using methods such as the Fourier transform or wavelet decomposition (Rosso et al., 2001). Although signals used within the medical field are predominantly presented in the time domain, representation in the frequency domain may provide advantages in certain applications. For example, studies have postulated that the frequency band with the highest strength correlates to the cycle length derived from time domain analysis (Ng et al., 2006), which is annotated as the dominant frequency (DF) (Sanders et al., 2005, 2006). This becomes potentially useful in signals with deflection, varying amplitudes, and more complex temporal patterns, wherein time domain measurements of the cycle length are likely to be inaccurate (Traykov et al., 2012). As this is often the case during AF, frequency-based analyses may provide a better measurement of the atrial rate (Traykov et al., 2012). It should be noted, however, that the frequency spectrum may also be determined by other factors outside of cycle length, such as morphology and amplitude (Ng et al., 2006; Elvan et al., 2009). As such, wavelet entropy methods that combine both entropy and frequency analysis may provide additional insights and more robust analyses in comparison to DF analysis alone (Ng et al., 2006; Elvan et al., 2009).

Specifically, wavelet entropy (WE) combines entropy and wavelet decomposition to provide an estimate of the degree of disorder present within a signal (Rosso et al., 2001). The wavelet entropy of a signal can be given by:

$$WE = - \sum_{j=1}^N E_j \log(E_j) \quad (11)$$

Where E_j is the relative energy associated with the wavelet coefficient at scale j and N the number of wavelet decomposition levels. Calculating entropy in this way provides a measurement of the amount of order or disorder in a signal, wherein WE will assume a value that is very low and close to zero for an extremely organized signal such as a periodic mono-frequency event, and high WE for random signals such as white noise (Rodenas et al., 2015). Consequently, EGM or ECG signals with greater complexity and irregularity will result in high WE.

TRANSFER ENTROPY

Transfer entropy (TE) is an information theoretic measure that can be used to understand the information transfer between joint processes (Barnett et al., 2009). In systems consisting of more than one component or variable, understanding information transfer between these variables can be extremely useful in determining its structure and mechanism. Many studies have attempted to study such relationships using an alternate information-theoretic measure known as mutual information (MI), which provides a model-free approach to

quantifying information overlap between two variables (Vicente et al., 2011). Specifically, this is achieved by measuring the amount of information that can be learnt from one random variable by observing another. Unfortunately, MI measures do not capture dynamical and directional information exchange, and hence poorly describe causal relationships (Schreiber, 2000). For example, MI is symmetric under the exchange of signals and cannot differentiate between response and driver systems. Secondly, MI captures only the amount of information that is shared by two signals, rather than the information being exchanged (which better relates to causal dependence) (Schreiber, 2000). To provide an asymmetric measure, delayed MI, which measures MI between a signal and another lagged signal, has been proposed. Though delayed MI reflects certain dynamical structures as a result of the time lag, it is still flawed and can cause issues when shared information from a common input or history is present (Schreiber, 2000). To address these problems, Schreiber et al. develop transfer entropy (TE) to provide an alternative information theoretic measure that shares some of the desired properties of mutual information, but also considers the dynamics and directionality of information transfer (Schreiber, 2000).

To measure TE between two variables X and Y , one needs to measure the amount of uncertainty (entropy) that is reduced in future values of Y by knowing past values of X , given the past values of Y . In mathematical notation, the TE between X and Y can be given by:

$$TE(X \rightarrow Y) = \sum_{y_{t+1}, y_t^n, x_t^m} p(y_{t+1}, y_t^n, x_t^m) \log \frac{p(y_{t+1} | y_t^n, x_t^m)}{p(y_{t+1} | y_t^n)} \quad (12)$$

where $x_t^m = (x_t, \dots, x_{t-m+1})$, $y_t^n = (y_t, \dots, y_{t-n+1})$, and m and n the orders of the Markov processes X and Y respectively (Vicente et al., 2011). Typically, TE estimations use the Shannon entropy algorithm during computation to provide a measure of the uncertainty between X and Y (Schreiber, 2000).

It can be noted that the concept of transfer entropy shares some overlap with the statistical notion of causal influence termed *Granger causality* (GC) (Barnett et al., 2009), which uses prediction via vector auto-regression to measure causality. Specifically, given sets of inter-dependent variables X and Y , Granger causality will say X Granger-causes Y if Y assists in predicting the future of X , beyond what X already predicts about its own future (Barnett et al., 2009). In contrast, the information theoretic notion of transfer entropy is framed in the context of *resolving uncertainty*. For example, it can be said that the transfer entropy from Y to X is the degree to which Y disambiguates the future of X , beyond what X already disambiguates about its own future (Barnett et al., 2009). This relationship was explicitly explored and detailed by Barnett et al. (2009), who shows that under Gaussian assumptions the concept of Granger Causality and Transfer entropy are in fact equivalent.

Although TE is prevalently used in neuroscience to understand the causal relationships between parts of the brain and responses to stimuli (Vicente et al., 2011), it has thus far received little attention in the cardiac space.

Limitations of Entropy

Although entropy is widely used in many fields, reliable estimation of information-theoretic quantities from empirical data can prove difficult. Firstly, the sensitivity of entropy estimates with respect to parameter selection can be problematic. Discretization of a time series using bins as commonly done in ShEn algorithms can pose potential problems, as inappropriately selecting bin-widths can lead to greater bias and reduce the accuracy of entropy estimates (Purwani et al., 2017).

Additionally, both ApEn and SampEn show significant 2-way and 3-way interactions between m , r , and N , hence are influenced heavily by the combination choice of these parameters (Yentes et al., 2013). Appropriate parameter selection is particularly critical when analyzing short data sets, as ensuring there is a sufficient number of matches can be problematic (Lake and Moorman, 2010). This can be seen in rapid diagnosis of AF. In such cases, choosing an m that is too large or r that is too small will result in too little template matches to estimate the conditional probabilities accurately. Conversely, if m is too small and r too large, all templates will match each other and cardiac different rhythms cannot be discerned (Lake and Moorman, 2010). Although SampEn is relatively more stable across varying data lengths in comparison to ApEn, inappropriate parameter selection, particularly in the choice of r , can still lead to inaccurate entropy estimates (Lake and Moorman, 2010).

In addition, although bipolar EGM entropy-based approaches of AF mapping (such as ShEn mapping) have been proposed for identification of rotational activity, problems may be encountered in areas where wave propagation dynamics mimic such rotational sources. For example, areas in which multiple waves precess and cross propagate in varying directions may instead appear to originate from a single rotational source and hence, result in high entropy estimates similar to those seen for rotors. This could potentially present problems for a targeted entropy guided ablation strategy in the future.

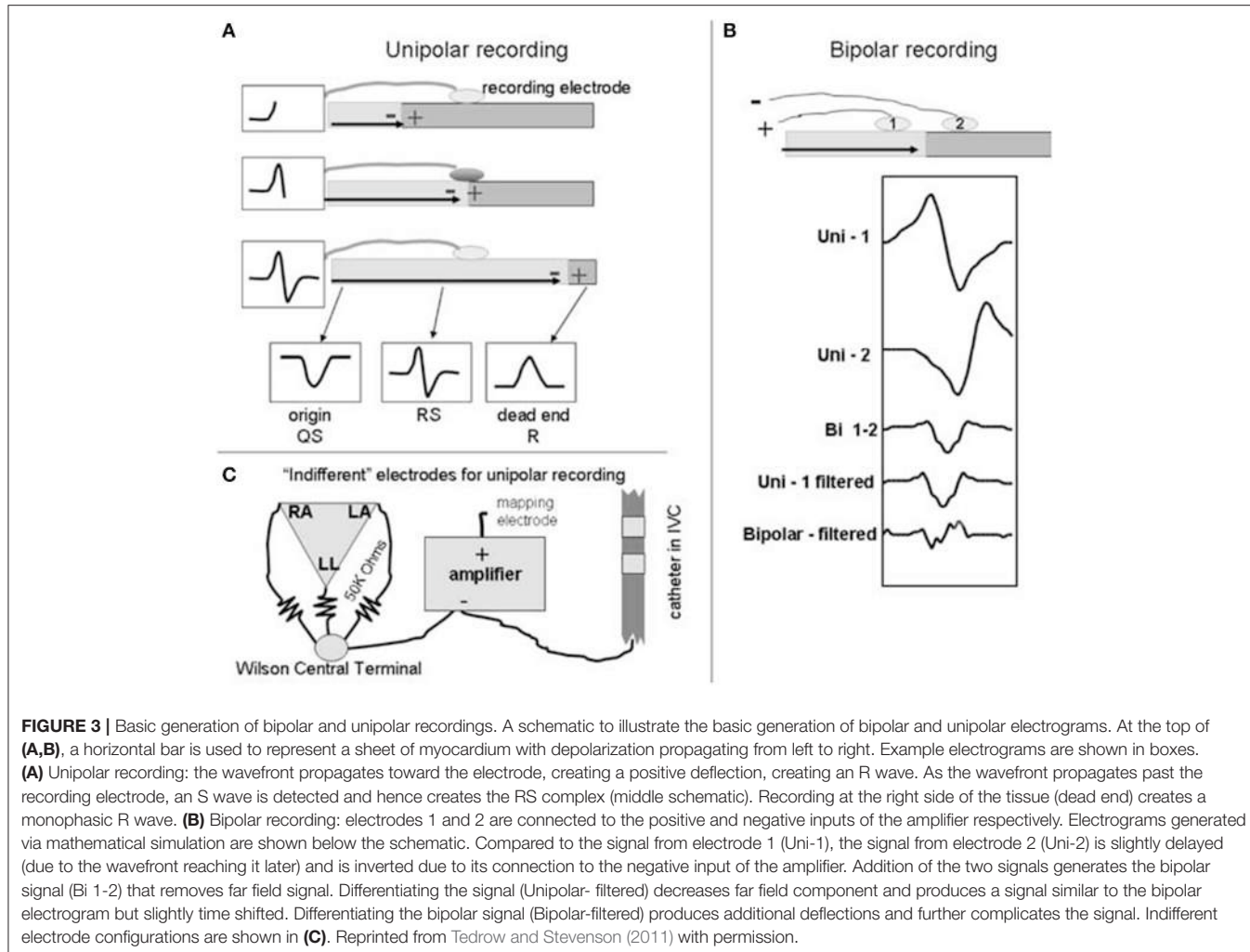
INFORMATION THEORY AND THE INTRACARDIAC ELECTROGRAM

To further discuss how information theory can be used in the context of AF mapping, we will first discuss the intracardiac electrogram. An intracardiac electrogram (EGM) is acquired by measuring the voltage difference between two recording electrodes (Tedrow and Stevenson, 2011). In the unipolar electrogram configuration, the anodal (positive) input of the amplifier is by convention connected to the exploring electrode, which is usually located at the tip of the catheter and in physical contact with the cardiac tissue (Tedrow and Stevenson, 2011; Baumert et al., 2016). Another intermediate electrode, often referred to as the reference electrode, that is distant from the heart is connected to the cathodal (negative) input of the amplifier (Tedrow and Stevenson, 2011; Baumert et al., 2016). As a product of this configuration, the resultant unipolar signal possesses a characteristic morphology due

to the passing of planar wavefronts toward the recording electrode (Figure 3) (Tedrow and Stevenson, 2011). A distinctive biphasic complex is created as the wavefront reaches and passes the electrode, causing the wavefront deflection to become steeply negative (Baumert et al., 2016). This generates an RS complex (Tedrow and Stevenson, 2011). One limitation of the unipolar EGM is its vulnerability to far field activity (electrical activity from other parts of the cardiac chamber), electromagnetic interference (mains noise) and in the case of AF mapping, interference from ventricular depolarization (Tedrow and Stevenson, 2011; Baumert et al., 2016). Few studies have utilized unipolar EGM for mapping, however, these issues have largely hindered their use within research (Konings et al., 1994, 1997; Allessie et al., 2010; Tedrow and Stevenson, 2011).

In contrast, bipolar electrograms are obtained via the subtraction of two unipolar EGMs recorded proximally, which is typically achieved by subtracting from adjacent poles of the catheter (Baumert et al., 2016). Due to this configuration, much of the ventricular contribution to the signal is largely eliminated, and as such, bipolar EGM are generally preferred in clinical settings (Tedrow and Stevenson, 2011; Baumert et al., 2016). Unfortunately, however, the timing of local activations is less defined in comparison to unipolar EGM, though in homogeneous tissue the initial peak coincides with local depolarization time (van der Does and de Groot, 2017). In AF, bipolar EGM morphologies are generally irregular and complex in comparison to their sinus rhythm counterpart, possessing many deflections (Baumert et al., 2016). EGM morphologies can be categorized into three types, as previously described by Wells et al. (1978) (Table 1).

Relating to the EGM morphology is the previously discussed concept of entropy. When applied to the intracardiac electrogram, entropy approaches have the potential to provide clinical insights into the underlying dynamics of AF. As entropy is linked to the information content of a signal, EGM with complex, non-uniform morphology will result in greater uncertainty and higher entropy. Conversely, an EGM with a regular, periodic morphology will result in lower entropy (Ganesan et al., 2012). This characteristic makes entropy particularly useful in AF applications in which the ability to distinguish between AF and non-AF signals is required (AF detection algorithms), and where changes in the EGM morphology are thought to correlate to important AF triggers or substrates (AF mapping). The identification and localization of rotors provides a particularly interesting application of entropy within the AF mapping space, as it has been demonstrated that the pivot zone of a rotor experiences greater spatial uncertainty of wavefront direction, resulting in less stable bipolar EGM morphologies that can be quantified by entropy (Ganesan et al., 2012, 2014; Arunachalam et al., 2015). Other wave propagation dynamics are less well explored in relation to entropy, though additional mechanisms of interest (such as complex wavelet interaction regions) may also yield useful entropy characteristics. If statistical information theoretic approaches such as entropy can be used to pinpoint such potentially important AF landmarks,



a targeted ablation strategy may become possible in the future.

In some ways, the concept of entropy shares some conceptual overlap with the notion of fractionation. Broadly speaking, the term fractionation is used to describe EGMs that possess multiple deflections and are prolonged (van der Does and de Groot, 2017), although no precise consensus definition currently exists (Baumert et al., 2016). As such, like entropy, CFAE essentially aims to provide some definition to describe the complexity of an electrogram. A number of sources are said to be responsible for fractionation, with the local collision of multiple wavelets, local re-entry and zones of slow conduction said to result in EGM fractionation during AF (de Bakker and Wittkampf, 2010; Waks and Josephson, 2014). Consequently, it is thought that there is some relationship between CFAE and the maintenance of AF (Waks and Josephson, 2014), thus CFAE mapping and CFAE guided ablation have previously been explored (Nademanee et al., 2004; Nademanee and Oketani, 2009; Berenfeld and Jalife, 2011; Hayward et al., 2011; Li et al., 2011; Chen et al., 2014). Though both CFAE and entropy aim to capture the qualitative property of signal fractionation to some degree, entropy is differentiated

TABLE 1 | Characterization of Atrial Fibrillation (AF) in Man as defined by Wells et al. (1978).

AF Type	Description
Type 1	Discrete atrial complexes with varying morphological appearance but with discrete isoelectric baseline
Type 2	Discrete beat-to-beat atrial complexes but no isoelectric baseline
Type 3	Complex and highly irregular atrial EGMs with no discrete complexes or isoelectric intervals

Characterization of AF into three AF types, which uses the bipolar EGM morphology during AF to provide classification.

from CFAE by having a quantitative definition rooted in signal processing and mathematics, and does not use empirically derived definitions.

Outside of fractionation, entropy-based analysis of the EGM also has the potential to provide insights about the complex wave propagation dynamics underlying AF (Kośna et al., 2015). For example, transfer entropy may possess the ability to

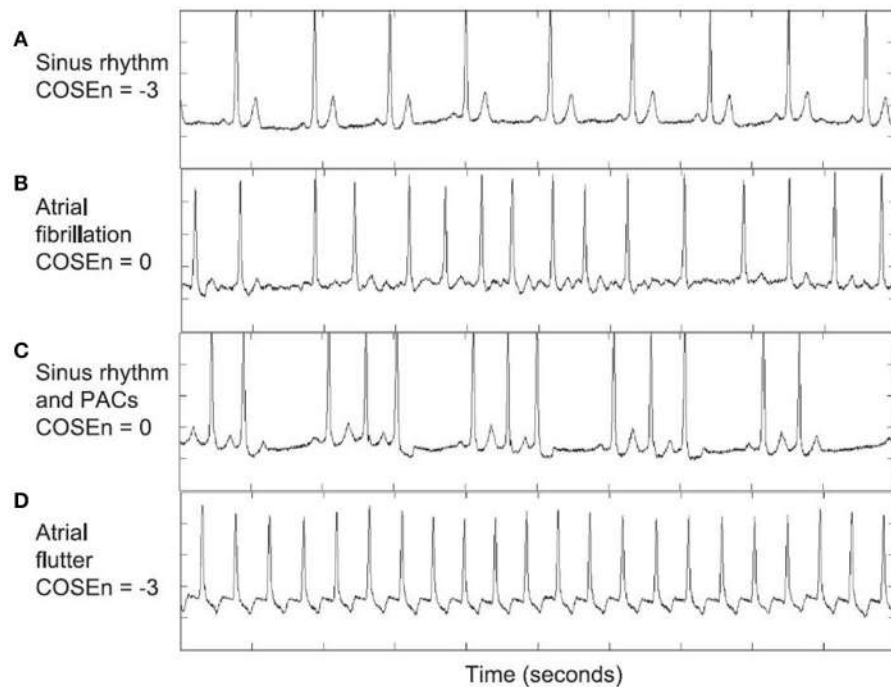


FIGURE 4 | AF detection using COSEn (Coefficient of sample entropy). CoSEn values for ECGs from the MIT-BIH atrial fibrillation database used by Lake and Moorman (2010) to test automated AF detection using SampEn. Although CoSEn was able to differentiate between normal sinus rhythm (**A**) and atrial fibrillation (**B**), sinus rhythm with ectopy (**C**), and atrial flutter (**D**) resulted in misclassification. This was due to (i) irregular RR intervals for sinus with ectopy, which increased SampEn and mimicked AF values for CoSEn and (ii) 2:1 AFL creating regular RR intervals, mimicking sinus values for CoSEn. Reprinted from Lake and Moorman (2010) with permission.

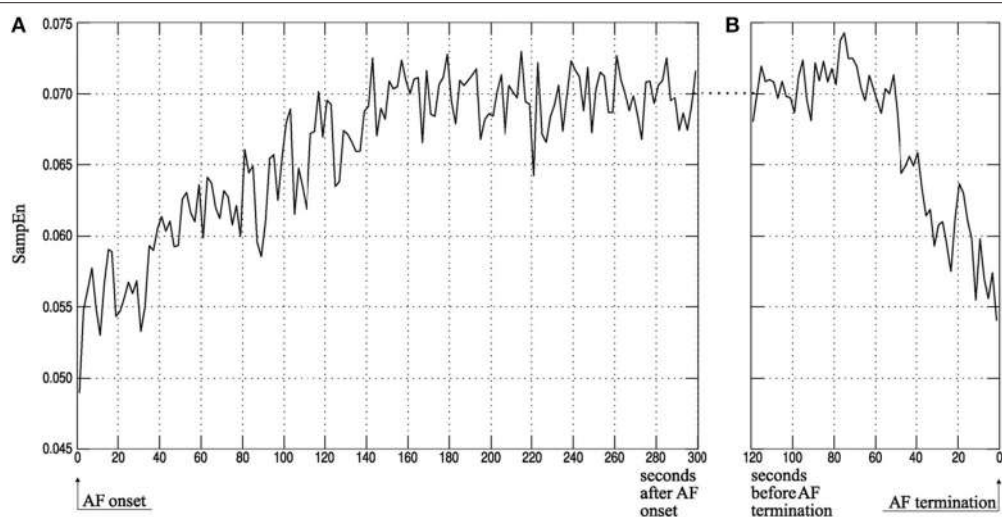


FIGURE 5 | Atrial activity organization time course of ECG recordings measured using SampEn. Average atrial activity (AA) organization, quantified using SampEn, for (**A**) the first 5 min after AF onset and (**B**) the last 2 min before AF termination as computed by Alcaraz and Rieta (2010). Findings show that SampEn, and in turn the AA organization, decreases in the first few minutes of AF onset and increases within the last minute of spontaneous AF termination. Reprinted from Alcaraz and Rieta (2010) with permission.

determine information flow during AF and in turn, uncover causality and electrophysiological pathways between various regions of the heart that may be involved during AF propagation.

Consequently, analysis of information flow may be useful for identifying the atrial regions central to maintaining AF (Kośna et al., 2015).

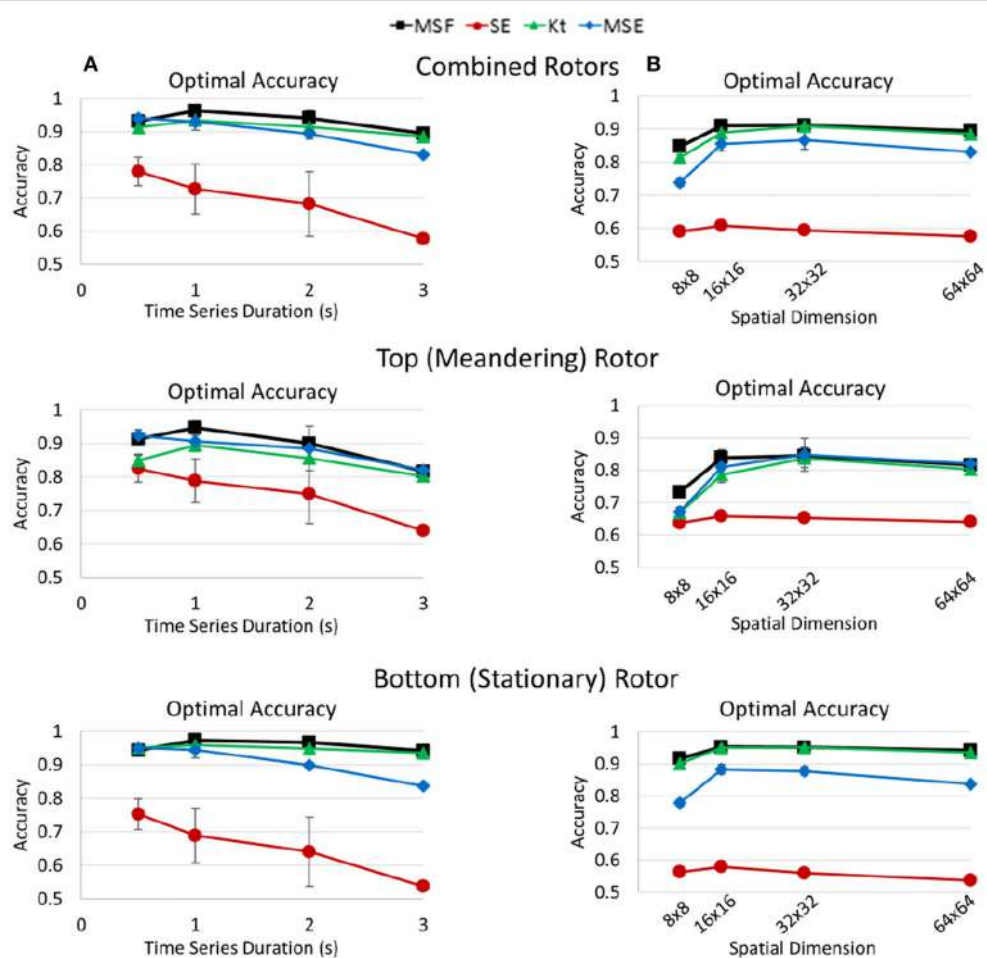


FIGURE 6 | Optimal accuracy of multiscale frequency (MSF), Shannon entropy (SE), kurtosis (Kt), and multiscale entropy (MSE) for the identification of rotors shown in. Optimal accuracies for MSF, SE, Kt, and MSE measures determined by Annoni et al. (2017). The optimal accuracies are shown for both rotors (**Top**), the top meandering rotor (**Middle**) and bottom stationary rotor (**Bottom**). Reprinted from Annoni et al. (2017) with permissions.

CURRENT STUDIES USING INFORMATION THEORETIC APPROACHES IN ATRIAL FIBRILLATION

Though information theoretic and entropy-based approaches remain relatively limited within atrial fibrillation research, a handful of studies have explored their use. Broadly speaking, the use of entropy in AF can be categorized into three groups, namely: (i) entropy for AF detection, (ii) entropy for AF characteristic determination, and lastly (iii) entropy for AF mapping. Some of the approaches using entropy in the current literature will be broadly discussed in the following, with particular focus on the role of entropy in AF mapping.

Entropy for AF Detection

Presently, with respect to the study of atrial fibrillation (AF), entropy is most widely used for the detection of AF in ECG recordings and Holter monitors. As AF

episodes occur paroxysmally in the majority of patients, human-based diagnosis of AF can oftentimes be difficult and time consuming, hence automated and computerized methods of AF detection have become a lucrative diagnostic application of entropy (Ródenas et al., 2015; Cui et al., 2017).

Many algorithms have been developed to detect AF, which can often be broadly categorized as being based on either (i) P-wave detection or (ii) RR interval (RRI) variability (Lee et al., 2011). Of these two methods, AF detection using the temporal variability of the RR interval has become a much more common approach in literature as analysis of the P-wave morphology is often difficult, as ECGs can be noisy and are prone to motion artifact. In addition, the determination of a P-wave fiducial point is challenging due to its low amplitude during AF which makes it more susceptible to corruption through noise, in turn lowering the signal-to-noise ratio (Dash et al., 2009; Lee et al., 2011; Ródenas et al., 2015).

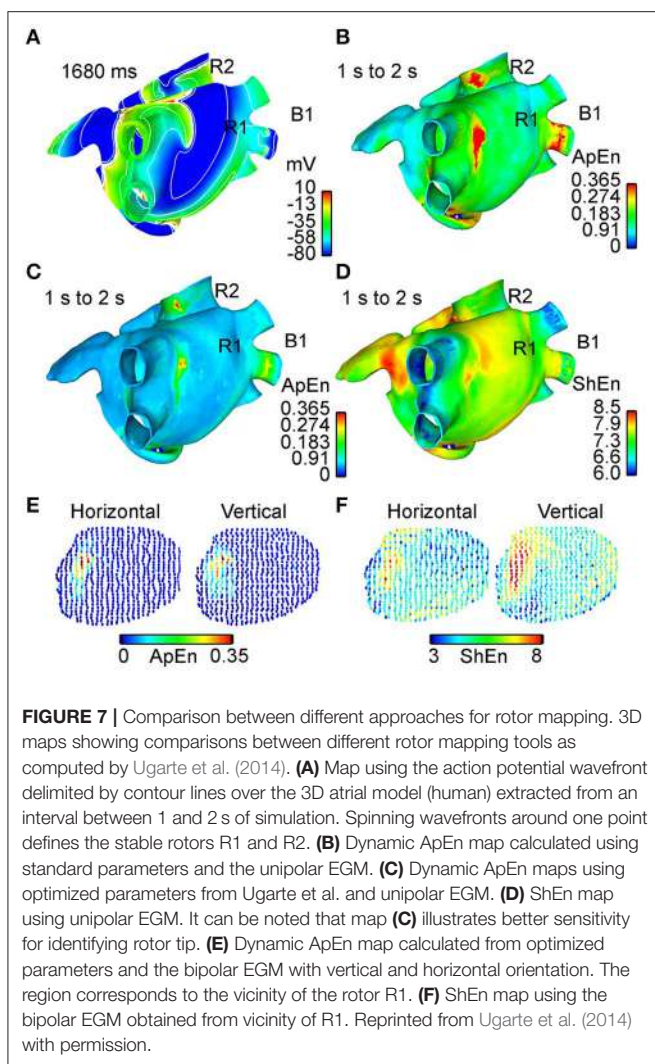


FIGURE 7 | Comparison between different approaches for rotor mapping. 3D maps showing comparisons between different rotor mapping tools as computed by Ugarte et al. (2014). **(A)** Map using the action potential wavefront delimited by contour lines over the 3D atrial model (human) extracted from an interval between 1 and 2 s of simulation. Spinning wavefronts around one point defines the stable rotors R1 and R2. **(B)** Dynamic ApEn map calculated using standard parameters and the unipolar EGM. **(C)** Dynamic ApEn maps using optimized parameters from Ugarte et al. and unipolar EGM. **(D)** ShEn map using unipolar EGM. It can be noted that map **(C)** illustrates better sensitivity for identifying rotor tip. **(E)** Dynamic ApEn map calculated from optimized parameters and the bipolar EGM with vertical and horizontal orientation. The region corresponds to the vicinity of the rotor R1. **(F)** ShEn map using the bipolar EGM obtained from vicinity of R1. Reprinted from Ugarte et al. (2014) with permission.

Various studies have used Shannon entropy (ShEn) in conjunction with various other measures of complexity such as the Turning Points Ratio (TPR) (Dash et al., 2009), Root Mean Square (RMS) of successive RR differences (Dash et al., 2009), symbolic dynamics (Zhou et al., 2014), and time-varying coherence functions (TVCF) (Lee et al., 2011), among others, to better capture the randomness in the signal and detect variability of the RRI time series (Dash et al., 2009; Lee et al., 2011; Zhou et al., 2014). As ShEn can be used to measure the level of uncertainty and information size in the signal, it can reflect whether the ECG morphology exhibits irregularities, and hence variability in the RRI time series. Results using these methods demonstrate high rates of sensitivity and specificity upwards of 95% (Dash et al., 2009; Lee et al., 2011; Zhou et al., 2014), indicating the feasibility of entropy for detecting RRI variability.

Although the RRI time series approach is frequently used, widely available and capable of providing adequate AF detection in a number of cases, entropy-based approaches have also been used independently to detect AF (Lake and Moorman, 2010;

Carrara et al., 2015a,b). Sample Entropy (SampEn) algorithms have been used to detect the probability that runs of AF will match with others within the time series (Richman and Moorman, 2000; Lake and Moorman, 2010) (Figure 4). A benefit of SampEn is its ability to use short runs or bursts of AF as a template for matching, hence avoiding issues relating to short AF episode durations that are common with RRI variability-based methods. These studies showed that SampEn provided a high degree of accuracy in distinguishing AF from sinus rhythm (~95%), but encountered errors when atrial or ventricular ectopy were present, as this increased the entropy of the signal (Lake and Moorman, 2010; Carrara et al., 2015a,b).

The use of wavelet entropy (WE) for AF detection has also been explored in single lead electrograms (Ródenas et al., 2015). This method was used under the premise that using entropy and wavelet decomposition in conjunction increases the robustness of the detection algorithm to noise, artifacts and non-stationarities (Ródenas et al., 2015). Ródenas et al. use this method to calculate the WE on a TQ interval to identify the presence and absence of the P-wave in each beat of the ECG, which in turn determines the presence of AF. Results demonstrated a discriminant ability of approximately 95%, which is comparable to results from other studies (Lake and Moorman, 2010; Carrara et al., 2015a,b).

Entropy for AF Prediction and Characteristic Determination

To effectively treat atrial fibrillation, an understanding of the arrhythmia itself is also crucial. As such, another application of entropy is its use in determining the various characteristics of AF. One such area that has been studied are the changes in the RR interval dynamics preceding the onset of postoperative AF, as studying these characteristics may enable prediction of postoperative AF episodes. It has been hypothesized that heart rate variability (HRV), which can be used as an indicator of cardiac sympathovagal balance, would alter before the onset of postoperative AF and could be measured using entropy algorithms (Hogue et al., 1998). Findings on this have been conflicting, however, with Hogue et al. showing a decrease in ApEn upon the onset of AF (Hogue et al., 1998), whilst other studies show entropy and HRV analyses provide little predictive value when studying the onset of postoperative AF (Amar et al., 2003; Chamchad et al., 2011).

Adding to this, it is argued that the ability to predict the spontaneous onset of AF for non-postoperative patients is also important as it may allow prevention using electrical stabilization and various pacing techniques (Tuzcu et al., 2006). A number of studies have used ApEn and SampEn to predict the onset of paroxysmal AF (PAF), as these measures have the ability to measure the regularity of the time series signal, and hence quantify the heart rate variability (HRV) (Vikman et al., 1999; Amar et al., 2003; Shin et al., 2006; Tuzcu et al., 2006). Findings showed that ApEn and SampEn could predict the onset of AF as entropy of the HRV reduced significantly in ECG preceding AF, in comparison to those distant from an AF episode (Vikman et al., 1999; Shin et al., 2006; Tuzcu et al., 2006).

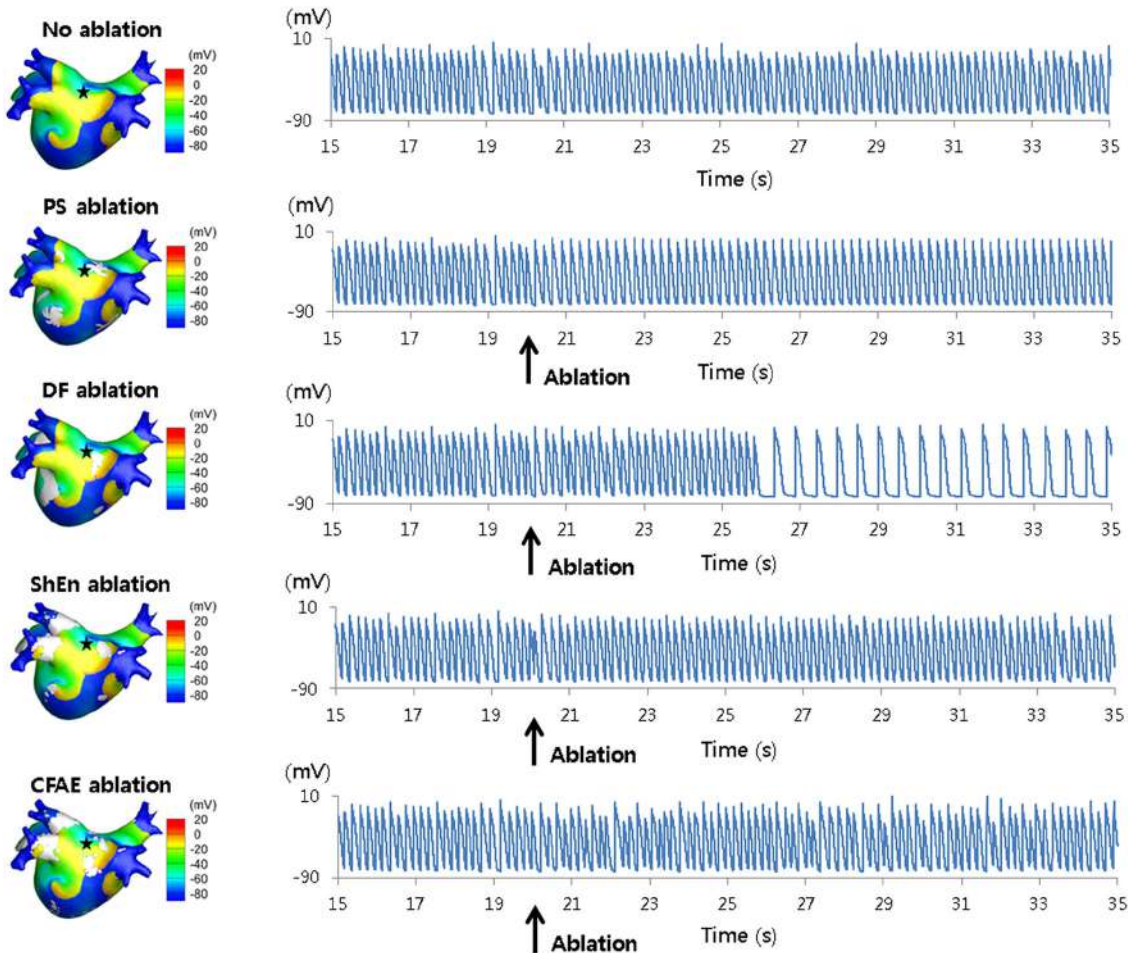


FIGURE 8 | 3D voltage maps and action potential curves during virtual ablation using phase singularity (PS), dominant frequency (DF), Shannon entropy (SE), and complex fractionated electrogram (CFAE) approaches. Results from simulated ablation using PS, DF, SE, and CFAE, as performed by Hwang et al. (2016). 3D heart voltage maps are shown on the (Left), with the black star indicating the action potential recording site. Action potential curves are shown on the (Right). Only simulated DF ablation resulted in changes of the action potential, converting AF into atrial tachycardia. Reprinted from Hwang et al. (2016) with permissions.

In the same breath, predicting the termination of PAF may also have clinical implications, as it may in turn help improve management of the arrhythmia and avoid unnecessary treatments (Alcaraz and Rieta, 2009a). Specifically, SampEn has been used to study the atrial activity (AA) organization from surface electrocardiograms (ECG) and predict the spontaneous termination of AF. It has been shown that SampEn of terminating AF episodes are lower in comparison to non-terminating episodes (Alcaraz and Rieta, 2009a,b, 2010) (Figure 5).

Lastly, analysis of the HRV complexity using SampEn have also been used to evaluate the characteristics of both PAF and persistent AF (Sungnoon et al., 2012). The study conducted by Sungnoon et al. aimed to test the hypothesis that impairment of cardiac autonomic control relates to increased irregularity in the AF signal. It was found that increased atrial signal irregularity as reflected by SampEn was consistent with an impairment of cardiac autonomic function in both PAF and persistent patients (Sungnoon et al., 2012).

Entropy for AF Mapping

AF mapping is pivotal to catheter ablation, as this helps locate AF triggers and substrates to guide the selection of ablation targets (Baumert et al., 2016). Unfortunately, although ectopic impulses from the pulmonary veins have been shown to initiate AF, catheter ablation of these ectopic foci have only shown limited success in persistent AF cases (Verma et al., 2015). Adding to this limited success is the fact that optimal ablation targets for persistent AF are still debated, as the mechanisms underlying this AF type are not yet well understood (Jalife et al., 2002). As a consequence of this, many approaches to AF mapping have been explored.

Masè et al. explore the use of entropy for quantifying synchronization during atrial fibrillation (Masè et al., 2005). In this study, a synchronization index (Sy) was developed using Shannon entropy (ShEn) (Shannon, 1948) to quantify the degree of synchronization during AF. Although AF is often described as being desynchronized, a certain amount

of synchronized electrical activity is in fact present, and quantifying this was thought to facilitate the identification of various propagation patterns that may be associated with AF, and hence improve understanding on AF mechanisms and treatment (Masè et al., 2005). Sy was defined by quantifying the complexity of the distribution of the time delays between sites using ShEn estimates. Findings from this study showed that a progressive and significant decrease in Sy correlated with increasing AF complexity (Masè et al., 2005), using definitions for complexity classes as defined by Wells et al. (1978) (Table 1). Sy was also calculated on the whole right atrial chamber, showing the existence of spatial heterogeneities (Masè et al., 2005).

Following this, a number of studies have also utilized entropy for the identification of rotors during AF (Ganesan et al., 2012, 2014; Orozco-Duque et al., 2013; Ugarte et al., 2014). There exists various schools of thought about the mechanisms driving an AF episode, with the rotor theory suggesting that AF is maintained by sites of rotational activation referred to as spiral waves or rotors (Jalife et al., 2002; Waks and Josephson, 2014). There is clinical and experimental evidence to support this theory, and as such, rotors are thought to be potentially effective targets for ablation (Schuessler et al., 1992; Skanes et al., 1998; Vaquero et al., 2008; Narayan et al., 2012). Building on this, Ganesan et al. hypothesized that rotors could be identified through regions of high Shannon entropy (Shannon, 1948), as wavefronts encircling the rotor pivot should result in broadening of the amplitude distribution of bipolar electrograms (EGM) due to their direction-dependent nature (Ganesan et al., 2012). Findings showed that maximum ShEn co-located with the rotor pivot in computer simulated spiral waves, rat and sheep models, and human AF (Ganesan et al., 2012). Ganesan et al. also further explored the characteristics of high ShEn regions at rotor pivot zones (Ganesan et al., 2014) to test the hypothesis that pivot points possess higher ShEn than electrograms recorded at the periphery (Ganesan et al., 2014). It was found that the rotor pivot not only coincided with higher ShEn than those found at the periphery of the spiral wave, but also that pivot zones consistently resulted in maximum ShEn, irrespective of bipolar electrode spacing, signal filtering and rotor meander (Ganesan et al., 2014).

In a following independent study, Arunachalam et al. supported the ability for ShEn to identify rotors in isolated rabbit hearts (Arunachalam et al., 2015). Specifically, ShEn-based mapping techniques were used to identify pivotal rotor points in optically mapped data acquired from the rabbit hearts, following which the mapping approach was applied to clinical intracardiac human data. Results demonstrated that ShEn could accurately identify the rotor pivot in optically mapped data with known pivot zones (Arunachalam et al., 2015), supporting findings published by Ganesan et al. (2012, 2014). In a more recent study, however, Annoni et al. report that the performance of ShEn is greatly affected by the presence of artifacts, suggesting that other techniques such as multiscale frequency (MSF), Kurtosis (Kt), and Multiscale Entropy (MSE) provide more accurate and robust detection of rotors (Annoni et al., 2017) (Figure 6).

In a similar vein, Orozco-Duque et al. utilize approximate entropy (ApEn) (Richman and Moorman, 2000) for localizing rotors, under the hypothesis that CFAE are generated by the pivot point of a rotor (Orozco-Duque et al., 2013). Findings suggest that regions of high ApEn also co-located with the rotor pivot (Orozco-Duque et al., 2013). Ugarte et al. also study the relationships between CFAE and the rotor pivot using ApEn (Ugarte et al., 2014) (Figure 7), under the argument that a non-linear dynamic measure will better capture the property of fractionation in comparison to the empirical definitions proposed in the original CFAE study (Nademanee et al., 2004). After simulating AF in a 3D human atrial model, results showed a positive correlation between ApEn and levels of fractionation, suggesting the ability of high ApEn regions to co-locate areas of high fractionation, and in turn the rotor pivot (Ugarte et al., 2014). Sample entropy (SampEn) based approaches have also been explored for this purpose, with Cirugeda-Roldán et al. using SampEn to characterize the degree of fractionation in atrial electrograms (Cirugeda-Roldán et al., 2015). A specificity of 86% and a sensitivity of 77% was reported when discerning between CFAE and non-CFAE electrogram signals (Cirugeda-Roldán et al., 2015).

Investigating the mapping of rotors further, Hwang et al. examined ablation approaches based on Shannon entropy (ShEn) in both 2D and 3D models (Hwang et al., 2016) (Figure 8). The study compared ShEn to other rotor mapping approaches commonly used in literature, namely: phase singularities (PS), dominant frequency (DF), and CFAE cycle length (CFAE-CL) (Hwang et al., 2016). Results from virtual ablation showed that ShEn, PS and CFAE-CL guided approaches did not result in AF termination or modify the AF into slow atrial tachycardia, whilst virtual DF ablation successfully achieved these end-points (Hwang et al., 2016). Additionally, in 2D and 3D *in-silico* models, ShEn was shown to overlap with 33.2 and 27.5% of the rotor tip trajectory respectively, which was outperformed by DF wherein a 71 and 39.7% overlap was seen in the 2D and 3D models respectively (Hwang et al., 2016).

Outside of rotor mapping, entropy can also be used to study causality and information flow. Transfer entropy (TE), which determines the directed exchange of information between two systems (Schreiber, 2000), can be used to investigate the direction and degree of information flow between electrograms. In a study conducted by Kośna et al., TE was used to study information flow between electrograms recorded in the high right atrium (HRA), coronary sinus (CS), and left atrial appendage (LAA) (Kośna et al., 2015). Findings demonstrated that information flow in the heart is symmetric, and that the direction and amount of information flowing between neighboring sites in the atria could be quantified using TE (Kośna et al., 2015). This suggests that studying information flow between different areas of the atria may provide useful insights into the complex wave propagation dynamics during AF.

Recalling the connections between transfer entropy and Granger causality (GC) as discussed previously, work published by Alcaine et al. (2017) uses Granger causality based definitions to develop a multi-variate predictability framework to study

information flow and causal relationships between different cardiac sites during AF. Using GC, causal interactions were analyzed between different atrial sites during different rhythms, by considering EGM as stochastic processes that interacts with neighboring atrial sites through information exchange that is driven by atrial activity (Alcaine et al., 2017). Predictability measures were also obtained from the residual variances of linear predictions performed with multivariate autoregressive (MVAR) modeling of involved EGM signals (Alcaine et al., 2017). As such, Alcaine's framework provides a measure of regularity for individual EGMs, in addition to the connectivity between neighboring sites. Using computational simulations and clinical basket catheter data acquired from patients in paroxysmal AF, the study showed that the framework not only allowed different rhythms to be identified (using the regularity measures), but also that the underlying cardiac activity, acquired from simultaneous multi-electrode basket recordings, could be tracked and mapped using GC-based definitions (Alcaine et al., 2017). Although GC is a statistical concept rather than an information theoretic approach, this study demonstrates its connection to transfer entropy and its ability to also study causal relationships.

RESEARCH GAPS AND POTENTIAL FUTURE DEVELOPMENTS

Within the past decade, a number of EGM-based quantitative approaches have been developed for AF analysis. These approaches have brought several developments to the study of AF, however, clinical application of these techniques have yet to be achieved due to lack of reproducibility of promising results (Baumert et al., 2016). Underlying this may be the qualitative nature of these approaches, or their need for empirically-based definitions, as well as the lack of understanding of the complex AF mechanism. With this in mind, information theoretic measures may have the potential to provide new insights from study of the statistical properties of signals in AF using a purely quantitative approach.

Thus far, few information theoretic approaches have been explored in the context of atrial fibrillation, particularly in AF mapping applications. Further studies are required to explore the various characteristics of measures such as entropy during AF, and understand their relation to the AF physiology. For example, there is room for future studies to observe the spatial and temporal stability of EGM entropy, as this is an area that has not been investigated thus far. Understanding the spatiotemporal characteristics of AF may determine the presence or absence of spatial and temporal stability, which is important for developing novel adjunctive or primary ablation strategies based on high entropy regions as targets.

In addition to this, the relationships between information theoretic approaches to the micro and anatomical structure of the atrium is also yet to be explored. Anatomical co-registration may further reveal regions with a predisposition to forming rotors or other mechanisms that perpetuate AF, as well as electrical

pathways that may be important to AF propagation. Using information theoretic and statistical approaches such as transfer entropy (TE) or Granger causality (GC) to observe information flow between regions of the atria may also help shed light on this, as analysis of connectivity between atrial regions may help infer the wave propagation dynamics of AF, which are highly complex and presently limit the determination of effective ablation targets. Understanding these wave dynamics may again provide potential clinical insight that may lead to more effective ablation strategies.

CONCLUSION

Unfortunately, although AF has been a long-standing topic of research, there remains continuing debate regarding the mechanisms underlying the dynamics of the heart rhythm disorder (Schotten et al., 2011). Currently, there is some consensus that AF is the result of an interplay between substrate and triggering mechanism, though it is agreed that this interaction is not yet completely understood, nor is the triggering mechanism responsible.

Due to the complexity in understanding the AF phenomenon, establishing effective mapping approaches have proven hugely difficult, especially for real-time methods that can be used for guided ablation. While direct wavefront mapping during clinical AF procedures would be extremely valuable, current challenges make this approach practically impossible. With this in mind, a logical substitute is to take advantage of the intracardiac electrogram (EGM), which is the primary recording modality currently employed in electrophysiology (EP) clinics. Quantitative analysis of the EGM signal properties using information theoretic approaches has the potential to provide not only a clinically interpretable direct translation to what is seen in practice, but also insights into the system dynamics underlying AF. Aiming to understand the AF dynamics indirectly through analysis of the signal properties is not a left-field approach, as other well studied methods such as CFAE and DF use similar principles. Unlike these techniques however, information theoretic approaches have the benefit of being less reliant on empirically derived definitions.

In summary, while information theory has proved a useful tool for analysis of physiological signals in other fields, it remains underutilized and under-explored in AF studies. As the AF phenomena is far from being understood, understanding the arrhythmia from a signal property perspective and using new approaches may be key to determining effective ablation targets and strategies for the ever increasing AF population.

AUTHOR CONTRIBUTIONS

DD conducted the literature review, drafted the article, provided critical revision of the article and final approval of the version to be published. LD, AM, PK, and KP provided critical revision of the article and final approval of the version to be published. AG drafted the article, provided critical revision of the article and final approval of the version to be published.

REFERENCES

- Aftab, O., Cheung, P., Kim, A., Thakkar, S., and Yeddanapudi, N. (2001). *Information Theory and the Digital Age*. (Massachusetts, MA: Bandwagon), 9–11.
- Alcaine, A., Mase, M., Cristoforetti, A., Ravelli, F., Nollo, G., Laguna, P., et al. (2017). A multi-variate predictability framework to assess invasive cardiac activity and interactions during atrial fibrillation. *IEEE Trans. Biomed. Eng.* 64, 1157–1168. doi: 10.1109/TBME.2016.2592953
- Alcaraz, R., and Rieta, J. (2010). A novel application of sample entropy to the electrocardiogram of atrial fibrillation. *Nonlinear Anal.* 11, 1026–1035. doi: 10.1016/j.nonrwa.2009.01.047
- Alcaraz, R., and Rieta, J. J. (2009a). Sample entropy of the main atrial wave predicts spontaneous termination of paroxysmal atrial fibrillation. *Med. Eng. Phys.* 31, 917–922. doi: 10.1016/j.medengphy.2009.05.002
- Alcaraz, R., and Rieta, J. J. (2009b). Non-invasive organization variation assessment in the onset and termination of paroxysmal atrial fibrillation. *Comput. Methods Programs Biomed.* 93, 148–154. doi: 10.1016/j.cmpb.2008.09.001
- Allessie, M. A., de Groot, N. M., Houben, R. P., Schotten, U., Boersma, E., Smeets, J. L., et al. (2010). Electrophysiological substrate of long-standing persistent atrial fibrillation in patients with structural heart disease: clinical perspective: longitudinal dissociation. *Circulation* 3, 606–615. doi: 10.1161/CIRCEP.109.910125
- Amar, D., Zhang, H., Miodownik, S., and Kadish, A. H. (2003). Competing autonomic mechanisms precede the onset of postoperative atrial fibrillation. *J. Am. Coll. Cardiol.* 42, 1262–1268. doi: 10.1016/S0735-1097(03)00955-0
- Annoni, E. M., Arunachalam, S. P., Kapa, S., Mulpuru, S. K., Friedman, P. A., and Talkachova, E. G. (2017). “Novel quantitative analytical approaches for rotor identification and associated implications for mapping,” in *IEEE Transactions on Biomedical Engineering* (Minnesota, MN)
- Arunachalam, S. P., Mulpuru, S. K., Friedman, P. A., and Tolkacheva, E. G. (2015). “Feasibility of visualizing higher regions of Shannon entropy in atrial fibrillation patients,” in *Engineering in Medicine and Biology Society (EMBC), 37th Annual International Conference of the IEEE, 2015* (Minnesota, MN: IEEE).
- Barnett, L., Barrett, A. B., and Seth, A. K. (2009). Granger causality and transfer entropy are equivalent for Gaussian variables. *Phys. Rev. Lett.* 103:238701. doi: 10.1103/PhysRevLett.103.238701
- Baumert, M., Sanders, P., and Ganesan, A. (2016). Quantitative-electrogram-based methods for guiding catheter ablation in atrial fibrillation. *Proc. IEEE* 104, 416–431. doi: 10.1109/JPROC.2015.2505318
- Ben-Mizrachi, A., Procaccia, I., and Grassberger, P. (1984). Characterization of experimental (noisy) strange attractors. *Phys. Rev. A* 29:975. doi: 10.1103/PhysRevA.29.975
- Berenfeld, O., and Jalife, J. (2011). Complex fractionated atrial electrograms: is this the beast to tame in atrial fibrillation? *Circ. Arrhythm. Electrophysiol.* 4, 426–428. doi: 10.1161/CIRCEP.111.964841
- Busa, M. A., and van Emmerik, R. E. (2016). Multiscale entropy: A tool for understanding the complexity of postural control. *J. Sport Health Sci.* 5, 44–51. doi: 10.1016/j.jshs.2016.01.018
- Carrara, M., Carozzi, L., Moss, T. J., de Pasquale, M., Cerutti, S., Ferrario, M., et al. (2015a). Heart rate dynamics distinguish among atrial fibrillation, normal sinus rhythm and sinus rhythm with frequent ectopy. *Physiol. Meas.* 36:1873. doi: 10.1088/0967-3334/36/9/1873
- Carrara, M., Carozzi, L., Moss, T. J., de Pasquale, M., Cerutti, S., Lake, D. E., et al. (2015b). Classification of cardiac rhythm using heart rate dynamical measures: validation in MIT-BIH databases. *J. Electrocardiol.* 48, 943–946. doi: 10.1016/j.jelectrocard.2015.08.002
- Chamchad, D., Horow, J. C., Samuels, L. E., and Nakhamchik, L. (2011). Heart rate variability measures poorly predict atrial fibrillation after off-pump coronary artery bypass grafting. *J. Clin. Anesth.* 23, 451–455. doi: 10.1016/j.jclinane.2010.12.016
- Chen, J., Lin, Y., Chen, L., Yu, J., Du, Z., Li, S., et al. (2014). A decade of complex fractionated electrograms catheter-based ablation for atrial fibrillation: literature analysis, meta-analysis and systematic review. *IJC Heart Vessels* 4, 63–72. doi: 10.1016/j.ijchv.2014.06.013
- Cirugeda-Roldán, E., Novak, D., Kremen, V., Cuesta-Frau, D., Keller, M., Luik, A., et al. (2015). Characterization of complex fractionated atrial electrograms by sample entropy: an international multi-center study. *Entropy* 17, 7493–7509. doi: 10.3390/e17117493
- Costa, M., and Healey, J. (2003). “Multiscale entropy analysis of complex heart rate dynamics: discrimination of age and heart failure effects,” in *Computers in Cardiology 2003* (Boston, MA: IEEE).
- Costa, M., Goldberger, A. L., and Peng, C.-K. (2002b). Multiscale entropy analysis of complex physiologic time series. *Phys. Rev. Lett.* 89:068102. doi: 10.1103/PhysRevLett.89.068102
- Costa, M., Goldberger, A. L., and Peng, C.-K. (2005). Multiscale entropy analysis of biological signals. *Phys. Rev. E* 71:021906. doi: 10.1103/PhysRevE.71.021906
- Costa, M., Goldberger, A., and Peng, C.-K. (2002a). Multiscale entropy to distinguish physiologic and synthetic RR time series. *Comput. Cardiol.* 29, 137–140 doi: 10.1109/CIC.2002.1166726
- Cover, T. M., and Thomas, J. A. (1991). Entropy, relative entropy and mutual information. *Elements Inform. Theor.* 2, 1–55.
- Cui, X., Chang, E., Yang, W. H., Jiang, B. C., Yang, A. C., and Peng, C.-K. (2017). Automated detection of paroxysmal atrial fibrillation using an information-based similarity approach. *Entropy* 19:677. doi: 10.3390/e19120677
- Dash, S., Chon, K., Lu, S., and Raeder, E. (2009). Automatic real time detection of atrial fibrillation. *Ann. Biomed. Eng.* 37, 1701–1709. doi: 10.1007/s10439-009-9740-z
- Dawes, G., Moulden, M., Sheila, O., and Redman, C. (1992). Approximate entropy, a statistic of regularity, applied to fetal heart rate data before and during labor. *Obstet. Gynecol.* 80, 763–768.
- de Bakker, J. M., and Wittkampf, F. H. (2010). The pathophysiologic basis of fractionated and complex electrograms and the impact of recording techniques on their detection and interpretation. *Circ. Arrhythm. Electrophysiol.* 3, 204–213. doi: 10.1161/CIRCEP.109.904763
- Eckmann, J. P., and Ruelle, D. (1985). “Ergodic theory of chaos and strange attractors,” in *The Theory of Chaotic Attractors*, eds B. R. Hunt, T. Y. Li, J. A. Kennedy, H. E. Nusse (New York, NY: Springer), 273–312.
- Elvan, A., Linnenbank, A. C., A. Misier, R. R., P. Delnoy, P. H., Beukema, W. P., and Jacques, M. (2009). Dominant frequency of atrial fibrillation correlates poorly with atrial fibrillation cycle length. *Circ. Arrhythm. Electrophysiol.* 2, 634–644. doi: 10.1161/CIRCEP.108.843284
- Ephremides, A. (2009). “How information theory changed the world—a brief review of the history of the information theory society,” in *2009 IEEE Conference on the History of Technical Societies* (IEEE).
- Faes, L., Porta, A., Javorka, M., and Nollo, G. (2017). Efficient computation of multiscale entropy over short biomedical time series based on linear state-space models. *Complexity* 2017:1768264. doi: 10.1155/2017/1768264
- Fleisher, L. A., Dipietro, J. A., Johnson, T. R., and Pincus, S. (1997). Complementary and non-coincident increases in heart rate variability and irregularity during fetal development. *Clin. Sci.* 92, 345–349. doi: 10.1042/cs0920345
- Fleisher, L. A., Pincus, S. M., and Rosenbaum, S. H. (1993). Approximate entropy of heart rate as a correlate of postoperative ventricular dysfunction. *Anesthesiology* 78, 683–692. doi: 10.1097/00000542-199304000-00011
- Ganesan, A. N., Kuklik, P., Gharaviri, A., Brooks, A., Chapman, D., Lau, D. H., et al. (2014). Origin and characteristics of high Shannon entropy at the pivot of locally stable rotors: insights from computational simulation. *PLoS ONE* 9:e110662. doi: 10.1371/journal.pone.0110662
- Ganesan, A. N., Kuklik, P., Lau, D. H., Brooks, A. G., Baumert, M., Lim, W. W., et al. (2012). Bipolar electrogram shannon entropy at sites of rotational activation: implications for ablation of atrial fibrillation. *Circ. Arrhythm. Electrophysiol.* 6, 48–57. doi: 10.1161/CIRCEP.112.976654
- Goldberger, A. L., Mietus, J. E., Rigney, D. R., Wood, M. L., and Fortney, S. M. (1994). Effects of head-down bed rest on complex heart rate variability: response to LBNP testing. *J. Appl. Physiol.* 77, 2863–2869. doi: 10.1152/jappl.1994.77.6.2863
- Grassberger, P. (1988). Finite sample corrections to entropy and dimension estimates. *Phys. Lett. A* 128, 369–373. doi: 10.1016/0375-9601(88)90193-4
- Grassberger, P., and Procaccia, I. (1983). Estimation of the Kolmogorov entropy from a chaotic signal. *Phys. Rev. A* 28:2591. doi: 10.1103/PhysRevA.28.2591
- Grassberger, P., Schreiber, T., and Schaffrath, C. (1991). Nonlinear time sequence analysis. *Int. J. Bifurc. Chaos* 1, 521–547. doi: 10.1142/S0218127491000403
- Gray, R. M. (2011). *Entropy and Information Theory*. New York, NY: Springer Science & Business Media.

- Haissaguerre, M., Jaïs, P., Shah, D. C., Takahashi, A., Hocini, M., Quiniou, G., et al. (1998). Spontaneous initiation of atrial fibrillation by ectopic beats originating in the pulmonary veins. *N. Engl. J. Med.* 339, 659–666. doi: 10.1056/NEJM199809033391003
- Hayward, R. M., Upadhyay, G. A., Mela, T., Ellinor, P. T., Barrett, C. D., Heist, E. K., et al. (2011). Pulmonary vein isolation with complex fractionated atrial electrogram ablation for paroxysmal and nonparoxysmal atrial fibrillation: a meta-analysis. *Heart Rhythm* 8, 994–1000. doi: 10.1016/j.hrthm.2011.02.033
- Ho, K. K., Moody, G. B., Peng, C.-K., Mietus, J. E., Larson, M. G., Levy, D., et al. (1997). Predicting survival in heart failure case and control subjects by use of fully automated methods for deriving nonlinear and conventional indices of heart rate dynamics. *Circulation* 96, 842–848. doi: 10.1161/01.CIR.96.3.842
- Hogue, C. W., Domitrovich, P. P., Stein, P. K., Despotis, G. D., Re, L., Schuessler, R. B., et al. (1998). RR interval dynamics before atrial fibrillation in patients after coronary artery bypass graft surgery. *Circulation* 98, 429–434. doi: 10.1161/01.CIR.98.5.429
- Humeau-Heurtier, A. (2015). The multiscale entropy algorithm and its variants: a review. *Entropy* 17, 3110–3123. doi: 10.3390/e17053110
- Hwang, M., Song, J.-S., Lee, Y.-S., Li, C., Shim, E. B., and Pak, H.-N. (2016). Electrophysiological rotor ablation in *in-silico* modeling of atrial fibrillation: comparisons with dominant frequency, Shannon entropy, and phase singularity. *PLoS ONE* 11:e0149695. doi: 10.1371/journal.pone.0149695
- Jalife, J., Berenfeld, O., and Mansour, M. (2002). Mother rotors and fibrillatory conduction: a mechanism of atrial fibrillation. *Cardiovasc. Res.* 54, 204–216. doi: 10.1016/S0008-6363(02)00223-7
- Konings, K. T., Smeets, J. L., Penn, O. C., Wellens, H. J., and Allessie, M. A. (1997). Configuration of unipolar atrial electrograms during electrically induced atrial fibrillation in humans. *Circulation* 95, 1231–1241. doi: 10.1161/01.CIR.95.5.1231
- Konings, K., Kirchhof, C., Smeets, J., Wellens, H., Penn, O. C., and Allessie, M. A. (1994). High-density mapping of electrically induced atrial fibrillation in humans. *Circulation* 89, 1665–1680. doi: 10.1161/01.CIR.89.4.1665
- Korpelainen, J. T., Sotaniemi, K. A., Mäkkilä, A., Huikuri, H. V., and Myllylä, V. V. (1999). Dynamic behavior of heart rate in ischemic stroke. *Stroke* 30, 1008–1013. doi: 10.1161/01.STR.30.5.1008
- Kośna, K., Steven, D., Willems, S., Zebrowski, J. J., and Kuklik, P. (2015). “Causality in Atrial Fibrillation determined by transfer entropy,” in *Computing in Cardiology Conference (CinC) 2015* (IEEE).
- Lake, D. E., and Moorman, J. R. (2010). Accurate estimation of entropy in very short physiological time series: the problem of atrial fibrillation detection in implanted ventricular devices. *Am. J. Physiol. Heart Circ. Physiol.* 300, H319–H325. doi: 10.1152/ajpheart.00561.2010
- Lee, J., McManus, D., and Chon, K. (2011). “Atrial Fibrillation detection using time-varying coherence function and Shannon Entropy,” in *Engineering in Medicine and Biology Society, EMBC, Annual International Conference of the IEEE, 2011* (Boston, MA: IEEE).
- Li, W.-J., Bai, Y.-Y., Zhang, H.-Y., Tang, R.-B., Miao, C.-J., Sang, C.-H., et al. (2011). Additional ablation of complex fractionated atrial electrograms after pulmonary vein isolation in patients with atrial fibrillation—clinical perspective: a meta-analysis. *Circ. Arrhyth. Electrophysiol.* 4, 143–148. doi: 10.1161/CIRCEP.110.958405
- Lipsitz, L. A., Pincus, S. M., Morin, R. J., Tong, S., Eberle, L. P., and Gootman, P. M. (1997). Preliminary evidence for the evolution in complexity of heart rate dynamics during autonomic maturation in neonatal swine. *J. Auton. Nerv. Syst.* 65, 1–9. doi: 10.1016/S0165-1838(97)00028-3
- Lombardi, O., Holik, F., and Vanni, L. (2016). What is Shannon information? *Synthese* 193, 1983–2012. doi: 10.1007/s11229-015-0824-z
- Mäkkilä, T. H., Ristimäe, T., Airaksinen, K. J., Peng, C.-K., Goldberger, A. L., and Huikuri, H. V. (1998). Heart rate dynamics in patients with stable angina pectoris and utility of fractal and complexity measures. *Am. J. Cardiol.* 81, 27–31. doi: 10.1016/S0002-9149(97)00799-6
- Mäkkilä, T. H., Seppänen, T., Niemelä, M., Airaksinen, K. J., Tulppo, M., and Huikuri, H. V. (1996). Abnormalities in beat to beat complexity of heart rate dynamics in patients with a previous myocardial infarction. *J. Am. Coll. Cardiol.* 28, 1005–1011. doi: 10.1016/S0735-1097(96)00243-4
- Masè, M., Faes, L., Antolini, R., Scaglione, M., and Ravelli, F. (2005). Quantification of synchronization during atrial fibrillation by Shannon entropy: validation in patients and computer model of atrial arrhythmias. *Physiol. Meas.* 26, 911–923. doi: 10.1088/0967-3334/26/6/003
- Nademanee, K., and Oktetani, N. (2009). The role of complex fractionated atrial electrograms in atrial fibrillation ablation: moving to the beat of a different drum. *J. Am. Coll. Cardiol.* 53, 790–791. doi: 10.1016/j.jacc.2008.11.022
- Nademanee, K., McKenzie, J., Kosar, E., Schwab, M., Sunsaneewitayakul, B., Vasavakul, T., et al. (2004). A new approach for catheter ablation of atrial fibrillation: mapping of the electrophysiologic substrate. *J. Am. Coll. Cardiol.* 43, 2044–2053. doi: 10.1016/j.jacc.2003.12.054
- Narayan, S. M., Krummen, D. E., Shivkumar, K., Clopton, P., Rappel, W.-J., and Miller, J. M. (2012). Treatment of atrial fibrillation by the ablation of localized sources: CONFIRM (Conventional Ablation for Atrial Fibrillation With or Without Focal Impulse and Rotor Modulation) trial. *J. Am. Coll. Cardiol.* 60, 628–636. doi: 10.1016/j.jacc.2012.05.022
- Nelson, J. C., Griffin, M. P., and Moorman, J. R. (1998). Probing the order within neonatal heart rate variability. *Pediatr. Res.* 43, 823–831. doi: 10.1203/00006450-199806000-00017
- Ng, J., Kadish, A. H., and Goldberger, J. J. (2006). Effect of electrogram characteristics on the relationship of dominant frequency to atrial activation rate in atrial fibrillation. *Heart Rhythm* 3, 1295–1305. doi: 10.1016/j.hrthm.2006.07.027
- Orozco-Duque, A., Ugarté, J. P., Tobón, C., Saiz, J., and Bustamante, J. (2013). “Approximate entropy can localize rotors, but not ectopic foci during chronic atrial fibrillation: a simulation study,” in *Computing in Cardiology Conference (CinC) 2013* (Zaragoza: IEEE).
- Palazzolo, J. A., Estafanous, F. G., and Murray, P. A. (1998). Entropy measures of heart rate variation in conscious dogs. *Am. J. Physiol. Heart Circ. Physiol.* 274, H1099–H1105. doi: 10.1152/ajpheart.1998.274.4.H1099
- Pincus, S. M. (1991). Approximate entropy as a measure of system complexity. *Proc. Natl. Acad. Sci. U.S.A.* 88, 2297–2301. doi: 10.1073/pnas.88.6.2297
- Pincus, S. M., Cummins, T. R., and Haddad, G. G. (1993). Heart rate control in normal and aborted-SIDS infants. *Am. J. Physiol. Regul. Integr. Comp. Physiol.* 264, R638–R646. doi: 10.1152/ajpregu.1993.264.3.R638
- Pincus, S. M., Gladstone, I. M., and Ehrenkranz, R. A. (1991). A regularity statistic for medical data analysis. *J. Clin. Monit.* 7, 335–345. doi: 10.1007/BF01619355
- Purwani, S., Nahar, J., and Twining, C. (2017). “Analyzing bin-width effect on the computed entropy,” in *AIP Conference Proceedings* (Yogyakarta: AIP Publishing).
- Richman, J. S., and Moorman, J. R. (2000). Physiological time-series analysis using approximate entropy and sample entropy. *Am. J. Physiol. Heart Circ. Physiol.* 278, H2039–H2049. doi: 10.1152/ajpheart.2000.278.6.H2039
- Richman, J. S., Lake, D. E., and Moorman, J. R. (2004). Sample entropy. *Meth. Enzymol.* 384, 172–184. doi: 10.1016/S0076-6879(04)84011-4
- Ródenas, J., García, M., Alcaraz, R., and Rieta, J. J. (2015). Wavelet entropy automatically detects episodes of atrial fibrillation from single-lead electrocardiograms. *Entropy* 17, 6179–6199. doi: 10.3390/e17096179
- Rosso, O. A., Blanco, S., Yordanova, J., Kolev, V., Figliola, A., Schürmann, M., et al. (2001). Wavelet entropy: a new tool for analysis of short duration brain electrical signals. *J. Neurosci. Methods* 105, 65–75. doi: 10.1016/S0165-0270(00)00356-3
- Ryan, S. M., Goldberger, A. L., Pincus, S. M., Mietus, J., and Lipsitz, L. A. (1994). Gender-and age-related differences in heart rate dynamics: are women more complex than men? *J. Am. Coll. Cardiol.* 24, 1700–1707. doi: 10.1016/0735-1097(94)90177-5
- Sanders, P., Berenfeld, O., Hocini, M., Jaïs, P., Vaidyanathan, R., Hsu, L.-F., et al. (2005). Spectral analysis identifies sites of high-frequency activity maintaining atrial fibrillation in humans. *Circulation* 112, 789–797. doi: 10.1161/CIRCULATIONAHA.104.517011
- Sanders, P., Nalliah, C. J., Dubois, R., Takahashi, Y., Hocini, M., Rotter, M., et al. (2006). Frequency mapping of the pulmonary veins in paroxysmal versus permanent atrial fibrillation. *J. Cardiovasc. Electrophysiol.* 17, 965–972. doi: 10.1111/j.1540-8167.2006.00546.x
- Schotten, U., Verheule, S., Kirchhof, P., and Goette, A. (2011). Pathophysiological mechanisms of atrial fibrillation: a translational appraisal. *Physiol. Rev.* 91, 265–325. doi: 10.1152/physrev.00031.2009
- Schreiber, T. (2000). Measuring information transfer. *Phys. Rev. Lett.* 85, 461–464. doi: 10.1103/PhysRevLett.85.461

- Schuckers, S. A. C. (1998). Use of approximate entropy measurements to classify ventricular tachycardia and fibrillation. *J. Electrocardiol.* 31, 101–105. doi: 10.1016/S0022-0736(98)90300-4
- Schuessler, R. B., Grayson, T. M., Bromberg, B. I., Cox, J. L., and Boineau, J. P. (1992). Cholinergically mediated tachyarrhythmias induced by a single extrastimulus in the isolated canine right atrium. *Circ. Res.* 71, 1254–1267. doi: 10.1161/01.RES.71.5.1254
- Shannon, C. (1948). A Mathematical Theory of Communication. *Bell Syst. Techn. J.* 27, 379–423, 623–656. doi: 10.1002/j.1538-7305.1948.tb00917.x
- Shin, D.-G., Yoo, C.-S., Yi, S.-H., Bae, J.-H., Kim, Y.-J., Park, J.-S., et al. (2006). Prediction of paroxysmal atrial fibrillation using nonlinear analysis of the RR interval dynamics before the spontaneous onset of atrial fibrillation. *Circ. J.* 70, 94–99. doi: 10.1253/circj.70.94
- Skanes, A. C., Mandapati, R., Berenfeld, O., Davidenko, J. M., and Jalife, J. (1998). Spatiotemporal periodicity during atrial fibrillation in the isolated sheep heart. *Circulation* 98, 1236–1248. doi: 10.1161/01.CIR.98.12.1236
- Sungnoon, R., Muengtaewpongsa, S., Kitipawong, P., Suwanprasert, K., and Ngarmukos, T. (2012). “Increased sample entropy in atrial fibrillation relates to cardiac autonomic dysfunction determined by heart rate variability: a preliminary study,” in *Biomedical Engineering International Conference (BMEICON) 2012* (Ubon Ratchathani: IEEE).
- Tedrow, U. B., and Stevenson, W. G. (2011). Recording and interpreting unipolar electrograms to guide catheter ablation. *Heart Rhythm* 8, 791–796. doi: 10.1016/j.hrthm.2010.12.038
- Traykov, V. B., Pap, R., and Sághy, L. (2012). Frequency domain mapping of atrial fibrillation-methodology, experimental data and clinical implications. *Curr. Cardiol. Rev.* 8, 231–238. doi: 10.2174/157340312803217229
- Tulppo, M. P., Makikallio, T., Takala, T., Seppanen, T., and Huikuri, H. V. (1996). Quantitative beat-to-beat analysis of heart rate dynamics during exercise. *Am. J. Physiol. Heart Circ. Physiol.* 271, H244–H252. doi: 10.1152/ajpheart.1996.271.1.H244
- Tuzcu, V., Nas, S., Börklü, T., and Ugur, A. (2006). Decrease in the heart rate complexity prior to the onset of atrial fibrillation. *Europace* 8, 398–402. doi: 10.1093/europace/eul031
- Ugarte, J. P., Orozco-Duque, A., Tobón, C., Kremen, V., Novak, D., Saiz, J., et al. (2014). Dynamic approximate entropy electroanatomic maps detect rotors in a simulated atrial fibrillation model. *PLoS ONE* 9:e114577. doi: 10.1371/journal.pone.0114577
- Vajapeyam, S. (2014). Understanding Shannon’s Entropy metric for Information. *arXiv preprint arXiv: 1405.2061*.
- Valencia, J. F., Porta, A., Vallverdu, M., Claria, F., Baranowski, R., Orlowska-Baranowska, E., et al. (2009). Refined multiscale entropy: application to 24-h holter recordings of heart period variability in healthy and aortic stenosis subjects. *IEEE Trans. Biomed. Eng.* 56, 2202–2213. doi: 10.1109/TBME.2009.2021986
- van der Does, L. J., and de Groot, N. M. (2017). Inhomogeneity and complexity in defining fractionated electrograms. *Heart Rhythm* 14, 616–624. doi: 10.1016/j.hrthm.2017.01.021
- Vaquero, M., Calvo, D., and Jalife, J. (2008). Cardiac fibrillation: from ion channels to rotors in the human heart. *Heart Rhythm* 5, 872–879. doi: 10.1016/j.hrthm.2008.02.034
- Verdu, S. (1998). Fifty years of Shannon theory. *IEEE Trans. Inform. Theor.* 44, 2057–2078. doi: 10.1109/18.720531
- Verma, A., Jiang, C.-Y., Betts, T. R., Chen, J., Deisenhofer, I., Mantovan, R., et al. (2015). *Approaches to Catheter Ablation for Persistent Atrial Fibrillation*. *New Engl. J. Med.* 372, 1812–1822. doi: 10.1056/NEJMoa1408288
- Vicente, R., Wibral, M., Lindner, M., and Pipa, G. (2011). Transfer entropy—a model-free measure of effective connectivity for the neurosciences. *J. Comput. Neurosci.* 30, 45–67. doi: 10.1007/s10827-010-0262-3
- Vikman, S., Mäkkilä, T. H., Yli-Mäyry, S., Pikkujämsä, S., Koivisto, A.-M., Reinikainen, P., et al. (1999). Altered complexity and correlation properties of RR interval dynamics before the spontaneous onset of paroxysmal atrial fibrillation. *Circulation* 100, 2079–2084. doi: 10.1161/01.CIR.100.2.2079
- Waks, J. W., and Josephson, M. E. (2014). Mechanisms of atrial fibrillation-reentry, rotors and reality. *Arrhythm. Electrophysiol. Rev.* 3, 90–100. doi: 10.15420/aer.2014.3.2.90
- Wells, J. L., Karp, R. B., Kouchoukos, N. T., Maclean, W. A., James, T. N., and Waldo, A. L. (1978). Characterization of atrial fibrillation in man: studies following open heart surgery. *Pacing Clin. Electrophysiol.* 1, 426–438. doi: 10.1111/j.1540-8159.1978.tb03504.x
- Wu, S.-D., Wu, C. W., Lin, S.-G., Wang, C.-C., and Lee, K.-Y. (2013). Time series analysis using composite multiscale entropy. *Entropy* 15, 1069–1084. doi: 10.3390/e15031069
- Xiong, W., Faes, L., and Ivanov, P. C. (2017). Entropy measures, entropy estimators, and their performance in quantifying complex dynamics: effects of artifacts, nonstationarity, and long-range correlations. *Phys. Rev. E* 95:062114. doi: 10.1103/PhysRevE.95.062114
- Yentes, J. M., Hunt, N., Schmid, K. K., Kaipust, J. P., McGrath, D., and Stergiou, N. (2013). The appropriate use of approximate entropy and sample entropy with short data sets. *Ann. Biomed. Eng.* 41, 349–365. doi: 10.1007/s10439-012-0668-3
- Zhang, Y.-C. (1991). Complexity and 1/f noise. A phase space approach. *J. Phys. I* 1, 971–977. doi: 10.1051/jp1:1991180
- Zhou, X., Ding, H., Ung, B., Pickwell-MacPherson, E., and Zhang, Y. (2014). Automatic online detection of atrial fibrillation based on symbolic dynamics and Shannon entropy. *Biomed. Eng. Online* 13:18. doi: 10.1186/1475-925X-13-18

Conflict of Interest Statement: The authors declare that the research was conducted in the absence of any commercial or financial relationships that could be construed as a potential conflict of interest.

Copyright © 2018 Dharmapran, Dykes, McGavigan, Kuklik, Pope and Ganesan. This is an open-access article distributed under the terms of the Creative Commons Attribution License (CC BY). The use, distribution or reproduction in other forums is permitted, provided the original author(s) and the copyright owner(s) are credited and that the original publication in this journal is cited, in accordance with accepted academic practice. No use, distribution or reproduction is permitted which does not comply with these terms.



A Heart for Diversity: Simulating Variability in Cardiac Arrhythmia Research

Haibo Ni, Stefano Morotti and Eleonora Grandi*

Department of Pharmacology, University of California, Davis, Davis, CA, United States

OPEN ACCESS

Edited by:

Oleg Aslanidi,
King's College London,
United Kingdom

Reviewed by:

Stefano Severi,
Università degli Studi di Bologna, Italy
Emilia Entcheva,
George Washington University,
United States

***Correspondence:**

Eleonora Grandi
ele.grandi@gmail.com

Specialty section:

This article was submitted to
Computational Physiology and
Medicine,
a section of the journal
Frontiers in Physiology

Received: 30 April 2018

Accepted: 29 June 2018

Published: 20 July 2018

Citation:

Ni H, Morotti S and Grandi E (2018) A Heart for Diversity: Simulating Variability in Cardiac Arrhythmia Research. *Front. Physiol.* 9:958.
doi: 10.3389/fphys.2018.00958

In cardiac electrophysiology, there exist many sources of inter- and intra-personal variability. These include variability in conditions and environment, and genotypic and molecular diversity, including differences in expression and behavior of ion channels and transporters, which lead to phenotypic diversity (e.g., variable integrated responses at the cell, tissue, and organ levels). These variabilities play an important role in progression of heart disease and arrhythmia syndromes and outcomes of therapeutic interventions. Yet, the traditional *in silico* framework for investigating cardiac arrhythmias is built upon a parameter/property-averaging approach that typically overlooks the physiological diversity. Inspired by work done in genetics and neuroscience, new modeling frameworks of cardiac electrophysiology have been recently developed that take advantage of modern computational capabilities and approaches, and account for the variance in the biological data they are intended to illuminate. In this review, we outline the recent advances in statistical and computational techniques that take into account physiological variability, and move beyond the traditional cardiac model-building scheme that involves averaging over samples from many individuals in the construction of a highly tuned composite model. We discuss how these advanced methods have harnessed the power of big (simulated) data to study the mechanisms of cardiac arrhythmias, with a special emphasis on atrial fibrillation, and improve the assessment of proarrhythmic risk and drug response. The challenges of using *in silico* approaches with variability are also addressed and future directions are proposed.

Keywords: **cardiac electrophysiology, physiological variability, computational modeling, arrhythmia mechanisms, big data**

INTRODUCTION

Beginning with the seminal paper by Hodgkin and Huxley, 1952, mathematical models of electrophysiology have proven to be valuable tools for better understanding many physiological processes, especially in cardiac arrhythmia research (Noble et al., 2012; Dibb et al., 2015). Fifty-six years after publication of the first cardiac model (Noble, 1962), there is currently a computational model for almost every cell type of the heart, including nodal, atrial, ventricular, and Purkinje cells (Beeler and Reuter, 1977; Difrancesco and Noble, 1985; Luo and Rudy, 1991; Inada et al., 2009; Maltsev and Lakatta, 2009; Sampson et al., 2010; Grandi et al., 2011; O'Hara et al., 2011), for

numerous species, and for various levels of complexity across multiple spatial scales (e.g., inclusion of disease-associated remodeling, drug action, contractile, energetics, and signaling modules) (Fink et al., 2011). Most of these models use average data from voltage-clamp experiments of individual ionic membrane currents, and while they have led to many important advances in studies of cardiac electrophysiology and pathology, especially cardiac arrhythmias (Sepulveda et al., 1989; Courtemanche and Winfree, 1991; Panfilov and Holden, 1991; Gray et al., 1995; Krogh-Madsen and Christini, 2012; Roberts et al., 2012; Bueno-Orovio et al., 2014), they typically represent the average behavior of a particular cell type. Because these models ignore evident inter- and intra-personal variability, they can fail to capture the properties of any given individual cell or cells in a given patient (Golowasch et al., 2002; Dokos and Lovell, 2004; Sarkar and Sobie, 2010; Marder, 2011; Zaniboni, 2011; Groenendaal et al., 2015; Pathmanathan et al., 2015). This is in part because incorporating variance that reflects biological data into cardiac models requires significant computational capacity, particularly as compared to what was available when mathematical modeling of electrophysiology first emerged. Given ever-increasing computational capabilities, new modeling approaches have been developed to reproduce and analyze the immense physiological diversity observed in electrophysiology.

In this review, we discuss the importance of accounting for variability when building models of cardiac electrophysiology in both physiological and diseased conditions, and describe new tools being developed to address the limitations of traditional modeling approaches. In particular, we focus on two computational approaches that have emerged as leading methodologies for studying variability in cardiac electrophysiology, which we will refer to as (1) population-based modeling and (2) sample-specific modeling. Both methodologies have provided valuable insights in the fields of neuroscience, cardiology, and pharmacology. Here we review how they have advanced our understanding of the basic mechanisms of cardiac arrhythmias, and particularly atrial fibrillation (AF). As these *in silico* approaches have led to important insights into arrhythmia risks, mechanisms of arrhythmogenesis, and variable response to drugs, they should be considered when determining the regulatory requirements for the proarrhythmia assessment and drug efficacy and safety evaluation of candidate compounds.

Abbreviations: AF, atrial fibrillation; AP, action potential; APD, AP duration; cAF, chronic AF; CaT, Ca^{2+} transient; CiPA, Comprehensive *in vitro* Proarrhythmia Assay; DAD, delayed afterdepolarization; dLQTS, drug-induced long QT syndrome; EAD, early afterdepolarization; ECG, electrocardiogram; FRD, forward rate dependence; GA, genetic algorithm; hERG, human *ether-a-go-go*-related gene; hMSCs, human mesenchymal stem cells; I_{CaL} , L-type Ca^{2+} current; I_{to} , transient outward K^{+} current; I_{Kur} , ultra-rapid delayed-rectifier K^{+} current; I_{Kr} , rapid delayed-rectifier K^{+} current; I_{ks} , slow delayed-rectifier K^{+} current; I_{K1} , inward rectifier K^{+} current; I_{Na} , fast Na^{+} current; I_{NaL} , late Na^{+} current; iPSC-CM, induced pluripotent stem-cell-derived cardiomyocyte; LHS, latin hypercube sampling; LQT3, long QT syndrome type 3; NCX, $\text{Na}^{+}/\text{Ca}^{2+}$ exchanger; nSR, normal sinus rhythm; SERCA, sarco/endoplasmic reticulum Ca^{2+} -ATPase; TdP, torsades de pointes.

IMPORTANCE OF TAKING INTO ACCOUNT VARIABILITY IN CARDIAC ELECTROPHYSIOLOGY

Sources of variability in cardiac electrophysiology encompass multiple spatial and temporal scales, and include inter-species (Sham et al., 1995; Su et al., 2003), inter-ethnic (Lau et al., 2012; Fender et al., 2014), inter-subject (Taneja et al., 2001; Batchvarov et al., 2002), regional (Feng et al., 1998; Yan et al., 1998), and temporal (Jeyaraj et al., 2012) differences. Variability in experimental electrophysiological data does not only represent natural physiological diversity, but also reflects, in part, differences in the experimental conditions in which electrophysiological measurements are performed (Groenendaal et al., 2015). These conditions can vary from laboratory to laboratory (Niederer et al., 2009; Fink et al., 2011), experiment to experiment, or during the same experiment, e.g., due to deterioration of the experimental preparations over time (Fink et al., 2011). There is also instrument noise (Mirams et al., 2016), artifacts, and use of non-physiological temperatures and solutions (Groenendaal et al., 2015), all of which impact the structure and function of the cellular or tissue components being studied. These sources of variation are difficult to control even for experienced electrophysiologists and are equally as challenging to account for by modelers.

Mathematical cardiomyocyte models have remained useful tools for unraveling physiological and pathophysiological mechanisms, including mechanisms of arrhythmia, and identifying antiarrhythmic strategies without accounting for variability (Sepulveda et al., 1989; Courtemanche and Winfree, 1991; Clancy and Rudy, 1999, 2002; Clancy et al., 2002; Rivolta et al., 2002; Gong et al., 2007; Noble et al., 2007; Tsujimae et al., 2007; Zhang et al., 2007; Zhu and Clancy, 2007; Campbell et al., 2008; Comtois et al., 2008; Kharche et al., 2008; Sale et al., 2008; Ahrens-Nicklas et al., 2009; Butters et al., 2010; Adeniran et al., 2012; Edwards et al., 2014; Grandi and Malek, 2016; Morotti et al., 2016; Ni et al., 2017). Although average models have also been successfully applied to the study of sources of variability, such as sexual and hormonal factors (Yang et al., 2010, 2017; Yang and Clancy, 2012), age (Behar and Yaniv, 2017), and circadian regulation (Fotiadis and Forger, 2013), the rationale for developing novel computational approaches that specifically account for electrophysiological variability can be summarized by two main reasons.

Average Data May Not Accurately Represent Any Specific Individual or Behavior Well

The traditional cardiac model-building scheme involves averaging over samples from multiple experiments from many individuals, both to parameterize the model and validate it, which may not represent any specific measured physiological behavior very well. This “failure of averaging” has been demonstrated in many fields, most recently in neuroscience (Golowasch et al., 2002; Marder, 2011), and was particularly well-documented in 1952, the same year that the seminal Hodgkin and Huxley paper

was published, when Lt. Gilbert S. Daniels of the U.S. Air Force published a Technical Note that highlighted the fundamental problem with fitting data to the mean (Daniels, 1952; Rose, 2017). Using data from 4,063 pilots, Lt. Daniels calculated the average of 10 physical dimensions believed to be most relevant for design of the cockpit on a plane, including a pilot's height, chest circumference, and sleeve length. Surprisingly, he found that a total of zero individuals fit within the middle 30% of the range of values for each dimension, and less than 3.5% of pilots would be average sized on any three dimensions. After this finding, the U.S. Air Force completely moved from standardizing all dimensions to an "average pilot," to making all the dimensions adjustable to each individual pilot, which immediately and drastically improved performance and was soon adopted by all branches of the American military. Modeling of electrophysiology is undergoing a similar evolution, which will likely improve the translational significance of the models.

Variability Has Implications on Genesis and Treatment of Arrhythmia

Variability plays an important role in arrhythmia generation and treatment, as exemplified by AF. The atria are characterized by a high degree of phenotypic variability in physiological properties, with broad and diverging distributions of biomarkers in patients in normal sinus rhythm (nSR) or chronic AF (cAF, **Figure 1A**) (Ravens et al., 2015), likely due to innate variability of the ionic currents (perhaps due to stochastic gating) that can affect whole cell and/or tissue proarrhythmic behavior (Pueyo et al., 2011; Heijman et al., 2013). This phenotypic variability can be captured by adding variability in the conductance parameters of a mathematical model of the action potential (AP, **Figures 1B,C**). In some circumstances, physiological variability itself can be the substrate for arrhythmia. For example, increased heterogeneity of refractoriness is important for the maintenance of AF (Moe et al., 1964; Boutjdir et al., 1986; Misier et al., 1992; Sato et al., 1992; Wang et al., 1995, 1996; Gaspo et al., 1997; Liu and Nattel, 1997; Ramirez et al., 2000), and regional differences in atrial ionic currents play a significant role in atrial arrhythmia initiation (Feng et al., 1998; Gaborit et al., 2007; Colman et al., 2013). Consequently, pharmacotherapy that increases dispersion of refractoriness is an adverse side effect of drugs for the treatment of AF (Ramanna et al., 2001; Soylu et al., 2003).

It is well-known that individuals may present largely different responses to same pharmacological interventions. As an example, it has been shown that drugs that block the hERG (human *ether-à-go-go*-related gene) channel are generally responsible for drug-induced long QT syndrome (dLQTS), but in a population this adverse response is highly variable, from minimum changes in the electrocardiogram (ECG) to induction of lethal ventricular arrhythmias (Singh et al., 2000; Kannankeril et al., 2011). Accounting for physiological variability may help better understand why some individuals display adverse side effects, while others do not. Given the different etiologies of many cardiac arrhythmias, such as AF, computational approaches that take into account variability may help us identify subpopulations in which a particular antiarrhythmic therapy will be effective and

safe, or toxic. Furthermore, when assessing the efficacy and safety of a drug administration for heart conditions, it is important to take into account physiological and pathological variabilities to make sure that results are quantified and valid at the population level. Such approaches will potentially be more clinically useful in simulating the effects of drugs and aiding the design of safer and more effective therapies (Britton et al., 2013, 2017a; Passini et al., 2016; Yang et al., 2016).

APPROACHES AND INSIGHT ON THE IMPACT OF VARIABILITY ON CARDIAC ELECTROPHYSIOLOGY

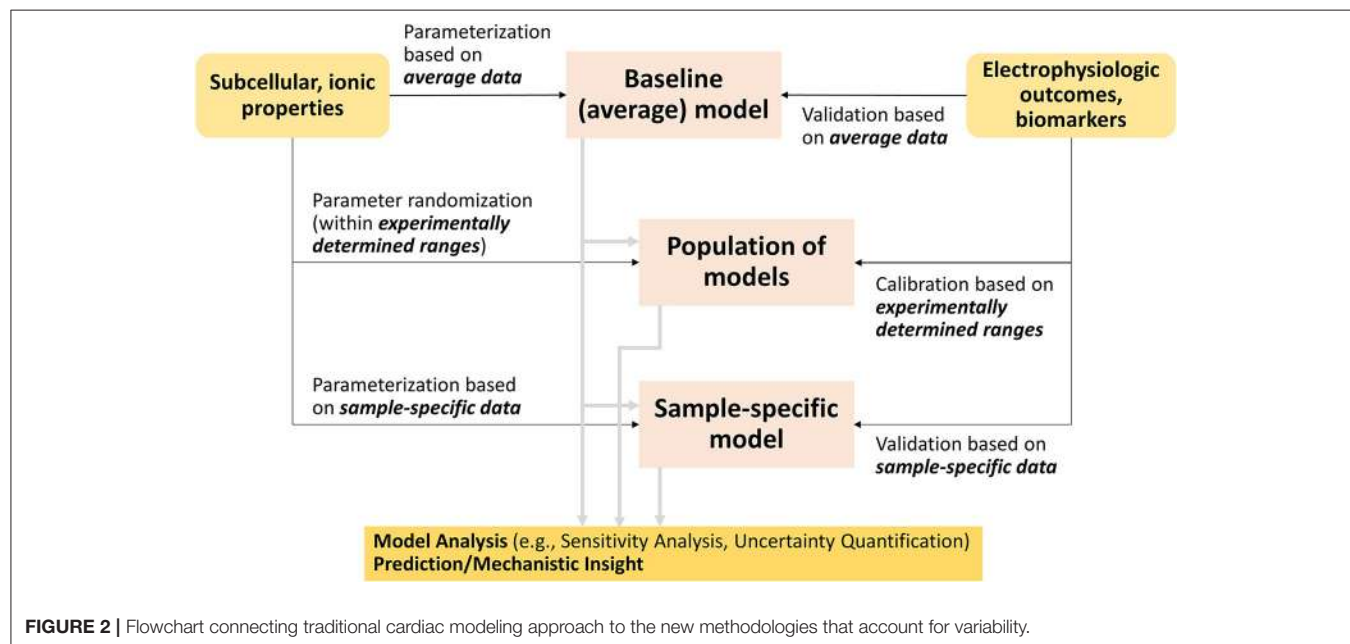
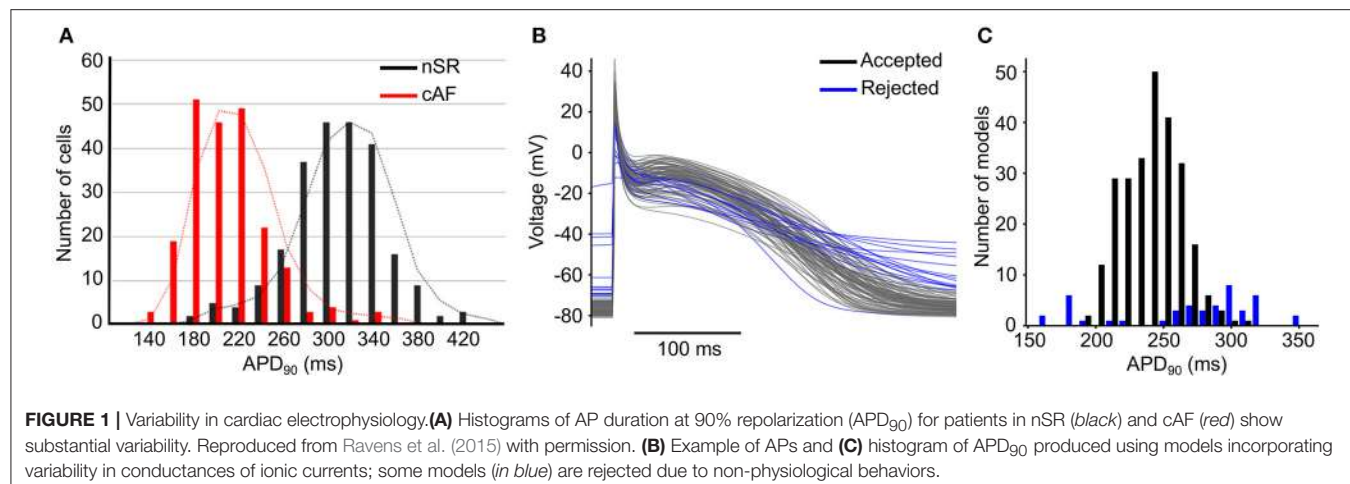
Although many methods have been developed, two families of approaches have emerged as leading methodologies to account for variability in cardiac electrophysiology: (1) population-based and (2) sample-specific modeling (**Figure 2**). Both methods generally start with the building or use of a baseline cardiac cell model, which has been parameterized and validated to average data. Population-based approaches generate model variants of the baseline model that fit given experimental distributions of electrophysiological outcomes or biomarkers, while sample-specific modeling approaches re-parameterize the baseline model based on cell- or patient-specific datasets (**Figure 2**). Because their implementation requires computational power, the advancements in computing capabilities and techniques (Pitt-Francis et al., 2006; Abramson et al., 2010), especially in parallel computing (Wang et al., 2011), have helped these methods gain traction in the last decade.

Population-Based Modeling

Population-based modeling approaches have been developed and employed to obtain results at the population level, which led to many novel insights into physiological and pathophysiological variabilities, and variable responses to drug administration. We refer the readers to a recent review from the Rodriguez group (Muszkiewicz et al., 2016), where this methodology is described in detail. Here, we briefly describe the general approach of population-based modeling, and summarize how it has contributed to advancing the field as exemplified by some important studies.

Creating Populations of AP Models

Populations of models are generally created by modifying sets of parameters in a baseline model (**Figure 2**). This process involves determination of the parameters to be varied, over what range, and a sampling method to select the parameter values. Frequently, maximal conductances or maximum transport rates of ion channels, pumps and transporters in AP models are selected to vary. The parameter space over which these model parameters vary can be chosen either to reflect the experimental range, when available, or theoretical upper and lower bounds. Then, populations of parameter sets are created by sampling the parameters within the predefined parameter spaces. Typically, four types of sampling methods have been applied to obtain the populations of parameter sets: uniform-interval sampling



(Romero et al., 2009, 2011; Corrias et al., 2011), log-normal sampling (Sobie, 2009; Sadrieh et al., 2013; Ellinwood et al., 2017a; Morotti and Grandi, 2017), Latin hypercube sampling (LHS) (Britton et al., 2013) and its variants such as orthogonal sampling (Burrage et al., 2015; Donovan et al., 2018), and sequential Monte Carlo sampling (Muszkiewicz et al., 2017).

After generating hundreds or thousands of model variants, calibration can be performed to exclude models that display non-physiological behaviors (Figure 2). This can be done, for example, by removing models showing repolarization failure (Sobie, 2009), or exhibiting AP duration (APD) more than three standard deviations from the population mean (Devenyi and Sobie, 2016). Population of models are also calibrated to measured data from patient samples, whereby model variants are selected based on simulated electrophysiological properties, such as APD, upstroke velocity, resting membrane potential and/or Ca²⁺ transient (CaT) (Britton et al., 2013, 2017a; Sanchez et al.,

2014; Passini et al., 2016; Rees et al., 2018). Other studies use additional information such as ionic current data (Muszkiewicz et al., 2017), or ECG data (Mann et al., 2016). This calibration step is meant to ensure that (1) variants displaying non-physiological properties are discarded before analysis, and (2) the simulated electrophysiological properties of models in a given population are in the same range as experimental data, or, more recently, correspond to the same distribution of observed experimental biomarkers (Lawson et al., 2018), thus possibly making inferences from *in silico* experiments more physiologically relevant.

Analyzing Populations of AP Models

Once a population of cardiac AP models is generated, and electrophysiological simulations have been performed corresponding to the scientific question at hand, mechanistic insights can be obtained using various analysis techniques. These analyses have contributed to our understanding of the

relative role of the underlying parameters in modulating the physiological properties of interest (i.e., sensitivity analysis), or revealing association of certain parameter ranges or properties with specific physiological behaviors (e.g., repolarization abnormalities, ectopic activity, drug response). Many relevant examples have recently been reviewed (Muszkiewicz et al., 2016). Here we highlight new recent developments and discuss details of parameter sensitivity analysis.

Performing parameter sensitivity analysis

A common systematic analysis of populations of models is sensitivity analysis. It assesses how model outputs, which typically represent whole cell behavior (e.g., APD), are sensitive to changes in model parameters, (e.g., conductances and maximum transport rates). Because many parameters are often varied to generate the populations of models, multivariable linear regression (Hair et al., 2010; Draper and Smith, 2014) has emerged as a frequently utilized tool to perform sensitivity analysis in cardiac electrophysiology. Moreover, as the number of independent parameters varied is used to predict a smaller set of dependent variables, sensitivity analysis is typically performed using partial least squares regression (Geladi and Kowalski, 1986; Sobie, 2009), as compared to standard multivariable regression. The result of linear regression is a set of coefficients (forming a “regression model”) describing how perturbing a particular parameter influences an output of interest. This method has been successfully utilized in other fields such as molecular biology (Janes et al., 2005) and neuroscience (Weaver and Wearne, 2008), and was first used in cardiac electrophysiology by Sobie (2009), who applied it to study sensitivities of properties such as APD and pacing rate threshold for inducing AP alternans. Since the regression model represents a linear approximation of a highly non-linear system, it is important to always check the goodness of fit. Several papers by the Sobie’s group have indeed shown that the linear approximation actually provides a very good fit of the AP biomarkers, which was not trivially predictable (Sarkar et al., 2012).

The approach of varying multiple ionic conductances at once in a systematic fashion (as opposed to one at a time) and employing sensitivity analysis using multivariable regression has led to many important insights in cardiac electrophysiology (Sarkar and Sobie, 2011; Mann et al., 2012; Heijman et al., 2013; Walmsley et al., 2013), some of which have been confirmed experimentally (Lee et al., 2013; Devenyi and Sobie, 2016; Devenyi et al., 2017). For example, it has been used to study how different diseased conditions affect the sensitivities of given electrophysiological properties (Sadrieh et al., 2013; Ellinwood et al., 2017a; Vagos et al., 2017; Koivumaki et al., 2018), mechanisms of physiological phenomena (Lee et al., 2013), and for constraining free parameters (Sarkar and Sobie, 2010). Through sensitivity analysis, Cummins et al. identified multiple potential ionic targets mediating forward rate dependence (FRD) of AP, and demonstrated that modulation of the inward rectifier K⁺ current (I_{K1}) or the Na⁺/K⁺ pump current was more likely to produce FRD (Cummins et al., 2014). Devenyi and Sobie performed sensitivity analysis of rat ventricular myocyte models, and quantitatively compared the modulatory role of transient

outward K⁺ current (I_{to}) and sarco/endoplasmic reticulum Ca²⁺-ATPase (SERCA) in CaT amplitude. They found that in rat epicardial cells I_{to} plays a more important role than SERCA in regulating CaT amplitude, and this was analogous to human atrial cells, where both I_{to} and ultra-rapid delayed-rectifier K⁺ current (I_{Kur}) had greater impacts on CaT amplitude than did SERCA (Devenyi and Sobie, 2016). These studies highlight how sensitivity analysis can be applied to compare and contrast roles of different ionic processes and Ca²⁺ handling in regulating physiological properties and behaviors between cell types and species. Sensitivity analysis has also been used to compare the dependence of AP biomarkers on ionic processes in healthy and diseased conditions. For example, Lee et al. compared the impact of ionic processes on APD in control and AF-remodeled cells and found that the Na⁺/Ca²⁺ exchanger (NCX) current has little influence on APD in control cells but more markedly impacts AF cells; the analysis also revealed that I_{K1} upregulation plays a dominant role in APD shortening in AF, and that the L-type Ca²⁺ current (I_{CaL}) significantly contributes to rate-dependent APD changes in both control and AF myocytes (Lee Y. S. et al., 2016). Most recently, Gong and Sobie described a novel use of regression models, cross-cell regression, to predict adult myocyte drug responses from induced pluripotent stem-cell-derived cardiomyocytes (iPSC-CMs) behaviors (Gong and Sobie, 2018).

Multivariable linear regression is used if the physiological output of interest is continuous, but, for the study of arrhythmia mechanisms, another particularly useful and efficient regression technique is logistic regression, which is used when the outcome of interest is Boolean (i.e., yes/no, true/false). Applying logistic regression in studies of physiology is well-described by Lee et al. who examined Ca²⁺ spark triggering (an all-or-none event), and demonstrated the accuracy of logistic regression using receiver operator characteristic curves (Lee et al., 2013). This method has since been used to study the probability that a certain arrhythmic event such as early afterdepolarizations (EADs) will occur and suggest underlying factors (Morotti and Grandi, 2017).

The main limitation of regression (both linear and logistic) analysis is that it only highlights how inputs are correlated to outputs, so the conclusions drawn from the analysis can be misleading if only a few outputs are considered. For example, it has been shown that completely different parameter combinations could produce essentially identical AP shapes but substantially different CaT amplitudes (Figure 3) (Sarkar and Sobie, 2010). However, sensitivity analysis can still help determine whether the relationships between inputs and outputs in computational models match experimental findings and assumptions, and whether there are particularly influential parameters that can be exploited therapeutically or targeted to better understand a given physiological phenomena (e.g., arrhythmia mechanism).

Comparing subpopulations of models

Comparing subgroups in a population of models (often using statistical difference tests of parameters of interest) can help identify underlying determinants of different phenotypes, behaviors, and pathological conditions (Sanchez et al., 2014;

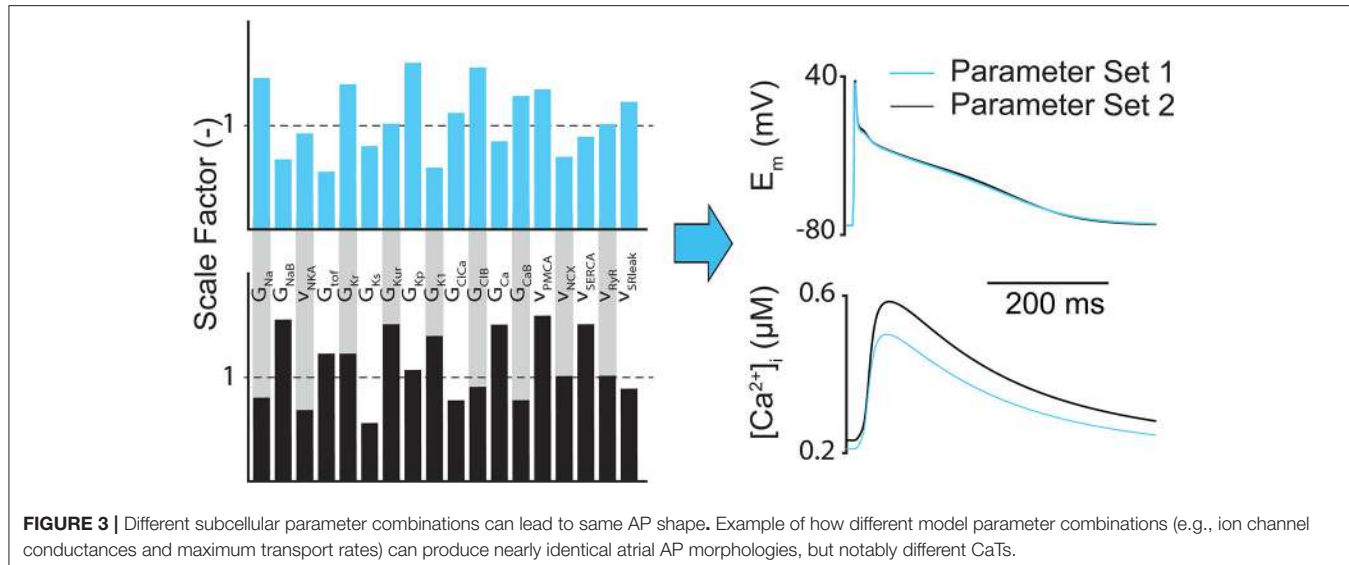


FIGURE 3 | Different subcellular parameter combinations can lead to same AP shape. Example of how different model parameter combinations (e.g., ion channel conductances and maximum transport rates) can produce nearly identical atrial AP morphologies, but notably different CaTs.

Zhou et al., 2016; Britton et al., 2017b; Muszkiewicz et al., 2017; Vagos et al., 2017; Lawson et al., 2018). For example, through characterizing ionic parameters of models that are prone to repolarization abnormalities, Britton et al. found that the electrogenic Na^+/K^+ pump is a key determinant of susceptibility to repolarization abnormalities in human ventricular cardiomyocytes by applying arrhythmia-provoking conditions to a population of experimentally-calibrated cardiac cells (Britton et al., 2017b). A population-based approach has also been used to tease out the ionic mechanisms underlying variability in iPSC-CMs (Paci et al., 2017). By calibrating generated subpopulations of human atrial myocyte models to ranges of experimental data from a large number of patients with nSR or cAF, Sanchez et al. characterized potential ionic determinants of inter-subject variability in AP biomarkers, and identified similar changes in $I_{\text{K}1}$, I_{Kur} , and I_{to} in cAF vs. nSR subpopulations that were consistent with experimentally reported AF-induced remodeling effects (Sanchez et al., 2014). In a more recent study, instead of calibrating population of models to the range of experimental dataset, Lawson et al. proposed a novel method to calibrate these models to the distributions of multiple experimentally measured biomarkers (Lawson et al., 2018), which led to an improved characterization of ionic differences between nSR and cAF. These studies focused on AP biomarkers at a fixed pacing rate. In a different study, Vagos et al. expanded the use of population of models to compare the steady state and dynamic restitution behaviors of AP in nSR and cAF populations (Vagos et al., 2017). By combining population-based modeling and experiments, Muszkiewicz et al. characterized variability in AP and ionic densities and their impact on CaT in atrial cells from right atrial appendage of patients exhibiting nSR (Muszkiewicz et al., 2017). In addition to calibrating model outputs to measured AP biomarkers, they also extended the experimental calibration of population of human atrial models to model parameter (inputs) by using experimental data of major ionic currents.

Quantifying drug modulatory effects, understanding variability in drug response, and identifying phenotype-specific therapy

By using a population of models that incorporate variabilities, drug modulatory effects on electrophysiological properties can be interpreted at a whole population level, which also contributes to limiting potential model-dependent results. For example, Yang et al. used a population-based approach to simulate effects of late Na^+ current (I_{NaL}) and hERG block and found that the selective I_{NaL} blocker GS-458967 could suppress proarrhythmic markers after hERG block in ventricular myocytes (Yang et al., 2016). Population-based modeling has also allowed for more rigorous quantitative comparison of modulatory effects between multiple drugs. A recent study by Britton et al. calibrated populations of ventricular models to specific individuals using data from human trabeculae (Britton et al., 2017a). They then assessed the effects of four different (selective and non-selective) blockers of the rapid delayed-rectifier K^+ current (I_{Kr}), dofetilide, sotalol, quinidine, and verapamil, to quantitatively compare changes in AP biomarkers, and demonstrated good agreement with experiments for the selective I_{Kr} blockers (dofetilide and sotalol) but not for the non-selective I_{Kr} inhibitors (quinidine and verapamil). Paci et al. utilized populations of *in silico* iPSC-CMs to evaluate antiarrhythmic effects of mexiletine and ranolazine to treat iPSC-CM long QT syndrome type 3 (LQT3) mutants and demonstrated that mexiletine stops spontaneous APs in more LQT3 models than ranolazine due to its stronger effects on the fast Na^+ current (I_{Na}) (Paci et al., 2017). In contrast to the traditional modeling approach using a single model, the population-based modeling can gain insights into the physiologically relevant variability of predictions made *in silico*, as demonstrated in these studies.

By taking a step further, simulations using populations of models incorporating variabilities can also help recognize the contributing factors underlying the variability observed in response to drugs. One relevant example is the variable

outcomes of hERG inhibition, which is frequently linked with dILQTS. Population-based modeling has offered insights into the mechanisms underlying the fact that individuals will not exhibit the same degree of QT interval prolongation after hERG block (Singh et al., 2000; Kannankeril et al., 2011; Weeke et al., 2014). Employing a population of models of ventricular myocytes, Sobie and Sarkar attributed the variable outcomes to the different ionic properties of the cells (Sarkar and Sobie, 2011). In another interesting application, Passini et al. implemented an *in silico* drug trial using experimentally-calibrated populations of AP models to investigate the risk of drug-induced arrhythmias, and to identify specific subpopulations at higher risk for proarrhythmic cardiotoxicity (Passini et al., 2017). Their methodology not only demonstrated higher accuracy than animal models in predicting arrhythmia risk, but also provided mechanistic insight into the underlying ionic contributors to repolarization/depolarization abnormalities.

Understanding the bases of variability in electrophysiological behavior and arrhythmia proclivity may also allow developing specific antiarrhythmic therapies for different disease phenotypes. For example, Liberos et al. compared AF models that had self-sustained vs. self-terminating reentries (Liberos et al., 2016). They found that AF maintenance was correlated with high I_{CaL} and I_{Na} , and that I_{CaL} block could be an effective treatment depending on the basal availability of Na^+ and Ca^{2+} ion channel conductivities (I_{Na} depression increased efficacy). Mayourian et al. employed a comprehensive integrated approach to study the mechanisms of cardiac contractility and arrhythmogenicity using experimentally-calibrated human mesenchymal stem cells (hMSCs) (Mayourian et al., 2017). In simulations testing proarrhythmic effects, they found that hMSCs paracrine signaling protected such adverse effects of heterocellular coupling at various levels of engraftment. This work highlights that antiarrhythmic strategies can move beyond simply considering repolarization abnormalities.

Sample-Specific Modeling

Instead of taking a baseline cardiac model and introducing variability by randomly varying the ionic conductances, optimization and statistical techniques can also be used to tailor the baseline model to describe a specific experimental sample. Depending on the characteristics of the dataset at hand, sample-specific models can be representative of either individual myocytes or a particular group of cells. The former approach, cell-specific modeling, can be helpful when integrating mathematical modeling into an experimental setup. For example, Ravagli et al. characterized the role of the “funny” current I_f in sinoatrial myocytes using the dynamic clamp technique by adapting the extent of injected I_f in a cell-specific fashion, i.e., based on the basal firing rate measured in each individual cell (Ravagli et al., 2016). Despite the use of average data, sample-specific models built from a group of cells (e.g., a cell line developed in a certain laboratory, myocytes isolated from disease models, iPSC-CMs derived from a single patient) can allow for specific characterization of conditions that are far from the average, or even of personalized physiology (Barichello et al., 2018). For example, monophasic AP data recorded in

AF patients undergoing ablation procedures have been used to construct atrial cell models that capture patient-specific electrophysiological properties (Lombardo et al., 2016). This approach has the promise of making patient-specific predictions given interventions such as arrhythmia-provoking protocols or drug application. Here we summarize methodologies for building and improving sample-specific cell models. For more detail, we refer the readers to a previous review on the topic (Krogh-Madsen et al., 2016).

Fitting Sample-Specific Models

Sample-specific models can be constructed by fitting the parameters of a baseline model so that the model outputs match the corresponding physiological behaviors seen in a single patient or myocyte (Figure 2). Cardiac electrophysiology models can be optimized using many different fitness functions (Druckmann et al., 2007; Tomaiuolo et al., 2012), such as global search heuristics (Vanier and Bower, 1999; Dokos and Lovell, 2004; Bueno-Orovio et al., 2008; Guo et al., 2010). Recently, many sample-specific models are generated using the genetic algorithm (GA), which traces its beginnings to evolutionary biology (Fraser and Burnell, 1970; Crosby, 1982), but is still being applied in new ways today (Chen and Guan, 2004; Hussein and El-Ghazaly, 2004; Leung et al., 2004; Vieira et al., 2004). Its use for optimization of ionic models is relatively new in both neuroscience (Achard and De Schutter, 2006; Gurkiewicz and Korngreen, 2007; Hobbs and Hooper, 2008; Ben-Shalom et al., 2012) and cardiac electrophysiology (Syed et al., 2005; Bot et al., 2012; Kaur et al., 2014; Groenendaal et al., 2015). Syed et al. demonstrated its feasibility for atrial cell models when they proved they could fit two different cell models (Courtemanche et al., 1998; Nygren et al., 1998) to any given atrial AP (Syed et al., 2005). Essentially, the GA optimization procedure is initialized in the same way as for the population-based approach (varying maximal conductance and/or transport rates), and then it iteratively evolves toward better solutions in generations, while the underlying parameters can be varied, swapped, or discarded. Sensitivity analysis can be used in conjunction with generating sample-specific models as it can inform the design of the error function (i.e., weights) by revealing the conductances that more significantly impact the electrophysiological outputs used for fitting. For example, Krogh-Madsen et al. recently combined sensitivity analysis and global optimization (using a GA) of a ventricular myocyte model to clinical long QT data and intracellular Ca^{2+} and Na^+ concentrations, to better constrain the model parameters (Krogh-Madsen et al., 2017). They found that this improved prediction of drug-induced *torsades de pointes* (TdP), especially in eliminating false-positive outcomes generated by the baseline model parameters.

Improving Fidelity of Sample-Specific Models

The final solution of an optimization procedure using some fitness function may not match experimental data well if only fitting to a single electrophysiological output such as a single AP, because multiple parameter combinations can potentially produce the same AP (Figure 3) (Syed et al., 2005; Druckmann et al., 2007; Sarkar and Sobie, 2010; Guo et al., 2013; Kaur

et al., 2014; Groenendaal et al., 2015). In this case, although fitness function itself can be improved, for example, by increasing the population size or diversity for GAs can improve the fit of a sample-specific model, it may not necessarily guarantee that the final solution relates to the global minimum. To address this issue, many methods have been developed using (1) additional electrophysiological properties for fitting and/or (2) more complex electrophysiological protocols to improve model fidelity. It has been shown that model faithfulness can be improved by adding membrane resistance as an objective (Kaur et al., 2014), by optimizing to Ca^{2+} handling (Dokos and Lovell, 2004; Sarkar and Sobie, 2010; Rees et al., 2018), or by accounting for experimental data generated from multiple pacing frequencies (Syed et al., 2005; Lombardo et al., 2016) or irregular pacing protocols (Guo et al., 2013; Groenendaal et al., 2015).

In addition to using multiple electrophysiological properties to improve the fit of sample-specific models, more intricate voltage-clamp protocols that capture complex and rich electrophysiological dynamics have been employed, as first demonstrated to improve the fit of Markov models of ionic currents with many parameters (Dokos and Lovell, 2004; Zhou et al., 2009; Beattie et al., 2018). These can be implemented over a short time frame and may be used to emphasize certain currents over others. In the absence of pharmacological isolation, Groenendaal et al. used only a 6-s protocol that effectively isolated I_{K_1} , I_{CaL} , and slow delayed-rectifier K^+ current (I_{K_s}) given their disproportionately large contribution at voltage steps of -120 , $+20$, $+40$, and -30 mV, respectively (Groenendaal et al., 2015). They found that using this protocol alone cannot isolate all ionic currents, and when used in combination with a stochastic pacing protocol there was a considerable improvement in parameter estimation. Developing short but information-rich protocols is useful especially when trying to improve the results of an optimization procedure for cell-specific modeling, because longer protocols take longer to implement experimentally and thus are difficult to perform in a single cell. In a recent study, Beattie et al. proposed an innovative experimental and mathematical modeling method that allows to concisely measure the dominant processes involved in hERG channel gating by applying a short (8-s long) “sum of sinusoids” voltage-clamp protocol (Beattie et al., 2018). The sinusoidal waves were able to provoke a wider range of non-equilibrium behavior than traditional square voltage steps, thus allowing rich and complete characterization of hERG channel kinetics in the same cell and efficient model fitting (**Figure 4A**).

The final step in improving fidelity of sample-specific models is to directly experimentally test the predictions of the model given new protocols (Groenendaal et al., 2015; Devenyi et al., 2017; Beattie et al., 2018). **Figure 4B** reports an example of such validation experiments, where predictions obtained with cell-specific I_{K_r} models (identified applying the sinusoidal protocol in **Figure 4A** in 9 cells) are compared to the I_{K_r} -voltage relationships experimentally determined in each cell (Beattie et al., 2018). The order of the panels in **Figure 4B** is based on an index of recording stability (lowest to highest difference in leak resistance between the vehicle and dofetilide recordings) that is associated to “data quality”. Cell-specific predictions are excellent

for cells 1–5 (higher data quality), but less accurate for cells 6–9 (lower data quality). The analysis also shows that cell-specific models provide better predictions than the average model for the cells with the highest data quality (cells 1–5). Experimental validation is an important last step in improving cell-specific models, as generating cell-specific models is potentially more susceptible to observational error. Devenyi et al. used a GA to re-parameterize the Livshitz-Rudy model of the guinea pig ventricular cardiomyocyte (Livshitz and Rudy, 2009), and predicted an increase in I_{K_r} and a drastic decrease in I_{K_s} given a dynamic clamp protocol as compared to the original model, and this was validated experimentally (Devenyi et al., 2017). Their adjusted model predicted that I_{K_s} can stabilize the AP and EADs better as compared to I_{K_r} —which improved the ability to assess arrhythmia risk, given the baseline model did not produce physiological behaviors that were quantitatively similar to their experiments.

Models of Patient-Specific Anatomy

While a detailed discussion of patient-specific anatomical models is beyond the scope of our review, recent studies have begun investigating how inter-patient differences in myocardial structure affects atrial arrhythmia, as reviewed by Barichello et al. (2018). For example, Zhao et al. developed a 3D human heart-specific atrial computer model integrating 3D high resolution structural and functional mapping data to test the impact of wall thickness, fibrosis, and myofiber orientation on AF induction, maintenance, and ablation strategies (Zhao et al., 2017). Deng et al. demonstrated that reentrant driver localization dynamics are influenced by inter-patient variability in the spatial distribution of atrial fibrosis, APD, and conduction velocity (Deng et al., 2017). This suggests that incorporating patient-specific electrophysiological models in patient-specific geometries might enhance their predictive value. We discuss the computational challenges associated to this task in the section entitled “Arrhythmia Research Requires Understanding Variability at Larger Spatial Scales”. Furthermore, obtaining patient-specific electrophysiological data might constitute another logistical roadblock.

Overall, methods that incorporate variability are particularly useful for (1) analyzing variability in cardiac electrophysiology, (2) assessing proarrhythmic risk, (3) determining the underlying factors contributing to variable drug response, and (4) identifying phenotype-specific (and in the future patient-specific) antiarrhythmic targets. **Table 1** summarizes applications of these approaches and new insights provided by the studies (shaded areas indicate atrial studies).

CHALLENGES AND FUTURE DIRECTIONS

We reviewed the most common methods used to account for variability in cardiac electrophysiology, which largely fall into the two categories of (1) population-based modeling and (2) sample-specific modeling. These methods complement each other well, as population-based methods can help characterize behavior in a particular patient group (healthy, diseased, stressed, etc.), and sample-specific modeling shows significant promise to

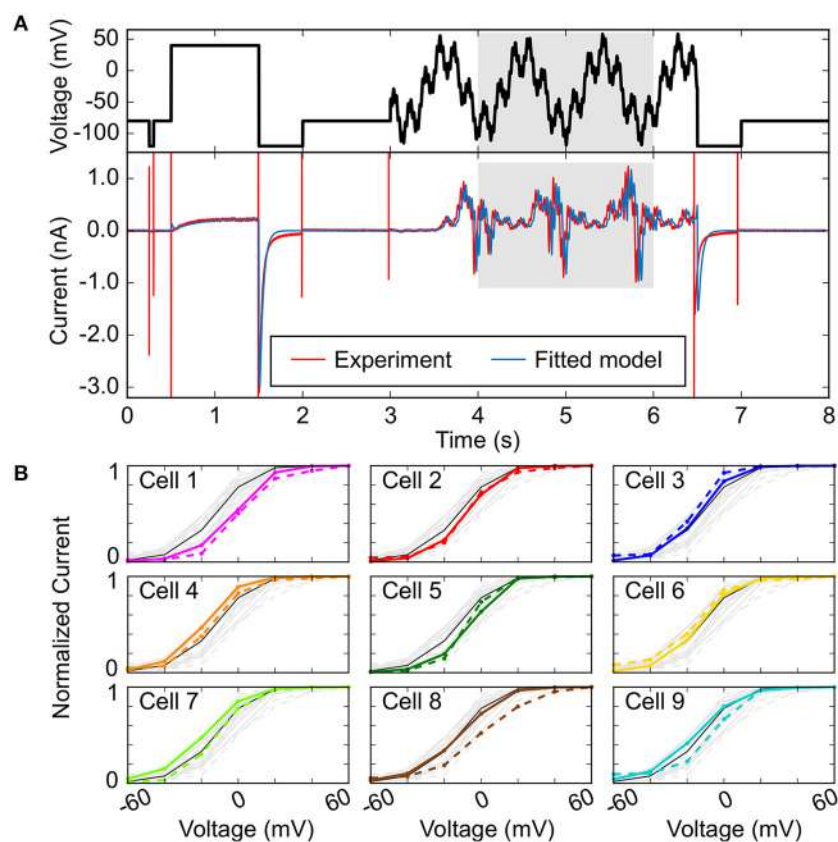


FIGURE 4 | Improving fit of sample-specific models. **(A)** Experimental and simulated I_{K_r} time courses (bottom) evoked in response to an efficient, information-rich sum-of-sinusoid voltage protocol (top) that allows rapid characterization of I_{K_r} behavior. **(B)** Steady-state peak I_{K_r} -voltage curves comparing cell-specific model predictions (bold, colored) to cell-specific experimental recordings (dashed, colored). The black lines in each plot are from the model calibrated to averaged sinusoidal data from all the cells (light gray). Reproduced from Beattie et al. (2018) with permission.

develop personalized medical approaches for individual patients. Both methods have led to many important insights into the mechanisms of arrhythmogenesis and antiarrhythmic strategies. However, there are several important limitations to consider, which suggest potential future developments in modeling of cardiac electrophysiology.

Analysis of Electrophysiology From Populations of Models May Require Different Statistical Methods

As opposed to the traditional approach of producing a single value from a single baseline model, models that incorporate variability have allowed statistical methods to be applied that can either ask new scientific questions or quantify the impact of variability on electrophysiological outputs, as performed in experimental studies. While the statistical analysis methods used in experimental studies can be directly applied in the *in silico* population-based studies, differences in the nature of experimental and simulation studies may need to be considered. For example, some population-based techniques generate model population sizes (often sample sizes in the 1000s) that are much greater than could be achieved by experiments (often sample

sizes of 3–12) or the traditional cardiac modeling approach alone. Therefore, given similar effects, results produced in the population-based simulations have greater statistical power to detect differences. Furthermore, because even very small effects can reach statistical significance with large samples, physiological significance should be assessed (White et al., 2014). Additionally, when evaluating drug effects on electrophysiology, in simulations of the same virtual cell (a single model out of the population-models) can be used to perform both control and with-drug studies, allowing for paired comparisons, which is often not practical in experimental studies. The methodologies for analyzing and interpreting the “big data” produced by the population of models should be carefully considered and standards should be established going forward.

Variability Does Not Fully Account for Uncertainty

Physiologic variability should be thought of in the context of the broader umbrella of uncertainty, which is the confidence (or precision) with which a quantity, such as an electrophysiological output, can be given a value (Mirams et al., 2016). While here we reviewed how cardiac electrophysiology models have

TABLE 1 | Applications and main findings of computational methods incorporating cardiac electrophysiological variability (**shaded areas indicate atrial studies).

Author, Year	Baseline Model	Model Generation	Approach	Insight
ANALYZING VARIABILITY				
Sobie, 2009	MVMMs: Luo and Rudy, 1991; Fox et al., 2002; Kurata et al., 2005	Sampled from LND	MLR	New method to rapidly identify ionic mechanisms shaping AP properties, CaT, and alternans
Sanchez et al., 2014	HAMMs: Courtemanche et al., 1998; Maleckar et al., 2009; Grandi et al., 2011	Sampled over a $\pm 100\%$ variation range around their baseline values as described by Marino et al. (2008); calibrated to AP recordings in atrial trabecula	Statistical difference tests	Ionic determinants of variability in human AP in nSR vs. cAF
Lee Y. S. et al., 2016	HAMM: Courtemanche et al., 1998	Sampled from LND	MLR	Comparison of parameter sensitivity between nSR and AF condition. Ionic contributions to rate-dependence and spiral wave dynamics in AF
Devenyi and Sobie, 2016	HAMM: Grandi et al., 2011; HVMM: Grandi et al., 2010; RVMM: Pandit et al., 2001	Sampled from LND	MLR	In human atrial myocytes, both I_{to} and I_{Kur} had greater impacts on CaT amplitude than did SERCA. This was similar in rat left ventricular epicardial cells, where I_{to} played a more important role than SERCA
Vagos et al., 2017	HAMM: Skibsbye et al., 2016	Sampled from Gaussian distribution	MLR	Ionic determinants of unstable behaviors in nSR vs. cAF
Ellinwood et al., 2017b	HAMM: Grandi et al., 2011	Sampled from LND	MLR	I_{Kur} impacts APD and effective refractory period more in cAF (even though it is downregulated) vs. nSR
Muszkiewicz et al., 2017	HAMMs: Courtemanche et al., 1998; Maleckar et al., 2009; Grandi et al., 2011	Sampled using LHS and sequential MC; calibrated to experimental recordings	PCCs, statistical difference tests	Ionic determinants of electrophysiological and CaT properties
Lawson et al., 2018	HAMM: Courtemanche et al., 1998	Sampled over a $\pm 100\%$ variation range around their baseline values; sequential MC; model calibrated based on distributions of biomarkers estimated from multivariate kernel density estimation	Statistical difference tests	Accurate identification of inherent variability within the experimental population and improved characterization of ionic differences between nSR and cAF
ASSESSING ARRHYTHMIA RISK				
Walmsley et al., 2013	HVMM: O'Hara et al., 2011	MC sampling from a uniform distribution ($\pm 30\%$); calibrated to mRNA expression data in failing and non-failing hearts	MLR	Combination of low SERCA activity and high I_{CaL} conductance impacted the formation of alternans the most in the non-failing heart population, but low hERG conductance was the main contributor to alternans in the failing heart population
Zhou et al., 2016	HVMM: O'Hara et al., 2011	Sampled using LHS; calibrated to <i>in vivo</i> recordings	PCCs, statistical difference tests	I_{CaL} and NCX current determine the cell-to-cell differences in repolarization alternans through intracellular and sarcoplasmic Ca^{2+} regulation
Britton et al., 2017b	HVMM: O'Hara et al., 2011	Sampled using LHS; calibrated to data in human ventricular trabeculae	Logistic regression, PCCs, statistical difference tests	Na^{+}/K^{+} pump is a key determinant of repolarization abnormality susceptibility
Morotti and Grandi, 2017	HAMM: Grandi et al., 2011	Sampled from LND	Logistic regression	EADs are particularly sensitive to conductances of I_{Na} , acetylcholine-sensitive and ultra-rapid K^{+} channels, and NCX transport rate
Devenyi et al., 2017	Guinea pig left ventricular myocyte model Livshitz and Rudy, 2009	Fit using GA; sampled from LND	Dynamic clamp data for fitting, MLR	I_{Ks} is more capable to stabilize AP and EADs as compared to I_{Kr}

(Continued)

TABLE 1 | Continued

Author, Year	Baseline Model	Model Generation	Approach	Insight
IDENTIFYING ANTIARRHYTHMIC TARGETS				
Cummins et al., 2014	MVMMs: Luo and Rudy, 1991; Fox et al., 2002; Hund and Rudy, 2004; Ten Tusscher et al., 2004; Ten Tusscher and Panfilov, 2006; Livshitz and Rudy, 2009; O'Hara et al., 2011	Sampled from LND	MLR	I_{K1} and Na^+/K^+ pump currents favor forward rate dependence
Liberos et al., 2016	HAMM: Skibbsbye et al., 2016	Sampled using LHS; calibrated to AP recordings in atrial trabeculae in patients with AF	PCCs, statistical difference tests	AF maintenance was correlated to high I_{CaL} and I_{NaL} , and I_{CaL} block could be an effective treatment depending on the basal availability of Na^+ and Ca^{2+} channel conductivities
Passini et al., 2016	HVMM: O'Hara et al., 2011	Sampled using LHS; calibrated to non-diseased and HCM myocytes AP recordings	Analysis of repolarization properties	I_{CaL} re-activation is the key mechanism for repolarization abnormalities in HCM myocytes, and combined NCX, I_{NaL} and I_{CaL} block is effective to partially reverse the HCM phenotype
Yang et al., 2016	Rabbit ventricular myocyte model Soltis and Saucerman, 2010	Randomly selected within $\pm 10\%$ of nominal value (uniform distribution)	Analysis of TRlAD pro-arrhythmic markers	GS-458967 suppressed proarrhythmic markers following HERG block
ASSESSING THE VARIABLE RESPONSE TO DRUGS				
Sarkar and Sobie, 2011	MVMMs: Fox et al., 2002; Hund and Rudy, 2004; Ten Tusscher et al., 2004; Kurata et al., 2005; Grandi et al., 2010	Sampled from LND	MLR	Individuals do not exhibit the same degree of QT interval prolongation due to different ionic ensembles
Britton et al., 2013	Adapted rabbit Purkinje cell model Corrias et al., 2011	Sampled using LHS; calibrated to experimental data	PCCs	Quantitatively predicted the arrhythmia risk of four concentrations of the K^+ channel blocker dofetilide; baseline I_{Kr} conductance is the primary determinant of APD prolongation caused by dofetilide
Lancaster and Sobie, 2016	HVMMs: Ten Tusscher et al., 2004; Grandi et al., 2010; O'Hara et al., 2011	Sampled from LND; calibrated to experimental data	PCA, ROC curves, TdP risk scores	TdP risk assessment could be improved by quantifying the impact of multiple cardiac ion channels (even those not typically considered to affect risk)
Britton et al., 2017a	HVMM: Adapted O'Hara et al., 2011	Sampled using LHS, calibrated to heart-specific ex vivo measurements	Coefficients of variation	Good agreement with experiments for selective I_{Kr} blockers, but notable differences for the non-selective I_{Kr} inhibitors
Passini et al., 2017	HVMM: O'Hara et al., 2011	Sampled using LHS; calibrated to experimental data	TdP scoring system	<i>In silico</i> drug trial demonstrated higher accuracy than animal models in predicting arrhythmia risk (89%); underlying ionic contributions to repolarization/depolarization abnormalities
Krogh-Madsen et al., 2017	HVMM: O'Hara et al., 2011	Fit using GA; optimized to clinical data	TdP risk prediction	TdP risk assessment could be improved by using global optimization methods and multi-variable objectives
Gong and Sobie, 2018	HVMM O'Hara et al., 2011 and human iPSC-CM models Paci et al., 2017	Sampled from LND	Cross-cell MLR	Cross-cell regression predicted adult ventricular myocyte drug responses from the behaviors of an iPSC-CM <i>in silico</i> population

HAMM, human atrial myocyte model; HCM, hypertrophic cardiomyopathy; HVMM, human ventricular myocyte model; LHS, Latin hypercube sampling; LND, log-normal distribution; MLR, multivariable linear regression; MVMM, mammalian ventricular myocyte model; RVMM, rat ventricular myocyte model; PCA, principal component analysis; PCC, partial correlation coefficient; ROC, receiver operator characteristic; MC, Monte Carlo; TRlAD, Triangulation, Reverse use dependence, beat-to-beat Instability of action potential duration, and temporal and spatial action potential duration Dispersion.

begun to account for physiological and experimental variability, uncertainty analysis should determine whether the baseline model itself is a valid representation of its physical system. The extent and rigor of validation during model development affects uncertainty, whereby the broader the set of constraints, e.g., the model recapitulates both voltage and Ca^{2+} responses, their pacing rate-dependence, short- and long-term behavior, the lesser the uncertainty in the obtained parameters. Uncertainty analysis should also verify that the experiments used to construct the model are appropriate. For example, in experiments, voltage-clamp protocols used to characterize ionic currents are often done using non-selective pharmacological block which may have unidentified effects, over a range narrower than the entire physiological range, or on larger cells that are easier to patch-clamp with intrinsically greater than normal maximal conductances (Courtemanche et al., 1998). All of these would lead to uncertainties in the initial parameters and conditions due to experimental error and lack of knowledge. Likewise, the choice of the computational methods or resources used to perform the model parameterization and simulations can produce uncertainty in model results. This is because cardiac models may use different mathematical equations to describe the same physiological process, perhaps based on different analyses or assumptions on the physical-world process. Using more than one (e.g., cell) model to confirm predictions or validate the mechanistic understanding of a process is therefore a useful strategy (see for example Sarkar and Sobie, 2011; Sanchez et al., 2014; Lancaster and Sobie, 2016; Muszkiewicz et al., 2017). Additionally, even the choice of the numerical solver used by the software can lead to variability in model outputs, i.e., simulator uncertainty (Pathmanathan et al., 2012). Moreover, uncertainty in model outputs may arise if the code has not been verified to truly represent the mathematical equations in the computational model (Niederer et al., 2011a). Finally, optimization procedures can also introduce uncertainty, whereby the choice of whether to optimize simplified models with few parameters (Bueno-Orovio et al., 2008; Al Abed et al., 2013; Guo et al., 2013) or detailed models but only a few properties (e.g., focusing on specific currents) (Zhou et al., 2009; Fink et al., 2011) can lead to multiple distinct models given the same experimental data.

Used in conjunction with the approaches discussed in this review that take into account electrophysiological variability, new methods have been developed that try to quantify uncertainty more generally (Marino et al., 2008). Uncertainty quantification methods aim to quantify uncertainties in model inputs and propagation through the model to see how they affect model predictions (Pathmanathan et al., 2015; Mirams et al., 2016). This is typically done by assigning probability distribution functions, rather than fixed values to model parameters, as done for example by Pathmanathan et al. and applied to the study of I_{Na} steady-state inactivation (Pathmanathan et al., 2015). However, this process can be slow and tedious (requiring lots of simulations), especially if using a Monte Carlo sampling method that chooses input values from a statistical distribution. Also, in some cases, this statistical distribution of input parameters can be difficult to obtain or justify experimentally. To solve this issue, uncertainty quantification analysis has developed surrogate

models or emulators (e.g., polynomial chaos expansions, and Gaussian process emulators; Chang et al., 2015), which are fast-running statistical approximations of the computational models and are quite powerful when fit to carefully constructed training data. Formal studies using uncertainty quantification in cardiac models are still limited, given the huge number of parameters in cardiac models, and may require the development of new methods or computational techniques (Johnstone et al., 2016).

Potential Covariance in Ionic Conductances Challenges the Current Method of Incorporating Variability

Currently, populations of cardiac models and sample-specific models typically calibrate or fit to maximal conductance values or transport rates of channels or receptors, based on the observation that changes in expression levels of ion channels and transport proteins are the primary contributors to (inter-species) variability (Rosati et al., 2008). However, this approach does not take into account that the expression of ion channels will vary over relatively short time scales given changes in transcription, translation, degradation, or even circadian rhythm. Moreover, with a few exceptions (Sarkar and Sobie, 2011; Cummins et al., 2014) these methods do not typically account for variability in ion channel kinetics, which is known to change especially in response to drugs (Clancy et al., 2007). The methods discussed in this review can attempt to account for these properties using additional parameters.

Although the correlation between parameters (i.e., maximal conductances) is assessed sometimes (Britton et al., 2013), neither population-based nor the sample-specific approaches account for possible covariance in ion channel conductances, despite the fact it has been observed in neurons (Schulz et al., 2006, 2007; Tobin et al., 2009) and cardiac tissue (Schram et al., 2002; Rosati and Mckinnon, 2004; Deschenes et al., 2008; Xiao et al., 2008; Banyasz et al., 2011; Milstein et al., 2012). The exact mechanisms responsible for these covariances are still being explored. Xiao et al. found that sustained reductions in I_{Kr} may lead to compensatory upregulation of I_{Ks} through post-transcriptional upregulation of underlying subunits (Xiao et al., 2008), which potentially underlie the observed phenomenon of repolarization reserve (Roden, 2008). Macromolecular complexes or post-transcriptional modifications could also facilitate coregulation of ionic conductances, as demonstrated by the observed structural or functional complex between I_{to} and I_{Na} (Deschenes et al., 2008). Rees et al. recently argued that sensing of aggregate CaT may be sufficient in itself to regulate ionic conductances (of K^+ and inward Ca^{2+}) to maintain normal Ca^{2+} handling (Rees et al., 2018). Moreover, knockout and knockdown studies are consistent with the idea that cardiac cells have compensatory mechanisms to maintain AP or CaTs (perhaps to prevent arrhythmias) (Guo et al., 1999; Zhou et al., 2003). The covariance of ionic conductance can have significant implications for both calibrating populations of models or fitting sample-specific models, because it could propose additional constraints for how the underlying parameters of the computational model can be varied. Thus, new methods have begun to be developed that

measure all ionic conductances at once, and can not only tease out how ionic conductances are correlated, but the extent to which they vary between cells (Banyasz et al., 2011; Groenendaal et al., 2015).

Arrhythmia Research Requires Understanding Variability at Larger Spatial Scales

Accounting for variability at tissue and organ-level scales is a logical, but not trivial (Elshrif and Cherry, 2014), next step. A thorough investigation of variability would first require including differences among the cells in the same tissue, and evaluating the impact of diverse geometrical distributions. One should also account for patient-specific structural differences, based on measures of tissue conductivity and anatomic properties, including heterogeneity in signaling due to non-uniform innervation. This last step can be particularly problematic when investigating diseased conditions affected by pronounced structural remodeling, such as fibrosis, organ dilation, and alterations in gap junction coupling. Where there has been meaningful progress in accounting for variability is in developing personalized atrial model structures based on medical images (Dossel et al., 2012; Trayanova, 2014). These methods have shown some promise in developing personalized ablation strategies (McDowell et al., 2015). For example, recently, Soor et al. implemented a modeling approach to optimize ablation times based on patient-specific atrial geometries to create lesions for a given atrial wall thickness (Soor et al., 2016). Combining these methods that utilize medical images with the methods described here, could significantly improve the clinical value of both methods alone (Hansen et al., 2017; Zhao et al., 2017). For example, Arevalo et al. developed personalized heart models based on cardiac imaging and published patch-clamp data to better predict arrhythmic events and possibly avoid unnecessary implantable cardioverter defibrillators (Arevalo et al., 2016). Developing multi-scale frameworks that account for variability is the next frontier in cardiac modeling that will greatly benefit from further advancements in computing capabilities. Beyond the availability of large experimental and clinical datasets, the development of novel techniques to speed model derivations and to integrate automation will be crucial to capture variability for different cell types and conditions at various scales.

Safety Pharmacology Requires Complementary Electrophysiological Experimental Methods

The *in silico* approaches described here are being combined with other state-of-the-art tools to improve the evaluation of drug safety. Of significance, these approaches can help further the mission of the CiPA (Comprehensive *in vitro* Proarrhythmia Assay) initiative, which aspires to develop better methods to predict TdP. Beyond exclusively using steady-state hERG block as the main predictor of arrhythmia and not at all using QT interval prolongation, the CiPA initiative attempts to gain

a more comprehensive understanding of proarrhythmic risk by combining (1) mechanistically-based *in vitro* assays, (2) *in silico* reconstructions of cardiac electrophysiology, and (3) confirmation using human iPSC-CMs (Colatsky et al., 2016). The methods described in this review are being utilized to help meet the mission of the CiPA initiative (Cummins et al., 2014; Lancaster and Sobie, 2016; Britton et al., 2017a; Passini et al., 2017). Most of the methods described here that assess the effects of drugs on populations of cardiac myocytes use simple pore block schemes. However, it is also clear that the sole use of steady-state hERG block assays is insufficient to predict arrhythmia risk, and thus studies are beginning to simulate the effects drug-binding kinetics and state-specific binding, which have been shown to affect electrophysiological outcomes (Lee W. et al., 2016; Dutta et al., 2017; Ellinwood et al., 2017b; Li et al., 2017). Incorporating more detailed drug-binding effects may allow studying the effects of populations of drugs characteristics (e.g., state-dependent block and kinetics) on populations of cardiomyocytes.

CONCLUSION

Computational approaches that have been developed over the past decade to account for variability in cardiac electrophysiology have led to important insights into mechanisms of arrhythmogenesis, etiology of disease, and variable response to drugs. The approaches outlined in this review are used in basic research studies, i.e., quite separately from actual clinical workflows, where decisions are made sometimes for a particular patient within minutes. Advanced computing facilities now allow near real-time simulations of anatomically realistic, biophysically detailed models of human cardiac electrophysiology (Niederer et al., 2011b; Okada et al., 2015, 2017). Such massively parallel processes could be optimized to run personalized cardiac simulations pre-determined to have clinical value. However, implementing these approaches more comprehensively into clinical workflows still presents challenges and simulation of variability may not find immediate application.

AUTHOR CONTRIBUTIONS

HN, SM, and EG reviewed the literature and wrote the manuscript.

ACKNOWLEDGMENTS

This work was supported by the American Heart Association grant 15SDG24910015 (EG); the National Institutes of Health (NIH) Stimulating Peripheral Activity to Relieve Conditions grant 1OT2OD023848-01 (EG), the National Heart, Lung, and Blood Institute R01HL131517 and R01HL141214 grants (EG) and K99HL138160 award (SM); and the Heart Rhythm Society post-doctoral fellowship 16OA9HRS (SM). An early version of this article was drafted by Dr. Nicholas Ellinwood.

REFERENCES

- Abramson, D., Bernabeu, M. O., Bethwaite, B., Burrage, K., Corrias, A., Enticott, C., et al. (2010). High-throughput cardiac science on the Grid. *Philos. Trans. A Math. Phys. Eng. Sci.* 368, 3907–3923. doi: 10.1098/rsta.2010.0170
- Achard, P., and De Schutter, E. (2006). Complex parameter landscape for a complex neuron model. *PLoS Comput. Biol.* 2:e94. doi: 10.1371/journal.pcbi.0020094
- Adeniran, I., El Harchi, A., Hancox, J. C., and Zhang, H. (2012). Proarrhythmia in KCNJ2-linked short QT syndrome: insights from modelling. *Cardiovasc. Res.* 94, 66–76. doi: 10.1093/cvr/cvs082
- Ahrens-Nicklas, R. C., Clancy, C. E., and Christini, D. J. (2009). Re-evaluating the efficacy of beta-adrenergic agonists and antagonists in long QT-3 syndrome through computational modelling. *Cardiovasc. Res.* 82, 439–447. doi: 10.1093/cvr/cvp083
- Al Abed, A., Guo, T., Lovell, N. H., and Dokos, S. (2013). Optimisation of ionic models to fit tissue action potentials: application to 3D atrial modelling. *Comput. Math. Methods Med.* 2013:951234. doi: 10.1155/2013/951234
- Arevalo, H. J., Vadakkumpadan, F., Guallar, E., Jebb, A., Malamas, P., Wu, K. C., et al. (2016). Arrhythmia risk stratification of patients after myocardial infarction using personalized heart models. *Nat. Commun.* 7:11437. doi: 10.1038/ncomms11437
- Banyasz, T., Horvath, B., Jian, Z., Izu, L. T., and Chen-Izu, Y. (2011). Sequential dissection of multiple ionic currents in single cardiac myocytes under action potential-clamp. *J. Mol. Cell. Cardiol.* 50, 578–581. doi: 10.1016/j.yjmcc.2010.12.020
- Barichello, S., Roberts, J. D., Backx, P., Boyle, P. M., and Laksman, Z. (2018). Personalizing therapy for atrial fibrillation: the role of stem cell and *in silico* disease models. *Cardiovasc. Res.* 114, 931–943. doi: 10.1093/cvr/cvy090
- Batchvarov, V. N., Ghuran, A., Smetana, P., Hnatkova, K., Harries, M., Dilaveris, P., et al. (2002). QT-RR relationship in healthy subjects exhibits substantial intersubject variability and high intrasubject stability. *Am. J. Physiol. Heart Circ. Physiol.* 282, H2356–H2363. doi: 10.1152/ajpheart.00860.2001
- Beattie, K. A., Hill, A. P., Bardenet, R., Cui, Y., Vandenberg, J. I., Gavaghan, D. J., et al. (2018). Sinusoidal voltage protocols for rapid characterisation of ion channel kinetics. *J. Physiol.* 596, 1813–1828. doi: 10.1113/JP275733
- Beeler, G. W., and Reuter, H. (1977). Reconstruction of the action potential of ventricular myocardial fibres. *J. Physiol.* 268, 177–210. doi: 10.1113/jphysiol.1977.sp011853
- Behar, J., and Yaniv, Y. (2017). Age-related pacemaker deterioration is due to impaired intracellular and membrane mechanisms: insights from numerical modeling. *J. Gen. Physiol.* 149, 935–949. doi: 10.1085/jgp.2017.1179
- Ben-Shalom, R., Aviv, A., Razon, B., and Korngreen, A. (2012). Optimizing ion channel models using a parallel genetic algorithm on graphical processors. *J. Neurosci. Methods* 206, 183–194. doi: 10.1016/j.jneumeth.2012.02.024
- Bot, C. T., Kherlopian, A. R., Ortega, F. A., Christini, D. J., and Krogh-Madsen, T. (2012). Rapid genetic algorithm optimization of a mouse computational model: benefits for anthropomorphization of neonatal mouse cardiomyocytes. *Front. Physiol.* 3:421. doi: 10.3389/fphys.2012.00421
- Boutjdir, M., Le Heuzey, J. Y., Lavergne, T., Chauvaud, S., Guize, L., Carpenter, A., et al. (1986). Inhomogeneity of cellular refractoriness in human atrium: factor of arrhythmia? *Pacing Clin. Electrophysiol.* 9, 1095–1100. doi: 10.1111/j.1540-8159.1986.tb06676.x
- Britton, O. J., Abi-Gerges, N., Page, G., Ghetti, A., Miller, P. E., and Rodriguez, B. (2017a). Quantitative comparison of effects of dofetilide, sotalol, quinidine, and verapamil between human *ex vivo* trabeculae and *in silico* ventricular models incorporating inter-individual action potential variability. *Front. Physiol.* 8:597. doi: 10.3389/fphys.2017.00597
- Britton, O. J., Bueno-Orovio, A., Van Ammel, K., Lu, H. R., Towart, R., Gallacher, D. J., et al. (2013). Experimentally calibrated population of models predicts and explains intersubject variability in cardiac cellular electrophysiology. *Proc. Natl. Acad. Sci. U.S.A.* 110, E2098–E2105. doi: 10.1073/pnas.1304382110
- Britton, O. J., Bueno-Orovio, A., Virag, L., Varro, A., and Rodriguez, B. (2017b). The Electrogenic Na(+)K(+) Pump is a key determinant of repolarization abnormality susceptibility in human ventricular cardiomyocytes: a population-based simulation study. *Front. Physiol.* 8:278. doi: 10.3389/fphys.2017.00278
- Bueno-Orovio, A., Cherry, E. M., and Fenton, F. H. (2008). Minimal model for human ventricular action potentials in tissue. *J. Theor. Biol.* 253, 544–560. doi: 10.1016/j.jtbi.2008.03.029
- Bueno-Orovio, A., Sánchez, C., Pueyo, E., and Rodriguez, B. (2014). Na/K pump regulation of cardiac repolarization: insights from a systems biology approach. *Pflugers Arch.* 466, 183–193. doi: 10.1007/s00424-013-1293-1
- Burrage, K., Burrage, P., Donovan, D., and Thompson, B. (2015). Populations of models, experimental designs and coverage of parameter space by latin hypercube and orthogonal sampling. *Procedia Comp. Sci.* 51, 1762–1771. doi: 10.1016/j.procs.2015.05.383
- Butters, T. D., Aslanidi, O. V., Inada, S., Boyett, M. R., Hancox, J. C., Lei, M., et al. (2010). Mechanistic links between Na⁺ channel (SCN5A) mutations and impaired cardiac pacemaking in sick sinus syndrome. *Circ. Res.* 107, 126–137. doi: 10.1161/CIRCRESAHA.110.219949
- Campbell, S. G., Flaim, S. N., Leem, C. H., and McCulloch, A. D. (2008). Mechanisms of transmurally varying myocyte electromechanics in an integrated computational model. *Philos. Trans. A Math. Phys. Eng. Sci.* 366, 3361–3380. doi: 10.1098/rsta.2008.0088
- Chang, E. T., Strong, M., and Clayton, R. H. (2015). Bayesian sensitivity analysis of a cardiac cell model using a gaussian process emulator. *PLoS ONE* 10: e0130252. doi: 10.1371/journal.pone.0130252
- Chen, Q., and Guan, S. U. (2004). Incremental multiple objective genetic algorithms. *IEEE Trans. Syst. Man. Cybern. B Cybern.* 34, 1325–1334. doi: 10.1109/TSMCB.2003.822958
- Clancy, C. E., and Rudy, Y. (1999). Linking a genetic defect to its cellular phenotype in a cardiac arrhythmia. *Nature* 400, 566–569. doi: 10.1038/23034
- Clancy, C. E., and Rudy, Y. (2002). Na(+) channel mutation that causes both Brugada and long-QT syndrome phenotypes: a simulation study of mechanism. *Circulation* 105, 1208–1213. doi: 10.1161/hc1002.105183
- Clancy, C. E., Tateyama, M., and Kass, R. S. (2002). Insights into the molecular mechanisms of bradycardia-triggered arrhythmias in long QT-3 syndrome. *J. Clin. Invest.* 110, 1251–1262. doi: 10.1172/JCI0215928
- Clancy, C. E., Zhu, Z. I., and Rudy, Y. (2007). Pharmacogenetics and anti-arrhythmic drug therapy: a theoretical investigation. *Am. J. Physiol. Heart Circ. Physiol.* 292, H66–H75. doi: 10.1152/ajpheart.00312.2006
- Colatsky, T., Fermini, B., Gintant, G., Pierson, J. B., Sager, P., Sekino, Y., et al. (2016). The Comprehensive *in Vitro* Proarrhythmia Assay (CiPA) initiative - Update on progress. *J. Pharmacol. Toxicol. Methods* 81, 15–20. doi: 10.1016/j.vascn.2016.06.002
- Colman, M. A., Aslanidi, O. V., Kharche, S., Boyett, M. R., Garratt, C., Hancox, J. C., et al. (2013). Pro-arrhythmogenic effects of atrial fibrillation-induced electrical remodelling: insights from the three-dimensional virtual human atria. *J. Physiol.* 591, 4249–4272. doi: 10.1113/jphysiol.2013.254987
- Comtois, P., Sakabe, M., Vigmond, E. J., Munoz, M., Texier, A., Shiroshita-Takeshita, A., et al. (2008). Mechanisms of atrial fibrillation termination by rapidly unbinding Na⁺ channel blockers: insights from mathematical models and experimental correlates. *Am. J. Physiol. Heart Circ. Physiol.* 295, H1489–H1504. doi: 10.1152/ajpheart.01054.2007
- Corrias, A., Giles, W., and Rodriguez, B. (2011). Ionic mechanisms of electrophysiological properties and repolarization abnormalities in rabbit Purkinje fibers. *Am. J. Physiol. Heart Circ. Physiol.* 300, H1806–H1813. doi: 10.1152/ajpheart.01170.2010
- Courtmanche, M., Ramirez, R. J., and Nattel, S. (1998). Ionic mechanisms underlying human atrial action potential properties: insights from a mathematical model. *Am. J. Physiol.* 275, H301–H321. doi: 10.1152/ajpheart.1998.275.1.H301
- Courtmanche, M., and Winfree, A. T. (1991). Re-entrant rotating waves in a beeler-reuter based model of two-dimensional cardiac electrical activity. *Int. J. Bifurcation Chaos* 1, 431–444. doi: 10.1142/S0218127491000336
- Crosby, J. L. (1982). *Computer Simulation in Genetics*. London, New York, NY: John Wiley.
- Cummins, M. A., Dalal, P. J., Bugana, M., Severi, S., and Sobie, E. A. (2014). Comprehensive analyses of ventricular myocyte models identify targets exhibiting favorable rate dependence. *PLoS Comput. Biol.* 10:e1003543. doi: 10.1371/journal.pcbi.1003543
- Daniels, G. S. (1952). *The Average Man?* Technical Note WCRD53-7, Wright Air Development Center, Ohio AD-10203.

- Deng, D., Murphy, M. J., Hakim, J. B., Franceschi, W. H., Zahid, S., Pashakhanloo, F., et al. (2017). Sensitivity of reentrant driver localization to electrophysiological parameter variability in image-based computational models of persistent atrial fibrillation sustained by a fibrotic substrate. *Chaos* 27, 093932. doi: 10.1063/1.5003340
- Deschênes, I., Armoundas, A. A., Jones, S. P., and Tomaselli, G. F. (2008). Post-transcriptional gene silencing of KChIP2 and Navbeta1 in neonatal rat cardiac myocytes reveals a functional association between Na and Ito currents. *J. Mol. Cell. Cardiol.* 45, 336–346. doi: 10.1016/j.yjmcc.2008.05.001
- Devenyi, R. A., Ortega, F. A., Groenendaal, W., Krogh-Madsen, T., Christini, D. J., and Sobie, E. A. (2017). Differential roles of two delayed rectifier potassium currents in regulation of ventricular action potential duration and arrhythmia susceptibility. *J. Physiol.* 595, 2301–2317. doi: 10.1113/JP27319
- Devenyi, R. A., and Sobie, E. A. (2016). There and back again: iterating between population-based modeling and experiments reveals surprising regulation of calcium transients in rat cardiac myocytes. *J. Mol. Cell. Cardiol.* 96, 38–48. doi: 10.1016/j.yjmcc.2015.07.016
- Dibb, K., Trafford, A., Zhang, H., and Eisner, D. (2015). A model model: a commentary on DiFrancesco and Noble (1985) 'A model of cardiac electrical activity incorporating ionic pumps and concentration changes'. *Philos. Trans. R Soc. Lond. B Biol. Sci.* 370:20140316. doi: 10.1098/rstb.2014.0316
- DiFrancesco, D., and Noble, D. (1985). A model of cardiac electrical activity incorporating ionic pumps and concentration changes. *Philos. Trans. R Soc. Lond. B Biol. Sci.* 307, 353–398. doi: 10.1098/rstb.1985.0001
- Dokos, S., and Lovell, N. H. (2004). Parameter estimation in cardiac ionic models. *Prog. Biophys. Mol. Biol.* 85, 407–431. doi: 10.1016/j.pbiomolbio.2004.02.002
- Donovan, D., Burrage, K., Burrage, P., McCourt, T. A., Thompson, B., and Yazici, E. S. (2018). Estimates of the coverage of parameter space by latin hypercube and orthogonal array-based sampling. *Appl. Math. Model.* 57, 553–564. doi: 10.1016/j.apm.2017.11.036
- Dössel, O., Krueger, M. W., Weber, F. M., Wilhelms, M., and Seemann, G. (2012). Computational modeling of the human atrial anatomy and electrophysiology. *Med. Biol. Eng. Comput.* 50, 773–799. doi: 10.1007/s11517-012-0924-6
- Draper, N. R., and Smith, H. (2014). *Applied Regression Analysis*. Hoboken; Somerset, NJ: John Wiley and Sons.
- Druckmann, S., Banitt, Y., Gidon, A., Schürmann, F., Markram, H., and Segev, I. (2007). A novel multiple objective optimization framework for constraining conductance-based neuron models by experimental data. *Front. Neurosci.* 1, 7–18. doi: 10.3389/neuro.01.1.001.2007
- Dutta, S., Chang, K. C., Beattie, K. A., Sheng, J., Tran, P. N., Wu, W. W., et al. (2017). Optimization of an *in silico* cardiac cell model for proarrhythmia risk assessment. *Front. Physiol.* 8:616. doi: 10.3389/fphys.2017.00616
- Edwards, A. G., Grandi, E., Hake, J. E., Patel, S., Li, P., Miyamoto, S., et al. (2014). Nonequilibrium reactivation of Na⁺ current drives early afterdepolarizations in mouse ventricle. *Circ. Arrhythm Electrophysiol.* 7, 1205–1213. doi: 10.1161/CIRCEP.113.001666
- Ellinwood, N., Dobrev, D., Morotti, S., and Grandi, E. (2017a). *In silico* assessment of efficacy and safety of IKur inhibitors in chronic atrial fibrillation: role of kinetics and state-dependence of drug binding. *Front. Pharmacol.* 8, 799. doi: 10.3389/fphar.2017.00799
- Ellinwood, N., Dobrev, D., Morotti, S., and Grandi, E. (2017b). Revealing kinetics and state-dependent binding properties of IKur-targeting drugs that maximize atrial fibrillation selectivity. *Chaos* 27, 093918. doi: 10.1063/1.5000226
- Elshrif, M. M., and Cherry, E. M. (2014). A quantitative comparison of the behavior of human ventricular cardiac electrophysiology models in tissue. *PLoS ONE* 9:e84401. doi: 10.1371/journal.pone.0084401
- Fender, E. A., Henrikson, C. A., and Tereshchenko, L. (2014). Racial differences in sudden cardiac death. *J. Electrocardiol.* 47, 815–818. doi: 10.1016/j.jelectrocard.2014.07.023
- Feng, J., Yue, L., Wang, Z., and Nattel, S. (1998). Ionic mechanisms of regional action potential heterogeneity in the canine right atrium. *Circ. Res.* 83, 541–551. doi: 10.1161/01.RES.83.5.541
- Fink, M., Niederer, S. A., Cherry, E. M., Fenton, F. H., Koivumäki, J. T., Seemann, G., et al. (2011). Cardiac cell modelling: observations from the heart of the cardiac physiome project. *Prog. Biophys. Mol. Biol.* 104, 2–21. doi: 10.1016/j.pbiomolbio.2010.03.002
- Fotiadis, P., and Forger, D. B. (2013). Modeling the effects of the circadian clock on cardiac electrophysiology. *J. Biol. Rhythms* 28, 69–78. doi: 10.1177/0748730412469499
- Fox, J. J., Mcharg, J. L., and Gilmour, R. F. (2002). Ionic mechanism of electrical alternans. *Am. J. Physiol. Heart Circ. Physiol.* 282, H516–H530. doi: 10.1152/ajpheart.00612.2001
- Fraser, A., and Burnell, D. (1970). *Computer Models in Genetics*. New York, NY: McGraw-Hill.
- Gaborit, N., Le Bouter, S., Szuts, V., Varro, A., Escande, D., Nattel, S., et al. (2007). Regional and tissue specific transcript signatures of ion channel genes in the non-diseased human heart. *J. Physiol.* 582, 675–693. doi: 10.1113/jphysiol.2006.126714
- Gasper, R., Bosch, R. F., Talajic, M., and Nattel, S. (1997). Functional mechanisms underlying tachycardia-induced sustained atrial fibrillation in a chronic dog model. *Circulation* 96, 4027–4035. doi: 10.1161/01.CIR.96.11.4027
- Geladi, P., and Kowalski, B. R. (1986). Partial least-squares regression - a tutorial. *Anal. Chim. Acta* 185, 1–17. doi: 10.1016/0003-2670(86)80028-9
- Golowasch, J., Goldman, M. S., Abbott, L. F., and Marder, E. (2002). Failure of averaging in the construction of a conductance-based neuron model. *J. Neurophys.* 87, 1129–1131. doi: 10.1152/jn.00412.2001
- Gong, J. Q. X., and Sobie, E. A. (2018). Population-based mechanistic modeling allows for quantitative predictions of drug responses across cell types. *NPJ. Syst. Biol. Appl.* 4, 11. doi: 10.1038/s41540-018-0047-2
- Gong, Y., Xie, F., Stein, K. M., Garfinkel, A., Culianu, C. A., Lerman, B. B., et al. (2007). Mechanism underlying initiation of paroxysmal atrial flutter/atrial fibrillation by ectopic foci: a simulation study. *Circulation* 115, 2094–2102. doi: 10.1161/CIRCULATIONAHA.106.656504
- Grandi, E., and Maleckar, M. M. (2016). Anti-arrhythmic strategies for atrial fibrillation: the role of computational modeling in discovery, development, and optimization. *Pharmacol. Ther.* 168, 126–142. doi: 10.1016/j.pharmthera.2016.09.012
- Grandi, E., Pandit, S. V., Voigt, N., Workman, A. J., Dobrev, D., Jalife, J., et al. (2011). Human atrial action potential and Ca²⁺ model: sinus rhythm and chronic atrial fibrillation. *Circ. Res.* 109, 1055–1066. doi: 10.1161/CIRCRESAHA.111.253955
- Grandi, E., Pasqualini, F. S., and Bers, D. M. (2010). A novel computational model of the human ventricular action potential and Ca transient. *J. Mol. Cell. Cardiol.* 48, 112–121. doi: 10.1016/j.yjmcc.2009.09.019
- Gray, R. A., Jalife, J., Panfilov, A., Baxter, W. T., Cabo, C., Davidenko, J. M., et al. (1995). Nonstationary vortexlike reentrant activity as a mechanism of polymorphic ventricular tachycardia in the isolated rabbit heart. *Circulation* 91, 2454–2469. doi: 10.1161/01.CIR.91.9.2454
- Groenendaal, W., Ortega, F. A., Kherlopian, A. R., Zygmunt, A. C., Krogh-Madsen, T., and Christini, D. J. (2015). Cell-specific cardiac electrophysiology models. *PLoS Comput. Biol.* 11:e1004242. doi: 10.1371/journal.pcbi.1004242
- Guo, T., Abed, A. A., Lovell, N. H., and Dokos, S. (2010). A generic ionic model of cardiac action potentials. *Conf. Proc. IEEE. Eng. Med. Biol. Soc.* 2010, 1465–1468. doi: 10.1109/IEMBS.2010.5626853
- Guo, T., Al Abed, A., Lovell, N. H., and Dokos, S. (2013). Optimisation of a generic ionic model of cardiac myocyte electrical activity. *Comput. Math. Methods Med.* 2013:706195. doi: 10.1155/2013/706195
- Guo, W., Xu, H., London, B., and Nerbonne, J. M. (1999). Molecular basis of transient outward K⁺ current diversity in mouse ventricular myocytes. *J. Physiol.* 521(Pt 3), 587–599. doi: 10.1111/j.1469-7793.1999.00587.x
- Gurkiewicz, M., and Korngreen, A. (2007). A numerical approach to ion channel modelling using whole-cell voltage-clamp recordings and a genetic algorithm. *PLoS Comput. Biol.* 3:e169. doi: 10.1371/journal.pcbi.0030169
- Hair, J. F., Black, W. C., Babin, B. J., and Anderson, R. E. (2010). *Multivariate Data Analysis*. Upper Saddle River, NJ: Pearson Prentice Hall.
- Hansen, B. J., Zhao, J., and Fedorov, V. V. (2017). Fibrosis and atrial fibrillation: computerized and optical mapping; a view into the human atria at submillimeter resolution. *JACC Clin. Electrophysiol.* 3, 531–546. doi: 10.1016/j.jacep.2017.05.002
- Heijman, J., Zaza, A., Johnson, D. M., Rudy, Y., Peeters, R. L., Volders, P. G., et al. (2013). Determinants of beat-to-beat variability of repolarization duration in the canine ventricular myocyte: a computational analysis. *PLoS Comput. Biol.* 9:e1003202. doi: 10.1371/journal.pcbi.1003202

- Hobbs, K. H., and Hooper, S. L. (2008). Using complicated, wide dynamic range driving to develop models of single neurons in single recording sessions. *J. Neurophysiol.* 99, 1871–1883. doi: 10.1152/jn.00032.2008
- Hodgkin, A. L., and Huxley, A. F. (1952). A quantitative description of membrane current and its application to conduction and excitation in nerve. *J. Physiol.* 117, 500–544. doi: 10.1113/jphysiol.1952.sp004764
- Hund, T. J., and Rudy, Y. (2004). Rate dependence and regulation of action potential and calcium transient in a canine cardiac ventricular cell model. *Circulation* 110, 3168–3174. doi: 10.1161/01.CIR.0000147231.69595.D3
- Hussein, Y. A., and El-Ghazaly, S. M. (2004). Modeling and optimization of microwave devices and circuits using genetic algorithms. *IEEE Trans. Microwave Theory Tech.* 52, 329–336. doi: 10.1109/TMTT.2003.820899
- Inada, S., Hancox, J. C., Zhang, H., and Boyett, M. R. (2009). One-dimensional mathematical model of the atrioventricular node including atrio-nodal, nodal, and nodal-his cells. *Biophys. J.* 97, 2117–2127. doi: 10.1016/j.bpj.2009.06.056
- Janes, K. A., Albeck, J. G., Gaudet, S., Sorger, P. K., Lauffenburger, D. A., and Yaffe, M. B. (2005). A systems model of signaling identifies a molecular basis set for cytokine-induced apoptosis. *Science* 310, 1646–1653. doi: 10.1126/science.1116598
- Jeyaraj, D., Haldar, S. M., Wan, X., Mccauley, M. D., Ripperger, J. A., Hu, K., et al. (2012). Circadian rhythms govern cardiac repolarization and arrhythmogenesis. *Nature* 483, 96–99. doi: 10.1038/nature10852
- Johnstone, R. H., Chang, E. T. Y., Bardenet, R., de Boer, T. P., Gavaghan, D. J., Pathmanathan, P., et al. (2016). Uncertainty and variability in models of the cardiac action potential: can we build trustworthy models? *J. Mol. Cell. Cardiol.* 96, 49–62. doi: 10.1016/j.yjmcc.2015.11.018
- Kannankeril, P. J., Norris, K. J., Carter, S., and Roden, D. M. (2011). Factors affecting the degree of QT prolongation with drug challenge in a large cohort of normal volunteers. *Heart Rhythm* 8, 1530–1534. doi: 10.1016/j.hrthm.2011.03.042
- Kaur, J., Nygren, A., and Vigmond, E. J. (2014). Fitting membrane resistance along with action potential shape in cardiac myocytes improves convergence: application of a multi-objective parallel genetic algorithm. *PLoS ONE* 9:e107984. doi: 10.1371/journal.pone.0107984
- Kharche, S., Garratt, C. J., Boyett, M. R., Inada, S., Holden, A. V., Hancox, J. C., et al. (2008). Atrial proarrhythmia due to increased inward rectifier current (I_{K1}) arising from KCNJ2 mutation—a simulation study. *Prog. Biophys. Mol. Biol.* 98, 186–197. doi: 10.1016/j.pbiomolbio.2008.10.010
- Koivumäki, J. T., Naumenko, N., Tuomainen, T., Takalo, J., Oksanen, M., Puttonen, K. A., et al. (2018). Structural immaturity of human iPSC-Derived cardiomyocytes: *in silico* investigation of effects on function and disease modeling. *Front. Physiol.* 9:80. doi: 10.3389/fphys.2018.00080
- Krogh-Madsen, T., and Christini, D. J. (2012). Nonlinear dynamics in cardiology. *Annu. Rev. Biomed. Eng.* 14, 179–203. doi: 10.1146/annurev-bioeng-071811-150106
- Krogh-Madsen, T., Jacobson, A. F., Ortega, F. A., and Christini, D. J. (2017). Global optimization of ventricular myocyte model to multi-variable objective improves predictions of drug-induced torsades de pointes. *Front. Physiol.* 8:1059. doi: 10.3389/fphys.2017.01059
- Krogh-Madsen, T., Sobie, E. A., and Christini, D. J. (2016). Improving cardiomyocyte model fidelity and utility via dynamic electrophysiology protocols and optimization algorithms. *J. Physiol.* 594, 2525–2536. doi: 10.1113/JP270618
- Kurata, Y., Hisatome, I., Matsuda, H., and Shibamoto, T. (2005). Dynamical mechanisms of pacemaker generation in IK1-downregulated human ventricular myocytes: insights from bifurcation analyses of a mathematical model. *Biophys. J.* 89, 2865–2887. doi: 10.1529/biophysj.105.060830
- Lancaster, M. C., and Sobie, E. A. (2016). Improved prediction of drug-induced torsades de pointes through simulations of dynamics and machine learning algorithms. *Clin. Pharmacol. Ther.* 100, 371–379. doi: 10.1002/cpt.367
- Lau, C. P., Tse, H. F., Siu, C. W., and Gbadebo, D. (2012). Atrial electrical and structural remodeling: implications for racial differences in atrial fibrillation. *J. Cardiovasc. Electrophysiol.* 23(Suppl. 1), S36–S40. doi: 10.1111/jce.12022
- Lawson, B. A. J., Drovandi, C. C., Cusimano, N., Burrage, P., Rodriguez, B., and Burrage, K. (2018). Unlocking data sets by calibrating populations of models to data density: a study in atrial electrophysiology. *Sci. Adv.* 4:e1701676. doi: 10.1126/sciadv.1701676
- Lee, W., Mann, S. A., Windley, M. J., Imtiaz, M. S., Vandenberg, J. I., and Hill, A. P. (2016). *In silico* assessment of kinetics and state dependent binding properties of drugs causing acquired LQTS. *Prog. Biophys. Mol. Biol.* 120, 89–99. doi: 10.1016/j.pbiomolbio.2015.12.005
- Lee, Y. S., Hwang, M., Song, J. S., Li, C., Joung, B., Sobie, E. A., et al. (2016). The contribution of ionic currents to rate-dependent action potential duration and pattern of reentry in a mathematical model of human atrial fibrillation. *PLoS ONE* 11:e0150779. doi: 10.1371/journal.pone.0150779
- Lee, Y. S., Liu, O. Z., Hwang, H. S., Knollmann, B. C., and Sobie, E. A. (2013). Parameter sensitivity analysis of stochastic models provides insights into cardiac calcium sparks. *Biophys. J.* 104, 1142–1150. doi: 10.1016/j.bpj.2012.12.055
- Leung, F. H. F., Lam, H. K., Ling, S. H., and Tam, P. K. S. (2004). Optimal and stable fuzzy controllers for nonlinear systems based on an improved genetic algorithm. *IEEE Trans. Indus. Electron.* 51, 172–182. doi: 10.1109/TIE.2003.821898
- Li, Z., Dutta, S., Sheng, J., Tran, P. N., Wu, W., Chang, K., et al. (2017). Improving the *in silico* assessment of proarrhythmia risk by combining herg (human ether-a-go-go-related gene) channel-drug binding kinetics and multichannel pharmacology. *Circ. Arrhythm. Electrophysiol.* 10:e004628. doi: 10.1161/CIRCEP.116.004628
- Liberos, A., Bueno-Orovio, A., Rodrigo, M., Ravens, U., Hernandez-Romero, I., Fernandez-Aviles, F., et al. (2016). Balance between sodium and calcium currents underlying chronic atrial fibrillation termination: an *in silico* intersubject variability study. *Heart Rhythm* 13, 2358–2365. doi: 10.1016/j.hrthm.2016.08.028
- Liu, L., and Nattel, S. (1997). Differing sympathetic and vagal effects on atrial fibrillation in dogs: role of refractoriness heterogeneity. *Am. J. Physiol.* 273, H805–H816. doi: 10.1152/ajpheart.1997.273.2.H805
- Livshitz, L., and Rudy, Y. (2009). Uniqueness and stability of action potential models during rest, pacing, and conduction using problem-solving environment. *Biophys. J.* 97, 1265–1276. doi: 10.1016/j.bpj.2009.05.062
- Lombardo, D. M., Fenton, F. H., Narayan, S. M., and Rappel, W. J. (2016). Comparison of detailed and simplified models of human atrial myocytes to recapitulate patient specific properties. *PLoS Comput. Biol.* 12:e1005060. doi: 10.1371/journal.pcbi.1005060
- Luo, C. H., and Rudy, Y. (1991). A model of the ventricular cardiac action potential. Depolarization, repolarization, and their interaction. *Circ. Res.* 68, 1501–1526. doi: 10.1161/01.RES.68.6.1501
- Maleckar, M. M., Greenstein, J. L., Giles, W. R., and Trayanova, N. A. (2009). K⁺ current changes account for the rate dependence of the action potential in the human atrial myocyte. *Am. J. Physiol. Heart Circ. Physiol.* 297, H1398–H1410. doi: 10.1152/ajpheart.00411.2009
- Maltsev, V. A., and Lakatta, E. G. (2009). Synergism of coupled subsarcolemmal Ca²⁺ clocks and sarcolemmal voltage clocks confers robust and flexible pacemaker function in a novel pacemaker cell model. *Am. J. Physiol. Heart Circ. Physiol.* 296, H594–H615. doi: 10.1152/ajpheart.01118.2008
- Mann, S. A., Imtiaz, M., Winbo, A., Rydberg, A., Perry, M. D., Couderc, J. P., et al. (2016). Convergence of models of human ventricular myocyte electrophysiology after global optimization to recapitulate clinical long QT phenotypes. *J. Mol. Cell. Cardiol.* 100, 25–34. doi: 10.1016/j.yjmcc.2016.09.011
- Mann, S. A., Otway, R., Guo, G., Soka, M., Karlsson, L., Trivedi, G., et al. (2012). Epistatic effects of potassium channel variation on cardiac repolarization and atrial fibrillation risk. *J. Am. Coll. Cardiol.* 59, 1017–1025. doi: 10.1016/j.jacc.2011.11.039
- Marder, E. (2011). Variability, compensation, and modulation in neurons and circuits. *Proc. Natl. Acad. Sci. U.S.A.* 108(Suppl. 3), 15542–15548. doi: 10.1073/pnas.1010674108
- Marino, S., Hogue, I. B., Ray, C. J., and Kirschner, D. E. (2008). A methodology for performing global uncertainty and sensitivity analysis in systems biology. *J. Theor. Biol.* 254, 178–196. doi: 10.1016/j.jtbi.2008.04.011
- Mayourian, J., Cashman, T. J., Ceholski, D. K., Johnson, B. V., Sachs, D., Kaji, D. A., et al. (2017). Experimental and computational insight into human mesenchymal stem cell paracrine signaling and heterocellular coupling effects on cardiac contractility and arrhythmogenicity. *Circ. Res.* 121, 411–423. doi: 10.1161/CIRCRESAHA.117.310796
- McDowell, K. S., Zahid, S., Vadakkumpadan, F., Blauer, J., Macleod, R. S., and Trayanova, N. A. (2015). Virtual electrophysiological study

- of atrial fibrillation in fibrotic remodeling. *PLoS ONE* 10:e0117110. doi: 10.1371/journal.pone.0117110
- Milstein, M. L., Musa, H., Balbuena, D. P., Anumonwo, J. M., Auerbach, D. S., Furspan, P. B., et al. (2012). Dynamic reciprocity of sodium and potassium channel expression in a macromolecular complex controls cardiac excitability and arrhythmia. *Proc. Natl. Acad. Sci. U.S.A.* 109, E2134–E2143. doi: 10.1073/pnas.1109370109
- Mirams, G. R., Pathmanathan, P., Gray, R. A., Challenor, P., and Clayton, R. H. (2016). Uncertainty and variability in computational and mathematical models of cardiac physiology. *J. Physiol.* 594, 6833–6847. doi: 10.1113/JP271671
- Misier, A. R., Ophof, T., Van Hemel, N. M., Defauw, J. J., de Bakker, J. M., Janse, M. J., et al. (1992). Increased dispersion of “refractoriness” in patients with idiopathic paroxysmal atrial fibrillation. *J. Am. Coll. Cardiol.* 19, 1531–1535. doi: 10.1016/0735-1097(92)90614-S
- Moe, G. K., Rheinboldt, W. C., And Abildskov, J. A. (1964). A computer model of atrial fibrillation. *Am. Heart J.* 67, 200–220. doi: 10.1016/0002-8703(64)90371-0
- Morotti, S., and Grandi, E. (2017). Logistic regression analysis of populations of electrophysiological models to assess proarrhythmic risk. *MethodsX* 4, 25–34. doi: 10.1016/j.mex.2016.12.002
- Morotti, S., McCulloch, A. D., Bers, D. M., Edwards, A. G., and Grandi, E. (2016). Atrial-selective targeting of arrhythmogenic phase-3 early afterdepolarizations in human myocytes. *J. Mol. Cell. Cardiol.* 96, 63–71. doi: 10.1016/j.yjmcc.2015.07.030
- Muszkiewicz, A., Britton, O. J., Gemmell, P., Passini, E., Sánchez, C., Zhou, X., et al. (2016). Variability in cardiac electrophysiology: using experimentally-calibrated populations of models to move beyond the single virtual physiological human paradigm. *Prog. Biophys. Mol. Biol.* 120, 115–127. doi: 10.1016/j.pbiomolbio.2015.12.002
- Muszkiewicz, A., Liu, X., Bueno-Orovio, A., Lawson, B. A. J., Burrage, K., Casadei, B., et al. (2017). From ionic to cellular variability in human atrial myocytes: an integrative computational and experimental study. *Am. J. Physiol. Heart Circ. Physiol.* 314, H895–H916. doi: 10.1152/ajpheart.00477.2017
- Ni, H., Whittaker, D. G., Wang, W., Giles, W. R., Narayan, S. M., and Zhang, H. (2017). Synergistic anti-arrhythmic effects in human atria with combined use of sodium blockers and acacatin. *Front. Physiol.* 8:946. doi: 10.3389/fphys.2017.00946
- Niederer, S. A., Fink, M., Noble, D., and Smith, N. P. (2009). A meta-analysis of cardiac electrophysiology computational models. *Exp. Physiol.* 94, 486–495. doi: 10.1113/expphysiol.2008.044610
- Niederer, S. A., Kerfoot, E., Benson, A. P., Bernabeu, M. O., Bernus, O., Bradley, C., et al. (2011a). Verification of cardiac tissue electrophysiology simulators using an N-version benchmark. *Philos. Trans. R. Soc. Math. Phys. Eng. Sci.* 369, 4331–4351. doi: 10.1098/rsta.2011.0139
- Niederer, S., Mitchell, L., Smith, N., and Plank, G. (2011b). Simulating human cardiac electrophysiology on clinical time-scales. *Front. Physiol.* 2:14. doi: 10.3389/fphys.2011.00014
- Noble, D. (1962). A modification of the Hodgkin–Huxley equations applicable to Purkinje fibre action and pace-maker potentials. *J. Physiol.* 160, 317–352. doi: 10.1113/jphysiol.1962.sp006849
- Noble, D., Gurney, A., and Noble, P. J. (2012). How the Hodgkin–Huxley equations inspired the Cardiac Physiome Project. *J. Physiol. Lond.* 590, 2613–2628. doi: 10.1113/jphysiol.2011.224238
- Noble, D., Sarai, N., Noble, P. J., Kobayashi, T., Matsuoka, S., and Noma, A. (2007). Resistance of cardiac cells to NCX knockout: a model study. *Ann. N. Y. Acad. Sci.* 1099, 306–309. doi: 10.1196/annals.1387.018
- Nygren, A., Fiset, C., Firek, L., Clark, J. W., Lindblad, D. S., Clark, R. B., et al. (1998). Mathematical model of an adult human atrial cell: the role of K⁺ currents in repolarization. *Circ. Res.* 82, 63–81. doi: 10.1161/01.RES.82.1.63
- O’Hara, T., Virág, L., Varró, A., and Rudy, Y. (2011). Simulation of the undiseased human cardiac ventricular action potential: model formulation and experimental validation. *PLoS Comput. Biol.* 7:e1002061. doi: 10.1371/journal.pcbi.1002061
- Okada, J. I., Washio, T., Nakagawa, M., Watanabe, M., Kadooka, Y., Kariya, T., et al. (2017). Multi-scale, tailor-made heart simulation can predict the effect of cardiac resynchronization therapy. *J. Mol. Cell. Cardiol.* 108, 17–23. doi: 10.1016/j.yjmcc.2017.05.006
- Okada, J., Yoshinaga, T., Kurokawa, J., Washio, T., Furukawa, T., Sawada, K., et al. (2015). Screening system for drug-induced arrhythmogenic risk combining a patch clamp and heart simulator. *Sci. Adv.* 1:e1400142. doi: 10.1126/sciadv.1400142
- Paci, M., Passini, E., Severi, S., Hyttinen, J., and Rodriguez, B. (2017). Phenotypic variability in LQT3 human induced pluripotent stem cell-derived cardiomyocytes and their response to antiarrhythmic pharmacologic therapy: an *in silico* approach. *Heart Rhythm* 14, 1704–1712. doi: 10.1016/j.hrthm.2017.07.026
- Pandit, S. V., Clark, R. B., Giles, W. R., and Demir, S. S. (2001). A mathematical model of action potential heterogeneity in adult rat left ventricular myocytes. *Biophys. J.* 81, 3029–3051. doi: 10.1016/S0006-3495(01)75943-7
- Panfilov, A. V., and Holden, A. V. (1991). Spatiotemporal irregularity in a two-dimensional model of cardiac tissue. *Int. J. Bifurcation Chaos* 1, 219–225. doi: 10.1142/S0218127491000142
- Passini, E., Britton, O. J., Lu, H. R., Rohrbacher, J., Hermans, A. N., Gallacher, D. J., et al. (2017). Human *in silico* drug trials demonstrate higher accuracy than animal models in predicting clinical pro-arrhythmic cardiotoxicity. *Front. Physiol.* 8:668. doi: 10.3389/fphys.2017.00668
- Passini, E., Mincholé, A., Coppini, R., Cerbai, E., Rodriguez, B., Severi, S., et al. (2016). Mechanisms of pro-arrhythmic abnormalities in ventricular repolarisation and anti-arrhythmic therapies in human hypertrophic cardiomyopathy. *J. Mol. Cell. Cardiol.* 96, 72–81. doi: 10.1016/j.yjmcc.2015.09.003
- Pathmanathan, P., Bernabeu, M. O., Niederer, S. A., Gavaghan, D. J., and Kay, D. (2012). Computational modelling of cardiac electrophysiology: explanation of the variability of results from different numerical solvers. *Int. J. Numer. Methods Biomed. Eng.* 28, 890–903. doi: 10.1002/cnm.2467
- Pathmanathan, P., Shortwell, M. S., Gavaghan, D. J., Cordeiro, J. M., and Gray, R. A. (2015). Uncertainty quantification of fast sodium current steady-state inactivation for multi-scale models of cardiac electrophysiology. *Prog. Biophys. Mol. Biol.* 117, 4–18. doi: 10.1016/j.pbiomolbio.2015.01.008
- Pitt-Francis, J., Gurney, A., and Gavaghan, D. (2006). Enabling computer models of the heart for high-performance computers and the grid. *Philos. Trans. A Math. Phys. Eng. Sci.* 364, 1501–1516. doi: 10.1098/rsta.2006.1783
- Pueyo, E., Corrias, A., Virág, L., Jost, N., Szél, T., Varró, A., et al. (2011). A multiscale investigation of repolarization variability and its role in cardiac arrhythmogenesis. *Biophys. J.* 101, 2892–2902. doi: 10.1016/j.bpj.2011.09.060
- Ramanna, H., Elvan, A., Wittkampf, F. H., de Bakker, J. M., Hauer, R. N., and Robles de Medina, E. O. (2001). Increased dispersion and shortened refractoriness caused by verapamil in chronic atrial fibrillation. *J. Am. Coll. Cardiol.* 37, 1403–1407. doi: 10.1016/S0735-1097(01)01132-9
- Ramirez, R. J., Nattel, S., and Courtemanche, M. (2000). Mathematical analysis of canine atrial action potentials: rate, regional factors, and electrical remodeling. *Am. J. Physiol. Heart Circ. Physiol.* 279, H1767–H1785. doi: 10.1152/ajpheart.2000.279.4.H1767
- Ravagli, E., Bucci, A., Bartolucci, C., Paina, M., Baruscotti, M., DiFrancesco, D., et al. (2016). Cell-specific Dynamic Clamp analysis of the role of funny If current in cardiac pacemaking. *Prog. Biophys. Mol. Biol.* 120, 50–66. doi: 10.1016/j.pbiomolbio.2015.12.004
- Ravens, U., Katircioglu-Öztürk, D., Wettwer, E., Christ, T., Dobrev, D., Voigt, N., et al. (2015). Application of the RIMARC algorithm to a large data set of action potentials and clinical parameters for risk prediction of atrial fibrillation. *Med. Biol. Eng. Comput.* 53, 263–273. doi: 10.1007/s11517-014-1232-0
- Rees, C., Yang, J.-H., Santolini, M., Lusis, A. J., Weiss, J. N., and Karma, A. (2018). Variability and compensation of cardiomyocyte ionic conductances at the population level. *bioRxiv* [Preprint]. doi: 10.1101/283275
- Rivolta, I., Clancy, C. E., Tateyama, M., Liu, H., Priori, S. G., and Kass, R. S. (2002). A novel SCN5A mutation associated with long QT-3: altered inactivation kinetics and channel dysfunction. *Physiol. Genomics* 10, 191–197. doi: 10.1152/physiolgenomics.00039.2002
- Roberts, B. N., Yang, P. C., Behrens, S. B., Moreno, J. D., and Clancy, C. E. (2012). Computational approaches to understand cardiac electrophysiology and arrhythmias. *Am. J. Physiol. Heart Circ. Physiol.* 303, H766–H783. doi: 10.1152/ajpheart.01081.2011
- Roden, D. M. (2008). Repolarization reserve: a moving target. *Circulation* 118, 981–982. doi: 10.1161/CIRCULATIONAHA.108.798918
- Romero, L., Carbonell, B., Trenor, B., Rodríguez, B., Saiz, J., and Ferrero, J. M. (2011). Systematic characterization of the ionic basis of rabbit cellular

- electrophysiology using two ventricular models. *Prog. Biophys. Mol. Biol.* 107, 60–73. doi: 10.1016/j.biopharmolbio.2011.06.012
- Romero, L., Pueyo, E., Fink, M., and Rodriguez, B. (2009). Impact of ionic current variability on human ventricular cellular electrophysiology. *Am. J. Physiol. Heart Circ. Physiol.* 297, H1436–H1445. doi: 10.1152/ajpheart.00263.2009
- Rosati, B., Dong, M., Cheng, L., Liou, S. R., Yan, Q., Park, J. Y., et al. (2008). Evolution of ventricular myocyte electrophysiology. *Physiol. Genomics* 35, 262–272. doi: 10.1152/physiolgenomics.00159.2007
- Rosati, B., and Mckinnon, D. (2004). Regulation of ion channel expression. *Circ. Res.* 94, 874–883. doi: 10.1161/01.RES.0000124921.81025.1F
- Rose, T. (2017). *End of Average*. London: Penguin Books.
- Sadrieh, A., Mann, S. A., Subbiah, R. N., Domanski, L., Taylor, J. A., Vandenberg, J. I., et al. (2013). Quantifying the origins of population variability in cardiac electrical activity through sensitivity analysis of the electrocardiogram. *J. Physiol.* 591, 4207–4222. doi: 10.1113/jphysiol.2013.251710
- Sale, H., Wang, J., O'Hara, T. J., Tester, D. J., Phartiyal, P., He, J. Q., et al. (2008). Physiological properties of hERG 1a/1b heteromeric currents and a hERG 1b-specific mutation associated with Long-QT syndrome. *Circ. Res.* 103, e81–95. doi: 10.1161/CIRCRESAHA.108.185249
- Sampson, K. J., Iyer, V., Marks, A. R., and Kass, R. S. (2010). A computational model of Purkinje fibre single cell electrophysiology: implications for the long QT syndrome. *J. Physiol.* 588, 2643–2655. doi: 10.1113/jphysiol.2010.187328
- Sánchez, C., Bueno-Orovio, A., Wetters, E., Loose, S., Simon, J., Ravens, U., et al. (2014). Inter-subject variability in human atrial action potential in sinus rhythm versus chronic atrial fibrillation. *PLoS ONE* 9:e105897. doi: 10.1371/journal.pone.0105897
- Sarkar, A. X., Christini, D. J., and Sobie, E. A. (2012). Exploiting mathematical models to illuminate electrophysiological variability between individuals. *J. Physiol.* 590, 2555–2567. doi: 10.1113/jphysiol.2011.223313
- Sarkar, A. X., and Sobie, E. A. (2010). Regression analysis for constraining free parameters in electrophysiological models of cardiac cells. *PLoS Comput. Biol.* 6:e1000914. doi: 10.1371/journal.pcbi.1000914
- Sarkar, A. X., and Sobie, E. A. (2011). Quantification of repolarization reserve to understand interpatient variability in the response to proarrhythmic drugs: a computational analysis. *Heart Rhythm* 8, 1749–1755. doi: 10.1016/j.hrtm.2011.05.023
- Sato, S., Yamauchi, S., Schuessler, R. B., Boineau, J. P., Matsunaga, Y., and Cox, J. L. (1992). The effect of augmented atrial hypothermia on atrial refractory period, conduction, and atrial flutter/fibrillation in the canine heart. *J. Thorac. Cardiovasc. Surg.* 104, 297–306.
- Schram, G., Pourrier, M., Melnyk, P., and Nattel, S. (2002). Differential distribution of cardiac ion channel expression as a basis for regional specialization in electrical function. *Circ. Res.* 90, 939–950. doi: 10.1161/01.RES.0000018627.89528.6F
- Schulz, D. J., Goaillard, J. M., and Marder, E. (2006). Variable channel expression in identified single and electrically coupled neurons in different animals. *Nat. Neurosci.* 9, 356–362. doi: 10.1038/nn1639
- Schulz, D. J., Goaillard, J. M., and Marder, E. E. (2007). Quantitative expression profiling of identified neurons reveals cell-specific constraints on highly variable levels of gene expression. *Proc. Natl. Acad. Sci. U.S.A.* 104, 13187–13191. doi: 10.1073/pnas.0705827104
- Sepulveda, N. G., Roth, B. J., and Wikswo, J. P. (1989). Current injection into a two-dimensional anisotropic bidomain. *Biophys. J.* 55, 987–999. doi: 10.1016/S0006-3495(89)82897-8
- Sham, J. S., Hatem, S. N., and Morad, M. (1995). Species differences in the activity of the Na⁺-Ca²⁺ exchanger in mammalian cardiac myocytes. *J. Physiol.* 488 (Pt 3), 623–631. doi: 10.1113/jphysiol.1995.sp020995
- Singh, S., Zoble, R. G., Yellen, L., Brodsky, M. A., Feld, G. K., Berk, M., et al. (2000). Efficacy and safety of oral dofetilide in converting to and maintaining sinus rhythm in patients with chronic atrial fibrillation or atrial flutter: the symptomatic atrial fibrillation investigative research on dofetilide (SAFIRE-D) study. *Circulation* 102, 2385–2390. doi: 10.1161/01.CIR.102.19.2385
- Skibbsby, L., Jespersen, T., Christ, T., Maleckar, M. M., Van den Brink, J., Tavi, P., et al. (2016). Refractoriness in human atria: time and voltage dependence of sodium channel availability. *J. Mol. Cell. Cardiol.* 101, 26–34. doi: 10.1016/j.yjmcc.2016.10.009
- Sobie, E. A. (2009). Parameter sensitivity analysis in electrophysiological models using multivariable regression. *Biophys. J.* 96, 1264–1274. doi: 10.1016/j.biophys.2008.10.056
- Soltis, A. R., and Saucerman, J. J. (2010). Synergy between CaMKII Substrates and beta-Adrenergic Signaling in Regulation of Cardiac Myocyte Ca²⁺ Handling. *Biophys. J.* 99, 2038–2047. doi: 10.1016/j.biophys.2010.08.016
- Soor, N., Morgan, R., Varela, M., and Aslanidi, O. V. (2016). Towards patient-specific modelling of lesion formation during radiofrequency catheter ablation for atrial fibrillation. *Conf. Proc. IEEE Eng. Med. Biol. Soc.* 2016, 489–492. doi: 10.1109/EMBC.2016.7590746
- Soylu, M., Demir, A. D., Ozdemir, O., Soylu, O., Topaloglu, S., Kunt, A., et al. (2003). Increased dispersion of refractoriness in patients with atrial fibrillation in the early postoperative period after coronary artery bypass grafting. *J. Cardiovasc. Electrophysiol.* 14, 28–31. doi: 10.1046/j.1540-8167.2003.02218.x
- Su, Z., Li, F., Spitzer, K. W., Yao, A., Ritter, M., and Barry, W. H. (2003). Comparison of sarcoplasmic reticulum Ca²⁺-ATPase function in human, dog, rabbit, and mouse ventricular myocytes. *J. Mol. Cell. Cardiol.* 35, 761–767. doi: 10.1016/S0022-2828(03)00119-6
- Syed, Z., Vigmond, E., Nattel, S., and Leon, L. J. (2005). Atrial cell action potential parameter fitting using genetic algorithms. *Med. Biol. Eng. Comput.* 43, 561–571. doi: 10.1007/BF02351029
- Taneja, T., Mahnert, B. W., Passman, R., Goldberger, J., and Kadish, A. (2001). Effects of sex and age on electrocardiographic and cardiac electrophysiological properties in adults. *Pacing Clin. Electrophysiol.* 24, 16–21. doi: 10.1046/j.1460-9592.2001.00016.x
- ten Tusscher, K. H., Noble, D., Noble, P. J., and Panfilov, A. V. (2004). A model for human ventricular tissue. *Am. J. Physiol. Heart Circ. Physiol.* 286, H1573–H1589. doi: 10.1152/ajpheart.00794.2003
- ten Tusscher, K. H., and Panfilov, A. V. (2006). Alternans and spiral breakup in a human ventricular tissue model. *Am. J. Physiol. Heart Circ. Physiol.* 291, H1088–H1100. doi: 10.1152/ajpheart.00109.2006
- Tobin, A. E., Cruz-Bermúdez, N. D., Marder, E., and Schulz, D. J. (2009). Correlations in ion channel mRNA in rhythmically active neurons. *PLoS ONE* 4:e6742. doi: 10.1371/journal.pone.0006742
- Tomaiuolo, M., Bertram, R., Leng, G., and Tabak, J. (2012). Models of electrical activity: calibration and prediction testing on the same cell. *Biophys. J.* 103, 2021–2032. doi: 10.1016/j.biophys.2012.09.034
- Trayanova, N. A. (2014). Mathematical approaches to understanding and imaging atrial fibrillation significance for mechanisms and management. *Circ. Res.* 114, 1516–1531. doi: 10.1161/CIRCRESAHA.114.302240
- Tsujimae, K., Suzuki, S., Murakami, S., and Kurachi, Y. (2007). Frequency-dependent effects of various IKr blockers on cardiac action potential duration in a human atrial model. *Am. J. Physiol. Heart Circ. Physiol.* 293, H660–H669. doi: 10.1152/ajpheart.01083.2006
- Vagos, M. R., Arevalo, H., de Oliveira, B. L., Sundnes, J., and Maleckar, M. M. (2017). A computational framework for testing arrhythmia marker sensitivities to model parameters in functionally calibrated populations of atrial cells. *Chaos* 27, 093941. doi: 10.1063/1.4999476
- Vanier, M. C., and Bower, J. M. (1999). A comparative survey of automated parameter-search methods for compartmental neural models. *J. Comput. Neurosci.* 7, 149–171. doi: 10.1023/A:1008972005316
- Vieira, D., Adriano, R. L. S., Vasconcelos, J. A., and Krahnenbuhl, L. (2004). Treating constraints as objectives in multiobjective optimization problems using niched pareto genetic algorithm. *IEEE Trans. Magn.* 40, 1188–1191. doi: 10.1109/TMAG.2004.825006
- Walmsley, J., Rodriguez, J. F., Mirams, G. R., Burrage, K., Efimov, I. R., and Rodriguez, B. (2013). mRNA expression levels in failing human hearts predict cellular electrophysiological remodeling: a population-based simulation study. *PLoS ONE* 8:e56359. doi: 10.1371/journal.pone.0056359
- Wang, J., Liu, L., Feng, J., and Nattel, S. (1996). Regional and functional factors determining induction and maintenance of atrial fibrillation in dogs. *Am. J. Physiol.* 271, H148–H158. doi: 10.1152/ajpheart.1996.271.1.H148
- Wang, W., Huang, H. H., Kay, M., and Cavazos, J. (2011). GPGPU accelerated cardiac arrhythmia simulations. *Conf. Proc. IEEE Eng. Med. Biol. Soc.* 2011, 724–727. doi: 10.1109/IEMBS.2011.6090164
- Wang, Z., Feng, J., and Nattel, S. (1995). Idiopathic atrial fibrillation in dogs: electrophysiologic determinants and mechanisms of

- antiarrhythmic action of flecainide. *J. Am. Coll. Cardiol.* 26, 277–286. doi: 10.1016/0735-1097(95)90845-F
- Weaver, C. M., and Wearne, S. L. (2008). Neuronal firing sensitivity to morphologic and active membrane parameters. *PLoS Comput. Biol.* 4:e11. doi: 10.1371/journal.pcbi.0040011
- Weeke, P., Mosley, J. D., Hanna, D., Delaney, J. T., Shaffer, C., Wells, Q. S., et al. (2014). Exome sequencing implicates an increased burden of rare potassium channel variants in the risk of drug-induced long QT interval syndrome. *J. Am. Coll. Cardiol.* 63, 1430–1437. doi: 10.1016/j.jacc.2014.01.031
- White, J. W., Rassweiler, A., Samhouri, J. F., Stier, A. C., and White, C. (2014). Ecologists should not use statistical significance tests to interpret simulation model results. *Oikos* 123, 385–388. doi: 10.1111/j.1600-0706.2013.01073.x
- Xiao, L., Xiao, J., Luo, X., Lin, H., Wang, Z., and Nattel, S. (2008). Feedback remodeling of cardiac potassium current expression: a novel potential mechanism for control of repolarization reserve. *Circulation* 118, 983–992. doi: 10.1161/CIRCULATIONAHA.107.758672
- Yan, G. X., Shimizu, W., and Antzelevitch, C. (1998). Characteristics and distribution of M cells in arterially perfused canine left ventricular wedge preparations. *Circulation* 98, 1921–1927. doi: 10.1161/01.CIR.98.18.1921
- Yang, P. C., and Clancy, C. E. (2012). *In silico* prediction of sex-based differences in human susceptibility to cardiac ventricular tachyarrhythmias. *Front. Physiol.* 3:360. doi: 10.3389/fphys.2012.00360
- Yang, P. C., El-Bizri, N., Romero, L., Giles, W. R., Rajamani, S., Belardinelli, L., et al. (2016). A computational model predicts adjunctive pharmacotherapy for cardiac safety via selective inhibition of the late cardiac Na current. *J. Mol. Cell. Cardiol.* 99, 151–161. doi: 10.1016/j.yjmcc.2016.08.011
- Yang, P. C., Kurokawa, J., Furukawa, T., and Clancy, C. E. (2010). Acute effects of sex steroid hormones on susceptibility to cardiac arrhythmias: a simulation study. *PLoS Comput. Biol.* 6:e1000658. doi: 10.1371/journal.pcbi.1000658
- Yang, P. C., Perissinotti, L. L., López-Redondo, F., Wang, Y., Demarco, K. R., Jeng, M. T., et al. (2017). A multiscale computational modelling approach predicts mechanisms of female sex risk in the setting of arousal-induced arrhythmias. *J. Physiol.* 595, 4695–4723. doi: 10.1113/JP273142
- Zaniboni, M. (2011). 3D current-voltage-time surfaces unveil critical repolarization differences underlying similar cardiac action potentials: a model study. *Math. Biosci.* 233, 98–110. doi: 10.1016/j.mbs.2011.06.008
- Zhang, Z. S., Tranquillo, J., Neplioueva, V., Bursac, N., and Grant, A. O. (2007). Sodium channel kinetic changes that produce Brugada syndrome or progressive cardiac conduction system disease. *Am. J. Physiol. Heart Circ. Physiol.* 292, H399–H407. doi: 10.1152/ajpheart.01025.2005
- Zhao, J., Hansen, B. J., Wang, Y., Csepe, T. A., Sul, L. V., Tang, A., et al. (2017). Three-dimensional integrated functional, structural, and computational mapping to define the structural “fingerprints” of heart-specific atrial fibrillation drivers in human heart *ex vivo*. *J. Am. Heart. Assoc.* 6:e005922. doi: 10.1161/JAHA.117.005922
- Zhou, J., Kodirov, S., Murata, M., Buckett, P. D., Nerbonne, J. M., and Koren, G. (2003). Regional upregulation of Kv2.1-encoded current, IK_{slow2}, in Kv1DN mice is abolished by crossbreeding with Kv2DN mice. *Am. J. Physiol. Heart Circ. Physiol.* 284, H491–H500. doi: 10.1152/ajpheart.00576.2002
- Zhou, Q., Zygmunt, A. C., Cordeiro, J. M., Siso-Nadal, F., Miller, R. E., Buzzard, G. T., et al. (2009). Identification of Ikr kinetics and drug binding in native myocytes. *Ann. Biomed. Eng.* 37, 1294–1309. doi: 10.1007/s10439-009-9690-5
- Zhou, X., Bueno-Orovio, A., Orini, M., Hanson, B., Hayward, M., Taggart, P., et al. (2016). *In vivo* and *in silico* investigation into mechanisms of frequency dependence of repolarization alternans in human ventricular cardiomyocytes. *Circ. Res.* 118, 266–278. doi: 10.1161/CIRCRESAHA.115.307836
- Zhu, Z. I., and Clancy, C. E. (2007). Genetic mutations and arrhythmia: simulation from DNA to electrocardiogram. *J. Electrocardiol.* 40, S47–50. doi: 10.1016/j.jelectrocard.2007.05.033

Conflict of Interest Statement: The authors declare that the research was conducted in the absence of any commercial or financial relationships that could be construed as a potential conflict of interest.

Copyright © 2018 Ni, Morotti and Grandi. This is an open-access article distributed under the terms of the Creative Commons Attribution License (CC BY). The use, distribution or reproduction in other forums is permitted, provided the original author(s) and the copyright owner(s) are credited and that the original publication in this journal is cited, in accordance with accepted academic practice. No use, distribution or reproduction is permitted which does not comply with these terms.



Atrial Rotor Dynamics Under Complex Fractional Order Diffusion

Juan P. Ugarte^{1*}, Catalina Tobón², António M. Lopes³ and J. A. Tenreiro Machado⁴

¹ Grupo de Investigación en Modelamiento y Simulación Computacional, Facultad de Ingenierías, Universidad de San Buenaventura, Medellín, Colombia, ² MATBIOM, Universidad de Medellín, Medellín, Colombia, ³ UISPA-LAETA/INEGI, Faculty of Engineering, University of Porto, Porto, Portugal, ⁴ Department of Electrical Engineering, Institute of Engineering, Polytechnic of Porto, Porto, Portugal

OPEN ACCESS

Edited by:

Pawel Kuklik,
Universitätsklinikum
Hamburg-Eppendorf, Germany

Reviewed by:

Nele Vandersickel,
Ghent University, Belgium
Arun V. Holden,
University of Leeds, United Kingdom

*Correspondence:

Juan P. Ugarte
juan.ugarte@usbmed.edu.co

Specialty section:

This article was submitted to
Computational Physiology and
Medicine,
a section of the journal
Frontiers in Physiology

Received: 30 March 2018

Accepted: 03 July 2018

Published: 24 July 2018

Citation:

Ugarte JP, Tobón C, Lopes AM and
Machado JAT (2018) Atrial Rotor
Dynamics Under Complex Fractional
Order Diffusion. *Front. Physiol.* 9:975.
doi: 10.3389/fphys.2018.00975

The mechanisms of atrial fibrillation (AF) are a challenging research topic. The rotor hypothesis states that the AF is sustained by a reentrant wave that propagates around an unexcited core. Cardiac tissue heterogeneities, both structural and cellular, play an important role during fibrillatory dynamics, so that the ionic characteristics of the currents, their spatial distribution and their structural heterogeneity determine the meandering of the rotor. Several studies about rotor dynamics implement the standard diffusion equation. However, this mathematical scheme carries some limitations. It assumes the myocardium as a continuous medium, ignoring, therefore, its discrete and heterogeneous aspects. A computational model integrating both, electrical and structural properties could complement experimental and clinical results. A new mathematical model of the action potential propagation, based on complex fractional order derivatives is presented. The complex derivative order appears of considering the myocardium as discrete-scale invariant fractal. The main aim is to study the role of a myocardial, with fractal characteristics, on atrial fibrillatory dynamics. For this purpose, the degree of structural heterogeneity is described through derivatives of complex order $\gamma = \alpha + j\beta$. A set of variations for γ is tested. The real part α takes values ranging from 1.1 to 2 and the imaginary part β from 0 to 0.28. Under this scheme, the standard diffusion is recovered when $\alpha = 2$ and $\beta = 0$. The effect of γ on the action potential propagation over an atrial strand is investigated. Rotors are generated in a 2D model of atrial tissue under electrical remodeling due to chronic AF. The results show that the degree of structural heterogeneity, given by γ , modulates the electrophysiological properties and the dynamics of rotor-type reentrant mechanisms. The spatial stability of the rotor and the area of its unexcited core are modulated. As the real part decreases and the imaginary part increases, simulating a higher structural heterogeneity, the vulnerable window to reentrant is increased, as the total meandering of the rotor tip. This *in silico* study suggests that structural heterogeneity, described by means of complex order derivatives, modulates the stability of rotors and that a wide range of rotor dynamics can be generated.

Keywords: rotor dynamics, atrial fibrillation, complex order diffusion, structural heterogeneity, electrical remodeling

1. INTRODUCTION

Atrial fibrillation (AF) represents an important socio-economic burden for world health systems (Kirchhof et al., 2016). Research efforts are focused on determining the AF underlying mechanisms (Zaman and Peters, 2014). Catheter ablation has improved the outcomes of therapeutic interventions for patients in early stages of the arrhythmia (Haïssaguerre et al., 1998; Atienza et al., 2014). However, as the AF perdures in time, the ablation effectiveness decreases significantly (Kirchhof et al., 2016; Lim et al., 2017). During this chronic AF (CAF) scenario, the pathophysiological substrate sustains a more complex form of the arrhythmia. The rotor hypothesis establishes that an AF episode is sustained by a single or several spiral waves known as rotors, activating the surrounding tissue at high rates and generating complex patterns of propagation (Jalife et al., 2002). A rotor is a functional reentry that circumvolves an excitable but unexcited core (Guillem et al., 2016). Recent clinical studies report high rates of success when targeting rotors as ablation sites in CAF patients (Narayan et al., 2012, 2013; Miller et al., 2017). This investigation provides evidence in favor of the rotor hypothesis, but controversy persists since some researchers were not able to replicate the results (Buch et al., 2016; Steinberg et al., 2017). Therefore, a better understanding of the rotor dynamics and the effect of structural heterogeneity, could lead to deeper knowledge for determining critical ablation targets.

The electrical and structural remodeling that the atrial tissue undergoes during CAF, yield a complex interplay in sustaining the arrhythmia (Trayanova et al., 2014). It is recognized that abnormal structural changes play a larger role in perpetuating of CAF than the electrical remodeling alone (Anné et al., 2007). Electrophysiological models were used for understanding the start-up and the perpetuation of rotors, since this task is not easy to develop in experimental terms. The proposed computational descriptions of rotors propagating in a structurally remodeled atrial tissue, provided insight of how rotors evolve under such circumstances (Trayanova et al., 2014; Zhao et al., 2015; Hansen et al., 2017). Structural heterogeneities are modeled through non-conducting elements, reduced conductivity elements and boundary conditions. However, a precise knowledge of tissular conditions is needed in order to set the model parameters (Stinstra et al., 2010). Furthermore, the commonly used standard diffusion equation that models the action potential (AP) propagation, assumes the myocardium as a continuous domain (Keener and Sneyd, 1998), while in the real case, conduction in cardiac tissue is inherently discontinuous (Shaw and Rudy, 2010).

Fractional differential equations, that generalize the classical derivatives/integrals of to real or complex valued orders (Oldham and Spanier, 2006), gained incidence in several fields of applied mathematics (Ionescu et al., 2017; Machado and Kiryakova, 2017; Sun et al., 2018). Cardiac electrophysiological fractional models were recently reported able to characterize the ventricular repolarization expressed by a structurally heterogeneous myocardial domain (Bueno-Orovio et al., 2014). Although it is recognized that fractional derivatives/integrals can better describe experimental data, how to physically interpret the

fractional order remains as an open problem whose answer is relative to the specific system under study. In Bueno-Orovio et al. (2014), the real valued fractional derivative is related with the average degree of tissular structural inhomogeneities. However, the estimation of the derivative order is bonded to the goodness of fit of the data. It would be desirable that a specific value of the derivative order could be translated to a tissular structure.

Fractal objects have been associated with distinct physical phenomena (Mandelbrot, 1982). The main feature of fractals is the self-similarity, meaning that the scaled parts resemble the whole, yielding to irregular patterns (Captur et al., 2016). Such patterns partially fill the embedding space, and in consequence a non integer dimension, or fractal dimension, describes the object. Thus, the overall morphologic complexity is measured by the fractal dimension (Bizzarri et al., 2011). Biological systems have been studied under the fractal perspective (Copley et al., 2012; Wedman et al., 2015; Lennon et al., 2016; Stankovic et al., 2016). There are reports suggesting that the fractal dimension discriminates between healthy and pathological conditions (Hiroshima et al., 2016; Zehani et al., 2016; Müller et al., 2017; Zhang et al., 2017; Popovic et al., 2018). In the cardiac context, structural remodeling generates significant fractal dimension variations (Zouein et al., 2014; Captur et al., 2016). Therefore, the fractal analysis could serve as a link between the geometrical complexity of the myocardium and the AP propagation dynamics under pathological conditions such as AF.

Bearing this ideas in mind, a new approach for assessing the effect of structural heterogeneous tissue on rotor dynamics based on complex fractional order derivatives is developed. We assume that the structurally remodeled myocardium undergoing CAF, has a fractal signature. Taking advantage of well developed mathematical theory, we relate the fractal dimension with the space fractional derivative order. It is evinced that complex valued orders arising if the fractal domain have the property of discrete-scale invariance. Previously, using a simplified cellular model, we found that the rotor stability is affected by real valued order derivatives (Ugarte et al., 2017). We extend the electrophysiological fractional system by means of complex order derivatives to assess the rotor dynamics and to implement a detailed atrial membrane formalism. The fractal structural heterogeneity of the tissue is then controlled by two parameters, namely the real and imaginary parts of the complex derivative. We test a set of discrete values for the complex derivative order and we analyze the stability of the rotors generated for each case. Our simulations include the standard diffusion solution given that it is a particular case of the new complex fractional order model.

2. MATERIAL AND METHODS

2.1. Electrical Potential Over a Fractal Myocardium With Discrete Scale Invariance

A fractal can be described by a fractional dimension and generalizes the Euclidean concept of integer space dimension (Mandelbrot, 1982). A fractal is a self-similar

object and such property implies scale invariance. An object $f(x)$ depending on the space variable x , is scale-invariant if after applying a scale factor ξ the following relation is obtained:

$$f(x) \sim \xi^\gamma f(\xi x), \quad (1)$$

where γ is the fractal dimension. The scale factor ξ controls the scale of magnification applied. The value of γ indicates how the object fills the space and it is a measure of the object irregularity (heterogeneity). The fractal dimension γ can be real or complex: if the self-similarity is fulfilled only at discrete scales of observation (i.e., at discrete zoom factors), then γ is a complex number and the object is discrete-scale invariant. If self-similarity is preserved at the full range of scales, then γ is a real number, and the object is continuous-scale invariant. A mathematical description is given in the Supplementary Material, and for a detailed theoretical explanation please refer to Sornette (1998).

Let us assume the punctual current source $s(x)$ over a discrete-scale invariant fractal myocardium. For simplicity, the myocardium is embedded on a one-dimensional space. We want to investigate, how the source $s(x)$ interacts with the fractal myocardium. For this purpose, the convolution integral (2) over the bounded myocardium Ω is calculated, such as:

$$\phi(x) = \int_{\Omega} P(x-u)s(u)du, \quad (2)$$

where $P(x)$ is the normalized fractal structure-factor of the myocardium. If the Fourier image of $P(x)$ converges for small and large values of the Fourier variable (Nigmatullin and Le Mehaute, 2005; Nigmatullin and Baleanu, 2013), then the function $P(x)$ has the form:

$$P(x) = A_0 \Psi_{\alpha} \frac{1}{|x|^{1-\alpha}} + A_1 \Psi_{\alpha+j\beta} \frac{1}{|x|^{1-\alpha-j\beta}} + \bar{A}_1 \Psi_{\alpha-j\beta} \frac{1}{|x|^{1-\alpha+j\beta}}, \quad (3)$$

with:

$$\Psi_{\alpha \pm j\beta} = \frac{1}{\pi} \Gamma(1 - \alpha \mp j\beta) \sin \left[\frac{(\alpha \pm j\beta)\pi}{2} \right], \quad (4)$$

where $\Gamma(\cdot)$ is the Gamma function, A_0 and A_1 are complex constants, the operator $\bar{\cdot}$ represents the complex conjugation, α is the fractal dimension of domain D_{Ω} and β correspond to a log-periodic correction to the fractal dimension.

Each term in the right side of (3) corresponds to the Green function of the fractional Laplacian operator (Pozrikidis, 2016). Therefore, Equation (2) can be expressed as:

$$\phi(x) = \left[-A_0(-\Delta)^{-\frac{\alpha}{2}} - A_1(-\Delta)^{-\frac{\alpha+j\beta}{2}} - \bar{A}_1(-\Delta)^{-\frac{\alpha-j\beta}{2}} \right] s(x), \quad (5)$$

where $\phi(x)$ can be interpreted as the electrical potential over a fractal domain generated by a electrical source $s(x)$. If the fractal myocardial structure is continuous-scale invariant, then the Laplacian complex-conjugates pair vanishes and the potential is governed by the real fractional Laplacian (recovering the model proposed in Bueno-Orovio et al., 2014). Equation (5)

describes the electrical potential over a discrete-scale invariant fractal myocardium. In what follows, we will evaluate the effect of the Laplacian conjugates pair over the electrical potential in a structurally remodeled myocardium (i.e., a discrete-scale invariant fractal structure) under CAF conditions.

2.2. Complex Fractional Order Diffusion Model

We propose that the AP propagation in a structurally heterogeneous two-dimensional (2D) domain can be modeled by the following equation

$$\frac{\partial V}{\partial t} = \kappa (H_x^\gamma V + H_y^\gamma V) + \frac{1}{C} I, \quad (6)$$

where V denotes the cellular membrane potential, I is the ionic transmembrane current, C is membrane capacitance, κ represents the diffusion coefficient assuming isotropic propagation, x and y are the spatial variables, t is the time variable, and $\gamma = \alpha + j\beta$ is the complex fractional order. The operator H_x^γ involves a pair of complex-conjugate derivative and is defined by:

$$H_x^\gamma = -\frac{1}{2} \left[\left(-\frac{\partial^2}{\partial x^2} \right)^{\gamma/2} + \left(-\frac{\partial^2}{\partial y^2} \right)^{\bar{\gamma}/2} \right], \quad (7)$$

where $\bar{\gamma} = \alpha - j\beta$ is the complex conjugate of γ . The operator H_y^γ in the Equation (6) is defined as in Equation (7) with respect to the variable x . The purpose on defining Equation (7) is to obtain a real-valued function after applying the complex order derivative (Machado, 2013; Hartley et al., 2016). Model (6) represents a generalization of the classical AP propagation model based on the standard diffusion operator (Trayanova et al., 2014).

2.3. Model of Chronic Atrial Fibrillation

The Courtemanche atrial membrane formalism (Courtemanche et al., 1998) is used to calculate the term I in Equation (6). The ionic conductances are adjusted in order to implement the electrical remodeling due to CAF. According to experimental data (Van Wagoner et al., 1997; Bosch et al., 1999; Dobrev et al., 2001) we modify the maximum conductances of the transient potassium current (I_{to}) and the L-type calcium current (I_{Cal}) by a factor of 0.65, the maximum conductance of delayed rectifier potassium current (I_{Kur}) is reduced by a factor 0.49, and the maximum conductance of the potassium time independent current (I_{K1}) is incremented by a factor of 2.1.

Cholinergic activity is known as a factor that promotes CAF. The cholinergic effect is included in the Courtemanche model by implementing the acetylcholine-dependent potassium current (I_{KACH}) (Kneller et al., 2002) and an acetylcholine concentration of 5 nM.

2.4. Stimulation Protocol

Rotors are generated by applying the S1-S2 cross-field stimulation protocol. In this protocol, S1 is a train of stimuli with a basic cycle length of 400 ms and is applied to a boundary of the 2D domain, aiming to generate plane propagation waves.

After S1, the S2 is a single premature stimulus applied at the lower quadrant that is adjacent to the S1 application boundary, when the last repolarization wave generated by S1 reaches the half of the domain. The coupling interval is measured as the difference between the time of the last S1 stimulus and the time when starting S2. A single stimulus is a rectangular wavefront current with a duration of 2 ms and an amplitude of twice the diastolic threshold. Restitution curves are calculated by applying a S1-S2 stimulation protocol. The S1 is a train of 10 stimuli with a basic cycle length (BCL) of 1000 ms, and S2 is the premature stimulus following S1. Measures of APD and CV are registered at the point located at two thirds of L from the stimulation point, provided that a wave of propagation is generated.

3. ATRIAL STRAND ANALYSIS

To assess the effect of β on the electrophysiological characteristics of the Courtemanche model, simulations over atrial strands are carried out. We use a set of test values for γ with $\alpha \in [1.1, 2]$ and $\beta \in [0, 0.28]$, according to stability conditions (see Supplementary Material).

We perform the analysis at microscopic scale with measures from a cell within the strand, and at mesoscopic with representing properties of the atrial strand. At the microscopic scale, the transmembrane ionic currents and action potential duration (APD) from the middle cell are measured. At the mesoscopic scale, the APD dispersion (dAPD), spatial peak currents profiles and restitution curves are registered. The APD is defined at 90% of repolarization. The CV is measured between the points located at one third and two thirds of L . The global dAPD is defined as the range of the APD values within the strand. The local dAPD is negative and is defined as the difference between the minimum APD within the strand and the local APD. The peak ionic current spatial profiles are build using the peak values of the corresponding ionic current at each cell of the strand.

3.1. Reentry Vulnerability and Rotor Dynamics Analysis

The reentry vulnerability analysis is accomplished by applying the S1-S2 protocol at different coupling intervals. We define the vulnerable window (VW) as the difference between the maximum and minimum coupling intervals that triggers a rotor sustaining for at least two rotations within the domain.

The analysis of the rotor dynamics requires calculating the rotor tip trajectory from the phase maps (Bray et al., 2001). The phase analysis defines the rotor tip as the singularity point where the phase is undefined. A phase map is calculated, based on the values of V over the space domain at a given time. The Hilbert transform is obtained from each V time series, and the phase is calculated from the relation of the imaginary part of the Hilbert transform and the corresponding V value at a given time. The rotor dynamics is characterized by the motion of the singularity through the tissue.

3.2. Simulation Setup

An atrial tissue is modeled as a 2D domain of $4 \times 4 \text{ cm}^2$ in surface and is discretized with uniform space steps of $\Delta x = \Delta y = 321.5$

μm . The time is discretized with a step of $\Delta t = 10^{-2}$ ms. The Equation (6) is numerically solved by splitting the operator (Marchuk, 1968; Strang, 1968). The complex order space derivative operator is calculated using a semi-spectral scheme (details are presented in the Supplementary Material). The time derivatives of the Courtemanche model are obtained using the explicit Euler approximation.

Initial conditions for the atrial tissue are set from unicellular simulations, where a single CAF remodeled cell is paced at a basic cycle length of 400 ms during 60 s. For assessing the rotors behavior for different degrees of structural heterogeneity, we define a set of test values for γ . The real part α is varied within the interval $[1.1, 2]$ with a step of 0.1. The range of the imaginary part β is bounded to ensure numerical stability of Equation (6) (see Supplementary Material). Taking this into account, the imaginary part assumes two values $\beta = \{0, 0.28\}$. The diffusion coefficient κ is adjusted in order to generate plane propagation with a conduction velocity (CV) of 63 cm/s, when the CAF remodeling is not applied to the Courtemanche model. Therefore, a specific value of κ is defined for each α with $\beta = 0$.

Prior to the rotor simulations, the effect of β over the electrophysiological characteristics of the CAF model are studied using a 1D model. An atrial strand is modeled as a 1D domain with $L = 2 \text{ cm}$ discretized at $N = 128$ points. Simulations for a dynamical evolution during 10 seconds are executed. The stimulation is applied at the left side of the strand at a BCL of 1000 ms. Microscopic measures are registered from the middle cell of the strand.

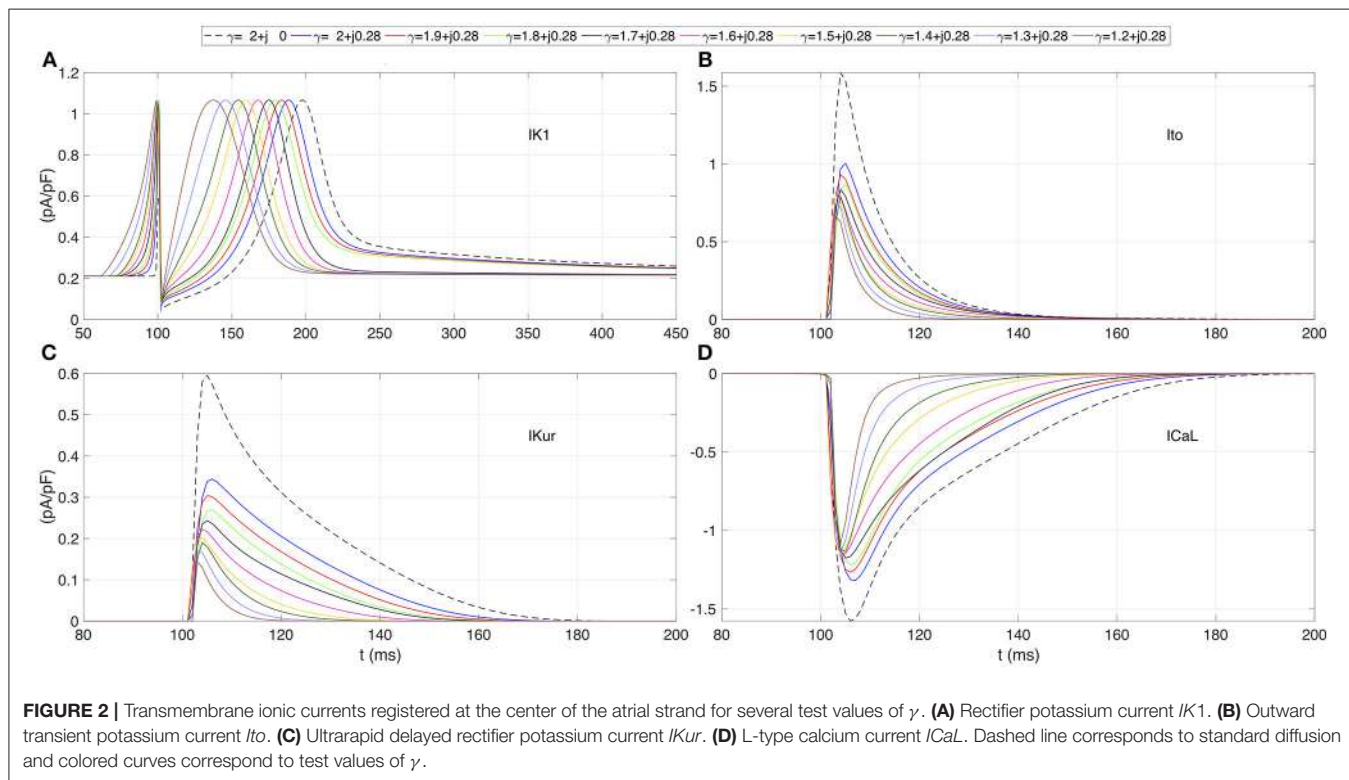
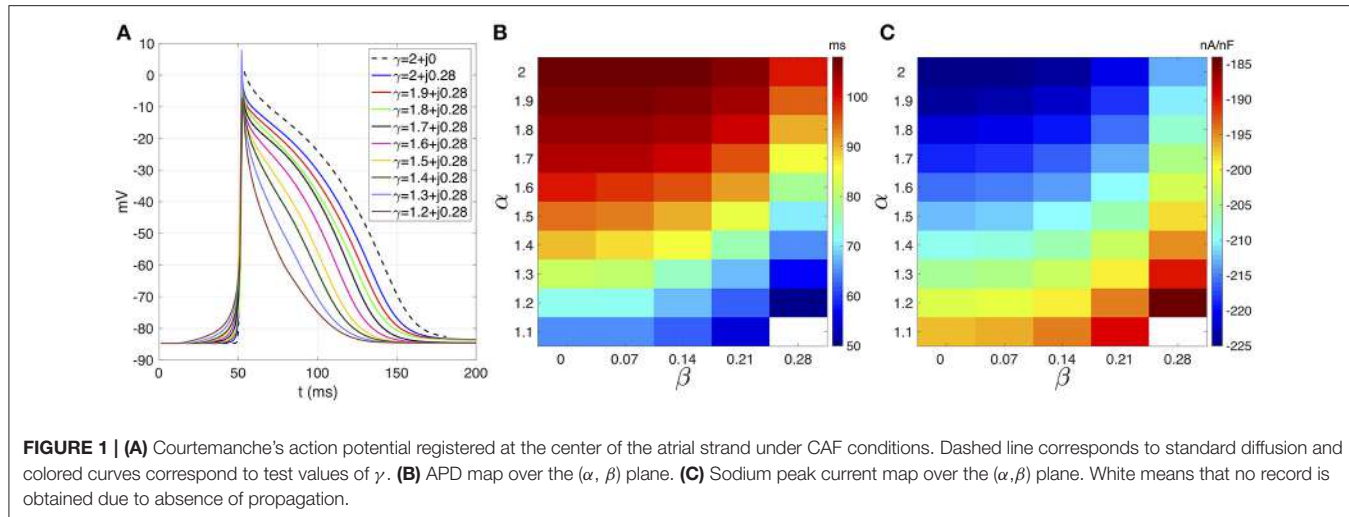
4. RESULTS

4.1. Atrial Electrophysiological Characteristics Under Complex Order Diffusion

4.1.1. Microscale Analysis

Figure 1A shows the action potentials (AP) registered from the middle cell within the strand for $\beta = 0.28$ fixed. The standard diffusion case ($\gamma = 2 + j0$, dotted line) is also shown. The AP foot during the depolarization phase describe a smoother transition from rest to activation as α decreases. The AP repolarization is also affected and reveals a decreasing APD as α decrease. In both cases, a significant difference between the standard diffusion and the new description with $\gamma = 2 + j0.28$ is observed. This is clarified in **Figure 1B**, that presents the APD map over the complex plane (α, β). The APD decrease smoothly as α decreases and β increases. However, β generates greater reductions of the APD than α . For example, a reduction of 9 ms is achieved by fixing $\alpha = 2$ and increasing β from 0 (APD = 108 ms) to 0.28 (APD = 99 ms). In order to generate such an APD reduction with $\beta = 0$, a reduction from 2 to 1.6 is needed.

The effects of β on the ionic currents are shown in **Figures 1C, 2**. **Figure 1C** depicts the map of the sodium peak current. Reducing α , or increasing β , increases the peak value, but the effect is more significant for β increments. **Figure 2** illustrates the effect of γ over the temporal series of representative ionic currents. Complex values of γ modulate the ionic current



transients which is in accordance with the modulations observed during the depolarization and repolarization phases of the atrial AP.

4.1.2. Mesoscale Analysis

Figure 3 shows the effect of γ over the dAPD. Figure 3A shows the map of the global dAPD over the complex plane (α, β) . The map suggests that the global dAPD increase with β and with decrements of α . Although the β modulation is stronger, the dAPD changes are smaller in magnitude than those observed in the microscopic analysis. Figure 3B shows the local dAPD

spatial profiles for three representative values of α . For α fixed, β modulates the local dAPD profiles, producing relevant changes for small α values.

The spatial profiles of ionic current peaks for INa , Ito , $IKur$, and $ICaL$ are illustrated in Figure 4. Complex values of γ generate a family of spatial profiles with differences in magnitude. Note the gap in magnitude between the profiles family generated with complex values of γ and the profile for the standard diffusion case ($\gamma = 2 + j0$, dashed line).

Finally, the restitution curves are shown in Figure 5. As it is characteristic of CAF, flat curves for APD and CV are generated

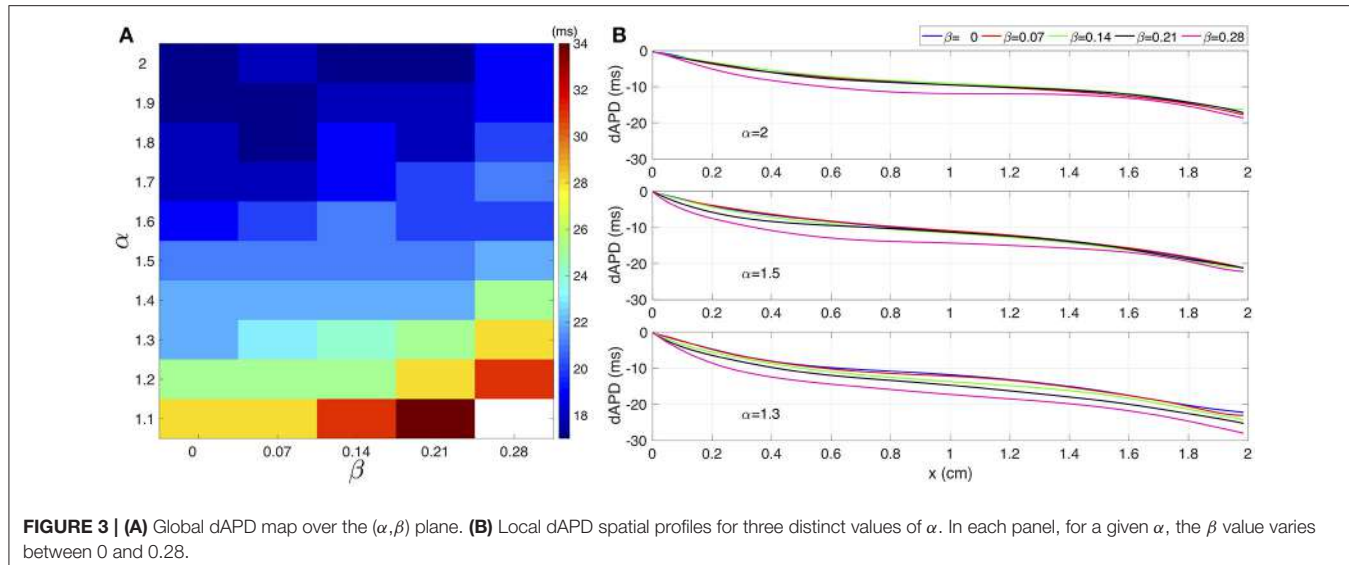


FIGURE 3 | (A) Global dAPD map over the (α, β) plane. **(B)** Local dAPD spatial profiles for three distinct values of α . In each panel, for a given α , the β value varies between 0 and 0.28.

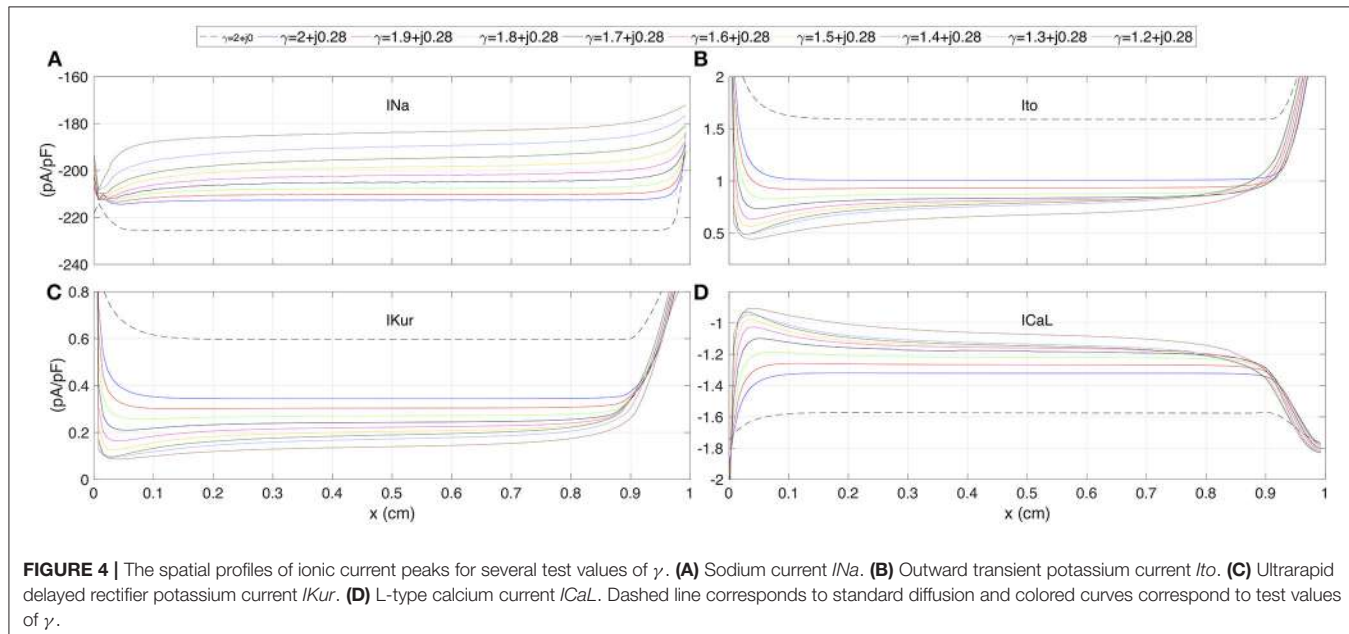


FIGURE 4 | The spatial profiles of ionic current peaks for several test values of γ . **(A)** Sodium current I_{Na} . **(B)** Outward transient potassium current I_{to} . **(C)** Ultrarapid delayed rectifier potassium current I_{Kur} . **(D)** L-type calcium current I_{CaL} . Dashed line corresponds to standard diffusion and colored curves correspond to test values of γ .

for complex values of γ . The coupling interval values for each family of restitutions curves suggest a non linear behavior: (i) in the interval $2 \geq \alpha > 1.2$, for decreasing values of α , the atrial strand generates propagation with premature stimulus; (ii) for $\alpha < 1.3$ premature stimulation is accepted for increasing values of α . For the CV restitutions curves, there is a notorious difference in magnitude between the standard diffusion case and the family of curves generated with γ complex. This difference is not evident for the APD restitutions curves.

4.2. Rotor Simulations

We present the results of rotor simulations using the novel model based on the complex fractional order diffusion operator.

In a unicellular environment, pacing is applied during 60 s to the Courtemanche model before and after applying the CAF electrical remodeling. The last AP generated for each case are shown in Figure 6. Modifications in the AP characteristics resulting from the CAF conditions can be summarized as: the action potential duration reduces from 309 ms to 96 ms and the resting membrane potential decreases from -80.98 mV to -84.67 mV.

We calculate κ for each variation of $\gamma = \alpha + j0$ for generating a CV of 63 cm/s without CAF. Table 1 shows the adjusted κ values and the corresponding CV for both physiological conditions. The CAF remodeling reduces the CV as α decreases or β increases. This behavior is depicted in the bar graph of Figure 6. The propagation generated with standard diffusion decreases the CV

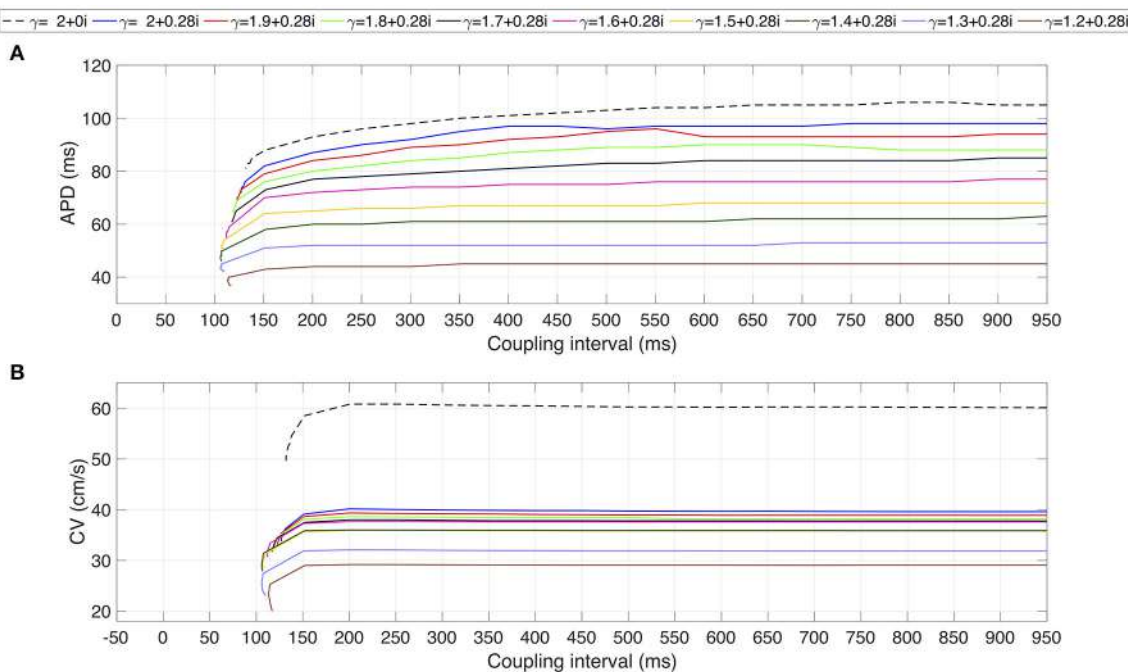


FIGURE 5 | Restitution curves for several test values of γ . **(A)** APD restitution curve. **(B)** CV restitution curve. Dashed line corresponds to standard diffusion and colored curves correspond to test values of γ .

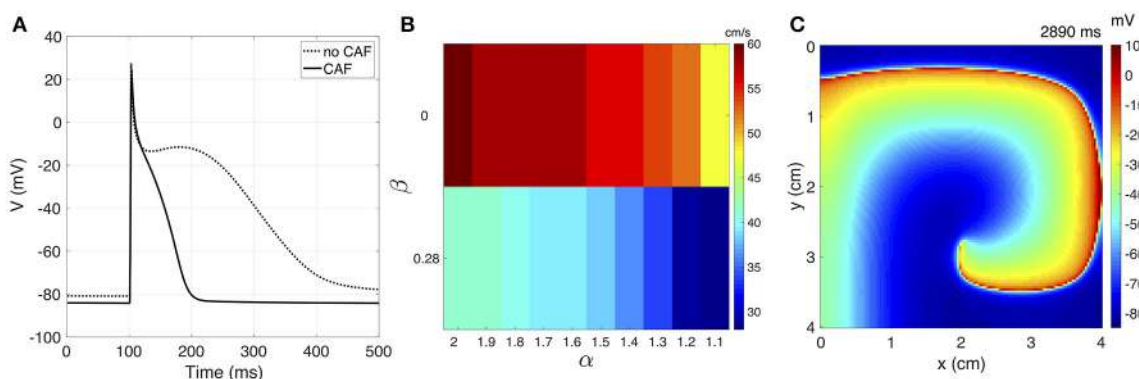


FIGURE 6 | **(A)** The unicellular AP curves for no CAF and CAF models. **(B)** CV map over the complex plane (α, β) under CAF conditions. **(C)** Sample frame of rotor propagation for $\gamma = 1.6 + j0.28$.

by 5%, while for $\gamma = 2 + j0$ and $\gamma = 1.2 + j0.28$ the CV decreases by 25% and 55%, respectively. For $\gamma = 1.1 + j0.28$ propagation cannot be generated under CAF conditions.

4.2.1. Vulnerable Window

The analysis of the reentry vulnerability of the tissue is performed by applying the S1-S2 protocol for each variation of γ and measuring the VW as detailed above. Under this scheme, we were not able to generate a sustained reentry for any couple interval value for $\gamma = \{1.2 + j0.28, 1.1 + j0.28\}$. **Table 2** shows the results. For $\beta = 0$ the VW increases as α increases. For $\beta = 0.28$ the VW tends to increase as α decreases, reaching a maximum with

$\alpha = 1.4$. The values of VW obtained with $\beta = 0.28$ are larger than those obtained with $\beta = 0$.

4.2.2. Rotor Dynamics

Fibrillation episodes in the 2D atrial tissue are simulated by generating rotor mechanisms. We apply the S1-S2 protocol for simulating fibrillatory episodes of 5 seconds. The variations of $\gamma = \alpha + j0.28$ with $\alpha \leq 1.3$ are excluded since propagation cannot be sustained. We study the effect of γ on the rotor tip trajectories through the phase singularity motion. **Figure 7** shows the filament of the phase singularity, that represents the temporal evolution of the rotor tip depicted in the tridimensional space

TABLE 1 | Adjusted values of κ that yield propagation at 63 cm/s under non-CAF conditions and $\beta = 0$. CV (cm/s) for CAF conditions with $\beta = \{0, 0.28\}$.

α		2	1.9	1.8	1.7	1.6	1.5	1.4	1.3	1.2	1.1
κ (cm ² /s)		0.40	0.59	0.87	1.26	1.84	2.68	3.81	5.38	7.52	10.28
CAF	CV, $\beta = 0$	60.10	57.87	57.87	57.87	57.87	55.80	55.80	53.88	52.08	47.35
	CV, $\beta = 0.28$	41.11	41.11	40.06	39.06	39.06	38.11	36.34	33.97	28.94	—

The mark—means no sustained propagation.

TABLE 2 | Values of VW (ms) measured for several test values of γ after applying the S1-S2 cross-field stimulation protocol to the tissue.

		α									
β		2	1.9	1.8	1.7	1.6	1.5	1.4	1.3	1.2	1.1
0		16	16	16	17	18	21	18	24	31	36
0.28		39	38	38	39	40	42	49	0	0	0

(x, y, t) . The filament corresponding to the standard diffusion case ($\gamma = 2 + j0$) stably evolves around an axis parallel to the t -axis. By varying α and β , the filaments describe distinct spatially complex trajectories. In order to quantify the effect of γ over the rotor spatial stability, we estimate the tip maximal displacement (D) as the maximum euclidean distance between two points that belongs to the singularity filament, assuming all points as coplanar:

$$D = \max \left\{ \sqrt{(x_j - x_k)^2 + (y_j - y_k)^2} \right\}, \quad (8)$$

where (x_j, y_j) and (x_k, y_k) are any couple of points within the filament. **Figure 8** shows the filaments within the same plane (x, y) . The red mark represents the core of the rotor. The black marks represent the farthest points within the filament, where the distance between them is equal to D . The standard diffusion generates the lowest value of D that can be interpreted as the most stable rotor dynamics among the γ variations. For $\beta = 0$, the value of D tends to increase as α decreases, depicting filaments with closed trajectories around the core of the rotor. For $\beta = 0.28$, different dynamics can be identified: for $\alpha > 1.6$ the rotor meanders without defining a stable core, and for $\alpha \leq 1.6$ the rotor meandering describe closed paths around a stable core. Note that the values of D with $\beta = 0.28$ are greater than their counterparts with $\beta = 0$.

5. DISCUSSION

The present computational study assesses the interplay between rotors and the structural heterogeneity of a CAF remodeled tissue. The structural remodeled tissue is modeled as fractal structure with discrete-scale invariance. Such structural heterogeneities are implemented using the complex derivative order $\gamma = \alpha + j\beta$, that represents the fractal dimension of the domain with log-periodic corrections. Thus, the proposed complex fractional order diffusion equation has two degrees of freedom (α and β) besides those imposed by the cellular

model (reactive term) and the diffusion coefficient (κ). Having the same electrical remodeling due to CAF, through the simulations we found that: the incremental changes of β generates electrophysiological modulation to a greater extent than the decremental changes of α . The quantitative and qualitative changes in the repolarization features (such, as APD, and ionic currents) generated by β are more visible on the microscale. At the mesoscale, the extent of β modulation depends on α . The observed restitution properties indicate that complex values of γ favors the premature propagation. This result suggests that increasing structural complexity of a discrete-scale invariant atrial strand, has proarrhythmic effects which is characteristic of CAF. The reentry vulnerability of the tissue can be modulated by γ , where the shortest VW achieved corresponds to the standard diffusion case. Furthermore, the extent in which the CAF remodeling reduces the CV depends on the value of γ , having the smaller reduction with the standard diffusion. Lastly, by varying γ the rotor dynamics is affected, generating meandering or drifting rotors, and modifying the area covered by the rotor core.

5.1. The Complex Order Model of AP Propagation

Fractal analysis and fractional differential equations have proven to be useful tools for describing real processes (Mandelbrot, 1982; Captur et al., 2016; Ionescu et al., 2017; Machado and Kiryakova, 2017). Although, there is a general agreement about a relation between both theories, the formal mathematical arguments supporting this relation are still being developed. Important advances in this regard have been made in the last two decades (Sornette, 1998; Nigmatullin and Le Mehaute, 2005; Nigmatullin and Baleanu, 2013; Calcagni, 2017; Nigmatullin et al., 2017). Therefore, this work contextualizes this theoretical frame and situates it within the scope of cardiac electrophysiological systems. A complex fractional order diffusion equation is proposed considering the propagation medium as a fractal object. The complex derivative order implies that the myocardium is discrete-scale invariant. Such

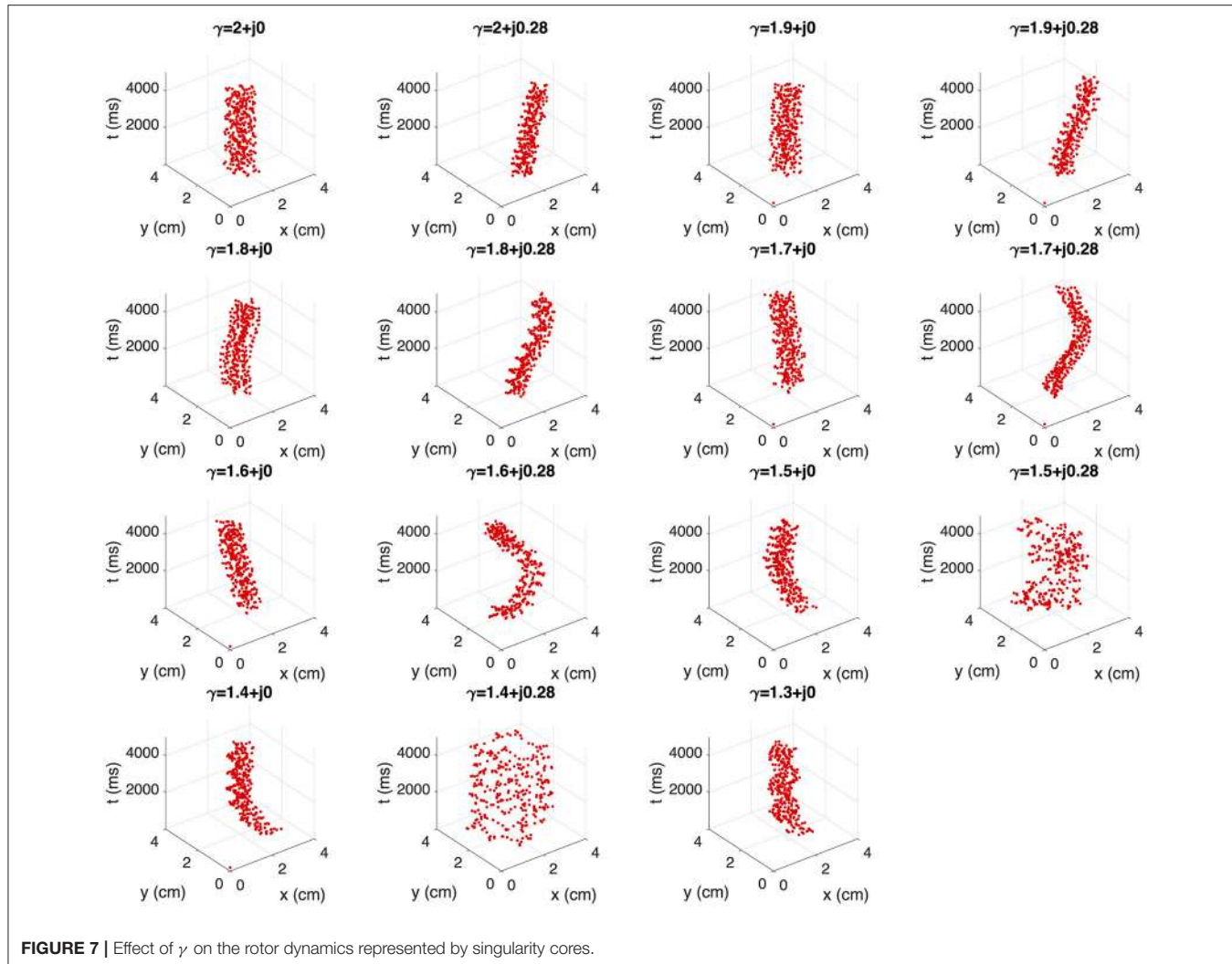


FIGURE 7 | Effect of γ on the rotor dynamics represented by singularity cores.

a property is characteristic of, for example, fractal trees, percolation and diffusion-limited aggregates (Sornette, 1998). These mathematical objects have been applied to describe cardiovascular components: (i) fractal trees are used to study the human coronary vasculature (Zamir, 1999; Zenin et al., 2007), the His-Purkinje conduction system (Goldberger and West, 1987; Berenfeld, 1991), and the atrial pectinate musculature (Goldberger and West, 1987; Goldberger et al., 1990); (ii) percolation clusters serve for modeling fibrosis (Vigmond et al., 2016), and a heterogeneous and discrete myocardium (Alonso and Bär, 2013); (iii) diffusion-limited aggregates are used to model fibroblast (Dickinson et al., 1994; Nogueira et al., 2011). The atrial tissue is composed by a discrete net of cardiomyocytes, a microscopic structure of capillaries, and non-myocyte cells such as the fibroblasts. This complex atrial architecture can be considered as a fractal object, whose mechanisms lead to discrete-scale invariance. Moreover, the fractal analysis has been applied to characterize structural pathological states (Cross, 1997; Fuseler et al., 2007; Zouein et al., 2014; Captur et al., 2015, 2016). Thus, the complex order

diffusion equation can serve as a good model of atrial structural remodeling.

Previous report of fractional electrophysiological model of cardiac propagation (Bueno-Orovio et al., 2014), justified the adoption of real fractional derivative order as a degree of structural heterogeneity between a homogeneous domain, dictated by the standard diffusion model ($\alpha = 2, \beta = 0$), and the domain inhomogeneities, dictated by the ballistic regime ($\alpha = 1, \beta = 0$). We want to stress here that our approach does not disagree with the one proposed in Bueno-Orovio et al. (2014). Indeed, a fractal dimension of $\gamma = 2 + j0$ corresponds to a full homogeneous domain. As the fractal dimension decreases ($\alpha \rightarrow 1$), the irregularity of the domain increases (i.e., the increasing structural heterogeneities). Thus, the transition between both regimes is preserved. A purely real derivative order would imply a system with no characteristic scale, and a given property is held regardless the scale of observations, also referred as a scale-free system. However, in real systems, physical cut-offs prevent the invariance spreading over all scales Khaluf et al. (2017). Therefore, the complex order derivative

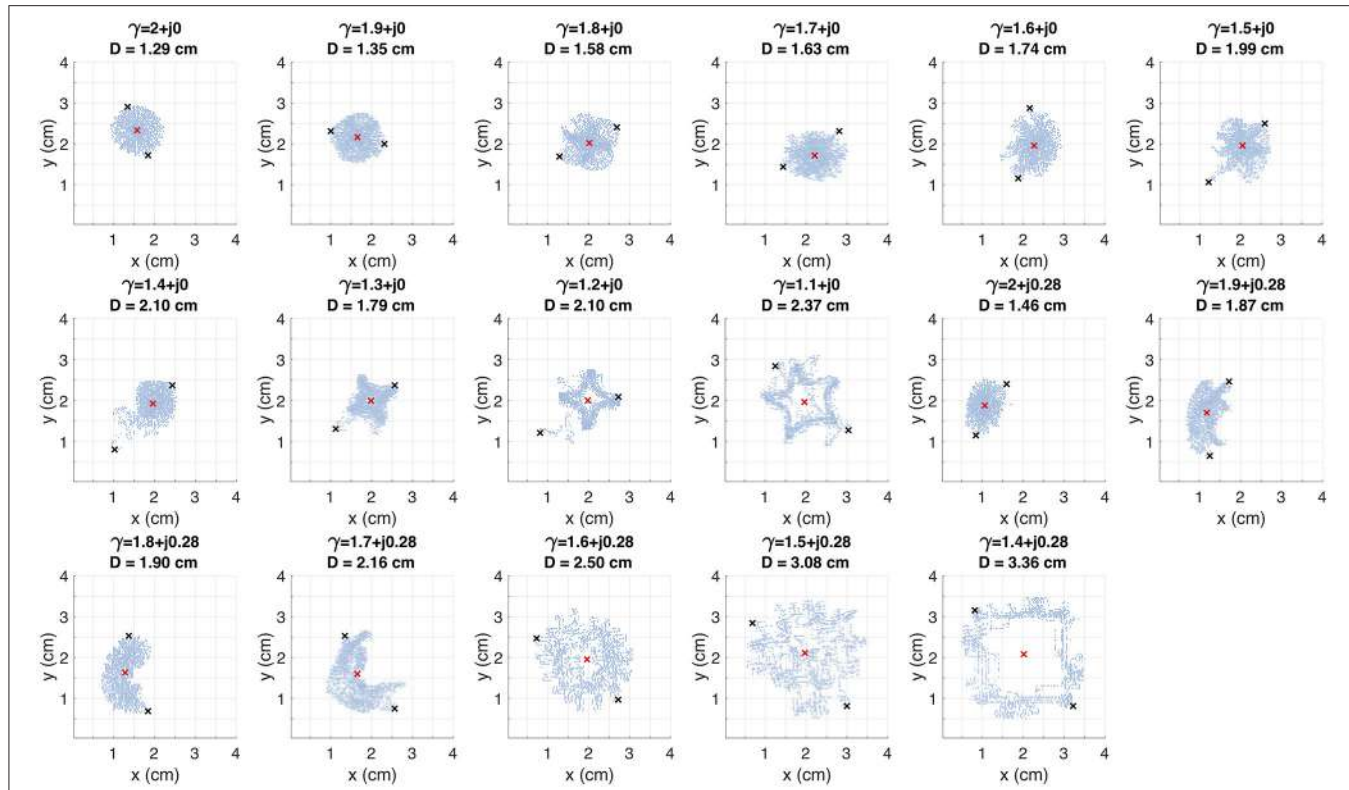


FIGURE 8 | Trajectory of the rotor tip within the spatial plane (x, y) for several test values of γ . The red mark indicates the rotor core. The D value corresponds to the distance between the black marks. These marks depict the farthest points within the trajectory.

yields a more realistic model of electrophysiological systems. The inclusion of the imaginary part β implies the existence of relevant length scales within the electrophysiological system (Sornette, 1998), one of these scales may be related with the size of a single cardiomyocyte. Through the complex derivative order, the characteristic scales that may play a role during the cardiac dynamics can be identified. For this reason, our complex order model extends the real fractional model, in order to enhance the comprehension of the cardiac structure effects on cardiac propagation.

5.2. The Modulation of Electrophysiological Properties Through the Complex Fractional Derivative

We evinced that the depolarization phase of the AP is modulated by complex derivative order. The slow down of the AP foot was related to structural heterogeneities in atrial and ventricular tissue from adult dogs (Spach et al., 1998). This observation agrees with the results obtained using the complex order diffusion model.

It is well recognized that the APD is reduced under CAF conditions due to the electrical remodeling (Wijffels et al., 1995; Bosch et al., 1999; Workman et al., 2001). Our results suggest that structural changes reduce the APD under CAF conditions. Experimental measures of APD reduction were obtained mainly

from unicellular patch clamp experiments. Determining the APD response to structural remodeling is a difficult task. In fact, there are some experimental studies reporting, through surrogate measures, that the APD decreases in patients undergoing CAF and structural remodeling (Morillo et al., 1995; Graux et al., 1998; Vasquez et al., 2010) and, therefore, our results agree with those observations.

Clinical studies described different behaviors for the dAPD in CAF patients, indicating a global increment of the dAPD (Boutjdir et al., 1986) and also reporting a regional dependence (Kamalvand et al., 1999). Our results suggest that, under similar electrical remodeling conditions, distinct degrees of global dAPD can be generated by means of γ . This can be used to represent different regions within the atria, which coincides with the description of Kamalvand et al. (1999). Furthermore, the local dAPD profiles obtained by means of the complex order model indicates a reduction of the APD in the direction of propagation. This gradient has been observed in rabbit atria, sinoatrial node zone (Boyett et al., 1999), rat ventricular cellular cultures (Badic and Bursac, 2009) and human ventricles (Hanson et al., 2009).

The reduction of CV plays an important role in the onset of AF, because it can favor the occurrence of reentry (Bosch et al., 1999). The structural remodeling under CAF conditions is a factor that alters the CV (Jalife and Kaur, 2014; Nattel and Harada, 2014). Our results agree with those observations: decreasing CV values are obtained when α decreases or β

increases and their combination represents different degrees of structural heterogeneities. The changes in CV result from varying the complex order γ under the same CAF electrical remodeling conditions, where the reductions in CV are greater when increasing the imaginary part β . Local structural characteristics in the atria are important to determine the propagation of the AP, meaning that the CV varies according on the region (Lesh et al., 1996). When the CAF electrical remodeling occurs, the extent of CV deterioration depends on the atrial zone (Markides et al., 2003; Xia et al., 2004; Lalani et al., 2012). Using the complex fractional model it is possible to simulate different atrial tissues with heterogeneous CV values that can represent distinct atrial regions.

5.3. Rotor Dynamics

The focal ectopic activity is an important source of reentrant propagation (Haïssaguerre et al., 1998; Arora et al., 2003). There is experimental evidence suggesting that the mechanisms determining the tissue vulnerability to reentry are related with structural and electrical remodeling interactions (Narayan et al., 2017). The complex fractional model reveals that increasing the degrees of structural heterogeneity increase the VW. Under the conditions of our simulations, these results indicate that increased vulnerability to reentry might be regulated by the underlying tissular structure. Additionally, we show that the VW values increase significantly with the imaginary part, so that β can be interpreted as a parameter representing a specific type of structural complexity.

The interest in rotor dynamics research has increased since clinical reports claim that rotor ablation improves the rates of success in human CAF treatment (Narayan et al., 2012). Using in silico models, mechanistic explanations and therapeutic approaches have been tested (Zhao et al., 2015; Berenfeld, 2016; Guillem et al., 2016; Tobón et al., 2017). In this work, we assessed the effect of structural heterogeneities on rotor propagation by varying the complex derivative order γ . For real values of γ (i.e., $\gamma = \alpha + j0$) meandering quasi-stable rotors, with a shape-changing core, are generated. For complex values of γ (i.e., $\gamma = \alpha + j0.28$) the rotor dynamics varies from drifting trajectories ($\alpha > 1.6$) to meandering trajectories whose core is markedly greater with respect to those with $\beta = 0$. As mentioned above, the inclusion of the imaginary part β yields a major modulation of electrophysiological features. In the case of the standard diffusion (i.e., $\gamma = 2 + j0$), corresponding to a structurally homogeneous tissue (Bueno-Orovio et al., 2014), the rotor meanders in a quasi-stable form and describes the minimum tip displacement among all γ variations. Therefore, by varying γ , the spatial stability of the rotor can be modulated, obtaining a wide range of rotor dynamics. Previous simulation studies report quasi-stable dynamics using the Courtemanche model (Cherry and Evans, 2008; Wilhelms et al., 2013). Our standard diffusion simulations agree with those reports. However, additionally we evinced that using the CAF remodeled Courtemanche formalism and keeping its parameters fixed, unstable rotor trajectories can be obtained through γ variations. Thus, we show that using the complex fractional order diffusion model, it is possible to simulate realistic CAF conditions in which meandering and

drifting rotors are observed. These dynamics can be related with increasing degrees of structural heterogeneity causing difficulties in accurately locating and ablating rotors. Under such conditions the CAF may be not reverted which agrees with experimental observations (Buch et al., 2016; Steinberg et al., 2017).

The growing evidence that structural remodeling has a relevant role in AF dynamics, leads the computational electrophysiology researchers to incorporate myocardial structure features in the AP propagation models. There is a lack of consensus on defining how purely structural properties has to be included in a computational model. Variable diffusion tensor (ranging from reduced conductivity to zero conductivity), boundary conditions and non-cardiomyocyte active models, are proposals for modeling the myocardial structure (Trayanova et al., 2014; Brown et al., 2015). There is a common element among these approaches: the standard diffusion equation that assumes the cardiac tissue as a continuum (Keener and Sneyd, 1998). Although these computational schemes have improved our knowledge about the CAF mechanisms, modeling the inherently discontinuous myocardium as a continuous domain is inconsistent with the cardiac histological structure (Shaw and Rudy, 2010). In this work, the cardiac structural heterogeneity is implemented using a complex conjugate derivative operator. The resulting mathematical model generalizes the previously established propagation models (Keener and Sneyd, 1998; Bueno-Orovio et al., 2014) without the restriction of assuming a homogeneous domain.

5.4. Limitations

The biophysical interpretation of the complex derivative order is built on the mathematical theory of smoothed functions averaged over fractal sets (Nigmatullin and Le Mehaute, 2005). This problem has been solved for fractional temporal derivatives and the relation with the complex dimension has been established (Nigmatullin et al., 2017). This theory is supported by experimental results (Nigmatullin et al., 2007, 2018). However, the solution for spatial derivative operators is a more complex problem and the averaging procedure only admits specific types of fractals (Nigmatullin and Baleanu, 2013). Therefore, although in this work a fractal as medium of propagation was assumed, the specific fractal that is related with the fractional Laplacian operator has not been established. Future investigations will look into this problem. The simulations are performed in 2D domains. Nevertheless the atrial tissue is a 3D complex domain, whose heterogeneities can impact the rotor dynamics (Kharche et al., 2015). For this reason, our results cannot be generalized until analyzing 3D experiments of rotor propagation. The lack of detailed experimental data describing the spatial distribution of atrial electrophysiological properties does not allow an exhaustive assessment of the simulation outcomes. Therefore, the results obtained in this work invite to design experimental setups in order validate them.

6. CONCLUSIONS

The new complex fractional order diffusion model allows the simulation of a wide range of rotor dynamics. The results

can be correlated with changes in the atrial tissular structure that have been observed in the clinical practice. This approach is a step toward an integral electrophysiological mathematical model that embodies the structural and electrical features of the myocardium.

AUTHOR CONTRIBUTIONS

All authors contributed to conception and design of the study; JU performed the simulations. JU and CT wrote the first draft of the manuscript. All authors contributed to manuscript revision, read and approved the submitted version.

REFERENCES

- Alonso, S., and Bär, M. (2013). Reentry near the percolation threshold in a heterogeneous discrete model for cardiac tissue. *Phys. Rev. Lett.* 110, 1–5. doi: 10.1103/PhysRevLett.110.158101
- Anné, W., Willems, R., Holemans, P., Beckers, F., Roskams, T., Lenaerts, I., et al. (2007). Self-terminating AF depends on electrical remodeling while persistent AF depends on additional structural changes in a rapid atrially paced sheep model. *J. Mol. Cell. Cardiol.* 43, 148–158. doi: 10.1016/j.yjmcc.2007.05.010
- Arora, R., Verheule, S., Scott, L., Navarrete, A., Katari, V., Wilson, E., et al. (2003). Arrhythmogenic substrate of the pulmonary veins assessed by high-resolution optical mapping. *Circulation* 107, 1816–1821. doi: 10.1161/01.CIR.0000058461.86339.7E
- Atienza, F., Almendral, J., Ormaetxe, J. M., Moya, Á., Martínez-Alday, J. D., Hernández-Madrid, A., et al. (2014). Comparison of radiofrequency catheter ablation of drivers and circumferential pulmonary vein isolation in atrial fibrillation: a noninferiority randomized multicenter RADAR-AF trial. *J. Am. Coll. Cardiol.* 64, 2455–2467. doi: 10.1016/j.jacc.2014.09.053
- Badie, N., and Bursac, N. (2009). Novel micropatterned cardiac cell cultures with realistic ventricular microstructure. *Biophys. J.* 96, 3873–3885. doi: 10.1016/j.bpj.2009.02.019
- Berenfeld, O. (1991). Simulation of High-Resolution QRS Complex Using a Ventricular Model With a Fractal Conduction System. Effects of Ischemia on High-Frequency QRS Potentials. *Circ. Res.* 68, 1751–1761. doi: 10.1161/01.RES.68.6.1751
- Berenfeld, O. (2016). The major role of I_{K1} in mechanisms of rotor drift in the atria: a computational study. *Clin. Med. Insights Cardiol.* 10, 71–79. doi: 10.4137/CMC.S39773
- Bizzarri, M., Giuliani, A., Cucina, A., D'Anselmi, F., Soto, A. M., and Sonnenschein, C. (2011). Fractal analysis in a systems biology approach to cancer. *Semi. Cancer Biol.* 21, 175–182. doi: 10.1016/j.semcancer.2011.04.002
- Bosch, R. F., Zeng, X., Grammer, J. B., Popovic, K., Mewis, C., and Kühlkamp, V. (1999). Ionic mechanisms of electrical remodeling in human atrial fibrillation. *Cardiovasc. Res.* 44, 121–131. doi: 10.1016/S0008-6363(99)00178-9
- Boutjdir, M., Le Heuzey, J. Y., Lavergne, T., Chauvaud, S., Guize, L., Carpenterier, A., et al. (1986). Inhomogeneity of Cellular Refractoriness in Human Atrium: Factor of Arrhythmia? L'hétérogénéité des périodes réfractaires cellulaires de l'oreillette humaine: un facteur d'arythmie? *Pacing Clin. Electrophysiol.* 9, 1095–1100. doi: 10.1111/j.1540-8159.1986.tb06676.x
- Boyett, M. R., Honjo, H., Yamamoto, M., Nikmaram, M. R., Niwa, R., and Kodama, I. (1999). Downward gradient in action potential duration along conduction path in and around the sinoatrial node. *Am. J. Physiol. Heart Circ. Physiol.* 276(2 Pt 2), H686–H698. doi: 10.1152/ajpheart.1999.276.2.H686
- Bray, M. A., Lin, S. F., Aliev, R. R., Roth, B. J., and Wikswo, J. P. (2001). Experimental and theoretical analysis of phase singularity dynamics in cardiac tissue. *J. Cardiovasc. Electrophysiol.* 12, 716–722. doi: 10.1046/j.1540-8167.2001.00716.x
- Brown, T. R., Krogh-Madsen, T., and Christini, D. J. (2015). Computational approaches to understanding the role of fibroblast-Myocyte interactions in cardiac arrhythmogenesis. *BioMed Res. Int.* 2015:465714. doi: 10.1155/2015/465714
- Buch, E., Share, M., Tung, R., Benharash, P., Sharma, P., Koneru, J., et al. (2016). Long-term clinical outcomes of focal impulse and rotor modulation for treatment of atrial fibrillation: a multicenter experience. *Heart Rhythm* 13, 636–641. doi: 10.1016/j.hrthm.2015.10.031
- Bueno-Orovio, A., Kay, D., Grau, V., Rodriguez, B., Burrage, K., and Interface, J. R. S. (2014). Fractional diffusion models of cardiac electrical propagation: role of structural heterogeneity in dispersion of repolarization. *J. R. Soc. Interf.* 11:20140352. doi: 10.1098/rsif.2014.0352
- Calcagni, G. (2017). Complex dimensions and their observability. *Phys. Rev. D* 96, 1–7. doi: 10.1103/PhysRevD.96.046001
- Captur, G., Karperien, A. L., Hughes, A. D., Francis, D. P., and Moon, J. C. (2016). The fractal heart-embracing mathematics in the cardiology clinic. *Nat. Rev. Cardiol.* 14, 56–64. doi: 10.1038/nrccardio.2016.161
- Captur, G., Karperien, A. L., Li, C., Zemrak, F., Tobon-Gomez, C., Gao, X., et al. (2015). Fractal frontiers in cardiovascular magnetic resonance: towards clinical implementation. *J. Cardiovasc. Magn. Reson.* 17, 1–10. doi: 10.1186/s12968-015-0179-0
- Cherry, E. M., and Evans, S. J. (2008). Properties of two human atrial cell models in tissue: Restitution, memory, propagation, and reentry. *J. Theor. Biol.* 254, 674–690. doi: 10.1016/j.jtbi.2008.06.030
- Copley, S. J., Giannarou, S., Schmid, V., Hansell, D., Wells, A., and Yang, G.-Z. (2012). Effect of aging on lung structure *in vivo*: assessment with densitometric and fractal analysis of high-resolution computed tomography data. *J. Thorac. Imaging* 27, 366–371. doi: 10.1097/RTI.0b013e31825148c9
- Courtemanche, M., Ramirez, R. J., and Nattel, S. (1998). Ionic mechanisms underlying human atrial action potential properties: insights from a mathematical model. *Am. J. Physiol.* 275(1 Pt 2), H301–H321. doi: 10.1152/ajpheart.1998.275.1.H301
- Cross, S. S. (1997). Fractals in pathology. *J. Pathol.* 182, 1–8. doi: 10.1002/(SICI)1096-9896(199705)182:1<1::AID-PATH808>3.0.CO;2-B
- Dickinson, R. B., Guido, S., and Tranquillo, R. T. (1994). Biased cell migration of fibroblasts exhibiting contact guidance in oriented collagen gels. *Anna. Biomed. Eng.* 22, 342–356. doi: 10.1007/BF02368241
- Dobrev, D., Graf, E., Wettwer, E., Himmel, H., Hála, O., Doerfel, C., et al. (2001). Molecular basis of downregulation of G-protein-coupled inward rectifying K⁺ current I(K,ACh) in chronic human atrial fibrillation: decrease in GIRK4 mRNA correlates with reduced I(K,ACh) and muscarinic receptor-mediated shortening of action potentials. *Circulation* 104, 2551–2557. doi: 10.1161/hc4601.099466
- Fuseler, J. W., Millette, C. F., Davis, J. M., and Carver, W. (2007). Fractal and image analysis of morphological changes in the actin cytoskeleton of neonatal cardiac fibroblasts in response to mechanical stretch. *Microsc. Microanal.* 13, 133–143. doi: 10.1017/S1431927607070225
- Goldberger, A. L., Rigney, D. R., and West, B. J. (1990). Chaos and fractals in human physiology. *Sci. Pic.* 262, 42–9.
- Goldberger, A. L., and West, B. J. (1987). Fractals in physiology and medicine. *Yale J. Biol. Med.* 60, 421–435.

FUNDING

This work was supported by the “Departamento Administrativo de Ciencia, Tecnología e Innovación – COLCIENCIAS” of Colombia, by research project #121065741044, and by the UdeM research project #890.

SUPPLEMENTARY MATERIAL

The Supplementary Material for this article can be found online at: <https://www.frontiersin.org/articles/10.3389/fphys.2018.00975/full#supplementary-material>

- Graux, P., Carlioz, R., Rivat, P., Bera, J., Guyomar, Y., and Dutoit, A. (1998). Wavelength and atrial vulnerability: an endocardial approach in humans. *Pacing Clin. Electrophysiol.* 21, 202–208. doi: 10.1111/j.1540-8159.1998.tb01089.x
- Guillem, M. S., Climent, A. M., Rodrigo, M., Fernandez-Aviles, F., Atienza, F., and Berenfeld, O. (2016). Presence and stability of rotors in atrial fibrillation: evidence and therapeutic implications. *Cardiovasc. Res.* 109, 480–492. doi: 10.1093/cvr/cvw011
- Haïssaguerre, M., Jaïs, P., Shah, D. C., Takahashi, A., Hocini, M., Quiniou, G., et al. (1998). Spontaneous initiation of atrial fibrillation by ectopic beats originating in the pulmonary veins. *N. Engl. J. Med.* 339, 659–666. doi: 10.1056/NEJM199809033391003
- Hansen, B. J., Zhao, J., and Fedorov, V. V. (2017). Fibrosis and atrial fibrillation: computerized and optical mapping: a view into the human atria at submillimeter resolution. *JACC Clin. Electrophysiol.* 3, 531–546. doi: 10.1016/j.jacep.2017.05.002
- Hanson, B., Suton, P., Elameri, N., Gray, M., Critchley, H., Gill, J. S., et al. (2009). Interaction of activation-repolarization coupling and restitution properties in humans. *Circ. Arrhyth. Electrophysiol.* 2, 162–170. doi: 10.1161/CIRCEP.108.785352
- Hartley, T. T., Tomhartleyolcom, E., Lorenzo, C. F., and Adams, J. L. (2016). “Conjugated-Order differintegrals,” in *ASME, International Design Engineering Technical Conferences and Computers and Information in Engineering Conference*, Vol. 6 (California, CA), 1597–1602.
- Hiroshima, Y., Shuto, K., Yamazaki, K., Kawaguchi, D., Yamada, M., Kikuchi, Y., et al. (2016). Fractal dimension of tc-99m dtpa gsa estimates pathologic liver injury due to chemotherapy in liver cancer patients. *Ann. Surg. Oncol.* 23, 4384–4391. doi: 10.1245/s10434-016-5441-7
- Ionescu, C., Lopes, A., Copot, D., Machado, J. A., and Bates, J. H. (2017). The role of fractional calculus in modeling biological phenomena: a review. *Commun. Nonlinear Sci. Numerical Simulat.* 51, 141–159. doi: 10.1016/j.cnsns.2017.04.001
- Jalife, J., Berenfeld, O., and Mansour, M. (2002). Mother rotors and fibrillatory conduction: a mechanism of atrial fibrillation. *Cardiovasc. Res.* 54, 204–216. doi: 10.1016/S0008-6363(02)00223-7
- Jalife, J., and Kaur, K. (2014). Atrial remodeling, fibrosis, and atrial fibrillation. *Trends Cardiovasc. Med.* 25, 475–484. doi: 10.1016/j.tcm.2014.12.015
- Kamalvand, K., Tan, K., Lloyd, G., Gill, J., Bucknall, C., and Sulke, N. (1999). Alterations in atrial electrophysiology associated with chronic atrial fibrillation in man. *Eur. Heart J.* 20, 888–895. doi: 10.1053/euhj.1998.1404
- Keener, J., and Sneyd, J. (1998). *Mathematical Physiology*. New York, NY: Springer-Verlag New York, Inc.
- Khaluf, Y., Ferrante, E., Simoens, P., and Huepe, C. (2017). Scale invariance in natural and artificial collective systems: a review. *J. R. Soc. Inter.* 14:20170662. doi: 10.1098/rsif.2017.0662
- Kharche, S. R., Biktasheva, I. V., Seemann, G., Zhang, H., and Biktashev, V. N. (2015). A computer simulation study of anatomy induced drift of spiral waves in the human atrium. *BioMed Res. Int.* 2015, 24–26. doi: 10.1155/2015/731386
- Kirchhof, P., Benussi, S., Kotecha, D., Ahlsson, A., Atar, D., Casadei, B., et al. (2016). 2016 ESC Guidelines for the management of atrial fibrillation developed in collaboration with EACTS. *Europace* 18, 1609–1678. doi: 10.1093/europace/euw295
- Kneller, J., Zou, R., Vigmond, E. J., Wang, Z., Leon, L. J., and Nattel, S. (2002). Cholinergic atrial fibrillation in a computer model of a two-dimensional sheet of canine atrial cells with realistic ionic properties. *Circ. Res.* 90, 73e–87. doi: 10.1161/01.RES.0000019783.88094.BA
- Lalani, G. G., Schricker, A., Gibson, M., Rostamian, A., Krummen, D. E., Narayan, S. M., et al. (2012). Atrial conduction slows immediately before the onset of human atrial fibrillation a Bi-Atrial contact mapping study of transitions to atrial fibrillation. *JAC* 59, 595–606. doi: 10.1016/j.jacc.2011.10.879
- Lennon, F. E., Cianci, G. C., Kanteti, R., Riehm, J. J., Arif, Q., Poroyko, V. A., et al. (2016). Unique fractal evaluation and therapeutic implications of mitochondrial morphology in malignant mesothelioma. *Sci. Rep.* 6:24578. doi: 10.1038/srep24578
- Lesh, M. D., Kalman, J. M., Olglin, J. E., and Ellis, W. S. (1996). The role of atrial anatomy in clinical atrial arrhythmias. *J. Electrocardiol.* 29(SUPPL.), 101–113. doi: 10.1016/S0022-0736(96)80039-2
- Lim, H. S., Hocini, M., Dubois, R., Denis, A., Derval, N., Zellerhoff, S., et al. (2017). Complexity and distribution of drivers in relation to duration of persistent atrial fibrillation. *J. Am. Coll. Cardiol.* 69, 1257–1269. doi: 10.1016/j.jacc.2017.01.014
- Machado, J. A., and Kiryakova, V. (2017). The Chronicles of Fractional Calculus. *Fract. Calc. Appl. Anal.* 20, 307–336. doi: 10.1515/fca-2017-0017
- Machado, J. A. T. (2013). Optimal Controllers with Complex Order Derivatives. *J. Optim. Theory Applic.* 156, 2–12. doi: 10.1007/s10957-012-0169-4
- Mandelbrot, B. (1982). *The Fractal Geometry of Nature*. Florence: Einaudi paperbacks 1997.
- Marchuk, G. I. (1968). On the construction and comparison of difference schemes. *Aplikace Matematiky* 13, 103–132.
- Markides, V., Schilling, R. J., Ho, S. Y., Chow, A. W., Davies, D. W., and Peters, N. S. (2003). Characterization of left atrial activation in the intact human heart. *Circulation* 107, 733–739. doi: 10.1161/01.CIR.0000048140.31785.02
- Miller, J. M., Kalra, V., Das, M. K., Jain, R., Garlie, J. B., Brewster, J. A., et al. (2017). Clinical benefit of ablating localized sources for human atrial fibrillation: the Indiana University FIRM registry. *J. Am. Coll. Cardiol.* 69, 1247–1256. doi: 10.1016/j.jacc.2016.11.079
- Morillo, C. A., Klein, G., Jones, D., and Guiraudon, C. (1995). Chronic rapid atrial pacing: Structural, functional, and electrophysiological characteristics of a new model of sustained atrial fibrillation. *Circulation* 91, 1588–1595. doi: 10.1161/01.CIR.91.5.1588
- Müller, A., Marschner, C., Kristensen, A., Wiinberg, B., Sato, A., Rubio, J., et al. (2017). Pulmonary vasculature in dogs assessed by three-dimensional fractal analysis and chemometrics. *Veter. Radiol. Ultras.* 58, 653–663. doi: 10.1111/vru.12536
- Narayan, S. M., Krummen, D. E., Clopton, P., Shivkumar, K., and Miller, J. M. (2013). Direct or coincidental elimination of stable rotors or focal sources may explain successful atrial fibrillation ablation: on-treatment analysis of the CONFIRM Trial (Conventional ablation for AF with or without focal impulse and rotor modulation). *J. Am. Coll. Cardiol.* 62, 138–147. doi: 10.1016/j.jacc.2013.03.021
- Narayan, S. M., Patel, J., Mulpuru, S., and Krummen, D. E. (2012). Focal impulse and rotor modulation ablation of sustaining rotors abruptly terminates persistent atrial fibrillation to sinus rhythm with elimination on follow-up A video case study. *Heart Rhythm.* 9, 1436–1439. doi: 10.1016/j.hrthm.2012.03.055
- Narayan, S. M., Vishwanathan, M. N., Kowalewski, C. A., Baykaner, T., Rodrigo, M., Zaman, J. A., et al. (2017). The continuous challenge of AF ablation: from foci to rotational activity. *Rev. Portug. Cardiol.* 36, 9–17. doi: 10.1016/j.repc.2017.09.007
- Nattel, S., and Harada, M. (2014). Atrial remodeling and atrial fibrillation: recent advances and translational perspectives. *J. Am. Coll. Cardiol.* doi: 10.1016/j.jacc.2014.02.555
- Nigmatullin, R. R., Arbuzov, A. A., Salehli, F., Giz, A., Bayrak, I., and Catalgil-Giz, H. (2007). The first experimental confirmation of the fractional kinetics containing the complex-power-law exponents: Dielectric measurements of polymerization reactions. *Phys. B Condensed Matter* 388, 418–434. doi: 10.1016/j.physb.2006.06.153
- Nigmatullin, R. R., and Baleanu, D. (2013). New relationships connecting a class of fractal objects and fractional integrals in space. *Fract. Calc. Appl. Anal.* 16, 911–936. doi: 10.2478/s13540-013-0056-1
- Nigmatullin, R. R., Budnikov, H. C., and Sidelnikov, A. V. (2018). Mesoscopic theory of percolation currents associated with quantitative description of VAGs: confirmation on real data. *Chaos Solit. Fract.* 106, 171–183. doi: 10.1016/j.chaos.2017.11.028
- Nigmatullin, R. R., and Le Mehaute, A. (2005). Is there geometrical/physical meaning of the fractional integral with complex exponent? *J. Non Crystall. Solids* 351, 2888–2899. doi: 10.1016/j.jnoncrysol.2005.05.035
- Nigmatullin, R. R., Zhang, W., and Gubaidullin, I. (2017). Accurate relationships between fractals and fractional integrals: new approaches and evaluations. *Fract. Calc. Appl. Anal.* 20, 1263–1280. doi: 10.1515/fca-2017-0066
- Nogueira, I. R., Alves, S. G., and Ferreira, S. C. (2011). Scaling laws in the diffusion limited aggregation of persistent random walkers. *Phys. A Stat. Mech. Applic.* 390, 4087–4094. doi: 10.1016/j.physa.2011.06.077

- Oldham, K., and Spanier, J. (2006). *The Fractional Calculus: Theory and Applications of Differentiation and Integration to Arbitrary Order*. Mineola, NY: Dover books on mathematics, Dover Publications.
- Popovic, N., Radunovic, M., Badnjar, J., and Popovic, T. (2018). Fractal dimension and lacunarity analysis of retinal microvascular morphology in hypertension and diabetes. *Microvasc. Res.* 118, 36–43. doi: 10.1016/j.mvr.2018.02.006
- Pozrikidis, C. (2016). *The Fractional Laplacian*. Boca Raton, FL: CRC Press.
- Shaw, R. M., and Rudy, Y. (2010). Cardiac muscle is not a uniform syncytium. *Biophys. J.* 98, 3102–3103. doi: 10.1016/j.bpj.2010.03.030
- Sornette, D. (1998). Discrete-scale invariance and complex dimensions. *Phys. Report* 297, 239–270. doi: 10.1016/S0370-1573(97)00076-8
- Spach, M. S., Heidlage, J. F., Dolber, P. C., and Barr, R. C. (1998). Extracellular discontinuities in cardiac muscle: evidence for capillary effects on the action potential foot. *Circ. Res.* 83, 1144–1164. doi: 10.1161/01.RES.83.11.1144
- Stankovic, M., Pantic, I., De Luka, S., Puskas, N., Zaletel, I., Milutinovic-Smiljanic, S., et al. (2016). Quantification of structural changes in acute inflammation by fractal dimension, angular second moment and correlation. *J. Microsc.* 261, 277–284. doi: 10.1111/jmi.12330
- Steinberg, J. S., Shah, Y., Bhatt, A., Sichrovsky, T., Arshad, A., Hansinger, E., et al. (2017). Focal impulse and rotor modulation: acute procedural observations and extended clinical follow-up. *Heart Rhythm* 14, 192–197. doi: 10.1016/j.hrthm.2016.11.008
- Stinstra, J., Macleod, R., and Henriquez, C. (2010). Incorporating Histology into a 3D Microscopic Computer Model of Myocardium to Study Propagation at a Cellular Level. *Ann. Biomed. Eng.* 38, 1399–1414. doi: 10.1007/s10439-009-9883-y
- Strang, G. (1968). On the construction and comparison of difference schemes. *J. Numerical Anal.* 5, 506–517. doi: 10.1137/0705041
- Sun, H., Zhang, Y., Baleanu, D., Chen, W., and Chen, Y. (2018). A new collection of real world applications of fractional calculus in science and engineering. *Commun. Nonlinear Sci. Num. Simul.* 64, 213–231. doi: 10.1016/j.cnsns.2018.04.019
- Tobón, C., Orozco-Duque, A., Ugarte, J. P., Becerra, M., and Saiz, J. (2017). “Chapter 08: Complexity of atrial fibrillation electrograms through nonlinear signal analysis: *in silico* approach,” in *Interpreting Cardiac Electrograms - From Skin to Endocardium*, ed K. A. Michael (Rijeka: InTech), 137–168.
- Trayanova, N. A., Boyle, P. M., Arevalo, H. J., and Zahid, S. (2014). Exploring susceptibility to atrial and ventricular arrhythmias resulting from remodeling of the passive electrical properties in the heart: a simulation approach. *Front. Physiol.* 5:435. doi: 10.3389/fphys.2014.00435
- Ugarte, J. P., Tobón, C., Orozco-Duque, A., and Andrade-Caicedo, H. (2017). Generation of fibrillatory dynamics in cardiac tissue : fractional diffusion as arrhythmogenic mechanism modelling tool. *Appl. Math. Sci.* 11, 637–650. doi: 10.12988/ams.2017.7136
- Van Wagoner, D. R., Pond, A. L., McCarthy, P. M., Trimmer, J. S., and Nerbonne, J. M. (1997). Outward K^+ current densities and $Kv1.5$ expression are reduced in chronic human atrial fibrillation. *Circ. Res.* 80, 772–781. doi: 10.1161/01.RES.80.6.772
- Vasquez, C., Mohandas, P., Louie, K., Benamer, N., Bapat, A., and Morley, G. (2010). Enhanced fibroblast-myocyte interactions in response to cardiac injury. *Circ. Res.* 107, 1011–1020. doi: 10.1161/CIRCRESAHA.110.227421
- Vigmond, E., Pashaei, A., Amraoui, S., Cochet, H., and Hassaguerre, M. (2016). Percolation as a mechanism to explain atrial fractionated electrograms and reentry in a fibrosis model based on imaging data. *Heart Rhythm*. 13, 1536–1543. doi: 10.1016/j.hrthm.2016.03.019
- Wedman, P., Aladhami, A., Beste, M., Edwards, M. K., Chumanevich, A., Fuseler, J. W., et al. (2015). A new image analysis method based on morphometric and fractal parameters for rapid evaluation of *in situ* mammalian mast cell status. *Microsc. Microanal.* 21, 1573–1581. doi: 10.1017/S1431927615015342
- Wijffels, M. C., Kirchhof, C. C., Dorland, R., and Allessie, M. A. (1995). Atrial fibrillation begets atrial fibrillation. *Circulation* 92, 1954–1968. doi: 10.1161/01.CIR.92.7.1954
- Wilhelms, M., Hettmann, H., Maleckar, M. M., Koivumäki, J. T., Dössel, O., and Seemann, G. (2013). Benchmarking electrophysiological models of human atrial myocytes. *Front. Physiol.* 3:487. doi: 10.3389/fphys.2012.00487
- Workman, A. J., Kane, K. A., and Rankin, A. C. (2001). The contribution of ionic currents to changes in refractoriness of human atrial myocytes associated with chronic atrial fibrillation. *Cardiovasc. Res.* 52, 226–235. doi: 10.1016/S0008-6363(01)00380-7
- Xia, Y., Hertervig, E., Kongstad, O., Ljungström, E., Pyotr, P., Holm, M., et al. (2004). Deterioration of interatrial conduction in patients with paroxysmal atrial fibrillation: electroanatomic mapping of the right atrium and coronary sinus. *Heart Rhythm*. 1, 548–553. doi: 10.1016/j.hrthm.2004.07.016
- Zaman, J. A., and Peters, N. S. (2014). The rotor revolution: conduction at the eye of the storm in atrial fibrillation. *Circ. Arrhythm. Electrophysiol.* 7, 1230–1236. doi: 10.1161/CIRCEP.114.002201
- Zamir, M. (1999). On fractal properties of arterial trees. *J. Theor. Biol.* 197, 517–526. doi: 10.1006/jtbi.1998.0892
- Zehani, S., Ouahabi, A., Oussalah, M., Mimi, M., and Taleb-Ahmed, A. (2016). “New and robust method for trabecular bone texture based on fractal dimension,” in *IECON 2016 - 42nd Annual Conference of the IEEE Industrial Electronics Society* (New York, NY), 992–997.
- Zenin, O. K., Kizilova, N. N., and Filippova, E. N. (2007). Studies on the structure of human coronary vasculature. *Biophysics* 52, 499–503. doi: 10.1134/S0006350907050089
- Zhang, Y.-D., Zhang, Y., Phillips, P., Dong, Z., and Wang, S. (2017). Synthetic minority oversampling technique and fractal dimension for identifying multiple sclerosis. *Fractals* 25:1740010. doi: 10.1142/S0218348X17400102
- Zhao, J., Kharche, S. R., Hansen, B. J., Csepe, T. A., Wang, Y., Stiles, M. K., et al. (2015). Optimization of catheter ablation of atrial fibrillation: insights gained from clinically-derived computer models. *Int. J. Mol. Sci.* 16, 10834–10854. doi: 10.3390/ijms160510834
- Zouein, F. A., Kurdi, M., Booz, G. W., and Fuseler, J. W. (2014). Applying fractal dimension and image analysis to quantify fibrotic collagen deposition and organization in the normal and hypertensive heart. *Microsc. Microanal.* 20, 1134–1144. doi: 10.1017/S1431927614001044

Conflict of Interest Statement: The authors declare that the research was conducted in the absence of any commercial or financial relationships that could be construed as a potential conflict of interest.

Copyright © 2018 Ugarte, Tobón, Lopes and Machado. This is an open-access article distributed under the terms of the Creative Commons Attribution License (CC BY). The use, distribution or reproduction in other forums is permitted, provided the original author(s) and the copyright owner(s) are credited and that the original publication in this journal is cited, in accordance with accepted academic practice. No use, distribution or reproduction is permitted which does not comply with these terms.



Stationary Atrial Fibrillation Properties in the Goat Do Not Entail Stable or Recurrent Conduction Patterns

Arne van Hunnik*, Stef Zeemering, Piotr Podziemski, Jorik Simons, Giulia Gatta, Laura Hannink, Bart Maesen, Marion Kuiper, Sander Verheule and Ulrich Schotten

Department of Physiology, Cardiovascular Research Institute Maastricht, Maastricht University, Maastricht, Netherlands

OPEN ACCESS

Edited by:

Gary Tse,
The Chinese University of Hong Kong,
Hong Kong

Reviewed by:

Arne V. Holden,
University of Leeds, United Kingdom
Bradley John Roth,
Oakland University, United States

*Correspondence:

Arne van Hunnik
a.vanhunnik@maastrichtuniversity.nl

Specialty section:

This article was submitted to
Computational Physiology and
Medicine,
a section of the journal
Frontiers in Physiology

Received: 30 April 2018

Accepted: 28 June 2018

Published: 27 July 2018

Citation:

van Hunnik A, Zeemering S, Podziemski P, Simons J, Gatta G, Hannink L, Maesen B, Kuiper M, Verheule S and Schotten U (2018) Stationary Atrial Fibrillation Properties in the Goat Do Not Entail Stable or Recurrent Conduction Patterns. *Front. Physiol.* 9:947. doi: 10.3389/fphys.2018.00947

Introduction: Electro-anatomical mapping of the atria is used to identify the substrate of atrial fibrillation (AF). Targeting this substrate by ablation in addition to pulmonary vein ablation did not consistently improve outcome in clinical trials. Generally, the assessment of the substrate is based on short recordings (≤ 10 s, often even shorter). Thus, targeting the AF substrate assumes spatiotemporal stationarity but little is known about the variability of electrophysiological properties of AF over time.

Methods: Atrial fibrillation (AF) was maintained for 3–4 weeks after pericardial electrode implantation in 12 goats. Within a single AF episode 10 consecutive minutes were mapped on the left atrial free wall using a 249-electrode array (2.25 mm inter-electrode spacing). AF cycle length, fractionation index (FI), lateral dissociation, conduction velocity, breakthroughs, and preferentiality of conduction (Pref) were assessed per electrode and AF property maps were constructed. The Pearson correlation coefficient (PCC) between the 10 AF-property maps was calculated to quantify the degree spatiotemporal stationarity of AF properties. Furthermore, the number of waves and presence of re-entrant circuits were analyzed in the first 60-s file. Comparing conduction patterns over time identified recurrent patterns of AF with the use of recurrence plots.

Results: The averages of AF property maps were highly stable throughout the ten 60-s-recordings. Spatiotemporal stationarity was high for all 6 property maps, PCC ranged from 0.66 ± 0.11 for Pref to 0.98 ± 0.01 for FI. High stationarity was lost when AF was interrupted for about 1 h. However, the time delay between the recorded files within one episode did not affect PCC. Yet, multiple waves (7.7 ± 2.3) were present simultaneously within the recording area and during $9.2 \pm 11\%$ of the analyzed period a re-entrant circuit was observed. Recurrent patterns occurred rarely and were observed in only 3 out of 12 goats.

Conclusions: During non-self-terminating AF in the goat, AF properties were stationary. Since this could not be attributed to stable recurrent conduction patterns during AF, it is suggested that AF properties are determined by anatomical and structural properties of the atria even when the conduction patterns are very variable.

Keywords: atrial fibrillation, mapping, conduction patterns, stationary patterns, recurrence quantification analysis, AF dynamics

INTRODUCTION

Mapping of conduction patterns has been of fundamental importance to understand mechanisms that maintain cardiac arrhythmias (Nattel et al., 2005). The importance of cardiac mapping in clinical practice was demonstrated by Haïssaguerre's et al. (1998) pivotal finding that atrial fibrillation (AF) was often initiated from the pulmonary veins (PV) and that ablation of ectopic sites in the PVs terminated AF. However, many patients experience recurrences of AF in the months following a PV isolation (Verma et al., 2015), suggesting that other regions in the atria may contribute to AF perpetuation as well.

Detailed mapping studies of AF, in both animal models (Berenfeld et al., 2000; Verheule et al., 2010) and humans (Konings et al., 1994; Allessie et al., 2010; Lee et al., 2014, 2015), have described fast, irregular and seemingly random conduction patterns. AF maintenance can be explained by different conceptual models such as multiple wavelets (Allessie et al., 1996, 2010), rotor activity (Jalife, 2011) and repetitive focal activity (Lee et al., 2015). Notably, these mechanisms are not mutually exclusive and different mechanisms may occur in an individual patient. Several electrophysiological parameters have been used to detect local sources of AF. Nedios et al. (2016) Complex fractionated atrial electrograms (CFAE) and high frequency zones are thought to reflect driver sites of rotational or focal activity or to correlate with areas demonstrating high complexity of AF. Unlike such electrogram parameters, with focal impulse and rotor mapping (FIRM) conduction patterns are identified that putatively describe focal and rotational activity. Narayan et al. (2012); Swarup et al. (2014) Unfortunately, targeting these substrate parameters has variable outcomes in clinical trials and need further validation (Gadenz et al., 2017; Krummen et al., 2017; van der Does and de Groot, 2017).

A potential factor contributing to the limited success rates are the limitations of the mapping techniques used. The atrial surface can only be mapped with a limited time and spatial resolution. A limited spatial resolution may lead to misinterpretation of conduction patterns (Kuklik et al., 2017; Roney et al., 2017). If higher spatial resolution is obtained, for example by point-by-point mapping typically relatively short recordings are acquired. It is unknown whether these recordings are representative for longer episodes of AF. Also, it is largely unexplored whether AF driver sites are stable across different AF episodes.

In this study we analyzed left atrial epicardial high-density recording in goats with 3 to 4 weeks of maintained AF. We studied the degree of stationarity of local AF properties derived from ten 60-s-long recordings within a single AF episode and between different AF episodes. Moreover, we analyzed complexity and stability of conduction patterns, and rotational activity. For the assessment of stability of conduction patterns, we made use of a new recurrence quantification analysis.

MATERIALS AND METHODS

Animal Model

This study was carried out in accordance with the principles of the Basel Declaration and regulations of European directive

2010/63/EU. The local ethical board for animal experimentation of the Maastricht University approved the protocol. In total 12 goats, 6 per study, weighing 60 ± 9.8 kg were included. Goats were anesthetized (sufentanil $6 \mu\text{g}/\text{kg}/\text{h}$ and propofol $5-10 \text{ mg}/\text{kg}/\text{h}$, i.v.) and electrodes were implanted on the pericardium above the left atrium (LA). After 2 weeks of recovery from surgery, AF was induced by repetitive burst of stimuli (1 s, 50 Hz, 2 times threshold with a maximum of 10 V) using subcutaneously implanted neurostimulator (Itrel 3 or 4, Medtronic, Minneapolis, Minnesota, USA). AF was subsequently maintained for 3–4 weeks. For open chest sacrifice experiments, goats were anesthetized with parenteral sufentanil $6 \mu\text{g}/\text{kg}/\text{h}$, propofol $10 \text{ mg}/\text{kg}/\text{h}$, and rocuronium $0.3 \text{ mg}/\text{kg}/\text{h}$.

Data Acquisition

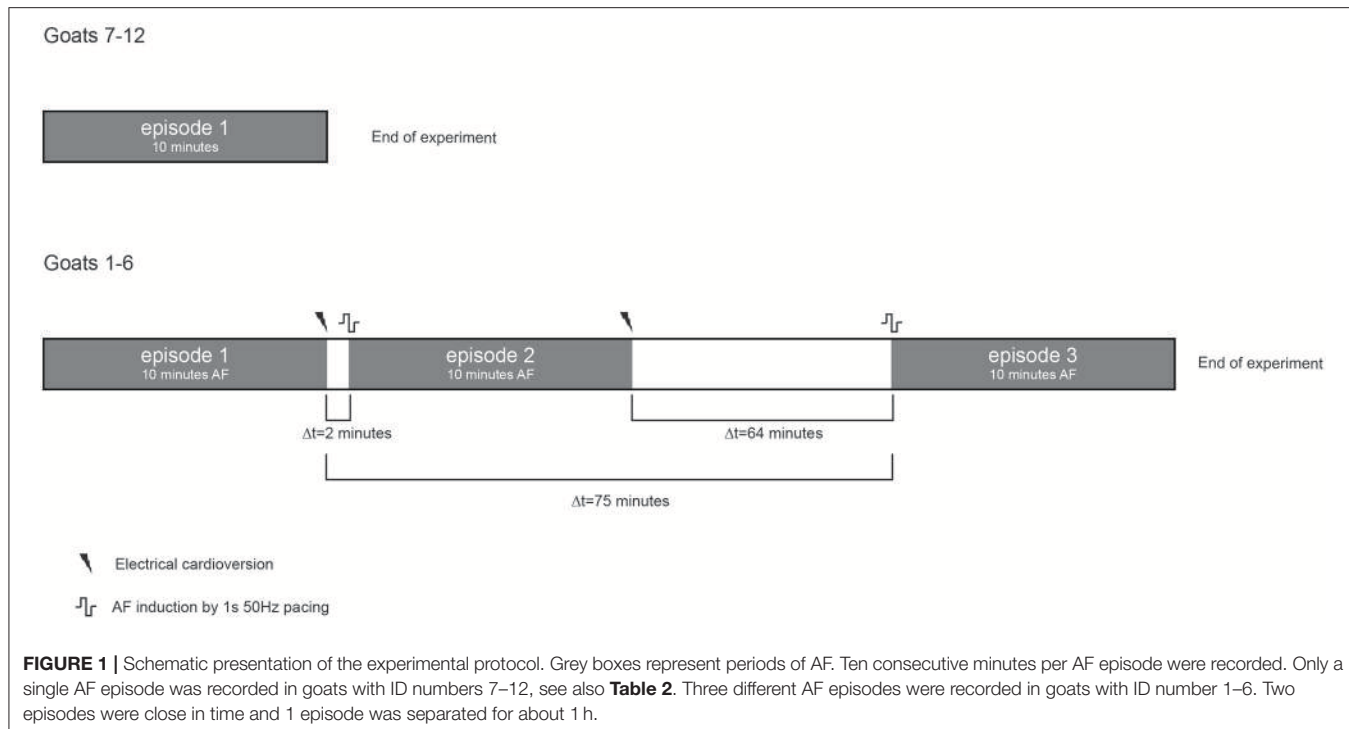
A circular mapping array containing 249 electrodes (2.4 mm inter-electrode distance, 14.3 cm^2 surface area) was placed on the left atrial (LA) free wall and kept in stable position throughout the experiment. Unipolar electrograms were recorded with 1.039 kHz sampling rate, bandwidth of 0.1–408 Hz and AD resolution of 16bit. In a 10-min window ten 60-s files were recorded during non-selfterminating AF. In a subset of 6 animals 2 additional 10-min windows were recorded (Figure 1). Electrical cardioversion of AF was performed using a ≤ 20 Joules synchronized DC shock (Physio-control lifepak 9 B, Medtronic, Minneapolis, Minnesota, USA). The DC shock was delivered on endocardial catheters of which one was placed in the coronary sinus and the other in the right atrial cavity.

Analysis of Local Activation Time and Direction

The recorded signals were analyzed offline using custom-made analysis software (MATLAB 8.1, The Mathworks, Inc., Natick, Massachusetts, USA). Local deflections, activation times, and unipolar fractionation index (FI) were identified using a probabilistic annotation algorithm, as previously described. Zeemering et al. (2012); Lau et al. (2015) Based on the activation times, the AF cycle length (AFCL) and conduction direction and velocity (CV) were determined. For calculation of conduction vectors, a plane was fitted through the central activation time and its direct neighbors in space and time (min. 3 max 8). If the conduction time of a neighboring electrode implied a CV of $<20 \text{ cm/s}$, the occurrence of conduction block was assumed and the activation time of that neighbor was excluded from plane fitting. Per electrode the degree for preferential direction of conduction (Pref) was calculated as $\text{Pref} = 1 - (\text{circular variance of all conduction vectors})$. The maximal time difference of activation times with its neighbors was calculated as a measure of epicardial lateral dissociation (LD).

AF Property Maps Analysis

Based on the results of the above-mentioned analysis, 6 different parameters, i.e., FI, AFCL, LD, CV, breakthroughs (BT), and Pref were obtained for each individual electrode and used to construct AF property maps. Per parameter the spatial Pearson correlation coefficient (PCC) between property maps, of all 45 possible comparisons within a 10-min window, was determined and averaged per animal, producing an intra-episode correlation



of property maps at various time points. To address potential correlations due to chance, we randomly reassigned electrodes in space and recalculated the average PCC. In a subset of 6 animals three 10-min windows were recorded from 3 different episodes of AF, in order to determine the inter-episode correlation.

Analysis of Epicardial Waves and Re-entrant Circuits

Next, we analyzed the fibrillation waves propagating on the epicardial surface as previously described by Zeemering et al. (2012). In short, waves were defined as clusters of activation times that are connected in space and time by an apparent CV of $> 20\text{cm/s}$. The earliest activation time that cannot be explained by its surrounding was identified as the starting point of the wave. This starting point was specified as peripheral, on the border of the electrode, or breakthrough, separated > 1 electrode from the border, (BT) origin. Furthermore, we analyzed re-entrant activity based on conduction paths that can be identified based on the activation times. Conduction paths were determined as the shortest contiguous trajectory between a starting and end point of a wave, considering $\text{CV} \geq 20\text{ cm/s}$. If the trajectory had ≥ 1 intersection(s) it was considered as a re-entrant circuit (RC).

Recurrence Analysis

For a recording with N time samples, a recurrence plot (an $N \times N$ scatter plot with time on the x- and y-axis) can be constructed. If an event occurs at two time points with sufficient similarity, it is considered to be recurrent and can be identified by a dot in the scatter plot. Here, we analyzed the recurrence of conduction patterns in 60-s-recordings. We considered a pattern to be recurrent if the wave front(s); (1) reached the same point in

space, (2) propagated in the same direction, and (3) had a similar shape. To achieve this, we developed a method that is based on local activation times and corresponding activation intervals. The linear phase ($-\pi$ to π) was interpolated for every individual interval (**Figure 2A**). This approach does not require Hilbert transformation or time embedding of the raw electrogram as frequently used for the identification of phase singularities.

Phase signals were down-sampled to 10 timesteps per AFCL because the recurrence analysis leads to a large number of comparisons $[(60\text{s} \cdot 1.039\text{kHz})^2 = 3.9\text{e}9]$ and long computation times would be required. Based on the phase signals, phase maps were constructed for all time steps. For individual electrodes, the difference in phase was calculated by comparing 2 phase maps. Based on all 249 phase differences, the average phase difference (aPD) was computed. This was executed for every possible comparison between time steps within the 60-s-recording. Recurrent patterns were identified at an aPD of $< \pi/4$, corresponding to 1/8 of the AFCL. The rate of recurrent patterns was calculated as the ratio of the number of observed recurrences to the number of expected recurrences if the pattern was fully recurrent. The number of unique recurrent patterns was subjectively scored (by AvH) with the help of conduction movies.

To illustrate the impact of conduction patterns on the aPD and consequent recurrence identification, we can consider the two hypothetical examples presented in **Figures 2B,C**.

Example 1, (**Figure 2B**) demonstrates the effect of time in the recurrence analysis. One large “recurrent” wave front was present in the middle mapping area in the first map, timepoint n . In the second map, $n + 2$ timesteps, the wave front had propagated somewhat further, resulting in an aPD of 1.46. This level of the

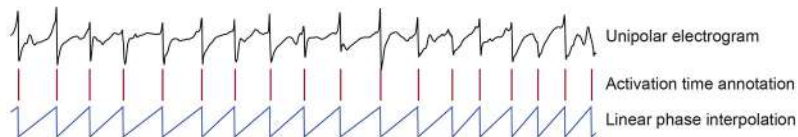
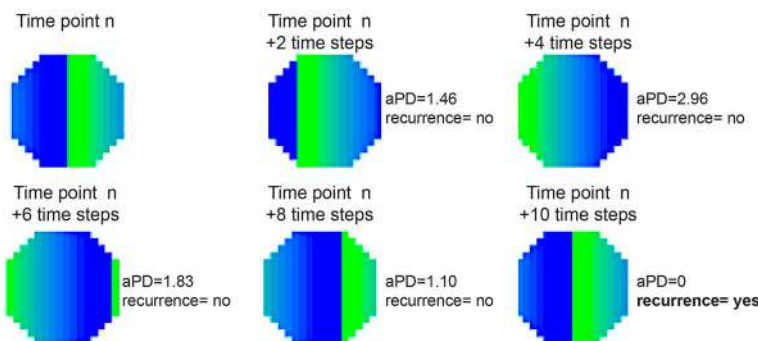
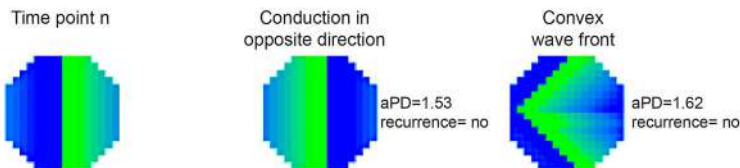
A Transformation from electrogram to phase**B Example 1. The effect of time****C Example 2. The effect of conduction direction and wave front shape**

FIGURE 2 | (A) Illustrates that based on the unipolar electrogram activation times (red columns) are identified. Based on the length of the interval, the linear phase from activation time to activation time was interpolated. **(B)** Demonstrates the effect of time on the recurrence analysis. One large “recurrent” wave front was present in the middle mapping area in the first map, timepoint n . In the second map, $n + 2$ timesteps, the wave front propagated somewhat further, resulting in an aPD of 1.46. This level of the aPD is above $\pi/4$ (0.7854) and therefore considered to be non-recurrent. At timestep $n + 4$, the aPD increased to a maximum of 2.96. In the following timesteps ($n + 6$ and $n + 8$), aPD decreased again until at $n + 10$ the wave front reoccurred at the same site like timepoint n . Here, the aPD was 0 and consequently considered to be recurrent. **(C)** Demonstrates the effect of direction and wave front shape. Map n is presented again as the first map. The wave front in the second map propagated in the opposite direction compared to map n . The aPD was now calculated to be 1.53, thus not recurrent. In the third map the wave did conduct in the same direction like map n . However, the wave front shape was now set to be convex instead of planar. The aPD between this map and map n was 1.62, thus also non-recurrent.

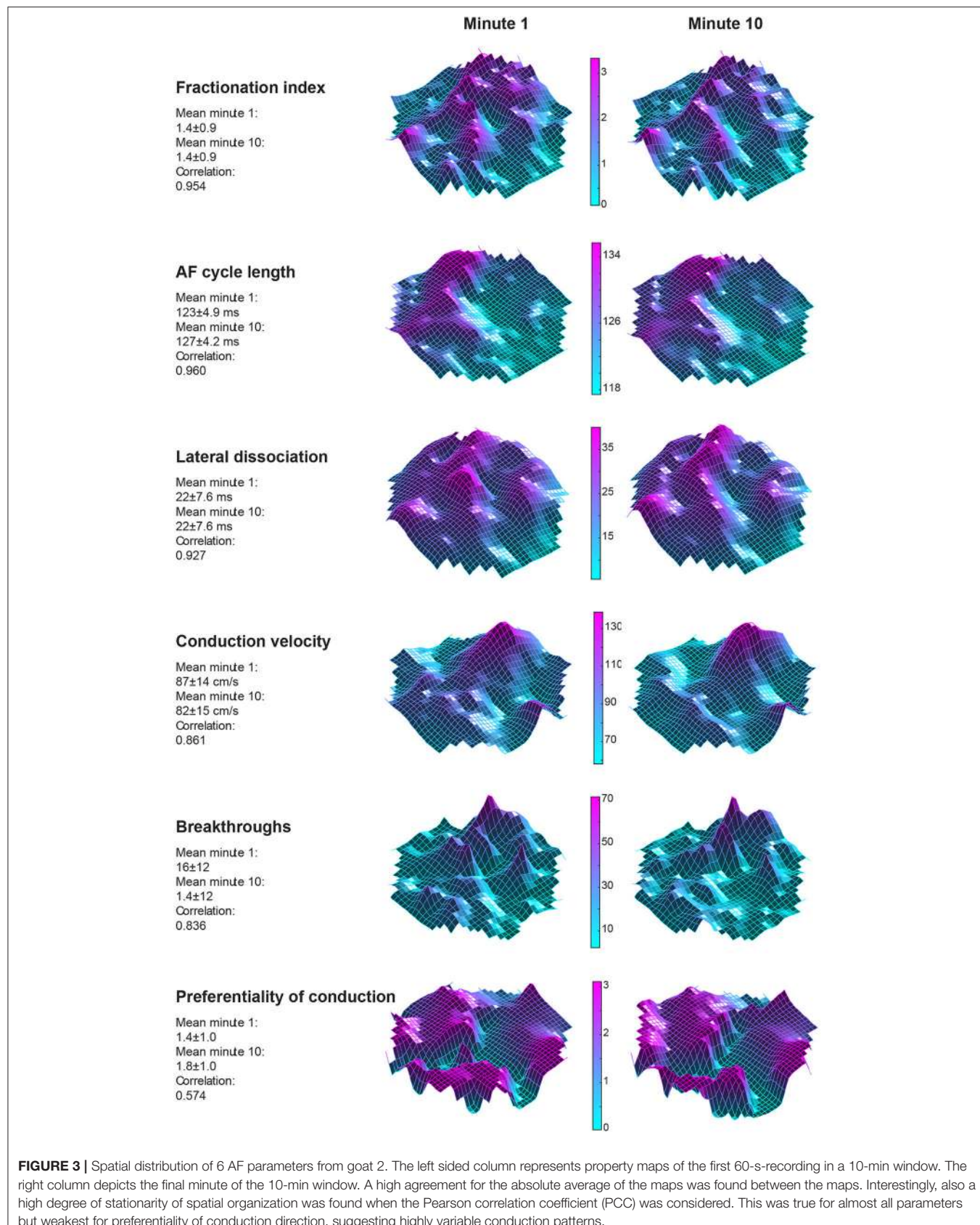
aPD is above $\pi/4$ (0.7854) and therefore considered to be non-recurrent. At timestep $n + 4$, the aPD increased to a maximum of 2.96. In the following timesteps ($n + 6$ and $n + 8$), aPD decreased until at $n + 10$ the wave front reoccurred at the same site like timepoint n . Here, the aPD was 0 and consequently the pattern was considered to be recurrent.

Example 2 (Figure 2C) demonstrates the effect of direction and wave front shape. Map n is again presented as the first map. The wave front in the second map propagated in the opposite direction compared to map n . The aPD was now calculated to be

1.53, thus non-recurrent. In the third map the wave did propagate in the same direction like map n . However, the wave front shape was now set to be convex instead of planar. The aPD between this map and map n was 1.62, therefore also non-recurrent.

Statistics

Data are presented as mean \pm sd. Data were tested for normality using a Kolmogorov-Smirnov test. The effect of time was tested using a repeated measure ANOVA. Intra- and inter-episode correlation between property maps was assessed using



Pearson correlation coefficient (PCC). A Bonferroni's correction was applied to correct for multiple comparisons. Inter-episode correlation differences were tested with a Wilcoxon rank sum test.

RESULTS

AF Property Maps

Twelve goats a 10-min period within a single AF episode was recorded. This 10-min period was divided into ten 60-s-recordings. In **Figure 3** two property maps, the first and last recording in a period, of goat 2 are presented. Only minor differences in the spatial distribution of the AF properties between the 2 recordings are apparent. This suggests that the AF properties remained very stable over this interval of 9 min. This high stability was found in all 6 parameters and all goats (**Figure 4**). We further addressed the spatial stationarity of the different parameters by exploring the correlation between AF property maps. From **Figure 4B** it can be appreciated that the average PCCs were very high, ranging from 0.66 ± 0.11 for Pref up to 0.98 ± 0.01 for FI and all PCCs were significant (**Table 1**). To underscore that this finding was not due to chance we broke the spatial coherence of the maps by randomly reassigning the electrodes within the map. This test diminished the average PCCs to almost 0 (right panel of **Figure 4B**). These observations demonstrate that both a high temporal and spatial stationarity was present.

We also looked at to what extent AF properties vary in space. High correlations between 60-s-recordings could have occurred due to a limited spatial diversity of the parameter. **Table 1** presents the coefficient of variation and range within the property maps. Within the AFCL-maps the coefficient of variation was very low ($4.3 \pm 2\%$), demonstrating a fairly homogeneous spatial distribution. By contrast, for FI-, preferentiality-, and breakthrough-maps the coefficient of variation was much larger, ranging from 50 to 78%. This indicates that discrete zones on the atrial epicardial surface exhibited different properties. In **Table 1** the overall characteristics of the 6 different property maps is presented.

All property maps are available in the Supplemental Materials. Raw data are not available online because of the large data size, 240 min for 249 unipolar channels at a sampling frequency of 1039 Hz. The raw data supporting the conclusions of this manuscript will be made available by the authors, without undue reservation, to any qualified researcher.

Short Term AF Dynamics

Potentially, stable conduction properties can be stable on a beat-to-beat level or at somewhat longer timespans, e.g., seconds, could have contributed to the stationary property maps within single AF episodes. Therefore, we explored dynamic behavior of AF (**Figure 5**). On a beat-to-beat level, the AFCL varied by 20 ± 3.7 ms, $16 \pm 3.6\%$ of the AFCL, and conduction direction varied with 66 ± 10 degrees. This high dynamic behavior was also reflected in the large average number of simultaneously present waves per cycle, 7.7 ± 2.3 . In total 453 re-entrant trajectories were found of which 25 lasted >2 rotations. On average re-entrant

activity was present for $9.2 \pm 11\%$. The lifespan of re-entrant circuits was 149 ± 18 ms. Hence, the average lifespan of re-entries was short and close to the AFCL with a lifespan to AFCL ratio of 1.2 ± 0.3 . These finding demonstrated a large beat-to-beat variability with high dynamic patterns that cannot explain stationary AF properties.

Recurrence of Conduction Patterns

On average, AF exhibited a highly dynamic behavior in terms frequency and patterns, nonetheless a high degree of spatiotemporal stationarity of AF properties was present. This could be explained by frequent recurrent patterns that dominate the property maps. We therefore investigated the occurrence of recurrent AF patterns.

In **Figure 6** a representation of the construction of a representative recurrence plot is presented. A segment of the AF recording with recurrent activity is depicted on the left series of maps in panel A. In the right side a series of maps with a segment with non-recurrent activity is presented. In **Figure 6B**, the recurrence plots over 3 cycles of these two segments are shown. The recurrent phase presented diagonal lines while during the segment with chaotic activity no recurrences were found. In the overall 60s-recurrence plot, we can observe that the non-recurrent phase was present throughout most of the time. The recurrent pattern appeared 3 times, at timepoints 32, 48, and 52s, in the 60-s-recordings.

Recurrence plots, wave and re-entrant circuit analysis for each individual animal are presented in **Table 2**. In the majority of goats (9 out of 12, goat number; 1, 3, 4, 6, and 8-12) no frequent or long lasting recurrent patterns were found. Only 3 goats had higher recurrence rates. Overall 1.6 ± 0.7 recurrent patterns per goat were found, with either peripheral or BT origins. Sixty-four percent of the reentrant circuits with >2 rotations were identified as recurrent events. No predominant origin of conduction pattern was found. Frequent disruption occurred, initiating unique states resulting in a recurrent pattern rate of 0.11 ± 0.19 (**Figure 7**). The association of recurrent pattern rate was strong with the number of waves but was weak with the number of reentrant circuits.

AF Property Maps and Effect of Time and AF Episode

Potentially, AF property maps could gradually change over a period of several minutes. Therefore, we investigated the effect of time on these property maps. In the section above we determined the average PCC for all comparisons within the 10-min period. Here we averaged the PCC for the different possible time intervals (1–9 min) between the recordings within the 10-min period (**Figure 8**). No changes in PCC occurred for all parameters at the various time intervals. Thus, within a single AF episode a high degree of spatiotemporal stationarity was found.

High stationarity could reflect the underlying anatomical structure. In that case one would expect that different AF episodes would display comparable AF property distribution. We therefore explored the spatiotemporal stationarity in 2 additional AF episodes ($n = 6$). We chose 2 episodes to be closely apart, 2.1 ± 1 min of AF interruption, and the third episode after

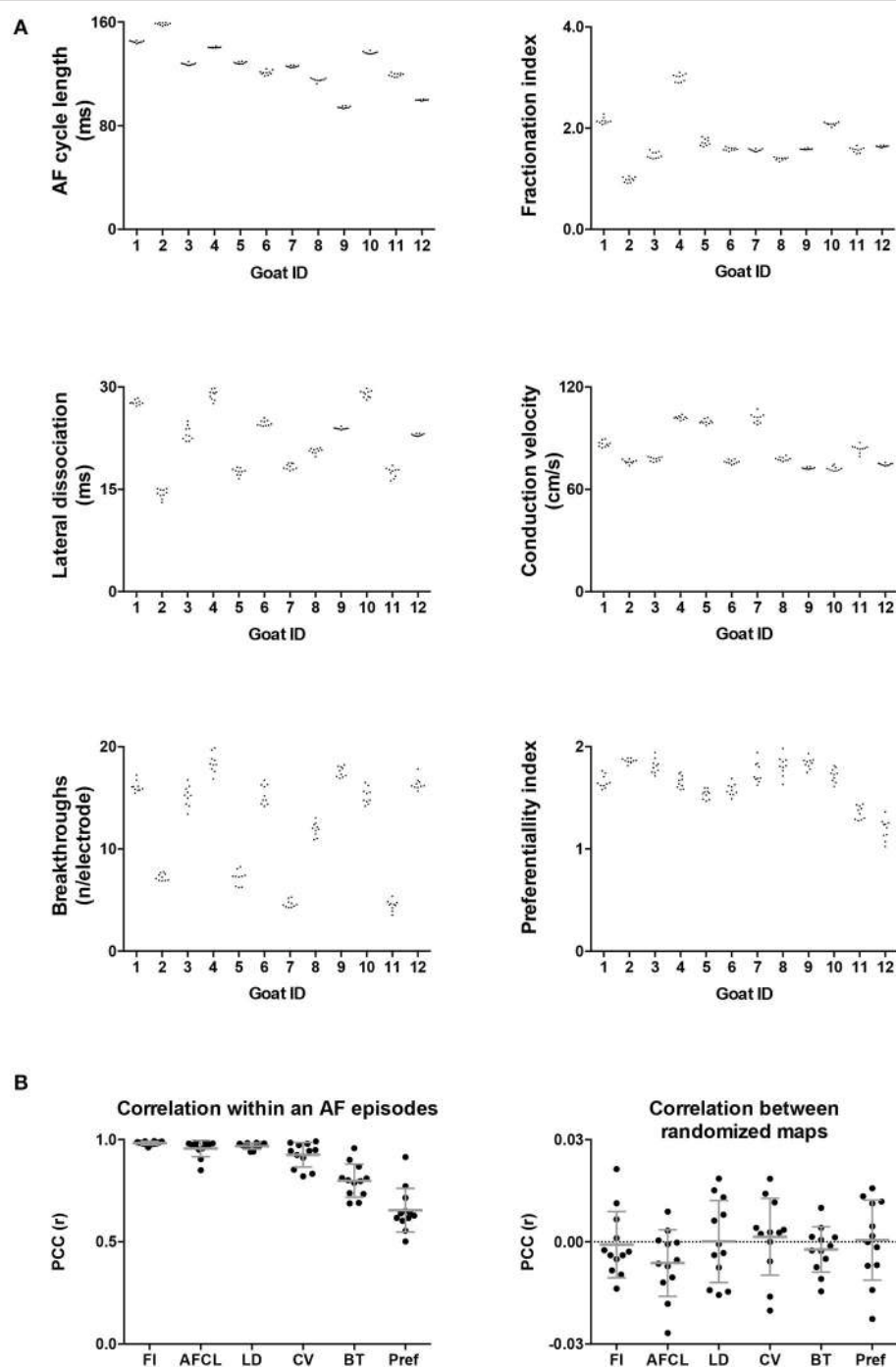


FIGURE 4 | (A) Intra-episode PCC for 6 different AF parameters. On the x-axis the individual animals are given. Panel A represents the absolute average of a map in a 60-s-recording. Per animal 10 values of the 10 consecutive maps are given. **(B)** In the first panel the average PCC, based on 45 correlations, is given per animal per parameter. The right-hand panel confirms that this high degree of stationarity did not occur due to chance since breaking the spatial coherence completely removed the correlation.

~1h of AF interruption. This resulted into a time difference of 63.4 ± 16.7 min for episode 2 vs. 3 and 75.3 ± 17.9 min for episode 1 vs. 3, (Figure 1, goats 1-6). The 2-min AF interruption led hardly to any changes in average PCC (Figure 9). However,

larger changes for some animals occurred than for others, specifically for CV. Interestingly, after the 60-min interruption of AF the PCC led to a large inter-individual variation. The decrease of PCC was significant for AFCL, CV, and FI.

DISCUSSION

Major Findings

In the goat model of persistent AF, we demonstrated that in 60-s-recordings the spatiotemporal distributions of AF parameters are stationary if measured within a single AF episode. A short interruption of an AF episode had little effect on this stationary behavior but interruption of longer duration changed AF parameters significantly. Sixty-second

recurrence analysis illustrated that recurrent patterns were scarce and only found in a minority of the animals. AF was also shown to have highly dynamic behavior at a beat-to-beat level. Therefore, stationary spatiotemporal properties could not be attributed to stable recurrent conduction patterns during AF suggesting that the atrial myocardium may determine average AF properties even when the conduction patterns are highly variable.

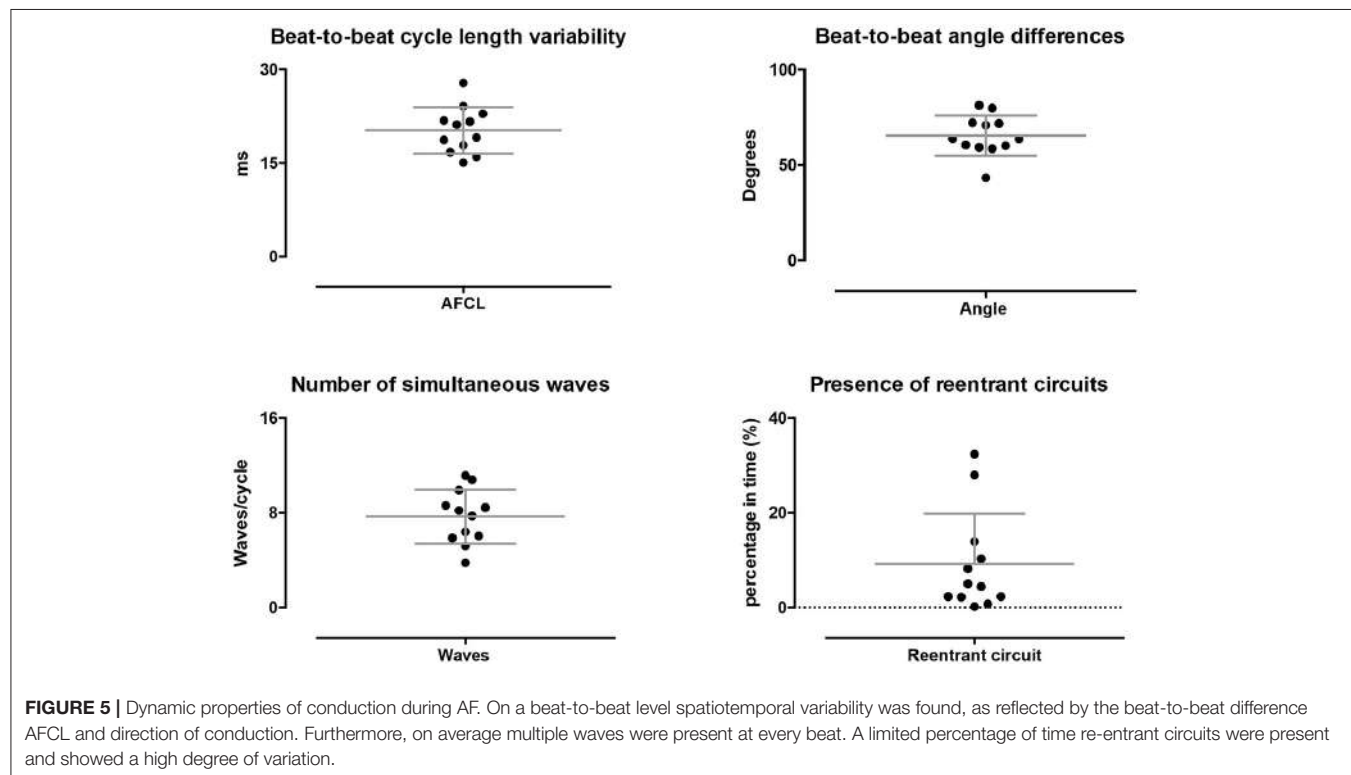
Stationarity of Ablation Targets

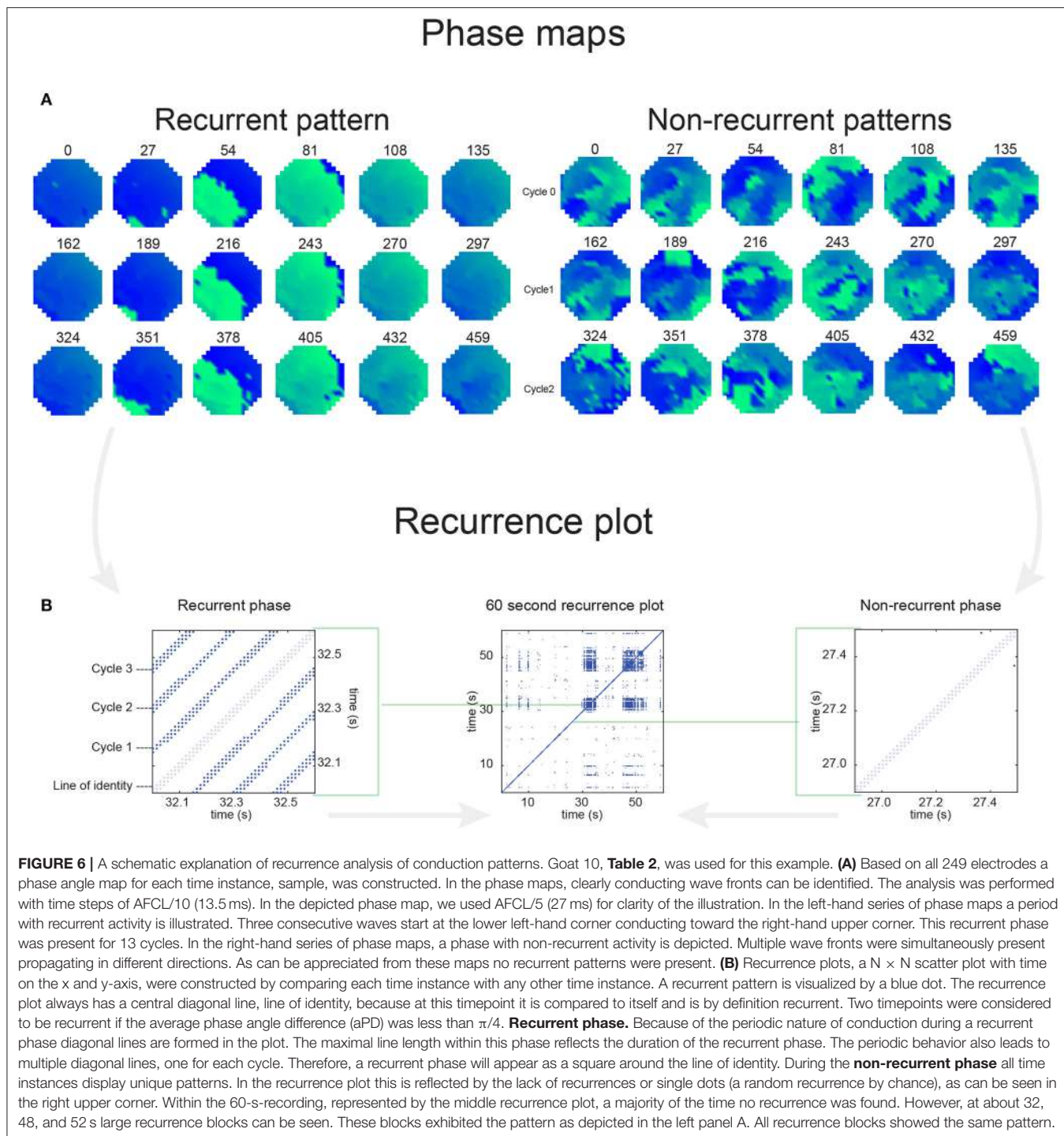
Complex fractionated electrograms (CFAE) were reported to occur during induced AF at sites of conduction block in Wolf-Parkinson-White patients and therefore reflect areas with higher complexity of AF (Konings et al., 1997). Consequently, they might reflect zones that act as sources for AF. It was hypothesized that CFAE sites might be suitable targets for AF ablation (Nademanee et al., 2004). Initially high success rates were reported but recent randomized controlled trials failed to show superiority of PV isolation + CFAE ablation above PV isolation alone (Verma et al., 2015; Vogler et al., 2015). In other studies, high dominant frequency (DF) was found to associate with rotor sites in cholinergic AF in sheep hearts (Berenfeld et al., 2000; Mandapati et al., 2000). This notion led to hypothesis that ablating DF sites might be a valid target for AF ablation (Mandapati et al., 2000; Sanders et al., 2005). Indeed, the presence of high frequency sites inversely correlated to procedural success rates (Gadenz et al., 2017; Kimata et al., 2018) but targeting DF sites did not consistently lead to improvement of clinical outcome (Atienza et al., 2014; Gadenz

TABLE 1 | Spatial variation (coefficient of variation and range) and stability in time (PCC) of the 6 different AF parameters.

	Coefficient of variation	Range	PCC(r)	PCC p-value
Fractionation index	50 ± 0.8%	4.60 ± 1.5	0.983 ± 0.01	p < 0.001
AFCL (ms)	4.3 ± 2%	21.2 ± 8.2	0.956 ± 0.04	p < 0.001
Lateral dissociation (ms)	28 ± 8%	29.8 ± 5.5	0.968 ± 0.01	p < 0.001
Conduction velocity (cm/s)	23 ± 14%	115 ± 76	0.926 ± 0.06	p < 0.001
BT (n/electrode/60 s)	78 ± 34%	53 ± 22	0.799 ± 0.08	p < 0.001
Preferentiality	53 ± 11%	3.1 ± 0.02	0.655 ± 0.11	p < 0.001

Per animal the average coefficient of variation and average range (max-min) of the 10 maps was calculated. The grand mean ± sd is presented in the table. The grand mean of the Pearson correlation coefficient (PCC) was based on all 45 comparisons per animal.





et al., 2017). It is unclear whether these negative outcomes entail that CFAE and high DF indicate bystander sites instead of AF driver sites or are due to technical limitations of the methods applied.

Irrespective of the applied methods, the intrinsic assumption entail that driver sites are stable in time and space. In most studies, DF and CFAE was determined on electrograms of 2-6 s.

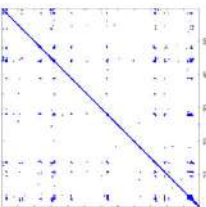
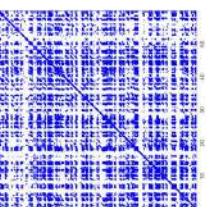
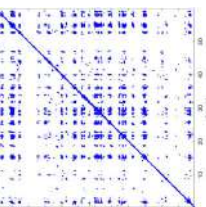
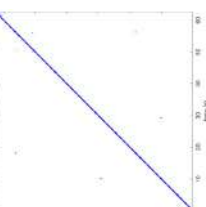
Lau et al. (2012), Gadenz et al. (2017) The question is whether these recording lengths are sufficient to capture potential transient appearances of CFAE's or DF's. Salinet et al. reported limited reproducibility of DF zones in non-contact intra-atrial electrograms (Salinet et al., 2014). However, continuous recordings of bipolar contact electrograms showed that about 75% of CFAE's remain stable in time (Lau et al., 2015). Similarly,

TABLE 2 | Overview of recurrence, wave and re-entry analysis for all 12 goats.

Goat ID	Recurrence map	Predominant recurrent pattern	Secondary recurrent pattern	Tertiary recurrent pattern	Rate of recurrent patterns	Waves/cycle	AFCL (ms)	RC presence (% in time)	RC lifespan (ms)
1		Wave type: PW Origin: NE→SW Time point: 58	NA	NA	0.021	9.9	150	2.30	159
2		Wave type: PW Origin: NW Time point: 26	Wave type: rBT Origin: SW→NE Time point: 26	Wave type: PW Origin: E→W Time point: 55.9	0.665	3.8	164	0.21	137
3		Wave type: PW Origin: NW	Wave type: rBT Origin: NW	Wave type: PW Origin: SE→NW Time point: 8.5	NA	0.063	7.8	132	8.21
4		Wave type: PW Origin: NE→SW	Wave type: PW Origin: SW→NE	Wave type: PW Origin: SW→NE	NA	0.014	10.8	144	0.74
5		Wave type: PW Origin: W→E	NA	NA	0.172	5.17	135	2.19	136

(Continued)

TABLE 2 | Continued

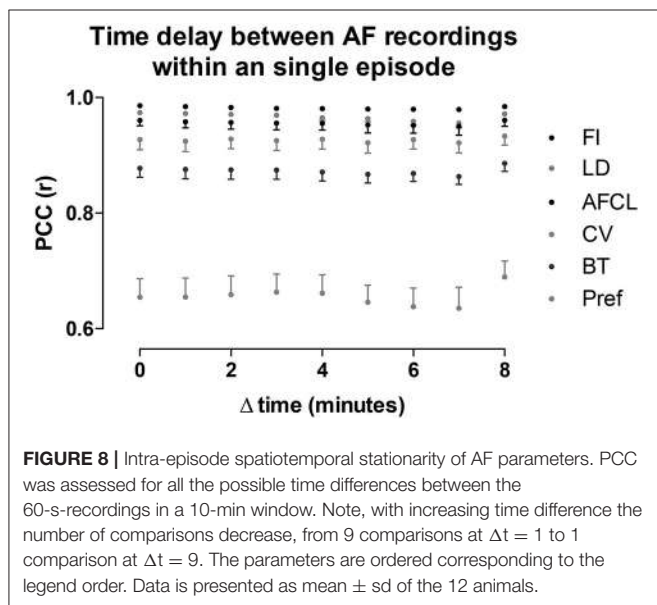
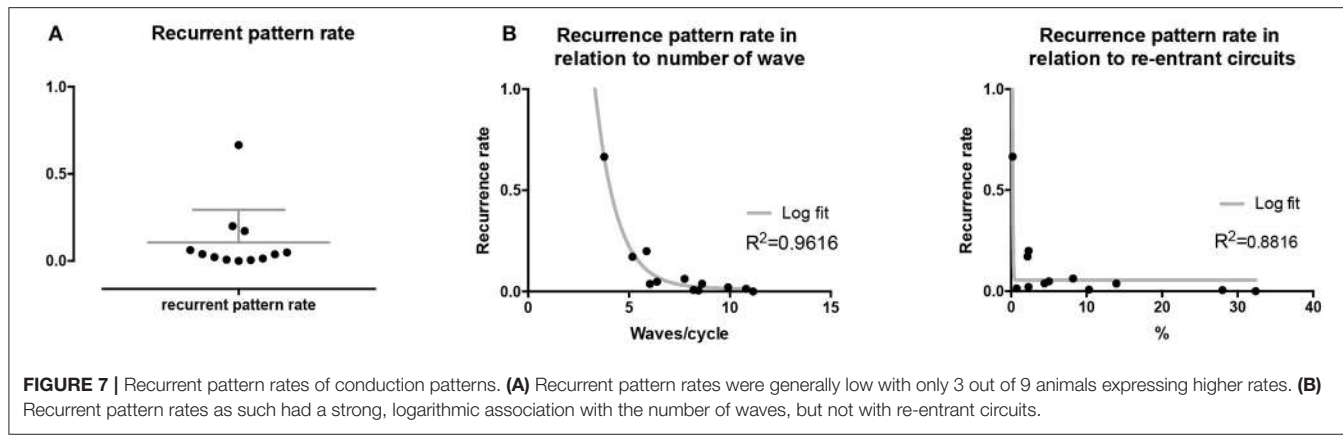
Goat ID	Recurrence map	Predominant recurrent pattern	Secondary recurrent pattern	Tertiary recurrent pattern	Rate of recurrent patterns	Waves/cycle	AFCL (ms)	RC presence (% in time)	RC lifespan (ms)
6		Wave type: Collision of 2 PW's Origin: N and S Time point: 3	NA	NA	0.008	8.20	128	10.3	147
7		Wave type: Collision of 2 PW Origin: S and N Time point: 5-8-10 etc.	NA	NA	0.200	5.87	127	2.32	151
8		Wave type: RBT Origin: NE Time point: 2-15-25 etc.	NA	NA	0.038	6.03	121	14.0	178
9		Wave type: - Origin: - Time point: -	NA	NA	0.001	11.2	103	32.4	158

(Continued)

TABLE 2 | Continued

Goat ID	Recurrence map	Predominant recurrent pattern	Secondary recurrent pattern	Tertiary recurrent pattern	Rate of recurrent patterns	Waves/cycle	AFCL (ms)	RC presence (% in time)	RC lifespan (ms)
10		rBT Origin: N Time point: 32-48 52	NA	NA	0.039	8.61	139	4.43	144
11		rBT Origin: N Time point: 4	PW Origin: NW-SE Time point: 21	PW Origin: South Time point: 14	0.049	6.38	122	5.00	129
12		rBT Origin: S Time point: 9 56	rBT Origin: N Time point: 30	NA	0.006	8.44	102	28.0	157

Recurrent patterns were subjectively scored to be most frequent (primary), second (secondary) or third (tertiary) in line. For each pattern the wave type, origin and time point of appearance (in seconds) is indicated. Acronyms used are: PW, peripheral wave; rBT, repetitive breakthrough; RC, reentrant circuit; N, north; E, east; S, south; W, west; NA, Not available.



we found very high spatiotemporal stationarity for both FI and AFCL. Recordings of 60 s within a single episode of AF were more than sufficient to reliably capture patterns. However, the determination of the minimal recording length to obtain representative information was not addressed in this study and would require further investigations, preferably in human recordings.

Stationarity of Conduction Properties

Both AFCL and FI are parameters that are derived from single electrograms. Therefore, they reflect AF properties of a limited area. Parameters that account for spatial characteristics of conduction, such as CV and LD had comparably high stationarity properties too. Stationarities were lower when AF patterns were taken into account. Preferentiality of conduction direction was subject to largest variability, indicative of dynamic conduction patterns. Breakthroughs were found at almost all electrodes and clear preferential regions of epicardial focal spread of activation

were present. Recurrence analysis revealed that half of the goats exhibit periods of repetitive BT's of variable durations. Whether these sites are important for the perpetuation of AF, as proposed by Lee et al. (Lee et al., 2015), warrants further investigation.

In general, AF wave and recurrence analysis revealed multiple propagating wave fronts with a small number of recurrent patterns. Hence, it is unlikely that the high degree of stationarity of AF property maps is caused by stable and frequent conduction patterns. Therefore, we conclude that the atrial structure and local electrophysiological properties are likely to determine average AF properties even if the conduction patterns as such are very variable. This might imply that the relatively large variation in AF complexity (3.8–11 waves/cycle), among animals without substantial structural remodeling (Verheule et al., 2010), may—at least partly—be driven by the individual atrial architecture.

Are AF Properties Independent From the AF Episode?

If AF properties would only be determined by the atrial architecture, then the initiation conditions should not affect AF properties. We therefore examined the effect of different episodes of AF. We found that stationarity is conserved if two AF episodes are relative close in time (~ 2 min). This observation is in line with Redfearn et al. who found that $\sim 80\%$ of CFAE regions were confirmed when the atria were remapped after a 10 min interval of sinus rhythm (Redfearn et al., 2009). This implies that atrial structure has a prominent role on conduction properties during AF. However, stationarity of AF properties was lower when AF was interrupted > 1 h. Because atrial structure does not change in this time interval, we propose that some form of acute recovery from electrical remodeling affected the atrial substrate. This observation might be of clinical importance since some symptomatic AF patients are cardioverted to sinus rhythm before AF ablation. Re-induction of AF during the procedure may reveal other AF patterns or drivers than originally were present with the risk that the leading mechanism cannot be identified.

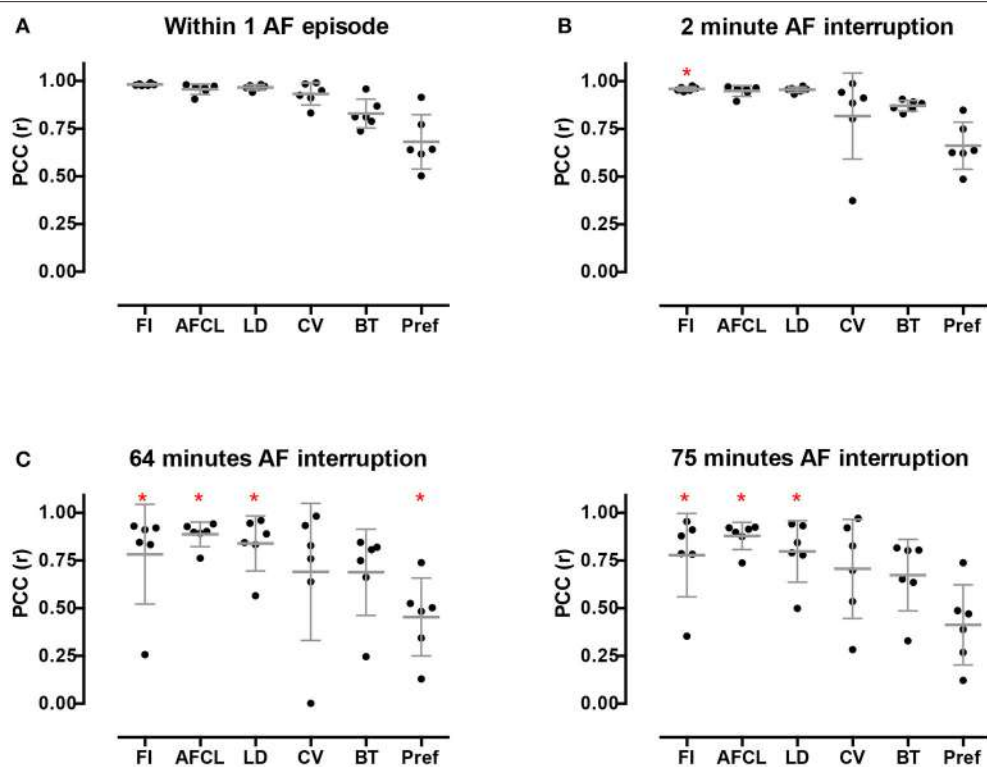


FIGURE 9 | Inter-episode spatiotemporal stationarity of AF parameters. Three different AF episodes were compared. **(A)** Intra-episode stationarity. The average PCC based on the 6 goats in the first episode. **(B)** PCC for inter-episodes stationarity with short time difference. **(C)** PCC for inter-episodes stationarity with ~ 1 h time difference. **(D)** PCC for inter-episodes stationarity with ~ 1.5 h time difference. Changes in PCC were tested with a Wilcoxon rank sum test without *post-hoc* analysis. $*p < 0.05$ vs within episode.

The Use of Recurrence Quantification Analysis

Recurrence quantification analysis is a technique to identify recurrent states in non-linear dynamical systems. Recurrence quantification analysis has been used in various biomedical disciplines, e.g., postural fluctuation and heart rate variability (Riley et al., 1999; Arcentales et al., 2011). In AF, recurrence analysis has been used mostly for (fractionated) electrogram morphology (Censi et al., 2000; Ng et al., 2014). We made a first step toward recurrent conduction pattern analysis by applying principal component analysis on all electrograms from a high-density array (Zeemering et al., 2015). This approach showed a good correlation with the number of waves but lacked directional and wave front information. Hence, recurrence of the degree of complexity but no recurrence of patterns could be discriminated. Here, we introduce a method accounting for both directionality and complexity of conduction patterns. An important finding is that recurrent patterns were scarce in the overall data set. The frequency of recurrent patterns was inversely related to the number of waves. Recurrent patterns mainly occurred in animals with a low degree of AF complexity. A recurrent pattern in animals with a higher average number of waves per cycle is more likely to be disrupted by other waves. In addition, if more independent wave fronts are present, than the likelihood that all

fronts show a recurrence, i.e., synchronize in time and space, is relatively low.

Future Perspectives

The introduced recurrence analysis allows addressing AF on a large time scale and may generate new ideas about AF perpetuation. For instance, the identification of a recurrent period within an episode of AF could indicate maintenance of AF by large circuits, while non-recurrent periods reflect more localized mechanisms. In that case the corresponding dimensions of the recurrence area that matches the local mechanism should be found. Alternatively, recurrent periods could reflect large transient reentrant circuits that act as oscillators of the fibrillation process. These resonators may speed up fibrillation rate with consequent breakdown in distant areas of the atria. Recurrent patterns may also occur before cardioversion of AF when AF complexity becomes low.

LIMITATIONS

An obvious limitation of this study is that the recordings were performed in the goat model of persistent AF in the presence of limited structural remodeling. Additional investigations are required to investigate whether similar patterns occur in patients

with AF. Also, the effect of the degree of structural remodeling on recurrent patterns should be addressed in future studies.

AUTHOR CONTRIBUTIONS

AvH conducted the experiments, analyzed data, scientific interpretation, developed the concept, and wrote the article. SZ developed analysis tools, analyzed data, scientific interpretation, developed of the concept, and contributed to the writing of the article. PP scientific interpretation, developed of the concept, and contributed to the writing of the article. JS developed analysis tools, analyzed data. GG conducted experiments. LH analyzed data. MK conducted experiments. BM contributed to the writing of the article. SV scientific interpretation, developed of the concept, and contributed to the writing of the article. US scientific interpretation, developed of the concept, and contributed to the writing of the article.

REFERENCES

- Allessie, M. A., de Groot, N. M., Houben, R. P., Schotten, U., Boersma, E., and Smeets, J. L. (2010). Electrophysiological substrate of long-standing persistent atrial fibrillation in patients with structural heart disease: longitudinal dissociation. *Circ. Arrhythm. Electrophysiol.* 3, 606–615. doi: 10.1161/CIRCEP.109.910125
- Allessie, M. A., Konings, K., Kirchhof, C. J., and Wijffels, M. (1996). Electrophysiologic mechanisms of perpetuation of atrial fibrillation. *Am. J. Cardiol.* 77, 10A–23A. doi: 10.1016/S0002-9149(97)89114-X
- Arcentales, A., Giraldo, B. F., Caminal, P., Benito, S., and Voss, A. (2011). “Recurrence quantification analysis of heart rate variability and respiratory flow series in patients on weaning trials,” in *2011 Annual International Conference of the IEEE Engineering in Medicine and Biology Society* (Boston, MA: IEEE), 2724–2727.
- Atienza, F., Almendral, J., Ormaetxe, J. M., Moya, A., Martínez-Alday, J. D., and Hernández-Madrid, A. (2014). Comparison of radiofrequency catheter ablation of drivers and circumferential pulmonary vein isolation in atrial fibrillation: a noninferiority randomized multicenter RADAR-AF trial. *J. Am. Coll. Cardiol.* 64, 2455–2467. doi: 10.1016/j.jacc.2014.09.053
- Berenfeld, O., Mandapati, R., Dixit, S., Skanes, A. C., Chen, J., and Mansour, M. (2000). Spatially distributed dominant excitation frequencies reveal hidden organization in atrial fibrillation in the Langendorff-perfused sheep heart. *J. Cardiovasc. Electrophysiol.* 11, 869–879. doi: 10.1111/j.1540-8167.2000.tb00066.x
- Censi, F., Barbaro, V., Bartolini, P., Calcagnini, G., Michelucci, A., and Gensini, G. F. (2000). Recurrent patterns of atrial depolarization during atrial fibrillation assessed by recurrence plot quantification. *Ann. Biomed. Eng.* 28, 61–70. doi: 10.1114/1.248
- Gadenz, L., Hashemi, J., Shariat, M. H., Gula, L., and Redfearn, D. P. (2017). Clinical role of dominant frequency measurements in atrial fibrillation ablation - a systematic review. *J. Atr. Fibrillation.* 9:1548. doi: 10.4022/jafib.1548
- Haïssaguerre, M., Jaïs, P., Shah, D. C., Takahashi, A., Hocini, M., Quiniou, G., et al. (1998). Spontaneous initiation of atrial fibrillation by ectopic beats originating in the pulmonary veins. *N. Engl. J. Med.* 339, 659–666. doi: 10.1056/NEJM199809033391003
- Jalife, J. (2011). Deja vu in the theories of atrial fibrillation dynamics. *Cardiovasc. Res.* 89, 766–775. doi: 10.1093/cvr/cvq364
- Kimata, A., Yokoyama, Y., Aita, S., Nakamura, H., Higuchi, K., and Tanaka, Y. (2018). Temporally stable frequency mapping using continuous wavelet transform analysis in patients with persistent atrial fibrillation. *J. Cardiovasc. Electrophysiol.* 29, 514–522. doi: 10.1111/jce.13440
- Konings, K. T., Kirchhof, C. J., Smeets, J. R., Wellens, H. J., Penn, O. C., and Allessie, M. A. (1994). High-density mapping of electrically induced atrial fibrillation in humans. *Circulation* 89, 1665–1680. doi: 10.1161/01.CIR.89.4.1665
- Konings, K. T., Smeets, J. L., Penn, O. C., Wellens, H. J., and Allessie, M. A. (1997). Configuration of unipolar atrial electrograms during electrically induced atrial fibrillation in humans. *Circulation* 95, 1231–1241. doi: 10.1161/01.CIR.95.5.1231
- Krummen, D. E., Baykaner, T., Schricker, A. A., Kowalewski, C. A. B., Swarup, V., and Miller, J. M. (2017). Multicentre safety of adding Focal Impulse and Rotor Modulation (FIRM) to conventional ablation for atrial fibrillation. *Europace* 19, 769–774. doi: 10.1093/europace/euw377
- Kuklik, P., Zeemering, S., van Hunnik, A., Maesen, B., Pison, L., and Lau, D. H. (2017). Identification of rotors during human atrial fibrillation using contact mapping and phase singularity detection: technical considerations. *IEEE Trans. Biomed. Eng.* 64, 310–318. doi: 10.1109/TBME.2016.2554660
- Lau, D. H., Maesen, B., Zeemering, S., Kuklik, P., van Hunnik, A., and Lankveld, T. A. (2015). Indices of bipolar complex fractionated atrial electrograms correlate poorly with each other and atrial fibrillation substrate complexity. *Heart Rhythm* 12, 1415–1423. doi: 10.1016/j.hrthm.2015.03.017
- Lau, D. H., Maesen, B., Zeemering, S., Verheule, S., Crijns, H. J., and Schotten, U. (2012). Stability of complex fractionated atrial electrograms: a systematic review. *J. Cardiovasc. Electrophysiol.* 23, 980–987. doi: 10.1111/j.1540-8167.2012.02335.x
- Lee, G., Kumar, S., Teh, A., Madry, A., Spence, S., and Larobina, M. (2014). Epicardial wave mapping in human long-lasting persistent atrial fibrillation: transient rotational circuits, complex wavefronts, and disorganized activity. *Eur. Heart J.* 35, 86–97. doi: 10.1093/eurheartj/eht267
- Lee, S., Sahadevan, J., Khrestian, C. M., Cakulev, I., Markowitz, A., and Waldo, A. L. (2015). Simultaneous biatrial high-density (510–512 Electrodes) epicardial mapping of persistent and long-standing persistent atrial fibrillation in patients: new insights into the mechanism of its maintenance. *Circulation* 132, 2108–2117. doi: 10.1161/CIRCULATIONAHA.115.017007
- Mandapati, R., Skanes, A., Chen, J., Berenfeld, O., and Jalife, J. (2000). Stable microreentrant sources as a mechanism of atrial fibrillation in the isolated sheep heart. *Circulation* 101, 194–199. doi: 10.1161/01.CIR.101.2.194
- Nademanee, K., McKenzie, J., Kosar, E., Schwab, M., and Sunsaneewitayakul, B., Vasavakul, T., et al. (2004). A new approach for catheter ablation of atrial fibrillation: mapping of the electrophysiologic substrate. *J. Am. Coll. Cardiol.* 43, 2044–2053. doi: 10.1016/j.jacc.2003.12.054
- Narayan, S. M., Krummen, D. E., Shivkumar, K., Clopton, P., Rappel, W. J., and Miller, J. M. (2012). Treatment of atrial fibrillation by the ablation of localized sources: CONFIRM (Conventional Ablation for Atrial Fibrillation With or Without Focal Impulse and Rotor Modulation) trial. *J. Am. Coll. Cardiol.* 60, 628–636. doi: 10.1016/j.jacc.2012.05.022

FUNDING

This work was supported by the Netherlands Heart Foundation (CVON2014-09, RACE V Reappraisal of Atrial Fibrillation: Interaction between hyperCoagulability, Electrical remodeling, and Vascular Destabilization in the Progression of AF), the European Union (CATCH ME: Characterizing Atrial fibrillation by Translating its Causes into Health Modifiers in the Elderly, No. 633196, the ITN Network AFibTrainNet, No. 675351, and the ERACoSysMED H2020 ERA-NET Cofund project Systems medicine for diagnosis and stratification of atrial fibrillation).

SUPPLEMENTARY MATERIAL

The Supplementary Material for this article can be found online at: <https://www.frontiersin.org/articles/10.3389/fphys.2018.00947/full#supplementary-material>

- Nattel, S., Shiroshita-Takeshita, A., Brundel, B., J., and Rivard, L. (2005). Mechanisms of atrial fibrillation: lessons from animal models. *Prog. Cardiovasc. Dis.* 48, 9–28. doi: 10.1016/j.pcad.2005.06.002
- Nedios, S., Sommer, P., Bollmann, A., and Hindricks, G. (2016). Advanced mapping systems to guide atrial fibrillation ablation: electrical information that matters. *J. Atr. Fibrillation.* 8:1337. doi: 10.4022/jafib.1337
- Ng, J., Gordon, D., Passman, R. S., Knight, B. P., Arora, R., and Goldberger, J. J. (2014). Electrogram morphology recurrence patterns during atrial fibrillation. *Heart Rhythm.* 11, 2027–2034. doi: 10.1016/j.hrthm.2014.08.002
- Redfearn, D. P., Simpson, C. S., Abdollah, H., and Baranchuk, A. M. (2009). Temporo-spatial stability of complex fractionated atrial electrograms in two distinct and separate episodes of paroxysmal atrial fibrillation. *Europace* 11, 1440–1444. doi: 10.1093/europace/eup287
- Riley, M. A., Balasubramaniam, R., and Turvey, M. T. (1999). Recurrence quantification analysis of postural fluctuations. *Gait Posture* 9, 65–78. doi: 10.1016/S0966-6362(98)00044-7
- Roney, C. H., Cantwell, C. D., Bayer, J. D., Qureshi, N. A., Lim, P. B., and Tweedy, J. H. (2017). Spatial resolution requirements for accurate identification of drivers of atrial fibrillation. *Circ. Arrhythm. Electrophysiol.* 10:e004899. doi: 10.1161/CIRCEP.116.004899
- Salinet, J. L., Tuan, J. H., Sandilands, A. J., Stafford, P. J., Schlindwein, F. S., and Ng, G. A. (2014). Distinctive patterns of dominant frequency trajectory behavior in drug-refractory persistent atrial fibrillation: preliminary characterization of spatiotemporal instability. *J. Cardiovasc. Electrophysiol.* 25, 371–379. doi: 10.1111/jce.12331
- Sanders, P., Berenfeld, O., Hocini, M., Jaïs, P., Vaidyanathan, R., and Hsu, L. F. (2005). Spectral analysis identifies sites of high-frequency activity maintaining atrial fibrillation in humans. *Circulation* 112, 789–797. doi: 10.1161/CIRCULATIONAHA.104.517011
- Swarup, V., Baykaner, T., Rostamian, A., Daubert, J. P., Hummel, J., and Krummel, D. E. (2014). Stability of rotors and focal sources for human atrial fibrillation: focal impulse and rotor mapping (FIRM) of AF sources and fibrillatory conduction. *J. Cardiovasc. Electrophysiol.* 25, 1284–1292. doi: 10.1111/jce.12559
- van der Does, L., J., and de Groot, N., M. (2017). Inhomogeneity and complexity in defining fractionated electrograms. *Heart Rhythm.* 14, 616–624. doi: 10.1016/j.hrthm.2017.01.021
- Verheule, S., Tuyls, E., van Hunnik, A., Kuiper, M., Schotten, U., and Allessie, M. (2010). Fibrillatory conduction in the atrial free walls of goats in persistent and permanent atrial fibrillation. *Circ. Arrhythm. Electrophysiol.* 3, 590–599. doi: 10.1161/CIRCEP.109.931634
- Verma, A., Jiang, C. Y., Betts, T. R., Chen, J., Deisenhofer, I., and Mantovan, R. (2015). Approaches to catheter ablation for persistent atrial fibrillation. *N. Engl. J. Med.* 372, 1812–1822. doi: 10.1056/NEJMoa1408288
- Vogler, J., Willems, S., Sultan, A., Schreiber, D., Lüker, J., Servatius, H., et al. (2015). Pulmonary vein isolation versus defragmentation: the CHASE-AF clinical trial. *J. Am. Coll. Cardiol.* 66, 2743–2752. doi: 10.1016/j.jacc.2015.09.088
- Zeemering, S., Bonizzi, P., Maesen, B., Peeters, R., and Schotten, U. (2015). Recurrence quantification analysis applied to spatiotemporal pattern analysis in high-density mapping of human atrial fibrillation. *Conf. Proc. IEEE Eng. Med. Biol. Soc.* 2015, 7704–7707. doi: 10.1109/EMBC.2015.7320177
- Zeemering, S., Maesen, B., Nijs, J., Lau, D. H., Granier, M., and Verheule, S. (2012). Automated quantification of atrial fibrillation complexity by probabilistic electrogram analysis and fibrillation wave reconstruction. *Conf Proc. IEEE Eng. Med. Biol. Soc.* 2012, 6357–6360. doi: 10.1109/EMBC.2012.6347448

Conflict of Interest Statement: The authors declare that the research was conducted in the absence of any commercial or financial relationships that could be construed as a potential conflict of interest.

Copyright © 2018 van Hunnik, Zeemering, Podziemski, Simons, Gatta, Hannink, Maesen, Kuiper, Verheule and Schotten. This is an open-access article distributed under the terms of the Creative Commons Attribution License (CC BY). The use, distribution or reproduction in other forums is permitted, provided the original author(s) and the copyright owner(s) are credited and that the original publication in this journal is cited, in accordance with accepted academic practice. No use, distribution or reproduction is permitted which does not comply with these terms.



Dispersion of Recovery and Vulnerability to Re-entry in a Model of Human Atrial Tissue With Simulated Diffuse and Focal Patterns of Fibrosis

Richard H. Clayton*

Department of Computer Science, Insigneo Institute for *in-silico* Medicine, University of Sheffield, Sheffield, United Kingdom

OPEN ACCESS

Edited by:

Jichao Zhao,
University of Auckland, New Zealand

Reviewed by:

Michael Alan Colman,
University of Leeds, United Kingdom

Haibo Ni,
University of California, Davis,
United States

***Correspondence:**

Richard H. Clayton
r.h.clayton@sheffield.ac.uk

Specialty section:

This article was submitted to
Computational Physiology and
Medicine,
a section of the journal
Frontiers in Physiology

Received: 25 April 2018

Accepted: 16 July 2018

Published: 07 August 2018

Citation:

Clayton RH (2018) Dispersion of Recovery and Vulnerability to Re-entry in a Model of Human Atrial Tissue With Simulated Diffuse and Focal Patterns of Fibrosis. *Front. Physiol.* 9:1052.
doi: 10.3389/fphys.2018.01052

Fibrosis in atrial tissue can act as a substrate for persistent atrial fibrillation, and can be focal or diffuse. Regions of fibrosis are associated with slowed or blocked conduction, and several approaches have been used to model these effects. In this study a computational model of 2D atrial tissue was used to investigate how the spatial scale of regions of simulated fibrosis influenced the dispersion of action potential duration (APD) and vulnerability to re-entry in simulated normal human atrial tissue, and human tissue that has undergone remodeling as a result of persistent atrial fibrillation. Electrical activity was simulated in a 10×10 cm square 2D domain, with a spatially varying diffusion coefficient as described below. Cellular electrophysiology was represented by the Courtemanche model for human atrial cells, with the model parameters set for normal and remodeled cells. The effect of fibrosis was modeled with a smoothly varying diffusion coefficient, obtained from sampling a Gaussian random field (GRF) with length scales of between 1.25 and 10.0 mm. Twenty samples were drawn from each field, and used to allocate a value of diffusion coefficient between 0.05 and 0.2 mm²/ms. Dispersion of APD was assessed in each sample by pacing at a cycle length of 1,000 ms, followed by a premature beat with a coupling interval of 400 ms. Vulnerability to re-entry was assessed with an aggressive pacing protocol with pacing cycle lengths decreasing from 450 to 250 ms in 25 ms intervals for normal tissue and 300–150 ms for remodeled tissue. Simulated fibrosis at smaller spatial scales tended to lengthen APD, increase APD dispersion, and increase vulnerability to sustained re-entry relative to fibrosis at larger spatial scales. This study shows that when fibrosis is represented by smoothly varying tissue diffusion, the spatial scale of fibrosis has important effects on both dispersion of recovery and vulnerability to re-entry.

Keywords: atrial fibrillation, Courtemanche model, Gaussian random field, fibrosis, computer model, cardiac electrophysiology

1. INTRODUCTION

Although atrial fibrillation (AF) is a common cardiac arrhythmia, the mechanisms that initiate and sustain it are complex and remain incompletely understood. Circulating waves of electrical activation and recovery, often called re-entrant waves or rotors, are believed to sustain AF (Nattel, 2002). The anatomy of the human atria is complex, and structural heterogeneity is considered

to be an important substrate for atrial arrhythmias (Haissaguerre et al., 2016; Zhao et al., 2017). Fibrosis is an important component of heterogeneity (Csépe et al., 2017), although the role played by regions of fibrosis in anchoring rotors remains controversial (Nguyen et al., 2014; Trayanova et al., 2014; Sohns et al., 2017). Magnetic resonance imaging of the heart using delayed enhancement enables regions of fibrosis to be imaged directly; this approach has been used to reveal the different spatial scales of fibrosis that are present (Tanaka et al., 2007), to stratify patients and guide intervention (Akoum et al., 2012), and to demonstrate an association between the presence of fibrosis and recurrent atrial arrhythmias in patients (Marrouche et al., 2014).

Fibrosis is hard to study in experimental preparations because it is difficult to control the extent of fibrosis and the size of individual lesions, and so computational models of cardiac cell and tissue electrophysiology have been used to examine how regions of simulated fibrosis affect activation and recovery in cardiac tissue, as well as vulnerability to arrhythmias (Trayanova et al., 2014). When regions of fibrosis are represented as inexcitable obstacles, diffuse fibrosis can act to slow activation and to destabilize re-entry in simulated ventricular tissue (Ten Tusscher and Panfilov, 2007). This approach was extended by representing fibroblasts as coupled elements with a fixed resting potential instead of inexcitable regions, and similar effects were found (Majumder et al., 2012). A more recent study has shown that the strength of coupling between normal tissue and simulated fibroblasts as well as the fibroblast resting potential can modify the tissue response (Sridhar et al., 2017). The density of simulated fibrosis was identified as important in a study that used detailed anatomical models of infarcted rabbit ventricles; intermediate densities increased susceptibility to arrhythmia whereas high densities suppressed arrhythmia (McDowell et al., 2011). In patient specific models of atrial fibrosis, the particular shape and configuration of fibrotic regions has been observed to have an important effect on rotor behavior (McDowell et al., 2015; Morgan et al., 2016). The effect of spatial scale of fibrosis has also been investigated in simulations where fibrosis was represented as regions of uncoupled and inexcitable ventricular tissue; this study found that an increasing amount of fibrosis and increasing spatial scale both acted to increase vulnerability to arrhythmia (Kazbanov et al., 2016). In simulated atrial tissue, the electrotonic effect of regions of fibrosis was studied using a coupled and detailed fibroblast model to demonstrate that the effect of fibroblasts could underlie the complex fractionated electrograms often seen in persistent atrial fibrillation (Ashihara et al., 2012).

The role of heterogeneous tissue properties in increasing vulnerability to atrial arrhythmias is well-established (Allessie et al., 1976; Vigmond et al., 2004; Haissaguerre et al., 2016; Gokhale et al., 2017), but the role played by the size or length scale of fibrosed regions is not well-understood. Some simulation studies have represented heterogeneity by a chequerboard, where the size of the squares can be modified to control the length scale (Xie et al., 2001; Clayton and Holden, 2005; Kazbanov et al., 2016). Other studies have based the configuration of fibrosis on experimental (Tanaka et al., 2007; Engelman et al., 2010) or clinical (Morgan et al., 2016; Zahid et al., 2016) images. However

the sharp boundaries imposed by these approaches where tissue is designated as either fibrosed or normal may not represent the smooth changes that might be expected in cardiac tissue.

One technique for representing smoothly varying quantities is a correlated random field, where the overall properties of the field are random, but neighboring regions are correlated so that the field varies smoothly according to a correlation length. One class of correlated random field is a Gaussian random field (GRF) with exponential covariance, which is specified by a mean, a variance, and a correlation length. In 2-dimensions (2D), a GRF can be sampled to produce a series of random fields. In each sample, the values of the field will be correlated in both principal directions, and will be normally distributed. However the configuration of fluctuations in the field will vary from sample to sample. This approach has been used in models of groundwater flow with varying hydraulic conductivity (Meerschaert et al., 2013), and the heterogeneous spread of disease (Baptista et al., 2016).

The aim of the present study was to use a GRF to generate samples of 2D atrial tissue with fibrosis represented as smoothly varying diffusion, and to investigate the effect of heterogeneous diffusion at different length scales on electrical activation, recovery, action potential duration (APD), vulnerability to re-entry, and dynamics of re-entry.

2. METHODS

2.1. Overall Approach

Electrical activation and recovery were simulated in a 2D sheet of atrial tissue, to enable the effect of cell and tissue electrophysiology to be examined without the additional complexity of anatomical structure. To represent the effect of fibrosis, the diffusion coefficient was set to vary smoothly from a low value representing regions of fibrosis, up to higher levels representing normal excitable tissue. The length scale of fluctuations in diffusion coefficient was varied by taking samples from GRFs with different correlation lengths. The effects of heterogeneities in diffusion at different length scales were examined by simulating normal beats during pacing at a steady cycle length, a single premature stimulus, vulnerability to re-entry during rapid decremental pacing, and behavior of an imposed spiral wave. These simulations were run using model parameters set to represent normal human atrial cells, and cells that have undergone remodeling as a consequence of persistent AF.

2.2. Cellular Electrophysiology Model and Implementation

Cardiac cellular electrophysiology was modeled using the Courtemanche-Ramirez-Nattel (CRN) model of human atrial cells (Courtemanche et al., 1998). To avoid instability resulting from drift in intracellular ion concentrations (Cherry and Evans, 2008; Wilhelms et al., 2012), $[Na^+]$ _i and $[K^+]$ _i were fixed at their default initial values of 11.17 and 139.00 mM, respectively. The CRN model was implemented in C, based on code automatically generated from the CellML repository (www.cellml.org).

Two variants of the cell model were used in this study. The first variant, denoted *CRNnormal*, used model parameters as

specified in the original paper (Courtemanche et al., 1998) and curated in CellML. This variant produces an action potential with a pronounced spike and dome, and an APD of around 300 ms. The second variant, denoted *CRNremodelled*, simulated the effects of cellular remodeling due to persistent AF. In *CRNremodelled*, the maximum conductance of I_{to} and $I_{Ca,L}$ were decreased by 65% (i.e., multiplied by 0.35), $I_{K,ur}$ was decreased by 49%, and the maximum conductance of I_{K1} was increased by 110%. These changes are based on those described in a previous study (Wilhelms et al., 2012), and produced a shortened action potential with a less prominent spike and dome that was consistent with experimental observations in cells from remodeled hearts (Workman et al., 2001). Initial conditions for gating and other variables in each simulation were set by pacing each variant at a cycle length of 1,000 ms for 40 beats.

2.3. Tissue Model and Gaussian Random Field

Cardiac tissue was simulated using the monodomain model (Clayton et al., 2011), where tissue conductivity can be represented as a diffusion coefficient. Electrical activation and recovery were studied in a 2D sheet of tissue, with 400×400 grid points representing dimensions of 10×10 cm, isotropic diffusion, and no-flux boundary conditions at each edge. The monodomain model was solved using a finite difference method, with a space step of 0.25 mm, and an adaptive time step that ranged between 0.1 and 0.01 ms (Rush and Larsen, 1978; Qu, 1999). With a uniform diffusion coefficient of $0.2 \text{ mm}^2\text{ms}^{-1}$, this configuration yielded a plane wave conduction velocity of 0.695 mm ms^{-1} for the *CRNnormal* variant, which is at the lower end of the range of conduction velocity observed in human atria (Weber et al., 2011).

Gaussian random fields (GRFs) can represent a smoothly varying field in space, and are composed of a mean and a covariance. The covariance function describes correlations between the value of the field at a single point and within its neighborhood. A squared exponential covariance function includes a correlation length δ , which can be used to vary the length scale of fluctuations in the field.

$$\text{Cov}(x, y) = \exp \left\{ \frac{(|x - y|)^2}{\delta^2} \right\} \quad (1)$$

Stationary GRFs with mean of 0, variance of 1.0, and an exponential covariance function were generated with length scales of 1.25, 2.50, 5.0, and 10.0 mm using the method of circulant embedding, which is detailed in Kroese and Botev (2015). Samples of these GRFs with a length scale of 1.25 and 10 mm are illustrated in **Figures 1A,B**. To translate these fields into a diffusion field, the raw GRF was offset by 2, and multiplied by 0.05. GRF raw values of -1, 0, and +1 therefore translated to diffusion coefficients of 0.05, 0.1, and $0.15 \text{ mm}^2\text{ms}^{-1}$, respectively. The value of the diffusion coefficient was capped at $0.2 \text{ mm}^2\text{ms}^{-1}$.

Regions with a diffusion coefficient less than $0.05 \text{ mm}^2\text{ms}^{-1}$ were designated areas of fibrosis, and were set to be coupled but inexcitable, with a diffusion coefficient of $0.05 \text{ mm}^2\text{ms}^{-1}$.

Inexcitability was imposed by setting the membrane current term in the monodomain equation to zero, while retaining the term describing voltage diffusion.

Figures 1C, D show the diffusion fields corresponding to **Figures 1A,B**, and the profile of the raw GRF as well as the diffusion coefficient for the central row of each sample are plotted in **Figures 1E,F**. The lower panel of **Figures 1** shows the distribution of diffusion coefficient in the samples of the GRF at each length scale. In these distributions the median is close to $0.1 \text{ mm}^2\text{ms}^{-1}$ as expected, and the effect of truncation at 0.05 and $0.2 \text{ mm}^2\text{ms}^{-1}$ can be seen.

Since the configuration of fibrotic regions would be expected to affect simulated tissue behavior, 20 samples of the GRF were obtained at each of the four length scales. The procedure described above was used to generate a set of 20 diffusion fields, and these were then used for simulations with the different pacing protocols described in the next section. Multiple samples enabled the effect of length scale to be assessed independent of the specific configuration of a single sample relative to pacing sites. Each sample was then used to simulate the different pacing protocols specified below, with both *CRNnormal* and *CRNremodelled* variants.

To compare the effect of the smooth variations in diffusion coefficient provided by the GRF with abrupt changes, a further set of diffusion fields were generated. For each length scale, a copy was made of each of the 20 diffusion fields obtained by sampling the GRF. These copies were then further processed so that they contained only two values of diffusion coefficient, with an abrupt change between the two. In the fibrotic regions, the diffusion coefficient of $0.05 \text{ mm}^2\text{ms}^{-1}$ was retained, but elsewhere it was set to $0.2 \text{ mm}^2\text{ms}^{-1}$.

Within the 20 diffusion fields generated at each length scale, the average proportion of simulated fibrotic tissue (i.e., locations where the diffusion coefficient was $0.05 \text{ mm}^2\text{ms}^{-1}$, and the cell model was set to be inexcitable) was 18.7, 18.0, 19.1, and 17.0% at length scales of 1.25, 2.50, 5.0, and 10.0 mm, respectively. The size and configuration of these regions was different in each of the 20 samples. At a length scale of 10 mm, the proportion of simulated fibrotic tissue ranged between 4.9 and 25.1% across the 20 samples. With a length scale of 1.25 mm, which was a smaller length scale relative to the size of the simulated tissue, the range was 17.9–19.6%.

2.4. Pacing Protocols

2.4.1. S1S2 Pacing

Activation and recovery of normal and remodeled tissue were studied with regular pacing for three beats at a cycle length of 1,000 ms followed by a premature stimulus with a coupling interval of 400 ms. Stimuli were delivered with a current injection of -2000 pA for 1 ms in a 2.5×2.5 mm square region in the lower left hand corner.

2.4.2. Decremental Pacing

The response of the each sample of the heterogenous tissue to rapid decremental pacing was examined by pacing from a circular region in the centre of the tissue with a with radius of 6.25 mm. Ten pacing stimuli with a current of $-2,000 \text{ pA}$ and duration of

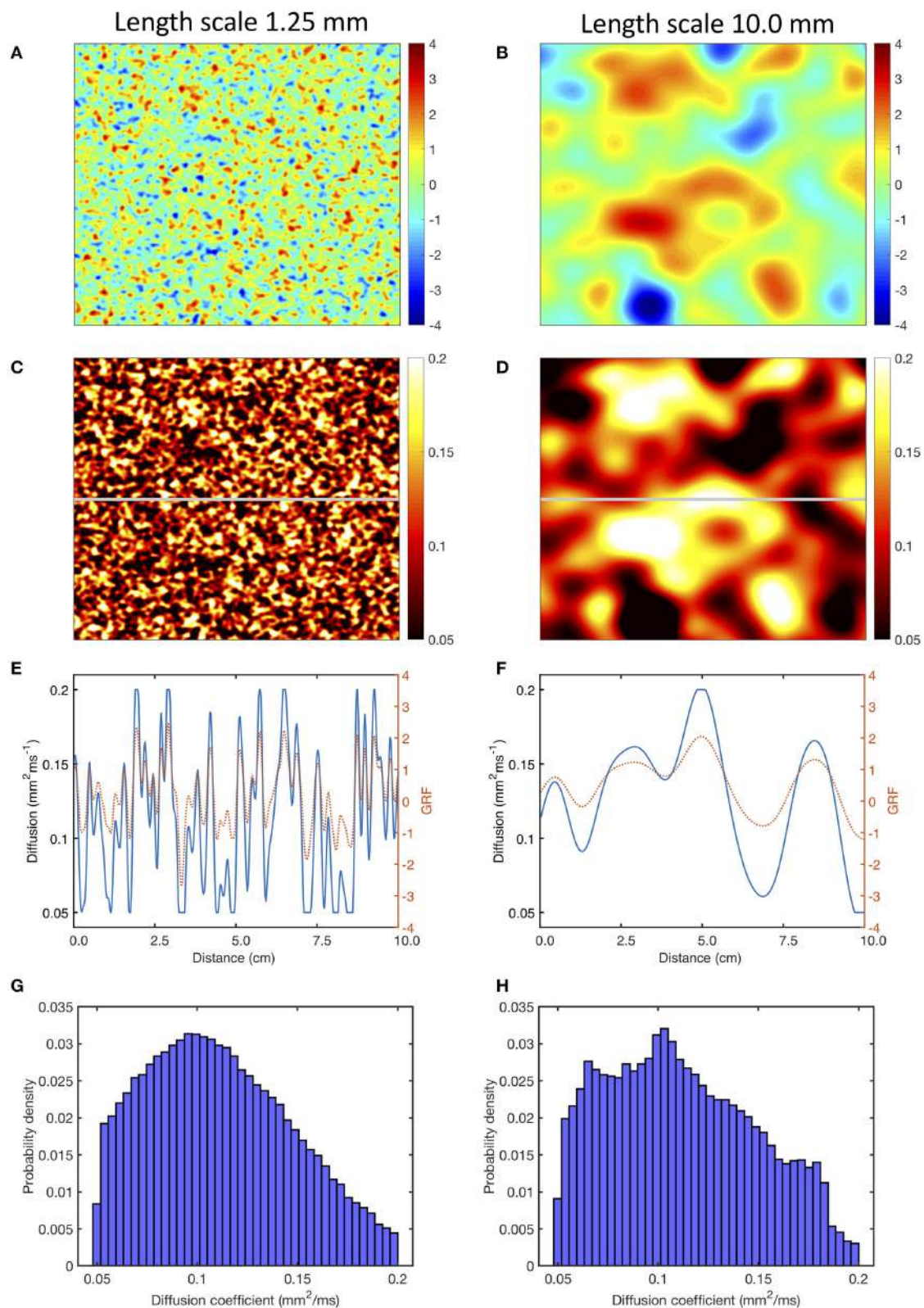


FIGURE 1 | Use of a Gaussian random field (GRF) to generate heterogeneous and smoothly varying diffusion. Panels (A, B) show samples of GRF with mean of 0 and variance of 1, with spatial length scales of 1.25 and 10 mm, respectively. Panels (C, D) corresponding diffusion fields, calculated as described in the main text, with a cut-off of 0.05 and $0.2 \text{ mm}^2 \text{ms}^{-1}$. Panels (E, F) show the profile of GRF (red, dotted) and diffusion coefficient (blue) across the middle row of each sample indicated by the horizontal gray line in (C, D). Lower panels (G, H) show the distribution of the diffusion fields shown in (C, D).

1 ms were delivered with an initial coupling interval of 450 ms for the *CRNnormal* variant and 300 ms for the *CRNremodelled* variant, decreasing by 25 ms with each successive stimulus to a final coupling interval of 250 ms for normal tissue and 150 ms for remodeled tissue (Zahid et al., 2016).

2.4.3. Dynamics of Re-entry

The dynamic behavior of re-entry in each sample of heterogeneous tissue was studied by imposing an Archimedean spiral on the model as an initial condition using the phase distribution method (Biktashev and Holden, 1998).

3. RESULTS

Examples of the effect of heterogeneous diffusion with a length scale of 1.25 mm and 10.0 mm on activation, repolarization, and APD are shown in **Figures 2B,C**, compared to results for simulated tissue with a uniform diffusion coefficient of $0.2 \text{ mm}^2 \text{ ms}^{-1}$ shown in **Figure 2A**. In each of these simulations, activation and recovery times were determined from excursions of the local action potential above a threshold of -73.0 mV , which corresponds approximately to the voltage at which repolarization is 90% complete in the CRN model. APD was the difference between repolarization time and activation time. Activation time, repolarization time, and APD were not calculated for regions of fibrotic tissue with diffusion set to $0.05 \text{ mm}^2 \text{ ms}^{-1}$, and these are indicated as white regions in **Figures 2B,C**.

With uniform diffusion, the activation isochrones were smooth, and recovery isochrones were modified by the boundary resulting in a slightly prolonged APD close to the stimulus site, and a slightly shortened APD on the top and right hand boundary (Cherry and Fenton, 2011). In this configuration, the conduction velocity was 0.507 mm ms^{-1} for the *CRNnormal* and 0.489 mm ms^{-1} *CRNremodelled* variants.

Heterogeneous diffusion with a length scale of 1.25 mm delayed activation by up to 120 ms, and recovery by up to 250 ms. As a result, conduction velocity was lower and APD was prolonged in regions of delayed recovery (**Figure 2B**). Heterogeneous diffusion with a length scale of 10 mm resulted in a similar delay of activation, but with smoother activation isochrones and a more tortuous activation sequence. Recovery was not prolonged to the same extent, and APD was only prolonged slightly compared to simulations with uniform diffusion (**Figure 2C**).

The overall effects on activation, recovery, and APD for all of the simulations are shown in **Figure 3**. In 14/160 simulations with smoothly varying diffusion, either S1 and S2 stimuli (9) or S2 stimuli only (5) were blocked by a region of simulated fibrosis close to the stimulus site at the lower left hand corner. Data from these simulations are not plotted. Activation delays relative to simulations with uniform diffusion were broadly similar for S1 and S2 stimuli, and for *CRNnormal* and *CRNremodelled* cell model variants. This finding reflects the reduced conduction velocity relative to uniform diffusion, resulting from the lower average diffusion in the heterogeneous simulations. The spread of both median and interquartile range activation delay increased somewhat with increasing length scale. This was attributed to

different configurations of low diffusion regions having a greater effect on activation pattern at larger length scales. **Figure 2C**, for example, shows activation that proceeds upwards along one edge before propagating from left to right.

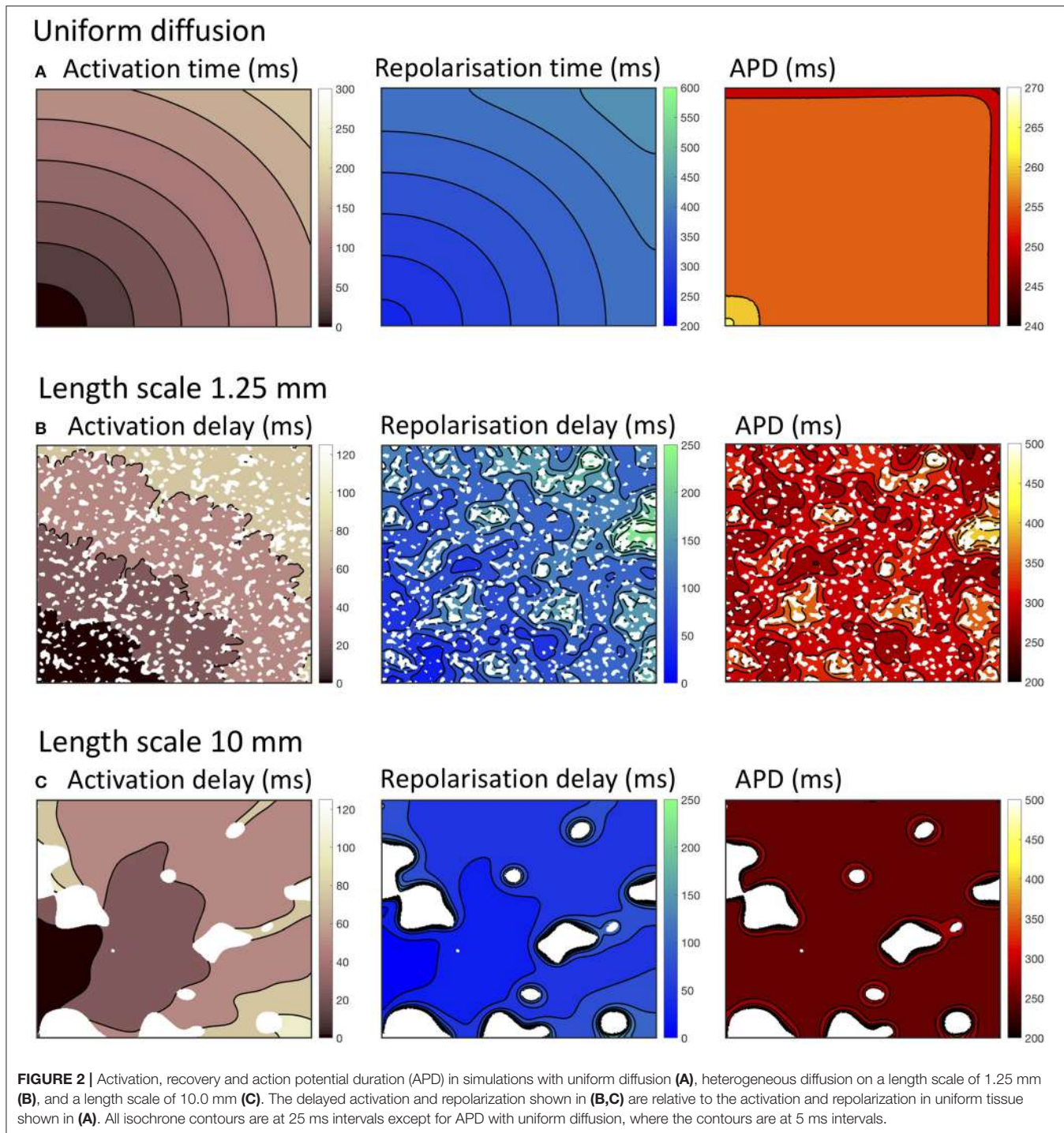
A further set of simulations was conducted using diffusion fields where the smoothly varying diffusion obtained from the GRF was replaced by an abrupt transition from a diffusion coefficient of $0.05 \text{ mm}^2 \text{ ms}^{-1}$ in fibrotic regions to a diffusion coefficient of $0.2 \text{ mm}^2 \text{ ms}^{-1}$ elsewhere. A modified version of **Figure 3** with these results superimposed is included as **Supplementary Figure A**. The delay in activation time compared to uniform diffusion was much smaller, but otherwise these simulations showed a broadly similar pattern of behavior.

Delay in recovery was greatest for S1 beats in simulations with the *CRNnormal* variant and a length scale between 1.25 and 5.0 mm. The interquartile range of recovery delay was also greatest for simulations with the *CRNnormal* variant and length scales of 2.5 and 5.0 mm. These delays produced the longest median APD for S1 beats in simulations with the *CRNnormal* variant and a length scale between 1.25 and 5.0 mm, and the greatest APD dispersion for length scales of 2.5 and 5.0 mm.

A more detailed view of the findings is given in **Figure 4**, where distributions of APD across all 20 simulations in each category are shown. For simulations with the *CRNnormal* variant, the distribution of APD became much narrower as length scale increased. The median and symmetry of APD distribution for the S2 beat was similar at all length scales, whereas the distribution for the S1 beat was positively skewed toward longer APD, especially with a length scale of 2.5 and 5.0 mm. In contrast, with the *CRNremodelled* variant, the distributions for both S1 and S2 beats became negatively skewed toward shorter APD at long length scales.

A possible explanation for these observations is explored in **Figure 5**, which shows examples of heterogeneous diffusion at length scale of 1.25 mm (**Figure 5A**) and 10 mm (**Figure 5B**), together with voltage time series recorded from locations with diffusion coefficients of 0.2, 0.1, and $0.05 \text{ mm}^2 \text{ ms}^{-1}$. In the model of fibrosis chosen for the present study, regions with a diffusion coefficient of $0.05 \text{ mm}^2 \text{ ms}^{-1}$ were deemed diffusively coupled but inexcitable. These regions could act as a current sink during activation, and as either a current source or a current sink during recovery. The magnitude of this effect was modulated by the length scale of heterogeneity. In **Figure 5A**, the voltage time series obtained from the inexcitable region with diffusion coefficient of $0.05 \text{ mm}^2 \text{ ms}^{-1}$ (shown in yellow) had a sharp upstroke, and an amplitude and recovery that were comparable in slope to the other time series shown. In contrast, the corresponding voltage time series shown for a length scale of 10 mm in **Figure 5B** had a much slower upstroke and downstroke, as well as a lower amplitude. For both length scales the shorter APD associated with the *CRNremodelled* variant produced a lower amplitude deflection in the inexcitable regions.

The interaction of local APD, heterogeneous diffusion, and the length scale of heterogeneities therefore appears to be complex, and this is emphasized by the range of action potential shapes seen in **Figure 5**. Heterogeneous diffusion acted to delay activation because inexcitable regions act as a current sink,



slowing the action potential upstroke, and the delay appeared to be broadly independent of length scale. However, during the action potential, the voltage of inexcitable regions increased from a resting value, by an amount that depended on both the length scale of heterogeneity and APD. A greater length scale combined with the shorter APD of the *CRNremodelled* variant resulted in a lower amplitude excursion. The lower amplitude excursion in the *CRNremodelled* variant in turn shortened the

recovery of neighboring excitable regions by acting as a current sink. At longer length scales, these neighboring regions were smaller in extent, which could explain in the skewed distribution toward shorter APD seen in the right hand panels of **Figure 4**, which became more marked at longer length scales. In contrast, the larger amplitude voltage excursion in inexcitable regions produced by the longer APD of the *CRNnormal* variant could act as a current source during recovery, acting to prolong APD, an

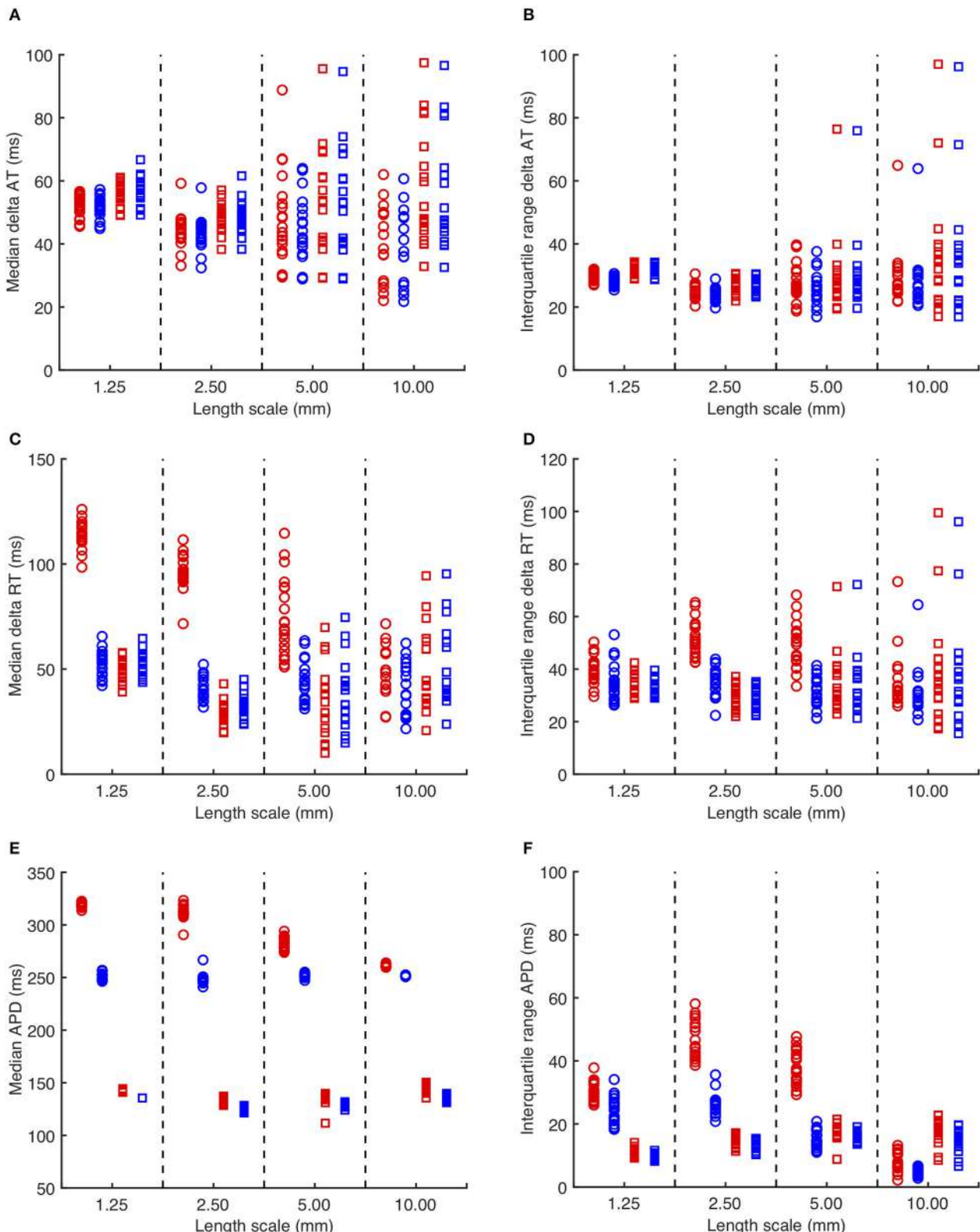


FIGURE 3 | (A) Median delay in activation time for each simulation with heterogeneous diffusion compared to uniform diffusion. Red symbols indicate activation following the third S1 stimulus, and blue symbols the S2 stimulus. Circles denote CRN_{normal}, and squares CRN_{remodelled}. **(B)** Corresponding interquartile range of activation time delay. **(C,D)** Median and interquartile range of recovery time delay. **(E,F)** median and interquartile range of APD.

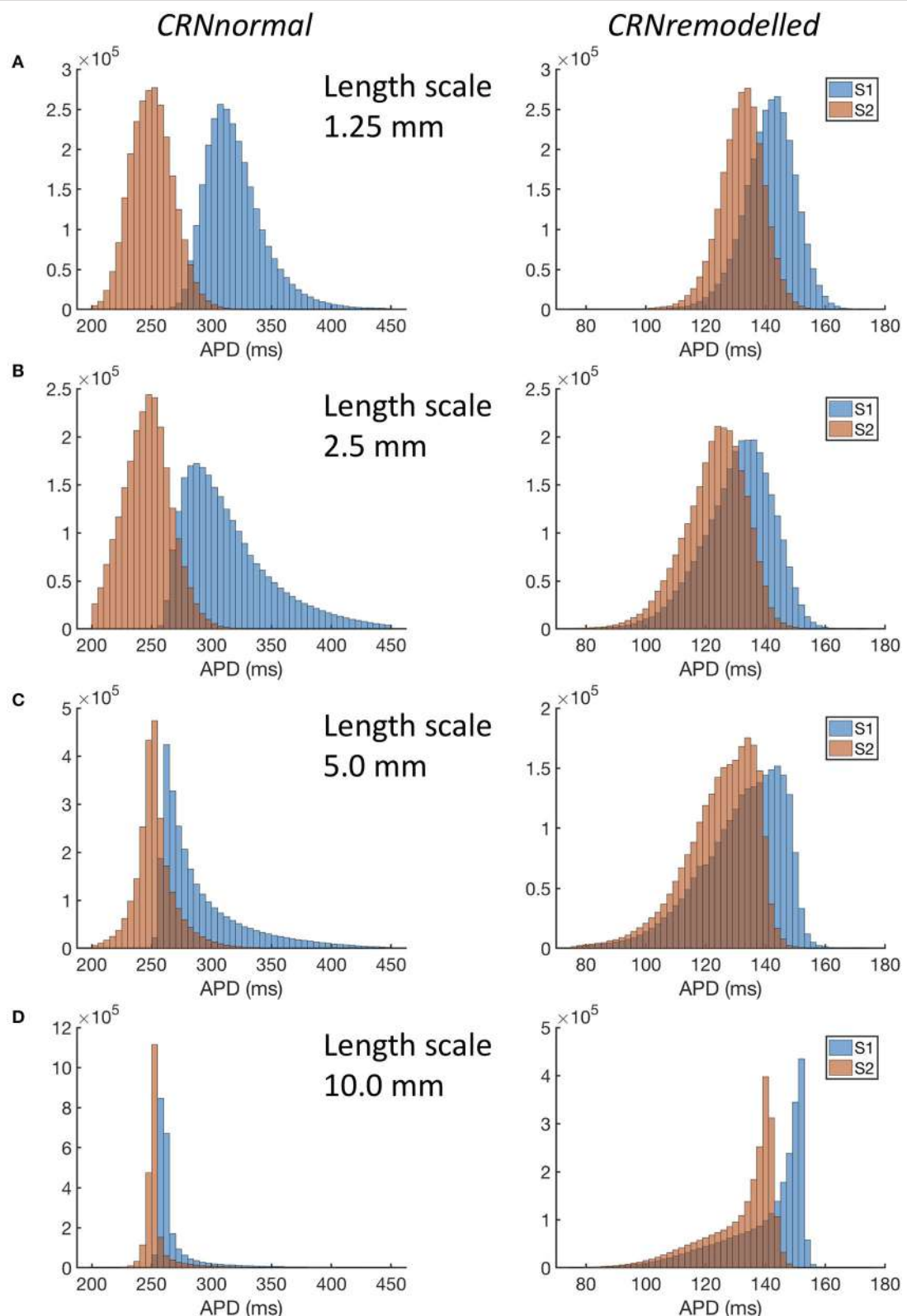
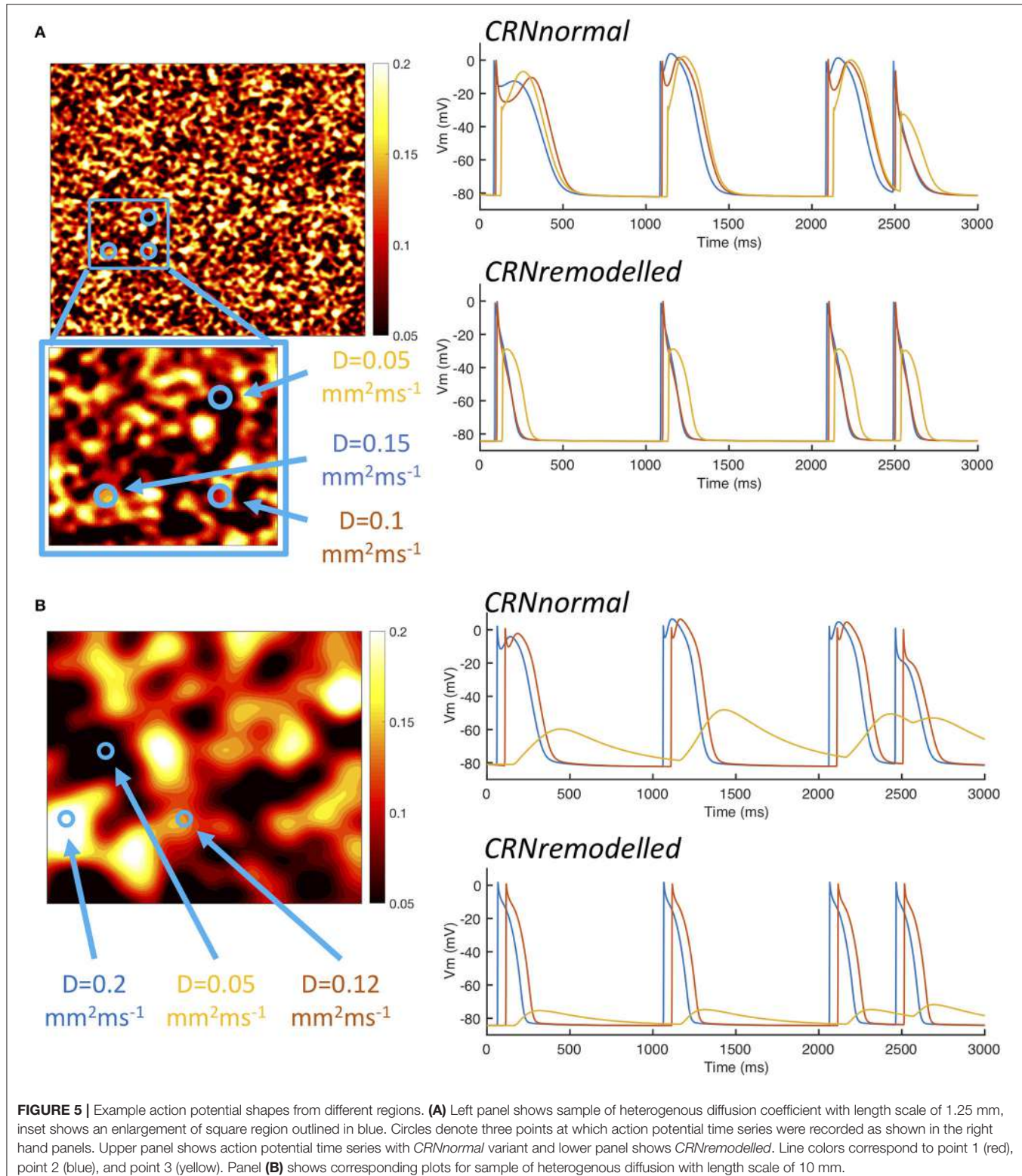
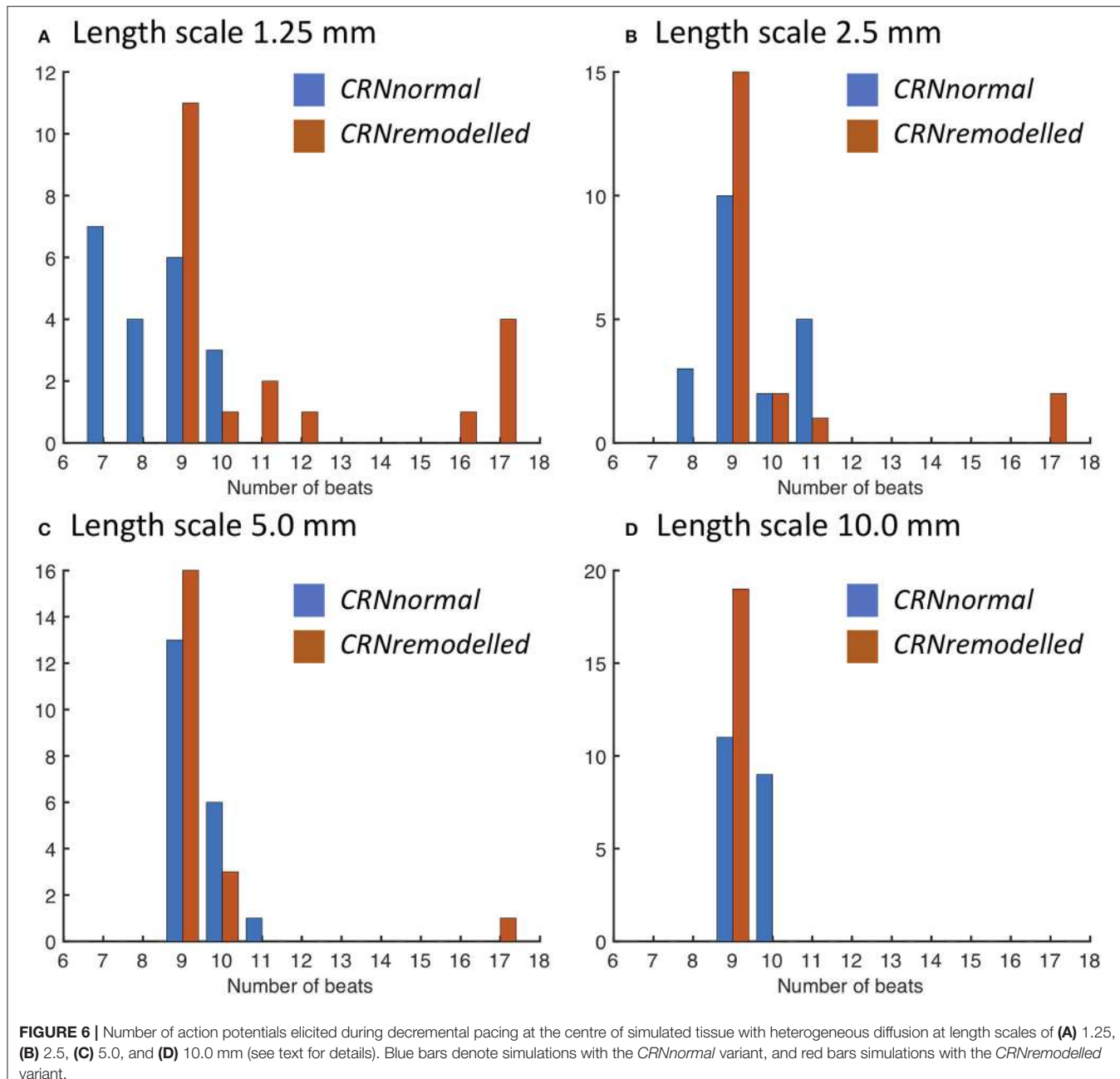


FIGURE 4 | Distribution of APD in simulations with *CRNnormal* (left) and *CRNremodelled* variants, at length scales of 1.25 mm through to 10.0 mm (A–D). Red bars denote APD following third S1 stimulus, and blue bars APD following S2 stimulus.



effect that would have had more impact on neighboring regions. This could explain the skew toward longer APD values seen in the left hand panels of **Figure 4**.

The response of this complex tissue model to decremental pacing with 9 stimuli is illustrated in **Figure 6**, which shows results from each group of 20 simulations. Additional action



potentials after the end of the pacing sequence, or sustained re-entry (deemed to be more than 15 beats), were observed in only a minority of the simulations. For simulations with the *CRNnormal* variant, some configurations of heterogeneity resulted in one or more of the pacing stimuli being blocked, and so the number of beats recorded was less than 9. However, this effect was not observed with the *CRNremodelled* variant, which could be attributed to the greater prolongation of APD in heterogeneous tissue with the *CRNnormal* variant described above. Overall, the prevalence of additional beats and re-entry was greater with the *CRNremodelled* variant, and with shorter length scales. Additional simulations were run using diffusion

fields where the smoothly varying diffusion obtained from the GRF was replaced by an abrupt transition, and the maximum number of beats elicited was 10. These data are included as **Supplementary Figure B**.

The precise configuration of regions with lower diffusion was important for eliciting re-entry, and this is illustrated in **Figure 7**. The first activation sequence in **Figure 7A** shows a lobe of delayed activation running down from the centre, and one side of this lobe provided the activation pathway for re-entry seen in **Figure 7B**. The narrow activation pathway running toward the bottom right from the centre in **Figure 7C** became blocked during decremental pacing, and provided a pathway for

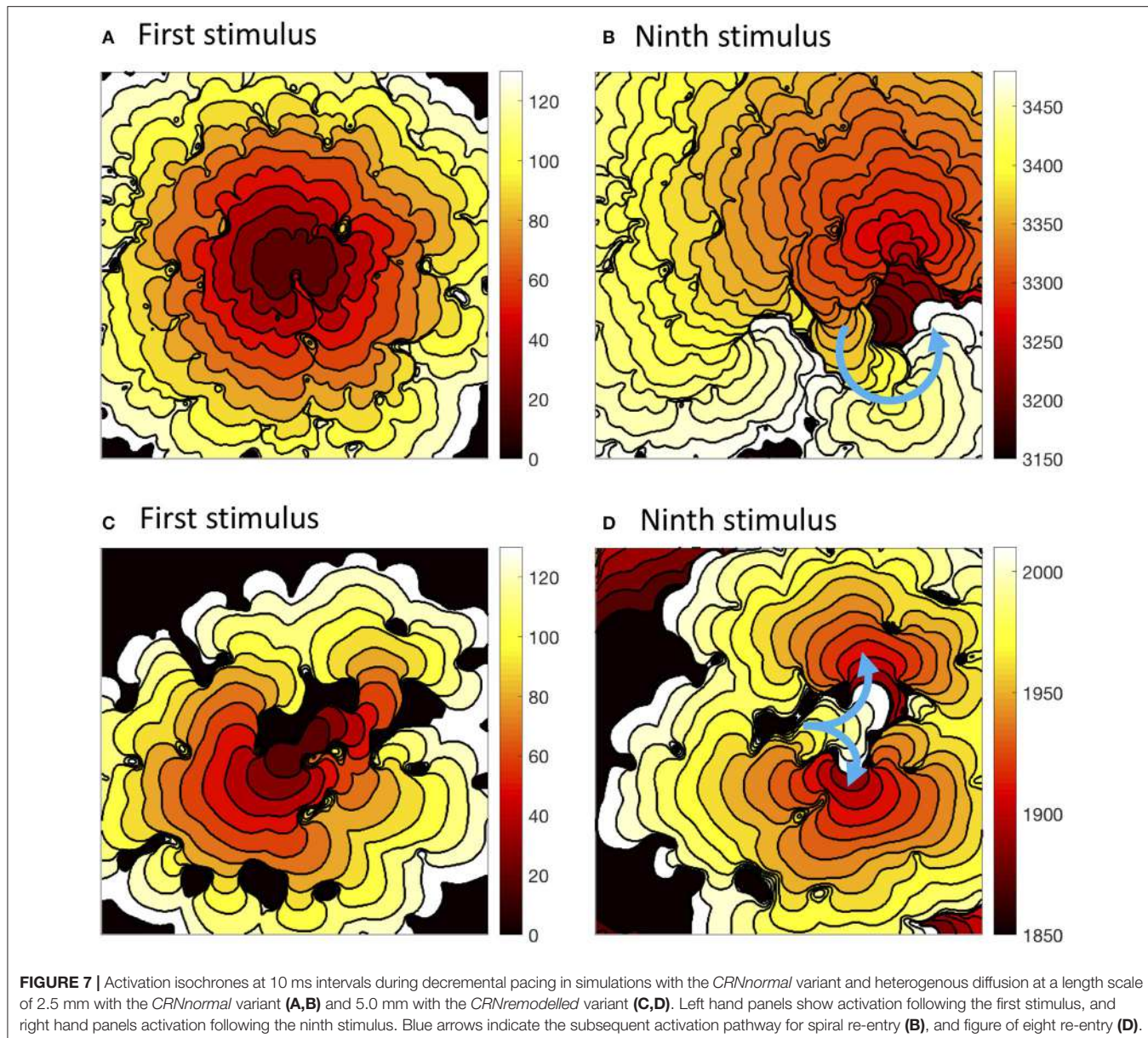


FIGURE 7 | Activation isochrones at 10 ms intervals during decremental pacing in simulations with the *CRNnormal* variant and heterogenous diffusion at a length scale of 2.5 mm with the *CRNnormal* variant **(A,B)** and 5.0 mm with the *CRNremodelled* variant **(C,D)**. Left hand panels show activation following the first stimulus, and right hand panels activation following the ninth stimulus. Blue arrows indicate the subsequent activation pathway for spiral re-entry **(B)**, and figure of eight re-entry **(D)**.

re-entry following the final stimulus in **Figure 7D**. Movies of these simulations are available as **Videos 1, 2**, and an additional example of sustained re-entry in a simulation with a length scale of 2.5 mm and the *CRNremodelled* model variant is illustrated in **Video 3**.

When a spiral wave was imposed as an initial condition, the configuration of heterogeneities again played a similar role. The number of beats resulting from spiral wave initiation are shown for each length scale in **Figure 8**. The majority of simulations with the *CRNremodelled* variant resulted in sustained re-entry of more than 2 beats, whereas simulations with the *CRNnormal* variant tended to result in non-sustained re-entry (see **Video 4**). The length scale of heterogeneity did not play a major role, although there was a slight tendency for less sustained re-entry at larger length scales.

The wavelength (minimum APD \times conduction velocity) is an important tissue property, and excitable tissue must be large enough to accommodate the wavelength in order to sustain re-entry. Heterogeneous diffusion modulates wavelength by slowing conduction velocity (delaying activation) and modifying APD, and so the behavior of re-entry was found to depend on the configuration of heterogeneities. **Figure 9** illustrates different wavelengths by showing activation isochrones during one cycle of re-entry in a simulation with the *CRNnormal* variant (**Figure 9A**), and one cycle in a simulation with the *CRNremodelled* variant. Both simulations had a length scale of 10.0 mm, and the heterogeneity in diffusion was identical. In both cases, re-entry propagates clockwise around an inexcitable region in the top left quadrant of the simulated tissue, and this is an example of re-entry “pinned” to a heterogeneity (Zahid et al.,

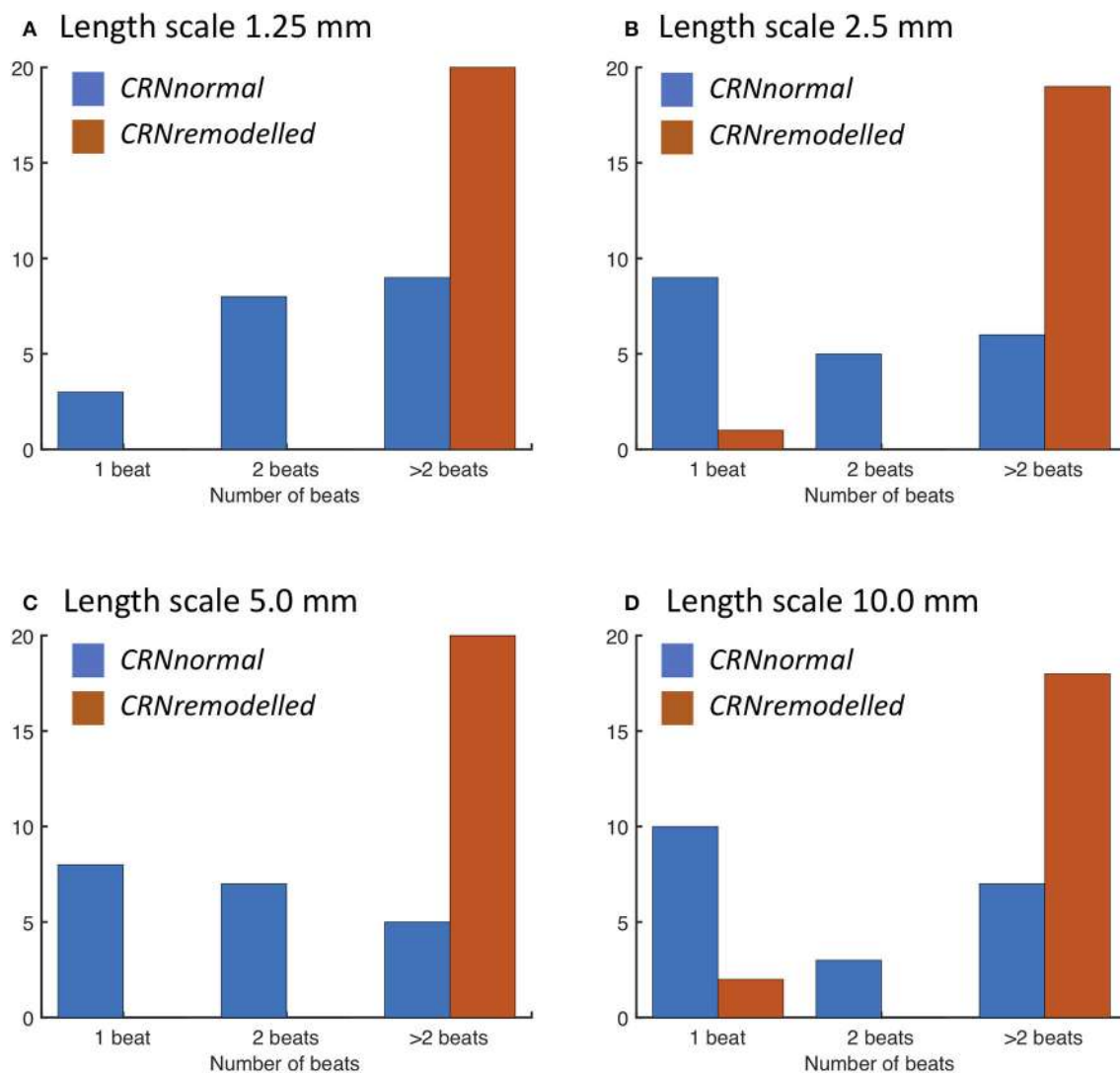


FIGURE 8 | Number of re-entry cycles following initiation with spiral wave with heterogeneous diffusion at length scales of **(A)** 1.25, **(B)** 2.5, **(C)** 5.0, and **(D)** 10.0 mm (see text for details). Blue bars denote simulations with the *CRNnormal* variant, and red bars simulations with the *CRNremodelled* variant.

2016; Deng et al., 2017). The activation pathway is illustrated by a blue arrow, and the wavelength is the distance between the wavefront (white regions), and the wave back (dark red). The short wavelength associated with the shorter APD in the *CRNremodelled* variant results in a compact re-entrant pathway (**Figure 9**), whereas the longer wavelength associated with the *CRNnormal* variant results in an extended re-entrant pathway (**Figure 9A**), and a much longer period of re-entry. Movies of these simulations are available as **Videos 5, 6**.

4. DISCUSSION AND CONCLUSIONS

It is well-known that electrical heterogeneity is an important factor for determining vulnerability to arrhythmias in cardiac tissue, and this has been investigated in experimental preparations (Allessie et al., 1976; Gokhale et al., 2017), in

intact atria (Haissaguerre et al., 2016), and in computer models (Xie et al., 2001; Vigmond et al., 2004; Clayton and Holden, 2005; McDowell et al., 2015; Kazbanov et al., 2016; Morgan et al., 2016). Fibrosis is believed to be associated with atrial fibrillation in the human heart, and regions of fibrosis can be focal or diffuse (McDowell et al., 2015). The present study investigated how heterogeneous diffusion varying on different length scales influenced electrical activation, electrical recovery, APD, vulnerability to re-entry, and dynamical behavior of re-entry in a model of human atrial tissue. Regions of concentrated fibrosis were represented by coupled but inexcitable tissue. The main findings of the study are as follows:

- It is possible to represent heterogeneity in cardiac tissue conductivity at different length scales using samples of a GRF.
- The length scale of heterogeneity did not markedly affect the median delay in activation time relative to simulations with

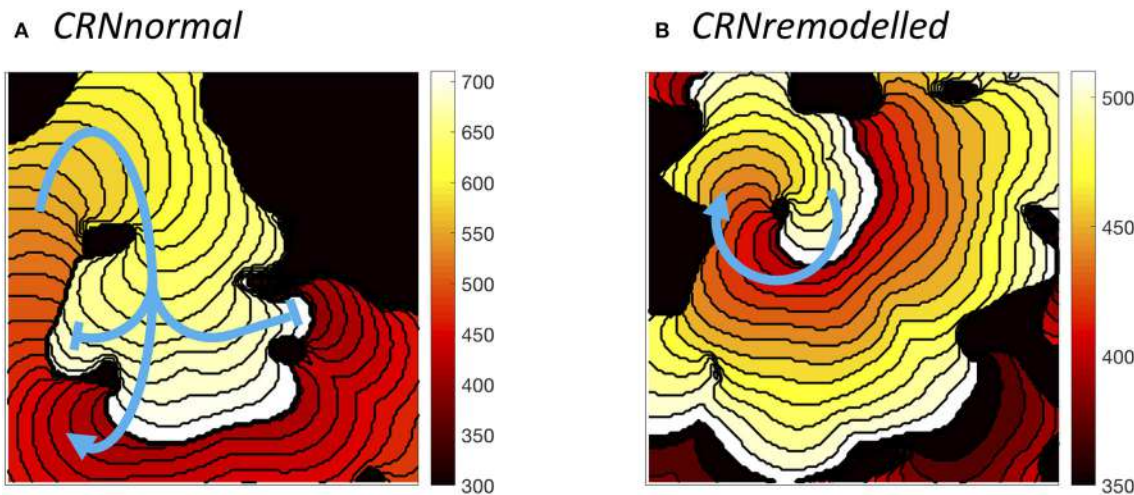


FIGURE 9 | Examples of sustained re-entry elicited by spiral wave initiation with the same pattern of heterogeneous diffusion at a length scale of 10 mm. **(A)** re-entry pathway with period of around 310 ms in simulated tissue with *CRNnormal* variant. **(B)** more compact re-entry pathway with much shorter period of around 130 ms in simulated tissue with *CRNremodelled* variant. Activation isochrones spaced at 10 ms intervals.

a uniform diffusion coefficient of $0.2 \text{ mm}^2\text{ms}^{-1}$, but larger length scales of 5.0 and 10.0 mm tended to produce a wider spread of activation delays.

- A delay in recovery relative to simulations with a uniform diffusion coefficient was found. This tended to be greater in simulations with heterogeneity on a smaller length scale, and greater with the *CRNnormal* variant rather than *CRNremodelled*.
- Distributions of APD tended to be positively skewed toward higher APD with the *CRNnormal* variant and negatively skewed toward lower APD with the *CRNremodelled* variant. This difference was attributed to inexcitable regions of simulated fibrosis acting as a current source during repolarization in simulations with the *CRNnormal* variant, and as a current sink in simulations with the *CRNremodelled* variant.
- With decremental pacing, simulations with smaller length scale heterogeneity and the *CRNremodelled* variant were most likely to result in sustained re-entry. However, the configuration of regions of simulated fibrosis also played an important role.
- With a spiral wave as an initial condition, simulations with smaller length scale heterogeneity and the *CRNremodelled* variant were also most likely to result in sustained re-entry

The interaction of heterogeneous diffusion, length scale, simulated fibrosis, and APD is complex and merits further investigation. The relationship of this study to previous work is discussed below.

4.1. Model of Fibrosis

The findings of the present study depend on the way that cellular electrophysiology and regions of fibrosis have been represented. In previous studies, regions of fibrosis have been represented in many different ways including inexcitable obstacles (Ten

Tusscher and Panfilov, 2007), coupled elements with a fixed resting potential (Majumder et al., 2012), and with detailed fibroblast models (Sachse et al., 2009; Ashihara et al., 2012; Morgan et al., 2016; Zahid et al., 2016). The extent of coupling between fibroblasts and myocytes in the heart remains controversial because detailed experimental study of fibroblasts embedded in native cardiac tissue is difficult (Kohl and Gourdie, 2014), but novel experimental techniques have shown that non-myocytes undergo voltage excursions close to the border of scar tissue (Quinn et al., 2016). Regions of fibrosis have often been represented as areas of reduced tissue conductivity or a lower diffusion coefficient in computational studies (Gonzales et al., 2014; McDowell et al., 2015; Zahid et al., 2016).

In the present study regions of diffuse fibrosis were represented by smoothly varying but reduced diffusion, and focal fibrosis was represented as inexcitable tissue with a fixed diffusion coefficient of $0.05 \text{ mm}^2\text{ms}^{-1}$. The slowed upstroke and lower amplitude of voltage excursion observed in simulated fibrosed regions compared to normal tissue was comparable to other studies that have used more detailed models of fibroblast electrophysiology (Ashihara et al., 2012; Zahid et al., 2016) as well as experimental observations (Kohl and Gourdie, 2014). Nevertheless, further work with more detailed fibroblast models would be a valuable extension to the present study.

An additional set of simulations was done to compare the effect of simulations that used smoothly varying diffusion fields with simulations where the diffusion coefficient was set to $0.05 \text{ mm}^2\text{ms}^{-1}$ in fibrosed regions and $0.2 \text{ mm}^2\text{ms}^{-1}$ elsewhere (see **Supplementary Figure A**). With the *CRNnormal* variant, simulations with abrupt changes in diffusion had a longer APD and greater APD dispersion, especially at shorter length scales, compared to simulations with smoothly varying diffusion. With both variants, the delay in activation time was much shorter compared to simulations with smoothly varying diffusion. The overall response to decremental pacing was also similar for

the *CRNnormal* variant, but it was not possible to elicit more than one additional beat with the *CRNremodelled* variant (see **Supplementary Figure B**). These findings indicate that there are important differences in the behavior of simulated tissue with abrupt and smooth changes in diffusion coefficient.

4.2. Effect of Length Scale

The length scale of heterogeneity was found to play a role in the prolongation and dispersion of APD, as well as in determining vulnerability to re-entry and rotor stability. A shorter length scale favored a longer APD, greater APD dispersion, and sustained re-entry. The configuration of simulated fibrotic regions was also important because a small isthmus of tissue often formed part of the activation pathway during re-entry as illustrated in **Figure 7**. Images of human left atria show fibrosis on a range of different length scales (McDowell et al., 2015), and the observations in the present study are consistent with result from patient specific models, where configuration of fibrotic regions was found to determine rotor location and stability (Zahid et al., 2016; Deng et al., 2017).

One of the aims of the present study was to investigate the effect of smooth changes in diffusion. Since diffusion was capped at 0.2 and $0.05 \text{ mm}^2\text{ms}^{-1}$, there were discontinuities at the boundary of these regions as illustrated in **Figures 1E,F**. While no obvious numerical problems were identified, a recent study indicates that numerical approximation of a continuum model may not capture the biophysics of heterogeneous tissue fully (Gokhale et al., 2017). The conduction velocity observed with a uniform diffusion coefficient (**Figure 2A**) in the present study was lower than those observed clinically (Weber et al., 2011), with an expected decrease in conduction velocity associated with fibrosis manifest as an activation delay (**Figure 3A**). For future work capping at a higher diffusion coefficient may be needed to better match conduction velocity, and this could potentially introduce numerical problems.

4.3. Effect of AF-Induced Remodeling

Persistent or permanent AF leads to changes in the electrophysiology of atrial myocytes, which act to shorten APD and hence wavelength, and these changes are consistent with the observed progression of AF from a short-lived paroxysmal arrhythmia to a permanent state (Nattel, 2002; Colman et al., 2013). In the present study, two variants of the CRN model were used, *CRNnormal* representing normal atrial myocytes, and *CRNremodelled* representing remodeled atrial myocytes (Wilhelms et al., 2012). The shorter APD of the *CRNremodelled* variant tended to modulate the effects of inexcitable fibrotic regions, and to increase vulnerability to re-entry. A further consequence of the shorter APD was the shorter wavelength of the *CRNremodelled* variant, which favored sustained re-entry in almost all simulations with the *CRNremodelled* variant and a spiral wave as an initial condition (**Figure 8**).

It is possible that more complex effects come into play in real cardiac tissue. Isolated atrial myocytes from canine right atrium show a wide range of action potential shapes (Feng et al., 1998), and the variability of APD measured in

human atrial cells indicate that a similar range of shape is likely in the human heart (Sánchez et al., 2014). A further consideration is changes in the Ca^{2+} handling mechanisms, which are affected by remodeling and also feed back into action potential shape (Grandi et al., 2011). These effects are likely to be important because in the present study, local source and sink effects acted to modify action potential shape in the absence of underlying cellular heterogeneity (**Figure 5A**).

4.4. Insights Into AF Mechanisms

The anatomy and configuration of fibrosis has recently been shown to be more important in determining rotor location than cellular electrophysiology (Deng et al., 2017). In the present study there were strong indications that the configuration of fibrosed regions, combined with length scale and electrical remodeling, acted together to determine APD dispersion and arrhythmogenic potential. Since configuration was found to be important, there was not a simple association between APD dispersion and vulnerability to re-entry. Extending this study to detailed anatomical representations of the human atria (Morgan et al., 2016; Varela et al., 2016) would begin to shed light on the underlying principles. While there is progress toward building patient specific models of human atria based on imaging of fibrosis as tools to guide therapy (Trayanova et al., 2014; Morgan et al., 2016), the present study indicates that there is more to learn about the way that electrical activation and recovery are modulated by heterogeneous diffusion. A better understanding of this complexity may in the future lead to improvements in our understanding of the factors that favor and sustain AF in some individuals and not others.

4.5. Study Limitations

This study used a very simple representation of fibrosis, as discussed above. There was no attempt to represent the detailed anatomy of the human atria, which would add a further layer of complexity to the findings. In particular, diffusion was assumed to be isotropic, although fibrosis is known to have a stronger effect on lateral connections between myocytes, acting to increase anisotropy (Kohl and Gourdie, 2014). In the human atria, the action potential acts to initiate and synchronize mechanical contraction, and fibrosis would be expected to alter the mechanical properties of atrial tissue. There was no attempt to include atrial mechanics in the present study, and heterogeneous contraction may add a further layer of complexity to the understanding of fibrosis and atrial arrhythmogenesis. Despite these limitations, this investigation has demonstrated a novel application of GRFs to represent heterogeneous diffusion at different length scales in cardiac tissue.

AUTHOR CONTRIBUTIONS

RC designed the study, wrote and implemented the computational model, ran the simulations, prepared the figures, and wrote the manuscript.

FUNDING

This work was funded by research grants EP/K037145/1 and EP/P010741/1 from the UK Engineering and Physical Sciences Research Council.

SUPPLEMENTARY MATERIAL

The Supplementary Material for this article can be found online at: <https://www.frontiersin.org/articles/10.3389/fphys.2018.01052/full#supplementary-material>

Supplementary Figure A | Image modified version of **Figure 3**, which includes results from simulations with abrupt transitions between normal and fibrotic regions.

Supplementary Figure B | Image modified version of **Figure 6**, which includes results from simulations with abrupt transitions between normal and fibrotic regions.

Video 1 | Video shows a movie of rapid pacing resulting in sustained re-entry in a simulation with a length scale of 2.5 mm and the *CRNnormal* model variant, corresponding to **Figures 7A,B**.

Video 2 | Video shows a simulation with a length scale of 5 mm and the *CRNremodelled* model variant, corresponding to **Figures 7C,D**.

Video 3 | Video shows a further example where rapid pacing results in sustained re-entry in a simulation with a length scale of 2.5 mm and the *CRNremodelled* model variant.

Video 4 | Video shows non-sustained re-entry following initiation with a spiral wave in a simulation with a length scale of 1.25 mm and the *CRNnormal* model variant.

Video 5 | Video shows sustained re-entry following initiation with a spiral wave in a simulation with a length scale of 10 mm and the *CRNnormal* model variant, corresponding to **Figure 9A**.

Video 6 | Video shows sustained re-entry following initiation with a spiral wave in a simulation with a length scale of 10 mm and the *CRNremodelled* model variant, corresponding to **Figure 9B**.

REFERENCES

- Akoum, N., Daccarett, M., McGann, C., Segerson, N., Vergara, G., Kuppahally, S., et al. (2012). Atrial fibrosis helps select the appropriate patient and strategy in catheter ablation of atrial fibrillation. *J. Cardiovasc. Electrophysiol.* 22, 16–22. doi: 10.1111/j.1540-8167.2010.01876.x
- Allessie, M. A., Bonke, F. I., and Schopmann, F. T. G. (1976). Circus movement in rabbit atrial muscle as a mechanism of tachycardia II. The role of nonuniform recovery of excitability in the occurrence of unidirectional block studied with multiple microelectrodes. *Circ. Res.* 39, 168–177. doi: 10.1161/01.RES.39.2.168
- Ashihara, T., Haraguchi, R., Nakazawa, K., Namba, T., Ikeda, T., Nakazawa, Y., et al. (2012). The role of fibroblasts in complex fractionated electrograms during persistent/permanent atrial fibrillation: implications for electrogram-based catheter ablation. *Circ. Res.* 110, 275–284. doi: 10.1161/CIRCRESAHA.111.255026
- Baptista, H., Mendes, J. M., MacNab, Y. C., Xavier, M., Caldas-De-Almeida, J., Lawson, A. B., et al. (2016). A Gaussian random field model for similarity-based smoothing in Bayesian disease mapping. *Stat. Methods Med. Res.* 25, 1166–1184. doi: 10.1177/0962280216660407
- Biktashev, V. N., and Holden, A. V. (1998). Reentrant waves and their elimination in a model of mammalian ventricular tissue. *Chaos* 8, 48–56. doi: 10.1063/1.166307
- Cherry, E. M., and Evans, S. J. (2008). Properties of two human atrial cell models in tissue: restitution, memory, propagation, and reentry. *J. Theor. Biol.* 254, 674–690. doi: 10.1016/j.jtbi.2008.06.030
- Cherry, E. M., and Fenton, F. H. (2011). Effects of boundaries and geometry on the spatial distribution of action potential duration in cardiac tissue. *J. Theor. Biol.* 285, 164–176. doi: 10.1016/j.jtbi.2011.06.039
- Clayton, R. H., Bernus, O., Cherry, E. M., Dierckx, H., Fenton, F. H., Mirabella, L., et al. (2011). Models of cardiac tissue electrophysiology: progress, challenges and open questions. *Prog. Biophys. Mol. Biol.* 104, 22–48. doi: 10.1016/j.pbiomolbio.2010.05.008
- Clayton, R. H., and Holden, A. (2005). Dispersion of cardiac action potential duration and the initiation of re-entry: a computational study. *Biomed. Eng.* 4:11. doi: 10.1186/1475-925X-4-11
- Colman, M. A., Aslanidi, O. V., Kharche, S., Boyett, M. R., Garratt, C. J., Hancock, J. C., et al. (2013). Pro-arrhythmogenic effects of atrial fibrillation induced electrical remodelling- insights from 3D virtual human atria. *J. Physiol.* 594, 4249–4272. doi: 10.1113/jphysiol.2013.254987
- Courtemanche, M., Ramirez, R. J., and Nattel, S. (1998). Ionic mechanisms underlying human atrial action potential properties: insights from a mathematical model. *Am. J. Physiol.* 275, H301–H321. doi: 10.1152/ajpheart.1998.275.1.H301
- Csepe, T. A., Zhao, J., Sul, L. V., Wang, Y., Hansen, B. J., Li, N., et al. (2017). Novel application of 3D contrast-enhanced CMR to define fibrotic structure of the human sinoatrial node *in vivo*. *Eur. Heart J. Cardiovasc. Imaging* 18, 862–869. doi: 10.1093/ehjci/jew304
- Deng, D., Murphy, M. J., Hakim, J. B., Franceschi, W. H., Zahid, S., Pasbakhshanloo, F., et al. (2017). Sensitivity of reentrant driver localization to electrophysiological parameter variability in image-based computational models of persistent atrial fibrillation sustained by a fibrotic substrate. *Chaos* 27:093932. doi: 10.1063/1.5003340
- Engelman, Z. J., Trew, M. L., and Smaill, B. H. (2010). Structural heterogeneity alone is a sufficient substrate for dynamic instability and altered restitution. *Circ. Arrhythmia Electrophysiol.* 3, 195–203. doi: 10.1161/CIRCEP.109.890459
- Feng, J., Yue, L., Wang, Z., and Nattel, S. (1998). Ionic mechanisms of regional action potential heterogeneity in the canine right atrium. *Circ. Res.* 83, 541–551. doi: 10.1161/01.RES.83.5.541
- Gokhale, T. A., Medvescek, E., and Henriquez, C. S. (2017). Modeling dynamics in diseased cardiac tissue: impact of model choice. *Chaos* 27:093909. doi: 10.1063/1.4999605
- Gonzales, M. J., Vincent, K. P., Rappel, W. J., Narayan, S. M., and McCulloch, A. D. (2014). Structural contributions to fibrillatory rotors in a patient-derived computational model of the atria. *Europace* 16, iv3–iv10. doi: 10.1093/europace/euu251
- Grandi, E., Pandit, S. V., Voigt, N., Workman, A. J., Dobrev, D., Jalife, J., et al. (2011). Human atrial action potential and Ca²⁺ model: sinus rhythm and chronic atrial fibrillation. *Circ. Res.* 109, 1055–1066. doi: 10.1161/CIRCRESAHA.111.253955
- Haissaguerre, M., Shah, A. J., Cochet, H., Hocini, M., Dubois, R., Efimov, I., et al. (2016). Intermittent drivers anchoring to structural heterogeneities as a major pathophysiological mechanism of human persistent atrial fibrillation. *J. Physiol.* 594, 2387–2398. doi: 10.1113/P270617
- Kazbanov, I. V., Ten Tusscher, K. H., and Panfilov, A. V. (2016). Effects of heterogeneous diffuse fibrosis on arrhythmia dynamics and mechanism. *Sci. Rep.* 6, 1–14. doi: 10.1038/srep20835
- Kohl, P., and Gourdie, R. G. (2014). Fibroblast-myocyte electrotonic coupling: Does it occur in native cardiac tissue? *J. Mol. Cell. Cardiol.* 70, 37–46. doi: 10.1016/j.yjmcc.2013.12.024
- Kroese, D. P., and Botev, Z. I. (2015). *Spatial Process Simulation*. Cham: Springer International Publishing.
- Majumder, R., Nayak, A. R., and Pandit, R. (2012). Nonequilibrium arrhythmic states and transitions in a mathematical model for diffuse fibrosis in human cardiac tissue. *PLoS ONE* 7:e45040. doi: 10.1371/journal.pone.0045040
- Marrouche, N. F., Wilber, D., Hindricks, G., Jais, P., Akoum, N., Marchlinski, F., et al. (2014). Association of atrial tissue fibrosis identified by delayed enhancement MRI and atrial fibrillation catheter ablation: The DECAAF study. *JAMA* 311, 498–506. doi: 10.1001/jama.2014.3

- McDowell, K. S., Arevalo, H. J., Maleckar, M. M., and Trayanova, N. A. (2011). Susceptibility to arrhythmia in the infarcted heart depends on myofibroblast density. *Biophys. J.* 101, 1307–1315. doi: 10.1016/j.bpj.2011.08.009
- McDowell, K. S., Zahid, S., Vadakkumpadan, F., Blauer, J., MacLeod, R. S., and Trayanova, N. A. (2015). Virtual electrophysiological study of atrial fibrillation in fibrotic remodeling. *PLoS ONE* 10:e0117110. doi: 10.1371/journal.pone.0117110
- Meerschaert, M. M., Dogan, M., Van Dam, R. L., Hyndman, D. W., and Benson, D. A. (2013). Hydraulic conductivity fields: Gaussian or not? *Water Resour. Res.* 49, 4730–4737. doi: 10.1002/wrcr.20376
- Morgan, R., Colman, M. A., Chubb, H., Seemann, G., and Aslanidi, O. V. (2016). Slow conduction in the border zones of patchy fibrosis stabilizes the drivers for atrial fibrillation: insights from multi-scale human atrial modeling. *Front. Physiol.* 7:474. doi: 10.3389/fphys.2016.00474
- Nattel, S. (2002). New ideas about atrial fibrillation 50 years on. *Nature* 415, 219–226. doi: 10.1038/415219a
- Nguyen, T. P., Qu, Z., and Weiss, J. N. (2014). Cardiac fibrosis and arrhythmogenesis: The road to repair is paved with perils. *J. Mol. Cell. Cardiol.* 70, 83–91. doi: 10.1016/j.yjmcc.2013.10.018
- Qu, Z. (1999). An advanced algorithm for solving partial differential equation in cardiac conduction. *Biomed. Eng. IEEE* 46, 1166–1168. doi: 10.1109/10.784149
- Quinn, T. A., Camelliti, P., Rog-Zielinska, E. A., Siedlecka, U., Poggiali, T., O'Toole, E. T., et al. (2016). Electrotomic coupling of excitable and nonexcitable cells in the heart revealed by optogenetics. *Proc. Natl. Acad. Sci. U.S.A.* 113, 14852–14857. doi: 10.1073/pnas.1611184114
- Rush, S. and Larsen, H. (1978). A practical algorithm for solving dynamic membrane equations. *IEEE Trans. Biomed. Eng.* 25, 389–392. doi: 10.1109/TBME.1978.326270
- Sachse, F. B., Moreno, A. P., Seemann, G., and Abildskov, J. A. (2009). A model of electrical conduction in cardiac tissue including fibroblasts. *Ann. Biomed. Eng.* 37, 874–889. doi: 10.1007/s10439-009-9667-4
- Sánchez, C., Bueno-Orovio, A., Wettwer, E., Loose, S., Simon, J., Ravens, U., et al. (2014). Inter-subject variability in human atrial action potential in sinus rhythm versus chronic atrial fibrillation. *PLoS ONE* 9:e105897. doi: 10.1371/journal.pone.0105897
- Sohns, C., Lemes, C., Metzner, A., Fink, T., Chmelevsky, M., Maurer, T., et al. (2017). First-in-man analysis of the relationship between electrical rotors from noninvasive panoramic mapping and atrial fibrosis from magnetic resonance imaging in patients with persistent atrial fibrillation. *Circ. Arrhythmia Electrophysiol.* 10, 1–12. doi: 10.1161/CIRCEP.116.004419
- Sridhar, S., Vandersickel, N., and Panfilov, A. V. (2017). Effect of myocyte-fibroblast coupling on the onset of pathological dynamics in a model of ventricular tissue. *Sci. Rep.* 7:40985. doi: 10.1038/srep40985
- Tanaka, K., Zlochiver, S., Vikstrom, K. L., Yamazaki, M., Moreno, J., Klos, M., et al. (2007). Spatial distribution of fibrosis governs fibrillation wave dynamics in the posterior left atrium during heart failure. *Circ. Res.* 101, 839–847. doi: 10.1161/CIRCRESAHA.107.153858
- Ten Tusscher, K. H., and Panfilov, A. V. (2007). Influence of diffuse fibrosis on wave propagation in human ventricular tissue. *Europace* 9(Suppl. 6), 38–45. doi: 10.1093/europace/eum206
- Trayanova, N. A., Boyle, P. M., Arevalo, H. J., and Zahid, S. (2014). Exploring susceptibility to atrial and ventricular arrhythmias resulting from remodeling of the passive electrical properties in the heart: a simulation approach. *Front. Physiol.* 5:435. doi: 10.3389/fphys.2014.00435
- Varela, M., Colman, M. A., Hancox, J. C., and Aslanidi, O. V. (2016). Atrial heterogeneity generates re-entrant substrate during atrial fibrillation and anti-arrhythmic drug action: mechanistic insights from canine atrial models. *PLoS Comput. Biol.* 12:e1005245. doi: 10.1371/journal.pcbi.1005245
- Vigmond, E., Tsoi, V., Kuo, S., Arevalo, H., Kneller, J., Nattel, S., et al. (2004). The effect of vagally induced dispersion of action potential duration on atrial arrhythmogenesis. *Heart Rhythm* 1, 334–344. doi: 10.1016/j.hrthm.2004.03.077
- Weber, F. M., Luik, A., Schilling, C., Seemann, G., Krueger, M. W., Lorenz, C., et al. (2011). Conduction velocity restitution of the human atrium—An efficient measurement protocol for clinical electrophysiological studies. *IEEE Trans. Biomed. Eng.* 58, 2648–2655. doi: 10.1109/TBME.2011.2160453
- Wilhelms, M., Hettmann, H., Maleckar, M. M., Koivumäki, J. T., Dössel, O., and Seemann, G. (2012). Benchmarking electrophysiological models of human atrial myocytes. *Front. Physiol.* 3:487. doi: 10.3389/fphys.2012.00487
- Workman, A. J., Kane, K. A., and Rankin, A. C. (2001). The contribution of ionic currents to changes in refractoriness of human atrial myocytes associated with chronic atrial fibrillation. *Cardiovasc. Res.* 52, 226–235. doi: 10.1016/S0008-6363(01)00380-7
- Xie, F. G., Qu, Z., Garfinkel, A., and Weiss, J. N. (2001). Electrophysiological heterogeneity and stability of reentry in simulated cardiac tissue. *Am. J. Physiol.* 280, H535–H545. doi: 10.1152/ajpheart.2001.280.2.H535
- Zahid, S., Cochet, H., Boyle, P. M., Schwarz, E. L., Whyte, K. N., Vigmond, E. J., et al. (2016). Patient-derived models link re-entrant driver localization in atrial fibrillation to fibrosis spatial pattern. *Cardiovasc. Res.* 110, 443–454. doi: 10.1093/cvr/cvw073
- Zhao, J., Hansen, B. J., Wang, Y., Csepe, T. A., Sul, L. V., Tang, A., et al. (2017). Three-dimensional integrated functional, structural, and computational mapping to define the structural “fingerprints” of heart-specific atrial fibrillation drivers in human heart *ex vivo*. *J. Am. Heart Assoc.* 6:e005922. doi: 10.1161/JAHA.117.005922

Conflict of Interest Statement: The author declares that the research was conducted in the absence of any commercial or financial relationships that could be construed as a potential conflict of interest.

Copyright © 2018 Clayton. This is an open-access article distributed under the terms of the Creative Commons Attribution License (CC BY). The use, distribution or reproduction in other forums is permitted, provided the original author(s) and the copyright owner(s) are credited and that the original publication in this journal is cited, in accordance with accepted academic practice. No use, distribution or reproduction is permitted which does not comply with these terms.



The Subcellular Distribution of Ryanodine Receptors and L-Type Ca^{2+} Channels Modulates Ca^{2+} -Transient Properties and Spontaneous Ca^{2+} -Release Events in Atrial Cardiomyocytes

OPEN ACCESS

Edited by:

Edward Joseph Vigmond,
Université de Bordeaux, France

Reviewed by:

Yael Yaniv,

Technion – Israel Institute of
Technology, Israel
Stefano Severi,
Università degli Studi di Bologna, Italy

*Correspondence:

Jordi Heijman
jordi.heijman@maastrichtuniversity.nl

[†]These authors have contributed
equally to this work

‡Present Address:

Bart van Sloun,
Maastricht Centre for Systems
Biology, Maastricht University,
Maastricht, Netherlands

Specialty section:

This article was submitted to
Computational Physiology and
Medicine,
a section of the journal
Frontiers in Physiology

Received: 06 March 2018

Accepted: 23 July 2018

Published: 14 August 2018

Citation:

Sutanto H, van Sloun B, Schönleitner P, van Zandvoort MAMJ, Antoons G and Heijman J (2018) The Subcellular Distribution of Ryanodine Receptors and L-Type Ca^{2+} Channels Modulates Ca^{2+} -Transient Properties and Spontaneous Ca^{2+} -Release Events in Atrial Cardiomyocytes. *Front. Physiol.* 9:1108.
doi: 10.3389/fphys.2018.01108

Henry Sutanto ^{1†}, Bart van Sloun ^{1†‡}, Patrick Schönleitner ², Marc A. M. J. van Zandvoort ³,
Gudrun Antoons ² and Jordi Heijman ^{1*}

¹ Department of Cardiology, CARIM School for Cardiovascular Diseases, Maastricht University, Maastricht, Netherlands

² Department of Physiology, CARIM School for Cardiovascular Diseases, Maastricht University, Maastricht, Netherlands

³ Department of Genetics and Cell Biology, Maastricht University, Maastricht, Netherlands

Spontaneous Ca^{2+} -release events (SCaEs) from the sarcoplasmic reticulum play crucial roles in the initiation of cardiac arrhythmias by promoting triggered activity. However, the subcellular determinants of these ScaEs remain incompletely understood. Structural differences between atrial and ventricular cardiomyocytes, e.g., regarding the density of T-tubular membrane invaginations, may influence cardiomyocyte Ca^{2+} -handling and the distribution of cardiac ryanodine receptors (RyR2) has recently been shown to undergo remodeling in atrial fibrillation. These data suggest that the subcellular distribution of Ca^{2+} -handling proteins influences proarrhythmic Ca^{2+} -handling abnormalities. Here, we employ computational modeling to provide an in-depth analysis of the impact of variations in subcellular RyR2 and L-type Ca^{2+} -channel distributions on Ca^{2+} -transient properties and ScaEs in a human atrial cardiomyocyte model. We incorporate experimentally observed RyR2 expression patterns and various configurations of axial tubules in a previously published model of the human atrial cardiomyocyte. We identify an increased ScaE incidence for larger heterogeneity in RyR2 expression, in which ScaEs preferentially arise from regions of high local RyR2 expression. Furthermore, we show that the propagation of Ca^{2+} waves is modulated by the distance between RyR2 bands, as well as the presence of experimentally observed RyR2 clusters between bands near the lateral membranes. We also show that incorporation of axial tubules in various amounts and locations reduces Ca^{2+} -transient time to peak. Furthermore, selective hyperphosphorylation of RyR2 around axial tubules increases the number of spontaneous waves. Finally, we present a novel model of the human atrial cardiomyocyte with physiological RyR2 and L-type Ca^{2+} -channel distributions that reproduces experimentally observed Ca^{2+} -handling properties. Taken together, these results significantly enhance our understanding of the structure-function relationship in cardiomyocytes, identifying that RyR2 and L-type Ca^{2+} -channel distributions have a major impact on systolic Ca^{2+} transients and ScaEs.

Keywords: calcium, sarcoplasmic reticulum, ryanodine receptor, spontaneous calcium releases, atrial fibrillation, subcellular distribution, computational modeling

INTRODUCTION

Despite the significant advances in the treatment of cardiovascular diseases during the past 50 years, the frequency of cardiac arrhythmias, particularly atrial fibrillation (AF), is projected to increase, placing a significant burden on modern healthcare systems (Chugh et al., 2014; Roth et al., 2015; Morillo et al., 2017). Ca^{2+} -handling abnormalities play a key role in ectopic activity and reentry, the two major arrhythmogenic mechanisms underlying AF (Heijman et al., 2014, 2016a; Landstrom et al., 2017). Dysfunctional ryanodine receptor type-2 (RyR2) channels, and/or SR Ca^{2+} overload can promote the occurrence of spontaneous sarcoplasmic reticulum (SR) Ca^{2+} -release events (SCaEs) (Heijman et al., 2016a), which transiently increase the cytosolic Ca^{2+} concentration, activating the $\text{Na}^+/\text{Ca}^{2+}$ -exchanger type-1 (NCX1), resulting in a depolarizing transient-inward current and promoting delayed after depolarizations (DADs) and triggered activity. Although potential proarrhythmic effects of changes in RyR2 expression and phosphorylation have been extensively discussed (Dobrev and Wehrens, 2014; Houser, 2014), these studies have generally employed tissue homogenates, ignoring the subcellular structure of Ca^{2+} -handling proteins. However, there is increasing evidence that differences in subcellular structure critically influence cardiomyocyte Ca^{2+} -handling. For example, there are important structural differences between atrial and ventricular cardiomyocytes that affect Ca^{2+} -handling, including a relative paucity of transverse T-tubular structures in atrial cardiomyocytes, resulting in a centripetal Ca^{2+} wave propagating from RyR2 opposing L-type Ca^{2+} channels (LTCC) at the sarcolemma to RyR2 in the cell center (Arora et al., 2017). On the other hand, there is increasing evidence for a role of axial tubules in atrial cardiomyocyte Ca^{2+} -handling (McNutt and Fawcett, 1969; Kirk et al., 2003; Dibb et al., 2013; Yue et al., 2017). Axial tubules promote a faster Ca^{2+} release from the SR in the center of the cell, which is partly mediated by coupling of LTCC to hyperphosphorylated RyR2 surrounding axial tubules (Brandenburg et al., 2016). Moreover, this axial tubular system undergoes extensive remodeling during cardiovascular disease, e.g., proliferating in the presence of atrial hypertrophy (Brandenburg et al., 2016) or disappearing in mice with atrial-specific knock-out of NCX1 (Yue et al., 2017). AF-related remodeling of the RyR2 distribution has also been reported, with RyR2 cluster fragmentation and redistribution in sheep with AF, which was associated with increased Ca^{2+} -spark frequency (Macquaide et al., 2015). However, the exact impact of the subcellular distribution of RyR2 and LTCC on cardiomyocyte Ca^{2+} -handling remains largely unknown. It is currently experimentally challenging to study both (sub)cellular structure and functional Ca^{2+} -handling in human atrial cardiomyocytes, as the former usually requires fixation of the cardiomyocyte

Abbreviations: AF, atrial fibrillation; Ca^{2+} , calcium; CICR, Ca^{2+} -induced Ca^{2+} -release; CRU, Ca^{2+} Release Unit; DAD, delayed after depolarization; IgG1, Immunoglobulin-G1; K^+ , potassium; LTCC, L-type Ca^{2+} channel; NA, Numerical Aperture; Na^+ , sodium; NCX1, $\text{Na}^+/\text{Ca}^{2+}$ exchanger type-1; RyR2, ryanodine receptor type-2; SCAE(s), spontaneous Ca^{2+} -release event(s); SR, sarcoplasmic reticulum; SERCA2a, SR Ca^{2+} -ATPase type-2a.

for antibody staining. The perfect control and observability provided by computational modeling may help to overcome this challenge (Heijman et al., 2016b).

A number of ventricular cardiomyocyte models have been developed that are able to simulate local Ca^{2+} -handling and SCAEs (Colman et al., 2017; Walker et al., 2017). Models of atrial subcellular Ca^{2+} -handling, on the other hand, are relatively scarce (Heijman et al., 2016b). We recently developed a human atrial cardiomyocyte model with stochastic gating of RyR2 channels and both transverse and longitudinal compartmentation of Ca^{2+} -handling. Our model has a simple cell-type specific subcellular structure with LTCC only present on the lateral membranes, reflecting the relative paucity of T-tubules in isolated atrial cardiomyocytes (Voigt et al., 2014). However, all currently available atrial and ventricular cardiomyocyte models assume a homogeneous distribution of Ca^{2+} -handling proteins. Here, we hypothesized that changes in the subcellular distribution of RyR2 and LTCC may promote proarrhythmic SCAEs. We employed both confocal microscopy and computational modeling to study for the first time the impact of the subcellular distribution of RyR2 and LTCC on Ca^{2+} -handling in atrial cardiomyocytes.

MATERIALS AND METHODS

A detailed overview of the experimental and computational methods can be found in the online Data Supplement. A brief summary is given below.

Animal Model, Cardiomyocyte Isolation, and Confocal Imaging

This investigation conformed with the Guide for the Care and Use of Laboratory Animals Published by the US National Institutes of Health (NIH Publications No. 85-23, revised 1996). All animal handling conformed with directive 2010/63/EU and experimental protocols were approved by the local ethical committee (DEC2014-112). New Zealand white rabbits (2.5–3.5 kg) were anesthetized and hearts were rapidly removed, excised, washed, perfused and cut into smaller pieces, as previously described (Greiser et al., 2014). Atrial cardiomyocytes were seeded on laminin coated coverslips. RyR2s were labeled with primary (mouse monoclonal (C3-33), IgG1, Sigma-Aldrich®, MO, 1:50) and secondary (Alexa® 488, goat anti-mouse, Abcam, UK, 1:100) antibodies (Dyba et al., 2003; Muller et al., 2012). The RyR2-stained atrial cardiomyocytes were imaged with a Leica TCS SP8 confocal microscope using a 63x objective (NA 1.40, oil immersion). The RyR2-Alexa® 488 antibody complex was detected at 420–520 nm under 488 nm laser illumination. Z-stacks were taken with a step size of 0.26 μm and an xy-resolution of 0.07 μm .

Image Processing

Image processing was employed to enable simulation with the experimental data (**Supplemental Figure 1**). The raw z-stacks were deconvolved using Huygens Professional (SVI,

Netherlands). A single slice from the z-stack was selected and rotated to obtain a horizontal alignment of the RyR2. The image was thresholded and overlaid with a grid of $\sim 1 \mu\text{m}^2$ units, in which the mean pixel intensity was calculated for every square of the grid as an indirect readout of local RyR2 density. The edges of the RyR2 expression matrix were detected and stretched to accommodate the rectangular dimensions of the virtual cardiomyocyte ($100 \times 18 \mu\text{m}$). The resulting RyR2 distribution matrix was implemented in the computational model and employed for simulation.

Computational Modeling

Simulations were based on a previously published model of the human atrial cardiomyocyte in which local Ca^{2+} -handling was simulated by dividing the virtual cardiomyocyte into 50 segments, each containing 18 subcellular Ca^{2+} domains located between two membrane domains (Voigt et al., 2014; Heijman et al., 2016b). The RyR2 expression in the published model was identical in every unit. We further optimized the 50-segment model with uniform RyR2 distribution based on experimental values (Tanaka et al., 2001; Woo et al., 2002; Kirk et al., 2003; Loughrey et al., 2004; Voigt et al., 2012, 2014; Greiser et al., 2014) of Ca^{2+} -handling properties and SCaE properties reported in previous publications (Supplemental Figures 2, 3). In the present work, the model was extended to enable simulations with heterogeneous RyR2 distributions. Heterogeneity in RyR2 distribution across all 50×18 units was incorporated by drawing a random number from a Gaussian distribution with mean 1.0 and standard deviation σ for each unit and subsequently scaling these numbers to achieve the desired total RyR2 density. We also developed a model with a higher longitudinal resolution (100 segments), enabling simulation of the experimentally observed banded expression of RyR2. Axial tubules were simulated in the 100-segment model by including LTCC in axial-tubule-associated Ca^{2+} domains. Parameters of the 100-segment model with uniform RyR2 expression were adjusted to achieve similar Ca^{2+} -handling properties as the 50-segment model (Supplemental Figures 2, 3) and heterogeneous RyR2 expression patterns were generated analogous to the 50-segment model. The values of the optimized parameters for both model versions are given in Supplemental Table 1. All results in the 100-segment model are provided following pacing for 250 beats at 0.5 Hz to achieve a quasi-steady state (Supplemental Figure 4). The source code for the model can be downloaded from the authors' website (<http://www.jordiheijman.net>).

Data Analysis and Statistics

Due to the stochastic nature of the simulations, each condition was simulated at least 6 times and data were expressed as mean \pm standard deviation. Statistical differences between conditions were evaluated using one- or two-way ANOVA with Tukey *post-hoc* test for multiple comparisons, or independent *t*-test, depending on the number of groups and the type of the data. Statistical analyses were performed using GraphPad Prism 7 (GraphPad Software Inc., La Jolla, CA).

RESULTS

Effects of Heterogeneity in RyR2 Distribution on SCaEs

The model with uniform RyR2 distribution ($\sigma = 0.0$) produced a few large Ca^{2+} waves and corresponding DADs during follow-up after pacing at 0.5 Hz, in line with experimental data (Supplemental Figure 2). Increasing the heterogeneity of RyR2 distribution from $\sigma = 0.0$ to $\sigma = 0.4$ while keeping the total number of RyR2 constant substantially increased the incidence of SCaEs, but decreased their size (Figures 1A–C). For example, with $\sigma = 0.4$, the incidence of SCaEs was $14 \times$ larger ($3.31 \pm 0.51 \text{ s}^{-1}$ vs. $0.23 \pm 0.04 \text{ s}^{-1}$, $n = 6$, $p < 0.05$) and the average size of a Ca^{2+} wave as fraction of cardiomyocyte volume was 5x smaller than with $\sigma = 0.0$ (0.18 ± 0.02 vs. 0.91 ± 0.11 , $n = 6$, $p < 0.05$). Increasing RyR2 heterogeneity also reduced the longitudinal ($100.94 \pm 3.66 \mu\text{m/s}$ vs. $211.24 \pm 7.24 \mu\text{m/s}$, $n = 6$, $p < 0.05$) and transversal ($102.81 \pm 3.94 \mu\text{m/s}$ vs. $210.79 \pm 14 \mu\text{m/s}$, $n = 6$, $p < 0.05$) velocity of Ca^{2+} waves. We compared the magnitude of the effect of altered RyR2 distribution to a 25% change in total RyR2 expression. In line with previous results (Voigt et al., 2014), increasing Ca^{2+} flux led to an increased number of SCaEs and smaller SCaE size (Figures 1B,C). Likewise, a 25% decrease in total RyR2 led to lower SCaE incidence and bigger SCaE size. Increasing RyR2 heterogeneity and total expression had synergistic effects on SCaE incidence.

Next, we investigated the origins of SCaEs in simulations with heterogeneous RyR2 distributions (crosses in Figure 2A). SCaEs preferentially arose from units with high local RyR2 expression. In agreement, comparison of the histograms of relative RyR2 expression of all 50×18 units with those of SCaE-inducing units revealed that SCaE-inducing units had significantly higher local RyR2 expression (Figure 2B). The difference in mean RyR2 expression between SCaE-inducing units and all units was most pronounced in simulations with large heterogeneity in RyR2 distribution (Figure 2C), establishing units with high local RyR2 expression as foci for SCaEs.

Simulation of Experimentally Characterized RyR2 Distributions

RyR2 distributions were studied in rabbit atrial cardiomyocytes. In line with previous results, we observed a banded RyR2 pattern with $\sim 2 \mu\text{m}$ inter-band distance (Figures 3A,B). We analyzed the average RyR2 intensity after image-processing of the confocal images based on a square grid with $1 \mu\text{m}^2$ units and identified a significant variation in RyR2 distribution along the bands (Figure 3C). The histogram of relative RyR2 expression showed a large peak at near-zero levels, reflecting the units between RyR2 bands and a normal distribution with standard deviation $\sigma = 0.253$ for the RyR2 intensity within the bands (Figure 3D). In order to simulate this physiological RyR2 distribution, we increased the resolution of our model, simulating 100 segments of $1 \mu\text{m}$ with alternating pattern of RyR2 expression (Supplemental Figure 5) and validated its Ca^{2+} -handling properties based on experimental data (Supplemental Figures 2, 3). We also incorporated the option to simulate the regional expression of LTCC localized in axial

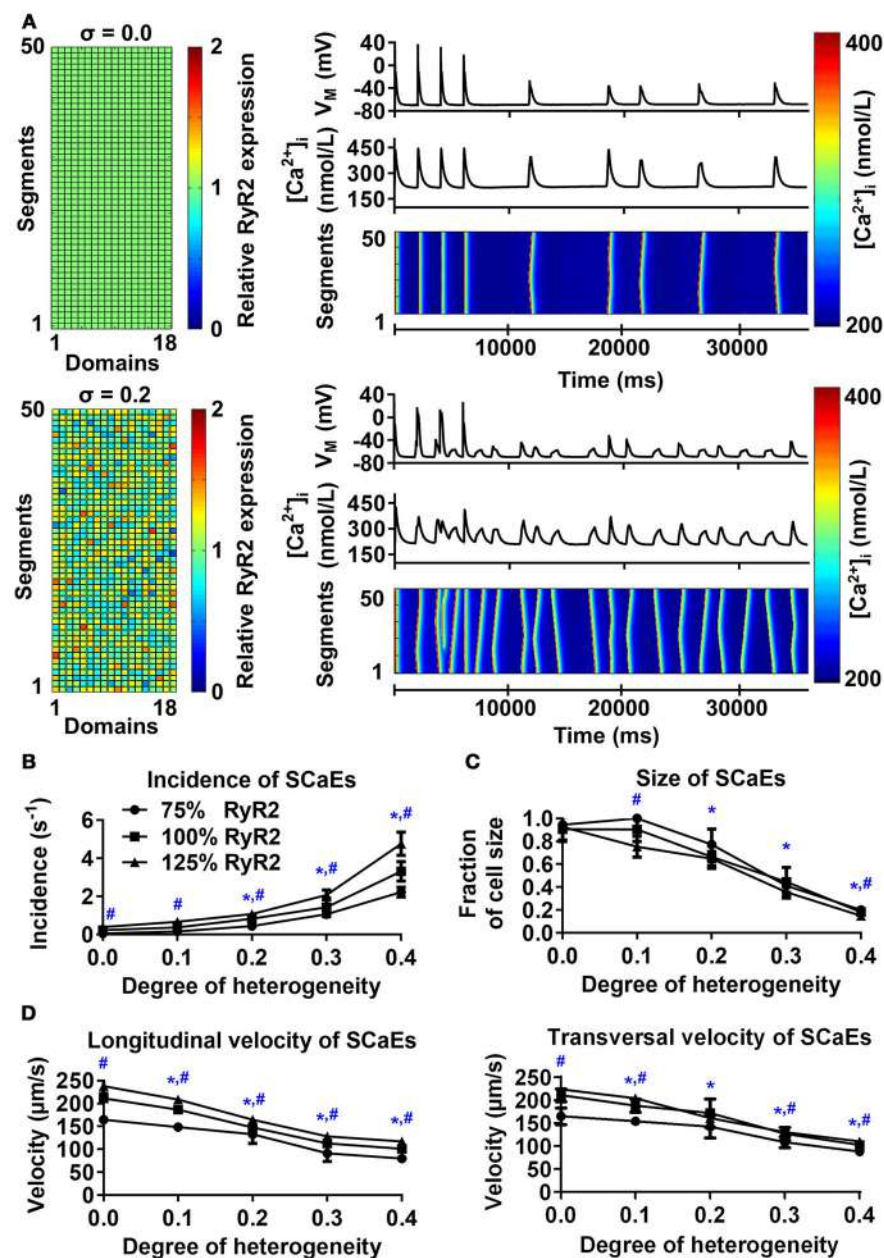


FIGURE 1 | Effects of RyR2 distribution heterogeneity on spontaneous Ca^{2+} -release events (SCaEs) in the 50-segment model. **(A)** Representative examples comparing heterogeneity (σ) of 0.0 (uniform expression, top) and 0.2 (bottom). The 50 \times 18 matrices (left) show the relative RyR2 distribution. The membrane potential (V_M), whole-cell Ca^{2+} concentration, and longitudinal line scan on the right show marked differences in number of SCaEs and corresponding delayed afterdepolarizations between both groups. **(B–D)** SCaE incidence **(B)** and size **(C)**, as well as longitudinal and transversal velocity of Ca^{2+} waves **(D)** as a function of RyR2 heterogeneity σ for different levels of total RyR2 expression (75% of control: circles; 100% of control: squares; 125% of control: triangles). SCaE incidence increases, while size decreases with increasing RyR2 heterogeneity. *indicates $P < 0.05$ vs. the group with heterogeneity 0.0 and # indicates statistically significant differences among three levels of RyR2 expression; $n = 6$ per condition.

tubules and the experimentally observed hyperphosphorylation of axial-tubule-associated RyR2 (discussed below). A schematic representation of the subcellular structure of the model is shown in Figure 4.

Similar to the 50-segment model, increasing heterogeneity of RyR2 expression in the 100-segment model led to an increase

in SCaE incidence and reduction in SCaE size, longitudinal and transversal velocity (Figure 5), with SCaEs originating from units with high local RyR2 expression (Supplemental Figure 6). However, despite similar SCaE-incidence with a uniform RyR2 distribution, the increase in SCaEs with increasing RyR2 heterogeneity was more pronounced in the 100-segment

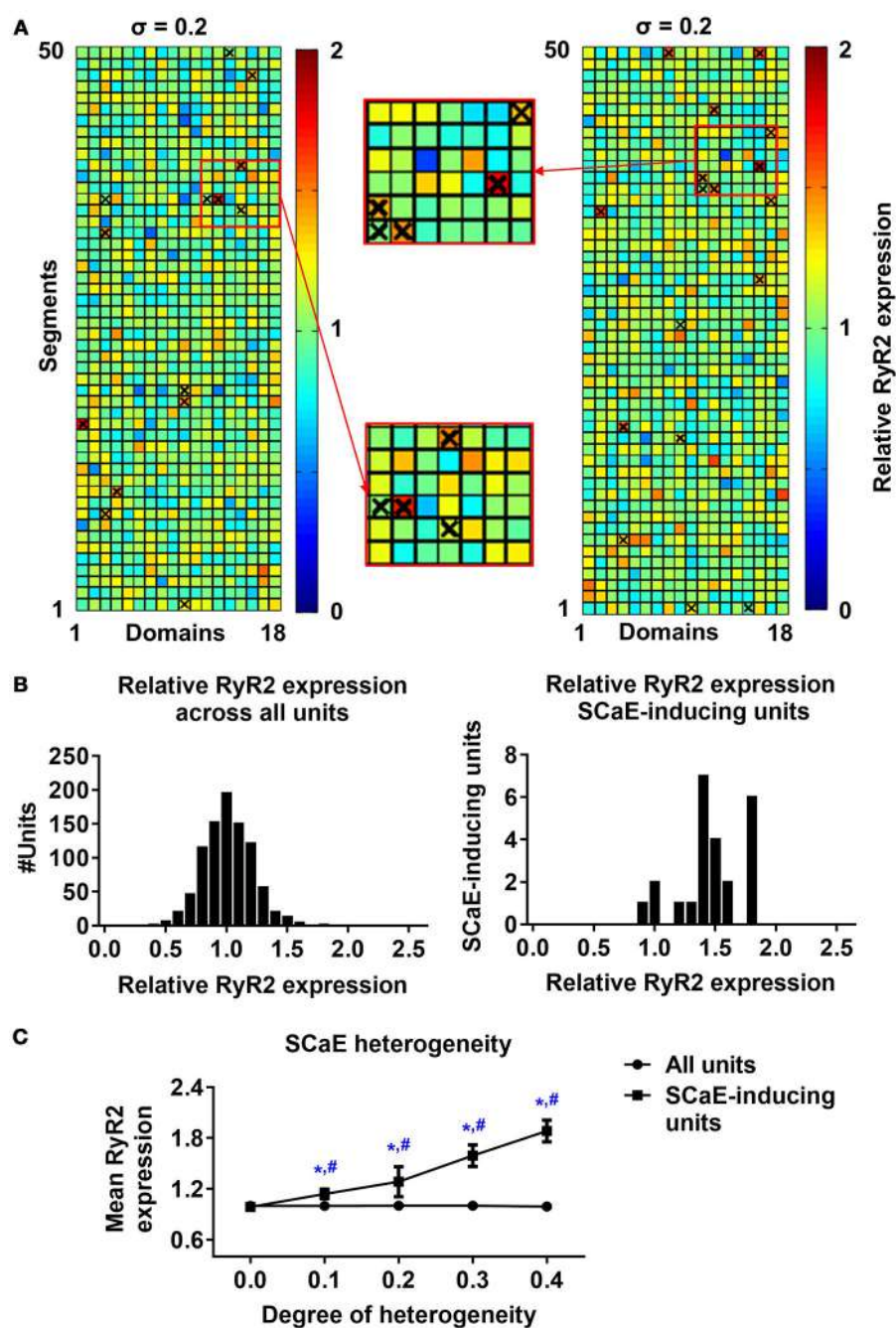


FIGURE 2 | Origins of spontaneous Ca^{2+} -release events (SCaEs). **(A)** Two representative examples of 50×18 matrices with heterogeneous RyR2 distribution ($\sigma = 0.2$). Red colors indicate high local RyR2 expression and blue colors low local RyR2 expression. The origins of individual Ca^{2+} waves are marked with crosses. Insets depict enlarged portions of the RyR2 distribution, showing that crosses mainly coincide with regions of high local RyR2 expression. **(B)** Histograms of relative RyR2 expression in all units (left) and units which were the origin of a SCaE (SCaE-inducing units). SCaEs arise mainly from units with high local RyR2 expression. **(C)** Mean relative RyR2 expression in SCaE-inducing units (squares) and all units (circles, 1.0 on average by definition) for different degrees of RyR2 heterogeneities. *indicates $P < 0.05$ vs. the group with heterogeneity 0.0 and #indicates $P < 0.05$ between mean relative RyR2 expression in SCaE-inducing units and all units; $n = 6$ per condition.

model (115-fold vs. 14-fold increase from $\sigma = 0.0$ to $\sigma = 0.4$ in the 100-segment and 50-segment models, respectively; **Supplemental Figure 7, Figure 1**). Implementation of the

experimentally observed RyR2 distribution pattern in the 100-segment model resulted in the occurrence of many small SCaEs, similar to our 100-segment simulations with heterogeneity (σ)

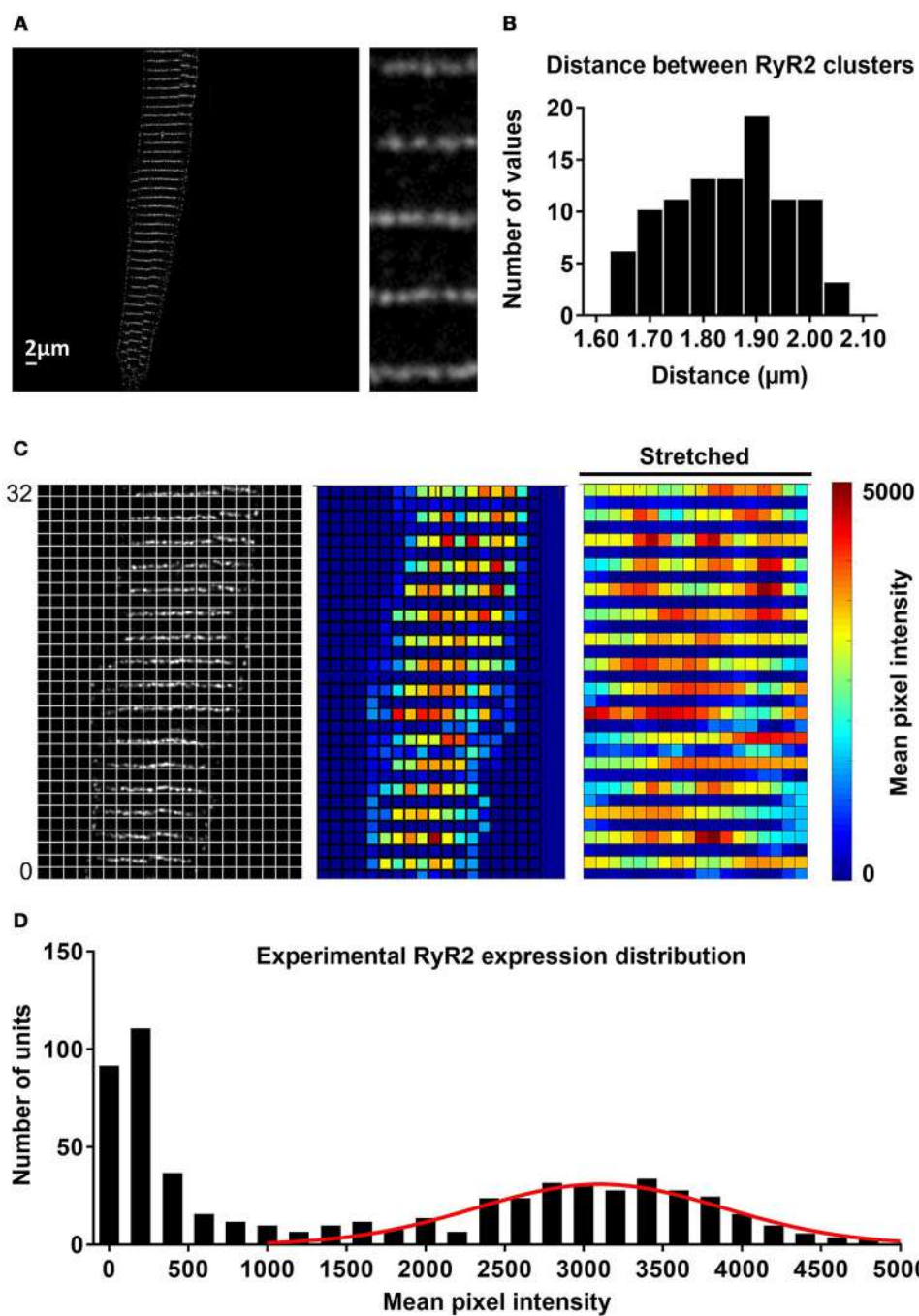


FIGURE 3 | Experimental distribution of RyR2 expression in atrial cardiomyocytes. **(A)** Confocal image of RyR2 staining in a rabbit atrial cardiomyocyte. Inset shows region of interest at higher magnification, revealing that RyR2 clusters assemble in a regular banded pattern along the Z-band. **(B)** Distribution of distances between RyR2 bands, showing that majority of these gaps were around 1.8–1.9 μm . **(C)** Image processing of confocal images and alignment with a regular grid of $\sim 1 \mu\text{m}^2$ units (left) enabled quantification of local RyR2 expression (right panel, red indicates high local RyR2 expression and blue low local RyR2 expression). **(D)** Histogram of experimental RyR2 expression distribution across all units with a large peak around 0, representing units between bands of RyR2 expression and a normal distribution of RyR2 expression within bands (line shows normal distribution with standard deviation of 0.253).

0.3 and 0.4 (with SCaE incidence of $12.96 \pm 0.28 \text{ s}^{-1}$ in the experimentally observed RyR2 distribution vs. $9.88 \pm 1.16 \text{ s}^{-1}$ in $\sigma = 0.3$ and $21.83 \pm 2.62 \text{ s}^{-1}$ in $\sigma = 0.4$, **Figure 5B** and

Supplemental Figure 7). Longitudinal and transversal velocity of SCaEs in the experimentally observed RyR2 distribution model were similar to 100-segment simulations with $\sigma = 0.2$

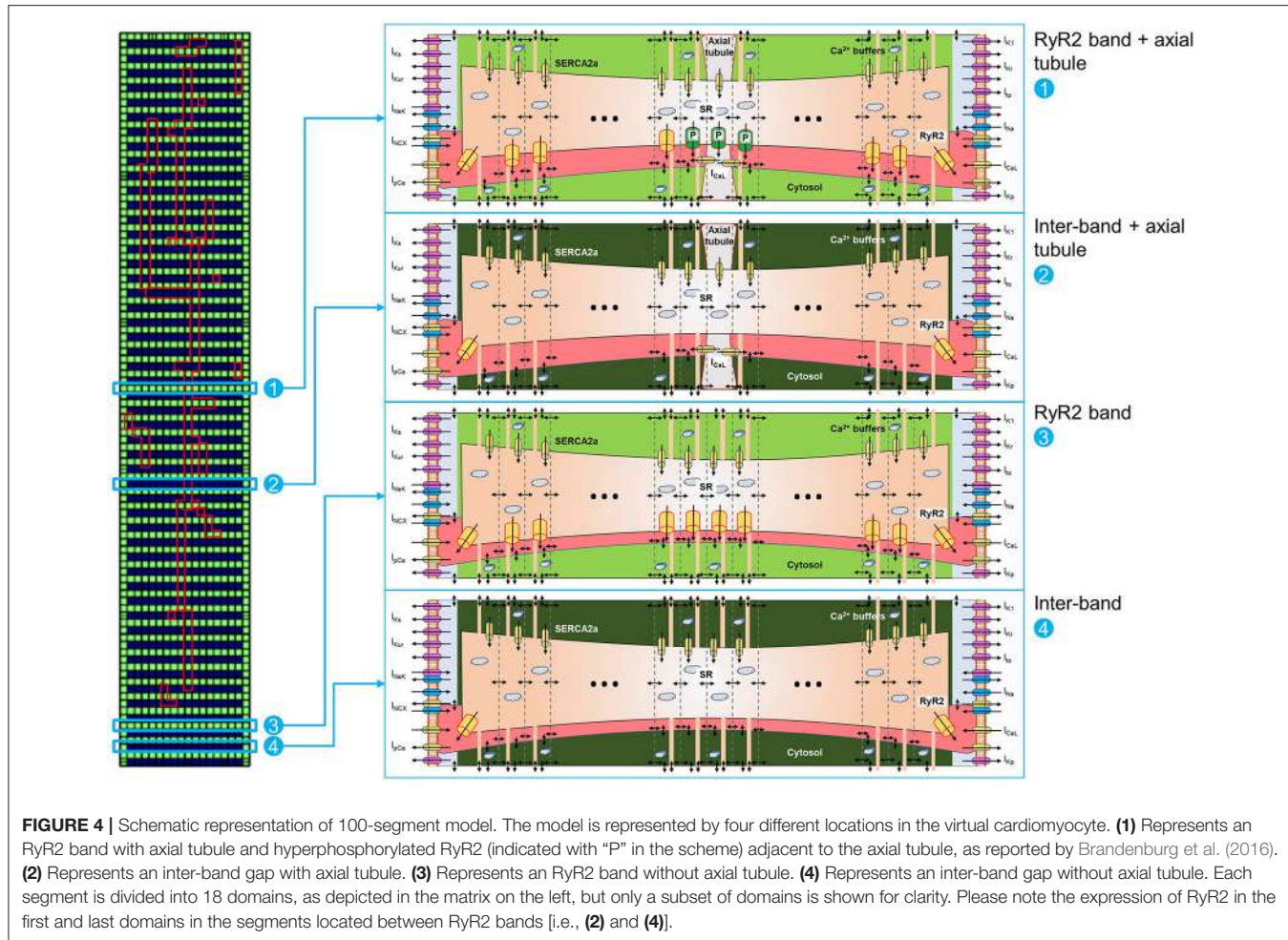


FIGURE 4 | Schematic representation of 100-segment model. The model is represented by four different locations in the virtual cardiomyocyte. (1) Represents an RyR2 band with axial tubule and hyperphosphorylated RyR2 (indicated with “P” in the scheme) adjacent to the axial tubule, as reported by Brandenburg et al. (2016). (2) Represents an inter-band gap with axial tubule. (3) Represents an RyR2 band without axial tubule. (4) Represents an inter-band gap without axial tubule. Each segment is divided into 18 domains, as depicted in the matrix on the left, but only a subset of domains is shown for clarity. Please note the expression of RyR2 in the first and last domains in the segments located between RyR2 bands [i.e., (2) and (4)].

(Figure 5D). Heterogeneities in RyR2 expression did not affect properties of the LTCC-triggered Ca^{2+} transient in the absence of preceding SCaEs (Supplemental Figure 8).

Modulation of SCaE Propagation by the Distance Between RyR2s and RyR2 Clusters at the Lateral Membrane

Previous studies have reported a closer spacing between RyR2s around the lateral membrane in rat atrial and ventricular cardiomyocytes (Chen-Izu et al., 2006; Galice et al., 2018), rabbit atrial (Musa et al., 2002), ventricular (Musa et al., 2002; Dan et al., 2007) and SA nodal cells (Musa et al., 2002), and human atrial cardiomyocytes (Brandenburg et al., 2016). We similarly observed a higher density of RyR2 clusters at the lateral membrane in rabbit atrial cardiomyocytes (Figure 6A) and accordingly incorporated RyR2 expression in the first and last Ca^{2+} unit of every segment of the virtual cardiomyocyte for the simulations of Figure 5. Next, we employed the model to assess the impact of these lateral RyR2s by comparing simulations with and without RyR2 in the outer Ca^{2+} units for segments located between RyR2 bands. The absence of RyR2s in the lateral region of the cardiomyocyte prevented the propagation of SCaEs, resulting in a reduced longitudinal velocity and numerous

small SR Ca^{2+} releases (Supplemental Figure 9A). This behavior could be fully restored by reducing the time constant of Ca^{2+} diffusion between segments and normalizing the total RyR expression (SCaE incidence of $0.24 \pm 0.04 \text{ s}^{-1}$ in the group with normalized RyR2 expression and corrected longitudinal velocity vs. $0.19 \pm 0.02 \text{ s}^{-1}$ in the control group, $n = 6$, $p > 0.05$; Supplemental Figure 9B).

Next, we investigated the effect of alterations in the distance between RyR2 bands by simulating two or three segments without RyR2 expression between bands (instead of one). Although an increased RyR2 inter-band distance indeed slowed down the longitudinal velocity of SCaEs, it surprisingly did not impair propagation of SCaEs and resulted in an increased SCaE incidence (Figure 6B, left column; Figures 6C–E). Subsequent analyses showed that the RyR2 expressed at the lateral membrane in segments without RyR2 bands are critical for the propagation of SCaEs. In particular, a similar increase in RyR2 inter-band distance in the model without lateral RyR2 between bands (but with corrected longitudinal velocity of SCaEs at baseline) resulted in failure of Ca^{2+} -wave propagation and many fragmented SCaEs (Figure 6B, right column). These data strongly suggest that the closer spacing of RyR2 at the lateral membrane that we observed experimentally may provide a safety factor for synchronous

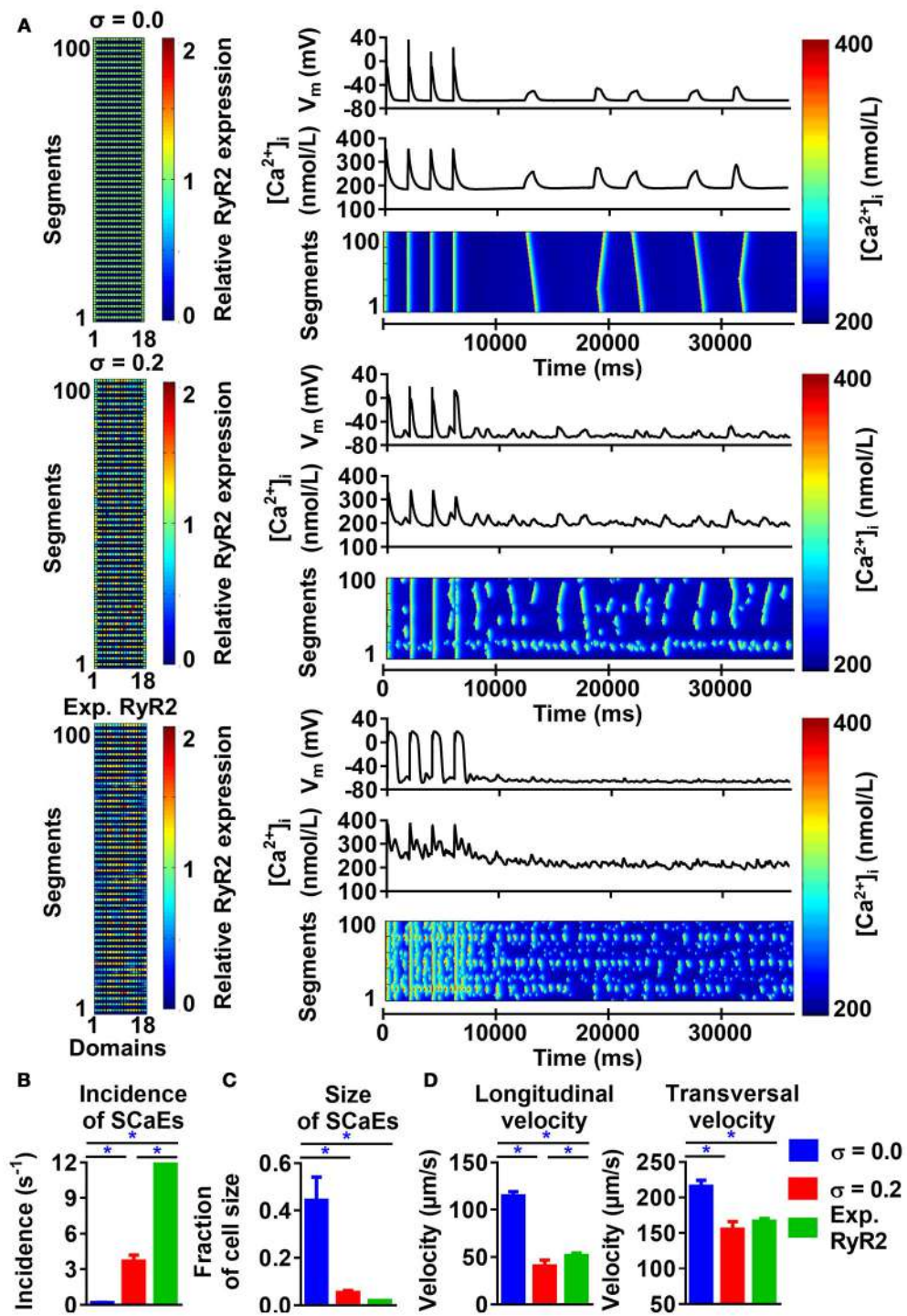


FIGURE 5 | Effects of RyR2 distribution heterogeneity on spontaneous Ca^{2+} -release events (SCaEs) in the 100-segment model. **(A)** Representative examples comparing heterogeneity (σ) of 0.0 (uniform expression, top), 0.2 (middle), and experimentally observed RyR2 expression patterns (bottom) on membrane potential (V_m), whole-cell Ca^{2+} -transient, and longitudinal line scan (right panels). The 100×18 matrices (left) of relative RyR2 expression incorporate the experimentally observed $2 \mu\text{m}$ inter-band distance. **(B–D)** SCAE incidence **(B)**, size **(C)**, as well as longitudinal and transversal velocity of Ca^{2+} waves **(D)** in 100-segment simulations with $\sigma = 0.0$, $\sigma = 0.2$, and experimentally observed RyR2 expression. Incorporation of the experimentally observed RyR2 expression in the original 100-segment model results in a large (non-physiological) number of small SCAEs. *indicates $P < 0.05$ between indicated groups; $n = 6$ per condition.

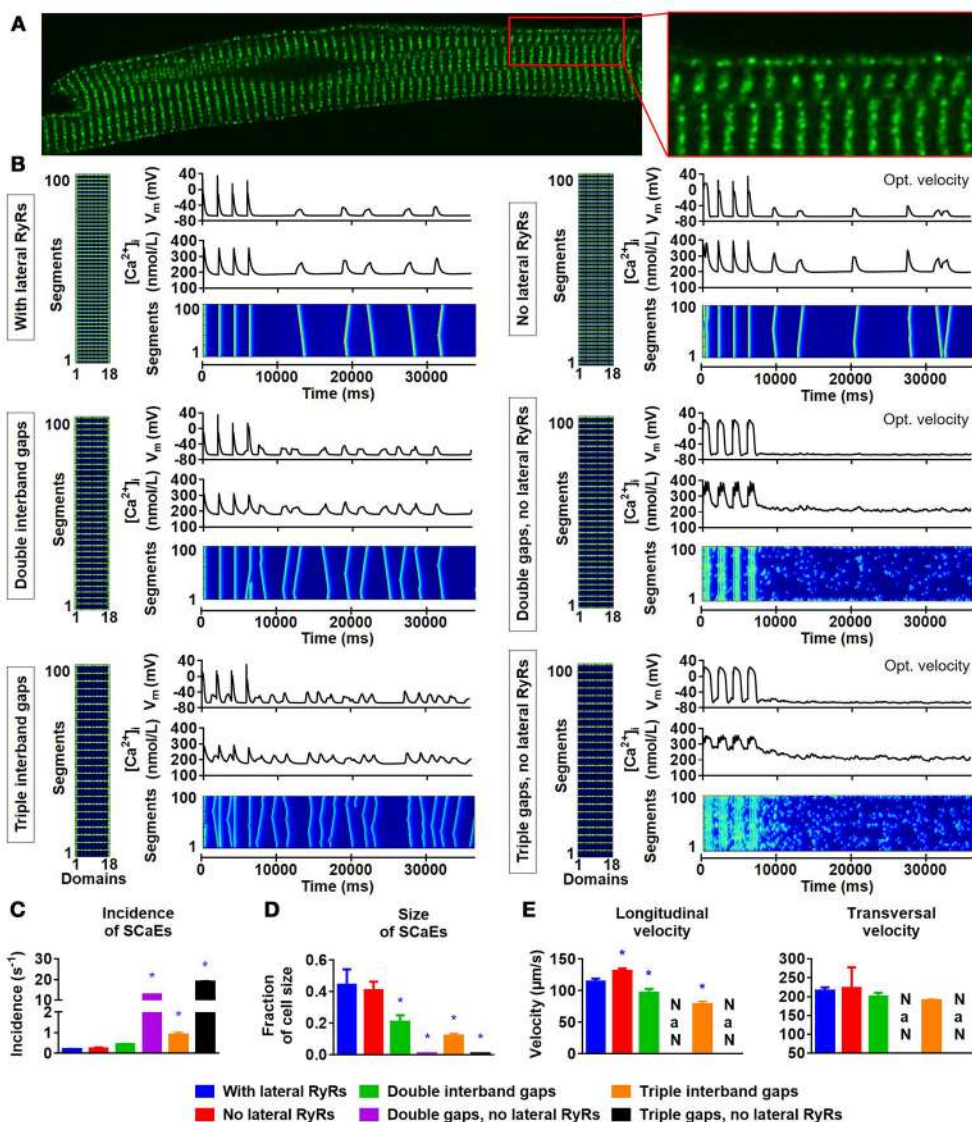


FIGURE 6 | Lateral RyR2s, inter-band distance and the propagation of SCaEs. **(A)** Confocal image showing an increased density of RyR2 close to the lateral membrane in a rabbit atrial cardiomyocyte. **(B)** Representative examples of membrane potential (V_m), whole-cell Ca^{2+} -transient, and longitudinal line scan for the 100-segment model with single ($\sim 2 \mu\text{m}$; top row), double (middle row) or triple (bottom row) inter-band distance, with (left column) or without (right column) expression of lateral RyR2s between bands. In all panels, the total number of RyR2 was adjusted to achieve a density of 2,772 RyR2 per unit. The time constant of longitudinal Ca^{2+} diffusion between SR release spaces was adjusted from 0.22 to 0.07 ms in the model without lateral RyR2 expression to obtain similar SCaE properties for physiological inter-band distances. **(C–E)** SCaE incidence **(C)**, size **(D)**, as well as longitudinal and transversal velocity of Ca^{2+} waves **(E)** for the six model versions. An increased inter-band distance increased the incidence of SCaEs, reduced their size and altered the longitudinal velocity without affecting the transversal velocity. *indicates $P < 0.05$ vs. the control model (100-segment model of single inter-band distance with lateral RyRs; blue bars), $n = 6$ per condition.

SR Ca^{2+} release but may also facilitate propagation of large proarrhythmic Ca^{2+} waves.

Inter-band RyR2 Expression and SCaEs

Similar to the results described by Macquaide et al. (2015), our confocal images also showed occasional RyR2 expression between individual bands. We employed the 100-segment model to better understand the functional effects of these inter-band RyR2 clusters. For any degree of heterogeneity, the presence

of inter-band RyR2 clusters resulted in fewer, slightly larger SCaEs compared to simulations without inter-band clusters (**Figures 7A–C**, compare blue and red bars), without affecting longitudinal and transversal velocity of SCaEs (**Figure 7D**). We hypothesized that the reduction in SCaEs was due to a reduction in maximal local RyR2 expression resulting from the redistribution of RyR2 from the bands to the inter-band clusters. RyR2 expression per unit was indeed lower in the homogeneous simulations with inter-band clusters (2,543 vs. 2,772 RyR2 per

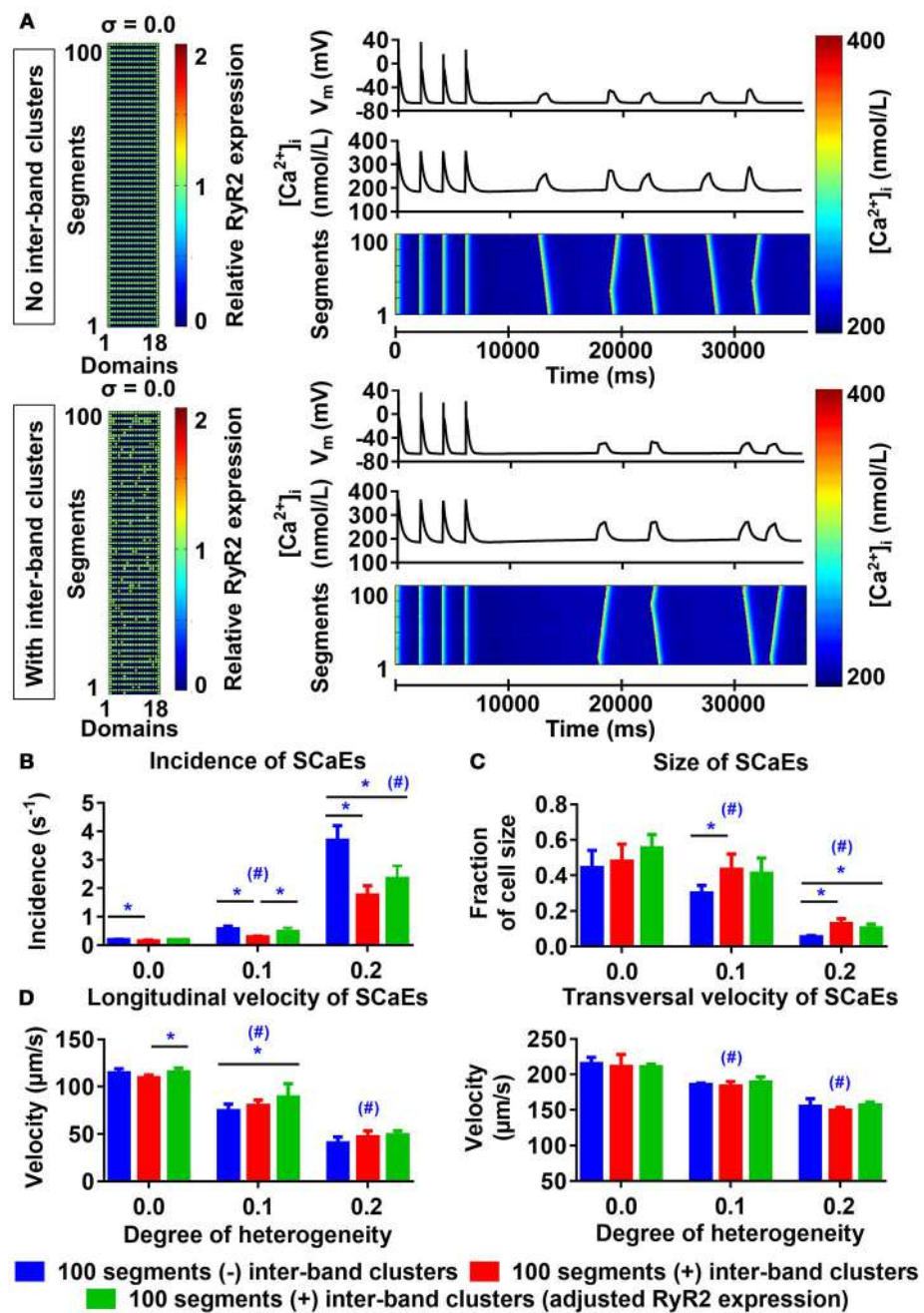


FIGURE 7 | Effects of inter-band RyR2 clusters on spontaneous Ca^{2+} waves (SCaEs). **(A)** Comparison of RyR2 expression matrix (left), membrane potential (V_M), whole-cell Ca^{2+} transient, and longitudinal line scan (right, top to bottom) in the model without inter-band RyR2 clusters (top) and with inter-band clusters (bottom) with uniform RyR2 expression ($\sigma = 0.0$). **(B–D)** SCAE incidence **(B)** and size **(C)**, as well as longitudinal and transversal velocity of Ca^{2+} waves **(D)** as a function of RyR2 heterogeneity σ (0.0–0.2) in the absence of inter-band RyR2 clusters (blue), in the presence of 10% inter-band RyR2 clusters (red), or in the presence of 10% inter-band RyR2 clusters with increased global RyR2 expression to ensure similar RyR2 density within the bands (green). *indicates $P < 0.05$ between groups and # indicates $P < 0.05$ between a given level of heterogeneity and the group with heterogeneity 0.0; $n = 6$ per condition.

unit) and increasing the total RyR2 expression of the 100-segment model with inter-band clusters to 2,772 in all units containing RyR2 normalized SCAE incidence for low levels of RyR2 heterogeneity ($0.185 \pm 0.015 \text{ s}^{-1}$ in the normalized RyR2

expression group vs. $0.191 \pm 0.018 \text{ s}^{-1}$ in the group without inter-band clusters ($\sigma = 0.0$), $p > 0.05$ and $0.470 \pm 0.138 \text{ s}^{-1}$ for normalized RyR2 expression vs. $0.565 \pm 0.105 \text{ s}^{-1}$ without inter-band clusters ($\sigma = 0.1$), $p > 0.05$; **Figure 7B**). For high

RyR2 heterogeneities, SCaE incidence remained lower in the presence of inter-band RyR2 cluster, even after adjusting the total RyR2 expression. Under these conditions, SCaEs are frequent, suggesting that annihilation or merging of small SCaEs arising around inter-band clusters contributes to a lower incidence of observed SCaEs, even after adjusting RyR2 expression.

The Impact of Axial Tubules on Atrial Ca^{2+} -Handling

Axial tubules are unique to atrial cardiomyocytes, but their role in Ca^{2+} -handling is not fully understood. Axial tubules contain LTCCs, modulating Ca^{2+} -induced Ca^{2+} release and centripetal Ca^{2+} -wave propagation. We incorporated various configurations of axial tubules in the 100-segment model and investigated their impact on depolarization-induced, LTCC-triggered Ca^{2+} transients and SCaEs. Addition of an axial tubule to the model reduced time-to-peak of the regional LTCC-triggered Ca^{2+} transient (based on a virtual transversal line scan through the region with the axial tubule) and slightly increased the Ca^{2+} -transient amplitude (**Figure 8**). Moreover, time to peak of the transversal-line-scan-based Ca^{2+} -transient is influenced by both the number of parallel axial tubules and their location. The reduction in time to peak was largest with an axial tubule located in the center of the virtual cardiomyocyte, and addition of two or more parallel axial tubules further reduced the time to peak (**Figure 8**). The impact of axial tubules on whole-cell Ca^{2+} -transient properties depended on axial-tubule length and was limited for short axial tubules (compare regional and whole-cell time to peak in **Figure 8B**). However, a longer axial tubule network, such as that observed experimentally (Brandenburg et al., 2016), also significantly shortened time to peak of the whole-cell Ca^{2+} transient (**Figure 8B**, rightmost columns).

There were no differences in the longitudinal Ca^{2+} -wave velocity between simulations with and without axial tubules. Similarly, the presence of axial tubules with LTCC did not affect the number of SCaEs (**Figures 9A,B**; compare red and blue bars), consistent with the idea that SCaEs result from stochastic RyR2 openings that are independent of LTCCs. However, a recent study (Brandenburg et al., 2016) noted that although RyR2 expression adjacent to the axial tubule was not different from other parts of the cardiomyocyte, these RyR2 near axial tubules were hyperphosphorylated. We simulated RyR2 hyperphosphorylation in our model by increasing RyR2 open probability for all RyR2 located in units surrounding axial tubules. In the presence of hyperphosphorylated RyR2 surrounding axial tubules, the number of SCaEs was increased, with a corresponding reduction in their size (**Figures 9B,C**). Of note, SCaEs indeed primarily originated around the axial tubule (**Figure 9D**, **Supplemental Figure 10**), although in the presence of a heterogeneous RyR2 distribution, regions with high local RyR2 expression may also act as foci (**Supplemental Figure 10**).

Predicting the Effects of Beta-Adrenergic Stimulation on SCaEs

Beta-adrenergic stimulation is an accepted promoter of SCaE-mediated triggered activity (Chen et al., 2014). Here, we

investigated the functional consequences of three established downstream targets of beta-adrenergic stimulation. Chronic AF is associated with a hyperphosphorylation-mediated 100–500% increase in RyR2 open probability (Voigt et al., 2012). Therefore, we first implemented a 100% increase of RyR2 open probability to simulate the effect of beta-adrenergic stimulation. This resulted in smaller and more frequent SCaEs compared to baseline (incidence of $2.03 \pm 0.09 \text{ s}^{-1}$ in the increased RyR2 open probability group vs. $0.19 \pm 0.02 \text{ s}^{-1}$ in the baseline group, $n = 6$, $p < 0.05$; **Supplemental Figure 11**). Second, we implemented an increased SERCA2a affinity for cytosolic Ca^{2+} to reflect phospholamban phosphorylation. In the presence of increased SERCA2a function, the incidence of SCaEs was increased without any statistically significant change in the size of SCaEs (**Supplemental Figure 12**). In addition, an increase in longitudinal and transversal velocities of SCaEs was observed. Third, we implemented a homogenous increase of LTCC function by doubling the maximum conductance of the channel, which resulted in an increased SCaE incidence without any statistically significant changes in the size and velocities of SCaEs (**Supplemental Figure 13**). The combination of all three modifications, reflecting maximal beta-adrenergic stimulation, produced a dramatic increase in SCaEs (incidence of $27.77 \pm 14.92 \text{ s}^{-1}$ vs. $0.19 \pm 0.02 \text{ s}^{-1}$ in the baseline group, $n = 6$, $p < 0.05$), including proarrhythmic triggered activity (**Supplemental Figure 14**).

A Computational Model Incorporating Physiological RyR2 and LTCC Distributions

Finally, we combined both the experimentally observed RyR2 distribution (**Figure 3**) and axial tubule network with LTCC in a novel model of the human atrial cardiomyocyte. When using the parameters established for the model with uniform RyR2 distribution and no axial tubules, this model showed a non-physiological number of small SCaEs, in line with the effects of the experimental RyR2 distribution in **Figure 5A**. As such, we performed a parameter optimization to reproduce the experimentally observed Ca^{2+} -handling properties in the combined model (**Figure 10**).

DISCUSSION

Recent studies have identified a major role for cardiomyocyte Ca^{2+} -handling abnormalities in cardiac arrhythmias and have provided insight into the underlying molecular mechanisms (Heijman et al., 2016a; Landstrom et al., 2017). However, the impact of the subcellular distribution of RyR2 and LTCC on cardiomyocyte Ca^{2+} -handling remains largely unknown. It is currently experimentally challenging to study both (sub)cellular structure and functional Ca^{2+} -handling in the same cardiomyocyte. Here, we extended a computational model of the human atrial cardiomyocyte with a more physiological subcellular structure, including heterogeneous RyR2 distributions and axial tubules with LTCC.

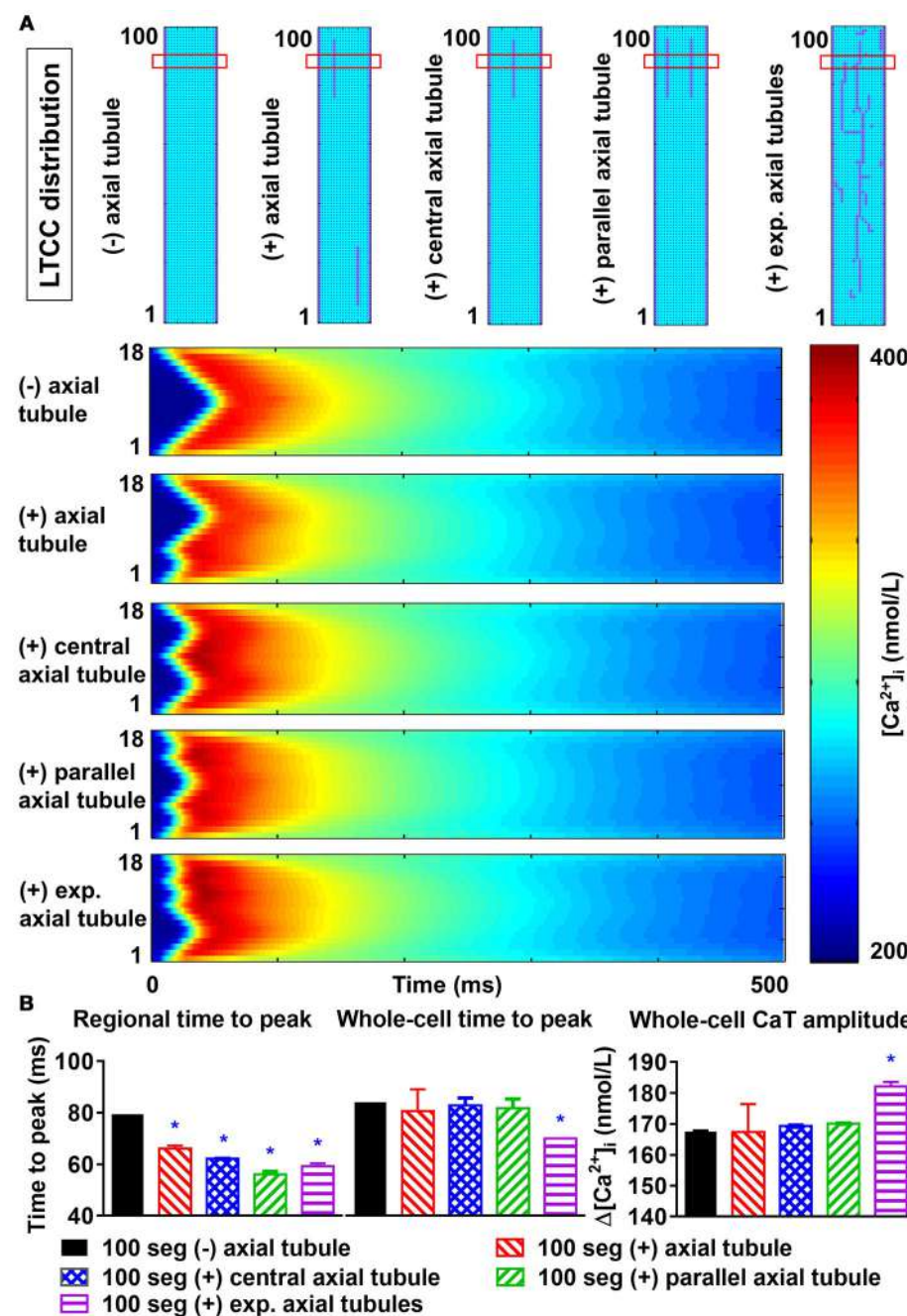


FIGURE 8 | Effects of axial tubule(s) on centripetal Ca^{2+} -wave propagation. **(A)** Schematic representations of model structure: no axial tubule (L-type Ca^{2+} -channels [LTCC] only at lateral membranes), single axial tubule at 33% of cell width, single central axial tubule at 50% of cell width, two parallel axial tubules at 33 and 66% of cell width, or experimentally observed axial tubules based on Brandenburg et al. (2016) (top) and corresponding transversal line scans of Ca^{2+} -induced Ca^{2+} release during an action potential, showing centripetal Ca^{2+} -wave propagation (bottom). **(B)** Quantification of time to peak (left) and Ca^{2+} -transient amplitude (right) for the indicated line scan in the four groups (“regional”) or for the whole-cell Ca^{2+} transient. Increasing numbers of axial tubules and more centrally located axial tubules decrease the time-to-peak and slightly increase the Ca^{2+} -transient amplitude. The magnitude of the increase depends on the number of axial tubules. *indicates $P < 0.05$ vs. the 100-segment group without axial tubules (black bars); $n = 6$ per condition.

Our computational analyses showed that increasing RyR2 heterogeneity resulted in more, smaller SCaEs arising from regions with high local RyR2 expression. LTCC located in axial

tubules produced a faster, more synchronous CICR, which was modulated by the location and extent of the axial tubular network. Moreover, hyperphosphorylation of RvR2 surrounding

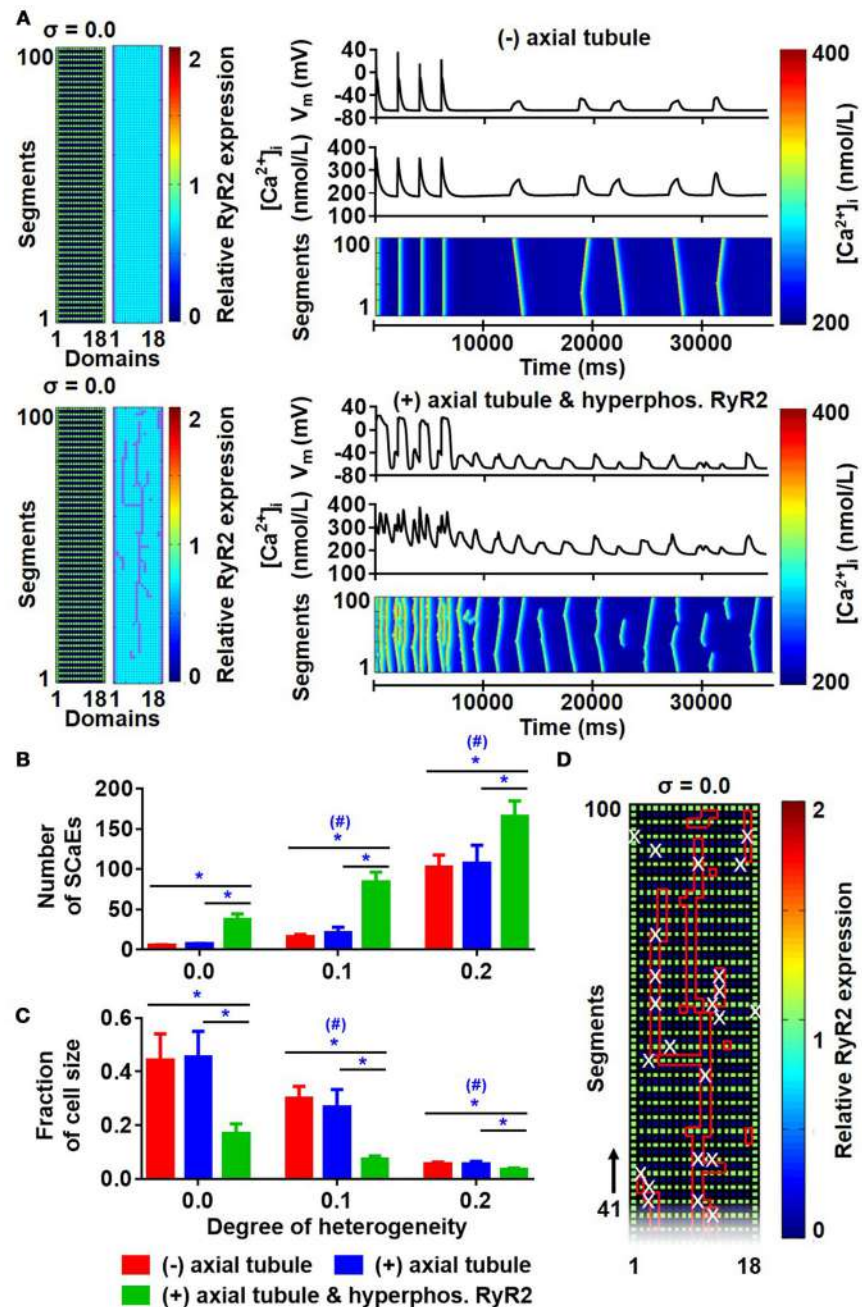


FIGURE 9 | Effects of axial tubules on SCaEs. **(A)** Comparison between the model without axial tubules and model with axial tubules with uniform RyR2 expression ($\sigma = 0.0$), but hyperphosphorylated RyR2 around axial tubules. **(B,C)** Number of Ca^{2+} waves **(B)** and SCaE size **(C)** in the absence of axial tubules (red bars), presence of axial tubules (blue bar), or presence of axial tubules with hyperphosphorylation of surrounding RyR2 (green bars). **(D)** Distribution of RyR2 expression and location of axial tubules (red lines) in relation to the origin of SCaEs (white crosses), showing that SCaEs primarily originated from RyR2 clusters adjacent to the axial tubules. *indicates $P < 0.05$ between groups and # indicates $P < 0.05$ between a given level of heterogeneity and the group with heterogeneity 0.0; $n = 6$ per condition.

axial tubules increased the incidence of SCaEs and DADs. Finally, we developed and validated a novel human atrial cardiomyocyte model with physiological RyR2 distribution and axial tubules with LTCC based on experimental observations, which can serve as a tool for future studies.

Role of Subcellular Structure in Cardiomyocyte Ca^{2+} -Handling

An increased SCaE incidence in atrial cardiomyocytes from patients with AF contributes to the initiation of DADs and cellular triggered activity (Hove-Madsen et al., 2004;

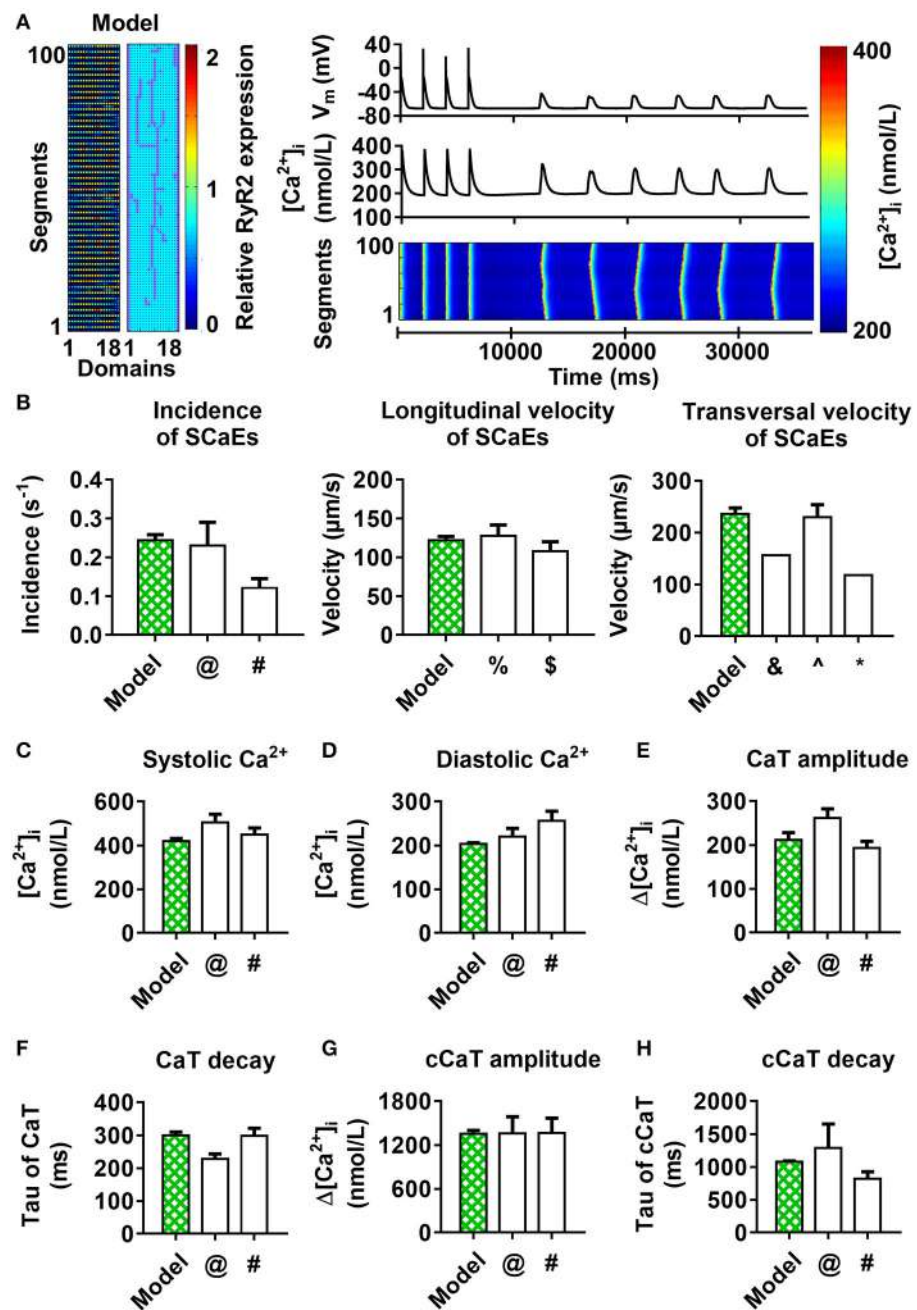


FIGURE 10 | 100-segment model with experimental RyR2 distribution and LTCC expression based on experimentally observed axial tubules, with RyR2 hyperphosphorylation around axial tubules. **(A)** Model structure (left panel) and longitudinal line scan of the optimized 100-segment model (“Model”). **(B–H)** Comparison of SCaE characteristics **(B)** and whole-cell Ca^{2+} -transient properties **(C–H)** of the model to previously published experimental data [§]Tanaka et al. (2001); [^]Woo et al. (2002); [&]Kirk et al. (2003); [%]Loughrey et al. (2004); [@]Voigt et al. (2012); [#]Voigt et al. (2014); ^{*}Greiser et al. (2014).

Voigt et al., 2012, 2014), which, when occurring at the tissue level, may act as initiators of AF or may sustain the arrhythmia when occurring repetitively at high frequency (Vincenti et al., 2006; Voigt et al., 2014). SCaEs are promoted by increased SR Ca^{2+} load leading to store-overload-induced SR Ca^{2+} release (MacLennan and Chen, 2009). In agreement, SERCA2a activity

is increased in patients with paroxysmal AF and is associated with increased SR Ca^{2+} load and a higher incidence of SCaEs (Voigt et al., 2014). In addition, RyR2 dysfunction can increase the incidence of SCaEs even in the absence of increased SR Ca^{2+} load. RyR2 mutations leading to catecholaminergic polymorphic ventricular tachycardia have been associated with familial AF

(Enriquez et al., 2016) and genetic mouse models with these mutations show pronounced atrial Ca^{2+} -handling abnormalities (Shan et al., 2012). Moreover, RyR2 open probability is increased, likely due to hyperphosphorylation of the RyR2 channel, in patients with long-standing persistent AF (Voigt et al., 2012). Besides changes in cardiomyocyte Ca^{2+} -handling, AF produces structural remodeling at the level of the single cardiomyocyte (atrial cellular hypertrophy, myolysis, alterations in size and distribution of mitochondria and SR) (Morillo et al., 1995; Brundel et al., 2002; Goette et al., 2016), suggesting a potential role for changes in subcellular structure in regulating cardiomyocyte Ca^{2+} -handling. Indeed, Macquaide et al. (2015) reported that ultrastructural reorganization of RyR2 clusters in atrial cardiomyocytes of sheep with persistent AF is associated with overactive Ca^{2+} release. In addition, Lenaerts et al. (2009) reported that in sheep with persistent AF, there was loss of T-tubule organization, fewer Ca^{2+} channel-RyR couplings, and reduced efficiency of the coupling at subsarcolemmal sites, which led to a reduction in SR Ca^{2+} release despite preserved SR Ca^{2+} content. Thus, there is substantial indirect evidence for a role of subcellular structure in cardiomyocyte Ca^{2+} -handling. However, a systematic analysis of the impact of changes in Ca^{2+} -handling protein distributions on whole-cell proarrhythmic Ca^{2+} -handling is lacking.

Consistent with previous publications (Hiess et al., 2015; Yue et al., 2017), our confocal images of rabbit atrial cardiomyocytes showed a banded RyR2 expression with inter-band distance of $\approx 1.9 \mu\text{m}$. Moreover, there appears to be a substantial heterogeneity of RyR2 density along the z-bands. We increased the spatial resolution of our computational model to enable simulations of the banded RyR2 pattern and incorporated the experimentally observed RyR2 distribution in our model. In line with the work by Macquaide et al. (2015), our simulations showed a pronounced impact of RyR2 distribution on SCaE incidence and size. Indeed, physiologically observed degrees of RyR2 heterogeneity had a larger impact on SCaEs than differences in total RyR2 expression observed between patients with sinus rhythm and paroxysmal AF (Voigt et al., 2014). Of note, our simulations identified regions with high local RyR2 expression as foci for SCaEs, which is in line with recent experimental work by Galice et al. (2018).

In ventricular cardiomyocytes, LTCC are primarily (but not exclusively, Best and Kamp, 2012) located in T-tubules, promoting synchronous SR Ca^{2+} release throughout the cell. Recent studies have identified a similar role for axial tubules in atrial cardiomyocytes (Dibb et al., 2013). For example, Brandenburg et al. (2016) reported the importance of axial tubules in atrial cardiomyocytes in maintaining Ca^{2+} -handling and Ca^{2+} -wave propagation to the center of atrial cardiomyocytes. Similarly, Yue et al. (2017) observed synchronous SR Ca^{2+} release in mouse atrial cells, which was ascribed to the presence of transverse-axial tubules. We employed the perfect control provided by computational models to study the exact effects of different locations, numbers, and distributions of such axial tubules on whole-cell Ca^{2+} -handling. Incorporation of axial tubules produced a more synchronous SR Ca^{2+} release, as evident from a W-shaped instead of V-shaped pattern in

simulated transversal line scans. The W-shaped patterns varied with different locations of the axial tubules, consistent with experimental findings (Kirk et al., 2003; Yue et al., 2017) noting that the presence and location of the transverse-axial tubular system determined the shape of the whole-cell Ca^{2+} transient and transversal Ca^{2+} waves. Our simulations showed that more centrally located and/or higher number of axial tubules reduced the local time-to-peak. However, in order to affect the global time-to-peak and global Ca^{2+} -transient amplitude, the length of the axial tubules had to be sufficiently long to affect a large part of the virtual cardiomyocyte. Brandenburg et al. (2016) reported that instead of an increase in the number of RyR2 adjacent to the axial tubules, there was a selective local RyR2 hyperphosphorylation, which led to a faster Ca^{2+} release at axial tubule locations residing inside the cell. Our simulations showed that the presence of axial tubules *per se* did not affect SCaEs, but that simulation of local hyperphosphorylation of RyR2 increased the number of SCaEs. Furthermore, we confirmed that regions with local hyperphosphorylation acted as the origins of SCaEs. However, these results depended on the amount of RyR2 heterogeneity and the number of axial tubules, with SCaEs also arising from regions with high local RyR2 expression independent of RyR2 hyperphosphorylation. Taken together, these findings underline the importance of the subcellular distribution of Ca^{2+} -handling proteins in atrial cardiomyocytes for cardiac arrhythmogenesis.

Previous publications (Musa et al., 2002; Chen-Izu et al., 2006; Dan et al., 2007; Brandenburg et al., 2016) have reported an increased RyR2 density at the lateral membrane using confocal microscopy. However, the role of these lateral RyR2 clusters remains unknown. Here, we employed a computational model with no expression of lateral RyR2s to investigate their role in the propagation of SCaEs. Our data show that lateral RyR2s hold a very important role as “bridges” that facilitate Ca^{2+} -wave propagation. Removal of lateral RyR2 clusters impaired Ca^{2+} -wave propagation and resulted in more, but smaller SCaEs, effectively converting proarrhythmic Ca^{2+} waves to Ca^{2+} sparks.

Comparison to Previous Models

Several computational models have been developed to study cardiomyocyte Ca^{2+} -handling abnormalities. These include, on the one hand, highly detailed models of a single Ca^{2+} -release unit (CRU) to study the molecular determinants of SR Ca^{2+} release. For example, Hake et al. (2012) developed a computational model with a highly detailed, electron microscopy-based computational geometry of a CRU from a mouse ventricular cardiomyocyte to simulate local Ca^{2+} sparks. Walker et al. (2014) developed a detailed three-dimensional model of a CRU incorporating diffusion, intracellular buffering systems, and stochastically gated RyRs and LTCCs to simulate local Ca^{2+} dynamics with a high spatial resolution. This work showed that perturbations to subspace dimensions strongly alter Ca^{2+} -spark dynamics. Similarly, Zahradníkova and Zahradník (2012) constructed virtual CRUs composed of a variable number of RyRs distributed in clusters in line with the experimentally observed cluster-size distribution to provide a description of Ca^{2+} -spark properties for spontaneous

and triggered Ca^{2+} sparks. These studies strongly suggest that the organization of the CRU plays a critical role in determining the characteristics of microscopic Ca^{2+} -release events (sparks) but have not simulated whole-cell Ca^{2+} -handling abnormalities, which would be relevant to study arrhythmogenesis.

On the other hand, a number of models have been developed to study whole-cell Ca^{2+} -handling: Walker et al. (2017) developed a biophysically detailed three-dimensional model of the ventricular cardiomyocyte with stochastic gating of RyR2 channels and determined the impact of cytosolic and SR Ca^{2+} concentrations, basal inward-rectifier K^+ current density, and gap junction conductance on DADs and triggered activity using this model. Likewise, Wescott et al. (2016) developed a mathematical whole-cell model, incorporating realistic stochastic gating of LTCCs and RyRs to investigate excitation-contraction coupling and Ca^{2+} -spark fidelity. Recently, Colman et al. (2017) developed a detailed three-dimensional multiscale model of a ventricular cardiomyocyte based on scanning electron microscopy data to examine the effects of a realistic SR structure on pro-arrhythmic Ca^{2+} dynamics, alternans, and SCaEs. Song et al. (2018) also investigated the influence of subcellular structure on Ca^{2+} -handling in a model with a three-dimensional network of CRUs representing different transverse tubule network structures, including uniform and random distribution of transverse tubules, to investigate Ca^{2+} sparks, DADs, and triggered activities. However, these studies were primarily done in ventricular cardiomyocytes, which have well-established differences in subcellular structures, notably the configuration and number of axial tubules and a different composition of ion channels from atrial cardiomyocytes.

Here, we developed an atrial cardiomyocyte model with atrial-specific subcellular structure and electrophysiology that can simulate multiple physiological properties of cardiomyocyte Ca^{2+} -handling, as well as proarrhythmic Ca^{2+} -handling abnormalities. This model has an intermediate level of detail, incorporating heterogeneous distributions of Ca^{2+} -handling proteins with micrometer resolution, a level that is of the same order of magnitude as the experimental information about the distributions obtained with confocal imaging. This level of detail is highly suitable to study the structural determinants of whole-cell Ca^{2+} -handling abnormalities that are relevant for arrhythmogenesis. Moreover, because of its relatively modest computational complexity, this model can also be employed in future studies to investigate the determinants of triggered activity at the tissue level, something that is not possible with the previously developed, highly detailed, three-dimensional models.

Potential Limitations

Our model with local Ca^{2+} -handling strongly suggested that the subcellular distribution of RyR2 and LTCC has a major impact on cardiomyocyte Ca^{2+} -handling. However, the model only considered a 2-dimensional representation of the cardiomyocyte, equivalent to a single slice from a z-stack. Previous computational studies using simpler 3-dimensional models have identified

that persistent Ca^{2+} waves can be generated through specific patterns of 3-dimensional Ca^{2+} -wave propagation (so-called “ping waves”) (Thul et al., 2012), suggesting a need to consider the 3-dimensional structure of cardiomyocytes. Furthermore, although we increased the spatial resolution of our previously published model (Voigt et al., 2014) in order to simulate the banded pattern of RyR2 expression, the resolution of the current model (units of $1 \mu\text{m}^2$) was insufficient to simulate local Ca^{2+} dynamics around a single Ca^{2+} -release unit (e.g., (sub)sparks). Detailed Ca^{2+} -release unit models have been developed (Hake et al., 2012; Zahradníkova and Zahradník, 2012; Walker et al., 2014) and could potentially be integrated in the present cell-level model in future studies, although this would significantly increase the computational complexity. Additionally, we acknowledge that our investigations into the effects of beta-adrenergic stimulation represent a highly simplified approach. Implementing a complete signaling pathway and its downstream effects on atrial electrophysiology, such as previously described for ventricular cardiomyocytes (Heijman et al., 2011) would be of interest, but was beyond the scope of the present study.

The resolution and quality of confocal imaging is limited by physical properties and quality of cell-isolation and antibody staining (particularly in rabbit samples). The use of super-resolution microscopy would be beneficial to obtain a more detailed overview of the 3-dimensional RyR2 distribution. In this case, dual staining of RyR2 and axial tubules should be performed to obtain information on both distributions in a single cardiomyocyte, which was not performed in the current study. Instead, a representative experimental axial tubule geometry from previously published work (Brandenburg et al., 2016) was used. Ideally, future experiments would be performed in human atrial cardiomyocytes to obtain a human-specific RyR2 distribution, rather than the rabbit atrial cardiomyocytes employed here, although their availability and cell-quality is generally much lower. Indeed, the experimental RyR2 distribution that formed the basis for the model with physiological RyR2 and LTCC distribution (Figure 10) was based on a limited number of rabbit atrial cardiomyocytes and may not be representative for diseased human atrial cardiomyocytes. Likewise, the current model requires stretching of the observed RyR2 expression pattern to match the 100×18 rectangular shape of the virtual cardiomyocyte. Finally, heterogeneous distributions of other Ca^{2+} -handling proteins such as NCX1 or SERCA2a may also impact whole-cell Ca^{2+} -handling and could be studied using the computational framework developed in the present study.

CONCLUSIONS

We employed the perfect control and observability provided by computer models to overcome experimental challenges in the analysis of the subcellular determinants of cardiomyocyte Ca^{2+} -handling. Our findings highlight the importance of atrial subcellular structures, especially RyR2 and LTCC distributions, in the genesis of SCaEs and DADs, which are well-known triggers

of cardiac arrhythmias. Importantly, whole-cell Ca^{2+} -handling properties are determined by non-linear interactions between heterogeneities in the properties (expression, phosphorylation) of both LTCC and RyR2, highlighting the need for detailed immunocytochemistry and functional studies to explain differences in whole-cell Ca^{2+} -handling properties between conditions.

AUTHOR CONTRIBUTIONS

HS, BvS, and JH conceived the study. PS, BvS, JH, MvZ, and GA performed and supervised the experiments. HS and JH performed the computational simulations and data analysis. HS and JH drafted the manuscript. All authors critically revised the manuscript and approved the final version.

REFERENCES

- Arora, R., Aistrup, G. L., Supple, S., Frank, C., Singh, J., Tai, S., et al. (2017). Regional distribution of T-tubule density in left and right atria in dogs. *Heart Rhythm* 14, 273–281. doi: 10.1016/j.hrthm.2016.09.022
- Best, J. M., and Kamp, T. J. (2012). Different subcellular populations of L-type Ca^{2+} channels exhibit unique regulation and functional roles in cardiomyocytes. *J. Mol. Cell. Cardiol.* 52, 376–387. doi: 10.1016/j.jmcc.2011.08.014
- Brandenburg, S., Kohl, T., Williams, G. S., Gusev, K., Wagner, E., Rog-Zielinska, E. A., et al. (2016). Axial tubule junctions control rapid calcium signaling in atria. *J. Clin. Invest.* 126, 3999–4015. doi: 10.1172/JCI88241
- Brundel, B. J. J. M., Henning, R. H., Kampinga, H. H., Van Gelder, I. C., and Crijns, H. J. G. M. (2002). Molecular mechanisms of remodeling in human atrial fibrillation. *Cardiovasc. Res.* 54, 315–324. doi: 10.1016/S0008-6363(02)00222-5
- Chen, P. S., Chen, L. S., Fishbein, M. C., Lin, S. F., and Nattel, S. (2014). Role of the autonomic nervous system in atrial fibrillation: pathophysiology and therapy. *Circ. Res.* 114, 1500–1515. doi: 10.1161/CIRCRESAHA.114.303772
- Chen-Izu, Y., McCulle, S. L., Ward, C. W., Soeller, C., Allen, B. M., Rabang, C., et al. (2006). Three-dimensional distribution of ryanodine receptor clusters in cardiac myocytes. *Biophys. J.* 91, 1–13. doi: 10.1529/biophysj.105.077180
- Chugh, S. S., Havmoeller, R., Narayanan, K., Singh, D., Rienstra, M., Benjamin, E. J., et al. (2014). Worldwide epidemiology of atrial fibrillation: a global burden of disease 2010 study. *Circulation* 129, 837–847. doi: 10.1161/CIRCULATIONAHA.113.005119
- Colman, M. A., Pinali, C., Trafford, A. W., Zhang, H., and Kitmitto, A., A (2017). Computational model of spatio-temporal cardiac intracellular calcium handling with realistic structure and spatial flux distribution from sarcoplasmic reticulum and t-tubule reconstructions. *PLoS Comput. Biol.* 13:e1005714. doi: 10.1371/journal.pcbi.1005714
- Dan, P., Lin, E., Huang, J., Bilin, P., and Tibbets, G. F. (2007). Three-dimensional distribution of cardiac $\text{Na}^+/\text{Ca}^{2+}$ exchanger and ryanodine receptor during development. *Biophys. J.* 93, 2504–2518. doi: 10.1529/biophysj.107.104943
- Dibb, K. M., Clarke, J. D., Eisner, D. A., Richards, M. A., and Trafford, A. W. (2013). A functional role for transverse (t-) tubules in the atria. *J. Mol. Cell. Cardiol.* 58, 84–91. doi: 10.1016/j.jmcc.2012.11.001
- Dobrev, D., and Wehrens, X. H. (2014). Role of RyR2 phosphorylation in heart failure and arrhythmias: controversies around ryanodine receptor phosphorylation in cardiac disease. *Circ. Res.* 114, 1311–1319. discussion: 1319. doi: 10.1161/CIRCRESAHA.114.300568
- Dyba, M., Jakobs, S., and Hell, S. W. (2003). Immunofluorescence stimulated emission depletion microscopy. *Nat. Biotechnol.* 21, 1303–1304. doi: 10.1038/nbt897
- Enriquez, A., Antzelevitch, C., Bismah, V., and Baranchuk, A. (2016). Atrial fibrillation in inherited cardiac channelopathies: from mechanisms to management. *Heart Rhythm* 13, 1878–1884. doi: 10.1016/j.hrthm.2016.06.008
- Galice, S., Xie, Y., Yang, Y., Sato, D., and Bers, D. M. (2018). Size matters: ryanodine receptor cluster size affects arrhythmogenic sarcoplasmic reticulum calcium release. *J. Am. Heart Assoc.* 7:e008724. doi: 10.1161/JAHA.118.008724
- Goette, A., Kalman, J. M., Aguinaga, L., Akar, J., Cabrera, J. A., Chen, S. A., et al. (2016). EHRA/HRS/APHRS/SOLAECE expert consensus on atrial cardiomyopathies: definition, characterization, and clinical implication. *Europace* 18, 1455–1490. doi: 10.1093/europace/euw161
- Greiser, M., Kerfant, B. G., Williams, G. S., Voigt, N., Harks, E., Dibb, K. M., et al. (2014). Tachycardia-induced silencing of subcellular Ca^{2+} signaling in atrial myocytes. *J. Clin. Invest.* 124, 4759–4772. doi: 10.1172/JCI70102
- Hake, J., Edwards, A. G., Yu, Z., Kekenes-Huskey, P. M., Michailova, A. P., McCammon, J. A., et al. (2012). Modelling cardiac calcium sparks in a three-dimensional reconstruction of a calcium release unit. *J. Physiol.* 590, 4403–4422. doi: 10.1113/jphysiol.2012.227926
- Heijman, J., Erfanian Abdoust, P., Voigt, N., Nattel, S., and Dobrev, D. (2016b). Computational models of atrial cellular electrophysiology and calcium handling, and their role in atrial fibrillation. *J. Physiol.* 594, 537–553. doi: 10.1113/JP271404
- Heijman, J., Schirmer, I., and Dobrev, D. (2016a). The multiple proarrhythmic roles of cardiac calcium-handling abnormalities: triggered activity, conduction abnormalities, beat-to-beat variability, and adverse remodelling. *Europace* 18, 1452–1454. doi: 10.1093/europace/euv417
- Heijman, J., Voigt, N., Nattel, S., and Dobrev, D. (2014). Cellular and molecular electrophysiology of atrial fibrillation initiation, maintenance, and progression. *Circ. Res.* 114, 1483–1499. doi: 10.1161/CIRCRESAHA.114.302226
- Heijman, J., Volders, P. G., Westra, R. L., and Rudy, Y. (2011). Local control of beta-adrenergic stimulation: effects on ventricular myocyte electrophysiology and Ca^{2+} -transient. *J. Mol. Cell. Cardiol.* 50, 863–871. doi: 10.1016/j.jmcc.2011.02.007
- Hiess, F., Vallmitjana, A., Wang, R., Cheng, H., ter Keurs, H. E., Chen, J., et al. (2015). Distribution and function of cardiac ryanodine receptor clusters in live ventricular myocytes. *J. Biol. Chem.* 290, 20477–20487. doi: 10.1074/jbc.M115.650531
- Houser, S. R. (2014). Role of RyR2 phosphorylation in heart failure and arrhythmias: protein kinase A-mediated hyperphosphorylation of the ryanodine receptor at serine 2808 does not alter cardiac contractility or cause heart failure and arrhythmias. *Circ. Res.* 114, 1320–1327. discussion: 1327. doi: 10.1161/CIRCRESAHA.114.300569
- Hove-Madsen, L., Llach, A., Bayes-Genis, A., Roura, S., Rodriguez Font, E., Aris, A., et al. (2004). Atrial fibrillation is associated with increased spontaneous calcium release from the sarcoplasmic reticulum in human atrial myocytes. *Circulation* 110, 1358–1363. doi: 10.1161/01.CIR.0000141296.59876.87
- Kirk, M. M., Izu, L. T., Chen-Izu, Y., McCulle, S. L., Wier, W. G., Balke, C. W., et al. (2003). Role of the transverse-axial tubule system in generating calcium sparks and calcium transients in rat atrial myocytes. *J. Physiol.* 547, 441–451. doi: 10.1113/jphysiol.2002.034355

FUNDING

This work was supported by the Netherlands Organization for Scientific Research (ZonMW Veni 91616057 to JH).

ACKNOWLEDGMENTS

The authors thank Helma Kuijpers for her excellent technical assistance.

SUPPLEMENTARY MATERIAL

The Supplementary Material for this article can be found online at: <https://www.frontiersin.org/articles/10.3389/fphys.2018.01108/full#supplementary-material>

- Landstrom, A. P., Dobrev, D. and Wehrens, X. H. T. (2017). Calcium signaling and cardiac arrhythmias. *Circ. Res.* 120, 1969–1993. doi: 10.1161/CIRCRESAHA.117.310083
- Lenaerts, I., Bito, V., Heinzel, F. R., Driesen, R. B., Holemans, P., D'Hooge, J., et al. (2009). Ultrastructural and functional remodeling of the coupling between Ca^{2+} influx and sarcoplasmic reticulum Ca^{2+} release in right atrial myocytes from experimental persistent atrial fibrillation. *Circ. Res.* 105, 876–885. doi: 10.1161/CIRCRESAHA.109.206276
- Loughrey, C. M., Smith, G. L., and MacEachern, K. E. (2004). Comparison of Ca^{2+} release and uptake characteristics of the sarcoplasmic reticulum in isolated horse and rabbit cardiomyocytes. *Am. J. Physiol. Heart Circ. Physiol.* 287, H1149–H1159. doi: 10.1152/ajpheart.00060.2004
- MacLennan, D. H., and Chen, S. R. (2009). Store overload-induced Ca^{2+} release as a triggering mechanism for CPVT and MH episodes caused by mutations in RYR and CASQ genes. *J. Physiol.* 587, 3113–3115. doi: 10.1113/jphysiol.2009.172155
- Macquaire, N., Tuan, H. T., Hotta, J., Sempels, W., Lenaerts, I., Holemans, P., et al. (2015). Ryanodine receptor cluster fragmentation and redistribution in persistent atrial fibrillation enhance calcium release. *Cardiovasc. Res.* 108, 387–398. doi: 10.1093/cvr/cvv231
- McNutt, N. S., and Fawcett, D. W. (1969). The ultrastructure of the cat myocardium. II. Atrial muscle. *J. Cell Biol.* 42, 46–67.
- Morillo, C. A., Banerjee, A., Perel, P., Wood, D., and Jouven, X. (2017). Atrial fibrillation: the current epidemic. *J. Geriatr. Cardiol.* 14, 195–203. doi: 10.11909/j.issn.1671-5411.2017.03.011
- Morillo, C. A., Klein, G. J., Jones, D. L., and Guiraudon, C. M. (1995). Chronic rapid atrial pacing. Structural, functional, and electrophysiological characteristics of a new model of sustained atrial fibrillation. *Circulation* 91, 1588–1595.
- Muller, T., Schumann, C., and Kraegeloh, A. (2012). STED microscopy and its applications: new insights into cellular processes on the nanoscale. *Chem. Phys. Chem.* 13, 1986–2000. doi: 10.1002/cphc.201100986
- Musa, H., Lei, M., Honjo, H., Jones, S. A., Dobrzynski, H., Lancaster, M. K., et al. (2002). Heterogeneous expression of Ca^{2+} handling proteins in rabbit sinoatrial node. *J. Histochem. Cytochem.* 50, 311–324. doi: 10.1177/002215540205000303
- Roth, G. A., Huffman, M. D., Moran, A. E., Feigin, V., Mensah, G. A., Naghavi, M., et al. (2015). Global and regional patterns in cardiovascular mortality from 1990 to 2013. *Circulation* 132, 1667–1678. doi: 10.1161/CIRCULATIONAHA.114.008720
- Shan, J., Xie, W., Betzenhauser, M., Reiken, S., Chen, B. X., Wronska, A., et al. (2012). Calcium leak through ryanodine receptors leads to atrial fibrillation in 3 mouse models of catecholaminergic polymorphic ventricular tachycardia. *Circ. Res.* 111, 708–717. doi: 10.1161/CIRCRESAHA.112.273342
- Song, Z., Liu, M. B., and Qu, Z. (2018). Transverse tubular network structures in the genesis of intracellular calcium alternans and triggered activity in cardiac cells. *J. Mol. Cell. Cardiol.* 114, 288–299. doi: 10.1016/j.yjmcc.2017.12.003
- Tanaka, H., Masumiya, H., Sekine, T., Kase, J., Kawanishi, T., Hayakawa, T., et al. (2001). Involvement of Ca^{2+} waves in excitation-contraction coupling of rat atrial cardiomyocytes. *Life Sci.* 70, 715–726. doi: 10.1016/S0024-3205(01)01436-9
- Thul, R., Coombes, S., and Bootman, M. D. (2012). Persistence of pro-arrhythmic spatio-temporal calcium patterns in atrial myocytes: a computational study of ping waves. *Front. Physiol.* 3:279. doi: 10.3389/fphys.2012.00279
- Vincenti, A., Brambilla, R., Fumagalli, M. G., Merola, R., and Pedretti, S. (2006). Onset mechanism of paroxysmal atrial fibrillation detected by ambulatory Holter monitoring. *Europace* 8, 204–210. doi: 10.1093/europace/euj043
- Voigt, N., Heijman, J., Wang, Q., Chiang, D. Y., Li, N., Karck, M., et al. (2014). Cellular and molecular mechanisms of atrial arrhythmogenesis in patients with paroxysmal atrial fibrillation. *Circulation* 129, 145–156. doi: 10.1161/CIRCULATIONAHA.113.006641
- Voigt, N., Li, N., Wang, Q., Wang, W., Trafford, A. W., Abu-Taha, I., et al. (2012). Enhanced sarcoplasmic reticulum Ca^{2+} leak and increased $\text{Na}^{+}\text{-Ca}^{2+}$ exchanger function underlie delayed afterdepolarizations in patients with chronic atrial fibrillation. *Circulation* 125, 2059–2070. doi: 10.1161/CIRCULATIONAHA.111.067306
- Walker, M. A., Gurev, V., Rice, J. J., Greenstein, J. L., and Winslow, R. L. (2017). Estimating the probabilities of rare arrhythmic events in multiscale computational models of cardiac cells and tissue. *PLoS Comput. Biol.* 13:e1005783. doi: 10.1371/journal.pcbi.1005783
- Walker, M. A., Williams, G. S., Kohl, T., Lehnart, S. E., Jafri, M. S., Greenstein, J. L., et al. (2014). Superresolution modeling of calcium release in the heart. *Biophys. J.* 107, 3018–3029. doi: 10.1016/j.bpj.2014.11.003
- Wescott, A. P., Jafri, M. S., Lederer, W. J., and Williams, G. S. (2016). Ryanodine receptor sensitivity governs the stability and synchrony of local calcium release during cardiac excitation-contraction coupling. *J. Mol. Cell. Cardiol.* 92, 82–92. doi: 10.1016/j.yjmcc.2016.01.024
- Woo, S. H., Cleemann, L., and Morad, M. (2002). Ca^{2+} current-gated focal and local Ca^{2+} release in rat atrial myocytes: evidence from rapid 2-D confocal imaging. *J. Physiol.* 543, 439–453. doi: 10.1113/jphysiol.2002.024190
- Yue, X., Zhang, R., Kim, B., Ma, A., Philipson, K. D., and Goldhaber, J. I. (2017). Heterogeneity of transverse-axial tubule system in mouse atria: remodeling in atrial-specific $\text{Na}^{+}\text{-Ca}^{2+}$ exchanger knockout mice. *J. Mol. Cell. Cardiol.* 108, 50–60. doi: 10.1016/j.yjmcc.2017.05.008
- Zahradnikova, A., and Zahradnik, I. (2012). Construction of calcium release sites in cardiac myocytes. *Front. Physiol.* 3:322. doi: 10.3389/fphys.2012.00322

Conflict of Interest Statement: The authors declare that the research was conducted in the absence of any commercial or financial relationships that could be construed as a potential conflict of interest.

Copyright © 2018 Sutanto, van Sloun, Schönleitner, van Zandvoort, Antoons and Heijman. This is an open-access article distributed under the terms of the Creative Commons Attribution License (CC BY). The use, distribution or reproduction in other forums is permitted, provided the original author(s) and the copyright owner(s) are credited and that the original publication in this journal is cited, in accordance with accepted academic practice. No use, distribution or reproduction is permitted which does not comply with these terms.



Morphological Substrates for Atrial Arrhythmogenesis in a Heart With Atrioventricular Septal Defect

Robert S. Stephenson ^{1*}, Jack Rowley-Nobel ², Caroline B. Jones ³, Rafael Guerrero ⁴, Tristan Lowe ⁵, Jichao Zhao ⁶, Henggui Zhang ² and Jonathan C. Jarvis ⁷

¹ Comparative Medicine Lab, Institute of Clinical Medicine, Aarhus University, Aarhus, Denmark, ² School of Physics and Astronomy, University of Manchester, Manchester, United Kingdom, ³ Department of Cardiology, Alder Hey Children's Hospital, Liverpool, United Kingdom, ⁴ Department of Cardiac Surgery, Alder Hey Children's Hospital, Liverpool, United Kingdom, ⁵ Manchester X-ray Imaging Facility, Photon Science Institute, University of Manchester, Manchester, United Kingdom, ⁶ Auckland Bioengineering Institute, Auckland University, Auckland, New Zealand, ⁷ School of Sport and Exercise Sciences, Liverpool John Moores University, Liverpool, United Kingdom

OPEN ACCESS

Edited by:

Joseph L. Greenstein,
Johns Hopkins University,
United States

Reviewed by:

Thomas Hund,
The Ohio State University,
United States
Jussi Tapani Koivumäki,
Tampere University of Technology,
Finland

*Correspondence:

Robert S. Stephenson
robert.stephenson@clin.au.dk

Specialty section:

This article was submitted to
Computational Physiology and
Medicine,
a section of the journal
Frontiers in Physiology

Received: 30 April 2018

Accepted: 17 July 2018

Published: 23 August 2018

Citation:

Stephenson RS, Rowley-Nobel J,
Jones CB, Guerrero R, Lowe T,
Zhao J, Zhang H and Jarvis JC (2018)
Morphological Substrates for Atrial
Arrhythmogenesis in a Heart With
Atrioventricular Septal Defect.
Front. Physiol. 9:1071.
doi: 10.3389/fphys.2018.01071

Due to advances in corrective surgery, congenital heart disease has an ever growing patient population. Atrial arrhythmias are frequently observed pre- and post-surgical correction. Pharmaceutical antiarrhythmic therapy is not always effective, therefore many symptomatic patients undergo catheter ablation therapy. In patients with atrioventricular septal defects (AVSD), ablation therapy itself has mixed success; arrhythmogenic recurrences are common, and because of the anatomical displacement of the atrioventricular node, 3-degree heart block post-ablation is a real concern. In order to develop optimal and safe ablation strategies, the field of congenital cardiac electrophysiology must combine knowledge from clinical electrophysiology with a thorough understanding of the anatomical substrates for arrhythmias. Using image-based analysis and multi-cellular mathematical modeling of electrical activation, we show how the anatomical alterations characteristic of an AVSD serve as arrhythmogenic substrates. Using ex-vivo contrast enhanced micro-computed tomography we imaged post-mortem the heart of a 5 month old male with AVSD at an isometric spatial resolution of 38 μ m. Morphological analysis revealed the 3D disposition of the cardiac conduction system for the first time in an intact heart with this human congenital malformation. We observed displacement of the compact atrioventricular node inferiorly to the ostium of the coronary sinus. Myocyte orientation analysis revealed that the normal arrangement of the major atrial muscle bundles was preserved but was modified in the septal region. Models of electrical activation suggest the disposition of the myocytes within the atrial muscle bundles associated with the "fast pathway," together with the displaced atrioventricular node, serve as potential substrates for re-entry and possibly atrial fibrillation. This study used archived human hearts, showing them to be a valuable resource for the mathematical modeling community, and opening new possibilities for the investigations of arrhythmogenesis and ablation strategies in the congenitally malformed heart.

Keywords: arrhythmias cardiac, atrial fibrillation (AF), re-entry, micro-computed tomography, mathematical modeling, myocyte orientation, congenital heart disease (CHD), atrioventricular septal defect

INTRODUCTION

The competency and success of corrective surgery is ever improving, as a result congenital heart disease has an ever growing patient population, with adults now outnumbering children (Khairy, 2008). Despite this, atrial arrhythmias are frequently observed pre- and post-surgical correction. Patients with atrioventricular septal defect (AVSD) or atrioventricular canal defect (AVCD) have a common atrioventricular connection, this occurs due to incorrect fusion of the endocardial cushions with the atrial septum and muscular ventricular septum (Anderson et al., 2000, 2008). Preoperative electrophysiological studies of AVSD patients have shown cases of atrioventricular re-entrant tachycardia (Khairy et al., 2007), atrial fibrillation (Daliento et al., 1991; Khairy et al., 2006) and supra-Hisian first degree AV block, and confirm inter-nodal conduction delay in the majority of patients (Fournier et al., 1986). Persistent AV block is present in up to 7% of patients in the immediate post-operative period and approximately 2% on follow up (Daliento et al., 1991; Boening et al., 2002), with atrial fibrillation or flutter noted in 5% of patients after surgical repair (Vetter and Horowitz, 1982; Daliento et al., 1991). Many symptomatic patients undergo catheter ablation therapy with varying success, arrhythmogenic recurrences are common. During ablation therapy the interventional cardiologist will target the major muscle bundles believed to be responsible for the inter-nodal conduction disturbance. These bundles have been described previously based on their anatomical appearance and the alignment of the myocyte chains within them (James, 1963; Merideth and Titus, 1968; Sanchez-Quintana et al., 1997). More recently these pathways have been described based on their electrophysiology using optical mapping, and are described in the context of the so-called dual pathway physiology (Hucker et al., 2008; Mani and Pavri, 2014; George et al., 2017). The pathways are termed the “slow” and “fast” pathways; in the healthy heart the “fast” pathway is the dominant conduction pathway between the sinus node and atrioventricular node. Anatomically the fast pathway courses the anterior-superior aspect of the inter-atrial septum and is associated proximally with the terminal crest and distally with the transitional cells surrounding the compact AV node [(Mani and Pavri, 2014; George et al., 2017); **Figure 1A**]. Conversely, the “slow” pathway has a less direct course, it runs inferior to the coronary sinus ostium and fossa ovalis, and is associated with the flutter isthmus and the inferior nodal extension. In AVSD the atrioventricular node is displaced. The compact atrioventricular node no longer lies at the apex of the triangle of Koch (**Figure 1A**), but in a posterior-inferior position, anterior to the ostium of the coronary sinus at the point where the posterior-inferior rims of muscular ventricular and atrial septa join [(Moorman et al., 1998); **Figure 1B**]. This inevitably changes the anatomical course of the “fast” and “slow” pathways (**Figure 1B**). Conduction disturbances in AVSD patients are associated with prolonged inter-nodal conduction times and numerous conduction disturbances (Waldo et al., 1973; Jacobsen et al., 1976; Fournier et al., 1986; Khairy et al., 2006), presumably because the inter-nodal muscle bundles are distorted or modified as they course the atria (Waldo et al., 1973).

Inter-nodal conduction is thus dictated by the location of the nodal tissues and the muscle bundles connecting them. In order to develop optimal and safe ablation strategies for congenitally malformed hearts, the field of congenital cardiac electrophysiology requires an integration of clinical electrophysiology with a thorough understanding of the anatomical substrates for arrhythmias. Guided by the available clinical electrophysiological data we hypothesize that anatomical displacement of the compact atrioventricular node and modification of the dual pathway physiology act as substrates for arrhythmogenesis in AVSD patients. We use image data acquired by micro-computed tomography (micro-CT), as described previously (Stephenson et al., 2012, 2017), to extract myocyte orientation and to identify the 3D disposition of the nodal tissue for the first time in an intact heart with AVSD. This information is then incorporated into electrophysiologically accurate mathematical models of electrical activation to assess the influence of these anatomical alterations on inter-nodal conduction. This study also demonstrates the suitability of long term stored archived human hearts as a resource for the mathematical modeling community in investigations of arrhythmogenesis in the congenitally malformed heart.

METHODS

Ethical Approval Statement

We obtained NHS ethical approval to scan congenitally malformed samples from the Alder Hey archive in Liverpool UK. Samples had been consented and placed in the archive in the 1970s.

Sample Preparation

We chose a sample from the archive free of clotted blood, and probably perfused via the coronary circulation prior to fixation. The sample was from a male who died aged 5 months, and has been in storage for approximately 50 years since the 1970s. The heart dimensions; max length ~70 mm, max width ~55 mm. The sample was prepared for scanning by immersion in 3.75% iodine/potassium iodide (I_2KI) in PBFS for 2 weeks, refreshing the solution at 1 week (Stephenson et al., 2017). Iodine molecules are progressively and differentially absorbed by the tissues, permitting discrimination of fat, working myocardium, conducting tissues, and fibrous tissue.

Scanning

The sample was scanned in the Nikon Metris XTEK 320 kV Custom Bay at the Manchester X-Ray Imaging Facility, University of Manchester, as previously described by Stephenson et al. (2012, 2017). Prior to scanning the sample was drained and rinsed in saline to remove excess contrast agent. Plastic wrap provided containment of the tissue, and maintained the original shape of the sample. The heart was immobilized in a plastic tube to reduce movement during the imaging process. Scans were acquired with an X-ray energy of ~95 kV. 360° scans were performed and data was collected from 3142 projections. A tungsten target was used for all scans, with a 0.25 mm aluminum filter. Total scan times were approximately 50 min.

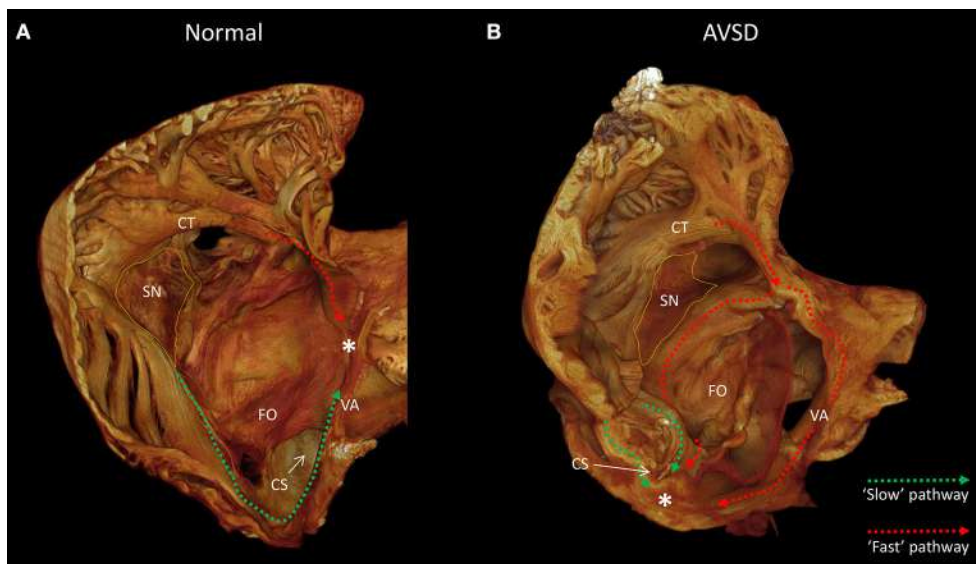


FIGURE 1 | The anatomy of the slow and fast pathways in the right atrium. **(A)** indicates the anatomical locations of the slow pathway (green), fast pathway (red), and compact atrioventricular node (*) in the normal heart, viewed from inferior-lateral position. **(B)** indicates the hypothesized anatomical location of the slow pathway (green) and fast pathway (red) in a heart with an atrioventricular septal defect, note the compact atrioventricular node (*) is displaced posterior-inferiorly. Images derived from micro-CT data. *Location of compact atrioventricular node; CS, coronary sinus; CT, terminal crest; FO, fossa ovalis; SN, sinus node; VA, valve annulus.

Data was reconstructed using filtered back-projection, resulting in tomographic image data with an isotropic voxel size of $38.5 \times 38.5 \times 38.5 \mu\text{m}$. After scanning, the sample was placed back in to formaldehyde solution to allow passive removal of the iodine.

Image Analysis

The datasets were examined using Amira (5.3.3) and analyzed using objective semi-automatic segmentation methods as described previously (Jarvis and Stephenson, 2013; Stephenson et al., 2017). Muscle bundles associated with the slow and fast pathways along with the terminal crest and common valve annulus were segmented based on the ability to visualize and trace the longitudinal chains of myocyte in the individual muscle bundles using the micro-CT image data. The specialized tissues of the cardiac conduction system were segmented based on their differential attenuation. The electrophysiological block zone, a region of slow conductance between the sinus node and atrial septum, was subjectively placed based on previous representations (Boyett et al., 2000). Myocyte orientation was extracted from the micro-CT data using eigen analysis of the 3D structure tensor as described previously (Ni et al., 2013). To generate myocyte orientation files the raw data was first down-sampled to a spatial resolution of 0.15 mm.

Modeling

To generate a geometrical model for the modeling protocols the raw data was down-sampled to an isotropic spatial resolution of 0.15 mm, which is close to the length of atrial myocytes. Virtual suturing of the dissected borders was

performed prior to modeling, such regions were assigned atrial electrophysiological characteristics. Muscle bundle and whole atria electrical activation was modeled using the Coleman-Ni-Zhang (CNZ) model (Ni et al., 2017). In this study cells of the conduction system and the segmented muscle bundles were all assigned as “CT” type. The cells of the atrial working myocardium were assigned as “RA” type. Cells in the region labeled as the “block zone” were assigned as “RA” type but with reduced excitability, this was achieved by reducing their calcium and sodium conductance to 50%. The diffusion parameters were set to a ratio of 8:1 (along the myocyte chain:perpendicular to the myocyte chain). Diffusion coefficients and spatial resolution gave a conduction velocity of 68.2 cm/s for the RA cells. This is within the range of (70.2 ± 9.9) cm/s measured experimentally in RA cells (Kojodjojo et al., 2006). A series of external stimuli with an amplitude of 20 pA/pF and a duration of 2 ms were applied to the sinus node cells in the standard protocols. At fast pacing rates, stimuli with an amplitude of 40 pA/pF and a duration of 4 ms were implemented. During the pacing protocols various S1-S2 intervals were investigated, these ranged from 250 to 400 ms.

RESULTS

Morphological Analysis by Micro-Computed Tomography

The contrast enhanced micro-CT data allowed fast and unequivocal classification of the congenital malformation. We confirmed the heart to have an atrioventricular septal defect with common atrioventricular junction

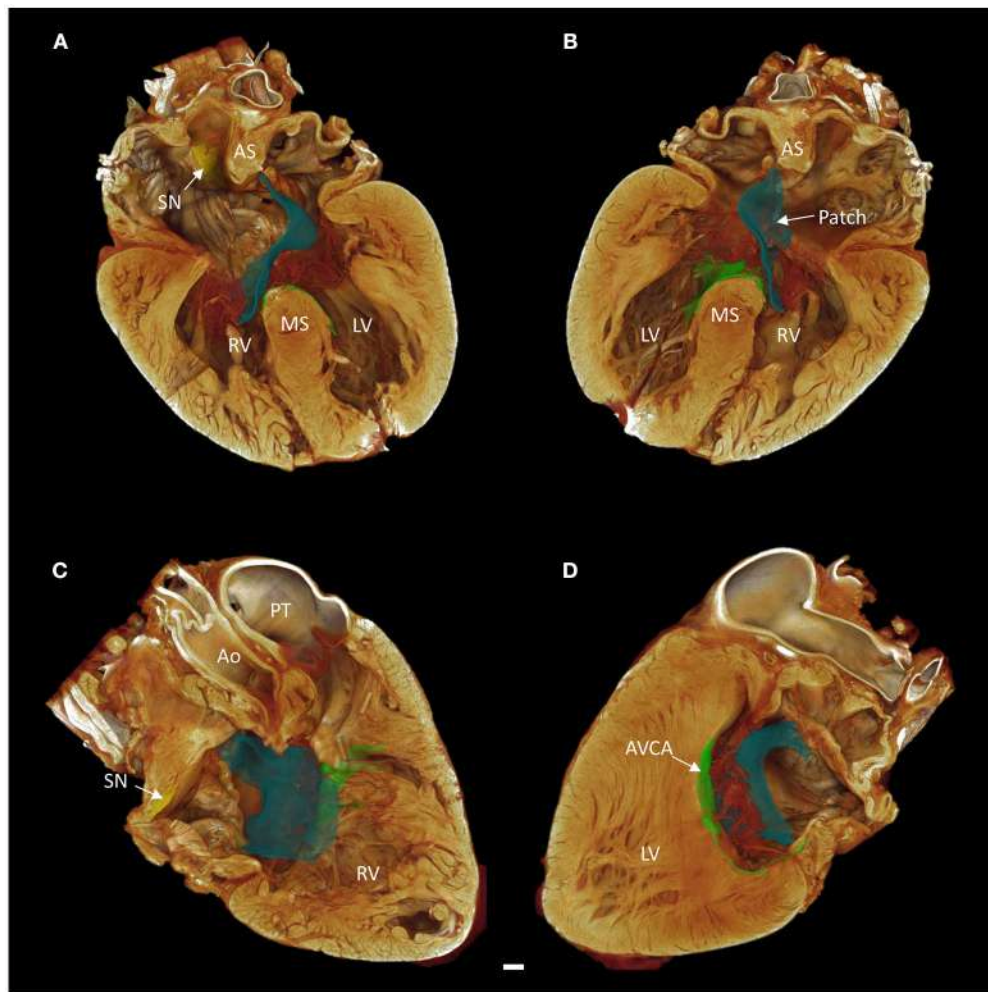


FIGURE 2 | Long axis volume renderings of a heart with atrioventricular septal defect (AVSD). **(A)** Anterior 4-chamber view, **(B)** posterior 4-chamber view, **(C)** right side two-chamber view, **(D)** left side two-chamber view. The sinus node is shown in yellow, the atrioventricular conduction axis in green, and the surgical patch in blue. Images derived from micro-CT data. Ao, aorta; AS, atrial septum; AVCA, atrioventricular conduction axis; LV, left ventricle; MS, muscular ventricular septum; PT, pulmonary trunk; RV, right ventricle; SN, sinus node. Scale bar represents 3 mm.

and aligned atrial and muscular ventricular septa (Figure 2).

Contrast enhancement permitted discrimination of multiple tissue types based on their differential attenuation of the x-ray source. As a result of differential iodine absorption; fat, myocardium, nodal tissues, and connective tissue presented decreasing voxel values respectively (Figure 3). The sinus node was located as a low attenuating (low voxel values) area in the intercaval region (Figures 1–3). The sinus node was seen to give off complex projections into the surrounding working myocardium, with a less pronounced paranodal region than that which is seen in the adult heart (Figure 3B). The compact atrioventricular node was notably displaced from its usual position at the apex of the triangle of Koch. The node was found in a posterior-inferior position anterior to the ostium of the coronary sinus at the point where the posterior-inferior rims of the muscular ventricular and atrial septa join, and was

therefore housed in the inferior nodal triangle (Figures 1–4). The atrioventricular conduction axis (AVCA) and the proximal aspects of the right and left bundle branches could also be identified based on their differential attenuation (Figures 3D, 4). The conduction axis was seen to take a long and tortuous path across the crest of the muscular ventricular septum, with the proximal connection between the compact node and the axis appearing quite tenuous. The sinus node and atrioventricular compact node could be identified objectively in both the micro-CT image data (Figure 3) and the derived volume renderings (Figure 1). This is the first time the 3-dimensional disposition of the cardiac conduction system has been presented in a heart with AVSD.

It was apparent the heart had undergone attempted correctional surgery, namely the implantation of a surgical patch. This patch itself and the accompanying pledges and suture lines could be identified in the micro-CT data

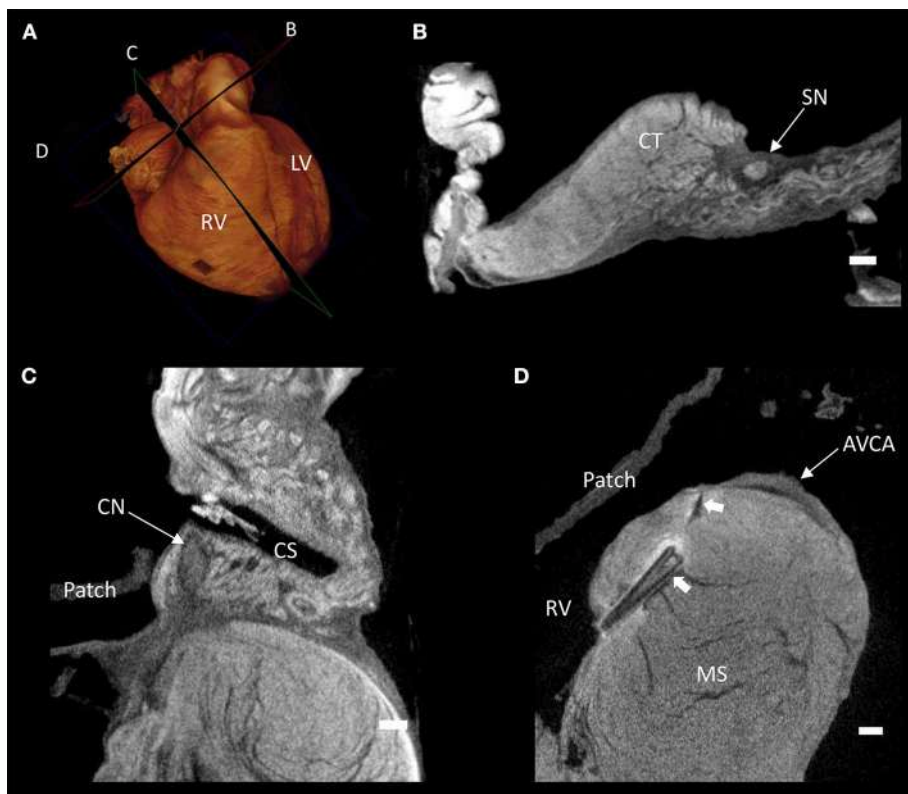


FIGURE 3 | Virtual histology of the cardiac conduction system in a heart with atrioventricular septal defect (AVSD). **(A)** Volume rendering of the whole heart illustrating the virtual cutting planes used in **(B–D)**. **(B)** Short axis micro-CT section of the sinus node, **(C)** two-chamber micro-CT section of the compact atrioventricular node, **(D)** 4-chamber micro-CT section of the atrioventricular conduction axis. AVCA, atrioventricular conduction axis; CN, compact atrioventricular node; CS, coronary sinus; CT, terminal crest; LV, left ventricle; MS, muscular ventricular septum; RV, right ventricle; SN, sinus node; solid arrow heads- plegget and suture line. Scale bars represents 1 mm.

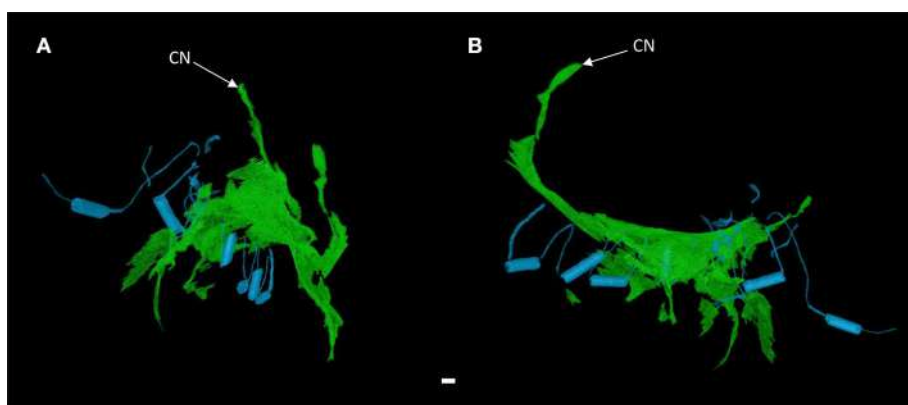


FIGURE 4 | 3-dimensional rendering of the atrioventricular conduction axis in a heart with atrioventricular septal defect (AVSD). Showing the conduction axis (green) and the surgically placed pledgets and sutures (blue) in anterior **(A)** and right lateral views **(B)**. Images derived from segmentation of micro-CT data. CN, compact atrioventricular node. Scale bar represents 1 mm.

(**Figures 3C,D**), and subsequently segmented and presented in 3-dimensions (**Figures 2, 4**). The patch had been attached superiorly at the free inferior margin of the atrial septum, which itself appeared hypoplastic. Inferiorly the pledgets and suture

lines were placed deep into the right-hand aspect of the muscular ventricular septum. The sutures appeared to pass directly through the nodal tissue, particularly the right bundle branch (**Figures 3D, 4**).

The high resolution micro-CT data allowed the major muscle bundles of the atria to be identified and separated objectively based on their relatively parallel myocyte orientation. The terminal crest, Bachmann's bundle, common valve annulus and the bundles associated with the “slow” and “fast” pathways were segmented (Figures 5, 6). These bundles collectively formed a continuous “circuit” (Figures 5, 6). Note, the region normally associated with the distal aspect of the “fast” pathway showed a continuous connection with the common valve annulus and a distinct muscle bundle traversing the atrial septum (Figures 1B, 5, 6: red dotted lines). The mean orientation of the myocyte chains could be appreciated by following longitudinal features in volume renderings (Figures 1, 5, 6) and in the micro-CT image data (Figure 3B). Myocyte orientation analysis (see methods for details) confirmed that the mean orientation of the myocyte chains followed the long axis of these identified muscle bundles.

Mathematical Modeling

NB: When describing the modeling results in the AVSD heart we use the term “slow” and “fast” pathway based on the traditional identification of their anatomical position in the normal human heart, this is not a reflection of their conduction time.

We performed mathematical modeling of the wave of electrical depolarisation in both the isolated muscle bundles and the whole atria. We used a multi-cellular approach, with different models used for the sinus node, block zone, muscle bundles, and the atrial myocardium (see methods). The results of the myocyte orientation analysis were also incorporated into the models by allowing for faster conduction in the long axis of the myocytes than in the orthogonal directions (anisotropic conduction).

Activation maps (comprising isochrones) of the isolated muscle bundles showed that the fastest route to the atrioventricular compact node in this heart was via the

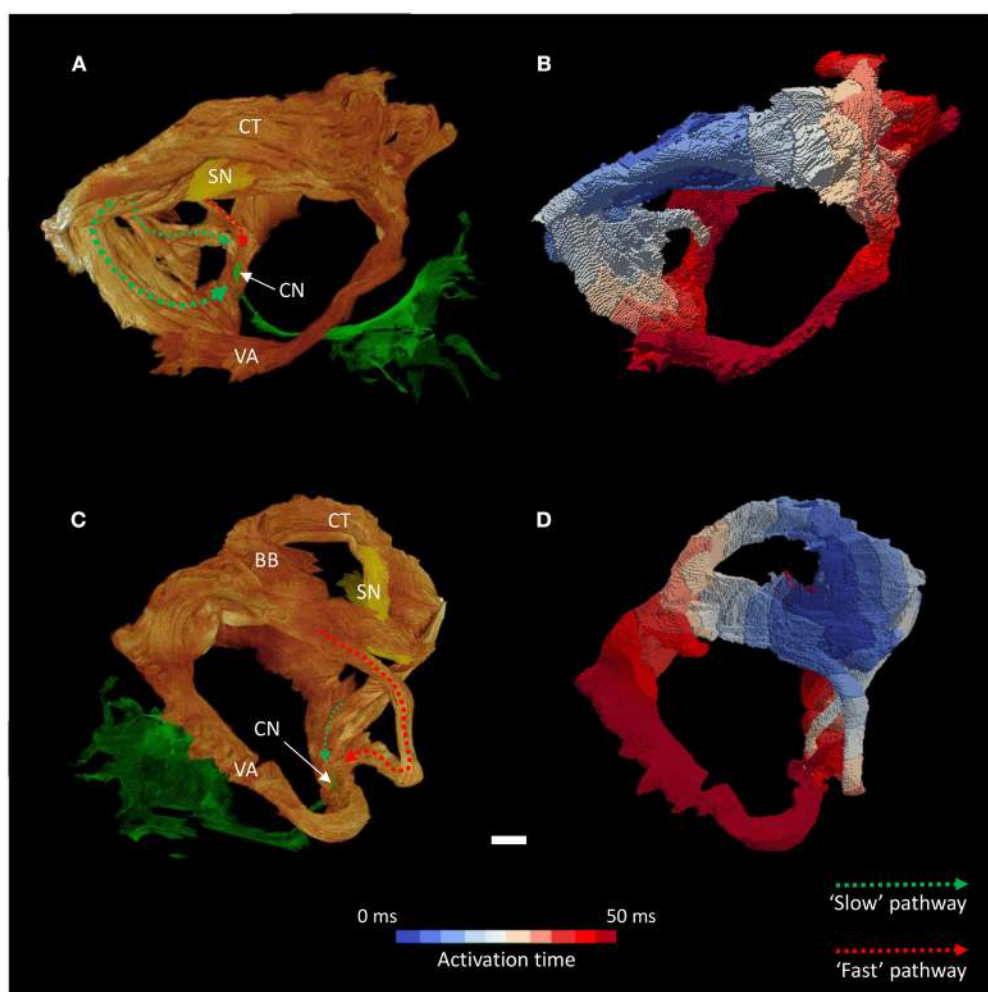


FIGURE 5 | Inter-nodal conduction through the atrial muscle bundles I. Volume renderings of the atrial muscle bundles in right lateral (A) and left lateral (C) views, the normal location and direction of the “slow” pathway (green), and the septal aspect of the elongated “fast” pathway (red) are indicated by dotted arrows. (B,D) Display the corresponding electrical activation maps, showing excitation of the distal aspect of the region normally associated with the “slow” pathway precedes that of the “fast” pathway. See methods for modeling parameters. BB, Bachmann's bundle; CN, compact atrioventricular node; CT, terminal crest; SN, sinus node; VA, valve annulus. Scale bar represents 3 mm.

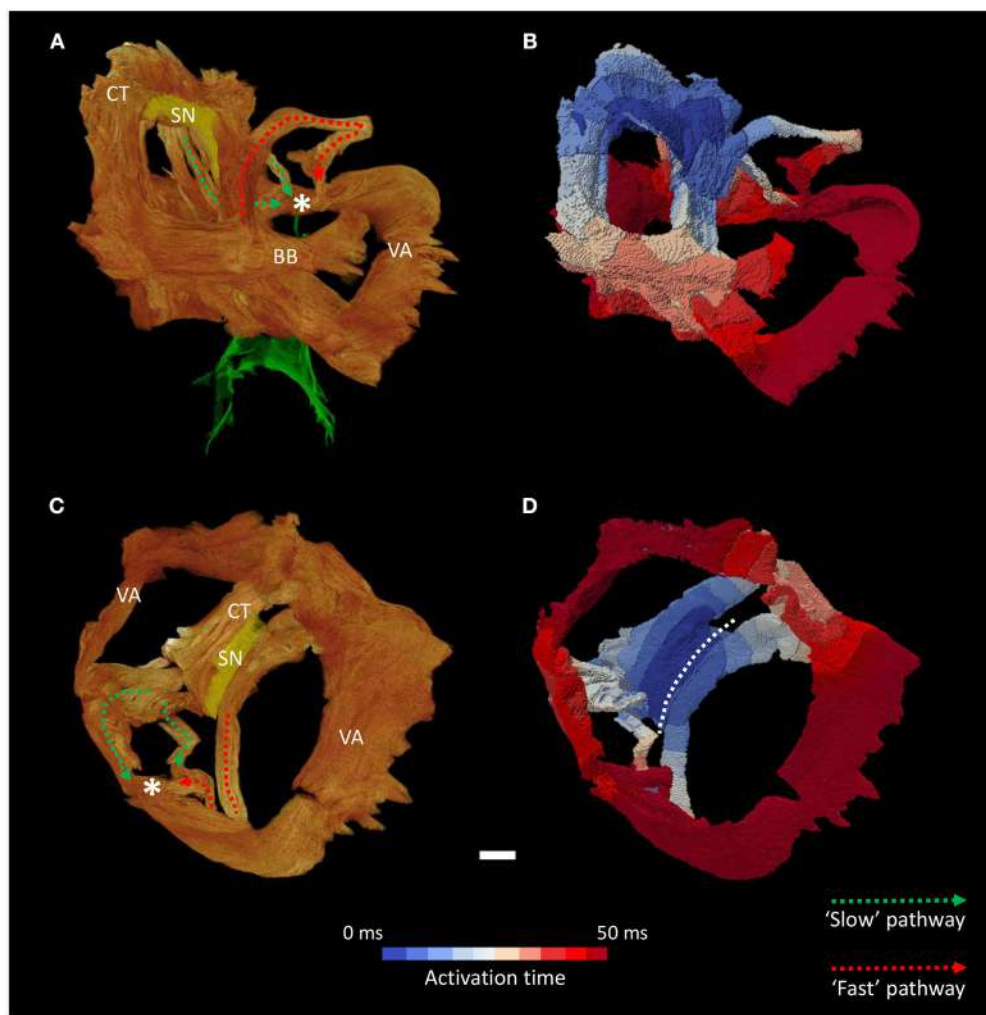


FIGURE 6 | Inter-nodal conduction through the atrial muscle bundles II. Volume renderings of the atrial muscle bundles in anterior (A) and inferior (C) views, the normal location and direction of the “slow” pathway (green), and the septal aspect of the elongated “fast” pathway (red) are indicated by dotted arrows. (B,D) Display the corresponding electrical activation maps, showing excitation of the distal aspect of the region normally associated with the “slow” pathway precedes that of the “fast” pathway. See methods for modeling parameters. *Location of compact atrioventricular node; BB, Bachmann’s bundle; CT, terminal crest; SN, sinus node; VA, valve annulus. Scale bar represents 3 mm.

“slow” pathway (Figures 5, 6). This is also clearly illustrated in **Supplementary Video 1**. The “fast” pathway connects with the compact node via the common valve annulus and a distinct septal muscle bundle traversing the atrial septum. Activation via this septal bundle arrived at the node 5–10 ms after the “slow” pathway (Figures 5, 6). The results therefore reflect a switch or flipping of the usual dual pathway physiology. The valve annulus provided the slowest route toward the compact node, and its activation was annihilated by stimulation via the “slow” and “fast” pathways in an anti-clockwise direction (**Supplementary Video 1**). These results were not affected by the presence or absence of the “block zone.”

Whole atrial modeling showed synchronous activation of the right and left atrial appendages and inter-atrial conduction preferentially via Bachmann’s bundle. The results described above for the conspicuous muscle bundles were mirrored

when modeling the whole atria, with the fastest route to the atrioventricular compact node seen to be via the “slow” pathway (Figure 7 and **Supplementary Video 2**). **Figure 7** suggests the “fast” pathway would be the preferential pathway to the compact node were the node housed in the “normal” location (Figures 7B–D- red asterisk). Pacing of the whole atria with a 400 ms stimulus interval brought about normal sequential atrial activation. S2 intervals <300 ms brought about atrial conduction block, with stimulus of the sinus node failing to elicit activation of the whole atria. In these scenarios the stimulus to atrial activation ratio approached 2:1. An S2 interval of 300 ms did, however, elicit atrial activation, but preferential activation of the compact node was no longer via the “slow” pathway. Preferential conductance and subsequent activation of the nodal region was provided by the “fast” pathway (Figures 8B,C). Nodal activation was followed by retrograde propagation up the “slow pathway” (Figure 8C).

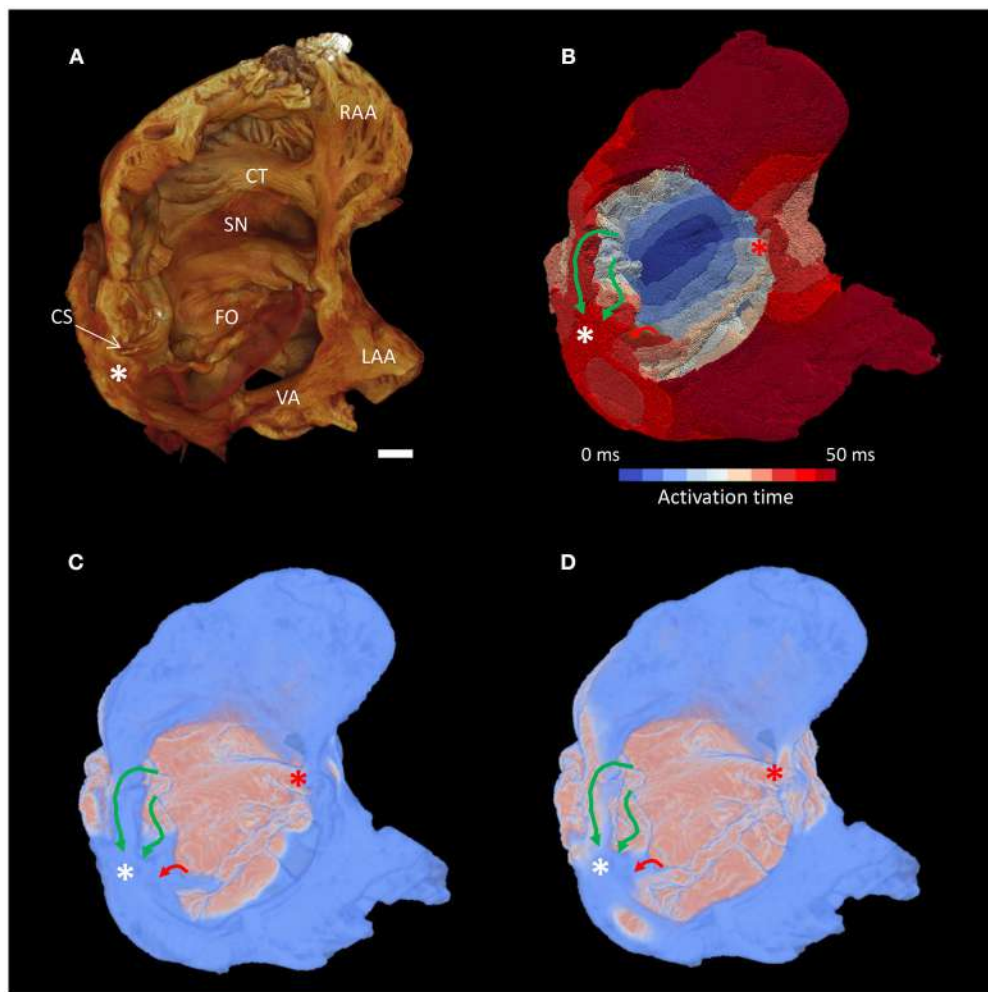


FIGURE 7 | Preferential inter-nodal conduction via the “slow” pathway in the atria of a heart with AVSD. **(A)** Volume rendering of the atrial cavity viewed from the inferior-lateral position. **(B)** Corresponding isochrone electrical activation map, the normal location and direction of the “slow” pathway (green), and the septal aspect of the elongated “fast” pathway (red) are indicated by solid arrows. **(C,D)** Snapshots taken from the **Supplementary Video 2** showing excitation of the distal aspect of the region normally associated with the “slow” pathway precedes that of the “fast” pathway, pink indicates activated myocardium, light blue indicates dormant myocardium. See methods for modeling parameters. White*, location of compact atrioventricular node in AVSD heart; Red*, approximate location of compact atrioventricular node in normal heart; CS, coronary sinus; CT, terminal crest; FO, fossa ovalis; LAA, left atrial appendage; RAA, right atrial appendage; SN, sinus node; VA, valve annulus. Scale bar represents 3 mm.

As a result the muscle bundles associated with “fast” pathway emerged from their refractory period before those of the “slow” pathway (Figure 8D). The pacing data presented in Figure 8 is presented as an animation in **Supplementary Video 3**.

DISCUSSION

In this study we show that contrast enhanced micro-CT is an effective non-destructive method for producing high-resolution, high-fidelity, 3-dimensional images of archived human hearts. From these images the 3-dimensional disposition of the cardiac conduction system and the complex arrangement of the myocyte chains can be resolved and quantified. To the best of our knowledge this is the first time such data has been presented for a heart with an AVSD. This high-resolution micro-anatomical

data was then used to inform mathematical models of electrical activation, offering a potential stepwise change in the structural fidelity of such models. The resultant simulations are comparable to *in-vivo* clinical assessment of electrophysiology in AVSD patients, suggesting this is a viable technique for the investigation of arrhythmogenesis in congenitally malformed hearts *ex-vivo*.

The Competencies of Micro-Computed Tomography

The nature of micro-CT data means that the morphological structure of this precious archived sample is forever preserved. This data is digital and thus will not degrade over time, and can be easily distributed and visualized using open source software. Thus, anatomists, surgeons, cardiologists, engineers, and teachers can easily make use of this new information.

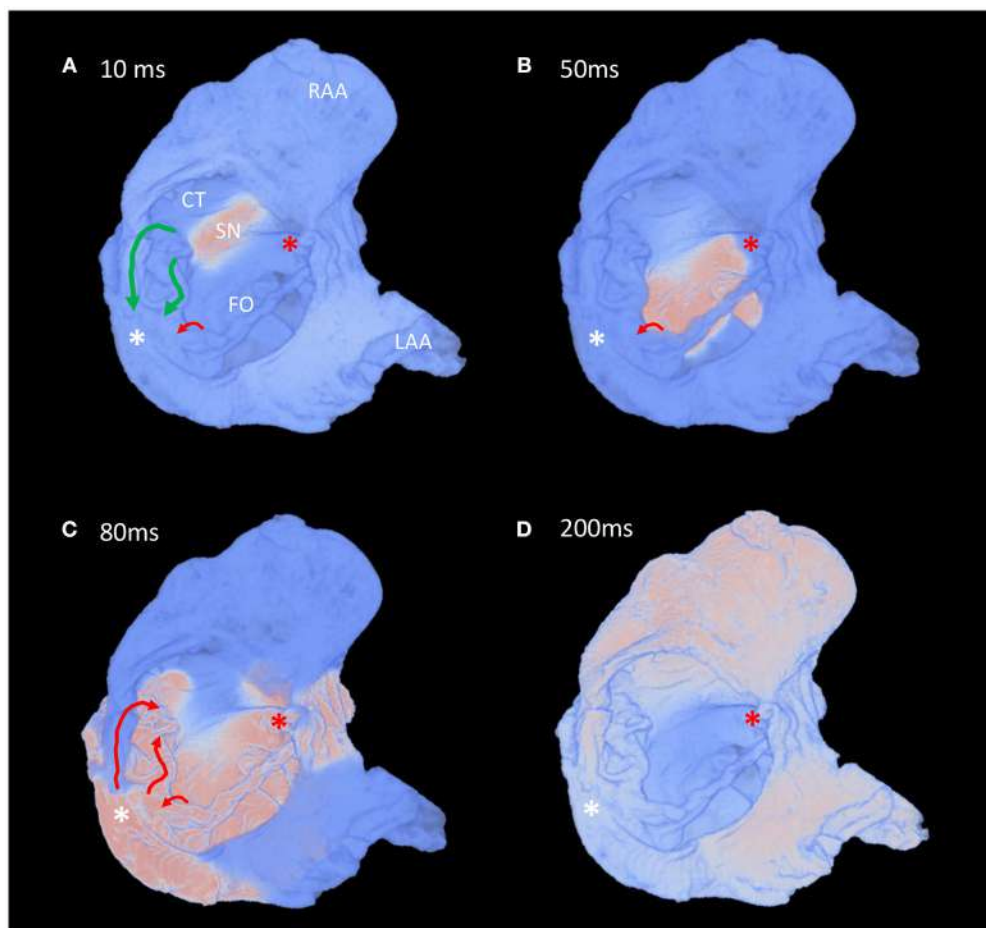


FIGURE 8 | Fast pacing elicits retrograde conduction via the “slow” pathway in the atria of a heart with AVSD. **(A–D)** Time-lapse snapshots taken from the **Supplementary Video 3** showing preferential inter-nodal conduction via the region normally associated with the “fast” pathway, and subsequent retrograde conduction up the “slow” pathway, during an atrial pacing protocol (s1-s2 interval 300 ms). Views are comparable to those presented in **Figure 7**. The normal location and direction of the “slow” pathway (green), and the septal aspect of the elongated “fast” pathway (red) are indicated by solid arrows. Pink indicates activated myocardium, light blue indicates dormant myocardium. See methods for modeling parameters. White*, location of compact atrioventricular node in AVSD heart; Red*, location of compact atrioventricular node in normal heart; CS, coronary sinus; CT, terminal crest; FO, fossa ovalis; LAA, left atrial appendage; RAA, right atrial appendage; SN, sinus node.

The micro-CT data allowed for fast diagnosis and classification of the defect. Virtual histology (**Figure 3**) and virtual dissection (**Figures 1, 2**) can be performed rapidly and non-destructively in an infinite number of planes. This has clear advantages over traditional destructive, laborious, and error prone techniques such as histology and blunt dissection. As described previously (Stephenson et al., 2012, 2017), contrast enhancement allowed the specialized cells of the cardiac conduction system to be resolved independent of the surrounding working myocardium and connective tissue. The disposition of the nodal tissues described in the present study is consistent with previous anatomical accounts of hearts with AVSD using traditional techniques (Anderson et al., 2000). Consistent with previous accounts in the adult human heart (Boyett et al., 2000; Sánchez-Quintana et al., 2005; Fedorov et al., 2010; Stephenson et al., 2017), the sinus node was irregular in

shape and occupied a large portion of the inter-caval region, and was seen to give off complex projections into the surrounding myocardium. The sinus node in the AVSD heart did however appear to have a less pronounced paranodal area compared with the adult (Chandler et al., 2011; Stephenson et al., 2017). The nature of the defect and the posterior-inferior displacement of the compact atrioventricular node made for an elongated AVCA, this has been described previously, and is thought to contribute to the prevalence of atrioventricular node block in these patients (Feldt et al., 1970; Anderson et al., 2000, 2008).

In the present study, and previously (Aslanidi et al., 2012; Ni et al., 2013; Stephenson et al., 2017), we have demonstrated how myocyte orientation can be extracted from high-resolution micro-CT data. Extraction of myocyte orientation is imperative to allow accurate modeling of cardiac electrical activation.

Conduction is known to be faster along a cardiomyocyte chain's longitudinal axis than across its short axis (Spach and Kootsey, 1983). The course of the cardiomyocyte chains and their aggregation into distinguishable muscle bundles, therefore, plays a crucial role in inter-nodal conduction. This is highlighted in modeling data presented in the current study (Figures 5–8), and illustrates the importance of the whole heart high-resolution data presented here.

Substrates for Arrhythmogenesis in a Heart With AVSD

NB: When describing the modeling results in the AVSD heart we use the term "slow" and "fast" pathway based on their anatomical position in the normal human heart, this is not a reflection of their conduction time.

The simulations of atrial activation produced in the present study show preferential activation of the compact atrioventricular node via the region normally associated with the "slow" pathway (Figures 5–7). This flipping of the dual pathway physiology is consistent with previous *in-vivo* three-dimensional electroanatomic mapping studies, in which the slowest pathway was located superior to AVCA, while the fastest pathway was identified posterior-inferior to the compact node (Khairy et al., 2007; Khairy and Balaji, 2009). The arrangement is best observed in the right hand and left hand views shown in Figure 5. This phenomenon is not surprising considering the displacement of the compact node implies a physical shortening of the "slow" pathway and a concomitant lengthening of the "fast" pathway (Figure 1). In this regard, we show how the distal aspect of the region normally associated with the "fast" pathway is continuous with a septal muscle bundle and the common valve annulus. Contrary to the findings of Khairy and associates (Khairy et al., 2007), our modeling data suggests conduction along the leftward aspect of the valve annulus is slow and is annihilated by the "slow" pathway (Supplementary Videos 1, 2). The preferential route for the "fast" pathway is, therefore, via the septal region. Our data therefore supports the suggestion of Waldo and associates that the middle and anterior (corresponding to the "fast" pathway) inter-nodal pathways may become distorted or modified due to the septal defect (Waldo et al., 1973).

The area anterior-inferior to the fossa ovale, which in the normal heart houses a distinct muscle bundle and the region of the inferior nodal extension, was seen to be hypoplastic and damaged by the suture placement associated with the patch implantation. This suggests, in this instance, that this region is not a viable route, and that inter-nodal conduction runs posterior-superior to the fossa ovale via a septal bundle. Patch placement in the ventricle can also have functional implications. It is hindered by the need to attach the patch to the right hand aspect of the muscular ventricular septum in order to close the defect. Fournier and associates observed right bundle branch block in 19 of 25 postoperative patients (Fournier et al., 1986). Right bundle branch block has historically been a problem in AVSD patients and the necessary placement of pledges and sutures in the current sample demonstrate the challenge facing the reconstructive surgical team (Figures 3D, 4). In this regard micro-CT data has potential implications in the planning of corrective surgery and ablation therapy, pathological

reporting, and for investigations into the history of surgical approaches.

Retrograde atrial activation via the fastest conducting pathway has been observed previously in AVSD patients (Khairy et al., 2007), and in this case cryomapping of the slowest conducting pathway can relieve the accompanying atrioventricular re-entry tachycardia (AVNRT). In the present study atrial pacing using a S2 interval of 300 ms elicited whole atrial activation, but preferential activation of the compact node was no longer via the "slow" pathway. Preferential conductance and subsequent activation of the nodal region was provided by the "fast" pathway (Figures 8B,C and Supplementary Video 3). Nodal activation was then followed by retrograde propagation up the "slow" pathway (Figure 8C and Supplementary Video 3). As a result the muscle bundles associated with "fast" pathway were seen to leave their refractory period before those of the "slow" pathway (Figure 8D and Supplementary Video 3). In this setting the dual pathway physiology therefore becomes desynchronised which could perpetuate both typical and atypical AVNRTs. This finding also provides reasoning for other electrical disturbances observed clinically, such as slow inter-nodal conduction, atrial fibrillation and atrioventricular block (Daliendo et al., 1991; Khairy et al., 2006). Furthermore, the data provides evidence to support ablation of the slowest conducting pathways in this setting.

Our findings suggest that displacement of the compact atrioventricular node and the accompanying structural modification of the dual pathway physiology provides morphological substrates for arrhythmogenesis in hearts with AVSD.

Future Perspectives

The methodologies and concepts presented in the current study provide the opportunity to investigate, and potentially resolve, controversies regarding the anatomical substrates for inter-nodal conduction (Anderson et al., 1981; Sanchez-Quintana et al., 1997; Hucker et al., 2008). Future studies using this dataset could include atrio-ventricular and whole heart modeling to investigate substrates and ablation strategies for ventricular tachycardia, atrioventricular block, and bundle branch block, all of which are frequently observed in this defect (Daliendo et al., 1991; Khairy, 2008; Khairy and Balaji, 2009). Furthermore, there are many other cardiac congenital malformations that are associated with specific electrical disturbances and arrhythmias. This study is a "proof of concept," opening the door for wide-scale investigation of arrhythmogenesis by topographical micro-anatomy combined with numerical simulation of electrical activity in the congenitally malformed heart.

STUDY LIMITATIONS

We recognize that this study lacks an age-matched healthy control to validate our findings, but such a sample would be extremely difficult to obtain. The major limitation of this study is the need to downsample the high-resolution information-rich micro-CT data into a form which is computationally manageable. The large file size, in this case ~10 GB, and the fine structural details, make the integration of such data into mathematical models, computationally and theoretically difficult.

This, however, highlights a new research challenge for the modeling and engineering community. While providing new challenges, high resolution micro-CT data does provide a step change in the quality of structural geometries available to groups working on mathematical models of cardiac depolarisation.

DATA AVAILABILITY

The datasets for this manuscript are not publicly available because: this patient data is sensitive and ethical approval is acquired on an individual basis. Requests to access the datasets should be directed to Dr. Robert Stanley Stephenson, email: robert.stephenson@clin.au.dk.

AUTHOR CONTRIBUTIONS

JJ, CJ, and RG acquisition of ethical approval for the study. JJ and RS sample preparation and RS, JJ, and TL data acquisition. JR-N, RS, and HZ data analysis and production of figures. RS writing and JR-N, CJ, RG, JZ, HZ, and JJ editing of manuscript.

REFERENCES

- Anderson, R. H., Baker, E. J., Yen Ho, S., Rigby, M. L., and Ebels, T. (2008). The morphology and diagnosis of atrioventricular septal defects. *Cardiol. Young* 1, 290–305. doi: 10.1017/S1047951100010362
- Anderson, R. H., Ho, S. Y., and Becker, A. E. (2000). Anatomy of the human atrioventricular junctions revisited. *Anat. Rec.* 260, 81–91. doi: 10.1002/1097-0185(20000901)260:1<81::AID-AR90>3.0.CO;2-3
- Anderson, R. H., Ho, S. Y., Smith, A., and Becker, A. E. (1981). The internodal atrial myocardium. *Anat. Rec.* 201, 75–82. doi: 10.1002/ar.1092010110
- Aslanidi, O., Nikolaidou, T., Zhao, J., Smaill, B., Gilbert, S., Jarvis, J., et al. (2012). Application of micro-computed tomography with iodine staining to cardiac imaging, segmentation and computational model development. *Med. Imaging IEEE Trans.* 32, 8–17. doi: 10.1109/TMI.2012.2209183
- Boening, A., Scheewe, J., Heine, K., Hedderich, J., Regensburger, D., Kramer, H. H., et al. (2002). Long-term results after surgical correction of atrioventricular septal defects. *Eur. J. Cardio Thoracic Surg.* 22, 167–173. doi: 10.1016/S1010-7940(02)00272-5
- Boyett, M. R., Honjo, H., and Kodama, I. (2000). The sinoatrial node, a heterogeneous pacemaker structure. *Cardiovasc. Res.* 47, 658–687. doi: 10.1016/S0008-6363(00)00135-8
- Chandler, N., Aslanidi, O., Buckley, D., Inada, S., Birchall, S., Atkinson, A., et al. (2011). Computer three-dimensional anatomical reconstruction of the human sinus node and a novel paranodal area. *Anat. Rec. Adv. Integr. Anat. Evol. Biol.* 294, 970–979. doi: 10.1002/ar.21379
- Daliento, L., Rizzoli, G., Marchiori, M. C., Buja, G., Milanesi, O., Valente, S., et al. (1991). Electrical instability in patients undergoing surgery for atrioventricular septal defect. *Int. J. Cardiol.* 30, 15–21. doi: 10.1016/0167-5273(91)90119-A
- Fedorov, V. V., Glukhov, A. V., Chang, R., Kostecki, G., Aferol, H., Hucker, W. J., et al. (2010). Optical mapping of the isolated coronary-perfused human sinus node. *J. Am. Coll. Cardiol.* 56, 1386–1394. doi: 10.1016/j.jacc.2010.03.098
- Feldt, R. H., Dushane, J. W., and Titus, J. I. (1970). The atrioventricular conduction system in persistent common atrioventricular canal defect. *Correlations Electrocadiogr.* 42, 437–444.
- Fournier, A., Young, M.-L., Garcia, O. L., Tamer, D. F., and Wolff, G. S. (1986). Electrophysiologic cardiac function before and after surgery in children with atrioventricular canal. *Am. J. Cardiol.* 57, 1137–1141. doi: 10.1016/0002-9149(86)90688-0
- George, S. A., Faye, N. R., Murillo-Berlioz, A., Lee, K. B., Trachiotis, G. D., and Efimov, I. R. (2017). At the Atrioventricular Crossroads: dual pathway electrophysiology in the atrioventricular node and its underlying heterogeneities. *Arrhythmia Electrophysiol. Rev.* 6, 179–185. doi: 10.15420/aer.2017.30.1
- Hucker, W. J., Fedorov, V. V., Foyil, K. V., Moazami, N., and Efimov, I. R. (2008). Optical mapping of the human atrioventricular junction. *Circulation* 117, 1474–1477. doi: 10.1161/CIRCULATIONAHA.107.733147
- Jacobsen, J. R., Gillette, P. C., Corbett, B. N., Rabinovitch, M., and McNamara, D. G. (1976). Intracardiac electrography in endocardial cushion defects. *Circulation* 54, 599–603. doi: 10.1161/01.CIR.54.4.599
- James, T. N. (1963). The connecting pathways between the sinus node and A-V node and between the right and the left atrium in the human heart. *Am. Heart J.* 66, 498–508. doi: 10.1016/0002-8703(63)90382-X
- Jarvis, J. C., and Stephenson, R. (2013). Studying the Microanatomy of the Heart in Three Dimensions: a practical update. *Front. Pediatr.* 1:26. doi: 10.3389/fped.2013.00026
- Khairiy, P. (2008). EP challenges in adult congenital heart disease. *Heart Rhythm* 5, 1464–1472. doi: 10.1016/j.hrthm.2008.05.026
- Khairiy, P., and Balaji, S. (2009). Cardiac Arrhythmias In Congenital Heart Diseases. *Indian Pacing Electrophysiol. J.* 9, 299–317.
- Khairiy, P., Dore, A., Talajic, M., Dubuc, M., Poirier, N., Roy, D., et al. (2006). Arrhythmias in adult congenital heart disease. *Expert Rev. Cardiovasc. Ther.* 4, 83–95. doi: 10.1586/14779072.4.1.83
- Khairiy, P., Mercier, L.-A., Dore, A., and Dubuc, M. (2007). Partial atrioventricular canal defect with inverted atrioventricular nodal input into an inferiorly displaced atrioventricular node. *Heart Rhythm* 4, 355–358. doi: 10.1016/j.hrthm.2006.10.012
- Kojodjojo, P., Kanagaratnam, P., Markides, V., Davies, W. D., and Peters, N. (2006). Age-related changes in human left and right atrial conduction. *J. Cardiovasc. Electrophysiol.* 17, 120–127. doi: 10.1111/j.1540-8167.2005.00293.x
- Mani, B. C., and Pavri, B. B. (2014). Dual Atrioventricular Nodal Pathways Physiology: a review of relevant anatomy, electrophysiology, and electrocardiographic manifestations. *Indian Pacing Electrophysiol. J.* 14, 12–25. doi: 10.1016/S0972-6292(16)30711-2
- Merideth, J., and Titus, J. I. (1968). The anatomic atrial connections between sinus and A-V node. *Circulation* 37, 566–579. doi: 10.1161/01.CIR.37.4.566
- Moorman, A. F. M., de Jong, F., Denyn, M. M. F. J., and Lamers, W. H. (1998). Development of the cardiac conduction system. *Circ. Res.* 82, 629–644. doi: 10.1161/01.RES.82.6.629

FUNDING

RS is a Marie Skłodowska-Curie Fellow of the European Union, This project has received funding from the European Union's Horizon 2020 research and innovation programme under the Marie Skłodowska-Curie grant agreement No 707663.

ACKNOWLEDGMENTS

We would like to acknowledge Alder Hey Children's Hospital, Liverpool, UK for granting us permission to access the tissue and conduct the study, and for their supportive role in the acquisition of ethical approval. The MXIF was established using EPSRC funding [EP/F007906; EP/F001452; EP/I02249X].

SUPPLEMENTARY MATERIAL

The Supplementary Material for this article can be found online at: <https://www.frontiersin.org/articles/10.3389/fphys.2018.01071/full#supplementary-material>

- Ni, H., Castro, S. J., Stephenson, R. S., Jarvis, J. C., Lowe, T., Hart, G., et al. (2013). Extracting myofibre orientation from micro-CT images: an optimisation study. *Paper Presented Comput. Cardiol.* 40, 823–826.
- Ni, H., Whittaker, D. G., Wang, W., Giles, W. R., Narayan, S. M., and Zhang, H. (2017). Synergistic anti-arrhythmic effects in human atria with combined use of sodium blockers and acacetin. *Front. Physiol.* 8:946. doi: 10.3389/fphys.2017.00946
- Sánchez-Quintana, D., Cabrera, J. A., Farré, J., Climent, V., Anderson, R. H., and Ho, S. Y. (2005). Sinus node revisited in the era of electroanatomical mapping and catheter ablation. *Heart* 91, 189–194. doi: 10.1136/heart.2003.031542
- Sanchez-Quintana, D., Wyn Davies, D., Yen Ho, S., Oslizlok, P., and Anderson, R. H. (1997). Architecture of the atrial musculature in and around the triangle of koch. *J. Cardiovasc. Electrophysiol.* 8, 1396–1407. doi: 10.1111/j.1540-8167.1997.tb01036.x
- Spach, M. S., and Kootsey, J. M. (1983). The nature of electrical propagation in cardiac muscle. *Am. J. Physiol. Heart Circulatory Physiol.* 244, H3–H22. doi: 10.1152/ajpheart.1983.244.1.H3
- Stephenson, R. S., Atkinson, A., Kottas, P., Perde, F., Jafarzadeh, F., Bateman, M., et al. (2017). High resolution 3-Dimensional imaging of the human cardiac conduction system from microanatomy to mathematical modeling. *Sci. Rep.* 7:1788. doi: 10.1038/s41598-017-07694-8
- Stephenson, R. S., Boyett, M. R., Hart, G., Nikolaidou, T., Cai, X., Corno, A. F., et al. (2012). Contrast enhanced micro-computed tomography resolves the 3-dimensional morphology of the cardiac conduction system in mammalian hearts. *PLoS ONE* 7:e35299. doi: 10.1371/journal.pone.0035299
- Vetter, V. L., and Horowitz, L. N. (1982). Electrophysiologic residua and sequelae of surgery for congenital heart defects. *Am. J. Cardiol.* 50, 588–604. doi: 10.1016/0002-9149(82)90328-9
- Waldo, A. L., Kaiser, G. A., Bowman, F. O., and Malm, J. R. (1973). Etiology of prolongation of the P-R interval in patients with an endocardial cushion defect. Further observations on internodal conduction and the polarity of the retrograde P Wave. *Circulation* 48, 19–26.

Conflict of Interest Statement: The authors declare that the research was conducted in the absence of any commercial or financial relationships that could be construed as a potential conflict of interest.

Copyright © 2018 Stephenson, Rowley-Nobel, Jones, Guerrero, Lowe, Zhao, Zhang and Jarvis. This is an open-access article distributed under the terms of the Creative Commons Attribution License (CC BY). The use, distribution or reproduction in other forums is permitted, provided the original author(s) and the copyright owner(s) are credited and that the original publication in this journal is cited, in accordance with accepted academic practice. No use, distribution or reproduction is permitted which does not comply with these terms.



The Fibrotic Substrate in Persistent Atrial Fibrillation Patients: Comparison Between Predictions From Computational Modeling and Measurements From Focal Impulse and Rotor Mapping

OPEN ACCESS

Edited by:

Jichao Zhao,

University of Auckland, New Zealand

Reviewed by:

Ning Li,

The Ohio State University,

United States

Richard Gray,

United States Food and Drug

Administration, China

Sanjay Ram Kharche,

University of Western Ontario, Canada

*Correspondence:

Natalia A. Trayanova

ntrayanova@jhu.edu

Specialty section:

This article was submitted to

Computational Physiology
and Medicine,

a section of the journal

Frontiers in Physiology

Received: 30 May 2018

Accepted: 31 July 2018

Published: 29 August 2018

Citation:

Boyle PM, Hakim JB, Zahid S, Franceschi WH, Murphy MJ, Prakosa A, Aronis KN, Zghaib T, Balouch M, Ipek EG, Chrispin J, Berger RD, Ashikaga H, Marine JE, Calkins H, Nazarian S, Spragg DD and Trayanova NA (2018) The Fibrotic Substrate in Persistent Atrial Fibrillation Patients: Comparison Between Predictions From Computational Modeling and Measurements From Focal Impulse and Rotor Mapping. *Front. Physiol.* 9:1151. doi: 10.3389/fphys.2018.01151

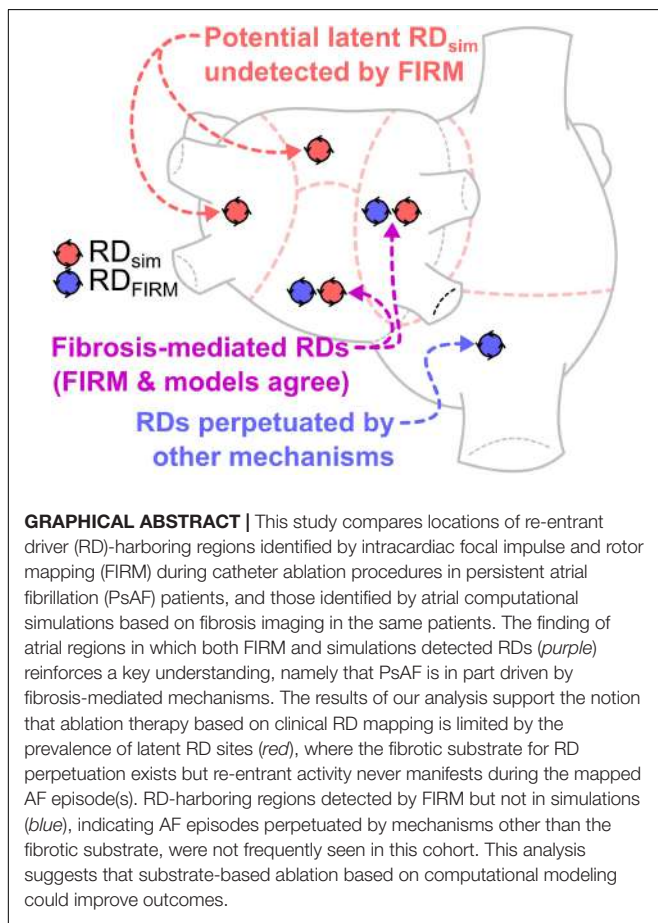
Patrick M. Boyle¹, Joe B. Hakim¹, Sohail Zahid¹, William H. Franceschi¹, Michael J. Murphy¹, Adityo Prakosa¹, Konstantinos N. Aronis², Tarek Zghaib², Muhammed Balouch², Esra G. Ipek², Jonathan Chrispin², Ronald D. Berger², Hiroshi Ashikaga², Joseph E. Marine², Hugh Calkins², Saman Nazarian³, David D. Spragg² and Natalia A. Trayanova^{1*}

¹ Department of Biomedical Engineering, Institute for Computational Medicine, Johns Hopkins University, Baltimore, MD, United States, ² Department of Cardiology, Johns Hopkins Hospital, Baltimore, MD, United States, ³ Penn Heart & Vascular Center, University of Pennsylvania, Philadelphia, PA, United States

Focal impulse and rotor mapping (FIRM) involves intracardiac detection and catheter ablation of re-entrant drivers (RDs), some of which may contribute to arrhythmia perpetuation in persistent atrial fibrillation (PsAF). Patient-specific computational models derived from late gadolinium-enhanced magnetic resonance imaging (LGE-MRI) has the potential to non-invasively identify all areas of the fibrotic substrate where RDs could potentially be sustained, including locations where RDs may not manifest during mapped AF episodes. The objective of this study was to carry out multi-modal assessment of the arrhythmogenic propensity of the fibrotic substrate in PsAF patients by comparing locations of RD-harboring regions found in simulations and detected by FIRM (RD_{sim} and RD_{FIRM}) and analyze implications for ablation strategies predicated on targeting RDs. For 11 PsAF patients who underwent pre-procedure LGE-MRI and FIRM-guided ablation, we retrospectively simulated AF in individualized atrial models, with geometry and fibrosis distribution reconstructed from pre-ablation LGE-MRI scans, and identified RD_{sim} sites. Regions harboring RD_{sim} and RD_{FIRM} were compared. RD_{sim} were found in 38 atrial regions (median [inter-quartile range (IQR)] = 4 [3; 4] per model). RD_{FIRM} were identified and subsequently ablated in 24 atrial regions (2 [1; 3] per patient), which was significantly fewer than the number of RD_{sim}-harboring regions in corresponding models ($p < 0.05$). Computational modeling predicted RD_{sim} in 20 of 24 (83%) atrial regions identified as RD_{FIRM}-harboring during clinical mapping. In a large number of cases, we uncovered RD_{sim}-harboring regions in which RD_{FIRM} were never observed (18/22 regions that differed between the two modalities; 82%); we termed such cases “latent” RD_{sim} sites. During follow-up (230 [180; 326] days), AF recurrence occurred in 7/11 (64%) individuals. Interestingly, latent RD_{sim} sites were observed in

all seven computational models corresponding to patients who experienced recurrent AF (2 [2; 2] per patient); in contrast, latent RD_{sim} sites were only discovered in two of four patients who were free from AF during follow-up (0.5 [0; 1.5] per patient; $p < 0.05$ vs. patients with AF recurrence). We conclude that substrate-based ablation based on computational modeling could improve outcomes.

Keywords: atrial fibrillation, re-entrant drivers, fibrotic remodeling, ablation, computational modeling, intracardiac electroanatomic mapping



INTRODUCTION

Atrial fibrillation (AF) affects up to 2% of the population, making it the most prevalent sustained arrhythmia (Andrade et al., 2014). Pulmonary vein isolation (PVI) via catheter ablation can effectively treat some forms of AF (Haissaguerre et al., 1998; Calkins et al., 2017), but recurrence rates remain unacceptably high (40–60%) in patients with persistent AF (PsAF) (Verma et al., 2015). A potential explanation for the relative ineffectiveness of ablation in these patients is the fact that PsAF is often associated with atrial fibrosis, establishing a substrate for which the arrhythmogenic propensity is beyond the area affected by PVI (Burstein and Nattel, 2008; Nattel et al., 2008; Yue et al., 2011). Thus, new methodologies are needed to accurately identify the ablation targets in the fibrotic substrate.

One approach used in recent studies is focal impulse and rotor mapping (FIRM), one aim of which is to determine the locations of the re-entrant drivers (RDs; i.e., rotors) that contribute to AF perpetuation by interpreting intracardiac electrogram signals from multi-electrode basket catheters inserted in the atria during ablation procedures; identified RD sites are then targeted for ablation (Narayan et al., 2012b, 2014). One potential explanation for the limited ability of FIRM-guided ablation to achieve freedom from AF in some cases (Mohanty et al., 2018) is the failure to modify the arrhythmogenic substrate sufficiently to eliminate its capacity to sustain RDs. This notion is supported by evidence from some studies that AF may be sustained by persistent RDs at different locations in cases of failed ablation (Lalani et al., 2016; Boyle et al., 2018). Notably, FIRM also aims to identify sources of triggered excitation (i.e., focal impulses) but these are beyond the scope of the present investigation.

Simulations conducted in patient-specific computational models reconstructed from late gadolinium-enhanced magnetic resonance imaging (LGE-MRI) scans have recently been used to develop insights into the perpetuation and ablation of PsAF in patients with atrial fibrosis (McDowell et al., 2012; Trayanova, 2014; Boyle et al., 2016, 2017; Zahid et al., 2016a). Our work using such models has identified specific spatial patterns of fibrotic tissue that promote AF perpetuation (Zahid et al., 2016a) and these findings are corroborated by clinical evidence (Cochet et al., 2018). Also, in a study complementary to the present work, we compared rotor harboring regions, as characterized by pre-ablation non-invasive electrocardiographic imaging (ECGI), with those predicted in patient-specific models reconstructed from LGE-MRI scans of the same patients (Boyle et al., 2018). These studies all pointed to a key advantage of the computational approach to fibrotic substrate characterization: namely, simulations are capable of identifying latent rotor sites that may not manifest during clinical mapping.

The aim of this study was to carry out multi-modal assessment of pro-arrhythmic properties in the fibrotic substrate in PsAF patients by comparing RD-harboring regions found in simulations and detected by FIRM (RD_{sim} and RD_{FIRM}) and analyze implications for ablation strategies predicated on targeting rotors. We retrospectively conducted simulations in personalized atrial models reconstructed from pre-procedure MRI scans for 11 PsAF patients who underwent FIRM-guided ablation at Johns Hopkins Hospital. Our study offers further insights into the importance of latent RD_{sim} sites in the fibrotic atria, which have implications for improving long-term outcomes of PsAF ablation procedures.

MATERIALS AND METHODS

Persistent AF Patient Cohort

Eleven patients with PsAF who underwent pre-ablation LGE-MRI and FIRM as an adjunct to PVI in 2015 were included in this study. All 11 patients have been included in previous studies by our group (Chrispin et al., 2016; Balouch et al., 2017); the other patients included in those previous studies could not be included here due to the fact that pre-ablation LGE-MRI scans were not obtained. PsAF was defined as sustained AF that lasts >7 days, which is consistent with AHA/ACC/HRS guidelines (Calkins et al., 2017). The approach used to obtain pre-ablation LGE-MRI scans has been described in previous papers (Khurram et al., 2014; Chrispin et al., 2016; Zahid et al., 2016b; Balouch et al., 2017). The Johns Hopkins Institutional Review Board approved, and all patients provided written informed consent for, retrospective study of data collected from these ablation procedures.

Reconstruction of Patient-Specific Computational Models of the Fibrotic Atria

The approach used to reconstruct atrial models, including patient-specific representations of atrial geometry and fibrotic tissue distribution has been presented in previous papers (McDowell et al., 2012; Roney et al., 2016; Zahid et al., 2016a,b; Deng et al., 2017; Boyle et al., 2018). Briefly, the atrial wall was segmented from MRI scans and LGE and non-LGE regions were delineated using an image intensity ratio approach (Khurram et al., 2014). Three-dimensional finite-element meshes were then constructed for each patient-specific model. These models included a realistic representation of atrial wall thickness. Average edge length ranged from 351.01 to 380.88 μm ; mesh size ranged from 1.34 to 2.65 million nodes. Fiber orientations in the atrial myocardium were estimated as described previously (McDowell et al., 2012). We begin with generalized fiber orientations from an atlas human atrial geometry, then use large deformation diffeomorphic metric mapping to morph vectors those onto each patient-specific atrial geometry (Beg et al., 2004; Vadakkumpadan et al., 2009; McDowell et al., 2013). As such, the fiber orientation tensor field is unique in each individual model.

Our methodology for modeling atrial electrophysiology in PsAF patients with fibrotic atria can be found in our published papers (Zahid et al., 2016a,b; Deng et al., 2017; Boyle et al., 2018). Briefly, at the cellular scale in non-fibrotic regions, we used a human chronic AF atrial action potential model (Courtemanche et al., 1998) with modifications to fit clinical monophasic action potential recordings from patients with AF (Krummen et al., 2012). In fibrotic regions, this model was further modified to match relevant experimental data, as described previously (Avila et al., 2007; Corradi et al., 2008; Nattel et al., 2008; Pedrotty et al., 2009; Kakkar and Lee, 2010; Ramos-Mondragon et al., 2011; Zahid et al., 2016a,b). At the tissue scale, as in previous studies (Zahid et al., 2016a,b; Deng et al., 2017; Boyle et al., 2018), conductivity tensor values

in both regions were calibrated to match clinical recordings. Briefly, parameters were adjusted in a test slab geometry (4.5 cm \times 4.5 cm \times 0.5 cm, uniform fiber orientation) to obtain a longitudinal conduction velocity (CV) of 43.39 cm/s, consistent with the range of values measured during clinically mapped AF in humans (38–54 cm/s) (Konings et al., 1994). When the calibrated parameters were used in a test model with patient-specific fiber orientations and regions of fibrotic remodeling, CV values were in the expected range (31.46 [28.38; 36.32] cm/s; min/max: 15.18/47.81 cm/s).

Identification and Comparison of RD Locations in Simulations and FIRM Data

In each model, rapid pacing was applied at 30 uniformly distributed sites to induce AF. Pacing cycle length was decreased from 300 to 150 ms with the following inter-beat coupling intervals, in ms: 300, 275, 250, 225, 200, 190, 180, 170, 160, 150, and 150. For all 12 stimuli, pulse duration was 5 ms and transmembrane current strength was 0.3 mA/cm². Induced AF episodes were simulated for 2.5 s following the end of pacing. Persistent RD locations observed in simulations (i.e., RD_{sim}) were identified by determining phase singularity trajectories (Gray et al., 1998; Eason and Trayanova, 2002), which were extracted using the dynamic wavefront tip trajectory analysis approach (Deng et al., 2017). Briefly, RD_{sim} wavefront “pivot points” were manually identified during a 1,000 ms analysis interval at the end of each simulation. This ensured that multiple RD_{sim} rotations were analyzed and that transient instability immediately following AF initiation was disregarded. In all cases, RD_{sim} persisted for at least two rotations and lasted at least 200 ms, which is consistent with the RD definition of in previous papers (Narayan et al., 2012a; Haissaguerre et al., 2014).

A description of the methodology used to identify RDs from FIRM data (i.e., RD_{FIRM}) can be found in previous publications (Chrispin et al., 2016; Balouch et al., 2017). Briefly, a 3D bi-atrial electroanatomical map was constructed with the CARTO system (Biosense Webster) and merged with geometry extracted from pre-ablation MRI scans. AF was induced in patients presenting in sinus rhythm by atrial burst pacing and isoprotenerol infusion. RD_{FIRM} were mapped using a 64-pole basket mapping catheter (FIRMap; Abbott) in both the left and right atria and projected onto the electroanatomical map. This involved the use of proprietary software (RhythmView, Abbott) to derive 2D graphical displays of endocardial activation patterns from basket catheter unipolar electrogram signals.

RD_{sim} and RD_{FIRM} locations were compared on a region-wise basis. Each atrial geometry was manually subdivided into seven anatomically defined regions, as described by Haissaguerre et al. (2014): four regions in the left atrium (LA), two in the right atrium (RA), and one in the interatrial septum. Each RD was classified as belonging to the region in which the majority the RD trajectory was located. Regional classification of RD locations was performed by three different individuals (PB, JH, and MM) who were blinded to each other’s annotations; no discrepancies in classification occurred. As in our previous study (Boyle et al., 2018), each atrial region in each patient was classified into one of

four categories: RD_{sim} and RD_{FIRM}, RD_{sim} only, RD_{FIRM} only, or no RD activity.

FIRM-Guided Ablation Protocol and Clinical Follow-Up

The FIRM-guided ablation protocol has also been described in our earlier papers (Chrispin et al., 2016; Balouch et al., 2017). Although all cases in this study were considered retrospectively, we provide a summary of the protocol here to put the acute and long-term outcomes of clinical ablation in context. Standard electrophysiological catheters were advanced to the high RA, his bundle region, and coronary sinus. If the participant was in sinus rhythm, AF was induced by a rapid atrial burst pacing protocol. A 3D mesh of the RA was constructed using the CARTO 3 system (Biosense Webster, Inc., Diamond Bar, CA, United States). Subsequently, a 64-pole basket catheter (50 or 60 mm; Abbott Electrophysiology, Menlo Park, CA, United States) was introduced in the RA. Unipolar electrograms were recorded from the basket catheter at a sampling frequency of 977 Hz and were filtered at 0.05 to 500 Hz (Cardiolab; GE Healthcare, Waukesha, WI, United States). The quality of unipolar electrograms was assessed by the operating physician and adjustments to the catheter position were made to maximize atrial coverage and signal to noise ratio. FIRM mapping was performed with 60 s of unipolar signals collected per epoch. These signals were analyzed using proprietary software (Rhythm View workstation, Abbott, Menlo Park, CA, United States) and RD_{FIRM} were identified as areas of stable rotational activation patterns. Raw basket electrograms were not analyzed in this study. Ablation was performed using a 3.5-mm-tip irrigated catheter (ThermoCool SmartTouch; Biosense Webster, Inc., Diamond Bar, CA, United States) with power at the discretion of the operator (generally 25 W on the posterior wall and 30 W in anterior, septal, and lateral regions for ~15–30 s at each location). Ablation was continued until abatement of local electrograms. A repeat RD_{FIRM} map was obtained, and any additional identified RD_{FIRM} were ablated. After completion of ablation of RD_{FIRM} located in RA, a transeptal puncture was performed, and the process was repeated in the LA. All observed stable RD_{FIRM} were ablated. In this cohort, focal drivers of AF were not specifically

tracked, nor were they targeted for ablation. After completion of the FIRM-guided ablation, PVI was performed using wide area circumferential ablation of the pulmonary vein antra until entrance and exit block was demonstrated for each pulmonary vein. Additional lines were ablated at the attending physician's discretion.

As described previously (Balouch et al., 2017), routine follow-up including electrocardiographic testing was performed at 3, 6, and 12 months. Additional follow-up for symptomatic patients was performed as needed. Any incidence of AF documented by ECG or a device-recording system lasting ≥ 30 s, outside of a 3-month post-procedure blanking period, was classified as recurrence.

Statistics

Continuous variables were expressed as median [IQR] and compared using either the Wilcoxon signed-rank test (for paired comparisons) or the Mann-Whitney test (for unpaired comparisons). After classifying RD_{sim}/RD_{FIRM} within anatomical regions, agreement between regions identified by the two modalities was assessed by calculating the modified Cohen's kappa statistic (κ_0) (Kraemer, 1980). All tests were two-tailed; $p < 0.05$ indicated statistical significance.

RESULTS

Demographic information about the patient cohort retrospectively analyzed in this study is provided in **Table 1**. No identifiable trends in potential confounding variables (age, sex, BMI, duration of AF prior to ablation, PsAF vs. long-standing PsAF, and proportion of fibrotic tissue as identified by LGE-MRI) were observed. Moreover, there were no differences between success and failure groups in terms of the number of RD_{FIRM} targets ablated or the number of RD_{FIRM}-harboring regions. For all 11 individuals, **Figure 1** shows long-term and acute success rates of FIRM-guided ablation procedures (follow-up duration: 230 [180; 326] days), anatomical regions where RD_{sim} and RD_{FIRM} were detected, and Venn diagrams summarizing the degree of overlap between RD_{sim} and RD_{FIRM}-harboring regions. As patient IDs were arbitrarily assigned in this retrospective

TABLE 1 | Demographic and FIRM-guided ablation procedure information for the cohort considered in this study.

Variable	Overall (n = 11)	Success (n = 4)	Failure (n = 7)	p-value*
Age	67 [55; 72]	69 [55.5; 72]	67 [55; 69]	0.7485
Male	10 (91)	4 (100)	6 (86)	>0.9999
BMI	29.2 [27.9; 35.3]	32.25 [28.9; 40.48]	28.4 [24.2; 35.3]	0.2515
PsAF	8 (73)	3 (75)	5 (71)	>0.9999
Long-standing PsAF	3 (27)	1 (25)	2 (29)	>0.9999
Duration of AF (y)	4 [2; 10]	2.25 [0.5; 10]	6 [2; 10]	0.3818
Fibrotic tissue (%)	29.1 [18; 47.1]	36.2 [13.73; 46.53]	29.1 [18; 53]	0.6485
RD _{FIRM} targets ablated (#)	3 [2; 6]	4 [2.25; 5.75]	3 [1; 6]	0.5364
RD _{FIRM} -harboring regions (#)	2 [1; 3]	2.5 [1.25; 3.75]	2 [1; 3]	0.5788

Long-term outcomes are defined in terms of freedom from AF during the follow-up period, which was classified as success. *Comparisons are between patients with different long-term FIRM ablation outcomes.

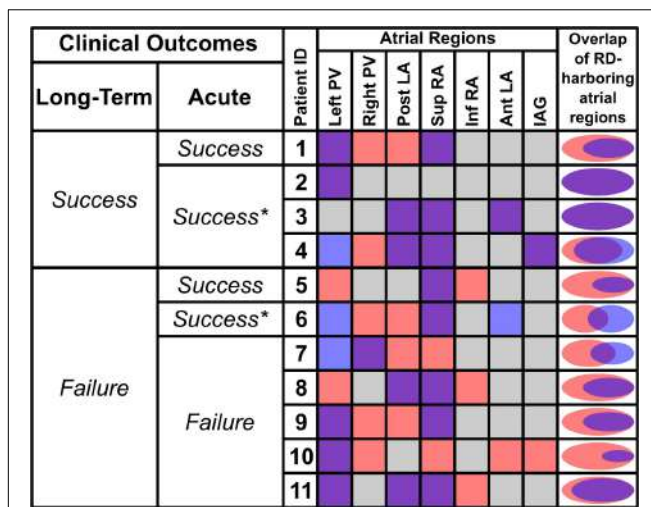


FIGURE 1 | Summary of RD_{sim} and RD_{FIRM}-harboring regions for all retrospectively studied individuals and corresponding patient-specific models. The first two columns show long-term and acute outcomes of catheter ablation; see **Table 1** for definition of long-term clinical outcomes. Acute outcomes are defined as Success (AF spontaneously terminated during FIRM-guided to ablation), Success* (AF organized to atrial flutter during FIRM-guided to ablation), or Failure (AF persisted for the duration of FIRM-guided ablation). Columns under “Atrial Regions” heading show color-coded classification of each part of the atria: purple = both RD_{sim} and RD_{FIRM}; gray = neither RD_{sim} nor RD_{FIRM}; red = RD_{sim} only; blue = RD_{FIRM} only. Rightmost column shows Venn diagrams (to scale) for each patient indicating degree of overlap between RD_{sim}- and RD_{FIRM}-harboring atrial regions. Data in this figure regarding overlap are based on region-wise comparison (i.e., if a particular atrial region was found to be both RD_{sim}-harboring and RD_{FIRM}-harboring, that region was deemed to have overlapping RD presence). Here, the concept of overlap is not intended to connote exact physical co-localization of RD_{sim} and RD_{FIRM} sites. PV, pulmonary vein; Post/Ant LA, posterior/anterior left atrium; Sup/Inf RA, superior/inferior right atrium; IAG, inter-atrial groove.

study, we were able to order the patients by long-term outcome then by acute outcome. Detailed information about all 11 clinical procedures, including notes on any ablations other than RD_{FIRM} targets or PVI that were performed, are provided in **Table 2**.

RD_{sim} were observed in 38 atrial regions (4 [3; 4] per patient); in contrast, RD_{FIRM} were only detected in 24 regions (2 [1; 3] per model; $p < 0.05$ vs. RD_{sim}). Classification of atrial regions (as RD-harboring or not) was in agreement between simulations and FIRM more frequently than it differed (5 [4; 6] vs. 2 [1; 3], $p < 0.05$, see **Table 3**). Analysis of inter-rater agreement yielded $\kappa_0 = 0.323$, which indicates a moderate degree of consensus (Kraemer, 1980). These findings are consistent with our expectation that RD_{sim} and RD_{FIRM} locations would only partially agree due to the fact that FIRM is capable of identifying only the specific RDs that are manifest during the procedure, whereas simulations can predict all potential RDs arising from the fibrotic substrate. Indeed, the majority of cases where regional classification differed (18/22; 82%) involved latent RD sites in regions where such activity was never detected during FIRM.

Distribution of RD_{sim} and RD_{FIRM}-harboring regions is summarized in **Figure 2**. The most common sites of RD_{sim}

occurrence (31/38; 82%) were the left and right PVs, the posterior LA, and the superior RA; in contrast, the majority of RD_{FIRM} were observed in the left PVs and the superior RA (16/24; 67%). This observation is reinforced by the fact that these two regions were the most likely to harbor latent RD sites (right PVs: 5/18, 28%; posterior LA: 4/18, 22%).

Side-by-side visualizations of RD_{sim} and RD_{FIRM} sites for four different patients are shown in **Figure 3**. In each case, the spatial distribution of fibrotic tissue in the same model is also included. For Patient 8 (**Figure 3A**), the example shown is for an RD_{sim} located in the posterior LA, roughly at the center of the plane formed by the four pulmonary veins; RD_{FIRM} was documented for the same patient at a similar location during FIRM (yellow highlighted region). For Patient 4 (**Figure 3B**), two examples are shown. First (top row), an RD_{sim} in the anterior part of the inter-atrial groove region, inferior to the right superior PV; second (bottom row), an RD_{sim} in the superior RA, near the base of the RA appendage. These sites correspond, respectively, to the blue and green highlighted regions in the FIRM schematic shown. For Patient 10 (**Figure 3C**), the case shown is for an RD_{sim} near the left PVs, which corresponded to a FIRM-mapped site (blue). Finally, for Patient 9 (**Figure 3D**), the highlighted RD_{sim} is found in the left PV region, between the left inferior PV and the mitral valve annulus, which is a direct match to the RD_{FIRM} area (pink). Notably, although this particular RD trajectory persists within a region that appears non-fibrotic from the epicardial surface, the underlying transmural and endocardial tissue in that area is quite fibrotic (see inset).

Four examples of latent RD_{sim} sites (i.e., located in regions that were not classified as RD_{FIRM}-harboring) are shown in **Figure 4**. Two separate AF episodes are shown for Patient 10, first for an RD_{sim} observed in the inter-atrial groove region on the

TABLE 2 | Details of ablation procedures for all 11 patients in the cohort.

Patient ID #	RD _{FIRM} targets ablated (#)	RD _{FIRM} -harboring regions (#)	Procedures notes (PVI, other lesions, etc.)
1	3	2	LA roof line
2	2	1	LA posterior roof and floor lines
3	5	3	LA roof line + 2 posterior LA lines
4	6	4	Coronary sinus isolation line
5	1	1	LA roof line
6	6	3	Cavo-tricuspid isthmus ablation (flutter)
7	2	2	LA roof line (flutter)
8	6	2	LA roof line
9	3	2	LA roof line
10	1	1	PVI deferred due to respiratory compensation; FIRM only
11	3	3	No additional lesions

In 2/11 cases, atypical LA flutter developed after PVI; additional ablation was performed as indicated.

TABLE 3 | For each patient model, number of atrial regions that were identified as RD_{sim}-harboring, RD_{FIRM}-harboring, both, or neither.

Patient ID #	# Regions that agreed			# Regions that differed		
	Both RD _{sim} and RD _{FIRM}	Neither RD _{sim} nor RD _{FIRM}	Total	RD _{sim} only	RD _{FIRM} only	Total
1	2	3	5	2	0	2
2	1	6	7	0	0	0
3	3	4	7	0	0	0
4	3	2	5	1	1	2
5	1	4	5	2	0	2
6	1	2	3	2	2	4
7	1	3	4	2	1	3
8	2	3	5	2	0	2
9	2	3	5	2	0	2
10	1	2	3	4	0	4
11	3	3	6	1	0	1
Total	20	35	55	18	4	22
Median [IQR]	2 [1; 3]	3 [2; 4]	5 [4; 6]	2 [1; 2]	0 [0; 1]	2 [1; 3]

anterior side of the RA near the superior vena cava (**Figure 4A**); second, for an RD_{sim} in the right PV region, near the carina between the right superior and inferior PVs (**Figure 4B**). For Patient 9, the example shown (**Figure 4C**) highlights simulated AF that was perpetuated by two simultaneous RD_{sim}, one very close to the right inferior PV and the other on the posterior LA, toward the left superior PV. This was the only case in which this particular dynamic (i.e., more than one stable RD_{sim} persisting simultaneously) was observed in this study; for purposes of RD_{sim} classification, this example led to both the right PV and posterior LA regions being annotated as RD_{sim}-harboring. Finally, for Patient 5, the RD_{sim} shown is in the inferior RA on the posterior side of the inferior vena cava (**Figure 4D**). In all four examples

presented above, RD_{FIRM} activity was not documented in the given atrial region during the clinical ablation procedure.

For this cohort, most of atrial regions in which RD_{FIRM} were observed were also found to be RD_{sim}-harboring during simulation analysis (20/24; 83%). Three examples of RD_{FIRM} that were not observed in the corresponding models are shown in **Figure 5**. For Patient 6, two instances are presented: first, two RD_{FIRM} in the left PV region (yellow and orange highlighted areas in **Figure 5A**); second, another two RD_{FIRM} on the anterior LA, at the base of the LA appendage (green highlighted areas in **Figure 5B**). For Patient 4, an RD_{FIRM} was identified in the left PV region (blue highlighted area in **Figure 5C**). In all of these cases, RD_{sim} were not observed in the corresponding regions

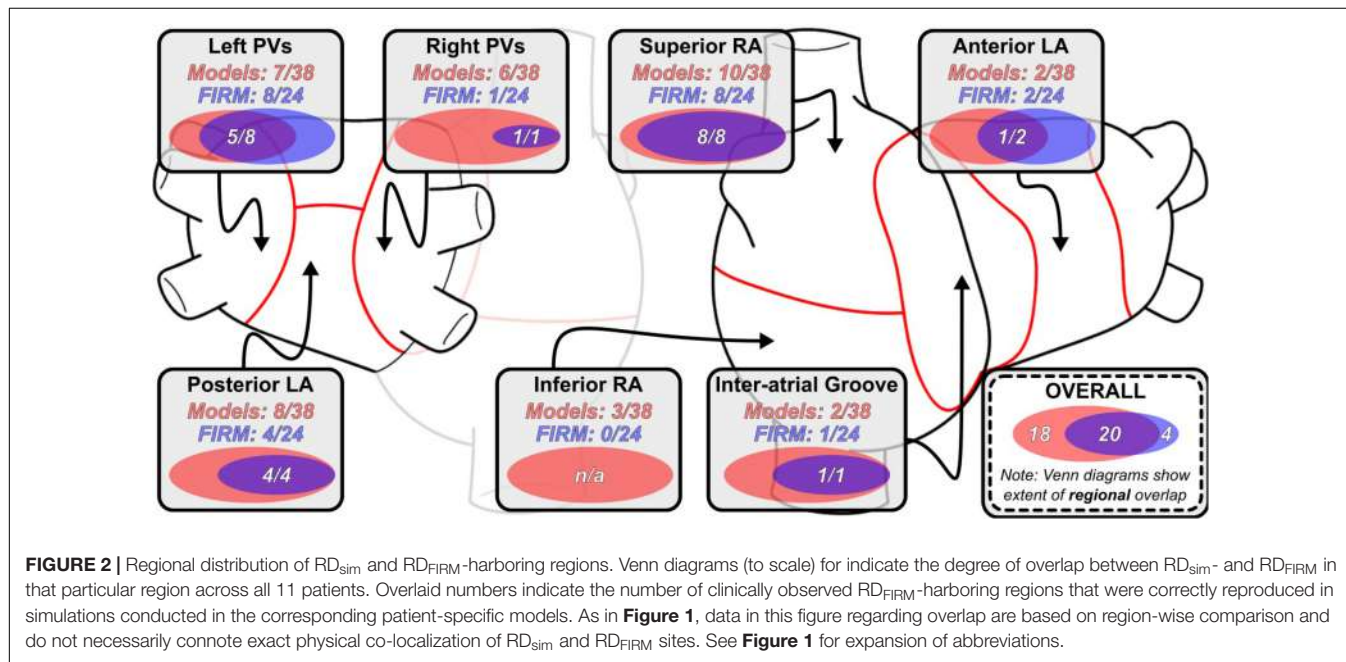


FIGURE 2 | Regional distribution of RD_{sim} and RD_{FIRM}-harboring regions. Venn diagrams (to scale) for indicate the degree of overlap between RD_{sim}- and RD_{FIRM} in that particular region across all 11 patients. Overlaid numbers indicate the number of clinically observed RD_{FIRM}-harboring regions that were correctly reproduced in simulations conducted in the corresponding patient-specific models. As in **Figure 1**, data in this figure regarding overlap are based on region-wise comparison and do not necessarily connote exact physical co-localization of RD_{sim} and RD_{FIRM} sites. See **Figure 1** for expansion of abbreviations.

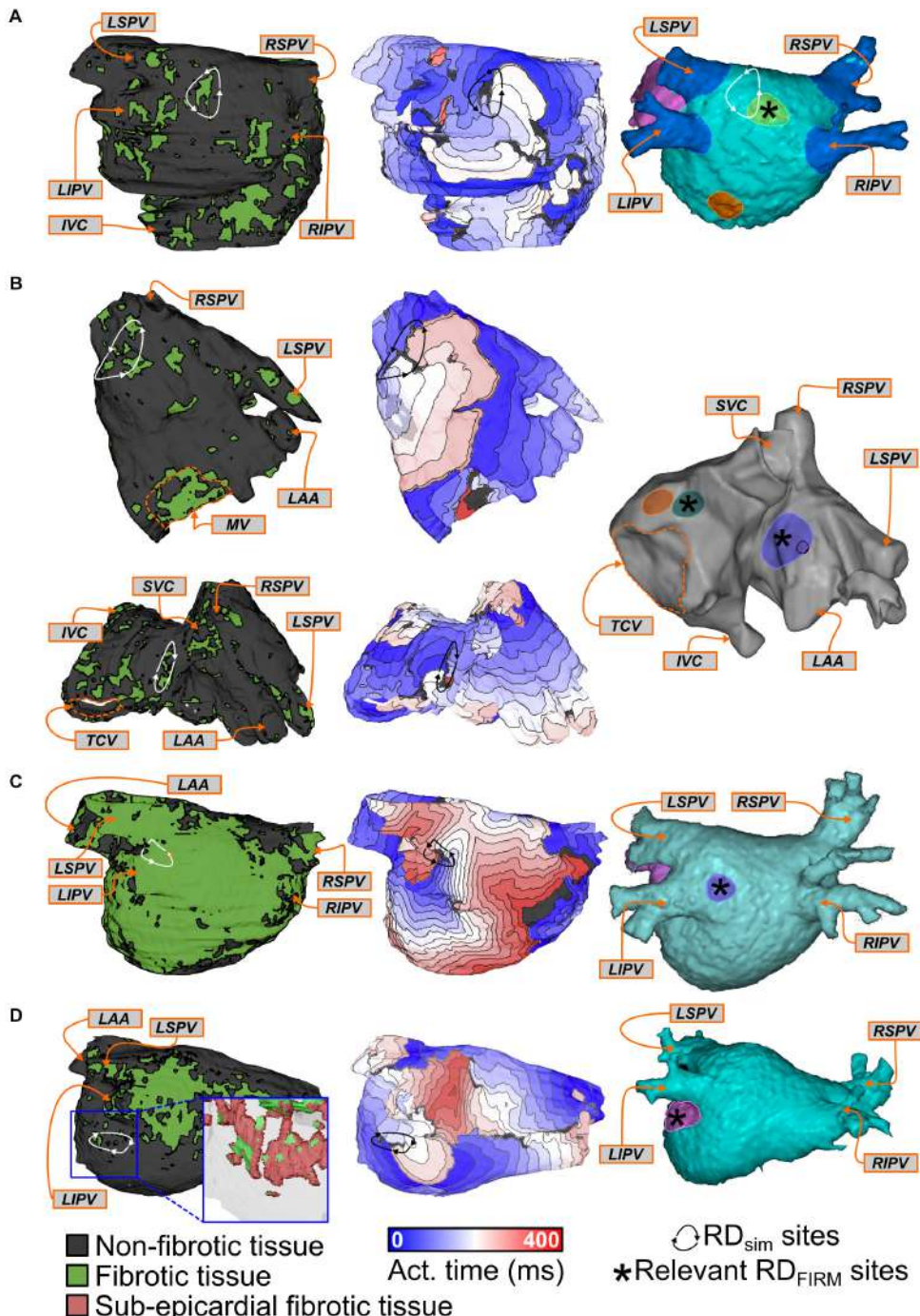


FIGURE 3 | Examples showing direct evidence of co-localization of RD_{sim} and RD_{fIRM}. Each row shows the distribution of fibrotic tissue in the patient-specific model (left), with anatomical labels (orange boxes and arrows) for ease of navigation; an activation map highlighting the location of an RD_{sim} that perpetuated AF during simulations (middle); and an annotated map exported from the electro-anatomical mapping system (right). Black regions indicate tissue that did not activate during the relevant interval; locations of RD_{fIRM} are highlighted by brightly colored regions. Some variability existed in the visual due to differences in the export process that could not be made consistent across all 11 cases. **(A)** Patient 8: Matching RD_{sim} and RD_{fIRM} (yellow) sites in the posterior LA region. Note that the figure also shows a second, more inferior posterior LA target (orange). The PVs and LA appendage were colored blue and pink for ease of clinical navigation (i.e., there were no RD_{fIRM} in these colored regions). **(B)** Patient 4: Matching RD_{sim} and RD_{fIRM} sites in the inter-atrial groove (FIRM annotation: blue) and superior RA (FIRM annotation: green) regions of the atria. A third RD_{fIRM} is shown deeper inside the RA appendage (orange). **(C)** Patient 10: Matching RD_{sim} and RD_{fIRM} (blue) sites in the left PV region. The LA appendage was colored pink for ease of clinical navigation. **(D)** Patient 9: Matching RD_{sim} and RD_{fIRM} (pink) sites in the left PV region. Inset: View of RD_{sim} region with non-fibrotic tissue rendered as semi-transparent to show 3D transmural distribution of fibrotic tissue, including extensive sub-epicardial fibrotic remodeling in this area (red).

of the patient-specific model. Another possibility that cannot be excluded is that these RD_{FIRM} sites are false positives.

In general, the number of RD_{sim}-harboring regions observed in computational models differed significantly between those reconstructed from MRI scans of patients who did not experience AF recurrence during follow-up vs. those in whom the procedure was classified as a long-term failure. There was a trend toward more RD_{sim}-harboring regions in the seven patients whose ablation failed compared to the four individuals in whom the procedure succeeded (Figure 6A; failure: 4 [3; 4] vs. success: 3.5 [1.5; 4], $p = \text{n.s.}$). Interestingly, this trend was reversed for RD_{FIRM}-harboring regions (Figure 6B; failure: 2 [1; 3] vs. success: 2.5 [1.25; 3.75], $p = \text{n.s.}$), although neither difference rose to the level of significance. In the four patients who had long-term freedom from AF, there were only three examples of latent RD_{sim} sites in two patients; in contrast, all patients who had recurrent AF during follow-up had at least one latent RD_{sim} site (Figure 6C; failure: 2 [2; 2] vs. 0.5 [0; 1.75], $p < 0.05$).

DISCUSSION

Our study has important implications for understanding of the fibrotic substrate for arrhythmia initiation and perpetuation in PsAF patients. Nearly all of the atrial regions (84%) where RD_{FIRM} were observed also harbored RD_{sim} in simulations, which reinforces the validity of our patient-specific modeling technique and supports the notion that many rotors mapped during clinical procedures are perpetuated by the fibrotic substrate. Interestingly, in the subset of patients ($n = 7$) in whom the long-term outcome of ablation was failure (AF recurred during follow-up), we uncovered a large number of additional RD_{sim}-harboring regions (2 [2; 2] per individual), within which rotor activity was never identified by FIRM. These locations, termed latent RD_{sim} sites, were significantly less prevalent in models corresponding to patients who remained free from AF for the duration of follow-up ($n = 4$; 0.5 [0; 1.75] per individual). These results suggest that one potential explanation for the failure of FIRM-guided ablation is the prevalence of latent RD_{sim} sites. It also suggests that ablation procedures based on custom-tailored plans to exhaustively target all potential RD_{sim} locations could lead to better long-term outcomes for PsAF patients.

Another interesting finding of our study was that the prevalence of latent RD_{sim} sites was particularly high in two specific atrial regions: the posterior LA and the right PVs. There are several potential explanations for this finding. On one hand, due to inter-patient variability in atrial geometry and fibrotic tissue distribution, it is possible that many individuals in this cohort happened to have the necessary substrate for rotor perpetuation in those regions but re-entrant activity did not happen to manifest there during mapped AF episodes. On the other hand, it is also conceivable that rotors *did* manifest in those atrial regions in some or all of the apparent latent RD_{sim} sites, but FIRM failed to uncover them as RD_{FIRM}. If the latter is the case, it is also unclear whether this is due to a shortcoming in the FIRM system's ability to record rotors in these regions or some other factor (e.g., the specific way the

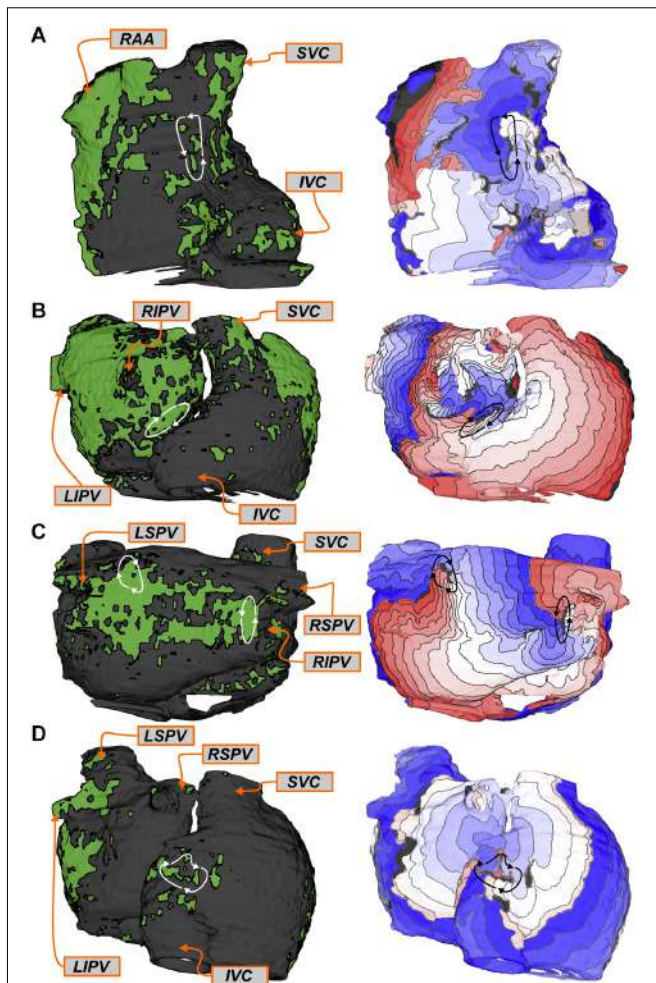
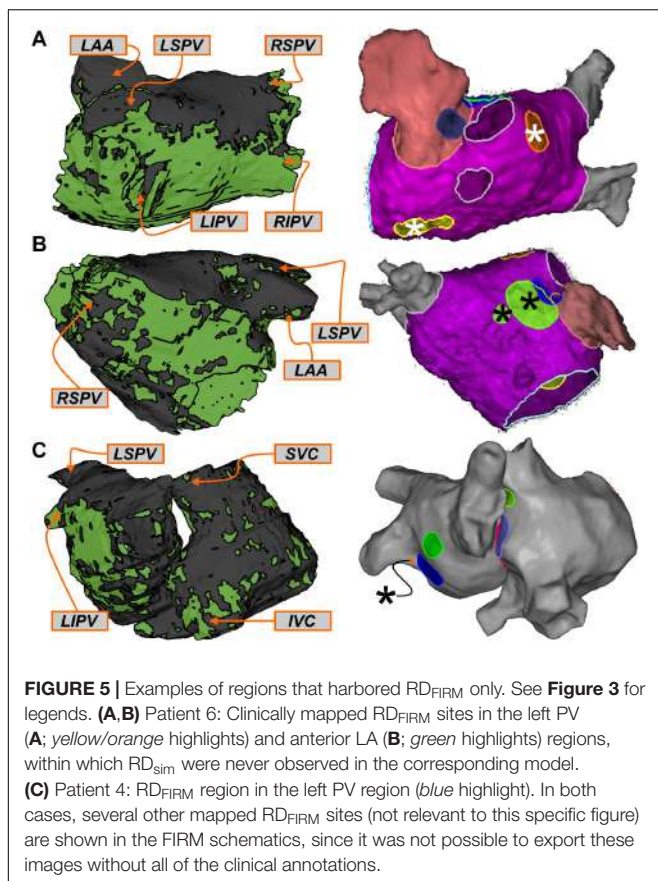


FIGURE 4 | Examples of regions that harbored RD_{sim} only (i.e., latent RD_{sim}). See Figure 3 for legends. **(A,B)** Patient 10: Latent RD_{sim} sites in the inter-atrial groove **(A)** and right PV **(B)** regions. **(C)** Patient 9: Latent RD_{sim} in the posterior LA (upper left) and right PV (right) regions; see text for further discussion of this unique case in which two RD_{sim} simultaneously persisted during a single simulated AF episode. **(D)** Patient 5: Latent RD_{sim} in the inferior RA.

basket catheter was deployed during the ablation procedures in question). Finally, since there is no gold standard for evaluating rotor presence during AF episodes or confirming their causative role in arrhythmia perpetuation, we cannot formally exclude the possibility that the prevalence of latent RD_{sim} sites is partly or wholly attributable to false positives in simulations; however, the fact that they were observed more frequently in models corresponding to patients who experienced AF recurrence during follow-up provides modest correlative evidence that this is not the case.

Previous studies, both from our group (Boyle et al., 2018) and others (Tanaka et al., 2007), have pointed to the left PV and posterior LA regions as the most likely to harbor rotors. For the patient-specific models considered in this study, we also observed numerous RD_{sim} in those regions (left PVs: 7/38 [18%]; posterior

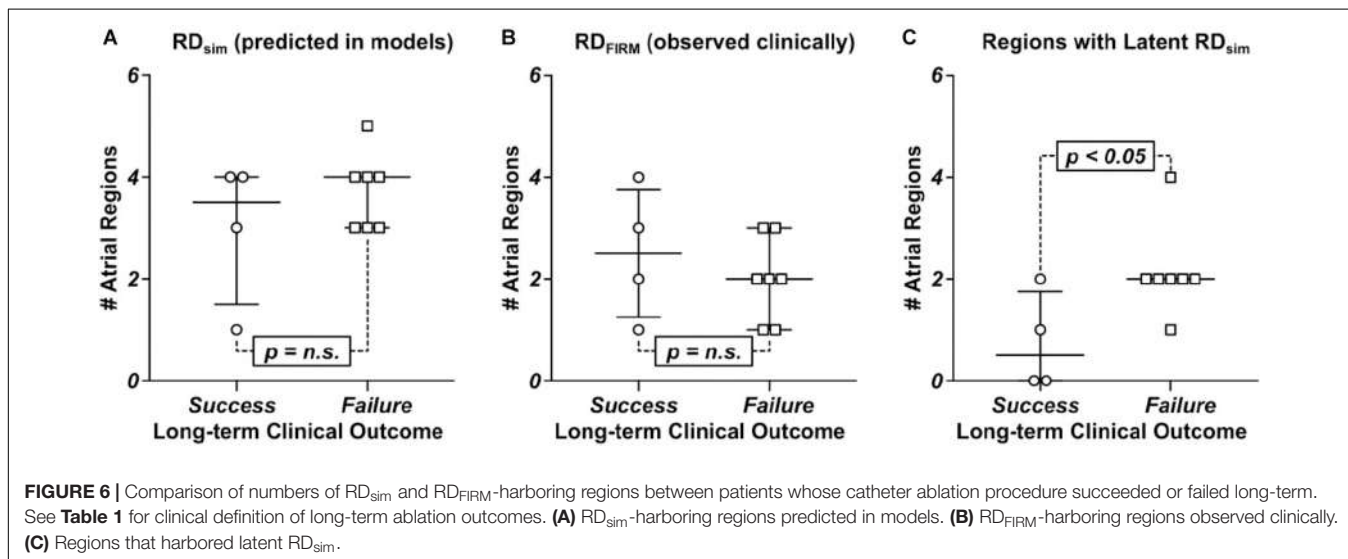


LA: 8/38 [21%]) but RD_{sim} were just as likely to manifest in the right PV and superior RA regions (6/38 [16%] and 10/38 [26%, respectively). This highlights the importance of attempting to map AF-perpetuating activity in the RA in addition to the LA, since many putative targets (in both simulations and FIRM) were identified in the upper part of that chamber. Notably, in

three of the four cases where the procedure resulted in long-term freedom from AF (see **Figure 1**), RD_{FIRM} were observed and ablated in areas that would not be targeted as part of a PVI procedure (superior RA, anterior LA, and/or inter-atrial groove), regardless of whether roof or floor lines were added in addition to standard circumferential lesions in the PV antra. This reinforces the general value of substrate-based ablation in the PsAF population.

In our earlier study (Boyle et al., 2018), which compared rotors detected by pre-ablation non-invasive ECGI to those predicted by simulations, the majority of atrial regions where the two modalities differed (23/32 [72%]) were cases where an RD_{sim} was not observed in the model even though it was recorded during mapped AF. In contrast, for the present study, the number of RD_{FIRM}-only regions was small (only four instances across all patients), meaning that the differences between FIRM and simulations were dominated by latent RD_{sim} sites. Previously, we primarily attributed the prevalence of rotors detected by ECGI but not predicted by simulations to rotors perpetuated by mechanisms other than the fibrotic substrate, but the present finding raises an intriguing alternative explanation. Namely, rotor detection via ECGI may be susceptible to a high rate of false positives (i.e., incorrect classification of non-rotor activity as an ablation targets), especially compared to RD_{FIRM} detection, which our findings conversely suggest is vulnerable to false negatives (i.e., the failure to observe latent RD_{sim} sites). This putative over-sensitivity of rotor detection via ECGI would also explain why the incidence of latent RD_{sim} in our previous study was low. However, a more systematic study involving rotor identification via all three methods in the same cohort, would be necessary in order to test this hypothesis. The development of a definitive gold standard for rotor identification would also be helpful in advancing knowledge in this area.

Finally, our discovery that latent RD_{sim} sites existed in all seven patients who had failed FIRM-guided ablation procedures but only two of the four individuals who benefited from treatment could explain why some recent trials have reported limited



efficacy of PVI + FIRM compared to PVI alone (Mohanty et al., 2018). However, the size of the cohort in our study is quite small ($n = 11$) and the number of patients who did not experience recurrent AF was even smaller ($n = 4$), thus it is difficult for us to draw definitive conclusions. Moreover, due to the retrospective nature of our study, the data presented here cannot definitively prove that latent RD_{sim} sites were the underlying cause of AF recurrence. Future work will need to test this hypothesis by determining prospectively if clinical ablation of all potential rotor sites, as identified by simulations conducted in patient-specific models of the fibrotic atria or by some other means, can deliver robust and long-term freedom from AF in PsAF patients.

As outlined in Section “Materials and Methods,” our model reconstruction approach uses a complex image-based technique to morph human atrial atlas fiber orientations onto each patient-specific geometry to create a unique conductivity tensor field. This is the most advanced approach currently undertaken, given clinical MRI has not yet developed to the point where it would be feasible to discern patient-specific fiber orientations or fine-grain structural details (e.g., endocardial bundles). Complexities of the atrial endocardial microstructure have recently been shown to influence RD localization in experiments and simulations conducted in models reconstructed from high-resolution *ex vivo* MRI scans (Hansen et al., 2015; Zhao et al., 2017). The data presented here provide important insights based on dynamic localization of RD_{sim} arising from the macroscopic distribution of fibrotic and non-fibrotic tissue (which can be obtained non-invasively via standard clinical imaging techniques), however, we cannot exclude the possibility that these mechanisms might interact with other potential factors (e.g., variability in myocardial thickness, endocardial bundles, etc.) to give rise to the complex behavior of AF-perpetuating rotors in patients.

The FIRM approach is capable of identifying both reentrant (i.e., RD_{FIRM}) and focal AF drivers. However, for the patient cohort examined in the present study, the incidence of focal drivers was not tracked. Since study was retrospective, we cannot offer any insights on the debate regarding the relative importance of focal vs. RDs. Moreover, since our computational approach is specifically designed to identify regions within each patient’s unique fibrotic substrate where RD_{sim} could potentially be sustained, it is not suitable for investigating the role(s) played by focal drivers in perpetuating AF.

Finally, a limitation of this project is that due to the retrospective nature of the study, we cannot evaluate the physical distance between RD_{FIRM} and RD_{sim} sites, as CARTO maps from

FIRM ablation procedures could not be co-registered with model geometry reconstructed from LGE-MRI. Because of that, rather than comparing specific RD_{FIRM} and RD_{sim} locations, we instead opted to compare RD_{FIRM}- and RD_{sim}-harboring *regions*, as done in previous work by us and others (Haissaguerre et al., 2014; Boyle et al., 2018), with the acknowledgment that these atrial regions are relatively large.

CONCLUSION

The presence of numerous atrial regions in multiple patients that were found to harbor both RD_{FIRM} and RD_{sim} reinforces our previous finding that PsAF is partly driven by fibrosis-mediated mechanisms and supports the validity of our computational modeling approach. Our analysis highlights the prevalence of latent RD_{sim} sites as a potential explanation for failed ablation procedures in PsAF patients. Finally, we show that long-term outcomes were better in patients where there were fewer latent RD_{sim} sites, suggesting that substrate-based ablation based on computational modeling may be able to identify a more exhaustive set of PsAF substrate ablation targets compared to intracardiac mapping.

AUTHOR CONTRIBUTIONS

PB, SZ, SN, DS, and NT conceived the idea. PB, JH, SZ, WF, and MM developed the patient-specific atrial models, ran the computational simulations, and analyzed the outputs thereof. PB, JH, SZ, WF, MM, AP, KA, TZ, MB, EI, JC, DS, and NT interpreted the imaging data, FIRM-guided ablation, and simulation results. JC, RB, HA, JM, HC, SN, and DS oversaw and carried out the FIRM-guided ablation procedures. PB and NT wrote the manuscript.

FUNDING

This study was supported by grants from AHA 16-SDG-30440006 (PB); NIH DP1-HL123271 (NT) and the Leducq Foundation (NT and HC). This study was also supported by the Roz and Marvin H. Weiner and Family Foundation; the Dr. Francis P. Chiaramonte Foundation; Marilyn and Christian Poindexeter; and the Norbert and Louise Grunwald Cardiac Arrhythmia Research Fund.

REFERENCES

- Andrade, J., Khairy, P., Dobrev, D., and Nattel, S. (2014). The clinical profile and pathophysiology of atrial fibrillation: relationships among clinical features, epidemiology, and mechanisms. *Circ. Res.* 114, 1453–1468. doi: 10.1161/CIRCRESAHA.114.303211
- Avila, G., Medina, I. M., Jimenez, E., Elizondo, G., and Aguilar, C. I. (2007). Transforming growth factor-beta1 decreases cardiac muscle L-type Ca₂₊ current and charge movement by acting on the Cav1.2 mRNA. *Am. J. Physiol. Heart Circ. Physiol.* 292, H622–H631. doi: 10.1152/ajpheart.00781.2006
- Balouch, M., Gucuk Ipek, E., Chrispin, J., Bajwa, R. J., Zghaib, T., Berger, R. D., et al. (2017). Impact of rotor tempospatial stability on acute and one-year atrial fibrillation ablation outcomes. *Clin. Cardiol.* 40, 383–389. doi: 10.1002/clc.22674
- Beg, M. F., Helm, P. A., McVeigh, E., Miller, M. I., and Winslow, R. L. (2004). Computational cardiac anatomy using MRI. *Magn. Reson. Med.* 52, 1167–1174. doi: 10.1002/mrm.20255
- Boyle, P. M., Hakim, J. B., Zahid, S., Franceschi, W. H., Murphy, M. J., Vigmond, E. J., et al. (2018). Comparing reentrant drivers predicted by image-based computational modeling and mapped by electrocardiographic imaging in persistent atrial fibrillation. *Front. Physiol.* 9:414. doi: 10.3389/fphys.2018.00414

- Boyle, P. M., Zahid, S., and Trayanova, N. A. (2016). Towards personalized computational modelling of the fibrotic substrate for atrial arrhythmia. *Europace* 18(Suppl. 4), iv136–iv145. doi: 10.1093/europace/euw358
- Boyle, P. M., Zahid, S., and Trayanova, N. A. (2017). Using personalized computer models to custom-tailor ablation procedures for atrial fibrillation patients: are we there yet? *Expert Rev. Cardiovasc. Ther.* 15, 339–341. doi: 10.1080/14779072.2017.1317593
- Burstein, B., and Nattel, S. (2008). Atrial fibrosis: mechanisms and clinical relevance in atrial fibrillation. *J. Am. Coll. Cardiol.* 51, 802–809. doi: 10.1016/j.jacc.2007.09.064
- Calkins, H., Hindricks, G., Cappato, R., Kim, Y. H., Saad, E. B., Aguinaga, L., et al. (2017). 2017 HRS/EHRA/ECAS/APHRS/SOLAECE expert consensus statement on catheter and surgical ablation of atrial fibrillation. *Heart Rhythm* 14, e275–e444. doi: 10.1016/j.hrthm.2017.05.012
- Chrispin, J., Gucuk Ipek, E., Zahid, S., Prakosa, A., Habibi, M., Spragg, D., et al. (2016). Lack of regional association between atrial late gadolinium enhancement on cardiac magnetic resonance and atrial fibrillation rotors. *Heart Rhythm* 13, 654–660. doi: 10.1016/j.hrthm.2015.11.011
- Cochet, H., Dubois, R., Yamashita, S., Al Jefairi, N., Berte, B., Sellal, J.-M., et al. (2018). Relationship between fibrosis detected on late gadolinium-enhanced cardiac magnetic resonance and re-entrant activity assessed with electrocardiographic imaging in human persistent atrial fibrillation. *JACC Clin. Electrophysiol.* 4, 17–29. doi: 10.1016/j.jacep.2017.09.019
- Corradi, D., Callegari, S., Maestri, R., Benussi, S., and Alfieri, O. (2008). Structural remodeling in atrial fibrillation. *Nat. Clin. Pract. Cardiovasc. Med.* 5, 782–796. doi: 10.1038/ncpcardio1370
- Courtemanche, M., Ramirez, R. J., and Nattel, S. (1998). Ionic mechanisms underlying human atrial action potential properties: insights from a mathematical model. *Am. J. Physiol.* 275(1 Pt 2), H301–H321. doi: 10.1152/ajpheart.1998.275.1.H301
- Deng, D., Murphy, M. J., Hakim, J. B., Franceschi, W. H., Zahid, S., Pashakhanloo, F., et al. (2017). Sensitivity of reentrant driver localization to electrophysiological parameter variability in image-based computational models of persistent atrial fibrillation sustained by a fibrotic substrate. *Chaos* 27:093932. doi: 10.1063/1.5003340
- Eason, J., and Trayanova, N. (2002). Phase singularities and termination of spiral wave reentry. *J. Cardiovasc. Electrophysiol.* 13, 672–679. doi: 10.1046/j.1540-8167.2002.00672.x
- Gray, R. A., Pertsov, A. M., and Jalife, J. (1998). Spatial and temporal organization during cardiac fibrillation. *Nature* 392, 75–78. doi: 10.1038/32164
- Haissaguerre, M., Hocini, M., Denis, A., Shah, A. J., Komatsu, Y., Yamashita, S., et al. (2014). Driver domains in persistent atrial fibrillation. *Circulation* 130, 530–538. doi: 10.1161/CIRCULATIONAHA.113.0421
- Haissaguerre, M., Jais, P., Shah, D. C., Takahashi, A., Hocini, M., Quiniou, G., et al. (1998). Spontaneous initiation of atrial fibrillation by ectopic beats originating in the pulmonary veins. *N. Engl. J. Med.* 339, 659–666. doi: 10.1056/NEJM19980903391003
- Hansen, B. J., Zhao, J., Csepe, T. A., Moore, B. T., Li, N., Jayne, L. A., et al. (2015). Atrial fibrillation driven by micro-anatomic intramural re-entry revealed by simultaneous sub-epicardial and sub-endocardial optical mapping in explanted human hearts. *Eur. Heart J.* 36, 2390–2401. doi: 10.1093/eurheartj/ehv233
- Kakkar, R., and Lee, R. T. (2010). Intramyocardial fibroblast myocyte communication. *Circ. Res.* 106, 47–57. doi: 10.1161/CIRCRESAHA.109.207456
- Khurram, I. M., Beinart, R., Zipunnikov, V., Dewire, J., Yarmohammadi, H., Sasaki, T., et al. (2014). Magnetic resonance image intensity ratio, a normalized measure to enable interpatient comparability of left atrial fibrosis. *Heart Rhythm* 11, 85–92. doi: 10.1016/j.hrthm.2013.10.007
- Konings, K. T., Kirchhof, C. J., Smeets, J. R., Wellens, H. J., Penn, O. C., and Allessie, M. A. (1994). High-density mapping of electrically induced atrial fibrillation in humans. *Circulation* 89, 1665–1680. doi: 10.1161/01.CIR.89.4.1665
- Kraemer, H. C. (1980). Extension of the kappa coefficient. *Biometrics* 36, 207–216. doi: 10.2307/2529972
- Krummen, D. E., Bayer, J. D., Ho, J., Ho, G., Smetak, M. R., Clopton, P., et al. (2012). Mechanisms of human atrial fibrillation initiation: clinical and computational studies of repolarization restitution and activation latency. *Circ. Arrhythm. Electrophysiol.* 5, 1149–1159. doi: 10.1161/CIRCEP.111.969022
- Lalani, G. G., Coysh, T., Baykaner, T., Zaman, J., Hopper, K., Schricker, A. A., et al. (2016). Organized sources are spatially conserved in recurrent compared to pre-ablation atrial fibrillation: further evidence for non-random electrical substrates. *J. Cardiovasc. Electrophysiol.* 27, 661–669. doi: 10.1111/jce.12964
- McDowell, K. S., Vadakkumpadan, F., Blake, R., Blauer, J., Plank, G., MacLeod, R. S., et al. (2012). Methodology for patient-specific modeling of atrial fibrosis as a substrate for atrial fibrillation. *J. Electrocardiol.* 45, 640–645. doi: 10.1016/j.jelectrocard.2012.08.005
- McDowell, K. S., Vadakkumpadan, F., Blake, R., Blauer, J., Plank, G., MacLeod, R. S., et al. (2013). Mechanistic inquiry into the role of tissue remodeling in fibrotic lesions in human atrial fibrillation. *Biophys. J.* 104, 2764–2773. doi: 10.1016/j.bpj.2013.05.025
- Mohanty, S., Mohanty, P., Trivedi, C., Gianni, C., Della Rocca, D. G., Di Biase, L., et al. (2018). Long-term outcome of pulmonary vein isolation with and without focal impulse and rotor modulation mapping: insights from a meta-analysis. *Circ. Arrhythm. Electrophysiol.* 11:e005789. doi: 10.1161/CIRCEP.117.005789
- Narayan, S. M., Baykaner, T., Clopton, P., Schricker, A., Lalani, G. G., Krummen, D. E., et al. (2014). Ablation of rotor and focal sources reduces late recurrence of atrial fibrillation compared with trigger ablation alone: extended follow-up of the CONFIRM trial (Conventional Ablation for Atrial Fibrillation With or Without Focal Impulse and Rotor Modulation). *J. Am. Coll. Cardiol.* 63, 1761–1768. doi: 10.1016/j.jacc.2014.02.543
- Narayan, S. M., Krummen, D. E., and Rappel, W. J. (2012a). Clinical mapping approach to diagnose electrical rotors and focal impulse sources for human atrial fibrillation. *J. Cardiovasc. Electrophysiol.* 23, 447–454. doi: 10.1111/j.1540-8167.2012.02332.x
- Narayan, S. M., Krummen, D. E., Shivkumar, K., Clopton, P., Rappel, W. J., and Miller, J. M. (2012b). Treatment of atrial fibrillation by the ablation of localized sources: confirm (Conventional Ablation for Atrial Fibrillation With or Without Focal Impulse and Rotor Modulation) trial. *J. Am. Coll. Cardiol.* 60, 628–636. doi: 10.1016/j.jacc.2012.05.022
- Nattel, S., Burstein, B., and Dobrev, D. (2008). Atrial remodeling and atrial fibrillation: mechanisms and implications. *Circ. Arrhythm. Electrophysiol.* 1, 62–73. doi: 10.1161/CIRCEP.107.754564
- Pedrotty, D. M., Klinger, R. Y., Kirkton, R. D., and Bursac, N. (2009). Cardiac fibroblast paracrine factors alter impulse conduction and ion channel expression of neonatal rat cardiomyocytes. *Cardiovasc. Res.* 83, 688–697. doi: 10.1093/cvr/cvp164
- Ramos-Mondragon, R., Vega, A. V., and Avila, G. (2011). Long-term modulation of Na⁺ and K⁺ channels by TGF-beta1 in neonatal rat cardiac myocytes. *Pflugers Arch.* 461, 235–247. doi: 10.1007/s00424-010-0912-3
- Roney, C. H., Bayer, J. D., Zahid, S., Meo, M., Boyle, P. M., Trayanova, N. A., et al. (2016). Modelling methodology of atrial fibrosis affects rotor dynamics and electrograms. *Europace* 18(Suppl. 4), iv146–iv155. doi: 10.1093/europace/euw365
- Tanaka, K., Zlochiver, S., Vikstrom, K. L., Yamazaki, M., Moreno, J., Klos, M., et al. (2007). Spatial distribution of fibrosis governs fibrillation wave dynamics in the posterior left atrium during heart failure. *Circ. Res.* 101, 839–847. doi: 10.1161/CIRCRESAHA.107.153858
- Trayanova, N. A. (2014). Mathematical approaches to understanding and imaging atrial fibrillation: significance for mechanisms and management. *Circ. Res.* 114, 1516–1531. doi: 10.1161/CIRCRESAHA.114.302240
- Vadakkumpadan, F., Rantner, L. J., Tice, B., Boyle, P., Prassl, A. J., Vigmond, E., et al. (2009). Image-based models of cardiac structure with applications in arrhythmia and defibrillation studies. *J. Electrocardiol.* 42, 157.e1–157.e10. doi: 10.1016/j.jelectrocard.2008.12.003
- Verma, A., Jiang, C. Y., Betts, T. R., Chen, J., Deisenhofer, I., Mantovan, R., et al. (2015). Approaches to catheter ablation for persistent atrial fibrillation. *N. Engl. J. Med.* 372, 1812–1822. doi: 10.1056/NEJMoa1408288
- Yue, L., Xie, J., and Nattel, S. (2011). Molecular determinants of cardiac fibroblast electrical function and therapeutic implications for atrial fibrillation. *Cardiovasc. Res.* 89, 744–753. doi: 10.1093/cvr/cvq329
- Zahid, S., Cochet, H., Boyle, P. M., Schwarz, E. L., Whyte, K. N., Vigmond, E. J., et al. (2016a). Patient-derived models link re-entrant driver localization

- in atrial fibrillation to fibrosis spatial pattern. *Cardiovasc. Res.* 110, 443–454. doi: 10.1093/cvr/cvw073
- Zahid, S., Whyte, K. N., Schwarz, E. L., Blake, R. C. III, Boyle, P. M., Chrispin, J., et al. (2016b). Feasibility of using patient-specific models and the “minimum cut” algorithm to predict optimal ablation targets for left atrial flutter. *Heart Rhythm* 13, 1687–1698. doi: 10.1016/j.hrthm.2016.04.009
- Zhao, J., Hansen, B. J., Wang, Y., Csepe, T. A., Sul, L. V., Tang, A., et al. (2017). Three-dimensional integrated functional, structural, and computational mapping to define the structural “Fingerprints” of heart-specific atrial fibrillation drivers in human heart ex vivo. *J. Am. Heart Assoc.* 6:e005922. doi: 10.1161/JAHA.117.005922

Conflict of Interest Statement: The authors declare that the research was conducted in the absence of any commercial or financial relationships that could be construed as a potential conflict of interest.

Copyright © 2018 Boyle, Hakim, Zahid, Franceschi, Murphy, Prakosa, Aronis, Zghaib, Balouch, Ipek, Chrispin, Berger, Ashikaga, Marine, Calkins, Nazarian, Spragg and Trayanova. This is an open-access article distributed under the terms of the Creative Commons Attribution License (CC BY). The use, distribution or reproduction in other forums is permitted, provided the original author(s) and the copyright owner(s) are credited and that the original publication in this journal is cited, in accordance with accepted academic practice. No use, distribution or reproduction is permitted which does not comply with these terms.



Automatic Detection of Atrial Fibrillation Based on Continuous Wavelet Transform and 2D Convolutional Neural Networks

Runnan He¹, Kuanquan Wang¹, Na Zhao¹, Yang Liu¹, Yongfeng Yuan¹, Qince Li^{1*} and Henggui Zhang^{1,2,3,4*}

¹ School of Computer Science and Technology, Harbin Institute of Technology, Harbin, China, ² School of Physics and Astronomy, The University of Manchester, Manchester, United Kingdom, ³ Space Institute of Southern China, Shenzhen, China, ⁴ Key Laboratory of Medical Electrophysiology, Ministry of Education, Collaborative Innovation Center for Prevention and Treatment of Cardiovascular Disease, Institute of Cardiovascular Research, Southwest Medical University, Luzhou, China

OPEN ACCESS

Edited by:

Jichao Zhao,

University of Auckland, New Zealand

Reviewed by:

Ahsan H. Khandoker,

Khalifa University,

United Arab Emirates

Neetika Nath,

Universitätsmedizin Greifswald,

Germany

*Correspondence:

Qince Li

qinceli@hit.edu.cn

Henggui Zhang

henggui.zhang@manchester.ac.uk

Specialty section:

This article was submitted to

Computational Physiology

and Medicine,

a section of the journal

Frontiers in Physiology

Received: 29 March 2018

Accepted: 10 August 2018

Published: 30 August 2018

Citation:

He R, Wang K, Zhao N, Liu Y, Yuan Y, Li Q and Zhang H (2018)

Automatic Detection of Atrial Fibrillation Based on Continuous Wavelet Transform and 2D Convolutional Neural Networks.

Front. Physiol. 9:1206.

doi: 10.3389/fphys.2018.01206

Atrial fibrillation (AF) is the most common cardiac arrhythmias causing morbidity and mortality. AF may appear as episodes of very short (i.e., proximal AF) or sustained duration (i.e., persistent AF), either form of which causes irregular ventricular excitations that affect the global function of the heart. It is an unmet challenge for early and automatic detection of AF, limiting efficient treatment strategies for AF. In this study, we developed a new method based on continuous wavelet transform and 2D convolutional neural networks (CNNs) to detect AF episodes. The proposed method analyzed the time-frequency features of the electrocardiogram (ECG), thus being different to conventional AF detecting methods that implement isolating atrial or ventricular activities. Then a 2D CNN was trained to improve AF detection performance. The MIT-BIH Atrial Fibrillation Database was used for evaluating the algorithm. The efficacy of the proposed method was compared with those of some existing methods, most of which implemented the same dataset. The newly developed algorithm using CNNs achieved 99.41, 98.91, 99.39, and 99.23% for the sensitivity, specificity, positive predictive value, and overall accuracy (ACC) respectively. As the proposed algorithm targets the time-frequency feature of ECG signals rather than isolated atrial or ventricular activity, it has the ability to detect AF episodes for using just five beats, suggesting practical applications in the future.

Keywords: atrial fibrillation, continuous wavelet transform, 2D convolutional neural networks, time-frequency features, practical applications

INTRODUCTION

Atrial fibrillation (AF) is recognized as a major cardiovascular disease, affecting a large number of the population (Zoniberisso et al., 2014; Potter and Le, 2015). AF is associated with increased risks of cardiovascular events, reducing the life quality of AF patients or even causing mortality (Hylek et al., 2003; Mathew et al., 2009). AF is also related to obesity, long-term alcoholism and obstructive sleep apnea, each of which promotes the development of AF (Gami et al., 2004; Mukamal et al., 2005; Miyasaka et al., 2006; Mathew et al., 2009, p. 25). Furthermore, the lack of a deep understanding for its pathophysiological mechanisms affects the diagnosis of AF (Censi et al., 2013). Therefore, an early detection of AF appears to be important for effective treatments of AF.

Based on the duration of episodes, AF can be classified into three main types, namely paroxysmal, persistent, and permanent (January et al., 2014). Paroxysmal AF is usually the primary condition of the arrhythmia, with which the episodes terminate spontaneously within 7 days after its initiation; whilst persistent and permanent AF can last for more than several months. For many AF patients they may initially suffer very short episodes, but the episodes increase in frequency and duration, leading to be persistent by a mechanism of AF begetting AF (de Vos et al., 2010). For this condition, AF may last longer than 7 days, to terminate which one may need interventions such as pharmacological or electrical cardioversion. Without treatment, persistent AF may turn into permanent AF, one of the most sustained cardiac arrhythmias (Zoniberisso et al., 2014).

Early detection of AF is essential for effective treatments. However, it is still not easy to address the early AF detection task though the use of long-term ECG recording devices is available. Proximal AF episodes often last only for a few beats in duration, therefore, it is very time-consuming to detect AF by visual inspection (Dash et al., 2009). Such a challenge calls for a wide variety of automatic AF detectors. For the past years, a series of sophisticated methods have been developed to tackle the challenges of AF detection (Kikillus et al., 2007; Couceiro et al., 2008; Babaeizadeh et al., 2009; Yaghoubi et al., 2010; Larburu et al., 2011; Parvaresh and Ayatollahi, 2011). Two classes of AF detection methods, the atrial activity analysis-based (Artis et al., 1991; Slocum et al., 1992; Lake and Moorman, 2011; Zhou et al., 2014; Ladavich and Ghoraani, 2015) and the ventricular response analysis-based (Moody and Mark, 1983; Tateno and Glass, 2001; Dash et al., 2009; Park et al., 2009; Huang et al., 2011; Lian et al., 2011; Yaghoubi et al., 2012; Lee et al., 2014) method, attract the interest of the most of studies. The first category methods utilize the absence of P waves or the presence of f-waves for diagnosis. The performance of this kind of method highly depended on the signal quality, which is hard to be guaranteed in the practice. The second category methods are based on the variability of RR intervals. Although these kinds of methods have a robust noise resistance, its diagnosis accuracy is unsatisfactory when a wide variety of rhythms need to be dealt with due to the limitation of the information conveyed by RR intervals (Petrutiu et al., 2006; Huang et al., 2011; Lian et al., 2011; Lee et al., 2014).

Over past years, algorithms based on convolutional neural networks (CNNs) have proved successful in information classification in many fields, such as object detection, speech, and image recognition (Lecun et al., 2015). However, CNNs-based

algorithms for stratifying cardiovascular diseases are not well-established due to limited availability of ECG database. Though a few previous studies have applied CNNs to detect cardiac arrhythmias (Rajpurkar et al., 2017; Vollmer et al., 2017), it still remains a challenge to develop an effective algorithm for detecting AF based on short episodes of ECGs.

The objective of this study was to address some potential drawbacks of existing AF classification methods by developing an accurate and reliable one for the fully automated classification of AF based on continuous wavelet transform (CWT) (Addison, 2005) and 2D CNNs (Krizhevsky et al., 2012) methods. Such possible drawbacks of traditional AF classification methods include: (i) manual extraction of ECG features that limits the accuracy of classification; (ii) low efficacy for fast AF detection with a short period of ECG signal data; and (iii) the use of atrial or ventricular only activities to classify AF and normal condition, lacking consideration of complete information of ECG signal. The advantage of the proposed algorithm over others lies at that we do not need to manually extract features of ECG signals. Instead, the proposed CNNs can automatically extract the spatio-temporal features of ECG patterns obtained by the CWT analysis with proper trainings. In addition, the proposed algorithm can detect AF by using only five beats to achieve a significant performance, suggesting potentials for clinical applications.

The developed method was tested and validated by the MIT-BIH Atrial Fibrillation Database (AFDB) (Goldberger et al., 2000).

The rest of this paper is organized as follows. In Section “Materials and Methods,” the method of three-stage AF classification is described in details. In Section “Implementation of the Algorithm,” some details about the implementation of the algorithm are presented. In Section “Results and Discussion,” the proposed method is evaluated using the AFDB, and its performance with varied CNNs parameters is analyzed. AF detection results by the presented method are compared with those from other existing algorithms. Finally, Section “Conclusion” concludes our study.

MATERIALS AND METHODS

The flowchart of the proposed AF detection method is shown in **Figure 1**. It includes four stages in two phases: phase 1 is for pre-processing (data denoising and data segmentation) and phase 2 for CWT and AF classification with CNNs. In phase 1,

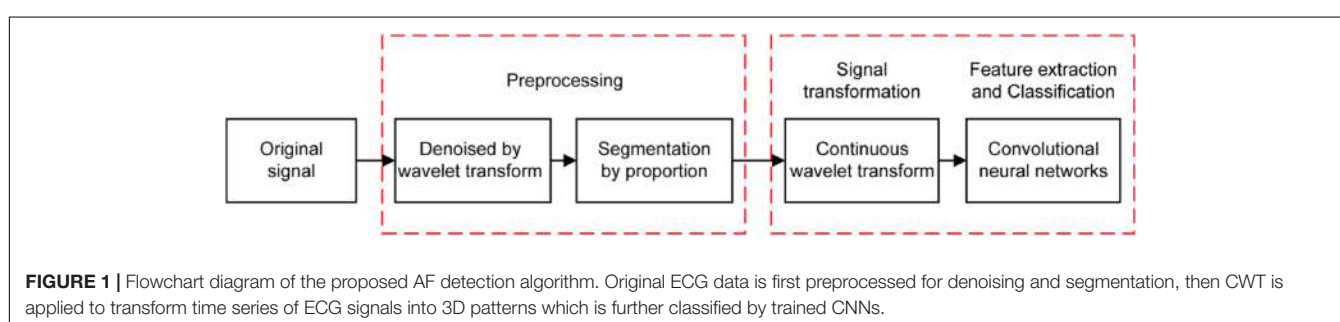


FIGURE 1 | Flowchart diagram of the proposed AF detection algorithm. Original ECG data is first preprocessed for denoising and segmentation, then CWT is applied to transform time series of ECG signals into 3D patterns which is further classified by trained CNNs.

the wavelet transform (WT) method is applied to remove the noise from the ECG signal, which is then segmented into a series of periods, each of which has duration of 1.2 s (i.e., 300 sample points given the sampling rate of 250 Hz). In phase 2, CWT is first employed to transform the five beats of the ECG signal in each segment to a 3D time-frequency representation of ECG patterns. Then, the proposed CNNs was properly trained to process the AF classification.

Database

The MIT-BIH AFDB was used to evaluate the performance of the developed AF detection method. The database contains 25 ECG recordings with about 10-h in duration length mainly from PAF patients, which were obtained with a 250 Hz sampling rate. However, in the present study four recordings in database were excluded because two raw recordings ("00735" and "03665") are not available, and the other two recordings ("04936" and "05091") have some incorrect reference annotations. The database contains 605 episodes for four different rhythms, among them 291 episodes are for AF, 14 episodes for atrial flutter, 12 episodes for junctional rhythm, and 288 episodes for other rhythms. For each ECG recording, it contains ECG signals from two leads, first of which was used for this study.

Noise Filtering

Raw data of ECG is contaminated by noises. Therefore, the WT method (Shyu et al., 2004; Gomes et al., 2010) is used to filter noises.

For a time series of ECG $f(t)$, its WT with respect to a given mother wavelet (ψ) is defined as the following (Shyu et al., 2004; Gomes et al., 2010):

$$W_{a,b}f(t) = \frac{1}{|a|^{1/2}} \int_{-\infty}^{\infty} f(t)\psi\left(\frac{t-b}{a}\right) dt \quad (1)$$

where a , b and $W_{a,b}$ are the scale factor, translational value and WT respectively. Letting $a = 2^j$ ($j \in \mathbb{Z}$, \mathbb{Z} is the integral set), the WT is regarded as dyadic WT, which represents better the multiscale characterization of ECG signals than the CWT does (Mallat and Zhong, 1992). For a discrete time series of $f(t)$, which is denoted as $f(n)$, $n = 1, 2, 3 \dots N$, the calculation of dyadic WT is derived from Equation (1) for low and high frequency components as represented as:

$$S_{2^j}f(n) = \sum_{k \in \mathbb{Z}} h_k S_{2^{j-1}}f(n - 2^{j-1}k) \quad (2)$$

$$W_{2^j}f(n) = \sum_{k \in \mathbb{Z}} g_k S_{2^{j-1}}f(n - 2^{j-1}k) \quad (3)$$

where S_{2^j} and W_{2^j} are the smoothing operator of the WT, and h_k and g_k are the coefficients of the corresponding high and low filters. In this study, we decomposed original ECG signal into seven scales (the corresponding frequency bands are 62.5–125, 31.25–62.5, 15.63–31.25, 7.81–15.63, 3.91–7.81, 1.95–3.91, and 0.98–1.95 Hz, respectively). By using the *Daubechies4* (*db4*) wavelet function (Daubechies, 1988), the input ECG signal $f(n)$ is decomposed into low frequency and high frequency components,

and the low frequency component is put into the next layer for further decomposition. The reason why we choose the *db4* wavelet is due to its good regularity, which makes the reconstruction of ECG signals smooth (Daubechies, 1988).

In numerical implementation, it was found that the high frequency noise was mainly determined by one to three scale bands. Therefore, the values of these three scales were set to zeros to filter the high-frequency noise. The filtered signals were used in subsequent processing, which are shown in **Figure 2** for AF and normal ECG signals.

Data Segmentation by Proportion

Segmentation of ECG signal into a series of time periods usually requires precise detection of boundaries and peak positions of the three characteristic of ECG waves (i.e., P, QRS, and T waves corresponding to the depolarization of the atria and ventricles, and repolarization of the ventricles respectively), which are termed as fiducial points. In this study, segmentation of ECG recordings into a series of time windows was based on the annotated R-peak locations of the database, allowing us to directly compare our results with the performance of other existing methods.

For each segmented time window of the ECG signal, it contains one heart beat cycle and has a length of 1.2 s (i.e., about 300 sampling points), starting at the 2/3 period of the previous RR interval (which is the interval between the peaks of the previous QRS complex to the current QRS peak, see **Figure 3**). Each segment contains the information of atrial and ventricular activities. The reason for the segment size to be chosen is to allow each segment contain most of the information in one heart beat cycle for both AF and normal conditions. An example of segmented ECG signals into five beats for AF and normal conditions are shown in **Figure 3**, with each beat being marked by two dotted lines with the same color. For normal ECG signal (**Figure 3A**), a clear P wave is present as shown by the encircled inset. For AF ECG signal (**Figure 3B**), no clear P wave is present. Instead, a series of continuous, rapid and irregular f-waves is present indicating AF (f-waves) (see the encircled inset).

Continuous Wavelet Transform

Feature extraction plays a key role for AF classification (Chazal and Reilly, 2006). Any information in the ECG signals that can be used to discriminate AF from normal condition is considered as one feature. The features can be extracted in various forms directly from the processed ECG signal in the time, frequency and time-frequency domains.

Previous studies have investigated various ways to extract ECG features, among them the WT methods are believed to be the most efficient for processing ECG signals (Guler and Ubeyli, 2005; Lin et al., 2008; Kutlu and Kuntalp, 2012). By WT, one can extract ECG information in both frequency and time domains, which is superior to the traditional Fourier transform, which can only analyze ECG information in the frequency domain (Dokur and Olmez, 2001). For various types of WT (Addison, 2005), the most popular one for ECG classification is the discrete wavelet transform (DWT) (Kozak et al., 2008). In addition to DWT, CWT has also been used to extract features from the

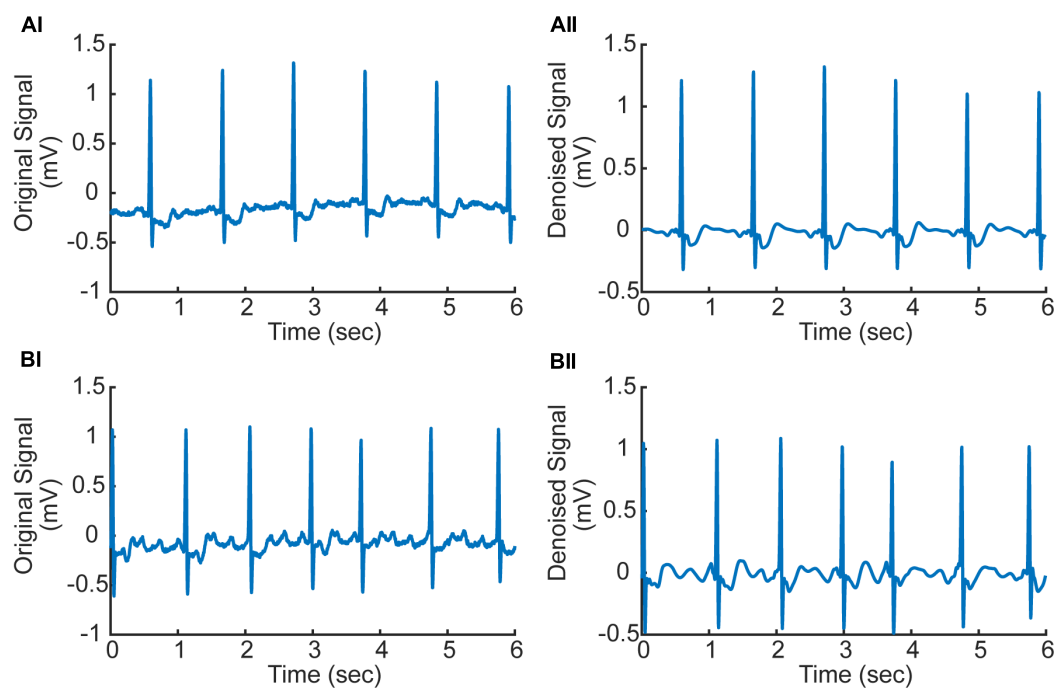


FIGURE 2 | (Ai,Aii) Original and denoised ECG signal in AF condition (ECG record 07910). **(Bi,Bii)** Original and denoised ECG signal in normal condition (ECG record 07910). f-Waves between two consecutive R-waves are apparent illustrating atrial fibrillation (AF).

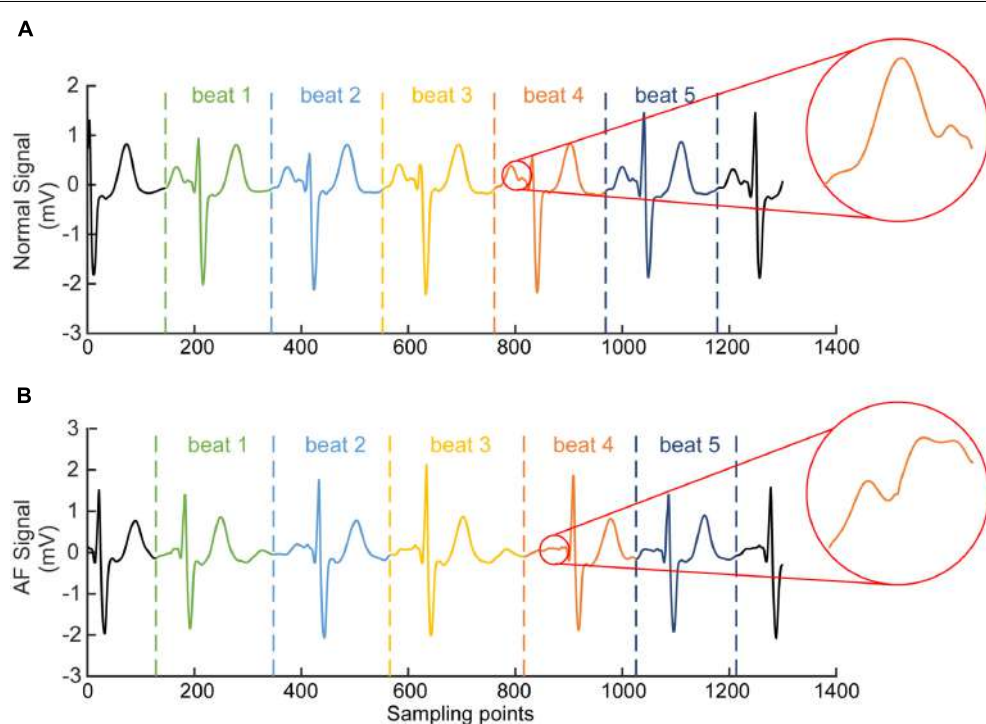


FIGURE 3 | Illustration of segmented ECG signals into five beats for normal **(A)** and AF **(B)** conditions. Each beat was marked by two dotted lines with the same color. In **(A)** for normal ECG, a clear normal P wave is present as shown by the encircled inset. In **(B)** for AF ECG, abnormal f-waves are apparent as shown in the encircled inset.

ECG signals, since it solves many of DWT defects, such as the coarseness of the representation and instability, which has been applied successfully for at least a decade ago (Addison, 2005).

In this study, we have employed CWT based Equation (1) with the *Daubechies5* (*db5*) wavelet to transform five beats to a series of five corresponding 2D CWT patterns, which can be regarded as a 3D time-frequency representation of ECG signals (Daubechies, 1988). **Figure 4** shows examples of the 2D patterns of CWT transformation from normal and AF ECG signals. In the figure, the color codes the density of the signal component in the corresponding frequency with brighter color representing a higher density. As shown in **Figures 4Ai,Aii**, there are some differences in the 1D time series of ECGs between normal and AF conditions. First, there is no clear or a dominant P wave in the AF ECG (**Figure 4Ai**) as compared to the normal ECG (instead, high frequency but low amplitude f-waves exist). Second, due to the filtering effect of atrioventricular node, there is no 1:1 ventricular response to the atrial excitation, therefore the RR interval is different between the AF and normal conditions. Consequentially during each segmented time window of the ECG signal (fixed for 1.2 s, i.e., 300 sampling points), one R wave presents in the AF ECG (**Figure 4Ai**) whilst two R waves presents in the normal ECG (**Figure 4Aii**). Such different information in the time domain are reflected by

the CWT, which converts the 1D time domain signal into the 2D pattern in the time-frequency domain of the distribution of frequency at different timings, which can be used to better differentiate AF from normal condition. The 2D CWT patterns for AF and normal conditions are shown in **Figures 4Aii,Bii** correspondingly.

The Basic Construction of Convolutional Neural Networks

Convolutional neural network has been shown to be able to automatically extract features of signals without any data pre-processing and pre-training algorithms (Arel et al., 2010). A traditional CNNs is composed of an input and an output layer, as well as multiple hidden layers which typically consist of convolutional layers, pooling layers, and fully connected layers (Hubel and Wiesel, 1959).

For convolutional layers, they are locally connected to extract and convolve the features by applying a set of weights which are called filter or kernel (Hubel and Wiesel, 1959). Basically, the relevant high-level features can be extracted with the increase of the number of the convolutional layers. The weights of the parameters of the convolutional kernels in each layer are trained with the backpropagation (BP) error algorithm (Rumelhart et al., 1988). For an activation function, a

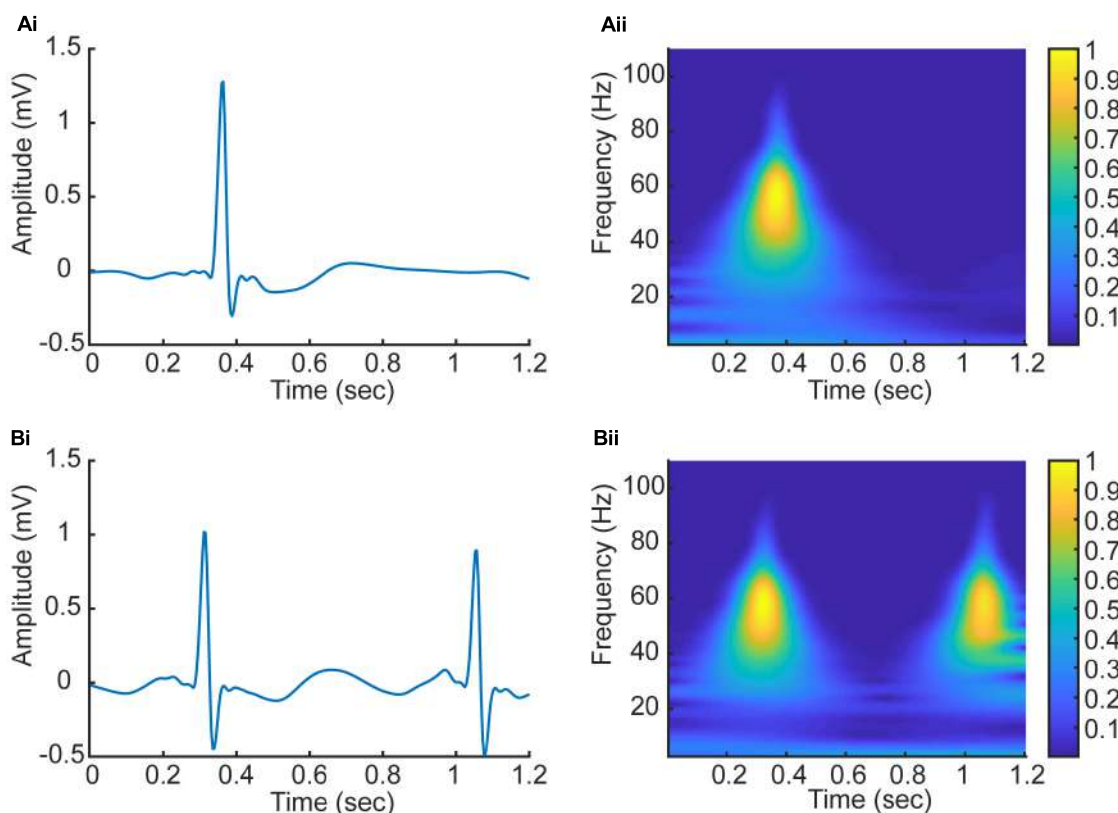


FIGURE 4 | (Ai,Aii) 1D time domain signal and 2D frequency-time pattern based on CWT in AF condition. **(Bi,Bii)** 1D time domain signal and 2D frequency-time pattern based on CWT in normal condition.

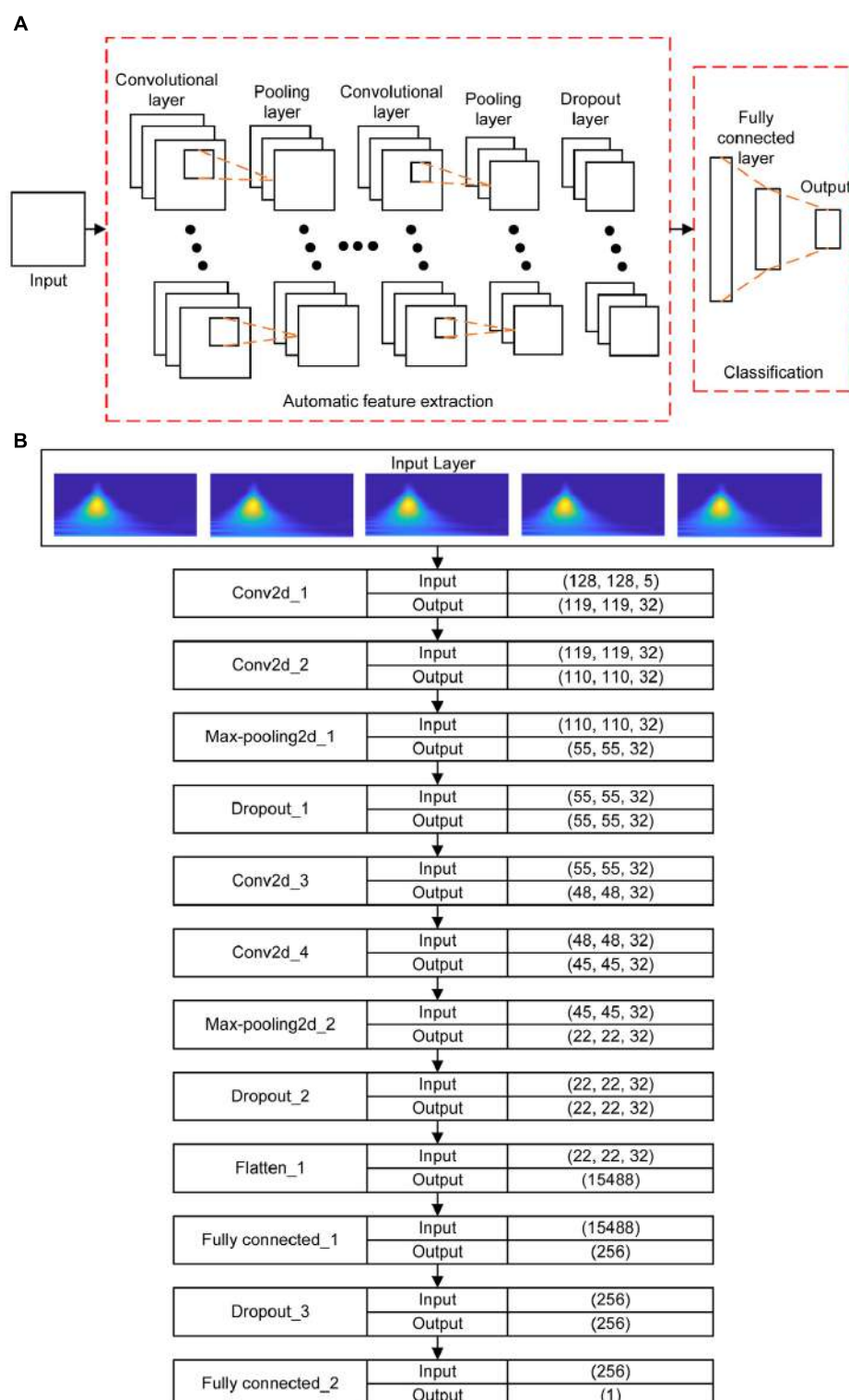


FIGURE 5 | (A) Schematic illustration of the basic construction of CNNs. **(B)** The architecture of the proposed CNNs. The input instance of the proposed CNNs is five 128×128 images representing the CWT spectrums of corresponding five beats. In the convolutional layer, the output size is denoted as (x, y, z) , where (x, y) is the size of the feature map in this layer, and z is the number of convolutional kernels. In the Max-pooling layer, the size of the feature map is reduced by half in both x and y axes. In the Dropout layer, the output size is the same as the output of previous layer. In the Flatten layer, the output is flattened to an 1D vector. In the Fully connected layer, the output size is the same as the number of neurons of the layer.

sigmoid function is usually applied to the convolved features as follows:

$$\alpha_i^k = W^k x_i + b^k \quad (4)$$

$$\beta_i^k = \frac{1}{1 + e^{-\alpha_i^k}} \quad (5)$$

where α_i^k represents the convolution result that is for the i th input and the k th feature map, W^k and b^k respectively represent the corresponding weights and bias terms for the k th feature map. The sigmoid function output β_i^k is applied to the k th feature map producing outputs. Furthermore, x_i denotes the i th training data which is an n -dimension vector.

After the convolution layer, the dimensionality of the extracted features is reduced in order to improve the speed of the training process, so the pooling layer is applied to the following hidden layer which is called the subsampling layer merging similar features into one. The action of the pooling layer is to compute the averaged convolved features within the neighboring neurons that are laid in the prior convolutional layer. In some cases, the dropout layer may be applied for random training network parameters to prevent over-fitting. After a given set of convolutional, pooling and dropout layers, one or more fully connected layers are employed whose neurons are jointed to the whole neurons from the previous layer at the end of the constructed CNNs. The major of CNNs parameters are generally produced by the fully connected layer parameters, which complete the mission of AF classification and determine the final classification results. The basic construction of CNNs is shown in **Figure 5A** including the common input convolutional, pooling, dropout, fully connected, and output layers.

In this paper, the CNNs architecture including the input, convolutional, max-pooling, dropout, flatten, fully connected, and output layers are designed in which the optimal parameters are described in Section "Implementation of the Algorithm." The whole construction of the proposed CNNs for AF classification is also demonstrated in Section "Implementation of the Algorithm."

IMPLEMENTATION OF THE ALGORITHM

The Division of Dataset

The original annotated time series of ECG signal is divided into a series of five segments, each of which contains one heart beat cycle. In total, 162,536 five beat data segments were used, among which 61,924 and 100,612 segments are for AF and normal condition respectively. It is obvious that the AF and normal samples are not balanced. To address this issue, we randomly selected the same number data of AF and normal conditions, which were assigned into training and test sets from different recordings, by which over-fitting resulted from training and testing data set from the same patient was also avoided. Eventually, we extracted a total of 100,000 samples into a training set and test set based on the proportion of 4:1, among which 80000 training and 20000 test data were used to build the model.

The Architecture of the Proposed CNNs

Continuous wavelet transform was used to transform the five beat time domain signals into time-frequency domain signals with the db5 wavelet (Daubechies, 1988), resulting in five corresponding 2D patterns of frequency density as a 3D input instance to the proposed CNNs.

With a 3D input instance, the structure of the proposed CNNs is designed as shown in **Figure 5B**. The CNNs structure contains four convolutional layers, three dropout layers, two max-pooling, two fully connected layers, and one flatten layer. Each of the first two convolutional layers has 32 convolution kernels with the kernel size of 10×10 . After the convolution operations, the first max-pooling layer with pooling size of 2×2 was used to reduce the size of the previous output followed by a dropout layer to suppress the complexity of the network. The number of kernel of the following two convolutional layers is the same as in the previous ones, but the sizes of the kernels are 8×8 and 4×4 respectively. Followings are the second max-pooling layer with the same pooling size as the first one and a dropout layer. After these operations, the output data is transformed to a 1D vector by a flatten layer, and then feed into two fully connected layers that have 256 and 1 neurons respectively, between which is a dropout layer.

In the CNNs, the learning rate, momentum and weight decay rates are set to 0.001, 0.8, and 10^{-6} respectively. To optimize these parameters, the stochastic gradient decent (SGD) algorithm (Rumelhart et al., 1988) was implemented. Furthermore, instead of large-size convolutional kernel, a multi-layer with small-scale convolutional kernel is used in order to reduce the

TABLE 1 | Optimal CNNs parameter set for AF arrhythmias classification.

The CNNs parameter	Value
Learning rate initial value	0.001
Moment coefficient	0.8
First convolutional layer kernel size	10
Weight decay rates	10^{-6}
Second convolutional layer kernel size	10
First max-pooling layer kernel size	2
Third convolutional layer kernel size	8
Forth convolutional layer kernel size	4
Max-pooling layer kernel size	2
The number of neurons in the first fully connected layer	256
The number of neurons in the second fully connected layer	1
Epoch number	50

TABLE 2 | Various learning rate for proposed CNNs.

Learning rate value	Testing samples classification accuracy (%)
0.0007	99.08
0.0008	99.12
0.0009	99.06
0.001	99.23
0.003	99.08
0.005	99.04

TABLE 3 | Various moment coefficient for proposed CNNs.

Moment coefficient	Testing samples classification accuracy (%)
0.7	99.18
0.75	99.15
0.8	99.23
0.85	99.06
0.9	99.16
0.95	98.90

number of parameters and increase the non-linearity of the network.

As shown in **Figure 5B**, the Conv2d_i ($i = 1, 2, 3, 4$) represent the four convolutional layers, which are followed by two Max-pooling2d_j ($j = 1, 2$) and Dropout_k ($k = 1, 2$) layers. In this paper, the input instance of the proposed network is a 3D vector with a size of (128, 128, 5) specifying the length, width and beat number of the CWT pattern. After four convolution and two max-pooling operations, the size of the instance is transformed into a pattern of (22, 22, 32), which specify the size of convolutional result of each kernel and the number of kernels in the last convolutional layer. Through the flatten layer, the output size of the previous layer is changed to 15488 ($22 \times 22 \times 32$), which is then input into the first Fully connected_1 layer containing 256 neurons. Finally, with the third Dropout_3 and the second Fully connected_2 layer, the classification results are decided.

RESULTS AND DISCUSSION

The proposed method was applied to the dataset of AFDB. From classification results, we calculated four parameters: correct AF classification number [true positives (TPs)], false normal classification number [false negatives (FNs)], correct normal classification number [true negatives (TNs)], and false AF classification number [false positives (FPs)]. In order to evaluate the performance of the proposed classification algorithm,

the sensitivity (Se), specificity (Sp), positive predictive value (PPV), and overall accuracy (ACC) were calculated using the following equations respectively.

$$Se = \frac{TP}{TP + FN} \times 100\% \quad (6)$$

$$Sp = \frac{TN}{TN + FP} \times 100\% \quad (7)$$

$$PPV = \frac{TP}{TP + FP} \times 100\% \quad (8)$$

$$Acc = \frac{TP + TN}{TP + FP + TN + FN} \times 100\% \quad (9)$$

In this study, the newly developed algorithm using CNNs with the AFDB have achieved 99.41, 98.91, 99.39, and 99.23% for the sensitivity, specificity, PPV, and overall accuracy respectively, which was better than most of other existing algorithms as detailed below.

Selection of Parameters

To obtain an optimal CNNs network structure to classify AF, the impacts of varied structural and training parameters of the network on output results were evaluated. By comparing the final error values of testing samples, a set of final CNNs parameters were obtained to achieve the minimum testing error, which are shown in **Table 1**.

The number of feature maps in the pooling layers is the same as the convolutional layers. The learning rate and moment are initialized at 0.001 and 0.8 during the training procession. The classification loss function about the training samples is stable after 50 epochs of CNNs. Because of the number of the training samples, the accuracy rate of the proposed method cannot be further increased by changing the number of convolutional and max-pooling layers.

In the following analysis, the impacts of different training and structural parameters about the proposed classification method are discussed.

TABLE 4 | Comparison of the performances of AF classification algorithms based on the same database of AFDB.

Algorithm	Year	WL (s)	Se (%)	Sp (%)	PPV (%)	ACC (%)
Moody and Mark	1983	60	87.54	95.14	92.29	92.12
Cerutti et al.	1997	90	96.10	81.55	75.76	83.38
Tateno and Glass	2001	50	94.40	97.20	96.10	—
Logan and Healey	2005	120	96.00	89.00	—	—
Couceiro et al.	2008	60	93.80	96.09	—	—
Babaeizadeh et al.	2009	>60	89.00	96.00	88.00	—
Dash et al.	2009	128 beats	94.40	95.10	—	—
Lake and Moorman	2011	12	91.00	94.00	—	—
Huang et al.	2011	101 beats	96.10	98.10	—	—
Ladavich and Ghorani	2015	7 beats	98.09	91.66	79.17	93.12
Asgari et al.	2015	9.8	97.00	97.10	—	97.10
Garcia et al.	2016	7 beats	91.21	94.53	—	93.32
Xia et al.	2018	5	98.79	97.87	—	98.63
Proposed Algorithm	2018	5 beats	99.41	98.91	99.39	99.23

Learning Rate

In this case, the original value of the learning rate is changed systematically from 0.0007 to 0.005. **Table 2** shows the testing samples classification accuracy of different learning rate values after 50 epochs. As the performance displayed in **Table 2**, results of the proposed CNNs are not improved whether the learning rate is increased or decreased. Therefore, the optimum value of the learning rate is set to 0.001.

Momentum Coefficient

In this case, the influences of altering the momentum coefficient on the results of the proposed CNNs are investigated. The classification accuracy about the testing samples during 50 epochs are calculated and presented in **Table 3** with the same CNNs structural parameters. As the performance shown in **Table 3**, the results of the proposed CNNs are not improved whether the momentum coefficient is increased or decreased. Therefore, the optimum momentum coefficient value is set to 0.8. About the momentum coefficient, it can avoid the neural network into a local minimum. However, it also may result in the unstable of the network structure when the value is set quite high.

CNNs Structural Parameters

In this study, the final values of the learning rate and momentum coefficient are respectively set to 0.001 and 0.8. Furthermore, the changes for the other CNNs structural parameters (the convolutional and max-pooling layer kernel size and the number of neurons in the fully connected layer max-pooling layer kernel size) also have been carried out based on experimentation experiences. According to the results, the performance is not improved for different structural parameter sets, as such the parameters shown in **Table 1** are still as optimum choice for proposed CNNs.

Comparison With Other Related Studies for AF Classification

In order to evaluate the performance of the proposed classification method, the proposed algorithm was compared with other existing algorithm employing five measurements containing the sensitivity, specificity, PPV, overall accuracy and the length of the window (WL) respectively. Many of the algorithms (Moody and Mark, 1983; Cerutti et al., 1997; Tateno and Glass, 2001; Logan and Healey, 2005; Couceiro et al., 2008; Babaeizadeh et al., 2009; Dash et al., 2009; Huang et al., 2011; Lake and Moorman, 2011; Asgari et al., 2015; Ladavich and Ghoraani, 2015; García et al., 2016; Xia et al., 2018) were chosen for comparison as the best performing results for various methods.

As shown in **Table 4**, the performance of the proposed method is better than all of other algorithms in comparison for classifying AF which implemented on the same database of AFDB. In addition, the present algorithm is capable of AF detection by using only five beats, which is superior to other algorithms. This is due to the implementation of finer CWT transform and better designed CNNs network of the

present algorithm as compared to the others, allowing a more accurate identification of AF by using shorter ECG segments based on automatically extracting pattern features of 2D CWT transformation patterns.

Clinical Relevance

The proposed method is able to classify AF with five beat cycles. It has potentials to be used as an assistant diagnosing tool for clinic uses. In general, AF is the main causes of strokes so it is essential to diagnose it in the early stage for AF patients. Upon a proper early diagnosis, efficient treatment plans like rate-control medication or anticoagulation therapy for AF patients can be made to reduce the occurrence of strokes. As the proposed algorithm requires only five beats, proximal AF data can be detected as AF with a high accuracy.

CONCLUSION

We developed a framework based on time-frequency representation of ECG signals and CNNs architectural model for automated classification of AF. The framework transforms 1D ECG signal into 2D patterns of frequency densities, allowing the state-of-the-art techniques of CNNs-based machine learning method to classify AF automatically. It analyzes the time-frequency features of both atrial and ventricular activities, allowing AF detection by using a very short period (five beats) of ECG. By testing it on the AFDB, a performance with 99.41, 98.91, 99.39, and 99.23% for the sensitivity, specificity, PPV, and overall accuracy respectively was achieved, which is superior to the most of the existing algorithms suggesting a great potential in clinical diagnosis in the future.

AUTHOR CONTRIBUTIONS

HZ conceived the study. RH performed the design and implementation of the algorithm. QL helped the algorithm design and implementation. RH, HZ, and QL wrote the manuscript. KW and YY commented on and approved the manuscript. NZ and YL contributed to the classification of AF. All authors read and approved the final manuscript.

FUNDING

The work was supported by the National Natural Science Foundation of China (NSFC) (Grant Nos. 61572152, 61571165, and 61601143 to HZ, KW, and QL), the Science Technology and Innovation Commission of Shenzhen Municipality (Grant Nos. JSGG20160229125049615 and JCYJ20151029173639477 to HZ), and the China Postdoctoral Science Foundation (Grant No. 2015M581448 to QL).

REFERENCES

- Addison, P. S. (2005). Wavelet transforms and the ECG: a review. *Physiol. Meas.* 26, R155–R199. doi: 10.1088/0967-3334/26/5/R01
- Arel, I., Rose, D. C., and Karnowski, T. P. (2010). Deep machine learning - a new frontier in artificial intelligence research. *IEEE Comput. Intell. Magazine* 5, 13–18. doi: 10.1109/TMI.2010.2833635
- Artis, S. G., Mark, R. G., and Moody, G. B. (1991). Detection of atrial fibrillation using artificial neural networks. *Comput. Cardiol.* 18, 173–176. doi: 10.1109/CIC.1991.169073
- Asgari, S., Mehrnia, A., and Moussavi, M. (2015). Automatic detection of atrial fibrillation using stationary wavelet transform and support vector machine. *Comput. Biol. Med.* 60, 132–142. doi: 10.1016/j.combiomed.2015.03.005
- Babaeizadeh, S., Gregg, R. E., Helfenbein, E. D., Lindauer, J. M., and Zhou, S. H. (2009). Improvements in atrial fibrillation detection for real-time monitoring. *J. Electrocardiol.* 42, 522–526. doi: 10.1016/j.jelectrocard.2009.06.006
- Censi, F., Cianfrocca, C., and Purificato, I. (2013). Atrial fibrillation and the 4P medicine. *Ann. Ist. Super. Sanita* 49, 247–248. doi: 10.4415/ANN_13_03_02
- Cerutti, S., Mainardi, L. T., Porta, A., and Bianchi, A. M. (1997). Analysis of the dynamics of RR interval series for the detection of atrial fibrillation episodes. *Comput. Cardiol.* 24, 77–80. doi: 10.1109/CIC.1997.647834
- Chazal, P. D., and Reilly, R. B. (2006). A patient-adapting heartbeat classifier using ECG morphology and 317 heartbeat interval features. *IEEE Trans. Biomed. Eng.* 53, 2535–2543. doi: 10.1109/TBME.2006.883802
- Couceiro, R., Carvalho, P., Henriques, J., and Antunes, M. (2008). Detection of atrial fibrillation using model-based ECG analysis. *Int. Conf. Pattern Recog.* 50, 1–5. doi: 10.1109/ICPR.2008.4761755
- Dash, S., Chon, K. H., Lu, S., and Raeder, E. A. (2009). Automatic real time detection of atrial fibrillation. *Ann. Biomed. Eng.* 37, 1701–1709. doi: 10.1007/s10439-009-9740-z
- Daubechies, I. (1988). Orthonormal bases of compactly supported wavelets. *Commun. Pure Appl. Math.* 41, 909–996. doi: 10.1002/cpa.3160410705
- de Vos, C. B., Pisters, R., Nieuwlaat, R., Prins, M. H., Tielemans, R. G., Coelen, R. J., et al. (2010). Progression from paroxysmal to persistent atrial fibrillation: clinical correlates and prognosis. *J. Am. Coll. Cardiol.* 55, 725–731. doi: 10.1016/j.jacc.2009.11.040
- Dokur, Z., and Olmez, T. (2001). ECG beat classification by a novel hybrid neural network. *Comput. Methods Programs Biomed.* 66, 167–181. doi: 10.1016/S0169-2607(00)00133-4
- Gami, A. S., Pressman, G., Caples, S. M., Kanagala, R., Gard, J. J., Davison, D. E., et al. (2004). Association of atrial fibrillation and obstructive sleep apnea. *Circulation* 13, 62–63.
- García, M., Rodenas, J., Alcaraz, R., and Rieta, J. J. (2016). Application of the relative wavelet energy to heart rate independent detection of atrial fibrillation. *Comput. Methods Programs Biomed.* 131, 157–168. doi: 10.1016/j.cmpb.2016.04.009
- Goldberger, A. L., Amaral, L. A. N., Glass, L., Hausdorff, J. M., Ivanov, P. C., Mark, R. G., et al. (2000). Physiobank, physiotoolkit, and physionet: components of a new research resource for complex physiologic signals. *Circulation* 101, e215–e220. doi: 10.1161/01.CIR.101.23.e215
- Gomes, P. R., Soares, F. O., Correia, J. H., and Lima, C. S. (2010). “ECG data-acquisition and classification system by using wavelet-domain hidden Markov models,” in *Proceedings of the Engineering in Medicine and Biology Society (EMBC), 2010 Annual International Conference*, Vol. 2010, (Buenos Aires: IEEE), 4670–4673. doi: 10.1109/EMBS.2010.5626456
- Guler, I., and Ubeyli, E. D. (2005). ECG beat classifier designed by combined neural network model. *Pattern Recog.* 38, 199–208. doi: 10.1016/j.patcog.2004.06.009
- Huang, C., Ye, S., Chen, H., Li, D., He, F., and Tu, Y. (2011). A novel method for detection of the transition between atrial fibrillation and sinus rhythm. *IEEE Trans. Biomed. Eng.* 58, 1113–1119. doi: 10.1109/TBME.2010.2096506
- Hubel, D. H., and Wiesel, T. N. (1959). Receptive fields of single neurones in the cat's striate cortex. *J. Physiol.* 148, 574–591. doi: 10.1113/jphysiol.1959.sp006308
- Hylek, E. M., Go, A. S., Chang, Y., Jenvsvald, N. G., Henault, L. E., Selby, J. V., et al. (2003). Effect of intensity of oral anticoagulation on stroke severity and mortality in atrial fibrillation. *N. Engl. J. Med.* 349, 1019–1026. doi: 10.1056/NEJMoa022913
- January, C. T., Wann, L. S., Alpert, J. S., Calkins, H., Cigarroa, J. E., Cleveland, J. C., et al. (2014). 2014 AHA/ACC/HRS guideline for the management of patients with atrial fibrillation: executive summary a report of the American college of cardiology/american heart association task force on practice guidelines and the heart rhythm society. *J. Am. Coll. Cardiol.* 64, 2246–2280. doi: 10.1016/j.jacc.2014.03.021
- Kikillus, N., Hammer, G., Lentz, N., and Stockwald, F. (2007). Three different algorithms for identifying patients suffering from atrial fibrillation during atrial fibrillation free phases of the ECG. *Comput. Cardiol.* 34, 801–804. doi: 10.1109/CIC.2007.4745607
- Kozak, C. A., Lawrence, J. B., and Ruddle, F. H. (2008). “Performance analysis of stationary and discrete wavelet transform for action potential detection from sympathetic nerve recordings in humans,” in *Proceedings of the International Conference of the IEEE Engineering in Medicine and Biology Society 2008*, (Vancouver, BC: IEEE), 2932–2935. doi: 10.1109/IEMBS.2008.4649817
- Krizhevsky, A., Sutskever, I., and Hinton, G. E. (2012). Imagenet classification with deep convolutional neural networks. *Int. Conf. Neural Inf. Process. Syst.* 60, 1097–1105.
- Kutlu, Y., and Kuntalp, D. (2012). Feature extraction for ECG heartbeats using higher order statistics of WPD coefficients. *Comput. Methods Programs Biomed.* 105, 257–267. doi: 10.1016/j.cmpb.2011.10.002
- Ladavich, S., and Ghoraani, B. (2015). Rate-independent detection of atrial fibrillation by statistical modeling of atrial activity. *Biomed. Sig. Process. Control* 18, 274–281. doi: 10.1016/j.bspc.2015.01.007
- Lake, D. E., and Moorman, J. R. (2011). Accurate estimation of entropy in very short physiological time series: the problem of atrial fibrillation detection in implanted ventricular devices. *Am. J. Physiol. Heart Circ. Physiol.* 300, H319–H325. doi: 10.1152/ajpheart.00561.2010
- Larburu, N., Lopetegi, T., and Romero, I. (2011). Comparative study of algorithms for atrial fibrillation detection. *Comput. Cardiol.* 38, 265–268.
- Lecun, Y., Bengio, Y., and Hinton, G. (2015). Deep learning. *Nature* 521, 436–444. doi: 10.1038/nature14539
- Lee, J., Reyes, B. A., Mcmanus, D. D., Maitas, O., and Chon, K. H. (2014). Atrial fibrillation detection using an iphone 4s. *IEEE Trans. Biomed. Eng.* 60, 203–206. doi: 10.1109/TBME.2012.2208112
- Lian, J., Wang, L., and Muessig, D. (2011). A simple method to detect atrial fibrillation using RR intervals. *Am. J. Cardiol.* 107, 1494–1497. doi: 10.1016/j.amjcard.2011.01.028
- Lin, C. H., Du, Y. C., and Chen, T. (2008). Adaptive wavelet network for multiple cardiac arrhythmias recognition. *Exp. Syst. Appl.* 34, 2601–2611. doi: 10.1016/j.eswa.2007.05.008
- Logan, B., and Healey, J. (2005). Robust detection of atrial fibrillation for a long term telemonitoring system. *Comput. Cardiol.* 32, 619–622. doi: 10.1109/CIC.2005.1588177
- Mallat, S., and Zhong, S. (1992). Characterization of signals from multiscale edges. *IEEE Trans. Pattern Anal. Machine Intell.* 14, 710–732. doi: 10.1109/34.142909
- Mathew, S. T., Patel, J., and Joseph, S. (2009). Atrial fibrillation: mechanistic insights and treatment options. *Eur. J. Int. Med.* 20, 672–681. doi: 10.1016/j.ejim.2009.07.011
- Miyasaka, Y., Barnes, M. E., Gersh, B. J., Cha, S. S., Bailey, K. R., Abhayaratna, W. P., et al. (2006). Secular trends in incidence of atrial fibrillation in Olmsted County, Minnesota, 1980 to 2000, and implications on the projections for future prevalence. *Circulation* 114, 119–125. doi: 10.1161/CIRCULATIONAHA.105.595140
- Moody, G. B., and Mark, R. R. (1983). New method for detecting atrial fibrillation using R-R intervals. *Comput. Cardiol.* 10, 227–230.
- Mukamal, K. J., Tolstrup, J. S., Friberg, J., Jensen, G., and Grønbæk, M. (2005). Alcohol consumption and risk of atrial fibrillation in men and women in the Copenhagen city heart study. *Circulation* 112, 1736–1742. doi: 10.1161/CIRCULATIONAHA.105.547844
- Park, J., Lee, S., and Jeon, M. (2009). Atrial fibrillation detection by heart rate variability in poincare plot. *Biomed. Eng. Online* 8, 1–12. doi: 10.1186/1475-925X-8-38
- Parvaresh, S., and Ayatollahi, A. (2011). “Automatic atrial fibrillation detection using autoregressive modeling,” in *Proceedings of the International Conference on Biomedical Engineering and Technology (ICBET)*, Singapore, 4–5.
- Petrutiu, S., Ng, J., Nijm, G. M., Alangari, H., Swiryn, S., and Sahakian, A. V. (2006). Atrial fibrillation and waveform characterization. A time domain perspective in the surface ECG. *IEEE Eng. Med. Biol. Mag.* 25, 24–30. doi: 10.1109/EMB-M.2006.250505

- Potter, B. J., and Le, L. J. (2015). Taking the pulse of atrial fibrillation. *Lancet* 386, 113–115. doi: 10.1016/S0140-6736(14)61991-7
- Rajpurkar, P., Hannun, A. Y., Haghpanahi, M., Bourn, C., and Ng, A. Y. (2017). Cardiologist-level arrhythmia detection with convolutional neural networks. *arXiv*:1707.01836.
- Rumelhart, D. E., Hinton, G. E., and Williams, R. J. (1988). Learning representations by back-propagating errors. *Read. Cogn. Sci.* 323, 399–421. doi: 10.1016/B978-1-4832-1446-7.50035-2
- Shyu, L. Y., Wu, Y. H., and Hu, W. (2004). Using wavelet transform and fuzzy neural network for VPC detection from the holter ECG. *IEEE Trans. Biomed. Eng.* 51, 1269–1273. doi: 10.1109/TBME.2004.824131
- Slocum, J., Sahakian, A., and Swiryn, S. (1992). Diagnosis of atrial fibrillation from surface electrocardiograms based on computer-detected atrial activity. *J. Electrocardiol.* 25, 1–8. doi: 10.1016/0022-0736(92)90123-H
- Tateno, K., and Glass, L. (2001). Automatic detection of atrial fibrillation using the coefficient of variation and density histograms of RR and ΔRR intervals. *Med. Biol. Eng. Comput.* 39, 664–671. doi: 10.1007/BF02345439
- Vollmer, M., Sodmann, P., Caanitz, L., Nath, N., and Kaderali, L. (2017). Can supervised learning be used to classify cardiac rhythms? *Comput. Cardiol.* 44, 1–4. doi: 10.22489/CinC.2017.347-176
- Xia, Y., Wulan, N., Wang, K., and Zhang, H. (2018). Detecting atrial fibrillation by deep convolutional neural networks. *Comput. Biol. Med.* 93, 84–92. doi: 10.1016/j.combiomed.2017.12.007
- Yaghoubi, F., Ayatollahi, A., Bahramali, R., and Yaghoubi, M. (2012). Robust genetic programming-based detection of atrial fibrillation using RR intervals. *Exp. Syst.* 29, 183–199.
- Yaghoubi, F., Ayatollahi, A., Bahramali, R., Yaghoubi, M., and Alavi, A. H. (2010). Towards automatic detection of atrial fibrillation: a hybrid computational approach. *Comput. Biol. Med.* 40, 919–930. doi: 10.1016/j.combiomed.2010.10.004
- Zhou, X., Ding, H., Ung, B., Pickwellmacpherson, E., and Zhang, Y. (2014). Automatic online detection of atrial fibrillation based on symbolic dynamics and shannon entropy. *Biomed. Eng. Online* 13, 1–18. doi: 10.1186/1475-925X-13-18
- Zoniberizzo, M., Lercari, F., Carazza, T., and Domenicucci, S. (2014). Epidemiology of atrial fibrillation: european perspective. *Clin. Epidemiol.* 6, 213–220. doi: 10.2147/CLEP.S47385

Conflict of Interest Statement: The authors declare that the research was conducted in the absence of any commercial or financial relationships that could be construed as a potential conflict of interest.

Copyright © 2018 He, Wang, Zhao, Liu, Yuan, Li and Zhang. This is an open-access article distributed under the terms of the Creative Commons Attribution License (CC BY). The use, distribution or reproduction in other forums is permitted, provided the original author(s) and the copyright owner(s) are credited and that the original publication in this journal is cited, in accordance with accepted academic practice. No use, distribution or reproduction is permitted which does not comply with these terms.



Loss of Side-to-Side Connections Affects the Relative Contributions of the Sodium and Calcium Current to Transverse Propagation Between Strands of Atrial Myocytes

OPEN ACCESS

Edited by:

Joseph L. Greenstein,
Johns Hopkins University,
United States

Reviewed by:

Thomas Hund,
The Ohio State University,
United States

Eleonora Grandi,

University of California, Davis,
United States

Correspondence:

Sander Verheule
s.verheule@maastrichtuniversity.nl

Specialty section:

This article was submitted to
Computational Physiology and
Medicine,
a section of the journal
Frontiers in Physiology

Received: 30 April 2018

Accepted: 13 August 2018

Published: 04 September 2018

Citation:

Zhao J, Schotten U, Smaill B and
Verheule S (2018) Loss of
Side-to-Side Connections Affects the
Relative Contributions of the Sodium
and Calcium Current to Transverse
Propagation Between Strands of Atrial
Myocytes. *Front. Physiol.* 9:1212.
doi: 10.3389/fphys.2018.01212

Jichao Zhao¹, Ulrich Schotten², Bruce Smaill¹ and Sander Verheule^{2*}

¹ Auckland Bioengineering Institute, University of Auckland, Auckland, New Zealand, ² Department of Physiology, Maastricht University, Maastricht, Netherlands

Background: Atrial fibrillation (AF) leads to a loss of transverse connections between myocyte strands that is associated with an increased complexity and stability of AF. We have explored the interaction between longitudinal and transverse coupling, and the relative contribution of the sodium (I_{Na}) and calcium (I_{Ca}) current to propagation, both in healthy tissue and under diseased conditions using computer simulations.

Methods: Two parallel strands of atrial myocytes were modeled (Courtemanche et al. ionic model). As a control condition, every single cell was connected both transversely and longitudinally. To simulate a loss of transverse connectivity, this number was reduced to 1 in 4, 8, 12, or 16 transversely. To study the interaction with longitudinal coupling, anisotropy ratios of 3, 9, 16, and 25:1 were used. All simulations were repeated for varying degrees of I_{Na} and I_{Ca} block and the transverse activation delay (TAD) between the paced and non-paced strands was calculated for all cases.

Results: The TAD was highly sensitive to the transverse connectivity, increasing from 1 ms at 1 in 1, to 25 ms at 1 in 4, and 100 ms at 1 in 12 connectivity. The TAD also increased when longitudinal coupling was increased. Both decreasing transverse connectivity and increasing longitudinal coupling enhanced the synchronicity of activation of the non-paced strand and increased the propensity for transverse conduction block. Even after long TADs, the action potential upstroke in the non-paced strand was still mainly dependent on the I_{Na} . Nevertheless, I_{Ca} in the paced strand was essential to provide depolarizing current to the non-paced strand. Loss of transverse connections increased the sensitivity to both I_{Na} and I_{Ca} block. However, when longitudinal coupling was relatively high, transverse propagation was more sensitive to I_{Ca} block than to I_{Na} block.

Conclusions: Although transverse propagation depends on both I_{Na} and I_{Ca} , their relative contribution, and sensitivity to channel blockade, depends on the distribution of transverse connections and the axial conductivity. This simple two-strand model helps to explain the nature of atrial discontinuous conduction during structural remodeling and provides an opportunity for more effective drug development.

Keywords: atrial fibrillation, transverse propagation, discontinuous conduction, sodium, calcium, fibrosis, structural remodeling

INTRODUCTION

Atrial fibrillation (AF)—the most common tachyarrhythmia in clinical practice—leads to remodeling of the atrial myocardium that promotes the maintenance of the arrhythmia (Schotten et al., 2011). Both the fast process of electrical remodeling (shortening of the action potential duration, occurring within 1–2 days) and the much slower process of structural remodeling (changes in cell and tissue structure, developing over months to years) contribute to AF stabilization (Schotten et al., 2011). Early in the disease process, sinus rhythm may be restored in patients by decreasing excitability (class I drugs, sodium channel blockers) (Crijns et al., 1988) or increasing action potential duration (class III drugs, potassium channel blockers) (Vos et al., 1998). However, when AF has been present for a longer time, both classes of drugs lose their efficacy, both in AF patients (Crijns et al., 1988; Vos et al., 1998) and in animal models (Eijsbouts et al., 2006; Verheule et al., 2010).

Whereas atrial myocytes form large intercalated discs with abundant gap junction channels at end-to-end connections, transverse connections between myocytes strands are more sparse (Spach and Dolber, 1986; Dolber and Spach, 1989). The structural changes—most notable endomysial fibrosis (also referred to as “interstitial fibrosis” and “microfibrosis”)—that results from aging (Spach and Dolber, 1986; Koura et al., 2002) or AF itself (Verheule et al., 2013) lead to a further loss of transverse connections. As a consequence, transverse propagation can become discontinuous, allowing reentrant conduction to take place in relatively small tissue areas (microreentry) (Spach and Josephson, 1994; Spach and Boineau, 1997).

In a seminal modeling study on longitudinal strands of ventricular myocytes, Shaw and Rudy have investigated the effects of reduced excitability (i.e., decreased sodium current) and gap junctional coupling (Shaw and Rudy, 1997). They showed that reduced sodium current amplitude led to a relatively small reduction in conduction velocity before conduction block occurred. By contrast, a reduction in gap junctional coupling allowed very slow conduction with a high safety factor (i.e., conduction that is unlikely to block). Under those conditions, electrical propagation became more dependent on the calcium current than on the rapidly inactivating sodium current. However, it has not been investigated how these ionic factors affect longitudinal and transverse propagation in strands of myocytes with transverse connections, and how structural remodeling (i.e., a loss of transverse connections) affects this interplay. We hypothesize that reduced transverse connectivity

is a pivotal contributor to the substrate for sustained AF. Better understanding of the ionic basis of propagation can aid the development of more effective drug treatment for AF patients. Therefore, we have constructed a simple model consisting of two parallel strands of atrial myocytes with varying discrete side-to-side connections (Figure 1A). With this model, we have investigated the effect of reduced transverse connectivity on transverse propagation delays (Figure 1B), the relative roles of the sodium and calcium currents, and the sensitivity to sodium and calcium channel blockade.

METHODS

Modeling Atrial Electrical Transverse and Longitudinal Propagation in 3D Cables

The two parallel myocyte cables with discrete transverse coupling were modeled in a 3D setting: $3 \times 3000 \times 3$ cells in the upper strand, $3 \times 3000 \times 3$ cells in the lower strand, transverse connections are composed as $3 \times 1 \times 3$ cells (Figure 1). The spread of electrical activation in the 3D cable can be estimated by solving the cardiac monodomain equation (Zhao et al., 2013)

$$\nabla \bullet (\sigma_i \nabla V_m) = A_m (C_m \frac{\partial V_m}{\partial t} + I_{ion})$$

where the tensor σ_i represents the conductivity vector in spatial space, V_m is the transmembrane voltage, while A_m and C_m are membrane cross-sectional area and membrane capacitance. I_{ion} is the net current carried by transmembrane ion channels. The monodomain version of the reaction-diffusion equation was solved on a 3D voxel-based finite difference grid and paralleled using a Message Passing Interface (MPI). In the 3D cable model, we employed the biophysically detailed human atrial cell electrophysiology model developed by Courtemanche et al. (1998). Simulations with the Courtemanche cell model with a time step of 0.0025 ms run on an IBM3850 (32 dual thread Intel chips, 256 GB shared memory, Linux operating system) (Zhao et al., 2013). To simulate the loss of transverse connections in the cable model, we removed the connected grids in the grid-based mesh between the two parallel cables in the 3D numerical solver. Axially, anisotropic electrical properties were assigned to the two 3D cables along the long-axis of the cables and transversely in the cell-to-cell connection regions. Conductivities in transverse directions were fixed and set at 0.1 ms, while the longitudinal conductivities were varied to investigate the influence of longitudinal impedance. To model the effects of

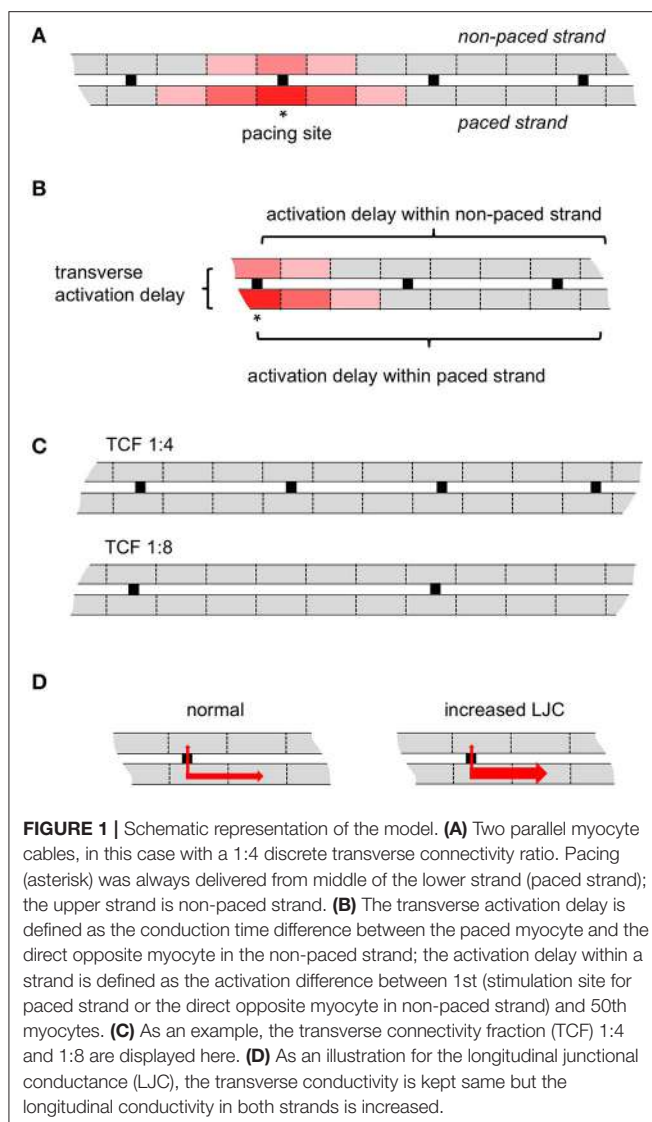


FIGURE 1 | Schematic representation of the model. **(A)** Two parallel myocyte cables, in this case with a 1:4 discrete transverse connectivity ratio. Pacing (asterisk) was always delivered from middle of the lower strand (paced strand); the upper strand is non-paced strand. **(B)** The transverse activation delay is defined as the conduction time difference between the paced myocyte and the direct opposite myocyte in the non-paced strand; the activation delay within a strand is defined as the activation difference between 1st (stimulation site for paced strand or the direct opposite myocyte in non-paced strand) and 50th myocytes. **(C)** As an example, the transverse connectivity fraction (TCF) 1:4 and 1:8 are displayed here. **(D)** As an illustration for the longitudinal junctional conductance (LJC), the transverse conductivity is kept same but the longitudinal conductivity in both strands is increased.

g_{Na} and $g_{Ca,L}$ channel blockers in the 3D cable, we used the percentage of conductance g_{Na} and $g_{Ca,L}$ of its baseline values.

Computer Simulation Design

In this study, we have performed three groups of computer simulations:

- 1) Reducing discrete transverse coupling (1:1, 1:4, 1:8, 1:12, and 1:16) to study the impact of gradual loss of transverse connections during structural remodeling (Figure 1C);
- 2) Increasing the longitudinal conductance while keeping the transverse conductance the same (the ratio of the two at 3:1, 9:1, 16:1, and 25:1) to investigate the influence of longitudinal impedance on transverse propagation (Figure 1D);
- 3) Testing different degrees (0 to 100%) of sodium or calcium current blockade to investigate the sensitivity of longitudinal and transverse propagation to channel block.

In each of these simulations, the middle of the lower strand was paced. At that pacing site, $3 \times 1 \times 3$ cells were paced with stimulus strength of 4 mA for 1 ms with 1 Hz. The results analyzed in this study were taken when the model reached its steady state (11th cycle). Atrial action potentials and sodium/calcium currents across the 3D myocyte cable were saved and analyzed, especially the site in the upper strand (the non-paced strand) that was directly opposed to the stimulus location (Figure 1B). A cut-off value of the membrane potential of -40 mV was used to determine whether a cell was activated or whether conduction had blocked. The time point with the maximal dV/dt was taken as the time point of activation.

RESULTS

Effects of Transverse Connectivity on Transverse Propagation

When the transverse connectivity fraction (TCF) was reduced from 1:1 to 1:4, 1:8, 1:12, and 1:16, the conduction velocity (CV) in the stimulated strand was not affected (~ 1 mm/ms; blue lines in Figure 2B). However, the shape of the action potential plateau in the electrically paced strand was affected by electrotonic interaction with the non-paced strand, which acted as a current sink before its moment of activation. Once the non-paced strand was activated, it acted as a current source and that elevated the potential in the paced strand (circled deflections in Figure 2A). With decreasing TCF, the delay between the earliest activation in the paced and non-paced strands dramatically increased (Figures 2B, 3). After this prolonged activation delay between the two strands, the activation propagated more rapidly in the non-paced strand than in the paced strand. Interestingly, the propagation within the non-paced strand became faster with a progressive loss of transverse connections, leading to a virtually simultaneous activation of the non-paced strand with a TCF of 1:12 (Figures 2A,B). A further reduction in TCF to 1:16 lead to transverse conduction block (not shown).

Effects of Axial Impedance on Transverse Propagation

When depolarizing current flows from the paced to the non-paced strand through a lateral connection, part of that current quickly dissipates in the axial direction within the non-paced strand. To investigate the strength of this effect, we increased the longitudinal junctional conductance (LJC), while keeping the transverse junctional conductance and transverse connectivity fraction unchanged. This corresponded to an anisotropy ratio (longitudinal vs. transverse conductance) varying from 3:1 to 25:1. Over this range, we observed an increase in CV in the paced strand as expected, as well as an increasing transverse activation delay (Figures 2C,D, 3). With a TCF of 1:4 and LJC 3:1, the average CV in the paced strand was 0.57 m/s, increasing 1.7 and 2.9-fold at an LJC of 9:1 and 25:1, respectively. Increasing the LJC caused a pronounced increase in transverse conduction delays, e.g., 8, 26, and 82 ms for LJC of 3:1, 9:1, and 25:1, respectively. After the transverse activation delay, the activation of the non-paced strand was more synchronous than that of the stimulated

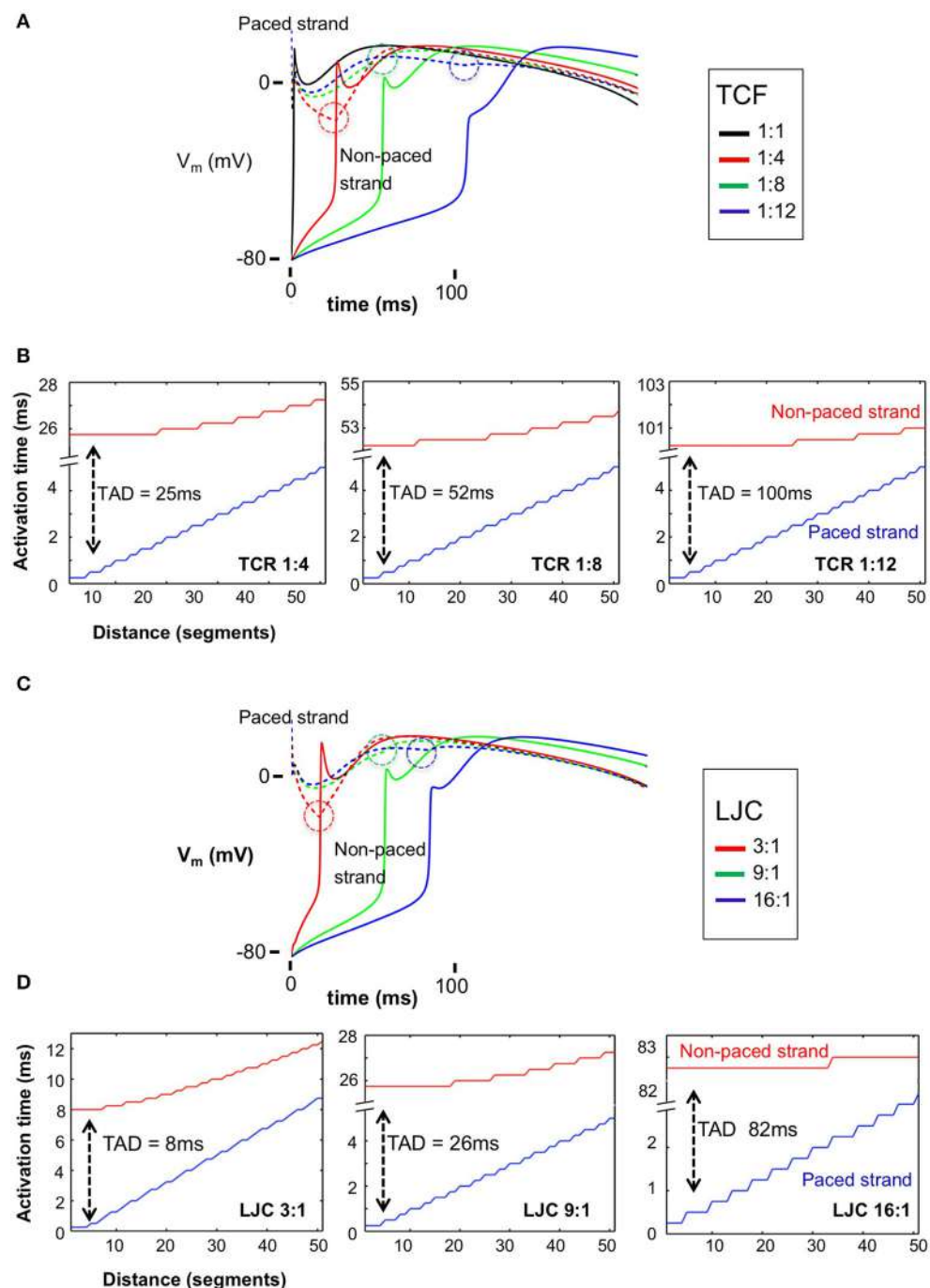


FIGURE 2 | Action potentials (APs) and transverse activation delay (TAD) for the paced and non-paced strands with varied discrete TCF and LJC. **(A)** APs for the stimulus location in the paced strand (dashed lines) and the directly opposite myocyte in the non-paced strand (solid lines) with TCF = 1:1, 1:4, 1:8, 1:12, respectively. The dashed circles highlight the timing of electrotonic interaction between the paced and non-paced strands; once the non-paced strand was activated, it acted as a current source and that elevated the potential in the paced strand. **(B)** TADs increased dramatically with decreased TCF from 25 ms (TCF = 1:4) to 100 ms (TCF = 1:12), while having little impact on conduction velocity in the paced strand. On the other hand, after a long TAD, activation of the non-paced strand is almost instantaneous. **(C)** APs for the stimulus location in the paced strand (dashed lines) and the directly opposite myocyte in the non-paced strand (solid lines) with LJC = 3, 9 and 16:1, respectively. The dashed circles highlight the timing of electrotonic interaction between the paced and non-paced strands. **(D)** TADs increased dramatically with increased LJC from 8 ms (LJC = 3) to 82 ms (LJC = 16), while having little impact on conduction velocity in the paced strand. With a higher LJC, and a longer TAD, the degree of synchronicity of activation within the non-paced strand increased.

TCF LJC	1:1	1:4	1:8	1:12	1:16	
3:1	8.8	8.8	8.8	8.8	8.5	paced
	0.0	8.0	16.0	25.8	35.8	TAD
	8.8	4.5	4.0	4.0	4.0	non-paced
9:1	5.8	5.0	5.0	5.0	5.0	paced
	1.3	25.8	52.3	100.3	block	TAD
	4.5	1.5	1.5	0.7	-	non-paced
12:1	5.3	4.5	4.5	4.5	4.5	paced
	1.3	34.0	76.8	block	block	TAD
	4.0	1.3	0.7	-	-	non-paced
16:1	4.8	3.8	3.8	3.8	3.8	paced
	1.5	45.5	block	block	block	TAD
	3.3	1.0	-	-	-	non-paced
25:1	4.0	3.3	x	x	x	paced
	1.5	82.5	block	block	block	TAD
	2.5	0.5	-	-	-	non-paced

Activation time differences (ms) {

- within the paced strand
- between the strands (TAD)
- within the non-paced strand

FIGURE 3 | Summarizing table for TAD and activation delays (in milliseconds) in both strands with varied TCF and LJC. Black blocks indicate the TAD; gray and light gray blocks contain entries for activation delays for the non-paced and paced strands, respectively.

strand. The synchronicity of activation was enhanced when the TCF was decreased and especially when the axial conductance was increased as well.

Effects of Sodium and Calcium Channel Blockade

To assess the effects of g_{Na} and $g_{Ca,L}$ channel blockers, a stepwise reduction of g_{Na} and $g_{Ca,L}$ conductance in the computer model was implemented until transverse conduction block was observed (Figure 4). With high transverse coupling (1:1 or 1:4) and relatively low LJC (3:1), transverse propagation was relatively more sensitive to sodium current blockade. Under these conditions, transverse propagation could be blocked by 70% g_{Na}

blockade, but still occurred with 100% $g_{Ca,L}$ blockade. Increasing axial conductance dramatically increased the sensitivity to calcium channel blockade, with transverse block occurring at 40 and 20% calcium channel blockade at an LJC of 9:1 and 25:1. Similarly, decreasing the TCF strongly enhanced the sensitivity to calcium channel blockade, with transverse block observed at 90 and 40% with a TCF of 1:8 and 1:12, respectively. Qualitatively, simulations with sodium channel blockade showed similar trends, but the sensitivity to changes in TCF and LJC was less pronounced. Whereas transverse propagation still occurred with 100% $g_{Ca,L}$ blockade at a TCF of 1:4 and a LJC of 3:1, transverse propagation failed at 40% $g_{Ca,L}$ blockade when TCF was lowered to 1:12 and at 20% g_{Ca} blockade when LJC was increased to 25:1. Under the same conditions, transverse

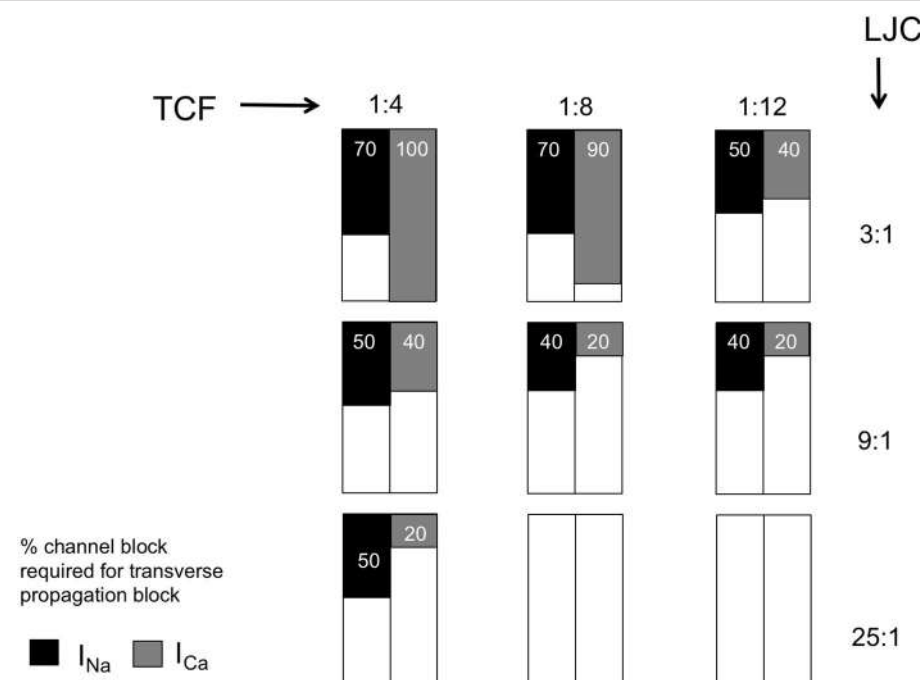


FIGURE 4 | Sensitivity of transverse propagation to sodium and calcium current (I_{Na} and I_{Ca}) block. Summarizing table with entries representing the minimal percentage of channel block required for transverse block with varied discrete TCF and LJC.

propagation failed at 70, 50, and 50% I_{Na} blockade, respectively (Figure 4). For the combination of LJC = 25:1 and low TCF (1:8 or 1:12), transverse propagation failure was always observed, even in the absence of sodium or calcium channel blockade.

These results demonstrate that both sodium and calcium current contribute to transverse propagation, because both sodium and calcium channel block can cause failure of transverse propagation.

The Roles of Sodium and Calcium in Transverse Propagation

The role of the sodium and calcium currents in the activation of both strands was distinctly different. With an LJC of 9:1 and a TCF of 1:8, there was a long transverse conduction delay of 52 ms (top left panel in Figure 5A). However, even after this long delay, the action potential upstroke in the non-paced strand is still dependent on the sodium current (bottom left panel in Figure 5A). At the moment of activation of the non-paced strand, the sodium current in the paced strand had already completely inactivated. Therefore, the calcium current maintaining the action potential plateau in the paced strand was essential in providing sufficient depolarizing current for the sodium-dependent upstroke to occur in the non-paced strand. In Figure 5A, the right panel plots the ratio of the amount of depolarizing charge carried by the sodium and calcium currents during the AP upstroke in the non-paced strand. Although this ratio Q_{Na}/Q_{Ca} strongly decreases when the TCF is reduced, the preponderance of the charge is still carried by the sodium current under all conditions in which transverse propagation occurs.

Figure 5B compares the action potential morphologies (LJC = 9:1 and TCF = 1:8) at 10% $I_{Ca,L}$ blockade, which still allows transverse propagation and 20% $I_{Ca,L}$ blockade, which leads to transverse propagation failure. When $I_{Ca,L}$ in the paced strand is sufficient to support transverse propagation, the AP in the paced strand is prolonged by the electrotonic influence of the activated non-paced strand (left panel). When transverse propagation fails at a slightly higher degree of $I_{Ca,L}$ blockade, the AP in the paced is markedly shorter (right panel).

DISCUSSION

Propagation of the activation waveform in cardiac tissue primarily depends on the I_{Na} current density and the degree of gap junctional coupling. In a seminal study, Shaw and Rudy have used a mathematical model of a single strand of myocytes to compare the effects of reductions in these two factors (Shaw and Rudy, 1997). They demonstrated that I_{Na} blockade conduction velocity decreased from 54 to 17 cm/s before conduction block occurred. However, when gap junctional coupling was reduced, a much lower conduction velocity of 0.26 cm/s was reached before conduction blocked. With strongly reduced gap junctional coupling, propagation became almost entirely dependent on $I_{Ca,L}$. This modeling study agrees with an earlier study in patterned cultures of neonatal myocytes, where a thin strip of myocytes widened into a broader monolayer (Rohr et al., 1997). Whereas conduction normally blocked at the widening point, the thin strip was able to excite the broader area during partial gap junctional

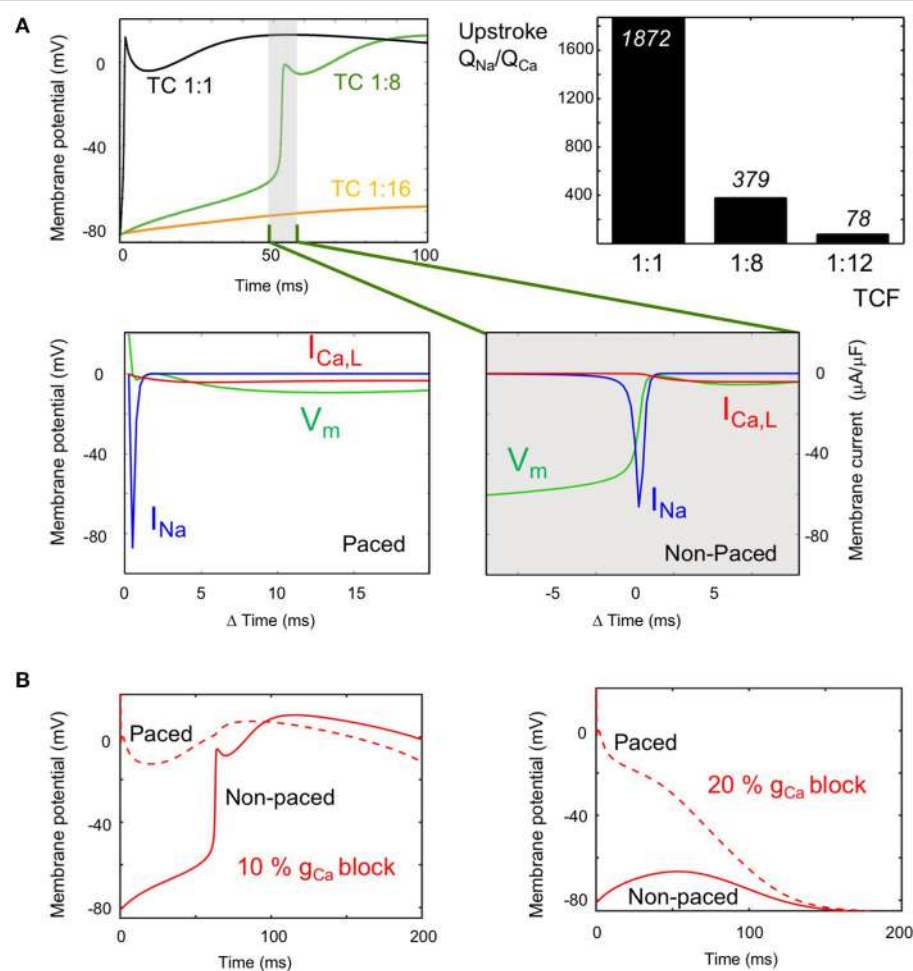


FIGURE 5 | Role of the sodium and calcium current (I_{Na} and I_{Ca}) in transverse propagation. **(A)** I_{Na} and I_{Ca} during the upstroke at long TADs ($LJC = 9:1$). Top left: Action potentials (APs) in the non-paced strand, at the site directly opposing the pacing site, with TCF 1:1 (black), 1:8 (long TAD, green), and 1:16 (propagation failure, orange). Bottom row: V_m (green), I_{Na} (blue) and I_{Ca} (red) during upstroke of the AP at a TCF of 1:8 are plotted for the paced strand (left panel) and the non-paced strand (right panel). The magnitude of I_{Na} during the upstroke in the non-paced strand is several hundred times of that of I_{Ca} . Top right panel: Calculated ratio of charge carried by the sodium and calcium current during the AP upstroke in the non-paced strand at various TCFs ($LJC = 9:1$). **(B)** Role of I_{Ca} in transverse propagation ($LJC = 9:1$, TCF 1:8). APs are displayed for the paced strand (dashed line) and non-paced strand (solid line) for 10% $I_{Ca,L}$ blockade, where transverse propagation was successful (left panel) and for 20% $I_{Ca,L}$ blockade, where transverse conduction block occurred (right panel).

uncoupling with octanol, illustrating that an increase in gap junctional resistance can paradoxically prevent conduction block.

In the normal adult myocardium, neighboring myocytes are well coupled at their end-to-end (longitudinal) connections (Desplantez et al., 2007). However, the distribution of transverse connections is more discrete and sparse, both between individual myocytes and between neighboring bundles. This sparsity of lateral connections differs between regions in the healthy heart (Dolber and Spach, 1987). For example, in Bachmann's bundle, the distance between lateral connections between funicles (sub-bundles) may amount to 2 mm (Dolber and Spach, 1989). The development of endomysial/ interstitial fibrosis specifically affects transverse connectivity, probably by increasing the sparsity of lateral connections between myocytes and myocyte bundles. This process occurs during

normal aging (Spach and Dolber, 1986; Koura et al., 2002; Spach et al., 2007) and is exacerbated by structural remodeling that occurs during AF. In a goat model, 6 months of AF caused endomysial fibrosis specifically in the thin epicardial layer of the atrial wall, selectively impairing transverse propagation of epicardial wavefronts (Verheule et al., 2013, 2014).

The central question of this study is how the sparse nature of lateral connections affects cardiac propagation and the relative contributions of the sodium and calcium currents to propagation. The main findings of our study can be summarized as follows, as discussed sequentially below:

- (1) Reducing transverse coupling increases the transverse activation delay; this is exacerbated when axial conductivity is high.

- (2) With reduced transverse coupling and increased axial conductivity, the spread of activation within the non-paced strand becomes faster.
- (3) Even after a long transverse activation delay, the action potential upstroke in the non-paced strand is still I_{Na} - dependent, but I_{Ca} is essential for transverse propagation by sustaining the plateau in the paced strand.
- (4) Increased axial conductivity or decreased transverse connectivity increases sensitivity to I_{Ca} block to a greater extent than the sensitivity to I_{Na} block.

Transverse Activation Delay (ad 1)

In our simulations, the TAD was highly sensitive to both the TCF and the LJC. When the TCF was decreased and the LJC was increased, the paced strand was completely activated before transverse propagation occurred. Thus, a loss of transverse connections precipitates discontinuous transverse propagation. As a starting condition, we used a TCF of 1:1, i.e., all units in the parallel strands were coupled transversely. Under this condition, the TAD was small at all LJC:s investigated. However, even in the healthy adult heart, the degree of transverse connectivity is probably much lower, especially in regions with a strong preferential fiber orientation such as Bachmann's bundle (Dolber and Spach, 1987, 1989). This normal sparsity of transverse connections between bundles would increase the propensity to longer TADs, and it would increase further when fibrosis leads to a loss of transverse connections.

We varied the LJC to assess to which extent transverse propagation is affected by a lower axial impedance. In theory, depolarizing current flowing through a transverse connection would more readily dissipate in the axial direction of the non-paced strand with a higher LJC. This would make it more difficult to reach the activation threshold of the non-paced strand, leading to a longer TAD or even transverse block. Indeed, our simulations show that the TAD is very sensitive to the LJC, increasing from 8 ms at an LJC of 3:1 to 83 ms at an LJC of 25:1 (TCF 1:4). With a further reduction in TCF, an increase in LJC quickly led to block of transverse propagation. In a single strand of myocytes, a "safety factor" for conduction can be calculated as the ratio between the charge generated by a cell upstream in the strand and the charge required to bring the next cell to threshold (Shaw and Rudy, 1997). In our model however, the charge generated by an activated myocyte in the paced strand not only flows to a connected myocyte in the non-paced strand, but to a larger extent to myocytes in the axial direction, precluding a straightforward determination of a safety factor. With an increase in axial conductivity and a decrease in transverse connectivity, the paced strand activates first, with the entire strand contributing to depolarization of the non-paced strand. In several experimental models, structural remodeling, and the concomitant loss of side-to-side connections and cellular hypertrophy primarily affects transverse propagation, with minor effects on longitudinal propagation (Stein et al., 2008; Glukhov et al., 2012). Based on cable theory, an increase in cell diameter should decrease axial impedance and increase longitudinal conduction velocity, as has indeed been shown

for hypertrophic ventricular myocardium in a rabbit model of heart failure (Wiegerinck et al., 2006). Structural remodeling caused by AF is characterized both by endomyocardial fibrosis and myocyte hypertrophy (Ausma et al., 2003; Verheule et al., 2013). These two factors may thus act synergistically to produce discontinuous transverse conduction and transverse conduction block.

Activation Pattern Within the Strands (ad 2)

As expected, activation of the paced strand became slightly faster with increasing LJC (activation time decreased from 8.8 ms at LJC 3:1 to 4 ms at LJC 25:1). By contrast, the activation of the paced strand was relatively insensitive to the TCF, indicating that current leak through transverse connections did not significantly affect longitudinal conduction in our model. As noted above, an increase in LJC and decrease in TCF increased the TAD. However, after this longer TAD, activation within the non-paced strand became faster (activation time 8.8 ms at TCF 1:1 and LJC 3:1 vs. 0.7 ms at TCF 1:8 and LJC 12:1, for example). With a long TAD, the paced strand has already activated completely, allowing depolarizing current to flow through numerous adjacent transverse connections, jointly bringing the non-paced strand to its activation threshold. Especially at high LJC and low TCF, the activation within the non-paced strand is essential synchronous. For this reason, a conduction velocity cannot be calculated for the non-paced strand. In effect, this near-instantaneous activation (after a long delay) translates to a 90-degree turn in propagation direction between the two simulated strands, from longitudinal in the paced strand to transverse in the non-paced strand. A loss of transverse connections may thus paradoxically precipitate discontinuous transverse propagation. Depending on local fiber architecture, this phenomenon would also promote sharp changes in propagation direction and may therefore in part explain experimental observations of zig-zag conduction (in canine atria as a result of aging) (Koura et al., 2002) and microreentry (in human atria) (Hansen et al., 2015).

Contribution of I_{Na} and I_{Ca} (ad 3)

In simulations on a single strand, the upstroke of the action potential became increasingly dependent on I_{Ca} when gap junctional conductance was reduced (Shaw and Rudy, 1997). The long TAC that occurs in our double strand model when LJC was increased and/ or TCF was decreased entails that I_{Na} had already completely inactivated when the non-paced strand was activated, and could therefore not supply depolarizing current over transverse connections at that point in time. Instead, I_{Ca} was responsible for maintaining the action potential plateau of the paced strand long enough for transverse propagation to occur. Nevertheless, even with long TADs, the majority of the current during the action potential upstroke of the non-paced strand was still carried by I_{Na} .

Sensitivity to Channel Block (ad 4)

The diverging roles of I_{Na} and I_{Ca} described above translate into different sensitivities to channel block under the conditions

we have tested. Overall, the degree of I_{Na} block required to block transverse propagation decreased both when TCF was decreased and when LJC was increased. However, the degree of I_{Ca} block required to block transverse propagation was much more sensitive to both parameters. At a TCF of 1:4 and an LJC of 3:1, transverse propagation still occurred with 100% I_{Ca} block, but 40% I_{Ca} block was sufficient to prevent transverse propagation with a TCF of 1:12 and 20% I_{Ca} block prevented transverse propagation with an LJC of 25:1. The dependence on TCF implies that sensitivity to I_{Ca} block increases strongly with a loss of transverse connections, i.e., during structural remodeling. Anti-arrhythmic drugs can be used for cardioversion at early stages in the pathogenesis of AF both in AF patients (Crijns et al., 1988) and in animal models, but their efficacy declines when structural remodeling develops (Eijsbouts et al., 2006; Verheule et al., 2010). Fibrillatory conduction in structurally remodeled atria is characterized by dissociated propagation patterns that are consistent with loss of transverse connectivity (Verheule et al., 2013). According to our model and earlier experimental and modeling studies this loss of transverse connectivity would favor discontinuous transverse propagation (Spach and Dolber, 1986; Spach and Boineau, 1997; Christensen et al., 2015). As an anti-arrhythmic strategy, I_{Ca} blockade has not been successful, (Villani et al., 2000; Manios et al., 2003; Hemels et al., 2006) possibly because potential anti-arrhythmic effects (prevention of calcium overload and discontinuous conduction) are offset by the pro-arrhythmic effect of action potential shortening. However, because of the different roles of I_{Na} and I_{Ca} in transverse propagation, a potential strategy would be combined treatment with an I_{Ca} blocker and an I_{Na} or I_K blocker. To our knowledge, this approach has not been investigated either in animal models of AF or in AF patients.

LIMITATIONS

Our “proof-of principle” model consists of two 3-dimensional strands. These strands correspond to small bundles or “funicles,” which have been demonstrated to be important determinants of microscopic conduction (Dolber and Spach, 1987, 1989). The model displayed long time delays in transverse propagation. We do not know to what extent the ranges in our simulations exceed the pathophysiological range, but discontinuous transverse propagation in the atria has been observed in isolated bundles and intact hearts (Spach et al., 1982; Verheule et al., 2010). It is likely that with more parallel bundles, TADs would become smaller, because more transverse connections can deliver depolarizing current from bundles that have already been activated to a bundle that is still at rest. However, we believe the same dependencies of transverse propagation on the transverse connectivity and axial conductance would still hold. In addition, TADs would become larger, also in 3-dimensional structures, during premature activations

or AF, (Spach et al., 2007) when I_{Na} and I_{Ca} cannot fully recover from inactivation, and this mechanism could thereby contribute to the dissociated fibrillation patterns observed in structurally remodeled atria (Verheule et al., 2010).

Several mathematical models are available for atrial cellular electrophysiology. We have used the Courtemanche model for a human atrial myocyte (Shaw and Rudy, 1997), a widely used and generally accepted model. However, we do not expect our findings to be model-dependent. The relative contributions of the sodium and calcium current in transverse propagation depend mainly on their current density and kinetics, which are quite similar between models. This does not mean that alterations in cellular electrophysiology will not have an effect. For example, AF-induced electrical remodeling shortens the APD. We expect that this would increase the propensity for transverse propagation failure, and failure would then occur already at a higher degree of transverse coupling. However, the nature of the dependencies on TCF and LJC would remain the same.

The study by Shaw and Rudy simulated the effects of LJC in a single, one-cell wide, strand of ventricular myocytes (Shaw and Rudy, 1997). Here, we have simulated thin 3-dimensional strands of atrial myocytes, because we believe that this is more pertinent to the tissue architecture of the atria. Although our study cannot be directly compared to the study by Shaw and Rudy in all respects, we propose that the sparse nature of transverse connection is an important determinant of cardiac propagation and that contribution and I_{Na} and I_{Ca} differs between longitudinal and transverse propagation.

AUTHOR CONTRIBUTIONS

JZ worked on computer simulations, data analysis, and writing. US and BS critically evaluated the manuscript. SV ensured the overall coordination of the article, and worked on data analysis and writing.

FUNDING

This work was supported by the Netherlands Heart Foundation (CVON2014-09, RACE V Reappraisal of Atrial Fibrillation: Interaction between hyperCoagulability, Electrical remodeling, and Vascular Destabilisation in the Progression of AF), the European Union (CATCH ME: Characterizing Atrial fibrillation by Translating its Causes into Health Modifiers in the Elderly, No. 633196, the ITN Network AFibTrainNet, No. 675351 and the ERACoSysMED H2020 ERA-NET Cofund project Systems medicine for diagnosis and stratification of atrial fibrillation and by the Health Research Council of New Zealand 16/385).

REFERENCES

- Ausma, J., van der Velden, H. M., Lenders, M. H., van Ankeren, E. P., Jongsma, H. J., Ramaekers, F. C., et al. (2003). Reverse structural and gap-junctional remodeling after prolonged atrial fibrillation in the goat. *Circulation* 107, 2051–2058. doi: 10.1161/01.CIR.0000062689.04037.3F
- Christensen, K., Manani, K. A., and Peters, N. S. (2015). Simple model for identifying critical regions in atrial fibrillation. *Phys. Rev. Lett.* 114:028104. doi: 10.1103/PhysRevLett.114.028104
- Courtemanche, M., Ramirez, R. J., and Nattel, S. (1998). Ionic mechanisms underlying human atrial action potential properties: insights from a mathematical model. *Am. J. Physiol.* 275, H301–H321.
- Crijns, H., van Wijk, L., van Gilst, W., Kingma, J., van Gelder, I., and Lie, K. (1988). Acute conversion of atrial fibrillation to sinus rhythm: clinical efficacy of flecainide acetate. Comparison of two regimens. *Eur. Heart J.* 9, 634–638. doi: 10.1093/oxfordjournals.eurheartj.a062553
- Desplantez, T., Dupont, E., Severs, N. J., and Weingart, R. (2007). Gap junction channels and cardiac impulse propagation. *J. Membr. Biol.* 218, 13–28. doi: 10.1007/s00232-007-9046-8
- Dolber, P. C., and Spach, M. S. (1987). Thin collagenous septa in cardiac muscle. *Anat. Rec.* 218, 45–55. doi: 10.1002/ar.1092180109
- Dolber, P. C., and Spach, M. S. (1989). Structure of canine Bachmann's bundle related to propagation of excitation. *Am. J. Physiol.* 257, H1446–H1457.
- Eijssbouts, S., Ausma, J., Blaauw, Y., Schotten, U., Duytschaever, M., and Allessie, M. (2006). Serial cardioversion by class IC Drugs during 4 months of persistent atrial fibrillation in the goat. *J. Cardiovasc. Electrophysiol.* 17, 648–654. doi: 10.1111/j.1540-8167.2006.00407.x
- Glukhov, A. V., Fedorov, V. V., Kalish, P. W., Ravikumar, V. K., Lou, Q., Janks, D., et al. (2012). Conduction remodeling in human end-stage nonischemic left ventricular cardiomyopathy. *Circulation* 125, 1835–1847. doi: 10.1161/CIRCULATIONAHA.111.047274
- Hansen, B. J., Zhao, J., Csepe, T. A., Moore, B. T., Li, N., Jayne, L. A., et al. (2015). Atrial fibrillation driven by micro-anatomic intramural re-entry revealed by simultaneous sub-epicardial and sub-endocardial optical mapping in explanted human hearts. *Eur. Heart J.* 36, 2390–2401. doi: 10.1093/eurheartj/ehv233
- Heimels, M. E., Van Noord, T., Crijns, H. J., Van Veldhuisen, D. J., Veeger, N. J., Bosker, H. A., et al. (2006). Verapamil versus digoxin and acute versus routine serial cardioversion for the improvement of rhythm control for persistent atrial fibrillation. *J. Am. Coll. Cardiol.* 48, 1001–1009. doi: 10.1016/j.jacc.2006.05.043
- Koura, T., Hara, M., Takeuchi, S., Ota, K., Okada, Y., Miyoshi, S., et al. (2002). Anisotropic conduction properties in canine atria analyzed by high-resolution optical mapping: preferential direction of conduction block changes from longitudinal to transverse with increasing age. *Circulation* 105, 2092–2098. doi: 10.1161/01.CIR.000015506.36371.0D
- Manios, E. G., Mavrakis, H. E., Kanoupakis, E. M., Kallergis, E. M., Dermitzaki, D. N., Kambouraki, D. C., et al. (2003). Effects of amiodarone and diltiazem on persistent atrial fibrillation conversion and recurrence rates: a randomized controlled study. *Cardiovasc. Drugs Ther.* 17, 31–39. doi: 10.1023/A:1024203824761
- Rohr, S., Kucera, J. P., Fast, V. G., and Kléber, A. G. (1997). Paradoxical improvement of impulse conduction in cardiac tissue by partial cellular uncoupling. *Science* 275, 841–844. doi: 10.1126/science.275.5301.841
- Schotten, U., Verheule, S., Kirchhof, P., and Goette, A. (2011). Pathophysiological mechanisms of atrial fibrillation: a translational appraisal. *Physiol. Rev.* 91, 265–325. doi: 10.1152/physrev.00031.2009
- Shaw, R. M., and Rudy, Y. (1997). Ionic mechanisms of propagation in cardiac tissue: roles of the sodium and L-type calcium currents during reduced excitability and decreased gap junction coupling. *Circ. Res.* 81, 727–741. doi: 10.1161/01.RES.81.5.727
- Spach, M., and Boineau, J. (1997). Microfibrosis produces electrical load variations due to loss of side-to-side cell connections: a major mechanism of structural heart disease arrhythmias. *Pacing Clin. Electrophysiol.* 20, 397–413. doi: 10.1111/j.1540-8159.1997.tb06199.x
- Spach, M. S., and Dolber, P. C. (1986). Relating extracellular potentials and their derivatives to anisotropic propagation at a microscopic level in human cardiac muscle. Evidence for electrical uncoupling of side-to-side fiber connections with increasing age. *Circ. Res.* 58, 356–371. doi: 10.1161/01.RES.58.3.356
- Spach, M. S., Heidlage, J. F., Dolber, P. C., and Barr, R. C. (2007). Mechanism of origin of conduction disturbances in aging human atrial bundles: experimental and model study. *Heart Rhythm* 4, 175–185. doi: 10.1016/j.hrthm.2006.10.023
- Spach, M. S., and Josephson, M. E. (1994). Initiating reentry: the role of nonuniform anisotropy in small circuits. *J. Cardiovasc. Electrophysiol.* 5, 182–209. doi: 10.1111/j.1540-8167.1994.tb01157.x
- Spach, M. S., Miller, W. T., Dolber, P. C., Kootsey, J. M., Sommer, J. R., and Mosher, C. E. (1982). The functional role of structural complexities in the propagation of depolarization in the atrium of the dog. Cardiac conduction disturbances due to discontinuities of effective axial resistivity. *Circ. Res.* 50, 175–191. doi: 10.1161/01.RES.50.2.175
- Stein, M., Noorman, M., van Veen, T. A., Herold, E., Engelen, M. A., Boulaksil, M., et al. (2008). Dominant arrhythmia vulnerability of the right ventricle in senescent mice. *Heart Rhythm* 5, 438–448. doi: 10.1016/j.hrthm.2007.10.033
- Verheule, S., Eckstein, J., Linz, D., Maesen, B., Bidar, E., Gharaviri, A., et al. (2014). Role of endo-epicardial dissociation of electrical activity and transmural conduction in the development of persistent atrial fibrillation. *Prog. Biophys. Mol. Biol.* 115, 173–185. doi: 10.1016/j.pbiomolbio.2014.07.007
- Verheule, S., Tuyls, E., Gharaviri, A., Hulmans, S., van Hunnik, A., Kuiper, M., et al. (2013). Loss of continuity in the thin epicardial layer due to endomyocardial fibrosis increases the complexity of atrial fibrillatory conduction. *Circ. Arrhyth. Electrophysiol.* 6, 202–211. doi: 10.1161/CIRCEP.112.975144
- Verheule, S., Tuyls, E., van Hunnik, A., Kuiper, M., Schotten, U., and Allessie, M. (2010). Fibrillatory conduction in the atrial free walls of goats in persistent and permanent atrial fibrillation. *Circ. Arrhyth. Electrophysiol.* 3, 590–599. doi: 10.1161/CIRCEP.109.931634
- Villani, G. Q., Piepoli, M. F., Terracciano, C., and Capucci, A. (2000). Effects of diltiazem pretreatment on direct-current cardioversion in patients with persistent atrial fibrillation: a single-blind, randomized, controlled study. *Am. Heart J.* 140:e12. doi: 10.1067/mhj.2000.107179
- Vos, M. A., Golitsyn, S. R., Stangl, K., Ruda, M. Y., Van Wijk, L. V., Harry, J. D., et al. (1998). Superiority of ibutilide (a new class III agent) over DL-sotalol in converting atrial flutter and atrial fibrillation. The Ibutilide/Sotalol Comparator Study Group. *Heart* 79, 568–575. doi: 10.1136/hrt.79.6.568
- Wiegerinck, R. F., Verkerk, A. O., Belterman, C. N., van Veen, T. A. B., Baartscheer, A., Ophof, T., et al. (2006). Larger cell size in rabbits with heart failure increases myocardial conduction velocity and QRS duration. *Circulation* 113, 806–813. doi: 10.1161/CIRCULATIONAHA.105.565804
- Zhao, J., Butters, T. D., Zhang, H., LeGrice, I. J., Sands, G. B., and Smaill, B. H. (2013). Image-based model of atrial anatomy and electrical activation: a computational platform for investigating atrial arrhythmia. *IEEE Trans. Med. Imaging* 32, 18–27. doi: 10.1109/TMI.2012.2227776

Conflict of Interest Statement: The authors declare that the research was conducted in the absence of any commercial or financial relationships that could be construed as a potential conflict of interest.

Copyright © 2018 Zhao, Schotten, Smaill and Verheule. This is an open-access article distributed under the terms of the Creative Commons Attribution License (CC BY). The use, distribution or reproduction in other forums is permitted, provided the original author(s) and the copyright owner(s) are credited and that the original publication in this journal is cited, in accordance with accepted academic practice. No use, distribution or reproduction is permitted which does not comply with these terms.



Computational Modeling of Electrophysiology and Pharmacotherapy of Atrial Fibrillation: Recent Advances and Future Challenges

OPEN ACCESS

Edited by:

Oleg Aslanidi,
King's College London,
United Kingdom

Reviewed by:

Alfonso Bueno-Orovio,
University of Oxford, United Kingdom
Arun V. Holden,
University of Leeds, United Kingdom

*Correspondence:

Jussi T. Koivumäki
jussi.koivumaki@iki.fi

[†]These authors share first authorship

[‡]These authors share senior authorship

Specialty section:

This article was submitted to
Computational Physiology
and Medicine,
a section of the journal
Frontiers in Physiology

Received: 31 May 2018

Accepted: 13 August 2018

Published: 04 September 2018

Citation:

Vagos MRSS, van Herck IGM, Sundnes J, Arevalo HJ, Edwards AG and Koivumäki JT (2018) Computational Modeling of Electrophysiology and Pharmacotherapy of Atrial Fibrillation: Recent Advances and Future Challenges. *Front. Physiol.* 9:1221.
doi: 10.3389/fphys.2018.01221

Márcia R. S. S. Vagos^{1,2†}, Ilsebeth G. M. van Herck^{1,2†}, Joakim Sundnes^{1,3},
Hermenegild J. Arevalo^{1,3}, Andrew G. Edwards^{1,3‡} and Jussi T. Koivumäki^{4,5*‡}

¹ Computational Physiology Department, Simula Research Laboratory, Lysaker, Norway, ² Department of Informatics, University of Oslo, Oslo, Norway, ³ Center for Cardiological Innovation, Oslo, Norway, ⁴ BioMediTech Institute and Faculty of Biomedical Sciences and Engineering, Tampere University of Technology, Tampere, Finland, ⁵ A.I. Virtanen Institute for Molecular Sciences, University of Eastern Finland, Kuopio, Finland

The pathophysiology of atrial fibrillation (AF) is broad, with components related to the unique and diverse cellular electrophysiology of atrial myocytes, structural complexity, and heterogeneity of atrial tissue, and pronounced disease-associated remodeling of both cells and tissue. A major challenge for rational design of AF therapy, particularly pharmacotherapy, is integrating these multiscale characteristics to identify approaches that are both efficacious and independent of ventricular contraindications. Computational modeling has long been touted as a basis for achieving such integration in a rapid, economical, and scalable manner. However, computational pipelines for AF-specific drug screening are in their infancy, and while the field is progressing quite rapidly, major challenges remain before computational approaches can fill the role of workhorse in rational design of AF pharmacotherapies. In this review, we briefly detail the unique aspects of AF pathophysiology that determine requirements for compounds targeting AF rhythm control, with emphasis on delimiting mechanisms that promote AF triggers from those providing substrate or supporting reentry. We then describe modeling approaches that have been used to assess the outcomes of drugs acting on established AF targets, as well as on novel promising targets including the ultra-rapidly activating delayed rectifier potassium current, the acetylcholine-activated potassium current and the small conductance calcium-activated potassium channel. Finally, we describe how heterogeneity and variability are being incorporated into AF-specific models, and how these approaches are yielding novel insights into the basic physiology of disease, as well as aiding identification of the important molecular players in the complex AF etiology.

Keywords: atrial fibrillation, computational modeling, drug therapies, *in silico* drug screening, pathophysiology, pharmacology, pharmacodynamics

INTRODUCTION

Atrial fibrillation (AF) is a complex and multifactorial disease and the most common sustained cardiac arrhythmia, afflicting about 2% of the population. Age is the most powerful predictor of risk: approximately 5% of 65-year-olds and 10% of 75-year-olds suffer from AF (Heeringa et al., 2006). AF is already a pervasive disease carrying an immense socioeconomic burden, and with increasing life expectancy both the human and economic costs are growing rapidly: AF prevalence in the European population is projected to increase to 3% by 2030 (Zoni-Berisso et al., 2014). Although rhythm control strategies are available, these are inadequate and there is at present an unmet need for safe and effective antiarrhythmic therapy for AF (Ehrlich and Nattel, 2009). Since 2010, the European Medicines Agency has not authorized any new drugs for treatment of AF. The most prominent explanations for this lack of new medicine are the limited understanding of this multi-etiological and progressive disease, as well as the challenge of designing compounds that are strongly specific for atrial rather than ventricular targets. As a result, the development of novel pharmacological therapies is necessarily coupled to a thorough understanding of the basic etiology and physiological mechanisms of AF.

Unlike most episodes of ventricular arrhythmia, which must either be terminated or are lethal, AF does not have immediate catastrophic consequences, and short episodes of self-terminating AF are often asymptomatic and go undetected. This allows prolonged AF episodes to drive pro-arrhythmic remodeling across all levels of physiology (Schotten et al., 2011), as is succinctly captured by the phrase “AF begets AF” (Wijffels et al., 1995). In turn, this remodeling allows the mechanisms and complexity of AF to be richer than ventricular arrhythmia and causes treatment to be a moving target as the disease progresses from paroxysmal (pAF) to chronic (cAF) stages.

Both ectopic activity and the generation of a vulnerable substrate are accepted contributors to AF initiation and maintenance, although their respective contributions are thought to change as disease progresses. Triggering events are generally thought to play a more prominent role in pAF than at later stages when gross tissue-level remodeling is widespread. A range of evidence has led to this general perspective, but some key observations include: (1) prominent focal initiation of spontaneous episodes of pAF near the pulmonary vein (PV) junctions in patients (Haïssaguerre et al., 1998), (2) the absence of major alterations to action potential (AP) morphology and the excitable tissue gap in pAF (Diker et al., 1998; Voigt et al., 2013b), (3) elevated frequency of cellular triggering events (Voigt et al., 2012, 2013b).

As AF progresses, electrical and structural remodeling becomes pronounced, and characteristic changes to conduction and refractoriness leave the atrial myocardium more vulnerable to reentrant circuit formation (Nattel and Harada, 2014). AP duration (APD) and the effective refractory period (ERP) are consistently shortened in cAF (Iwasaki et al., 2011; Skibbsby et al., 2016), conduction is slowed (Lalani et al., 2012; Zheng et al., 2016), and the threshold for alternans induction, a key component of vulnerable substrate generation, is reduced

(Narayan et al., 2011). Electrical remodeling exacerbates regional heterogeneities and promotes dispersion of refractoriness. Additionally, formation of fibrotic regions, collagen patches, and fibroblast differentiation, as part of structural remodeling, enhances tissue anisotropy and is non-uniform throughout the atria, thus further promoting the development of a reentrant substrate. Moreover, contractile remodeling (atrial dilatation and increased wall compliance) is both a consequence and effector of AF (Schotten et al., 2003). All these identified mechanisms of progressive remodeling, resulting from recurrent rapid pacing or paroxysms of AF, generate positive feedback loops that ultimately set the conditions for sustained AF. These processes are likely to be important in determining the dynamic characteristics of reentrant circuit formation, and in certain cases may be important for understanding drug action. For example, the efficacy of class Ic antiarrhythmics depends on the dynamics inherent to spiral wave propagation (Comtois et al., 2005; Kneller et al., 2005). However, currently, we do not have sufficient understanding of the tissue-level dynamics driving AF at various stages, to focus pharmacologic design efforts on correcting specific tissue-level dynamical characteristics. For this reason, our discussion below focuses on remodeling occurring at subcellular and cellular levels and their implications in AF progression, and acknowledge that the sustaining effect of tissue-level electrical and structural remodeling causes antiarrhythmic targeting in cAF to be extremely challenging. The major components, interactions, and contributions of the characteristic processes at the various stages of disease progression are summarized in **Figure 1**.

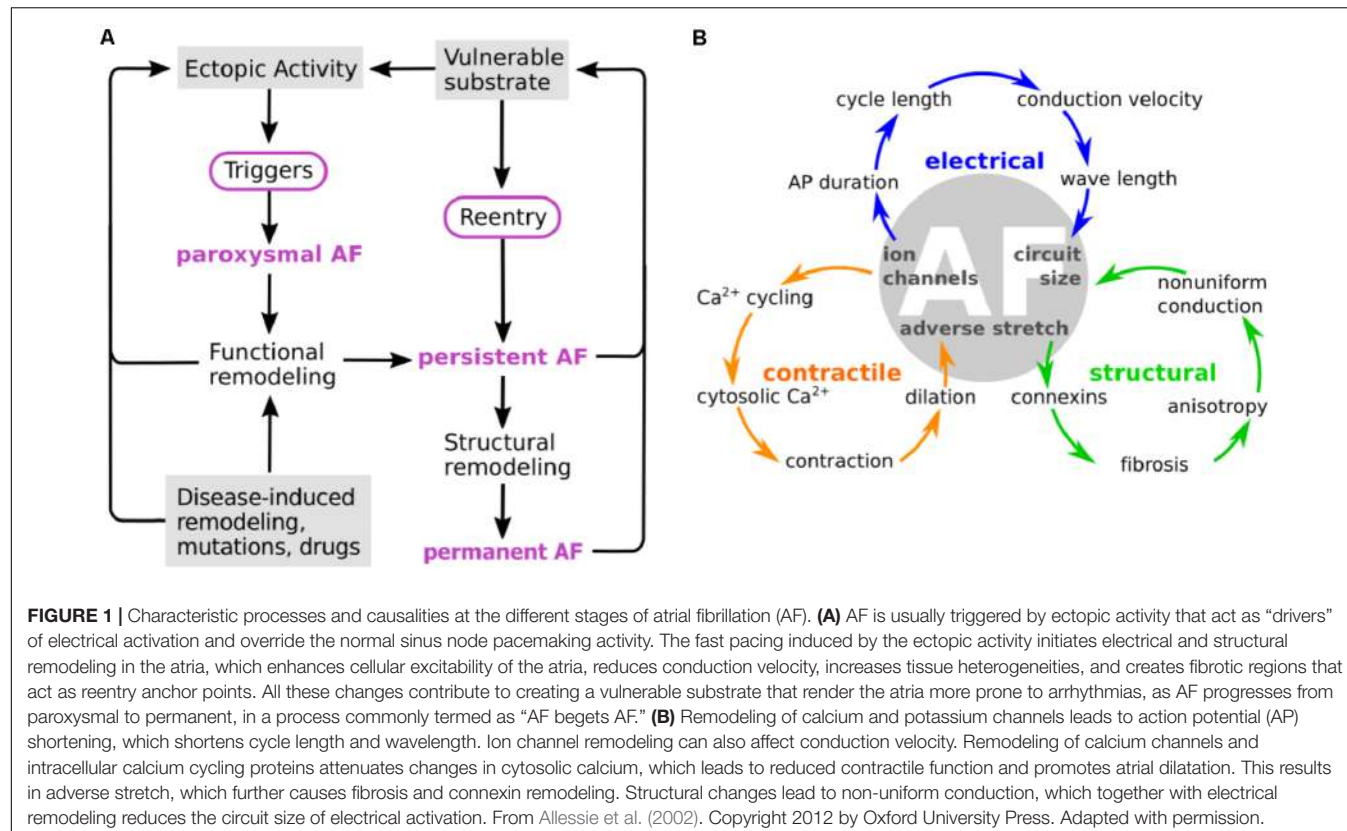
In the following four sections, we first briefly introduce the basic aspects of AF mechanisms and their related experimental findings (see the section “Arrhythmogenic Mechanisms of AF”). We then review current computational approaches for modeling atrial physiology and AF pathophysiology (see the section “*In silico* Atrial Modeling”). We present an overview of how drug-target interactions and their outcomes have been simulated in the heart, followed by current efforts to explore novel strategies for AF drug targeting (see the section “Computational Pharmacology in AF”). Finally, in the section “Modeling Variability and Uncertainty at the Cell Level,” we describe how variability and stochasticity can be incorporated into computational models to increase their robustness and predictive power in AF drug therapy.

ARRHYTHMOGENIC MECHANISMS OF AF

Remodeling of Cellular Electrophysiology, Ultrastructure, and Calcium Handling

Pathological Changes to Sarcolemmal Current Carriers

Human atrial cardiomyocytes (hA-CMs) exhibit a range of AP morphologies that differ markedly from those apparent in the ventricle. This is primarily due to differing expression levels of ion channel subunits, and consequent ion current densities.



The atrial AP exhibits a less pronounced plateau phase, largely due to the prominent expression of the fast-activating potassium currents, particularly the ultra rapidly activating delayed rectifier current (I_{Kur}), which is virtually absent in the ventricle. Atrial APs also exhibit relatively slow late repolarization (phase 3), elevated resting potential, and slower AP upstroke, all of which are strongly influenced by a reduced density of the inward-rectified potassium current (I_{K1}) relative to human ventricular CMs (hV-CMs). Like I_{Kur} , the small conductance calcium-activated potassium current ($I_{K,Ca}$) is only present in hA-CMs, and it is thought to assist hA-CM repolarization, although its relative contribution remains contentious. The major differences in atrial and ventricular AP morphology and underlying ion currents are summarized in **Figures 2A,B**.

The pathophysiology of cAF is characterized by several prototypical changes in current expression that result in both marked deceleration of early repolarization, and acceleration of late repolarization (Schotten et al., 2011). The two most prominent molecular changes that drive these outcomes are: (1) augmentation of inward-rectified potassium currents (increase of I_{K1} expression and constitutive activity of the acetylcholine-activated inward rectifier current; $I_{K,ACh}$), and (2) simultaneous decrease in the L-type calcium current (I_{CaL}). The major counteractive changes are carried by increased sodium-calcium exchanger (NCX) expression, and reductions in the major rapidly activating outward currents, namely I_{Kur} and the fast component of the transient outward potassium current (herein simply referred to as I_{to}). Together, these five alterations (I_{K1} ,

I_{CaL} , NCX, I_{Kur} , and I_{to}) constitute the majority of the known modulators of repolarization trajectory in cAF (**Figure 3**). Overall these effects result in the shortening of ERP, and a slightly more negative resting membrane potential (Ravens et al., 2014; Skibbsby et al., 2014, 2016), both of which expand the window for reentrant excitation. However, as discussed further below, they are accompanied by a range of changes to cellular ultrastructure and to the function of major calcium- and sodium-handling proteins, such that predicting the integrated outcomes from any subset of changes is non-trivial and necessitates quantitative approaches.

Ultrastructural Contributions to AF Pathogenesis

Although there is important species-specificity of atrial CM ultrastructure, it has been generally observed that healthy atrial CMs exhibit a varied and relatively sparse membrane ultrastructure compared to ventricular CMs. This results in important baseline differences in excitation-contraction coupling. Most prominently, atrial CMs have a less developed T-tubule network (Dibb et al., 2013), particularly in rodents, as illustrated in **Figures 2C,D**. This morphological difference has implications for intracellular calcium diffusion. In the absence of T-tubules, Ca^{2+} enters the cells largely from the periphery, and thus must diffuse centripetally to engage the contractile machinery. Correspondingly, the localization of Ca^{2+} handling proteins is very different in ventricular and atrial CMs. In hA-CMs, as in hV-CMs, L-type Ca^{2+} channels interact with clusters of sarcoplasmic reticulum (SR) Ca^{2+} release channels

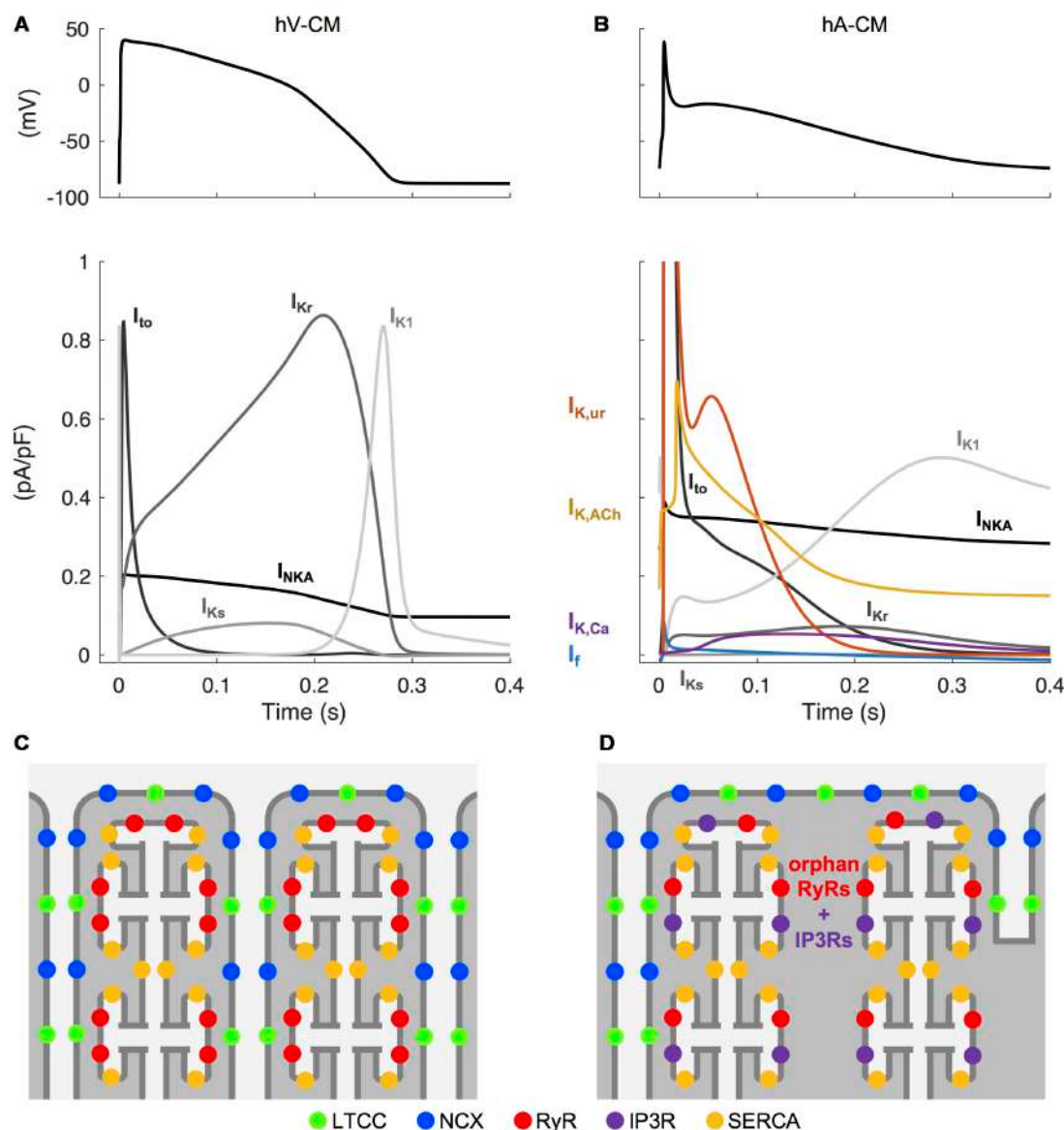


FIGURE 2 | Unique electrophysiological and structural characteristics of atrial cardiomyocytes. Simulated AP in human ventricular **(A)** and atrial **(B)** CMs, as well the differences in underlying repolarizing potassium currents, obtained with the hV-CM (O'Hara et al., 2011) and hA-CM (Skibbsbye et al., 2016) models, at 1 Hz pacing. Please, note that in order to visualize the weaker currents, the peaks of atrial transient outward potassium current (I_{to}) (~ 11 pA/pF) and the ultra rapidly activating delayed rectifier potassium current (I_{Kur}) (~ 4.6 pA/pF) are cut off. The atria-specific ion currents funny current (I_f), I_{Kur} , the acetylcholine-activated potassium current ($I_{K,ACh}$), and the small conductance calcium-activated potassium current ($I_{K,Ca}$) are highlighted with colored lines. Illustration of the relative positioning of some of the key components involved in intracellular calcium dynamics in hV-CMs **(C)** and hA-CMs **(D)**.

(RyRs; ryanodine receptors) located in the junctional SR to trigger Ca^{2+} -induced Ca^{2+} release (CICR). However, in hA-CMs, a higher proportion of RyR clusters are concentrated in non-junctional SR, and this is a distinguishing structural characteristic. These orphan or non-junctional RyRs contribute to the fire-diffuse-fire propagation of Ca^{2+} , which is augmented by inositol 1,4,5-trisphosphate receptors (IP3Rs) that are also embedded in the SR membrane (Lipp et al., 2000; Yamada et al., 2001; Zima and Blatter, 2004; Li et al., 2005; Wullschleger et al., 2017). The importance of IP3Rs is generally greater in atrial

than ventricular CMs – in ventricle, they are generally only observed in disease states, such as heart failure (Go et al., 1995). These features of the calcium signaling system fundamentally alter the essential structure-function relationships governing calcium handling in atrial versus ventricular CMs, where the extensive and highly organized T-tubule network shortens the diffusion distances so that fast and uniform CICR is possible. The physiological outcome for the atrial CM is a slower rise phase of the intracellular Ca^{2+} transient (CaT) (Hatem et al., 1997; Greiser et al., 2014) and contractile force (Frisk et al., 2014), and

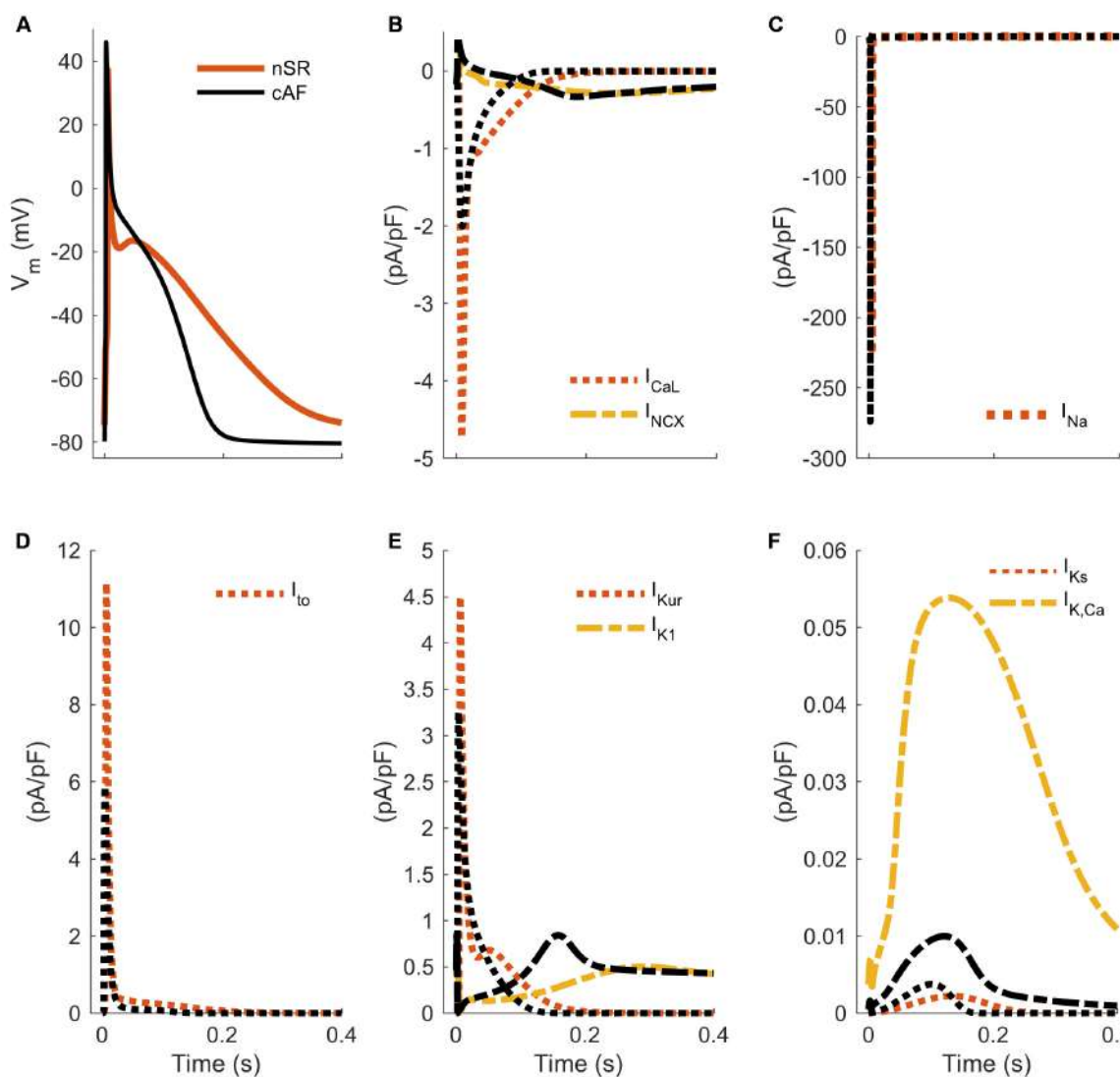


FIGURE 3 | Hallmarks of altered electrophysiology of human atrial myocytes in AF. APs (**A**) and underlying ion currents (**B–F**) in normal sinus rhythm and chronic AF variants of a hA-CM model (Skibsbye et al., 2016). The cAF model variant accounts for increased/decreased ion current conductance I_{Na} (-18%), I_{CaL} (-59%), I_{to} (-62%), I_{Kur} (-38%), I_{K1} ($+62\%$), I_{Ks} ($+170\%$), $I_{K,Ca}$ (-50%) and I_{NCX} ($+50\%$), as summarized in Koivumäki et al. (2014b) and Skibsbye et al. (2016).

~100 ms delayed CaT at the center of the CM comparatively to the periphery (Hatem et al., 1997; Tanaami et al., 2005; Greiser et al., 2014), resulting from spatial (particularly centripetal) propagation of intracellular Ca^{2+} during atrial systole.

This unique membrane ultrastructure of atrial CMs is now also thought to contribute to AF pathogenesis. Recently, it has been shown that T-tubule density in atrial cells is reduced in sheep and canine models of AF (Lenaerts et al., 2009; Wakili et al., 2010); however, supporting human atrial data is lacking. The putative loss of T-tubules may lead to contractile dysfunction, but is also strongly implicated in arrhythmogenesis. In particular, the increased spatial heterogeneity in subcellular Ca^{2+} signaling has been shown to promote CaT and APD alternans (Gaeta et al., 2009; Li et al., 2012), and incomplete excitation–contraction (E–C) coupling (Greiser et al., 2014). Reorganization of RyR

clusters adds a further dimension to AF-related ultrastructural remodeling. It has been shown to be associated with more frequent Ca^{2+} sparks in a sheep model of cAF, and is thought to increase the probability of the propagating Ca^{2+} release underlying arrhythmogenic calcium waves (Macquaide et al., 2015). However, there are no human data available to corroborate the possible change in organization of RyRs in AF patients. Thus, additional structural and functional data from patients would be valuable for understanding the functional role of structural degradation in this disease.

Cell dilation/hypertrophy is also a common finding in cAF patient samples, where increases of 12% (Neef et al., 2010) and 16–54% (Schotten et al., 2001; Neef et al., 2010; Corradi et al., 2012) have been reported for length and diameter, respectively. In line with these findings, cell surface area in patients with cAF was

reported to be \sim 40% larger (Wouters et al., 2000). The increased cell volume and diameter reduce CaT amplitude and slow centripetal Ca^{2+} diffusion, respectively (Koivumäki et al., 2014b). As hA-CMs are likely to have very few (if any) T-tubules in cAF, slower Ca^{2+} diffusion is thought to exacerbate dyssynchrony of the AP and CaT, thus potentially contributing to alternans. At the tissue level, increased capacitance of CM membrane causes conduction slowing (Oliveira et al., 2015).

As mentioned above, tissue-level remodeling, inflammatory signaling, and mechanical dysregulation also make a major contribution to AF pathology, particularly in the advanced stages of disease. We mention these aspects briefly here, but the remainder of this article will focus on classical electrophysiologic and ionic mechanisms of AF, particularly those targeted for acute cardioversion early in disease development. Reduced I_{CaL} in cAF promotes contractile dysfunction and atrial dilatation (atrial stretch). These mechanical perturbations are thought to be a major contributor to the widespread deposition of interstitial collagen, lateralization of gap junctions (connexin remodeling), and proliferation of myofibroblasts and potentially adipocyte infiltration observed in many animal models of chronic disease (Ravelli and Allessie, 1997; Schotten et al., 2003; Lau et al., 2017). While these characteristics are widely thought to be similarly prominent in humans, corroborating data remain relatively sparse because *in vivo* measures are technically challenging. Functional indicators (e.g., complex fractionated atrial electrograms) have often been used as primary measures of fibrosis, although gadolinium-enhanced MRI protocols have also been shown capable of quantifying *in vivo* differences between paroxysmal and more advanced disease (Daccarett et al., 2011). These changes in atrial tissue structure have profound consequences for tissue conductivity, wave propagation, and potential for reentry, and are thus likely to pose an insurmountable challenge to pharmacotherapy in later disease stages. For this reason, interventions targeting the suppression of the signaling pathways that results in these gross changes to atrial structure, have recently become an area of substantial interest (Nattel and Harada, 2014).

Role of Remodeled Calcium Homeostasis in AF

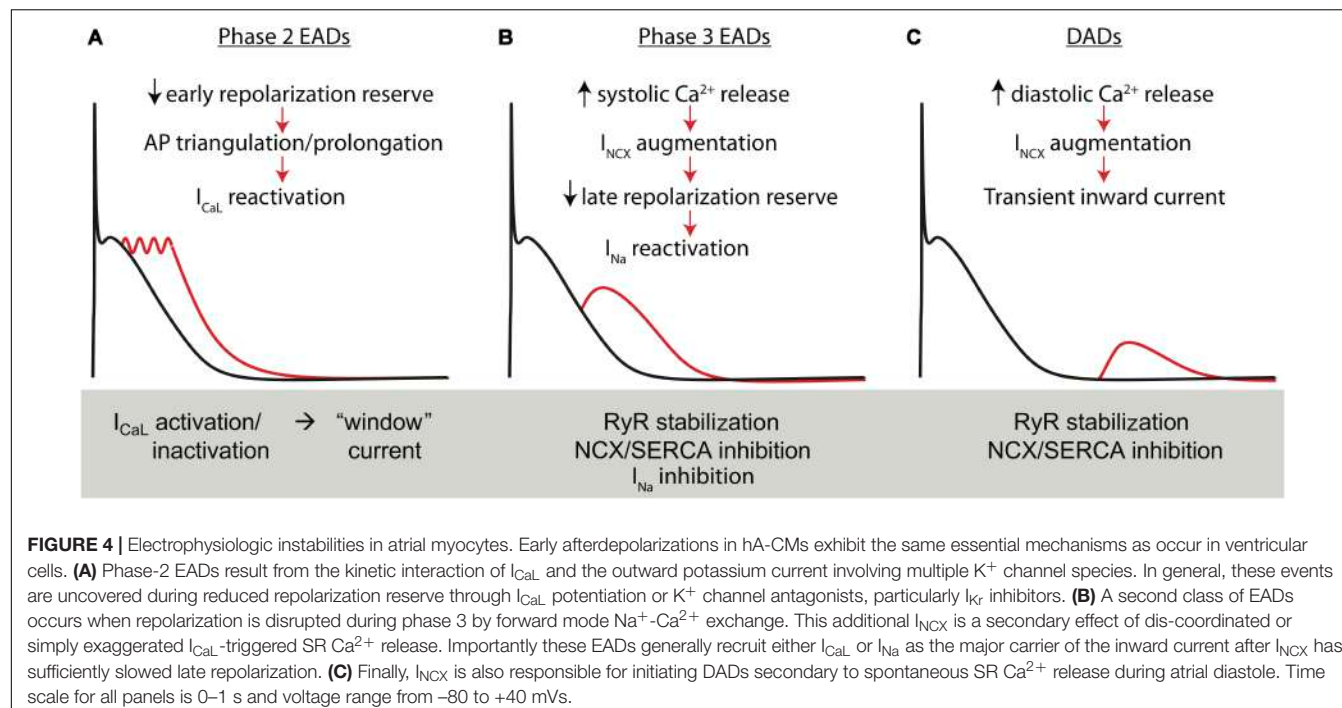
Alterations to calcium handling are intrinsically linked to the ultrastructural changes described above, but further remodeling of expression or regulation of the major intracellular transporters is also likely to contribute. In general, the role for these mechanisms in AF, particularly pAF, has become well supported in recent years, and ion transporters involved in calcium handling and their regulatory proteins seem to be promising targets for drug therapy of AF. As mentioned above, cAF is associated with increased NCX expression in patients (Gaborit et al., 2005; El-Armouche et al., 2006; Neef et al., 2010). There is also strong evidence of an increased coupling gain between intracellular Ca^{2+} load and I_{NCX} in cAF (Grandi et al., 2011; Voigt et al., 2012) and larger I_{NCX} amplitudes have also been reported in cAF patient samples (Christ et al., 2016). The data on altered RyR function in AF is less conclusive. Increased RyR activity has been reported in cAF patients (Neef et al., 2010; Voigt et al., 2012), whereas, RyR expression has been reported to be both

reduced (Ohkusa et al., 1999; Oh et al., 2010) and unchanged (Shanmugam et al., 2011; Voigt et al., 2012) in cAF patients. Hyperphosphorylation of RyRs has been reported to increase their Ca^{2+} sensitivity and open probability, increasing Ca^{2+} leak from the SR into the cytosol (Vest et al., 2005; Neef et al., 2010; Voigt et al., 2012). One further player in the game of calcium remodeling is the SR Ca^{2+} -ATPase (SERCA), which pumps Ca^{2+} back into the SR from the cytosol. SERCA function is regulated by two inhibitory proteins: phospholamban and sarcolipin, and the phosphorylation levels of these regulatory proteins has an impact on the amplitude of the CaT and SR Ca^{2+} load. Reduced SERCA protein expression accompanied by increased activity was found in both pAF patients (Voigt et al., 2013b), while a rabbit model of rapid atrial pacing has shown remodeling-induced reduction in expression levels of SERCA with unchanged activity (Greiser et al., 2014). Although SERCA plays an important role in the modulation of SR Ca^{2+} load and, indirectly, in the extent of arrhythmogenic Ca^{2+} leak, there is currently no published *in vitro* human data on the AF-related change in function of SERCA, and the protein expression data is not conclusive.

Cellular Electrophysiologic Instability in AF

As described above, one of the proposed mechanisms of AF initiation is the generation of triggered activity in the atria in early stages of AF. These triggering events are classified as they are in the ventricle. That is, instabilities in AP repolarization are named early afterdepolarizations (EADs), and diastolic instabilities initiating from resting potential are delayed afterdepolarizations (DADs). Several of the established mechanisms of EADs and DADs are described in Figure 4. Because repolarization is hastened and I_{CaL} is reduced in cAF, AP triangulation is also reduced and the conditions for EAD generation via conventional I_{CaL} reactivation are generally impaired (Ming et al., 1994; Burashnikov and Antzelevitch, 2006). However, a body of literature supports that EADs initiating late in phase 3 of the AP may be important in some atrial regions and contexts, particularly focal arrhythmia initiating in the PV sleeves (Burashnikov and Antzelevitch, 2003; Patterson et al., 2006; Morotti et al., 2014, 2016). These EADs are driven by enhanced Ca^{2+} signaling, which in turn exaggerates I_{NCX} , slows late repolarization, and thereby promotes I_{Na} reactivation (Morotti et al., 2014, 2016).

The decreased Ca^{2+} influx via I_{CaL} , enhanced calcium extrusion due to increased NCX expression, and a leaky population of RyR, has generally been observed to result in marked depletion of the intracellular Ca^{2+} in cAF. In and of itself, this would be expected to reduce the incidence of spontaneous Ca^{2+} waves and DADs, and the ability of these diastolic events to drive focal arrhythmia. Indeed, the majority of studies support silencing of Ca^{2+} signaling as a cardioprotective mechanism and a reduced role for spontaneous Ca^{2+} release in cAF (Schotten et al., 2007; Christ et al., 2014; Greiser et al., 2014; Koivumäki et al., 2014b). However, opposite findings have also been reported in hA-CMs from cAF patients (Voigt et al., 2012). Importantly, rather than being reduced, SR Ca^{2+} load



was maintained in that study, and thus the elevated RyR activity and NCX expression readily translated to increased Ca^{2+} waves and DADs. Data from patients in pAF suggest that SR Ca^{2+} load is either not depleted (Hove-Madsen et al., 2004), or may in fact be exacerbated at these early stages of disease (Voigt et al., 2013b). Thus, the conditions explaining the observed increases in magnitude and frequency of spontaneous Ca^{2+} waves are more obvious and consistent. Viewing this collection of studies together, the most parsimonious interpretation is that the molecular drivers of increased Ca^{2+} wave frequency (RyR hyperphosphorylation, possibly increased SERCA activity) may precede those that strongly deplete intracellular Ca^{2+} (NCX expression). Thus, the increase in spontaneous Ca^{2+} release observed early in AF may be lost as the delayed molecular adaptations, particularly increased NCX expression, act to shift Ca^{2+} flux balance toward extrusion, thus depleting the Ca^{2+} store and silencing Ca^{2+} signaling, even during tachycardia (Greiser et al., 2014). This conceptual model of how Ca^{2+} -driven diastolic instability develops during AF is largely hypothetical, and further characterization of the specific temporal development of these molecular and functional maladaptations during disease is highly desirable.

Another proposed mechanism of triggered diastolic activity in the atria has stemmed from the discovery of expression of hyperpolarization-activated cation channels (HCN), carriers of the pacemaker current (I_f), in the left atrial appendage (Zorn-Pauly et al., 2004; Scheruebel et al., 2014). Furthermore, I_f properties are altered in cAF (Stillitano et al., 2013), lending weight to the hypothesis of abnormal cell automaticity as an additional mechanism of diastolic triggered activity in the remodeled myocardium. HCN channels could, therefore, constitute a novel potential target for antiarrhythmic drug

therapy. However, the lack of conclusive experimental human data thus far has rendered this mechanism a less attractive option for pharmacotherapy discovery.

Finally, the role of APD alternans in driving AF initiation is increasingly becoming appreciated after the observation that it immediately precedes AF in patients (Narayan et al., 2011). While the mechanisms capable of driving APD alternans are diverse, dynamic, and interactive, a growing body of evidence suggests that the proximal driver at the cellular level is a period 2 instability in Ca^{2+} cycling (Gaeta et al., 2009). In ventricular CMs this form of instability was initially thought to be driven by a kinetic mismatch in SR Ca^{2+} reuptake leading to variable refractoriness of Ca^{2+} release at high pacing frequencies (Diaz et al., 2004). However, more recently the role of subcellular heterogeneities in Ca^{2+} dynamics has emerged as a central aspect to the link between APD and Ca^{2+} transient alternans (Shiferaw and Karma, 2006; Gaeta et al., 2009, 2010; Gaeta and Christini, 2012). The intrinsic variability in atrial CM ultrastructure would be expected to promote these behaviors, particularly in AF, and this relationship between structure and dysfunction in AF requires stronger investigation by computational approaches.

IN SILICO ATRIAL MODELING

Existing hA-CM Models and AF Model Variants

Models for cardiac cellular electrophysiology and ion dynamics have been developed for more than five decades (Noble, 1962), and the first atria-specific hA-CM models were published by Courtemanche et al. (1998) and Nygren et al. (1998). These model lineages have been retroactively extended with novel

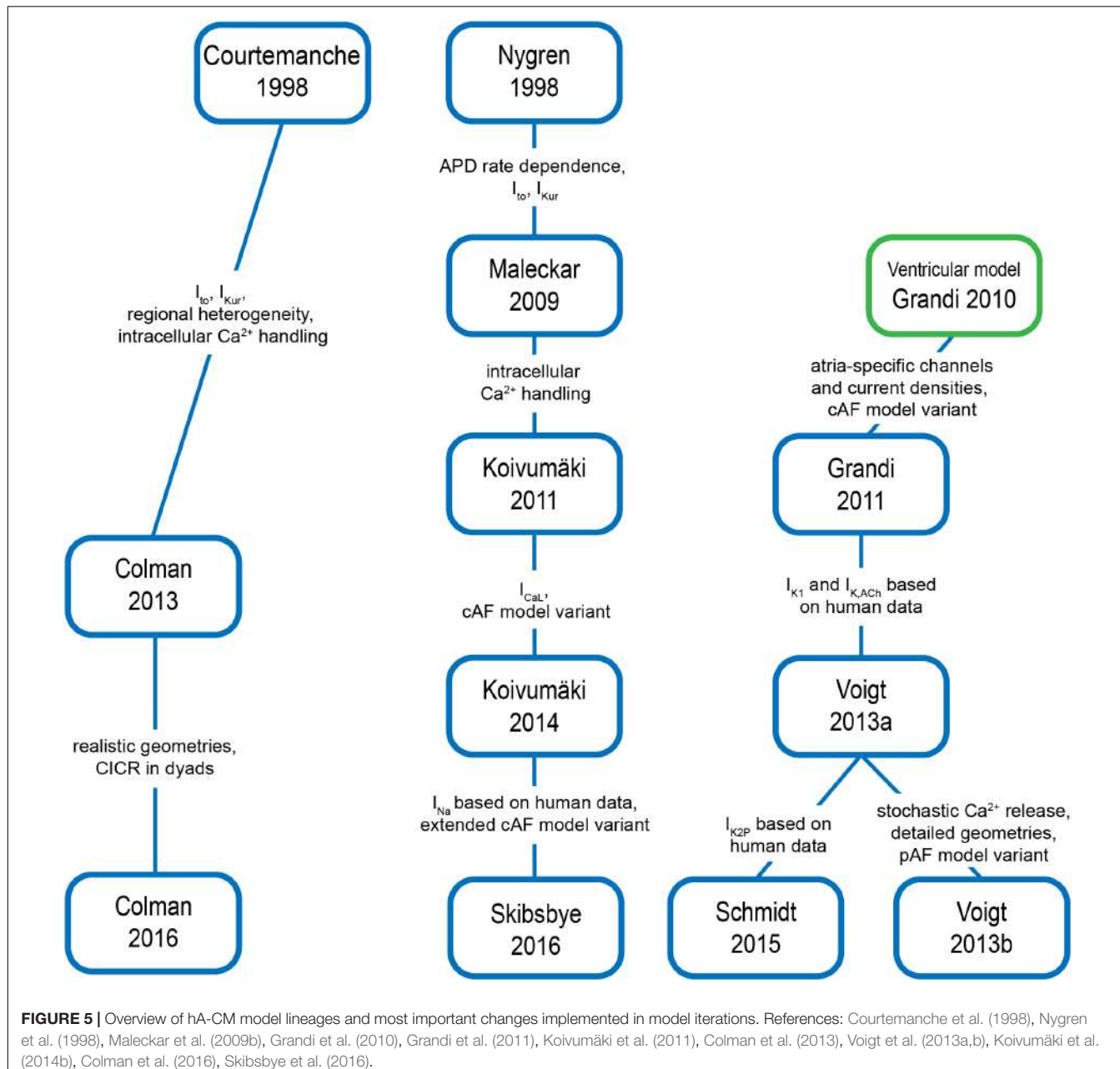


FIGURE 5 | Overview of hA-CM model lineages and most important changes implemented in model iterations. References: Courtemanche et al. (1998), Nygren et al. (1998), Maleckar et al. (2009b), Grandi et al. (2010), Grandi et al. (2011), Koivumäki et al. (2011), Colman et al. (2013), Voigt et al. (2013a,b), Koivumäki et al. (2014b), Colman et al. (2016), Skibsbye et al. (2016).

features, and new models have also been introduced as shown in **Figure 5**. The Courtemanche, Nygren–Maleckar–Koivumäki and Grandi model lineages, were benchmarked in detail (Wilhelms et al., 2013), and shown to be based on varying datasets and assumptions. As Wilhelms et al. (2013) reported, there are substantial differences in AP and CaT morphology, and rate adaptation properties among these models. For example, the AP repolarization in the Courtemanche model depends more on I_{Kr} and less on I_{Kur} compared to the other models. The Nygren model has a substantially larger contribution of the I_{Ks} current. Furthermore, several models include ion currents not incorporated in the others. For example, $I_{K,ACh}$ (Maleckar and Grandi models); I_f (Koivumäki model); plateau potassium

current, the Ca^{2+} dependent chloride current and background chloride current (Grandi model).

With accumulating experimental (human) data supporting the unique characteristics of atrial Ca^{2+} handling and its role in AF pathophysiology and arrhythmogenesis, the foundational hA-CM models have been updated to particularly include more complex intracellular Ca^{2+} signaling and ion channel localization. To account for the centripetal diffusion of calcium due to the lack of T-tubules in hA-CMs, Voigt et al. (2013b) extended the Grandi model with a spatial representation of Ca^{2+} handling based on longitudinal and transverse division of the intracellular space, and included stochastic RyR gating. Colman et al. (2016) also presented an atrial model with spatial

representation of the calcium handling system to assess the role of variable T-tubule density on intracellular calcium waves and alternans. These efforts have generally attempted to approach more realistic Ca^{2+} handling representations by drawing on data describing the T-tubule structure in particular. For instance, it may be possible to replicate the approach now being taken in ventricular CMs, where realistic SR and T-tubule geometries resolved by serial scanning electron microscopy have made it possible to reconstruct large sections of the cell directly from data (Colman et al., 2017). When applied to atrial CMs, this approach may provide a more realistic basis for simulating the effects of subcellular structure on macroscopic E-C coupling and arrhythmogenesis.

In addition to recapitulating physiology of healthy hA-CMs, all the above-mentioned cell models have variants to mimic cellular remodeling related to AF. The principle of 'AF begets AF' (Wijffels et al., 1995) emphasizes the need to represent the pathophysiological changes at different stages of AF progression with dedicated models. So far, the only pAF model variant has been published by Voigt et al. (2013b), accounting for early dysregulation of SR Ca^{2+} release and enhanced uptake, with no significant changes to sarcolemmal current carriers, and AP morphology. Conversely, cAF involves a much more advanced and complex remodeling (Schotten et al., 2011), which has been implemented in the *in silico* models to varying degrees of detail. The vast majority of cAF model variants have focused on electrical remodeling as distinct from remodeling of subcellular structure and Ca^{2+} handling machinery. These efforts have generally included the decreased I_{to} , I_{CaL} and I_{Kur} , and increased I_{K1} , as described in the section "Arrhythmogenic Mechanisms of AF." More recently, cAF models that also account for the remodeling of intracellular Ca^{2+} handling have been developed (Grandi et al., 2011; Colman et al., 2013; Voigt et al., 2013a; Koivumäki et al., 2014b). Furthermore, AF-related structural remodeling, specifically cell dilation, has been represented in one hA-CM model (Koivumäki et al., 2014b). First steps in accounting for the role of changes to regulatory signaling have also been taken by Grandi et al. (2011), who showed dramatic APD shortening as a result of parasympathetic activation of $I_{\text{K,ACh}}$. However, the overly simplified $I_{\text{to}} - I_{\text{CaL}} - I_{\text{Kur}} - I_{\text{K1}}$ approach of cAF modeling is still commonly used. As the accumulating experimental evidence suggests a central role for altered E-C coupling and intracellular Ca^{2+} handling in AF pathophysiology, a greater emphasis should be put on these components in future modeling studies.

In silico hA-CM models are comprehensive tools, complementing the *in vitro* experiments, for increasing the understanding of AF mechanisms and discovering potential pharmacological targets. The diversity of hA-CM models adds a layer of complexity to modeling of pharmacodynamics, as the outcome of pharmacological interventions *in silico* will vary between different models. This will be discussed in detail in the section "Computational Pharmacology in AF." As the physiological accuracy and robustness of atrial CM models have improved over the years, and continues to progress, so do their utility in higher

dimensional and organ scale simulations, as discussed further below.

1D and 2D Models of Electrical Conduction in the Atria

Modeling Electrical Propagation in Tissue

Early observations of electrograms during AF revealed the presence of chaotic activity in the atria. Recent technological advancements in high-resolution AF mapping have shown that AF is maintained by one or multiple spiral waves or rotors, which may be stationary or meander around anatomical structures (Guillem et al., 2016). Several studies have further supported that AF is maintained by high-frequency reentrant activity, compatible with the mother rotor hypothesis, as recently reviewed (Waks and Josephson, 2014; Guillem et al., 2016). However, several open questions still remain regarding the exact dynamical drivers of AF. Computational models of electrical propagation in the atria have contributed to elucidating the mechanisms of arrhythmia by enabling the simulation of electrical propagation in the heart through simplified models of single cell myocyte networks, mainly in the form of 1D and 2D architectures representing atrial fibers or patches of atrial tissue.

Characteristics of electrical activation in the myocardium, such as conduction velocity (CV), ERP, CV restitution, and APD restitution are known to modulate impulse propagation, with CV and refractoriness largely determining rotor dynamics and reentry stability (Sánchez et al., 2012). This commonly cited conceptual model is termed "leading circle" reentry, and states that a reentrant waveform is permitted to follow a circular path of minimal length equal to the wavelength ($\text{CV}^* \text{ERP}$), with the core remaining continuously refractory. Reported values of CV measured in the atria lie between ~ 50 to ~ 120 cm/s (Dössel et al., 2012), and are reduced by $\sim 15\%$ in AF (Feld et al., 1997). Conduction slowing and ERP shortening are two hallmarks of AF-induced remodeling, which result in reduced wavelength and higher susceptibility to reentry (Starmer et al., 1991; Nattel et al., 2008; Wakili et al., 2011; King et al., 2013). Conveniently, ERP and changes to ERP resulting from pharmacotherapy, can be implemented in 0D cell models, and CV can then be assessed by applying simple cable theory to couple such 0D implementations in series. The resulting 1D simulation frameworks are often used to arrive at basic indications of pharmacologic impacts on susceptibility to reentry, without actually permitting reentrant excitation.

At a higher level, 2D patches of tissue have been employed in simulations to reproduce the effects of structural and electrical remodeling on conduction barriers and exacerbated electrophysiological heterogeneities leading to unidirectional block and spiral wave breakup. As will be further discussed in the section " I_{Na} ," these frameworks have been very important for establishing the role of spiral wave dynamics in explaining the efficacy and subtype specificity of I_{Na} blockade. Aslanidi et al. (2009b) used 2D models of the atria to study activation patterns in the absence and presence of electrical heterogeneity, independently of structural effects or conduction anisotropy.

Results of 2D simulations show that APD gradients across the atria alone can reproduce different activation patterns in different regions of the atria (LA versus RA) (Aslanidi et al., 2009b). More recently, Gharaviri et al. (2017) studied the effect of transmural conduction using a dual sheet model of atrial tissue. They found that reducing the number of connections between the endo- and epicardial layers resulted in increased endo-epicardial dyssynchrony of electrical activity and in enhanced AF stability, in agreement with experimental findings in patients and animals (Verheule et al., 2013; Hansen et al., 2015).

Additionally, computational tissue models have helped elucidate the molecular mechanisms that give rise to spatially discordant alternans (SDAs), a mechanism that has been linked to the development of an arrhythmogenic substrate and increased reentry incidence (Pastore and Rosenbaum, 2000). Clinical data has shown that AP alternans precede episodes of AF in patients (Narayan et al., 2011), and another study in healthy controls and persistent AF patients showed that rapid pacing-induced SDA were associated with AF incidence, and could be terminated by verapamil administration (Hiromoto et al., 2005). These findings highlight the potential arrhythmogenic role of alternans, and the need to further elucidate the contribution of SDA to AF. Experimental studies in whole heart (Pruvot et al., 2004) and modeling studies in both 1D and 2D ventricular tissue have shown that SDA can be attributed to different mechanisms, in particular, Ca^{2+} instabilities (Sato et al., 2006, 2013), steep APD and CV restitution, (Qu et al., 2000) and tissue heterogeneities (Watanabe et al., 2001).

Because these 1D and 2D tissue models remain relatively computationally efficient, they can also be used to assess the ionic determinants that modulate conduction and rate adaptation in the atria during rapid pacing or other processes involving manipulation of the electrophysiologic steady state (Starmer et al., 2003; Krummen et al., 2012; Hunnik et al., 2016). In these contexts, extracting measures from simulated reentrant circuits allows quantitative comparisons of the impact of different ionic mechanisms and model conditions on the incidence and magnitude of AF, commonly quantified in terms of dominant frequency (DF), organization index, rotor meandering (RM), and duration of reentry.

Fibrosis in 1D and 2D Models

Tissue models of the atria have recently been expanded to include the effect of fibrosis in AF maintenance. Myofibroblasts, or simply fibroblasts (Fb), compose about 10–15% of myocardium volume, although they largely outnumber myocytes (Shiraishi et al., 1992). Fibroblasts can exhibit APs when electrically coupled to CMs through gap junction channels (Camelliti et al., 2004; Wang et al., 2006), and have long been recognized to play an important role in modulating the electrical function of the myocardium (Kohl and Noble, 1996; Kamkin et al., 1999; Kohl et al., 2005; Tanaka et al., 2007). The fibroblasts can act as either current sources or sinks during a myocyte excitation, disturbing normal electrical propagation, and their proliferation has also been linked to abnormal automaticity in the atria, whereby Fb-CM coupling can induce a depolarizing current during the diastolic phase and elicit APs (Miragoli et al., 2007).

In agreement with *in vitro* experimental data, modeling studies in 1D and 2D models have shown that proliferation of fibroblasts (or more generically, non-myocytes) in the atrial tissue, and their coupling with myocytes through gap junctions, lead to alterations of the AP shape, RMP, upstroke velocity and CV. The significance of the alterations, and their arrhythmogenic potential, depends on several factors, such as fibroblast density and distribution, the strength of Fb-CM coupling, and RMP of the fibroblast (Jacquemet and Henriquez, 2008; Maleckar et al., 2009a; Koivumäki et al., 2014a; Seemann et al., 2017), as reviewed in Yue et al. (2011). Additionally, Fb-CM coupling can lower or raise the APD alternans threshold, depending on whether APD is shortened or prolonged (Xie et al., 2009). Furthermore, in cAF, the hyperpolarization of the membrane potential has been shown to render the remodeled myocytes less sensitive to coupling with fibroblasts (Sánchez J. et al., 2017). In another study, the APD shortening effect of dofetilide and vardenafil was enhanced with increasing amount of coupled fibroblasts, showing the importance of including Fb-CM coupling in pharmacological modeling studies (Gao et al., 2017).

Although human data is still sparse, and the precise contribution of fibrosis to ectopic activity and reentry in AF remains poorly understood, it seems clear that fibrotic tissue is a key promoter of AF progression. Therefore, therapeutic approaches that prevent fibroblast proliferation, secretion and connexin expression, by targeting for example fibroblast ion channels and signaling pathways, could constitute a potential strategy for upstream regulation of AF progression (Yue et al., 2011).

3D Models of the Atria

Single cell models of atrial electrophysiology have significantly contributed to increase our understanding of the cellular mechanisms of arrhythmia and underpinning novel pharmacotherapeutic targets (Heijman et al., 2015). However, multiscale models of the atria are necessary to understand the complexity of atrial arrhythmias and capture the essential dynamics of this disease. This need is accentuated by challenges associated with obtaining reliable AF activation maps, especially in patients, which has pressed the need for more elaborate *in silico* whole atrial models. Three-dimensional (3D) models of atrial electroconduction have been developed to enable simulation of normal atrial function and arrhythmogenesis in the context of full structural complexity of the atrial geometry, and incorporating many of the regional electrical heterogeneities present in the intact organ.

Electrical heterogeneities in the atria are mainly characterized by regional variations of ion current and connexin expression. However, as human data are sparse, these regional differences are generally incorporated from studies conducted in other species, mostly canine. The complex structural heterogeneities in the atria are also challenging to accurately represent in computational models, but are believed to be important for the understanding of AF dynamics. Thus, in recent years a considerable amount of effort has been devoted to the incorporation of detailed anatomic, structural and electrophysiological information in the modeling pipeline.

Incorporating Heterogeneity Into 3D Models of the Atria

The first attempts to develop 3D models of the atria relied on simplistic geometries with limited anatomical detail, such as spherical surfaces (Blanc et al., 2001), or geometrical surfaces designed to resemble the atria (Harrild and Henriquez, 2000; Vigmond et al., 2003; Ruiz-Villa et al., 2009). Additionally, most of these first models did not consider regional differences in electrophysiology (Harrild and Henriquez, 2000; Blanc et al., 2001; Virag et al., 2002). In their first stage of development, 3D models of the atria were mostly focused on the role of atrial geometry and structural heterogeneity on the development of a proarrhythmic substrate (Harrild and Henriquez, 2000; Blanc et al., 2001; Virag et al., 2002). Although useful in discerning the basic mechanisms underlying atrial arrhythmias, these studies recognized the importance of incorporating electrical and more detailed structural heterogeneity into the models in order to faithfully reproduce complex arrhythmogenic patterns. Vigmond et al. (2003) presented the first atrial model, a canine model, containing all the major structural features of the atria, electrical propagation according to fiber orientation (constructed with a series of interconnected cables), AP heterogeneity, and electrical remodeling. The study provided new insight into the role of structural and electrical heterogeneity of atrial tissue on reentry and fibrillation maintenance, and confirmed the importance of including electrophysiological variations in atrial tissue models.

Since these earlier efforts, regional differences in AP morphology have typically been incorporated by varying ion channel maximum conductances and gating variables of the Courtemanche hA-CM model. **Figure 6** shows an example of different AP morphologies in the different regions of the atria modeled in this way (Colman et al., 2013). These are mainly due to differences in expression of I_{Kr} , I_{Ks} , I_{to} , I_{Kur} , I_{K1} , and I_{CaL} . We will not describe these regional characteristics in detail, but a comprehensive overview of current densities and APD in the different atrial regions, and of the original experimental data sources, can be found in Krueger et al. (2013). With these model variants as a baseline for electrical variation

throughout the atria, it has been possible to begin understanding the role of electrophysiological heterogeneity both in normal atrial activation, and in AF arrhythmogenesis. During normal activation, the gradient in APD from the sino-atrial node (SAN) toward the atrio-ventricular node (AVN) and the left atrium (LA) (Ridler et al., 2006), is thought to facilitate conduction from the SAN toward the AVN and impede uni-directional conduction block during normal sinus rhythm. However, the role of these APD gradients in atrial arrhythmias is not fully understood, and the manner in which change associated with AF electrical remodeling contribute to arrhythmia is very complex (Colman et al., 2013). Patchy tissue heterogeneities in left versus right atria are known to promote AF initiation (Luca et al., 2015), and it has often been suggested that left-right gradients in ion current expression increase dispersion of refractoriness and thereby promote reentrant substrate (Voigt et al., 2010). However, computational studies of the effect of right-left APD gradients in a canine model has found these gradients to be a protective mechanism against reentry, while increasing the complexity of arrhythmia patterns (Ridler et al., 2006, 2011). These studies highlight the complex effect of atrial heterogeneities and the need for a systematic characterization of the role of spatial variation of cell and tissue properties in AF.

In addition to the varying AP morphology, the atria present significant regional differences in CV and fiber orientation. These differences can be represented in models by spatially varying tissue conductivities according to tensor vectors obtained from fiber direction information. Fiber direction can be obtained with rule based methods (Seemann et al., 2006; Aslanidi et al., 2011; Colman et al., 2013), based on anatomical data obtained from *ex vivo* diffusion-tensor imaging (Pashakhanloo et al., 2016), or histological slices (Butters et al., 2013; Tobón et al., 2013).

Seemann et al. (2006) published the first model implementing realistic full 3D atrial geometries with regional heterogeneity. This model incorporated heterogeneity based on both human and animal experimental data of several atrial structures: Crista terminalis (CT), pectinate muscles (PM), Bachmann's bundle, atrial working myocardium, atrial appendage, and SAN. More

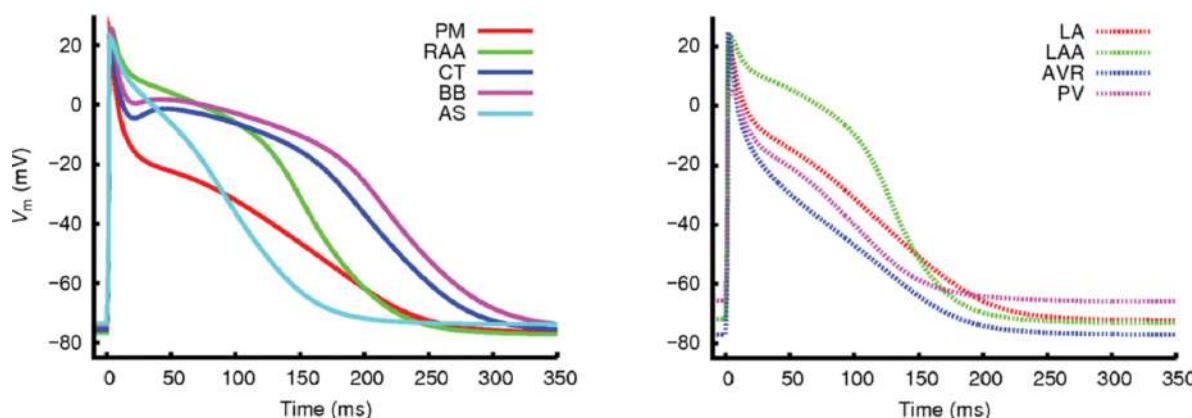


FIGURE 6 | Regional differences in AP morphologies in the different atrial regions obtained with a hA-CM model. From Colman et al. (2013). Creative Commons Attribution License BY.

recently, Krueger et al. (2013) developed an extended model with patient-specific anatomical data and additional segmentation of atrial regions: the PVs, atrial septum, the tricuspid valve ring, the mitral valve ring, and the fossa ovalis. Colman et al. (2013) have also published a similarly comprehensive model of the whole human atria incorporating both local heterogeneities and AF remodeling. **Figure 7** shows examples of 3D atrial models constructed via regional segmentation and incorporating heterogeneous AP morphologies (**Figure 7A**). Segmentation into different regions is often carried out manually based on known anatomical features.

Given the relative abundance of animal data sources, computational models of animal atria anatomy and electrophysiology are an important tool for studying arrhythmia mechanisms. Therefore, models of other animal species have also been developed, such as the rabbit atrial model from Aslanidi et al. (2009a), the canine models from Colman et al. (2014) and Varela et al. (2016), and the sheep model from Butters et al. (2013). All these models have contributed to further elucidating of the mechanisms underlying atrial arrhythmogenesis, and exemplify the importance of considering models of other animal species, integrating available experimental data, in studies of

AF mechanisms and in the discovery of novel therapeutic approaches (Nishida et al., 2010). Other 3D models of human atria developed in recent years have been reviewed in Dössel et al. (2012).

Importance of Modeling Heterogeneities in AF Studies

Several modeling studies have shown the importance of considering realistic anatomical structures, fiber orientation, and AP heterogeneity in the initiation and maintenance of reentry in both human (Seemann et al., 2006; Colman et al., 2013; Krueger et al., 2013; Luca et al., 2015; Zhao et al., 2017) and animal models (Aslanidi et al., 2009a; Butters et al., 2013; Varela et al., 2016). Studies have shown the role of anisotropy, mainly due to fiber orientation, in maintenance of AF, and the role of electrical heterogeneity in the initiation of AF (Butters et al., 2013). In particular, it has been shown that the abrupt anisotropy in fiber orientation between the posterior LA and the PVs is critical for wave break leading to reentry (Klos et al., 2008).

Butters et al. (2013) were the first to investigate computationally the mechanisms of initiation and maintenance of AF by describing the individual contributions of electrical heterogeneity and anisotropy, employing an anatomically detailed model of the sheep atria with regional AP variation. This study confirmed that the abrupt changes in tissue anisotropy between the LA and PVs provide an important AF substrate. This was primarily due to the complexity of the fiber structure of the PV region and the RA (in particular, the CT and PMs), as compared to the LA, which is relatively homogeneous. More recently, Zhao et al. (2017) extended human 3D models by incorporating transmural fibrosis, atrial wall thickness, and 3D myofiber architecture, based on *ex vivo* functional and structural imaging of the atria. This study found that the structural characteristics of regions driving AF were characterized by intermediate wall thickness and fibrotic density, as well as twisted myofiber structure.

Although data supports the involvement of atrial fibrosis in the development of AF, whether this is a cause or consequence of AF is still an open question (Schotten et al., 2016). A study on post-mortem human samples from several locations of the atria supported the existence of a correlation between the extent of atrial fibrosis and fatty tissue infiltrations, and the development and severity of AF (Platonov et al., 2011). As described in the previous section, simulation studies have contributed with some insight into the role of fibrosis in AF development. For example, Maleckar et al. (2009a), showed that CM excitability, repolarization, and rate-adaptation properties are strongly modulated by CM-myofibroblast electrotonic coupling, in particular the strength of coupling, number of coupled myofibroblasts, and the pacing rate. These findings suggest that myofibroblast proliferation during structural remodeling may exacerbate repolarization heterogeneities and decrease tissue excitability, thus facilitating abnormal conduction patterns (e.g., conduction block) and the development of a reentrant substrate.

McDowell et al. (2013) included the effect of fibrotic lesions on the initiation and progression of AF in a whole atrial model, finding that atrial fibrosis contributes to dispersion

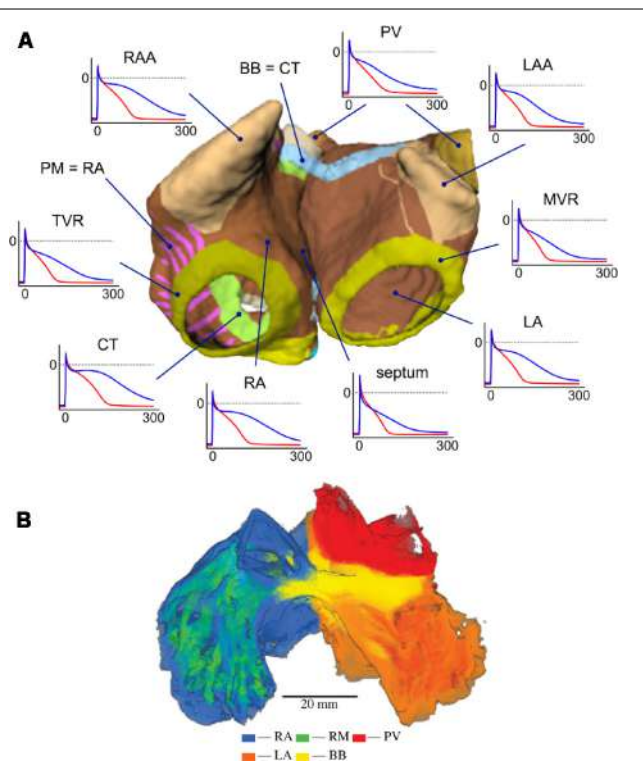


FIGURE 7 | (A) Three-dimensional atrial model with segmented regions and corresponding APs in physiological (blue) and AF-remodeled conditions (red), obtained with the Courtemanche model. From Krueger (2013). Creative Commons Attribution License BY-NC-ND. **(B)** Regional segmentation of an atrial sheep model into right atrium (RA), left atrium (LA), pectinate muscles (PM), pulmonary veins (PV), and Bachmann's Bundle (BB). From Butters et al. (2013). Copyright 2013 by Royal Society (United Kingdom). Reprinted with permission.

of APD due to gap-junction remodeling, as well as to the proliferation of myofibroblasts. The study showed that the latter was a sufficient condition for unidirectional conduction block following an ectopic beat from the PV region, while myofibroblast proliferation in the fibrotic region was sufficient to trigger reentry. In agreement with the previous study by Maleckar et al. (2009a) they found that the presence of myofibroblasts in the fibrotic region caused alterations of the transmembrane potential, in particular, shortening of APD and elevation of RMP, and these changes were exacerbated by the presence of collagen deposition. However, their proposed mechanism by which myofibroblasts cause inhomogeneous conduction slowing was through the remodeling of the potassium currents responsible for the repolarization phase of the AP, rather than by electrotonic effects resulting from the formation of direct connections between the myofibroblasts and CMs. Another computational study from the same group including the effects of atrial fibrosis, concluded that initiation of AF is independent of pacing location, and instead depends on the distance between the pacing location and the closest fibrotic region (McDowell et al., 2015).

Although much is still unknown about the role of structural and electrophysiological heterogeneities in AF, computational studies have contributed to the systematic characterization of the mechanisms of arrhythmogenesis. In some cases, these have highlighted the importance of patient-specific aspects for clinical therapy, as, for instance, the role of patient-specific fibrosis patterns for guiding catheter ablation procedures (McDowell et al., 2015; Boyle et al., 2016; Deng et al., 2017; Cochet et al., 2018).

COMPUTATIONAL PHARMACOLOGY IN AF

Lessons From Existing Rhythm Control Strategies in AF

The available compounds and therapeutic guidelines for AF cardioversion provide important context for AF drug design, and highlight key points of lacking knowledge that may be aided by computational approaches. Effective compounds include class III [amiodarone/dronedarone, intravenous ibutilide, vernakalant (in Europe), dofetilide, and sotalol], class Ic (flecainide and propafenone), and class V agents (cardiac glycosides). Computational studies have addressed their predominant modulatory targets: potassium channels, sodium channels, and NKA, respectively. Computational contributions to increase functional and mechanistic understanding of clinically relevant antiarrhythmic drugs are listed in **Table 1**. Most often these compounds are administered intravenously in the early stages of AF to achieve cardioversion, but flecainide and propafenone are also used orally as pill-in-the-pocket strategies. A critical consideration for choosing among these options is whether structural disease is present. Flecainide and propafenone are contraindicated for all NYHA heart failure classes, while ibutilide and vernakalant are inappropriate for patients with class III-IV disease. These specific characteristics of therapy and

contraindications provide an important general hierarchy for understanding the links between the mechanisms of drug action and their clinical utility in AF.

First, agents with QT prolonging actions are broadly contraindicated, as even relatively subtle effects on ventricular APD limit their use in AF treatment due to high comorbidity with structural disease. Additionally, Na^+ channel antagonists may be effective if they do not simultaneously reduce the atrial ERP or increase QT (thus eliminating both classes Ia and Ib). It is probable that the efficacy of class Ic agents is largely due to prolonged ERP accompanying their slow dissociation kinetics, which promotes termination of spiral wave reentry (Comtois et al., 2005; Kneller et al., 2005), but they may also limit triggering ectopy particularly early in disease development (Watanabe et al., 2009; Liu et al., 2011). Lastly, non-cardiac contraindications and drug interactions are a significant consideration, particularly for anticoagulant therapy, a core prophylactic for AF-induced thrombosis.

Given these core characteristics of drugs with established efficacy, major current AF strategies can be classified into two broad groups: (1) those that focus on extending the atrial ERP through atria-specific K^+ channel targeting, (2) combined therapies that leverage multi-target outcomes and minimize contraindications. In the case of ERP modulators, the key challenge is to improve atrial selectivity and reduce non-cardiac contraindications. For this reason channels that contribute to atrial repolarization but have little role in the ventricle (e.g., I_{Kur} , $\text{I}_{\text{K,Ca}}$, $\text{I}_{\text{K,Ach}}$) are the most attractive targets. Approaches targeting Ca^{2+} -handling are largely mechanism-driven, and address disturbances to calcium homeostasis, particularly via RyR hyperactivity and calcium overload secondary to dysregulated Na^+ homeostasis and CaMKII signaling (Heijman et al., 2015). Finally, recently developed multi-target therapies particularly seek to combine the efficacy of Na^+ channel blockade with repolarization modulators to generate ideal compound profiles (Ni et al., 2017).

Computational approaches are being applied to all of these avenues. Below, we briefly review major computational methods applied to rational drug design, and then highlight approaches where simulations may be crucial in integrating information taken from high-throughput screening, and traditional *in vitro* and *in vivo* electrophysiology.

Pharmacological Modeling Approaches

Modeling drug interactions can start at the molecular level with molecular docking or dynamic simulations to test small molecule binding sites and structural protein changes (see **Table 1** for structural modeling contributions for AF drugs). These approaches are attractive because they permit estimation of binding affinities (and kinetics in some cases) based on available 3D-structures. However, the availability of these structures has traditionally been quite limited for ion channel targets, largely due to difficulties in crystallizing transmembrane proteins. With recent advances in cryoelectron microscopy, structure-based drug discovery for integral membrane targets is quickly gaining traction (Lengauer and Rarey, 1996; Shoichet et al., 2002; Meng et al., 2011; Yarov-Yarovoy et al., 2014), and is thought to

TABLE 1 | Summary of AF drugs, ionic targets, and related computational work.

Drug	Class	Target	Computational work
Flecainide	IC	I_{Na} (Roden and Woosley, 1986) I_{to} , I_{Kur} , I_{Kr} (Tamargo et al., 2004)	<u>Functional:</u> - Flecainide and lidocaine state specific binding models incorporating detailed voltage- and pH-dependence (Moreno et al., 2011) <u>Structural:</u> Gómez et al. (2014) and Melgari et al. (2015)
Propafenone	IC	I_{Na} , I_{to} , I_{K1} , I_K (Duan et al., 1993) I_{to} , I_{Kur} , I_{Kr} , I_{Ks} (Tamargo et al., 2004) $I_{K,2P}$ (Schmidt et al., 2013)	<u>Functional:</u> - State-specificity and kinetics of binding via genetic algorithm search (Pásek and Simurda, 2004) <u>Structural:</u> Gómez et al. (2014) and Ngo et al. (2016)
Amiodarone	III	I_{Kr} , I_{Ks} , I_{to} , I_{Kur} (Tamargo et al., 2004) I_{Na} , I_{Ca} (Nattel et al., 1992) $I_{K,2P}$ (Gerten et al., 2010)	<u>Functional:</u> - Multi-target modeling of drug action in AF via Hill-type conductance-only block (Loewe et al., 2014) - Pharmacodynamic modeling of drug–drug interactions (Chen et al., 2015) - Effect of pharmacologically altered I_{Na} kinetics on post-repolarization refractoriness and APD prolongation (Franz et al., 2014) - Mechanistic understanding of amiodarone effects in 1D and 3D, focus on QT prolongation (Wilhelms et al., 2012) - Amiodarone targeting I_{NaL} in failing human myocardium simulations (Maltsev et al., 2001) <u>Structural:</u> Zhang et al. (2016)
Dronedarone	III	I_{Kr} , I_{Ks} , I_{K1} , I_{Na} , I_{CaL} (Gautier et al., 2003) I_{Kr} , I_{Ks} (Tamargo et al., 2004)	<u>Functional:</u> - Frequency and concentration dependent effects in cAF remodeled hearts (Loewe et al., 2014) - Drug–drug interaction dronedarone (Denisov et al., 2018)
Ibutilide	III	I_{Kr} (Tamargo et al., 2004)	<u>Functional:</u> - Clinical intervention with ibutilide linked with simulated phase synchrony between tissue regions (Vidmar et al., 2015)
Vernakalant	III	I_{to} , I_{Kr} , I_{Kur} , $I_{K,ACh}$, I_{Na} (Fedida, 2007) $I_{K,2P}$ (Seyler et al., 2014)	<u>Functional:</u> - Multi-target, cellular mode of action (Loewe et al., 2015) - AF termination simulated by I_{Na} block with rapid dissociation through decreased wavebreak and blocked rotor generation (Comtois et al., 2008) <u>Structural:</u> Eldstrom and Fedida (2009)
Dofetilide	III	I_{Kr} (Tamargo et al., 2004)	<u>Functional:</u> - Multiscale cardiac toxicity (TdP risk) predictor (Costabal et al., 2018) - Contribution of fibroblasts to cardiac safety pharmacology (Gao et al., 2017) - Interaction of hERG channel kinetics and putative inhibition schemes in long QT syndrome (Romero et al., 2014) - New hERG Markov model including drug-binding dynamics for early drug safety assessment (Di Veroli et al., 2012) - Gender and age on dofetilide induced QT prolongation (Gonzalez et al., 2010) <u>Structural:</u> Dux-Santoy et al. (2011), Saiz et al. (2011) and Varkevisser et al. (2013)
Sotalol	III	I_{Kr} (Kpaeyeh and Wharton, 2016) I_K (Carmeliet, 1985)	<u>Functional:</u> - Prediction of drug effects at therapeutic doses in controlled clinical trials and real-life conditions (Chain et al., 2013) - Identifying total area of the ECG T-wave as a biomarker for drug toxicity (Jie et al., 2010) <u>Structural:</u> DeMarco et al. (2018)
Ranolazine	I, anti- anginal drug	I_{NaL} , late I_{Ca} , peak I_{Ca} , I_{NCX} , I_{Kr} , I_{Ks} (Antzelevitch et al., 2004)	<u>Functional:</u> - Antiarrhythmic drug effect specifically in inherited long-QT syndrome and heart failure-induced remodeling (Moreno et al., 2013) - Prevention of late phase-3 EADs (Morotti et al., 2016) - Combined antiarrhythmic and torsadogenic effect of I_{NaL} and I_{Kr} block on hV-CMs (Trenor et al., 2013) <u>Structural:</u> Du et al. (2014)
Cardiac glycosides (digitalis compounds)	V	NKA (Vivo et al., 2008; Schmidt et al., 2018) Vagal stimulation (Falk, 1991)	<u>Functional:</u> - Effect NKA on cell and tissue refractoriness and rotor dynamics (Sánchez et al., 2012) - Physiologically based PK model (Neuhoff et al., 2013) - Two compartment PK-PD model for clinical dosage effect (Jelliffe et al., 2014) <u>Structural:</u> Weiss (2007)

hold great promise as a support for drug development in the future.

Besides modeling molecular binding sites, one may focus on functionally driven drug-ion channel interactions, based on the classical Hodgkin and Huxley (HH) formalism or more recent Markov modeling formulations. For both HH and Markov formulations, the foundation for modeling the effects of antagonists on observable myocyte electrophysiology has been driven by two major frameworks for conceptualizing drug-binding: (1) the “modulated receptor” hypothesis (Hille, 1977), and (2) the “slow inactivation” hypothesis (Khodorov, 1979). The modulated receptor hypothesis states that drug-binding exhibits selectivity for the functional states of the channel, and that this selectivity can be readily expressed by different association and dissociation kinetics (and resulting affinities) for drug binding to each state (Hondegem and Katzung, 1977; Hondegem, 1987). Conversely, the synergistic-inactivation hypothesis is essentially an allosteric mechanism, which suggests that a drug does not need to exhibit selective binding for specific functional states, but instead, once the drug is bound it promotes transition to states in which channels are non-conducting. This mode of block has become somewhat popular for calcium channels (Hering, 2002). Broadly speaking, the modulated receptor hypothesis has been more often applied across various drug–channel interactions, and modified to include the popular “guarded receptor” derivatives. Structure-based modeling will surely refine the application of these approaches in coming years.

Because the states are defined by function, these approaches are largely independent of protein structure, but through the binding kinetics can incorporate both time- and voltage-dependent characteristics of drug interaction. Of course, such approaches require well-defined functional models representing the baseline function of the channel target, as well as any disease-related alterations to channel conductance and gating. Markov models of ion channels have the advantage of being able to more accurately represent inter-dependence of state transitions which can considerably impact the outcome of drug binding simulations. However, more complex Markov formulations are often subject to insufficient data or contradictory parameterization requirements when trying to fit multiple experimental data sets.

Drug modeling with intended clinical application need to take pharmacokinetic (PK), additionally to pharmacodynamic (PD), modeling into account. The focus of this review is on PD modeling, the mechanism and effect of drugs, but the spread of drugs and off-target effects should be acknowledged. For recent reviews on (multiscale) PK/PD modeling in systems pharmacology and drug-induced cardiovascular effects (Collins et al., 2015; Clancy et al., 2016; Danhof, 2016). A good example of the importance is the conversion of drug from amiodarone to its derivative dronedarone. Both drugs share the main structure (removed iodine and added methanesulfonyl group) and electropharmacologic profile, with different relative effects on individual ion channels (Pamukcu and Lip, 2011; Rosa et al., 2014). Amiodarone accumulates in tissue due to a longer half-life and iodine is known to negatively affect thyroid function (Cohen-Lehman et al., 2010). The development of amiodarone

TABLE 2 | Summary of ion currents included in the hA-CM models.

Model (reference)	$I_{K,ACh}$	I_{bCl}	$I_{Cl,Ca}$	I_f	$I_{K,2P}$	$I_{K,Ca}$	cAF variant
Courtemanche et al., 1998							
Colman et al., 2013							X
Colman et al., 2016							
Nygren et al., 1998							
Maleckar et al., 2009b					X		
Koivumäki et al., 2011						X	
Koivumäki et al., 2014b						X	X
Skibbsbye et al., 2016	X					X	X
Grandi et al., 2011	X	X	X				X
Voigt et al., 2013a	X	X	X				X
Schmidt et al., 2015	X	X	X			X	X
Voigt et al., 2013b	X	X	X				X

Ion currents that are common to all models include: I_{Na} , I_{CaL} , I_{to} , I_{Kur} , I_{Kr} , I_{KS} , I_{NKA} , I_{NCX} , I_{PMCA} , I_{bNa} , and I_{bCa} . Those models that have a comprehensive cAF variant are marked in the right most column.

to dronedarone was motivated by PK and off-target PD effects, to optimize drug efficacy and limit clinical side effects. PK/PD modeling should be taken into account for drug development, but should be preceded by establishing the effect of targeting (a combination of) ion channels as possible drug targets.

Modeling Specific Ion Channels as Drug Targets

As mentioned above, various potassium channels are remodeled during AF and several of them are almost only expressed in the atria (I_{Kur} , $I_{K,ACh}$, $I_{K,2P}$, and $I_{K,Ca}$) (Ravens and Christ, 2010; Hancox et al., 2016). Pharmacological inhibition of these channels prolongs the AP and therefore extends the atrial ERP. **Table 2** summarizes which ion currents are included in published the hA-CM models. The majority of clinically relevant drugs, targets or affects I_{Na} and/or I_{NaL} as antiarrhythmic strategy. Below, we focus on computational approaches to the pharmacological modeling of sodium channels and the range of potassium channels that are still considered viable targets for AF rhythm control.

I_{Na}

The dynamics and pharmacologic properties of the cardiac sodium current are among the best-characterized of any electrophysiologic drug target. I_{Na} inhibitors, first quinidine and then the local anesthetics, were observed to have antiarrhythmic efficacy in the first half of the 20th century, and were adopted for treatment well before their molecular actions were known (Nattel, 1993; Rosen and Janse, 2010). Once modern voltage and patch clamp techniques were developed, pharmacologic properties such as state-specificity and association–dissociation kinetics were extensively characterized for a number of compounds (Bean et al., 1983; Rosen and Janse, 2010). The ability of class I compounds (particularly Ic) to suppress premature ventricular complexes spurred the beginning of major clinical trials (CAST 1 and 2, IMPACT) to assess their overall efficacy. The overwhelming failure of these

trials (treatment-induced mortality), has driven scientists and clinicians to reconsider both the key pharmacologic characteristics of major antiarrhythmics (particularly I_{Na} antagonists), and the antiarrhythmic classification systems used to guide clinical development (Rosen and Janse, 2010). Computational approaches have been key for understanding several major dynamical characteristics that determine the positive and negative outcomes of I_{Na} -targeted drugs in different contexts of arrhythmia.

The modulated receptor and guarded receptor approaches have been essential in understanding the myocyte-level outcomes of I_{Na} antagonists. Early efforts in particular, made useful contributions to distinguish the characteristics of the different subclasses of Na^+ channel blockers by applying this approach to very simple baseline models of channel gating (Cohen et al., 1981; Bean et al., 1983). The findings of these efforts still define the major characteristics of these subclass distinctions. For example, the role that slow class Ic dissociation kinetics play in determining the utility of this subclass for extending atrial ERP and antagonizing AF is thought to result from the brevity of the atrial AP (Starmer et al., 2003). That brevity in turn prevents fast-dissociating inactive-state antagonists (e.g., class 1b agents) from being effective in AF. This general mechanism of class Ic efficacy is likely to be particularly potent in terminating spiral wave dynamics by expanding both the core and the curvature of the wavefront, thus increasing the size of primary circuits and organizing the fibrillatory pattern (Kneller et al., 2005).

I_{Kr}

I_{Kr} is expressed in both human atria and ventricles, and its inhibition prolongs APD in both regions. While I_{Kr} block remains a viable strategy for AF targeting, it presents many challenges of ventricular contraindication. Dofetilide is an example of a drug that specifically blocks I_{Kr} , and was approved for AF treatment (Elming et al., 2003), but for which safety remains a significant concern (Mounsey and DiMarco, 2000; Abraham et al., 2015; Cho et al., 2017). For this reason, computational approaches are an attractive means for screening compounds with atrial-selective of targeting of I_{Kr} , but so far this goal has not been addressed convincingly. Below, we highlight several aspects that should be considered when applying computational approaches to address the role of I_{Kr} antagonists in AF.

The manner in which I_{Kr} targeting compounds promote ventricular AP and QT interval prolongation is a topic of major interest in toxicology screening, and we will not cover it comprehensively here. However, it is worthwhile noting that a classical parameter for characterizing the ventricular arrhythmogenicity of I_{Kr} -targeting compounds, reverse-rate-dependence, is also important in atrial drug design. Strong frequency-dependence is highly desirable for AF cardioversion due to very high frequencies of tissue activation during AF. As such, modeling approaches that do not permit accurate assessment of this characteristic are of limited value. To this end, the commonly used Courtemanche model does not reproduce the reverse-frequency-dependency of I_{Kr} block on atrial APD (Tsujimae et al., 2007). By adding a slow activation parameter to

the Hodgkin-Huxley model formulation and inhibiting varying combinations of fast and slow gating variables, Tsujimae et al. (2007) reproduced the inhibition dynamics and the frequency dependence of known I_{Kr} blockers (quinidine, vesnarinone, and dofetilide). More recent models have attempted to define I_{Kr} pharmacology in a more detailed manner. For example, Li et al. (2016) first developed a detailed Markov model of I_{Kr} gating, and then embedded it in the O'Hara-Rudy hV-CM model to provide a basis for characterizing compounds with known and varying TdP risk (Li et al., 2017). As a result they found that a mechanism of trapping in the hERG pore (carrier of the I_{Kr} current) represented by an additional Markov state in the pharmacological model, created a better predictability of TdP risk by I_{Kr} inhibitors. Applying models of this detail in atrial and ventricular CM models may provide a basis for better establishing the potential of I_{Kr} blockade for targeting AF. We are not aware that such an approach, especially with the focus on atrial I_{Kr} in AF, has been pursued to date.

I_{Kur}

Due to atria-specific expression, pharmacological inhibition of I_{Kur} allows for atrial selective APD prolongation with minimal adverse effects in the ventricles (Nattel and Carlsson, 2006). Experimental investigation of I_{Kur} and pharmacological properties is complicated by the lack of drug selectivity and overlap of I_{Kur} block with other currents, such as I_{to} (Ravens and Wettwer, 2011). Furthermore, first clinical trials have controversially shown no decrease in AF burden in patients upon treatment with an I_{Kur} blocker (Shunmugam et al., 2018).

Experimental complications can be overcome by using *in silico* models to assess I_{Kur} involvement in AF and AF treatment. Tsujimae et al. (2008) extended the Courtemanche et al. (1998) I_{Kur} formulation with voltage- and time-dependent pharmacological scaling factor to computationally investigate the voltage- and time-dependent block of I_{Kur} to mimic experimental drug inhibition and effects on AP characteristics. In simulations incorporating AF remodeling, they showed overall APD prolongation for a blocker with fast association kinetics and frequency-dependent APD prolongation when association kinetics were slow, particularly when dissociation was also slow. The same I_{Kur} formulation was used to show that rotor termination in chronic AF depends on binding kinetics of I_{Kur} inhibitors (Scholz et al., 2013).

Computational approaches have also been used to define the kinetic properties of the ideal I_{Kur} antagonist: maximum effect in disease, minimum effect in healthy cells and no (non-cardiac) adverse effects. Ellinwood et al. (2017b) used a six-state Markov model of I_{Kur} fitted with voltage clamp data from hA-CMs and expanded the model with drug-bound states. Incorporating the detailed channel model and drug interactions in the Grandi hA-CM model enabled *in silico* assessment of necessary drug characteristics, showing that drug binding to both open and inactive states yields the largest prolongation of APD and ERP. This inhibition was most efficient at

intermediate rates of association, and exhibited similar positive-frequency-dependence independent of binding mode (Ellinwood et al., 2017a,b). These simulations have largely supported the perspective that I_{Kur} is an attractive AF target, and future simulations are likely to be useful for assessing whether the specific binding characteristics and multi-target effects of specific I_{Kur} blockers are capable of realizing this potential.

$I_{K,ACh}$

$I_{K,ACh}$ is selectively present in the atria and thus may hold potential as an AF treatment target (Ehrlich et al., 2008). Its response to acetylcholine is decreased in cAF (Dobrev et al., 2001), exhibiting constitutive activity (Ehrlich et al., 2004; Dobrev et al., 2005). Single channel patch clamp experiments of $I_{K,ACh}$ expressed in canine atrial CMs suggest an increase in opening frequency and open probability after tachycardia-induced remodeling, while open-duration, channel conductance, and membrane density were unchanged (Voigt et al., 2007). Bingen et al. (2013) showed that $I_{K,ACh}$ blockade decreased restitution-driven alternans, reduced AF inducibility, and promoted AF termination in rat atrial CM cultures and intact atria. These findings agree with tertiapin block of $I_{K,ACh}$ prolonging ERP and terminating AF in a canine model (Hashimoto et al., 2006).

The importance and involvement of $I_{K,ACh}$ in human atrial electrophysiology and fibrillation is well established, but computational models of this channel are still limited. The models of $I_{K,ACh}$ in human atria are based on various data sources, but show a similar and prototypical involvement in the atrial AP: activation of $I_{K,ACh}$ results in hyperpolarization and pronounced AP abbreviation. Maleckar et al. (2009b) implemented a model of $I_{K,ACh}$ based on patch clamp experiments in canine atria, comprising of current-voltage relationship in combination with a scaling factor depending on half-activation and acetylcholine concentration (Kneller et al., 2002) and extended it with dose dependency. The first model incorporating $I_{K,ACh}$ based on human data was the Grandi model (Grandi et al., 2011), yielding the expected dose-dependent reduction in APD and CaT amplitude with increasing concentration of acetylcholine.

Pharmacological block of $I_{K,ACh}$ in *in vitro* and *ex vivo* experiments showed promising antiarrhythmic effects. However, recent studies have found $I_{K,ACh}$ block to be ineffective both in increasing the left-atrial ERP *in vivo* (Walfridsson et al., 2015) and reducing AF burden in clinical trials (Podd et al., 2016). Pharmacological effects and pathways activated by acetylcholine that are currently not implemented in the existing computational models (e.g., crosstalk with CaMKII and β -adrenergic stimulation) might explain the disagreement between *in vitro*, *in silico*, and clinical studies. *In silico* investigation may help to resolve these discrepancies, and confirm whether this ion channel holds potential as an AF target. Future computational work should address these possibilities, and better describe the effects of regional heterogeneity in $I_{K,ACh}$ expression and acetylcholine release in the atria (Kneller et al., 2002; Jones et al., 2012), as the role of these ion channels in spatial aspects of parasympathetically driven AF remains poorly understood.

$I_{K,2P}$

The background potassium current mediated by the TWIK protein-related acid-sensitive K^+ channel (TASK)-1, a two-pore domain K^+ channel (K2P), $I_{K,2P}$, has been shown to contribute to APD in hA-CMs (Limberg et al., 2011). TASK-1 encoded by KCNK3 has also been genetically associated with familial AF and early-onset lone AF (Liang et al., 2014). Furthermore, TASK-1 channels are expressed predominantly in the atria (Ellinghaus et al., 2005; Gaborit et al., 2007; Limberg et al., 2011; Schmidt et al., 2015), thus they are a potential atria-specific antiarrhythmic target in AF. However, there is some discrepancy in the direction of association between TASK-1 channels and AF. Some studies reported increased channel expression in cAF (Barth et al., 2005; Schmidt et al., 2015, 2017), while no change was found by others (Ellinghaus et al., 2005; Gaborit et al., 2005). Similarly, functional measurements have shown both increased (Schmidt et al., 2015, 2017) and diminished (Harleton et al., 2015) $I_{K,2P}$ amplitudes in cAF.

The first computational models of $I_{K,2P}$, was published by Limberg et al. (2011). They developed a three-state Markov model of the TASK-1 channel with voltage-dependent transitions between the two closed states, and one open state. The channel model was further integrated to the Courtemanche et al. (1998) hA-CM model to simulate effects of $I_{K,2P}$ on AP, showing that current block led to increased APD (−13%). More recently, Schmidt et al. (2015) published a channel model with less mechanistic detail, using a Hodgkin–Huxley formulation with voltage-dependent activation/deactivation kinetics and steady-state activation. To simulate the effect of $I_{K,2P}$ on AP, the authors integrated their TASK-1 channel model to the Voigt et al. (2013a) hA-CM model.

Pharmacological block of $I_{K,2P}$ with A293 *in vitro* has been shown to increase APD₉₀ by +19% (Limberg et al., 2011), +17% (Schmidt et al., 2015) in sinus rhythm hA-CMs, whereas in cAF the reported have been much larger: +58% (Schmidt et al., 2015) and +74% (Schmidt et al., 2017). These findings match well with dynamic patch clamp results, showing +19% and −16% changes in APD₉₀ in sinus rhythm with $I_{K,2P}$ subtraction and doubling, respectively (Limberg et al., 2011). The (patho-)physiological significance of the above data has, however, not been yet corroborated *ex vivo* in AP measurements with human atrial trabeculae; isolated hA-CMs are known to have compromised repolarization reserve (Rajamani et al., 2006). Furthermore, TASK-1 channel is also inhibited by some of the commonly used AF drugs, such as amiodarone (Gerten et al., 2010) and vernakalant (Seyler et al., 2014). There is definitely a need for more comprehensive computational studies, investigating the role $I_{K,2P}$ at different stages of AF.

$I_{K,Ca}$

All subtypes of SK (small conductance Ca^{2+} -activated potassium channel; SK1-3), carrying $I_{K,Ca}$, have been found in the atria, with SK2 and SK3 exhibiting the most atria-specific expression in human cells (Xu et al., 2003; Tuteja et al., 2005; Skibsbye et al., 2014). SK3 encoded by KCNN3 has also been

genetically associated with AF (Ellinor et al., 2010; Olesen et al., 2011). The role of SK channels in AF progression appears especially interesting since recent *in vivo* animal studies have showed that their inhibition can reduce the duration of, or even protect against, pacing-induced AF (Diness et al., 2010, 2011, 2017; Skibbsby et al., 2011; Haugaard et al., 2015). However, some studies have also suggested a pro-arrhythmic effect of SK current inhibition (Hsueh et al., 2013). At the cellular level, SK inhibitors NS8593 and ICAGEN induce APD prolongation in hA-CMs (Skibbsby et al., 2014), supporting a role for SK channels in atrial repolarization and encouraging the development of SK-antagonists as an antiarrhythmic strategy. Indeed, the first clinical trial with an SK inhibitor for AF treatment has recently been announced (NTR7012, compound AP30663¹).

At the pharmacodynamic level, drug-dependent regulation of SK function has been established for several different drugs, but the mechanisms and binding sites are still being examined (Weatherall et al., 2010, 2011; Dilly et al., 2011). In canine atria, inhibition of the SK channels by UCL1684 or apamin prolonged APD (Rosa et al., 1998). Even though the SK channel is a promising target for AF treatment, most drugs targeting SK channels have been shown to have significant affinity for other ion channels (particularly I_{Kr}), and as such have often fallen victim to toxicological exclusion.

The most detailed computational modeling effort of SK channels to date has focused on incorporating dynamics from single channel patch clamp experiments in rat SK2 (Hirschberg et al., 1998). This study established two Markov gating binding schemes, each consisting of four closed and two open states, which differentiated two modes of channel gating associated with different mean open probabilities. These models recapitulate observed kinetic components of Ca^{2+} -dependent activation and the varied macroscopic open probabilities of single channels, and thus provide a mechanistic basis for interrogating state-dependent drug interaction with SK. However, a comprehensive understanding of SK channel gating is still lacking, particularly as it relates to heteromeric channels, signaling-dependent effects, and to explain the apparent modal gating observed by Hirschberg et al. (1998). Additionally, in the context of the intact atrial CM, subcellular localization and possible colocalization with calcium sources or regulatory proteins remains largely unknown, and is surely important for constructing realistic whole cell models incorporating SK function (Ren et al., 2006; Dolga et al., 2013; Zhang et al., 2018).

There is currently no cardiac-specific computational model that represents both the complex kinetics and pharmacology of SK channels, and their interaction with cardiac Ca^{2+} dynamics. A detailed computational model of the SK channel would enhance our ability to interrogate both the pharmacologic targeting of SK, and the fundamental physiology of SK currents in the atria and in AF. In combination with a hA-CM model with realistic definition of subcellular Ca^{2+} gradients in healthy and AF CMs, the antiarrhythmic

effect of SK channels can be probed and drug development optimized.

Multi-Target Drug Modeling

The strategies described in the previous section focused on specific potassium channels. While these approaches provide simplicity of interpretation, it is well known that virtually all drugs in clinical use have multiple targets in the therapeutic dose range. In some contexts, these effects are thought to be counterproductive, and in others they appear advantageous. AF is a disease that has been particularly well targeted by the so-called 'dirty drugs,' namely amiodarone, dronedarone, and most recently in Europe, vernakalant (**Table 1**). Various research fields take advantage of multi-target drug design to discover new treatment options or targets (Ma et al., 2010; Koutsoukas et al., 2011). In AF and other cardiac diseases, existing knowledge has been largely incorporated in computational models, and provides a strong basis for guiding these multi-target therapies.

In general, amiodarone, dronedarone, and vernakalant are thought to be effective in AF for their ability to prolong the atrial ERP through multiple modes of action (Ni et al., 2017), and also to a lesser extent through inhibiting triggered activity via I_{Na} inhibition. Using these drugs as a base, an effort is now being made both computationally and experimentally to define idealized compounds (or personalized multi-therapy approaches), where dual I_{Na} and I_K targeting may yield the best therapies. In the case of vernakalant, the primary potassium current target is I_{Kur} , while for amiodarone/dronedarone it is I_{Kr} (Heijman et al., 2016). To this end, recent efforts have established a useful line of computational work to describe what idealized versions of these multi-target schemes may be. First, a key requirement was to understand how to limit adverse effects of Na^+ channel block by optimizing state-dependent block, as shown by (Aguilar-Shardonofsky et al., 2012). Following this, the same group showed improved theoretical AF selectivity by combining Na^+ current inhibition with I_{Kr} or putative I_{Kur} inhibition (Aguilar et al., 2015). Combined I_{Na}/I_{Kr} block improved atrial selectivity over I_{Na} alone, but still exhibited ventricular outcomes (Aguilar et al., 2015). Both that study, and a subsequent investigation only concerning combined I_{Na}/I_{Kur} inhibition (Ni et al., 2017), established that selective I_{Kur} blockade could be combined with idealized I_{Na} block to provide more atria-selective antiarrhythmic properties than is achievable via dual I_{Na}/I_{Kr} targeting. Adding some complexity to the clinical interpretation of these approaches, Morotti et al. (2016) applied a detailed Markov model to assess the ability of ranolazine to prevent AF re-initiation by blocking I_{Na} reactivation. Like amiodarone, ranolazine is a known antagonist of both I_{Na} and I_{Kr} , and while only the I_{Na} interaction was modeled in that study, their results suggest that multiple types of I_{Na} antagonism should be considered for permitting atrial-selectivity.

Additional novel targets, including those described above, as well as calcium handling targets, such as RyR, are likely to offer additional potential through multi-target approaches, particularly once disease-stage specific aspects of AF pathophysiology are better understood. It is already known that the class Ic compounds flecainide and propafenone have

¹<http://www.trialregister.nl/trialreg/admin/rctview.asp?TC=7012>

RyR blocking activity, which is thought to contribute to their ventricular efficacy (Watanabe et al., 2009, 2011; Galimberti and Knollmann, 2011). *In silico* models will surely be necessary for integrating and further characterizing these multi-target outcomes, and thereby find the most suitable treatment option and guide drug development for various stages of AF.

MODELING VARIABILITY AND UNCERTAINTY AT THE CELL LEVEL

In silico drug-screening studies have typically been based on a mechanistic approach where the effect of drug binding is simulated by altering the conductance or the gating kinetics of the target ion channel, as detailed in the previous section. More recently, studies of the mechanistic effects of drug binding on CM electrophysiology have been combined with approaches that allow incorporating natural variability into CM models. This methodology is based on the previously proposed so-called ‘Population of Models’ (PoMs) approach for the study of arrhythmia mechanisms. Simulation studies incorporating the effect of drugs in populations of ventricular myocyte (Passini et al., 2017) and induced pluripotent stem cell-derived CM models (Gong and Sobie, 2018) have shown that incorporating variability into the modeling pipeline allows for a more robust analysis of model predictions of, for instance, the ionic modulators of proarrhythmic mechanisms, the proarrhythmic effects of disease-related remodeling, and drug binding in cardiotoxicity studies of antiarrhythmic drugs.

Sources of Variability

As discussed in the section “1D and 2D Models of Electrical Conduction in the Atria,” atrial tissue has natural regional heterogeneity both at the cell and tissue (structural) levels. Furthermore, experimental findings have revealed a wide variability in measured APs and ionic current densities that cannot be attributed to regional variations. This intrinsic variability has been demonstrated in numerous reports of experimental data on atrial electrophysiology, both in healthy and pathological conditions, and spanning from the single cell to organ levels. Variability in experimental data has been observed in electrophysiological measurements of both different individuals (inter-subject) and CMs of the same individual (intra-subject). This arises from several sources, in particular, varying expression levels and post-transcriptional changes of ion channels, leading to variable ionic current densities, and of calcium handling proteins in CMs. Additional variability arises from local differences in cellular morphology and shape, and even from circadian rhythms. For a more detailed overview of sources of variability and uncertainty in experimental measurements and models of cardiac electrophysiology (Johnstone et al., 2016; Muszkiewicz et al., 2016).

Population of Models Approach

Single cell models are typically constructed by fitting the model to average values of experimental measurements, with the aim of deriving a single representative model.

The available experimental data have permitted the development of increasingly detailed and refined mathematical hA-CM models. However, the fact that these models are matched to specific data sources, obtained under different experimental settings, often results in families of models that are overfitted to a single source of experimental data. As mentioned above, electrophysiological properties, such as APD, RMP, and repolarization reserve, may vary substantially between the different model lineages, which raises questions about their applicability in a general setting. The PoM approach thus allows to expand the applicability of single cell models by representing a diversity of phenotypes, and may uncover new emergent phenomena that are not observed in the traditionally single “averaged” model. Another application of PoMs is to perform sensitivity analysis on cell models to uncover the ‘global’ effect of model parameters on arrhythmogenic behavior, such as ectopic activity, and reentry. For further reading on PoMs and sensitivity analysis, we refer the reader to a review published in this same issue (Ni et al., 2018).

In order to capture the variability observed in experimental data, the PoM approach has been proposed for the study of cellular electrophysiological mechanisms. This approach, first introduced by Prinz et al. (2003) to model neurons, and later applied to cardiac cell models by Sobie (2009), generally refers to a set of models sharing the same ionic and molecular formulations, but with variable parameters to reflect observed variability in experimental measurements of the biomarkers. Allowing multiple parameters to vary within large ranges can easily lead to unphysiological models, and thus the PoMs typically need to be calibrated. The calibration step can be experimentally driven, by using experimental data to set the boundaries of maximum and minimum values of electrophysiological biomarkers, more typically AP characteristics. Alternatively, defined biomarker distributions can be used to select models from the population, when experimental data is not available. Different approaches to varying parameters and restraining physiological models in the population have been employed (Muszkiewicz et al., 2016), but most commonly these PoMs are built with the aim at reflecting particular conditions or a specific mechanism of interest.

Extending PoM to Incorporate Drug Effects and Remodeling

One major advantage of using PoMs is that it allows to study the effect of drugs on a wide range of cellular phenotypes and thus provides a better prediction tool of the effect of drugs on the ionic currents. This can be done both in control conditions, and incorporating drug binding effects. The PoM approach has become part of the routine when assessing drug risk with computational models. It has also been adopted by the CiPA initiative as part of the framework for assessing the risk of TdP development in ventricular CMs under antiarrhythmic drug treatment (Colatsky et al., 2016). The combination of PoM approach and drug binding offers a tool for systematically assessing pro-arrhythmic risk of drugs including inter- and intra-subject variability and tissue heterogeneities. Studies

have suggested that comprehensive CM models incorporating variability and uncertainty can provide more robust and reliable arrhythmia risk markers and metrics (Pathmanathan et al., 2015; Passini et al., 2017).

Population of model studies incorporating AF remodeling have also shown interesting differences in the ionic determinants of AP characteristics and rate adaptation in normal and AF remodeling conditions (Sánchez et al., 2014; Lee et al., 2016), supporting the role of ion channel remodeling, and RyR kinetics in the development arrhythmogenic alternans (Chang et al., 2014; Lee et al., 2016; Vagos M.R. et al., 2017). Additionally, PoMs offers a strategy for incorporating single myocyte electrophysiological variability into tissue models, representing “population of tissues,” and assessing the ionic determinants of arrhythmic activity. Liberos et al. (2016) used a population of 3D spherical tissues incorporating patient variability to uncover mechanisms of DF and RM during reentry. They DF and RM to be highly dependent on I_{Na} , and I_{K1} , while RM was inversely correlated to I_{CaL} conductance. In addition to demonstrating the use of PoMs in uncovering the underlying mechanisms of AF perpetuation, this study suggested a dependency of the efficacy of I_{CaL} blockers on I_{Na} and I_{K1} , and provided further evidence for the benefits of a combined drug target approach or multi-target agents in the treatment of AF. In another modeling study, Sánchez C. et al., 2017 used a calibrated PoMs of atrial myocytes to build whole atrial models representing six different AP phenotypes with long and short APD, and studied their effects on reentry dynamics. They found that differences in APD resulted in different activation patterns of fibrillatory activity, such as regularity of reentry, conduction block, and interatrial differences of rotor dynamics indices. Interestingly, partial block of I_{K1} , I_{Na} , and I_{NaK} promoted a slight increase in wave meandering, activation irregularity, and reentry disorganization, which were more pronounced in the phenotypes with shorter APD at early stages of repolarization. This study shed light on the mechanisms of fibrillatory dynamics in the presence of electrophysiological variability and ion channel blockade, suggesting that prolongation of the early phase of repolarization could be a potential antiarrhythmic strategy and corroborating experimental findings on the pro-arrhythmic effect of I_{K1} and I_{Na} block via rotor destabilization. In another study, the authors used PoMs to replicate experimentally measured effects of nNOS-induced shortening of AP by increasing the conductance of I_{Kur} , I_{to} , I_{K1} , and I_{CaL} , showing a more pronounced role of I_{Kur} and I_{K1} over the remainder ionic currents in the altered AP phenotype (Reilly et al., 2016).

Figure 8 illustrates the use of the PoM approach in the assessment of the effects of two commonly used drugs in AF rhythm control, dofetilide and flecainide, on repolarization instabilities (here considered as either failed repolarization or afterdepolarizations). The PoM was constructed by varying the density of the major ionic currents in a hA-CM model (Skibbsby et al., 2016) within $\pm 30\%$ following a Gaussian distribution, and the populations were calibrated against experimental data (Sánchez et al., 2014). This study indicated an increased incidence (or probability) of repolarization abnormalities in the

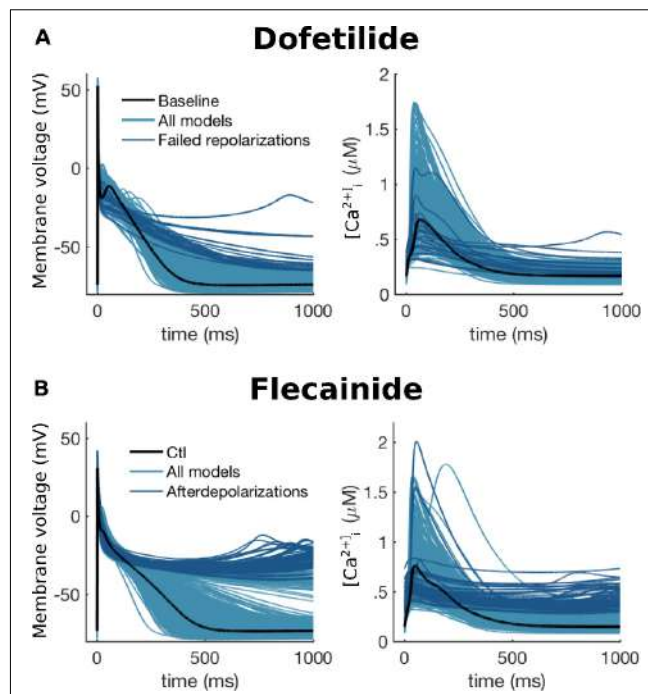


FIGURE 8 | Population of models approach to modeling drug binding effects of dofetilide and flecainide on repolarization abnormalities with an atrial myocyte model. APs (left) and calcium transient (right) traces of dofetilide (A) and flecainide (B) at 10-fold free plasma concentration are shown. Black lines represent the baseline (control) model, light blue traces represent all models in the populations, and dark blue lines show the models that presented repolarization abnormalities. Simulation results were published in preliminary form in abstract at the Vago M. et al. (2017).

populations with both drugs (dark blue to light blue traces ratio), with a 10-fold free plasma concentration, while the baseline (black traces) was mostly unaffected. This example showcases the advantage of using a PoM approach instead of a single averaged model in predicting drug binding outcomes.

Thus, PoMs provide a useful platform for the systematic study of arrhythmia mechanisms at both the single cell and tissue levels, and to obtain a more robust mechanistic insight into, and prediction of drug action on repolarization instabilities, triggered activity, and reentry.

CONCLUDING REMARKS AND FUTURE PERSPECTIVES

- Computational modeling of AF has progressed rapidly in the past two decades and has yielded a body of knowledge surrounding AF disease complexity that could not have been achieved with experimental approaches alone. Although current models are generally oversimplified and computational approaches are not yet truly multiscale with respect to pharmacology, aspects of current approaches, such as idealized drug modeling, are critically involved in the cycle of hypothesis generation and testing.

- As described in the section “Computational Pharmacology in AF,” much work still needs to be done in order to develop functionally detailed models of the ion channels thought to offer therapeutic potential in AF. These models, and the cell models in which they are tested, will rely upon new experimental data, not just of the drug–channel interaction but also key aspects of AF pathophysiology, particularly the time course of mechanistic changes during disease progression. New experimental data on the metabolic pathways, such as signaling cascades and phosphorylation of regulatory proteins, involved in remodeling processes and calcium homeostasis dysfunction could be a meaningful addition to hA-CM models. This is especially relevant to models of advanced stages of AF, where pathological phenotype is largely an interplay of several concurrent mechanisms.
- Methods that permit a more direct path from experimental characterization to model generation will improve efficiency and constrain uncertainty in the drug–target models. Structure-based approaches may eventually be very useful in this way. Integrated activities of experimentalists and computational scientists will also be essential to determine the most important knowledge for future modeling efforts, particularly as it relates to the stages of AF progression, and personalization. These efforts should be fostered, and cross the boundary between academic and commercial pharmacology.
- Personalized approaches will eventually be the ultimate goal of model-based treatment, although in the short-term, applications outside ablation therapy are still relatively distant. Using models as a foundation for developing general rules about the interaction of pharmacologic

REFERENCES

- Abraham, J. M., Saliba, W. I., Vekstein, C., Lawrence, D., Bhargava, M., Bassiouny, M., et al. (2015). Safety of oral dofetilide for rhythm control of atrial fibrillation and atrial flutter. *Circ. Arrhythm. Electrophysiol.* 8, 772–776. doi: 10.1161/CIRCEP.114.002339
- Aguilar, M., Xiong, F., Qi, X. Y., Comtois, P., and Nattel, S. (2015). Potassium channel blockade enhances atrial fibrillation-selective antiarrhythmic effects of optimized state-dependent sodium channel blockade. *Circulation* 132, 2203–2211. doi: 10.1161/CIRCULATIONAHA.115.018016
- Aguilar-Shardonofsky, M., Vigmond, E. J., Nattel, S., and Comtois, P. (2012). In silico optimization of atrial fibrillation-selective sodium channel blocker pharmacodynamics. *Biophys. J.* 102, 951–960. doi: 10.1016/j.bpj.2012.01.032
- Allessie, M., Ausma, J., and Schotten, U. (2002). Electrical, contractile and structural remodeling during atrial fibrillation. *Cardiovasc. Res.* 54, 230–246. doi: 10.1016/S0008-6363(02)00258-4
- Antzelevitch, C., Belardinelli, L., Zygmunt, A. C., Burashnikov, A., Di Diego, J. M., Fish, J. M., et al. (2004). Electrophysiological effects of ranolazine, a novel antianginal agent with antiarrhythmic properties. *Circulation* 110, 904–910. doi: 10.1161/01.CIR.0000139333.83620.5D
- Aslanidi, O. V., Boyett, M. R., Dobrzynski, H., Li, J., and Zhang, H. (2009a). Mechanisms of transition from normal to reentrant electrical activity in a model of rabbit atrial tissue: interaction of tissue heterogeneity and anisotropy. *Biophys. J.* 96, 798–817. doi: 10.1016/j.bpj.2008.09.057
- Aslanidi, O. V., Robinson, R., Cheverton, D., Boyett, M. R., and Zhang, H. (2009b). “Electrophysiological substrate for a dominant reentrant source during atrial fibrillation,” in *Proceedings of the 2009 Annual International Conference of the IEEE Engineering in Medicine and Biology Society*, Minneapolis, MN, 2819–2822. doi: 10.1109/EMBS.2009.5333573
- Aslanidi, O. V., Colman, M. A., Stott, J., Dobrzynski, H., Boyett, M. R., Holden, A. V., et al. (2011). 3D virtual human atria: a computational platform for studying clinical atrial fibrillation. *Prog. Biophys. Mol. Biol.* 107, 156–168. doi: 10.1016/j.pbiomolbio.2011.06.011
- Barth, A. S., Merk, S., Arnoldi, E., Zwermann, L., Kloos, P., Gebauer, M., et al. (2005). Reprogramming of the human atrial transcriptome in permanent atrial fibrillation expression of a ventricular-like genomic signature. *Circ. Res.* 96, 1022–1029. doi: 10.1161/01.RES.0000165480.82737.33
- Bean, B. P., Cohen, C. J., and Tsien, R. W. (1983). Lidocaine block of cardiac sodium channels. *J. Gen. Physiol.* 81, 613–642. doi: 10.1085/jgp.81.5.613
- Bingen, B. O., Neshati, Z., Askar, S. F. A., Kazbanov, I. V., Ypey, D. L., Panfilov, A. V., et al. (2013). Atrium-specific Kir3.x determines inducibility, dynamics, and termination of fibrillation by regulating restitution-driven alternans. *Circulation* 128, 2732–2744. doi: 10.1161/CIRCULATIONAHA.113.005019
- Blanc, O., Virag, N., Vesin, J. M., and Kappenberger, L. (2001). A computer model of human atria with reasonable computation load and realistic anatomical properties. *IEEE Trans. Biomed. Eng.* 48, 1229–1237. doi: 10.1109/10.959315
- Boyle, P. M., Zahid, S., and Trayanova, N. A. (2016). Towards personalized computational modelling of the fibrotic substrate for atrial arrhythmia. *Europace* 18, iv136–iv145. doi: 10.1093/europace/euw358
- Burashnikov, A., and Antzelevitch, C. (2003). Reinduction of atrial fibrillation immediately after termination of the arrhythmia is mediated by late

targeting with geometric characteristics and disease-stage will provide an important intermediate step to the clinic, and one that can be approached in the short to medium term.

AUTHOR CONTRIBUTIONS

All authors contributed to drafting the article and reviewing it critically for important intellectual content, as well as, approved the final version of the manuscript.

FUNDING

MV and IvH were supported by funding from the European Union’s Horizon 2020 MSCA ITN AFib-TrainNet, under grant agreement no. 675351. JS was funded by the SysAFib project (ERACoSysMed program, Call JTC-1, proposal number 82). HA was funded by the Novo Nordisk Foundation. AE was supported through the SURPh program, an initiative of the Norwegian Department of Research and Education. JK was supported by the Paavo Nurmi Foundation, the Finnish Foundation for Cardiovascular Research, and the Academy of Finland, Centre of Excellence in Body-on Chip Research (Grant No. 312412).

ACKNOWLEDGMENTS

The authors acknowledge the contribution of Bernardo Lino de Oliveira to the simulation results presented in **Figure 8**.

- phase 3 early afterdepolarization-induced triggered activity. *Circulation* 107, 2355–2360. doi: 10.1161/01.CIR.0000065578.00869.7C
- Burashnikov, A., and Antzelevitch, C. (2006). Late-phase 3 EAD: a unique mechanism contributing to initiation of atrial fibrillation. *Pacing Clin. Electrophysiol.* 29, 290–295. doi: 10.1111/j.1540-8159.2006.00336.x
- Butters, T. D., Aslanidi, O. V., Zhao, J., Smaill, B., and Zhang, H. (2013). A novel computational sheep atria model for the study of atrial fibrillation. *Interface Focus* 3, 20120067. doi: 10.1098/rsfs.2012.0067
- Camelliti, P., Devlin, G. P., Matthews, K. G., Kohl, P., and Green, C. R. (2004). Spatially and temporally distinct expression of fibroblast connexins after sheep ventricular infarction. *Cardiovasc. Res.* 62, 415–425. doi: 10.1016/j.cardiores.2004.01.027
- Carmeliet, E. (1985). Electrophysiologic and voltage clamp analysis of the effects of sotalol on isolated cardiac muscle and Purkinje fibers. *J. Pharmacol. Exp. Ther.* 232, 817–825.
- Chain, A. S. Y., Dieleman, J. P., Noord, C., van Hofman, A., Stricker, B. H. C., Danhof, M., et al. (2013). Not-in-trial simulation I: bridging cardiovascular risk from clinical trials to real-life conditions. *Br. J. Clin. Pharmacol.* 76, 964–972. doi: 10.1111/bcpt.12151
- Chang, K. C., Bayer, J. D., and Trayanova, N. A. (2014). Disrupted calcium release as a mechanism for atrial alternans associated with human atrial fibrillation. *PLoS Comput. Biol.* 10:e1004011. doi: 10.1371/journal.pcbi.1004011
- Chen, Y., Mao, J., and Hop, C. E. (2015). Physiologically based pharmacokinetic modeling to predict drug-drug interactions involving inhibitory metabolite: a case study of amiodarone. *Drug Metab. Dispos.* 43, 182–189. doi: 10.1124/dmd.114.059311
- Cho, J. H., Youn, S. J., Moore, J. C., Kyriakakis, R., Vekstein, C., Militello, M., et al. (2017). Safety of oral dofetilide reloading for treatment of atrial arrhythmias. *Circ. Arrhythm. Electrophysiol.* 10:e005333. doi: 10.1161/CIRCEP.117.005333
- Christ, T., Kovács, P. P., Acsai, K., Knaut, M., Eschenhagen, T., Jost, N., et al. (2016). Block of Na⁺/Ca²⁺ exchanger by SEA0400 in human right atrial preparations from patients in sinus rhythm and in atrial fibrillation. *Eur. J. Pharmacol.* 788, 286–293. doi: 10.1016/j.ejphar.2016.06.050
- Christ, T., Rozmaritsa, N., Engel, A., Berk, E., Knaut, M., Metzner, K., et al. (2014). Arrhythmias, elicited by catecholamines and serotonin, vanish in human chronic atrial fibrillation. *Proc. Natl. Acad. Sci. U.S.A.* 111, 11193–11198. doi: 10.1073/pnas.1324132111
- Clancy, C. E., An, G., Cannon, W. R., Liu, Y., May, E. E., Orteleva, P., et al. (2016). Multiscale modeling in the clinic: drug design and development. *Ann. Biomed. Eng.* 44, 2591–2610. doi: 10.1007/s10439-016-1563-0
- Cochet, H., Dubois, R., Yamashita, S., Al Jefairi, N., Berte, B., Sellal, J.-M., et al. (2018). Relationship between fibrosis detected on late gadolinium-enhanced cardiac magnetic resonance and re-entrant activity assessed with electrocardiographic imaging in human persistent atrial fibrillation. *JACC Clin. Electrophysiol.* 4, 17–29. doi: 10.1016/j.jacep.2017.07.019
- Cohen, C. J., Bean, B. P., Colatsky, T. J., and Tsien, R. W. (1981). Tetrodotoxin block of sodium channels in rabbit Purkinje fibers. Interactions between toxin binding and channel gating. *J. Gen. Physiol.* 78, 383–411. doi: 10.1085/jgp.78.4.383
- Cohen-Lehman, J., Dahl, P., Danzi, S., and Klein, I. (2010). Effects of amiodarone therapy on thyroid function. *Nat. Rev. Endocrinol.* 6, 34–41. doi: 10.1038/nrendo.2009.225
- Colatsky, T., Fermin, B., Gintant, G., Pierson, J. B., Sager, P., Sekino, Y., et al. (2016). The Comprehensive in Vitro Proarrhythmia Assay (CiPA) initiative – Update on progress. *J. Pharmacol. Toxicol. Methods* 81, 15–20. doi: 10.1016/j.vascn.2016.06.002
- Collins, T. A., Bergenholm, L., Abdulla, T., Yates, J. W. T., Evans, N., Chappell, M. J., et al. (2015). Modeling and simulation approaches for cardiovascular function and their role in safety assessment. *CPT Pharmacometrics Syst. Pharmacol.* 4, 175–188. doi: 10.1002/psp.418
- Colman, M. A., Aslanidi, O. V., Kharche, S., Boyett, M. R., Garratt, C. J., Hancock, J. C., et al. (2013). Pro-arrhythmogenic effects of atrial fibrillation induced electrical remodelling- insights from 3D virtual human atria. *J. Physiol.* 591, 4249–4272. doi: 10.1113/jphysiol.2013.254987
- Colman, M. A., Pinali, C., Trafford, A. W., Zhang, H., and Kitmitto, A. (2017). A computational model of spatio-temporal cardiac intracellular calcium handling with realistic structure and spatial flux distribution from sarcoplasmic reticulum and t-tubule reconstructions. *PLoS Comput. Biol.* 13:e1005714. doi: 10.1371/journal.pcbi.1005714
- Colman, M. A., Sarathy, P. P., MacQuaide, N., and Workman, A. J. (2016). “A new model of the human atrial myocyte with variable T-tubule organization for the study of atrial fibrillation,” in *Proceedings of the 2016 Computing in Cardiology Conference (CinC)*, Vancouver, 221–224. doi: 10.23919/CIC.2016.7868719
- Colman, M. A., Varela, M., Hancock, J. C., Zhang, H., and Aslanidi, O. V. (2014). Evolution and pharmacological modulation of the arrhythmogenic wave dynamics in canine pulmonary vein model. *Europace* 16, 416–423. doi: 10.1093/europace/eut349
- Comtois, P., Kneller, J., and Nattel, S. (2005). Of circles and spirals: bridging the gap between the leading circle and spiral wave concepts of cardiac reentry. *Europace* 7, S10–S20. doi: 10.1016/j.eupc.2005.05.011
- Comtois, P., Sakabe, M., Vigmond, E. J., Munoz, M., Texier, A., Shiroshita-Takeshita, A., et al. (2008). Mechanisms of atrial fibrillation termination by rapidly unbinding Na⁺ channel blockers: insights from mathematical models and experimental correlates. *Am. J. Physiol. Heart Circ. Physiol.* 295, H1489–H1504. doi: 10.1152/ajpheart.01054.2007
- Corradi, D., Callegari, S., Maestri, R., Ferrara, D., Mangieri, D., Alinovi, R., et al. (2012). Differential structural remodeling of the left-atrial posterior wall in patients affected by mitral regurgitation with or without persistent atrial fibrillation: a morphological and molecular study. *J. Cardiovasc. Electrophysiol.* 23, 271–279. doi: 10.1111/j.1540-8167.2011.02187.x
- Costabal, F. S., Yao, J., and Kuhl, E. (2018). Predicting the cardiac toxicity of drugs using a novel multiscale exposure–response simulator. *Comput. Methods Biomed. Eng.* 21, 232–246. doi: 10.1080/10255842.2018.1439479
- Courtemanche, M., Ramirez, R. J., and Nattel, S. (1998). Ionic mechanisms underlying human atrial action potential properties: insights from a mathematical model. *Am. J. Physiol. Heart Circ. Physiol.* 275, H301–H321. doi: 10.1152/ajpheart.1998.275.1.H301
- Daccarett, M., Badger, T. J., Akoum, N., Burgeon, N. S., Mahnkopf, C., Vergara, G., et al. (2011). Association of left atrial fibrosis detected by delayed-enhancement magnetic resonance imaging and the risk of stroke in patients with atrial fibrillation. *J. Am. Coll. Cardiol.* 57, 831–838. doi: 10.1016/j.jacc.2010.09.049
- Danhof, M. (2016). Systems pharmacology – towards the modeling of network interactions. *Eur. J. Pharm. Sci.* 94, 4–14. doi: 10.1016/j.ejps.2016.04.027
- DeMarco, K. R., Bekker, S., Clancy, C. E., Noskov, S. Y., and Vorobyov, I. (2018). Digging into lipid membrane permeation for cardiac ion channel blocker d-sotalol with all-atom simulations. *Front. Pharmacol.* 9:26. doi: 10.3389/fphar.2018.00026
- Deng, D., Murphy, M. J., Hakim, J. B., Franceschi, W. H., Zahid, S., Pashakhianloo, F., et al. (2017). Sensitivity of reentrant driver localization to electrophysiological parameter variability in image-based computational models of persistent atrial fibrillation sustained by a fibrotic substrate. *Chaos* 27:093932. doi: 10.1063/1.5003340
- Denisov, I. G., Baylon, J. L., Grinkova, Y. V., Tajkhorshid, E., and Sligar, S. G. (2018). Drug–drug interactions between atorvastatin and dronedarone mediated by monomeric CYP3A4. *Biochemistry* 57, 805–816. doi: 10.1021/acs.biochem.7b01012
- Di Veroli, G. Y., Davies, M. R., Zhang, H., Abi-Gerges, N., and Boyett, M. R. (2012). High-throughput screening of drug-binding dynamics to HERG improves early drug safety assessment. *Am. J. Physiol. Heart Circ. Physiol.* 304, H104–H117. doi: 10.1152/ajpheart.00511.2012
- Diaz, M. E., O’Neill, S. C., and Eisner, D. A. (2004). Sarcoplasmic reticulum calcium content fluctuation is the key to cardiac alternans. *Circ. Res.* 94, 650–656. doi: 10.1161/01.RES.0000119923.64774.72
- Dibb, K. M., Clarke, J. D., Eisner, D. A., Richards, M. A., and Trafford, A. W. (2013). A functional role for transverse (t-) tubules in the atria. *J. Mol. Cell. Cardiol.* 58, 84–91. doi: 10.1016/j.yjmcc.2012.11.001
- Diker, E., Özdemir, M., Aydoğdu, S., Tezcan, U. K., Korkmaz, S., Küük, E., et al. (1998). Dispersion of repolarization in paroxysmal atrial fibrillation. *Int. J. Cardiol.* 63, 281–286. doi: 10.1016/S0167-5273(97)00327-6
- Dilly, S., Lamy, C., Marion, N. V., Liégeois, J.-F., and Seutin, V. (2011). Ion-channel modulators: more diversity than previously thought. *Chembiochem* 12, 1808–1812. doi: 10.1002/cbic.201100236
- Diness, J. G., Skibbsby, L., Jespersen, T., Bartels, E. D., Sørensen, U. S., Hansen, R. S., et al. (2011). Effects on atrial fibrillation in aged hypertensive rats by Ca²⁺-activated K⁺ channel inhibition. *Hypertension* 57, 1129–1135. doi: 10.1161/HYPERTENSIONAHA.111.170613

- Diness, J. G., Skibsbye, L., Simó-Vicens, R., Santos, J. L., Lundsgaard, P., Citterni, C., et al. (2017). Termination of vernakalant-resistant atrial fibrillation by inhibition of small-conductance Ca^{2+} -activated K^+ channels in pigs. *Circ. Arrhythm. Electrophysiol.* 10:e005125. doi: 10.1161/CIRCEP.117.005125
- Diness, J. G., Sørensen, U. S., Nissen, J. D., Al-Shahib, B., Jespersen, T., Grunnet, M., et al. (2010). Inhibition of small-conductance Ca^{2+} -activated K^+ channels terminates and protects against atrial fibrillation. *Circ. Arrhythm. Electrophysiol.* 3, 380–390. doi: 10.1161/CIRCEP.110.957407
- Dobrev, D., Friedrich, A., Voigt, N., Jost, N., Wettwer, E., Christ, T., et al. (2005). The G protein-gated potassium current IK_{ACh} is constitutively active in patients with chronic atrial fibrillation. *Circulation* 112, 3697–3706. doi: 10.1161/CIRCULATIONAHA.105.575332
- Dobrev, D., Graf, E., Wettwer, E., Himmel, H. M., Hala, O., Doerfel, C., et al. (2001). Molecular basis of downregulation of G-protein-coupled inward rectifying K^+ current (IK_{ACh}) in chronic human atrial fibrillation: decrease in GIRK4 mRNA correlates with reduced IK_{ACh} and muscarinic receptor-mediated shortening of action potentials. *Circulation* 104, 2551–2557. doi: 10.1161/hc4601.099466
- Dolga, A. M., Netter, M. F., Perocchi, F., Doti, N., Meissner, L., Tobaben, S., et al. (2013). Mitochondrial small conductance SK2 channels prevent glutamate-induced oxytosis and mitochondrial dysfunction. *J. Biol. Chem.* 288, 10792–10804. doi: 10.1074/jbc.M113.453522
- Dössel, O., Krueger, M., Weber, F., Wilhelms, M., and Seemann, G. (2012). Computational modeling of the human atrial anatomy and electrophysiology. *Med. Biol. Eng. Comput.* 50, 773–799. doi: 10.1007/s11517-012-0924-6
- Du, C., Zhang, Y., El Harchi, A., Dempsey, C. E., and Hancox, J. C. (2014). Ranolazine inhibition of hERG potassium channels: drug-pore interactions and reduced potency against inactivation mutants. *J. Mol. Cell. Cardiol.* 74, 220–230. doi: 10.1016/j.yjmcc.2014.05.013
- Duan, D., Fermini, B., and Nattel, S. (1993). Potassium channel blocking properties of propafenone in rabbit atrial myocytes. *J. Pharmacol. Exp. Ther.* 264, 1113–1123.
- Dux-Santoy, L., Sebastian, R., Felix-Rodriguez, J., Ferrero, J. M., and Saiz, J. (2011). Interaction of specialized cardiac conduction system with antiarrhythmic drugs: a simulation study. *IEEE Trans. Biomed. Eng.* 58, 3475–3478. doi: 10.1109/TBME.2011.2165213
- Ehrlich, J. R., Biliczki, P., Hohnloser, S. H., and Nattel, S. (2008). Atrial-selective approaches for the treatment of atrial fibrillation. *J. Am. Coll. Cardiol.* 51, 787–792. doi: 10.1016/j.jacc.2007.08.067
- Ehrlich, J. R., Cha, T. J., Zhang, L., Chartier, D., Villeneuve, L., Hébert, T. E., et al. (2004). Characterization of a hyperpolarization-activated time-dependent potassium current in canine cardiomyocytes from pulmonary vein myocardial sleeves and left atrium. *J. Physiol.* 557, 583–597. doi: 10.1113/jphysiol.2004.061119
- Ehrlich, J. R., and Nattel, S. (2009). Novel approaches for pharmacological management of atrial fibrillation. *Drugs* 69, 757–774. doi: 10.2165/00003495-200969070-00001
- El-Armouche, A., Boknik, P., Eschenhagen, T., Carrier, L., Knaut, M., Ravens, U., et al. (2006). Molecular determinants of altered Ca^{2+} handling in human chronic atrial fibrillation. *Circulation* 114, 670–680. doi: 10.1161/CIRCULATIONAHA.106.636845
- Eldstrom, J., and Fedida, D. (2009). Modeling of high-affinity binding of the novel atrial anti-arrhythmic agent, vernakalant, to Kv1.5 channels. *J. Mol. Graph. Model.* 28, 226–235. doi: 10.1016/j.jmgm.2009.07.005
- Ellinghaus, P., Scheubel, R. J., Dobrev, D., Ravens, U., Holtz, J., Huetter, J., et al. (2005). Comparing the global mRNA expression profile of human atrial and ventricular myocardium with high-density oligonucleotide arrays. *J. Thorac. Cardiovasc. Surg.* 129, 1383–1390. doi: 10.1016/j.jtcvs.2004.08.031
- Ellinor, P. T., Lunetta, K. L., Glazer, N. L., Pfeifer, A., Alonso, A., Chung, M. K., et al. (2010). Common variants in KCNN3 are associated with lone atrial fibrillation. *Nat. Genet.* 42, 240–244. doi: 10.1038/ng.537
- Ellinwood, N., Dobrev, D., Morotti, S., and Grandi, E. (2017a). In silico assessment of efficacy and safety of IKur inhibitors in chronic atrial fibrillation: role of kinetics and state-dependence of drug binding. *Front. Pharmacol.* 8:799. doi: 10.3389/fphar.2017.00799
- Ellinwood, N., Dobrev, D., Morotti, S., and Grandi, E. (2017b). Revealing kinetics and state-dependent binding properties of IKur-targeting drugs that maximize atrial fibrillation selectivity. *Chaos* 27:093918. doi: 10.1063/1.5000226
- Elming, H., Brendorp, B., Pedersen, O. D., Køber, L., and Torp-Petersen, C. (2003). Dofetilide: a new drug to control cardiac arrhythmia. *Expert Opin. Pharmacother.* 4, 973–985. doi: 10.1517/14656566.4.6.973
- Falk, R. H. (1991). Digoxin for atrial fibrillation: a drug whose time has gone? *Ann. Intern. Med.* 114, 573–575. doi: 10.7326/0003-4819-114-7-573
- Fedida, D. (2007). Vernakalant (RSD1235): a novel, atrial-selective antifibrillatory agent. *Expert Opin. Investig. Drugs* 16, 519–532. doi: 10.1517/13543784.16.4.519
- Feld, G. K., Mollerup, M., Birgersdotter-Green, U., Fujimura, O., Bahnson, T. D., Boyce, K., et al. (1997). Conduction velocity in the tricuspid valve-inferior vena cava isthmus is slower in patients with type I atrial flutter compared to those without a history of atrial flutter. *J. Cardiovasc. Electrophysiol.* 8, 1338–1348. doi: 10.1111/j.1540-8167.1997.tb01030.x
- Franz, M. R., Gray, R. A., Karasik, P., Moore, H. J., and Singh, S. N. (2014). Drug-induced post-repolarization refractoriness as an antiarrhythmic principle and its underlying mechanism. *Europace* 16, iv39–iv45. doi: 10.1093/europace/euu274
- Frisk, M., Koivumäki, J. T., Norseng, P. A., Maleckar, M. M., Sejersted, O. M., and Louch, W. E. (2014). Variable t-tubule organization and Ca^{2+} homeostasis across the atria. *Am. J. Physiol. Heart Circ. Physiol.* 307, H609–H620. doi: 10.1152/ajpheart.00295.2014
- Gaborit, N., Le Bouter, S., Szuts, V., Varro, A., Escande, D., Nattel, S., et al. (2007). Regional and tissue specific transcript signatures of ion channel genes in the non-diseased human heart. *J. Physiol.* 582, 675–693. doi: 10.1113/jphysiol.2006.126714
- Gaborit, N., Steenman, M., Lamirault, G., Le Meur, N., Le Bouter, S., Lande, G., et al. (2005). Human atrial ion channel and transporter subunit gene-expression remodeling associated with valvular heart disease and atrial fibrillation. *Circulation* 112, 471–481. doi: 10.1161/CIRCULATIONAHA.104.506857
- Gaeta, S., and Christini, D. J. (2012). Non-linear dynamics of cardiac alternans: subcellular to tissue-level mechanisms of arrhythmia. *Front. Physiol.* 3:157. doi: 10.3389/fphys.2012.00157
- Gaeta, S. A., Bub, G., Abbott, G. W., and Christini, D. J. (2009). Dynamical mechanism for subcellular alternans in cardiac myocytes. *Circ. Res.* 105, 335–342. doi: 10.1161/CIRCRESAHA.109.197590
- Gaeta, S. A., Krogh-Madsen, T., and Christini, D. J. (2010). Feedback-control induced pattern formation in cardiac myocytes: a mathematical modeling study. *J. Theor. Biol.* 266, 408–418. doi: 10.1016/j.jtbi.2010.06.041
- Galimberti, E. S., and Knollmann, B. C. (2011). Efficacy and potency of class I antiarrhythmic drugs for suppression of Ca^{2+} waves in permeabilized myocytes lacking calsequestrin. *J. Mol. Cell. Cardiol.* 51, 760–768. doi: 10.1016/j.yjmcc.2011.07.002
- Gao, X., Engel, T., Carlson, B. E., and Wakatsuki, T. (2017). Computational modeling for cardiac safety pharmacology analysis: contribution of fibroblasts. *J. Pharmacol. Toxicol. Methods* 87, 68–73. doi: 10.1016/j.vascn.2017.04.011
- Gautier, P., Guillemaire, E., Marion, A., Bertrand, J.-P., Tourneur, Y., and Nisato, D. (2003). Electrophysiologic characterization of dronedarone in guinea pig ventricular cells. *J. Cardiovasc. Pharmacol.* 41, 191–202. doi: 10.1097/00002434-200302000-00007
- Gharaviri, A., Verheule, S., Eckstein, J., Potse, M., Kuklik, P., Kuijpers, N. H. L., et al. (2017). How disruption of endo-epicardial electrical connections enhances endo-epicardial conduction during atrial fibrillation. *Europace* 19, 308–318. doi: 10.1093/europace/euv445
- Giertzen, J., Ficker, E., Bloehs, R., Schweizer, P. A., Zitron, E., Scholz, E., et al. (2010). The human cardiac K2P3.1 (TASK-1) potassium leak channel is a molecular target for the class III antiarrhythmic drug amiodarone. *Naunyn Schmied. Arch. Pharmacol.* 381, 261–270. doi: 10.1007/s00210-009-0454-4
- Go, L. O., Moschella, M. C., Watras, J., Handa, K. K., Fyfe, B. S., and Marks, A. R. (1995). Differential regulation of two types of intracellular calcium release channels during end-stage heart failure. *J. Clin. Invest.* 95, 888–894. doi: 10.1172/JCI117739
- Gómez, R., Caballero, R., Barana, A., Amorós, I., De Palm, S.-H., Matamoros, M., et al. (2014). Structural basis of drugs that increase cardiac inward rectifier Kir2.1 currents. *Cardiovasc. Res.* 104, 337–346. doi: 10.1093/cvr/cvu203
- Gong, J. Q. X., and Sobie, E. A. (2018). Population-based mechanistic modeling allows for quantitative predictions of drug responses across cell types. *NPJ Syst. Biol. Appl.* 4:11. doi: 10.1038/s41540-018-0047-2

- Gonzalez, R., Gomis-Tena, J., Corrias, A., Ferrero, J. M., Rodriguez, B., and Saiz, J. (2010). "Sex and age related differences in drug induced QT prolongation by dofetilide under reduced repolarization reserve in simulated ventricular cells," in *Proceedings of the 2010 Annual International Conference of the IEEE Engineering in Medicine and Biology*, Buenos Aires, 3245–3248. doi: 10.1109/IEMBS.2010.5627415
- Grandi, E., Pandit, S. V., Voigt, N., Workman, A. J., Dobrev, D., Jalife, J., et al. (2011). Human atrial action potential and Ca^{2+} model: sinus rhythm and chronic atrial fibrillation. *Circ. Res.* 109, 1055–1066. doi: 10.1161/CIRCRESAHA.111.253955
- Grandi, E., Pasqualini, F. S., and Bers, D. M. (2010). A novel computational model of the human ventricular action potential and Ca transient. *J. Mol. Cell. Cardiol.* 48, 112–121. doi: 10.1016/j.yjmcc.2009.09.019
- Greiser, M., Kurfant, B.-G., Williams, G. S. B., Voigt, N., Harks, E., Dibb, K. M., et al. (2014). Tachycardia-induced silencing of subcellular Ca^{2+} signaling in atrial myocytes. *J. Clin. Invest.* 124, 4759–4772. doi: 10.1172/JCI70102
- Guillem, M. S., Climent, A. M., Rodrigo, M., Fernández-Avilés, F., Atienza, F., and Berenfeld, O. (2016). Presence and stability of rotors in atrial fibrillation: evidence and therapeutic implications. *Cardiovasc. Res.* 109, 480–492. doi: 10.1093/cvr/cvw011
- Haïssaguerre, M., Jaïs, P., Shah, D. C., Takahashi, A., Hocini, M., Quiniou, G., et al. (1998). Spontaneous initiation of atrial fibrillation by ectopic beats originating in the pulmonary veins. *N. Engl. J. Med.* 339, 659–666. doi: 10.1056/NEJM19980903391003
- Hancox, J. C., James, A. F., Marrion, N. V., Zhang, H., and Thomas, D. (2016). Novel ion channel targets in atrial fibrillation. *Expert Opin. Ther. Targets* 20, 947–958. doi: 10.1517/14728222.2016.1159300
- Hansen, B. J., Zhao, J., Csepe, T. A., Moore, B. T., Li, N., Jayne, L. A., et al. (2015). Atrial fibrillation driven by micro-anatomic intramural re-entry revealed by simultaneous sub-epicardial and sub-endocardial optical mapping in explanted human hearts. *Eur. Heart J.* 36, 2390–2401. doi: 10.1093/eurheartj/ehv233
- Harleton, E., Besana, A., Chandra, P., Danilo, P., Rosen, T. S., Rosen, M. R., et al. (2015). TASK-1 current is inhibited by phosphorylation during human and canine chronic atrial fibrillation. *Am. J. Physiol. Heart Circ. Physiol.* 308, H126–H134. doi: 10.1152/ajpheart.00614.2014
- Harrild, D., and Henriquez, C. (2000). A computer model of normal conduction in the human atria. *Circ. Res.* 87, E25–E36.
- Hashimoto, N., Yamashita, T., and Tsuruzoe, N. (2006). Tertiapin, a selective IKACH blocker, terminates atrial fibrillation with selective atrial effective refractory period prolongation. *Pharmacol. Res.* 54, 136–141. doi: 10.1016/j.phrs.2006.03.021
- Hatem, S. N., Benardeau, A., Rucker-Martin, C., Marty, I., de Chamisso, P., Villaz, M., et al. (1997). Different compartments of sarcoplasmic reticulum participate in the excitation-contraction coupling process in human atrial myocytes. *Circ. Res.* 80, 345–353. doi: 10.1161/01.RES.80.3.345
- Haugaard, M. M., Hesselkilde, E. Z., Pehrson, S., Carstensen, H., Flethøj, M., Præstegaard, K. F., et al. (2015). Pharmacologic inhibition of small-conductance calcium-activated potassium (SK) channels by NS8593 reveals atrial antiarrhythmic potential in horses. *Heart Rhythm* 12, 825–835. doi: 10.1016/j.hrthm.2014.12.028
- Heeringa, J., Kuip, D. A. M., van der Hofman, A., Kors, J. A., Herpen, G., van, et al. (2006). Prevalence, incidence and lifetime risk of atrial fibrillation: the Rotterdam study. *Eur. Heart J.* 27, 949–953. doi: 10.1093/eurheartj/ehi825
- Heijman, J., Algalarondo, V., Voigt, N., Melka, J., Wehrens, X. H. T., Dobrev, D., et al. (2015). The value of basic research insights into atrial fibrillation mechanisms as a guide to therapeutic innovation: a critical analysis. *Cardiovasc. Res.* 109, 467–479. doi: 10.1093/cvr/cvv275
- Heijman, J., Algalarondo, V., Voigt, N., Melka, J., Wehrens, X. H. T., Dobrev, D., et al. (2016). The value of basic research insights into atrial fibrillation mechanisms as a guide to therapeutic innovation: a critical analysis. *Cardiovasc. Res.* 109, 467–479. doi: 10.1093/cvr/cvv275
- Hering, S. (2002). β -Subunits: fine tuning of Ca^{2+} channel block. *Trends Pharmacol. Sci.* 23, 509–513. doi: 10.1016/S0165-6147(02)02104-1
- Hille, B. (1977). Local anesthetics: hydrophilic and hydrophobic pathways for the drug-receptor reaction. *J. Gen. Physiol.* 69, 497–515. doi: 10.1085/jgp.69.4.497
- Hiromoto, K., Shimizu, H., Furukawa, Y., Kanemori, T., Mine, T., Masuyama, T., et al. (2005). Discordant repolarization alternans-induced atrial fibrillation is suppressed by verapamil. *Circ. J.* 69, 1368–1373. doi: 10.1253/circj.69.1368
- Hirschberg, B., Maylie, J., Adelman, J. P., and Marrion, N. V. (1998). Gating of recombinant small-conductance Ca -activated K^+ channels by calcium. *J. Gen. Physiol.* 111, 565–581. doi: 10.1085/jgp.111.4.565
- Hondeghem, L. M. (1987). Antiarrhythmic agents: modulated receptor applications. *Circulation* 75, 514–520. doi: 10.1161/01.CIR.75.3.514
- Hondeghem, L. M., and Katzung, B. G. (1977). Time- and voltage-dependent interactions of antiarrhythmic drugs with cardiac sodium channels. *Biochim. Biophys. Acta* 472, 373–398. doi: 10.1016/0304-4157(77)90003-X
- Hove-Madsen, L., Llach, A., Bayes-Genis, A., Roura, S., Font, E. R., Aris, A., et al. (2004). Atrial fibrillation is associated with increased spontaneous calcium release from the sarcoplasmic reticulum in human atrial myocytes. *Circulation* 110, 1358–1363. doi: 10.1161/01.CIR.0000141296.59876.87
- Hsueh, C.-H., Chang, P.-C., Hsieh, Y.-C., Reher, T., Chen, P.-S., and Lin, S.-F. (2013). Proarrhythmic effect of blocking the small conductance calcium activated potassium channel in isolated canine left atrium. *Heart Rhythm* 10, 891–898. doi: 10.1016/j.hrthm.2013.01.033
- Hunnik, A., van Lau, D. H., Zeemering, S., Kuiper, M., Verheule, S., and Schotten, U. (2016). Antiarrhythmic effect of vernakalant in electrically remodeled goat atria is caused by slowing of conduction and prolongation of postrepolarization refractoriness. *Heart Rhythm* 13, 964–972. doi: 10.1016/j.hrthm.2015.12.009
- Iwasaki, Y., Nishida, K., Kato, T., and Nattel, S. (2011). Atrial fibrillation pathophysiology: implications for management. *Circulation* 124, 2264–2274. doi: 10.1161/CIRCULATIONAHA.111.019893
- Jacquemet, V., and Henriquez, C. S. (2008). Loading effect of fibroblast-myocyte coupling on resting potential, impulse propagation, and repolarization: insights from a microstructure model. *Am. J. Physiol. Heart Circ. Physiol.* 294, H2040–H2052. doi: 10.1152/ajpheart.01298.2007
- Jelliffe, R. W., Milman, M., Schumitzky, A., Bayard, D., and Van Guilder, M. (2014). A two-compartment population pharmacokinetic-pharmacodynamic model of digoxin in adults, with implications for dosage. *Ther. Drug Monit.* 36, 387–393. doi: 10.1097/FTD.0000000000000023
- Jie, X., Rodriguez, B., and Pueyo, E. (2010). "A new ECG biomarker for drug toxicity: a combined signal processing and computational modeling study," in *Proceedings of the 2010 Annual International Conference of the IEEE Engineering in Medicine and Biology*, Buenos Aires, 2565–2568. doi: 10.1109/IEMBS.2010.562864
- Johnstone, R. H., Chang, E. T. Y., Bardenet, R., de Boer, T. P., Gavaghan, D. J., Pathmanathan, P., et al. (2016). Uncertainty and variability in models of the cardiac action potential: can we build trustworthy models? *J. Mol. Cell. Cardiol.* 96, 49–62. doi: 10.1016/j.yjmcc.2015.11.018
- Jones, D. L., Tuomi, J. M., and Chidiac, P. (2012). Role of cholinergic innervation and RGS2 in atrial arrhythmia. *Front. Physiol.* 3:239. doi: 10.3389/fphys.2012.00239
- Kamkin, A., Kiseleva, I., Wagner, K. D., Lammerich, A., Bohm, J., Persson, P. B., et al. (1999). Mechanically induced potentials in fibroblasts from human right atrium. *Exp. Physiol.* 84, 347–356. doi: 10.1111/j.1469-445X.1999.01794.x
- Khodorov, B. (1979). Some aspects of the pharmacology of sodium channels in nerve membrane. Process of inactivation. *Biochem. Pharmacol.* 28, 1451–1459. doi: 10.1016/0006-2952(79)90457-X
- King, J. H., Huang, C. L.-H., and Fraser, J. A. (2013). Determinants of myocardial conduction velocity: implications for arrhythmogenesis. *Front. Physiol.* 4:154. doi: 10.3389/fphys.2013.00154
- Klos, M., Calvo, D., Yamazaki, M., Zlochiver, S., Mironov, S., Cabrera, J.-A., et al. (2008). Atrial septopulmonary bundle of the posterior left atrium provides a substrate for atrial fibrillation initiation in a model of vagally mediated pulmonary vein tachycardia of the structurally normal heart. *Circ. Arrhythm. Electrophysiol.* 1, 175–183. doi: 10.1161/CIRCEP.107.760447
- Kneller, J., Kalifa, J., Zou, R., Zaitsev, A. V., Warren, M., Berenfeld, O., et al. (2005). Mechanisms of atrial fibrillation termination by pure sodium channel blockade in an ionically-realistic mathematical model. *Circ. Res.* 96, e35–e47. doi: 10.1161/01.RES.0000160709.49633.2b
- Kneller, J., Zou, R., Vignmond, E. J., Wang, Z., Leon, L. J., and Nattel, S. (2002). Cholinergic atrial fibrillation in a computer model of a two-dimensional sheet of canine atrial cells with realistic ionic properties. *Circ. Res.* 90, E73–E87. doi: 10.1161/01.RES.0000019783.88094.BA

- Kohl, P., Camelliti, P., Burton, F. L., and Smith, G. L. (2005). Electrical coupling of fibroblasts and myocytes: relevance for cardiac propagation. *J. Electrocardiol.* 38, 45–50. doi: 10.1016/j.jelectrocard.2005.06.096
- Kohl, P., and Noble, D. (1996). Mechanosensitive connective tissue: potential influence on heart rhythm. *Cardiovasc. Res.* 32, 62–68. doi: 10.1016/S0008-6363(95)00224-3
- Koivumäki, J. T., Clark, R. B., Belke, D., Kondo, C., Fedak, P. W. M., Maleckar, M. M. C., et al. (2014a). Na⁺ current expression in human atrial myofibroblasts: identity and functional roles. *Front. Physiol.* 5:275. doi: 10.3389/fphys.2014.00275
- Koivumäki, J. T., Seemann, G., Maleckar, M. M., and Tavi, P. (2014b). In silico screening of the key cellular remodeling targets in chronic atrial fibrillation. *PLoS Comput. Biol.* 10:e1003620. doi: 10.1371/journal.pcbi.1003620
- Koivumäki, J. T., Korhonen, T., and Tavi, P. (2011). Impact of sarcoplasmic reticulum calcium release on calcium dynamics and action potential morphology in human atrial myocytes: a computational study. *PLoS Comput. Biol.* 7:e1001067. doi: 10.1371/journal.pcbi.1001067
- Koutsoukas, A., Simms, B., Kirchmair, J., Bond, P. J., Whitmore, A. V., Zimmer, S., et al. (2011). From in silico target prediction to multi-target drug design: current databases, methods and applications. *J. Proteom.* 74, 2554–2574. doi: 10.1016/j.jprot.2011.05.011
- Kpaeyeh, J. A. Jr., and Wharton, J. M. (2016). Sotalol. *Card. Electrophysiol. Clin.* 8, 437–452. doi: 10.1016/j.ccep.2016.02.007
- Krueger, M. W. (2013). *Personalized Multi-Scale Modeling of the Atria: Heterogeneities, Fiber Architecture, Hemodialysis and Ablation Therapy*. Ph. D. thesis, KIT Scientific Publishing, Karlsruhe. doi: 10.5445/KSP/1000031226
- Krueger, M. W., Dorn, A., Keller, D. U. J., Holmqvist, F., Carlson, J., Platонов, P. G., et al. (2013). In-silico modeling of atrial repolarization in normal and atrial fibrillation remodeled state. *Med. Biol. Eng. Comput.* 51, 1105–1119. doi: 10.1007/s11517-013-1090-1
- Krummen, D. E., Bayer, J. D., Ho, J., Ho, G., Smetak, M. R., Clopton, P., et al. (2012). Mechanisms of human atrial fibrillation initiation: clinical perspective clinical and computational studies of repolarization restitution and activation latency. *Circ. Arrhythm. Electrophysiol.* 5, 1149–1159. doi: 10.1161/CIRCEP.111.969022
- Lalani, G. G., Schricker, A., Gibson, M., Rostamian, A., Krummen, D. E., and Narayan, S. M. (2012). Atrial conduction slows immediately before the onset of human atrial fibrillation: a bi-atrial contact mapping study of transitions to atrial fibrillation. *J. Am. Coll. Cardiol.* 59, 595–606. doi: 10.1016/j.jacc.2011.10.879
- Lau, D. H., Linz, D., Schotten, U., Mahajan, R., Sanders, P., and Kalman, J. M. (2017). Pathophysiology of paroxysmal and persistent atrial fibrillation: rotors, foci and fibrosis. *Heart Lung Circ.* 26, 887–893. doi: 10.1016/j.hlc.2017.05.119
- Lee, Y.-S., Hwang, M., Song, J.-S., Li, C., Joung, B., Sobie, E. A., et al. (2016). The contribution of ionic currents to rate-dependent action potential duration and pattern of reentry in a mathematical model of human atrial fibrillation. *PLoS One* 11:e0150779. doi: 10.1371/journal.pone.0150779
- Lenaerts, I., Bito, V., Heinzel, F. R., Driesen, R. B., Holemans, P., D'hooge, J., et al. (2009). Ultrastructural and functional remodeling of the coupling between Ca²⁺ influx and sarcoplasmic reticulum Ca²⁺ release in right atrial myocytes from experimental persistent atrial fibrillation. *Circ. Res.* 105, 876–885. doi: 10.1161/CIRCRESAHA.109.206276
- Lengauer, T., and Rarey, M. (1996). Computational methods for biomolecular docking. *Curr. Opin. Struct. Biol.* 6, 402–406. doi: 10.1016/S0959-440X(96)80061-3
- Li, Q., O'Neill, S. C., Tao, T., Li, Y., Eisner, D., and Zhang, H. (2012). Mechanisms by which cytoplasmic calcium wave propagation and alternans are generated in cardiac atrial myocytes lacking t-tubules—insights from a simulation study. *Biophys. J.* 102, 1471–1482. doi: 10.1016/j.biophys.2012.03.007
- Li, X., Zima, A. V., Sheikh, F., Blatter, L. A., and Chen, J. (2005). Endothelin-1-induced arrhythmogenic Ca²⁺ signaling is abolished in atrial myocytes of inositol-1,4,5-trisphosphate(IP3)-receptor type 2-deficient mice. *Circ. Res.* 96, 1274–1281. doi: 10.1161/01.RES.0000172556.05576.4c
- Li, Z., Dutta, S., Sheng, J., Tran, P. N., Wu, W., Chang, K., et al. (2017). Improving the in silico assessment of proarrhythmia risk by combining hERG (Human Ether-à-go-go-Related Gene) channel-drug binding kinetics and multichannel pharmacology. *Circ. Arrhythm. Electrophysiol.* 10, e004628. doi: 10.1161/CIRCEP.116.004628
- Li, Z., Dutta, S., Sheng, J., Tran, P. N., Wu, W., and Colatsky, T. (2016). A temperature-dependent in silico model of the human ether-à-go-go-related (hERG) gene channel. *J. Pharmacol. Toxicol. Methods* 81, 233–239. doi: 10.1016/j.jpharmtox.2016.05.005
- Liang, B., Soka, M., Christensen, A. H., Olesen, M. S., Larsen, A. P., Knop, F. K., et al. (2014). Genetic variation in the two-pore domain potassium channel, TASK-1, may contribute to an atrial substrate for arrhythmogenesis. *J. Mol. Cell. Cardiol.* 67, 69–76. doi: 10.1016/j.yjmcc.2013.12.014
- Liberos, A., Bueno-Orovio, A., Rodrigo, M., Ravens, U., Hernandez-Romero, I., Fernandez-Aviles, F., et al. (2016). Balance between sodium and calcium currents underlying chronic atrial fibrillation termination: an in silico intersubject variability study. *Heart Rhythm* 13, 2358–2365. doi: 10.1016/j.hrthm.2016.08.028
- Limberg, S. H., Netter, M. F., Rolfs, C., Rinné, S., Schlichthörl, G., Zuzarte, M., et al. (2011). TASK-1 channels may modulate action potential duration of human atrial cardiomyocytes. *Cell. Physiol. Biochem.* 28, 613–624. doi: 10.1159/000335757
- Lipp, P., Laine, M., Tovey, S. C., Burrell, K. M., Berridge, M. J., Li, W., et al. (2000). Functional InsP₃ receptors that may modulate excitation–contraction coupling in the heart. *Curr. Biol.* 10, 939–942. doi: 10.1016/S0960-9822(00)00624-2
- Liu, N., Denegri, M., Ruan, Y., Avelino-Cruz, J. E., Perissi, A., Negri, S., et al. (2011). Short communication: flecainide exerts an antiarrhythmic effect in a mouse model of catecholaminergic polymorphic ventricular tachycardia by increasing the threshold for triggered activity novelty and significance. *Circ. Res.* 109, 291–295. doi: 10.1161/CIRCRESAHA.111.247338
- Loewe, A., Lutz, Y., Wilhelms, M., Sinnecker, D., Barthel, P., Scholz, E. P., et al. (2014). In-silico assessment of the dynamic effects of amiodarone and dronedarone on human atrial patho-electrophysiology. *Europace* 16, iv30–iv38. doi: 10.1093/europace/euu230
- Loewe, A., Xu, Y., Scholz, E. P., Dössel, O., and Seemann, G. (2015). Understanding the cellular mode of action of vernakalant using a computational model: answers and new questions. *Curr. Dir. Biomed. Eng.* 1, 418–422. doi: 10.1515/cdbme-2015-0101
- Luca, A., Jacquemet, V., Virag, N., and Vesin, J. M. (2015). “Influence of right and left atrial tissue heterogeneity on atrial fibrillation perpetuation,” in *Proceedings of the 2015 Computing in Cardiology Conference (CinC)*, Nice, 449–452. doi: 10.1109/CIC.2015.7408683
- Ma, X. H., Shi, Z., Tan, C., Jiang, Y., Go, M. L., Low, B. C., et al. (2010). In-silico approaches to multi-target drug discovery. *Pharm. Res.* 27, 739–749. doi: 10.1007/s11095-010-0065-2
- Macquaide, N., Tuan, H.-T. M., Hotta, J., Sempels, W., Lenaerts, I., Holemans, P., et al. (2015). Ryanodine receptor cluster fragmentation and redistribution in persistent atrial fibrillation enhance calcium release. *Cardiovasc. Res.* 108, 387–398. doi: 10.1093/cvr/cvv231
- Maleckar, M. M., Greenstein, J. L., Giles, W. R., and Trayanova, N. A. (2009a). Electrotonic coupling between human atrial myocytes and fibroblasts alters myocyte excitability and repolarization. *Biophys. J.* 97, 2179–2190. doi: 10.1016/j.biophys.2009.07.054
- Maleckar, M. M., Greenstein, J. L., Giles, W. R., and Trayanova, N. A. (2009b). K⁺ current changes account for the rate dependence of the action potential in the human atrial myocyte. *Am. J. Physiol. Heart Circ. Physiol.* 297, H1398–H1410. doi: 10.1152/ajpheart.00411.2009
- Maltsev, V. A., Sabbah, H. N., and Undrovinas, A. I. (2001). Late sodium current is a novel target for amiodarone: studies in failing human myocardium. *J. Mol. Cell. Cardiol.* 33, 923–932. doi: 10.1006/jmcc.2001.1355
- McDowell, K. S., Vadakkumpadan, F., Blake, R., Blauer, J., Plank, G., MacLeod, R. S., et al. (2013). Mechanistic inquiry into the role of tissue remodeling in fibrotic lesions in human atrial fibrillation. *Biophys. J.* 104, 2764–2773. doi: 10.1016/j.biophys.2013.05.025
- McDowell, K. S., Zahid, S., Vadakkumpadan, F., Blauer, J., MacLeod, R. S., and Trayanova, N. A. (2015). Virtual electrophysiological study of atrial fibrillation in fibrotic remodeling. *PLoS One* 10:e0117110. doi: 10.1371/journal.pone.0117110
- Melgari, D., Zhang, Y., Harchi, A. E., Dempsey, C. E., and Hancox, J. C. (2015). Molecular basis of hERG potassium channel blockade by the class Ic antiarrhythmic flecainide. *J. Mol. Cell. Cardiol.* 86, 42–53. doi: 10.1016/j.yjmcc.2015.06.021

- Meng, X.-Y., Zhang, H.-X., Mezei, M., and Cui, M. (2011). *Molecular Docking: A Powerful Approach for Structure-Based Drug Discovery. Current Computer-Aided Drug Design*. Available at: <http://www.eurekaselect.com/74117/article> [accessed May 7, 2018]
- Ming, Z., Nordin, C., and Aronson, R. S. (1994). Role of L-type calcium channel window current in generating current-induced early afterdepolarizations. *J. Cardiovasc. Electrophysiol.* 5, 323–334. doi: 10.1111/j.1540-8167.1994.tb01169.x
- Miragoli, M., Salvarani, N., and Rohr, S. (2007). Myofibroblasts induce ectopic activity in cardiac tissue. *Circ. Res.* 101, 755–758. doi: 10.1161/CIRCRESAHA.107.160549
- Moreno, J. D., Yang, P.-C., Bankston, J. R., Grandi, E., Bers, D. M., Kass, R. S., et al. (2013). Ranolazine for congenital and acquired late ina-linked arrhythmias. *Circ. Res.* 113, e50–e61. doi: 10.1161/CIRCRESAHA.113.301971
- Moreno, J. D., Zhu, Z. I., Yang, P.-C., Bankston, J. R., Jeng, M.-T., Kang, C., et al. (2011). A computational model to predict the effects of class I anti-arrhythmic drugs on ventricular rhythms. *Sci. Transl. Med.* 3:98ra83. doi: 10.1126/scitranslmed.3002588
- Morotti, S., Edwards, A. G., McCulloch, A. D., Bers, D. M., and Grandi, E. (2014). A novel computational model of mouse myocyte electrophysiology to assess the synergy between Na^+ loading and CaMKII. *J. Physiol.* 592, 1181–1197. doi: 10.1113/jphysiol.2013.266676
- Morotti, S., McCulloch, A. D., Bers, D. M., Edwards, A. G., and Grandi, E. (2016). Atrial-selective targeting of arrhythmogenic phase-3 early afterdepolarizations in human myocytes. *J. Mol. Cell. Cardiol.* 96, 63–71. doi: 10.1016/j.yjmcc.2015.07.030
- Mounsey, J. P., and DiMarco, J. P. (2000). Dofetilide. *Circulation* 102, 2665–2670. doi: 10.1161/01.CIR.102.21.2665
- Muszkiewicz, A., Britton, O. J., Gemmell, P., Passini, E., Sánchez, C., Zhou, X., et al. (2016). Variability in cardiac electrophysiology: using experimentally-calibrated populations of models to move beyond the single virtual physiological human paradigm. *Prog. Biophys. Mol. Biol.* 120, 115–127. doi: 10.1016/j.pbiomolbio.2015.12.002
- Narayan, S. M., Franz, M. R., Clopton, P., Pruvot, E. J., and Krummen, D. E. (2011). Repolarization alternans reveals vulnerability to human atrial fibrillation. *Circulation* 123, 2922–2930. doi: 10.1161/CIRCULATIONAHA.110.977827
- Nattel, S. (1993). Comparative mechanisms of action of antiarrhythmic drugs. *Am. J. Cardiol.* 72, F13–F17. doi: 10.1016/0002-9149(93)90959-G
- Nattel, S., Burstein, B., and Dobrev, D. (2008). Atrial remodeling and atrial fibrillation: mechanisms and implications. *Circ. Arrhythm. Electrophysiol.* 1, 62–73. doi: 10.1161/CIRCEP.107.754564
- Nattel, S., and Carlson, L. (2006). Innovative approaches to anti-arrhythmic drug therapy. *Nat. Rev. Drug Discov.* 5, 1034–1049. doi: 10.1038/nrd2112
- Nattel, S., and Harada, M. (2014). Atrial remodeling and atrial fibrillation: recent advances and translational perspectives. *J. Am. Coll. Cardiol.* 63, 2335–2345. doi: 10.1016/j.jacc.2014.02.555
- Nattel, S., Talajic, M., Fermin, B., and Roy, D. (1992). Amiodarone: pharmacology, clinical actions, and relationships between them. *J. Cardiovasc. Electrophysiol.* 3, 266–280. doi: 10.1111/j.1540-8167.1992.tb00972.x
- Neef, S., Dybkova, N., Sossalla, S., Ort, K. R., Fluschnik, N., Neumann, K., et al. (2010). CaMKII-dependent diastolic SR Ca^{2+} leak and elevated diastolic Ca^{2+} levels in right atrial myocardium of patients with atrial fibrillation. *Circ. Res.* 106, 1134–1144. doi: 10.1161/CIRCRESAHA.109.203836
- Neuhoff, S., Yeo, K. R., Barter, Z., Jamei, M., Turner, D. B., and Rostami-Hodjegan, A. (2013). Application of permeability-limited physiologically-based pharmacokinetic models: part I—digoxin pharmacokinetics incorporating P-glycoprotein-mediated efflux. *J. Pharm. Sci.* 102, 3145–3160. doi: 10.1002/jps.23594
- Ngo, S. T., Fang, S.-T., Huang, S.-H., Chou, C.-L., Huy, P. D. Q., Li, M. S., et al. (2016). Anti-arrhythmic medication propafenone a potential drug for Alzheimer's disease inhibiting aggregation of $\text{A}\beta$: in silico and in vitro studies. *J. Chem. Inf. Model.* 56, 1344–1356. doi: 10.1021/acs.jcim.6b00029
- Ni, H., Morotti, S., and Grandi, E. (2018). A heart for diversity: simulating variability in cardiac arrhythmia research. *Front. Physiol.* 9:958. doi: 10.3389/fphys.2018.00958
- Ni, H., Whittaker, D. G., Wang, W., Giles, W. R., Narayan, S. M., and Zhang, H. (2017). Synergistic anti-arrhythmic effects in human atria with combined use of sodium blockers and acacetin. *Front. Physiol.* 8:946. doi: 10.3389/fphys.2017.00946
- Nishida, K., Michael, G., Dobrev, D., and Nattel, S. (2010). Animal models for atrial fibrillation: clinical insights and scientific opportunities. *Europace* 12, 160–172. doi: 10.1093/europace/eup328
- Noble, D. (1962). A modification of the Hodgkin–Huxley equations applicable to Purkinje fibre action and pace-maker potentials. *J. Physiol.* 160, 317–352. doi: 10.1113/jphysiol.1962.sp006849
- Nygren, A., Fiset, C., Firek, L., Clark, J. W., Lindblad, D. S., Clark, R. B., et al. (1998). Mathematical model of an adult human atrial cell: the role of K^+ currents in repolarization. *Circ. Res.* 82, 63–81. doi: 10.1161/01.RES.82.1.63
- Oh, S., Kim, K.-B., Ahn, H., Cho, H.-J., and Choi, Y.-S. (2010). Remodeling of Ion channel expression in patients with chronic atrial fibrillation and mitral valvular heart disease. *Korean J. Intern. Med.* 25, 377–385. doi: 10.3904/kjim.2010.25.4.377
- O'Hara, T., Virág, L., Varró, A., and Rudy, Y. (2011). Simulation of the undiseased human cardiac ventricular action potential: model formulation and experimental validation. *PLoS Comput. Biol.* 7:e1002061. doi: 10.1371/journal.pcbi.1002061
- Ohkusa, T., Ueyama, T., Yamada, J., Yano, M., Fujumura, Y., Esato, K., et al. (1999). Alterations in cardiac sarcoplasmic reticulum Ca^{2+} regulatory proteins in the atrial tissue of patients with chronic atrial fibrillation. *J. Am. Coll. Cardiol.* 34, 255–263. doi: 10.1016/S0735-1097(99)00169-2
- Olesen, M. S., Jabbari, J., Holst, A. G., Nielsen, J. B., Steinbrüchel, D. A., Jespersen, T., et al. (2011). Screening of KCNN3 in patients with early-onset lone atrial fibrillation. *Europace* 13, 963–967. doi: 10.1093/europace/eur007
- Oliveira, B. L., de Pfeiffer, E. R., Sundnes, J., Wall, S. T., and McCulloch, A. D. (2015). Increased cell membrane capacitance is the dominant mechanism of stretch-dependent conduction slowing in the rabbit heart: a computational study. *Cell. Mol. Bioeng.* 8, 237–246. doi: 10.1007/s12195-015-0384-9
- Pamukcu, B., and Lip, G. Y. (2011). Dronedarone as a new treatment option for atrial fibrillation patients: pharmacokinetics, pharmacodynamics and clinical practice. *Expert Opin. Pharmacother.* 12, 131–140. doi: 10.1517/14656566.2011.540800
- Pásek, M., and Simurda, J. (2004). Quantitative modelling of interaction of propafenone with sodium channels in cardiac cells. *Med. Biol. Eng. Comput.* 42, 151–157. doi: 10.1007/BF02344625
- Pashakhloo, F., Herzka, D. A., Ashikaga, H., Mori, S., Gai, N., Bluemke, D. A., et al. (2016). Myofiber architecture of the human atria as revealed by submillimeter diffusion tensor imaging. *Circ. Arrhythm. Electrophysiol.* 9, e004133. doi: 10.1161/CIRCEP.116.004133
- Passini, E., Britton, O. J., Lu, H. R., Rohrbacher, J., Hermans, A. N., Gallacher, D. J., et al. (2017). Human in silico drug trials demonstrate higher accuracy than animal models in predicting clinical pro-arrhythmic cardiotoxicity. *Front. Physiol.* 8:668. doi: 10.3389/fphys.2017.00668
- Pastore, J. M., and Rosenbaum, D. S. (2000). Role of structural barriers in the mechanism of alternans-induced reentry. *Circ. Res.* 87, 1157–1163. doi: 10.1161/01.RES.87.12.1157
- Pathmanathan, P., Shotwell, M. S., Gavaghan, D. J., Cordeiro, J. M., and Gray, R. A. (2015). Uncertainty quantification of fast sodium current steady-state inactivation for multi-scale models of cardiac electrophysiology. *Prog. Biophys. Mol. Biol.* 117, 4–18. doi: 10.1016/j.pbiomolbio.2015.01.008
- Patterson, E., Lazzara, R., Szabo, B., Liu, H., Tang, D., Li, Y.-H., et al. (2006). Sodium-calcium exchange initiated by the Ca^{2+} transient: an arrhythmia trigger within pulmonary veins. *J. Am. Coll. Cardiol.* 47, 1196–1206. doi: 10.1016/j.jacc.2005.12.023
- Platonov, P. G., Mitrofanova, L. B., Orshanskaia, V., and Ho, S. Y. (2011). Structural abnormalities in atrial walls are associated with presence and persistency of atrial fibrillation but not with age. *J. Am. Coll. Cardiol.* 58, 2225–2232. doi: 10.1016/j.jacc.2011.05.061
- Podd, S. J., Freemantle, N., Furniss, S. S., and Sulke, N. (2016). First clinical trial of specific IKACh blocker shows no reduction in atrial fibrillation burden in patients with paroxysmal atrial fibrillation: pacemaker assessment of BMS 914392 in patients with paroxysmal atrial fibrillation. *Europace* 18, 340–346. doi: 10.1093/europace/euv263
- Prinz, A. A., Billimoria, C. P., and Marder, E. (2003). Alternative to hand-tuning conductance-based models: construction and analysis of databases

- of model neurons. *J. Neurophysiol.* 90, 3998–4015. doi: 10.1152/jn.00641.2003
- Pruvot, E. J., Katra, R. P., Rosenbaum, D. S., and Laurita, K. R. (2004). Role of calcium cycling versus restitution in the mechanism of repolarization alternans. *Circ. Res.* 94, 1083–1090. doi: 10.1161/01.RES.0000125629.72053.95
- Qu, Z., Garfinkel, A., Chen, P. S., and Weiss, J. N. (2000). Mechanisms of discordant alternans and induction of reentry in simulated cardiac tissue. *Circulation* 102, 1664–1670. doi: 10.1161/01.CIR.102.14.1664
- Rajamani, S., Anderson, C. L., Valdivia, C. R., Eckhardt, L. L., Foell, J. D., Robertson, G. A., et al. (2006). Specific serine proteases selectively damage KCNH2 (hERG1) potassium channels and IKr. *Am. J. Physiol. Heart Circ. Physiol.* 290, H1278–H1288. doi: 10.1152/ajpheart.00777.2005
- Ravelli, F., and Allessie, M. (1997). Effects of atrial dilatation on refractory period and vulnerability to atrial fibrillation in the isolated langendorff-perfused rabbit heart. *Circulation* 96, 1686–1695. doi: 10.1161/01.CIR.96.5.1686
- Ravens, U., and Christ, T. (2010). Atrial-selective drugs for treatment of atrial fibrillation. *Herzschrittmacherther. Elektrophysiol.* 21, 217–221. doi: 10.1007/s00399-010-0088-8
- Ravens, U., Katircioglu-Öztürk, D., Wettwer, E., Christ, T., Dobrev, D., Voigt, N., et al. (2014). Application of the RIMARC algorithm to a large data set of action potentials and clinical parameters for risk prediction of atrial fibrillation. *Med. Biol. Eng. Comput.* 53, 263–273. doi: 10.1007/s11517-014-1232-0
- Ravens, U., and Wettwer, E. (2011). Ultra-rapid delayed rectifier channels: molecular basis and therapeutic implications. *Cardiovasc. Res.* 89, 776–785. doi: 10.1093/cvr/cvq398
- Reilly, S. N., Liu, X., Carnicer, R., Recalde, A., Muszkiewicz, A., Jayaram, R., et al. (2016). Up-regulation of miR-31 in human atrial fibrillation begets the arrhythmia by depleting dystrophin and neuronal nitric oxide synthase. *Sci. Transl. Med.* 8:340ra74. doi: 10.1126/scitranslmed.aac4296
- Ren, Y., Barnwell, L. F., Alexander, J. C., Lubin, F. D., Adelman, J. P., Pfaffinger, P. J., et al. (2006). Regulation of surface localization of the small conductance Ca^{2+} -activated potassium channel, Sk2, through direct phosphorylation by cAMP-dependent protein kinase. *J. Biol. Chem.* 281, 11769–11779. doi: 10.1074/jbc.M513125200
- Ridler, M., McQueen, D. M., Peskin, C. S., and Vigmond, E. (2006). “Action potential duration gradient protects the right atrium from fibrillating,” in *Proceedings of the 2006 International Conference of the IEEE Engineering in Medicine and Biology Society*, New York, NY, 3978–3981. doi: 10.1109/IEMBS.2006.260522
- Ridler, M.-E., Lee, M., McQueen, D., Peskin, C., and Vigmond, E. (2011). Arrhythmogenic consequences of action potential duration gradients in the atria. *Can. J. Cardiol.* 27, 112–119. doi: 10.1016/j.cjca.2010.12.002
- Roden, D. M., and Woosley, R. L. (1986). Flecainide. *N. Engl. J. Med.* 315, 36–41. doi: 10.1056/NEJM198607033150106
- Romero, L., Trenor, B., Yang, P.-C., Saiz, J., and Clancy, C. E. (2014). In silico screening of the impact of hERG channel kinetic abnormalities on channel block and susceptibility to acquired long QT syndrome. *J. Mol. Cell. Cardiol.* 72, 126–137. doi: 10.1016/j.yjmcc.2014.02.018
- Rosa, G. M., Bianco, D., Parodi, A., Valbusa, A., Zawaideh, C., Bizzarri, N., et al. (2014). Pharmacokinetic and pharmacodynamic profile of dronedarone, a new antiarrhythmic agent for the treatment of atrial fibrillation. *Expert Opin. Drug Metab. Toxicol.* 10, 1751–1764. doi: 10.1517/17425255.2014.974551
- Rosa, J. C., Galanakis, D., Ganellin, C. R., Dunn, P. M., and Jenkinson, D. H. (1998). Bis-Quinolinium Cyclophanes: 6,10-Diaza-3(1,3),8(1,4)-dibenzo-1,5(1,4)- diquinolinacyclodecaphane (UCL 1684), the first nanomolar, non-peptidic blocker of the apamin-sensitive Ca^{2+} -activated K^+ channel. *J. Med. Chem.* 41, 2–5. doi: 10.1021/jm970571a
- Rosen, M. R., and Janse, M. J. (2010). Concept of the vulnerable parameter: the sicilian gambit revisited. *J. Cardiovasc. Pharmacol.* 55, 428–437. doi: 10.1097/FJC.0b013e3181bfaddc
- Ruiz-Villa, C., Tobón, C., Rodríguez, J., Ferrero, J., Hornero, F., and Saíz, J. (2009). “Influence of atrial dilatation in the generation of re-entries caused by ectopic activity in the left atrium,” in *Proceedings of the 2009 36th Annual Computers in Cardiology Conference (CinC)*, Park City, UT, 457–460.
- Saiz, J., Gomis-Tena, J., Monserrat, M., Ferrero, J. M., Cardona, K., and Chorro, J. (2011). Effects of the antiarrhythmic drug dofetilide on transmural dispersion of repolarization in ventricle. A computer modeling study. *IEEE Trans. Biomed. Eng.* 58, 43–53. doi: 10.1109/TBME.2010.2077292
- Sánchez, C., Bueno-Orovio, A., Pueyo, E., and Rodriguez, B. (2017). Atrial fibrillation dynamics and ionic block effects in six heterogeneous human 3D virtual atria with distinct repolarization dynamics. *Front. Bioeng. Biotechnol.* 5:29. doi: 10.3389/fbioe.2017.00029
- Sánchez, J., Trénor, B., and Saiz, J. (2017). “In silico analysis of the effects of fibroblasts coupling to atrial myocytes under conditions of atrial fibrillation remodeling,” in *Proceedings of the 2017 Computing in Cardiology (CinC)*, Valencia, 1–4. doi: 10.22489/CinC.2017.122-310
- Sánchez, C., Bueno-Orovio, A., Wettwer, E., Loose, S., Simon, J., Ravens, U., et al. (2014). Inter-subject variability in human atrial action potential in sinus rhythm versus chronic atrial fibrillation. *PLoS One* 9:e105897. doi: 10.1371/journal.pone.0105897
- Sánchez, C., Corrias, A., Bueno-Orovio, A., Davies, M., Swinton, J., Jacobson, I., et al. (2012). The Na^+/K^+ pump is an important modulator of refractoriness and rotor dynamics in human atrial tissue. *Am. J. Physiol. Heart Circ. Physiol.* 302, H1146–H1159. doi: 10.1152/ajpheart.00668.2011
- Sato, D., Bers, D. M., and Shiferaw, Y. (2013). Formation of spatially discordant alternans due to fluctuations and diffusion of calcium. *PLoS One* 8:e85365. doi: 10.1371/journal.pone.0085365
- Sato, D., Shiferaw, Y., Garfinkel, A., Weiss, J. N., Qu, Z., and Karma, A. (2006). Spatially discordant alternans in cardiac tissue: role of calcium cycling. *Circ. Res.* 99, 520–527. doi: 10.1161/01.RES.0000240542.03986.e7
- Scheruebel, S., Koyani, C. N., Hallström, S., Lang, P., Platzer, D., Mächler, H., et al. (2014). If blocking potency of ivabradine is preserved under elevated endotoxin levels in human atrial myocytes. *J. Mol. Cell. Cardiol.* 72, 64–73. doi: 10.1016/j.yjmcc.2014.02.010
- Schmidt, C., Wiedmann, F., Gaubatz, A.-R., Ratte, A., Katus, H. A., and Thomas, D. (2018). New targets for old drugs: cardiac glycosides inhibit atrial-specific K_{2P3.1} (TASK-1) channels. *J. Pharmacol. Exp. Ther.* 365, 614–623. doi: 10.1124/jpet.118.247692
- Schmidt, C., Wiedmann, F., Schweizer, P. A., Becker, R., Katus, H. A., and Thomas, D. (2013). Class I antiarrhythmic drugs inhibit human cardiac two-pore-domain K₊ (K_{2P}) channels. *Eur. J. Pharmacol.* 721, 237–248. doi: 10.1016/j.ejphar.2013.09.029
- Schmidt, C., Wiedmann, F., Voigt, N., Zhou, X.-B., Heijman, J., Lang, S., et al. (2015). Upregulation of K_{2P3.1} K₊ current causes action potential shortening in patients with chronic atrial fibrillation. *Circulation* 132, 82–92. doi: 10.1161/CIRCULATIONAHA.114.012657
- Schmidt, C., Wiedmann, F., Zhou, X.-B., Heijman, J., Voigt, N., Ratte, A., et al. (2017). Inverse remodelling of K_{2P3.1} K₊ channel expression and action potential duration in left ventricular dysfunction and atrial fibrillation: implications for patient-specific antiarrhythmic drug therapy. *Eur. Heart J.* 38, 1764–1774. doi: 10.1093/eurheartj/ehw559
- Scholz, E. P., Carrillo-Bustamante, P., Fischer, F., Wilhelms, M., Zitron, E., Dössel, O., et al. (2013). Rotor termination is critically dependent on kinetic properties of IKur inhibitors in an in silico model of chronic atrial fibrillation. *PLoS One* 8:e83179. doi: 10.1371/journal.pone.0083179
- Schotten, U., Ausma, J., Stellbrink, C., Sabatschus, I., Vogel, M., Frechen, D., et al. (2001). Cellular mechanisms of depressed atrial contractility in patients with chronic atrial fibrillation. *Circulation* 103, 691–698. doi: 10.1161/01.CIR.103.5.691
- Schotten, U., de Haan, S., Verheule, S., Harks, E. G. A., Frechen, D., Bodewig, E., et al. (2007). Blockade of atrial-specific K₊-currents increases atrial but not ventricular contractility by enhancing reverse mode $\text{Na}^+/\text{Ca}^{2+}$ -exchange. *Cardiovasc. Res.* 73, 37–47. doi: 10.1016/j.cardiores.2006.11.024
- Schotten, U., Dobrev, D., Platonov, P. G., Kottkamp, H., and Hindricks, G. (2016). Current controversies in determining the main mechanisms of atrial fibrillation. *J. Intern. Med.* 279, 428–438. doi: 10.1111/joim.12492
- Schotten, U., Neuberger, H.-R., and Allessie, M. A. (2003). The role of atrial dilatation in the domestication of atrial fibrillation. *Prog. Biophys. Mol. Biol.* 82, 151–162. doi: 10.1016/S0079-6107(03)00012-9
- Schotten, U., Verheule, S., Kirchhof, P., and Goette, A. (2011). Pathophysiological mechanisms of atrial fibrillation: a translational appraisal. *Physiol. Rev.* 91, 265–325. doi: 10.1152/physrev.00031.2009

- Seemann, G., Hoper, C., Sachse, F. B., Dossel, O., Holden, A. V., and Zhang, H. (2006). Heterogeneous three-dimensional anatomical and electrophysiological model of human atria. *Philos. Trans. A Math. Phys. Eng. Sci.* 364, 1465–1481. doi: 10.1098/rsta.2006.1781
- Seemann, G., Loewe, A., and Wülfers, E. M. (2017). “Effects of fibroblasts coupling on the electrophysiology of cardiomyocytes from different regions of the human atrium: a simulation study,” in *Proceedings of the 2017 Computing in Cardiology (CinC)*, Rennes, 1–4. doi: 10.22489/CinC.2017.380-451
- Seyler, C., Li, J., Schweizer, P. A., Katus, H. A., and Thomas, D. (2014). Inhibition of cardiac two-pore-domain K⁺ (K2P) channels by the antiarrhythmic drug vernakalant – Comparison with flecainide. *Eur. J. Pharmacol.* 724, 51–57. doi: 10.1016/j.ejphar.2013.12.030
- Shanmugam, M., Molina, C. E., Gao, S., Severac-Bastide, R., Fischmeister, R., and Babu, G. J. (2011). Decreased sarcolipin protein expression and enhanced sarco(endo)plasmic reticulum Ca²⁺ uptake in human atrial fibrillation. *Biochem. Biophys. Res. Commun.* 410, 97–101. doi: 10.1016/j.bbrc.2011.05.113
- Shiferaw, Y., and Karma, A. (2006). Turing instability mediated by voltage and calcium diffusion in paced cardiac cells. *Proc. Natl. Acad. Sci. U.S.A.* 103, 5670–5675. doi: 10.1073/pnas.0511061103
- Shiraishi, I., Takamatsu, T., Minamikawa, T., Onouchi, Z., and Fujita, S. (1992). Quantitative histological analysis of the human sinoatrial node during growth and aging. *Circulation* 85, 2176–2184. doi: 10.1161/01.CIR.85.6.2176
- Shoichet, B. K., McGovern, S. L., Wei, B., and Irwin, J. J. (2002). Lead discovery using molecular docking. *Curr. Opin. Chem. Biol.* 6, 439–446. doi: 10.1016/S1367-5931(02)00339-3
- Shunmugam, S. R., Sugihara, C., Freemantle, N., Round, P., Furniss, S., and Sulke, N. (2018). A double-blind, randomised, placebo-controlled, crossover study assessing the use of XEN-D0103 in patients with paroxysmal atrial fibrillation and implanted pacemakers allowing continuous beat-to-beat monitoring of drug efficacy. *J. Interv. Card. Electrophysiol.* 51, 191–197. doi: 10.1007/s10840-018-0318-2
- Skibsgaard, L., Diness, J. G., Sørensen, U. S., Hansen, R. S., and Grunnet, M. (2011). The duration of pacing-induced atrial fibrillation is reduced in vivo by inhibition of small conductance Ca²⁺-activated K⁺ Channels. *J. Cardiovasc. Pharmacol.* 57, 672–681. doi: 10.1097/FJC.0b013e318217943d
- Skibsgaard, L., Jespersen, T., Christ, T., Maleckar, M. M., van den Brink, J., Tavi, P., et al. (2016). Refractoriness in human atria: time and voltage dependence of sodium channel availability. *J. Mol. Cell. Cardiol.* 101, 26–34. doi: 10.1016/j.yjmcc.2016.10.009
- Skibsgaard, L., Poulet, C., Diness, J. G., Bentzen, B. H., Yuan, L., Kappert, U., et al. (2014). Small conductance calcium activated potassium (SK) channels contribute to action potential repolarisation in human atria. *Cardiovasc. Res.* 103, 156–167. doi: 10.1093/cvr/cvu121
- Sobie, E. A. (2009). Parameter sensitivity analysis in electrophysiological models using multivariable regression. *Biophys. J.* 96, 1264–1274. doi: 10.1016/j.bpj.2008.10.056
- Starmer, C. F., Grant, A. O., and Colatsky, T. J. (2003). What happens when cardiac Na channel function is compromised? 2. Numerical studies of the vulnerable period in tissue altered by drugs. *Cardiovasc. Res.* 57, 1062–1071. doi: 10.1016/S0008-6363(02)00727-7
- Starmer, C. F., Lastra, A. A., Nesterenko, V. V., and Grant, A. O. (1991). Proarrhythmic response to sodium channel blockade. Theoretical model and numerical experiments. *Circulation* 84, 1364–1377. doi: 10.1161/01.CIR.84.3.1364
- Stillitano, F., Lonardo, G., Giunti, G., Del Lungo, M., Coppini, R., Spinelli, V., et al. (2013). Chronic atrial fibrillation alters the functional properties of if in the human atrium. *J. Cardiovasc. Electrophysiol.* 24, 1391–1400. doi: 10.1111/jce.12212
- Tamargo, J., Caballero, R., Gómez, R., Valenzuela, C., and Delpón, E. (2004). Pharmacology of cardiac potassium channels. *Cardiovasc. Res.* 62, 9–33. doi: 10.1016/j.cardiores.2003.12.026
- Tanaami, T., Ishida, H., Seguchi, H., Hirota, Y., Kadono, T., Genka, C., et al. (2005). Difference in propagation of Ca²⁺ release in atrial and ventricular myocytes. *Jpn. J. Physiol.* 55, 81–91. doi: 10.2170/jjphysiol.R2077
- Tanaka, K., Zlochiver, S., Vikstrom, K. L., Yamazaki, M., Moreno, J., Klos, M., et al. (2007). Spatial distribution of fibrosis governs fibrillation wave dynamics in the posterior left atrium during heart failure. *Circ. Res.* 101, 839–847. doi: 10.1161/CIRCRESAHA.107.153858
- Tobón, C., Ruiz-Villa, C. A., Heidenreich, E., Romero, L., Hornero, F., and Saiz, J. (2013). A three-dimensional human atrial model with fiber orientation, electrograms and arrhythmic activation patterns relationship. *PLoS One* 8:e50883. doi: 10.1371/journal.pone.0050883
- Trenor, B., Gomis-Tena, J., Cardona, K., Romero, L., Rajamani, S., Belardinelli, L., et al. (2013). In silico assessment of drug safety in human heart applied to late sodium current blockers. *Channels* 7, 249–262. doi: 10.4161/chan.24905
- Tsujimae, K., Murakami, S., and Kurachi, Y. (2008). In silico study on the effects of IK_{ur} block kinetics on prolongation of human action potential after atrial fibrillation-induced electrical remodeling. *Am. J. Physiol. Heart Circ. Physiol.* 294, H793–H800. doi: 10.1152/ajpheart.01229.2007
- Tsujimae, K., Suzuki, S., Murakami, S., and Kurachi, Y. (2007). Frequency-dependent effects of various IK_r blockers on cardiac action potential duration in a human atrial model. *Am. J. Physiol. Heart Circ. Physiol.* 293, H660–H669. doi: 10.1152/ajpheart.01083.2006
- Tuteja, D., Xu, D., Timofeyev, V., Lu, L., Sharma, D., Zhang, Z., et al. (2005). Differential expression of small-conductance Ca²⁺-activated K⁺ channels SK1, SK2, and SK3 in mouse atrial and ventricular myocytes. *Am. J. Physiol. Heart Circ. Physiol.* 289, H2714–H2723. doi: 10.1152/ajpheart.00534.2005
- Vagos, M. R., Arevalo, H., de Oliveira, B. L., Sundnes, J., and Maleckar, M. M. (2017). A computational framework for testing arrhythmia marker sensitivities to model parameters in functionally calibrated populations of atrial cells. *Chaos* 27:093941. doi: 10.1063/1.4999476
- Vagos, M., Lino de Oliveira, B., Arevalo, H., and Sundnes, J. (2017). An *in silico* population approach to study the effect of drugs on arrhythmia marker sensitivities of atrial cells. in *Poster at the Cardiac Physiome Workshop*, Toronto.
- Varela, M., Colman, M. A., Hancox, J. C., and Aslanidi, O. V. (2016). Atrial heterogeneity generates re-entrant substrate during atrial fibrillation and anti-arrhythmic drug action: mechanistic insights from canine atrial models. *PLoS Comput. Biol.* 12:e1005245. doi: 10.1371/journal.pcbi.1005245
- Varkevisser, R., Houtman, M. J. C., Linder, T., Git, K. C. G., de Beekman, H. D. M., Tidwell, R. R., et al. (2013). Structure-activity relationships of pentamidine-affected ion channel trafficking and dofetilide mediated rescue. *Br. J. Pharmacol.* 169, 1322–1334. doi: 10.1111/bph.12208
- Verheule, S., Tuyls, E., Gharaviri, A., Hulsmans, S., Hunnik, A., van Kuiper, M., et al. (2013). Loss of continuity in the thin epicardial layer because of endomyocardial fibrosis increases the complexity of atrial fibrillatory conduction. *Circ. Arrhythm. Electrophysiol.* 6, 202–211. doi: 10.1161/CIRCEP.112.975144
- Vest, J. A., Wehrens, X. H. T., Reiken, S. R., Lehnart, S. E., Dobrev, D., Chandra, P., et al. (2005). Defective cardiac ryanodine receptor regulation during atrial fibrillation. *Circulation* 111, 2025–2032. doi: 10.1161/01.CIR.0000162461.67140.4C
- Vidmar, D., Narayan, S. M., and Rappel, W.-J. (2015). Phase synchrony reveals organization in human atrial fibrillation. *Am. J. Physiol. Heart Circ. Physiol.* 309, H2118–H2126. doi: 10.1152/ajpheart.00407.2015
- Vigmond, E. J., Ruckdeschel, R., and Trayanova, N. (2003). Reentry in a morphologically realistic atrial model. *J. Cardiovasc. Electrophysiol.* 12, 1046–1054. doi: 10.1046/j.1540-8167.2001.01046.x
- Virag, N., Jacquemet, V., Henriquez, C. S., Zozor, S., Blanc, O., Vesin, J.-M., et al. (2002). Study of atrial arrhythmias in a computer model based on magnetic resonance images of human atria. *Chaos* 12, 754–763. doi: 10.1063/1.1483935
- Vivo, R. P., Krim, S. R., Perez, J., Inklab, M., Tenner, T., and Hodgson, J. (2008). Digoxin: current use and approach to toxicity. *Am. J. Med. Sci.* 336, 423–428. doi: 10.1097/MAJ.0b013e318176b94d
- Voigt, N., Friedrich, A., Bock, M., Wettwer, E., Christ, T., Knaut, M., et al. (2007). Differential phosphorylation-dependent regulation of constitutively active and muscarinic receptor-activated IK_{ACh} channels in patients with chronic atrial fibrillation. *Cardiovasc. Res.* 74, 426–437. doi: 10.1016/j.cardiores.2007.02.009
- Voigt, N., Heijman, J., Trausch, A., Mintert-Jancke, E., Pott, L., Ravens, U., et al. (2013a). Impaired Na⁺-dependent regulation of acetylcholine-activated inward-rectifier K⁺ current modulates action potential rate dependence in patients with chronic atrial fibrillation. *J. Mol. Cell. Cardiol.* 61, 142–152. doi: 10.1016/j.yjmcc.2013.03.011
- Voigt, N., Heijman, J., Wang, Q., Chiang, D. Y., Li, N., Karck, M., et al. (2013b). Cellular and molecular mechanisms of atrial arrhythmogenesis in patients

- with paroxysmal atrial fibrillation. *Circulation* 129, 145–156. doi: 10.1161/CIRCULATIONAHA.113.006641
- Voigt, N., Li, N., Wang, Q., Wang, W., Trafford, A. W., Abu-Taha, I., et al. (2012). Enhanced sarcoplasmic reticulum Ca^{2+} leak and increased Na^{+} - Ca^{2+} exchanger function underlie delayed afterdepolarizations in patients with chronic atrial fibrillation. *Circulation* 125, 2059–2070. doi: 10.1161/CIRCULATIONAHA.111.067306
- Voigt, N., Trausch, A., Knaut, M., Matschke, K., Varró, A., Van Wagoner, D. R., et al. (2010). Left-to-right atrial inward rectifier potassium current gradients in patients with paroxysmal versus chronic atrial fibrillation. *Circ. Arrhythm. Electrophysiol.* 3, 472–480. doi: 10.1161/CIRCEP.110.954636
- Wakili, R., Voigt, N., Kääb, S., Dobrev, D., and Nattel, S. (2011). Recent advances in the molecular pathophysiology of atrial fibrillation. *J. Clin. Invest.* 121, 2955–2968. doi: 10.1172/JCI46315
- Wakili, R., Yeh, Y.-H., Yan Qi, X., Greiser, M., Chartier, D., Nishida, K., et al. (2010). Multiple potential molecular contributors to atrial hypocontractility caused by atrial tachycardia remodeling in dogs / clinical perspective. *Circ. Arrhythm. Electrophysiol.* 3, 530–541. doi: 10.1161/CIRCEP.109.933036
- Waks, J. W., and Josephson, M. E. (2014). Mechanisms of atrial fibrillation – reentry, rotors and reality. *Arrhythm. Electrophysiol. Rev.* 3, 90–100. doi: 10.15420/aer.2014.3.2.90
- Walfridsson, H., Anfinsen, O.-G., Berggren, A., Frison, L., Jensen, S., Linhardt, G., et al. (2015). Is the acetylcholine-regulated inwardly rectifying potassium current a viable antiarrhythmic target? Translational discrepancies of AZD2927 and A7071 in dogs and humans. *Europace* 17, 473–482. doi: 10.1093/europace/euu192
- Wang, Y.-J., Sung, R. J., Lin, M.-W., and Wu, S.-N. (2006). Contribution of BKCa-channel activity in human cardiac fibroblasts to electrical coupling of cardiomyocytes-fibroblasts. *J. Membr. Biol.* 213, 175–185. doi: 10.1007/s00232-007-0027-8
- Watanabe, H., Chopra, N., Laver, D., Hwang, H. S., Davies, S. S., Roach, D. E., et al. (2009). Flecainide prevents catecholaminergic polymorphic ventricular tachycardia in mice and humans. *Nat. Med.* 15, 380–383. doi: 10.1038/nm.1942
- Watanabe, H., Steele, D. S., and Knollmann, B. C. (2011). Mechanism of antiarrhythmic effects of flecainide in catecholaminergic polymorphic ventricular tachycardia. *Circ. Res.* 109, 712–713. doi: 10.1161/CIRCRESAHA.111.251322
- Watanabe, M. A., Fenton, F. H., Evans, S. J., Hastings, H. M., and Karma, A. (2001). Mechanisms for discordant alternans. *J. Cardiovasc. Electrophysiol.* 12, 196–206. doi: 10.1046/j.1540-8167.2001.00196.x
- Weatherall, K. L., Goodchild, S. J., Jane, D. E., and Marrion, N. V. (2010). Small conductance calcium-activated potassium channels: from structure to function. *Prog. Neurobiol.* 91, 242–255. doi: 10.1016/j.pneurobio.2010.03.002
- Weatherall, K. L., Seutin, V., Liégeois, J.-F., and Marrion, N. V. (2011). Crucial role of a shared extracellular loop in apamin sensitivity and maintenance of pore shape of small-conductance calcium-activated potassium (SK) channels. *Proc. Natl. Acad. Sci. U.S.A.* 108, 18494–18499. doi: 10.1073/pnas.1110724108
- Weiss, M. (2007). Mechanistic modeling of digoxin distribution kinetics incorporating slow tissue binding. *Eur. J. Pharm. Sci.* 30, 256–263. doi: 10.1016/j.ejps.2006.11.012
- Wijffels, M. C., Kirchhof, C. J., Dorland, R., and Allessie, M. A. (1995). Atrial fibrillation begets atrial fibrillation: a study in awake chronically instrumented goats. *Circulation* 92, 1954–1968. doi: 10.1161/01.CIR.92.7.1954
- Wilhelms, M., Hettman, H., Maleckar, M. M., Koivumäki, J. T., Dössel, O., and Seemann, G. (2013). Benchmarking electrophysiological models of human atrial myocytes. *Front. Physiol.* 3:487. doi: 10.3389/fphys.2012.00487
- Wilhelms, M., Rombach, C., Scholz, E. P., Dössel, O., and Seemann, G. (2012). Impact of amiodarone and cisapride on simulated human ventricular electrophysiology and electrocardiograms. *Europace* 14, v90–v96. doi: 10.1093/europace/eus281
- Wouters, L., Guo-Shu, L., Flameng, W., Thijssen, V. L. J. L., Thone, F., and Borgers, M. (2000). Structural remodelling of atrial myocardium in patients with cardiac valve disease and atrial fibrillation. *Exp. Clin. Cardiol.* 5, 158–163. doi: 10.1093/icvts/ivu095
- Wullechleger, M., Blanch, J., and Egger, M. (2017). Functional local crosstalk of inositol 1,4,5-trisphosphate receptor- and ryanodine receptor-dependent Ca^{2+} release in atrial cardiomyocytes. *Cardiovasc. Res.* 113, 542–552. doi: 10.1093/cvr/cvx020
- Xie, Y., Garfinkel, A., Weiss, J. N., and Qu, Z. (2009). Cardiac alternans induced by fibroblast-myocyte coupling: mechanistic insights from computational models. *Am. J. Physiol. Heart Circ. Physiol.* 297, H775–H784. doi: 10.1152/ajpheart.00341.2009
- Xu, Y., Tuteja, D., Zhang, Z., Xu, D., Zhang, Y., Rodriguez, J., et al. (2003). Molecular identification and functional roles of a $Ca(2+)$ -activated K^{+} channel in human and mouse hearts. *J. Biol. Chem.* 278, 49085–49094. doi: 10.1074/jbc.M307508200
- Yamada, J., Ohkusa, T., Nao, T., Ueyama, T., Yano, M., Kobayashi, S., et al. (2001). Up-regulation of inositol 1,4,5 trisphosphate receptor expression in atrial tissue in patients with chronic atrial fibrillation. *J. Am. Coll. Cardiol.* 37, 1111–1119. doi: 10.1016/S0735-1097(01)01144-5
- Yarov-Yarovoy, V., Allen, T. W., and Clancy, C. E. (2014). Computational models for predictive cardiac ion channel pharmacology. *Drug Discov. Today Dis. Models* 14, 3–10. doi: 10.1016/j.ddmod.2014.04.001
- Yue, L., Xie, J., and Nattel, S. (2011). Molecular determinants of cardiac fibroblast electrical function and therapeutic implications for atrial fibrillation. *Cardiovasc. Res.* 89, 744–753. doi: 10.1093/cvr/cvq329
- Zhang, X.-D., Coulibaly, Z. A., Chen, W. C., Ledford, H. A., Lee, J. H., Sirish, P., et al. (2018). Coupling of SK channels, L-type Ca^{2+} channels, and ryanodine receptors in cardiomyocytes. *Sci. Rep.* 8:4670. doi: 10.1038/s41598-018-22843-3
- Zhang, Y., Colenso, C. K., El Harchi, A., Cheng, H., Witchel, H. J., Dempsey, C. E., et al. (2016). Interactions between amiodarone and the hERG potassium channel pore determined with mutagenesis and in silico docking. *Biochem. Pharmacol.* 113, 24–35. doi: 10.1016/j.bcp.2016.05.013
- Zhao, J., Hansen, B. J., Wang, Y., Csepe, T. A., Sul, L. V., Tang, A., et al. (2017). Three-dimensional integrated functional, structural, and computational mapping to define the structural “Fingerprints” of heart-specific atrial fibrillation drivers in human heart ex vivo. *J. Am. Heart Assoc.* 6:e005922. doi: 10.1161/JAHA.117.005922
- Zheng, Y., Xia, Y., Carlson, J., Kongstad, O., and Yuan, S. (2016). Atrial average conduction velocity in patients with and without paroxysmal atrial fibrillation. *Clin. Physiol. Funct. Imaging* 37, 596–601. doi: 10.1111/cpf.12342
- Zima, A. V., and Blatter, L. A. (2004). Inositol-1,4,5-trisphosphate-dependent Ca^{2+} signalling in cat atrial excitation-contraction coupling and arrhythmias. *J. Physiol.* 555, 607–615. doi: 10.1113/jphysiol.2003.058529
- Zoni-Berisso, M., Lercari, F., Carazza, T., and Domenicucci, S. (2014). Epidemiology of atrial fibrillation: European perspective. *Clin. Epidemiol.* 6, 213–220. doi: 10.2147/CLEP.S47385
- Zorn-Pauly, K., Schaffer, P., Pelzmann, B., Lang, P., Machler, H., Rigler, B., et al. (2004). If in left human atrium: a potential contributor to atrial ectopy. *Cardiovasc. Res.* 64, 250–259. doi: 10.1016/j.cardiores.2004.07.001

Conflict of Interest Statement: The authors declare that the research was conducted in the absence of any commercial or financial relationships that could be construed as a potential conflict of interest.

Copyright © 2018 Vagos, van Herck, Sundnes, Arevalo, Edwards and Koivumäki. This is an open-access article distributed under the terms of the Creative Commons Attribution License (CC BY). The use, distribution or reproduction in other forums is permitted, provided the original author(s) and the copyright owner(s) are credited and that the original publication in this journal is cited, in accordance with accepted academic practice. No use, distribution or reproduction is permitted which does not comply with these terms.



Characterizing Electrogram Signal Fidelity and the Effects of Signal Contamination on Mapping Human Persistent Atrial Fibrillation

David Vidmar¹, Mahmood I. Alhusseini², Sanjiv M. Narayan² and Wouter-Jan Rappel^{1*}

¹ Department of Physics, University of California, San Diego, San Diego, CA, United States, ² Division of Cardiology, Department of Medicine, Stanford University, Stanford, CA, United States

OPEN ACCESS

Edited by:
Jichao Zhao,
University of Auckland, New Zealand

Reviewed by:
Martin Stiles,
University of Auckland, New Zealand
Dennis Lau,
University of Adelaide, Australia

***Correspondence:**
Wouter-Jan Rappel
rappel@physics.ucsd.edu

Specialty section:
This article was submitted to
Computational Physiology and
Medicine,
a section of the journal
Frontiers in Physiology

Received: 26 April 2018

Accepted: 15 August 2018

Published: 05 September 2018

Citation:

Vidmar D, Alhusseini MI, Narayan SM and Rappel W-J (2018) Characterizing Electrogram Signal Fidelity and the Effects of Signal Contamination on Mapping Human Persistent Atrial Fibrillation. *Front. Physiol.* 9:1232.
doi: 10.3389/fphys.2018.01232

Objective: Determining accurate intracardiac maps of atrial fibrillation (AF) in humans can be difficult, owing primarily to various sources of contamination in electrogram signals. The goal of this study is to develop a measure for signal fidelity and to develop methods to quantify robustness of observed rotational activity in phase maps subject to signal contamination.

Methods: We identified rotational activity in phase maps of human persistent AF using the Hilbert transform of sinusoidally recomposed signals, where localized ablation at rotational sites terminated fibrillation. A novel measure of signal fidelity was developed to quantify signal quality. Contamination is then introduced to the underlying electrograms by removing signals at random, adding noise to computations of cycle length, and adding realistic far-field signals. Mean tip number N and tip density δ , defined as the proportion of time a region contains a tip, at the termination site are computed to compare the effects of contamination.

Results: Domains of low signal fidelity correspond to the location of rotational cores. Removing signals and altering cycle length accounted for minor changes in tip density, while targeted removal of low fidelity electrograms can result in a significant increase in tip density and stability. Far-field contamination was found to obscure rotation at the termination site.

Conclusion: Rotational activity in clinical AF can produce domains of low fidelity electrogram recordings at rotational cores. Observed rotational patterns in phase maps appear most sensitive to far-field activation. These results may inform novel methods to map AF in humans which can be tested directly in patients at electrophysiological study and ablation.

Keywords: atrial fibrillation, phase map, signal fidelity, signal contamination, modeling

INTRODUCTION

Fibrillation is the most common form of cardiac arrhythmia. Ventricular fibrillation (VF) is life-threatening and responsible for over 300,000 cases of sudden cardiac arrest per year (Nichol et al., 2008; Tracy et al., 2012), while atrial fibrillation (AF) affects 30 million people worldwide and is a major cause of stroke and debility (Chugh et al., 2014; January et al., 2014). Despite decades of research, the precise mechanisms underlying fibrillation are still debated (Pandit and Jalife, 2013; Nattel et al., 2017). Progress is slow in large part due to the inherent difficulty in mapping complex rhythms in humans where optical mapping, commonly used in animal studies (Gray et al., 1995; Mandapati et al., 2000), is not feasible. Therefore, the most accurate clinical determination of activation patterns of human AF and VF must come from the use of high density electrode arrays (Narayan et al., 2012a; Krummen et al., 2014) or non-invasive body surface mappings (Ramanathan et al., 2004).

Recent studies using intracardiac basket electrodes have revealed that during VF and AF spiral waves, or rotors, may underlie the irregular tissue activity (Narayan et al., 2012a,b; Krummen et al., 2015), recently confirmed by other intracardiac methods (Daoud et al., 2017; Grace et al., 2017) and with non-invasive mapping techniques (Haissaguerre et al., 2014). The relevance of these spiral waves have been supported by computational studies (Rappel et al., 2015) and by targeted ablation (Narayan et al., 2012c) and may more rapidly result in AF termination than traditional ablation to electrically isolate the pulmonary veins (Haissaguerre et al., 2014). Furthermore, the 1-year success of such ablation techniques is higher than the 40–60% reported for pulmonary vein ablation alone in many studies (Haissaguerre et al., 2014; Sommer et al., 2016; Miller et al., 2017; Spitzer et al., 2017) although meta-analyses show variable outcomes between centers (Ramirez et al., 2017; Baykaner et al., 2018; Parameswaran et al., 2018).

Nevertheless, these data are debated since <50% of patients show acute termination, and some groups report difficulties obtaining good clinical results with heterogeneity in meta-analyses (Ramirez et al., 2017; Baykaner et al., 2018; Parameswaran et al., 2018). One possible explanation for discrepant results, particularly in patients who have failed multiple prior procedures, might be variations in signal quality with subsequent degradation of mapping accuracy. In this study, we propose a method for quantifying signal fidelity and systematically determine how signal contamination affects stable rotational activation during clinical AF using an intracardiac electrode array. To show the potential of the fidelity metric and the possible effects of signal contamination, we focus on data obtained from several patients with AF. In future work we plan to apply these results to improve mapping and ablation in large patient cohorts.

METHODS

Data Processing

We will focus here on signals recorded from 64-pole basket electrodes on an 8×8 grid, recorded clinically during AF at a

sampling rate of 977 Hz upsampled to 1,000 Hz. These data were recorded in the left atrium of patients with persistent AF in whom anti-arrhythmic medications had been withheld for 72 h prior to ablation. During the procedure, carried out at the Stanford University Hospital, Palo Alto, CA, ablation acutely terminated persistent AF to sinus rhythm. The study was approved by the IRB.

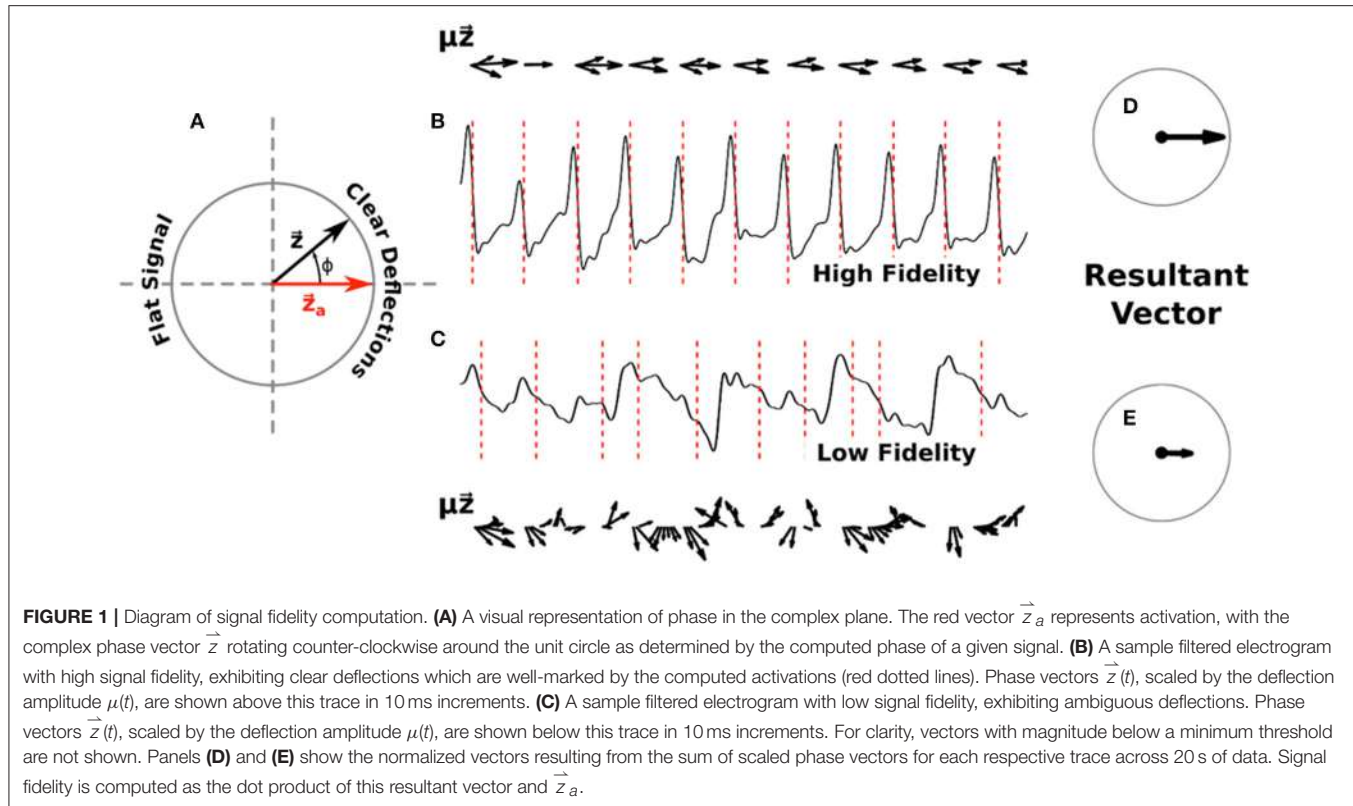
Quality of electrogram signals in AF was determined using a signal fidelity measure developed below, from which the majority of electrograms signals were of high quality with few contaminants. Electrograms spanning a time interval of 20 s, corresponding to over 400 cycles of AF, are analyzed. QRS contamination is removed from each signal by subtracting the average QRS complex from the electrode signal at each R wave. All traces are filtered with a 1.5–25 Hz Butterworth bandpass filter.

In order to allow for computation of phase maps from these signals we use a technique, recently proposed by Kuklik et al. (Kuklik et al., 2015, 2016), of sinusoidally recomposing the signals before applying the Hilbert Transform. In contrast to some other techniques, this technique is published and publicly available (<http://narayanlab.stanford.edu>). This technique has been compared to distinct mapping methods, and shows rotational activity in AF at similar sites, including sites of termination of persistent AF by ablation (Alhusseini et al., 2017). Briefly, the dominant cycle length of each electrogram is computed as that with largest power between 130 and 280 ms in the Welch spectral density estimate of the signal (window size = 2,000 ms, overlap = 1,000 ms). A recomposed signal is then computed as a sum of single-period sinusoidal waves, with period corresponding to the dominant cycle length and with amplitude corresponding to the deflection amplitude of the signal ($-dV/dt$, with positive deflections set to zero). To obtain spatial maps of the activation patterns, we apply the Hilbert Transform (Gray et al., 1998; Bray et al., 2001; Umapathy et al., 2010) to compute complex analytic signals which are interpolated in space and used to determine instantaneous phase. All spatial maps in this study are interpolated using linear interpolation to a grid with 225×225 points.

Signal Fidelity

We defined a measure of signal fidelity to determine the faithfulness of phase maps to underlying electrograms. Let us represent the computed phase $\phi(t)$ of a given signal as a complex phase vector $\vec{z}(t) = e^{i\phi(t)}$ with each activation occurring as this vector passes the positive real axis, denoted as \vec{z}_a . This unit vector can be visualized as a counterclockwise rotating vector, as depicted in **Figure 1A**.

To define a time-averaged signal fidelity, Γ , for each electrogram we note that signals which exhibit high fidelity should have distinct negative deflections, i.e., large $-dV/dt$, at the times when \vec{z} is near an activation \vec{z}_a , and should have minimal deflections otherwise. Conversely, signals with low fidelity might exhibit ambiguous deflections occurring when \vec{z} is not near \vec{z}_a , or could have small negative deflections around \vec{z}_a . Thus, we can



define

$$\Gamma = \left[\frac{\sum_t \mu(t) \vec{z}(t)}{\sum_t \mu(t)} \right] \cdot \vec{z}_a = \frac{\sum_t \mu(t) \cos \phi(t)}{\sum_t \mu(t)} \quad (1)$$

where μ is equal to the magnitude of the derivative of the signal if it is negative (i.e., $\mu = |-\text{d}V/\text{dt}|$) and zero otherwise, and where the sum is over the entire time interval. This fidelity ranges from -1 to $+1$, with larger values corresponding to easily interpretable and high fidelity signals and smaller values indicating low fidelity signals with relatively indistinct deflections.

In **Figures 1B,C** we show example computations of the signal fidelity measure across multiple deflections for two sample electrograms, one with high fidelity ($\Gamma = 0.90$) and one with low fidelity ($\Gamma = 0.43$). These electrograms were taken from a 67 years old female patient with a left atrial size of 55 mm and a left ventricular ejection fraction of 36%. On the top/bottom of these signals we show the weighted vectors $\mu \vec{z}$ from Equation (1) in increments of 10 ms. Summing up all of these vectors for the entire trace and normalizing gives us the resultant vectors shown in **Figures 1D,E**. Signal fidelity is then the dot product of this resultant vector and \vec{z}_a .

All of the vectors \vec{z} in the high fidelity trace occurring at or near activations also exhibit large deflections μ , with vectors \vec{z} occurring away from activations exhibiting small or non-negative deflections. The sum in Equation (1), therefore,

is taken over coherent vectors pointing mostly along the real axis resulting in a high fidelity measure. In the low fidelity trace, however, many vectors \vec{z} occurring at phases different from activation also exhibit large deflections. The origin of these large deflections at times different from activation are currently not clear but may include far-field effects, structural heterogeneities, and motion artifacts. The sum of these incoherent vectors, which can vary in direction as well as amplitude, results in a smaller resultant vector indicating a lower fidelity measure.

Tip Density

To quantify rotational dynamics we compute phase singularities (PS) on our phase maps using a standard approach (Gray et al., 1998; Bray et al., 2001; Umapathy et al., 2010), corresponding to the location of spiral wave tips, and determine the mean total number of tips N . Further, we can define phase singularity maps which quantify the amount of clockwise, $\Omega_{\text{CW}}(t)$, and counter-clockwise rotation, $\Omega_{\text{CCW}}(t)$, such that $\Omega = 1$ if there is a phase singularity of the given chirality within a distance of 28 interpolated grid points of each location, and $\Omega = 0$ otherwise. Note that this distance is slightly smaller than the spacing of one electrode. Because we are primarily interested in stable, rather than transient, rotational patterns, we compute the density of spiral tips over time as

$$\delta \stackrel{\text{def}}{=} \frac{1}{T} \sum_t [\Omega_{\text{CW}}(t) - \Omega_{\text{CCW}}(t)], \quad (2)$$

where T is the total duration of the signal. This density ranges from -1 to $+1$, with larger positive (negative) values indicating a region of tissue which experienced consistent clockwise (counter-clockwise) rotation for a significant portion of the episode. In addition, for each chirality we can then use k-means clustering, via MATLAB function k-means, to determine the largest spatial cluster of PS locations.

Signal Contamination

In this study, we investigated three potential sources of signal contamination in AF recordings: (1) Non-viable data due to signal saturation, (2) reduced signal quality due to poor electrode contact, and (3) false deflections from far-field activity. We quantified the effects of these sources on the mean tip number and tip density using a large number of random trials, further specified below.

First, we randomly removed signals from our recordings to simulate saturated data. This is motivated by clinical observations of electrogram data in which revealed that $>5\text{--}10\%$ of electrode sides may exhibit poor quality electrograms. Possible causes for loss of quality include poor size match of the basket with intermittent contact [which we circumvent clinically using matched basket sizes and multiple positions (Zaman et al., 2017)], electrical interference such as contact with an ablation electrode causing saturation, or other factors.

Along each affected spline, linear interpolation/extrapolation of recomposed signals was used to account for electrodes with no data and we quantify the corresponding effect as a function of the number of removed signals. Second, to determine the effects of incorrect cycle length determination due to poor signal quality we add independent normally distributed noise with standard deviation σ to the computed dominant cycle lengths of each electrogram. Third, we choose a single region of raw electrogram signal exhibiting a clear deflection to use as a surrogate deflection for far-field activity. Such far-field activity might arise from structural heterogeneities, including differences in wall thickness. This surrogate deflection is added at random times to the raw electrograms, being sure not to overlap surrogates. The amplitude of these deflections is set to some constant multiplied with the standard deviation of the filtered signal. Both the constant and number of deflections are varied.

RESULTS

Signal Fidelity

We first examine the signal fidelity map of AF for the patient whose electrograms are shown in **Figure 1**. This map shows two distinct domains of fidelity values, with a majority of the tissue exhibiting large values of fidelity and a minority exhibiting low values of fidelity (**Figure 2A**). The corresponding tip density map for this episode is shown in **Figure 2B**, where regions of elevated positive or negative values of density correlate well with visually-observed rotational activity in animations

of phase maps (see **Supplementary Video**). Particularly, the region of peak CCW rotation in these tip density maps, shown in dark blue, corresponds to the site where ablation terminated AF in this patient. The peak magnitude of CW and CCW tip densities are 0.36 and 0.43, respectively. Due to the spatial meander of the computed phase singularities, as reported in our earlier clinical reports (Narayan et al., 2012a, 2013) and in animal studies (Zlochiver et al., 2008), the tip density map shows spatially extended regions for both CW and CCW rotational activity. Interestingly, the region of elevated tip density also coincided with low values of fidelity.

With our method of computing signal fidelity we can quantify the expected faithfulness of signals to the underlying conduction. Signals which have low fidelity, then, can be discarded and interpolated over if desired. A convenient method of partitioning our signals into groups of either high or low fidelity uses k-means clustering, an iterative algorithm which clusters observations into N groups with similar values (Hartigan, 1975). We demonstrate this in **Figure 2C**, where we use k-means clustering on all values of signal fidelity to partition each signal into one of two groups. This separates our recordings into a domain of signals with high fidelity ($n = 44$) and those with low fidelity ($n = 20$). The signals marked by k-means as belonging to the low fidelity group are discarded. As outlined in Methods, discarded signals are accounted for through interpolation/extrapolation of recomposed signals along each spline. This removal of poor quality signals, in this case potentially due to fractionation expected at the core of rotational activity (Nademanee et al., 2004), results in a significant increase in the magnitudes of CW and CCW tip densities to 0.61 and 0.94, respectively.

Two additional patients in whom ablation acutely terminated persistent AF to sinus rhythm are presented in **Figures 2D–H**. One patient, a 66 years old gentleman, had a left atrial size of 47 mm and a left ventricular ejection fraction of 59%. Computing phase maps and phase singularities revealed a region of elevated CCW tip density as shown by the blue area in the **Figure 2D**. The location of this CCW rotor coincided with the ablation target which converted AF to sinus rhythm. As in the patient of **Figures 2A–C**, this region also coincided with low values of fidelity (**Figure 2E**) and removing electrodes with small values of fidelity (in this case the $n = 16$ electrodes for which $\Gamma < 0.5$) increased the tip density (**Figure 2F**). In this case, however, the increase was modest (approximately 10%).

The other additional patient was a 49 years old gentleman with a left atrial size of 53 mm and a left ventricular ejection fraction of 51%. The phase density maps reveal a more complex pattern with a clear CCW and several CW rotors (**Figure 2G**). Again, the location of these elevated regions of rotation correlate well with regions of low fidelity (**Figure 2H**). Furthermore, the location of the CW rotation (red) corresponds with the site of ablation that terminated AF to sinus rhythm. Likely due to the complexity of the pattern, removal of electrodes was not successful in increasing the phase singularity density.

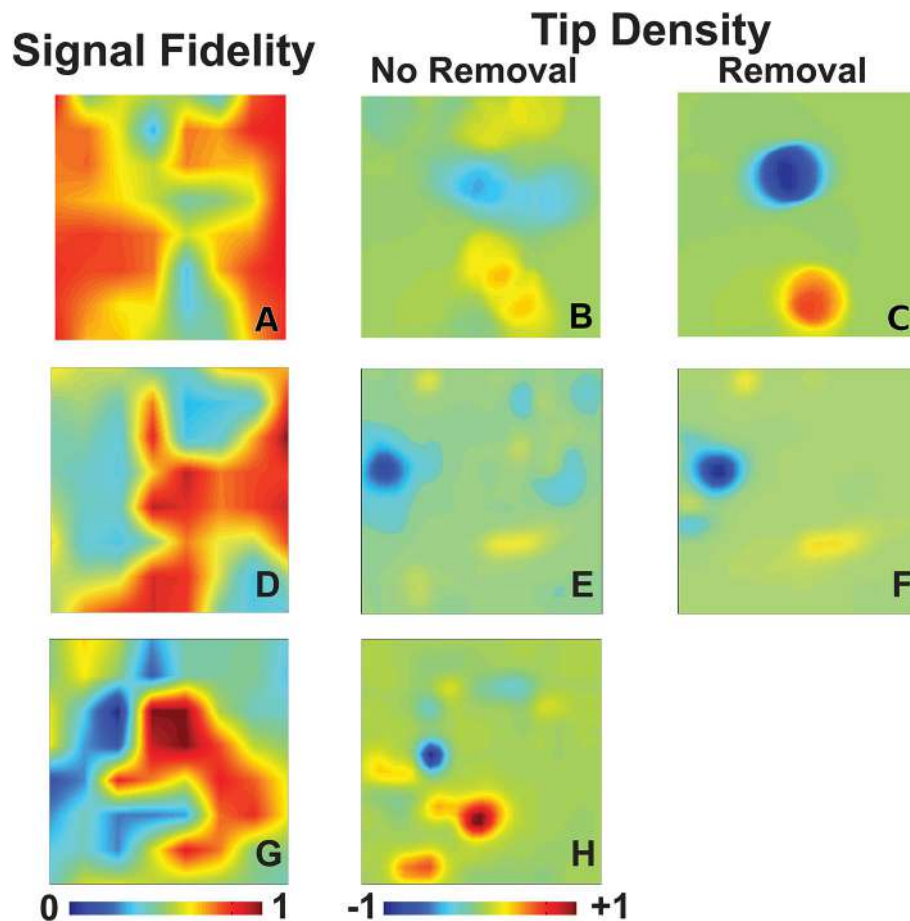


FIGURE 2 | Signal fidelity in patients during AF. **(A–C)** Signal fidelity map **(A)** for an episode of human AF corresponding to the electrograms shown in **Figure 1** (67 years-old female patient). The corresponding tip density map, with clockwise rotations in red and counter-clockwise rotations in blue, and tip density map after k-means removal, and interpolation over, electrogram recordings with low fidelity are shown in **(B)** and **(C)**, respectively. High values of tip density show concordance with domains of low fidelity. The magnitude of maximum tip density around the termination site (blue peak) was 0.43. The magnitude of maximum tip density around the termination site increases significantly to 0.94. **(D–F)** Signal fidelity map **(D)**, tip density map **(E)**, and tip density map after removal of low fidelity electrodes **(F)** corresponding to an episode of human AF of a 66 years old male patient. **(G–H)** Signal fidelity map for an episode of human AF of a 49 years old male patient **(G)** and the corresponding tip density map **(H)**.

Effect of Non-viable Signals

Next we examined the impact of various sources of contamination on the ability to identify rotational activity in phase maps, taking the patient corresponding to **Figures 2A–C** as an example. We first removed signals at random from our grid, leaving at least two electrodes on any spline since complete loss of a spline is rare, to simulate saturation rendering some signals non-interpretable. In **Figure 3A** we plot the peak tip density δ around the termination site, as well as the mean tip number N in **Figure 3B**, as a function of the number of removed signals. Both of these plots are normalized to their respective values when no electrodes have been removed and are computed as the mean result over 200 random trials. **Figure 3A** shows that as more and more electrodes are randomly removed, the magnitude of tip density first increases, then reaches a plateau. In **Figure 3B**, mean tip number, however, continually decreases as we increase the number of removed electrodes across our entire

range. Note that for both figures the standard deviation equals 0 for $N_{cut} = 0$ and becomes larger when the number of randomly removed electrodes is increased.

In addition to determining the effect on the phase maps, we also examined the accuracy of interpolating over removed signals. To do this we removed between 1 and 5 signals along each spline and interpolate across these signals. This was repeated for each permutation of removed electrodes along each spline. We then compared the resulting phase from this interpolated signal $\phi(t)$ to the phase from the original removed signal $\phi_0(t)$ to determine how well our interpolated phase matches with the original phase.

To quantify concordance we computed time-averaged dot product of the interpolated phase vector \vec{z} with the original phase vector \vec{z}_0 . This dot product ranges from -1 to 1 , with large positive values implying very similar phase progression and

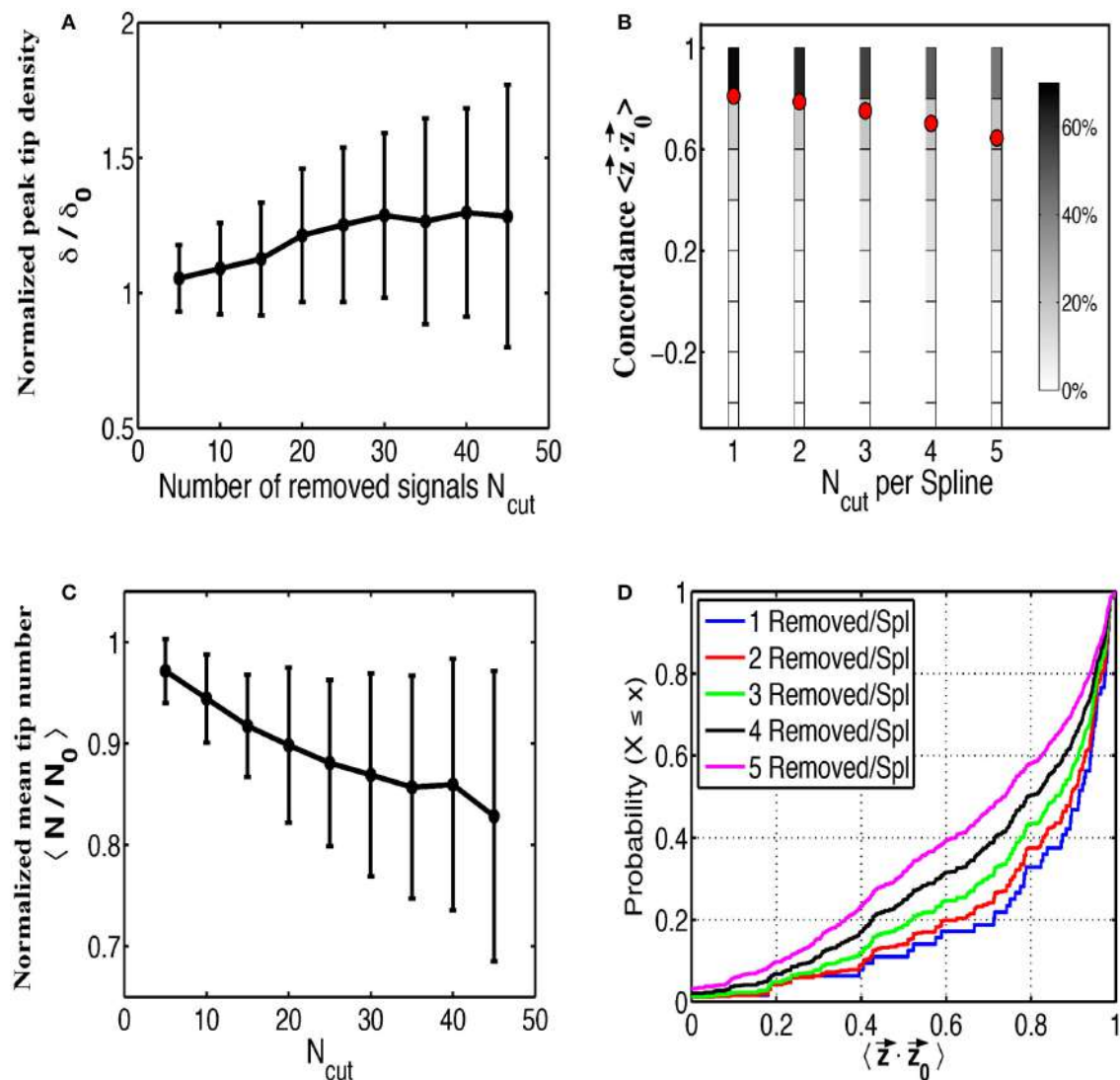


FIGURE 3 | The effects of random removal of electrodes. Normalized plots of peak tip density around the site of termination (A), and mean number of tips (B), as a function of the number of electrodes removed are shown for 200 trials. Error bars show standard deviation. Electrodes are then systematically removed per spline and the concordance between the interpolated phase vectors \vec{z} and the original phase vectors \vec{z}_0 is shown as multiple histograms in (C), with red dots marking the mean, and as cumulative distribution functions in (D).

negative values corresponding to an interpolated phase that is, on average, out of phase with the original phase. The results of this procedure over all permutations and for all number of removed electrodes, are shown in Figure 3C as multiple histograms with red dots denoting the average. This plot demonstrates that interpolation shows relatively high concordance with the missing data, particularly if fewer electrodes are missing per spline. With increasing number of removed electrodes per spline, the distribution of concordance values becomes less peaked near unity implying a greater chance that interpolated phase poorly represents the underlying missing data. Cumulative distribution functions for each number of removed electrodes per spline are shown in Figure 3D for a more precise comparison of the concordance distributions.

Effect of Varying Cycle Length

A critical part in the sinusoidal reconstruction of our underlying signal is the estimation of the dominant cycle length. To examine the possibility of poor quality recordings resulting in inaccurate cycle lengths, we add a noise term to each computed value of dominant cycle length before reconstructing the signals. We set a minimum cycle length of 50 ms to ensure that this never results in a negative cycle length. The results of this process as a function of the standard deviation σ of our normally-distributed noise term are shown in Figure 4. As the standard deviation of our noise term increased, tip density at the termination site decreased and the total number of tips increases. This effect was further examined in Figure 4C, where we systematically added values from -150

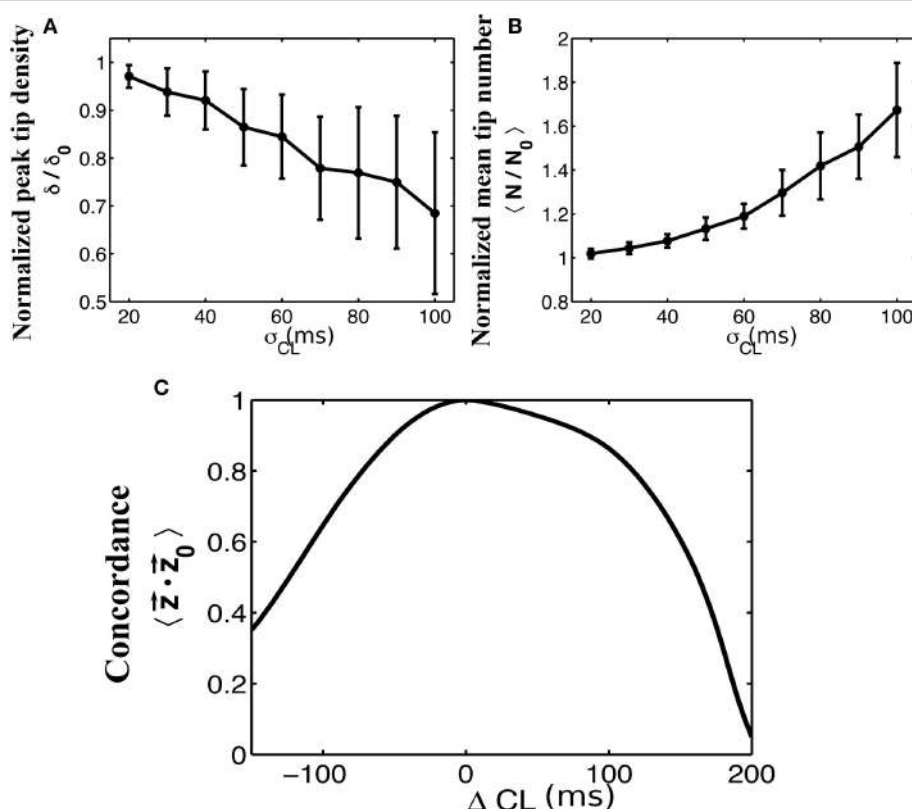


FIGURE 4 | The effects of adding normally distributed noise to the dominant cycle length. Normalized plots of peak tip density around the site of termination **(A)**, and mean number of tips **(B)**, as a function of the standard deviation of noise added to the dominant cycle lengths are shown for 50 trials. Error bars show standard deviation. A minimum cycle length of 50 ms is used throughout all trials. **(C)** Mean concordance between the resulting phase vectors \vec{z} and the original phase vectors \vec{z}_0 after systematically adding values between -150 and 200 to the originally determined cycle lengths.

to 200 to each computed dominant cycle length. Again, we measured the resulting average concordance between phase vectors \vec{z} resulting from these altered cycle lengths and the original phase vectors \vec{z}_0 .

Effect of Far-Field Contamination

To evaluate the effects of far-field contamination we add surrogate deflections at random to the raw electrograms, as is shown in **Figures 5A,B**, and compute phase maps. The resulting tip density and tip number are shown as heatmaps in **Figure 5** for different deflection amplitudes (0.5–5.0 times the standard deviation of the filtered signal, increments of 0.5) and different percentages of altered signal (5–50% signal altered, increments of 5%). **Figure 5C** shows that for large values of both frequency and amplitude of far field deflections, the tip density at the termination site decreases to less than half its original value. Similarly, **Figure 5D** shows that in this same domain the mean tip number increases by a factor of three, implying that far-field deflections can cause an increase in false detection of transient rotational activity.

DISCUSSION

In this study we set out to quantify the impact of variations in signal fidelity and the effects of electrogram contamination on mapping human AF to identify potential rotational drivers. Using recordings from patients in whom ablation at a site of stable rotational activity terminated persistent AF, we generated phase maps using a validated, non-proprietary method. Systematic addition of contamination and other perturbations revealed two main findings. First, sites of stable rotational activity in the animated phase maps corresponded to regions of low signal fidelity. Second, we found that observed rotational activity in AF was relatively robust to both removing signals at random and to altering dominant cycle lengths, whereas it was sensitive to the addition of surrogate far-field deflections. These findings have implications for future improvements in AF mapping, which may help to improve ablation targeting and patient outcomes.

Signal Fidelity at Rotor Core Sites

The concept that electrograms at rotational cores should exhibit unique characteristics has been proposed in many different forms, whether through complex fractionation (CFAE) (Nademanee et al., 2004), larger values of Shannon entropy in

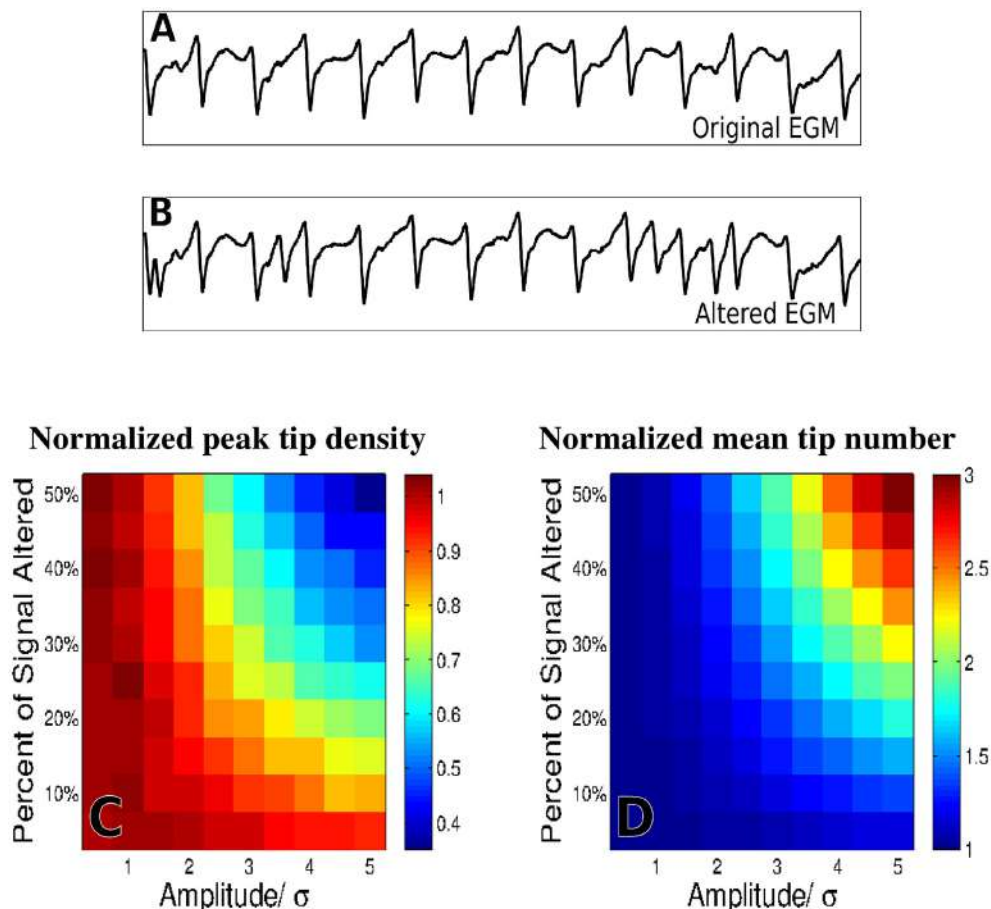


FIGURE 5 | The effects of adding false deflections to electrograms. A sample EGM before adding false deflections **(A)** and after altering 30% of the signal with deflections of amplitude/σ = 3 **(B)**. Normalized heat maps of peak tip density around the site of termination **(C)**, and mean number of tips **(D)**, as a function of both amplitude and frequency of added deflections are shown for 50 trials.

bipolar electrograms (Ganesan et al., 2013), or higher dominant frequency (Zlochiver et al., 2008). While recent studies reported difficulty in finding distinguishing characteristics in electrograms at sites of rotational activity (Narayan et al., 2013; Benharash et al., 2015), this study shows that such sites may be identified by our proposed metric of electrogram signal fidelity. Our measure of signal fidelity, which quantifies how distinct the deflections of an electrogram are from their baseline, may be able to identify spiral wave cores. Although the precise reason for this observed lower fidelity is not clear, we postulate that increased tip meander and reduced electrogram amplitudes may contribute to more irregular electrograms. Studies are ongoing to validate this finding and to pinpoint the responsible mechanism in larger series in our Institutions.

The developed measure of signal fidelity may enable the targeted removal of signals which are difficult to mark, using information from high fidelity neighboring electrodes to infer their value. As a result of the removal of the electrodes near the spiral tip, electrodes that capture the spiral arms define the activation pattern, potentially improving spiral wave identification. Using a clustering algorithm, such as k-means, or

removing electrodes with a lower fidelity than a certain threshold, this can be automated. In this study, the k-means removal of low fidelity recordings significantly increased peak tip density while the removal of 25% of electrodes, corresponding to those with the lowest fidelity, resulted in a modest increase in peak tip density. These possibly surprising findings are important because it implies that the original regions of elevated tip density were not a result of the low fidelity recordings (implying false positive tip detection), but rather that elevated tip density may have been a direct result of large-domain rotational circuits surrounding low fidelity regions. Thus, the low signal fidelity observed may be a result of rotational activity, as suggested theoretically (Pandit and Jalife, 2013) and consistent with recent reports which estimated the required spatial resolution for rotational activity (Rappel and Narayan, 2013).

Insensitivity of Mapping Rotational Activity to Signal “Dropout”

Observed rotational activity in this study was relatively robust to both removing signals at random and to altering dominant

cycle lengths, yet sensitive to the addition of surrogate far-field deflections. These results are summarized in **Figures 3–5**, where we ran multiple trials adding in these contaminants at random for the patient corresponding to **Figures 2A–C**. Of note, by removing signals at random and interpolating over the missing signals the tip density at the termination site actually increases. This is true even when removing over half of the signals present. Again, this suggests that observed rotational activity is not due to a small handful of signals but is rather an emergent behavior of the system as a whole. Removing any given electrode did not appear to have a significant impact, and in fact removing certain low-fidelity electrodes, as previously discussed, improved the detection of rotational activity. Whether this finding is generalizable will likely depend on the spatial domain of rotational circuits, because small domain rotations spanning only a handful of electrodes may be easily obscured by electrogram removal. Moreover, as more electrodes are removed, their interpolation becomes less reliable as is shown in **Figures 3C,D**.

Far-Field Contamination Degraded AF Mapping

Of the three means of signal contamination explored in this study, observed rotational activity was most degraded by far-field deflections. This is due to the ambiguity introduced when a given method attempts to mark the phase of an electrogram with multiple peaks and complex morphologies. During AF, signals have been shown to exhibit such complex morphologies as well as deflections due to far-field activity (Narayan et al., 2011). While some methods explicitly attempt to filter out these far-field effects (Gray et al., 1995), it is often difficult to distinguish far-field from near-field activity in electrograms. Innovations in accurately computing the phase of complex electrograms with significant far-field contamination could lead to more accurate phase maps, particularly in cases with sub-optimal electrode contact.

In addition, it should be possible to further investigate the effect of signal contamination and fidelity using computational studies. Such studies, successfully applied to investigate multiple aspects of activation mapping (Aslanidi et al., 2011; Gonzales et al., 2014; Labarthe et al., 2014; McDowell et al., 2015; Rappel et al., 2015; Boyle et al., 2018), can address questions not easily accessible in clinical studies, including questions regarding spatial heterogeneities, wave front collisions, and spatial resolution (Rappel and Narayan, 2013; Roney et al., 2017). We are currently planning to use computational studies to address these questions.

REFERENCES

- Alhusseini, M., Vidmar, D., Meckler, G. L., Kowalewski, C. A., Shenasa, F., Rappel, P. J., et al. (2017). Two independent mapping techniques identify rotational activity patterns at sites of local termination during persistent atrial fibrillation. *J. Cardiovasc. Electrophysiol.* 28, 615–622. doi: 10.1111/jce.13177

Limitations

The current study has several limitations. First, it has been argued that rotational sources identified with phase maps can be artificial and due to chance (Kuklik et al., 2016). While transient rotational activity can arise in phase maps, rotational activity observed in AF in this study occurred intermittently throughout the entire 20 s duration, with conserved chirality and spatial location, which is extremely unlikely due to chance. Moreover, clinical intervention (ablation) at the rotational site terminated persistent AF, supporting a mechanistic role in perpetuating the fibrillatory state. Second, we analyzed AF from a limited number of patients since the study was designed to develop a fidelity measure to quantify which signal contaminants most affect stable rotational activity in an index case with high quality electrograms and few contaminants. While we cannot generalize from this computational study to all specific signal contaminants, our prior work in larger series shows similar characteristics at sites of termination of persistent AF (Alhusseini et al., 2017; Kowalewski et al., 2018; Zaman et al., 2018). We are planning a systematic analysis of episodes in more patients, with varying degrees of signal complexity.

AUTHOR CONTRIBUTIONS

DV and W-JR conceived the study. SN collected the data. Model construction was performed by DV, MA, and W-JR. Data analysis was performed by DV and MA. The manuscript was written by DV, SN, and W-JR. All authors reviewed and approved the manuscript.

FUNDING

This work was supported in part by the National Institutes of Health R01 HL122384 (W-JR), R01 HL83359 (SN), K24 103800 (SN) and the American Heart Association 16PRE30930015 (DV).

SUPPLEMENTARY MATERIAL

The Supplementary Material for this article can be found online at: <https://www.frontiersin.org/articles/10.3389/fphys.2018.01232/full#supplementary-material>

Supplementary Video | Animated phase maps of AF for 4 seconds of data. Color scales from 0 (blue) to 2π (red), with primary phase singularities marked with a green dot (CCW) or blue dot (CW) as chosen by K-means clustering. Targeted ablation at the CCW rotational pattern resulted in AF termination.

- Aslanidi, O. V., Colman, M. A., Stott, J., Dobrzynski, H., Boyett, M. R., Zhang, H., et al. (2011). 3D virtual human atria: a computational platform for studying clinical atrial fibrillation. *Prog. Biophys. Mol. Biol.* 107, 156–168. doi: 10.1016/j.pbiomolbio.2011.06.011
- Baykaner, T., Rogers, A. J., Meckler, G. L., Zaman, J. A., Navara, R., Heidenreich, P. A., et al. (2018). Clinical Implications of ablation of drivers

- for atrial fibrillation: a systematic review and meta-analysis. *Circ. Arrhythm. Electrophysiol.* 11:e006119. doi: 10.1161/CIRCEP.117.006119
- Benharash, P., Buch, E., Frank, P., Share, M., Tung, R., Shirkumar, K., et al. (2015). Quantitative analysis of localized sources identified by focal impulse and rotor modulation mapping in atrial fibrillation. *Circ. Arrhythm. Electrophysiol.* 8, 554–561. doi: 10.1161/CIRCEP.115.002721
- Boyle, P. M., Hakim, J. B., Zahid, S., Franceschi, W. H., Murphy, M. J., Jais, P., et al. (2018). Comparing reentrant drivers predicted by image-based computational modeling and mapped by electrocardiographic imaging in persistent atrial fibrillation. *Front. Physiol.* 9:414. doi: 10.3389/fphys.2018.00414
- Bray, M. A., Lin, S. F., Aliev, R. R., Roth, B. J., and Wikswo, J. P. (2001). Experimental and theoretical analysis of phase singularity dynamics in cardiac tissue. *J. Cardiovasc. Electrophysiol.* 12, 716–722. doi: 10.1046/j.1540-8167.2001.00716.x
- Chugh, S. S., Havmoeller, R., Narayanan, K., Singh, D., Rienstra, M., Benjamin, E., et al. (2014). Worldwide epidemiology of atrial fibrillation: a global burden of disease 2010 study. *Circulation* 129, 837–847. doi: 10.1161/CIRCULATIONAHA.113.005119
- Daoud, E. G., Zeidan, Z., Hummel, J. D., Weiss, R., Houmssse, M., Kalbfleisch, S. J., et al. (2017). Identification of repetitive activation patterns using novel computational analysis of multielectrode recordings during atrial fibrillation and flutter in humans. *JACC Clin. Electrophysiol.* 3, 207–216. doi: 10.1016/j.jacep.2016.08.001
- Ganesan, A. N., Kuklik, P., Lau, D. H., Brooks, A. G., Baumert, M., Sanders, P., et al. (2013). Bipolar electrogram shannon entropy at sites of rotational activation: implications for ablation of atrial fibrillation. *Circ. Arrhythm. Electrophysiol.* 6, 48–57. doi: 10.1161/CIRCEP.112.976654
- Gonzales, M. J., Vincent, K. P., Rappel, W. J., Narayan, S. M., and McCulloch, A. D. (2014). Structural contributions to fibrillatory rotors in a patient-derived computational model of the atria. *Europace* 16, iv3–iv10. doi: 10.1093/europace/euu251
- Grace, A., Verma, A., and Willems, S. (2017). Dipole density mapping of atrial fibrillation. *Eur. Heart J.* 38, 5–9. doi: 10.1093/eurheartj/ehw585
- Gray, R. A., Jalife, J., Panfilov, A. V., Baxter, W. T., Cabo, C., Pertsov, A. M., et al. (1995). Mechanisms of cardiac fibrillation. *Science* 270, 1222–1223; author reply 1224–1225.
- Gray, R. A., Pertsov, A. M., and Jalife, J. (1998). Spatial and temporal organization during cardiac fibrillation. *Nature* 392, 75–78. doi: 10.1038/32164
- Haissaguerre, M., Hocini, M., Denis, A., Shah, A. J., Komatsu, Y., Dubois, R., et al. (2014). Driver domains in persistent atrial fibrillation. *Circulation* 130, 530–538. doi: 10.1161/CIRCULATIONAHA.113.005421
- Hartigan, J. A. (1975). *Clustering Algorithms*. New York, NY: Wiley.
- January, C. T., Wann, L. S., Alpert, J. S., Calkins, H., Cleveland, J. C., Yancy, C. W., et al. (2014). 2014 AHA/ACC/HRS guideline for the management of patients with atrial fibrillation: a report of the American College of Cardiology/American Heart Association Task Force on practice guidelines and the Heart Rhythm Society. *Circulation* 130, 2071–2104. doi: 10.1161/CIR.000000000000040
- Kowalewski, C. A. B., Rodrigo, M., Klopton, P., Shenasa, F., Meckler, G. L., Narayan, S. M., et al. (2018). Interaction of localized drivers and disorganized activation coexist in persistent AF? Reconciling putative mechanisms using multiple mapping techniques. *Circ. Arrhythm. Electrophysiol.* 11:e005846. doi: 10.1161/CIRCEP.117.005846
- Krummen, D. E., Hayase, J., Morris, D. J., Ho, J., Smetak, M. R., Narayan, S. M., et al. (2014). Rotor stability separates sustained ventricular fibrillation from self-terminating episodes in humans. *J. Am. Coll. Cardiol.* 63, 2712–2721. doi: 10.1016/j.jacc.2014.03.037
- Krummen, D. E., Hayase, J., Vampola, S. P., Ho, G., Schricker, A. A., Narayan, S. M., et al. (2015). Modifying ventricular fibrillation by targeted rotor substrate ablation: proof-of-concept from experimental studies to clinical VF. *J. Cardiovasc. Electrophysiol.* 26, 1117–1126. doi: 10.1111/jce.12753
- Kuklik, P., Zeemering, S., Maesen, B., Maessen, J., Crijns, H. J., Schotten, U., et al. (2015). Reconstruction of instantaneous phase of unipolar atrial contact electrogram using a concept of sinusoidal recombination and Hilbert transform. *IEEE Trans. Biomed. Eng.* 62, 296–302. doi: 10.1109/TBME.2014.2350029
- Kuklik, P., Zeemering, S., van Hunnik, A., Maesen, B., Pison, L., Lau, D., et al. (2016). Identification of rotors during human atrial fibrillation using contact mapping and phase singularity detection: technical considerations. *IEEE Trans. Biomed. Eng.* 64, 310–318. doi: 10.1109/TBME.2016.2554660
- Labarthe, S., Bayer, J., Coudière, Y., Henry, J., Cochet, H., Jaïs, P., et al. (2014). A bilayer model of human atria: mathematical background, construction, and assessment. *Europace* 16, iv21–iv29. doi: 10.1093/europace/euu256
- Mandapati, R., Skanes, A., Chen, J., Berenfeld, O., and Jalife, J. (2000). Stable microreentrant sources as a mechanism of atrial fibrillation in the isolated sheep heart. *Circulation* 101, 194–199. doi: 10.1161/01.CIR.101.2.194
- McDowell, K. S., Zahid, S., Vadakkumpadan, F., Blauer, J., MacLeod, R. S., and Trayanova, N. A. (2015). Virtual electrophysiological study of atrial fibrillation in fibrotic remodeling. *PLoS ONE* 10:e0117110. doi: 10.1371/journal.pone.0117110
- Miller, J. M., Kalra, V., Das, M. K., Jain, R., Garlie, J. B., Dandamudi, G., et al. (2017). Clinical benefit of ablating localized sources for human atrial fibrillation: the Indiana University FIRM registry. *J. Am. Coll. Cardiol.* 69, 1247–1256. doi: 10.1016/j.jacc.2016.11.079
- Nademanee, K., McKenzie, J., Kosar, E., Schwab, M., Sunsaneewitayakul, B., Vasavakul, T., et al. (2004). A new approach for catheter ablation of atrial fibrillation: mapping of the electrophysiologic substrate. *J. Am. Coll. Cardiol.* 43, 2044–2053. doi: 10.1016/j.jacc.2003.12.054
- Narayan, S. M., Krummen, D. E., Enyeart, M. W., and Rappel, W. J. (2012a). Computational mapping identifies localized mechanisms for ablation of atrial fibrillation. *PLoS ONE* 7:e46034. doi: 10.1371/journal.pone.0046034
- Narayan, S. M., Krummen, D. E., and Rappel, W. J. (2012b). Clinical mapping approach to diagnose electrical rotors and focal impulse sources for human atrial fibrillation. *J. Cardiovasc. Electrophysiol.* 23, 447–454. doi: 10.1111/j.1540-8167.2012.02332.x
- Narayan, S. M., Krummen, D. E., Shivkumar, K., Clopton, P., Rappel, W. J., and Miller, J. M. (2012c). Treatment of atrial fibrillation by the ablation of localized sources: CONFIRM (conventional ablation for atrial fibrillation with or without focal impulse and rotor modulation) trial. *J. Am. Coll. Cardiol.* 60, 628–636. doi: 10.1016/j.jacc.2012.05.022
- Narayan, S. M., Shivkumar, K., Krummen, D. E., Miller, J. M., and Rappel, W. J. (2013). Panoramic electrophysiological mapping but not electrogram morphology identifies stable sources for human atrial fibrillation: stable atrial fibrillation rotors and focal sources relate poorly to fractionated electrograms. *Circ. Arrhythm. Electrophysiol.* 6, 58–67. doi: 10.1161/CIRCEP.111.977264
- Narayan, S. M., Wright, M., Derval, N., Jadidi, A., Forclaz, A., Nault, I., et al. (2011). Classifying fractionated electrograms in human atrial fibrillation using monophasic action potentials and activation mapping: evidence for localized drivers, rate acceleration and non-local signal etiologies. *Heart Rhythm* 8, 244–253. doi: 10.1016/j.hrthm.2010.10.020
- Nattel, S., Xiong, F., and Aguilar, M. (2017). Demystifying rotors and their place in clinical translation of atrial fibrillation mechanisms. *Nat. Rev. Cardiol.* 14, 509–520. doi: 10.1038/nrcardio.2017.37
- Nichol, G., Thomas, E., Callaway, C. W., Hedges, J., Powell, J. L., Stiell, I., et al. (2008). Regional variation in out-of-hospital cardiac arrest incidence and outcome. *JAMA* 300, 1423–1431. doi: 10.1001/jama.300.12.1423
- Pandit, S. V., and Jalife, J. (2013). Rotors and the dynamics of cardiac fibrillation. *Circ. Res.* 112, 849–862. doi: 10.1161/CIRCRESAHA.111.300158
- Parameswaran, R., Voskoboinik, A., Gorelik, A., Lee, G., Kistler, P. M., Kalman, J. M., et al. (2018). Clinical impact of rotor ablation in atrial fibrillation: a systematic review. *Europace* 20, 1099–1106. doi: 10.1093/europace/eux370
- Ramanathan, C., Ghanem, R. N., Jia, P., Ryu, K., and Rudy, Y. (2004). Noninvasive electrocardiographic imaging for cardiac electrophysiology and arrhythmia. *Nat. Med.* 10, 422–428. doi: 10.1038/nm1011
- Ramirez, F. D., Birnie, D. H., Nair, G. M., Szczotka, A., Redpath, C. J., Nery, P. B., et al. (2017). Efficacy and safety of driver-guided catheter ablation for atrial fibrillation: a systematic review and meta-analysis. *J. Cardiovasc. Electrophysiol.* 28, 1371–1378. doi: 10.1111/jce.13313
- Rappel, W.-J., and Narayan, S. M. (2013). Theoretical considerations for mapping activation in human cardiac fibrillation. *Chaos* 23:023113. doi: 10.1063/1.4807098
- Rappel, W. J., Zaman, J. A., and Narayan, S. M. (2015). Mechanisms for the termination of atrial fibrillation by localized ablation: computational and clinical studies. *Circ. Arrhythm. Electrophysiol.* 8, 1325–1333. doi: 10.1161/CIRCEP.115.002956

- Roney, C. H., Cantwell, C. D., Bayer, J. D., Qureshi, N. A., Lim, P. B., Ng, F. S., et al. (2017). Spatial resolution requirements for accurate identification of drivers of atrial fibrillation. *Circ. Arrhythm. Electrophysiol.* 10:e004899. doi: 10.1161/CIRCEP.116.004899
- Sommer, P., Kircher, S., Rolf, S., John, S., Arya, A., Dinov, B., et al. (2016). Successful repeat catheter ablation of recurrent longstanding persistent atrial fibrillation with rotor elimination as the procedural endpoint: a case series. *J. Cardiovasc. Electrophysiol.* 27, 274–280. doi: 10.1111/jce.12874
- Spitzer, S. G., Károlyi, L., Rämmler, C., Scharfe, F., Weinmann, T., Zieschank, M., et al. (2017). Treatment of recurrent nonparoxysmal atrial fibrillation using focal impulse and rotor mapping (FIRM)-guided rotor ablation: early recurrence and long-term outcomes. *J. Cardiovasc. Electrophysiol.* 28, 31–38. doi: 10.1111/jce.13110
- Tracy, C. M., Epstein, A. E., Darbar, D., DiMarco, J. P., Dunbar, S. B., Link, M. S., et al. (2012). 2012 ACCF/AHA/HRS focused update of the 2008 guidelines for device-based therapy of cardiac rhythm abnormalities: a report of the American College of Cardiology Foundation/American Heart Association Task Force on practice guidelines. *J. Thorac. Cardiovasc. Surg.* 144, e127–e145. doi: 10.1016/j.jtcvs.2012.08.032
- Umapathy, K., Nair, K., Masse, S., Krishnan, S., Rogers, J., Nash, M., et al. (2010). Phase mapping of cardiac fibrillation. *Circ. Arrhythm. Electrophysiol.* 3, 105–114. doi: 10.1161/CIRCEP.110.853804
- Zaman, J. A., Baykaner, T., Clopton, P., Swarup, V., Kowal, R. C., Krummen, D. E., et al. (2017). Recurrent post-ablation paroxysmal atrial fibrillation shares substrates with persistent atrial fibrillation: an 11-center study. *JACC Clin. Electrophysiol.* 3, 393–402. doi: 10.1016/j.jacep.2016.10.006
- Zaman, J. A. B., Sauer, W. H., Alhusseini, M. I., Baykaner, T., Borne, R. T., Viswanathan, M. N., et al. (2018). Identification and characterization of sites where persistent atrial fibrillation is terminated by localized ablation. *Circ. Arrhythm. Electrophysiol.* 11:e005258. doi: 10.1161/CIRCEP.117.005258
- Zlochiver, S., Yamazaki, M., Kalifa, J., and Berenfeld, O. (2008). Rotor meandering contributes to irregularity in electrograms during atrial fibrillation. *Heart Rhythm* 5, 846–854. doi: 10.1016/j.hrthm.2008.03.010

Conflict of Interest Statement: W-JR and SN are coauthors of intellectual property owned by the University of California Regents, licensed to Abbott. W-JR and DV have filed patent applications related to the identification of fibrillation sources. SN received honoraria from Medtronic and St. Jude Medical.

The reviewer MS and handling Editor declared their shared affiliation at the time of the review.

The remaining author declares that the research was conducted in the absence of any commercial or financial relationships that could be construed as a potential conflict of interest.

Copyright © 2018 Vidmar, Alhusseini, Narayan and Rappel. This is an open-access article distributed under the terms of the Creative Commons Attribution License (CC BY). The use, distribution or reproduction in other forums is permitted, provided the original author(s) and the copyright owner(s) are credited and that the original publication in this journal is cited, in accordance with accepted academic practice. No use, distribution or reproduction is permitted which does not comply with these terms.



Description of the Human Atrial Action Potential Derived From a Single, Congruent Data Source: Novel Computational Models for Integrated Experimental-Numerical Study of Atrial Arrhythmia Mechanisms

Michael A. Colman^{1*}, Priyanka Saxena², Sarah Kettlewell² and Antony J. Workman²

OPEN ACCESS

Edited by:

Oleg Aslanidi,
King's College London,
United Kingdom

Reviewed by:

Yael Yaniv,
Technion – Israel Institute
of Technology, Israel
Eleonora Grandi,
University of California, Davis,
United States

*Correspondence:

Michael A. Colman
m.a.colman@leeds.ac.uk

Specialty section:

This article was submitted to
Computational Physiology
and Medicine,
a section of the journal
Frontiers in Physiology

Received: 03 May 2018

Accepted: 13 August 2018

Published: 07 September 2018

Citation:

Colman MA, Saxena P, Kettlewell S
and Workman AJ (2018) Description
of the Human Atrial Action Potential
Derived From a Single, Congruent
Data Source: Novel Computational
Models for Integrated
Experimental-Numerical Study of
Atrial Arrhythmia Mechanisms.
Front. Physiol. 9:1211.
doi: 10.3389/fphys.2018.01211

¹ Leeds Computational Physiology Lab, School of Biomedical Sciences, University of Leeds, Leeds, United Kingdom,

² Institute of Cardiovascular and Medical Sciences, College of Medical, Veterinary and Life Sciences, University of Glasgow, Glasgow, United Kingdom

Introduction: The development of improved diagnosis, management, and treatment strategies for human atrial fibrillation (AF) is a significant and important challenge in order to improve quality of life for millions and reduce the substantial social-economic costs of the condition. As a complex condition demonstrating high variability and relation to other cardiac conditions, the study of AF requires approaches from multiple disciplines including single-cell experimental electrophysiology and computational modeling. Models of human atrial cells are less well parameterized than those of the human ventricle or other mammal species, largely due to the inherent challenges in patch clamping human atrial cells. Such challenges include, frequently, unphysiologically depolarized resting potentials and thus injection of a compensatory hyperpolarizing current, as well as detecting certain ion currents which may be disrupted by the cell isolation process. The aim of this study was to develop a laboratory specific model of human atrial electrophysiology which reproduces exactly the conditions of isolated-cell experiments, including testing of multiple experimental interventions.

Methods: Formulations for the primary ion currents characterized by isolated-cell experiments in the Workman laboratory were fit directly to voltage-clamp data; the fast sodium-current was parameterized based on experiments relating resting membrane potential to maximal action potential upstroke velocity; compensatory hyperpolarizing current was included as a constant applied current. These formulations were integrated with three independent human atrial cell models to provide a family of novel models. Extrapolated intact-cell models were developed through removal of the hyperpolarizing current and introduction of terminal repolarization potassium currents.

Results: The isolated-cell models quantitatively reproduced experimentally measured properties of excitation in both control and pharmacological and dynamic-clamp interventions. Comparison of isolated and intact-cell models highlighted the importance

of reproducing this cellular environment when comparing experimental and simulation data.

Conclusion: We have developed a laboratory specific model of the human atrial cell which directly reproduces the experimental isolated-cell conditions and captures human atrial excitation properties. The model may be particularly useful for directly relating model to experiment, and offers a complementary tool to the available set of human atrial cell models with specific advantages resulting from the congruent input data source.

Keywords: atrial fibrillation, human atrial model, ion channel currents, computational model, action potential

INTRODUCTION

The incidence of atrial fibrillation (AF) is growing in epidemic proportions (Ceornodolea et al., 2017): the current prevalence of 2% in western countries is more than double that of over a decade ago (Zoni-Berisso et al., 2014) and its association with aging has led to projections of significant increase in the next few decades (Krijthe et al., 2013). AF increases the risk of death, mainly as a consequence of the associated four to fivefold increased risk of stroke, and results in significant costs to worldwide healthcare systems (Casajuana et al., 2018). Presently available treatment strategies are far from ideal: pharmacological intervention has sub-optimal efficacy in patients, and also risks adverse effects in certain patient groups; catheter ablation is invasive and may require repeated procedures (Kirchhof et al., 2016; Kirchhof and Calkins, 2017). The development of improved diagnosis, management, and treatment strategies for AF is therefore a significant and important challenge in order to improve quality of life for millions and reduce the substantial socio-economic costs of the condition.

The mechanisms driving the sustained rapid and irregular excitation during AF are controlled partly at the cellular level by the non-linear interactions of multiple ion currents underlying the action potential (AP), and thus these currents also influence the impact of pharmacological or surgical interventions. It is therefore vital to fully characterize the dynamics of these ion currents. Compounding the problem, expression and kinetics of these currents can be highly variable (e.g., Lawson et al., 2018), are modified by autonomic control (e.g., Chen and Tan, 2007; Workman, 2010), and can remodel in the long-term presence of AF (e.g., Workman et al., 2001); excitation dynamics at the tissue-scale may also be highly non-linear and unpredictable from single-cell studies alone (e.g., Colman et al., 2017b). It is therefore a significant challenge to comprehensively quantify the role of ion currents (and their variation, modulation, and remodeling) in the mechanisms of atrial arrhythmia.

Computational modeling has proved to be an increasingly valuable tool to assess and dissect the impact of ion channel function and anatomical structure on normal and arrhythmic human atrial electrical dynamics (Colman et al., 2014; Trayanova, 2014; Heijman et al., 2016): the number of simulation studies has significantly increased over the last decade and there are currently multiple contemporary models of the human atrial AP and calcium handling available (e.g., Courtemanche et al., 1998;

Nygren et al., 1998; Malekar et al., 2009; Grandi et al., 2011; Koivumäki et al., 2011; Colman et al., 2013). Despite the successes of simulation studies, human atrial cell models are in general less well parameterized than ventricular cell models, and they still rely on model components formulated on data from different sources, cell-types, and even species (Wilhelms et al., 2013); integration of components from different sources is non-trivial and often requires enforced parameter modification. Even integration of human atrial specific data from multiple sources is non-trivial due to the challenges of obtaining reliable data (Nattel, 2006), including substantial inter-patient, inter-isolate, and inter-cell variability. Also, subtle inter-laboratory differences, as well as variations in operative techniques and concomitant therapies, may influence the outcome of experiments in major ways, making multi-center studies challenging and providing uncertainty in the combination of mathematical descriptions based on data from multiple laboratories. Moreover, the recent trend has been toward introducing more components and additional complexity and sophistication; whereas this has proved useful in teasing apart ionic contributions to health and disease, it nevertheless provides more potential sources of error and reliance on a larger set of unknowns and/or *ad hoc* parameters. There is therefore motivation to derive a computational model based on human atrial data with the fewest non-specific additional components, and also specifically on data from a single source (i.e., consistent cell source and experimental environment and protocols).

There are numerous further challenges in obtaining reliable experimental data for developing a human atrial-specific cell model. These include inherent difficulties in acquiring human atrial tissues and acutely isolating cardiomyocytes from them, since they cannot be arterially perfused with enzymes. The “chunk technique” (Yue et al., 1996), in which small chunks of tissue are superfused with enzymes, is used to overcome this problem, but also has recognized limitations including potential disruption of ion currents such as the delayed rectifier potassium currents I_{Kr} and/or I_{Ks} (Yue et al., 1996; Workman et al., 2006), relatively low cell yield, and often an unphysiologically depolarized resting membrane potential (RMP; Escande et al., 1987; Bénarreau et al., 1996; Van Wagoner et al., 1999; Dobrev et al., 2001; Workman et al., 2006) to the extent that the fast sodium current (I_{Na}) may be unavailable. RMP depolarization can be mitigated in various ways, none without limitations, including injecting a constant background (hyperpolarizing) current during recording, as used routinely in the Workman

laboratory (WL). This method permits full repolarization of the AP and thus I_{Na} availability, but must be used sparingly and with caution; see Workman et al. (2006) for details. Computational models of atrial cells therefore do not necessarily directly translate to the isolated-cell experiments on which they are validated and which they themselves inform. There is therefore also motivation to develop a cell model which reproduces specifically the conditions of isolated whole-cell-patch current- and voltage-clamp experiments, for full congruence between experimental and simulation studies.

The aim of this study was to develop a human atrial isolated- and intact-cell model based primarily on specific human atrial cellular data from the WL, with motivation to introduce the fewest additional components from other sources. The model was tested for its ability to reproduce experimental observations for AP properties and their modulation by pharmacological and dynamic-clamp interventions. Furthermore, the descriptions of the set of the primary currents were integrated with contemporary human atrial cell models to provide a novel set of modified cell models, and used to assess the importance of the isolated-cell environment in AP morphology and response to various interventions. The resulting models therefore form a complementary tool to the available set of human atrial cell models, providing both a minimal approach with the emphasis on congruent input data which allows direct interaction between simulation and experiment, and a family of cell models suitable for mechanistic evaluation of atrial arrhythmias.

MATERIALS AND METHODS

In this study, novel formulations of the primary ion currents underlying human atrial electrophysiology and characterized in the WL were developed (sections “Isolated-Cell Experiments” and “Ion Current Formulations”). The formulations were integrated with multiple contemporary human atrial cell models, including both isolated- and intact-cell variants (section “Computational models”). The Courtemanche et al. (1998) model (hAM_CRN), Nygren et al. (1998) model (Nygren-Giles, hAM_NG), and Grandi et al. (2011) [Grandi-Bers, hAM_GB – specifically, the implementation of Chang et al. (2014)] were selected as these represent the baseline cell models underlying the primary distinct lines of human atrial cell model development [not including spatial cell models such as Koivumäki et al. (2011) and Voigt et al. (2014)]. Full model equations and parameters are provided in the **Supplementary Material** and model code in C/C++ is available from the GitHub repository¹.

Isolated-Cell Experiments

Isolated-cell experiments described pertain to both previously published and unpublished data characterizing the primary human atrial ion currents: fast sodium current (I_{Na}); transient-outward current (I_{to}); L-type calcium current (I_{CaL}); ultra-rapid, or sustained, potassium current ($I_{Kur/sus}$); and the time-independent potassium current (I_{K1}); as well as additional

intracellular calcium concentration ($[Ca^{2+}]_i$) data associated with the calcium transient (CaT).

A summary of the experimental conditions associated with each study is provided in **Table 1** and described briefly. Right atrial tissues were obtained from consenting patients undergoing cardiac surgery between 1999 and 2018. All patients were in sinus rhythm unless otherwise stated, and were taking a variety of drug treatments as detailed in the following publications. The whole-cell patch clamp technique and fluorescence microscopy were used to record ion currents, APs, effective refractory period (ERP), and intracellular Ca^{2+} concentration ($[Ca^{2+}]_i$), at 35–37°C, in the absence and presence of a variety of drugs, from atrial myocytes enzymatically isolated from these tissues. Procedures were approved by the West of Scotland Research Ethics Service (REC 99MC002 and REC 17/WS/0134). The chunk method of cell isolation used is detailed in Workman et al. (2001), and all the experimental conditions, patch-clamp configurations, recording protocols, and solutions used, are included in Workman et al. (2006, 2012) and Marshall et al. (2012). Specific data on individual ion currents, APs, or ERP are derived from the following WL published sources: APs, current magnitudes, and ERP: Workman et al. (2001, 2006) (referred to in short as WL_2001; WL_2006); I_{K1} : Marshall et al. (2012) (referred to as WL_2012_IK1); I_{to} and I_{sus} : Workman et al. (2012) (WL_2012_ITO); I_{CaL} : Pau et al. (2007) (WL_2007_ICAL). WL_2006 was considered the most representative collective data and was therefore used to set the relative magnitudes of the currents in the computational models.

I_{Na} data were derived using recent unpublished data obtained from human atrial isolated myocytes (by Priyanka Saxena in the WL) on the relationship between current-clamped RMP and AP phase 0 maximum upstroke velocity (dV/dt_{max}) as a surrogate for the voltage-dependence of I_{Na} (which cannot be directly measured accurately) in these cells. $[Ca^{2+}]_i$ data (unpublished) were recently recorded in human atrial isolated myocytes (by Sarah Kettlewell in the WL), using identical techniques to those employed earlier in rabbit atrial myocytes in this laboratory (Kettlewell et al., 2013).

Only specific data on the ion currents were used to derive the mathematical model; AP, excitation, and intervention data were used for validation and comparison only, and not to further train the model.

Ion Current Formulations

Workman-Laboratory Characterized Currents: I_{K1} and I_{hyp}

The current–voltage (IV) relationship for the time-independent current, I_{K1} , was considered from both WL_2012_IK1 [Figure 1A(i)] and WL_2006 [Figure 1A(ii)], where the former data correspond to Ba^{2+} -sensitive specific I_{K1} , and the latter may more accurately refer to a general voltage-dependent, time-independent current. Integrating the formulation of the current from WL_2012_IK1 with the background currents of the selected baseline human atrial cell models led to maintained RMP of below -70 mV in all models. The apparent reversal in the WL_2006 data and formulation of approximately -40 mV [Figure 1A(ii)] was necessary to result in the unphysiologically

¹https://github.com/michaelcolman/hAM_WL

depolarized RMP of isolated-cells. These formulations were therefore suitable for use in the intact- and isolated-cell models, respectively, and are thus referred as I_{K1}^{intact} (WL_2012_IK1 data) and $I_{K1}^{isolated}$ (WL_2006 data) for clarity. The IV relationship associated with I_{K1} in the primary, independent human atrial cell models is shown for reference in the I_{K1}^{intact} panel [Figure 1A(i)].

The relationship between RMP and the magnitude of the hyperpolarizing current (I_{hyp}) for isolated-cell models with three different magnitudes of I_{K1} (0.5, 1, and $2 \times$ maximum of -4 pA/pF at -120 mV; Workman et al., 2006) demonstrates hyperpolarizing currents of 0.4 – 1.4 pA/pF were necessary for maintaining a RMP of ~ -80 mV [Figure 1A(iii)], congruent with the magnitude of current used and reported in the isolated-cell experiments. An I_{hyp} of 0.63 pA/pF was used with the default scaling of I_{K1} for the baseline cell model, giving a

RMP of -82 mV when integrated with the hAM_CRN calcium handling system and background currents. This value of I_{hyp} closely matched that reported in experiments, e.g., 0.62 pA/pF (Workman et al., 2006). This value also maintained a RMP of ~ -80 mV when combined with the background currents and calcium handling system in the hAM_NG (-75 mV) and hAM_GB (-80 mV) models. To ensure consistent conditions between models, this value of I_{hyp} was maintained rather than imposing identical RMP.

Workman-Laboratory Characterized Currents: I_{to} and I_{sus}

The formulations for the transient-outward (I_{to}) and sustained/ultra-rapid potassium (I_{sus}/I_{Kur}) currents were derived from the voltage-clamp (100 ms pulse in 10 mV steps from -50 to 70 mV) data from WL_2012_ITO.

TABLE 1 | Control experimental conditions used for human atrial cell electrophysiological recordings, including intra- and extra-cellular ionic constituents, $[Ca^{2+}]_i$ -buffering and temperature (all closely matching and within mammalian physiological ranges), recording configurations and measurements taken.

Study	WL_2001 (Workman et al., 2001)	WL_2006 (Workman et al., 2006)	WL_2007_ICAL (Pau et al., 2007)	WL_2012_IK1 (Marshall et al., 2012)	WL_2012_ITO (Workman et al., 2012)
Intracellular solution constituents (mM, pH)	L-aspartate (110), KCl (20), $MgCl_2$ (1.0), EGTA (0.15), Na_2ATP (4.0), Na_2GTP (0.4), HEPES (5.0), pH 7.3	For ruptured-patch: K-aspartate (110), KCl (20), $MgCl_2$ (1.0), EGTA (0.15), Na_2ATP (4.0), Na_2GTP (0.4), HEPES (5.0), nystatin (0.18); pH 7.3 For perforated-patch: KCl (30), HEPES (5.0), $MgCl_2$ (1.0), K methane-sulfonic acid (100), $NaCl$ (5.0); pH 7.3	KCl (30), HEPES (5), $MgCl_2$ (1), K methane-sulfonic acid (100), $NaCl$ (5), nystatin (0.18); pH 7.3	K-aspartate (110), KCl (20), $MgCl_2$ (1.0), EGTA (0.15), Na_2ATP (4.0), Na_2GTP (0.4), HEPES (5.0); pH 7.3	K-aspartate (130), KCl (15), $NaCl$ (10), $MgCl_2$ (1), HEPES (10), EGTA (0.1); pH 7.3
Extracellular solution constituents (mM, pH)	NaCl (130), KCl (4.0), $CaCl_2$ (2.0), $MgCl_2$ (1.0), glucose (10), HEPES (10), pH 7.4	NaCl (130), KCl (4.0), $CaCl_2$ (2.0), $MgCl_2$ (1.0), glucose (10), HEPES (10); pH 7.4	NaCl (130), KCl (4.0), $CaCl_2$ (2.0), $MgCl_2$ (1.0), glucose (10), HEPES (10); pH 7.4	NaCl (130), KCl (4.0), $CaCl_2$ (2.0), $MgCl_2$ (1.0), glucose (10), HEPES (10); pH 7.4	NaCl (140), KCl (4.0), $CaCl_2$ (1.8), $MgCl_2$ (1.0), glucose (11), HEPES (10); pH 7.4
LLJP correction	Yes	Yes	Yes	Yes	Yes
Recording temperature	35–37°C	35–37°C	35–37°C	35–37°C	35–37°C
$[Ca^{2+}]_i$ -buffering	Minimal (0.15 mM EGTA)	Minimal (0.15 mM EGTA for ruptured-patch; zero EGTA for perforated-patch)	Minimal (zero EGTA as perforated-patch)	Minimal (0.15 mM EGTA)	Minimal (0.10 mM EGTA)
Cell isolation enzyme	Collagenase (Type 1, Worthington, 400 U/ml)	Collagenase (Type 1, Worthington, 400 U/ml)	Collagenase (Type 1, Worthington, 400 U/ml)	Collagenase (Type 1, Worthington, 400 U/ml)	Collagenase (Type 1, Worthington, 400 U/ml)
Patch configuration	Ruptured patch	Ruptured patch Nystatin-perforated patch	Nystatin-perforated patch	Ruptured patch	Ruptured patch
Patch-clamp amplifier	Axopatch-1D (Axon)	Axopatch-1D (Axon)	Axopatch-1D (Axon)	Axopatch-1D (Axon)	AxoClamp 2B (Axon)
Recording configuration	Current-clamp Voltage-clamp	Current-clamp Voltage-clamp	Current-clamp Voltage-clamp	Voltage-clamp	Current-clamp Voltage-clamp Dynamic-clamp
Measurements	APs, ERP, I_{CaL} , I_{to} , I_{K1} , I_{sus}	APs, ERP, I_{CaL} , I_{to} , I_{K1} , I_{sus}	APs, ERP, I_{CaL}	I_{to} , I_{K1} , I_{sus}	APs, I_{to}

LLJP, liquid-liquid junction potential; AP, action potential; ERP, cellular effective refractory period; I_{CaL} , L-type Ca^{2+} current; I_{to} , transient outward K^+ current; I_{K1} , inward rectifier K^+ current; I_{sus} , sustained outward K^+ current (mainly I_{Kur}).

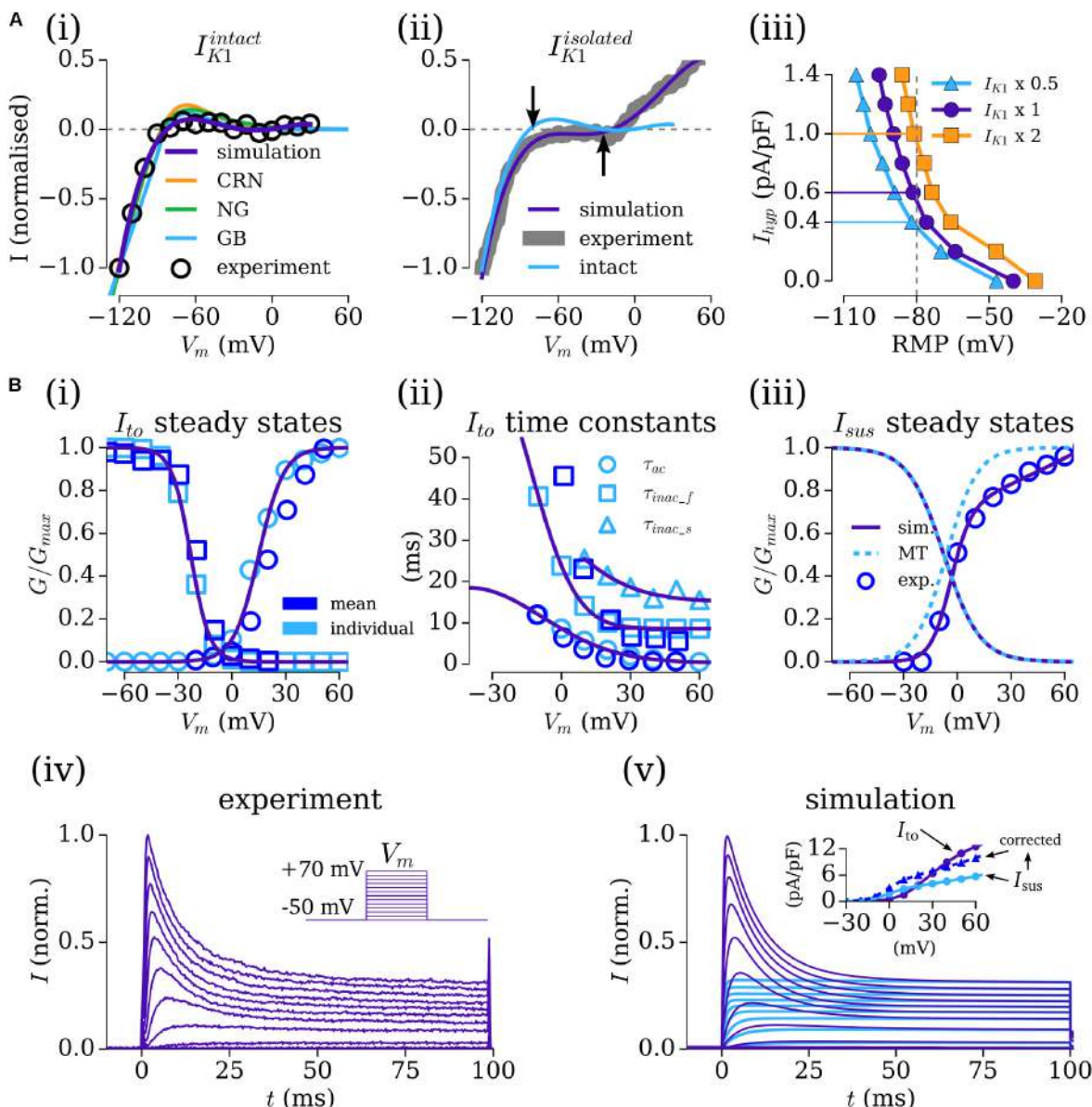
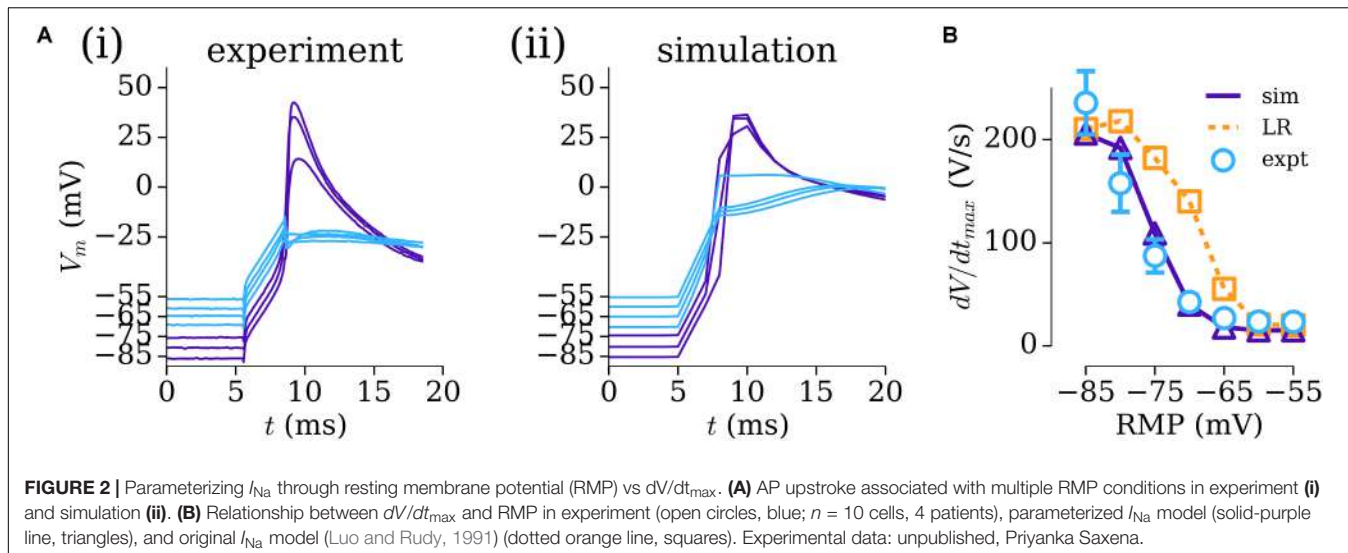


FIGURE 1 | Fitting the Workman-lab K⁺ characterized currents. **(A)** Fitting I_{K1} and the hyperpolarizing current (I_{hyp}). **(i)** I_{K1} measured in the WL_2012_IK1 study [Marshall et al., 2012], considered “intact” (black circles) and simulation fits from the new formulations (purple) and the three human atrial models [orange – CRN(Courtemanche et al., 1998); green – NG (Nygren et al., 1998); blue – GB (Grandi et al., 2011)]. **(ii)** I_{K1} measured in the WL_2006 (Workman et al., 2006) study, considered “isolated” (gray) and model fit (purple). The form of the “intact” current is shown for reference, with arrows indicating the difference in reversal between the intact and isolated variants. **(iii)** Relationship between resting membrane Potential (RMP) and I_{hyp} at three different amplitudes of I_{K1} ^{isolated} (baseline – closed circles, purple; $I_{K1} \times 2$ – closed squares, orange; $I_{K1} \times 0.5$ – closed triangles, blue). **(B,i-iii)** Fitting of the gating variable parameters for I_{to} and I_{sus} to the voltage-clamp data of WL_2012_ITO (Workman et al., 2012) **(iv)** and resulting simulated current traces **(v)** and IV relationship (inset). Open, light blue symbols refer to values calculated from fitting to individual current traces. Open, dark blue symbols refer to mean current data from WL_2012_ITO (Workman et al., 2012). The formulation from Maleckar et al. (2009) is shown for reference in panel **iii**. In the inset for panel **iv**, I_{to} is shown in purple, I_{sus} in light blue, and corrected I_{sus} in dark blue. Figure created using data from: Workman et al. (2006, 2012) and Marshall et al. (2012).

The baseline formulation for I_{to} was the same as that presented in the original study. The baseline formulation for I_{sus} was taken from Maleckar et al. (2009), derived on human atrial cell data. First, the maximum conductances (g_{to} , g_{sus}) were set to give the appropriate magnitude current at the +70 mV clamp step (where each channel

is considered to be fully activated). Then, each current was fit to individual, representative experimental current traces [using a least-squares optimization algorithm implemented in Python (Python Software Foundation²)]

²<https://www.python.org/>



to provide steady-state and time constant values for the activation and inactivation gates at each voltage step, optimized for the numerical solution of the governing equations. The voltage dependence functions describing the steady-states and time constants were then fit to a combination of these values (from a single experiment) and the mean measured values from all experiments [Figures 1B(i-iii)], producing current traces from a combined I_{to} - I_{sus} voltage-clamp which match well to experiment [Figures 1B(iv,v)].

The conductance parameters were adjusted to reflect the data described in WL_2006 (Workman et al., 2006); setting g_{to} , the maximal conductance of I_{to} , to 0.103 nS/pF gave a peak current of 12.5 pA/pF at +60 mV; the proportionally set maximal conductance of 0.040 nS/pF for I_{sus} gave a peak current of 5.17 pA/pF, below the value of 10.6 ± 0.8 pA/pF described in the data. Therefore, a corrected I_{sus} maximal conductance of 0.068 μ S/pF was set to reflect these data [Figure 1B(v-inset)].

Parameterizing the Fast Sodium Current, I_{Na}

To overcome the challenge of characterizing the voltage-dependence of I_{Na} , previously unpublished human atrial experimental data (from Priyanka Saxena in the WL) relating the RMP to dV/dt_{max} were used to modify the parameters of the formulation for I_{Na} originally presented by Luo and Rudy, 1991 and used as the baseline in multiple contemporary AP models including those of the human atria (Courtemanche et al., 1998; Grandi et al., 2011). These experimental data were obtained using the same patch-clamp amplifier (chosen for its accurate voltage-following) and recording solutions (including accurate liquid–liquid junction potential correction) as in WL_2012_ITO (Workman et al., 2012) and dV/dt_{max} measured using WinWCP software (John Dempster). Re-parameterization of this formulation to the data resulted in good agreement between experiment and simulation in the AP upstroke [Figures 2A(i,ii)] and dependence of

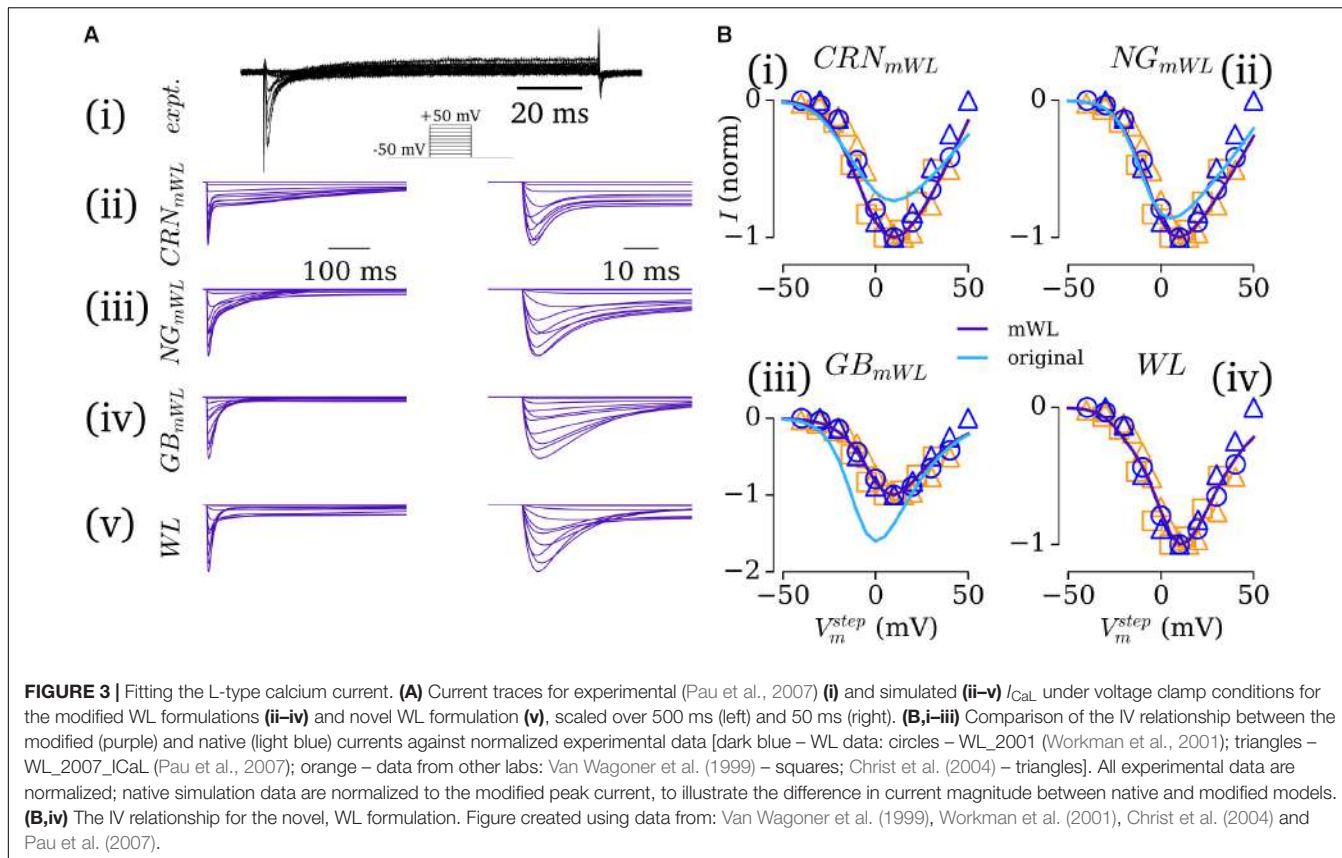
dV/dt_{max} on RMP (Figure 2B), which was significantly different to that observed with the original, ventricular formulation (Figure 2B).

Workman-Laboratory Characterized Currents: I_{CaL}

The L-type calcium current, I_{CaL} , presents a larger challenge to model than the previous currents described due to its tight coupling with the intracellular calcium handling system: the current is responsible for initiating intracellular calcium-induced-calcium-release (CICR) and also has implicit calcium-induced inactivation gating. Detailed electrophysiological data for the human-atrial calcium handling system, and calcium-induced inactivation of I_{CaL} , are limited (with notable exceptions, e.g., Voigt et al., 2014), and there is limited CaT data available from the WL. Therefore, the formulation for I_{CaL} was considered in conjunction with the computational models of the calcium-handling system implemented. Each of the three selected models (hAM_CRN; hAM_NG; hAM_GB; see sections “Materials and Methods” and “Computational Models”) contain different descriptions of CICR and calcium-induced inactivation of I_{CaL} , and model stability and homeostasis can be sensitive to these components.

In the first instance, the native formulations of I_{CaL} in each of these models was retained, with only the voltage dependence being modified to fit the experimental IV relationship presented in WL_2007_ICAL and WL_2001 (Figure 3), and the maximum conductance set to give a peak current of -5 pA/pF, as reported in WL_2006. Models implementing these formulations of I_{CaL} are referred to as the modified-WL models (see section “Computational Models”).

In the second instance, a new formulation for I_{CaL} was developed which more closely reproduces the time-course of the experimentally measured current [Figure 3A(i)] and was suitable for implementation with both the hAM_CRN and hAM_GB calcium handling systems. The hAM_NG



calcium handling system was not used for this purpose due to its sensitivity to changes in I_{CaL} and unphysiological CaT magnitude and morphology. The novel formulation implemented the dynamic conductance of I_{CaL} of hAM_GB, and was designed to work with both the differing calcium-induced inactivation formulations and CaT time-course associated with each model. This was achieved through first fitting the current formulations (comprising voltage-induced activation and inactivation only) to the voltage clamp data of WL_2007_ICaL, using the same approach as I_{to}/I_{sus} (see section “Workman-Laboratory Characterized Currents: I_{to} and I_{sus} ”). Then, the equations were modified to account for calcium-induced inactivation, with priority on maintaining uniformity in behavior between implementation with each calcium-handling system [Figures 3A(v),B(iv)]. This was the formulation used for the full WL models (see section “Computational Models”).

Computational Models

A family of human atrial cell models is presented which incorporate the formulations for the ion currents described above. First, a minimal approach was used to develop novel models of the isolated-cell human atrial AP: the novel formulations for I_{Na} , I_{to} , I_{sus} , I_{CaL} , I_{K1}^{isolated} , and I_{hyp} were integrated with the intracellular calcium handling models associated with hAM_CRN and hAM_GB (see section “Workman-Laboratory Characterized Currents: I_{CaL} ”); the

additional membrane current components necessary for intracellular homeostasis (and unquestionably present in human atrial myocytes; I_{NaCa} , I_{NaK} , I_{CaP} , I_{Cab} , I_{Nab}) were introduced using the formulations associated with each calcium handling system. Implementation with the hAM_GB model also retained additional background currents (I_{Kb} , I_{Clb}) and other components (I_{ClCa}). These models, fit as completely as possible to the experimental observations of the WL, are referred to as hAM_WL_{CRN}^{isolated} and hAM_WL_{GB}^{isolated}. Intact-cell variants of these models (hAM_WL_{CRN}^{intact}, hAM_WL_{GB}^{intact}) were derived by removal of I_{hyp} , replacing I_{K1}^{isolated} with I_{K1}^{intact} , and then minimally introducing I_{Kr} and I_{Ks} as necessary (see section “Intact-Cell Model”) to maintain physiological human atrial AP duration.

Second, the selected human atrial cell models were modified to reproduce the isolated-cell experimental environments and incorporate the novel ion current formulations: isolated-cell modifications (hAM_X^{isolated}) were implemented by the introduction of the new formulation for I_{K1}^{isolated} and I_{hyp} , and setting the conductances of I_{Kr} and I_{Ks} to zero. Modified cell models (hAM_X_{mWL}), for both isolated and intact-cells, were implemented by replacing the native formulations of I_{Na} , I_{to} , I_{sus} , and I_{K1} with the novel formulations presented, and the formulation of I_{CaL} with the modified variants associated with each calcium handling system (see section “Workman-Laboratory Characterized Currents: I_{CaL} ”). Thus, the present study considers the following models: the three hAM_CRN,

hAM_NG and hAM_GB as originally presented; the two novel presented WL based models (hAM_WL_{CRN/GB}); and the three modified WL models (hAM_CRN/NG/GB_{mWL}); all with isolated an intact variants.

Action potentials were initiated using a train of applied stimuli of magnitude -13.5 pA/pF for 3 ms. All models were paced to stable-state before results were obtained, with a minimum of 200 s pre-pacing stimuli.

RESULTS

Isolated-Cell Model Characteristics and Validation

The time-courses of the AP for the five novel model variants all exhibit very similar morphologies [Figure 4A(i)]; the differences in morphology observed are primarily a result of either the different I_{CaL} formulations (see section “Workman-Laboratory Characterized Currents: $ICaL$ ”), calcium-induced inactivation dependent on the CaT morphology, or the interaction with calcium-handling currents such as I_{NCX} . Comparison between the model and experimental APs shows good agreement in duration and morphology with the typical WL AP, exhibiting the low and triangular-like plateau morphology [Figures 4A(ii,iii)]. APD restitution also matches well with experimental data from WL_2001 [Figure 4B(i)], which is in general shorter than the data presented by other groups (Franz et al., 1997; Bosch et al., 1999). The different model variants exhibited different rate dependence of the MDP, with all but the hAM_NG_{mWL} model closely matching the experimental data [Figure 4B(ii)]. Comparison of APD₉₀ and dv/dt_{max} between model and experiment (WL_2001 and WL_2006) at 75 BPM showed all of the models exhibit properties close to the experimental value, with variation in dv/dt_{max} between the models being larger than that for the APD₉₀. This is a result of the different RMPs maintained by the consistent hyperpolarizing current.

The intracellular CaT exhibited large differences between model variants dependent on the underlying calcium handling system [Figure 4C(i)]: the hAM_NG_{mWL} model retained the very rapid and large amplitude spike associated with the NG model; the CRN and GB variants (WL and modified) exhibited more prolonged CaTs within the physiologically expected amplitude range (~ 0.4 – 0.5 μ M). The CRN model variants most closely reproduced the time-course of the CaT [Figure 4C(ii)]; the GB model variants exhibited a similar morphology but with a delayed onset. The GB model variants reproduced the diastolic and peak values most closely compared to mean experimental data [Figure 4C(iii)].

Interventions

The five novel model variants (novel WL with CRN/GB calcium handling; CRN/NG/GB WL-modified models) were compared against experimental data from the WL under the application of various pharmacological or dynamic-clamp intervention. The role of I_{to} was assessed through comparison to the dynamic-clamp data of WL_2012_ITO [Figure 5A(i)]: the magnitude of I_{to}

was scaled by a factor of zero to two, reproducing the subtraction and addition of up to the full magnitude of current in experiment. All novel model variants reproduced the main features of the intervention, most pertinently the negative correlation between I_{to} magnitude and terminal repolarization duration (Figure 5A). However, the magnitude of the impact of I_{to} modulation was different among the different model variants. As all models contain the same formulation for I_{to} , these differences were due to either (a) the impact of AP morphology and/or (b) the differing formulations for I_{CaL} , calcium handling system, and background currents.

The role of I_{CaL} was assessed through the application of nifedipine (channel blocker, WL_2001 data, modeled by 30–90% current block) and 5HT (channel enhancer, WL_2007_ICaL data, modeled by a three-fold increase in the current magnitude). The impact of nifedipine was in general overestimated in the cell models [Figure 5B – except for than the hAM_NG_{mWL} variant; Figure 5B(v)]; 5HT displayed more variable match between model and experiment, with some models overestimating its effects whereas others underestimated it (Figure 5E). After-depolarizations or non-repolarizing APs were observed in the hAM_WL_{CRN} and hAM_NG_{mWL} model variants under a large increase in I_{CaL} . Qualitatively, all models reproduced the features of these two interventions: nifedipine reducing the AP dome/plateau phase and accelerating terminal repolarization, whereas 5HT enhanced this plateau phase and extended terminal repolarization.

The impact of 4-AP (50% block of I_{to} and I_{sus}) was well reproduced by all model variants, displaying an elevation of the AP plateau and extension of terminal repolarization (Figure 4C). Similarly, the match between simulation and experiment for the application of 4-AP combined with nifedipine was strong, wherein all models reproduce the triangular morphology, prolonged phase-1 repolarization, and accelerated terminal repolarization (Figure 5D). The extent of APD shortening differed between the model variants, although all displayed some but not extensive shortening, as observed in experiment.

Intact-Cell Model

The intact-cell models (for future tissue-scale simulations) were derived through first exchanging the formulation of I_{K1} from the isolated to intact version (see Figure 1 and section “Workman-Laboratory Characterized Currents: $IK1$ and $Ihyp$ ”), and subsequent removal of the hyperpolarizing current. The RMP maintained in the cell model variants was ~ -74 mV, similar to that of the native hAM_GB and hAM_NG models, and less hyperpolarized than the isolated-cell model variants, the hAM_CRN model, and WL experiments of ~ -80 mV. For the case of the modified cell models (hAM_X_{mWL}), I_{Kr} and I_{Ks} were modeled as originally presented to preserve the modified nature of the cell models; in case of the WL models (hAM_WL_{CRN/GB}), the currents were incrementally introduced by scaling the maximum conductance of the associated model current formulation to preserve the minimal approach: factor of $\times 0$ – 1.5 for the hAM_WL_{CRN} model, and $\times 0$ – 5.0 in the hAM_WL_{GB} model. With the conductances set to zero, neither model maintained an APD expected of the intact healthy human

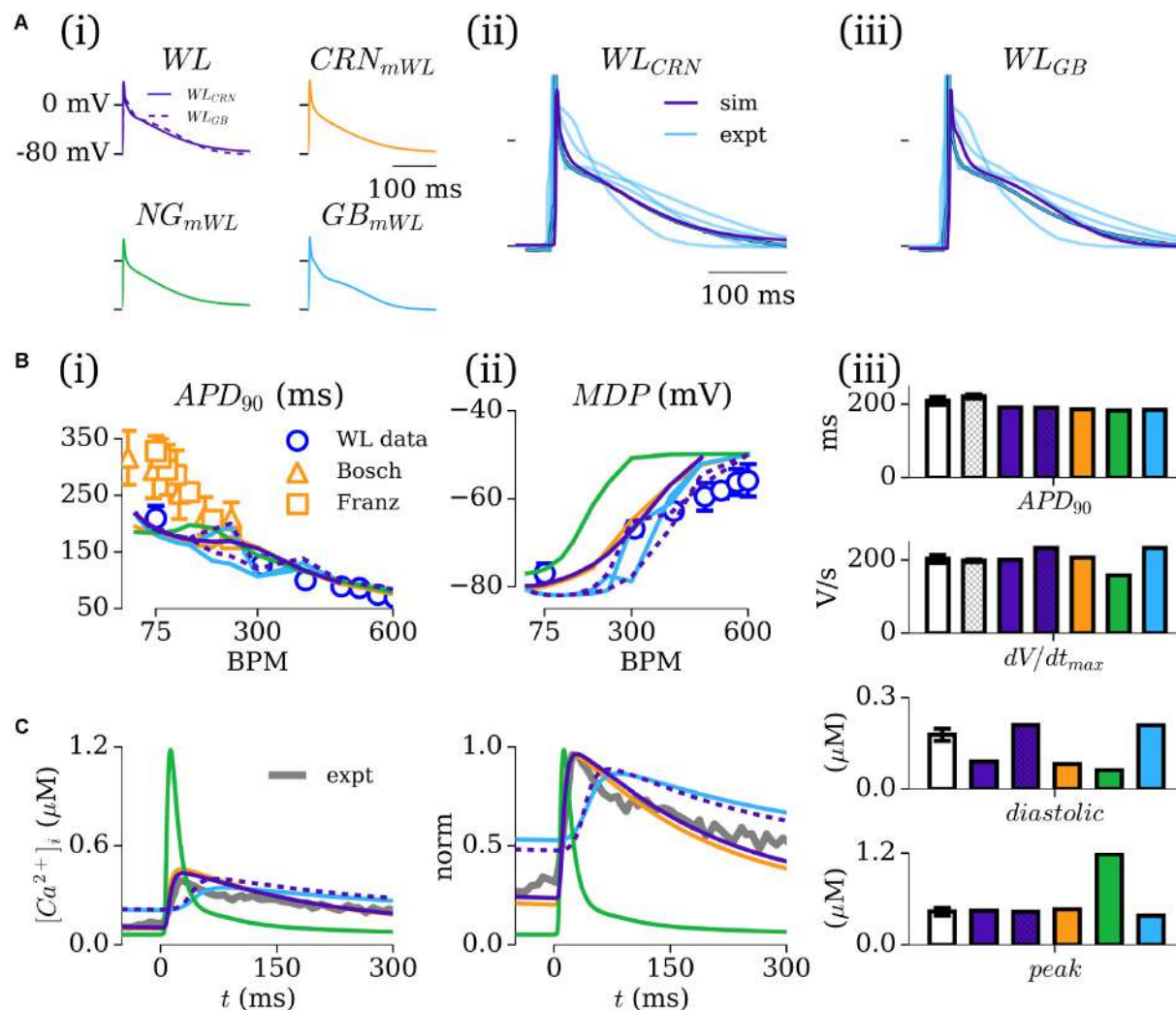


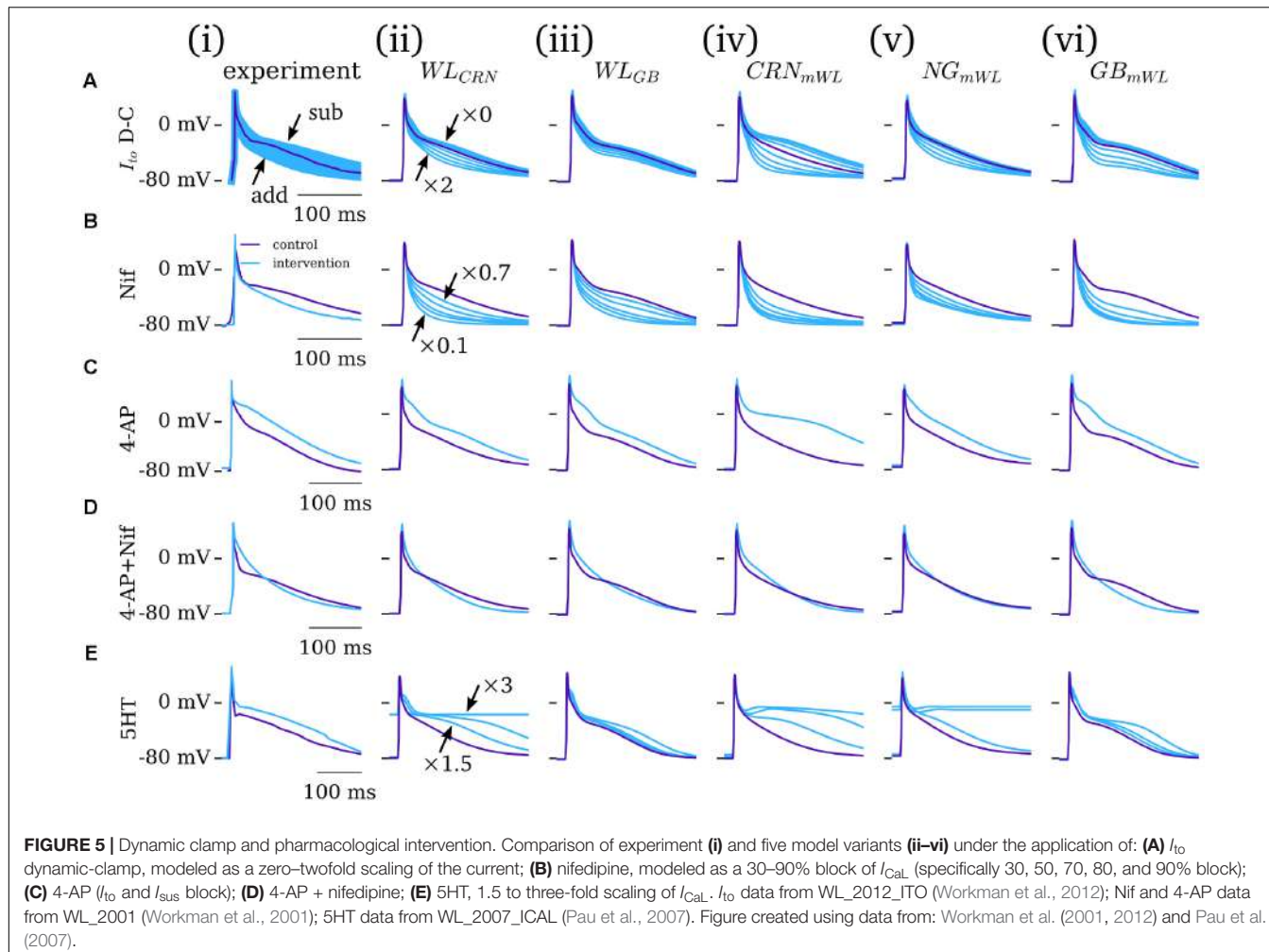
FIGURE 4 | Simulated AP and CaT characteristics and validation. **(A,i)** Action potential (AP) traces associated with the five novel model variants, paced at 75 BPM; **(A,ii,iii)** Comparison between the WL models (purple) and available experimental traces (blue; Workman et al., 2001, 2006, 2012; Pau et al., 2007 + Kettlewell unpublished Ca²⁺ data), with the "typical" Workman laboratory trace emphasized. **(B,i)** APD₉₀ restitution for the five models [colored lines – colors correspond to those in A(i)] compared to experimental data from the Workman laboratory (blue circles; WL_2001; Workman et al., 2001) as well as from other groups for additional context [orange triangles (Bosch et al., 1999); orange squares (Franz et al., 1997)]. **(B,ii)** Rate dependence of MDP in the five models and Workman laboratory data (WL_2001). **(B,iii)** Comparison of APD₉₀ and dV/dt_{max} at 75 BPM in the five models (colors; purple hatched bars corresponds to WL_{GB}) and experiment (white: WL_2001, open bars; WL_2006, hatched bars). **(C)** Intracellular calcium transients in the five model variants (colored lines) and single experimental trace from the Workman laboratory (black; unpublished Sarah Kettlewell WL data), shown on absolute **(i)** and normalized **(ii)** scales. **(iii)** Comparison of the diastolic and peak calcium in the five models with mean data ($n = 24$ cells, 5 patients) from the Workman laboratory Kettlewell experiments. Figure created using data from Franz et al. (1997), Bosch et al. (1999), Workman et al. (2001, 2006, 2012) and Pau et al. (2007).

atria, exhibiting non-repolarizing APs [Figures 6A,B(i,ii)]. In the hAM_WL_{CRN} model, introducing the currents with the conductance set to that presented originally was sufficient to maintain an APD of <400 ms [Figures 6A,B(i)]; in the hAM_WL_{GB} model, larger conductances (relative to the original study – note that the GB model has much smaller I_{Kr}/I_{Ks} than the CRN model) were necessary to maintain APD [Figures 6A,B(ii)]. All intact models with a duration of <400 ms displayed either a spike-and-dome (hAM_CRN_{mWL}) or low-plateau/dome (all other variants) morphology [Figures 6A,B(i–v)], and such durations could be achieved with relatively low

current magnitudes (i.e., an order of magnitude smaller than the peak in I_{to} , I_{sus} , and I_{CaL}).

Role of the Hyperpolarizing Current

The importance of the hyperpolarizing current, and isolated-cell conditions (i.e., $I_{K1}^{isolated}$ with a reversal of ~ -40 mV; insignificant I_{Kr}/I_{Ks}) was assessed by comparison of the intact and isolated-cell variants of the hAM_CRN, hAM_NG and hAM_GB models (Figure 7). For all three models, the isolated-cell variant exhibited a shorter APD₉₀ with more rapid terminal repolarization (Figure 7Aa). The dome associated with the



hAM_CRN model was flattened, and the long tail associated with the hAM_GB model was significantly reduced. The CaT was significantly reduced in isolated-cells in both the hAM_CRN and hAM_GB models, whereas the hAM_NG model, in general, showed the most similarity between isolated and intact [Figure 7A(ii)]. APD restitution was affected similarly, with APD₉₀ being significantly shortened at all except the fastest pacing rates (shortest cycle lengths), where convergence between isolated and intact-cell models in the hAM_CRN and hAM_NG model was observed (Figure 7Ac).

Analysis of the response of the AP to various interventions revealed some significant differences between isolated- and intact-cell model variants, pertaining both to proportional and behavioral differences. Selected examples illustrate the most significant differences observed (Figure 7B): the dynamic clamp I_{to} intervention in the hAM_CRN^{isolated} model matched well to the experimental data (Figure 5A), wherein terminal repolarization duration negatively correlated with I_{to} magnitude, whereas in hAM_CRN^{intact}, a positive correlation was observed, wherein initial elevation of the plateau under current block led to more rapid and thus shorter terminal repolarization [Figure 7B(i)]. The response to 4-AP in the hAM_CRN model

variants demonstrated the same feature: APD₉₀ was prolonged in the isolated-cell model but shortened in the intact-cell model [Figure 7B(ii)]. In the hAM_GB model variants, modulation of I_{CaL} exhibited the largest differences between isolated- and intact-cell models: the application of nifedipine (i.e., I_{CaL} current block) exhibited differences in the graded response to gradually increasing current block [Figure 7B(iii)]; the application of 5HT (i.e., I_{CaL} current enhancement) resulted in early-after-depolarizations (EADs) in the intact-cell model which were not observed in the isolated-cell model [Figure 7B(iv)].

Comparison Between Models

The IV relationship and current traces under voltage clamp for the novel formulations and inherited cell models demonstrate the variability between the different cell models (Figure 8). The IV curves for I_{to} in the CRN, NG, and GB models all demonstrate a takeoff potential of -30 to -20 mV, whereas the WL formulation exhibits a takeoff potential of -10 to 0 mV, and a smaller current magnitude [Figure 8A(i)]. The GB model (i.e., Malek et al., 2009 formulation) had the slowest decay time, with all other models being more similar [Figure 8B(i)]. I_{sus} is largest in the WL model, but exhibits similar voltage dependence to the NG and

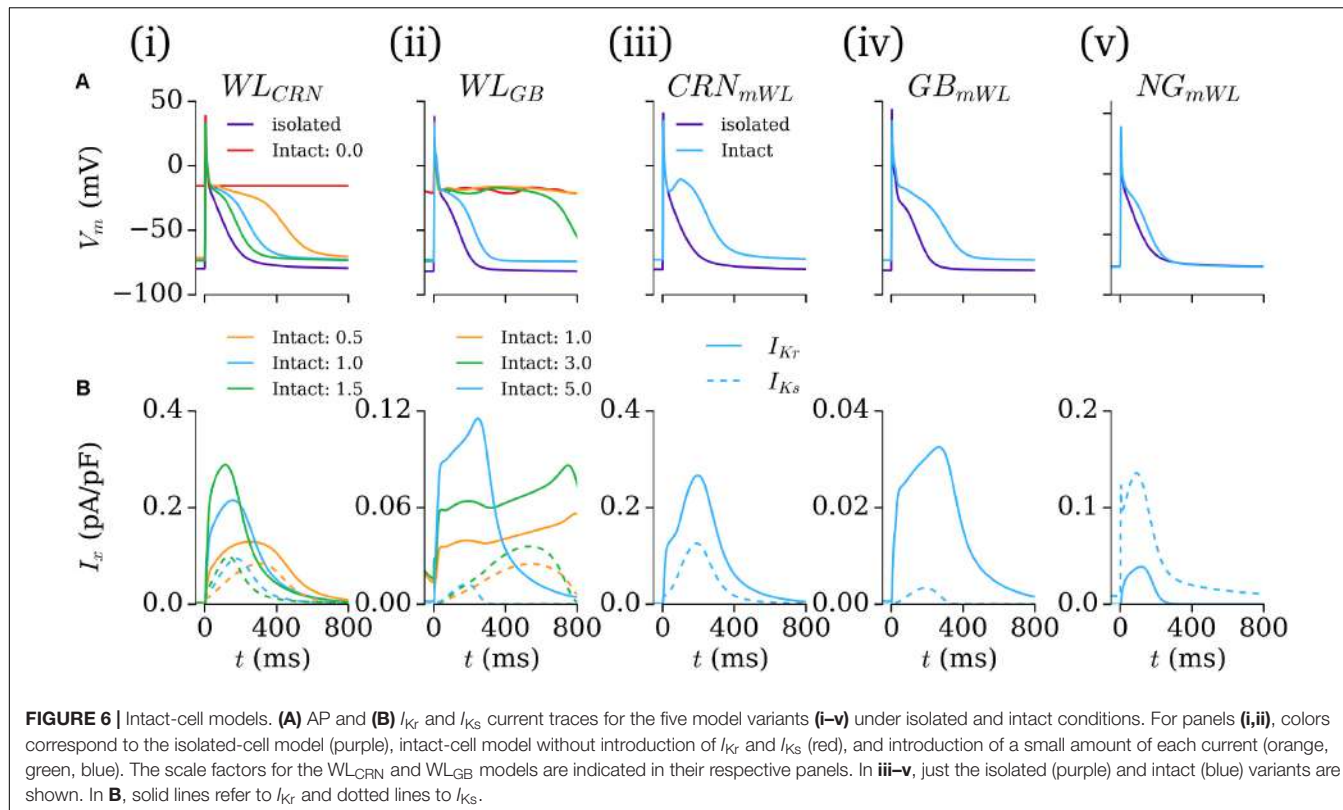


FIGURE 6 | Intact-cell models. **(A)** AP and **(B)** I_{K_r} and I_{K_s} current traces for the five model variants **(i–v)** under isolated and intact conditions. For panels **(i,ii)**, colors correspond to the isolated-cell model (purple), intact-cell model without introduction of I_{K_r} and I_{K_s} (red), and introduction of a small amount of each current (orange, green, blue). The scale factors for the WL_{CRN} and WL_{GB} models are indicated in their respective panels. In **iii–v**, just the isolated (purple) and intact (blue) variants are shown. In **B**, solid lines refer to I_{K_r} and dotted lines to I_{K_s} .

GB models [Figure 8A(ii)]. The model I_{CaL} formulations show similar voltage dependence and magnitude for the WL, CRN, and NG models, with the GB model being both larger and with a negative shift in its voltage dependence [Figure 8A(iii)]. The inter-model differences in the time-course of I_{CaL} traces during voltage clamp are larger, with the WL model showing the fastest decay.

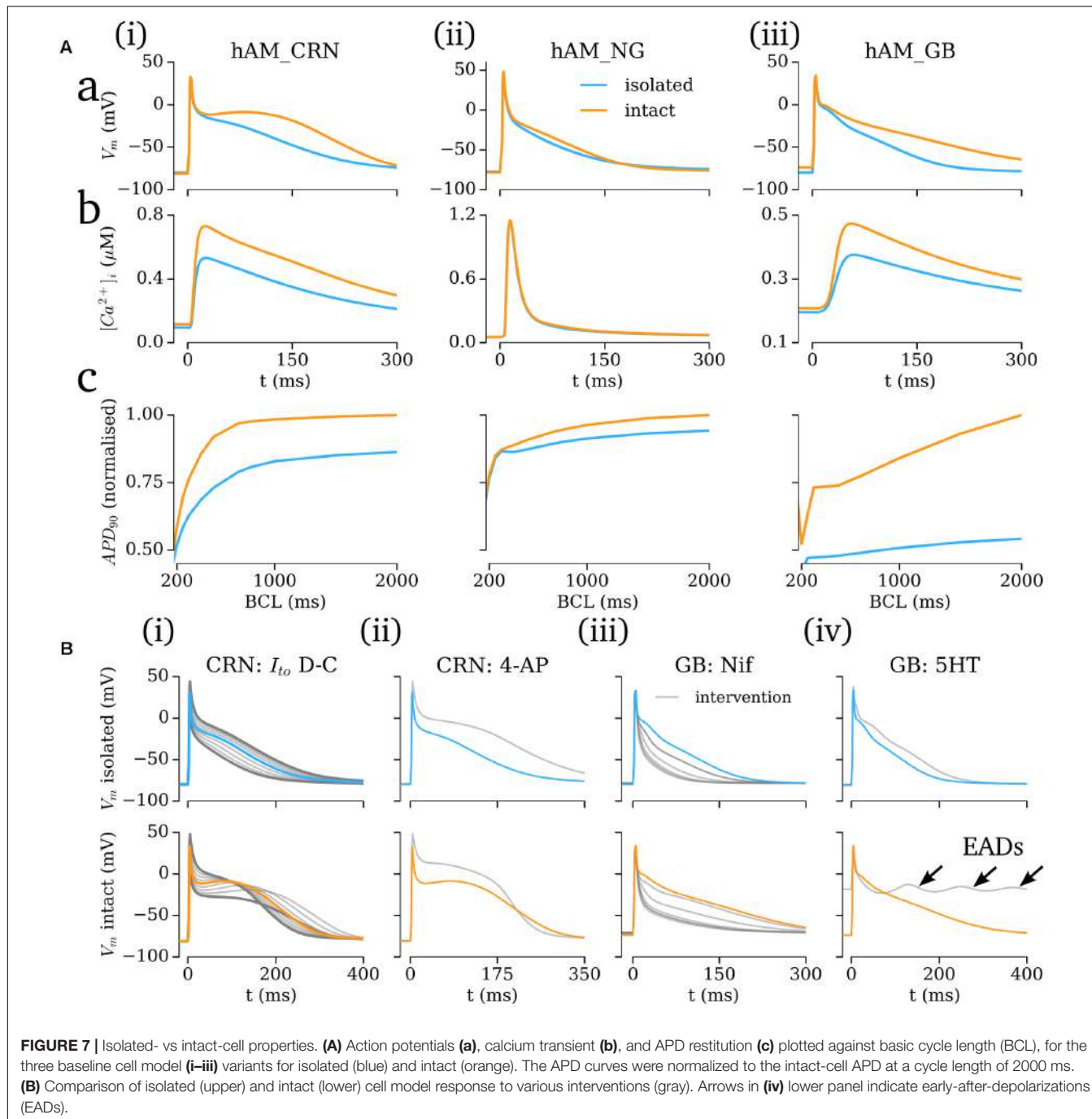
The influence of the novel current formulations on atrial AP morphology is illustrated through comparisons of the native (hAM_X), modified (hAM_X_{mWL}), and novel (hAM_WL_X) cell models (Figure 9A). In both isolated and intact-cell environments, the AP morphology and time-course of the various currents exhibits significant differences between the native and novel versions, with the isolated modified versions in general exhibiting closer features to the WL AP morphology and duration. The time-courses for the novel I_{to} and I_{sus} lie somewhat intermediary to those associated with the hAM_CRN and hAM_GB models.

The contribution of ion current balance (i.e., relative magnitudes of the different currents) and kinetics to the differences observed was assessed by comparing the native and mWL models with variants in which the current magnitudes of the native models were scaled to the same data as the WL models (WL_2006). These data highlight that both current magnitude and specific kinetics contribute to the differences observed in the mWL models, as the rescaled model variant did not reproduce the morphology of the mWL model (Figure 9B).

DISCUSSION

Summary

In this study, mathematical descriptions of the primary ion currents underlying human atrial electrophysiology were developed based primarily on congruent human atrial cell data from a single source, and specifically reproducing the environment of isolated atrial cardiomyocyte whole-cell-patch current- and voltage-clamp experiments, including the frequently observed unphysiologically depolarized RMP and injected compensating hyperpolarizing current. Formulations describing the currents I_{to} , I_{sus} , I_{CaL} , and I_{K1} were all fit to voltage-clamp data from the WL (Figures 1, 3); I_{Na} was parameterized using experiments relating RMP to dV/dt_{max} (Figure 2). The formulations were integrated with multiple available existing models of human atrial electrophysiology which include descriptions of intracellular calcium handling, to produce a family of novel and modified models of the human atrial myocyte (Figure 4). The models were compared to experimental data describing AP morphology, APD, rate-adaption, and current magnitudes (Figure 4) as well as pharmacological and dynamic clamp interventions (Figure 5); model variants were also compared to each other to elucidate the role of the primary ion current parameters in human atrial cell dynamics (Figures 8, 9), and the important differences between isolated- and intact-cell environments were characterized (Figure 7).



Comparison to Previous Work

There are many available models describing human atrial electrophysiology developed by multiple groups. Comprehensive reviews and comparisons of these models can be found in Wilhelms et al. (2013), Trayanova (2014), and Heijman et al. (2016), but these models can be briefly categorized into a few independent models (Courtemanche et al., 1998; Nygren et al., 1998; Grandi et al., 2011) and variants of these, introducing, for example, reformulations due to new data (Malek et al., 2009), mutant ion channel variants (Colman et al., 2017a),

parameterization to patient specific data (Lombardo et al., 2016), or population variability models (Ellinwood et al., 2017; Lawson et al., 2018; Ni et al., 2018). Whereas these models are typically based on data from multiple sources, cell-types, or species, the ion current formulations developed in the present study are derived directly from human atrial specific data from a single laboratory. Importantly, where many previous studies have adjusted current parameters to reproduce AP properties, no such modifications were made in the present study, ensuring that the relative balance and time-courses of the primary

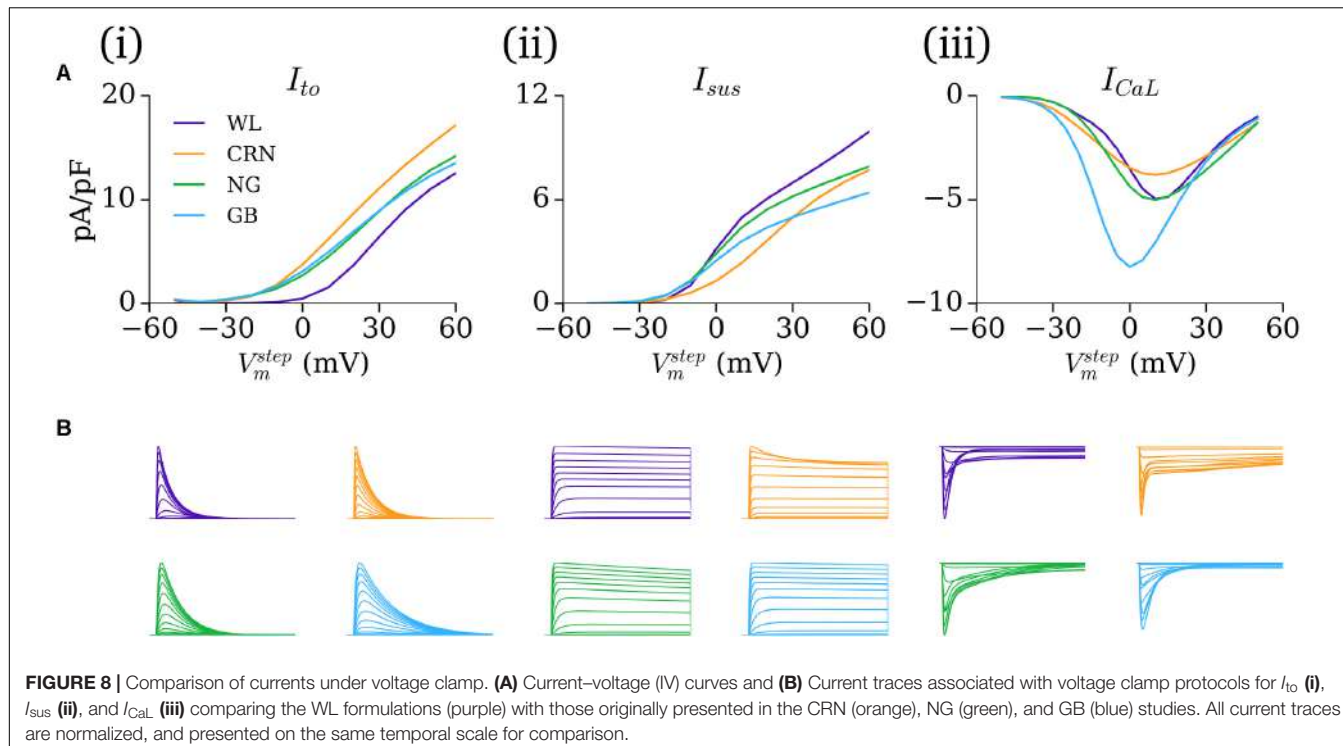


FIGURE 8 | Comparison of currents under voltage clamp. **(A)** Current–voltage (IV) curves and **(B)** Current traces associated with voltage clamp protocols for I_{to} **(i)**, I_{sus} **(ii)**, and I_{CaL} **(iii)** comparing the WL formulations (purple) with those originally presented in the CRN (orange), NG (green), and GB (blue) studies. All current traces are normalized, and presented on the same temporal scale for comparison.

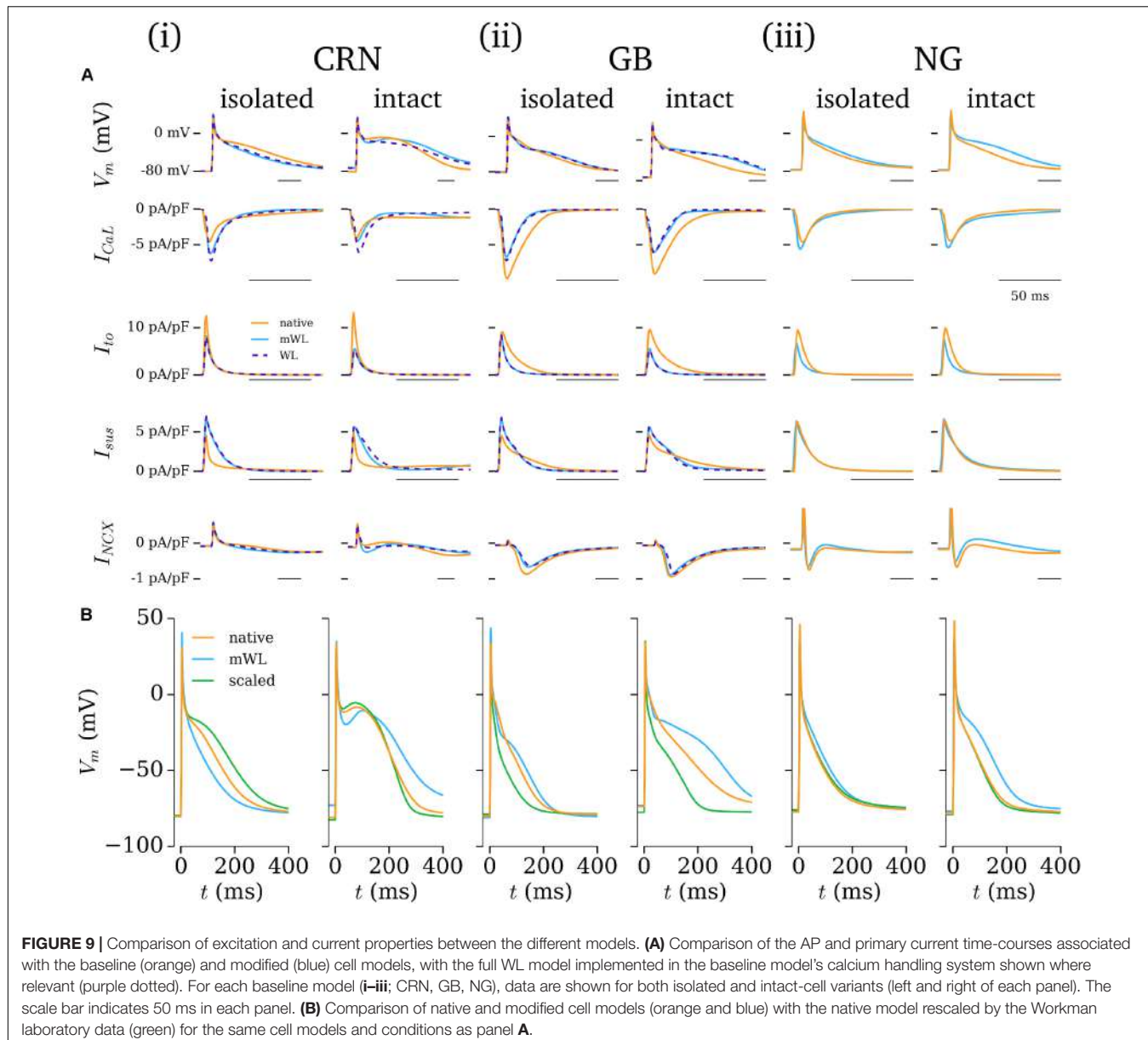
currents is experimentally justified. Furthermore, the model presented is the first to explicitly implement the conditions of isolated-cell experiments and to specifically differentiate isolated- and intact-cells. Analysis presented in this study highlights the importance of reproducing these isolated-cell environmental conditions when considering validation and comparison of AP response to intervention (sections “Role of the Hyperpolarizing Current” and “The Importance of the Isolated-Cell Environment”). Therefore, the models presented offer advantages for general integrated experimental-numerical investigation compared to previously presented models which do not reproduce these conditions, as well as for direct integration with experiments in the WL for which the model is tailored. Similar approaches could be applied to develop specific models for other laboratories and experimental environments; incidentally, a comparison of such models may provide the best means to fully assess the impact of inter-laboratory differences and elucidate the role and variation of ion currents in human atrial electrophysiology.

The single-source approach implemented theoretically provides a higher level of confidence than previous models, due to the absence of arbitrary or results-based parameter modification and lack of ambiguity in combination of the formulations of the primary ion currents. However, this is far from a claim that it is therefore superior, or that the previous models are “less-valid”; rather, at the very least, the formulations presented in this study, and the models which implement them, exhibit differences to those previous models (section “Comparison Between Models”) and therefore represent complementary tools which may assist in multi-model studies to provide a further,

independent perspective and thus achieve model-independent conclusions.

The Importance of the Isolated-Cell Environment

Isolated human atrial cardiomyocytes frequently feature unphysiologically depolarized RMP (Escande et al., 1987; Bénardeau et al., 1996; Dobrev et al., 2001; Workman et al., 2006) and apparent reversal of I_{K1} at ~ 40 mV. This issue has been addressed in a variety of ways; e.g., by current-clamping with a small, constant, hyperpolarizing current (Le Grand et al., 1994; Bénardeau et al., 1996; Workman et al., 2001). However, the previous models do not explicitly account for such RMP depolarization or hyperpolarizing current application (although studies in ventricular cells have investigated the effect of applied constant currents on APD at different rates, e.g., Grandi et al., 2010). Results presented in this study (section “Role of the Hyperpolarizing Current”), and based on the available, well-established human atrial cell models (i.e., independent of novel ion current formulations), demonstrated that these features can lead to significantly different behavior compared to “intact”-cells (i.e., the models as natively presented, with I_{K1} reversal $\sim E_K$ and a well maintained RMP of more negative than -70 mV): all isolated-cell model variants exhibited a shorter APD_{90} and a smaller CaT than the intact equivalents. In the hAM_CRN model, the different environments resulted in the difference between “spike-and-dome” versus “low-dome/triangulated” AP morphologies, which may have a significant impact on model dynamics.



Furthermore, the models responded differently to the application of interventions, in some cases in significant ways such as APD shortening vs lengthening, or the emergence of EADs. Some of these differences may simply be a result of AP morphology and its influence on the time-course of the underlying ion currents, but it is also highly likely that the more positive reversal potential and constant, injected hyperpolarizing current, as well as the absence of I_{Kr}/I_{Ks} , more directly underlies these differences to at least some extent (I_{Kr} and I_{Ks} , for example, being responsible for accelerated terminal repolarization associated with AP plateau elevation in intact-cell models).

These results therefore highlight the considerations which must be taken when validating human atrial cell models against experimental data attained under these isolated-cell

conditions, for translation of phenomena observed under perturbed conditions to the tissue scale, and for experimentally assessing model predictions attained without accounting for these conditions.

Potential Contributions of I_{Kr} and I_{Ks} to Human Atrial Repolarization

Due to I_{Ks} and I_{Kr} being very small or absent (Firek and Giles, 1995; Amos et al., 1996; Schreieck et al., 2000; Caballero et al., 2010) in isolated human atrial cells, these currents were not included in the isolated-cell model. Repolarization kinetics and duration properties matched well with experimental traces, indicating that these currents are not required for repolarization under these conditions. Extrapolation to the intact-cell model, in

which I_{hyp} was removed, indicated that I_{Kr}/I_{Ks} may be required in the intact human atria to maintain repolarization, as cell models exhibited prolonged (>700 ms) or non-repolarizing APs without inclusion of these currents. However, inclusion of these currents to only a relatively small magnitude was sufficient to maintain AP repolarization.

Limitations

Whereas the primary ion currents controlling the AP model were fit to detailed data from a single laboratory, the intracellular Ca^{2+} handling system was not parameterized to the same extent to human atrial data, and only limited CaT data were available for validation from the WL. For this reason, the current formulations were integrated with multiple contemporary human atrial calcium handling systems, rather than performing development and parameterization of a novel calcium handling system. However, the development of a more rigorously derived human atrial specific calcium handling system (for example, an extension of the spatial cell model presented in Voigt et al., 2014) would be a natural improvement to a full human atrial single-source model. Furthermore, integration with multiple, independent systems provided challenges for modeling the L-type calcium current homogeneously across the different models, due to the tight and sensitive coupling between this current and the calcium handling system. This led to a degree of uncertainty and subjectivity in the selection of parameters from non-unique solutions, which contrasts with the single-source and objective philosophy of the approach.

In general, the models and variants overestimated the impact of high concentrations of nifedipine on human atrial AP shortening. Whereas this feature is common to many models of the human atria, and in particular in the isolated-cell variants as presented in this study, its emergence in a model containing accurately reproduced dynamics for the main ion currents characterized in experiments suggests a potential important role of inward currents active at potentials more negative than -30 mV not captured in the model, possibly because I_{NCX} is too small, or the presence of larger background Ca^{2+} and Na^{2+} currents. This type of insight, however, supports a primary purpose of the model: for example, the potential role of incorrect relative current magnitude balance in the formulations of the primary currents underlying this discrepancy can be largely eliminated.

Variability was not investigated in the present study, although the single-source approach may offer the perfect tool to interpret data attained from the implementation of a full population variability approach and/or quantification through sensitivity analysis (Chang et al., 2015; Devenyi et al., 2017; Ellinwood et al., 2017; Sánchez et al., 2017; Lawson et al., 2018; Ni et al., 2018).

Due to the single-source, minimalist philosophy of the approach, there are many factors which play a role in human atrial electrophysiology which have not been included, due to a lack of well characterized and human atrial specific data. For example, the models do not contain detailed descriptions of phosphorylation due to PKA, or the impact of CaMKII (and serine and threonine; Heijman et al., 2014, 2017; Mesubi

and Anderson, 2016), or additional currents such as small conductance potassium channels (Skibbsye et al., 2014), which may have an important influence on human atrial cell dynamics in control and perturbed conditions. Exclusion of these components is not a claim that they are unimportant, but rather follows from the motivation not to introduce sophistication and complexity by including components which have not been well characterized in the human atria (and specifically the WL) and thus contain potential sources of error, *ad hoc* parameters, or inaccurately scaled contributions. We hope that in future further, well-characterized components will be added to the model as part of the long-term ambition of the biophysically detailed and biomedically accurate virtual human heart.

CONCLUSION

We have developed a family of biophysically detailed models of human atrial electrophysiology based primarily on data from a single laboratory and reproducing the conditions of isolated-cell experiments. The models reproduce human atrial excitation properties and the impact of various interventions, and the importance of the isolated-cell environment was highlighted. We therefore present a tool which can be used directly in conjunction with experiments to dissect the ionic mechanisms of atrial arrhythmias, and complementary to the available contemporary cell models for general mechanistic investigation.

AUTHOR CONTRIBUTIONS

MC and AW conceived and designed the study. MC carried out simulations, and acquired and analyzed the data. PS, SK, and AW performed isolated-cell experiments, and acquired and analyzed the data. MC prepared all the figures. MC prepared and all authors edited the drafts and manuscript. All authors approved the final version of the manuscript, interpreted the data, and agreed to be accountable for all aspects of the work in ensuring that questions related to the accuracy or integrity of any part of the work are appropriately investigated and resolved.

FUNDING

This work was supported by a Medical Research Council Strategic Skills Fellowship to MC (MR/M014967/1) and British Heart Foundation Project Grants (AW, SK, and PS) or Basic Science Lectureships (AW) funding (PG/99030, BS/2001001, FS/02/036, PG/04/084, FS/04/087, BS/06/003, PG/13/31/30156, and PG/16/42/32142).

SUPPLEMENTARY MATERIAL

The Supplementary Material for this article can be found online at: <https://www.frontiersin.org/articles/10.3389/fphys.2018.01211/full#supplementary-material>

REFERENCES

- Amos, G. J., Wettwer, E., Metzger, F., Li, Q., Himmel, H. M., and Ravens, U. (1996). Differences between outward currents of human atrial and subepicardial ventricular myocytes. *J. Physiol.* 491(Pt 1), 31–50. doi: 10.1113/jphysiol.1996.sp021194
- Bénarreau, A., Hatem, S. N., Rücker-Martin, C., Le Grand, B., Macé, L., Dervanian, P., et al. (1996). Contribution of $\text{Na}^+/\text{Ca}^{2+}$ exchange to action potential of human atrial myocytes. *Am. J. Physiol.* 271(3 Pt 2), H1151–H1161. doi: 10.1152/ajpheart.1996.271.3.H1151
- Bosch, R. F., Zeng, X., Grammer, J. B., Popovic, K., Mewis, C., and Kühlkamp, V. (1999). Ionic mechanisms of electrical remodeling in human atrial fibrillation. *Cardiovasc. Res.* 44, 121–131. doi: 10.1016/S0008-6363(99)0178-9
- Caballero, R., de la Fuente, M. G., Gómez, R., Barana, A., Amorós, I., Dolz-Gaitón, P., et al. (2010). In humans, chronic atrial fibrillation decreases the transient outward current and ultrarapid component of the delayed rectifier current differentially on each atria and increases the slow component of the delayed rectifier current in both. *J. Am. Coll. Cardiol.* 55, 2346–2354. doi: 10.1016/j.jacc.2010.02.028
- Casajuana, M., Giner-Soriano, M., Roso-Llorach, A., Vedia, C., Violan, C., and Morros, R. (2018). Annual costs attributed to atrial fibrillation management: cross-sectional study of primary healthcare electronic records. *Eur. J. Health Econ.* doi: 10.1007/s10198-018-0961-7 [Epub ahead of print].
- Ceornodolea, A. D., Bal, R., and Severens, J. L. (2017). Epidemiology and management of atrial fibrillation and stroke: review of data from four European countries. *Stroke Res. Treat.* 2017:8593207. doi: 10.1155/2017/8593207
- Chang, E. T. Y., Strong, M., and Clayton, R. H. (2015). Bayesian sensitivity analysis of a cardiac cell model using a gaussian process emulator. *PLoS One* 10:e0130252. doi: 10.1371/journal.pone.0130252
- Chang, K. C., Bayer, J. D., and Trayanova, N. A. (2014). Disrupted calcium release as a mechanism for atrial alternans associated with human atrial fibrillation. *PLoS Comput. Biol.* 10:e1004011. doi: 10.1371/journal.pcbi.1004011
- Chen, P. S., and Tan, A. Y. (2007). Autonomic nerve activity and atrial fibrillation. *Heart Rhythm.* 4(Suppl. 3), S61–S64. doi: 10.1016/j.hrthm.2006.12.006
- Christ, T., Boknik, P., Wöhrl, S., Wettwer, E., Graf, E. M., Bosch, R. F., et al. (2004). L-Type Ca^{2+} current downregulation in chronic human atrial fibrillation is associated with increased activity of protein phosphatases. *Circulation* 110, 2651–2657. doi: 10.1161/01.CIR.0000145659.80212.6A
- Colman, M. A., Aslanidi, O. V., Kharche, S., Boyett, M. R., Garratt, C., Hancox, J. C., et al. (2013). Pro-arrhythmogenic effects of atrial fibrillation-induced electrical remodelling: insights from the three-dimensional virtual human atria. *J. Physiol.* 591, 4249–4272. doi: 10.1113/jphysiol.2013.254987
- Colman, M. A., Castro, S. J., Alday, E. A. P., Hancox, J. C., Garratt, C., and Zhang, H. (2014). Recent progress in multi-scale models of the human atria. *Drug Discov. Today* 14, 23–32. doi: 10.1016/j.ddmod.2014.04.003
- Colman, M. A., Ni, H., Liang, B., Schmitt, N., and Zhang, H. (2017a). In silico assessment of genetic variation in KCNA5 reveals multiple mechanisms of human atrial arrhythmogenesis. *PLoS Comput. Biol.* 13:e1005587. doi: 10.1371/journal.pcbi.1005587
- Colman, M. A., Perez Alday, E. A., Holden, A. V., and Benson, A. P. (2017b). Trigger vs. Substrate: multi-dimensional modulation of QT-prolongation associated arrhythmic dynamics by a hERG channel activator. *Front. Physiol.* 8:757. doi: 10.3389/fphys.2017.00757
- Courtemanche, M., Ramirez, R. J., and Nattel, S. (1998). Ionic mechanisms underlying human atrial action potential properties: insights from a mathematical model. *Am. J. Physiol.* 275(1 Pt 2), H301–H321. doi: 10.1152/ajpheart.1998.275.1.H301
- Dobrev, D., Graf, E., Wettwer, E., Himmel, H. M., Hála, O., Doerfel, C., et al. (2001). Molecular basis of downregulation of G-protein-coupled inward rectifying K^+ current ($\text{I}_{\text{K},\text{ach}}$) in chronic human atrial fibrillation decrease in GIRK4 mRNA correlates with reduced $\text{I}_{\text{K},\text{ACH}}$ and muscarinic receptor-mediated shortening of action potentials. *Circulation* 104, 2551–2557 doi: 10.1161/hc4601.099466
- Devenyi, R. A., Ortega, F. A., Groenendaal, W., Krogh-Madsen, T., Christini, D. J., and Sobie, E. A. (2017). Differential roles of two delayed rectifier potassium currents in regulation of ventricular action potential duration and arrhythmia susceptibility. *J. Physiol.* 595, 2301–2317. doi: 10.1113/JP273191
- Ellinwood, N., Dobrev, D., Morotti, S., and Grandi, E. (2017). *In silico* assessment of efficacy and safety of I_{Kur} inhibitors in chronic atrial fibrillation: role of kinetics and state-dependence of drug binding. *Front. Pharmacol.* 8:799. doi: 10.3389/fphar.2017.00799
- Escande, D., Coulombe, A., Faivre, J. F., Deroubaix, E., and Corabœuf, E. (1987). Two types of transient outward currents in adult human atrial cells. *Am. J. Physiol.* 252(1 Pt 2), H142–H148. doi: 10.1152/ajpheart.1987.252.1.H142
- Firek, L., and Giles, W. R. (1995). Outward currents underlying repolarization in human atrial myocytes. *Cardiovasc. Res.* 30, 31–38. doi: 10.1016/S0008-6363(95)00014-3
- Franz, M. R., Karasik, P. L., Li, C., Moubarak, J., and Chavez, M. (1997). Electrical remodeling of the human atrium: similar effects in patients with chronic atrial fibrillation and atrial flutter. *J. Am. Coll. Cardiol.* 30, 1785–1792. doi: 10.1016/S0735-1097(97)00385-9
- Grandi, E., Pandit, S. V., Voigt, N., Workman, A. J., Dobrev, D., Jalife, J., et al. (2011). Human atrial action potential and Ca^{2+} model: sinus rhythm and chronic atrial fibrillation. *Circ. Res.* 109, 1055–1066. doi: 10.1161/CIRCRESAHA.111.253955
- Grandi, E., Pasqualini, F. S., and Bers, D. M. (2010). A novel computational model of the human ventricular action potential and Ca transient. *J. Mol. Cell. Cardiol.* 48, 112–121. doi: 10.1016/j.yjmcc.2009.09.019
- Heijman, J., Erfanian Abdoust, P., Voigt, N., Nattel, S., and Dobrev, D. (2016). Computational models of atrial cellular electrophysiology and calcium handling, and their role in atrial fibrillation. *J. Physiol.* 594, 537–553. doi: 10.1113/JP271404
- Heijman, J., Ghezelbash, S., Wehrens, X. H., and Dobrev, D. (2017). Serine/Threonine phosphatases in atrial fibrillation. *J. Mol. Cell. Cardiol.* 103, 110–120. doi: 10.1016/j.yjmcc.2016.12.009
- Heijman, J., Voigt, N., Wehrens, X. H., and Dobrev, D. (2014). Calcium dysregulation in atrial fibrillation: the role of CaMKII. *Front. Pharmacol.* 5:30. doi: 10.3389/fphar.2014.00030
- Kettlewell, S., Burton, F. L., Smith, G. L., and Workman, A. J. (2013). Chronic myocardial infarction promotes atrial action potential alternans, afterdepolarizations, and fibrillation. *Cardiovasc. Res.* 99, 215–224. doi: 10.1093/cvr/cvt078
- Kirchhof, P., Breithardt, G., Bax, J., Benninger, G., Blomstrom-Lundqvist, C., Borlani, G., et al. (2016). A roadmap to improve the quality of atrial fibrillation management: proceedings from the fifth atrial fibrillation network/European heart rhythm association consensus conference. *Europace* 18, 37–50. doi: 10.1093/europace/euv304
- Kirchhof, P., and Calkins, H. (2017). Catheter ablation in patients with persistent atrial fibrillation. *Eur. Heart J.* 38, 20–26. doi: 10.1093/eurheartj/ehw260
- Koivumäki, J. T., Korhonen, T., and Tavi, P. (2011). Impact of sarcoplasmic reticular calcium release on calcium dynamics and action potential morphology in human atrial myocytes: a computational study. *PLoS Comput. Biol.* 7:e1001067. doi: 10.1371/journal.pcbi.1001067
- Krijthe, B. P., Kunst, A., Benjamin, E. J., Lip, G. Y., Franco, O. H., Hofman, A., et al. (2013). Projections on the number of individuals with atrial fibrillation in the European union, from 2000 to 2060. *Eur. Heart J.* 34, 2746–2751. doi: 10.1093/eurheartj/eht280
- Lawson, B. A. J., Drovandi, C. C., Cusimano, N., Burrage, P., Rodriguez, B., and Burrage, K. (2018). Unlocking data sets by calibrating populations of models to data density: a study in atrial electrophysiology. *Sci. Adv.* 4:e1701676. doi: 10.1126/sciadv.1701676
- Le Grand, B. L., Hatem, S., Deroubaix, E., Couétil, J. P., and Corabœuf, E. (1994). Depressed transient outward and calcium currents in dilated human atria. *Cardiovasc. Res.* 28, 548–556. doi: 10.1093/cvr/28.4.548
- Lombardo, D. M., Fenton, F. H., Narayan, S. M., and Rappel, W. J. (2016). Comparison of detailed and simplified models of human atrial myocytes to recapitulate patient specific properties. *PLoS Comput. Biol.* 12:e1005060. doi: 10.1371/journal.pcbi.1005060
- Luo, C. H., and Rudy, Y. (1991). A model of the ventricular cardiac action potential. depolarization, repolarization, and their interaction. *Circ. Res.* 68, 1501–1526. doi: 10.1161/01.RES.68.6.1501
- Malekar, M. M., Greenstein, J. L., Giles, W. R., and Trayanova, N. A. (2009). K^+ current changes account for the rate dependence of the action potential in the

- human atrial myocyte. *Am. J. Physiol. Heart Circ. Physiol.* 297, H1398–H1410. doi: 10.1152/ajpheart.00411.2009
- Marshall, G. E., Russell, J. A., Tellez, J. O., Jhund, P. S., Currie, S., Dempster, J., et al. (2012). Remodelling of human atrial K⁺ currents but not ion channel expression by chronic β -blockade. *Pflugers Arch.* 463, 537–548. doi: 10.1007/s00424-011-1061-z
- Mesubi, O. O., and Anderson, M. E. (2016). Atrial remodelling in atrial fibrillation: CaMKII as a nodal proarrhythmic signal. *Cardiovasc. Res.* 109, 542–557. doi: 10.1093/cvr/cvw002
- Nattel, S. (2006). Preoperative atrial cardiomyocyte ionic currents and postoperative AF: important insights into what is not the mechanism. *J. Cardiovasc. Electrophysiol.* 17, 1239–1241. doi: 10.1111/j.1540-8167.2006.00625.x
- Ni, H., Morotti, S., and Grandi, E. (2018). A heart for diversity: simulating variability in cardiac arrhythmia research. *Front. Physiol.* 9:958. doi: 10.3389/fphys.2018.00958
- Nygren, A., Fiset, C., Firek, L., Clark, J. W., Lindblad, D. S., Clark, R. B., et al. (1998). Mathematical model of an adult human atrial cell: the role of K⁺ currents in repolarization. *Circ. Res.* 82, 63–81. doi: 10.1161/01.RES.82.1.63
- Pau, D., Workman, A. J., Kane, K. A., and Rankin, A. C. (2007). Electrophysiological and arrhythmogenic effects of 5-hydroxytryptamine on human atrial cells are reduced in atrial fibrillation. *J. Mol. Cell. Cardiol.* 42, 54–62. doi: 10.1016/j.yjmcc.2006.08.007
- Sánchez, C., Bueno-Orovio, A., Pueyo, E., and Rodríguez, B. (2017). Atrial fibrillation dynamics and ionic block effects in six heterogeneous human 3D virtual atria with distinct repolarization dynamics. *Front. Bioeng. Biotechnol.* 5:29. doi: 10.3389/fbioe.2017.00029
- Schreieck, J., Wang, Y., Overbeck, M., Schömig, A., and Schmitt, C. (2000). Altered transient outward current in human atrial myocytes of patients with reduced left ventricular function. *J. Cardiovasc. Electrophysiol.* 11, 180–192. doi: 10.1111/j.1540-8167.2000.tb00318.x
- Skibbye, L., Poulet, C., Diness, J. G., Bentzen, B. H., Yuan, L., Kappert, U., et al. (2014). Small-conductance calcium-activated potassium (SK) channels contribute to action potential repolarization in human atria. *Cardiovasc. Res.* 103, 156–167. doi: 10.1093/cvr/cvu121
- Trayanova, N. A. (2014). Mathematical approaches to understanding and imaging atrial fibrillation: significance for mechanisms and management. *Circ. Res.* 114, 1516–1531. doi: 10.1161/CIRCRESAHA.114.302240
- Van Wagoner, D. R., Pond, A. L., Lamorgese, M., Rossie, S. S., McCarthy, P. M., and Nerbonne, J. M. (1999). Atrial L-type Ca²⁺ currents and human atrial fibrillation. *Circ. Res.* 85, 428–436. doi: 10.1161/01.RES.85.5.428
- Voigt, N., Heijman, J., Wang, Q., Chiang, D. Y., Li, N., Karck, M., et al. (2014). Cellular and molecular mechanisms of atrial arrhythmogenesis in patients with paroxysmal atrial fibrillation. *Circulation* 129, 145–156. doi: 10.1161/CIRCULATIONAHA.113.006641
- Wilhelms, M., Hettmann, H., Malek, M. M., Koivumäki, J. T., Dössel, O., and Seemann, G. (2013). Benchmarking electrophysiological models of human atrial myocytes. *Front. Physiol.* 3:487. doi: 10.3389/fphys.2012.00487
- Workman, A. J. (2010). Cardiac adrenergic control and atrial fibrillation. *Naunyn Schmiedebergs Arch. Pharmacol.* 381, 235–249. doi: 10.1007/s00210-009-0474-0
- Workman, A. J., Kane, K. A., and Rankin, A. C. (2001). The contribution of ionic currents to changes in refractoriness of human atrial myocytes associated with chronic atrial fibrillation. *Cardiovasc. Res.* 52, 226–235. doi: 10.1016/S0008-6363(01)00380-7
- Workman, A. J., Marshall, G. E., Rankin, A. C., Smith, G. L., and Dempster, J. (2012). Transient outward K⁺ current reduction prolongs action potentials and promotes afterdepolarizations: a dynamic-clamp study in human and rabbit cardiac atrial myocytes. *J. Physiol.* 590, 4289–4305. doi: 10.1113/jphysiol.2012.235986
- Workman, A. J., Pau, D., Redpath, C. J., Marshall, G. E., Russell, J. A., Kane, K. A., et al. (2006). Post-operative atrial fibrillation is influenced by beta-blocker therapy but not by pre-operative atrial cellular electrophysiology. *J. Cardiovasc. Electrophysiol.* 17, 1230–1238. doi: 10.1111/j.1540-8167.2006.00592.x
- Yue, L., Feng, J., Li, G. R., and Nattel, S. (1996). Transient outward and delayed rectifier currents in canine atrium: properties and role of isolation methods. *Am. J. Physiol.* 270(6 Pt 2), H2157–H2168. doi: 10.1152/ajpheart.1996.270.6.H2157
- Zoni-Berisso, M., Lercari, F., Carazza, T., and Domenicucci, S. (2014). Epidemiology of atrial fibrillation: European perspective. *Clin. Epidemiol.* 6, 213–220. doi: 10.2147/CLEP.S47385

Conflict of Interest Statement: The authors declare that the research was conducted in the absence of any commercial or financial relationships that could be construed as a potential conflict of interest.

Copyright © 2018 Colman, Saxena, Kettlewell and Workman. This is an open-access article distributed under the terms of the Creative Commons Attribution License (CC BY). The use, distribution or reproduction in other forums is permitted, provided the original author(s) and the copyright owner(s) are credited and that the original publication in this journal is cited, in accordance with accepted academic practice. No use, distribution or reproduction is permitted which does not comply with these terms.



Wavelength and Fibrosis Affect Phase Singularity Locations During Atrial Fibrillation

Mirabeau Saha^{1,2†}, Caroline H. Roney^{3†}, Jason D. Bayer^{1,2}, Marianna Meo^{1,2}, Hubert Cochet^{1,2}, Remi Dubois^{1,2} and Edward J. Vigmond^{1,2*}

¹ IMB, UMR 5251, University of Bordeaux, Pessac, France, ² IHU Liryc, Electrophysiology and Heart Modeling Institute, Fondation Bordeaux University, Pessac, France, ³ Department of Biomedical Engineering, King's College London, London, United Kingdom

OPEN ACCESS

Edited by:

Jichao Zhao,
University of Auckland, New Zealand

Reviewed by:

Sanjay Ram Kharche,
University of Western Ontario, Canada
Wouter-Jan Rappel,
University of California, Davis,
United States

*Correspondence:

Edward J. Vigmond
edward.vigmond@u-bordeaux.fr

[†]These authors have contributed
equally to this work

Specialty section:

This article was submitted to
Computational Physiology and
Medicine,
a section of the journal
Frontiers in Physiology

Received: 30 April 2018

Accepted: 10 August 2018

Published: 10 September 2018

Citation:

Saha M, Roney CH, Bayer JD,
Meo M, Cochet H, Dubois R and
Vigmond EJ (2018) Wavelength and
Fibrosis Affect Phase Singularity
Locations During Atrial Fibrillation.
Front. Physiol. 9:1207.
doi: 10.3389/fphys.2018.01207

The mechanisms underlying atrial fibrillation (AF), the most common sustained cardiac rhythm disturbance, remain elusive. Atrial fibrosis plays an important role in the development of AF and rotor dynamics. Both electrical wavelength (WL) and the degree of atrial fibrosis change as AF progresses. However, their combined effect on rotor core location remains unknown. The aim of this study was to analyze the effects of WL change on rotor core location in both fibrotic and non-fibrotic atria. Three patient specific fibrosis distributions (total fibrosis content: 16.6, 22.8, and 19.2%) obtained from clinical imaging data of persistent AF patients were incorporated in a bilayer atrial computational model. Fibrotic effects were modeled as myocyte-fibroblast coupling + conductivity remodeling; structural remodeling; ionic current changes + conductivity remodeling; and combinations of these methods. To change WL, action potential duration (APD) was varied from 120 to 240ms, representing the range of clinically observed AF cycle length, by modifying the inward rectifier potassium current (I_{K1}) conductance between 80 and 140% of the original value. Phase singularities (PSs) were computed to identify rotor core locations. Our results show that I_{K1} conductance variation resulted in a decrease of APD and WL across the atria. For large WL in the absence of fibrosis, PSs anchored to regions with high APD gradient at the center of the left atrium (LA) anterior wall and near the junctions of the inferior pulmonary veins (PVs) with the LA. Decreasing the WL induced more PSs, whose distribution became less clustered. With fibrosis, PS locations depended on the fibrosis distribution and the fibrosis implementation method. The proportion of PSs in fibrotic areas and along the borders varied with both WL and fibrosis modeling method: for patient one, this was 4.2–14.9% as I_{K1} varied for the structural remodeling representation, but 12.3–88.4% using the combination of structural remodeling with myocyte-fibroblast coupling. The degree and distribution of fibrosis and the choice of implementation technique had a larger effect on PS locations than the WL variation. Thus, distinguishing the fibrotic mechanisms present in a patient is important for interpreting clinical fibrosis maps to create personalized models.

Keywords: atrial fibrillation, computer simulation, phase singularity mapping, Fibrosis, repolarization heterogeneity

1. INTRODUCTION

Cardiac arrhythmia is a major cause of death, with considerable health and economic impacts. Atrial Fibrillation (AF) is the most common cardiac arrhythmia. It leads to heart failure and stroke (Kannel et al., 1998). The understanding of the pathophysiology of AF remains incomplete despite numerous experimental and clinical studies, as well as several *in-silico* studies (Wolf et al., 1991; Courtemanche et al., 1998; Labarthe et al., 2014). Currently, because of its easy reproducibility, its inexpensiveness and its non-invasiveness, computational modeling is widely used to investigate the mechanisms underlying AF.

The underlying atrial substrate is essential for AF maintenance (Kostin et al., 2002). For many patients, the success of anti-arrhythmic drug therapy is low. Thus, catheter ablation is used to eliminate arrhythmogenic electrical sources by destroying the underlying tissue substrate (for example by isolating the pulmonary veins or by targeting potential reentrant sources) using localized energy delivery (Earley et al., 2006). However, AF is recurrent in 30–50% of patients (Calkins et al., 2012). The sub-optimal success rate of AF treatment by catheter ablation procedures is confounded by a lack of consensus between clinicians on the precise locations to be targeted (Schotten et al., 2011; Calkins et al., 2012).

AF dynamics are strongly influenced by heterogeneities in the electrophysiological tissue properties (Kottkamp et al., 2016) and the spatial pattern of tissue structural changes, which are patient specific. Cardiac wavelength (WL)—the distance traveled by the depolarization wave during the functional refractory period (Jacquemet et al., 2005)—is shortened by structural and electrical remodeling in tissue with chronic or persistent AF (Krogh-Madsen et al., 2012). Previous studies have shown that modifying WL properties (through action potential duration, APD, variation) affects AF dynamics (Qu et al., 1999). However, Deng et al. (2017) found that with modest changes in electrophysiological properties, reentrant drivers localized to the same areas, at the edges of high fibrotic regions.

Furthermore, myocardial fibrosis affects AF maintenance (Morgan et al., 2016; Cochet et al., 2018). Fibrotic remodeling is multi-factorial, and includes interstitial fibrosis (the deposition of collagen between fiber bundles), replacement fibrosis, gap junctional remodeling due to downregulation of connexin 43, fibroblast coupling and paracrine factors. These factors may initiate and sustain AF by modifying conduction pathways. Previous studies have suggested targeting fibrotic areas during catheter ablation procedures.

In this study, we investigate how WL affects AF driver location using a computational bilayer model of the human atria, incorporating fibrosis distributions based on late gadolinium enhancement (LGE) Magnetic Resonance Imaging (MRI) scans from patients with persistent AF. In comparison with previous studies, we explore a larger range of clinically observed APD, consider multiple techniques for modeling atrial fibrosis, and directly compare with clinical rotor core trajectory data.

2. METHODS

2.1. AF Bilayer Model

We used our previously described human batrial biophysically-detailed bilayer model (Labarthe et al., 2014), with AF simulated as in our former work (Bayer et al., 2016). Briefly, the bilayer model is a finite element model composed of discretely connected 2D layers. The right atrium (RA) consists of an epicardial layer and a layer for the crista terminalis (CT) and the pectinate muscles (PM). The left atrium (LA) comprises endocardial and epicardial layers. Each node on the LA endocardium and RA endocardial structures (the CT and PM) is connected by a discrete resistance to the closest node on the LA or RA epicardial surface, respectively. Interatrial connections include Bachmann's bundle, the rim of the fossa ovalis, and the muscular sheath of the coronary sinus. The mesh contains 363561 nodes with an edge length of approximately 300 μm . Atrial action potentials (AP) vary from region to region (Gelband et al., 1972). As in previous work (Bayer et al., 2016; Roney et al., 2018), the Courtemanche-Ramirez-Nattel human atrial ionic model (Courtemanche et al., 1998) was used and ionic channel conductances varied to recreate the observed heterogeneity (Aslanidi et al., 2011; Krueger et al., 2013). This ionic model is sufficient since we are mainly concerned with APD restitution, and not the detailed subcellular processes seen in newer models which carry significantly increased computational costs. We also incorporate heterogeneous coupling, resulting in different conduction velocities (CVs) in different anatomical regions, according to human data (Lemery et al., 2007; Bayer et al., 2016). Furthermore, to simulate chronic AF, the following electrical remodeling was incorporated: a 50% decrease in the conductance of the atrial-specific ultra-rapid potassium current I_{Kur} , a 50% decrease in the conductance of the transient outward current I_{to} , and a 70% decrease in the conductance of the L-type calcium current I_{CaL} (Courtemanche et al., 1999).

2.2. Wavelength Variation

WL is the product of the effective refractory period (ERP) and CV (Jacquemet et al., 2005), which we approximate as $\text{APD} \times \text{CV}$. Changing the conductance of I_{K1} alone does not affect CV (Entz and William, 2018; Nobles et al., 2018; Valli et al., 2018). Pandit and Jalife (2013) found that the inward rectifier K^+ channel (I_{K1}) has an important role on the spatiotemporal organization of AF drivers across different parts of the heart. Specifically, changes in I_{K1} conductance lead to variation of rotor (AF driver) frequency and tip meander because of changes in APD and in the resting level of the membrane potential (which in turn affects cardiac excitability). Previous studies have investigated the effects of I_{K1} conductance on APD (Dhamoon and Jalife, 2005; Pandit et al., 2005; Lee et al., 2016). We multiplied I_{K1} conductance by 80, 95, 100, 120, and 140 to modify the APD, and thereby the WL. These values were chosen to give tissue AF cycle lengths in the clinically reported range of 120–240 ms (Konings et al., 1994; Ng et al., 2006).

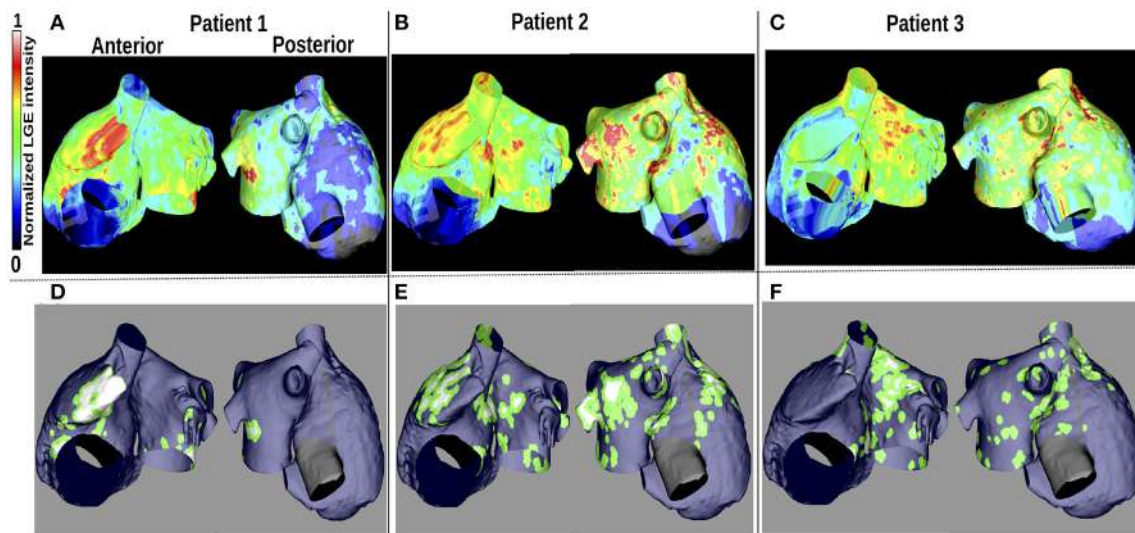


FIGURE 1 | Patient LGE data and fibrosis distribution used for modeling. **(A–C)**: Normalized LGE intensity. **(D–F)**: Fibrotic tissue (white), non-fibrotic areas (blue), and the border between them (green) are shown. The inferior vena cava and line of block regions of the model are electrically inactive and displayed in black in **(D–F)**.

2.3. Patient Fibrosis Data and Fibrosis Modeling

2.3.1. Patient Data

LGE-MRI intensity data from three patients with persistent AF (Cochet et al., 2015) were projected onto the aforementioned computational atrial bilayer model to assign a fibrosis distribution. For each patient, these intensity values were assigned for each point on an endocardial surface mesh as the maximum value through the atrial wall. These distributions of LGE intensity values were then mapped to the atrial bilayer model using an iterative closest point algorithm (Roney et al., 2016; Cochet et al., 2018). Each of the patients gave informed written consent. The ethics committee of the University of Bordeaux approved the study and it complies with the declaration of Helsinki. **Figures 1A–C** show the distribution maps of LGE intensity, normalized with respect to the highest value for each patient. We considered an identical LGE intensity distribution on the LA epicardium and endocardium. For the RA, we included atrial fibrosis in the epicardial layer of the model, but not on the endocardial structures. To incorporate atrial fibrosis in the models, nodes with normalized LGE intensity greater than 0.7 were defined to be fibrotic. This corresponds to 13.2, 27.2, and 27.5% of the LA tissue being classified as fibrotic, for patients 1, 2, and 3 respectively (16.6, 22.8, and 19.2% of the entire atria). Since previous studies have found phase singularities (PSs) on the border between fibrosis and normal myocardium (Zahid et al., 2016; Cochet et al., 2018), we defined nodes within 0.75 mm of the boundary to be in the border region (**Figures 1A–F**). This distance, representing a region about five elements wide, allowed us to be specific, while respecting clinical resolution. This width is less than an ablation line, which is usually greater than 2 mm (Bhaskaran et al., 2016). Therefore, we ensure that if the ablation strategy follows such a border, the

entire width of the border would be ablated. This border region is only considered for post-processing analyses and does not affect the model construction. The border region corresponds to 38.2, 62.4, and 71.9% of the total fibrotic area (normalized LGE intensity greater than 0.7) for patient 1–3, respectively.

2.3.2. Fibrosis Implementation Methods

Computational modeling studies use different methodologies to model fibrosis (Morgan et al., 2016; Vigmond et al., 2016; Zahid et al., 2016), and previous studies show that the reentry dynamics are affected by the fibrosis implementation method. To study how rotor core position changes when WL is varied in fibrotic atria, we used three different implementation methods: structural remodeling, ionic remodeling and fibroblast coupling, as well as two combinations: structural + ionic changes, and structural changes + fibroblast coupling.

Structural Remodeling

Vigmond et al. (2016) and Roney et al. (2016) give detailed descriptions of this method. It consists of randomly removing elements from the mesh, with a probability depending on the normalized LGE intensity.

Ionic Remodeling

To incorporate ionic remodeling, we rescaled the ionic conductances of the human atrial AF ionic cell model, following Zahid et al. (2016). Specifically, in fibrotic regions, ionic conductances were rescaled as follows: 50% reduction in inward rectifier potassium current (I_{K1}), 50% reduction in L-type calcium current (I_{CaL}), and 40% reduction in the sodium current (I_{Na}). To take into account the impact of fibrosis on the intermyocyte coupling, the longitudinal conductivity in the fibrotic regions of the model was reduced by 30%, and then the longitudinal-to-transverse anisotropy ratio was increased to

8:1 to model additional slowing of velocity in the transverse direction.

Fibroblast Coupling

We used the Morgan et al. (2016) model of atrial fibroblasts. Briefly, the interaction between fibroblast and myocyte cells is modeled with a gap junctional conductance of $0.5nS$. For each patient, the normalized LGE intensity was divided into six intervals ($0 - 0.27 - 0.4 - 0.55 - 0.69 - 0.82 - 1$). These intervals correspond to one non-fibrotic region and five different degrees of fibrotic remodeling, ranging from diffuse (1 and 2 fibroblasts per myocyte) to patchy (3 and 4 fibroblasts per myocyte) and dense (5 fibroblasts per myocyte). The myocyte-myocyte longitudinal coupling conductivity was decreased from 100% (in regions with no fibroblast coupling) to 20% of the baseline value (in regions with coupling to 5 fibroblasts per myocyte), following Morgan et al. (2016).

2.4. Simulation Protocol

We used the monodomain formulation and solved it with the Cardiac Arrhythmia Research Package (CARP) simulator (Vigmond et al., 2003). For each case, we first simulated the model for 2 seconds without electrical stimulation, followed by 3.5 s of sinus rhythm with a cycle length of 0.7 seconds (Roney et al., 2016). Five rapid pacing pulses, with a cycle length in the range 112–184 ms, depending on model inducibility, were applied to the upper right pulmonary vein (URPV) to initiate AF. We simulated each model for 2.1 s to allow AF arrhythmia dynamics to stabilize and the final 2.1 seconds were used for analysis for a total simulation time of 9.7 s. All models were inducible.

2.5. Analysis of the Effects of Wavelength Variations on PS Positions

To estimate WL, action potential duration at 90% repolarization (APD90) and CV were calculated over the atrial mesh for each simulation set-up during sinus rhythm. Local CV was computed as the magnitude of conduction velocity. WL was then estimated as the product of APD90 and CV for each node of the mesh.

PSs were located by the intersection of the isopotential line $V_m = -20$ mV and the line of $dV_m/dt = 0$ (Bishop and Plank, 2012). We plotted and analyzed changes in the percentage (defined as the number of PSs in an area over the total number of PSs in the model) and number of PSs per time unit (each ms) located in each atrial region as I_{K1} was varied. We analyzed the following atrial regions separately: the PVs [the upper left pulmonary vein (ULPV), the upper right pulmonary vein (URPV), the left lower pulmonary vein (LLPV) and the lower right pulmonary vein (LRPV)], the fossa-ovalis (FO), the superior vena cava (SVC), the LA and the RA. In models with fibrosis, we analyzed the PS content of the fibrotic areas and their borders. To reduce the computation time, parameters were evaluated on a reduced mesh, excluding the electrically inactive regions (the inferior vena cava and the septal line of block), Bachmann's bundle, the crista terminalis, and the pectinate muscles.

3. RESULTS

3.1. Physiological Changes Due to I_{K1} Variation

APD90, CV, and WL were computed for 5 values of I_{K1} conductance. For each of these measurements, the maximum values were located in the same atrial region for all of the I_{K1} values; this was also the case for the minimum values. Maps of these quantities are illustrated in Figure 2. The maximum and minimum APD90 changed when I_{K1} was varied, as shown in Table 1. As I_{K1} conductance was increased from 80% to 140% of the control value, APD_{min} decreased from 139.9 to 120.5 ms and APD_{max} from 312.9 to 227.1 ms, respectively. The maximum and minimum CV were ~ 1.1 and ~ 0.15 m/s, respectively. The CV extrema exhibit little variation as I_{K1} increased from 80% to 140% of control. The minimum and maximum WL decreased from 35.9 to 28.4 mm, and from 312.4 to 225.6 mm, respectively, when I_{K1} varied from 80 to 140% of control as shown in Table 1. These WL calculations are local and based on nonuniform propagation; APD and CV are influenced by wavefront curvature, changes in fiber direction, propagation into inexcitable borders, and wavefront collision.

The APD90 map is almost uniform on the LA posterior wall. On the LA anterior wall, the APD is higher around Bachmann's bundle than on the rest of the wall. This results in a large gradient of APD around the connection area. The CV and WL are higher on the LA wall area close to the LAA and inferior PV intersections. The highest APD, CV and WL values are seen on the RA posterior wall at the crista terminalis and pectinate muscles, and near the anterior SVC junction. There are gradients in APD and WL around the intersections of the LA wall with the PVs.

3.2. PS Location With No Fibrosis

Figures 3A–E show changes in PS density as I_{K1} is varied, and Figure 3F shows a corresponding map indicating the PS locations. For small I_{K1} values (corresponding to large APD values), rotor organizing centers were more likely to appear on the LA than the RA, in the center of the anterior wall and around the lower PVs intersections, where the APD gradients are high (see Figure 2). As the WL decreased (corresponding to increased I_{K1}), the PS density became less clustered and more widespread over the LA. In addition, PS trajectories covered larger areas of the RA. Concurrently, in the LA, the PS density decreased progressively as WL decreased, and more PS positions appeared.

Figure 4 shows how the number and locations of PSs change in different areas as the I_{K1} conductance was varied. The percentage of PS positions on the LA decreases from $\sim 90\%$ for large APD values to $\sim 60\%$ for short APD values, while it increases in the RA and PVs from $\sim 5\%$ each to $\sim 22\%$ and $\sim 18\%$, respectively. The number of PSs increases with I_{K1} conductance for all regions. There were a greater number of PSs on the LA than on the RA for all I_{K1} conductance values.

The LA had ~ 1.6 PS positions per time unit compared to ~ 0.1 in the RA for large APD, while for short APD, the LA had ~ 2.3 compared to ~ 0.9 in the RA. The lower PVs (Figure 4C) had an order of magnitude more PSs than the upper PVs (Figure 4D).

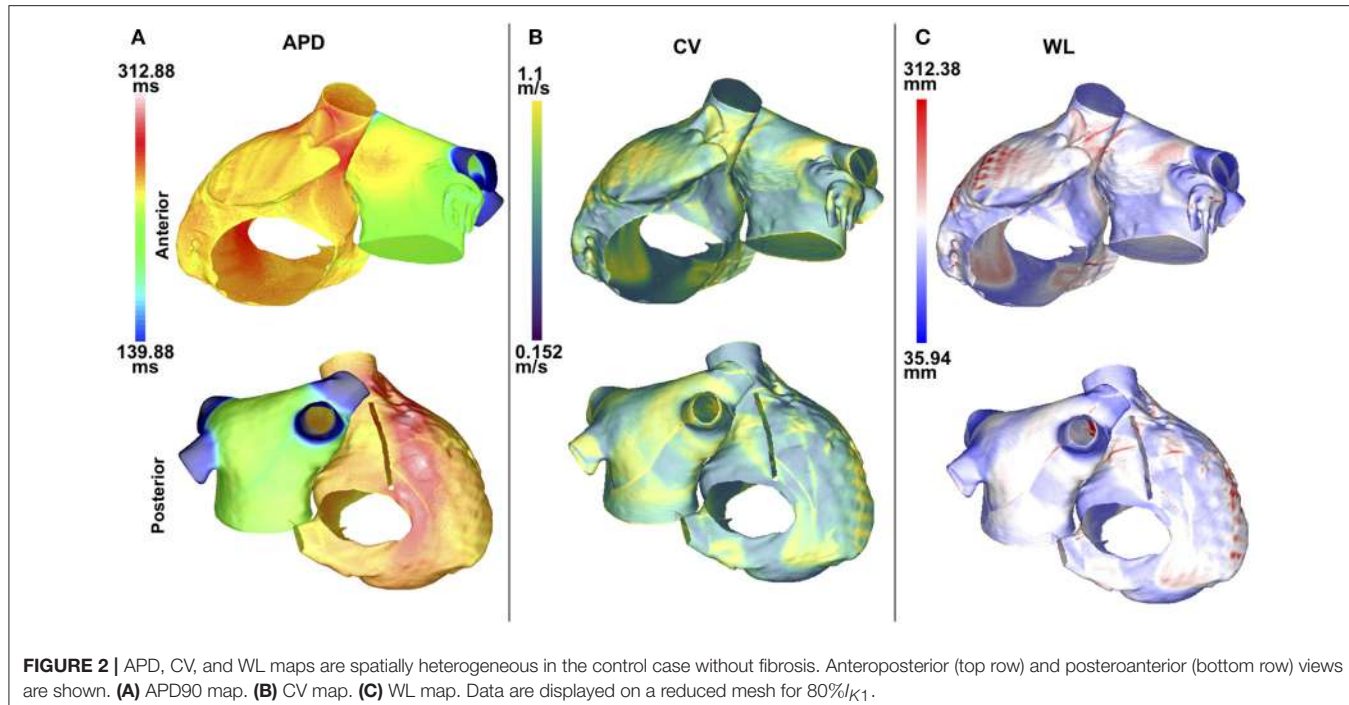


FIGURE 2 | APD, CV, and WL maps are spatially heterogeneous in the control case without fibrosis. Anteroposterior (top row) and posteroanterior (bottom row) views are shown. **(A)** APD90 map. **(B)** CV map. **(C)** WL map. Data are displayed on a reduced mesh for 80% I_{K1} .

TABLE 1 | Physiological changes due to I_{K1} variation.

I_{K1} percentage	80%	95%	100%	120%	140%
APD90min (ms)	139.9	134.7	133.1	127.3	120.5
APD90max (ms)	312.9	285.5	269.1	245.1	227.1
WLmin (mm)	35.9	30.1	28.2	29.3	28.4
WLmax (mm)	312.4	281.7	274.2	246.0	225.6

APDmin and APDmax are minimum and maximum APD, respectively. WLmin and WLmax are minimum and maximum WL, respectively.

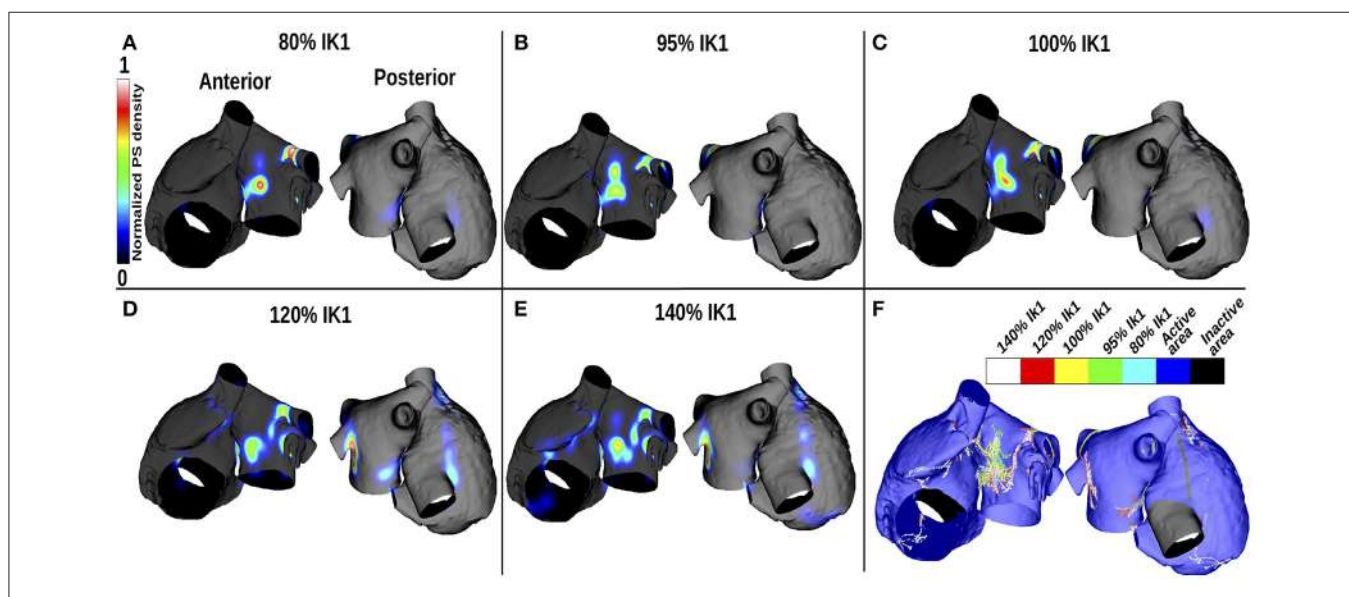


FIGURE 3 | PS density maps change with APD variation for the control case of no atrial fibrosis. Each subfigure shows anteroposterior (left) and posteroanterior (right) views. **(A–E)** display PS density distributions for 5 I_{K1} values. **(F)** Shows PS positions displayed on the same mesh for the different I_{K1} values.

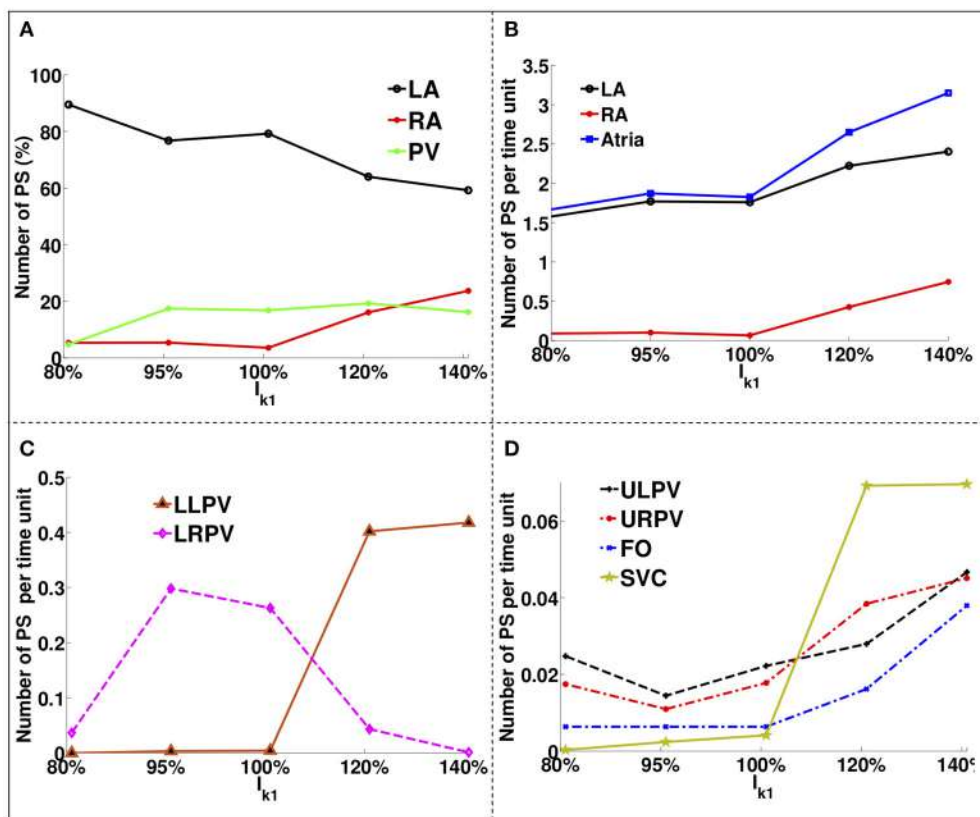


FIGURE 4 | PS location variation as a function of I_{K1} for atria with no fibrosis. **(A)** Percentage of PS locations on the LA body, on the RA and on the PVs. **(B)** Number of PSs per unit time on the entire LA, on the RA and on the whole atria. **(C)** Number of PSs per time unit on the LLPV and on the LRPV. **(D)** Number of PSs per unit time on the ULPV, URPV, FO, and SVC.

The number of PSs on the FO and SVC increased monotonically with I_{K1} conductance. For large APD values, there were no PS located on the LLPV or on the SVC, but as APD was decreased, the number of PS on both the LLPV and SVC increased.

3.3. PS Location Analyses for Cases With Fibrosis

Rotor core location depends on both fibrosis distribution and WL. Results are presented in full for one patient; similar results for the other patients are presented in the **Supplementary Material**.

Figure 5 presents PS location maps for patient 2 as I_{K1} conductance was varied from 80 to 140% for the five fibrosis implementation methods: structural changes, ionic current remodeling, myocyte-fibroblast coupling, the combination of structural + ionic current remodeling, and the combination of structural changes + myocyte-fibroblast coupling. An area of moderate PS density on the anterior wall of the LA and RA is seen in the clinical data (Figure 5F), and also in each of the simulations. This area of agreement is present for all of the fibrosis implementations. There is an area of high PS density on the posterior wall of the LA in the clinical, as presented in Figure 5F, that is not reproduced in the simulation results.

Supplementary Figure 1 presents PS density maps corresponding to long and short APD values for each of the fibrosis modeling methodologies, for each of the patients. In general, there is a good visual correspondence between PS density maps for long and short APDs, and a much larger variation in PS density maps between fibrosis implementation methods. The correlation between PS density maps as APD is varied is greatest for the ionic method (see **Supplementary Tables 1–3**), and generally lower for the structural remodeling method.

Figure 5A shows that for the structural remodeling method, reentry cores were more likely to be located outside of the fibrotic areas than either inside the fibrotic areas or in the border regions, regardless of APD variation. PSs are also more likely to be in the fibrosis border region than in the fibrosis region itself. Figure 6A quantifies this for structural remodeling in terms of the percentages of PS positions on the border and in the fibrosis area for each patient as APD changes: more than 60% of the PS positions are located outside of the fibrotic area, regardless of the fibrosis distribution.

For the ionic current remodeling method (Figures 5B, 6B), PSs tend to cluster more on the border and in the fibrotic areas than using the structural remodeling methodology or the combination methodologies. With this fibrosis implementation, the number of PS per unit time in the

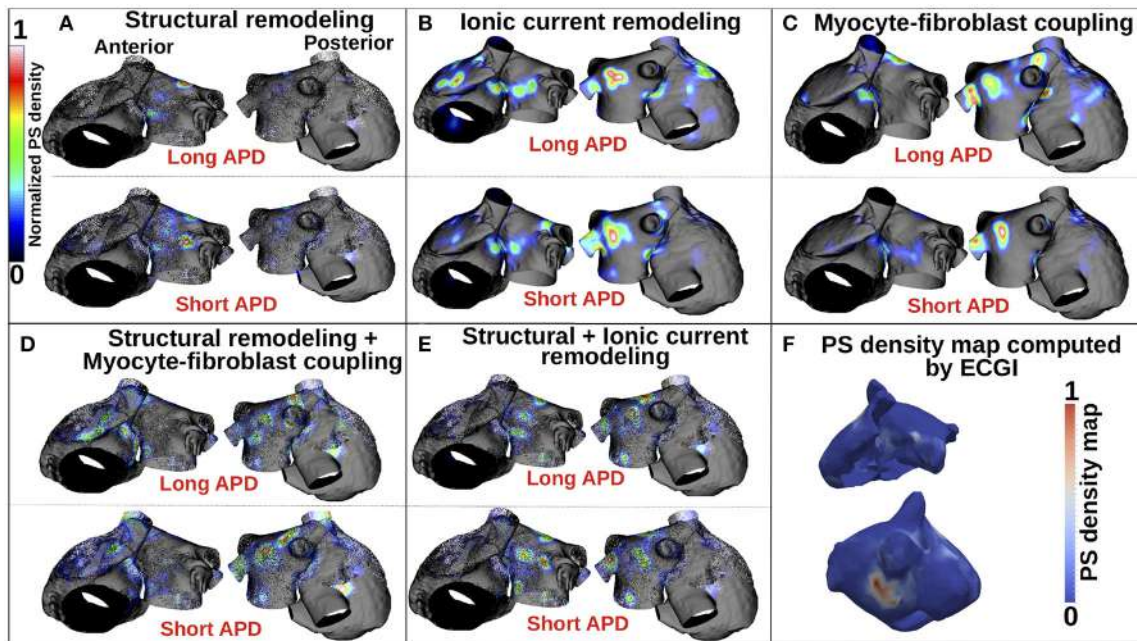


FIGURE 5 | PS density maps depend on both fibrosis implementation method and APD. **(A–E)** Show PS density maps for the 5 fibrosis implementation methods: structural remodeling, ionic current remodeling, myocyte-fibroblast coupling, structural remodeling + myocyte-fibroblast coupling, and structural + ionic current remodeling, respectively. **(F)** Clinical PS density map computed using electrocardiographic imaging (ECGI). These data are for patient 2; see Supplementary Figure 1 for patients 1 and 3.

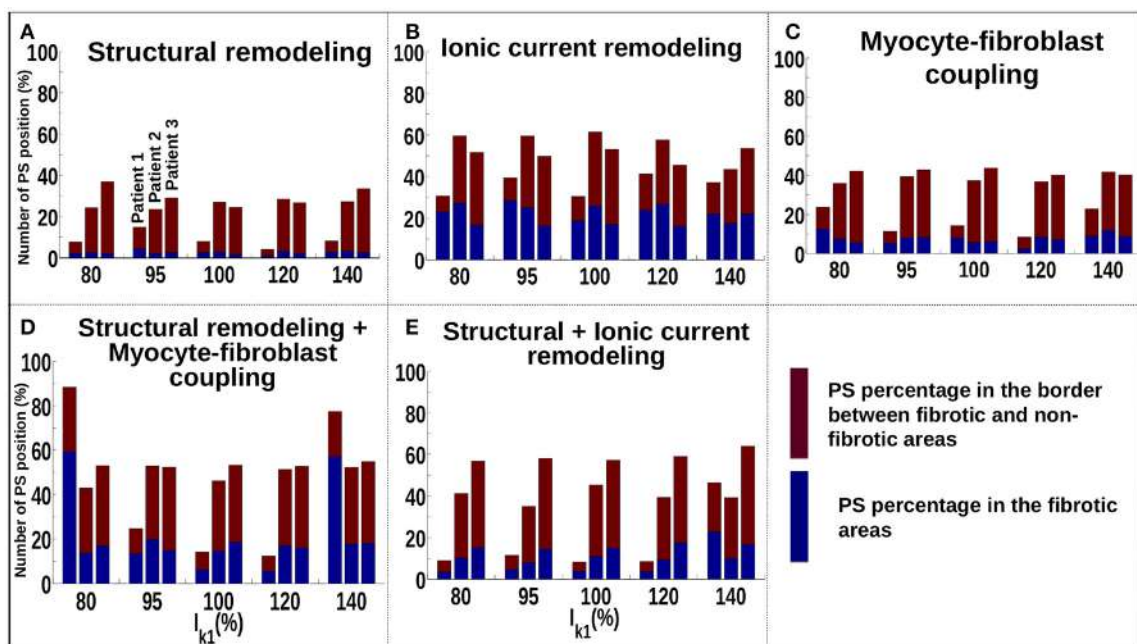
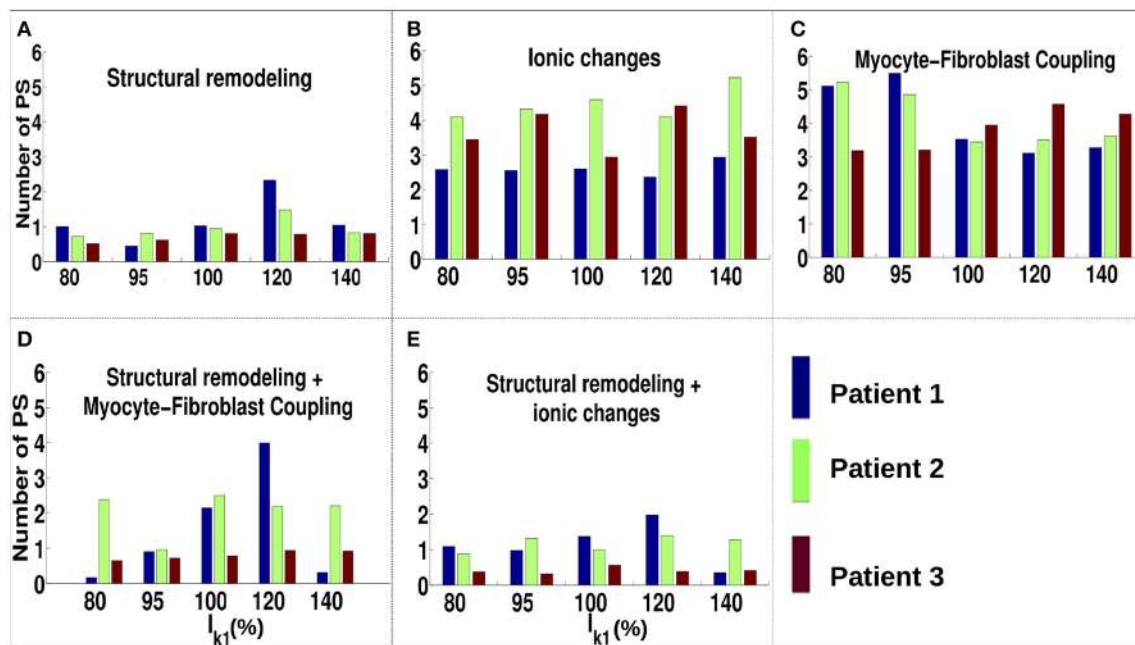


FIGURE 6 | Number of PSs located in the border and in the fibrosis area for patients 1–3 for different fibrosis modeling methodologies, corresponding to: **(A)** structural remodeling, **(B)** ionic current remodeling, **(C)** myocyte-fibroblast coupling, **(D)** structural remodeling and myocyte-fibroblast coupling, **(E)** structural and ionic current remodeling.



entire atria (Figure 7B) is higher (mean $\sim 3.53 \pm 0.84$ PS per unit time) than for methodologies incorporating structural remodeling (Figures 7A,D,E; mean values: $\sim 0.95 \pm 0.44$, $\sim 1.45 \pm 1.02$, and $\sim 0.92 \pm 0.48$, respectively). The number of PS is higher and the distribution is less scattered using ionic current remodeling than using methodologies incorporating structural remodeling.

For the myocyte-fibroblast coupling method (Figures 5C, 6C), the proportion of PSs within the fibrotic area and its border is higher than the equivalent measures for structural changes, but lower than for the ionic current remodeling method. The number of PS per time unit in the entire atria (Figure 7C) using the myocyte-fibroblast coupling method is $\sim 4.02 \pm 0.80$. Thus, it is higher than the number of PSs using implementations including structural remodeling. For the two combination methods (Figures 5D,E, 6D,E), PSs tend to cluster more in the border and the fibrotic areas than using the structural remodeling method alone, but the number of PS per time unit in the entire atria remains low ($\sim 1.45 \pm 1.02$ and $\sim 0.92 \pm 0.48$ for Figures 7D,E, respectively). The myocyte-fibroblast coupling method and the ionic method result in a larger number of PSs than the structural remodeling or combination methods, and the PS density maps for these methods are more similar to each other than to the structural remodeling method (see Supplementary Figure 1). For each of the fibrosis implementation methods together with the different patient-specific fibrosis distributions, the number of PSs varies non-monotonically as the APD is decreased.

As for the control case without fibrosis, we investigated how the quantity of reentry cores located in different parts of

the atria varies with APD. For each patient and each fibrosis implementation method, the variation in the percentage of PS located on all the PVs, on the LA and on the RA are presented in Supplementary Figure 2. The relative distribution of PSs in the LA compared to the RA changes between the fibrosis modeling methodologies. For example, for patient 3, there is a higher number of PSs in the RA compared to the LA for structural remodeling ($\sim 62.28 \pm 10.57\%$ of PS located on RA vs. $\sim 30.13 \pm 11.16\%$ on LA) and also for combining structural remodeling and ionic current changes (RA $\sim 47.24 \pm 5.82\%$ vs. LA $\sim 37.99 \pm 3.60\%$). Whereas, there is a higher number in the LA than the RA for the other modeling methodologies (ionic current changes: RA $\sim 28.48 \pm 5.97\%$ vs. LA $\sim 52.08 \pm 5.48\%$; fibroblast coupling method alone: RA $\sim 31.50 \pm 6.75\%$ vs. LA $\sim 49.11 \pm 8.16\%$; and combining structural remodeling and fibroblast coupling techniques: RA $\sim 28.35 \pm 3.45\%$ vs. LA $\sim 50.14 \pm 5.64\%$).

The number of PS per unit time located on the LA, on the RA, around the FO, on the SVC and on each PV are shown in Supplementary Figure 3 for different WLs. These quantities vary with WL. Using the structural remodeling method for fibrosis, patient 1 has ~ 7.7 , ~ 14.9 , ~ 7.97 , ~ 4.18 , and $\sim 8.29\%$ of PS located in fibrosis areas and borders for the 5 increasing values of I_{K1} , respectively (Figure 6A). Combining structural remodeling with myocyte-fibroblast coupling, the number of PS in fibrosis areas and borders are: ~ 88.41 , ~ 24.69 , ~ 14.20 , ~ 12.34 , and $\sim 77.53\%$, respectively (Figure 6D), demonstrating that the effect of the fibrosis implementation formulation may be greater than the effect of the variation of WL.

4. DISCUSSION

In this study, we used computer modeling to investigate the effects of WL variation on reentry in both fibrotic atria and non-fibrotic atria for three different patient-specific fibrosis distributions, with five known fibrosis implementation methods, on the same atrial mesh to exclude geometrical effects. Our study is unique in that it explores a broader range of APDs, closer to the range seen clinically, as well as investigating the effects of different AF modeling implementations. We further elucidated how structural and electrophysiological remodeling interact to determine rotor core location.

In the case of AF without fibrosis, PSs anchor on the center of the LA anterior wall and near the LA/PV junction for large APD values (Figure 3). These areas have high APD gradients (Figure 2). Decreasing the WL increases the number of PS and the distribution becomes less focused. In the case of fibrotic atria, propagation is constrained by the distribution of fibrosis through the physiological and/or structural changes made to the tissue, depending on the formulation of the implementation method. Previous clinical and computational studies have shown that tissue areas with higher fibrosis density attract more reentrant activity than other areas (Deng et al., 2017; Cochet et al., 2018), but the trajectories can change, particularly when there are several fibrotic areas close to each other.

There is more variation in the number and location of PSs as I_{K1} varies in our simulations without fibrosis, demonstrating that the effects of WL will depend on the degree of fibrosis (comparing Figures 4, 7). The fibrosis modeling method has a large effect on the number of PSs in the fibrosis areas and its border. WL has a larger effect on rotor location for the myocyte-fibroblast coupling method and the structural remodeling method than for the other methodologies.

Incorporating atrial fibrosis in the model changed the relationship between WL and number of PSs. Figure 7 shows that there is no consistent relationship between I_{K1} conductance and the number of PSs for any of the fibrosis implementation methodologies. The number of PSs, and their locality to the fibrotic areas (Figure 6), shows a greater dependence on the fibrosis type than the I_{K1} conductance. In addition, there are large differences in the proportion of PSs located in regions of fibrosis between fibrosis implementation types. Clinically, there is evidence both for (Cochet et al., 2018) and against (Chrispin et al., 2016) the delocalization of rotational activity with high LGE-intensity. These differences may be because of variations in the type of atrial remodeling. LGE imaging does not have the resolution required to capture microscale fibrotic factors; the effects of which may change as AF progresses.

The structural remodeling method localizes less PSs in areas with high fibrosis intensity, but combining the structural remodeling method with either ionic current remodeling or fibroblast-myocyte coupling forms electrical heterogeneities that better anchor the reentrant drivers. In particular, reentry anchors around areas of fibrosis for the ionic remodeling method due to the longer APD and lower CV with this fibrosis implementation method. Similar results were found in our previous work (Roney et al., 2016), in which differences in the amounts of rotational

activity and wavebreak were found between models. Zou et al. (2005) showed that AF initiation, maintenance and dynamics are strongly affected by substrate size. In addition, Panfilov (2006) suggested that the number of fibrillatory sources is proportional to the effective tissue size. In our study, the low presence of PS locations in high fibrosis density zones when modeling structural changes alone may be explained by the large quantity of elements that are removed in these regions, making the effective size of the tissue per unit surface area too small for rotor creation. The effective tissue size per surface unit is also low for cases with structural remodeling combined with ionic remodeling or fibroblast coupling, leading to a low presence of PS locations in high fibrosis density regions. Incorporating ionic remodeling or fibroblast coupling alone to implement fibrosis does not affect the effective tissue size per unit area, and results in a larger quantity of PSs. The higher number of PSs obtained with the fibroblast coupling method compared to the ionic remodeling method may be explained by the way in which the gradient of the physiological parameters is implemented for the two methods. The ionic remodeling method imposes an abrupt decrease in the conductivity at the border between fibrotic and non-fibrotic zones, whereas the fibroblast coupling method has five different levels of conductivity, changing from non-fibrotic to the highly fibrotic zones. This suggests that a more gradual spatial change in conductivity may lead to a larger number of PSs.

Deng et al. (2017) investigated the sensitivity of rotor location to variations in APD and CV, for simulations incorporating fibrosis modeled with modified ionic and conductivity properties. In their simulations, rotors were overwhelmingly located in border regions between fibrotic and healthy tissue regardless of APD and CV values; however, the specific border regions that contained rotors varied depending on the APD and CV parameters. A subset of rotor locations in the modified APD and CV cases were also present in the baseline case (35–80% agreement). The ionic remodeling fibrosis modeling methodology in our study is similar to the methodology used by Deng et al. (2017). We found a higher proportion of PSs in the fibrosis area and its border using this methodology than either the structural remodeling or fibroblast coupling method, and this proportion was high for all I_{K1} values. For the ionic fibrosis implementation, the number and distribution of PSs was similar for the different I_{K1} values. As such, our findings for the ionic fibrosis implementation agree with those of Deng et al. (2017) since we also see PSs in the fibrosis border zone, with some sites preserved as well as some different sites emerging as I_{K1} is varied.

However, in our simulations, there were also a significant proportion of PSs outside of the fibrosis area and border region, particularly around areas with significant APD gradient - for example the LA/PV junction. PS locations were found in areas of long APD (Figure 3), which is consistent with previous studies showing that areas of long APD attract PSs more strongly than inexcitable obstacles (Calvo et al., 2014; Defauw et al., 2014). Our model includes regional heterogeneity between atrial regions, resulting in APD heterogeneities in addition to those from the fibrosis distribution. Further differences in behavior may be attributable to model differences which include our representation of a bilayer mesh with discrete interatrial

connections as opposed to a continuous three-dimensional (3D) mesh.

The parameters used for the fibrosis modeling methodologies will affect PS distributions. For the ionic current remodeling method, a threshold intensity must be chosen to assign fibrotic regions, while for the myocyte-fibroblast coupling method, the number of fibroblasts must be chosen. The ionic and fibroblast methods include different degrees of conductivity changes. Matching simulation results with clinical data depends on these parameters. Parameter choice sensitivity was investigated in previous studies (Morgan et al., 2016; Roney et al., 2016; Zahid et al., 2016).

Catheter ablation therapy typically focuses on the LA. Our results show that the proportion of PSs in the RA is typically low for longer APD values; however, this increases as APD decreases (see **Figure 4A**). This suggests that for shorter WLs, the RA may play a larger role in driving the arrhythmia and RA ablation may be required. In addition, for the control case without fibrosis, the number of PSs and arrhythmia complexity increases as WL is decreased (see **Figure 4B**). Thus, estimating WL (as the product of AF cycle length and CV) during a procedure may help with therapy planning.

Multiple studies have investigated the effects of ERP, CV and tissue area on the probability that AF sustains. For example, Ravelli and Allessie (1997) found that ERP shortening induced by atrial stretch increased AF vulnerability; Zhuang et al. (2011) report that AF recurrence is more likely in dilated atria because of the increase in size; and Lee et al. (2013) found that both ERP and area affect the probability that AF sustains. Rensma et al. (1988) suggested that ERP and CV alone are poor predictors of susceptibility to reentry, and that the combined measure of WL is a better predictor. Reentry occurs when the path length taken by the wavefront is longer than the WL. WL changes as AF progresses due to increased electrical and structural remodeling. AF susceptibility can then be considered in terms of a critical WL value (Jacquemet et al., 2005), or a fibrillation number, which combines the atrial area and WL into a single measure that is higher in patients with post PV isolation AF inducibility (Hwang et al., 2015). In our study, the number of PSs increases with decreasing WL for simulations without fibrosis, meaning that shorter WL AF simulations are more likely to sustain. However, this was not the case for simulations with fibrosis. Fareh et al. (1998) found that ERP heterogeneity was more important than WL in predicting AF susceptibility, which may be the case for our simulations with fibrosis in which the presence of fibrosis results in conduction and depolarization gradients.

Reentry dynamics depend on both depolarization gradients, with increased PS density in regions of high APD gradient (for example the LA/PV junction), and fibrosis distribution. PS density maps show a closer correspondence with LGE-MRI intensity and are less affected by WL for ionic remodeling and myocyte-fibroblast coupling than for structural remodeling. The effects of fibrosis may outweigh the effects of WL variation in later stages of AF when the fibrosis burden is higher. During the onset of AF, WL and electrophysiology may be more important since electrical remodeling typically occurs before substrate remodeling.

5. LIMITATIONS

To investigate the effects of WL and fibrosis in isolation, we used the same atrial geometry for all simulations. However, patient-specific geometry and volume will affect AF dynamics (Cochet et al., 2018). The choice of human atrial cell model affects PS locations (Cherry and Evans, 2008; Wilhelms et al., 2013), but we did not investigate this. We changed WL through variations in ERP, but CV will also affect WL and reentry dynamics (Lim et al., 2017). In addition, we use a 2D bilayer model of the atria, rather than a full 3D model, so we cannot account for the effects of atrial thickness on rotor dynamics (Dutta et al., 2016). We used identical fibrosis distributions for the endocardial and epicardial surfaces of the LA and only included fibrosis on the RA epicardium; however, fibrosis is known to occur in the pectinate muscles (Spach et al., 1988) and the development of atrial fibrosis varies across the atrial thickness (Verheule et al., 2014), starting in the epicardial layer. We normalized LGE intensity to the maximum value for each patient, rather than working with either a number of standard deviations above the blood pool mean or the image intensity ratio for defining fibrotic tissue, which means that the amount of fibrosis included in each model does not necessarily reflect the Utah score for the patient. The choice of LGE-MRI intensity threshold used to define fibrotic and non-fibrotic areas in the image processing and modeling pipeline will affect the resulting AF dynamics, but the optimum value is unknown. For the fibroblast-myocyte coupling model of fibrosis, the fibroblast-myocyte gap-junction conductance value remains experimentally uncertain; *in vivo* measurements are required to validate fibroblast-myocyte coupling properties used in the simulations.

6. CONCLUSION

Cardiac WL affects reentry dynamics. Without fibrotic remodeling, increasing the cardiac WL decreased arrhythmia complexity, such that reentrant activities anchored and the number of PSs reduced. WL variation also modified reentry dynamics in fibrotic atria; however, this relationship is more complicated, as it also depends on the fibrosis distribution and fibrosis implementation method. The effects of WL, electrophysiology and APD heterogeneity should be included in computational simulations of AF. With higher fibrosis content, simulated PSs are less affected by WL and more likely to be found close to fibrotic patches. This has implications for model personalization as it suggests that it is important to tune WL for patients with a low degree of fibrotic remodeling, whilst LGE maps alone may be sufficient to predict behavior for patients with significant fibrosis, for which fibrosis implementation method is important.

AUTHOR CONTRIBUTIONS

MS ran the computational simulations, analyzed data and generated graphs. CR and EV conceived and designed the study and wrote analysis tools for the project. MS, CR, and EV drafted the manuscript. JB provided technical input on the simulation

tools. MM and RD analyzed the CardioInsight clinical data. HC segmented the LGE-MRI data.

FUNDING

The funding for this study was provided by the FRM (Fondation de la Recherche Medicale) grant SPF20160936220. CR acknowledges a Lefoulon-Delalande Foundation fellowship administered by the Institute of France. This study received financial support from the French Government as part of the Investments of the Future program managed by the National Research Agency (ANR), grant reference ANR-10-IAHU-04.

REFERENCES

- Aslanidi, O. V., Colman, M. A., Stott, J., Dobrzynski, H., Boyett, M. R., Holden, A. V., et al. (2011). 3d virtual human atria: A computational platform for studying clinical atrial fibrillation. *Progr. Biophys. Mol. Biol.* 107, 156–168. doi: 10.1016/j.pbiomolbio.2011.06.011
- Bayer, J. D., Roney, C. H., Pashaei, A., Jaïs, P., and Vigmond, E. J. (2016). Novel radiofrequency ablation strategies for terminating atrial fibrillation in the left atrium: a simulation study. *Front. Physiol.* 7:108. doi: 10.3389/fphys.2016.00108
- Bhaskaran, A., Chik, W., Pouliopoulos, J., Nalliah, C., Qian, P., Barry, T., et al. (2016). Five seconds of 50–60 w radio frequency atrial ablations were transmural and safe: an *in vitro* mechanistic assessment and force-controlled *in vivo* validation. *Europace* 19, 874–880. doi: 10.1093/europace/euw077
- Bishop, M. J., and Plank, G. (2012). The role of fine-scale anatomical structure in the dynamics of reentry in computational models of the rabbit ventricles. *J. Physiol.* 590, 4515–4535. doi: 10.1113/jphysiol.2012.229062
- Calkins, H., Kuck, K. H., Cappato, R., Brugada, J., Camm, A. J., Chen, S.-A., et al. (2012). 2012 HRS/EHRA/ECAS Expert consensus statement on catheter and surgical ablation of atrial fibrillation: recommendations for patient selection, procedural techniques, patient management and follow-up, definitions, endpoints, and research trial design. *Heart Rhythm* 9, 632–696. doi: 10.1016/j.hrthm.2011.12.016
- Calvo, C. J., Deo, M., Zlochiver, S., Millet, J., and Berenfeld, O. (2014). Attraction of rotors to the pulmonary veins in paroxysmal atrial fibrillation: a modeling study. *Biophys. J.* 106, 1811–1821. doi: 10.1016/j.bpj.2014.02.030
- Cherry, E. M., and Evans, S. J. (2008). Properties of two human atrial cell models in tissue: restitution, memory, propagation, and reentry. *J. Theor. Biol.* 254, 674–690. doi: 10.1016/j.jtbi.2008.06.030
- Chrissin, J., Ipek, E. G., Zahid, S., Prakosa, A., Habibi, M., Spragg, D., et al. (2016). Lack of regional association between atrial late gadolinium enhancement on cardiac magnetic resonance and atrial fibrillation rotors. *Heart Rhythm* 13, 654–660. doi: 10.1016/j.hrthm.2015.11.011
- Cochet, H., Dubois, R., Yamashita, S., Al Jefairi, N., Berte, B., Sellal, J.-M., et al. (2018). Relationship between fibrosis detected on late gadolinium-enhanced cardiac magnetic resonance and re-entrant activity assessed with electrocardiographic imaging in human persistent atrial fibrillation. *JACC Clin. Electrophysiol.* 4, 17–29. doi: 10.1016/j.jacep.2017.07.019
- Cochet, H., Mouries, A., Nivet, H., Sacher, F., Derval, N., Denis, A., et al. (2015). Age, atrial fibrillation, and structural heart disease are the main determinants of left atrial fibrosis detected by delayed-enhanced magnetic resonance imaging in a general cardiology population. *J. Cardiovasc. Electrophysiol.* 26, 484–492. doi: 10.1111/jce.12651
- Courtemanche, M., Ramirez, R. J., and Nattel, S. (1998). Ionic mechanisms underlying human atrial action potential properties: insights from a mathematical model. *Am. J. Physiol. Heart Circ. Physiol.* 275, H301–H321. doi: 10.1152/ajpheart.1998.275.1.H301
- Courtemanche, M., Ramirez, R. J., and Nattel, S. (1999). Ionic targets for drug therapy and atrial fibrillation-induced electrical remodeling: insights from a mathematical model. *Cardiovasc. Res.* 42, 477–489. doi: 10.1016/S0008-6363(99)00034-6
- EV acknowledges PRACE for awarding access to Marconi at CINECA, Italy, and to ARCHER UK National Supercomputing Service. JB gratefully acknowledges the French National Research Agency for the grant ANR-16-CE19-0009. This work was also supported by the Wellcome/EPSRC Center for Medical Engineering [WT 203148/Z/16/Z].
- ## SUPPLEMENTARY MATERIAL
- The Supplementary Material for this article can be found online at: <https://www.frontiersin.org/articles/10.3389/fphys.2018.01207/full#supplementary-material>

- approach for ablation of atrial fibrillation. *J. Cardiovasc. Electrophysiol.* 27, 22–30. doi: 10.1111/jce.12870
- Krogh-Madsen, T., Abbott, G. W., and Christini, D. J. (2012). Effects of electrical and structural remodeling on atrial fibrillation maintenance: a simulation study. *PLoS Comput. Biol.* 8:e1002390. doi: 10.1371/journal.pcbi.1002390
- Krueger, M. W., Dorn, A., Keller, D. U., Holmqvist, F., Carlson, J., Platonov, P. G., et al. (2013). *in-silico* modeling of atrial repolarization in normal and atrial fibrillation remodeled state. *Med. Biol. Eng. Comput.* 51, 1105–1119. doi: 10.1007/s11517-013-1090-1
- Labarthe, S., Bayer, J., Coudière, Y., Henry, J., Cochet, H., Jaïs, P., et al. (2014). A bilayer model of human atria: mathematical background, construction, and assessment. *Europace* 16, iv21–iv29. doi: 10.1093/europace/euu256
- Lee, A. M., Aziz, A., Didesch, J., Clark, K. L., Schuessler, R. B., and Damiano, R. J. (2013). Importance of atrial surface area and refractory period in sustaining atrial fibrillation: testing the critical mass hypothesis. *J. Thoracic Cardiovasc. Surg.* 146, 593–598. doi: 10.1016/j.jtcvs.2012.04.021
- Lee, Y.-S., Hwang, M., Song, J.-S., Li, C., Joung, B., Sobie, E. A., et al. (2016). The contribution of ionic currents to rate-dependent action potential duration and pattern of reentry in a mathematical model of human atrial fibrillation. *PLoS ONE* 11:e0150779. doi: 10.1371/journal.pone.0150779
- Leamy, R., Birnie, D., Tang, A. S., Green, M., Gollob, M., Hendry, M., et al. (2007). Normal atrial activation and voltage during sinus rhythm in the human heart: an endocardial and epicardial mapping study in patients with a history of atrial fibrillation. *J. Cardiovasc. Electrophysiol.* 18, 402–408. doi: 10.1111/j.1540-8167.2007.00762.x
- Lim, B., Hwang, M., Song, J.-S., Ryu, A.-J., Joung, B., Shim, E. B., et al. (2017). Effectiveness of atrial fibrillation rotor ablation is dependent on conduction velocity: an *in-silico* 3-dimensional modeling study. *PLoS ONE* 12:e0190398. doi: 10.1371/journal.pone.0190398
- Morgan, R., Colman, M. A., Chubb, H., Seemann, G., and Aslanidi, O. V. (2016). Slow conduction in the border zones of patchy fibrosis stabilizes the drivers for atrial fibrillation: insights from multi-scale human atrial modeling. *Front. Physiol.* 7:474. doi: 10.3389/fphys.2016.00474
- Ng, J., Kadish, A. H., and Goldberger, J. J. (2006). Effect of electrogram characteristics on the relationship of dominant frequency to atrial activation rate in atrial fibrillation. *Heart Rhythm* 3, 1295–1305. doi: 10.1016/j.hrthm.2006.07.027
- Nobles, M., Montaigne, D., Sebastian, S., Birnbaumer, L., and Tinker, A. (2018). Differential effects of inhibitory g-protein isoforms on g-protein gated inwardly rectifying K^+ currents in adult murine atria. *Am. J. Physiol. Cell Physiol.* 314, C616–C626. doi: 10.1152/ajpcell.00271.2016
- Pandit, S. V., Berenfeld, O., Anumonwo, J. M., Zaritski, R. M., Kneller, J., Nattel, S., et al. (2005). Ionic determinants of functional reentry in a 2-D model of human atrial cells during simulated chronic atrial fibrillation. *Biophys. J.* 88, 3806–3821. doi: 10.1529/biophysj.105.060459
- Pandit, S. V., and Jalife, J. (2013). Rotors and the dynamics of cardiac fibrillation. *Circ. Res.* 112, 849–862. doi: 10.1161/CIRCRESAHA.111.300158
- Panfilov, A. V. (2006). Is heart size a factor in ventricular fibrillation? or how close are rabbit and human hearts? *Heart Rhythm* 3, 862–864. doi: 10.1016/j.hrthm.2005.12.022
- Qu, Z., Weiss, J. N., and Garfinkel, A. (1999). Cardiac electrical restitution properties and stability of reentrant spiral waves: a simulation study. *Am. J. Physiol. Heart Circ. Physiol.* 276, H269–H283. doi: 10.1152/ajpheart.1999.276.1.H269
- Ravelli, F., and Allessie, M. (1997). Effects of atrial dilatation on refractory period and vulnerability to atrial fibrillation in the isolated Langendorff-perfused rabbit heart. *Circulation* 96, 1686–1695. doi: 10.1161/01.CIR.96.5.1686
- Rensma, P. L., Allessie, M. A., Lammers, W. J., Bonke, F. I., and Schalij, M. J. (1988). Length of excitation wave and susceptibility to reentrant atrial arrhythmias in normal conscious dogs. *Circ. Res.* 62, 395–410. doi: 10.1161/01.RES.62.2.395
- Roney, C. H., Bayer, J. D., Cochet, H., Meo, M., Dubois, R., Jaïs, P., et al. (2018). Variability in pulmonary vein electrophysiology and fibrosis determines arrhythmia susceptibility and dynamics. *PLoS Comput. Biol.* 14:e1006166. doi: 10.1371/journal.pcbi.1006166
- Roney, C. H., Bayer, J. D., Zahid, S., Meo, M., Boyle, P. M., Trayanova, N. A., et al. (2016). Modelling methodology of atrial fibrosis affects rotor dynamics and electrograms. *EP Europace* 18(Suppl. 4), iv146–iv155. doi: 10.1093/europace/euw365
- Schotten, U., Verheule, S., Kirchhof, P., and Goette, A. (2011). Pathophysiological mechanisms of atrial fibrillation: a translational appraisal. *Physiol. Rev.* 91, 265–325. doi: 10.1152/physrev.00031.2009
- Spach, M. S., Dolber, P. C., and Heidlage, J. F. (1988). Influence of the passive anisotropic properties on directional differences in propagation following modification of the sodium conductance in human atrial muscle. A model of reentry based on anisotropic discontinuous propagation. *Circ. Res.* 62, 811–832. doi: 10.1161/01.RES.62.4.811
- Valli, H., Ahmad, S., Jiang, A. Y., Smyth, R., Jeevaratnam, K., Matthews, H. R., et al. (2018). Cardiomyocyte ionic currents in intact young and aged murine $pgc-1\beta/-$ atrial preparations. *Mech. Ageing Develop.* 169, 1–9. doi: 10.1016/j.mad.2017.11.016
- Verheule, S., Eckstein, J., Linz, D., Maesen, B., Bidar, E., Gharaviri, A., et al. (2014). Role of endo-epicardial dissociation of electrical activity and transmural conduction in the development of persistent atrial fibrillation. *Progr. Biophys. Mol. Biol.* 115, 173–185. doi: 10.1016/j.biopharmolbio.2014.07.007
- Vigmond, E., Pashaei, A., Amraoui, S., Cochet, H., and Haïssaguerre, M. (2016). Percolation as a mechanism to explain atrial fractionated electrograms and reentry in a fibrosis model based on imaging data. *Heart Rhythm* 13, 1536–1543. doi: 10.1016/j.hrthm.2016.03.019
- Vigmond, E. J., Hughes, M., Plank, G., and Leon, L. J. (2003). Computational tools for modeling electrical activity in cardiac tissue. *J. Electrocardiol.* 36, 69–74. doi: 10.1016/j.jelectrocard.2003.09.017
- Wilhelms, M., Hettmann, H., Maleckar, M. M. C., Koivumäki, J. T., Dössel, O., and Seemann, G. (2013). Benchmarking electrophysiological models of human atrial myocytes. *Front. Physiol.* 3:487. doi: 10.3389/fphys.2012.00487
- Wolf, P. A., Abbott, R. D., and Kannel, W. B. (1991). Atrial fibrillation as an independent risk factor for stroke: the Framingham study. *Stroke* 22, 983–988. doi: 10.1161/01.STR.22.8.983
- Zahid, S., Cochet, H., Boyle, P. M., Schwarz, E. L., Whyte, K. N., Vigmond, E. J., et al. (2016). Patient-derived models link re-entrant driver localization in atrial fibrillation to fibrosis spatial pattern. *Cardiovasc. Res.* 110, 443–454. doi: 10.1093/cvr/cvw073
- Zhuang, J., Wang, Y., Tang, K., Li, X., Peng, W., Liang, C., et al. (2011). Association between left atrial size and atrial fibrillation recurrence after single circumferential pulmonary vein isolation: a systematic review and meta-analysis of observational studies. *Europace* 14, 638–645. doi: 10.1093/europace/eur364
- Zou, R., Kneller, J., Leon, L. J., and Nattel, S. (2005). Substrate size as a determinant of fibrillatory activity maintenance in a mathematical model of canine atrium. *Am. J. Physiol. Heart Circ. Physiol.* 289, H1002–H1012. doi: 10.1152/ajpheart.00252.2005

Conflict of Interest Statement: The authors declare that the research was conducted in the absence of any commercial or financial relationships that could be construed as a potential conflict of interest.

Copyright © 2018 Saha, Roney, Bayer, Meo, Cochet, Dubois and Vigmond. This is an open-access article distributed under the terms of the Creative Commons Attribution License (CC BY). The use, distribution or reproduction in other forums is permitted, provided the original author(s) and the copyright owner(s) are credited and that the original publication in this journal is cited, in accordance with accepted academic practice. No use, distribution or reproduction is permitted which does not comply with these terms.



Targeting the Substrate in Ablation of Persistent Atrial Fibrillation: Recent Lessons and Future Directions

Martin K. Stiles^{1,2*}, Prashanthan Sanders³ and Dennis H. Lau³

¹ Waikato Clinical School, University of Auckland, Hamilton, New Zealand, ² Department of Cardiology, Waikato District Health Board, Hamilton, New Zealand, ³ Centre for Heart Rhythm Disorders (CHRD), South Australian Health and Medical Research Institute (SAHMRI), The University of Adelaide and Royal Adelaide Hospital, Adelaide, SA, Australia

OPEN ACCESS

Edited by:

Gary Tse,
The Chinese University of Hong Kong,
Hong Kong

Reviewed by:

Muayad Alasady,
Australian National University, Australia
Raymond Sy,
Royal Prince Alfred Hospital, Australia
Matthew Webber,
Capital & Coast District Health Board,
New Zealand

*Correspondence:

Martin K. Stiles
martin.stiles@waikatodhb.health.nz

Specialty section:

This article was submitted to
Computational Physiology and
Medicine,
a section of the journal
Frontiers in Physiology

Received: 25 April 2018

Accepted: 02 August 2018

Published: 18 September 2018

Citation:

Stiles MK, Sanders P and Lau DH
(2018) Targeting the Substrate in
Ablation of Persistent Atrial Fibrillation:
Recent Lessons and Future
Directions. *Front. Physiol.* 9:1158.
doi: 10.3389/fphys.2018.01158

While isolation of the pulmonary veins is firmly established as effective treatment for the majority of paroxysmal atrial fibrillation (AF) patients, there is recognition that patients with persistent AF have substrate for perpetuation of arrhythmia existing outside of the pulmonary veins. Various computational approaches have been used to identify targets for effective ablation of persistent AF. This paper aims to discuss the clinical aspects of computational approaches that aim to identify critical sites for treatment. Various analyses of electrogram characteristics have been performed with this aim. Leading techniques for electrogram analysis are Complex Fractionated Atrial Electrograms (CFAE) and Dominant Frequency (DF). These techniques have been the subject of clinical trials of which the results are discussed. Evaluation of the activation patterns of atria in AF has been another avenue of research. Focal Impulse and Rotor Modulation (FIRM) mapping and forms of Body Surface Mapping aim to characterize multiple atrial wavelets, macro-reentry and focal sources which have been proposed as basic mechanisms perpetuating AF. Both invasive and non-invasive activation mapping techniques are reviewed. The presence of atrial fibrosis causes non-uniform anisotropic impulse propagation. Therefore, identification of fibrosis by imaging techniques is an avenue of potential research. The leading contender for imaging-based techniques is Cardiac Magnetic Resonance (CMR). As this technology advances, improvements in resolution and scar identification have positioned CMR as the mode of choice for analysis of atrial structure. AF has been demonstrated to be associated with obesity, inactivity and diseases of modern life. An opportunity exists for detailed computational analysis of the impact of risk factor modification on atrial substrate. This ranges from microstructural investigation through to examination at a population level via registries and public health interventions. Computational analysis of atrial substrate has moved from basic science toward clinical application. Future directions and potential limitations of such analyses are examined in this review.

Keywords: atrial fibrillation, ablation techniques, lifestyle interventions, mapping & localization, fibrosis, imaging, three-dimensional, imaging

INTRODUCTION

While isolation of the pulmonary veins (PVI) is firmly established as effective treatment for the majority of paroxysmal atrial fibrillation (AF) patients, (Calkins et al., 2017) there is recognition that patients with persistent AF have substrate for perpetuation of arrhythmia existing outside of the pulmonary veins. Computational approaches have been attempted in the search to identify targets for effective ablation of persistent AF. We aim to discuss the clinical aspects of computational approaches that seek to identify critical sites for ablation in the treatment of persistent AF. We explore the initial approach of electrogram-based analyses through to more topical panoramic mapping of AF substrate. We look at the role of imaging to identify atrial scar as a potential AF ablation target and the recent recognition that lifestyle management is very important in reducing AF burden. Lastly, we explore potential future directions to advance AF care via computational approaches.

Electrogram-Based Approach

Complex Fractionated Atrial Electrograms

Electrophysiologists skilled in ablation of arrhythmias have sought to look for characteristics of electrograms that might identify critical sites for ablation. The elimination of complex fractionated atrial electrograms (CFAE) has been shown in some studies to be an effective strategy of catheter ablation (Nademanee et al., 2004, 2008) Fractionated or prolonged electrograms have been demonstrated to identify areas acting as pivot points, slowed conduction, anisotropy, localized circuits or rotors, all of which are capable of sustaining re-entry (Spach and Dolber, 1986; Konings et al., 1994; Haïssaguerre et al., 2006). Accurately identifying such electrograms may allow targeted ablation to halt wavelet re-entry and prevent the perpetuation of AF.

Initially, CFAE were defined as fractionated electrograms composed of ≥ 2 deflections, perturbation of the baseline with continuous deflection of a prolonged activation complex, or atrial electrograms with a cycle length ≤ 120 ms (Nademanee et al., 2004) However, as this method of ablation became more widespread, a more consistent definition of ablation targets was desired, particularly if one wanted to perform a multi-center trial where standardization across hospitals was paramount. Hence, computer algorithms were designed to provide consistent definitions of CFAE, independent of the operator's discretion. These included the CFAE software module (CARTO, Biosense Webster, CA, USA) and the CFE-mean tool (NavX, Abbott, CA, USA).

The CFE-mean tool was used to test the usefulness of CFAE ablation in addition to PVI and linear lesions in the BOCA study of 130 persistent AF patients (Wong K. C. et al., 2015) This trial found no additional benefit in the patients randomized to CFAE ablation, despite longer procedure and ablation times. There was an excess of organized atrial arrhythmia, in particular gap-related macro-re-entrant flutter, in the patients randomized to CFAE ablation. In the multi-center STAR-AF II trial (Verma et al., 2015) the use of a computerized algorithm to detect standardized CFAE electrograms was employed. This trial showed no additional

benefit of CFAE ablation as guided by the CFE-mean tool in addition to PVI alone, in patients with persistent AF. Indeed, some have used this trial to suggest that CFAE-targeted ablation is detrimental to long-term outcome (Conti and Verma, 2016) The CHASE-AF trial produced similar conclusions, where no benefit from the addition of a CFAE-based ablation strategy over non-CFAE ablation was seen (Vogler et al., 2015) A recent meta-analysis confirmed that the addition of extra-pulmonary substrate ablation such as that of CFAE in persistent AF patients, was associated with declining efficacy as compared to PVI ablation alone (Clarnette et al., 2017).

However, strong proponents of CFAE-based ablation argue that computer-derived 3D maps of fractionation are inaccurate and lead to different areas being targeted, compared to the areas targeted when visual recognition of CFAEs are made by experienced operators (Oketani et al., 2016) For example, the semi-automated CFAE algorithms from the NavX and CARTO systems were found to correlate poorly with each other or AF complexity measures that may explain the variable results of CFAE-based ablation. Furthermore, the dynamic nature of CFAE with poor temporal stability may be another challenge for CFAE-based ablation based on point-by-point mapping (Lau et al., 2012) Novel indices such as unipolar fractionation index or spatiotemporal stability index of CFAE have been shown to demonstrate superior physiological relevance to AF dynamics (Lau et al., 2015; Thanigaimani et al., 2017a) Therefore, there perhaps remains a role for novel computerized algorithms used in combination with higher density mapping catheter that could better direct electrophysiologists to critical AF-sustaining sites.

Dominant Frequency

Dominant frequency (DF) analysis aims to distill the local activation frequency from highly complex electrograms. This utilizes computer algorithms (usually fast fourier transform) to assign a fundamental frequency of electrical activation. The DF can then be displayed on a 3D map to guide the ablator to sites of high DF thought to be driving the AF (focal source or rotor). The aim of such analysis is to detect sites of high frequency that have been hypothesized to "drive" the fibrillation process (Jalife et al., 2002) These sites have been shown by retrospective analysis to identify effective ablation areas (Sanders et al., 2005) In an elegant animal study by Kalifa et al, areas of fractionation were demonstrated at the periphery of areas of high dominant frequency (Kalifa et al., 2006) The proximity of high DF and CFAE sites has also been demonstrated in high-density mapping of human AF (Stiles et al., 2008) Of note, most studies examining DF guided ablation have used off-line analysis, although real-time analysis has also been reported albeit without incremental outcome (Atienza et al., 2014) In a systematic review of DF-based approaches, Gadenz et al concluded that DF-based approaches are a useful marker of ablation outcome; however, direct intervention targeting DF sites appears premature with mixed results and too few studies (Gadenz et al., 2017) A more recent study using a novel frequency analysis algorithm and longer duration of AF electrograms in search for temporally stable AF drivers has shown some promise (Kimata et al., 2018) Ongoing work will help refine our armamentarium toward future

targeting of high DF sites to improve outcomes (Sanders et al., 2018).

Shannon Entropy

The detection of points of high Shannon Entropy has been postulated as a way of mapping drivers of AF (Ganesan et al., 2014) In particular, ablation at the point of “phase singularity” has been shown to lead to termination of atrial fibrillation (Narayan et al., 2012) Recordings at the center of a rotor should have less directional information in the local bipolar electrogram than recordings away from the center. Maximum Shannon Entropy has been shown to be co-located at the center of rotational activity from experimental models of atrial fibrillation (Ganesan et al., 2014) Furthermore, Shannon Entropy of bipolar electrograms has been shown to be consistent across models and differences in electrode spacing, signal filtering and rotor meander (Ganesan et al., 2014) Studies examining ablation outcome based on Shannon Entropy guided ablation are ongoing.

With the number of promising computational approaches seeking to gather additional information from electrograms, some have sought to show which technique is best, or whether a hybrid approach combining multiple approaches is superior. Hwang et al looked at phase singularity, DF, Shannon entropy and CFAE cycle length with subsequent ablation in 2D and 3D simulation models and found that DF-based ablation was superior for AF termination (Hwang et al., 2016) However, no human AF studies have been able to replicate such data and it remains an area where computational based approaches to electrogram analysis may yet yield insights into effective ablation targets for human AF.

Panoramic Mapping of AF Mechanisms

Over the last decade, the field has progressed from electrogram-based AF mapping to focus on activation and phase mapping to detect AF drivers in the form of rotational (“rotors”) and ectopic focal (“foci”) activations. First descriptions of rotational activations were from studies that undertook sequential mapping with multi-polar spiral catheter (Atienza et al., 2011; Ghoraani et al., 2013) The Focal Impulse and Rotor Modulation (FIRM) guided technique was the first panoramic mapping study that showed high success rates with ablating AF drivers (Narayan et al., 2012). Other panoramic mapping techniques included body surface potentials mapping with inverse-solution electrocardiographic imaging (ECGI) (Haissaguerre et al., 2014) mapping of wavefront propagation using intracardiac multipolar catheter (CARTOFINDER) (Honarbakhsh et al., 2018) and non-contact mapping using a multielectrode array catheter (ENSITE) (Yamabe et al., 2016; Lee et al., 2017). **Table 1** summarizes the different panoramic mapping techniques utilized toward detection of AF rotors and foci.

Focal Impulse and Rotor Modulation (FIRM)

The FIRM technique is facilitated by a 64-pole basket type catheter with phase-based signal processing to detect AF rotors or foci. The algorithm has remained proprietary, with utilization of electrogram data such as local refractoriness and restitution. The initial study reported a mean of 2.1 sources (rotors or foci) per

TABLE 1 | Clinical panoramic mapping for AF rotors and foci.

	FIRM	ECGI	CARTOFINDER	Ensite
Mapping tool	64-electrode Basket type catheter	252-electrode body surface vest	20-electrode PentaRay or 64-electrode Basket type catheter	Ensite multielectrode array catheter
Contact mapping, Surface	Yes, Endocardial	No, Epicardial	Yes, Endocardial	No, Endocardial
Mapping window, Electrogram	Unknown, Unipolar and Bipolar	9 s, Unipolar surface potentials	30 s, Unipolar	7.5 s, Virtual unipolar
Signal processing algorithm	Phase mapping (proprietary)	Wavelet and phase mapping (proprietary)	Phase or Activation mapping	Activation mapping only
No. of persistent AF patients studied (n)	>500	>100	33	30
Key Findings	• AF rotors/foci are sustained • Variable outcomes from meta-analysis	• AF Rotors/foci are non-sustained • Outcome data from single-centre only	• Rotors/foci are non-sustained • Variable processing algorithms and limited outcome data	• Limited evidence of transient rotors • No outcome data to date

patient that conserved for tens of minutes. In this study, FIRM-guided ablation was superior to conventional ablation with 86 vs. 20% acute termination or slowing of AF, and 82.4% vs. 44.9% freedom from AF after a median of 9 months (Narayan et al., 2012). Further, follow-up of these patients to 3 years showed durable success with 77.8% of the FIRM-guided ablation group remained free of AF vs. 38.5% in the conventional group after a mean of 1.2 procedures (Narayan et al., 2014).

However, subsequent studies have shown a wide variability in the reported outcomes from FIRM-guided ablation. A recent meta-analysis (10 studies, $n = 527$ patients) showed a pooled estimate of single-procedure freedom from AF of only 59.2% in non-paroxysmal AF at a mean follow-up of 12.9 months, with a high level of heterogeneity seen among studies ($I^2 = 88.3\%$) (Parameswaran et al., 2018). The variability in outcomes could be due to the limitations in the use of the basket type catheter including suboptimal electrode contact or chamber coverage where potential absence of septal coverage and <25% of overall left atrial surface area coverage have been reported (Pathik et al., 2018). The assumption that the electrodes of the basket catheter are evenly spread over a 2-D grid as opposed to the actual variable spread in a 3-D orientation may contribute to potential errors in phase-based signal analysis of focal sources (Pathik et al., 2018). Further, it is unclear whether electrode density or spacing of the basket catheter may also affect detection of focal sources (Walters et al., 2016; Kuklik et al., 2017). There are also concerns regarding the validity of the FIRM technique whereby comparative assessments failed to identify the same temporally stable rotors as identified by FIRM, with absence of distinctive electrophysiological characteristics of rotors in terms of dominant frequency and Shannon Entropy (Benharash et al., 2015; Halbfass et al., 2017). Several ongoing randomized trials will provide further guidance on the utility of FIRM guided ablation.

Electrocardiographic Imaging (ECGI)

The ECGI is a non-invasive body surface potentials mapping technique using a 252-electrode vest with inverse solution to derive virtual potentials on the epicardial atrial surface localized with thoracic computed tomography. Additional signal processing of wavelet transform and phase mapping are then applied to detect AF sources. Initial report of ECGI mapping in 26 AF patients found mainly multiple wavelets and ectopic foci with rare rotor activities seen in 15% only (Cuculich et al., 2010). More recent ECGI mapping study of 103 persistent AF patients showed a median of 4 driver regions per patient that consisted of non-sustained repetitive rotors (median 2.6 rotations) with substantial meandering as well as ectopic focal sources that fired a mean of 6 times. In this study, the rotors accounted for 80.5% of all AF drivers with the remaining 19.5% consisted of ectopic foci. Importantly, ablation of these drivers resulted in AF termination in 80% and in these cohort of patients, AF freedom was 85% at 1 year follow-up (Haissaguerre et al., 2014). In addition, the ECGI data from the same group also demonstrated increased complexity of these AF drivers with prolonged AF duration. Specifically, longer duration of AF was associated with

increased numbers of rotors and ectopic foci, increased number of regions with these AF drivers and extrapulmonary drivers, such as from the infero-posterior left atrium and the anterior left atrium/septal region. Ablation targeting these driver sites resulted in AF termination in 70% of the persistent AF patients (Lim et al., 2017). However, there are several shortcomings with this mapping modality such as the inability to detect activations in the interatrial septum or the ridge between the pulmonary vein and left atrial appendage, reduced ability to detect low amplitude signals as well as the inability to distinguish between micro-entry and epicardial breakthrough activations (Cuculich et al., 2010; Haissaguerre et al., 2014).

CARTOFINDER

This is a mapping approach that utilizes existing CARTO 3-D electroanatomical mapping system (Biosense Webster, CA, USA) with a module called CARTOFINDER which is still in the development phase. The first report using this system included 13 persistent AF patients where mapping was performed with the PentaRay catheter in both the right and left atrium. In brief, it utilizes unipolar electrograms for phase analysis using Hilbert Transform to detect rotors as well as bipolar electrograms for dominant frequency analysis to gauge ablation efficacy. A mean of 1.8 rotor domains (mean 9.2 rotations) was seen in each patient while ablation of these sites resulted in reduction in dominant frequency, acute termination to sinus rhythm in 2 out of 13 patients (15%) and 1-year freedom from AF rate of 70% (Calvo et al., 2017). In another CARTOFINDER study, activation mapping was performed with the basket catheter in 20 persistent patients without using phase based analysis. Here, the AF drivers were transient (mostly ≤ 4 cycles) but repetitive in separate maps while ablation of these resulted in significant effect of termination or slowing of cycle length in 85% (Honarbakhsh et al., 2018). More outcome data are awaited as this system matures in its development.

Ensite Non-contact Multi-Electrode Array

Several groups have used the Ensite multi-electrode array catheter (St Jude Medical, MN, USA) for panoramic non-contact AF mapping (Yamabe et al., 2016; Lee et al., 2017). This is a commercially available system that affords recording of unipolar virtual electrograms that can be superimposed onto the 3-D endocardial geometry to display wavefront propagation as animated isopotential color map. Using this technique, transient AF rotors were seen in 1 out of 15 persistent AF and 10 out of 60 paroxysmal AF patients that lasted for a mean of 6.1 s in one study (Yamabe et al., 2016). In another study, the Ensite non-contact mapping system failed to identify any focal sources in 15 persistent AF patients (Lee et al., 2017). There are no data available regarding ablation of AF rotors or foci detected with this system.

Electrophysiological Characterization of AF Drivers

The various panoramic mapping methods described above represent intensive research in the field in search of AF driver sites. Many studies have provided increasing insights regarding the electrophysiological characteristics of these drivers despite

apparent differences seen in the dynamics of AF drivers. For example, all panoramic mapping modalities have found AF driver sites to be non-sustained except for the FIRM technique where AF drivers lasted for tens of minutes. The transient nature of AF drivers is in keeping with direct contact mapping studies in long-lasting persistent AF patients (Lee et al., 2014; Walters et al., 2015). Nevertheless, there appears to be agreement on the meandering nature of these drivers that appear repetitively at similar locations in the same patient, namely near the pulmonary vein ostia, left atrial appendages, septum and coronary sinus-inferior left atrium. The anatomical clustering of AF drivers is in keeping with the known importance of structures annexed to the left atrium and the presence of complex muscle fiber orientations at such sites (Haïssaguerre et al., 2005).

Further analysis of the ECGI detected driver sites have unveiled increased electrogram fractionation and their proximity to areas with increased fibrosis as assessed by late gadolinium-enhanced magnetic resonance imaging (LGE-MRI) (Haïssaguerre et al., 2016). However, others have not been able to show the same relationship between AF drivers and LGE-MRI detected fibrotic regions (Chrispin et al., 2016; Sohns et al., 2017). Nevertheless, novel 3-D computational framework provides evidence that AF drivers may be identifiable by a distinct structural “fingerprints” that consist of intermediate wall thickness, intermediate fibrosis and twisted myofiber orientation (Zhao et al., 2017). Taken together, further work is needed to refine our understanding of AF drivers and resolve the differences seen in the their dynamics to guide ablative therapy. The non-disclosures of proprietary algorithms in the detection of AF drivers may be a major obstacle toward rapid translation into clinical practice. Advancement in catheter technology and design to afford better chamber coverage with higher electrode density will also aid in the search of AF drivers amidst the irregularly irregular atrial activations of this highly complex arrhythmia.

Targeting Atrial Fibrosis

Atrial fibrosis is known to result in non-uniform anisotropic impulse propagation and increased conduction heterogeneity that may perpetuate AF by favoring re-entry and anchoring of AF drivers (Maesen et al., 2013; Haïssaguerre et al., 2016). These structural and conduction changes have been consistently seen in different atrial substrates such as hypertension, obesity, heart failure, valvular heart disease, diabetes, aging and obstructive sleep apnea (Sanders et al., 2003; Kistler et al., 2004; Kato et al., 2006; John et al., 2008; Lau et al., 2010, 2011a, 2013b; Medi et al., 2011; Dimitri et al., 2012; Abed et al., 2013a; Iwasaki et al., 2014). In addition, AF itself can result in increased atrial fibrosis in the absence of any risk factors (Stiles et al., 2009; Verheule et al., 2013; Corradi et al., 2014). The signaling mechanisms involved in atrial fibrosis are highly complex and remain incompletely understood (Thanigaimani et al., 2017b). Several agents have been studied in experimental models and have been found to be effective in attenuating or preventing atrial fibrosis: renin-angiotensin-aldosterone inhibitors, (Li et al., 2001; Milliez et al., 2005) n-3 polyunsaturated fatty acids,

(Lau et al., 2011b) HMG-CoA reductase inhibitors, (Shiroshita-Takeshita et al., 2007) and various anti-fibrotics such as tranilast, pirfenidone and relaxin (Lee et al., 2006; Nakatani et al., 2013; Parikh et al., 2013; Henry et al., 2016). Unfortunately, human studies of these agents remain lacking for translation into clinical practice.

Traditional assessment of atrial electrical changes has been facilitated by 3-D electroanatomical maps to evaluate atrial voltage, conduction velocity and electrogram fractionation (**Figure 1**; Lau et al., 2017). Advances in cardiac imaging have facilitated non-invasive quantification of atrial fibrosis by means of LGE-MRI (Oakes et al., 2009). Atrial fibrosis assessed with LGE-MRI has been shown to associate well with regions of low bipolar left atrial voltage as determined by 3-D electroanatomical systems (Malcolme-Lawes et al., 2013; Zghaib et al., 2018). In addition, it has been demonstrated that the degree of atrial fibrosis detected by LGE-MRI increased with AF persistence and the presence of more AF risk factors (Daccarett et al., 2011; McGann et al., 2014). Importantly, atrial fibrosis defined by LGE-MRI has been shown to be independently associated with AF recurrence in patients undergoing catheter ablation in the delayed-enhancement MRI determinant of successful radiofrequency catheter ablation of AF (DECAAF) study (Marrouche et al., 2014). Further analysis of 177 of the DECAAF patients who underwent repeat LGE-MRI scanning 90 days post-ablation showed that the greater overlap of ablation induced scarring over pre-ablation fibrosis, the better the arrhythmia free survival (Akoum et al., 2015). Ongoing prospective multi-center randomized controlled trial (DECAAF-II) will examine the efficacy of targeting LGE-MRI detected atrial fibrosis in persistent AF patients.

However, several technical challenges with LGE-MRI detection of atrial fibrosis have been acknowledged. These include issues such as spatial resolution given the thin atrial walls, motion artifact especially when the patient is not in sinus rhythm, the lack of standardized image acquisition protocols and the all-important quantitation of the amount of LGE that can be subjective and labor intensive even if signal intensity thresholding was employed over visual assessment (Appelbaum and Manning, 2014; Pontecorbo et al., 2017). It is also noted that there remains a paucity of good quality data whereby LGE-MRI detected atrial fibrosis or post-ablation scars have been histologically validated (Harrison et al., 2014; McGann et al., 2014). Therefore, it is of no surprise that the reproducibility of LGE-MRI analysis has been questioned and the diagnostic accuracy of this modality to detect ablation lesions has been shown to be suboptimal (Hunter et al., 2013; Pontecorbo et al., 2017). Alternatively, post-contrast cardiac MRI atrial T1 relaxation time mapping has been shown to be a reliable index of atrial fibrosis that correlated with atrial voltage and ablation outcome (Ling et al., 2014). However, the inability of T1 mapping technique to provide spatial distribution of atrial fibrosis will hamper its ultimate usage to guide ablative therapy. Hopefully, the LGE-MRI technique will mature toward standardization of image acquisition, automation of image analysis, improved image resolution and validation in the not too distant future.

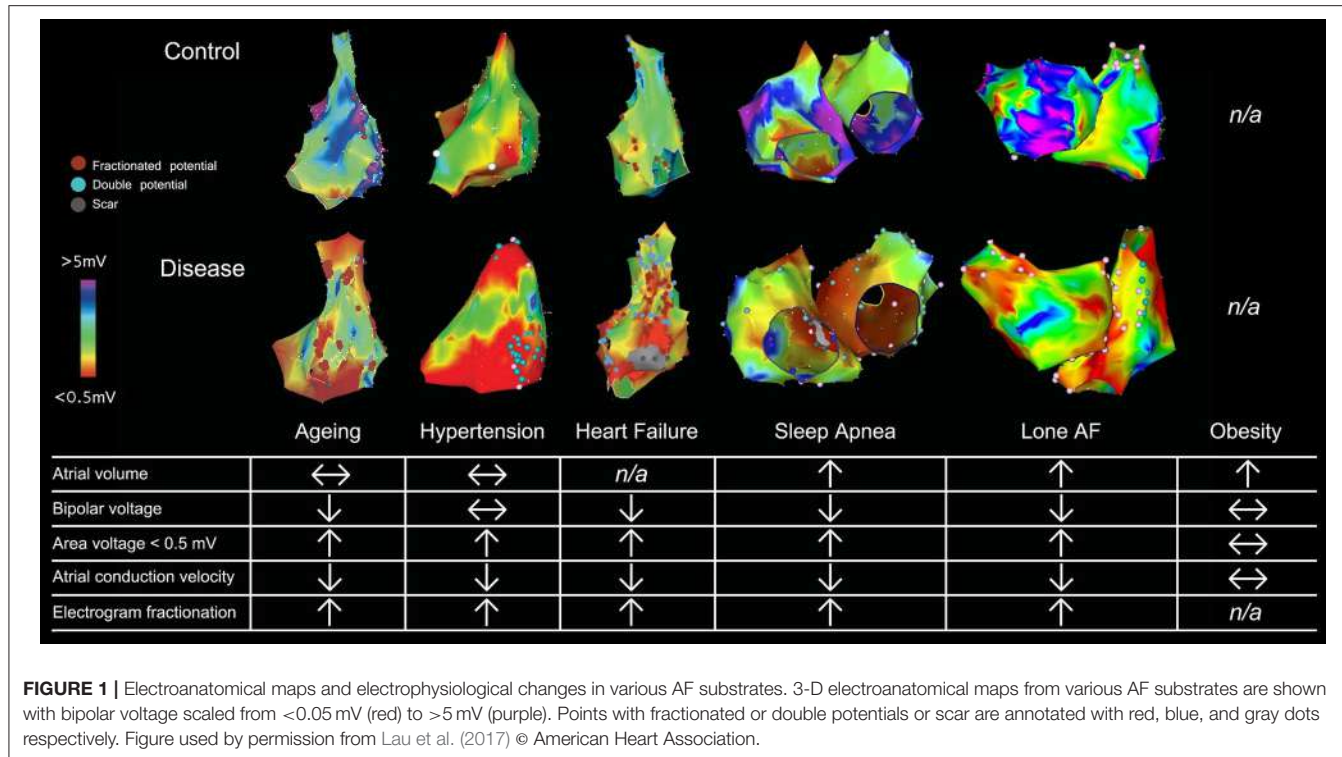


FIGURE 1 | Electroanatomical maps and electrophysiological changes in various AF substrates. 3-D electroanatomical maps from various AF substrates are shown with bipolar voltage scaled from <0.05 mV (red) to >5 mV (purple). Points with fractionated or double potentials or scar are annotated with red, blue, and gray dots respectively. Figure used by permission from Lau et al. (2017) © American Heart Association.

Targeting the AF Risk Factors

Despite the advances in catheter ablation technology and strategies over the last two decades, the field has not witnessed a significant improvement in ablation success especially in those with persistent AF (Brooks et al., 2010; Clarnette et al., 2017). It is well recognized that there is a long-term attrition in sinus rhythm maintenance following initially successful catheter ablation (Ganesan et al., 2013). In addition, progressive atrial substrate changes have been documented in individuals despite a successful AF ablation procedure (Teh et al., 2012). A myriad of AF risk factors have been identified to contribute to the progressive AF substrate and recurrences post catheter ablation procedures. These include: aging, left atrial enlargement, heart failure, hypertension, aortic stiffness, valvular heart disease, obesity, pericardial fat, diabetes mellitus, dyslipidemia and obstructive sleep apnea (de Vos et al., 2010; Ng et al., 2011; Wong et al., 2011; Mohanty et al., 2012; Lau et al., 2013a; Jacobs et al., 2015; Proietti et al., 2015; Wong C. X. et al., 2015; Linz et al., 2018). Therefore, efforts must be placed to target these risk factors to maximize rhythm control outcome in patients with AF.

There is prospective randomized evidence showing that a targeted weight loss intervention reduced atrial dilatation, left ventricular hypertrophy, and AF symptom burden and severity in highly symptomatic overweight and obese patients with AF (Abed et al., 2013b). Tight control of systolic blood pressure to under 130 mmHg has been shown to reduce incident and recurrent AF in hypertensive subjects although a more recent study reported neutral results (Thomas et al., 2008; Okin et al., 2015; Parkash et al., 2017). Continuous positive airway pressure therapy has been shown to improve sinus rhythm

maintenance in patients with obstructive sleep apnea undergoing electrical cardioversion and catheter ablation (Linz et al., 2018). A structured, physician-driven, and goal-directed weight and risk factor management strategy has been applied in overweight and obese patients with AF to good success, as seen in the ARREST-AF (Aggressive Risk Factor Reduction Study for Atrial Fibrillation and Implications for the Outcome of Ablation) and LEGACY (Long-Term Effect of Goal Directed Weight Management on an Atrial Fibrillation Cohort) studies (Figure 2). In brief, this program involved weight management by dietary modification, tailored moderate-intensity exercise to improve cardiorespiratory fitness, targeted strict systolic blood pressure control to <130 mm Hg, lipid and glycemic management aiming for low-density lipoprotein <2.6 mmol/L and hemoglobin A1c <6.5%, active screening and treatment of obstructive sleep apnea with continuous positive airways pressure therapy, smoking cessation and alcohol reduction to <3 standard drinks per week. In addition, gain in cardiorespiratory fitness was found to confer greater freedom from AF independent of weight loss.

Additional evidence on the benefits of exercise in AF can be seen from the study by Malmo and co-workers with aerobic interval training for 12 weeks (Malmo et al., 2016). Similarly, weight and exercise intervention has been shown to confer equivalent benefits to re-do catheter ablation in a study in patients with post-ablation AF recurrences (Mohanty et al., 2014). More recently, in persistent AF patients with heart failure, a multi-center prospective randomized study has demonstrated that additional intervention targeting the underlying conditions with cardiac rehabilitation including physical activity, dietary restrictions, and counseling, mineralocorticoid receptor

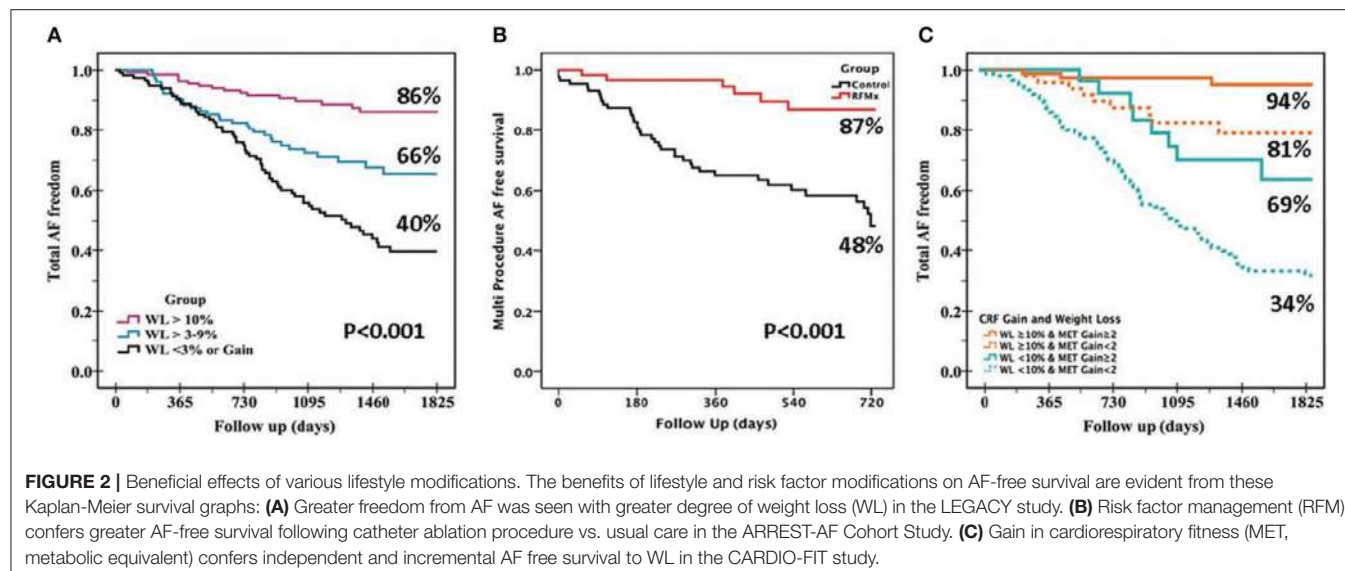


FIGURE 2 | Beneficial effects of various lifestyle modifications. The benefits of lifestyle and risk factor modifications on AF-free survival are evident from these Kaplan-Meier survival graphs: **(A)** Greater freedom from AF was seen with greater degree of weight loss (WL) in the LEGACY study. **(B)** Risk factor management (RFM) confers greater AF-free survival following catheter ablation procedure vs. usual care in the ARREST-AF Cohort Study. **(C)** Gain in cardiorespiratory fitness (MET, metabolic equivalent) confers independent and incremental AF free survival to WL in the CARDIO-FIT study.

antagonist, HMG-CoA reductase inhibitor and angiotensin converting enzyme inhibitors and/or receptor blockers resulted in improved sinus rhythm maintenance at 1 year (Rienstra et al., 2018). Taken together, the mounting evidence regarding the benefits of these lifestyle and risk factor management approaches and their cost-effectiveness warrants their incorporation as routine “4th pillar” of AF care to maximize outcomes (Lau et al., 2017; Pathak et al., 2017). This can be achieved by combining the risk factor management component with a wider integrated AF clinic to optimize care delivery (Hendriks et al., 2012).

Future Directions

Novel computational approaches that help identify the arrhythmogenic substrate of AF have the potential to advance the field of AF ablation. The progression of electrogram analysis through to dynamic substrate mapping has been increasingly reliant on the computational approach. Recognition that atrial microstructure is critical to the maintenance of persistent AF should stimulate future analyses to benefit from the increasing resolution of imaging studies, particularly MRI. However, with increasing resolution comes reliance on computing power and bespoke algorithms to take best advantage of it.

As we move into the world of meta-data and wearable technology, a computational approach to analysis of the data may afford increased detection of AF as well as giving additional insights to physical activity and its impact on AF incidence. Personalized exercise and weight reduction programmes for

patients with AF delivered via smartphone technology will integrate with aggressive risk factor management clinics. Computational analysis of effectiveness and the consequent outcomes for AF will no doubt be an important future application.

CONCLUSION

Recent developments in computational approaches to ablation of atrial fibrillation have focused on identifying drivers for the perpetuation of this arrhythmia. The future of detecting critical sites for ablation depends largely on a computational approach. However, large data analyses may also play a role in lifestyle adjustment which is now recognized to be an important part of a comprehensive patient management programme for AF.

AUTHOR CONTRIBUTIONS

MS and DL wrote sections of the manuscript and proofread each other’s section. PS proofread the manuscript and provided guidance on the overall direction of the manuscript. All authors critically appraised the final version of the paper.

FUNDING

DL is supported by the Robert J. Craig Lectureship from the University of Adelaide. PS is supported by Practitioner Fellowships from the NHMRC and NHF of Australia.

REFERENCES

- Abed, H. S., Samuel, C. S., Lau, D. H., Kelly, D. J., Royce, S. G., Alasady, M., et al. (2013a). Obesity results in progressive atrial structural and electrical remodeling: implications for atrial fibrillation. *Heart Rhythm* 10, 90–100. doi: 10.1016/j.hrthm.2012.08.043

- Abed, H. S., Wittert, G. A., Leong, D. P., Shirazi, M. G., Bahrami, B., Middeldorp, M. E., et al. (2013b). Effect of weight reduction and cardiometabolic risk factor management on symptom burden and severity in patients with atrial fibrillation: a randomized clinical trial. *JAMA* 310, 2050–2060. doi: 10.1001/jama.2013.280521

- Akoum, N., Wilber, D., Hindricks, G., Jais, P., Cates, J., Marchlinski, F., et al. (2015). MRI Assessment of ablation-induced scarring in atrial fibrillation: analysis from the DECAAF study. *J. Cardiovasc. Electrophysiol.* 26, 473–480. doi: 10.1111/jce.12650
- Appelbaum, E., and Manning, W. J. (2014). Left atrial fibrosis by late gadolinium enhancement cardiovascular magnetic resonance predicts recurrence of atrial fibrillation after pulmonary vein isolation: do you see what I see? *Circ. Arrhythm Electrophysiol.* 7, 2–4. doi: 10.1161/CIRCEP.114.001354
- Atienza, F., Almendral, J., Ormaetxe, J. M., Moya, A., Martínez-Alday, J. D., Hernández-Madrid, A., et al. (2014). Comparison of radiofrequency catheter ablation of drivers and circumferential pulmonary vein isolation in atrial fibrillation: a noninferiority randomized multicenter RADAR-AF trial. *J. Am. Coll. Cardiol.* 64, 2455–2467. doi: 10.1016/j.jacc.2014.09.053
- Atienza, F., Calvo, D., Almendral, J., Zlochiver, S., Grzeda, K. R., Martínez-Alzamora, N., et al. (2011). Mechanisms of fractionated electrograms formation in the posterior left atrium during paroxysmal atrial fibrillation in humans. *J. Am. Coll. Cardiol.* 57, 1081–1092. doi: 10.1016/j.jacc.2010.09.066
- Benharash, P., Buch, E., Frank, P., Share, M., Tung, R., Shivkumar, K., et al. (2015). Quantitative analysis of localized sources identified by focal impulse and rotor modulation mapping in atrial fibrillation. *Circ. Arrhythm Electrophysiol.* 8, 554–561. doi: 10.1161/CIRCEP.115.002721
- Brooks, A. G., Stiles, M. K., Laborderie, J., Lau, D. H., Kuklik, P., Shipp, N. J., et al. (2010). Outcomes of long-standing persistent atrial fibrillation ablation: a systematic review. *Heart Rhythm* 7, 835–846. doi: 10.1016/j.hrthm.2010.01.017
- Calkins, H., Hindricks, G., Cappato, R., Kim, Y. H., Saad, E. B., Aguinaga, L., et al. (2017). 2017 HRS/EHRA/ECAS/APHRS/SOLAECE expert consensus statement on catheter and surgical ablation of atrial fibrillation. *Heart Rhythm* 14, e275–e444. doi: 10.1016/j.hrthm.2017.05.012
- Calvo, D., Rubín, J., Pérez, D., Moris, C., (2017). Ablation of rotor domains effectively modulates dynamics of human: long-standing persistent atrial fibrillation. *Circ. Arrhythm Electrophysiol.* 10:e005740. doi: 10.1161/CIRCEP.117.005740
- Chrisipin, J., Gucuk Ipek, E., Zahid, S., Prakosa, A., Habibi, M., Spragg, D., et al. (2016). Lack of regional association between atrial late gadolinium enhancement on cardiac magnetic resonance and atrial fibrillation rotors. *Heart Rhythm* 13, 654–660. doi: 10.1016/j.hrthm.2015.11.011
- Clarnette, J. A., Brooks, A. G., Mahajan, R., Elliott, A. D., Twomey, D. J., Pathak, R. K., et al. (2017). Outcomes of persistent and long-standing persistent atrial fibrillation ablation: a systematic review and meta-analysis. *Europace.* doi: 10.1093/europace/eux297. [Epub ahead of print].
- Conti, S., and Verma, A. (2016). Ablation of complex fractionated electrograms may not be useful for catheter ablation of persistent atrial fibrillation. *Heart Rhythm* 13, 2101–2103. doi: 10.1016/j.hrthm.2016.06.037
- Corradi, D., Callegari, S., Manotti, L., Ferrara, D., Goldoni, M., Alinovi, R., et al. (2014). Persistent lone atrial fibrillation: clinicopathologic study of 19 cases. *Heart Rhythm* 11, 1250–1258. doi: 10.1016/j.hrthm.2014.02.008
- Cuculich, P. S., Wang, Y., Lindsay, B. D., Faddis, M. N., Schuessler, R. B., Damiano, R. J., et al. (2010). Noninvasive characterization of epicardial activation in humans with diverse atrial fibrillation patterns. *Circulation* 122, 1364–1372. doi: 10.1161/CIRCULATIONAHA.110.945709
- Daccarett, M., Badger, T. J., Akoum, N., Burgon, N. S., Mahnkopf, C., Vergara, G., et al. (2011). Association of left atrial fibrosis detected by delayed-enhancement magnetic resonance imaging and the risk of stroke in patients with atrial fibrillation. *J. Am. Coll. Cardiol.* 57, 831–838. doi: 10.1016/j.jacc.2010.09.049
- de Vos, C. B., Pisters, R., Nieuwlaat, R., Prins, M. H., Tielemans, R. G., Coelen, R. J., et al. (2010). Progression from paroxysmal to persistent atrial fibrillation clinical correlates and prognosis. *J. Am. Coll. Cardiol.* 55, 725–731. doi: 10.1016/j.jacc.2009.11.040
- Dimitri, H., Ng, M., Brooks, A. G., Kuklik, P., Stiles, M. K., Lau, D. H., et al. (2012). Atrial remodeling in obstructive sleep apnea: implications for atrial fibrillation. *Heart Rhythm* 9, 321–327. doi: 10.1016/j.hrthm.2011.10.017
- Gadenz, L., Hashemi, J., Shariat, M. H., Gula, L., and Redfearn, D. P. (2017). Clinical role of dominant frequency measurements in atrial fibrillation ablation - a systematic review. *J. Atr. Fibrillation* 9:1548. doi: 10.4022/jafib.1548
- Ganesan, A. N., Kuklik, P., Gharaviri, A., Brooks, A., Chapman, D., Lau, D. H., et al. (2014). Origin and characteristics of high Shannon entropy at the pivot of locally stable rotors: insights from computational simulation. *PLoS ONE* 9:e110662. doi: 10.1371/journal.pone.0110662
- Ganesan, A. N., Shipp, N. J., Brooks, A. G., Kuklik, P., Lau, D. H., Lim, H. S., et al. (2013). Long-term outcomes of catheter ablation of atrial fibrillation: a systematic review and meta-analysis. *J. Am. Heart. Assoc.* 2:e004549. doi: 10.1161/JAHA.112.004549
- Ghorbani, B., Dalvi, R., Gizararson, S., Das, M., Ha, A., Suszko, A., et al. (2013). Localized rotational activation in the left atrium during human atrial fibrillation: relationship to complex fractionated atrial electrograms and low-voltage zones. *Heart Rhythm* 10, 1830–1838. doi: 10.1016/j.hrthm.2013.09.007
- Haïssaguerre, M., Hocini, M., Sanders, P., Takahashi, Y., Rotter, M., Sacher, F., et al. (2006). Localized sources maintaining atrial fibrillation organized by prior ablation. *Circulation* 113, 616–625. doi: 10.1161/CIRCULATIONAHA.105.546648
- Haïssaguerre, M., Sanders, P., Hocini, M., Takahashi, Y., Rotter, M., Sacher, F., et al. (2005). Catheter ablation of long-lasting persistent atrial fibrillation: critical structures for termination. *J. Cardiovasc. Electrophysiol.* 16, 1125–1137. doi: 10.1111/j.1540-8167.2005.00307.x
- Haïssaguerre, M., Hocini, M., Denis, A., Shah, A. J., Komatsu, Y., Yamashita, S., et al. (2014). Driver domains in persistent atrial fibrillation. *Circulation* 130, 530–538. doi: 10.1161/CIRCULATIONAHA.113.005421
- Haïssaguerre, M., Shah, A. J., Cochet, H., Hocini, M., Dubois, R., Efimov, I., et al. (2016). Intermittent drivers anchoring to structural heterogeneities as a major pathophysiological mechanism of human persistent atrial fibrillation. *J. Physiol.* 594, 2387–2398. doi: 10.1113/jphysiol.2016.201607
- Halbfass, P., Müller, P., Nentwich, K., Sonne, K., Hamm, K., Barth, S., et al. (2017). Repetitive atrial activation during ongoing atrial fibrillation-comparison using different mapping algorithms: preliminary findings. *J. Interv. Card Electrophysiol.* 49, 67–74. doi: 10.1007/s10840-017-0244-8
- Harrison, J. L., Jensen, H. K., Peel, S. A., Chiribiri, A., Grøndal, A. K., Bloch, L. Ø., et al. (2014). Cardiac magnetic resonance and electroanatomical mapping of acute and chronic atrial ablation injury: a histological validation study. *Eur. Heart J.* 35, 1486–1495. doi: 10.1093/europheartj/eht560
- Hendriks, J. M., de Wit, R., Crijns, H. J., Vrijhoef, H. J., Prins, M. H., Pisters, R., et al. (2012). Nurse-led care vs. usual care for patients with atrial fibrillation: results of a randomized trial of integrated chronic care vs. routine clinical care in ambulatory patients with atrial fibrillation. *Eur. Heart J.* 33, 2692–2699. doi: 10.1093/eurheartj/ehs071
- Henry, B. L., Gabris, B., Li, Q., Martin, B., Giannini, M., Parikh, A., et al. (2016). Relaxin suppresses atrial fibrillation in aged rats by reversing fibrosis and upregulating Na^+ channels. *Heart Rhythm* 13, 983–991. doi: 10.1016/j.hrthm.2015.12.030
- Honarbakhsh, S., Schilling, R. J., Dhillon, G., Ullah, W., Keating, E., Providencia, R., et al. (2018). A novel mapping system for panoramic mapping of the left atrium: application to detect and characterize localized sources maintaining atrial fibrillation. *JACC Clin. Electrophysiol.* 4, 124–134. doi: 10.1016/j.jacep.2017.09.177
- Hunter, R. J., Jones, D. A., Boubertakh, R., Malcolm-Lawes, L. C., Kanagaratnam, P., Juli, C. F., et al. (2013). Diagnostic accuracy of cardiac magnetic resonance imaging in the detection and characterization of left atrial catheter ablation lesions: a multicenter experience. *J. Cardiovasc. Electrophysiol.* 24, 396–403. doi: 10.1111/jce.12063
- Hwang, M., Song, J. S., Lee, Y. S., Li, C., Shim, E. B., and Pak, H. N., et al. (2016). Electrophysiological rotor ablation in *in-silico* modeling of atrial fibrillation: comparisons with dominant frequency, shannon entropy, and phase singularity. *PLoS ONE* 11:e0149695. doi: 10.1371/journal.pone.0149695
- Iwasaki, Y. K., Kato, T., Xiong, F., Shi, Y. F., Naud, P., Maguy, A., et al. (2014). Atrial fibrillation promotion with long-term repetitive obstructive sleep apnea in a rat model. *J. Am. Coll. Cardiol.* 64, 2013–2023. doi: 10.1016/j.jacc.2014.05.077
- Jacobs, V., May, H. T., Bair, T. L., Crandall, B. G., Cutler, M., Day, J. D., et al. (2015). The impact of risk score (CHADS2 versus CHA2DS2-VASc) on long-term outcomes after atrial fibrillation ablation. *Heart Rhythm* 12, 681–686. doi: 10.1016/j.hrthm.2014.12.034
- Jalife, J., Berenfeld, O., and Mansour, M. (2002). Mother rotors and fibrillatory conduction: a mechanism of atrial fibrillation. *Cardiovasc. Res.* 54, 204–216. doi: 10.1016/S0008-6363(02)00223-7

- John, B., Stiles, M. K., Kuklik, P., Chandy, S. T., Young, G. D., Mackenzie, L., et al. (2008). Electrical remodelling of the left and right atria due to rheumatic mitral stenosis. *Eur. Heart J.* 29, 2234–2243. doi: 10.1093/eurheartj/ehn329
- Kalifa, J., Tanaka, K., Zaitsev, A. V., Warren, M., Vaidyanathan, R., Auerbach, D., et al. (2006). Mechanisms of wave fractionation at boundaries of high-frequency excitation in the posterior left atrium of the isolated sheep heart during atrial fibrillation. *Circulation* 113, 626–633. doi: 10.1161/CIRCULATIONAHA.105.575340
- Kato, T., Yamashita, T., Sekiguchi, A., Sagara, K., Takamura, M., Takata, S., et al. (2006). What are arrhythmogenic substrates in diabetic rat atria? *J. Cardiovasc. Electrophysiol.* 17, 890–894. doi: 10.1111/j.1540-8167.2006.00528.x
- Kimata, A., Yokoyama, Y., Aita, S., Nakamura, H., Higuchi, K., Tanaka, Y., et al. (2018). Temporally stable frequency mapping using continuous wavelet transform analysis in patients with persistent atrial fibrillation. *J. Cardiovasc. Electrophysiol.* 29, 514–522. doi: 10.1111/jce.13440
- Kistler, P. M., Sanders, P., Fynn, S. P., Stevenson, I. H., Spence, S. J., Vohra, J. K., et al. (2004). Electrophysiologic and electroanatomic changes in the human atrium associated with age. *J. Am. Coll. Cardiol.* 44, 109–116. doi: 10.1016/j.jacc.2004.03.044
- Konings, K. T., Kirchhof, C. J., Smeets, J. R., Wellens, H. J., Penn, O. C., and Allessie, M. A. (1994). High-density mapping of electrically induced atrial fibrillation in humans. *Circulation* 89, 1665–1680. doi: 10.1161/01.CIR.89.4.1665
- Kuklik, P., Zeemering, S., van Hunnik, A., Maesen, B., Pison, L., Lau, D. H., et al. (2017). Identification of rotors during human atrial fibrillation using contact mapping and phase singularity detection: technical considerations. *IEEE Trans. Biomed. Eng.* 64, 310–318. doi: 10.1109/TBME.2016.2554660
- Lau, D. H., Mackenzie, L., Kelly, D. J., Psaltis, P. J., Worthington, M., Rajendram, A., et al. (2010). Short-term hypertension is associated with the development of atrial fibrillation substrate: a study in an ovine hypertensive model. *Heart Rhythm* 7, 396–404. doi: 10.1016/j.hrthm.2009.11.031
- Lau, D. H., Maesen, B., Zeemering, S., Kuklik, P., van Hunnik, A., Lankveld, T. A., et al. (2015). Indices of bipolar complex fractionated atrial electrograms correlate poorly with each other and atrial fibrillation substrate complexity. *Heart Rhythm* 12, 1415–1423. doi: 10.1016/j.hrthm.2015.03.017
- Lau, D. H., Maesen, B., Zeemering, S., Verheule, S., Crijns, H. J., and Schotten, U. (2012). Stability of complex fractionated atrial electrograms: a systematic review. *J. Cardiovasc. Electrophysiol.* 23, 980–987. doi: 10.1111/j.1540-8167.2012.02335.x
- Lau, D. H., Middeldorp, M. E., Brooks, A. G., Ganesan, A. N., Roberts-Thomson, K. C., Stiles, M. K., et al. (2013a). Aortic stiffness in lone atrial fibrillation: a novel risk factor for arrhythmia recurrence. *PLoS ONE* 8:e76776. doi: 10.1371/journal.pone.0076776
- Lau, D. H., Nattel, S., Kalman, J. M., and Sanders, P. (2017). Modifiable risk factors and atrial fibrillation. *Circulation* 136, 583–596. doi: 10.1161/CIRCULATIONAHA.116.023163
- Lau, D. H., Psaltis, P. J., Carbone, A., Kelly, D. J., Mackenzie, L., Worthington, M., et al. (2011b). Atrial protective effects of n-3 polyunsaturated fatty acids: a long-term study in chronic heart failure. *Heart Rhythm* 8, 575–582. doi: 10.1016/j.hrthm.2010.12.009
- Lau, D. H., Psaltis, P. J., Mackenzie, L., Kelly, D. J., Carbone, A., Worthington, M., et al. (2011a). Atrial remodeling in an ovine model of anthracycline-induced nonischemic cardiomyopathy: remodeling of the same sort. *J. Cardiovasc. Electrophysiol.* 22, 175–182. doi: 10.1111/j.1540-8167.2010.01851.x
- Lau, D. H., Shipp, N. J., Kelly, D. J., Thanagaimani, S., Neo, M., Kuklik, P., et al. (2013b). Atrial arrhythmia in ageing spontaneously hypertensive rats: unraveling the substrate in hypertension and ageing. *PLoS ONE* 8:e72416. doi: 10.1371/journal.pone.0072416
- Lee, G., Kumar, S., Teh, A., Madry, A., Spence, S., Larobina, M., et al. (2014). Epicardial wave mapping in human long-lasting persistent atrial fibrillation: transient rotational circuits, complex wavefronts, and disorganized activity. *Eur. Heart J.* 35, 86–97. doi: 10.1093/eurheartj/eht267
- Lee, G., McLellan, A. J., Hunter, R. J., Lovell, M. J., Finlay, M., Ullah, W., et al. (2017). Panoramic characterization of endocardial left atrial activation during human persistent AF: insights from non-contact mapping. *Int. J. Cardiol.* 228, 406–411. doi: 10.1016/j.ijcard.2016.11.085
- Lee, K. W., Everett, T. H., Rahmutula, D., Guerra, J. M., Wilson, E., Ding, C., et al. (2006). Pirfenidone prevents the development of a vulnerable substrate for atrial fibrillation in a canine model of heart failure. *Circulation* 114, 1703–1712. doi: 10.1161/CIRCULATIONAHA.106.624320
- Li, D., Shinagawa, K., Pang, L., Leung, T. K., Cardin, S., Wang, Z., et al. (2001). Effects of angiotensin-converting enzyme inhibition on the development of the atrial fibrillation substrate in dogs with ventricular tachypacing-induced congestive heart failure. *Circulation* 104, 2608–2614. doi: 10.1161/hc4601.099402
- Lim, H. S., Hocini, M., Dubois, R., Denis, A., Derval, N., Zellerhoff, S., et al. (2017). Complexity and distribution of drivers in relation to duration of persistent atrial fibrillation. *J. Am. Coll. Cardiol.* 69, 1257–1269. doi: 10.1016/j.jacc.2017.01.014
- Ling, L. H., McLellan, A. J., Taylor, A. J., Iles, L. M., Ellims, A. H., Kumar, S., et al. (2014). Magnetic resonance post-contrast T1 mapping in the human atrium: validation and impact on clinical outcome after catheter ablation for atrial fibrillation. *Heart Rhythm* 11, 1551–1559. doi: 10.1016/j.hrthm.2014.06.012
- Linz, D., McEvoy, R. D., Cowie, M. R., Somers, V. K., Nattel, S., Lévy, P., et al. (2018). Associations of obstructive sleep apnea with atrial fibrillation and continuous positive airway pressure treatment: a review. *JAMA Cardiol.* 3, 532–540. doi: 10.1001/jamacardio.2018.0095
- Maesen, B., Zeemering, S., Afonso, C., Eckstein, J., Burton, R. A., van Hunnik, A., et al. (2013). Rearrangement of atrial bundle architecture and consequent changes in anisotropy of conduction constitute the 3-dimensional substrate for atrial fibrillation. *Circ. Arrhythm Electrophysiol.* 6, 967–975. doi: 10.1161/CIRCEP.113.000050
- Malcolme-Lawes, L. C., Juli, C., Karim, R., Bai, W., Quest, R., Lim, P. B., et al. (2013). Automated analysis of atrial late gadolinium enhancement imaging that correlates with endocardial voltage and clinical outcomes: a 2-center study. *Heart Rhythm* 10, 1184–1191. doi: 10.1016/j.hrthm.2013.04.030
- Malmo, V., Nes, B. M., Amundsen, B. H., Tjonna, A. E., Stoylen, A., Rossqvist, O., et al. (2016). Aerobic interval training reduces the burden of atrial fibrillation in the short term: a randomized trial. *Circulation* 133, 466–473. doi: 10.1161/CIRCULATIONAHA.115.018220
- Marrouche, N. F., Wilber, D., Hindricks, G., Jais, P., Akoum, N., Marchlinski, F., et al. (2014). Association of atrial tissue fibrosis identified by delayed enhancement MRI and atrial fibrillation catheter ablation: the DECAAF study. *JAMA* 311, 498–506. doi: 10.1001/jama.2014.3
- McGann, C., Akoum, N., Patel, A., Kholmovski, E., Revelo, P., Damal, K., et al. (2014). Atrial fibrillation ablation outcome is predicted by left atrial remodeling on MRI. *Circ. Arrhythm Electrophysiol.* 7, 23–30. doi: 10.1161/CIRCEP.113.000689
- Medi, C., Kalman, J. M., Spence, S. J., Teh, A. W., Lee, G., Bader, I., et al. (2011). Atrial electrical and structural changes associated with longstanding hypertension in humans: implications for the substrate for atrial fibrillation. *J. Cardiovasc. Electrophysiol.* 22, 1317–1324. doi: 10.1111/j.1540-8167.2011.02125.x
- Milliez, P., Deangelis, N., Rucker-Martin, C., Leenhardt, A., Vicaut, E., Robidel, E., et al. (2005). Spironolactone reduces fibrosis of dilated atria during heart failure in rats with myocardial infarction. *Eur. Heart J.* 26, 2193–2199. doi: 10.1093/eurheartj/ehi478
- Mohanty, S., Mohanty, P., Di Biase, L., Bai, R., Pump, A., Santangeli, P., et al. (2012). Impact of metabolic syndrome on procedural outcomes in patients with atrial fibrillation undergoing catheter ablation. *J. Am. Coll. Cardiol.* 59, 1295–1301. doi: 10.1016/j.jacc.2011.11.051
- Mohanty, S., Mohanty, P., Di Biase, L., Bai, R., Trivedi, C., Santangeli, P., et al. (2014). Long-term outcome of catheter ablation in atrial fibrillation patients with coexistent metabolic syndrome and obstructive sleep apnea: impact of repeat procedures versus lifestyle changes. *J. Cardiovasc. Electrophysiol.* 25, 930–938. doi: 10.1111/jce.12468
- Nademanee, K., McKenzie, J., Kosar, E., Schwab, M., Sunsaneewitayakul, B., Vasavakul, T., et al. (2004). A new approach for catheter ablation of atrial fibrillation: mapping of the electrophysiologic substrate. *J. Am. Coll. Cardiol.* 43, 2044–2053. doi: 10.1016/j.jacc.2003.12.054
- Nademanee, K., Schwab, M. C., Kosar, E. M., Karwecki, M., Moran, M. D., Visessoook, N., et al. (2008). Clinical outcomes of catheter substrate ablation for high-risk patients with atrial fibrillation. *J. Am. Coll. Cardiol.* 51, 843–849. doi: 10.1016/j.jacc.2007.10.044
- Nakatani, Y., Nishida, K., Sakabe, M., Kataoka, N., Sakamoto, T., Yamaguchi, Y., et al. (2013). Tranilast prevents atrial remodeling and development of

- atrial fibrillation in a canine model of atrial tachycardia and left ventricular dysfunction. *J. Am. Coll. Cardiol.* 61, 582–588. doi: 10.1016/j.jacc.2012.11.014
- Narayan, S. M., Baykaner, T., Clopton, P., Schricker, A., Lalani, G. G., Krummen, D. E., et al. (2014). Ablation of rotor and focal sources reduces late recurrence of atrial fibrillation compared with trigger ablation alone: extended follow-up of the CONFIRM trial (Conventional Ablation for Atrial Fibrillation With or Without Focal Impulse and Rotor Modulation). *J. Am. Coll. Cardiol.* 63, 1761–1768. doi: 10.1016/j.jacc.2014.02.543
- Narayan, S. M., Krummen, D. E., Shivkumar, K., Clopton, P., Rappel, W. J., and Miller, J. M. (2012). Treatment of atrial fibrillation by the ablation of localized sources: CONFIRM (Conventional Ablation for Atrial Fibrillation With or Without Focal Impulse and Rotor Modulation) trial. *J. Am. Coll. Cardiol.* 60, 628–636. doi: 10.1016/j.jacc.2012.05.022
- Ng, C. Y., Liu, T., Shehata, M., Stevens, S., Chugh, S. S., and Wang, X. (2011). Meta-analysis of obstructive sleep apnea as predictor of atrial fibrillation recurrence after catheter ablation. *Am. J. Cardiol.* 108, 47–51. doi: 10.1016/j.amjcard.2011.02.343
- Oakes, R. S., Badger, T. J., Kholmovski, E. G., Akoum, N., Burgon, N. S., Fish, E. N., et al. (2009). Detection and quantification of left atrial structural remodeling with delayed-enhancement magnetic resonance imaging in patients with atrial fibrillation. *Circulation* 119, 1758–1767. doi: 10.1161/CIRCULATIONAHA.108.811877
- Oketani, N., Seitz, J., Salazar, M., Pisapia, A., Kalifa, J., Smit, J. J., et al. (2016). Ablation of complex fractionated electrograms is useful for catheter ablation of persistent atrial fibrillation: protagonist point of view. *Heart Rhythm* 13, 2098–2100. doi: 10.1016/j.hrthm.2016.06.036
- Okin, P. M., Hille, D. A., Larstorp, A. C., Wachtell, K., Kjeldsen, S. E., Dahlöf, B., et al. (2015). Effect of lower on-treatment systolic blood pressure on the risk of atrial fibrillation in hypertensive patients. *Hypertension* 66, 368–373. doi: 10.1161/HYPERTENSIONAHA.115.05728
- Parameswaran, R., Voskoboinik, A., Gorelik, A., Lee, G., Kistler, P. M., Sanders, P., et al. (2018). Clinical impact of rotor ablation in atrial fibrillation: a systematic review. *Europace* 20, 1099–1106 doi: 10.1093/europace/eux370
- Parikh, A., Patel, D., McTiernan, C. F., Xiang, W., Haney, J., Yang, L., et al. (2013). Relaxin suppresses atrial fibrillation by reversing fibrosis and myocyte hypertrophy and increasing conduction velocity and sodium current in spontaneously hypertensive rat hearts. *Circ. Res.* 113, 313–321. doi: 10.1161/CIRCRESAHA.113.301646
- Parkash, R., Wells, G. A., Sapp, J. L., Healey, J. S., Tardif, J. C., Greiss, I., et al. (2017). Effect of aggressive blood pressure control on the recurrence of atrial fibrillation after catheter ablation: a randomized, open-label clinical trial (smac-af [substrate modification with aggressive blood pressure control]). *Circulation* 135, 1788–1798. doi: 10.1161/CIRCULATIONAHA.116.026230
- Pathak, R. K., Evans, M., Middeldorp, M. E., Mahajan, R., Mehta, A. B., Meredith, M., et al. (2017). Cost-effectiveness and clinical effectiveness of the risk factor management clinic in atrial fibrillation. *JACC Clin. Electrophysiol.* 3, 436–447. doi: 10.1016/j.jacep.2016.12.015
- Pathik, B., Kalman, J. M., Walters, T., Kuklik, P., Zhao, J., Madry, A., et al. (2018). Absence of rotational activity detected using 2-dimensional phase mapping in the corresponding 3-dimensional phase maps in human persistent atrial fibrillation. *Heart Rhythm* 15, 182–192. doi: 10.1016/j.hrthm.2017.09.010
- Pontecorbo, G., Figueras Ventura R. M., Carlosena, A., Benito, E., Prat-Gonzales, S., Mont, L., et al. (2017). Use of delayed-enhancement magnetic resonance imaging for fibrosis detection in the atria: a review. *Europace* 19, 180–189. doi: 10.1093/europace/euw053
- Proietti, R., Hadjis, A., AlTurki, A., Thanassoulis, G., Roux, J. F., Verma, A., et al. (2015). A systematic review on the progression of paroxysmal to persistent atrial fibrillation. *JACC: Clin. Electrophysiol.* 1, 105–115. doi: 10.1016/j.jacep.2015.04.010
- Rienstra, M., Hobbel, A. H., Alings, M., Tijssen, J. G. P., Smit, M. D., Brügmann, J., et al. (2018). Targeted therapy of underlying conditions improves sinus rhythm maintenance in patients with persistent atrial fibrillation: results of the RACE 3 trial. *Eur. Heart J.* doi: 10.1093/eurheartj/ehx739. [Epub ahead of print].
- Sanders, P., Berenfeld, O., Hocini, M., Jaïs, P., Vaidyanathan, R., Hsu, L. F., et al. (2005). Spectral analysis identifies sites of high-frequency activity maintaining atrial fibrillation in humans. *Circulation* 112, 789–797. doi: 10.1161/CIRCULATIONAHA.104.517011
- Sanders, P., Mishima, R. S., Linz, D., and Lau, D. H. (2018). In search of atrial fibrillation driver sites: is temporally stable frequency mapping a new armamentarium? *J. Cardiovasc. Electrophysiol.* 29, 523–525. doi: 10.1111/jce
- Sanders, P., Morton, J. B., Davidson, N. C., Spence, S. J., Vohra, J. K., Sparks, P. B., et al. (2003). Electrical remodeling of the atria in congestive heart failure: electrophysiological and electroanatomic mapping in humans. *Circulation* 108, 1461–1468. doi: 10.1161/01.CIR.0000090688.49283.67
- Shiroshita-Takeshita, A., Brundel, B. J., Burstein, B., Leung, T. K., Mitamura, H., Ogawa, S., et al. (2007). Effects of simvastatin on the development of the atrial fibrillation substrate in dogs with congestive heart failure. *Cardiovasc. Res.* 74, 75–84. doi: 10.1016/j.cardiores.2007.01.002
- Sohns, C., Lemes, C., Metzner, A., Fink, T., Chmelevsky, M., Maurer, T., et al. (2017). First-in-Man analysis of the relationship between electrical rotors from noninvasive panoramic mapping and atrial fibrosis from magnetic resonance imaging in patients with persistent atrial fibrillation. *Circ. Arrhythm Electrophysiol.* 10:e004419. doi: 10.1161/CIRCEP.116.004419
- Spach, M. S., and Dolber, P. C. (1986). Relating extracellular potentials and their derivatives to anisotropic propagation at a microscopic level in human cardiac muscle. Evidence for electrical uncoupling of side-to-side fiber connections with increasing age. *Circ. Res.* 58, 356–371. doi: 10.1161/01.RES.58.3.356
- Stiles, M. K., Brooks, A. G., Kuklik, P., John, B., Dimitri, H., Lau, D. H., et al. (2008). High-density mapping of atrial fibrillation in humans: relationship between high-frequency activation and electrogram fractionation. *J. Cardiovasc. Electrophysiol.* 19, 1245–1253. doi: 10.1111/j.1540-8167.2008.01253.x
- Stiles, M. K., John, B., Wong, C. X., Kuklik, P., Brooks, A. G., Lau, D. H., et al. (2009). Paroxysmal lone atrial fibrillation is associated with an abnormal atrial substrate: characterizing the “second factor”. *J. Am. Coll. Cardiol.* 53, 1182–1191. doi: 10.1016/j.jacc.2008.11.054
- Teh, A. W., Kistler, P. M., Lee, G., Medi, C., Heck, P. M., Spence, S. J., et al. (2012). Long-term effects of catheter ablation for lone atrial fibrillation: progressive atrial electroanatomic substrate remodeling despite successful ablation. *Heart Rhythm* 9, 473–480. doi: 10.1016/j.hrthm.2011.11.013
- Thanigaimani, S., Brooks, A. G., Kuklik, P., Twomey, D. J., Franklin, S., Noschka, E., et al. (2017a). Spatiotemporal characteristics of atrial fibrillation electrograms: a novel marker for arrhythmia stability and termination. *J. Arrhythmia* 33, 40–48. doi: 10.1016/j.joa.2016.05.009
- Thanigaimani, S., Lau, D. H., Agbaedeng, T., Elliott, A. D., Mahajan, R., and Sanders, P. (2017b). Molecular mechanisms of atrial fibrosis: implications for the clinic. *Exp. Rev. Cardiovasc. Ther.* 15, 247–256. doi: 10.1080/14779072.2017.1299005
- Thomas, M. C., Dublin, S., Kaplan, R. C., Glazer, N. L., Lumley, T., Longstreth, Jr. W. T., et al. (2008). Blood pressure control and risk of incident atrial fibrillation. *Am. J. Hypertens.* 21, 1111–1116. doi: 10.1038/ajh.2008.248
- Verheule, S., Tuyls, E., Gharaviri, A., Hulsmans, S., van Hunnik, A., Kuiper, M., et al. (2013). Loss of continuity in the thin epicardial layer because of endomyocardial fibrosis increases the complexity of atrial fibrillatory conduction. *Circ. Arrhythm Electrophysiol.* 6, 202–211. doi: 10.1161/CIRCEP.112.975144
- Verma, A., Jiang, C. Y., Betts, T. R., Chen, J., Deisenhofer, I., Mantovan, R., et al. (2015). Approaches to catheter ablation for persistent atrial fibrillation. *N. Engl. J. Med.* 372, 1812–1822. doi: 10.1056/NEJMoa1408288
- Vogler, J., Willems, S., Sultan, A., Schreiber, D., Lüker, J., Servatius, H., et al. (2015). Pulmonary vein isolation versus defragmentation: the chase-of clinical trial. *J. Am. Coll. Cardiol.* 66, 2743–2752. doi: 10.1016/j.jacc.2015.09.088
- Walters, T. E., Lee, G., Morris, G., Spence, S., Larobina, M., Atkinson, V., et al. (2015). Temporal stability of rotors and atrial activation patterns in persistent human atrial fibrillation. *JACC Clin. Electrophysiol.* 1, 14–24. doi: 10.1016/j.jacep.2015.02.012
- Walters, T. E., Lee, G., Spence, S., and Kalman, J. M. (2016). The effect of electrode density on the interpretation of atrial activation patterns in epicardial mapping of human persistent atrial fibrillation. *Heart Rhythm* 13, 1215–1220. doi: 10.1016/j.hrthm.2016.01.030
- Wong, C. X., Abed, H. S., Molaei, P., Nelson, A. J., Brooks, A. G., Sharma, G., et al. (2011). Pericardial fat is associated with atrial fibrillation severity and

- ablation outcome. *J. Am. Coll. Cardiol.* 57, 1745–1751. doi: 10.1016/j.jacc.2010.11.045
- Wong, C. X., Sullivan, T., Sun, M. T., Mahajan, R., Pathak, R. K., Middeldorp, M., et al. (2015). Obesity and the risk of incident, post-operative, and post-ablation atrial fibrillation. *JACC: Clin. Electrophysiol.* 1, 139–152. doi: 10.1016/j.jacep.2015.04.004
- Wong, K. C., Paisey, J. R., Sopher, M., Balasubramaniam, R., Jones, M., Qureshi, N., et al. (2015). No benefit of complex fractionated atrial electrogram ablation in addition to circumferential pulmonary vein ablation and linear ablation: benefit of complex ablation study. *Circ. Arrhythm. Electrophysiol.* 8, 1316–1324. doi: 10.1161/CIRCEP.114.002504
- Yamabe, H., Kanazawa, H., Ito, M., Kaneko, S., and Ogawa, H. (2016). Prevalence and mechanism of rotor activation identified during atrial fibrillation by noncontact mapping: lack of evidence for a role in the maintenance of atrial fibrillation. *Heart Rhythm* 13, 2323–2330. doi: 10.1016/j.hrthm.2016.07.030
- Zghaib, T., Keramati, A., Chrispin, J., Huang, D., Balouch, M. A., Ciuffo, L., et al. (2018). multimodal examination of atrial fibrillation substrate: correlation of left atrial bipolar voltage using multi-electrode fast automated mapping, point-by-point mapping, and magnetic resonance image intensity ratio. *JACC Clin. Electrophysiol.* 4, 59–68. doi: 10.1016/j.jacep.2017.10.010
- Zhao, J., Hansen, B. J., Wang, Y., Csepe, T. A., Sul, L. V., Tang, A., et al. (2017). Three-dimensional integrated functional, structural, and computational mapping to define the structural “fingerprints” of heart-specific atrial fibrillation drivers in human heart ex vivo. *J. Am. Heart Assoc.* 6:e005922. doi: 10.1161/JAHA.117.005922
- Conflict of Interest Statement:** PS reports having served on the advisory board of Biosense-Webster, Medtronic, Abbott, Boston Scientific and CathRx. PS reports that the University of Adelaide receives on his behalf lecture and/or consulting fees from Biosense-Webster, Medtronic, Abbott, and Boston Scientific. PS reports that the University of Adelaide receives on his behalf research funding from Medtronic, Abbott, Boston Scientific, Biotronik and Liva Nova. DL reports that the University of Adelaide has received on his behalf lecture or consulting fees from St Jude Medical, Boehringer Ingelheim, Bayer, and Pfizer.
- The remaining author declares that the research was conducted in the absence of any commercial or financial relationships that could be construed as a potential conflict of interest.
- Copyright © 2018 Stiles, Sanders and Lau. This is an open-access article distributed under the terms of the Creative Commons Attribution License (CC BY). The use, distribution or reproduction in other forums is permitted, provided the original author(s) and the copyright owner(s) are credited and that the original publication in this journal is cited, in accordance with accepted academic practice. No use, distribution or reproduction is permitted which does not comply with these terms.



A Computational Framework to Benchmark Basket Catheter Guided Ablation in Atrial Fibrillation

Martino Alessandrini¹, Maddalena Valinoti¹, Laura Unger², Tobias Oesterlein², Olaf Dössel², Cristiana Corsi¹, Axel Loewe^{2*} and Stefano Severi²

¹ Department of Electronic Engineering and Information Technology, University of Bologna, Cesena, Italy; ² Institute of Biomedical Engineering, Karlsruhe Institute of Technology, Karlsruhe, Germany

OPEN ACCESS

Edited by:

Jichao Zhao,
University of Auckland, New Zealand

Reviewed by:

Sanjay Ram Kharche,
University of Western Ontario, Canada

Rheeda Ali,
Johns Hopkins University,
United States

*Correspondence:

Axel Loewe
publications@ibt.kit.edu

Specialty section:

This article was submitted to
Computational Physiology and
Medicine,
a section of the journal
Frontiers in Physiology

Received: 31 May 2018

Accepted: 20 August 2018

Published: 21 September 2018

Citation:

Alessandrini M, Valinoti M, Unger L, Oesterlein T, Dössel O, Corsi C, Loewe A and Severi S (2018) A Computational Framework to Benchmark Basket Catheter Guided Ablation in Atrial Fibrillation. *Front. Physiol.* 9:1251.
doi: 10.3389/fphys.2018.01251

Catheter ablation is a curative therapeutic approach for atrial fibrillation (AF). Ablation of rotational sources based on basket catheter measurements has been proposed as a promising approach in patients with persistent AF to complement pulmonary vein isolation. However, clinically reported success rates are equivocal calling for a mechanistic investigation under controlled conditions. We present a computational framework to benchmark ablation strategies considering the whole cycle from excitation propagation to electrogram acquisition and processing to virtual therapy. Fibrillation was induced in a patient-specific 3D volumetric model of the left atrium, which was homogeneously remodeled to sustain reentry. The resulting extracellular potential field was sampled using models of grid catheters as well as realistically deformed basket catheters considering the specific atrial anatomy. The virtual electrograms were processed to compute phase singularity density maps to target rotor tips with up to three circular ablations. Stable rotors were successfully induced in different regions of the homogeneously remodeled atrium showing that rotors are not constrained to unique anatomical structures or locations. Density maps of rotor tip trajectories correctly identified and located the rotors (deviation < 10 mm) based on catheter recordings only for sufficient resolution (inter-electrode distance \leq 3 mm) and proximity to the wall (\leq 10 mm). Targeting rotor sites with ablation did not stop reentries in the homogeneously remodeled atria independent from lesion size (1–7 mm radius), from linearly connecting lesions with anatomical obstacles, and from the number of rotors targeted sequentially (\leq 3). Our results show that phase maps derived from intracardiac electrograms can be a powerful tool to map atrial activation patterns, yet they can also be misleading due to inaccurate localization of the rotor tip depending on electrode resolution and distance to the wall. This should be considered to avoid ablating regions that are in fact free of rotor sources of AF. In our experience, ablation of rotor sites was not successful to stop fibrillation. Our comprehensive simulation framework provides the means to holistically benchmark ablation strategies *in silico* under consideration of all steps involved in electrogram-based therapy and, in future, could be used to study more heterogeneously remodeled disease states as well.

Keywords: atrial fibrillation, ablation, basket catheter, computational modeling, rotor

INTRODUCTION

Atrial fibrillation (AF) is one of the major health challenges that modern societies are facing. AF is projected to develop in 25% of currently 40-year-old adults in their later life (Schnabel et al., 2015). Catheter ablation of the pulmonary veins (PVs) is the cornerstone of curative AF therapy and effective in 75% of patients with paroxysmal AF (Kuck et al., 2016). However, isolation of the PVs alone for persistent/permanent AF or AF with concurrent cardiac diseases is not sufficient in about half of the patients (Verma et al., 2015). Regrettably, several other ablation approaches did not yield better results in persistent AF patients in the large STAR AF II trial (Verma et al., 2015). Hence, the optimal ablation strategy for persistent AF patients remains an open question.

Lately, it has been suggested that AF may be driven by discrete reentrant drivers (Narayan et al., 2014; Haissaguerre et al., 2016). Ablation of rotational centers, so-called rotors, guided by electrograms acquired with basket catheters has attracted attention. However, the reported success rates are equivocal ranging from 21 to 82% (Narayan et al., 2014; Buch et al., 2016; Dukkipati and Reddy, 2017; Miller et al., 2017; Mohanty et al., 2018) demanding mechanistic investigation of this tailored ablation approach (Loewe and Dössel, 2017; Trayanova et al., 2018).

We present a framework to computationally evaluate basket catheter guided ablation mechanistically under controlled conditions. We tested this approach using an anatomically personalized model of a human AF patient. This study builds on our previous work (Alessandrini et al., 2017), which is extended in several ways: the sensitivity of the rotor trajectory estimated from catheter signals to the distance between the catheter and the atrial wall is studied; simulated acquisitions of a realistic Constellation basket catheter are considered in addition to simple 2D grid catheters; the basket-guided FIRM ablation protocol is simulated including the treatment by implementing up to three successive ablations.

MATERIALS AND METHODS

Clinical Data

Magnetic resonance (MR) was used to image the atria of one paroxysmal AF patient selected for radio-frequency ablation. A 1.5 T MR scanner (Achieva, Philips Medical System) was used with a 3D spoiled gradient recalled sequence. Contrast enhanced 3D MR angiographic (MRA) images were acquired (echo time: 1.12 ms, repetition time: 3.74 ms, flip angle: 25°, in-plane resolution $0.7 \times 0.7 \text{ mm}^2$ and slice thickness 3 mm with 1.5 mm overlap) with gadolinium injection of 0.1 mmol/kg followed by a 20 ml saline flush. Acquisition was ECG triggered and in breath hold. The study was approved by the Ethics IRST, IRCCS AVR Committee (CEIIAV n. 1456 prot. 6076/2015 I.5/220). Informed consent was obtained from the subject.

Anatomical Model

Left atrial (LA) blood pool, LA appendage (LAA) and the four pulmonary veins (PVs) were segmented semi-automatically

from the MRA data using in-house software (Valinoti et al., 2018). The 3D segmentation was obtained by stacking 2D segmentations along the cross-slice direction. The segmented volume was resampled at a uniform voxel size of $0.33 \times 0.33 \times 0.33 \text{ mm}^3$. Gaussian smoothing was employed to remove the staircase artifacts coming from the anisotropic voxel size of the MR system. The atrial epicardium was obtained by extruding the endocardial segmentation to a uniform wall thickness of 3 mm (Platonov et al., 2008; Krueger et al., 2013b). The LA model was augmented with myofiber directions in each cell of the anatomical model using a rule-based algorithm (Wachter et al., 2015). Hereto, a set of 13 anatomical landmarks was manually identified on the LA surface and used to identify the main fiber bundles. The resulting fiber distribution is illustrated in **Figure 1**. The same algorithm was used to label relevant tissue classes: atrial body, PVs, LAA and mitral valve ring (Krueger et al., 2013a). Additionally, Bachmann bundle and fossa ovalis were annotated manually and used to simulate sinus rhythm activation, as discussed in the following. Tissue classes are illustrated in **Figure 2**. Ablation lesions were modeled as non-conducting transmural structures.

Simulating Atrial Activation

The monodomain model was used to simulate excitation propagation in the LA based on a heterogeneous version (Loewe et al., 2015) of the Courtemanche membrane model (Courtemanche et al., 1998) accounting for AF related ionic remodeling (Loewe et al., 2014). The monodomain conductivity and its anisotropy were set as in (Loewe et al., 2015) besides altering the common LA properties homogeneously to account for AF-induced remodeling (reduced conductivity 8.9 mS/m and increased anisotropy of 10). Sinus activation was simulated by pacing the model at the insertion point of the Bachmann bundle and at the Fossa Ovalis with a physiological delay of 26 ms (Loewe et al., 2016). In order to initiate reentry, an extra stimulus was placed in a circular area with a radius of 5 mm. By changing the location of this area it was possible, in several cases, to cause unidirectional block and subsequent reentry (see Results). Transmembrane voltages and current densities were computed by the monodomain reaction-diffusion solver acCELLerate (Seemann et al., 2010; Niederer et al., 2011) using a finite element scheme. The ordinary differential equations of the cell model were integrated using the Rush-Larsen scheme for the gating variables and a forward Euler scheme for the remaining variables. Constant time stepping of 20 μs was used. The membrane models were initialized in a single cell environment to reach steady-state at a basic cycle length of 800 ms.

Multielectrode Catheters

Grid Catheters

To study the sensitivity of rotor tracking to spatial sampling density (i.e., intra-electrode distance) and distance to the atrial wall, we employed two “toy” catheters. The two catheters were obtained by positioning 9×9 (respectively, 5×5) electrodes on a square grid with an inter-electrode distance of 3 mm (respectively, 6 mm), as shown in **Figure 3**. As such, the total size of the 2D patch was $24 \times 24 \text{ mm}^2$ in both setups. The 2D

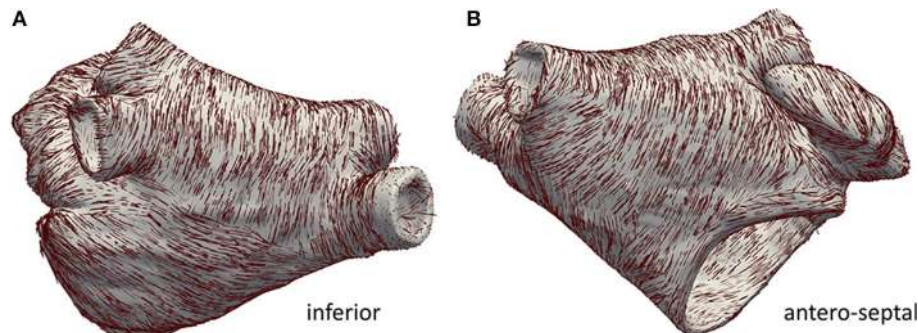


FIGURE 1 | Anatomical model with annotated fiber bundles. In **(A)** the inferior wall is shown, in **(B)** the anterior/septal wall is shown.

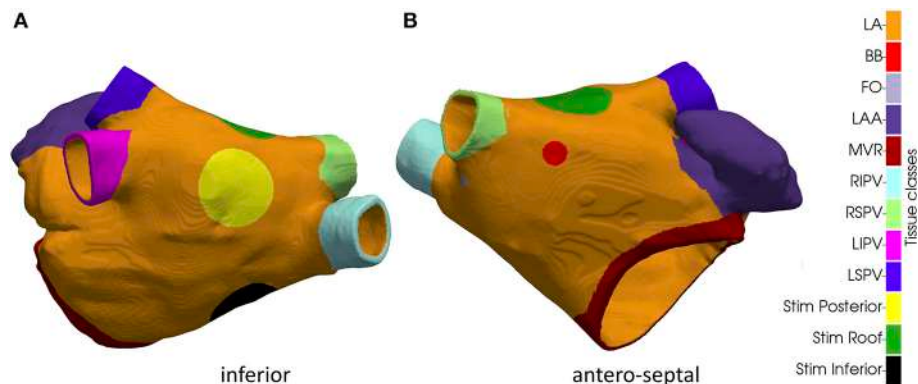


FIGURE 2 | Inferior **(A)** and antero-septal **(B)** aspect of the anatomical model with tissue classes. LA bulk, Bachmann's bundle insertion point (BB), fossa ovalis (FO), left atrial appendage (LAA), mitral valve ring (MVR), right inferior pulmonary vein (RIPV), right superior pulmonary vein (RSPV), left inferior pulmonary vein (LIPV) left superior pulmonary vein (LSPV). The three circular regions in which the extra stimuli were applied to initiate reentry in the three simulated AF scenarios are indicated as well.

grid catheters were then positioned in the 3D atrial model such that the tissue region of interest was covered at a given distance from the atrial wall. Catheter positioning was implemented as follows. An initial 3D rigid transform was employed to align the grid catheter with a given region of interest. Hereto, the center point of the desired region of interest was selected manually on the atrial endocardium and used as origin of the local coordinate system. The set of endocardial mesh nodes falling within a radius of 5 mm from the selected point were then used to fit a 2D plane and, hence, define the 3 axes of the local coordinate system: two tangential to the endocardial surface and one perpendicular to it. After 3D rotation, the catheter was adapted to the specific atrial shape by repositioning each electrode to its closest position on the atrial endocardium. To modify the distance between the electrode and the atrial wall, all electrodes were moved rigidly along the inwards normal direction defined by the local coordinate system used for rotation.

Basket Catheters

We used the algorithm presented in Oesterlein et al. (2016) to position a simulated basket catheter inside the specific atrial anatomy. In brief, a set of Frenet-Serret parameterized spline

pairs of a given size are deformed to minimize the inner tension energy while fulfilling the constraints posed by the atrial surface as well as the distal and proximal end of the basket catheter. We chose the Constellation basket size that best fit our geometry. Hereto, a commercially available 48 mm basket with 8 splines and 4 mm inter-electrode spacing was positioned inside the atrial geometry. The position was optimized with the objective of maximizing the coverage of the rotor trajectory with basket electrodes. The basket catheter is illustrated in Figure 4.

Simulated Electrograms

Unipolar electrograms (EGMs) $\phi(\mathbf{x}, t)$ at point electrode positions \mathbf{x} were computed from the monodomain current density distributions $I(\mathbf{x}, t)$ under the simplifying assumption of an unbounded volume conductor:

$$\phi(\mathbf{x}, t) = \frac{1}{4\pi\sigma} \sum_V \frac{I(\mathbf{x}_i, t)}{\|\mathbf{x}_i - \mathbf{x}\|}$$

where σ is the electrical conductivity of the volume conductor, \mathbf{x} is the sampling position (i.e., the electrode position), \mathbf{x}_i is the coordinate of the i th cell of the atrial mesh and V comprises the whole atrial wall. Simulated EGMS were sampled at 1 kHz.

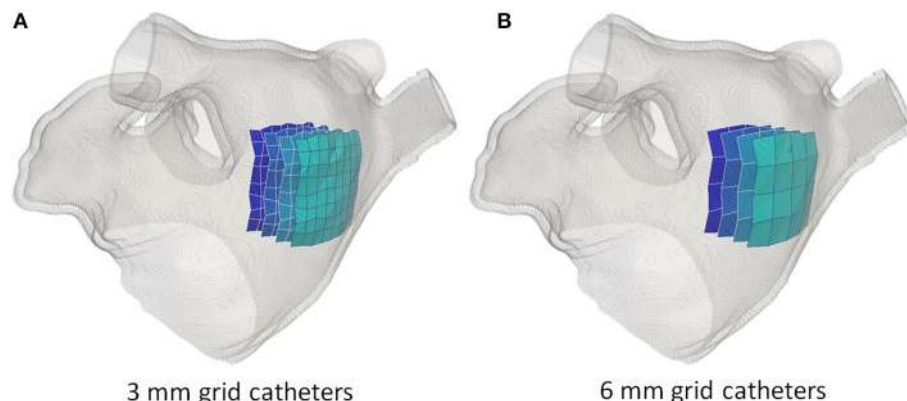


FIGURE 3 | Simulated grid catheters. In **(A)** the catheter with a 3 mm inter-electrode spacing. In **(B)** the catheter with a 6 mm inter-electrode spacing. In both cases, four catheters are illustrated corresponding to a distance to the atrial wall of 0 mm (lightest blue), 5, 10, and 15 mm (darkest blue).

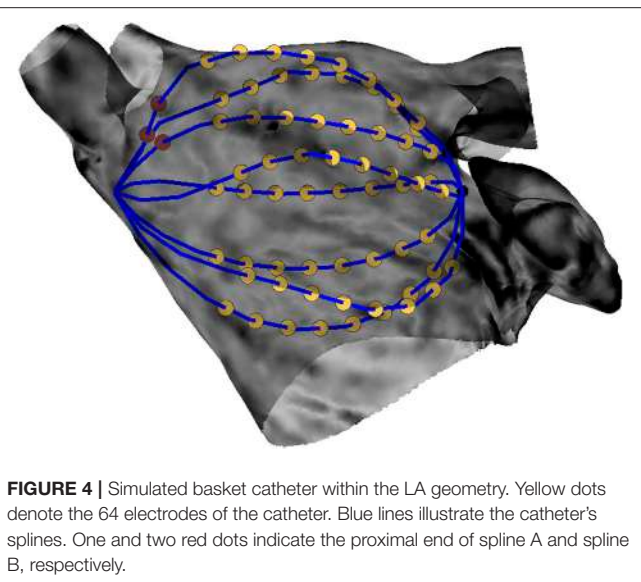


FIGURE 4 | Simulated basket catheter within the LA geometry. Yellow dots denote the 64 electrodes of the catheter. Blue lines illustrate the catheter's splines. One and two red dots indicate the proximal end of spline A and spline B, respectively.

Rotor Tracking From Multi-Electrode Acquisitions

We used the method presented in Valinoti et al. (2017) to detect and track electrical reentries from the simulated electrograms. Briefly, rotor detection is based on the concept of phase singularities (PS). Hereto, the simulated electrograms were first converted into phase signals by using a modified version of the sinusoidal decomposition approach (Kuklik et al., 2015). The extracted phase values were then mapped from the electrode positions to the 3D geometry by nearest neighbor interpolation with a cut-off value of 13 mm. The algorithm then looked for closed loops with monotonically increasing/decreasing phase values and a jump of at least π as per definition of a PS. The search was progressively extended to neighboring regions, i.e., sharing an interface in the 3D reconstruction. Rotors were identified by tracking the persistence of PS in the same region in subsequent

time frames. The PS persistence was estimated considering a threshold on the maximum distance between the coordinates of its location estimated frame by frame. The threshold was fixed at 8 mm for the 3 mm grid, 17 mm for the 6 mm grid and 20 mm for the basket. As such, a tip trajectory was estimated for each rotor in each of the simulations and the rotor with the longest lifespan was considered as ablation target.

Trajectory Density Maps and Evaluation of Tracking Accuracy

The ground truth rotor tip trajectory was tracked from the high resolution electrical activation maps. Hereto, the transmembrane potential time courses $V_m(t, \mathbf{x}_i)$ of each vertex \mathbf{x}_i were converted into phase signals by computing the phase of the complex-valued analytical signal $z(t, \mathbf{x}_i)$:

$$z(t, \mathbf{x}_i) = V_m(t, \mathbf{x}_i) + jH\{V_m(t, \mathbf{x}_i)\},$$

with $H\{\cdot\}$ being the Hilbert transform and j being the imaginary unit. The rotor tip was identified as a singularity in the reconstructed phase maps. Tracking accuracy was then assessed by comparing the trajectory estimated by the tracking algorithm vs. the ground truth. Hereto, instead of a pointwise comparison of the two trajectories, we used “trajectory density maps” as a way to represent temporal persistence of a rotor in a given atrial region over a given time interval Δt . If we denote by $\mathbf{y}(t_j)$ the rotor tip position at time t_j , then the density value d_i at a mesh node \mathbf{x}_i was computed as:

$$d_i = A \cdot \sum_{t_j \in \Delta t} f(\|\mathbf{y}(t_j) - \mathbf{x}_i\|), \text{ with } f(z) = e^{-z^2/2\sigma^2}$$

where σ defines the spatial extent of the smoothing kernel f . A is used to normalize peak density to one. In this study, we used an integrating time interval $\Delta t = 2$ s and $\sigma = 3$ mm. Hence, tracking accuracy was evaluated by comparing the position of the peak in the estimated trajectory map \mathbf{d} vs. the ground truth one as ultimately, peak density was used to guide rotor ablation, as described in the following.

Simulated Rotor-Ablation Protocol

Radiofrequency ablation was simulated by setting zero conductivities (longitudinal and transverse) for mesh elements pertaining to the ablation lesions (circular regions of 7 mm radius Bayer et al., 2016, unless otherwise specified). For a given tissue simulation and positioning of the multi-electrode catheter, rotor-driven ablation was simulated by repeating the following steps:

- EGM signal recordings were simulated for a period of 2 s, as described in section Simulated electrograms;
- The rotor trajectory was reconstructed from the simulated EGM signals with the custom rotor tracking algorithm, as described in section Rotor tracking from multi-electrode acquisitions;
- The trajectory density map was computed from the estimated rotor trajectory, as described in section Trajectory density maps and evaluation of tracking accuracy;
- The circular ablation site was centered in the maximum of the estimated density map;

As such, up to three ablations were incrementally applied.

RESULTS

Simulation of Rotor-Based Sustained Atrial Activation

Using the methods described in section Simulating atrial activation it was possible to induce complex propagation patterns maintained by stable rotors. In particular, we obtained three different sustained patterns by changing the location of the extra stimulus applied to induce reentry: one at the inferior wall (“Simulation Inferior,” **Supplemental Video 1**); one at the posterior wall toward the roof (“Simulation Posterior,” **Supplemental Video 2**); one at the roof (“Simulation Roof,” **Supplemental Video 3**). The position of the extra stimulus used to induce reentry in the three cases is illustrated in **Figure 2**.

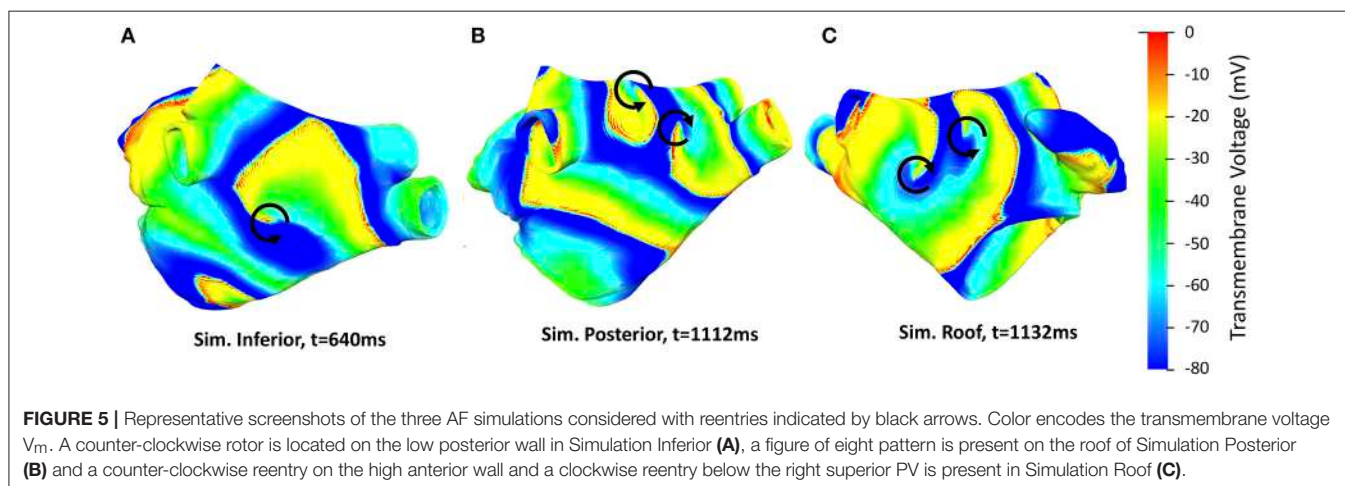
In all cases, this procedure generated “figure of eight” reentries (i.e., two reentries with opposite chirality). In Simulation Inferior

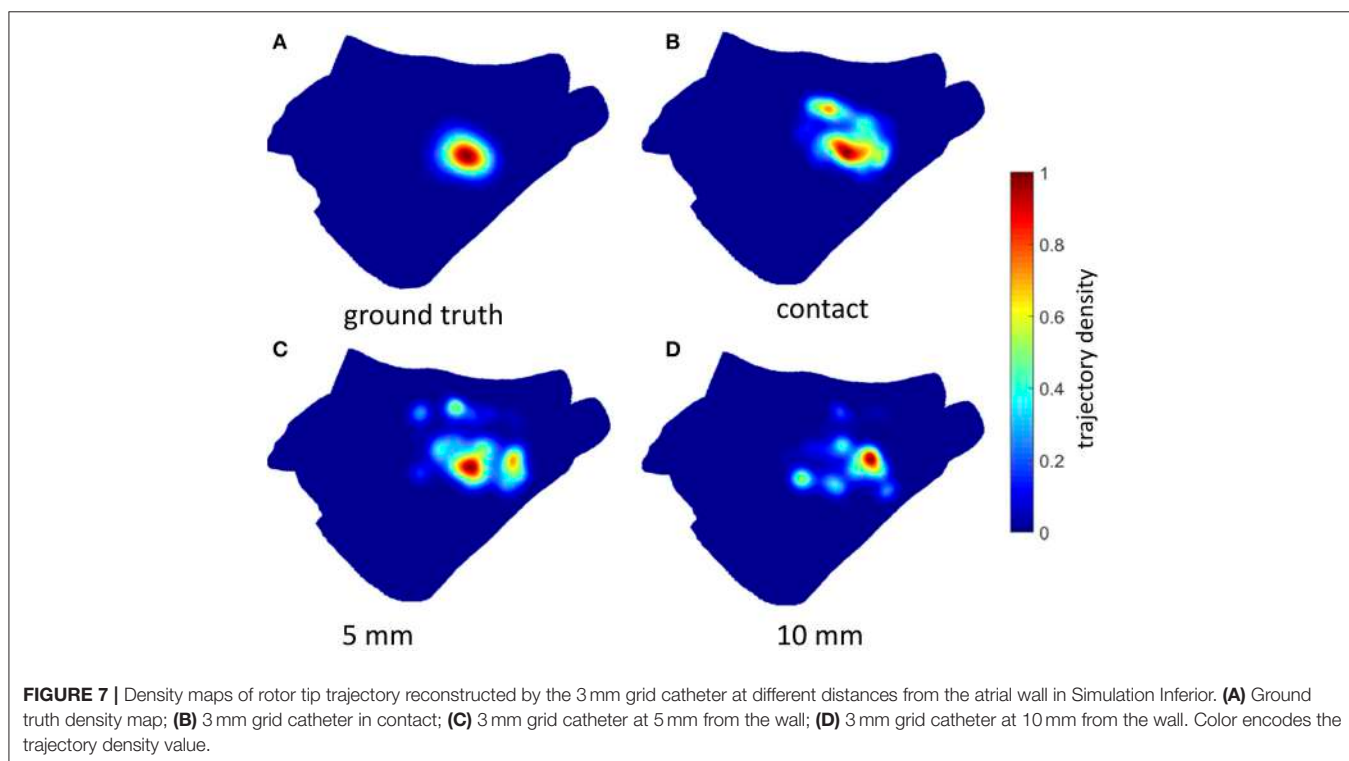
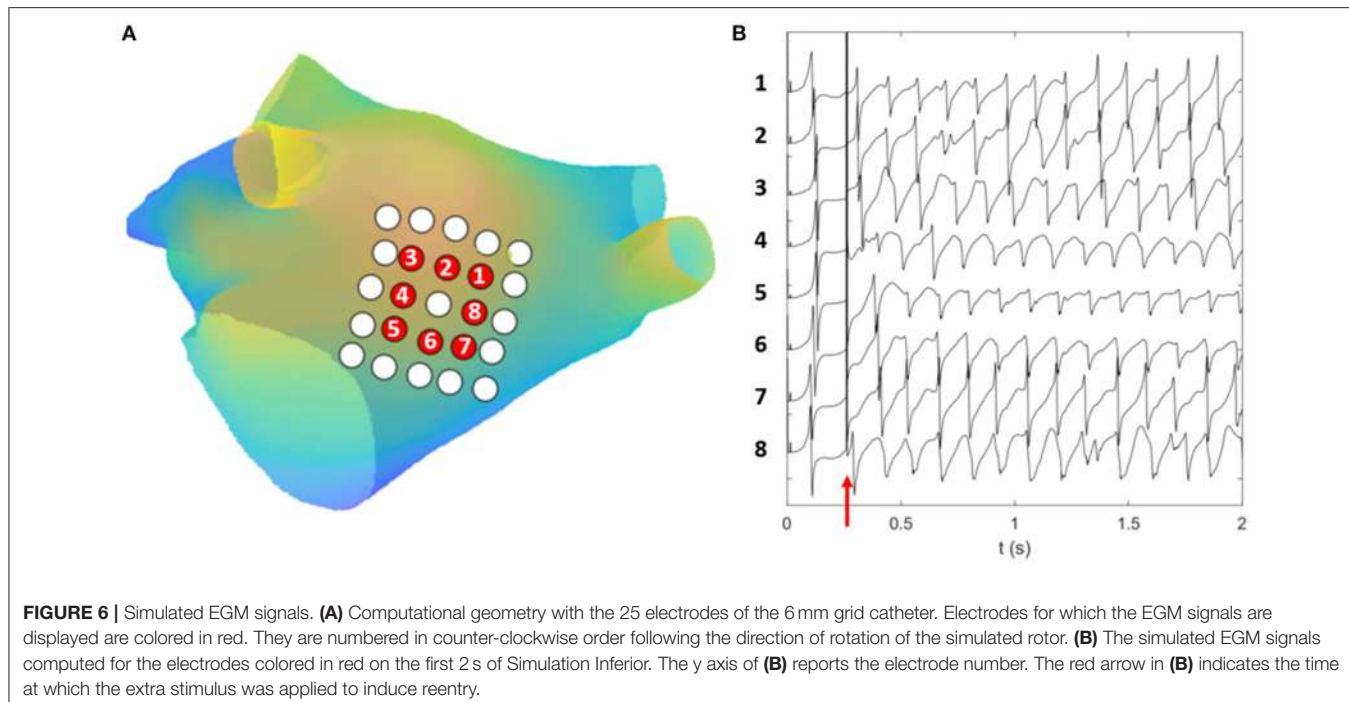
the counter-clockwise rotor was located in the low posterior wall moving toward the septum below the right inferior PV in the last part of the simulation. The clockwise rotor was stably located at the septum, above the mitral valve. In Simulation Posterior a rather stable figure of eight was formed by two highly interacting opposite reentries, which were located close to each other: one on the high posterior wall roughly midway between the right and left inferior PVs and the second one on the roof toward the left superior PV. At $t = 1.05$ s, a second figure of eight appeared at the septum, below the right superior PV. In Simulation Roof, one counter-clockwise reentry was stable in the high part of the anterior wall while a clockwise reentry was initially centered at the roof toward the right PVs. At time $t = 0.8$ s, a third, clockwise, reentry started below the right superior PV, most likely due to wavebreak caused by the local change in fiber direction. Consequently, the second reentry gradually shifted toward the posterior wall and vanished, while a stable figure of eight was formed by the first and third reentries. Representative screenshots are shown in **Figure 5** while the videos are provided in the **Supplemental Material**.

Simulation of Grid Catheters: Effect of Electrode-Wall Distance and Inter-Electrode Distance on Rotor Tracking

For each of the three simulated excitation patterns, we computed the electrograms and the corresponding phase maps from eight grid catheters, characterized by different inter-electrode spacing (3/6 mm) and distances to the atrial wall [0 mm (i.e., in contact), 5, 10, and 15 mm]. Example of simulated EGM signals for the 6 mm catheter from Simulation Inferior are illustrated in **Figure 6**. The grid catheters were positioned to cover as much as possible of the ground truth rotor trajectory and were used to assess the rotor tracking algorithm’s sensitivity to electrode spacing and wall distance.

The estimated rotor tip density maps in the case of Simulation Inferior are shown in **Figure 7** (3 mm inter-electrode spacing) and **Figure 8** (6 mm inter-electrode spacing). Due to the





reduction of the spatial resolution of the electrical activity by sampling with a limited number of electrodes, several spurious peaks in the rotor tip density maps were observed. Nevertheless, when the distance from the atrial wall was below 10 mm, it was possible to correctly locate the maximum peak density

(error < 9 mm) using the 3 mm inter-electrode spacing catheter (**Figure 7**).

On the contrary, when using 6 mm inter-electrode spacing, a systematic error (>11 mm) in the location of the density peak was observed independently of the distance from the atrial wall

(Figure 8). The accuracy of the rotor tracking algorithm on all three simulated activation patterns is presented in Table 1.

Simulation of Sequential Ablation of Rotors Based on Basket Catheter Mapping

For each simulation, the acquisition from a realistic basket geometry (cf. section Basket catheters) was analyzed to locate rotors as potential targets for ablation.

Simulation Inferior

The sustained activity (Supplemental Videos 1, 4) was mapped with the basket catheter (Figure 4) and the corresponding rotor tip density map (Figure 9A, mid) correctly located a peak at the low posterior wall, where one of the driving rotors was meandering. While only a smaller amplitude peak in the density map was found in correspondence of the septal rotor. The highest peak was targeted with circular tissue ablation (Figure 9A, mid), which caused a reentry around the lesion first, which was

then (at $t = 2.5$ s) overdriven by the second rotor located in the septum above the mitral valve, which was unaffected by this ablation (Supplemental Video 5). An illustrative screenshot showing the stable rotor on the septum is depicted in Figure 9B (left).

We then tested the effect of ablation lesion size. By reducing the dimension of the circular lesion, it was possible to change its interaction with the reentry, however without stopping it. A 3.5 mm radius lesion was the smallest one which caused reentry around the lesion (Supplemental Video 6). A 2 mm radius lesion interacted with the spiral but was too small to sustain the reentry around it; the reentry extended inferior-septally and toward the roof to form a larger functional obstacle first. Later on, the core moved toward the roof and the lesion did not play a role anymore (Supplemental Video 7). A 1 mm radius lesion did not affect the reentry at all (Supplemental Video 8).

The stable rotor in the septum, which became dominant after the first ablation (Supplemental Video 5) was then mapped

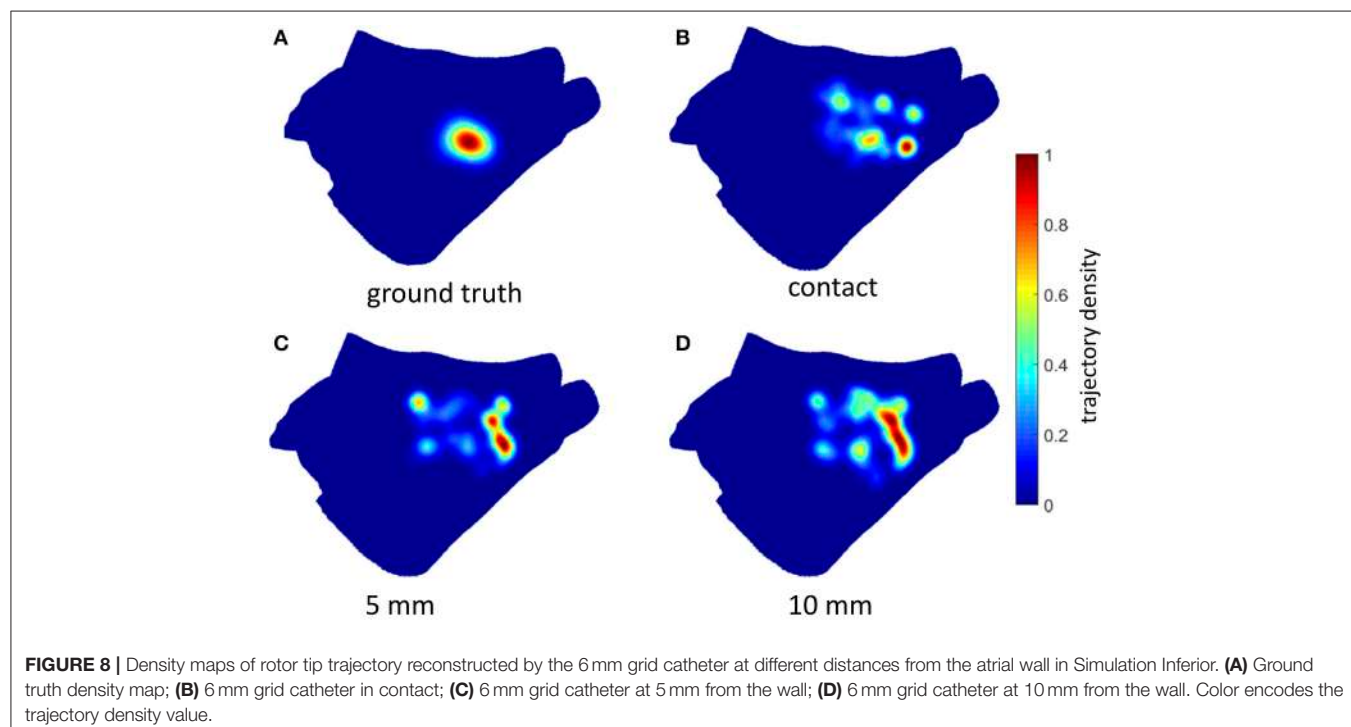


FIGURE 8 | Density maps of rotor tip trajectory reconstructed by the 6 mm grid catheter at different distances from the atrial wall in Simulation Inferior. **(A)** Ground truth density map; **(B)** 6 mm grid catheter in contact; **(C)** 6 mm grid catheter at 5 mm from the wall; **(D)** 6 mm grid catheter at 10 mm from the wall. Color encodes the trajectory density value.

TABLE 1 | Peak to peak distance (in mm) between ground truth and estimated rotor density map from grid catheter with different resolution (3 or 6 mm inter-electrode distance) and distance from the atrial wall.

		Distance from the atrial wall			
		0 mm (contact)	5 mm	10 mm	15 mm
Grid resolution	3 mm	1.2 (0.9/1.7/1.9)	5 (0.6/3.9/ 0.5)	8.4 (8.9/3.9/12.4)	11.5 (11.7/9.0/13.8)
	6 mm	11.8 (12.9/15.8/6.6)	10.3 (12.6/6.0/12.3)	12.1 (11.7/6.5/18.2)	16.4 (16.0/18.5/14.6)

Distances are given as average value and individual values for all three excitation patterns (Simulation Inferior/Simulation Posterior/Simulation Roof), for each distance-resolution combination.

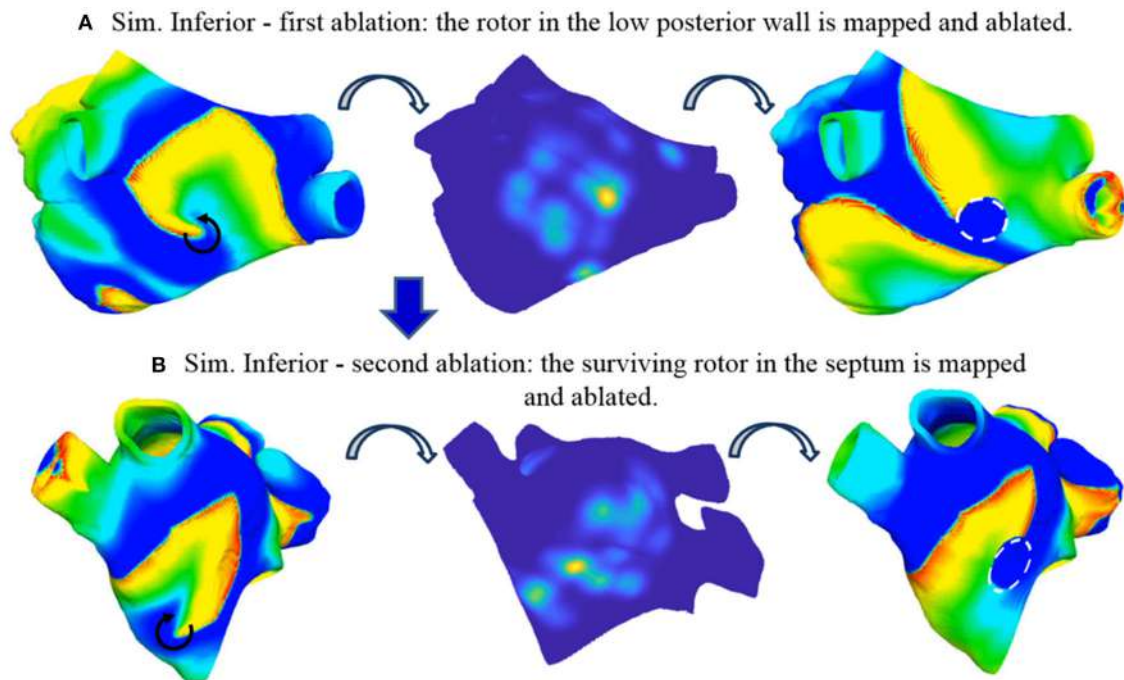


FIGURE 9 | Simulated ablation of Simulation Inferior. Two reentries are present before ablation: one in the posterior wall (**A**, left) and one in the septum (not visible from this view, see **Supplemental Video 4**). The basket-reconstructed density map identifies the first reentry (**A**, mid) which is ablated with a circular region (**A**, right, dashed white circle). After ablation, AF is sustained by the second reentry in the septum (**B**, left), which is mapped (**B**, mid) and ablated (**B**, right, dashed white circle). Two coupled reentries arose around the anatomical obstacles formed by the two lesions induced by sequential ablation (see **Supplemental Videos 4–11**). Color code is identical to **Figure 5** (left and right) and **Figure 7** (mid).

again with the 8-spline basket (**Figure 4**). In this case, the localization of the rotor tip based on the density map was less precise (**Figure 9B**, mid), probably due to the low-resolution basket coverage of the rotor. The peak of the density map was targeted by a second circular ablation (**Figure 9B**, right). This second ablation (**Supplemental Video 9**) led back to a pattern similar to the initial one: two coupled (figure of eight) reentries arose around the anatomical obstacles formed by the two lesions induced by sequential ablation.

Linear lesions toward anatomical obstacles were tested in order to stop reentry but were unsuccessful. A linear ablation connecting the lesion at the septum with the mitral valve was able to stop the reentry anchored around that lesion but did not affect the reentry around the other lesion, therefore it was not sufficient to stop sustained activity (**Supplemental Video 10**). An additional linear ablation connecting the lesion at the low posterior wall with the right inferior PV induced a combined larger reentry around the two lesions and the anatomical obstacles (**Supplemental Video 11**).

Simulation Posterior

The sustained activity shown in **Supplemental Video 2** was mapped with the basket catheter (**Figure 4**); the corresponding rotor tip density map (**Figure 10A**, mid) correctly pinpoints a peak at the roof, where one of the driving rotors was meandering. This peak was targeted by a circular ablation (**Figure 10A**, right), which stopped the reentry without affecting neither the

coupled reentry nor the other figure of eight located at the septum (**Supplemental Video 12**). Illustrative screenshots after the ablation are shown in **Figure 10A** (right) and **Figure 10B** (left). The atrium was mapped again with the 8-spline basket (**Figure 4**), in the attempt to locate the second rotor at the roof as a target for ablation. But it was not possible, based on the density map, to precisely locate the rotor tip. Indeed, the peak was clearly shifted to the left, toward the left PVs, with respect to the actual rotor tip (**Figure 10B**, mid). By trusting the results of the low-resolution catheter map, i.e., ablating a circular region centered in the position of the density peak, it was not possible to stop the second rotor, which indeed kept rotating close to the rather narrow space between the two lesions (**Figure 10B**, left, and **Supplemental Video 13**). However, after the second ablation, the rotor moved slightly toward the anterior wall leading to a collision with one of the two rotors at the septum. At the end, only two coupled rotors survived. When a third rotor-guided ablation was performed as intended in the FIRM protocol (**Figure 10C** and **Supplemental Video 14**), the sustained activity did not stop. The rotors moved slightly and after a transient phase, two reentries became stable: a rotor in the anterior wall and an anatomical reentry around the right superior PV.

Simulation Roof

The sustained activity shown in **Supplemental Video 3** was mapped with the basket catheter (**Figure 4**) and the

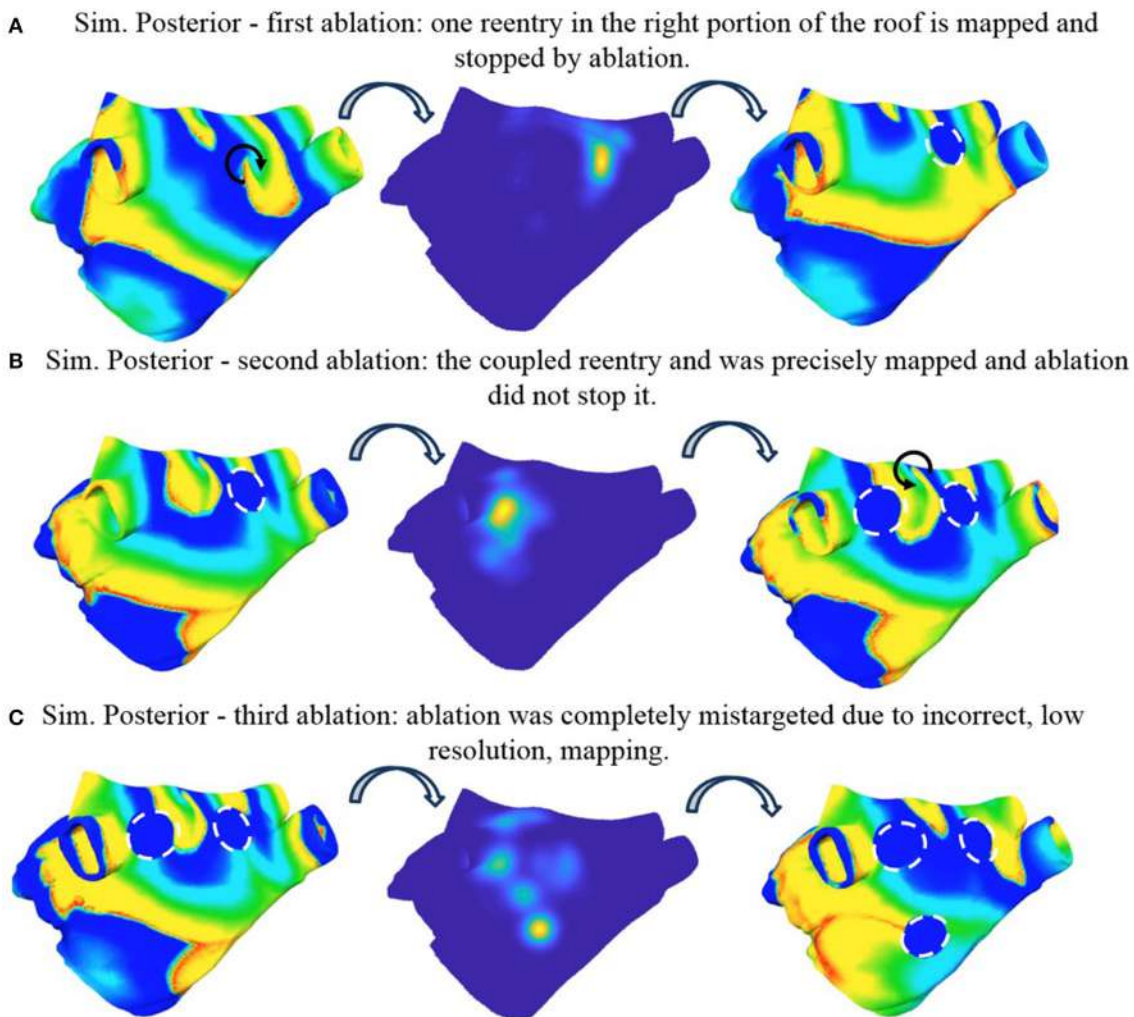


FIGURE 10 | Simulated ablation of Simulation Posterior. Three ablations are applied incrementally. First ablation correctly identifies one reentry in the right portion of the roof and stopped it (**A**). The second ablation was not precisely targeted to the coupled reentry and was not able to stop it (**B**). The third ablation was completely mistargeted due to incorrect, low resolution mapping (**C**) (see **Supplemental Videos 2, 12–14**). Color code is identical to **Figure 5** (left and right) and **Figure 7** (mid).

corresponding rotor tip density map (**Figure 11A, Mid**) correctly pinpoints a peak below the right superior PV, where one of the driving rotors was meandering. This peak was targeted by a circular ablation, which stopped this reentry. One rotor remained at the anterior wall while a second one appeared at the right inferior PV (**Supplemental Video 15**). An illustrative screenshot after the ablation is shown in **Figure 11A** (Left).

The atrium was mapped again with the basket (**Figure 4**) to locate the rotor at the anterior wall as a target for ablation. After the second ablation, the targeted rotor was stopped (**Figure 11B**); after an initial reentry around the anatomical obstacles produced by the ablations the disorganized activity in the entire atrium was driven by the rotor at the right inferior PV (**Supplemental Video 16**). Due to its position, within the initial tract of the PV, it was not possible to map this rotor with the basket catheter.

DISCUSSION

Main Findings

The accuracy of localizing rotors using multielectrode catheters and the efficacy of ablating the derived targets cannot be easily assessed *in vivo*, since the actual fibrillatory activation patterns are not known in great detail in clinical practice. We have implemented a computational framework to benchmark basket catheter guided ablation *in silico*.

Our results show that (i) in a simulated homogeneously remodeled atrium, stable rotors can be induced in different regions, depending on the timing and the location of an extra stimulus; this means that rotors are not constrained to unique anatomical structures or locations; (ii) Rotors may be identified and located with clinically sufficient accuracy by phase maps built from basket catheter recordings only if resolution and distance

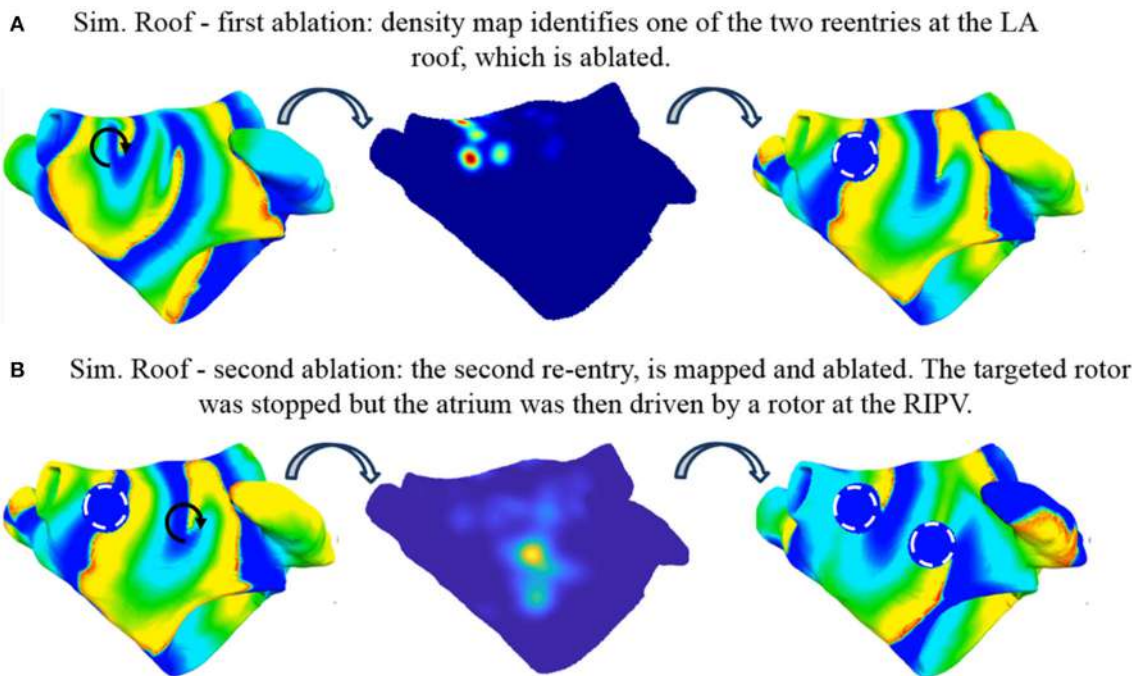


FIGURE 11 | Simulated ablation of Simulation Roof. Two coupled reentries are present before ablation (A, left). The basket-reconstructed density map identifies one of them (A, mid) which is ablated with a circular region (A, right, dashed white circle). After ablation, AF is sustained by the second reentry (B, left), which is mapped (B, mid) and ablated (B, right, dashed white circle). The targeted rotor was stopped but the atrium was then driven by a rotor at the right inferior PV (see [Supplemental Videos 3, 15, 16](#)). Color code is identical to [Figure 5](#) (left and right) and [Figure 7](#) (middle).

from the wall are appropriate; (iii) Ablation of rotor sites does not stop reentry in homogeneously remodeled atria.

Simulation of Rotor-Based Sustained Atrial Activation

It was possible to induce rotor-based sustained atrial activity by using a model that does not take into account transmural heterogeneity/uncoupling nor the presence of fibrosis. Not considering these effects is of course a limitation of the model and further studies with more detailed models are warranted. On the other hand, our results demonstrate that such elements are not strictly needed in order to obtain stable rotors in human atria and that stable rotors are not unique patterns constrained by the presence of a specific heterogeneous substrate. Zhao et al. (2017) used a 3D human heart-specific atrial model integrating local wall thickness and transmural fibrosis data and found that reentrant AF drivers were uninducible when fibrosis and myofiber anisotropy were removed from the model. Taken together these results suggest that myofiber anisotropy, which was included in our model too, can be the key factor for inducibility. On the other hand, also the patient-specific anatomy or the different pacing protocols used to induce the reentrant activity might play a role. In particular, in a preliminary study we were not able to induce reentry by using a single point burst pacing protocol.

In our hands, while keeping exactly the same substrate, stable rotors were induced in multiple different positions of the left

atrium. Thus, it is not surprising that ablation of the rotor core might be unsuccessful since rotors can move or arise somewhere else in the atrium. In many computational studies, this aspect was not investigated since only one sustained activation pattern was analyzed (e.g., Martinez-Mateu et al., 2018) or different patterns were induced by changing the underlying substrate (e.g., Vigmond et al., 2004 by changing the acetylcholine level). However, in some previous studies (McDowell et al., 2012; Gonzales et al., 2014; Krueger et al., 2014; Zhao et al., 2017) rotors were shown to be sustained and stabilized by fibrosis, and more recently a relationship between fibrosis and reentrant activity has been clinically reported (Cochet et al., 2018). Nevertheless, the causal effect and the impact of fibrosis on the ablation success rate is not completely clarified yet and deserves further studies. With this study, we contribute insight based on a simple structural model with a limited number of free parameters, which can be well controlled and analyzed.

Simulation of Electrogram Acquisition: Effect of Electrode-Wall Distance and Inter-electrode Distance on Rotor Tracking

Rotors in our simulations were not perfectly stable in space, some meandering was always observed. However, by tracking their movement, a quite concentrated ground truth core trajectory density was observed ([Figures 7, 8, Top Left](#)). Conversely, when looking at the estimated core trajectory density based on simulated electrogram recordings, a number of spurious peaks

were always present (**Figures 8, 9**) even for catheters in contact with or close to the endocardial wall. This is mainly due to the discretization, i.e., the low resolution of the EGM acquisition as shown by Roney et al. (2017). Different kinds of interpolation were suggested to increase the apparent spatial EGM sampling resolution and therefore the resolution of the estimated phase map. We preferred not to interpolate for two reasons: (i) It has recently been shown in a simulation setting quite similar to ours that interpolation between electrodes can generate artifact “phantom” rotors (Martinez-Mateu et al., 2018). (ii) We wanted to reproduce phase maps similar to those clinically available in the Topera format with the relevant difference that maps are directly computed on a patient-specific atrial anatomy rather than a fixed isotropic 8×8 grid (Oesterlein et al., 2016). Due to the observed dispersion of estimated core trajectories, it seems important to rely on an integral measure such as the density peak over time.

Localization of rotors worked well (i.e., with errors less or equal to the dimension of a lesion produced by the ablating catheter in a real procedure) for inter-electrode spacing of 3 mm and distances to the wall below 10 mm. This is in agreement with the recent observations by Martinez-Mateu et al. (2018) that rotor detection by the basket maps varied depending on the basket’s position and the electrode-wall distance. While it is difficult to establish a cut-off threshold for these parameters, two warnings can be derived for clinical panoramic mapping with basket catheters: (i) it is important to include an estimate of the distance of each electrode from the wall when estimating the phase map in order to exclude those too far to give reliable contributions, (ii) the commercially available basket catheters seem not to assure a sufficient resolution if used in the fully open position to simultaneously acquire EGMs from (almost) the entire atrial chamber.

Simulation of Sequential Ablation of Rotors Based on Basket Catheter Mapping

We found that ablation of rotor sites did not stop reentry in homogeneously remodeled atria. This was observed for all three reentry scenarios and independent from lesion size. By computing the phase maps and then the rotor trajectories directly on the atrial anatomy, it was possible to define the targets for rotor ablation very precisely. This could prove to be better than analysing and visualizing the phase map in a two-dimensional surface and then manually locate the ablation target on the atrial anatomy (Oesterlein et al., 2016). Indeed, as shown in one of our simulated scenarios (Simulation Posterior), relatively modest errors in rotor localization might lead to ablation with no effect on the rotor itself. This underlines the importance of sufficient spatial resolution and coverage when using panoramic mapping to guide rotor ablation.

Several AF ablation strategies have been studied using computational models as reviewed by Zhao et al. (2015) and Jacquemet (2016). Besides rotor ablation, sites of local electrical dyssynchrony have recently been studied as potential targets for ablation *in silico* (Kuklik et al., 2016). Compared to previous *in silico* studies of rotor ablation (McDowell et al., 2012, 2015;

Gonzales et al., 2014; Krueger et al., 2014; Ugarte et al., 2015; Bayer et al., 2016; Hwang et al., 2016; Zahid et al., 2016; Lim et al., 2017), the work presented here is, to the best of our knowledge, the first which considers the full workflow from signal acquisition using realistic catheter models via rotor tip estimation to virtual ablation.

While most previous studies considered spatial fibrosis distribution (McDowell et al., 2012, 2015; Gonzales et al., 2014; Krueger et al., 2014; Bayer et al., 2016; Zahid et al., 2016), we chose to focus on the basic mechanisms in a homogeneously remodeled substrate. Lim et al. (2017) chose a similar homogeneous approach, however high dominant frequency regions were targeted instead of rotors. Ugarte et al. (2015) only considered linear ablation patterns. Hwang et al. (2016) targeted rotors with virtual ablation in 2D and 3D models and obtained similar results. Sequential phase singularity-based ablation with a radius of 1 mm up to a maximum ablated area of 5% of the LA did not stop the arrhythmia. Instead, the rotor turned to a reentry encircling the ablated area. Combination of these findings is well in line with our results (observing sustained reentry with both permanent and transient anchoring to ablation lesions) as well as clinical data reporting that the majority of atrial tachycardias in patients undergoing a repeat procedure after prior FIRM guided ablation appeared to have little relationship to previous FIRM ablation sites (Latanich et al., 2018).

Limitations

The model employed in this study has several limitations. While considering gross anatomy and well-established atrial electrophysiology and structure, heterogeneous fibrosis distribution and transmural uncoupling are relevant factors that were intentionally neglected in this study. Both these aspects are integral aspects of current hypotheses on AF mechanisms (Schotten et al., 2016) and can lead to spatially heterogeneous alterations of conductive and ionic properties. However, we chose to focus on studying the fundamental principles in a simple setting of homogeneous remodeling, first. Moreover, variability in the LA anatomy as well as the interplay between excitations in the left and right atrium are beyond the scope of this study. Moreover, the algorithm for phase analysis in (cf. section Rotor tracking from multi-electrode acquisitions) might decrease its accuracy in the case of fractionated electrograms, since sinusoidal recomposition is expected to result in a single phase inversion detection in correspondence of a local atrial activation characterized by two deflections or more. However, this evaluation falls out of the scope of this paper.

Despite these limitations, our work can be considered a promising starting point to build a clinically relevant computational framework to benchmark basket catheter guided ablation and allows, in its present form, to investigate and discuss basic relations.

CONCLUSION

We presented a simulation framework covering the whole cycle from excitation propagation to electrogram acquisition

and processing to virtual ablation. The application to basket catheter guided rotor ablation suggests that local ablation of rotor tips does not terminate reentry in homogeneously remodeled atria. While phase maps based on intracardiac catheter electrograms are a powerful tool to map atrial activation patterns, they can also mislead physicians due to inaccurate localization of the rotor tip depending on electrode resolution and distance to the wall. This might entail ablation in atrial regions that are in fact free of rotor sources of AF.

AUTHOR CONTRIBUTIONS

MA conception of the study, software development, simulations, analysis of the results, manuscript drafting, figure preparation, revision of manuscript. MV image acquisition and processing, software development, analysis of simulated EGMs, phase mapping, rotor detection. LU software development, simulation of basket catheter, revision of the manuscript. TO simulation of basket catheter, software development. OD supervision of the study. CC conception of the study, image processing, software development, analysis of the results, figure preparation, revision of manuscript. AL conception of the study, software development, simulations, analysis of the results, manuscript drafting, video preparation, revision of manuscript. SS conception of the study, software development, analysis of the

results, manuscript drafting, revision of manuscript, supervision of the study.

FUNDING

This project received funding from MIUR-DAAD Joint Mobility Program GA: 57268231 including funds from the German Ministry of Education and Research (BMBF). MA received funding from the European Union's Horizon 2020 research and innovation programme under the Marie Skłodowska-Curie grant agreement No 659082. We gratefully acknowledge financial support by the Deutsche Forschungsgemeinschaft (DFG) through CRC 1173 and DO 637/22-3 and Open Access Publishing Fund of Karlsruhe Institute of Technology.

ACKNOWLEDGMENTS

We thank Dr Roberto Mantovan and Dr Antonio Pasini of the Bufalini Hospital (Cesena, Italy) for support with clinical data acquisition.

SUPPLEMENTARY MATERIAL

The Supplementary Material for this article can be found online at: <https://www.frontiersin.org/articles/10.3389/fphys.2018.01251/full#supplementary-material>

REFERENCES

- Alessandrini, M., Valinoti, M., Loewe, A., Oesterlein, T., Dössel, O., Corsi, C., et al. (2017). "A computational framework to benchmark basket catheter guided ablation," in *Computing in Cardiology Conference* (Rennes).
- Bayer, J. D., Roney, C. H., Pashaei, A., Jaïs, P., and Vigmond, E. J. (2016). Novel radiofrequency ablation strategies for terminating atrial fibrillation in the left atrium: a simulation study. *Front. Physiol.* 7:108. doi: 10.3389/fphys.2016.00108
- Buch, E., Share, M., Tung, R., Benharash, P., Sharma, P., Koneru, J., et al. (2016). Long-term clinical outcomes of focal impulse and rotor modulation for treatment of atrial fibrillation: a multi-center experience. *Heart Rhythm* 13, 636–641. doi: 10.1016/j.hrthm.2015.10.031
- Cochet, H., Dubois, R., Yamashita, S., Al Jefairi, N., Berte, B., Sellal, J. M., et al. (2018). Relationship between fibrosis detected on late gadolinium-enhanced cardiac magnetic resonance and re-entrant activity assessed with electrocardiographic imaging in human persistent atrial fibrillation. *JACC: Clin. Electrophysiol.* 4, 17–29. doi: 10.1016/j.jacep.2017.07.019
- Courtemanche, M., Ramirez, R. J., and Nattel, S. (1998). Ionic mechanisms underlying human atrial action potential properties: insights from a mathematical model. *Am. J. Physiol.* 275, H301–H321. doi: 10.1152/ajpheart.1998.275.1.H301
- Dukkipati, S. R., and Reddy, V. Y. (2017). Catheter ablation of "Rotors" for the treatment of AF: should we drink the Kool-Aid? *J. Am. Coll. Cardiol.* 69, 1270–1274. doi: 10.1016/j.jacc.2017.01.026
- Gonzales, M. J., Vincent, K. P., Rappel, W. J., Narayan, S. M., and McCulloch, A. D. (2014). Structural contributions to fibrillatory rotors in a patient-derived computational model of the atria. *Europace* 16(Suppl. 4):iv3–iv10. doi: 10.1093/europace/euu251
- Haissaguerre, M., Shah, A. J., Cochet, H., Hocini, M., Dubois, R., Efimov, I., et al. (2016). Intermittent drivers anchoring to structural heterogeneities as a major pathophysiological mechanism of human persistent atrial fibrillation. *J. Physiol.* 594:2387–2398. doi: 10.1113/JP270617
- Hwang, M., Song, J.S., Lee, Y.S., Li, C., Shim, E. B., and Pak, H.N. (2016). Electrophysiological rotor ablation in in-silico modeling of atrial fibrillation: comparisons with dominant frequency, shannon entropy, and phase singularity. *PLoS ONE* 11:e0149695. doi: 10.1371/journal.pone.0149695
- Jacquemet, V. (2016). Lessons from computer simulations of ablation of atrial fibrillation. *J. Physiol.* 594, 2417–2430. doi: 10.1113/JP271660
- Krueger, M. W., Dorn, A., Keller, D. U., Holmqvist, F., Carlson, J., Platonov, P. G., et al. (2013a). In-silico modeling of atrial repolarization in normal and atrial fibrillation remodeled state. *Med. Biol. Eng. Comput.* 51, 1105–1119. doi: 10.1007/s11517-013-1090-1
- Krueger, M. W., Rhode, K. S., O'Neill, M. D., Rinaldi, C. A., Gill, J., Razavi, R., et al. (2014). Patient-specific modeling of atrial fibrosis increases the accuracy of sinus rhythm simulations and may explain maintenance of atrial fibrillation. *J. Electrocardiol.* 47, 324–328. doi: 10.1016/j.jelectrocard.2013.11.003
- Krueger, M. W., Seemann, G., Rhode, K., Keller, D. U. J., Schilling, C., Arujuna, A., et al. (2013b). Personalization of atrial anatomy and electrophysiology as a basis for clinical modeling of radio-frequency ablation of atrial fibrillation. *IEEE Trans. Med. Imaging* 32, 73–84. doi: 10.1109/TMI.2012.2201948
- Kuck, K.-H., Brugada, J., Fürnkranz, A., Metzner, A., Ouyang, F., Chun, K. R. J., et al. (2016). Cryoballoon or radiofrequency ablation for paroxysmal atrial fibrillation. *N. Engl. J. Med.* 374, 2235–2245. doi: 10.1056/NEJMoa1602014
- Kuklik, P., Scha, B., Sultan, A., Steven, D., Scriver, D., Moser, J. M., et al. (2016). Local electrical dyssynchrony during atrial fibrillation: theoretical considerations and initial catheter ablation results. *PLoS ONE* 6:e164236. doi: 10.1371/journal.pone.0164236
- Kuklik, P., Zeemering, S., Maesen, B., Maessen, J., Crijns, H.J., Verheule, S., et al. (2015). Reconstruction of instantaneous phase of unipolar atrial contact electrogram using a concept of sinusoidal recombination and Hilbert transform. *IEEE Trans. Biomed. Eng.* 62, 296–302. doi: 10.1109/TBME.2014.2350029
- Latanich, C., Voss, J., Alhaj, E., Henry, C. A., Hushion, M., Cytron, J. A., et al. (2018). Mechanisms of recurrent atrial arrhythmias following firm guided ablations. *Heart Rhythm* 15:S532. doi: 10.1016/j.hrthm.2018.03.028

- Lim, B., Hwang, M., Song, J.S., Ryu, A.J., Joung, B., Shim, E. B., et al. (2017). Effectiveness of atrial fibrillation rotor ablation is dependent on conduction velocity: an in-silico 3-dimensional modeling study. *PLoS ONE* 12:e0190398. doi: 10.1371/journal.pone.0190398
- Loewe, A., and Dössel, O. (2017). Commentary: virtual in-silico modeling guided catheter ablation predicts effective linear ablation lesion set for longstanding persistent atrial fibrillation: multicenter prospective randomized study. *Front. Physiol.* 8:1113. doi: 10.3389/fphys.2017.01113
- Loewe, A., Krueger, M. W., Holmqvist, F., Dössel O., Seemann, G., and Platonov, P. G. (2016). Influence of the earliest right atrial activation site and its proximity to interatrial connections on P-wave morphology. *Europace* 18(Suppl. 4):iv35–iv43. doi: 10.1093/europace/euw349
- Loewe, A., Krueger, M. W., Platonov, P. G., Holmqvist, F., Dössel, O., and Seemann, G. (2015). "Left and right atrial contribution to the P-wave in realistic computational models," in *Lecture Notes in Computer Science 9126 (Functional Imaging and Modeling of the Heart)*, eds H. van Assen, P. Bovendeerd, and T. Delhaas (Karlsruhe: KIT Scientific Publishing), 439–447. doi: 10.1007/978-3-319-20309-6_50
- Loewe, A., Wilhelms, M., Dössel, O., and Seemann, G. (2014). Influence of chronic atrial fibrillation induced remodeling in a computational electrophysiological model. *Biomed. Tech. Biomed. Eng.* 59, S929–S932. doi: 10.1515/bmt-2014-5012
- Martinez-Mateu, L., Romero, L., Ferrer-Albero, A., Sebastian, R., Rodriguez Matas, J. F., Jalife, J., et al. (2018). Factors affecting basket catheter detection of real and phantom rotors in the atria: a computational study. *PLoS Comput. Biol.* 14:e1006017. doi: 10.1371/journal.pcbi.1006017
- McDowell, K. S., Vadakkumpadan, F., Blake, R., Blauer, J., Plank, G., Macleod, R. S., et al. (2012). Methodology for patient-specific modeling of atrial fibrosis as a substrate for atrial fibrillation. *J. Electrocardiol.* 45, 640–645. doi: 10.1016/j.jelectrocard.2012.08.005
- McDowell, K. S., Zahid, S., Vadakkumpadan, F., Blauer, J., MacLeod, R. S., and Trayanova, N. A. (2015). Virtual electrophysiological study of atrial fibrillation in fibrotic remodeling. *PLoS ONE* 10:e0117110. doi: 10.1371/journal.pone.0117110
- Miller, J. M., Kalra, V., Das, M. K., Jain, R., Garlie, J. B., Brewster, J. A., et al. (2017). Clinical benefit of ablating localized sources for human atrial fibrillation: the Indiana University FIRM Registry. *J. Am. Coll. Cardiol.* 69, 1247–1256. doi: 10.1016/j.jacc.2016.11.079
- Mohanty, S., Mohanty, P., Trivedi, C., Gianni, C., Della Rocca, D. G., Di Biase, L., et al. (2018). Long-term outcome of pulmonary vein isolation with and without focal impulse and rotor modulation mapping: insights from a meta-analysis. *Circ. Arrhythm. Electrophysiol.* 11:e005789. doi: 10.1161/CIRCEP.117.005789
- Narayan, S. M., Baykaner, T., Clopton, P., Schricker, A., Lalani, G. G., Krummen, D. E., et al. (2014). Ablation of rotor and focal sources reduces late recurrence of atrial fibrillation compared with trigger ablation alone: extended follow-up of the CONFIRM trial (Conventional Ablation for Atrial Fibrillation With or Without Focal Impulse and Rotor Modulation). *J. Am. Coll. Cardiol.* 63, 1761–1768. doi: 10.1016/j.jacc.2014.02.543
- Niederer, S. A., Kerfoot, E., Benson, A. P., Bernabeu, M. O., Bernus, O., Bradley, C., et al. (2011). Verification of cardiac tissue electrophysiology simulators using an N-version benchmark. *Philos. Trans. A Math. Phys. Eng. Sci.* 369, 4331–4351. doi: 10.1098/rsta.2011.0139
- Oesterlein, T., Frisch, D., Loewe, A., Seemann, G., Schmitt, C., Dössel, O., et al. (2016). Basket-type catheters: diagnostic pitfalls caused by deformation and limited coverage. *Biomed. Res. Int.* 2016:5340574. doi: 10.1155/2016/5340574
- Platonov, P. G., Ivanov, V., Ho, S. Y., and Mitrofanova, L. (2008). Left atrial posterior wall thickness in patients with and without atrial fibrillation: data from 298 consecutive autopsies. *J. Cardiovasc. Electrophysiol.* 19, 689–692. doi: 10.1111/j.1540-8167.2008.01102.x
- Roney, C. H., Cantwell, C. D., Bayer, J. D., Qureshi, N. A., Lim, P. B., Tweedy, J. H., et al. (2017). Spatial resolution requirements for accurate identification of drivers of atrial fibrillation. *Circ. Arrhythm. Electrophysiol.* 10:e004899. doi: 10.1161/CIRCEP.116.004899
- Schnabel, R. B., Yin, X., Gona, P., Larson, M. G., Beiser, A. S., McManus, D. D., et al. (2015). 50 year trends in atrial fibrillation prevalence, incidence, risk factors, and mortality in the Framingham Heart Study: a cohort study. *Lancet* 386, 154–162. doi: 10.1016/S0140-6736(14)61774-8
- Schotten, U., Dobrev, D., Platonov, P. G., Kottkamp, H., and Hindricks, G. G. (2016). Current controversies in determining the main mechanisms of atrial fibrillation. *J. Intern. Med.* 279, 428–438. doi: 10.1111/joim.12492
- Seemann, G., Sachse, F. B., Karl, M., Weiss, D. L., Heuveline, V., and Dössel, O. (2010). Framework for modular, flexible and efficient solving the cardiac bidomain equation using PETSc. *Math. Ind.* 15, 363–369. doi: 10.1007/978-3-642-12110-4_55
- Trayanova, N. A., Boyle, P. M., and Nikolov, P. P. (2018). Personalized imaging and modeling strategies for arrhythmia prevention and therapy. *Curr. Opin. Biomed. Eng.* 5, 21–28. doi: 10.1016/j.cobme.2017.11.007
- Ugarte, J. P., Tobón, C., Orozco-Duque, A., Becerra, M. A., and Bustamante, J. (2015). Effect of the electrograms density in detecting and ablating the tip of the rotor during chronic atrial fibrillation: an in silico study. *Europace* 17(Suppl. 2), ii97–ii104. doi: 10.1093/europace/euv244
- Valinoti, M., Bertoni, F., Alessandrini, M., Mantovan, R., Loewe, A., Dössel, O., et al. (2017). "Phase analysis of endoatrial electrograms for 3D rotor detection in atrial fibrillation," in *Computing in Cardiology Conference* (Rennes).
- Valinoti, M., Fabbri, C., Turco, D., Mantovan, R., Pasini, A., and Corsi, C. (2018). 3D patient-specific models for left atrium characterization to support ablation in atrial fibrillation patients. *Magn. Reson. Imaging* 45, 51–57. doi: 10.1016/j.mri.2017.09.012
- Verma, A., Jiang, C.Y., Betts, T. R., Chen, J., Deisenhofer, I., Mantovan, R., et al. (2015). Approaches to catheter ablation for persistent atrial fibrillation. *N. Engl. J. Med.* 372, 1812–1822. doi: 10.1056/NEJMoa1408288
- Vigmond, E. J., Tsoi, V., Kuo, S., Arevalo, H., Kneller, J., Nattel, S., et al. (2004). The effect of vagally induced dispersion of action potential duration on atrial arrhythmogenesis. *Heart Rhythm* 1, 334–344. doi: 10.1016/j.hrthm.2004.03.077
- Wachter, A., Loewe, A., Krueger, M. W., Dössel, O., and Seemann, G. (2015). Mesh structure-independent modeling of patient-specific atrial fiber orientation. *Curr. Dir. Biomed. Eng.* 1, 409–412. doi: 10.1515/cdbme-2015-0099
- Zahid, S., Whyte, K. N., Schwarz, E. L., Blake, R. C., Boyle, P. M., Chrispin, J., et al. (2016). Feasibility of using patient-specific models and the 'minimum Cut' algorithm to predict optimal ablation targets for left atrial flutter. *Heart Rhythm* 13, 1687–98. doi: 10.1016/j.hrthm.2016.04.009
- Zhao, J., Hansen, B. J., Wang, Y., Csepe, T. A., Sul, L. V., Tang, A., et al. (2017). Three-dimensional integrated functional, structural, and computational mapping to define the structural "Fingerprints" of heart-specific atrial fibrillation drivers in human heart *ex vivo*. *J. Am. Heart Assoc.* 6:e005922. doi: 10.1161/JAHA.117.005922
- Zhao, J., Kharche, S. R., Hansen, B. J., Csepe, T. A., Wang, Y., Stiles, M. K., et al. (2015). Optimization of catheter ablation of atrial fibrillation: insights gained from clinically-derived computer models. *Int. J. Mol. Sci.* 16, 10834–10854. doi: 10.3390/ijms160510834

Conflict of Interest Statement: The authors declare that the research was conducted in the absence of any commercial or financial relationships that could be construed as a potential conflict of interest.

Copyright © 2018 Alessandrini, Valinoti, Unger, Oesterlein, Dössel, Corsi, Loewe and Severi. This is an open-access article distributed under the terms of the Creative Commons Attribution License (CC BY). The use, distribution or reproduction in other forums is permitted, provided the original author(s) and the copyright owner(s) are credited and that the original publication in this journal is cited, in accordance with accepted academic practice. No use, distribution or reproduction is permitted which does not comply with these terms.



Image-Based Computational Evaluation of the Effects of Atrial Wall Thickness and Fibrosis on Re-entrant Drivers for Atrial Fibrillation

Aditi Roy, Marta Varela and Oleg Aslanidi*

Department of Biomedical Engineering, School of Biomedical Engineering & Imaging Sciences, King's College London, King's Health Partners, St Thomas' Hospital, London, United Kingdom

OPEN ACCESS

Edited by:

Joseph L. Greenstein,
Johns Hopkins University,
United States

Reviewed by:

Arun V. Holden,
University of Leeds, United Kingdom

Olivier Bernus,

Université de Bordeaux, France

Patrick M. Boyle,

Johns Hopkins University,
United States

*Correspondence:

Oleg Aslanidi
oleg.aslanidi@kcl.ac.uk

Specialty section:

This article was submitted to
Computational Physiology
and Medicine,
a section of the journal
Frontiers in Physiology

Received: 22 April 2018

Accepted: 06 September 2018

Published: 04 October 2018

Citation:

Roy A, Varela M and Aslanidi O (2018) Image-Based Computational Evaluation of the Effects of Atrial Wall Thickness and Fibrosis on Re-entrant Drivers for Atrial Fibrillation. *Front. Physiol.* 9:1352.
doi: 10.3389/fphys.2018.01352

Introduction: Catheter ablation (CA) is a common treatment for atrial fibrillation (AF), but the knowledge of optimal ablation sites, and hence clinical outcomes, are suboptimal. Increasing evidence suggest that ablation strategies based on patient-specific substrates information, such as distributions of fibrosis and atrial wall thickness (AWT), may be used to improve therapy. We hypothesized that competing influences of large AWT gradients and fibrotic patches on conductive properties of atrial tissue can determine locations of re-entrant drivers (RDs) sustaining AF.

Methods: Two sets of models were used: (1) a simple model of 3D atrial tissue slab with a step change in AWT and a synthetic fibrosis patch, and (2) 3D models based on patient-specific right atrial (RA) and left atrial (LA) geometries. The latter were obtained from four healthy volunteers and two AF patients, respectively, using magnetic resonance imaging (MRI). A synthetic fibrotic patch was added in the RA and fibrosis distributions in the LA were obtained from gadolinium-enhanced MRI of the same patients. In all models, 3D geometry was combined with the Fenton-Karma atrial cell model to simulate RDs.

Results: In the slab, RDs drifted toward, and then along the AWT step. However, with additional fibrosis, the RDs were localized in regions between the step and fibrosis. In the RA, RDs drifted toward and anchored to a large AWT gradient between the crista terminalis (CT) region and the surrounding atrial wall. Without such a gradient, RDs drifted toward the superior vena cava (SVC) or the tricuspid valve (TSV). With additional fibrosis, RDs initiated away from the CT anchored to the fibrotic patch, whereas RDs initiated close to the CT region remained localized between the two structures. In the LA, AWT was more uniform and RDs drifted toward the pulmonary veins (PVs). However, with additional fibrotic patches, RDs either anchored to them or multiplied.

Conclusion: In the RA, RD locations are determined by both fibrosis and AWT gradients at the CT region. In the LA, they are determined by fibrosis due to the absence of large AWT gradients. These results elucidate mechanisms behind the stabilization of RDs sustaining AF and can help guide ablation therapy.

Keywords: atrial fibrillation, atrial wall thickness, fibrosis, modeling, MR imaging

INTRODUCTION

Atrial fibrillation (AF), the most common sustained cardiac arrhythmia, is characterized by rapid and irregular activations of the upper chambers of the heart (Nattel et al., 2008). AF is independently associated with a twofold increase in all-cause mortality and increased morbidity, particularly stroke, heart failure, and cognitive impairment (Kirchhof et al., 2016). AF affects about 33.5 million people worldwide, and a progressive increase in the prevalence and incidence of AF, accompanied by high morbidity and mortality, is predicted over the coming decades (Chugh et al., 2014).

Catheter ablation (CA) is a well-established strategy for the restoration of sinus rhythm in AF patients who do not respond well to anti-arrhythmic drugs, with success rates of up to 70% in patients with episodes of AF lasting less than 1 week (paroxysmal AF). It typically relies on the insertion of a catheter into the atria, where it delivers high amounts of localized energy for the destruction and isolation of arrhythmogenic substrates without affecting the surrounding areas (Nattel, 2002). The widely accepted CA strategy to restore sinus rhythm is the electrical isolation of pulmonary vein (PV) sleeves in the left atrium (LA), which are believed to be the primary substrate for the generation of the ectopic beats and/or anchoring of re-entrant drivers (RDs) responsible for triggering and sustaining AF in the LA (Gray et al., 1998; Oral et al., 2002; Sahadevan et al., 2004). However, approximately 30% of AF patients are asymptomatic, which leads to delayed diagnosis and the development of persistent AF. In these patients, the success rate with CA drops to 42% (Ganesan et al., 2013), often requiring additional ablation procedures. A potential factor for the failure of CA in these patients is the presence of high degrees of electrophysiological and structural remodeling, which alters the AF substrate, making it harder to predict the locations of AF drivers. Therefore, by changing the focus of ablation strategies from anatomic to patient-specific functional targets, the efficiency of CA could be greatly improved.

Recent advances in catheter and electro-anatomic mapping technologies have enabled the development of more patient-specific ablation strategies that complement standard approaches, such as PV isolation (PVI), in persistent AF. These can directly target: (i) AF sources (ectopic triggers or RDs) identified invasively using basket catheters (Narayan et al., 2014) or non-invasively using body surface electrodes (Haissaguerre et al., 2014) and (ii) regions where the atrial substrate is expected to be arrhythmogenic, such as low voltage areas (Kottkamp et al., 2016). The role of RDs as drivers for AF has been long recognized (Gray et al., 1998; Sahadevan et al., 2004). However, RD-guided ablation is limited by the challenges of mapping and visualizing electrical activity on the endocardial surface with sufficiently high resolution. This can explain contradictory outcomes of multi-centre trials, some of which have shown favorable outcomes of RD-guided ablation (Miller et al., 2017), while others have failed to find advantages in this approach compared to PVI (Mohanty et al.,

2018). However, with the advancement of novel imaging tools the paradigm is shifting toward non-invasive identification of patient-specific regions where the atrial substrate can be arrhythmogenic (Kottkamp et al., 2015; Cochet et al., 2018).

Atrial fibrosis is the most studied example of an arrhythmogenic substrate in AF patients and it has been reported to correlate with both AF incidence and post-ablation recurrence (McGann et al., 2014). Moreover, the level of fibrosis can be used for patient stratification, as CA procedures have a higher success rate in patients with less fibrotic burden (Mahnkopf et al., 2010). Recent clinical studies have reported that low-voltage areas on the endocardial surface represent abnormal atrial substrate caused by fibrosis and can be directly targeted by ablation (Blandino et al., 2017). While mapping RDs or low-voltage areas is invasive and time-consuming, fibrosis can be imaged noninvasively using late gadolinium enhancement (LGE) MRI (Siebermair et al., 2017). Modeling studies based on patient-specific LGE MRI reconstructions of fibrosis have suggested that slow conducting border zones around fibrosis (Morgan et al., 2016) are common anchoring sites for RDs. Moreover, Zahid et al. (2016) showed that RDs anchor at the border zone locations with specific spatial patterns of fibrosis. This suggests that the dynamics of RDs may depend on patient-specific fibrosis distribution.

In order to predict optimal target locations for ablation, a better understanding of the mechanistic influence of fibrosis on AF should be considered in combination with other structural factors, which have been shown to also influence the dynamics of RDs. Theoretical studies have highlighted the role of fiber orientation (Varela et al., 2016), surface curvature (Dierckx et al., 2013), and tissue thickness gradients (Biktasheva et al., 2015) on the dynamics of RDs. The prediction that RDs can drift and stabilize at borders between thin and thick tissue is arguably best supported by experimental evidence. Optical recordings in the sheep right atrium (RA) have shown that RDs tend to localize in bordering regions between thin and thick pectinate muscles (Yamazaki et al., 2012). Moreover, association of complex fractionated electrograms with atrial wall thickness (AWT) of the LA has also been reported (Park et al., 2014), pointing to the presence of AF substrate in these regions.

These findings show a potential of AWT gradients as a marker for identifying RD locations in the atria. However, neither the influence of AWT gradients on the RD dynamics in realistic atrial geometries nor comparative effects of AWT gradients and fibrotic patches on RDs have been investigated. Reconstruction of the atrial wall from imaging (Varela et al., 2017b) provides basis for computational modeling of the RD dynamics in patient-specific atrial geometries, to understand the role of AWT gradients in influencing RD locations. Elucidating the relationships between AWT gradients, fibrosis, and RD locations can lead to an improved understanding of AF mechanisms, and ultimately help identify patient-specific ablation targets, improving the efficacy of treatment.

This study aims to investigate the mechanistic influence of two structural factors: (i) AWT and (ii) fibrosis on the dynamics of RDs sustaining AF. To this end, computational simulations of atrial electrophysiology will be performed on (1) an idealized 3D atrial slab with a sharp change in thickness and (2) realistic RA and LA geometries obtained from MRI of six patients. Our working hypothesis is that competing influences of AWT gradients and fibrotic patches on conductive properties of atrial tissue determine anchoring locations of RDs in 3D atrial models.

MATERIALS AND METHODS

The study consists of three parts summarized in **Table 1**. In Study 1, we perform simulations in an idealized 3D atrial slab with a varying thickness step to evaluate the mechanistic influence of AWT on the RDs dynamics (Study 1a). A single cylindrical fibrotic patch was subsequently included in the slab to investigate the competing effects of fibrosis and AWT (Study 1b). In Studies 2 and 3, we extend these simulations to realistic models of atrial

geometries derived from MRI data, which were created using the general workflow shown in **Figure 1**. We first investigate the role of AWT and morphology of the RA (Study 2) and LA (Study 3) on the RD dynamics. The effect of a single cylindrical fibrotic patch on the RD dynamics in the RA is also investigated (Study 2b). Finally, we incorporate atrial fibrosis from patient-specific LGE MRI into our LA models to evaluate its influence on RDs relative to the effects of AWT and atrial geometry (Study 3b).

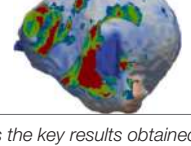
Modeling Atrial Electrophysiology

All simulations were performed by solving the standard monodomain equation:

$$\frac{\partial V}{\partial t} = \nabla \cdot (D \nabla V) - \frac{I_{\text{ion}}}{C_m}$$

Here, ∇ is the vector differential operator, V (mV) is the membrane potential and t is time (ms). D is the tensor with diffusion coefficients ($\text{mm}^2 \text{ ms}^{-1}$) that characterizes the spread of voltage within the tissue, C_m (pF) is the membrane capacitance, and I_{ion} is the total membrane ionic current

TABLE 1 | Effects of AWT and fibrosis of the RD dynamics.

	Geometry	Thickness	Fibrosis	RD outcome
Study 1: 3D atrial slab	a) 	✓ Height of the step	✗ None	<ul style="list-style-type: none"> • RDs drift and anchor to the step. • The sensitivity of the RD to the step increased with increase in the step height.
	b) 	✓ Height of the step	✓ Cylindrical fibrotic patch	<ul style="list-style-type: none"> • RDs anchor between the step and fibrotic patch. • The relative locations of the step and the fibrotic patch together influence the dynamics of the RDs.
Study 2: right atrium (RA)	a) 	✓ AWT for the RA geometry	✗ None	<ul style="list-style-type: none"> • RDs anchor to the CT region only in RA with large thickness gradient at the CT.
	b) 	✓ AWT for the RA geometry	✓ Spherical fibrotic patch	<ul style="list-style-type: none"> • RDs stabilize either at the CT region or the fibrotic patch, or the region between them, depending on their initial distance from these features.
Study 3: left atrium (LA)	a) 	✓ AWT for the LA geometry	✗ None	<ul style="list-style-type: none"> • RDs stabilize either near the PVs or the mitral valve. No effect of thickness noticed, since AWT is near-uniform.
	b) 	✓ AWT for the LA geometry	✓ Fibrosis from LGE-MRI	<ul style="list-style-type: none"> • RDs either anchor to or multiply into multiple RDs at the fibrotic patches.

The table summarizes the key results obtained from the current study aimed at investigating the competing influence of AWT and fibrosis on RDs sustaining AF.

(pA). Our model was isotropic and the diffusion tensor was replaced by a scalar diffusion coefficient $D = 0.1 \text{ mm}^2 \text{ ms}^{-1}$, carefully chosen to match an atrial conduction velocity (CV) of 0.60 m s^{-1} typical of AF (Zheng et al., 2017). For I_{ion} , we used the Fenton-Karma electrophysiology model (Fenton et al., 2008) modified to accurately described the restitution properties of remodeled atrial cells (Goodman et al., 2005). This atrial Fenton-Karma (aFK) cell model accurately captures the main characteristics of atrial action potentials and its restitution properties, while keeping the computational time relatively short. Equation (1) with no-flux boundary conditions was solved using forward Euler and centered finite differences schemes with temporal and spatial steps of 0.005 ms and 0.3 mm , respectively. In order to check independence of the simulation results on the choice of model, a subset of the simulations in Study 1 was repeated using the Courtemanche-Ramirez-Nattel (CRN) model (Courtemanche et al., 1998), which describes atrial myocyte in more detail. The latter has also been modified to match the restitution properties of remodeled atrial cells (Colman et al., 2013). The diffusion coefficient for the CRN model was chosen as $0.16 \text{ mm}^2 \text{ ms}^{-1}$ to produce the atrial CV of 0.60 m s^{-1} , same as that simulated with the FK model. The spatial step of 0.3 mm and temporal step of 0.005 ms were used for modified CRN model, for which numerical stability has been shown previously (Aslanidi et al., 2011).

Note that finite elements methods may have an advantage in terms of implementing zero-flux boundary conditions. However, benchmarks of cardiac electrophysiology models show that finite difference and finite elements solver have similar accuracy and convergence for spatial integration steps below 0.5 mm (Niederer et al., 2011). Moreover, both methods have been equally used for modeling of 3D atrial electrophysiology (Aslanidi et al.,

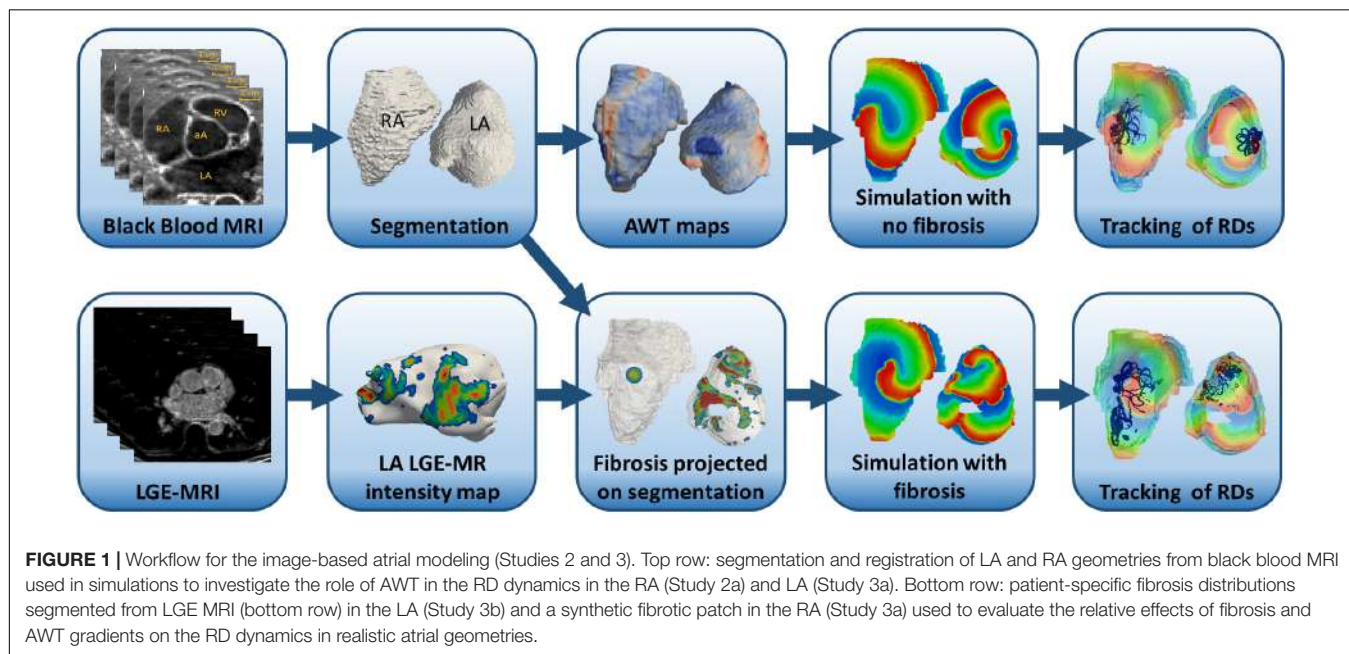
2011; Zhao et al., 2017; vs. Roney et al., 2016; Zahid et al., 2016).

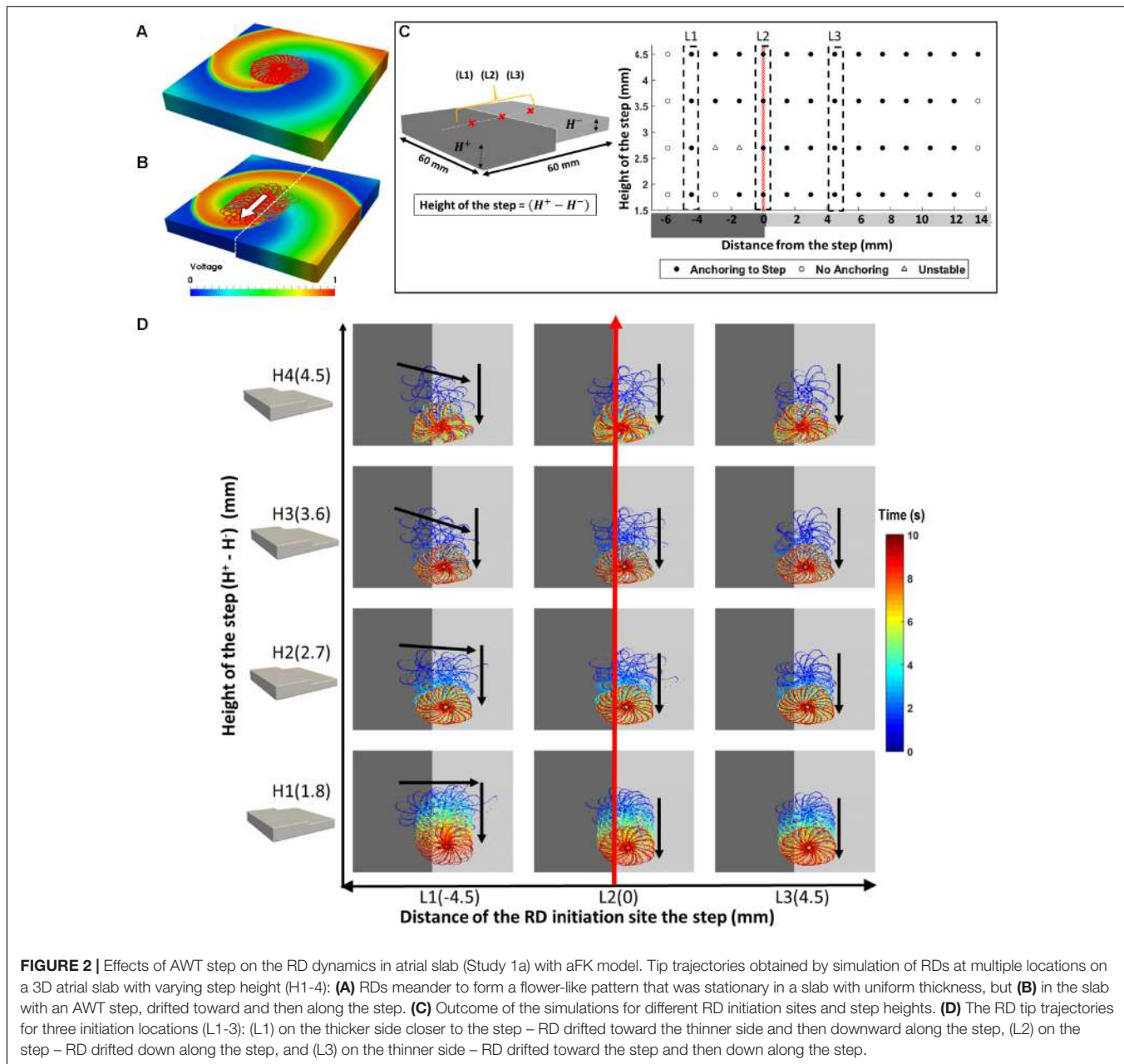
To model patchy fibrosis, we adopted the methodology from the study of Morgan et al. (2016). Each fibrotic patch was divided into five distinct levels representing increasingly severe fibrosis. The method for segmenting the fibrotic patches into these distinct levels for all the studies are described in their respective sections below. The diffusion coefficient D was progressively decreased by 16.67% to model the effect of fibrosis on slowing atrial conduction in fibrotic regions: level 0 corresponded to healthy tissue and $D = 0.1 \text{ mm}^2 \text{ ms}^{-1}$; inside the fibrosis patch, the value of D for levels 1-5 was $0.083, 0.067, 0.050, 0.033$, and $0.017 \text{ mm}^2 \text{ ms}^{-1}$, respectively. We did not use the value $D = 0$ for level 5, because there is no experimental evidence suggesting that dense fibrotic regions are completely non-conductive.

Study 1: 3D Atrial Tissue Slab

Simulations were conducted on a 3D atrial slab of $200 \times 200 \times 25$ voxels corresponding to tissue size of $60 \text{ mm} \times 60 \text{ mm} \times 7.5 \text{ mm}$ with a surface area of 3600 mm^2 , similar to that of the LA (Varela et al., 2017a). High frequency sources of electrical activity have been observed in clinical studies in AF patients (Haïssaguerre et al., 1998; Sanders et al., 2005) with frequencies in a broad range from 5.5 to 10.5 Hz (corresponding cycle lengths, CL from 95-180 ms). The frequency of RDs in our simulations varied between 6 and 10 Hz, which agrees with the clinical observations. Given CV of 0.6 m/s , these CL values correspond to the wavelengths estimate ($WL = CV \times CL$) between 57 and 108 mm. Therefore, the RD wavelength was comparable with linear dimensions of the slab and the LA.

A thickness step was introduced at the middle of the slab, with thickness of the right-hand side fixed at 7.5 mm and that of the left-hand side was varied between 5.7 and 3 mm (Figure 2, H1-4). In Study 1a, we investigated the mechanistic influence of

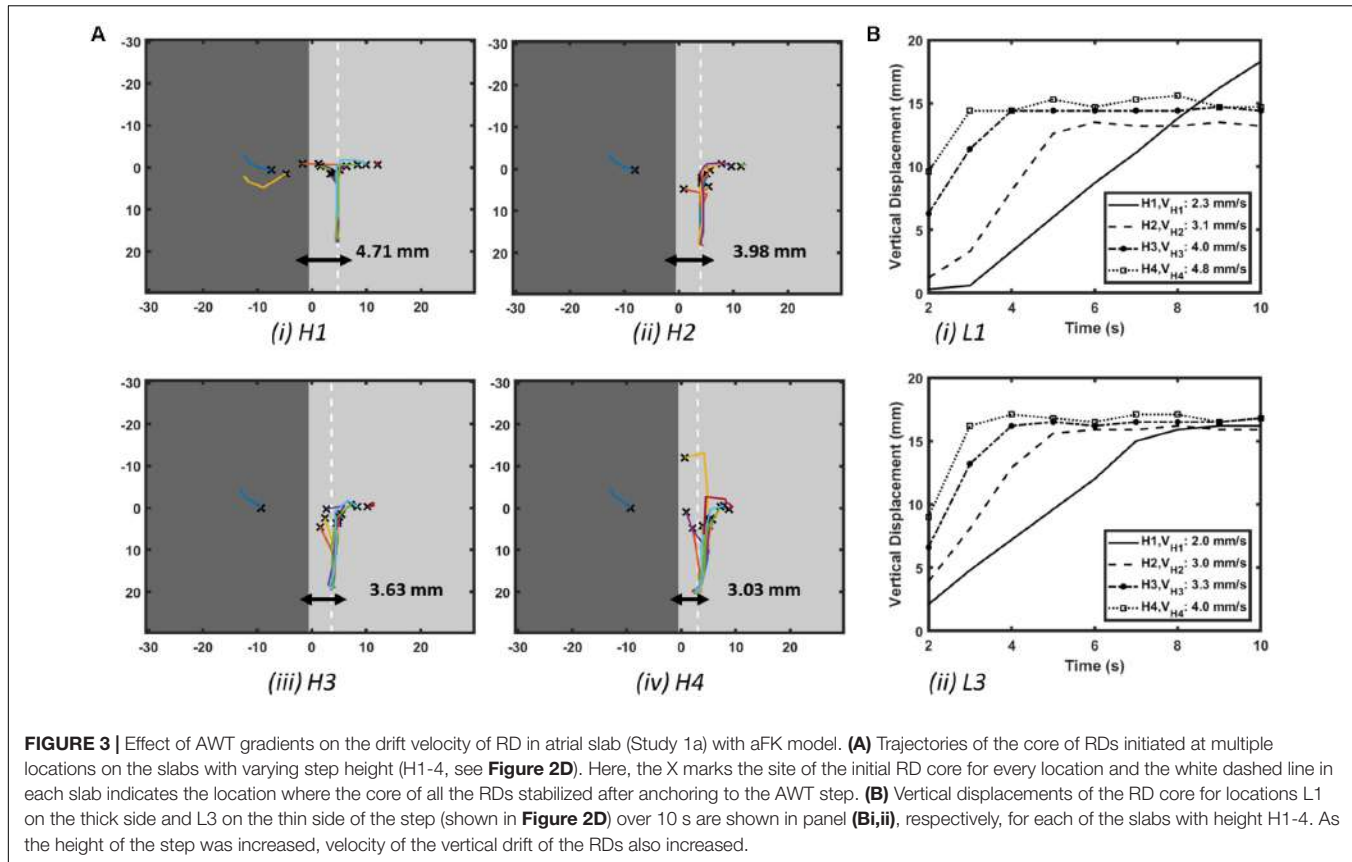




thickness gradients on the RD dynamics (Figures 2, 3). RDs were initiated using a cross-field protocol, where S2 pulse was applied at multiple distances from the AWT step, starting from 6 mm on the thick side to 13.5 mm on the thin side, and moving with a step of 1.5 mm (detailed information provided in the **Supplementary Material**). The trajectory of the RDs tip was tracked for 10 s in each simulation. Study 1a was also repeated using the CRN model to check the independence of results on the model choice (Supplementary Figure S2).

In Study 1b, the comparative effect of AWT and fibrosis on the RD dynamics were also investigated by incorporating a cylindrical fibrotic patch of 9-mm diameter positioned 10.5 mm away from the AWT step on the thinner side (Figure 4). This was

done for slab H2 with the step height of 2.7 mm. The rationale of placing the fibrotic region on the thinner side of the step was to mimic conditions when fibrotic tissue could be present in regions surrounding thick structures such as the crista terminalis (CT) in the RA. The cylindrical patch was divided into five concentric regions of gradually decreasing diameter representing increasingly dense fibrosis. RDs were initiated at multiple sites using the cross-field protocol, with varying relative distance from the step and the fibrotic patch: (i) 4.5 mm away from the step on the thick side (Figure 4D, column P), (ii) on the step (Figure 4D, column Q), (iii) 7.5 mm (Figure 4D, column R), and (iv) 15 mm (Figure 4D, column S) away from the step on the thin side. The RD tip trajectories were analyzed to explore their dynamics in



each case. The choice of 4.5 mm as the extreme limit of the RD initiation distance to the left of the patch was to ensure that the RDs were sensitive only to the AWT gradient and not the fibrotic patch. Likewise, the choice of 15 mm as the extreme limit on the right side was to ensure the sensitivity of RDs only to the fibrotic patch.

Studies 2 and 3: Right and Left Atria

Atrial geometries and fibrosis distributions were extracted from MRI to create 3D human atrial models, as described in previous studies (Varela et al., 2017b) and shown in the diagram in Figure 1.

Reconstruction of Atrial Geometries and AWT

Four healthy volunteers and two paroxysmal AF patients have been imaged (Varela et al., 2017b). Briefly, a black-blood MRI protocol (1.5 T, cardiac and respiratory gating, acquisition resolution: $1.4 \text{ mm} \times 1.4 \text{ mm} \times 1.4 \text{ mm}$) has been used to obtain patient-specific AWT maps non-invasively. Further details can be found in the previous publication (Varela et al., 2017b). The right (RA) and left atrial (LA) geometries of healthy volunteers and patients, respectively, were obtained by manual segmentation using ITK-SNAP (Kitware). A previously published method (Varela et al., 2017b) was used to generate patient-specific AWT maps, on which the computed RD tip trajectories were subsequently overlaid. In the RA, the region with the highest AWT ($5.10 \pm 1.00 \text{ mm}$ against $1.8 \pm 0.4 \text{ mm}$ in

the surrounding RA wall) can be identified as the CT (Sánchez-Quintana et al., 2002). We refer to this region as the CT in the following text. In some patients, this region was characterized by a large AWT gradient ($4.75 \pm 0.95 \text{ mm}$ in the CT region against $2.91 \pm 0.60 \text{ mm}$ in the RA wall), whereas in other patients, the region was less prominent ($2.90 \pm 1.04 \text{ mm}$ against $2.45 \pm 0.54 \text{ mm}$ in the RA wall).

Patient-Specific Fibrosis in the LA

The two paroxysmal AF patients have also undergone LGE MRI in the same scanning session and in the same phase of the cardiac cycle as the black-blood MRI acquisition, to detect fibrosis in the LA (1.5 T, cardiac and respiratory gating, acquisition resolution: $1.3 \text{ mm} \times 1.3 \text{ mm} \times 2 \text{ mm}$).

For Study 3b, the segmentation of fibrotic LA tissue was performed by analyzing the image intensity ratio (IIR), computed by dividing individual voxel intensities by the mean blood pool intensity. IIR values >1.08 were classified as interstitial fibrosis and >1.32 as dense fibrosis. The IIR threshold of 1.08 was obtained as an average of the previously proposed values of 1.2 (Benito et al., 2017) and 0.97 (Khurram et al., 2014). Transition from diffuse to dense fibrosis was represented by labelling segmented fibrotic tissue from 1 to 5 according to LGE-MRI intensity, where level 5 corresponded to dense fibrosis (regions with $\text{IIR} > 1.32$) and levels 1-4 corresponded to variable degree of diffuse fibrosis (regions with $1.08 < \text{IIR} < 1.32$ split into four equal intervals). These fibrotic regions were then nonlinearly

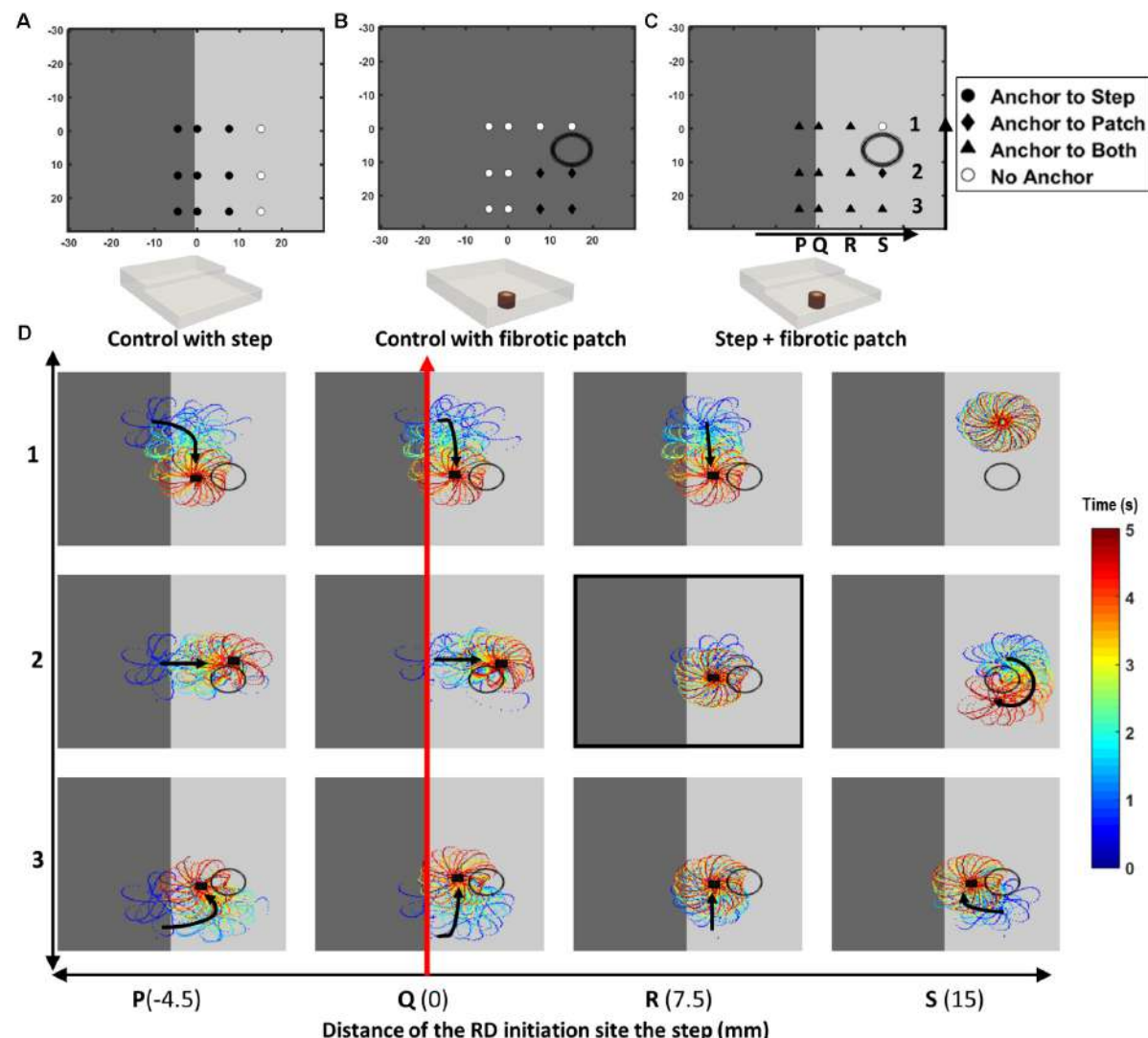


FIGURE 4 | Competing effects of AWT and fibrosis in the 3D atrial slab (Study 1b). Outcomes of the RD simulations performed for 12 initiation locations (P1 to S3) with: **(A)** a step change in AWT, **(B)** a cylindrical fibrotic patch (shown with a black circle), and **(C)** both AWT step and fibrosis. In cases **(A,B)**, RDs anchored to the step (for locations marked with filled black circle) and fibrotic patch (for locations marked with black diamond), respectively. White circles mark locations where the RDs did not anchor to either. In case **(C)**, majority of the RDs anchored between the AWT step and fibrotic patch (for locations marked with black triangle). These RD tip trajectories on the top surface of the 3D slab are shown for the 12 locations (P1 to S3) in the panel **(D)**. Black arrows indicates the direction of RD core drift, and black squares marks locations where they became stationary and anchored.

registered using MIRTK (Rueckert, 1999) and projected onto the LA geometries with transmural uniformity for the same patients using Paraview (Kitware) and Matlab (Mathworks, Inc.).

Synthetic Fibrosis in the RA

In the RA, due to lack of patient-specific fibrosis data, we added a synthetic 3D spherical fibrotic patch of diameter 9 mm, with similar labels 1-5 as done before for the 3D slab, in a region near the thick RA muscle bundle of the CT. This enabled a direct comparison of the effect of AWT and fibrosis on the RD dynamics in the RA (Study 2b). The choice of 9 mm diameter was based on calculating an average fibrotic patch size in the LA (Study 3).

Simulation Protocol for RD Initiation

A single RD was initiated using a cross-field protocol at different locations within the atrial geometries. In the RA, RDs were initiated in the vicinity of the CT region at six to nine different locations, where a large AWT gradient was typically observed. In the LA, four initiation locations were selected across the atrial wall. Simulations were performed in both geometries with and without fibrosis for a duration of at least 3 s. For each simulation, movement of the RD was tracked by recording location of its tip (organizing center around which a RD rotates) for each time step over duration of the entire simulation (Fenton et al., 2008). The resultant RD trajectories were then overlaid separately on

the AWT and fibrosis maps for each patient-specific atrial geometry.

RESULTS

Study 1: 3D Atrial Slab

The RDs initiated in the 3D atrial tissue slab meandered to form a characteristic hypotrochoidal (“flower-like”) pattern, with the RD tip moving along the “petals” in the outward clockwise direction around a central core. In a slab with uniform thickness, the flower pattern was stable, its radius was 10.4 mm, and the RD tip motion to complete the whole pattern took 500 ms (Figure 2A). However, with the introduction of a step change in AWT (Figure 2B), in addition to meandering around the core, the RD also drifted in a direction perpendicular to the direction of AWT change. The direction of RD drift also depended on its initiation location in the slab. The RD tip trajectories for multiple initiation locations are shown in the Supplementary Figure S1 (H1-4), and the drift directions are summarized in Figures 2C,D.

The core of RDs initiated on the thicker side (L1) first drift toward the AWT step, eventually crossing it and drifting along it on the thinner side. The core of RDs initiated on the thinner side (L2-3), otherwise, drifted toward the step and along it, but did not cross over to the thicker side. Besides, RDs that were initiated far away from the step (Supplementary Figure S1) were not influenced by the AWT gradient and remained stationary. For the default aFK model settings, RDs anchored to the AWT gradient in the range from 1.8 to 4.5 mm (H1-4), when they were initiated less than 4.5 mm from the step on the thick side, or less than 12 mm (H1-3)/15 mm (H4) on the thin side. Moreover, after an RD anchored to the step, its core moved vertically along the step at a specific distance from it. The core always drifted on the thinner side, and its distance from the step decreased with increasing the step height (Figure 3Ai-iv).

Simulations of the 3D slab with the CRN atrial cell model demonstrated similar behavior of the RDs (Supplementary Figure S2). The RD tip in the CRN-based model also meandered to form a flower-like pattern with radius of 12 mm and one complete rotation around the pattern taking about 700 ms. Similar to the aFK-based model, anchoring of the RDs to the AWT step was observed, indicating that the anchoring phenomena was model independent.

The RD drift along the AWT step became faster as the height of the step (H1-4) was increased. The drift velocity (DV) was computed by measuring the vertical displacement of the RD core over time, which was done for each step height (H1-4) as shown in Figure 3B. DV was 2.3 mm/s for H1 and 4.8 mm/s for a larger step H4, both measured for the initial location L1 on the thick side. Similarly, for the initial location L3 on the thin side, DV was 2 mm/s for H1 and 4 mm/s for H4. Therefore, DV of the RD core increased with increasing the AWT gradient. Note that the direction in which the RD meanders to form the petals (clockwise in these simulations), and hence the direction of drift along the step (downward here) is determined by the cross-field initiation protocol. However, the anchoring of the RD to the thickness step does not depend on the wave’s chirality.

Results of the simulations comparing the effects of AWT and fibrosis in the 3D slab are shown in Figure 4 for 12 different locations of the RD initiation, with the AWT step height (H2, 2.7 mm) and location of the synthetic fibrotic patch kept constant. In control cases of the AWT step only and the fibrotic patch only (Figures 4A,B, respectively), the RDs either drifted toward and anchored to the step (9 out of 12 locations) or anchored to the fibrotic patch and drifted in a clockwise direction around it (4 out of 12 locations). However, in the presence of both (Figure 4C), the majority of the RDs stabilized and anchored between the patch and the AWT step (8 out of 12 locations). Analyzing the RD trajectories in the latter case (Figure 4D), we found that RDs initiated on the thicker side, which were insensitive to the fibrotic patch alone, now drifted toward the patch located in the thinner region due to the influence of the AWT gradient. Once the RDs reached the region between the AWT step and the fibrotic patch, they could either drift downward along the step or drift rightward and rotate clockwise around the patch. Opposing influences from the AWT step and the fibrotic patch in this case can cancel each other out, with the RD becoming stationary and anchoring between the two structures.

For location R2 on the thinner side (highlighted in Figure 4D), increasing the step height from H2 to H4 caused the RDs to anchor to the step (Supplementary Figure S3D). However, increasing the distance between the step and the RD initiation site (from 7.5 to 15 mm), while preserving the distance between the initiation site and the patch, resulted in the RD anchoring to the patch (Supplementary Figure S3E).

Study 2: Right Atrial Geometry

The average AWT values computed in the CT region and the surrounding RA wall of Persons 1 (Figure 5A; CT: 3.45 ± 0.86 mm; RA: 2.09 ± 0.38 mm) and 2 (Figure 5B; CT: 4.75 ± 0.95 mm; RA: 2.91 ± 0.60 mm) showed a higher gradient in AWT compared to Persons 3 (Figure 5C; CT: 3.04 ± 0.65 mm; RA: 3.00 ± 0.54 mm) and 4 (Figure 5D; CT: 2.90 ± 1.04 mm; RA: 2.45 ± 0.54 mm). Hence, Persons 1 and 2 had a more prominent CT region compared to Persons 3 and 4.

In these patients, 55% of the RDs initiated at different locations drifted toward the CT region, either anchoring to it (Figures 5Ai, 5Bi) or crossing over it to the posterior side of the RA (Figures 5Aii, 5Bii). As an example, the 3D atrial voltage map in Person 1 is shown in Supplementary Figure S3. However, in the RA of Persons 3 and 4 (Figures 5C,D), the CT regions had thickness comparable to the remaining RA wall. Hence, the RDs neither drifted toward the CT, nor anchored at any location (Figures 5Ci,Di). Instead, they either drifted toward the superior vena cava (SVC) or the tricuspid valve (TSV) or terminated.

When the RA simulations were repeated in the presence of a synthetic fibrotic patch, the RD trajectories were affected in all patients, as shown in Figures 6, 7. For the RAs with a prominent CT region (Figure 6A), RDs initiated closer to the fibrotic patch either stabilized between the CT region and the patch (Figure 6Bii), or anchored to the latter (Figure 6Cii), depending on the distance from their initiation site to either structure. The critical proximity to the CT region and the patch

is challenging to determine in realistic RA geometry because, unlike AWT in a rectangular slab, the CT region is not a simple straight line. However, in an example provided for Person 1 (**Figure 7**), RDs initiated at the middle between edges of the CT region and the fibrotic patch (~3 mm from either structure horizontally and 6.6 mm vertically) (**Figure 7**, location A1), stabilized and anchored between them. Increasing the horizontal distance between the RD and the CT to 13 mm (**Figure 7**, location B1) led to the RD anchoring to the fibrotic patch. However, in the RAs with no distinguishable thickness gradient at the CT region (**Figure 6D**), all RDs anchored to the fibrotic patch (**Figures 6Eii,Fii**).

Study 3: Left Atrial Geometry

The AWT maps computed for LA geometry of Person 5 (**Figure 8A**) showed higher AWT in the LA roof (4.77 ± 0.60 mm) compared to the rest of the atrial wall (2.96 ± 0.31 mm). Therefore, in the respective simulations RDs drifted toward and along the LA roof (**Figure 8Ci**) when initiated in its proximity, but drifted toward the PVs (**Figure 8Bi**) if initiated further away. The LA of Person 6 (**Figure 8D**) was characterized by roughly uniform AWT (2.53 ± 1.20 mm), and RDs initiated in this geometry drifted either toward the PVs (**Figure 8Ei**) or the mitral valve (**Figure 8Fii**).

In the LA, LGE MRI intensity-based segmentations yielded different fibrosis distributions in the two AF patients, as shown in **Figures 8A,D**. Both Persons 5 and 6 had fibrotic

tissue in the LA regions surrounding the PVs, with a higher degree of fibrosis in one patient (14% of the atrial volume, **Figure 8A**) compared to the other (10%, **Figure 8D**). In Person 5, LA simulations repeated with the presence of fibrosis showed either stable RD anchoring to the border zones of fibrotic tissue (**Figure 8Cii**) or transient anchoring where RDs stabilized at a fibrotic patch in the first 1 s of simulation and then drifted to a new location in another fibrotic region and stabilized there (**Figure 8Bii**). 3D atrial voltage maps for the cases shown in **Figure 8Ci,ii** are illustrated in **Figures 9A,B**, respectively. In one particular case, we also observed the breakdown of the primary RD into multiple wavelets meandering between fibrotic patches (**Supplementary Figure S5B**). However, in Person 6, simulations repeated with the presence of fibrosis in the LA showed either stable RDs forming *macroscopic re-entry* around the PVs (**Figure 8Eii**) or RDs anchored to a fibrotic region (**Figure 8Fii**) near the PV.

DISCUSSION

The computational study performed on the 3D atrial tissue slabs and MRI-based realistic 3D atrial geometries enabled us to successfully evaluate the mechanistic influence of AWT and fibrosis distribution on the drift and anchoring of the RDs sustaining AF. In the 3D slabs, the AWT gradients acted as anchoring points for RDs in the absence of

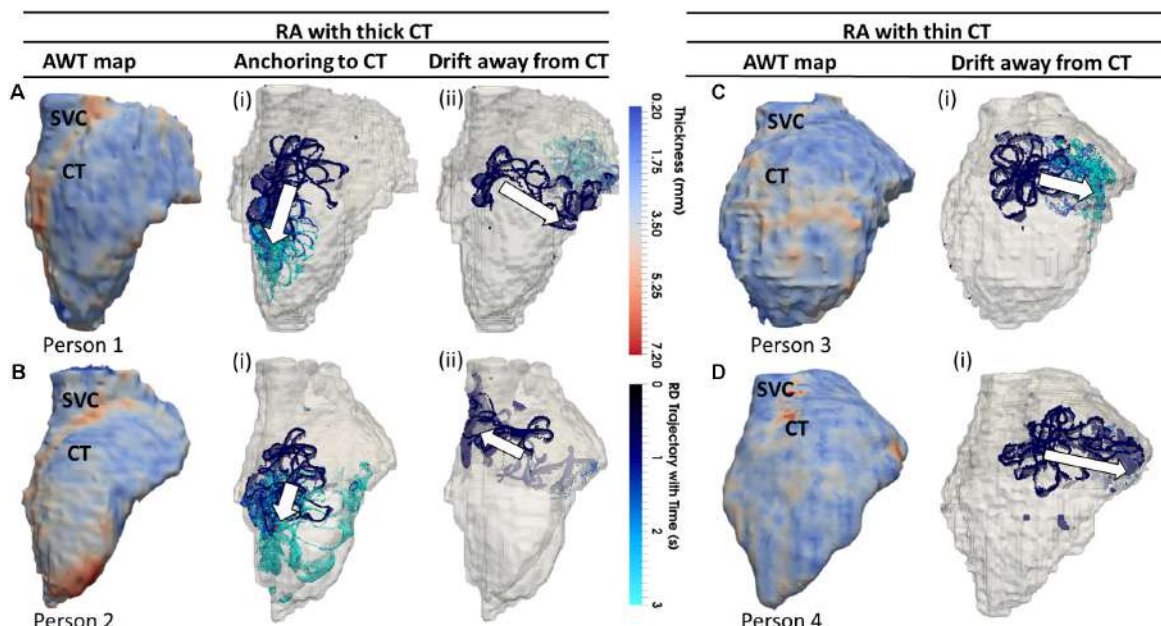


FIGURE 5 | Effects of AWT on the RD dynamics on the RA. Trajectories of RDs (blue), initiated at four to nine locations in the RA, are overlaid on the AWT map for four different subjects. In Persons 1 (**A**) and 2 (**B**), the CT region had a higher AWT compared to rest of the RA wall, while in Persons 3 (**C**) and 4 (**D**), the CT region was not distinguishable by thickness. The majority of RDs initiated in Person 1 (six out of nine sites) and Person 2 (four out of nine sites) drifted toward the thick CT region and anchored to it (**Aii,Bii**), but some also drifted toward the opposite side of the RA geometry (**Aii,Bii**). However, none on four RDs initiated in Person 3 and Person 4 anchored to the CT region, drifting away toward the SVC or TCV instead (**Ci,Di**). Here and below, white arrows indicate the direction of RD drift after initiation. More detailed illustration of RDs initiated at nine different locations in panel (**A**) is presented in **Supplementary Figure S4**.

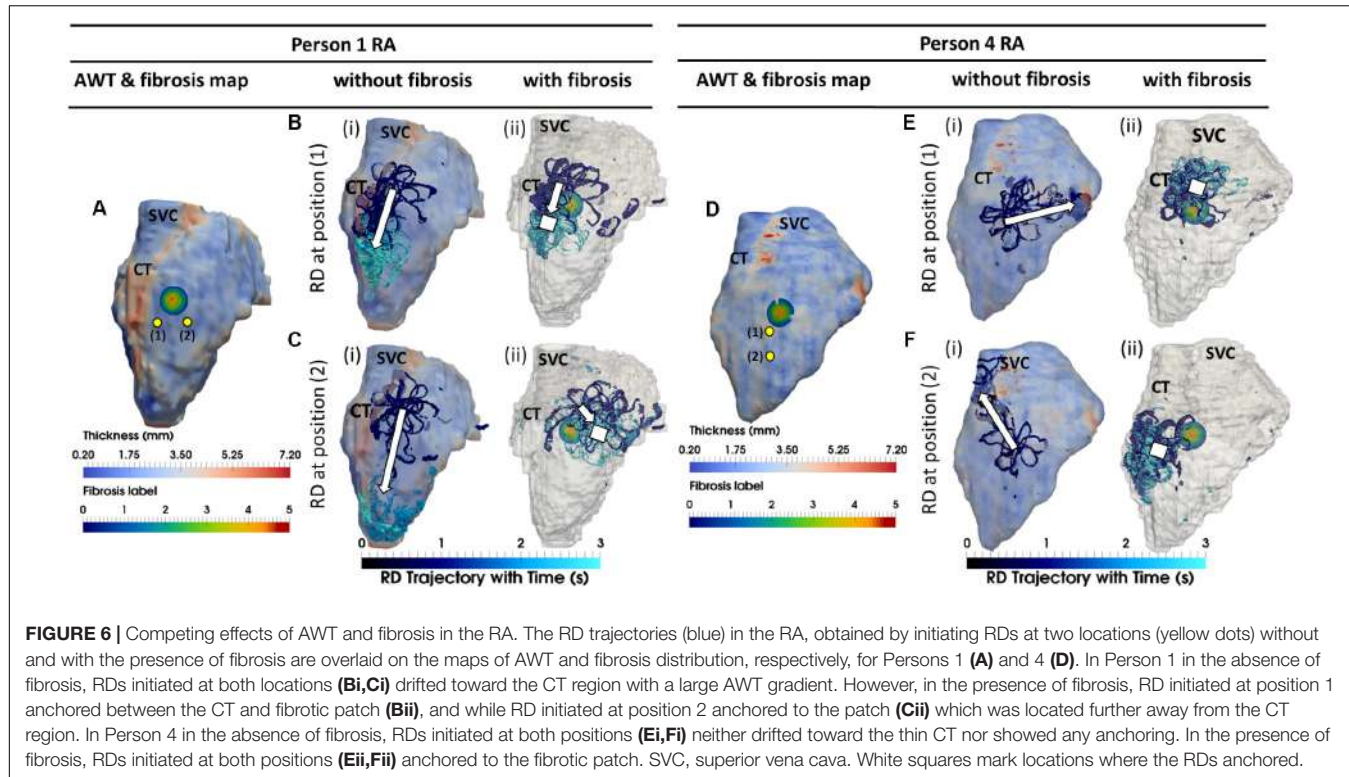


FIGURE 6 | Competing effects of AWT and fibrosis in the RA. The RD trajectories (blue) in the RA, obtained by initiating RDs at two locations (yellow dots) without and with the presence of fibrosis are overlaid on the maps of AWT and fibrosis distribution, respectively, for Persons 1 (A) and 4 (D). In Person 1 in the absence of fibrosis, RDs initiated at both locations (B*i*,C*i*) drifted toward the CT region with a large AWT gradient. However, in the presence of fibrosis, RD initiated at position 1 anchored between the CT and fibrotic patch (B*ii*), and while RD initiated at position 2 anchored to the patch (C*ii*) which was located further away from the CT region. In Person 4 in the absence of fibrosis, RDs initiated at both positions (E*i*,F*i*) neither drifted toward the thin CT nor showed any anchoring. In the presence of fibrosis, RDs initiated at both positions (E*ii*,F*ii*) anchored to the fibrotic patch. SVC, superior vena cava. White squares mark locations where the RDs anchored.

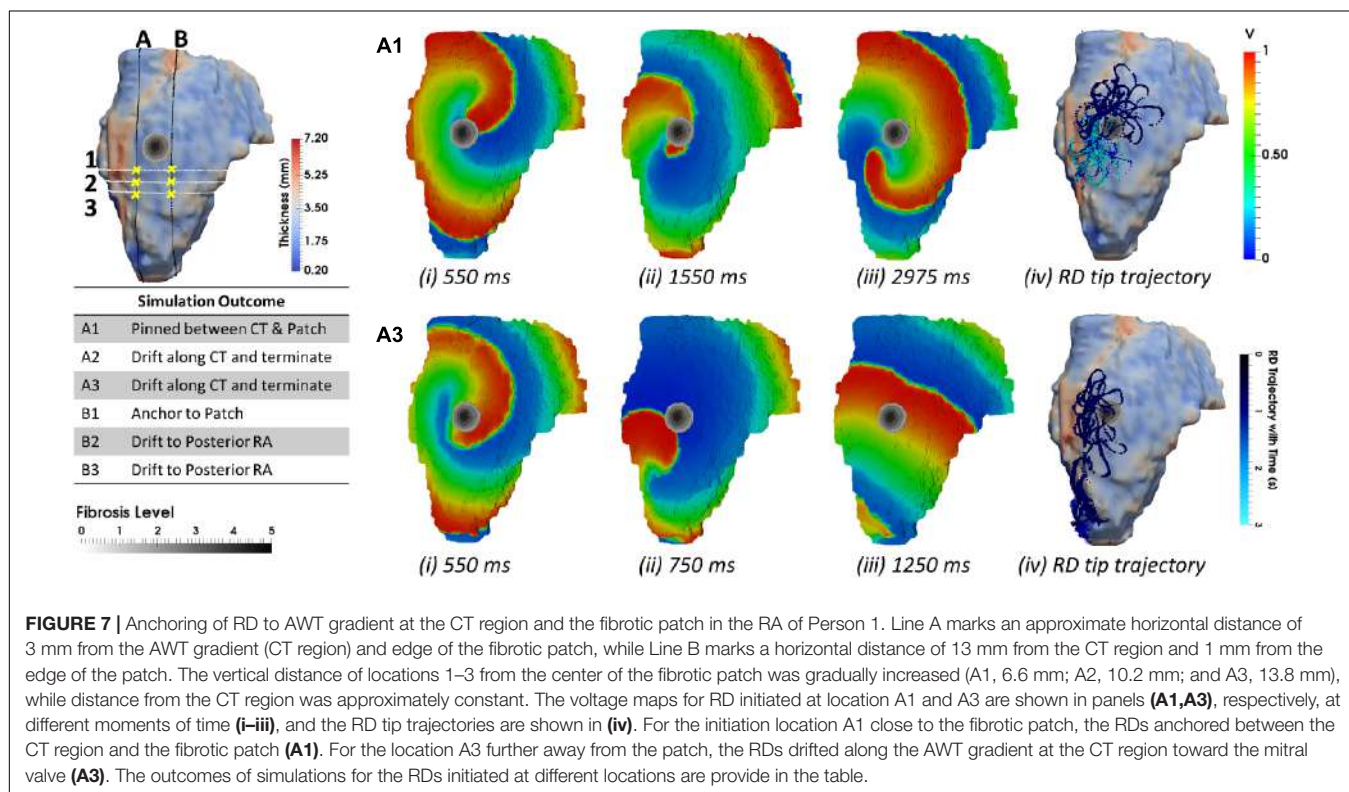


FIGURE 7 | Anchoring of RD to AWT gradient at the CT region and the fibrotic patch in the RA of Person 1. Line A marks an approximate horizontal distance of 3 mm from the AWT gradient (CT region) and edge of the fibrotic patch, while Line B marks a horizontal distance of 13 mm from the CT region and 1 mm from the edge of the patch. The vertical distance of locations 1–3 from the center of the fibrotic patch was gradually increased (A1, 6.6 mm; A2, 10.2 mm; and A3, 13.8 mm), while distance from the CT region was approximately constant. The voltage maps for RD initiated at location A1 and A3 are shown in panels (A1,A3), respectively, at different moments of time (i–iii), and the RD tip trajectories are shown in (iv). For the initiation location A1 close to the fibrotic patch, the RDs anchored between the CT region and the fibrotic patch (A1). For the location A3 further away from the patch, the RDs drifted along the AWT gradient at the CT region toward the mitral valve (A3). The outcomes of simulations for the RDs initiated at different locations are provide in the table.

fibrosis, while additional fibrotic patches provided competing attractors for the RDs. The results obtained from the RA and LA model simulations confirmed that drift direction and

anchoring points of RDs are determined by the interplay of competing influences of the patient-specific AWT gradients and fibrosis.

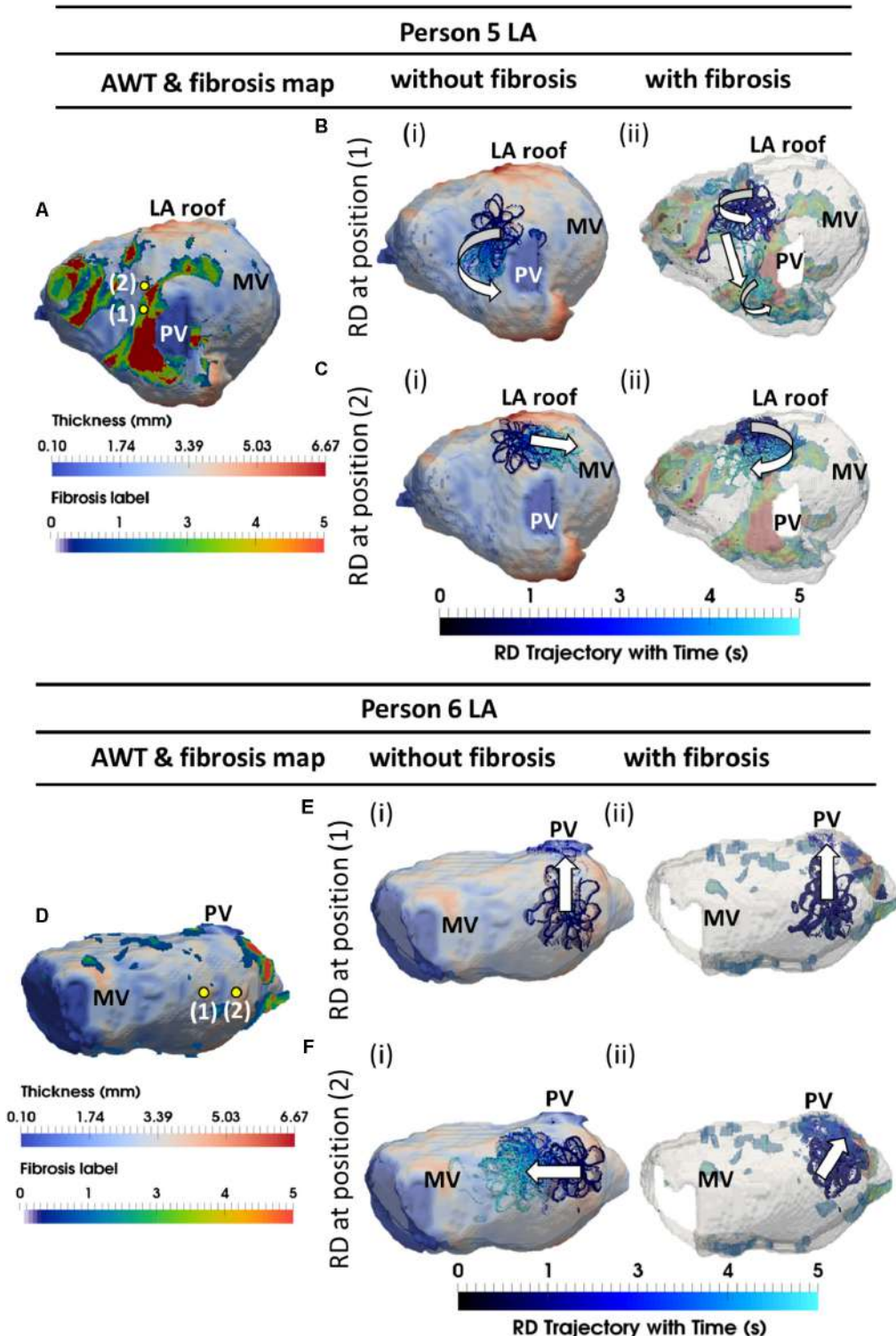


FIGURE 8 | Competing effects of AWT and fibrosis in the LA. The RDs trajectories (blue) in the LA, obtained by initiating RDs at two locations (yellow dots), without and with the presence of fibrosis, are overlaid on the AWT map and fibrosis distribution (A, D), respectively, for Person 5 (top) and 6 (bottom). In Person 5 in the absence of fibrosis, RDs initiated at positions 1 and 2 drifted toward the PVs [(B*i* and LA roof **C*i*]), respectively. With additional fibrosis, RDs drifted from its initial location to a new location (**B*ii***) for position 1 and anchored to the fibrotic patch (**C*ii***) for position 2. In Person 6 without fibrosis, RDs initiated at positions 1 and 2 drifted toward the PVs (**E*i***) and MV (**F*i***), respectively. With fibrosis, RDs continued to drift toward the PVs (**E*ii***) for position 1, but anchored to the fibrotic patch (**F*ii***) for position 2. PV, pulmonary vein; MV, mitral valve.**

Mechanistic Influence of AWT on the RD Dynamics

Simulations with both 3D atrial slabs and realistic 3D atrial geometries showed large AWT gradients provide anchoring locations for RDs. These results are in agreement with previous experimental observations in animal models of AF (Yamazaki et al., 2012). Moreover, larger AWT gradients have a stronger influence on the RD dynamics, forcing the RDs to drift with an increased velocity toward and then along the gradient. The underlying mechanism that enables the anchoring of RDs to these locations is likely to be based on a large source-to-sink mismatch in regions of high AWT gradient. The resulting current changes CV in tissue surrounding the AWT gradient, which helps stabilize the RDs in these locations. These results are in agreement with theoretical results using asymptotic theory based on simple three-variable ionic models (Biktasheva et al., 2015). We illustrated the tendency of RDs to anchor to regions with a high thickness gradient using the FK ionic model for remodeled atrial cells. Moreover, these results were reproduced using the CRN model that provides a detailed description of ionic currents and action potential in atrial cells (Supplementary Figure S2). This suggests that the anchoring of RDs to regions with large AWT gradients is model independent.

Note that, in addition to the influence of AWT gradients, anchoring of RDs to junction between thin and thick tissue observed by Yamazaki et al. could also be explained by the presence of pectinate muscles and activity of stretch-activated channels. Recent evidence also suggest that AF substrate can be provided by 3D structure of the atrial wall, which may cause epicardial and the endocardial discordance (Gutbrod et al., 2015). The latter may be explained by the formation of transmural RDs stabilized by interstitial fibrosis in the network of pectinate muscles (Hansen et al., 2015).

In this study, image-based RA and LA geometries from four healthy volunteers and two paroxysmal AF patients were used to assess the link between RD activity and regions of large AWT gradients. The subject-specific AWT was computed using previously published protocol from Varela et al. (2017b). Our results showed that RDs anchored to the CT region in subjects with a large AWT relative to the surrounding RA tissue. This findings can explain the presence of RD activity at the CT region, which has been reported in previous clinical (Kalman et al., 1998) and modeling (Gonzales et al., 2014) studies. However, RDs in this region can also be generated due to its high anisotropy (Aslanidi et al., 2011). In the atria with more homogeneous AWT (two RA models and all LA models), there was no clear link between the RD dynamics and specific AWT features. Instead, the direction of RD drift was always toward the TSV in the RA or the PVs and MV annulus in the LA. Our findings suggest that information from AWT may aid in designing personalized ablation strategies in patients whose atria are characterized by large gradients in thickness. Patient MRI can be used to reconstruct 3D atrial structure and identify patient-specific areas of large AWT gradients and fibrosis prior to CA procedures. Patient-specific models built based on such data can then predict the likely RD locations, and therefore aid in selecting the optimal ablation strategy for a given patient.

Competing Influence of Fibrosis and AWT on RDs

Our 3D model simulations using both atrial slabs and realistic atrial geometries revealed the interplay between the effects AWT and fibrosis on the dynamics of RDs. Previous imaging-based computational studies have reported anchoring of RDs at fibrotic patches in the LA (Gonzales et al., 2014; Morgan et al., 2016; Zahid et al., 2016). However, to the best of our knowledge, our

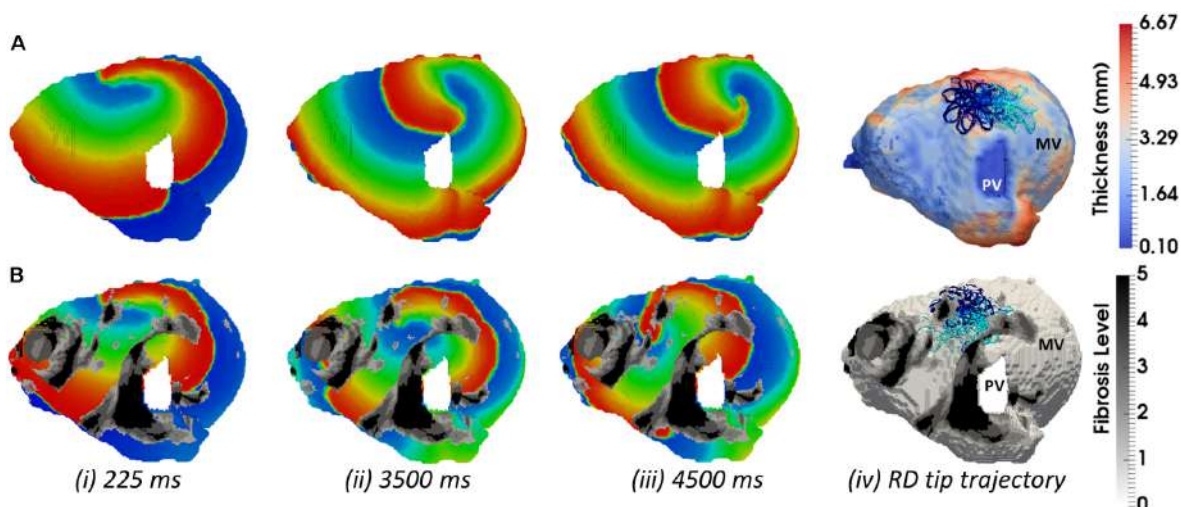


FIGURE 9 | Competing effects of AWT and fibrosis in the LA. The voltage map for RD initiated at Position 2 (shown in **Figure 8A**) are shown at different moments of time (i-iii). Rows **A** and **B** correspond to simulations without and with fibrosis, respectively. For each simulation, the RD tip trajectories (blue) are overlaid on their corresponding AWT and fibrosis map (iv). **(A)** RD initiated without fibrosis drifts along the large AWT gradient at the LA roof, while in the presence of fibrosis **(B)**, the same RD anchors to the fibrotic patch.

study is the first to explore the competing effects fibrosis and AWT gradients on the dynamics of RDs in both atria.

Simulations performed in both the 3D slab and realistic RA geometries produced similar results, with RDs anchoring between a region with a large AWT gradient (such as the CT region) and local fibrosis patches. Hence, locations of the RDs stabilization can be strongly influenced by both the presence of fibrosis, as predicted by previous studies (Morgan et al., 2016; Zahid et al., 2016), and the AWT gradients in the atria. These results can be explained by relative effects of (i) fibrotic patches providing slow conduction zones anchoring RDs and (ii) large AWT gradients creating substantial source-to-sink mismatches. The latter facilitate faster condition in the direction along the gradients. As the drift velocity of RDs along the AWT gradients increases with the increased gradient magnitude (**Figure 3B**), the RDs are more likely to drift along a large gradient, anchoring to it. Therefore, atrial tissue regions between a fibrotic patch and a large AWT gradient experience both competing influences and are most likely to anchor RDs. In addition, our simulations in both 3D slab and RA showed that RDs anchored to the fibrotic patch only when they were initiated further away from the structural features (thickness step, CT region) with large AWT gradients. Hence, anchoring of the RDs to either the AWT gradients or fibrotic patches may depend on (1) their comparative ability to provide suitable substrate and (2) their relative distance from the RD initiation site.

Our results could explain why the correlation between LGE-derived fibrosis and RDs locations reported by Cochet et al. (2018) was weaker in the RA than the LA. This may be explained by the higher variability in AWT in the RA compared to the LA, with the AWT gradients in the RA providing alternative anchoring locations for the RDs. Note that in this study, we used a synthetic cylindrical fibrotic patch in the RA, which was a simplified approximation of fibrotic patches of irregular geometry obtained from patient LGE MRI. The lack of patient-specific RA fibrosis data in our study was due to routine pre-ablation LGE MRI scans being restricted to the LA. Previous studies (Zahid et al., 2016) have linked RD behavior to the heterogeneity of the shape of the fibrotic patch. While a simple cylindrical patch in the RA was not patient-specific, using it enabled us to focus on the relative mechanistic influences of slow-conducting fibrotic tissue and AWT gradients, without considering additional complex effects of the fibrosis shape.

In LA model simulations in the absence of patient-specific fibrosis distribution, RDs were mostly localized in regions surround the PVs and MV openings. Such a lack of influence of AWT on the RD stabilization in the LA could be explained by the absence of structural features with large AWT gradient in most patients. The only exception was Person 5, where the RD anchored to a large AWT gradient at the LA roof. However, when the LA simulations were repeated with LGE MRI-derived fibrotic patches, a clear stabilization of RDs near the patches was observed in all patients. In the exceptional case of Person 5 (**Figure 8**), who had high fibrosis burden, RDs were unstable and formed multiple wavelets meandering between fibrotic patches.

These results contribute to the understanding of why PVI is effective for paroxysmal AF patients with low fibrosis burden (Akoum et al., 2011). Even in paroxysmal AF, the number of RDs near the PVs is higher than the number of focal triggers (Narayan et al., 2013) – the presence of RDs near the PVs, and therefore the success of PVI, in those patients may be explained by the lack of other anchoring locations, such as large AWT gradients or fibrotic patches. However, for AF patients with high fibrosis burden, the altered atrial substrates can result in the drift and multiplication of RDs in regions of slow conduction, such as the border zones of fibrotic tissue (Morgan et al., 2016). Therefore, assessment of patient-specific fibrosis distribution in the LA of persistent AF patients, facilitated by LGE MRI, may assist in the prediction of RD locations. In future, this could be tested by a retrospective study on a patient cohort that have been successfully ablated after LGE MRI mapping of fibrosis.

Limitations

In our study, fibrosis was modeled as regions of progressively slow conduction linked with LGE MRI intensity. The LGE MRI threshold of 1.08 IIR (level 1) and 1.32 IIR (level 5) was obtained from previous studies validated by electro-anatomical mapping data (Khurram et al., 2014; Benito et al., 2017), but the IIR threshold values for splitting the border zone into levels 1-4 was not validated due to lack of experimental data. However, correlation between decrease in CV and increase in IIR has been reported (Fukumoto et al., 2016). Therefore, our approach of gradually decreasing CV across fibrosis levels 0-5 is in agreement with patient studies. Recent studies have also shown that additional small effects of fibroblast-myocyte coupling (Morgan et al., 2016) and paracrine effects (Roney et al., 2016) could also influence the RD stabilization. However, data on such effects in human are unavailable, and modification of the model parameters based on *ex vivo* animal data can produce results that are inconsistent with clinical data (Roney et al., 2016). Therefore, such effects were not considered in this study.

Our study did not consider the influence of other patient-specific factors such as atrial anisotropy and electrophysiological heterogeneity, which may contribute to drift of the RDs observed in the realistic LA and RA geometries (Varela et al., 2016). Atrial fiber orientation is known to be complex (Ho and Sánchez-Quintana, 2009) and can have significant effects on atrial conduction (Aslanidi et al., 2011; Varela et al., 2016). However, fiber orientation was not incorporated in this study due to the absence of patient-specific data. Future studies will aim to incorporate information about fiber orientation into patient-specific atrial models based on recently proposed rule-based approaches (Fastl et al., 2018).

Note also that aFK model developed by Goodman et al. was based on data from tachypaced sheep atrial cells, due to a lack of equivalent human data. However, comparison of APD between the aFK model and in the CRN model for a remodeled human atrial myocyte showed a good agreement between the two models: less than 5% difference in APD in the considered range of frequencies between 6 and 10 Hz. Moreover, the main result of the study – that RDs anchor to regions with large AWT

gradients – was qualitatively similar between the aFK and CRN models.

Finally, LA wall dilation and heterogeneous wall thinning can occur with the disease progression from PAF to permanent AF (Nakamura et al., 2011). Therefore, results of this study, which are based on data from healthy volunteers and PAF patients, cannot be extended to persistent AF. Future studies will aim to characterize AWT changes in persistent AF and evaluate the arising effects on AF drivers.

CONCLUSION

This study elucidated the role of AWT as a substrate for RDs and marker for the identification of RD locations in the patient-specific atria, and compared the AWT effects with the respective effects of fibrosis. In the RA, RDs stabilized around structural features with large AWT gradients, while the addition of fibrotic patches provided an alternative attractor for the RDs. In the LA that had more uniform AWT distributions, RD locations were determined by the distribution of fibrotic patches or by anatomical features (e.g., the PVs). These findings corroborate our hypothesis that anchoring locations of RDs are dependent on the relative influence of gradients in AWT and fibrosis, and suggests the non-invasive assessment of AWT and fibrosis using MRI may inform clinical interventions in AF patients.

REFERENCES

- Akoum, N., Daccarett, M., McGann, C., Segerson, N., Vergara, G., Kuppahally, S., et al. (2011). Atrial fibrosis helps select the appropriate patient and strategy in catheter ablation of atrial fibrillation: a DE-MRI guided approach. *J. Cardiovasc. Electrophysiol.* 22, 16–22. doi: 10.1111/j.1540-8167.2010.01876.x
- Aslanidi, O. V., Colman, M. A., Stott, J., Dobrzynski, H., Boyett, M. R., Holden, A. V., et al. (2011). 3D virtual human atria: a computational platform for studying clinical atrial fibrillation. *Prog. Biophys. Mol. Biol.* 107, 156–168. doi: 10.1016/j.pbiomolbio.2011.06.011
- Benito, E. M., Carlosena-Remirez, A., Guasch, E., Prat-González, S., Perea, R. J., Figueras, R., et al. (2017). Left atrial fibrosis quantification by late gadolinium-enhanced magnetic resonance: a new method to standardize the thresholds for reproducibility. *Europace* 19, 1272–1279. doi: 10.1093/europace/euw219
- Biktasheva, I. V., Dierckx, H., and Biktashev, V. N. (2015). Drift of scroll waves in thin layers caused by thickness features: asymptotic theory and numerical simulations. *Phys. Rev. Lett.* 114, 1–12. doi: 10.1103/PhysRevLett.114.068302
- Blandino, A., Bianchi, F., Grossi, S., Biondi-Zocca, G., Conte, M. R., Gaido, L., et al. (2017). Left atrial substrate modification targeting low-voltage areas for catheter ablation of atrial fibrillation: a systematic review and meta-analysis. *Pacing Clin. Electrophysiol.* 40, 199–212. doi: 10.1111/pace.13015
- Chugh, S. S., Havmoeller, R., Narayanan, K., Singh, D., Rienstra, M., Benjamin, E. J., et al. (2014). Worldwide epidemiology of atrial fibrillation. *Circulation* 129, 837–847. doi: 10.1161/CIRCULATIONAHA.113.005119
- Cochet, H., Dubois, R., Yamashita, S., Al Jefairi, N., Berte, B., Sellal, J. M., et al. (2018). Relationship between fibrosis detected on late gadolinium-enhanced cardiac magnetic resonance and re-entrant activity assessed with electrocardiographic imaging in human persistent atrial fibrillation. *JACC Clin. Electrophysiol.* 4, 17–29. doi: 10.1016/j.jacep.2017.07.019
- Colman, M. A., Aslanidi, O. V., Kharche, S., Boyett, M. R., Garratt, C., Hancox, J. C., et al. (2013). Pro-arrhythmogenic effects of atrial fibrillation-induced electrical remodelling: insights from the three-dimensional virtual human atria. *J. Physiol.* 591, 4249–4272. doi: 10.1113/jphysiol.2013.254987
- Courtemanche, M., Ramirez, R. J., and Nattel, S. (1998). Ionic mechanisms underlying human atrial action potential properties: insights from a mathematical model. *Am. J. Physiol.* 275(1 Pt 2), H301–H321. doi: 10.1152/ajpheart.1998.275.1.H301
- Dierckx, H., Brisard, E., Verschelde, H., and Panfilov, A. V. (2013). Drift laws for spiral waves on curved anisotropic surfaces. *Phys. Rev. E* 88:012908. doi: 10.1103/PhysRevE.88.012908
- Fastl, T. E., Tobon-Gomez, C., Crozier, A., Whitaker, J., Rajani, R., McCarthy, K. P., et al. (2018). Personalized computational modeling of left atrial geometry and transmural myofiber architecture. *Med. Image Anal.* 47, 180–190. doi: 10.1016/j.media.2018.04.001
- Fenton, F., Karma, A., Fenton, F., and Karma, A. (2008). Vortex dynamics in three-dimensional continuous myocardium with fiber rotation: filament instability and fibrillation. *Chaos* 20, 20–47. doi: 10.1063/1.166311
- Fukumoto, K., Habibi, M., Ipek, E. G., Zahid, S., Khurram, I. M., Zimmerman, S. L., et al. (2016). Association of left atrial local conduction velocity with late gadolinium enhancement on cardiac magnetic resonance in patients with atrial fibrillation. *Circ. Arrhythmia. Electrophysiol.* 9:e002897. doi: 10.1161/CIRCEP.115.002897
- Ganesan, A. N., Shipp, N. J., Brooks, A. G., Kuklik, P., Lau, D. H., Lim, H. S., et al. (2013). Long-term outcomes of catheter ablation of atrial fibrillation: a systematic review and meta-analysis. *J. Am. Heart Assoc.* 2:e004549. doi: 10.1161/JAHA.112.004549
- Gonzales, M. J., Vincent, K. P., Rappel, W. J., Narayan, S. M., and McCulloch, A. D. (2014). Structural contributions to fibrillatory rotors in a patient-derived computational model of the atria. *Europace* 16, iv3–iv10. doi: 10.1093/europace/euu251
- Goodman, A. M., Oliver, R. A., Henriquez, C. S., and Wolf, P. D. (2005). A membrane model of electrically remodelled atrial myocardium derived

AUTHOR CONTRIBUTIONS

All authors have made substantial contributions to this study. AR and OA conceived and designed the study, and drafted the manuscript. AR substantially contributed to data analysis and computer simulations, and OA substantially contributed to the interpretation of the results. AR, MV, and OA contributed to data analysis, computer simulations, and manuscripts editing. All authors have also approved the final version to be published while agreeing to be accountable for all aspects of the work in ensuring that questions related to the accuracy or integrity of any part of the work are appropriately investigated and resolved.

FUNDING

This work was supported by the Engineering and Physical Sciences Research Council (EPSRC) (EP/L015226/1), the British Heart Foundation (PG/15/8/31138), and the Wellcome/EPSRC Centre for Medical Engineering (WT 203148/Z/16/Z).

SUPPLEMENTARY MATERIAL

The Supplementary Material for this article can be found online at: <https://www.frontiersin.org/articles/10.3389/fphys.2018.01352/full#supplementary-material>

- from in vivo measurements. *Europace* 7, 135–145. doi: 10.1016/j.eupc.2005.04.010
- Gray, R. A., Pertsov, A. M., and Jalife, J. (1998). Spatial and temporal organization during cardiac fibrillation. *Nature* 392, 75–78. doi: 10.1038/32164
- Gutbrod, S. R., Walton, R., Gilbert, S., Meillet, V., Jais, P., Hocini, M., et al. (2015). Quantification of the transmural dynamics of atrial fibrillation by simultaneous endocardial and epicardial optical mapping in an acute sheep model. *Circ. Arrhythm. Electrophysiol.* 8, 456–465. doi: 10.1161/CIRCEP.114.002545
- Haissaguerre, M., Hocini, M., Denis, A., Shah, A. J., Komatsu, Y., Yamashita, S., et al. (2014). Driver domains in persistent atrial fibrillation. *Circulation* 130, 530–538. doi: 10.1161/CIRCULATIONAHA.113.005421
- Haïssaguerre, M., Jaïs, P., Shah, D. C., Takahashi, A., Hocini, M., Quiniou, G., et al. (1998). Spontaneous initiation of atrial fibrillation by ectopic beats originating in the pulmonary veins. *N. Engl. J. Med.* 339, 659–666. doi: 10.1056/NEJM199809033391003
- Hansen, B. J., Zhao, J., Csepe, T. A., Moore, B. T., Li, N., Jayne, L. A., et al. (2015). Atrial fibrillation driven by micro-anatomic intramural re-entry revealed by simultaneous sub-epicardial and sub-endocardial optical mapping in explanted human hearts. *Eur. Heart J.* 36, 2390–2401. doi: 10.1093/eurheartj/ehv233
- Ho, S. Y., and Sánchez-Quintana, D. (2009). The importance of atrial structure and fibers. *Clin. Anat.* 22, 52–63. doi: 10.1002/ca.20634
- Kalman, J. M., Olglin, J. E., Karch, M. R., Hamdan, M. H., Lee, R. J., and Lesh, M. D. (1998). "Cristal tachycardias": origin of right atrial tachycardias from the crista terminalis identified by intracardiac echocardiography. *J. Am. Coll. Cardiol.* 31, 451–459. doi: 10.1016/S0735-1097(97)00492-0
- Khurram, I. M., Beinart, R., Zipunnikov, V., Dewire, J., Yarmohammadi, H., Sasaki, T., et al. (2014). Magnetic resonance image intensity ratio, a normalized measure to enable interpatient comparability of left atrial fibrosis. *Heart Rhythm* 11, 85–92. doi: 10.1016/j.hrthm.2013.10.007
- Kirchhof, P., Benussi, S., Kotecha, D., Ahlsson, A., Atar, D., Casadei, B., et al. (2016). 2016 ESC guidelines for the management of atrial fibrillation developed in collaboration with EACTS. *Eur. Heart J.* 37, 2893–2962. doi: 10.1093/eurheartj/ehw210
- Kottkamp, H., Bender, R., and Berg, J. (2015). Catheter ablation of atrial fibrillation: how to modify the substrate? *J. Am. Coll. Cardiol.* 65, 196–206. doi: 10.1016/j.jacc.2014.10.034
- Kottkamp, H., Berg, J., Bender, R., Rieger, A., and Schreiber, D. (2016). Box isolation of fibrotic areas (BIFA): a patient-tailored substrate modification approach for ablation of atrial fibrillation. *J. Cardiovasc. Electrophysiol.* 27, 22–30. doi: 10.1111/jce.12870
- Mahnkopf, C., Badger, T. J., Burgon, N. S., Daccarett, M., Haslam, T. S., Badger, C. T., et al. (2010). Evaluation of the left atrial substrate in patients with lone atrial fibrillation using delayed-enhanced MRI: implications for disease progression and response to catheter ablation. *Heart Rhythm* 7, 1475–1481. doi: 10.1016/j.hrthm.2010.06.030
- McGann, C., Akoum, N., Patel, A., Kholmovski, E., Revelo, P., Damal, K., et al. (2014). Atrial fibrillation ablation outcome is predicted by left atrial remodeling on MRI. *Circ. Arrhythm. Electrophysiol.* 7, 23–30. doi: 10.1161/CIRCEP.113.000689
- Miller, J. M., Kalra, V., Das, M. K., Jain, R., Garlie, J. B., Brewster, J. A., et al. (2017). Clinical benefit of ablating localized sources for human atrial fibrillation: the Indiana University firm registry. *J. Am. Coll. Cardiol.* 69, 1247–1256. doi: 10.1016/j.jacc.2016.11.079
- Mohanty, S., Mohanty, P., Trivedi, C., Gianni, C., Della Rocca, D. G., Di Biase, L., et al. (2018). Long-term outcome of pulmonary vein isolation with and without focal impulse and rotor modulation mapping: insights from a meta-analysis. *Circ. Arrhythm. Electrophysiol.* 11:e005789. doi: 10.1161/CIRCEP.117.005789
- Morgan, R., Colman, M. A., Chubb, H., Seemann, G., and Aslanidi, O. V. (2016). Slow conduction in the border zones of patchy fibrosis stabilizes the drivers for atrial fibrillation: insights from multi-scale human atrial modeling. *Front. Physiol.* 7:474. doi: 10.3389/fphys.2016.00474
- Nakamura, K., Funabashi, N., Uehara, M., Ueda, M., Murayama, T., Takaoka, H., et al. (2011). Left atrial wall thickness in paroxysmal atrial fibrillation by multislice-CT is initial marker of structural remodeling and predictor of transition from paroxysmal to chronic form. *Int. J. Cardiol.* 148, 139–147. doi: 10.1016/j.ijcard.2009.10.032
- Narayan, S. M., Baykaner, T., Clopton, P., Schricker, A., Lalani, G. G., Krummen, D. E., et al. (2014). Ablation of rotor and focal sources reduces late recurrence of atrial fibrillation compared with trigger ablation alone: extended follow-up of the confirm trial (conventional ablation for atrial fibrillation with or without focal impulse and rotor modulation). *J. Am. Coll. Cardiol.* 63, 1761–1768. doi: 10.1016/j.jacc.2014.02.543
- Narayan, S. M., Krummen, D. E., Clopton, P., Shivkumar, K., and Miller, J. M. (2013). Direct or coincidental elimination of stable rotors or focal sources may explain successful atrial fibrillation ablation: on-treatment analysis of the confirm trial (conventional ablation for AF with or without focal impulse and rotor modulation). *J. Am. Coll. Cardiol.* 62, 138–147. doi: 10.1016/j.jacc.2013.03.021
- Nattel, S. (2002). New ideas about atrial fibrillation 50 years on. *Nature* 415, 219–226. doi: 10.1038/415219a
- Nattel, S., Burstein, B., and Dobrev, D. (2008). Atrial remodeling and atrial fibrillation: mechanisms and implications. *Circ. Arrhythm. Electrophysiol.* 1, 62–73. doi: 10.1161/CIRCEP.107.754564
- Niederer, S. A., Kerfoot, E., Benson, A. P., Bernabeu, M. O., Bernus, O., Bradley, C., et al. (2011). Verification of cardiac tissue electrophysiology simulators using an N-version benchmark. *Philos. Trans. A Math. Phys. Eng. Sci.* 369, 4331–4351. doi: 10.1098/rsta.2011.0139
- Oral, H., Knight, B. P., Tada, H., Özaydin, M., Chugh, A., Hassan, S., et al. (2002). Pulmonary vein isolation for paroxysmal and persistent atrial fibrillation. *Circulation* 105, 1077–1081. doi: 10.1161/hc0902.104712
- Park, J., Park, C. H., Lee, H. J., Wi, J., Uhm, J. S., Pak, H. N., et al. (2014). Left atrial wall thickness rather than epicardial fat thickness is related to complex fractionated atrial electrogram. *Int. J. Cardiol.* 172, e411–e413. doi: 10.1016/j.ijcard.2013.12.255
- Roney, C. H., Bayer, J. D., Zahid, S., Meo, M., Boyle, P. M., Trayanova, N. A., et al. (2016). Modelling methodology of atrial fibrosis affects rotor dynamics and electrograms. *Europace* 18, iv146–iv155. doi: 10.1093/europace/euw365
- Rueckert, D. (1999). Nonrigid registration using free-form deformations: application to breast mr images. *IEEE Trans. Med. Imaging* 18, 712–721. doi: 10.1109/42.796284
- Sahadevan, J., Ryu, K., Peltz, L., Khrestian, C. M., Stewart, R. W., Markowitz, A. H., et al. (2004). Epicardial mapping of chronic atrial fibrillation in patients: preliminary observations. *Circulation* 110, 3293–3299. doi: 10.1161/01.CIR.0000147781.02738.13
- Sánchez-Quintana, D., Anderson, R. H., Cabrera, J. A., Climent, V., Martin, R., Farré, J., et al. (2002). The terminal crest: morphological features relevant to electrophysiology. *Heart* 88, 406–411.
- Sanders, P., Berenfeld, O., Hocini, M., Jaïs, P., Vaidyanathan, R., Hsu, L.-F., et al. (2005). Spectral analysis identifies sites of high-frequency activity maintaining atrial fibrillation in humans. *Circulation* 112, 789–797. doi: 10.1161/CIRCULATIONAHA.104.517011
- Siebermair, J., Kholmovski, E. G., and Marrouche, N. (2017). Assessment of left atrial fibrosis by late gadolinium enhancement magnetic resonance imaging: methodology and clinical implications. *JACC Clin. Electrophysiol.* 3, 791–802. doi: 10.1016/j.jacep.2017.07.004
- Varela, M., Bisbal, F., Zácur, E., Berrezo, A., Aslanidi, O. V., Mont, L., et al. (2017a). Novel computational analysis of left atrial anatomy improves prediction of atrial fibrillation recurrence after ablation. *Front. Physiol.* 8:68. doi: 10.3389/fphys.2017.00068
- Varela, M., Colman, M. A., Hancox, J. C., and Aslanidi, O. V. (2016). Atrial heterogeneity generates re-entrant substrate during atrial fibrillation and anti-arrhythmic drug action: mechanistic insights from canine atrial models. *PLOS Comput. Biol.* 12:e1005245. doi: 10.1371/journal.pcbi.1005245
- Varela, M., Morgan, R., Theron, A., Dillon-Murphy, D., Chubb, H., Whitaker, J., et al. (2017b). Novel MRI technique enables non-invasive measurement of atrial wall thickness. *IEEE Trans. Med. Imaging* 36, 1607–1614. doi: 10.1109/TMI.2017.2671839
- Yamazaki, M., Mironov, S., Taravant, C., Brec, J., Vaquero, L. M., Bandaru, K., et al. (2012). Heterogeneous atrial wall thickness and stretch promote scroll waves anchoring during atrial fibrillation. *Cardiovasc. Res.* 94, 48–57. doi: 10.1093/cvr/cvr357
- Zahid, S., Cochet, H., Boyle, P. M., Schwarz, E. L., Whyte, K. N., Vigmond, E. J., et al. (2016). Patient-derived models link re-entrant driver localization

- in atrial fibrillation to fibrosis spatial pattern. *Cardiovasc. Res.* 110, 443–454. doi: 10.1093/cvr/cvw073
- Zhao, J., Hansen, B. J., Wang, Y., Csepe, T. A., Sul, L. V., Tang, A., et al. (2017). Three-dimensional Integrated Functional, Structural, and Computational Mapping to Define the Structural “Fingerprints” of Heart-Specific atrial fibrillation drivers in human heart *ex vivo*. *J. Am. Heart Assoc.* 6, e005922. doi: 10.1161/JAHA.117.05922
- Zheng, Y., Xia, Y., Carlson, J., Kongstad, O., and Yuan, S. (2017). Atrial average conduction velocity in patients with and without paroxysmal atrial fibrillation. *Clin. Physiol. Funct. Imaging* 37, 596–601. doi: 10.1111/cpf.12342

Conflict of Interest Statement: The authors declare that the research was conducted in the absence of any commercial or financial relationships that could be construed as a potential conflict of interest.

The reviewer PB and handling Editor declared their shared affiliation.

Copyright © 2018 Roy, Varela and Aslanidi. This is an open-access article distributed under the terms of the Creative Commons Attribution License (CC BY). The use, distribution or reproduction in other forums is permitted, provided the original author(s) and the copyright owner(s) are credited and that the original publication in this journal is cited, in accordance with accepted academic practice. No use, distribution or reproduction is permitted which does not comply with these terms.



Myocyte Remodeling Due to Fibro-Fatty Infiltrations Influences Arrhythmogenicity

Tim De Coster^{1,2*}, Piet Claus², Gunnar Seemann³, Rik Willems², Karin R. Sipido² and Alexander V. Panfilov^{1,4,5*}

¹ Department of Physics and Astronomy, Ghent University, Ghent, Belgium, ² Department of Cardiovascular Sciences, KU Leuven, Leuven, Belgium, ³ Institute for Experimental Cardiovascular Medicine, University Heart Centre Freiburg • Bad Krozingen, Medical Center – University of Freiburg, and Faculty of Medicine, University of Freiburg, Freiburg, Germany, ⁴ Laboratory of Experimental Cardiology, Department of Cardiology, Heart Lung Centre Leiden, Leiden University Medical Center, Leiden, Netherlands, ⁵ Laboratory of Computational Biology and Medicine, Ural Federal University, Ekaterinburg, Russia

OPEN ACCESS

Edited by:

Oleg Aslanidi,
King's College London,
United Kingdom

Reviewed by:

Stefano Morotti,
University of California, Davis,
United States
Arun V. Holden,
University of Leeds, United Kingdom

*Correspondence:

Tim De Coster
tim.j.decoster@ugent.be
Alexander V. Panfilov
alexander.panfilov@ugent.be

Specialty section:

This article was submitted to
Computational Physiology and
Medicine,
a section of the journal
Frontiers in Physiology

Received: 30 April 2018

Accepted: 11 September 2018

Published: 04 October 2018

Citation:

De Coster T, Claus P, Seemann G, Willems R, Sipido KR and Panfilov AV (2018) Myocyte Remodeling Due to Fibro-Fatty Infiltrations Influences Arrhythmogenicity. *Front. Physiol.* 9:1381. doi: 10.3389/fphys.2018.01381

The onset of cardiac arrhythmias depends on the electrophysiological and structural properties of cardiac tissue. Electrophysiological remodeling of myocytes due to the presence of adipocytes constitutes a possibly important pathway in the pathogenesis of atrial fibrillation. In this paper we perform an *in-silico* study of the effect of such myocyte remodeling on the onset of atrial arrhythmias and study the dynamics of arrhythmia sources—spiral waves. We use the Courtemanche model for atrial myocytes and modify their electrophysiological properties based on published cellular electrophysiological measurements in myocytes co-cultured with adipocytes (a 69–87 % increase in APD_{90} and an increase of the RMP by 2.5–5.5 mV). In a generic 2D setup we show that adipose tissue remodeling substantially affects the spiral wave dynamics resulting in complex arrhythmia and such arrhythmia can be initiated under high frequency pacing if the size of the remodeled tissue is sufficiently large. These results are confirmed in simulations with an anatomically accurate model of the human atria.

Keywords: atrial fibrillation, adipose tissue, ionic modeling, arrhythmogenicity, computational modeling

1. INTRODUCTION

Atrial fibrillation (AF) forms an economic burden on modern health care (Stewart et al., 2004). It affects approximately 1.5 % of the population (Lip et al., 2007) and as much as 9% of people above the age of 80 (Go et al., 2001). AF is a progressive disease and results in increased mortality, morbidity, and impaired quality of life (Thrall et al., 2006). AF is therefore a major problem in cardiac electrophysiology and obtaining insights into the mechanism of this arrhythmia is of great interest to progress therapeutic strategies.

Several risk factors for AF have been identified. Of interest here, obesity increases the risk of AF by 49% in the general population, and the risk rises with an increased body mass index (Wanahita et al., 2008). It was shown that it is an independent risk factor for the occurrence of AF or progression of AF severity in the absence of other risk factors like heart failure, alcohol use, or hypertension (Wang et al., 2004; Dublin et al., 2006; Tsang et al., 2008). Recent experiments have shown significant correlations between adipose infiltrations and arrhythmias (Pantanowitz, 2001; Samanta et al., 2016; Haemers et al., 2017).

Risk factors result in physiological stimuli for the atrial myocardium resulting in a substrate for AF. Traditionally, structural factors like fibrosis, but also heterogeneities in atrial action potential have been identified. However, adipose tissue can affect the onset of arrhythmias as it produces both structural and electrophysiological (Lin et al., 2010) changes.

Recently a new detailed study examined the relationship between fatty infiltrations in the atrial myocardium and the development of AF substrate (Haemers et al., 2017). There, a direct relation between fibro-fatty infiltrations and arrhythmia was shown. Induction of AF in a sheep model resulted in a fibrotic remodeling of subepicardial adipose tissue infiltrates from pure fatty to dense fibro-fatty infiltrations and smaller adipocytes in the atrial wall. This remodeling was associated with cellular inflammation.

Adipose tissue creates in-excitable regions inside the heart similar to fibrosis (Pantanowitz, 2001). Structural dependency of arrhythmogenicity on adipocytes was recently studied *in-silico* in a generic two-dimensional model (De Coster et al., 2018). It was shown that a substrate with adipocytes is less arrhythmogenic than with fibrotic tissue and thus during remodeling of fatty into fibro-infiltrations the propensity to arrhythmias increases, confirming the results of Haemers et al. (2017).

In addition to creation of in-excitable regions inside the heart, adipose tissue also causes electrophysiological changes in the adjacent myocytes. Co-culture of rabbit atrial myocytes and epicardial adipocytes, results in remodeling of the myocyte action potential (Lin et al., 2012). The consequences at organ level of this remodeling have not yet been studied. However, they may substantially contribute to arrhythmogenesis in addition to structural effects. Furthermore, these changes can be more abundant as electrophysiological changes do not require infiltration of fat into cardiac tissue and occur even due to the presence of epicardial fat.

In this paper, we describe changes in properties of myocytes adjacent to adipocytes on the basis of an experimental study (Lin et al., 2012). The aim of this study was to investigate the effect of this adipose remodeling on the wave dynamics of spirals, onset of arrhythmias, and influence on its surroundings. We performed use *in-silico* simulations in a generic two dimensional setup and in a realistic anatomical model of human atria.

2. METHODS

2.1. Mathematical Model

To study the effect of remodeled myocytes in the vicinity of adipocytes in human cardiac tissue, we integrated a newly developed single cell model (explained in the next subsection: myocyte remodeling) together with the Courtemanche model (Courtemanche et al., 1998, 1999) for normal human atrial myocytes. The transmembrane voltage (V) is calculated in millivolts (mV) according to the mono-domain equations for cardiac tissue (Equation 1):

$$\frac{\partial V}{\partial t} = \nabla \cdot (\mathbf{D} \nabla V) - \frac{I_{ion}}{C_m}, \quad (1)$$

where t is time in milliseconds (ms), I_{ion} is the total ionic current density in microamperes per square centimeter ($\mu\text{A}/\text{cm}^2$) and is dependent on V , on the gating variables, and on the concentrations of intracellular calcium, C_m is the specific membrane capacitance in microfarad per square centimeters ($\mu\text{F}/\text{cm}^2$), and \mathbf{D} is the diffusion tensor, whose components are related to the myocyte orientation and gap junction distribution which create anisotropy.

A maximum velocity planar wave propagation of 54.71 cm/s at a stimulation frequency of 1 Hz was obtained for regular tissue.

For the human atrial morphology, data and fiber directions were obtained from Dössel et al. (2012). The ionic cell models that were used are the regular and the AF-induced electrically remodeled human atrial Courtemanche model (Courtemanche et al., 1998, 1999) (taken from CellML Yu et al., 2011 with the use of Myokit Clerx et al., 2016 and transformed to GPU-usable code).

We used an S1-S2 cross-field protocol to generate spiral and scroll waves. In human atrial monolayers, we assumed isotropy. Thus, the diffusion tensor of Equation (1) could be replaced by a scalar coefficient D . However, in 3D, to account for the anisotropy of realistic cardiac tissue, the diffusion tensor components D_{ij} were scaled according to the fiber direction tensor. The transverse diffusion coefficient (D_t , for signal propagation across the fibers) was assumed to be 9 times less than the longitudinal diffusion coefficient (D_l , for signal propagation along the fibers) giving rise to a realistic conduction velocity ratio (Liu et al., 2004; Aslanidi et al., 2011). Explicitly,

$$D_{ij} = (D_l - D_t)\alpha_i\alpha_j + D_t\delta_{ij}, \quad (2)$$

where α_i are components of the unit vector that is oriented along the direction of a fiber and $D_l = 1.3 \text{ cm}^2/\text{s}$.

2.2. Myocyte Remodeling

We used the Courtemanche model for both the normal (Courtemanche et al., 1998) and AF remodeled (Courtemanche et al., 1999) human atrial myocyte. The total ionic current consists of the following currents:

$$I_{ion} = I_{Na} + I_{CaL} + I_{K1} + I_{to} + I_{NaCa} + I_{NaK} + I_{Kur} + I_{Kr} + I_{Ks} + I_{bNa} + I_{bCa} + I_{pCa}. \quad (3)$$

Here I_{Na} represents the fast Na^+ current, I_{CaL} , the L-type Ca^{2+} current, I_{K1} , the inward-rectifier K^+ current, I_{to} , the transient outward K^+ current, I_{NaCa} , the $\text{Na}^+/\text{Ca}^{2+}$ exchanger current, I_{NaK} , the Na^+/K^+ pump current, I_{Kur} , the ultra-rapid-delayed rectifier K^+ current, I_{Kr} , the rapid-delayed rectifier K^+ current, I_{Ks} , the slow-delayed rectifier K^+ current, I_{bNa} , the background Na^+ current, I_{bCa} , the background Ca^{2+} current, and I_{pCa} , the plateau Ca^{2+} current.

The AF remodeled atrial cell model has changes in 3 of these ionic currents, namely a 70% reduction in I_{CaL} , a 50% reduction in I_{to} and a 50% reduction in I_{Kur} , resulting in a decreased action potential duration (APD).

Co-culture of adipocytes and left atrial myocytes has revealed important changes in ionic currents in a rabbit atrial model

(Lin et al., 2012). Measurements were made for co-culture of myocytes with adipose tissue from different regions in the heart (epicardial, retrosternal), abdominal adipose tissue, and adipocytes-conditioned supernatant for 2–4 h. We focused on remodeling due to epicardial adipose tissue as we aim to look at the arrhythmogenic effect of infiltrates. Based on these experimental data, we adapted 6 ion currents for adipose induced myocyte remodeling, namely I_{CaL} , I_{to} , I_{Kur} , I_{Na} , I_{Ks} , and I_{K1} . In Lin et al. (2012) the tail component of I_{Kr} was measured. Its dynamics resembles strongly I_{Ks} and it was therefore chosen as a replacement since the Courtemanche model does not have a tail component of I_{Kr} current. Experimental data points and corresponding error bars were extracted for the I-V plots in Lin et al. (2012). In **Figure 1B**, we present a *relative* I-V plot for the six relevant ion currents in remodeled myocytes. To obtain these plots, the remodeled peak currents were divided by the peak current of the normal myocyte. The obtained data points together with their corresponding error bar are denoted in green. These ratio's are assumed to be species independent and are consequently used to validate ionic changes made to a human atrial myocyte model. To inflict these changes, a combination of functions was tested to rescale the gating variables of the selected currents. These functions were either linear, parabolic or a sigmoid (see **Table 1**). After rescaling, simulations were run in a single cell, mimicking patch clamp experiments, to construct a current-voltage (I-V) relationship from *in silico* data. Model curves (**Figure 1A**) represent peak currents measured during 3,000 ms voltage steps to various potentials from a holding potential of -80 mV (This method was validated against earlier results, see **Figure S1** in the Supplementary Information). The peak values of adipose remodeled and regular cells were divided by each other to obtain a factor that can be compared with the experimental one. These data were presented by means of a full or orange dotted line on top of the experimental data (see rows denoted by the letter B in **Figure 1**). It can be seen that all executed conduction factor changes make for results that are in correspondence with experiment.

The final results of the rescaling factors can be found in **Table 1** and are used to scale the conductances. E.g. the new maximal conductance for the sodium current I_{Na} would now be $g'(V)_{Na} * g_{Na}$, where $g'(V)_{Na}$ is the measured curve, and g_{Na} is the standard maximal conductance. A table with all maximal conductances for all four models can be found in **Table S1** in the Supplementary Information.

2.3. Pacing Protocols

For all single cell simulations, we paced at a frequency of 1 Hz and considered the 12th action potential in agreement with previously published APs.

For 1D simulations, we obtained a restitution curve by means of a dynamic pacing protocol. The tissue was paced from one side at a basic cycle length (BCL) of 1,100 ms for six pulses. The BCL was progressively lowered with a step equal to 1 percent of the current BCL. This was done up until a step size of 1 ms was reached, after which we always went down with this minimal step size of 1 ms. This was repeated until conduction became impossible.

In the same cable configuration we obtained measurements of the conduction velocity from the twelfth pulse.

A variety of pacing protocols was tested in tissue monolayers. Firstly, we induced spirals by means of an S1S2-protocol. The first pulse was from one side of the tissue, while the second one comprised one eighth of the tissue just behind the waveback, going from the top of the tissue until halfway in the y-direction and from one quarter until the middle in the x-direction.

Secondly, to determine the minimal size of a remodeled patch to induce arrhythmia, we used an S1S2 protocol where the first pulse was from one side of the tissue, while the second pulse was delivered by a point located at the edge of the remodeled tissue patch.

Thirdly, a burst-pacing protocol for spontaneous spiral induction that consisted of 10 pulses at different BCL (1,000, 900, 800, 700, 600, 500, 450, 400, 350, 320, 300, 290, 280, 270, 260, 250, 240, 230, 220, all in ms) was used.

For anatomically correct human atrial data we used an induced spiral protocol. The spiral was induced at four locations, twice at a location in the left atrium and twice at a location in the right atrium and obtained by means of an S1S2-protocol. The first pulse was initiated from one side of the atria (the left atrium was chosen), while the second pulse is a slice through the whole atrium right after the waveback and perpendicular to the first pulse.

2.4. Implementation

We integrated the system of coupled ordinary differential equations Equation 1 in time using the forward Euler method with time step $\delta t = 0.005$ ms, and in space, using the centered finite-differencing scheme with space step $\delta x = \delta y = 0.0300$ cm in monolayers, and also 0.0300 cm in whole atria, subject to “no flux” boundary conditions. Our monolayer domains contained 1024×1024 grid points, so that the physical size of the simulated tissue was 30.72×30.72 cm to reduce possible boundary effects. The simulation domain for the whole atria contained 2,173,891 grid points. The gating variables in the electrophysiological model for the human cardiomyocyte were integrated using the Rush and Larsen scheme (Rush and Larsen, 1978).

The numerical solver was implemented with the C and C++ programming languages, using the CUDA toolkit for performing the majority of computations on graphical processing units. Visualization of results was done with the help of the Python programming language and ParaView (Kitware). Computations were performed with single precision and run on an Intel Core i7-3930K machine with two GeForce GTX TITAN Black graphics cards.

3. RESULTS

3.1. Single Cell

Differences in the ionic currents of four models (regular, regular + AF remodeling, adipose remodeling, adipose remodeling + AF remodeling) resulted in differences in action potential shapes. **Figure 1** shows these changes for 1 Hz pacing.

The results are shown in the rows denoted by the letter A in **Figure 1**. Epicardial adipocyte-incubated myocytes have larger

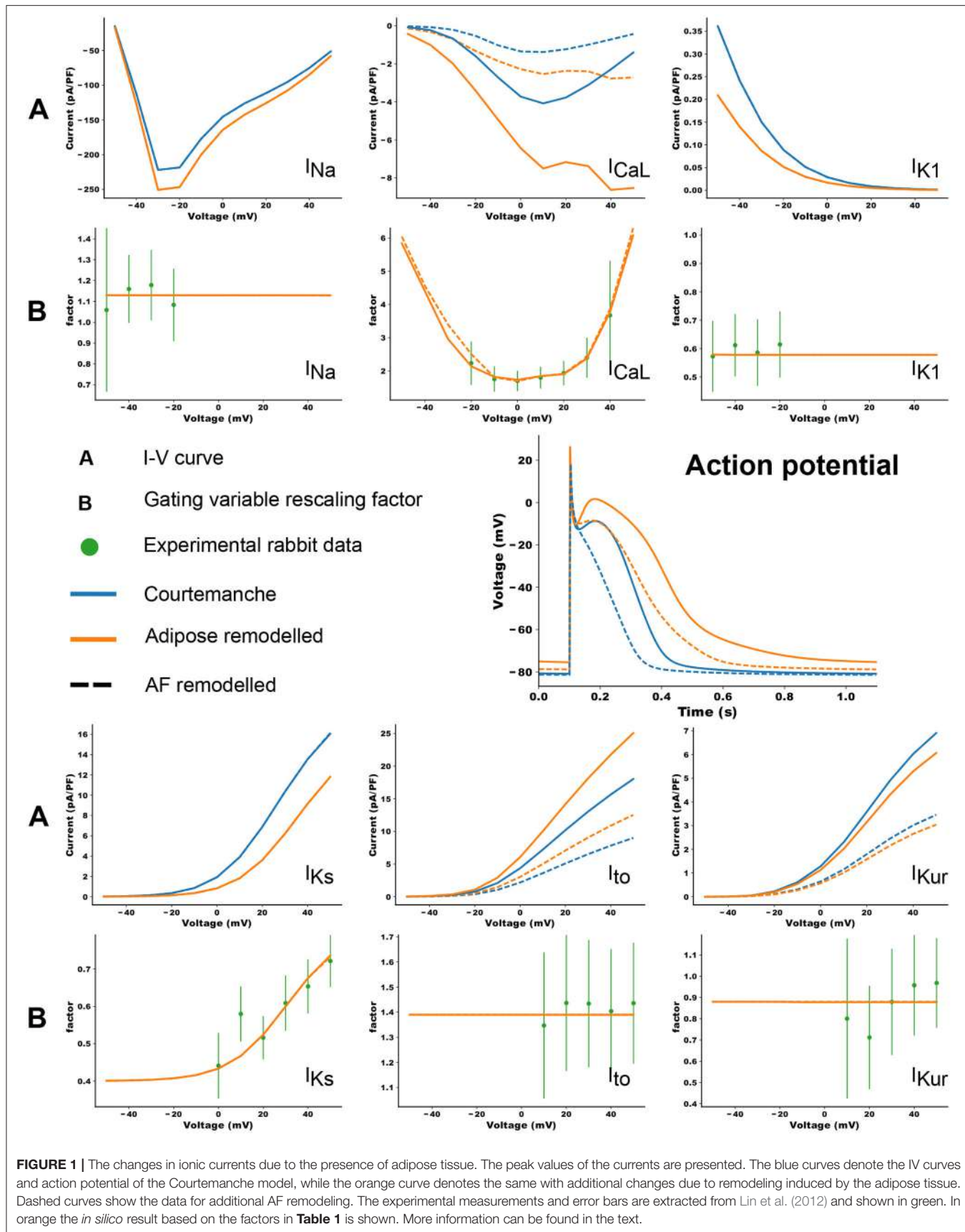


FIGURE 1 | The changes in ionic currents due to the presence of adipose tissue. The peak values of the currents are presented. The blue curves denote the IV curves and action potential of the Courtemanche model, while the orange curve denotes the same with additional changes due to remodeling induced by the adipose tissue. Dashed curves show the data for additional AF remodeling. The experimental measurements and error bars are extracted from Lin et al. (2012) and shown in green. In orange the *in silico* result based on the factors in **Table 1** is shown. More information can be found in the text.

late sodium currents (I_{Na}), L-type calcium currents (I_{CaL}) with an extra increase around its maximal value, and transient outward potassium currents (I_{to}) than control myocytes. On the other hand we see smaller delayed rectifier potassium (I_{Kr} and I_{Ks}) and inward rectifier potassium currents (I_{K1}). The extent of change of these currents due to remodeling corresponds to the experimental values.

These changes in ionic currents result in the following changes in the cellular action potential. In adipose-remodeled myocytes, the resting membrane potential (RMP) increases, making depolarization of the cell easier. The action potential amplitude (APA) remains similar resulting in a higher maximal voltage reached. An increased calcium current results in a higher plateau-level and prolongation of the APD_{50} . The decreased potassium rectifiers cause elongation of the tail (phase 3) of the remodeled AP, resulting in noticeable elongation of APD_{90} . Numerical values for all aforementioned properties (RMP, APA, and APD) can be found in **Table 2**.

Separate contributions of each current to the changes in action potential shape were also examined and can be found in the Supplementary Information: **Figure S2**.

3.2. 1D Propagation

3.2.1. Conduction Velocity

We calculated the conduction velocity in a 1D cable configuration. For a 1 Hz stimulation frequency the conduction velocities of the four different models with the standard value

TABLE 1 | Correction factors for selected currents in the human atrial model, based on measurements and fits to rabbit atrial data (rows denoted by the letter B in **Figure 1**).

	Best fit	Value
$g'(V)_{Na}$	Constant	1.13
	Parabolic	$V < 0 \text{ mV}$: $0.0017V^2 + 1.955$
$g'(V)_{CaL}$	Sigmoid	$0 \text{ mV} < V < 20 \text{ mV}$: $2.071 + \frac{1.949 - 2.071}{1 + e^{0.4 \times (V - 7.82 \text{ mV})}}$
	Parabolic	$V > 20 \text{ mV}$: $0.005 \times (V - 20.0)^2 + 2.07$
$g'(V)_{to}$	Constant	1.39
$g'(V)_{Kur}$	Constant	0.880
$g'(V)_{Ks}$	Sigmoid	$0.8 + \frac{0.4 - 0.8}{1 + e^{0.08 \times (V - 30 \text{ mV})}}$
$g'(V)_{K1}$	Sigmoid	$0.578 + \frac{0.805 - 0.578}{1 + e^{0.3 \times (V + 70 \text{ mV})}}$

The new maximal conductivity factor for the sodium current I_{Na} would now be $g'(V)_{Na} \cdot g_{Na}$.

TABLE 2 | Action potential properties for four models used in simulations.

	Courtemanche	Adipose remodeled	AF remodeled	AF + adipose remodeled
APD_{90} (ms)	299.910	507.545	215.425	403.330
APD_{50} (ms)	180.725	272.970	86.475	185.930
APD_{20} (ms)	5.680	4.635	7.660	6.235
RMP (mV)	-80.857	-75.466	-81.370	-78.841
APA (mV)	105.651	103.523	106.251	107.565

Adipose remodeling makes the RMP higher, elongates the tail of the APD (The difference in APD_{90} is much larger than the other APD-measurements), and increases the action potential amplitude (APA) of the APD.

of the diffusion coefficient of $1.3 \text{ cm}^2/\text{s}$ are: 50.94 cm/s for the Courtemanche model, 50.96 cm/s for the AF remodeled Courtemanche model, 56.04 cm/s for the adipose remodeled atrial myocyte, and 54.88 cm/s for the AF and adipose remodeled atrial myocyte. These results are consistent and correspond to conduction velocities observed in experiment (AF that was characterized by one or two non-uniformly conducting wavelets corresponds to $54 \pm 4 \text{ cm/s}$; Konings et al., 1994).

3.2.2. Restitution Curve

With the same configuration, we investigated the APD restitution properties of all four models. The results can be seen in **Figure 2**.

The Courtemanche model, depicted in green, has a regular restitution curve with a decrease in APD for low diastolic intervals (DIs). The AF remodeled Courtemanche model (the red line) shows a slow decrease in APD which becomes more steep for lower DI (see also Supplementary Information **Figure S3**). When adipose remodeling is considered, restitution curves change. Adipose tissue remodeling of the regular Courtemanche model (the blue line), results in substantial prolongation of APDs and a decrease happens at lower DIs with a slope similar to that of the Courtemanche model. Adipose remodeling of the AF Courtemanche model (the orange line) results in an almost flat dependency for long DIs and slow decrease at small DIs. There is also substantial difference in maximal pacing rate between the models. For the normal Courtemanche model the maximal frequency of pacing was 4.9 Hz, for the AF remodeled Courtemanche model it is 6.1 Hz, however for the adipose remodeled tissue it was 1.4 Hz and for the AF remodeled adipose tissue it was 2.1 Hz.

3.3. Tissue Monolayers

Next we study how observed changes in electrophysiological properties will affect 2D dynamics of the arrhythmias generated by spiral waves for the four different models as well as for combinations of the models in case of heterogeneous cardiac tissue.

3.3.1. Properties of Spiral Waves in Normal and Remodeled Tissue

We induced a spiral wave by an S1-S2 protocol in 2D homogeneous tissue for each of the four tissue types and studied its dynamics. The representative snapshots and the voltage recordings at one selected point are presented in **Figure 3**. Full movies can be found in the Supplementary Information.

In the Courtemanche model (top row in **Figure 3**) we can see a meandering spiral. The action potential trace shows small variation of atrial APs in time due to the meandering, but the changes are small. This is in line with previous observations in the Courtemanche model (Courtemanche et al., 1998). The AF remodeled Courtemanche model (second row in **Figure 3**) also shows a stable spiral with almost completely periodic action potentials. Compared to the normal Courtemanche model, the core of the spiral and the wavelength becomes much smaller.

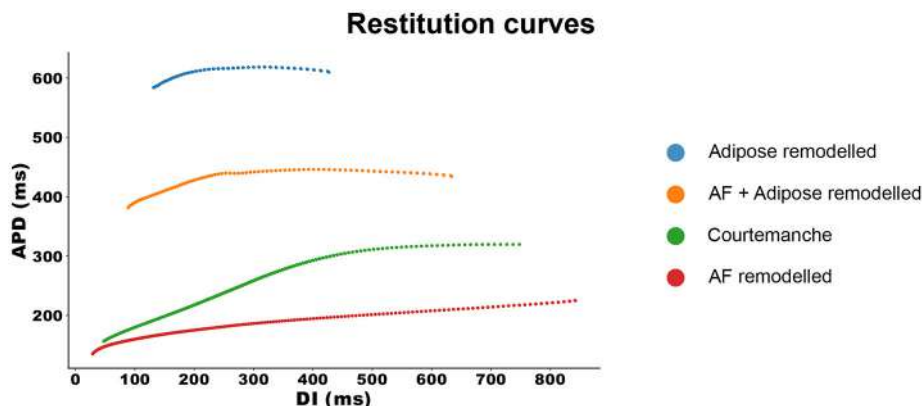


FIGURE 2 | Restitution curves for all four models. The APD measurements are made at 90% repolarization.

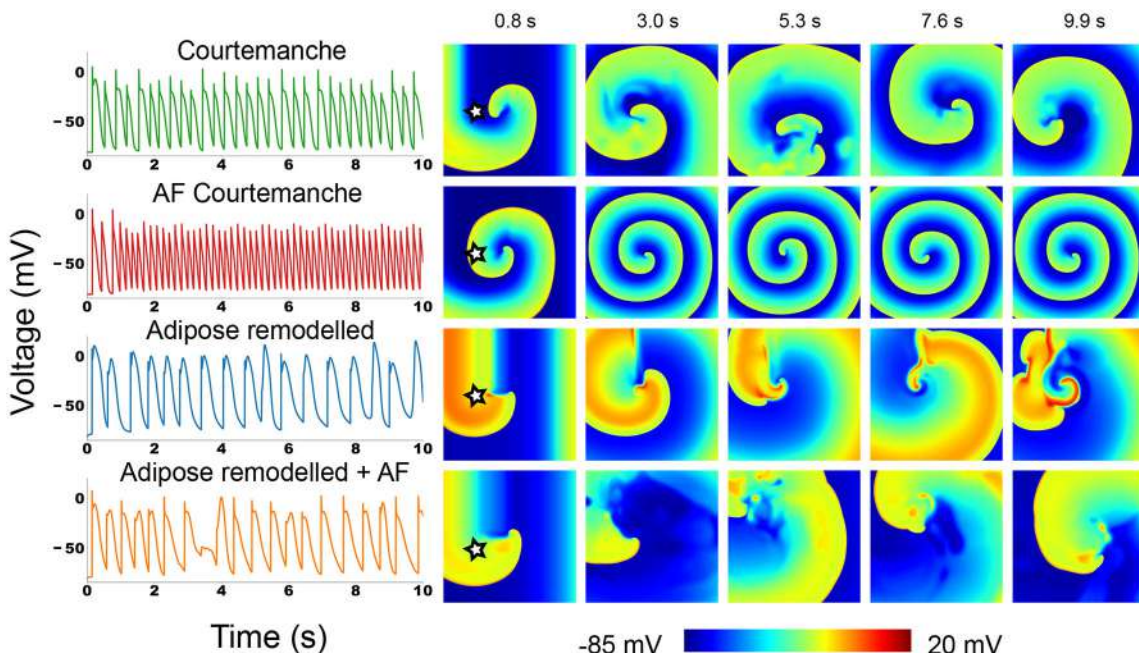


FIGURE 3 | Action potential traces and voltage snapshots of an S1S2 induced spiral in all four of the studied atrial myocyte models. The action potential traces were taken at the point denoted by a star in the first depicted time frame.

These dynamics also correspond to what has previously been observed for this model (Courtemanche et al., 1999).

For adipose remodeled tissue in both cases we observe completely different dynamics: the complexity of the pattern increases due to multiple successive break-ups of the spiral.

The regular Courtemanche model with adipose remodeling (third row in Figure 3) shows initially regular spiral behavior. However, temporary block in the rotating spiral makes for interesting changes in the behavior of the cells. The characteristic feature of the observed pattern are the high voltage plateaus (see Supplementary Information Video S1). They create block that initializes the first spots where reentry can occur. However, due to the elongated tail of the action potential when a wave passes

this region, its propagation is further disturbed which again can mediate block. In this way an irregular pattern is slowly generated that remains present. The spatio-temporal irregularity increases in time.

In the model where both AF remodeling and adipose remodeling were applied (bottom row in Figure 3), we see similar behavior. The initial spiral undergoes multiple break-ups in the course of time. We can see that this is due to calcium dynamics. The break-up is however less pronounced than in the previous case. The disturbance is lower than in the previous case, but is still able to produce temporal block. On top of this phenomenon, we observe that the spiral rotation period decreases due to the AF remodeling. This makes that after such a temporal block, a

quick rotation follows. This makes the curvature of the wavefront become too large and results in additional breaks. Once again this results in complex spatio-temporal excitation patterns.

Overall we can conclude that adding the adipose remodeling results in larger complexity of the spiral wave dynamics.

3.3.2. Effect of an Adipose Remodeled Patch on Spiral Wave Dynamics

In normal conditions the epicardial fat occupies only a part of the atrial tissue. We therefore also studied how the presence of a patch of a certain size of adipose remodeled tissue will affect the dynamics of an existing spiral wave. We investigated circular adipose remodeled patches placed into normal or AF remodeled tissue. We induced arrhythmia by an S1S2 mechanism.

Depending on the size of the arrhythmia and the combination of tissue, different cases of wave dynamics are observed (**Figure 4**).

The first case consists of spiral wave anchoring. Upon initiation of the spiral, it quickly attaches itself to the boundary of the adipose remodeled patch, after which it rotates around and, due to its longer APD duration periodically invades the patch itself. This is the case for the two smallest radii (1.536 and 3.072 cm) when having the normal Courtemanche model with an adipose remodeled patch. In case of the AF Courtemanche model with an AF and adipose remodeled patch, this behavior occurs for larger radii as well (up to 6.144 cm). In both cases, the spiral takes longer to anchor itself the larger the radius of the patch is in case it gets initiated in the center of the patch. For the smallest radius of the regular Courtemanche model with adipose remodeled patch, this was difficult to accomplish and it can be seen that it takes a while before this happens (see **Video S2**).

The second case consists of spiral wave spatio-temporal irregularity. When the spiral is initiated in the middle of the patch, it creates wave-blocks by means of the methods described earlier. This process stays inside the patch and creates irregular activation patterns. The radii where this behavior occurs are the five largest ones for the leftmost tissue configuration presented in **Figure 4** (6.144, 7.680, 9.216, 10.752, and 12.288 cm), and the four largest ones for the rightmost configuration.

And finally, the third case consists of a spiral influencing remodeled patch. It was observed in one instance: a radius of 4.608 cm with a Courtemanche and adipose remodeled patch configuration. Inside the patch some irregular behavior is present. Over the course of time, this irregular behavior produces waves which it pushes outside of the patch which can be seen in **Figure 4** in the 5 s frame. These irregularities influence the spiral wave behavior, making that the spiral doesn't attach to the patch but rather moves in close proximity of it. This case can be seen in the Supplementary Information in **Video S3**.

Upon inducing a spiral inside a remodeled patch, the arrhythmia is sustained but varies in complexity depending on the radius of the patch.

3.3.3. Effect of an Adipose Remodeled Patch on Spiral Wave Initiation

We have also studied the possibility to induce arrhythmia by high frequency pacing due to the presence of an adipose remodeled patch.

In the previous section a spiral was induced *ad-hoc*. We also looked at spontaneous induction of spirals. We did this by means of an S1S2 protocol that could initialize a figure of 8 reentry pattern. However, when trying this protocol on both cases (regular and an adipose remodeled patch, and AF remodeled and an AF plus adipose remodeled patch), it was observed that patches are needed that have an unphysical dimension (radius larger than 11 cm) to induce this kind of reentry. Therefore, in real atria, arrhythmia will not spontaneously induce itself at low frequencies as the patch sizes that can fit in an atrium are smaller.

Since the size of a patch is a limit to its arrhythmogenicity, we looked to the minimal frequency to get arrhythmia in a patch as well. The size we used to measure this minimal frequency is a radius of 4.608 cm. This radius was chosen for both cases, regular and adipose remodeled patch, and AF remodeled and AF plus adipose remodeled patch. This particular choice was made since that radius constitutes the regime where you switch between an attached spiral and spiral wave spatio-temporal irregularity. We found that in the first case, with regular tissue and an adipose remodeled patch, the first spontaneous break-up occurs between a frequency of 1.3 and 1.4 Hz or otherwise said a BCL shorter than 800 ms, but larger than 700 ms. When we look at AF remodeled tissue with an AF plus adipose remodeled patch, we observe a minimal frequency between 2.0 and 2.2 Hz or a BCL that has to be smaller than 500 ms but larger than 450 ms.

3.4. Realistic Human Atria

After studying effects of adipose remodeling in two dimensions, we performed similar studies in an anatomical model of human atria. Clinical and experimental observations show that epicardial fat occurs at the left or right atrial appendages. **Figure 5** shows the anatomy of the human atria in our model and also highlights the appendages and the fiber directions.

3.4.1. S1S2 Spiral Induction

We have first studied dynamics of spiral waves induced by an S1-S2 protocol for three configurations. The first one consisted of the homogeneous atrium with the Courtemanche model. The second one was the same but with both atrial appendages adipose remodeled. The third configuration consisted of the whole tissue being AF remodeled and the atrial appendages being AF and adipose remodeled. Spirals were induced outside of the atrial appendages to see what the effect of the remodeled appendages would be on the dynamics of the arrhythmia. We considered two placements of the spiral wave: in the left atrium and in the right atrium. Each case was simulated twice: two locations for the spiral were chosen in the right atrium, and two in the left atrium. Results were similar for different locations of the spiral in the left or right atrium. The results of one of the locations in each half of the atria can be seen in **Figure 5**. One representative frame out of each simulation is shown.

3.4.2. Spiral Wave Dynamics

Upon initiation of the spiral wave for the first case (regular Courtemanche model everywhere), we are able to see that the spiral remains in the atria at all times and does not create additional complexity or break-up. Some distortions of the wavefront are observed however, though they do not change the

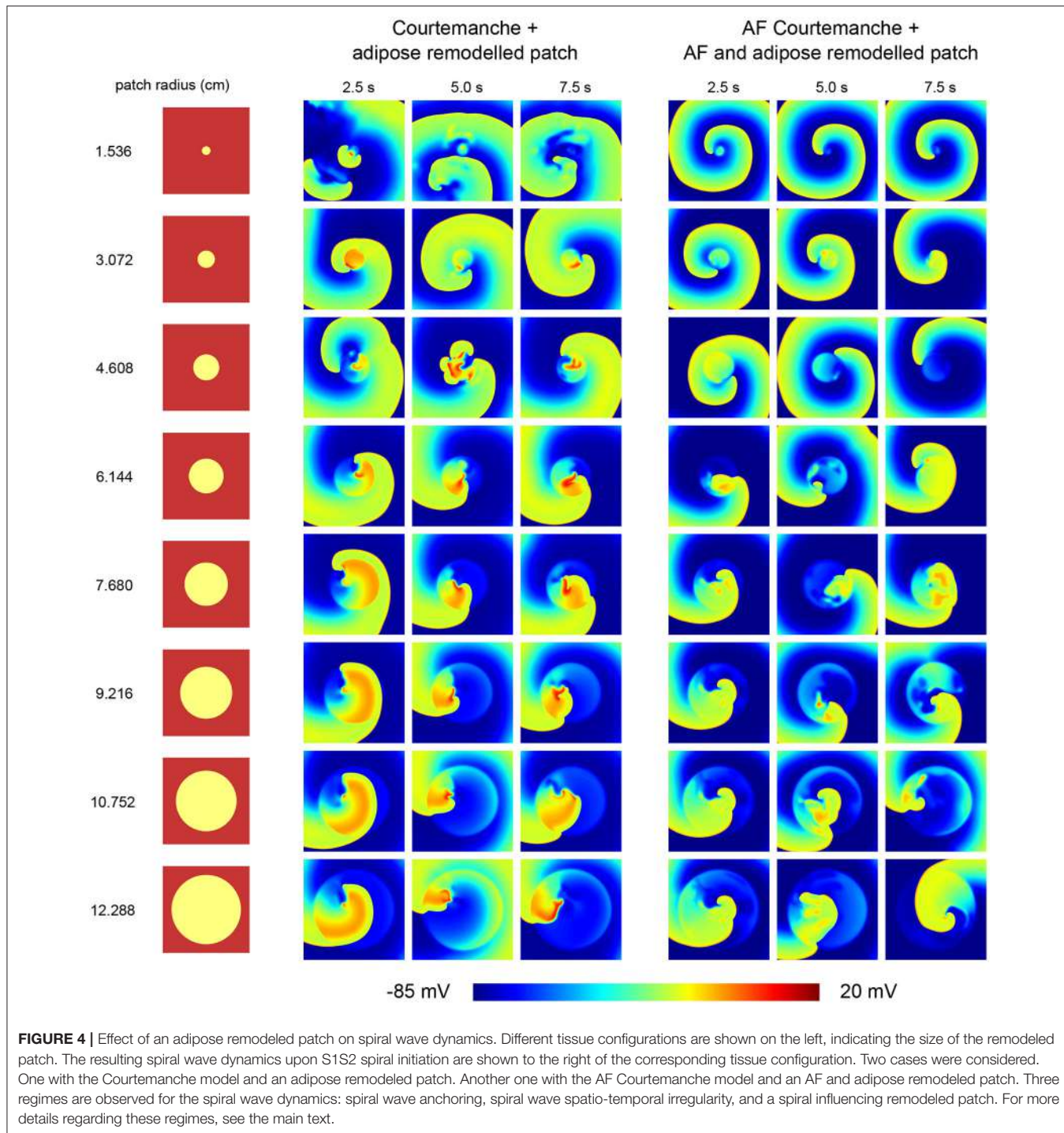


FIGURE 4 | Effect of an adipose remodeled patch on spiral wave dynamics. Different tissue configurations are shown on the left, indicating the size of the remodeled patch. The resulting spiral wave dynamics upon S1S2 spiral initiation are shown to the right of the corresponding tissue configuration. Two cases were considered. One with the Courtemanche model and an adipose remodeled patch. Another one with the AF Courtemanche model and an AF and adipose remodeled patch. Three regimes are observed for the spiral wave dynamics: spiral wave anchoring, spiral wave spatio-temporal irregularity, and a spiral influencing remodeled patch. For more details regarding these regimes, see the main text.

overall dynamics of the arrhythmia, neither in the left nor the right atrium. The single stable spiral can be seen in **Figure 5**. The core of the spiral is denoted by an open circle in the leftmost panel of the RA-spiral and the rightmost panel in the LA-spiral on the top row of the voltage patterns.

For the second case, where the appendages are adipose remodeled, the observed dynamics is more complex. Both in the case of the right and the left atrium we obtain break-ups that

disappear again over the course of time. The break-ups always occur in the right atrium. When the spiral is present in the right atrium, the breaks occur mostly around the atrial appendage and the *crista terminalis* (see the middle panel of the RA-spiral in **Figure 5** in the second row of the voltage patterns). When the spiral is present in the left atrium, some breaks occur around the right atrial appendage (see the leftmost panel of the LA-spiral in **Figure 5** in the second row of the voltage patterns). The reason

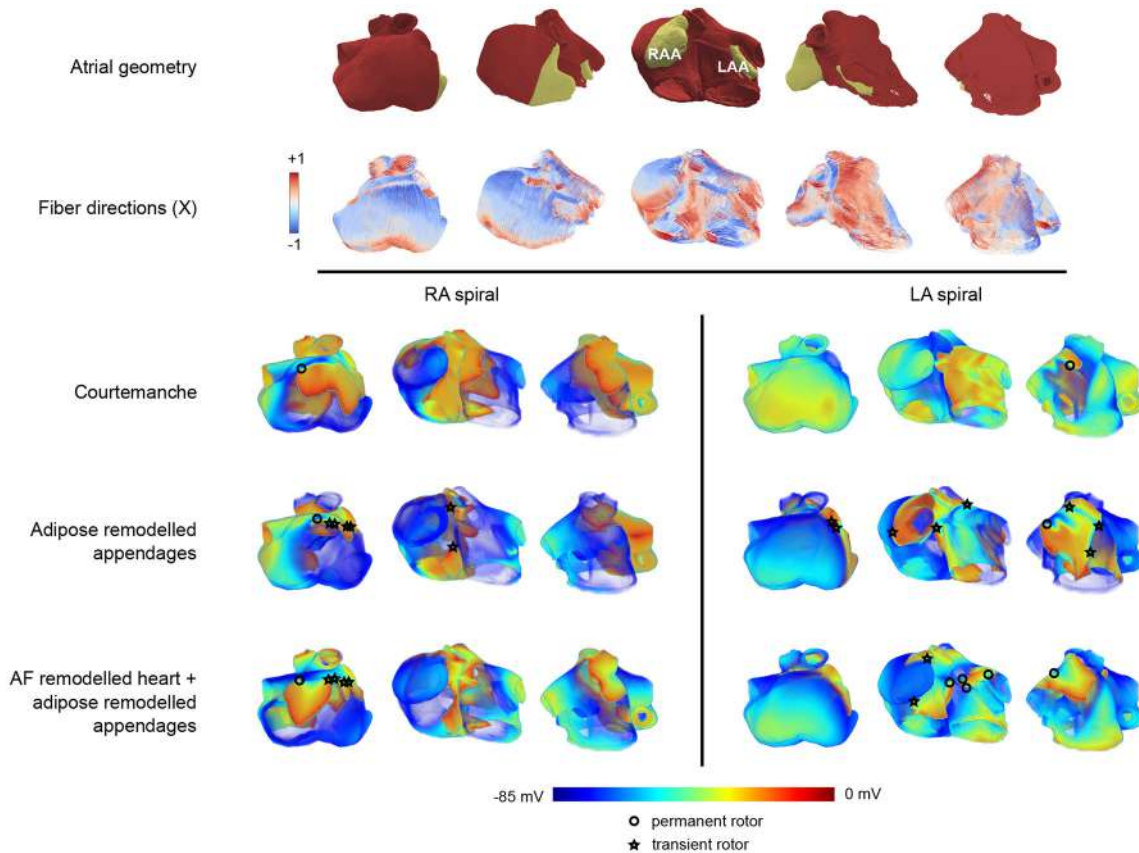


FIGURE 5 | Arrhythmia patterns in three dimensional realistic atria. The top two rows of panels show the configuration in five different orientations. The top row provides a view on the geometry of the atria where the appendages are colored in yellow, and the remaining part of the atria is colored in red. The second row provides the corresponding fiber orientation colored according to its orientation along one of the axes (X). In these five panels, the leftmost orientation provides a view on the right atrium, while the rightmost one provides a view on the left atrium. The panels in between show a rotation between those two configurations showing the front view of the atria. In the voltage maps at the bottom only the leftmost, middle, and rightmost configuration are presented. The three lower rows (split into two columns) show one frame out of an S1-S2 induced arrhythmia in three different orientations. Each row corresponds to the tissue types that were used (Courtemanche, Courtemanche + adipose remodeled appendages, AF Courtemanche + AF and adipose remodeled appendages). Each column corresponds to the location where the arrhythmia was initialized (in the right atrium, or in the left atrium). One can see different kinds of electrical wave propagation complexity for the different combinations present. The cores of spirals are denoted by either circles or stars. The circle denotes a rotor that remains during the whole arrhythmia simulation. The star indicates that the rotor disappears over the course of time.

breaks occur in the opposite atrium are due to the larger size of the right atrial appendage which has a high influence on its surroundings. In this last case of the spiral in the left atrium we can also see increased complexity of the wave pattern in the left atrium itself. Break-ups do occur, but are short-lived. A clear increase in complexity can be seen with respect to the previous case. The spiral in the left atrium also creates a more complex pattern than the one in the right atrium.

In the third case, with AF remodeled tissue together with AF and adipose remodeled appendages, even more complexity is observed. In both the cases of RA-spiral and LA-spiral additional transient spirals occur. In the RA-spiral case they appear mainly around the *crista terminalis* due to its fiber orientation, although some spirals may be observed around the right atrial appendage as well. In the case of the LA-spiral the disappearing spirals occur once again in the right atrium. There are however also new spirals created in the left atrium which do not disappear

but instead remain active over the course of time. They occur due to the presence of the strongly pronounced fiber direction of Bachmann's bundle in combination with the waveblock that occurs due to the left atrial appendage. A total of five spirals is observed. Just as in the previous cases, all spiral cores are denoted by circles (permanent) or stars (transient) in Figure 5. It is again clear that the spiral in the left atrium makes for a more complex pattern than the one in the right atrium.

For all cases, movies can be found in the **Supplementary Information**.

4. DISCUSSION

4.1. Findings

Adipose tissue is an important factor that contributes to arrhythmias. The fat is mainly located on the epicardial wall of the atria, or infiltrating in it. Epicardial adipose tissue infiltrates

can cause local inflammation which results in fibrosis (Haemers et al., 2017). The arrhythmogenic consequences of fibro-fatty remodeling have been discussed earlier (De Coster et al., 2018). The possible effects for electrophysiological remodeling of neighboring myocytes by these adipocytes are not yet studied. Experimental data using patch clamp has revealed adipocyte induced remodeling of the cardiomyocyte electrophysiology (Lin et al., 2012). We use these results measured on rabbit atria, project them to human tissue and investigate the possible effects of the observed remodeling.

While only focusing on the ionic changes that happened to the cell, we were able to reproduce the correct cell-membrane voltage behavior. There is an increase in RMP, a higher plateau level and APD lengthening. Therefore, our model provides the same qualitative results as were observed experimentally.

In chronic AF, one typically observes shortening of APD duration (Nattel et al., 2008). The observed prolongation of the APD by adipocytes was therefore proposed as the possible mechanism for induction of the arrhythmia, by inducing further heterogeneity in APD within the atria. We observed in the model that due to ionic changes we have a more-positive resting membrane potential and a longer APD. These changes reduce the depolarizing threshold and result in easier induction of arrhythmia.

We show that in 2D monolayers complex spiral wave dynamics are seen. It is observed that heterogeneities cause arrhythmias, however, they terminate spontaneously. The minimal size of an adipose remodeled patch to create arrhythmia is substantially large. For smaller patches, the arrhythmia can be induced but it normally passes through and terminates. This would correspond to transient atrial flutter. Short episodes of arrhythmia occur as a result of high frequency pacing, however to be sustained the spiral should be able to rotate inside the adipose remodeled patch. This has to do with symmetry breaking. When a spiral is spontaneously induced inside a circular patch it will need more space since two symmetric spirals should be able to rotate. When the symmetry is broken, smaller sizes are needed to keep the arrhythmia alive. For spontaneously induced arrhythmia this means that one needs a large patch (larger than the atrial appendages in realistic human atria), while the S1S2 induced arrhythmias could be sustained in patches that are comparable to the size of a human atrial appendage.

We studied induced spirals in fully remodeled tissue as well and can see that they are persistent and create additional breaks. The arrhythmias are more complex under adipose remodeling than without it, both in the case of regular Courtemanche as AF Courtemanche. A single rotor seems to be necessary in realistic atria (smaller patches) to create AF. These rotors could be created, for example, due to structural remodeling of adipose tissue or fibrosis (De Coster et al., 2018). Once the spiral core is present inside the adipose remodeled patch, an increase in complexity of the spiral wave pattern, can be seen, corresponding to AF.

For realistic human atria, additional factors need to be taken into account. One of them is the geometry, another one is the fiber structure.

We see that arrhythmia complexity increases from regular Courtemanche to the adipose remodeled appendages model,

and further for the AF and adipose remodeled appendages model. The arrhythmias were obtained by inducing a spiral with an S1S2-protocol. Spontaneously generating an arrhythmia was not successful. This can be attributed to the small size of the appendages.

The left atrium was clearly more prone to rotors than the right one due to the fact that the fiber orientation is inherently different in the left and right atrium. The current model has the fiber directions obtained from a mathematical model based on some measurements of anisotropy in few regions of atria (Dössel et al., 2012). Measuring of anisotropy of full atria would enhance the accuracy of simulation. Currently the left atrial appendage is not sufficiently large to obtain sustained arrhythmia. However, in AF it is known that the atria dilate which increases the size of the left atrial appendage. It would therefore be interesting to obtain anatomical data on dilated atrial appendages and study how it will affect the results on induction of the arrhythmia.

4.2. Limitations

Although the results show pronounced arrhythmogenic effects, we need to consider them with caution. Despite the adaptation of the model toward the human atrial myocyte, the original measurements of the ionic current remodeling were based on rabbit data. The experimental measurements were also performed with a short amount of time in co-culture (Lin et al., 2012). Chronic remodeling occurs over much longer time frames, which might result in different effects on the currents.

Rabbit atrial cells don't behave exactly the same as human atrial cells however, despite the fact they show many similarities. The most notable difference is in the transient outward potassium current I_{to} (Wang et al., 1999). This current repolarizes slower for rabbit than for human. Since we looked at relative changes, it is assumed that no effects due to this different time-dependence will occur.

The temperature of the measured currents in Lin et al. (2012) was at room temperature. The temperature changes are present in both the regular myocytes as well as the adipose remodeled myocytes. We are always looking at relative changes in currents. Therefore, the parts that get affected by the temperature are assumed to cancel out once you take the relative value. For this reason, temperature dependence of the measured currents is not taken into account here. In addition, in Lin et al. (2012) only differences in the peak I-V values of major currents are measured. However, remodeling can affect not only the peak values, but also activation and inactivation kinetics of the currents. Changes in time kinetics of the channels may add additional effects on adipose remodeling and its effect on onset of arrhythmias. To account for these effects, more measurements of currents and their activation-inactivation kinetics in co-cultures with human atrial myocytes at body temperature should be done for different durations of contact with adipocytes. With that kind of data it will be possible to represent adipose remodeling not as voltage-dependent scaling factors but through a novel formulation of equations for each current separately. This can subsequently be used to study more accurately effects of adipose remodeling on arrhythmogenicity.

In our paper we used the standard Courtemanche model for normal and AF remodeled atrial tissue (Courtemanche et al.,

1998, 1999). This model is one of the most widely used ones in atrial modeling (see e.g., Nattel et al., 2007; Pandit and Jalife, 2013). Recently new models for atrial remodeling were proposed. For example Loewe et al. (2014) proposed a model which accounts for chronic atrial fibrillation changes. It does so by changing potassium currents and increasing the cell capacitance based on a literature study. It will be interesting to find out if adipose tissue remodeling will have similar effects in this model and this should be addressed in a subsequent study. Possible dependency of the results of cardiac modeling on the cell model used, was also stressed in a recent study (Muszkiewicz et al., 2017), which investigated how variability in specific ionic currents impacts the phenotypic variability observed in human atrial cells. The authors compared three models: Courtemanche et al. (1998), Malek et al. (2009), and Grandi et al. (2011) and found that in order to reproduce the same experimental data, models need to be changed differently and thus the same changes in conductances of ionic currents in different model can produce different effects.

It should be noted that the readjustment factors of the currents derived from these measurements are only important for large values of the currents. When the current is close to zero, the form of the readjustment factor does not matter that much. Hence a plot that uses either a constant or a parabolic factor (e.g., I_{Na}) is only important near the points where the current is non-zero ($-80 \text{ mV} < V < -20 \text{ mV}$). As in this range the readjustment factor is constant we chose the constant approximation. Even if outside of this range we can have substantial deviations from this approximation it will not affect the results. Another issue is the presence of an extra peak at 40 mV for I_{CaL} in the I-V curve. This peak does not look physiological and occurs due to the combination of the behavior of the Courtemanche model together with our fit of the scaling factors. We decided to keep this representation and make no further adjustments for voltages $V > 30 \text{ mV}$, as such voltage range is not reached in our simulations. However, it is obviously a limitation of this approach and should be possibly corrected in the future.

Earlier, chronic AF remodeling was already mentioned. It has been shown that adipose infiltrates are the beginning stage in the development toward chronic AF. We are therefore modeling the beginning stages of full scale chronic arrhythmia. The model that was currently used is the Courtemanche model and the AF model from Courtemanche. We apply adipose remodeling to both these models to look for possible effects on wave dynamics. However, it would be interesting to follow up these models and see how they evolve. More ionic changes as a result of adipose arrhythmogenicity could make the system end up in the cAF model from Loewe et al. (2014), or it might end up in an adipose remodeled version of that model. More research will need to be conducted to look at the time evolution of the models such that they can end up in chronic atrial fibrillation.

In our 2D simulations with an adipose remodeled patch, the spiral wave was sustained only if it was rotating inside this patch. Such tendency of attachment of the spiral to the patch region can be understood as drift of the spiral wave to the regions with longer period. This was observed in various models

of cardiac tissue (Rudenko and Panfilov, 1983; Ten Tusscher and Panfilov, 2003). In addition, such heterogeneities can potentially attract existing rotors, leading to anchoring Defauw et al. (2014) as it could be seen in the case of the smallest radius with the Courtemanche model and adipose remodeled patch.

In our simulations, spiral waves were initiated by an S1S2 protocol. It would also be interesting to study other mechanisms of initiation of spiral waves, such as due to curvature effects (Pertsov et al., 1983), or heterogeneity in the refractory period (Panfilov and Vasiev, 1991). One can then study if the mechanism of initiation will affect the dynamics of spiral waves. In addition, it would be interesting to study if ionic remodeling can affect the process of defibrillation of cardiac tissue (Keener and Panfilov, 1996).

We also did not study combined structural and ionic remodeling. This was done due to the size difference between our study of structural remodeling and the one of ionic remodeling. The three-dimensional model would not be able to distinguish between adipocyte obstacles and fibrotic obstacles. It would be interesting to do however when more detailed heart data will be available. A recent example of such data can be found in Stephenson et al. (2017). Such study will also be interesting because recent work by Morgan et al. (2016), showed that myocyte-fibroblast coupling in the atria also increases the resting membrane potential of the myocytes, similar to adipose remodeling. Thus, a combined consideration of fibrotic and adipose remodeling can further attenuate possible arrhythmogenic effects.

5. CONCLUSION

As an outlook toward further studies, we can say that the obstacle nature of an adipocyte creates conditions for the onset of arrhythmia, while the remodeling part makes it more persistent and increases complexity. Together they form the basis of an arrhythmia that is difficult to terminate.

This gives rise to two ways of handling adipose induced arrhythmias. On the one hand by focusing on prevention of adipose infiltrates themselves such that one can take and remove the trigger mechanism. On the other hand one could suppress the adipocytes from changing ionic properties which helps to make arrhythmias less complex.

We have shown that adipose tissue remodeling substantially affects the dynamics of existing cardiac arrhythmias leading to breakup and an increasing complexity of the activation pattern. However, onset of new arrhythmias requires that this remodeling occurs in substantially large regions. We also discussed the implications of the presence of adipose tissue and combined effects of AF and adipose remodeling.

AUTHOR CONTRIBUTIONS

TDC and AP designed the numerical experiments. TDC wrote and tested the implementation of the model, performed the numerical experiments and did post-processing. GS provided the

anatomical atrial voxel model. TDC, PC, and AP analyzed the results and prepared the draft of the manuscript. TDC, PC, GS, RW, KS, and AP critically revised the manuscript.

FUNDING

This work was supported by the Interuniversity Attraction Poles (IAP P7/10) Program, Belgium (to RW, KS, and AP), and a KU

Leuven Program Financing grant (PF 10/014), Belgium (to PC and KS).

SUPPLEMENTARY MATERIAL

The Supplementary Material for this article can be found online at: <https://www.frontiersin.org/articles/10.3389/fphys.2018.01381/full#supplementary-material>

REFERENCES

- Aslanidi, O. V., Colman, M. A., Stott, J., Dobrzynski, H., Boyett, M. R., Holden, A. V., et al. (2011). 3D virtual human atria: a computational platform for studying clinical atrial fibrillation. *Prog. Biophys. Mol. Biol.* 107, 156–168. doi: 10.1016/j.pbiomolbio.2011.06.011
- Clerx, M., Collins, P., de Lange, E., and Volders, P. G. A. (2016). Myokit: a simple interface to cardiac cellular electrophysiology. *Prog. Biophys. Mol. Biol.* 120, 100–114. doi: 10.1016/j.pbiomolbio.2015.12.008
- Courtemanche, M., Ramirez, R. J., and Nattel, S. (1998). Ionic mechanisms underlying human atrial action potential properties: insights from a mathematical model. *Am. J. Physiol. Heart Circ. Physiol.* 275, H301–H321.
- Courtemanche, M., Ramirez, R. J., and Nattel, S. (1999). Ionic targets for drug therapy and atrial fibrillation-induced electrical remodeling: insights from a mathematical model. *Cardiovasc. Res.* 42, 477.
- De Coster, T., Claus, P., Kazbanov, I. V., Haemers, P., Willems, R., Sipido, K. R., et al. (2018). Arrhythmogenicity of fibro-fatty infiltrations. *Sci. Rep.* 8:2050. doi: 10.1038/s41598-018-20450-w
- Defauw, A., Vandersickel, N., Dawyndt, P., and Panfilov, A. V. (2014). Small size ionic heterogeneities in the human heart can attract rotors. *Am. J. Physiol. Heart Circ. Physiol.* 307, H1456–H1468. doi: 10.1152/ajpheart.00410.2014
- Dössel, O., Krueger, M. W., Weber, F. M., Wilhelms, M., and Seemann, G. (2012). Computational modeling of the human atrial anatomy and electrophysiology. *Med. Biol. Eng. Comput.* 50, 773–799. doi: 10.1007/s11517-012-0924-6
- Dublin, S., French, B., Glazer, N. L., Wiggins, K. L., Lumley, T., Psaty, B. M., et al. (2006). Risk of new-onset atrial fibrillation in relation to body mass index. *Arch. Intern. Med.* 166, 2322–2328. doi: 10.1001/archinte.166.21.2322
- Go, A. S., Hylek, E. M., Phillips, K. A., Chang, Y., Henault, L. E., Selby, J. V., et al. (2001). Prevalence of diagnosed atrial fibrillation in adults: national implications for rhythm management and stroke prevention: the anticoagulation and risk factors in atrial fibrillation (atria) study. *JAMA* 285, 2370–2375. doi: 10.1001/jama.285.18.2370
- Grandi, E., Pandit, S. V., Voigt, N., Workman, A. J., Dobrev, D., Jalife, J., et al. (2011). Human atrial action potential and Ca^{2+} model: sinus rhythm and chronic atrial fibrillation. *Circ. Res.* 109, 1055–1066. doi: 10.1161/CIRCRESAHA.111.253955
- Haemers, P., Hamdi, H., Guedj, K., Suffee, N., Farahmand, P., Popovic, N., et al. (2017). Atrial fibrillation is associated with the fibrotic remodelling of adipose tissue in the subepicardium of human and sheep atria. *Eur. Heart J.* 38, 53–61. doi: 10.1093/eurheartj/ehv625
- Keener, J. P., and Panfilov, A. (1996). A biophysical model for defibrillation of cardiac tissue. *Biophys. J.* 71, 1335.
- Konings, K., Kirchhof, C., Smeets, J., Wellens, H., Penn, O. C., and Allessie, M. A. (1994). High-density mapping of electrically induced atrial fibrillation in humans. *Circulation* 89, 1665–1680.
- Lin, Y. K., Chen, Y. C., Chen, J. H., Chen, S. A., and Chen, Y. J. (2012). Adipocytes modulate the electrophysiology of atrial myocytes: implications in obesity-induced atrial fibrillation. *Basic Res. Cardiol.* 107:293. doi: 10.1007/s00395-012-0293-1
- Lin, Y. K., Chen, Y. J., and Chen, S. A. (2010). Potential atrial arrhythmogenicity of adipocytes: implications for the genesis of atrial fibrillation. *Med. Hypotheses* 74, 1026–1029. doi: 10.1016/j.mehy.2010.01.004
- Lip, G. Y. H., Kakar, P., and Watson, T. (2007). Atrial fibrillation—the growing epidemic. *Heart* 93, 542–543. doi: 10.1136/hrt.2006.110791
- Liu, T. Y., Tai, C. T., Huang, B. H., Higa, S., Lin, Y. J., Huang, J. L., et al. (2004). Functional characterization of the crista terminalis in patients with atrial flutter: implications for radiofrequency ablation. *J. Am. Coll. Cardiol.* 43, 1639–1645. doi: 10.1016/j.jacc.2003.11.057
- Loewe, A., Lutz, Y., Wilhelms, M., Sinnecker, D., Barthel, P., Scholz, E. P., et al. (2014). *In-silico* assessment of the dynamic effects of amiodarone and dronedarone on human atrial patho-electrophysiology. *Europace* 16(Suppl. 4), iv30–iv38. doi: 10.1093/europace/euu230
- Malek, M. M., Greenstein, J. L., Giles, W. R., and Trayanova, N. A. (2009). K^{+} current changes account for the rate dependence of the action potential in the human atrial myocyte. *Am. J. Physiol. Heart Circ. Physiol.* 297, H1398–H1410. doi: 10.1152/ajpheart.00411.2009
- Morgan, R., Colman, M. A., Chubb, H., Seemann, G., and Aslanidi, O. V. (2016). Slow conduction in the border zones of patchy fibrosis stabilizes the drivers for atrial fibrillation: insights from multi-scale human atrial modeling. *Front. Physiol.* 7:474. doi: 10.3389/fphys.2016.00474
- Muszkiewicz, A., Liu, X., Bueno-Orovio, A., Lawson, B. A., Burrage, K., Casadei, B., et al. (2017). From ionic to cellular variability in human atrial myocytes: an integrative computational and experimental study. *Am. J. Physiol. Heart Circ. Physiol.* 314, H895–H916. doi: 10.1152/ajpheart.00477.2017
- Nattel, S., Burstein, B., and Dobrev, D. (2008). Atrial remodeling and atrial fibrillation: mechanisms and implications. *Circ. Arrhythm. Electrophysiol.* 1, 62–73. doi: 10.1161/CIRCEP.107.754564
- Nattel, S., Maguy, A., Le Bouter, S., and Yeh, Y. H. (2007). Arrhythmogenic ion-channel remodeling in the heart: heart failure, myocardial infarction, and atrial fibrillation. *Physiol. Rev.* 87, 425–456. doi: 10.1152/physrev.00014.2006
- Pandit, S. V., and Jalife, J. (2013). Rotors and the dynamics of cardiac fibrillation. *Circ. Res.* 112, 849–862. doi: 10.1161/CIRCRESAHA.111.300158
- Panfilov, A., and Vasiev, B. (1991). Vortex initiation in a heterogeneous excitable medium. *Phys. D Nonlinear Phenomena* 49, 107–113.
- Pantanowitz, L. (2001). Fat infiltration in the heart. *Heart* 85:253. doi: 10.1136/heart.85.3.253
- Pertsov, A. M., Panfilov, A. V., and Medvedeva, F. U. (1983). Instabilities of autowaves in excitable media associated with critical curvature phenomena. *Biofizika* 28, 100–102.
- Rudenko, A., and Panfilov, A. (1983). Drift and interaction of vortices in two-dimensional heterogeneous active medium. *Stud. Biophys.* 98, 183–188.
- Rush, S., and Larsen, H. (1978). A practical algorithm for solving dynamic membrane equations. *IEEE Trans. Biomed. Eng.* 25, 389–392.
- Samanta, R., Pouliopoulos, J., Thiagalingam, A., and Kovoov, P. (2016). Role of adipose tissue in the pathogenesis of cardiac arrhythmias. *Heart Rhythm* 13, 311–320. doi: 10.1016/j.hrthm.2015.08.016
- Stephenson, R. S., Atkinson, A., Kottas, P., Perde, F., Jafarzadeh, F., Bateman, M., et al. (2017). High resolution 3-dimensional imaging of the human cardiac conduction system from microanatomy to mathematical modeling. *Sci. Rep.* 7:7188. doi: 10.1038/s41598-017-07694-8
- Stewart, S., Murphy, N., Walker, A., McGuire, A., and McMurray, J. (2004). Cost of an emerging epidemic: an economic analysis of atrial fibrillation in the UK. *Heart* 90, 286–292. doi: 10.1136/heart.2002.008748
- Ten Tusscher, K., and Panfilov, A. V. (2003). Reentry in heterogeneous cardiac tissue described by the luo-rudy ventricular action potential model. *Am. J. Physiol. Heart Circ. Physiol.* 284, H542–H548. doi: 10.1152/ajpheart.00608.2002
- Thrall, G., Lane, D., Carroll, D., and Lip, G. Y. (2006). Quality of life in patients with atrial fibrillation: a systematic review. *Am. J. Med.* 119, 448.e1–448.e19. doi: 10.1016/j.amjmed.2005.10.057

- Tsang, T. S., Barnes, M. E., Miyasaka, Y., Cha, S. S., Bailey, K. R., Verzosa, G. C., et al. (2008). Obesity as a risk factor for the progression of paroxysmal to permanent atrial fibrillation: a longitudinal cohort study of 21 years. *Eur. Heart J.* 29, 2227–2233. doi: 10.1093/eurheartj/ehn324
- Wanahita, N., Messerli, F. H., Bangalore, S., Gami, A. S., Somers, V. K., and Steinberg, J. S. (2008). Atrial fibrillation and obesity—results of a meta-analysis. *Am. Heart J.* 155, 310–315. doi: 10.1016/j.ahj.2007.10.004
- Wang, T. J., Parise, H., Levy, D., D'Agostino, R. B., Wolf, P. A., Vasan, R. S., et al. (2004). Obesity and the risk of new-onset atrial fibrillation. *JAMA* 292, 2471–2477. doi: 10.1001/jama.292.20.2471
- Wang, Z., Feng, J., Shi, H., Pond, A., Nerbonne, J. M., and Nattel, S. (1999). Potential molecular basis of different physiological properties of the transient outward K^+ current in rabbit and human atrial myocytes. *Circ. Res.* 84, 551–561.
- Yu, T., Lloyd, C. M., Nickerson, D. P., Cooling, M. T., Miller, A. K., Garny, A., et al. (2011). The physiome model repository 2. *Bioinformatics* 27, 743–744. doi: 10.1093/bioinformatics/btq723

Conflict of Interest Statement: The authors declare that the research was conducted in the absence of any commercial or financial relationships that could be construed as a potential conflict of interest.

Copyright © 2018 De Coster, Claus, Seemann, Willems, Sipido and Panfilov. This is an open-access article distributed under the terms of the Creative Commons Attribution License (CC BY). The use, distribution or reproduction in other forums is permitted, provided the original author(s) and the copyright owner(s) are credited and that the original publication in this journal is cited, in accordance with accepted academic practice. No use, distribution or reproduction is permitted which does not comply with these terms.



Commentary: Atrial Rotor Dynamics Under Complex Fractional Order Diffusion

Alfonso Bueno-Orovio*

Department of Computer Science, University of Oxford, Oxford, United Kingdom

Keywords: cardiac tissue, structural heterogeneity, electrical propagation, fractional diffusion, wavefront curvature

A Commentary on

Atrial Rotor Dynamics Under Complex Fractional Order Diffusion

by Ugarte, J. P., Tobón, C., Lopes, A. M., and Tenreiro Machado, J. A. (2018). *Front. Physiol.* 9:975. doi: 10.3389/fphys.2018.00975

OPEN ACCESS

Edited by:

Jichao Zhao,

University of Auckland, New Zealand

Reviewed by:

Juan Pablo Ugarte,

Universidad de San Buenaventura,

Medellín, Colombia

Arun V. Holden,

University of Leeds, United Kingdom

*Correspondence:

Alfonso Bueno-Orovio

alfonso.bueno@cs.ox.ac.uk

Specialty section:

This article was submitted to Computational Physiology and Medicine,

a section of the journal *Frontiers in Physiology*

Received: 30 August 2018

Accepted: 11 September 2018

Published: 04 October 2018

Citation:

Bueno-Orovio A (2018) Commentary: Atrial Rotor Dynamics Under Complex Fractional Order Diffusion. *Front. Physiol.* 9:1386. doi: 10.3389/fphys.2018.01386

Even at healthy states, cardiac tissue conforms one of the most representative cases of a highly heterogeneous and composite biological medium, whose spatial complexity has for long been known to modulate electrical conduction (Frank and Langer, 1974; Spach et al., 1981). How to capture its intricate structural heterogeneity at a tractable cost remains an open challenge in computational physiology and medicine, as traditional approaches such as the monodomain or bidomain equations inherently assume that the tissue behaves as an averaged syncytium with negligible contribution of its composite microstructure.

To overcome some of these limitations, we recently pioneered the use of fractional diffusion for the description of cardiac conduction (Bueno-Orovio et al., 2014b). Our proposed framework took the form

$$\partial_t V = -(-\nabla \cdot \mathbf{D} \nabla V)^{\alpha/2} - \frac{1}{C_m} (I_{\text{ion}} - I_{\text{stim}}), \quad (1)$$

where $-(-\nabla \cdot \mathbf{D} \nabla V)^{\alpha/2}$ is the so-called fractional Laplacian of real order $1 < \alpha \leq 2$. For $\alpha = 2$, the model clearly recovers the standard monodomain equation, and could equally be extended to the bidomain setting. The well-founded potential theory around the fractional Laplacian allowed us to establish its biophysical interpretation, showing it represents the modulation of the electrical field of a homogeneous conductor by the secondary electrical sources associated with its inhomogeneities. The model further helped elucidating formerly unrelated effects of tissue microstructure on cardiac conduction, including widespread of the action potential foot during depolarization, action potential shortening along the activation pathway, and the modulated dispersion of repolarization. Experimentally, the model has been supported by diffusion spectrum imaging in *ex-vivo* hearts, indicating fractional diffusion metrics as indices of myocardial microstructure (Bueno-Orovio et al., 2016), as well as by high-resolution optical mapping on cardiac tissue preparations, demonstrating fractional scaling in the propagation of the cardiac wavelength (Loppini et al., 2018).

In the work under comment, Ugarte et al. build and expand on these ideas to present a two-dimensional isotropic fractional diffusion framework of complex order, of the form

$$\partial_t V = \kappa_\gamma (H_x^\gamma V + H_y^\gamma V) - \frac{1}{C_m} (I_{\text{ion}} - I_{\text{stim}}), \quad (2)$$

with operators H_x^γ and H_y^γ involving pairs of complex-conjugate fractional derivatives defined by

$$H_x^\gamma V = -\frac{1}{2} \left[(-\partial_x^2 V)^{\gamma/2} + (-\partial_x^2 V)^{\bar{\gamma}/2} \right], \quad (3)$$

where $\gamma = \alpha + j\beta$ is the complex fractional order, and $\bar{\gamma}$ its complex conjugate. The authors' interpretation of their complex-order model newly builds on potential theory, which connects potential distributions over fractal domains and the complex-order fractional Laplacian. Indeed, the inclusion of the imaginary part β implies that cardiac tissue must satisfy a discrete-scale fractal structure (self-similarity at discrete scales). Whilst such a self-similarity could perhaps be arguable for the main volumetric constituents of cardiac tissue (cardiomyocytes), other components might very well exhibit a fractal structure (e.g., microvasculature). Importantly, such a complex-order fractional framework holds a great potential for consideration of structural remodeling, shall the associated structures (e.g. fibrotic clefts) be proved to have a fractal nature.

However, an important limitation of Ugarte et al. (2018) is that their proposed model is not consistent with the fractional Laplacian in which the authors base their analysis. Taking $\beta = 0$ for simplicity, Equations (2), (3) then reduce to

$$\partial_t V = -\kappa_\alpha \left((-\partial_x^2 V)^{\alpha/2} + (-\partial_y^2 V)^{\alpha/2} \right) - \frac{1}{C_m} (I_{\text{ion}} - I_{\text{stim}}), \quad (4)$$

known as a fractional Riesz operator (fractional derivatives independently applied in each spatial coordinate). Conversely, under two-dimensional isotropic conditions, the fractional Laplacian model given by Equation (1) becomes

$$\partial_t V = -\kappa_\alpha \left(-\partial_x^2 V - \partial_y^2 V \right)^{\alpha/2} - \frac{1}{C_m} (I_{\text{ion}} - I_{\text{stim}}), \quad (5)$$

where for clarity the same notation κ_α has been used for the equivalent diffusion coefficient. Comparing (4) and (5),

it becomes evident that the proposed fractional model is only equivalent to the fractional Laplacian under the standard diffusion case, given by $\alpha = 2$.

The implications of these subtle but important discrepancies on cardiac conduction are exemplified in **Figure 1**. Simulations illustrate isotropic conduction for both models under decreasing fractional order α , with ion dynamics described for simplicity by Fenton and Karma (1998). Whereas the fractional Laplacian (**Figure 1A**) correctly replicates for all α the circular propagation patterns observed on isotropic cardiac monolayers as the simplest yet inhomogeneous *in-vitro* model of cardiac tissue (Badie and Bursac, 2009; Bian et al., 2014; Molitoris et al., 2016), the fractional Riesz operator (**Figure 1B**) induces increasingly larger curvature artifacts on wavefront conduction for decreasing α . Such curvature artifacts indeed translate into the results of Ugarte et al. (2018), as evidenced by their square-like spiral wavefronts and rotor trajectories. Given the well-known curvature-related modulation of conduction velocity and therefore wavefront-waveback interactions (Fast and Kléber, 1997; Comtois and Vinet, 1999; Comtois et al., 2005; Kadota et al., 2012), their results on vulnerability to re-entry and associated rotor biomarkers thus must be cautiously interpreted.

It is nevertheless relevant to note that more squared propagation patterns have been reported in both optical mapping (Koura et al., 2002; de Diego et al., 2011) and computational (He and Liu, 2010) studies. This was however under marked anisotropic conduction, not accounted in the isotropic model by Ugarte et al. (2018). In addition, fractional Riesz operators have been also used in modeling electrical propagation (Liu et al., 2013, 2015; Zeng et al., 2014). Such works, more centered in numerical analysis than in gaining physiological insights, might be additionally contributing to spreading the inconsistencies between these two types of fractional diffusion operators. Finally, a too coarse spatial resolution for atrial dynamics compared to previous studies (Wilhelms et al., 2013) could also contribute to partially unresolved re-entrant patterns. Although minimized by the high-order approach on which the authors base their

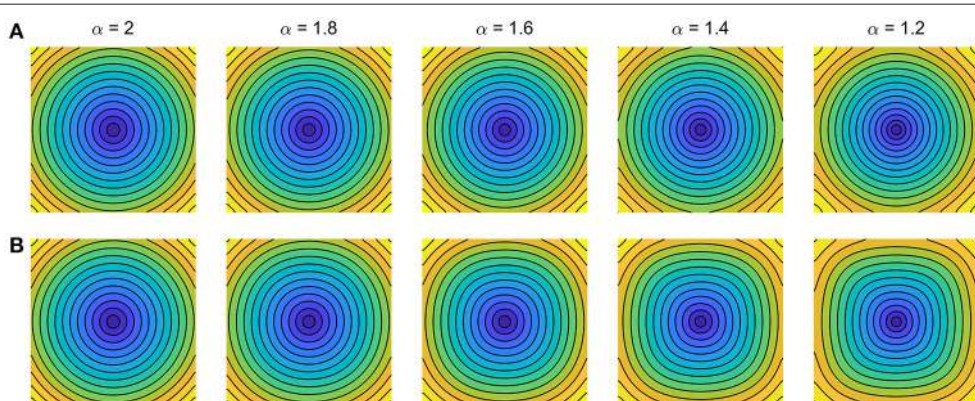


FIGURE 1 | Impact of fractional diffusion operators on cardiac conduction for decreasing order α . Activation maps for central domain stimulation are shown (5 ms separation isochrones). **(A)** Fractional Laplacian (Bueno-Orovio et al., 2014b). **(B)** Fractional Riesz operator (Ugarte et al., 2018). Diffusion coefficients were optimized to match standard diffusion conduction velocity at the center of 5 cm fiber strands. Ionic term: Fenton-Karma (modified Beeler-Reuter) dynamics; domain size: 5 × 5 cm; space discretisation: 512 × 512 points; time resolution: 0.025 ms.

numerical methods (Bueno-Orovio et al., 2014a), allowing considerably larger space steps than traditional stencils, this aspect certainly deserves further consideration.

As previously discussed, the ideas presented in Ugarte et al. (2018) hold a great potential for advancing the field of fractional diffusion applied to cardiac tissue, in order to promote our understanding of the role of tissue microstructure and structural remodeling in modulating wavefront propagation. However, this contribution raises awareness on the definition of suitable fractional diffusion models, exemplifying that simply recovering standard diffusion for a specific value of the considered tissue parameters is not a sufficient condition for realistic cardiac conduction. In this regard, frameworks that are consistent with the fractional Laplacian (Bueno-Orovio

et al., 2014b; Cusimano et al., 2015; Cusimano and Gerardo-Giorda, 2018) seem a more suitable modeling approach to correctly capture the characteristic electrotonic loading of cardiac tissue.

AUTHOR CONTRIBUTIONS

The author confirms being the sole contributor of this work and has approved it for publication.

FUNDING

AB-O holds a British Heart Foundation Intermediate Basic Science Research Fellowship (FS/17/22/32644).

REFERENCES

- Badie, N., and Bursac, N. (2009). Novel micropatterned cardiac cell cultures with realistic ventricular microstructure. *Biophys. J.* 96, 3873–3885. doi: 10.1016/j.bpj.2009.02.019
- Bian, W., Jackman, C. P., and Bursac, N. (2014). Controlling the structural and functional anisotropy of engineered cardiac tissues. *Biofabrication* 6:024109. doi: 10.1088/1758-5082/6/2/024109
- Bueno-Orovio, A., Kay, D., and Burrage, K. (2014a). Fourier spectral methods for fractional-in-space reaction-diffusion equations. *BIT Numer. Math.* 54, 937–954. doi: 10.1186/s40064-016-3295-x
- Bueno-Orovio, A., Kay, D., Grau, V., Rodriguez, B., and Burrage, K. (2014b). Fractional diffusion models of cardiac electrical propagation: role of structural heterogeneity in dispersion of repolarization. *J. R. Soc. Interface* 11:20140352. doi: 10.1098/rsif.2014.0352
- Bueno-Orovio, A., Teh, I., Schneider, J. E., Burrage, K., and Grau, V. (2016). Anomalous diffusion in cardiac tissue as an index of myocardial microstructure. *IEEE Trans. Med. Imaging* 35, 2200–2207. doi: 10.1109/TMI.2016.2548503
- Comtois, P., Kneller, J., and Nattel, S. (2005). Of circles and spirals: bridging the gap between the leading circle and spiral wave concepts of cardiac reentry. *Europace* 7, S10–S20. doi: 10.1016/j.eucp.2005.05.011
- Comtois, P., and Vinet, A. (1999). Curvature effects on activation speed and repolarization in an ionic model of cardiac myocytes. *Phys. Rev. E* 60:4619.
- Cusimano, N., Bueno-Orovio, A., Turner, I., and Burrage, K. (2015). On the order of the fractional Laplacian in determining the spatio-temporal evolution of a space-fractional model of cardiac electrophysiology. *PLoS ONE* 10:e0143938. doi: 10.1371/journal.pone.0143938
- Cusimano, N., and Gerardo-Giorda, L. (2018). A space-fractional monodomain model for cardiac electrophysiology combining anisotropy and heterogeneity on realistic geometries. *J. Comput. Phys.* 362, 409–424. doi: 10.1016/j.jcp.2018.02.034
- de Diego, C., Chen, F., Xie, Y., Pai, R. K., Slavin, L., Parker, J., et al. (2011). Anisotropic conduction block and reentry in neonatal rat ventricular myocyte monolayers. *Am. J. Physiol. Heart Circ. Physiol.* 300, H271–H278. doi: 10.1152/ajpheart.00758.2009
- Fast, V. G., and Kléber, A. G. (1997). Role of wavefront curvature in propagation of cardiac impulse. *Cardiovasc. Res.* 33, 258–271. doi: 10.1016/S0008-6363(96)00216-7
- Fenton, F., and Karma, A. (1998). Vortex dynamics in three-dimensional continuous myocardium with fiber rotation: filament instability and fibrillation. *Chaos* 8, 20–47. doi: 10.1063/1.166311
- Frank, J. S., and Langer, G. A. (1974). The myocardial interstitium: its structure and its role in ionic exchange. *J. Cell Biol.* 60, 586–601. doi: 10.1083/jcb.60.3.586
- He, Z. Z., and Liu, J. (2010). Effect of cardiac tissue anisotropy on three-dimensional electrical action potential propagation. *Mod. Phys. Lett. B* 24, 1847–1853. doi: 10.1142/S0217984910024237
- Kadota, S., Kay, M. W., Magome, N., and Agladze, K. (2012). Curvature-dependent excitation propagation in cultured cardiac tissue. *JETP Lett.* 94, 824–830. doi: 10.1134/S0021364011230044
- Koura, T., Hara, M., Takeuchi, S., Ota, K., Okada, Y., Miyoshi, S., et al. (2002). Anisotropic conduction properties in canine atria analyzed by high-resolution optical mapping: preferential direction of conduction block changes from longitudinal to transverse with increasing age. *Circulation* 105, 2092–2098. doi: 10.1161/01.CIR.0000015506.36371.0D
- Liu, F., Turner, I., Anh, V., Yang, Q., and Burrage, K. (2013). A numerical method for the fractional Fitzhugh–Nagumo monodomain model. *ANZIAM J.* 54, C608–C629. doi: 10.21914/anziamj.v54i0.6372
- Liu, F., Zhuang, P., Turner, I., Anh, V., and Burrage, K. (2015). A semi-alternating direction method for a 2-D fractional FitzHugh–Nagumo monodomain model on an approximate irregular domain. *J. Comput. Phys.* 293, 252–263. doi: 10.1016/j.jcp.2014.06.001
- Loppini, A., Gizzi, A., Cherubini, C., Cherry, E. M., Fenton, F. H., and Filippi, S. (2018). Spatiotemporal correlation uncovers fractional scaling in cardiac tissue. *arXiv* [preprint] arXiv:1806.04507.
- Molitoris, J. M., Paliwal, S., Sekar, R. B., Blake, R., Park, J., Trayanova, N. A., et al. (2016). Precisely parameterized experimental and computational models of tissue organization. *Integr. Biol.* 8, 230–242. doi: 10.1039/C5IB00270B
- Spach, M. S., Miller III, W. T., Geselowitz, D. B., Barr, R. C., Kootsey, J. M., and Johnson, E. A. (1981). The discontinuous nature of propagation in normal canine cardiac muscle. Evidence for recurrent discontinuities of intracellular resistance that affect the membrane currents. *Circ. Res.* 48, 39–54. doi: 10.1161/01.RES.48.1.39
- Ugarte, J. P., Tobón, C., Lopes, A. M., and Tenreiro Machado, J. A. (2018). Atrial rotor dynamics under complex fractional order diffusion. *Front. Physiol.* 9:975. doi: 10.3389/fphys.2018.00975
- Wilhelms, M., Hettmann, H., Maleckar, M. M., Koivumäki, J. T., Dössel, O., and Seemann, G. (2013). Benchmarking electrophysiological models of human atrial myocytes. *Front. Physiol.* 3:487. doi: 10.3389/fphys.2012.00487
- Zeng, F., Liu, F., Li, C., Burrage, K., Turner, I., and Anh, V. (2014). A Crank–Nicolson ADI spectral method for a two-dimensional Riesz space fractional nonlinear reaction-diffusion equation. *SIAM J. Numer. Anal.* 52, 2599–2622. doi: 10.1137/130934192

Conflict of Interest Statement: The author declares that the research was conducted in the absence of any commercial or financial relationships that could be construed as a potential conflict of interest.

Copyright © 2018 Bueno-Orovio. This is an open-access article distributed under the terms of the Creative Commons Attribution License (CC BY). The use, distribution or reproduction in other forums is permitted, provided the original author(s) and the copyright owner(s) are credited and that the original publication in this journal is cited, in accordance with accepted academic practice. No use, distribution or reproduction is permitted which does not comply with these terms.



Atrial Fibrillation Mechanisms and Implications for Catheter Ablation

Ghassen Cheniti^{1,2,3*}, Konstantinos Vlachos^{1,2}, Thomas Pambrun^{1,2}, Darren Hooks⁴, Antonio Frontera^{1,2}, Masateru Takigawa^{1,2}, Felix Bourier^{1,2}, Takeshi Kitamura^{1,2}, Anna Lam^{1,2}, Claire Martin^{1,2}, Carole Dumas-Pommier¹, Stephane Puyo², Xavier Pillois¹, Josselin Duchateau^{1,2}, Nicolas Klotz^{1,2}, Arnaud Denis^{1,2}, Nicolas Derval^{1,2}, Pierre Jais^{1,2}, Hubert Cochet^{2,5}, Meleze Hocini^{1,2}, Michel Haissaguerre^{1,2} and Frederic Sacher^{1,2}

OPEN ACCESS

Edited by:

Gary Tse,
The Chinese University of Hong Kong,
Hong Kong

Reviewed by:

Martin Stiles,
University of Auckland, New Zealand
Henggui Zhang,
University of Manchester,
United Kingdom

*Correspondence:

Ghassen Cheniti
ghassen.cheniti@gmail.com

Specialty section:

This article was submitted to
Computational Physiology and
Medicine,
a section of the journal
Frontiers in Physiology

Received: 30 April 2018

Accepted: 26 September 2018

Published: 17 October 2018

Citation:

Cheniti G, Vlachos K, Pambrun T, Hooks D, Frontera A, Takigawa M, Bourier F, Kitamura T, Lam A, Martin C, Dumas-Pommier C, Puyo S, Pillois X, Duchateau J, Klotz N, Denis A, Derval N, Jais P, Cochet H, Hocini M, Haissaguerre M and Sacher F (2018) Atrial Fibrillation Mechanisms and Implications for Catheter Ablation. *Front. Physiol.* 9:1458. doi: 10.3389/fphys.2018.01458

AF is a heterogeneous rhythm disorder that is related to a wide spectrum of etiologies and has broad clinical presentations. Mechanisms underlying AF are complex and remain incompletely understood despite extensive research. They associate interactions between triggers, substrate and modulators including ionic and anatomic remodeling, genetic predisposition and neuro-humoral contributors. The pulmonary veins play a key role in the pathogenesis of AF and their isolation is associated to high rates of AF freedom in patients with paroxysmal AF. However, ablation of persistent AF remains less effective, mainly limited by the difficulty to identify the sources sustaining AF. Many theories were advanced to explain the perpetuation of this form of AF, ranging from a single localized focal and reentrant source to diffuse bi-atrial multiple wavelets. Translating these mechanisms to the clinical practice remains challenging and limited by the spatio-temporal resolution of the mapping techniques. AF is driven by focal or reentrant activities that are initially clustered in a relatively limited atrial surface then disseminate everywhere in both atria. Evidence for structural remodeling, mainly represented by atrial fibrosis suggests that reentrant activities using anatomical substrate are the key mechanism sustaining AF. These reentries can be endocardial, epicardial, and intramural which makes them less accessible for mapping and for ablation. Subsequently, early interventions before irreversible remodeling are of major importance. Circumferential pulmonary vein isolation remains the cornerstone of the treatment of AF, regardless of the AF form and of the AF duration. No ablation strategy consistently demonstrated superiority to pulmonary vein isolation in preventing long term recurrences of atrial arrhythmias. Further research that allows accurate identification of the mechanisms underlying AF and efficient ablation should improve the results of PsAF ablation.

Keywords: atrial fibrillation, reentrant drivers, catheter ablation, fibrosis, mapping, pulmonary vein ablation

INTRODUCTION

Atrial fibrillation (AF) is the most common cardiac arrhythmia. It represents a major cause of mortality and morbidity, mainly related to embolic events and heart failure (Benjamin et al., 1998; Ruigomez et al., 2002, 2009; Pedersen et al., 2006; Miyasaka et al., 2007; Potpara et al., 2013; Pandey et al., 2017; Eggimann et al., 2018; Reddy et al., 2018). AF is a heterogeneous rhythm disorder that is related to a wide spectrum of etiologies and has broad clinical presentations. Despite extensive research, the mechanisms underlying AF remain incompletely understood. AF results from interactions between triggers, responsible for its initiation, and the substrate responsible for its perpetuation. In addition, ionic and anatomic remodeling, genetic predisposition, and neuro-humoral contributors make these interactions more complex.

The pulmonary veins play a key role in the pathogenesis of AF and their isolation is associated to high rates of AF freedom in patients with paroxysmal AF (PAF). However, ablation of persistent AF (PsAF) remains less effective, mainly limited by the difficulty to identify the sources sustaining AF outside the pulmonary veins.

We aimed to review the mechanisms underlying AF and their implications for catheter ablation.

AF PATHOPHYSIOLOGY

The mechanisms underlying AF are classically described as mechanisms responsible for its initiation (triggers) and mechanisms responsible for its perpetuation (Figure 1). This classification is clinically relevant as it allows to identify therapeutic targets.

AF Triggers

Haïssaguerre et al. (1998) first reported the essential role of the pulmonary veins (PVs) in the initiation and maintenance of paroxysmal AF (PAF). Ectopic activities originating from the PVs were identified in 94% of patients suffering from frequent pre-procedural AF episodes. Discrete ablation targeting the site of origin of the ectopic activities abolished the arrhythmia and prevented its recurrence in 62% of the cases after a follow-up of 8 months. The role of the PVs in triggering AF was confirmed in multiple subsequent studies (Chen et al., 1999; Wu et al., 2001; Sanders et al., 2002; Mahida et al., 2015).

Compared to the atrial cells, the PVs cardiomyocytes have specific action potential properties that predispose to arrhythmogenesis. In fact, the PVs cells have a higher resting membrane potential, a lower amplitude of the action potential, a smaller maximum phase 0 upstroke velocity and a shorter action potential duration (APD). Slow and rapid delayed rectifier currents are greater in the PVs whereas transient outward K⁺ current and L-type Ca²⁺ current are smaller (Ehrlich et al., 2003).

The initial premature beats arising from the PVs are focal (Arentz et al., 2007). These beats are likely automatic or triggered and related to calcium handling abnormalities and subsequent delayed afterdepolarizations (DAD) (Hirose and Laurita, 2007;

Takahara et al., 2011; Heijman et al., 2014). They are modulated by acute stressors like atrial stretch (Kalifa et al., 2003) and neural activation (Patterson et al., 2005; Lu et al., 2009). Early after depolarization due to prolonged action potential duration are mainly described in models of long QT syndrome (Lemoine et al., 2011). Subsequent firing is either related to DAD due to abnormal diastolic spontaneous calcium release (Chou et al., 2005; Nattel and Dobrev, 2016) or to reentrant activity at the junction between the PVs and left atrium. In fact, atrial myocytes at the entrance of the PV have abrupt changes in their fiber orientation, leading to slow conduction and reentry (Hocini et al., 2002). In addition, ionic mechanisms facilitate the occurrence of reentry by shortening the APD (increased rapid [I_{Kr}] and slow [I_{Ks}] delayed rectifier K⁺ currents) and slowing the conduction via the inactivation of Na⁺ currents (Nattel and Dobrev, 2016).

Additional ectopic sources triggering AF were identified outside the PVs. They can be located in the vena cavae, the crista terminalis, the coronary sinus, the ligament of Marshall, the inter-atrial septum, the appendages... (Mansour et al., 2002; Lin et al., 2003; Shah et al., 2003; Lee et al., 2005; Yamada et al., 2006; Pastor et al., 2007; Hwang and Chen, 2009; Yamaguchi et al., 2010; Elayi et al., 2013; Enriquez et al., 2017). Lin et al. (2003) identified non-PV triggers in 20% of the ectopic beats initiating PAF. Non PV triggers were predicted by female gender (odds ratio 2.00, 95% confidence interval 1.02–3.92) and left atrial enlargement (odds ratio 2.34, 95% confidence interval 1.27–4.32) in patients with PAF (Lee et al., 2005) and are more prevalent in AF of longer duration (Hung et al., 2017). Mechanisms underlying extra-PV triggers are less well-elucidated.

Perpetuation of AF

Mechanisms underlying the perpetuation of AF are still debated. Multiple wavelets and localized (focal or reentrant) sources are largely accepted to drive AF. These mechanisms are summarized in Figure 2.

Multiple Wavelets Hypothesis

Multiple wavelets were suggested to perpetuate AF in a mathematical model performed by Moe et al. (1964). In this model, multiple waves randomly propagate through the atria, cause wavebreaks, and give birth to new “daughter” wavelets. Theoretically, the number and the stability of these wavelets prevent AF termination. AF would be sustained as long as the number of wavelets exceeds a critical level. The presence of independent wavelets has been demonstrated in more recent studies (Chen et al., 2000; Reumann et al., 2007; De Groot et al., 2016). However, an important question is whether these wavelets are driving AF or they are just passive and result from the breakup of more organized waves remains unanswered. Chen et al. (2000) analyzed the individual wavelets during sustained AF by identifying the phase singularities using optical mapping. In their models, the wavelets existed for less than one rotation in 98% of the cases. In addition, the number of wavelets decreased between the entrance and the exit of the mapping field. These results suggested that wavelets essentially result from the breakup of high frequency organized waves and as such they are not an independent mechanism that maintains of AF. Recording

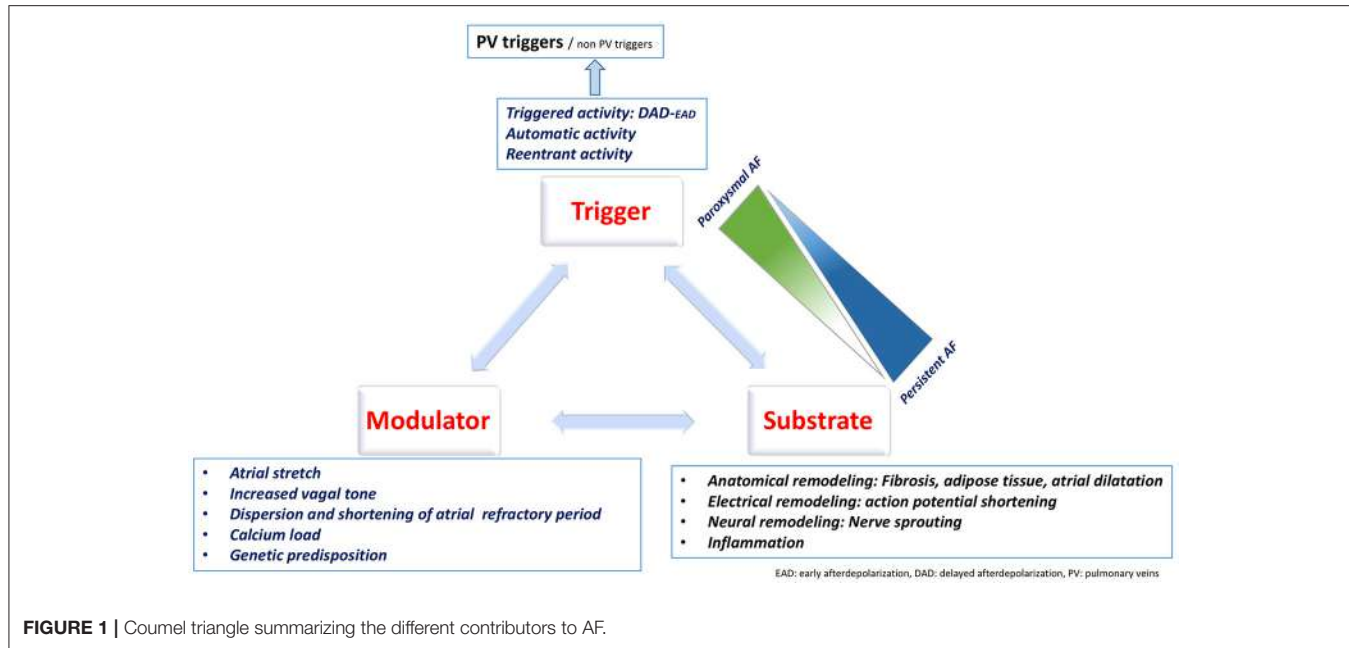


FIGURE 1 | Coumel triangle summarizing the different contributors to AF.

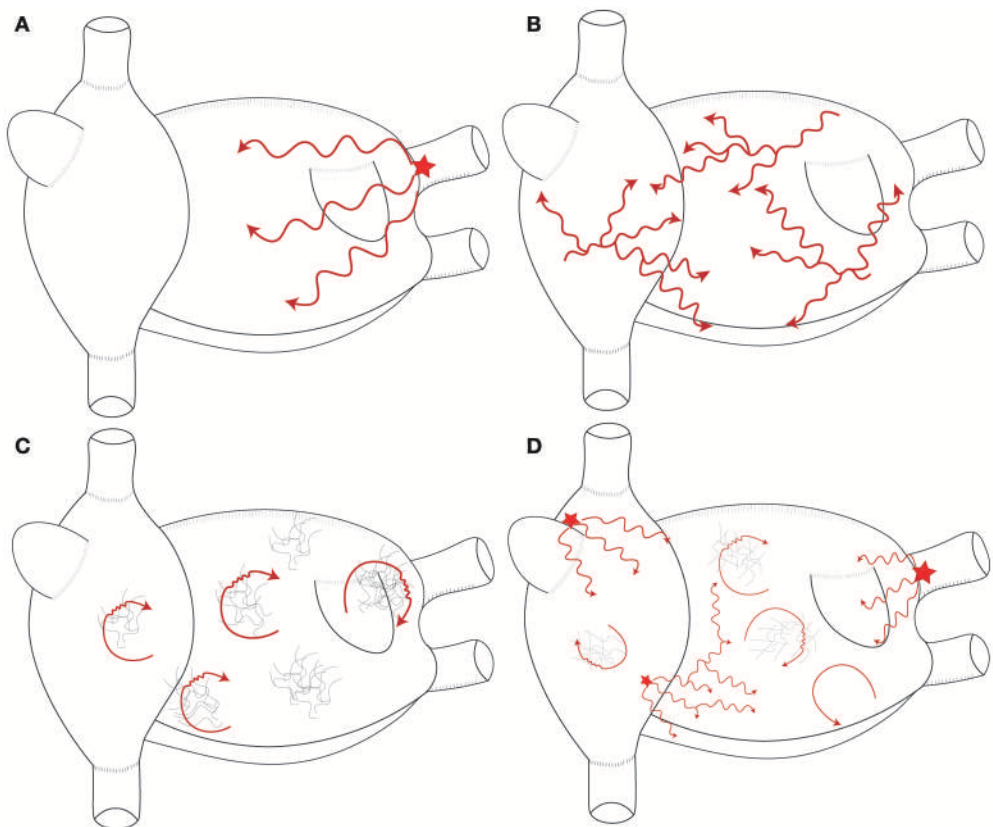


FIGURE 2 | Schematic representation of the mechanisms maintaining AF. **(A)** Single stable focal or reentrant source (star) with fibrillatory conduction. **(B)** Multiple wavelets: multiple waves propagate randomly and give birth to new daughter wavelets. **(C)** Multiple reentries (red arrows) around areas of scar and fibrosis. **(D)** Combination of the different mechanisms that sustain AF in humans. These mechanisms are typically meandering and last for few consecutive beats.

multiple wavelets during firing from the PVs is an example that supports the passive role these wavelets.

Localized AF Drivers: (Figure 3)

There is no specific definition of AF drivers. Hansen et al. (2016) defined AF drivers as localized sources of fast, repetitive activity from which activation propagates and breaks down into fibrillatory conduction in the rest of the atria. This definition refers to localized activities without specifying the underlying mechanism. The driving role of these activities is demonstrated by ablation slowing or terminating AF.

Functional reentry

Functional reentry refers to reentrant activity in the absence of underlying substrate and of anatomical obstacles.

The leading circle concept: This concept was developed by Allessie et al. (1977). In this theory, centripetal waves moving toward the center maintain this latter refractory. A functional reentry establishes itself in the shortest circuit defined as the shortest distance the impulse travels during the refractory period. The presence of slow conduction velocity (CV) or brief refractoriness (RP) produces a small wavelength (WL) and makes spontaneous termination of AF unlikely. In fact, as $WL = CV * RP$, the occurrence of a steady state where the WL is adapted to the circuit length would stabilize the reentry and would perpetuate AF.

Spiral wave reentry= rotor concept: Spiral wave reentry or “rotor” is a region of specific reentry where the curved wavefront and wavetail meet each other at a singularity, and where the central tissue is not refractory (Vaquero et al., 2008; Pandit and Jalife, 2013; Nattel et al., 2017).

Evidence for spiral wave reentry was first demonstrated in simulation studies (Winfree, 1973; Goldbeter, 1975; Lechleiter et al., 1991; Pertsov et al., 1993a). Its presence in cardiac tissue was demonstrated using optical mapping by Davidenko et al. (1990). The authors induced sustained reentrant activity by using a single appropriately timed premature electrical stimulus applied perpendicularly to the wake of a propagating quasiplanar wavefront. Reentry pivots at high frequency (5–7Hz) around a relatively small group of cells that show only minimal depolarizations (phaseless region) throughout the cycle.

Mandapati et al. (2000) identified micro-reentrant sources localized in 80% of the cases at the posterior LA, close to the left veins. The authors identified high frequency periodic activity limited to small area (10.4 ± 2.8 mm of core perimeter and 3.8 ± 2.8 mm² area). Using high resolution video imaging, the localized sources correspond to vortex like reentry.

Spatio-temporal characterization of the rotor activities was facilitated thanks to phase transformation. Gray et al. (1998) analyzed phase singularities during fibrillation and demonstrated a spatial and temporal organization that under certain conditions give rise to rotors. Phase represents the different stages within 1 cycle of a signal divided into 360° or 2π radians (Umapathy et al., 2010).

Phase analysis characterization of the recorded signals lacks temporal accuracy, Bray and Wikswo (2002) developed an algorithm capable of establishing proper orbits without the need

to specify “Tau.” Using the Hilbert transform, phase singularities could be localized closer to the point of initial formation than was possible previously. This transformation is important for the purposes of singularity tracking and investigating electrodynamic interactions. Phase transformation allows to identify the center of the pivoting rotor as an area of undefined phase and is called phase singularity. This center is surrounded by phases ranging between $-\pi$ and $+\pi$ (Figure 5).

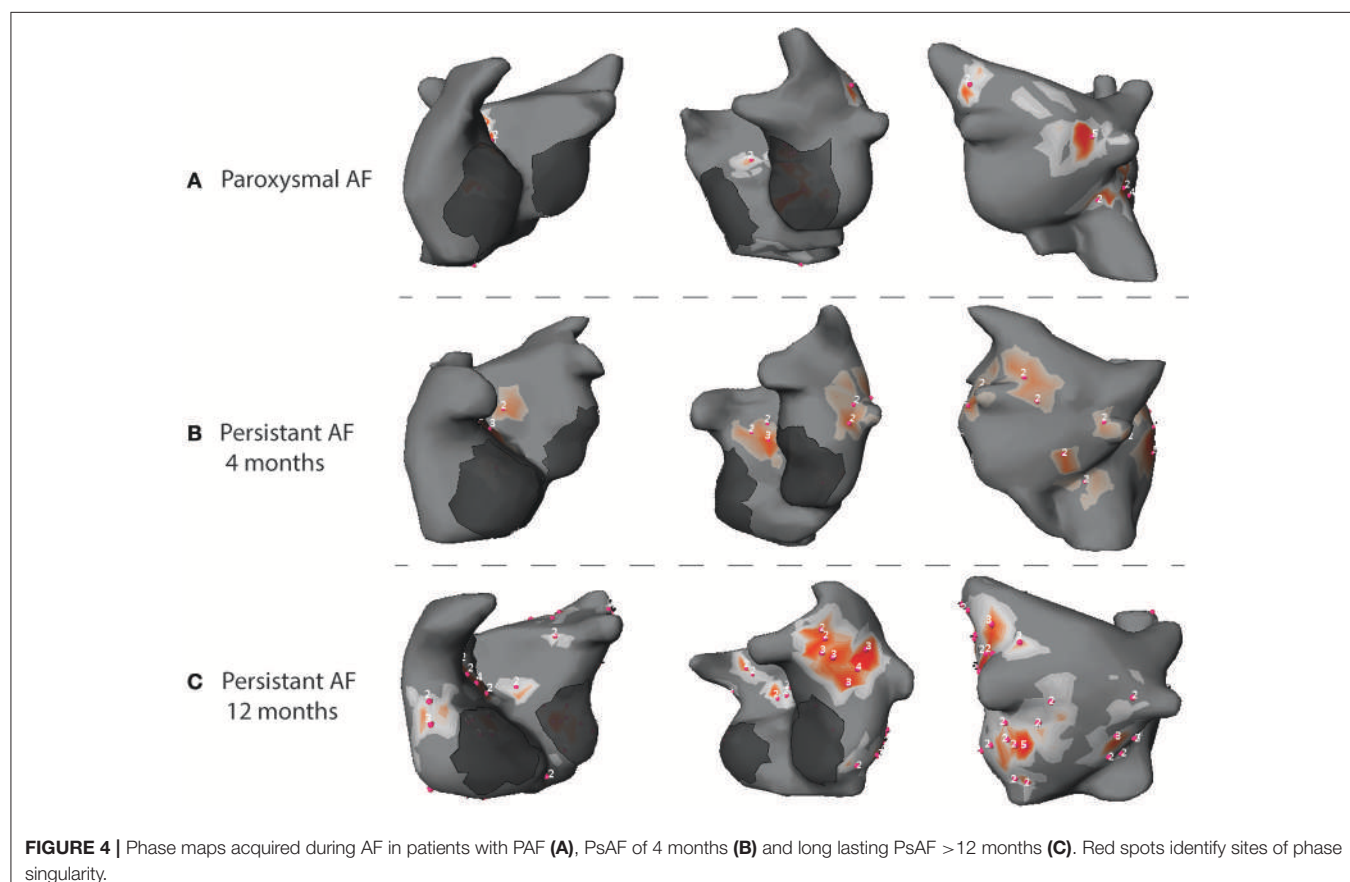
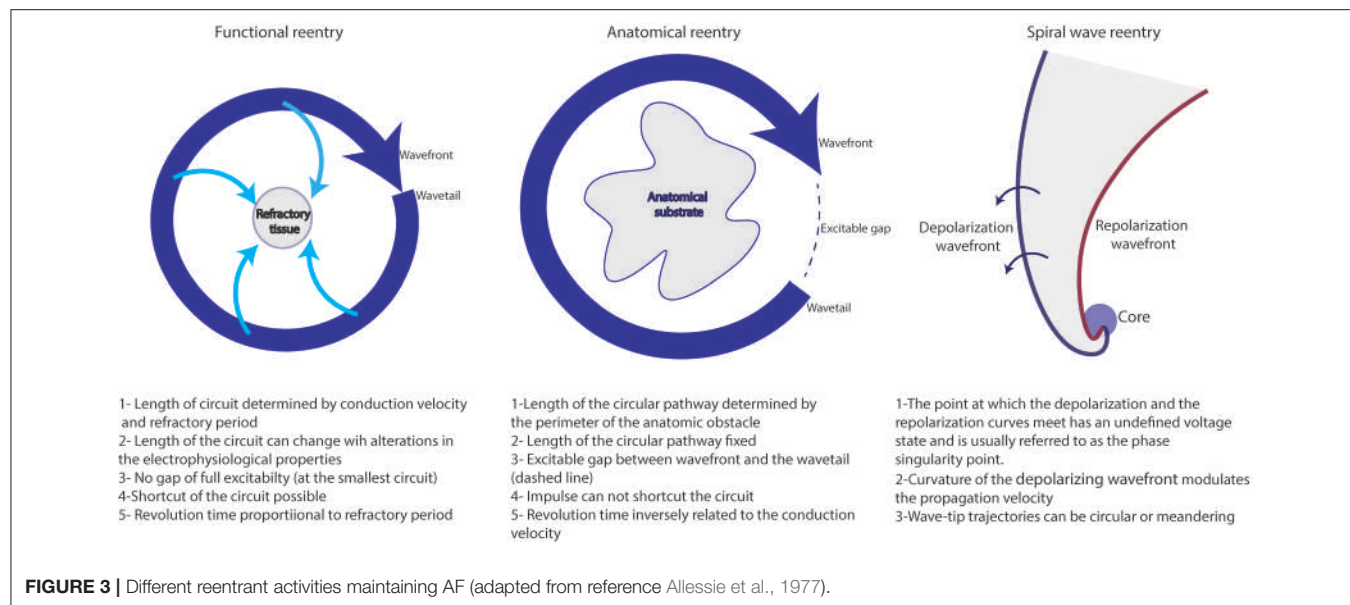
Anatomical reentry

Localized reentries play a key role in the maintenance of AF. Reentry occurs in the presence of unidirectional block and of slow conduction that makes the wavelength shorter than the length of the circuit. Such conditions are commonly encountered in the atria of patients with AF, mainly in the presence of fibrosis.

The role of reentry in maintaining AF was demonstrated by Schuessler et al. (1992). In their model, the authors induced AF using a single extra-stimulus and increasing concentrations of acetylcholine and mapped the right atrial activation. They noted an increase in the number of wavelets that tended to stabilize to small, single, relatively stable reentrant circuit in the absence of anatomical barriers. These reentries are facilitated by the occurrence of lines of functional block at the crista terminalis.

Spach et al. (1988) showed micro-anatomic reentry (within 1–2 mm area) that occur in the presence of non-uniform anisotropic conduction and micro-fibrosis of the pectinate bundles of the right atrium (Spach and Dolber, 1986). Hansen et al. (2015) provided the evidence for intramural reentries that anchor to fibrosis insulated atrial bundles. The authors induced AF in explanted Human hearts and mapped intramural activation of the right atrial wall using high resolution optical mapping. They noted stable reentries that anchor to areas with complex architecture marked by increased transmural fiber angle differences and interstitial fibrosis. The majority of the reentries were mapped from the endocardial surface and discrete ablation terminated AF which confirms their driving role. These micro-reentries were also identified in the left atrium (Zhao et al., 2015) at the junction between the left atrial roof and the posterior wall of the left atrium, at an area with abrupt changes in the myocardial fiber orientation. Ablation of the driver maintain AF can unmask drivers with longer cycle length (Hansen et al., 2015). The presence of several temporally competing drivers and secondary drivers may underlie the absence of acute termination by ablation and should motivate repeated mapping of AF.

AF drivers are more frequently recorded in the left atrium. This is attested by shorter AF CL in the left atrium with a gradient LA-RA, the higher rate of AF termination in the LA. Mansour et al. (2001) analyzed left atrial and right atrial dominant frequencies and identified left to right activation gradient that increased after the ablation of the Bachmann bundle and of the inferoposterior interatrial pathway. This observation supports the higher prevalence of AF drivers in the left atrium with fibrillatory conduction to the right atrium. Hocini et al. (2010) tracked the evolution of AF cycle length at the right and atrial appendages. In 70% of the cases, an increase of both cycle lengths occurred after left atrial ablation. Right atrial drivers were recorded in 20% of the cases.



Atrial Remodeling

Atrial remodeling includes structural and functional alterations including electric, structural, and autonomic remodeling that promote atrial arrhythmias.

Electrical remodeling

AF and rapid arrhythmias alter the expression and/or the function of ion channels in a way that promotes arrhythmias (Allessie et al., 2002; Schotten et al., 2011; Wakili et al., 2011;

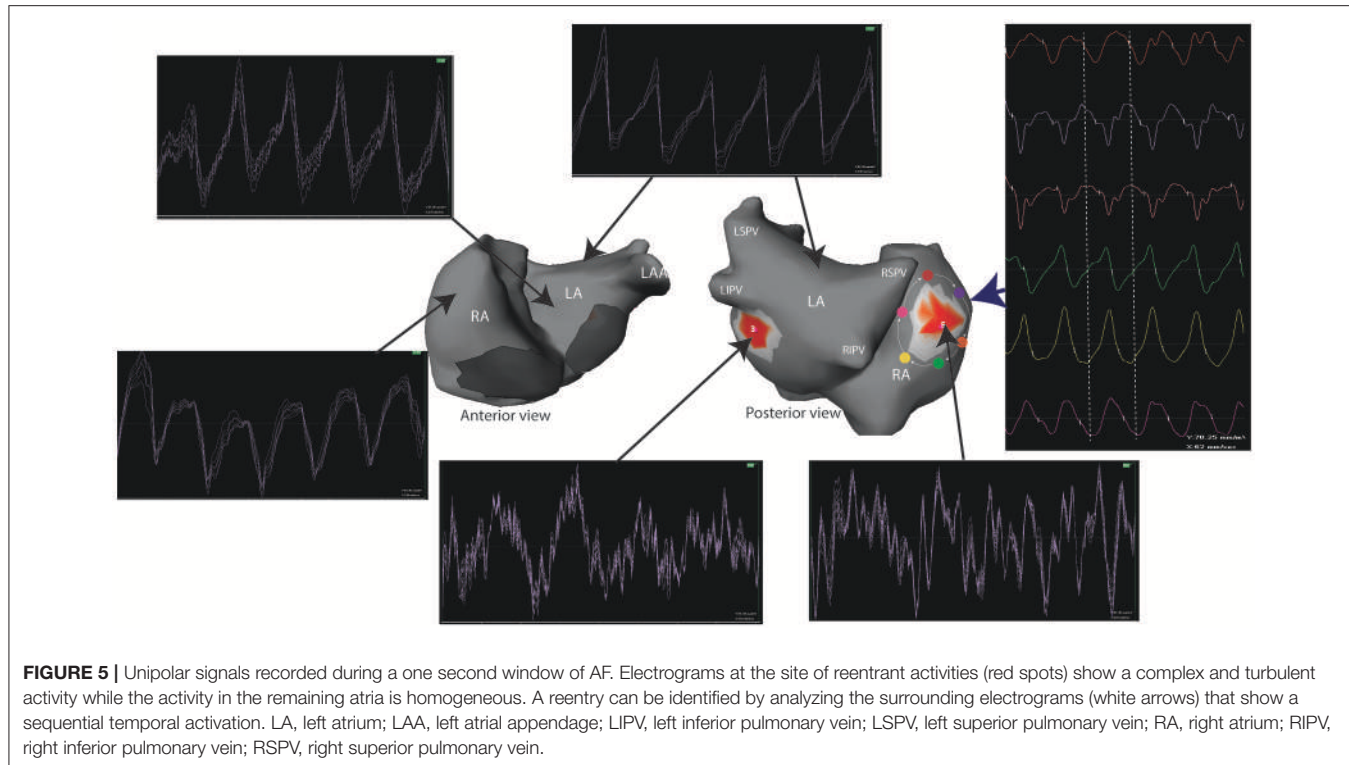


FIGURE 5 | Unipolar signals recorded during a one second window of AF. Electrograms at the site of reentrant activities (red spots) show a complex and turbulent activity while the activity in the remaining atria is homogeneous. A reentry can be identified by analyzing the surrounding electrograms (white arrows) that show a sequential temporal activation. LA, left atrium; LAA, left atrial appendage; LIPV, left inferior pulmonary vein; LSPV, left superior pulmonary vein; RA, right atrium; RIPV, right inferior pulmonary vein; RSPV, right superior pulmonary vein.

Heijman et al., 2014; Nattel and Harada, 2014). In fact, rapid atrial rate during AF initiates auto-protective mechanisms to reduce the entry of Ca^{2+} inside the cell (Iwasaki et al., 2011). These mechanisms aim to inactivate the Ca^{2+} currents, downregulate I_{CaL} , and enhance the inward rectifier K^{+} current. Subsequently, the action potential duration becomes shorter which increases the atrial vulnerability to atrial arrhythmias and stabilizes the mechanisms sustaining AF (Figure 5) (Allessie et al., 2002; Nattel, 2002; Schotten et al., 2011; Wakili et al., 2011). In addition, impaired calcium handling leads to contractile dysfunction and subsequent tachycardia-induced atrial cardiomyopathy (Sun et al., 1998).

Structural remodeling

Fibrosis represents the most important structural remodeling that promotes AF.

Fibrosis can be reactive (located at the interstitial space) or reparative (replaces dead myocytes) (Silver et al., 1990; Burstein and Nattel, 2008).

Animal studies identified atrial fibrosis in the presence of hypertension (Kistler et al., 2006; Lau et al., 2010a,b, 2013), heart failure (Li et al., 1999; Shi et al., 2002; Shinagawa et al., 2002; Lau et al., 2011), diabetes (Linz et al., 2016), obesity (Abed et al., 2013),... In humans, AF is more frequent in the presence of external stressors predisposing to fibrosis (Sanders et al., 2003; John et al., 2008; Roberts-Thomson et al., 2009; Medi et al., 2011, 2012; Dimitri et al., 2012; Vlachos et al., 2016; Anter et al., 2017; Karam et al., 2017). In addition, when left untreated, AF promotes the expression of genes that enhance the proliferation of fibroblasts and increase extra-cellular matrix

secreting function (Burstein et al., 2007; Guo et al., 2012). This underlies the progression of AF to permanent forms by creating a long-term positive feedback loop (Platonov et al., 2011; Yue et al., 2011); the so called AF begets AF hypothesis (Wijffels et al., 1995; Rostock et al., 2008).

Fibrosis increases the separation of the myocytes within sub-endocardial atrial bundles and between the endocardial and epicardial layers leading to endo-epicardial dissociation (Spach and Dolber, 1986; Verheule et al., 2013; Hansen et al., 2017). It forms barriers to the propagation of the activation wavefronts and isolates atrial myocytes. These obstacles affect the wavefront shape and can induce spiral waves through vortex shedding or by causing localized conduction block in narrow isthmuses (Panfilov and Keener, 1993; Cabo et al., 1996; Starobin et al., 1996). The interaction between the wavefront and the boundaries of the fibrotic area are determinant for the wavefront curvature by influencing the propagation velocities and the refractory periods (Comtois and Vinet, 1999; Sampson and Henriquez, 2002). This stabilizes rotor activity (Morgan et al., 2016; Roney et al., 2016) and anchors them to the scar boundaries (Davidenko et al., 1992; Pertsov et al., 1993b; Morgan et al., 2016).

In addition, the fibrotic pattern affects the velocity of the activation wavefront (Kawara et al., 2001; Comtois and Nattel, 2011). In a mathematical model, Tusscher and Panfilov (2005) demonstrated that an increasing number of small and randomly distributed obstacles decrease the conduction velocity but increase the inducibility of wavebreaks and spiral waves in 2D and 3D excitable media. Kawara et al. (2001) analyzed the wavefront activation in explanted human hearts and identified different conduction curves according to the

fibrotic pattern. The zones of dense, patchy fibrosis with long fibrotic strands were associated with prominent activation delay. The conduction curve in this situation was dependent on the fiber direction. Conversely, dense, diffuse fibrosis with short fibrotic strands only marginally affected conduction curves.

In a recent study, Vigmond et al. (2016) demonstrated the possibility to induce percolation in a computer model of fibrotic tissue. Percolation was produced as a result of micro-source-sink mismatch with the fibrotic region. This produced low amplitude and long lasting electrograms. Decreasing the cycle length increased the delay needed for the wavefront to exit the remodeled zones and induced reentrant activities. Additional studies demonstrated the occurrence of reentry near the percolation threshold in heterogeneous cardiac tissue including fibrosis (Alonso and Bar, 2013; Alonso et al., 2016).

In addition to fibrosis, structural atrial remodeling includes atrial fatty infiltration, inflammatory infiltration, necrosis and amyloid deposition (Frustaci et al., 1997; Rocken et al., 2002; Leone et al., 2004; Nguyen et al., 2009; Hatem and Sanders, 2014; Venticlef et al., 2015). The role of the adipose tissue in the pathogenesis of AF is well-demonstrated. Adipose tissue has a paracrine effect through the release of adipokines with pro-fibrotic properties. It also forms barriers to wavefront conduction and favor reentrant circuits (Hatem and Sanders, 2014).

Autonomic and neural remodeling

The heart has a rich and complex extrinsic and intrinsic autonomic innervation (Janes et al., 1986; Armour et al., 1997; Armour, 2008). The role of this system in the initiation and maintenance of AF is well-demonstrated (Arora, 2012; Chen et al., 2014) and is supported by the circadian variation in the incidence of AF (Viskin et al., 1999; Mitchell et al., 2003).

Neural remodeling including an increase in the atrial innervation occurs in different clinical situations. Animal studies (Jayachandran et al., 2000; Chang et al., 2001; Arora et al., 2008; Ng et al., 2011) demonstrated an increase in the density of sympathetic and parasympathetic innervation with AF. Gould et al. (2006) collected the atrial appendages in patients with AF undergoing cardiac surgery and demonstrated an increased atrial sympathetic innervation in patients with PsAF.

Neural remodeling also occurs after myocardial infarction (Han et al., 2012; Nguyen et al., 2012; Ajijola et al., 2015) and in the presence of cardiomyopathy (Ajijola et al., 2012) and contributes to the occurrence of AF in these populations. Recent therapeutic strategies aiming to modulate the autonomic tone successfully reduced the AF burden in animal models (Richer et al., 2008; Ogawa et al., 2009; Leiria et al., 2011; Shen et al., 2011) and in humans (Pappone et al., 2004; Scanavacca et al., 2006; Po et al., 2009; Katritsis et al., 2013; Pokushalov et al., 2013).

It is important to note that, in contrast with the electrical remodeling, structural remodeling and fibrosis are not reversible and lead to the perpetuation of AF in more complex forms. Early interventions are of major importance to avoid such progression of the disease.

Genetic Predisposition

Genetic predisposition plays an important role in the occurrence of AF. It is responsible for familial cases with early onset of AF independently of concomitant cardiovascular conditions (Fox et al., 2004; Lubitz et al., 2010; Oyen et al., 2012). AF incidence also shows racial differences, being less prevalent in Blacks, Hispanics and Asians compared to Whites (Dewland et al., 2013).

Up to one-third of the patients with AF had genetic variants that increase the risk of AF. So far, the genome wide association study (GWAS) and international collaborative metaanalysis identified at least 30 gene loci associated to AF (Gudbjartsson et al., 2007; Benjamin et al., 2009; Ellinor et al., 2010, 2012; Sinner et al., 2014; Low et al., 2017; Bapat et al., 2018; Campbell and Wehrens, 2018). Variants located close to the paired-like homeodomain 2 (PITX2) gene on chromosome 4q25 have the highest association to AF (Lubitz et al., 2014; Low et al., 2017). The majority of mutations underlying AF affect genes that encode transcription factors related to cardiopulmonary development, cardiac-expressed ion channels and cell signaling molecules (Roberts and Gollob, 2010, 2014; Ellinor et al., 2012). Genome wide association studies have allowed identification of variants potentially linked to AF (Christophersen et al., 2017; Lee et al., 2017; Low et al., 2017; Nielsen et al., 2018a,b; Roselli et al., 2018). These variants frequently require further classification to confirm or eliminate their pathogenicity. Genetic predisposition may influence the response to AF therapies (Darbar et al., 2007; Parvez et al., 2012; Benjamin Shoemaker et al., 2013; Huang and Darbar, 2016) and can allow specific and based-mechanism therapies (Roberts and Gollob, 2010; Campbell et al., 2013; Faggioni et al., 2014; Darbar, 2016).

MAPPING OF AF

Mapping represents a crucial step to understand the mechanisms of AF and improve the results of ablation. However, it is important to note that the spatial resolution of the mapping technique can significantly affect the interpretation of the underlying AF mechanism (Roney et al., 2017).

Invasive Mapping of Reentrant and Focal Activities

Narayan et al. (2012b) used a 64 pole-basket catheter (48 mm diameter, 4 mm electrode spacing; or 60 mm diameter, 5 mm electrode spacing) introduced through a venous femoral access to map AF activities from the right and the left atria. They included 97 patients who underwent 107 consecutive ablation procedures for PAF or PsAF. AF electrograms at 64–128 electrodes are combined with repolarization dynamics acquired using monophasic action potentials (MAP) and conduction dynamics to construct spatiotemporal AF maps (Narayan et al., 2012a). These maps were used to locate the focal impulses (defined as centrifugal activation contours from an origin) and rotors (defined as sequential clockwise or counterclockwise activation contours around a center of rotation emanating outwards to control local AF activation). Rotors and focal impulses were present in 97% cases with sustained AF. The majority of the

AF sources were rotors (70%) and predominantly located in the left atrium (76%). In contrast to our experience, no fragmented signals were recorded at the rotors site. The mean AF sources was 2.1 ± 1.0 and was significantly higher in PsAF than PAF and in spontaneous than induced AF. A group of patients underwent ablation targeting Focal Impulse and Rotor Modulation (FIRM guided ablation). Compared to patients undergoing conventional AF ablation, FIRM guided ablation was associated to a higher acute success and a better outcome.

Different systems were developed to invasively map rotational activities (Daoud et al., 2017; Grace et al., 2017; Honarbakhsh et al., 2017). The systems use different approaches and more studies are needed to evaluate their clinical usefulness.

Limitations of Invasive Mapping of Reentrant and Focal Activities

The FIRM approach needs the use of two basket catheters for concomitant bi-atrial analysis. Poor electrode contact and inefficient deployment may significantly alter the recorded signals (Laughner et al., 2016; Oesterlein et al., 2016). In addition, low resolution of mapping the atria may lead to false detections (Roney et al., 2017). Offline analysis is needed which prolongs the duration of the procedure and limits the reproducibility of the results (Benharash et al., 2015; Buch et al., 2016). In addition, there are significant discrepancies between 2D and 3D phase maps where rotors identified using 2-D maps were absent in 3D maps (Pathik et al., 2018).

Non-invasive Mapping

Principles of Non-invasive Mapping

Electrocardiographic mapping (ECGi) is a technology that allows to map the activation of AF from chest recordings in a beat-to-beat manner (Oster et al., 1997; Ramanathan et al., 2004; Cuculich et al., 2010; Frontera et al., 2018a). This technique is particularly useful to map focal sources and non-sustained arrhythmia (Jia et al., 2006; Wang et al., 2011; Shah et al., 2013; Zhang et al., 2013; Cochet et al., 2014).

Recording of the cardiac activity is acquired from the torso using a 252 electrode vest. The cardiac geometry and the position of each electrode is registered using high-resolution cross sectional non-contrast computed tomography. The ECGi algorithm computes epicardial unipolar electrograms from the input geometry and torso potentials by solving the inverse problem (Gulrajani et al., 1988; Rudy and Messinger-Rapport, 1988; Rudy and Oster, 1992; Ramanathan et al., 2003; Rudy, 2013). To avoid the superposition of the QRS, windows with long R-R interval exceeding one second allow to analyze the fibrillatory waves.

Additional algorithms can be applied to acquire different maps. Activation maps are computed using the unipolar electrogram intrinsic deflection (dV/dt) based method. Phase analysis identifies reentrant and focal activities. Reentrant activity is identified as a phase singularity formed at the intersection of depolarization and repolarization isolines (Gray et al., 1998). Focal breakthroughs are shown as activities raising from discrete points and showing a negative pattern of the local electrogram.

Results From Non-invasive Mapping

Cuculich et al. (2010) first used ECGi to map AF in 26 patients. The spatial accuracy for determining different pacing sites was 6 ± 4 mm. The authors identified multiple wavelets (defined as contiguous area of epicardial activation lasting ≥ 5 ms) as the most common pattern (92% of the patients). Rotor activity was present in 15% of the cases, only in patients with non-paroxysmal AF. The authors defined a complexity index as the sum of the number of wavelets and focal activities and showed an increased complexity with duration of AF.

Data from our laboratory (Haissaguerre et al., 2014; Lim et al., 2017) reported the results of 103 patients with PsAF. The analysis of cumulative windows of 9 ± 1 s of AF were performed using phase mapping. AF was driven by two to three regions of reentrant and focal activities during the first months. Drivers activity spread in more regions and became bi-atrial in PsAF of longer duration (Figure 4). Reentrant drivers were located in the PV antra and surrounding structures, the left atrial appendage and septum in nearly all the cases. Focal breakthroughs rose predominantly from the PV ostia and left and right appendages.

In the AFACART study (Knecht et al., 2017), ECGi was used to guide ablation in 118 patients with PsAF lasting <1 year. Reentrant activities were identified in all patients and were more frequently located around the PVs, at the anterior interatrial groove and the posterior and inferior left atrium. Focal breakthroughs were mapped in 95% of the cases and were more commonly located in the PVs and both appendages.

Metzner et al. (2017) used a noninvasive epicardial and endocardial system (NEEES) and compared the epicardial and the endocardial reentrant activity. The authors acquired phase maps from 6 patients with PsAF. The majority of the epicardial rotor activity was located in two to three anatomical clusters. These results were reproduced using invasive mapping by a multipolar catheter.

The effects of antiarrhythmic drugs were analyzed in a group of 13 patients who underwent ablation for PsAF (Amraoui et al., 2016). ECGi recordings were acquired before and after the infusion of flecainide. Flecainide infusion reduced the number of regions that hosted reentrant activity (7–4 regions, $p < 0.001$). Importantly, AF was terminated to sinus rhythm in 11 cases, by targeting the regions remaining after flecainide infusion in 9/11 cases. This result suggests that anti arrhythmic drugs select more stable and important regions that sustain AF. Similarly, amiodarone was used in patients with structural heart disease and PsAF and allowed to terminate AF using a shorter duration of radiofrequency (Cheniti et al., 2016). In our practice, an antiarrhythmic drug is used before ablation for PsAF order to limit the effects of the electrical remodeling.

Limitations of Non-invasive Mapping

Non-invasive mapping has some limitations that should be considered for optimal use. Cardiac signals are attenuated while crossing the thorax, leading to a “blurred vision” by the recording electrode on the torso. Subsequently, the recorded signals by each electrode on the torso represents the average of multiple signals. However, areas with turbulent activity can still be distinguished from areas with more organized activity (Figure 5).

ECGi does not explore intra-mural and endocardial activities. Subsequently, it is unable to discern the mechanisms of focal activities that may be microreentry, epicardial breakthrough of endocardial activity, focal activity (Cuculich et al., 2010). It is also unable to accurately analyze the septal activity where wavefronts from the left and right atria can be projected. In addition, phase transformation can produce phase generated non-rotational singularity points and false rotors (Vijayakumar et al., 2016). In our practice, signals at the reentrant site are manually validated by showing electrograms that cover all the cycle length.

Invasive Mapping of AF

Invasive mapping is limited by the inability to map simultaneously both atria, by contact issues, by mechanical movement of the atrial walls, by the inability to explore intra-mural and epicardial activities. The meandering nature of the sources maintaining AF is an additional major limitation to conventional sequential invasive mapping. Multipolar catheters with small electrodes improved the mapping of AF by acquiring high density maps and reducing the influence of farfield signals.

Findings During Invasive Mapping of AF

Konings et al. (1994) used a spoon shaped electrode containing 244 unipolar electrodes to map right atrial free wall in patients undergoing surgical ablation of accessory pathways. The authors identified 4 major patterns of activation according to the complexity of the atrial activation. Single broad wavefronts propagating uniformly across the right atrium were recorded in 40% of the cases. One or two non-uniformly conducting wavelets were recorded in 32% of the cases. Highly fragmented signals with more than two wavelets and variable direction of propagation were less frequent and recorded in 28% of the cases. The authors correlated the morphology of the signals recorded to the underlying mechanism (Konings et al., 1997). Unipolar signals were different according to the underlying mechanisms, showing single potentials in uniform conduction, short double potentials in areas of collision, long double potentials in areas with conduction block and fragmented potentials in pivoting points and in the presence of slow conduction. No preferential anatomic sites for double or fragmented potentials were found in the right atrium. The authors hypothesized that electrograms spanning the entire cycle length of the AF could identify localized reentries and areas where electrograms displayed fractionation could be pivotal points of these circuits. Fragmented signals with long duration are referred to as complex fractionated atrial electrograms (CFAE) and represented an important target for AF ablation (Nademanee et al., 2004). Different algorithms were developed in order to automatically locate the areas of CFAEs (Scherr et al., 2007; Verma et al., 2008; Seitz et al., 2013; Nahooi et al., 2015).

Rostock et al. (2006) performed high density endocardial mapping during AF using a 20-pole catheter. The authors identified two patterns of local activation. In the majority of the cases, they recorded nearly simultaneous activation covering only a limited part of the cycle length ($\leq 30\%$ of the AF cycle length). This pattern was correlated to passive activation. More rarely,

they recorded complex activation covering more than 75% of the cycle length. These signals were correlated either to local burst activity with activation gradient in the adjacent splines and may be related to localized reentry.

Haissaguerre et al. (2006) used a 20-pole catheter with 5 radiating splines covering 3.5-cm diameter to map both atria. The authors identified activity spanning 75–100% of the cycle length suggesting a complex localized activity or localized reentry. Ablation targeting these areas significantly prolonged the AF cycle length demonstrating the critical role of these reentries in the maintenance of AF. This result is consistent with the findings of Hansen et al. (2016) identified micro-reentrant activity with average area around 15* 6 mm with 3 mm depth. As such, these reentries may be mapped using high resolution catheters, but only if they are located on the endocardial or epicardial surface.

High density endocardial mapping at the drivers' area identified prolonged fractionated signals. These signals were more frequent in the driving area than in the remaining areas (62 vs. 40%, $p < 0.001$). Most importantly, electrograms recorded on the multispline catheter spanned across a greater part of AF cycle length in the driver regions than elsewhere (71 vs. 47% of the AF cycle length, $P < 0.001$) (Haissaguerre et al., 2014). This suggests a slow conduction or a localized reentry. These electrograms were rarely recorded for more than five consecutive beats indicating an unstable local propagation (Haissaguerre et al., 2016). In addition, these signals may show dynamic changes that are dependent on the local cycle length (Rostock et al., 2006). The instability of the electrograms is suggested by the smoothing of the local activity which shows a turbulent activity. In fact, unipolar signals at the site of reentry identified complex and turbulent activity spanning all the cycle length, while activation in the remaining atria are more homogeneous (Figure 5). In our experience, the persistence of complex activity at driver sites after ablation is associated to the persistence of AF and demonstrates the necessity for further ablation.

Limitations of the Mapping of Fragmented Signals

Multiple parameters may affect the accuracy of invasive mapping. The electrode size, the inter-electrode spacing, the proximity to the atrial wall and the duration of the mapping at each site represent the main parameters. Mapping catheters with small electrodes provide a higher sensitivity to near-field signals compared to 4 mm tip catheters (Stinnett-Donnelly et al., 2012; Berte et al., 2015). In addition, fractionation increases as interelectrode spacing increases (Correa De Sa et al., 2011; Lau et al., 2015).

The correlation between the fragmented signals and the underlying mechanism is poor. In fact, complex and fragmented signals may result from artifacts, inappropriate filtering, remote activation related to adjacent structure or overlying structures and alterations in conduction velocities related to wavefront curvature and tissue discontinuities (De Bakker and Wittkampf, 2010). In addition, these fragmented signals are frequently passive. Jadidi et al. (2012) acquired high density atrial maps during sinus rhythm, CS pacing and during AF. The distribution of the fragmented electrograms was different according to the site and the rate of activation. During sinus rhythm and

CS pacing, electrogram fragmentation mainly resulted from wavefront collision.

Recent work from our laboratory characterized the mechanism underlying the different types of electrograms using high density mapping (Rhythmia, Boston Scientific) during atrial tachycardia. Frontera et al. (2018b) analyzed electrograms at the sites of slow conduction areas, at the lines of block, at areas of collision and at pivot sites. Areas with slow conduction had a significantly lower amplitude and a long duration. Areas of wavefront collision had a shorter amplitude and a higher voltage. Electrograms at the lines of block were not fragmented, the block lines being defined as areas where the activation completely stopped with the front making a detour around the obstacle, the downstream activation proceeding toward the line of block being in an opposite direction to the upstream one. These characteristics should be assessed during AF.

Contribution of Imaging Modalities to AF Mapping

Cardiac magnetic resonance (CMR) studies demonstrated a higher proportion of atrial fibrosis in patients with AF compared to healthy patients (Oakes et al., 2009) and in patients with PsAF compared to those with PAF (Oakes et al., 2009; Daccarett et al., 2011).

Oakes et al. (2009) validated a processing protocol to detect atrial fibrosis by using late gadolinium enhancement (LGE) on CMR. This technique was used to characterize the atrial substrate in a group of 81 patients undergoing PV isolation. Fibrosis was present in all cases and its extent predicted the recurrence of AF after PVI. In the DECAAF study (Marrouche et al., 2014), Marrouche et al. demonstrated that an increase of 1% in the proportion of atrial fibrosis was associated to 6% increase in rate of recurrent arrhythmia after catheter ablation. In addition, residual fibrosis on MRI, defined as preablation atrial fibrosis not covered by ablation scar, was associated to the recurrence of AF (Akoum et al., 2015). These studies confirm the key role of fibrosis in the pathogenesis of AF.

Electrograms at the areas with fibrosis were analyzed by Jadidi et al. (2013) in a group of patients undergoing ablation for persistent and long-lasting PsAF. Atrial fibrosis was associated with lower amplitude and a slower and more organized activity. However, complex fractionated atrial electrograms were recorded outside the areas of fibrosis in 90% of the cases.

Haissaguerre et al. (2016) analyzed the presence of fibrosis and its density within each 2.5 mm spherical atrial volume in 13 patients undergoing CMR. The borders of the fibrotic areas hosted the majority of the reentrant activities. In fact, 80% of the reentrant activities were located in areas with a fibrotic density >70%. Conversely, only 10% of the non-driver region harbored such a high fibrotic density.

In a recent study, Cochet et al. (2018) used high resolution LGE-CMR to characterize atrial fibrosis in patients with AF undergoing ECGi guided catheter ablation. The authors characterized LGE density at the reentrant sites. Fibrosis was significantly associated with the number of reentrant regions,

to the left atrial volume and to the AF duration. Interestingly, reentrant activities were predominantly clustered at the LGE borders. Moreover, areas with high reentrant activity had a significantly higher local LGE density.

Fibrosis identified by CMR was shown to be an independent factor of AF recurrence after catheter ablation. In a post-analysis of the DECAAF study, Akoum et al. (2015) analyzed LGE CMR 3 months after the ablation in 177 cases. Baseline fibrosis and residual fibrosis were significantly correlated to the need for repeat catheter ablation. Similar results were reported in other studies (Oakes et al., 2009; Malcolme-Lawes et al., 2013; Khurram et al., 2016). Interestingly, CMR studies demonstrated a low rate of complete encirclement of the four pulmonary veins, only in around 7% of the cases (Badger et al., 2010; Akoum et al., 2015). Incomplete PVI is associated to higher recurrence after AF ablation (Peters et al., 2009; Badger et al., 2010). These results raise multiple questions about the efficiency and the durability of lesions caused by ablation.

IMPLICATIONS FOR AF ABLATION

Clinical AF ablation provides clues about the understanding of AF pathophysiology. In **Table 1** are presented the results of the main studies and the outcome after percutaneous AF ablation. Unfortunately, there is a significant heterogeneity between the different studies leading to poor reproducibility of the results.

Catheter ablation is superior to antiarrhythmic drugs in preventing AF recurrence (Hazard ratio = 0.53) as reported in the CABANA trial. However, the best strategy is still to be identified.

Despite the different techniques, CPVI remains the cornerstone of the treatment of AF, regardless of the AF form and of the AF duration (Voskoboinik et al., 2017). No strategy consistently demonstrated superiority to CPVI in preventing long term recurrences of atrial arrhythmias.

It is notable that higher rates of success are reported after multiple procedures (Ganesan et al., 2013). This raises questions about the identification of the mechanisms underlying AF and the efficiency and the durability of the lesions created during index procedures.

Paroxysmal AF

PV isolation (PVI) is the most widely used technique to treat PAF. The initial strategy targeted the earliest activation site by performing a focal and discrete ablation (Haissaguerre et al., 1998). However, this technique was associated to high rates of pulmonary vein stenosis (Rostamian et al., 2014). Later, wide area circumferential ablation that disconnects the PV two by two became the strategy of choice. This technique is thought to have better results (Lo et al., 2007) by targeting the trigger sources and the ostial drivers and also by autonomic denervation (Redfearn et al., 2007).

PVI is associated with high rates of freedom from AF recurrence. The freedom rate from AF recurrence varies between 60 and 79% (Katritsis et al., 2008; Takigawa et al., 2015a; Straube et al., 2016; Kis et al., 2017), 60 and 72% at 3 years (Vogt et al., 2013; Takigawa et al., 2015a; Takarada et al., 2017) and decreases

TABLE 1 | Summary of the different approaches of percutaneous ablation of AF.

References	Population	Ablation technique	Acute results/main findings	Long term outcome
PVI				
Haïssaguerre et al., 1998	45 PAF	Earliest site of activation of the ectopic beat initiating AF	69 ectopic sites, 94% originating from the PV	62% AF freedom after 8 ± 6months
Chen et al., 1999	79 PAF	Earliest site of activation of the ectopic beat initiating AF	116 ectopic foci, 88.8% originating from the PV	86% AF freedom after 6 ± 2 months, Focal stenosis in 42.4% of the PVs
Haïssaguerre et al., 2000	70 PAF	PV isolation (except RIPV) by targeting atrial breakthroughs		73% AF freedom after 4± 5 months, (29 patients had re-ablation session)
Deisenhofer et al., 2003	• 69 PAF • 6 PsAF	Segmental PVI	PVI achieved in 89% of the veins	51% AF freedom after 230 ± 133 days 40% underwent second procedure: 90% due to PV reconnection + 40% extra-PV foci
Arentz et al., 2003	• 37 PAF • 18 PsAF	Segmental PVI	PVI achieved in 99% of the veins	27 pts underwent a second procedure 62% event free after one-year follow-up 70% for PAF, 44% for PsAF
SMART AF Natale et al., 2014	• 172 PAF	• 160 PVI using contact force sensing catheter additional atrial ablation in 50% of the cases		• Atrial arrhythmia freedom after 1-year follow-up ◦ 74% = symptomatic arrhythmia ◦ 69.9% = symptomatic and asymptomatic arrhythmia Contact force within the selected range ≥80% of the time significantly increased the 12 month AF/AT freedom (88% vs. 66%)
STAR-AF study Verma et al., 2015	589 PsAF	67: CPVI, 263: CPVI plus CFAE, 259: CPVI plus linear lesions (roof, mitral isthmus)		CPVI + CFAE and CPVI + lines were not superior to CPVI alone after 18% follow-up (AF freedom = 49,46, 59% respectively, $P=0.15$)
CHASE-AF trial Vogler et al., 2015	153 PsAF	78 pts PVI alone, 75 full defragmentation,	• PVI group: SR achieved with electrical cardioversion • Full defragmentation group: AF termination in 60% (AT= 60%, SR= 40%)	No difference in the AF freedom after 1-year follow-up: 61.4% in the PVI group, vs. 58.3% in the full-defrag group
FIRE AND ICE trial Kuck et al., 2016a	762 PAF	• 378: PVI using cryoablation 384: Segmental PVI using radiofrequency ablation	• Successful PVI • 97.9% in radiofrequency group • 98.9% in the cryoballoon group	• AF and AT freedom without anti-arrhythmic drugs after a mean of 1.5-year follow-up was not different between the two groups: ◦ 65.4% in the cryoballoon group ◦ 64.1% in the radiofrequency group
Alster-Lost-AF Trial Fink et al., 2017	• 69 PsAF 6- 12 months 49 PsAF ≥ 12 months	• 61 pts CPVI-only • 57 pts Substrate-modification group, (CPVI + CFAEs and linear ablation)	• AF termination ◦ CPVI alone= 3% ◦ Substrate modification $n = 19\%$ ($P=0.007$)	• AF freedom after 1 year follow-up and a single procedure without AAD: ◦ 39% in the CPVI group ◦ 323% in the substrate modification group • AF freedom after 1-year follow-up and a single procedure ± AAD: ◦ 54% in the CPVI group ◦ 57% in the substrate modification group • AF freedom after 1-year follow-up and multiple procedures • 69% in the CPVI group • 86% in the substrate modification group

(Continued)

TABLE 1 | Continued

References	Population	Ablation technique	Acute results/main findings	Long term outcome
CASTLE AF trial Marrouche et al., 2018	<ul style="list-style-type: none"> 363 pts NYHA II,III,IV with PAF or PsAF, LVEF $\leq 35\%$ and an ICD 118 PAF 245 PsAF 106 PsAF > 12months 	<ul style="list-style-type: none"> Ablation = 179 pts vs. medical therapy= 184 Ablation consisted in PVI plus additional lesions at the discretion of the operator 		<ul style="list-style-type: none"> Ablation significantly reduced death from any cause and hospitalizations for worsening heart failure <ul style="list-style-type: none"> 28.5% after ablation 44.6% with medical treatment (hazard ratio, 0.62; 95% confidence interval, 0.43 to 0.87; $P=0.007$)
Tilz et al., 2018	161 PAF	CPVI using EAM and double-Lasso technique	<ul style="list-style-type: none"> All PVI were isolated during the index procedure Up to 5 redo procedures were performed Recurrence were mainly due to PV reconnections 	<ul style="list-style-type: none"> 10-year AF freedom <ul style="list-style-type: none"> 32.9% after a single procedure 62.7% after multiple procedures 6.2% progression to persistent AF after 10 years
CFAE ABLATION				
Nademanee et al., 2004	<ul style="list-style-type: none"> 57 PAF 64 PsAF 	CFAE ablation	<ul style="list-style-type: none"> Acute termination without antiarrhythmic drugs <ul style="list-style-type: none"> PAF: 86% PsAF: 62% 	<ul style="list-style-type: none"> AF freedom after 1 procedure at 1year follow-up= 76% Overall 91% AF freedom after 1 year follow-up
Oral et al., 2007	100 PsAF	CFAE ablation	Acute termination without antiarrhythmic drug: 16%	<ul style="list-style-type: none"> AF freedom after 14 \pm 7 months = 33% Redo ablation = 44% Overall AF freedom after 13 \pm 7 months = 57%
Oral et al., 2009	119 long lasting PsAF	<ul style="list-style-type: none"> 19 PVI 50 CFAE ablation 50 cardioversion 	<ul style="list-style-type: none"> AF termination by PVI only= 16% Acute AF termination during CFAE ablation $n = 18$ 	<ul style="list-style-type: none"> AF freedom after 1 procedure: 36% in the absence of CFAE ablation and 34% after CFAE ablation ($P=NS$) →No benefit of additional CFAE ablation
SELECT-AF study Verma et al., 2014	<ul style="list-style-type: none"> 48 PsAF 28 PAF 	<ul style="list-style-type: none"> 38 pts: CPVI and all CFAE 39 pts: CPVI and selective CFAE with continuous electrical activity 	<ul style="list-style-type: none"> CFAE ablation prolonged AF cycle length and resulted in similar rates of AF termination (37% vs. 28%; $P=0.42$) 	<ul style="list-style-type: none"> AF, AFL and AT freedom without anti-arrhythmic drugs after 1-year follow-up significantly lower after selective CFAE ablation (28% vs.50%)
Atienza et al., 2014 RADAR-AF	<ul style="list-style-type: none"> PAF= 115, AF induced in 95 pts PsAF= 117, AF induced in 22pts 	<ul style="list-style-type: none"> PAF= CPVI or high frequency sources ablation (HFSA) PSAF= CPVI or CPVI+ HFSA 	<ul style="list-style-type: none"> AF termination <ul style="list-style-type: none"> PAF CPVI= 38% HFSA= 58% PsAF CPVI= 26% CPVI + HFSA= 46% 	<ul style="list-style-type: none"> AF/AT freedom after 1 year-follow-up after a single procedure <ul style="list-style-type: none"> PAF 79% after CPVI 81% after HFSA PsAF <ul style="list-style-type: none"> 72% after CPVI 76% after CPVI + HFSA AF freedom after a first procedure at 1-year follow up significantly higher in the stepwise group: <ul style="list-style-type: none"> 73.3% in the stepwise group 53.3% after PVI ($p<0.01$) Similar results after a second procedure
Faustino et al., 2015	PAF: 150	<ul style="list-style-type: none"> 75 PVI alone 75 PVI + stepwise ablation (CFAEs + linear ablation) 	AF termination and non-inducibility achieved in 100% of the stepwise approach	<ul style="list-style-type: none"> AF freedom after a first procedure at 1-year follow up significantly higher in the stepwise group: <ul style="list-style-type: none"> 73.3% in the stepwise group 53.3% after PVI ($p<0.01$) Similar results after a second procedure
Seitz et al., 2017	33 PAF 119 PsAF	<ul style="list-style-type: none"> 105= ablation only regions displaying electrogram dispersion during AF 47= PVI and stepwise approach 	<ul style="list-style-type: none"> Ablation only at dispersion areas terminated AF in 95% of the pts. PVI/stepwise approach terminated AF in 60% of the pts 	<ul style="list-style-type: none"> AF freedom after a mean of 1.5 procedures per patient procedures after 18 month-follow-up: <ul style="list-style-type: none"> 85%= ablation only at regions displaying electrogram dispersion 59% = PVI/Stepwise approach ($P<0.001$)

(Continued)

TABLE 1 | Continued

References	Population	Ablation technique	Acute results/main findings	Long term outcome
ROTOR ABLATION AND FIRM ABLATION				
Cuculich et al., 2010	<ul style="list-style-type: none"> • PAF: 11 • PsAF \leq12 months: 19 • PsAF >12 months:6 	Driver domains identified by ECGi	<ul style="list-style-type: none"> • Multiple wavelets: most common pattern (92% of the patients) • Rotor activity detected in only 15% of the cases and only in patients with PsAF • AF complexity increased with the AF duration 	N/A
Haissaguerre et al., 2014	<ul style="list-style-type: none"> • PsAF in SR= 26 • PsAF AF \leq12 months= 57 • PsAF > 12 months= 20 	Driver domains identified by ECGi	80% AF termination after 28 \pm minutes of RF ablation. AF complexity increased with AF duration	85% AF freedom at 12 months in group, no difference compared to the control group
Lim et al., 2017	<ul style="list-style-type: none"> • PsAF in SR= 32 • PsAF AF \leq12 months= 45 • PsAF > 12 months= 28 	Driver domains identified by ECGi	<ul style="list-style-type: none"> • 70% AF termination, • Increased AF complexity and reduced success rate with the increase of AF duration 	NA
Knecht et al., 2017	<ul style="list-style-type: none"> • PsAF in SR= 32 • PsAF AF \leq12 months= 45 	Driver domains identified by ECGi in 8 different centers	64% AF termination after 46 \pm 28min RF ablation	<ul style="list-style-type: none"> • AF freedom after 1-year follow-up was 77% • Of the patients with no AF recurrence, 49% experienced at least one episode of atrial tachycardia (AT) which required either continued AAD therapy, cardioversion, or repeat ablation
Narayan et al., 2012b	<ul style="list-style-type: none"> • PAF= 31 • PsAF= 76 	FIRM guided: 36 Conventional ablation: 71	FIRM guided AF termination in 56% of the cases vs. 9% with conventional ablation	82% in the FIRM guided ablation vs. 45% AF freedom after 9 months
Pappone et al., 2018	PsAF: 81	<ul style="list-style-type: none"> • Group I: ablation of repetitive-regular activities followed by modified CPVI (mapping group; $n = 41$) • Group II: modified CPVI (control group; $n = 40$) 	61% (25/41) AF termination in the mapping- guided ablation vs. 30% (12/40) with conventional strategy ($P < 0.007$)	<ul style="list-style-type: none"> • AF freedom after 1-year follow-up <ul style="list-style-type: none"> ◦ 73.2% AF-free recurrence in the mapping group ◦ 50% in the control group ($P = 0.03$)
Honarbakhsh et al., 2017	20 PsAF	<ul style="list-style-type: none"> • Driver domains identified by basket catheters • Drivers identified using global activation propagation and not phase mapping 	<ul style="list-style-type: none"> • 30 potential drivers: 19 showing rotational activity and 11 focal • 26 drivers were ablated with a predefined response 84% of the cases (AF terminated with 12 and CL showed prolongation \geq30 ms with 10) 	N/A
Cochet et al., 2018	PsAF = 41	Driver domains identified using ECGi during AF	<ul style="list-style-type: none"> • Left atrial (LA)LGE imaging significantly associated with the number of re-entrant regions ($R = 0.52$; $P = 0.001$) • Clustering of re-entrant activity at LGE borders • Areas with high re-entrant activity showed higher local LGE density as compared with the remaining atrial areas • Failure to achieve AF termination during ablation was associated with higher LA LGE burden, higher number of re-entrant regions and longer AF duration 	AF freedom after 11 +/1 2 month-follow-up 25/34 (74%) pts.

(Continued)

TABLE 1 | Continued

References	Population	Ablation technique	Acute results/main findings	Long term outcome
LINEAR ABLATION				
Jais et al., 2004	PAF= 100	PVI + MI line vs. PVI + CTI line	PVI was achieved in all the pts, MI block was achieved in 92% of the pts	87% AF freedom without anti arrhythmic drugs after MI ablation after 1-year follow-up vs. 69 in the PVI group
Fassini et al., 2005	• PAF= 126 • PsAF= 61	Randomization: 92 PVI vs. 95 PVI + MI line	MI block was achieved in 72% of the pts	AF freedom at 1-year follow-up: PsAF: 74% after MI line vs. 36%, $p < 0.01$ PAF: 76% after MI line vs. 62%, $p < 0.05$
Hocini et al., 2005	• PAF= 90	• PVI + roof line • PVI • Ablation of CTI and ostial PV fragmented signals and non PV triggers in all cases	Roof line blocked in 96% of the cases Perimitral flutter inducible in 22% of the cases	87% Af freedom after roof line after 15month-follow-up vs. 69% in the PVI group
Gaita et al., 2008	• PAF=125 • PsAF and long lasting PsAF=79	• 67 PVI alone (41 PAF + 26 PsAF) • 137 PVI plus left linear lesions (84 PAF + 53PsAF/Long-standing AF)	• PVI was acutely achieved in all pts. • MI block in 31% of the cases • Roof block in 92% of the cases • CTI block in all patients	• AF freedom after a single procedure at 12-month follow-up, ◦ PVI alone= 46% for PAF ◦ PVI alone= 27% for PsAF ◦ PVI + lines= 57% for PAF ◦ PVI + lines= 45% for PsAF • AF freedom after a single procedure at 3-year follow-up, ◦ PVI alone: 29% for PAF ◦ PVI alone: 19% for PsAF ◦ PVI + lines: 53% for PAF ◦ PVI + lines: 41% for PsAF • After a second procedure (in about 50% of the cases), long term AF freedom without AAD: ◦ PVI: 62% for PAF ◦ PVI: 39% for PsAF ◦ PVI + lines: 85% for PAF ◦ PVI + lines: 75% for PsAF • AF freedom after 15.6 \pm 5 months of follow-up, ◦ 88.5% = CPVI ◦ 78.8% = CPVI + roof line ◦ 80.8% = CPVI + posterior ($P=0.44$)
Mun et al., 2012	• PAF= 156	• 52= CPVI, • 52= CPVI+ roof line • 52= CPVI+ posterior box	• CPVI = 100%, • CPVI +Roof line block= 80.8% • CPVI + posterior box= 59.6%	• AF freedom after 16.3 \pm 4-month follow-up without AAD: ◦ CPVI= 88% ◦ CPVI + posterior box + anterior line= 84%
Kim et al., 2015	• PAF= 100	• 50 CPVI • 50 CPVI + posterior box lesion and anterior linear ablation	• CPVI + CTI block= 100% • Anterior Line block= 68% • Posterior box isolatio $n = 60$ %	• AF freedom after 1-year follow-up ◦ 81% after roof line vs. ◦ 74% after PVI ($p = \text{NS}$)
Kettering et al., 2017	PsAF= 250	• CPVI + roof line • CPVI alone • Additional MI line (6 pts), and right atrial ablation (11 pts)	• Roof blocked in all cases	• AF freedom after 3-year follow-up ◦ 72% after roof line 63% after PVI, $P= 0.04$
SUBSTRATE MODIFICATION (FIBROTIC AREAS AND LOW VOLTAGE AREAS)				
Jadidi et al., 2016	PsAF=151	• Group 1: 85: PVI + ablation at low-voltage areas (LVA <0.5 mV in AF) with fractionated activity or rotational activity or discrete rapid local activity • Group 2: 66: PVI (control group)	• AF termination targeting LVAs with specific electrogram patterns = 73% • AF termination sites colocalized within LVA in 80% and at border zones in 20%	• Single- procedural AF-free survival after 13-month follow-up ◦ 69% = group 1 ◦ 47% = group 2 ($P < 0.001$)

(Continued)

TABLE 1 | Continued

References	Population	Ablation technique	Acute results/main findings	Long term outcome
Yamaguchi et al., 2016	PsAF= 117	<ul style="list-style-type: none"> Group I: 101= targeting low-voltage areas (<0.5 mV in SR) <ul style="list-style-type: none"> Group Ia:39 = PVI + ablation of LVA Group Ib:62 = PVI only (LVA not identified) Group II: 16= LVA non ablated group, only PVI 	<ul style="list-style-type: none"> Complete low voltage areas elimination in 92% of the cases Additional linear lesions in 82% of the cases in group Ia 	<ul style="list-style-type: none"> AF freedom after a single procedure after 18 ± 7 months <ul style="list-style-type: none"> 72% = No LVA identified 79% LVA ablation 38% No LVA ablation
BIFA trial Schreiber et al., 2017	<ul style="list-style-type: none"> PAF= 34 PsAF= 49 Long lasting PsAF= 9 	<ul style="list-style-type: none"> 92 PVI + box isolation of fibrotic area (BIFA) (<0.5 mV bipolar signals in sinus rhythm) 49 PVI (no fibrotic area identified during mapping) 	<ul style="list-style-type: none"> Different stages of Fibrotic atrial cardiomyopathy (FACM) <ul style="list-style-type: none"> 0= no detectable voltage < 1.5 mV I= very limited severe fibrosis II= confluence scar fibrotic areas (< 0.5 mV) III= pronounced ≥ 2 scar fibrotic areas (<0.5 mV) IV= diffuse fibrosis ("strawberry") AF termination in STABLER-SR group =12.3% AF termination in stepwise group=32.5% 	<ul style="list-style-type: none"> AF freedom after 16 ± 8 months <ul style="list-style-type: none"> Single procedure=69% Multiple procedures= 83% The extent of fibrosis significantly associated to AF recurrence
STABLE SR Yang et al., 2017	PsAF=229 pts	<ul style="list-style-type: none"> STABLE-SR group: 114=CPVI + CTI + ablation-homogenization of areas with low-voltage (LVZ 0.1–0.4 mV in SR) and complex electrograms Stepwise group:115= CPVI + linear lesions + CFAEs 	<ul style="list-style-type: none"> AF termination in STABLER-SR group =12.3% AF termination in stepwise group=32.5% 	<ul style="list-style-type: none"> AF-free survival after 18-month follow-up STABLE-SR group: 74% Stepwise group: 71.5% ($P=0.325$)

AF, atrial fibrillation; AFL, atrial flutter; AT, atrial tachycardia; CTI, cavo-tricuspid isthmus; EAM, electro-anatomical mapping; LVEF, left ventricular ejection fraction; CPVI, circumferential pulmonary veins isolation; MI, mitral isthmus; PAF, paroxysmal AF; PsAF, persistent AF; PVI, pulmonary veins isolation.

to 53–68% at 5 years (Neumann et al., 2013; Takigawa et al., 2015a, 2017; Kis et al., 2017). The long term freedom from AF may reach 77% (Vogt et al., 2013) after redo PVI. AF recurrence may be related to non PV triggers in one half of cases (Takigawa et al., 2015b) and to the reconnection of the PVs in the remaining cases.

Substrate modification in addition to PVI was tested by Di Biase et al. (2009) who randomly assigned 103 consecutive patients undergoing PAF to PVI alone ($n = 35$), PVI followed by CFAE ablation ($n = 34$) or CFAE ablation alone ($n = 34$). There was no difference in terms of success rate between PVI alone and PVI followed by CFAE ablation. However, CFAE ablation alone was associated with the highest rates of AF recurrence after 1-year follow-up. Similar results were reported in subsequent studies (Deisenhofer et al., 2009; Chen et al., 2011; Hayward et al., 2011). In addition, techniques aiming at incomplete PVI (Kuck et al., 2016b) or not isolating PV (Mikhaylov et al., 2011) were associated to worse results.

CFAE Ablation

Targeting the complex fractionated signals was commonly used as a strategy to ablate PsAF forms. Originally in 2004; Nademanee et al. (2004) included 121 patients with paroxysmal AF (57 patients) or chronic AF (64 patients) and performed ablation by targeting fragmented electrograms without additional PVI. They reported a high rate of acute success by targeting areas of CFAE (without PVI) with 95% of AF termination by ablation (associated to ibutilide in 28% of the cases) and 76% of AF

freedom at 1-year follow-up after one procedure. However, this result was not reproduced by Oral et al. (2007) who included 100 patients with chronic AF where they ablated CFAEs in the left atrium and the coronary sinus without performing PVI. Only 33% of the patients were free from AF or AT recurrence after a follow-up of 14 ± 7 months after one procedure. A second procedure was performed in 44% of the patients, pulmonary vein tachycardia originating from the targeted veins sustained atrial tachycardia in all cases.

Oral et al. (2009) performed a randomized study and included 119 consecutive patients with long-lasting PsAF. All patients underwent PVI that allowed termination to sinus rhythm in 19 (16%) of the cases. In the remaining 100 cases, patients were equally assessed to either electrical cardioversion or ablation of the CFAE in the left atrium or the coronary sinus. After 10 ± 3 -month follow-up, there was no difference in the rate of sinus rhythm without anti-arrhythmic drugs between the 3 groups.

In the STAR AF II study, Verma et al. (2015) performed a prospective randomized multicenter study that included 589 patients with PsAF. Ablation consisted in PVI alone in 67 patients, PVI and ablation of complex fractionated electrograms (263 patients) or PVI and additional linear ablation (259 patients). Acute termination of AF during ablation was significantly higher in patients undergoing PVI and complex electrograms ablation or PVI and linear ablation than patients undergoing PVI alone. However, the freedom from AF was not different between the three groups.

AF Drivers' Ablation

In a recent meta-analysis, Parameswaran et al. (2018) analyzed the outcome after rotor ablation in 11 studies with a total of 556 patients undergoing FIRM ablation for paroxysmal AF ($n = 166$) or PsAF ($n = 390$). Pooled single-procedure freedom from AF was around 37.8% PAF and 59.2% for PsAF after a mean follow-up of 1 year. Heterogeneity between the different studies was significantly high.

In the AFACART study (Knecht et al., 2017), non-invasive mapping was used to guide the ablation for 118 patients with PsAF lasting <1 year. Ablation targeted the drivers identified by the system, followed by PV isolation and linear ablation when AF could not be terminated. Ablation targeting the drivers' sites terminated AF in 64% of the cases after a mean radiofrequency ablation duration of 46 ± 28 min. AF termination rate increased to 72% when additional PVI and atrial linear ablation were performed. Extra-PV sources played a key role in the maintenance of PsAF and their ablation is associated with the termination of AF in the majority of the cases and arrhythmia freedom up to 77% at a 1-year follow-up.

Surgical Treatment for AF

Surgical treatment for AF was first described by Dr Cox (Cox, 1991). The surgery consisted in linear incisions of the atrial walls that aimed to interrupt the multiple wavelets and reentrant circuits and subsequently direct atrial activation through a maze-like system involving both atria. Different surgical techniques were developed later (Fragakis et al., 2012; Xu et al., 2016), all associated to high rates of arrhythmia free outcome (Prasad et al.,

2003; Ballaux et al., 2006; Barnett and Ad, 2006; Weimar et al., 2012; Gillinov et al., 2015).

Hybrid approach (Tahir et al., 2018) overcomes the limitations of the catheter based ablation and of the surgical ablation. Epicardial thoracoscopic ablation followed by endocardial ablation is associated to high rates of long term freedom from AF recurrence exceeding 70% in patients with paroxysmal or PsAF (Krul et al., 2011; Pison et al., 2012, 2014; La Meir et al., 2013; Kurfurst et al., 2014; Bulava et al., 2015).

CONCLUSION

Mechanisms underlying AF are complex and remain incompletely understood despite extensive research. Translating AF mechanisms described in basic science to the clinical practice remains challenging. In contrast with PAF, therapeutic interventions for PsAF are still inadequate, mainly limited by the identification of the sources maintaining AF. PsAF is driven by focal and reentrant activity which are initially clustered in a relatively limited atrial surface. These drivers disseminate everywhere because of the atrial remodeling which increases the complexity of AF. Accurate mapping techniques that consider the spatio-temporal variation of AF are essential to identify these sources.

AUTHOR CONTRIBUTIONS

All authors listed have made a substantial, direct and intellectual contribution to the work, and approved it for publication.

REFERENCES

- Abed, H. S., Samuel, C. S., Lau, D. H., Kelly, D. J., Royce, S. G., Alasady, M., et al. (2013). Obesity results in progressive atrial structural and electrical remodeling: implications for atrial fibrillation. *Heart Rhythm.* 10, 90–100. doi: 10.1016/j.hrthm.2012.08.043
- Ajijola, O. A., Wisco, J. J., Lambert, H. W., Mahajan, A., Stark, E., Fishbein, M. C., et al. (2012). Extracardiac neural remodeling in humans with cardiomyopathy. *Circ. Arrhythm. Electrophysiol.* 5, 1010–1116. doi: 10.1161/CIRCEP.112.972836
- Ajijola, O. A., Yagishita, D., Reddy, N. K., Yamakawa, K., Vaseghi, M., Downs, A. M., et al. (2015). Remodeling of stellate ganglion neurons after spatially targeted myocardial infarction: neuropeptide and morphologic changes. *Heart Rhythm.* 12, 1027–1035. doi: 10.1016/j.hrthm.2015.01.045
- Akoum, N., Wilber, D., Hindricks, G., Jais, P., Cates, J., Marchlinski, F., et al. (2015). MRI Assessment of ablation-induced scarring in atrial fibrillation: analysis from the DECAAF study. *J. Cardiovasc. Electrophysiol.* 26, 473–480. doi: 10.1111/jce.12650
- Allessie, M., Ausma, J., and Schotten, U. (2002). Electrical, contractile and structural remodeling during atrial fibrillation. *Cardiovasc. Res.* 54, 230–246. doi: 10.1016/S0008-6363(02)00258-4
- Allessie, M. A., Bonke, F. I., and Schopman, F. J. (1977). Circus movement in rabbit atrial muscle as a mechanism of tachycardia. III. The "leading circle" concept: a new model of circus movement in cardiac tissue without the involvement of an anatomical obstacle. *Circ. Res.* 41, 9–18. doi: 10.1161/01.RES.41.1.9
- Alonso, S., and Bar, M. (2013). Reentry near the percolation threshold in a heterogeneous discrete model for cardiac tissue. *Phys. Rev. Lett.* 110:158101. doi: 10.1103/PhysRevLett.110.158101
- Alonso, S., Dos Santos, R. W., and Bär, M. (2016). Reentry and ectopic pacemakers emerge in a three-dimensional model for a slab of cardiac tissue with diffuse microfibrosis near the percolation threshold. *PLoS ONE* 11:e0166972. doi: 10.1371/journal.pone.0166972
- Amraoui, S., Pomier, C., Sacher, F., Derval, N., Denis, A., Massoullié, G., et al. (2016). 209-05: does flecainide pre-treatment help to identify the most important players? *EP Europace* 18, i141–i141. doi: 10.1093/europace/18.suppl_1.i141
- Anter, E., Di Biase, L., Contreras-Valdes, F. M., Gianni, C., Mohanty, S., Tschabrunn, C. M., et al. (2017). Atrial substrate and triggers of paroxysmal atrial fibrillation in patients with obstructive sleep apnea. *Circ. Arrhythm. Electrophysiol.* 10:e005407. doi: 10.1161/CIRCEP.117.005407
- Arentz, T., Haegeli, L., Sanders, P., Weber, R., Neumann, F. J., Kalusche, D., et al. (2007). High-density mapping of spontaneous pulmonary vein activity initiating atrial fibrillation in humans. *J. Cardiovasc. Electrophysiol.* 18, 31–38. doi: 10.1111/j.1540-8167.2006.00682.x
- Arentz, T., Von Rosenthal, J., Blum, T., Stockinger, J., Burkle, G., Weber, R., et al. (2003). Feasibility and safety of pulmonary vein isolation using a new mapping and navigation system in patients with refractory atrial fibrillation. *Circulation* 108, 2484–2490. doi: 10.1161/01.CIR.0000097118.75179.83
- Armour, J. A. (2008). Potential clinical relevance of the 'little brain' on the mammalian heart. *Exp. Physiol.* 93, 165–176. doi: 10.1113/expphysiol.2007.041178
- Armour, J. A., Murphy, D. A., Yuan, B. X., Macdonald, S., and Hopkins, D. A. (1997). Gross and microscopic anatomy of the human intrinsic cardiac nervous system. *Anat Rec.* 247, 289–298.
- Arora, R. (2012). Recent insights into the role of the autonomic nervous system in the creation of substrate for atrial fibrillation – implications for therapies targeting the atrial autonomic nervous system. *Circ. Arrhythm. Electrophysiol.* 5, 850–859. doi: 10.1161/CIRCEP.112.972273
- Arora, R., Ulphani, J. S., Villuendas, R., Ng, J., Harvey, L., Thordson, S., et al. (2008). Neural substrate for atrial fibrillation: implications for targeted

- parasympathetic blockade in the posterior left atrium. *Am. J. Physiol. Heart Circ. Physiol.* 294, H134–H144. doi: 10.1152/ajpheart.00732.2007
- Atienza, F., Almendral, J., Ormaetxe, J. M., Moya, A., Martinez-Alday, J. D., Hernandez-Madrid, A., et al. (2014). Comparison of radiofrequency catheter ablation of drivers and circumferential pulmonary vein isolation in atrial fibrillation: a noninferiority randomized multicenter RADAR-AF trial. *J. Am. Coll. Cardiol.* 64, 2455–2467. doi: 10.1016/j.jacc.2014.09.053
- Badger, T. J., Daccarett, M., Akoum, N. W., Adjei-Poku, Y. A., Burgon, N. S., Haslam, T. S., et al. (2010). Evaluation of left atrial lesions after initial and repeat atrial fibrillation ablation: lessons learned from delayed-enhancement MRI in repeat ablation procedures. *Circ. Arrhythm. Electrophysiol.* 3, 249–259. doi: 10.1161/CIRCEP.109.868356
- Ballaux, P. K., Geuzebroek, G. S., Van Hemel, N. M., Kelder, J. C., Dossche, K. M., Ernst, J. M., et al. (2006). Freedom from atrial arrhythmias after classic maze III surgery: a 10-year experience. *J. Thorac. Cardiovasc. Surg.* 132, 1433–1440. doi: 10.1016/j.jtcvs.2006.06.048
- Bapat, A., Anderson, C. D., Ellinor, P. T., and Lubitz, S. A. (2018). Genomic basis of atrial fibrillation. *Heart* 104, 201–206. doi: 10.1136/heartjnl-2016-311027
- Barnett, S. D., and Ad, N. (2006). Surgical ablation as treatment for the elimination of atrial fibrillation: a meta-analysis. *J. Thorac. Cardiovasc. Surg.* 131, 1029–1035. doi: 10.1016/j.jtcvs.2005.10.020
- Benharash, P., Buch, E., Frank, P., Share, M., Tung, R., Shivkumar, K., et al. (2015). Quantitative analysis of localized sources identified by focal impulse and rotor modulation mapping in atrial fibrillation. *Circ. Arrhythm. Electrophysiol.* 8, 554–561. doi: 10.1161/CIRCEP.115.002721
- Benjamin Shoemaker, M., Muhammad, R., Parvez, B., White, B. W., Streur, M., Song, Y., et al. (2013). Common atrial fibrillation risk alleles at 4q25 predict recurrence after catheter-based atrial fibrillation ablation. *Heart Rhythm.* 10, 394–400. doi: 10.1016/j.hrthm.2012.11.012
- Benjamin, E. J., Rice, K. M., Arking, D. E., Pfeifer, A., Van Noord, C., Smith, A. V., et al. (2009). Variants in ZFHX3 are associated with atrial fibrillation in individuals of European ancestry. *Nat. Genet.* 41, 879–881. doi: 10.1038/ng.416
- Benjamin, E. J., Wolf, P. A., D'agostino, R. B., Silbershatz, H., Kannel, W. B., and Levy, D. (1998). Impact of atrial fibrillation on the risk of death: the framingham heart study. *Circulation* 98, 946–952. doi: 10.1161/01.CIR.98.10.946
- Berte, B., Relan, J., Sacher, F., Pillois, X., Appetiti, A., Yamashita, S., et al. (2015). Impact of electrode type on mapping of scar-related VT. *J. Cardiovasc. Electrophysiol.* 26, 1213–1223. doi: 10.1111/jce.12761
- Bray, M. A., and Wikswo, J. P. (2002). Considerations in phase plane analysis for nonstationary reentrant cardiac behavior. *Phys. Rev. E Stat. Nonlin. Soft Matter Phys.* 65:051902. doi: 10.1103/PhysRevE.65.051902
- Buch, E., Share, M., Tung, R., Benharash, P., Sharma, P., Koneru, J., et al. (2016). Long-term clinical outcomes of focal impulse and rotor modulation for treatment of atrial fibrillation: a multicenter experience. *Heart Rhythm.* 13, 636–641. doi: 10.1016/j.hrthm.2015.10.031
- Bulava, A., Mokrakek, A., Hanis, J., Kurfirst, V., Eisenberger, M., and Pesl, L. (2015). Sequential Hybrid Procedure for Persistent Atrial Fibrillation. *Journal of the American Heart Association.* 4:e001754. doi: 10.1161/JAHA.114.001754
- Burstein, B., and Nattel, S. (2008). Atrial fibrosis: mechanisms and clinical relevance in atrial fibrillation. *J. Am. Coll. Cardiol.* 51, 802–809. doi: 10.1016/j.jacc.2007.09.064
- Burstein, B., Qi, X. Y., Yeh, Y. H., Calderone, A., and Nattel, S. (2007). Atrial cardiomyocyte tachycardia alters cardiac fibroblast function: a novel consideration in atrial remodeling. *Cardiovasc. Res.* 76, 442–452. doi: 10.1016/j.cardiores.2007.07.013
- Cabo, C., Pertsov, A. M., Davidenko, J. M., Baxter, W. T., Gray, R. A., and Jalife, J. (1996). Vortex shedding as a precursor of turbulent electrical activity in cardiac muscle. *Biophys. J.* 70, 1105–1111.
- Campbell, C. M., Campbell, J. D., Thompson, C. H., Galimberti, E. S., Darbar, D., Vanoye, C. G., et al. (2013). Selective targeting of gain-of-function KCNQ1 mutations predisposing to atrial fibrillation. *Circ. Arrhythm. Electrophysiol.* 6, 960–966. doi: 10.1161/CIRCEP.113.000439
- Campbell, H. M., and Wehrens, X. H. T. (2018). Genetics of atrial fibrillation: an update. *Curr. Opin. Cardiol.* 33, 304–310. doi: 10.1097/HCO.0000000000000505
- Chang, C. M., Wu, T. J., Zhou, S., Doshi, R. N., Lee, M. H., Ohara, T., et al. (2001). Nerve sprouting and sympathetic hyperinnervation in a canine model of atrial fibrillation produced by prolonged right atrial pacing. *Circulation* 103, 22–25. doi: 10.1161/01.CIR.103.1.22
- Chen, J., Mandapati, R., Berenfeld, O., Skanes, A. C., Gray, R. A., and Jalife, J. (2000). Dynamics of wavelets and their role in atrial fibrillation in the isolated sheep heart. *Cardiovasc. Res.* 48, 220–232. doi: 10.1016/S0008-6363(00)00177-2
- Chen, M., Yang, B., Chen, H., Ju, W., Zhang, F., Tse, H. F., et al. (2011). Randomized comparison between pulmonary vein antral isolation versus complex fractionated electrogram ablation for paroxysmal atrial fibrillation. *J. Cardiovasc. Electrophysiol.* 22, 973–981. doi: 10.1111/j.1540-8167.2011.02051.x
- Chen, P.-S., Chen, L. S., Fishbein, M. C., Lin, S.-F., and Nattel, S. (2014). Role of the autonomic nervous system in atrial fibrillation: pathophysiology and therapy. *Circ. Res.* 114, 1500–1515. doi: 10.1161/CIRCRESAHA.114.303772
- Chen, S. A., Hsieh, M. H., Tai, C. T., Tsai, C. F., Prakash, V. S., Yu, W. C., et al. (1999). Initiation of atrial fibrillation by ectopic beats originating from the pulmonary veins: electrophysiological characteristics, pharmacological responses, and effects of radiofrequency ablation. *Circulation* 100, 1879–1886. doi: 10.1161/01.CIR.100.18.1879
- Chenit, G., Takigawa, M., Denis, A., Thompson, N., Amraoui, S., Antonio, F., et al. (2016). 216–28: electrophysiological effects of amiodarone in patients with persistent atrial fibrillation. *EP Europace* 18, i148–i148. doi: 10.1093/europace/18.suppl_1.i148
- Chou, C. C., Nihei, M., Zhou, S., Tan, A., Kawase, A., Macias, E. S., et al. (2005). Intracellular calcium dynamics and anisotropic reentry in isolated canine pulmonary veins and left atrium. *Circulation* 111, 2889–2897. doi: 10.1161/CIRCULATIONAHA.104.498758
- Christophersen, I. E., Rienstra, M., Roselli, C., Yin, X., Geelhoed, B., Barnard, J., et al. (2017). Large-scale analyses of common and rare variants identify 12 new loci associated with atrial fibrillation. *Nat. Genet.* 49, 946–952. doi: 10.1038/ng.3843
- Cochet, H., Dubois, R., Sacher, F., Derval, N., Sermesant, M., Hocini, M., et al. (2014). Cardiac arrhythmias: multimodal assessment integrating body surface ECG mapping into cardiac imaging. *Radiology* 271, 239–247. doi: 10.1148/radiol.13131331
- Cochet, H., Dubois, R., Yamashita, S., Al Jefairi, N., Berte, B., Sellal, J. M., et al. (2018). Relationship between fibrosis detected on late gadolinium-enhanced cardiac magnetic resonance and re-entrant activity assessed with electrocardiographic imaging in human persistent atrial fibrillation. *JACC Clin Electrophysiol.* 4, 17–29. doi: 10.1016/j.jacep.2017.07.019
- Comtois, P., and Nattel, S. (2011). Interactions between cardiac fibrosis spatial pattern and ionic remodeling on electrical wave propagation. *Conf. Proc. IEEE Eng. Med. Biol. Soc.* 2011, 4669–4672. doi: 10.1109/IEMBS.2011.6091156
- Comtois, P., and Vinet, A. (1999). Curvature effects on activation speed and repolarization in an ionic model of cardiac myocytes. *Physical Review E.* 60, 4619–4628. doi: 10.1103/PhysRevE.60.4619
- Correa De Sa, D. D., Thompson, N., Stinnett-Donnelly, J., Znokiewicz, P., Habel, N., Muller, J. G., et al. (2011). Electrogram fractionation: the relationship between spatiotemporal variation of tissue excitation and electrode spatial resolution. *Circ. Arrhythm. Electrophysiol.* 4, 909–916. doi: 10.1161/CIRCEP.111.965145
- Cox, J. L. (1991). The surgical treatment of atrial fibrillation. IV. Surgical technique. *J. Thorac. Cardiovasc. Surg.* 101, 584–592.
- Cuculich, P. S., Wang, Y., Lindsay, B. D., Faddis, M. N., Schuessler, R. B., Damiano, R. J. Jr. et al. (2010). Noninvasive characterization of epicardial activation in humans with diverse atrial fibrillation patterns. *Circulation* 122, 1364–1372. doi: 10.1161/CIRCULATIONAHA.110.945709
- Daccarett, M., Badger, T. J., Akoum, N., Burgon, N. S., Mahnkopf, C., Vergara, G., et al. (2011). Association of left atrial fibrosis detected by delayed-enhancement magnetic resonance imaging and the risk of stroke in patients with atrial fibrillation. *J. Am. Coll. Cardiol.* 57, 831–838. doi: 10.1016/j.jacc.2010.09.049
- Daoud, E. G., Zeidan, Z., Hummel, J. D., Weiss, R., Houmsse, M., Augostini, R., et al. (2017). Identification of repetitive activation patterns using novel computational analysis of multielectrode recordings during atrial fibrillation and flutter in humans. *JACC Clin. Electrophysiol.* 3, 207–216. doi: 10.1016/j.jacep.2016.08.001
- Darbar, D. (2016). The role of pharmacogenetics in atrial fibrillation therapeutics: is personalized therapy in sight? *J. Cardiovasc. Pharmacol.* 67, 9–18. doi: 10.1097/FJC.0000000000000280

- Darbar, D., Motsinger, A. A., Ritchie, M. D., Gainer, J. V., and Roden, D. M. (2007). Polymorphism modulates symptomatic response to antiarrhythmic drug therapy in patients with lone atrial fibrillation. *Heart Rhythm*. 4, 743–749. doi: 10.1016/j.hrthm.2007.02.006
- Davidenko, J. M., Kent, P. F., Chialvo, D. R., Michaels, D. C., and Jalife, J. (1990). Sustained vortex-like waves in normal isolated ventricular muscle. *Proc. Natl. Acad. Sci. U.S.A.* 87, 8785–8789. doi: 10.1073/pnas.87.22.8785
- Davidenko, J. M., Pertsov, A. V., Salomonsz, R., Baxter, W., and Jalife, J. (1992). Stationary and drifting spiral waves of excitation in isolated cardiac muscle. *Nature* 355, 349–351. doi: 10.1038/355349a0
- De Bakker, J. M., and Wittkampf, F. H. (2010). The pathophysiologic basis of fractionated and complex electrograms and the impact of recording techniques on their detection and interpretation. *Circ. Arrhythm. Electrophysiol.* 3, 204–213. doi: 10.1161/CIRCEP.109.904763
- De Groot, N., Van Der Does, L., Yaksh, A., Lanters, E., Teuwen, C., Knops, P., et al. (2016). Direct proof of endo-epicardial asynchrony of the atrial wall during atrial fibrillation in humans. *Circ. Arrhythm. Electrophysiol.* 9:e003648. doi: 10.1161/CIRCEP.115.003648
- Deisenhofer, I., Estner, H., Reents, T., Fichtner, S., Bauer, A., Wu, J., et al. (2009). Does electrogram guided substrate ablation add to the success of pulmonary vein isolation in patients with paroxysmal atrial fibrillation? A prospective, randomized study. *J. Cardiovasc. Electrophysiol.* 20, 514–521. doi: 10.1111/j.1540-8167.2008.01379.x
- Deisenhofer, I., Schneider, M. A. E., Böhnen-Knauf, M., Zrenner, B., Ndrepepa, G., Schmieder, S., et al. (2003). Circumferential mapping and electric isolation of pulmonary veins in patients with atrial fibrillation. *Am. J. Cardiol.* 91, 159–163. doi: 10.1016/S0002-9149(02)03102-8
- Dewland, T. A., Olglin, J. E., Vittinghoff, E., and Marcus, G. M. (2013). Incident atrial fibrillation among Asians, Hispanics, Blacks, and Whites. *Circulation* 128, 2470–2477. doi: 10.1161/CIRCULATIONAHA.113.002449
- Di Biase, L., Elayi, C. S., Fahmy, T. S., Martin, D. O., Ching, C. K., Barrett, C., et al. (2009). Atrial fibrillation ablation strategies for paroxysmal patients: randomized comparison between different techniques. *Circ. Arrhythm. Electrophysiol.* 2, 113–119. doi: 10.1161/CIRCEP.108.798447
- Dimitri, H., Ng, M., Brooks, A. G., Kuklik, P., Stiles, M. K., Lau, D. H., et al. (2012). Atrial remodeling in obstructive sleep apnea: implications for atrial fibrillation. *Heart Rhythm*. 9, 321–327. doi: 10.1016/j.hrthm.2011.10.017
- Eggimann, L., Blum, S., Aeschbacher, S., Reusser, A., Ammann, P., Erne, P., et al. (2018). Risk factors for heart failure hospitalizations among patients with atrial fibrillation. *PLoS ONE* 13:e0191736. doi: 10.1371/journal.pone.0191736
- Ehrlich, J. R., Cha, T. J., Zhang, L., Chartier, D., Melnyk, P., Hohnloser, S. H., et al. (2003). Cellular electrophysiology of canine pulmonary vein cardiomyocytes: action potential and ionic current properties. *J. Physiol.* 551, 801–813. doi: 10.1113/jphysiol.2003.046417
- Elayi, C. S., Di Biase, L., Bai, R., Burkhardt, J. D., Mohanty, P., Santangeli, P., et al. (2013). Administration of isoproterenol and adenosine to guide supplemental ablation after pulmonary vein antrum isolation. *J. Cardiovasc. Electrophysiol.* 24, 1199–1206. doi: 10.1111/jce.12252
- Ellinor, P. T., Lunetta, K. L., Albert, C. M., Glazer, N. L., Ritchie, M. D., Smith, A. V., et al. (2012). Meta-analysis identifies six new susceptibility loci for atrial fibrillation. *Nat. Genet.* 44, 670–675. doi: 10.1038/ng.2261
- Ellinor, P. T., Lunetta, K. L., Glazer, N. L., Pfeufer, A., Alonso, A., Chung, M. K., et al. (2010). Common variants in KCNN3 are associated with lone atrial fibrillation. *Nat. Genet.* 42, 240–244. doi: 10.1038/ng.537
- Enriquez, A., Liang, J. J., Santangeli, P., Marchlinski, F. E., and Riley, M. P. (2017). Focal atrial fibrillation from the superior vena cava. *J. Atr. Fibrillation*. 9:1593. doi: 10.4022/jafib.1593
- Faggioni, M., Savio-Galimberti, E., Venkataraman, R., Hwang, H. S., Kannankeril, P. J., Darbar, D., et al. (2014). Suppression of spontaneous ca elevations prevents atrial fibrillation in calsequestrin 2-null hearts. *Circ. Arrhythm. Electrophysiol.* 7, 313–320. doi: 10.1161/CIRCEP.113.000994
- Fassini, G., Riva, S., Chiodelli, R., Trevisi, N., Berti, M., Carbucicchio, C., et al. (2005). Left mitral isthmus ablation associated with PV Isolation: long-term results of a prospective randomized study. *J. Cardiovasc. Electrophysiol.* 16, 1150–1156. doi: 10.1111/j.1540-8167.2005.50192.x
- Faustino, M., Pizzi, C., Agricola, T., Xyheri, B., Costa, G. M., Flacco, M. E., et al. (2015). Stepwise ablation approach versus pulmonary vein isolation in patients with paroxysmal atrial fibrillation: randomized controlled trial. *Heart Rhythm*. 12, 1907–1915. doi: 10.1016/j.hrthm.2015.06.009
- Fink, T., Schluter, M., Heeger, C. H., Lemes, C., Maurer, T., Reissmann, B., et al. (2017). Stand-alone pulmonary vein isolation versus pulmonary vein isolation with additional substrate modification as index ablation procedures in patients with persistent and long-standing persistent atrial fibrillation: the randomized alster-lost-AF Trial (Ablation at St. Georg Hospital for Long-Standing Persistent Atrial Fibrillation). *Circ. Arrhythm. Electrophysiol.* 10:e005114. doi: 10.1161/CIRCEP.117.005114
- Fox, C. S., Parise, H., D'agostino, R. B. Sr, Lloyd-Jones, D. M., Vasan, R. S., Wang, T. J., et al. (2004). Parental atrial fibrillation as a risk factor for atrial fibrillation in offspring. *JAMA* 291, 2851–2855. doi: 10.1001/jama.291.23.2851
- Fragakis, N., Pantos, I., Younis, J., Hadjipavlou, M., and Katritsis, D. G. (2012). Surgical ablation for atrial fibrillation. *Europace* 14, 1545–1552. doi: 10.1093/europace/eus081
- Frontera, A., Cheniti, G., Martin, C. A., Takigawa, M., Duchateau, J., Puyo, S., et al. (2018a). Frontiers in non-invasive cardiac mapping: future implications for arrhythmia treatment. *Minerva Cardioangiologica*. 66, 75–82. doi: 10.23736/S0026-4725.17.04463-2
- Frontera, A., Takigawa, M., Martin, R., Thompson, N., Cheniti, G., Massoulié, G., et al. (2018b). Electrogram signature of specific activation patterns: analysis of atrial tachycardias at high-density endocardial mapping. *Heart Rhythm*. 15, 28–37. doi: 10.1016/j.hrthm.2017.08.001
- Frustaci, A., Chimenti, C., Bellocchi, F., Morgante, E., Russo, M. A., and Maseri, A. (1997). Histological substrate of atrial biopsies in patients with lone atrial fibrillation. *Circulation* 96, 1180–1184. doi: 10.1161/01.CIR.96.4.1180
- Gaita, F., Caponi, D., Scaglione, M., Montefusco, A., Corleto, A., Di Monte, F., et al. (2008). Long-term clinical results of 2 different ablation strategies in patients with paroxysmal and persistent atrial fibrillation. *Circ. Arrhythm. Electrophysiol.* 1, 269–275. doi: 10.1161/CIRCEP.108.774885
- Ganesan, A. N., Shipp, N. J., Brooks, A. G., Kuklik, P., Lau, D. H., Lim, H. S., et al. (2013). Long-term outcomes of catheter ablation of atrial fibrillation: a systematic review and meta-analysis. *J. Am. Heart Assoc.* 2:e004549. doi: 10.1161/JAHA.112.0004549
- Gillinov, A. M., Gelijns, A. C., Parides, M. K., Deroze, J. J. Jr, Moskowitz, A. J., Voisine, P., et al. (2015). Surgical ablation of atrial fibrillation during mitral-valve surgery. *N. Engl. J. Med.* 372, 1399–1409. doi: 10.1056/NEJMoa1500528
- Goldbeter, A. (1975). Mechanism for oscillatory synthesis of cyclic AMP in Dictyostelium discoideum. *Nature* 253, 540–542. doi: 10.1038/253540a0
- Gould, P. A., YII, M., McLean, C., Finch, S., Marshall, T., Lambert, G. W., et al. (2006). Evidence for increased atrial sympathetic innervation in persistent human atrial fibrillation. *Pacing Clin. Electrophysiol.* 29, 821–829. doi: 10.1111/j.1540-8159.2006.00447.x
- Grace, A., Verma, A., and Willems, S. (2017). Dipole density mapping of atrial fibrillation. *Eur. Heart J.* 38, 5–9. doi: 10.1093/eurheartj/ehw585
- Gray, R. A., Pertsov, A. M., and Jalife, J. (1998). Spatial and temporal organization during cardiac fibrillation. *Nature* 392, 75–78. doi: 10.1038/32164
- Gudbjartsson, D. F., Arnar, D. O., Helgadottir, A., Gretarsdottir, S., Holm, H., Sigurdsson, A., et al. (2007). Variants conferring risk of atrial fibrillation on chromosome 4q25. *Nature* 448, 353–357. doi: 10.1038/nature06007
- Gulrajani, R. M., Savard, P., and Roberge, F. A. (1988). The inverse problem in electrocardiography: solutions in terms of equivalent sources. *Crit. Rev. Biomed. Eng.* 16, 171–214.
- Guo, Y., Lip, G. Y., and Apostolakis, S. (2012). Inflammation in atrial fibrillation. *J. Am. Coll. Cardiol.* 60, 2263–2270. doi: 10.1016/j.jacc.2012.04.063
- Haïssaguerre, M., Hocini, M., Sanders, P., Takahashi, Y., Rotter, M., Sacher, F., et al. (2006). Localized sources maintaining atrial fibrillation organized by prior ablation. *Circulation*. 113, 616–625. doi: 10.1161/CIRCULATIONAHA.105.546648
- Haïssaguerre, M., Jais, P., Shah, D. C., Takahashi, A., Hocini, M., Quiniou, G., et al. (1998). Spontaneous initiation of atrial fibrillation by ectopic beats originating in the pulmonary veins. *N. Engl. J. Med.* 339, 659–666. doi: 10.1056/NEJM199809033391003
- Haïssaguerre, M., Shah, A. J., Cochet, H., Hocini, M., Dubois, R., Efimov, I., et al. (2016). Intermittent drivers anchoring to structural heterogeneities as a major

- pathophysiological mechanism of human persistent atrial fibrillation. *J. Physiol.* 594, 2387–2398. doi: 10.1113/JP270617
- Haissaguerre, M., Shah, D. C., Jais, P., Hocini, M., Yamane, T., Deisenhofer, I., et al. (2000). Electrophysiological breakthroughs from the left atrium to the pulmonary veins. *Circulation* 102, 2463–2465. doi: 10.1161/01.CIR.102.20.2463
- Han, S., Kobayashi, K., Joung, B., Piccirillo, G., Maruyama, M., Vinters, H. V., et al. (2012). Electroanatomic remodeling of the left stellate ganglion after myocardial infarction. *J. Am. Coll. Cardiol.* 59, 954–961. doi: 10.1016/j.jacc.2011.11.030
- Hansen, B. J., Csepe, T. A., Zhao, J., Ignazzi, A. J., Hummel, J. D., and Fedorov, V. V. (2016). Maintenance of atrial fibrillation: are reentrant drivers with spatial stability the key? *Circ. Arrhythm. Electrophysiol.* 9:e004398. doi: 10.1161/CIRCEP.116.004398
- Hansen, B. J., Zhao, J., Csepe, T. A., Moore, B. T., Li, N., Jayne, L. A., et al. (2015). Atrial fibrillation driven by micro-anatomic intramural re-entry revealed by simultaneous sub-epicardial and sub-endocardial optical mapping in explanted human hearts. *Eur. Heart J.* 36, 2390–2401. doi: 10.1093/eurheartj/ehv233
- Hansen, B. J., Zhao, J., and Fedorov, V. V. (2017). Fibrosis and atrial fibrillation: computerized and optical mapping; a view into the human atria at submillimeter resolution. *JACC Clin. Electrophysiol.* 3, 531–546. doi: 10.1016/j.jacep.2017.05.002
- Hatem, S. N., and Sanders, P. (2014). Epicardial adipose tissue and atrial fibrillation. *Cardiovasc. Res.* 102, 205–213. doi: 10.1093/cvr/cvu045
- Hayward, R. M., Upadhyay, G. A., Mela, T., Ellinor, P. T., Barrett, C. D., Heist, E. K., et al. (2011). Pulmonary vein isolation with complex fractionated atrial electrogram ablation for paroxysmal and nonparoxysmal atrial fibrillation: a meta-analysis. *Heart Rhythm*, 994–1000. doi: 10.1016/j.hrthm.2011.02.033
- Heijman, J., Voigt, N., Nattel, S., and Dobrev, D. (2014). Cellular and molecular electrophysiology of atrial fibrillation initiation, maintenance, and progression. *Circ. Res.* 114, 1483–1499. doi: 10.1161/CIRCRESAHA.114.302226
- Hirose, M., and Laurita, K. R. (2007). Calcium-mediated triggered activity is an underlying cellular mechanism of ectopy originating from the pulmonary vein in dogs. *Am. J. Physiol. Heart Circ. Physiol.* 292, H1861–H1867. doi: 10.1152/ajpheart.08262.2006
- Hocini, M., Ho, S. Y., Kawara, T., Linnenbank, A. C., Potse, M., Shah, D., et al. (2002). Electrical conduction in canine pulmonary veins: electrophysiological and anatomic correlation. *Circulation* 105, 2442–2448. doi: 10.1161/01.CIR.0000016062.80020.11
- Hocini, M., Jais, P., Sanders, P., Takahashi, Y., Rotter, M., Rostock, T., et al. (2005). Techniques, evaluation, and consequences of linear block at the left atrial roof in paroxysmal atrial fibrillation: a prospective randomized study. *Circulation* 112, 3688–3696. doi: 10.1161/CIRCULATIONAHA.105.541052
- Hocini, M., Nault, I., Wright, M., Veenhuzzen, G., Narayan, S. M., Jais, P., et al. (2010). Disparate evolution of right and left atrial rate during ablation of long-lasting persistent atrial fibrillation. *J. Am. Coll. Cardiol.* 55, 1007–1016. doi: 10.1016/j.jacc.2009.09.060
- Honarbakhsh, S., Schilling, R. J., Dhillon, G., Ullah, W., Keating, E., Providencia, R., et al. (2017). A novel mapping system for panoramic mapping of the left atrium. application to detect and characterize localized sources maintaining AF. *JACC Clin. Electrophysiol.* 4, 124–134. doi: 10.1016/j.jacep.2017.09.177
- Huang, H., and Darbar, D. (2016). Genotype influence in responses to therapy for atrial fibrillation. *Expert Rev. Cardiovasc. Ther.* 14, 1119–1131. doi: 10.1080/14779072.2016.1210510
- Hung, Y., Lo, L. W., Lin, Y. J., Chang, S. L., Hu, Y. F., Chung, F. P., et al. (2017). Characteristics and long-term catheter ablation outcome in long-standing persistent atrial fibrillation patients with non-pulmonary vein triggers. *Int. J. Cardiol.* 241, 205–211. doi: 10.1016/j.ijcard.2017.04.050
- Hwang, C., and Chen, P. S. (2009). Ligament of Marshall: why it is important for atrial fibrillation ablation. *Heart Rhythm.* 6, S35–S40. doi: 10.1016/j.hrthm.2009.08.034
- Iwasaki, Y. K., Nishida, K., Kato, T., and Nattel, S. (2011). Atrial fibrillation pathophysiology: implications for management. *Circulation* 124, 2264–2274. doi: 10.1161/CIRCULATIONAHA.111.019893
- Jadidi, A. S., Cochet, H., Shah, A. J., Kim, S. J., Duncan, E., Miyazaki, S., et al. (2013). Inverse relationship between fractionated electrograms and atrial fibrosis in persistent atrial fibrillation: combined magnetic resonance imaging and high-density mapping. *J. Am. Coll. Cardiol.* 62, 802–812. doi: 10.1016/j.jacc.2013.03.081
- Jadidi, A. S., Duncan, E., Miyazaki, S., Lellouche, N., Shah, A. J., Forclaz, A., et al. (2012). Functional nature of electrogram fractionation demonstrated by left atrial high density mapping. *Circ. Arrhythm. Electrophysiol.* 5, 32–42. doi: 10.1161/CIRCEP.111.964197
- Jadidi, A. S., Lehrmann, H., Keyl, C., Sorrel, J., Markstein, V., Minners, J., et al. (2016). Ablation of Persistent Atrial Fibrillation Targeting Low-Voltage Areas With Selective Activation Characteristics. *Circ. Arrhythm. Electrophysiol.* 9:e002962. doi: 10.1161/CIRCEP.115.002962
- Jais, P., Hocini, M., Hsu, L. F., Sanders, P., Scavee, C., Weerasooriya, R., et al. (2004). Technique and results of linear ablation at the mitral isthmus. *Circulation* 110, 2996–3002. doi: 10.1161/01.CIR.0000146917.75041.58
- Janes, R. D., Brandy, J. C., Hopkins, D. A., Johnstone, D. E., Murphy, D. A., and Armour, J. A. (1986). Anatomy of human extrinsic cardiac nerves and ganglia. *Am. J. Cardiol.* 57, 299–309. doi: 10.1016/0002-9149(86)9008-2
- Jayachandran, J. V., Sih, H. J., Winkle, W., Zipes, D. P., Hutchins, G. D., and Olglin, J. E. (2000). Atrial fibrillation produced by prolonged rapid atrial pacing is associated with heterogeneous changes in atrial sympathetic innervation. *Circulation* 101, 1185–1191. doi: 10.1161/01.CIR.101.10.1185
- Jia, P., Ramanathan, C., Ghanem, R. N., Ryu, K., Varma, N., and Rudy, Y. (2006). Electrocardiographic imaging of cardiac resynchronization therapy in heart failure: observation of variable electrophysiologic responses. *Heart Rhythm.* 3, 296–310. doi: 10.1016/j.hrthm.2005.11.025
- John, B., Stiles, M. K., Kuklik, P., Chandy, S. T., Young, G. D., Mackenzie, L., et al. (2008). Electrical remodelling of the left and right atria due to rheumatic mitral stenosis. *Eur. Heart J.* 29, 2234–2243. doi: 10.1093/eurheartj/ehn329
- Kalifa, J., Jalife, J., Zaitsev, A. V., Bagwe, S., Warren, M., Moreno, J., et al. (2003). Intra-atrial pressure increases rate and organization of waves emanating from the superior pulmonary veins during atrial fibrillation. *Circulation* 108, 668–671. doi: 10.1161/01.CIR.0000086979.39843.7B
- Karam, B. S., Chavez-Moreno, A., Koh, W., Akar, J. G., and Akar, F. G. (2017). Oxidative stress and inflammation as central mediators of atrial fibrillation in obesity and diabetes. *Cardiovasc. Diabetol.* 16:120. doi: 10.1186/s12933-017-0604-9
- Katritsis, D., Ellenbogen, K. A., Giazitzoglou, E., Sougiannis, D., Paxinos, G., Fragakis, N., et al. (2008). Clinical outcome of left atrial ablation for paroxysmal atrial fibrillation is related to the extent of radiofrequency ablation. *J. Interv. Card. Electrophysiol.* 22, 31–37. doi: 10.1007/s10840-008-9247-9
- Katritsis, D. G., Pokushalov, E., Romanov, A., Giazitzoglou, E., Siontis, G. C., Po, S. S., et al. (2013). Autonomic denervation added to pulmonary vein isolation for paroxysmal atrial fibrillation: a randomized clinical trial. *J. Am. Coll. Cardiol.* 62, 2318–2325. doi: 10.1016/j.jacc.2013.06.053
- Kawara, T., Derkzen, R., De Groot, J. R., Coronel, R., Tasseron, S., Linnenbank, A. C., et al. (2001). Activation delay after premature stimulation in chronically diseased human myocardium relates to the architecture of interstitial fibrosis. *Circulation* 104, 3069–3075. doi: 10.1161/hc5001.100833
- Kettering, K., Yim, D. H., and Gramley, F. (2017). Catheter ablation of persistent atrial fibrillation: circumferential pulmonary vein ablation: beneficial effect of an additional linear lesion at the roof of the left atrium on the long-term outcome. *Herzschriftmacherther. Elektrophysiol.* 28, 328–334. doi: 10.1007/s00399-017-0519-x
- Khurram, I. M., Habibi, M., Gucuk Ipek, E., Chrispin, J., Yang, E., Fukumoto, K., et al. (2016). Left atrial LGE and arrhythmia recurrence following pulmonary vein isolation for paroxysmal and persistent AF. *JACC Cardiovasc. Imaging* 9, 142–148. doi: 10.1016/j.jcmg.2015.10.015
- Kim, T. H., Park, J., Park, J. K., Uhm, J. S., Joung, B., Hwang, C., et al. (2015). Linear ablation in addition to circumferential pulmonary vein isolation (Dallas lesion set) does not improve clinical outcome in patients with paroxysmal atrial fibrillation: a prospective randomized study. *Europace* 17, 388–395. doi: 10.1093/europace/euu245
- Kis, Z., Muka, T., Franco, O. H., Bramer, W. M., De Vries, L. J., Kardos, A., et al. (2017). The short and long-term efficacy of pulmonary vein isolation as a sole treatment strategy for paroxysmal atrial fibrillation: a systematic review and meta-analysis. *Curr. Cardiol. Rev.* 13, 199–208. doi: 10.2174/1573403X13666170117125124
- Kistler, P. M., Sanders, P., Dodic, M., Spence, S. J., Samuel, C. S., Zhao, C., et al. (2006). Atrial electrical and structural abnormalities in an ovine model of chronic blood pressure elevation after prenatal corticosteroid exposure:

- implications for development of atrial fibrillation. *Eur. Heart J.* 27, 3045–3056. doi: 10.1093/eurheartj/ehl360
- Knecht, S., Sohal, M., Deisenhofer, I., Albenque, J. P., Arentz, T., Neumann, T., et al. (2017). Multicentre evaluation of non-invasive biatrial mapping for persistent atrial fibrillation ablation: the AFACART study. *Europace* 19, 1302–1309. doi: 10.1093/europace/euw168
- Konings, K. T., Kirchhof, C. J., Smeets, J. R., Wellens, H. J., Penn, O. C., and Allessie, M. A. (1994). High-density mapping of electrically induced atrial fibrillation in humans. *Circulation* 89, 1665–1680. doi: 10.1161/01.CIR.89.4.1665
- Konings, K. T., Smeets, J. L., Penn, O. C., Wellens, H. J., and Allessie, M. A. (1997). Configuration of unipolar atrial electrograms during electrically induced atrial fibrillation in humans. *Circulation* 95, 1231–1241. doi: 10.1161/01.CIR.95.5.1231
- Krul, S. P. J., Driessen, A. H. G., Van Boven, W. J., Linnenbank, A. C., Geuzebroek, G. S. C., Jackman, W. M., et al. (2011). Thoracoscopic video-assisted pulmonary vein antrum isolation, ganglionated plexus ablation, and periprocedural confirmation of ablation lesions: first results of a hybrid surgical-electrophysiological approach for atrial fibrillation. *Circ. Arrhythm. Electrophysiol.* 4, 262–270. doi: 10.1161/CIRCEP.111.961862
- Kuck, K. H., Brugada, J., Furnkranz, A., Metzner, A., Ouyang, F., Chun, K. R., et al. (2016a). Cryoballoon or radiofrequency ablation for paroxysmal atrial fibrillation. *N. Engl. J. Med.* 374, 2235–2245. doi: 10.1056/NEJMoa1602014
- Kuck, K. H., Hoffmann, B. A., Ernst, S., Wegscheider, K., Treszl, A., Metzner, A., et al. (2016b). Impact of complete versus incomplete circumferential lines around the pulmonary veins during catheter ablation of paroxysmal atrial fibrillation: results from the gap-atrial fibrillation-german atrial fibrillation competence network 1 trial. *Circ. Arrhythm. Electrophysiol.* 9:e003337. doi: 10.1161/CIRCEP.115.003337
- Kurfurst, V., Mokráček, A., Bulava, A., Canádyová, J., Haniš, J., and Pešl, L. (2014). Two-staged hybrid treatment of persistent atrial fibrillation: short-term single-centre results[†]. *Interact. Cardiovasc. Thorac. Surg.* 18, 451–456. doi: 10.1093/icvts/ivt538
- La Meir, M., Gelsomino, S., Lucà, F., Pison, L., Parise, O., Colella, A., et al. (2013). Minimally invasive surgical treatment of lone atrial fibrillation: early results of hybrid versus standard minimally invasive approach employing radiofrequency sources. *Int. J. Cardiol.* 167, 1469–1475. doi: 10.1016/j.ijcard.2012.04.044
- Lau, D. H., Mackenzie, L., Kelly, D. J., Psaltis, P. J., Brooks, A. G., Worthington, M., et al. (2010a). Hypertension and atrial fibrillation: evidence of progressive atrial remodeling with electrostructural correlate in a conscious chronically instrumented ovine model. *Heart Rhythm* 7, 1282–1290. doi: 10.1016/j.hrthm.2010.05.010
- Lau, D. H., Mackenzie, L., Kelly, D. J., Psaltis, P. J., Worthington, M., Rajendram, A., et al. (2010b). Short-term hypertension is associated with the development of atrial fibrillation substrate: a study in an ovine hypertensive model. *Heart Rhythm* 7, 396–404. doi: 10.1016/j.hrthm.2009.11.031
- Lau, D. H., Maesen, B., Zeemering, S., Kuklik, P., Van Hunnik, A., Lankveld, T. A., et al. (2015). Indices of bipolar complex fractionated atrial electrograms correlate poorly with each other and atrial fibrillation substrate complexity. *Heart Rhythm* 12, 1415–1423. doi: 10.1016/j.hrthm.2015.03.017
- Lau, D. H., Psaltis, P. J., Mackenzie, L., Kelly, D. J., Carbone, A., Worthington, M., et al. (2011). Atrial remodeling in an ovine model of anthracycline-induced nonischemic cardiomyopathy: remodeling of the same sort. *J. Cardiovasc. Electrophysiol.* 22, 175–182. doi: 10.1111/j.1540-8167.2010.01851.x
- Lau, D. H., Shipp, N. J., Kelly, D. J., Thanigaimani, S., Neo, M., Kuklik, P., et al. (2013). Atrial arrhythmia in ageing spontaneously hypertensive rats: unraveling the substrate in hypertension and ageing. *PLoS ONE* 8:e72416. doi: 10.1371/journal.pone.0072416
- Laughner, J., Shome, S., Child, N., Shuros, A., Neuzil, P., Gill, J., et al. (2016). Practical considerations of mapping persistent atrial fibrillation with whole-chamber basket catheters. *JACC Clin. Electrophysiol.* 2, 55–65. doi: 10.1016/j.jacep.2015.09.017
- Lechleiter, J., Girard, S., Peralta, E., and Clapham, D. (1991). Spiral calcium wave propagation and annihilation in *Xenopus laevis* oocytes. *Science* 252, 123–126. doi: 10.1126/science.2011747
- Lee, J. Y., Kim, T. H., Yang, P. S., Lim, H. E., Choi, E. K., Shim, J., et al. (2017). Korean atrial fibrillation network genome-wide association study for early-onset atrial fibrillation identifies novel susceptibility loci. *Eur. Heart J.* 38, 2586–2594. doi: 10.1093/eurheartj/ehx213
- Lee, S. H., Tai, C. T., Hsieh, M. H., Tsao, H. M., Lin, Y. J., Chang, S. L., et al. (2005). Predictors of non-pulmonary vein ectopic beats initiating paroxysmal atrial fibrillation: implication for catheter ablation. *J. Am. Coll. Cardiol.* 46, 1054–1059. doi: 10.1016/j.jacc.2005.06.016
- Leiria, T. L., Glavinovic, T., Armour, J. A., Cardinal, R., De Lima, G. G., and Kus, T. (2011). Longterm effects of cardiac mediastinal nerve cryoablation on neural inducibility of atrial fibrillation in canines. *Auton. Neurosci.* 161, 68–74. doi: 10.1016/j.autneu.2010.12.006
- Lemoine, M. D., Duverger, J. E., Naud, P., Chartier, D., Qi, X. Y., Comtois, P., et al. (2011). Arrhythmogenic left atrial cellular electrophysiology in a murine genetic long QT syndrome model. *Cardiovasc. Res.* 92, 67–74. doi: 10.1093/cvr/cvr166
- Leone, O., Boriani, G., Chiappini, B., Pacini, D., Cenacchi, G., Martin Suarez, S., et al. (2004). Amyloid deposition as a cause of atrial remodelling in persistent valvular atrial fibrillation. *Eur. Heart J.* 25, 1237–1241. doi: 10.1016/j.ehj.2004.04.007
- Li, D., Fareh, S., Leung, T. K., and Nattel, S. (1999). Promotion of atrial fibrillation by heart failure in dogs: atrial remodeling of a different sort. *Circulation* 100, 87–95. doi: 10.1161/01.CIR.100.1.87
- Lim, H. S., Hocini, M., Dubois, R., Denis, A., Derval, N., Zellerhoff, S., et al. (2017). Complexity and distribution of drivers in relation to duration of persistent atrial fibrillation. *J. Am. Coll. Cardiol.* 69, 1257–1269. doi: 10.1016/j.jacc.2017.01.014
- Lin, W. S., Tai, C. T., Hsieh, M. H., Tsai, C. F., Lin, Y. K., Tsao, H. M., et al. (2003). Catheter ablation of paroxysmal atrial fibrillation initiated by non-pulmonary vein ectopy. *Circulation* 107, 3176–3183. doi: 10.1161/01.CIR.0000074206.52056.2D
- Linz, D., Hohl, M., Dhein, S., Ruf, S., Reil, J. C., Kabiri, M., et al. (2016). Cathepsin A mediates susceptibility to atrial tachyarrhythmia and impairment of atrial emptying function in Zucker diabetic fatty rats. *Cardiovasc. Res.* 110, 371–380. doi: 10.1093/cvr/cvw071
- Lo, L. W., Tai, C. T., Lin, Y. J., Chang, S. L., Wongcharoen, W., Hsieh, M. H., et al. (2007). Mechanisms of recurrent atrial fibrillation: comparisons between segmental ostial versus circumferential pulmonary vein isolation. *J. Cardiovasc. Electrophysiol.* 18, 803–807. doi: 10.1111/j.1540-8167.2007.00848.x
- Low, S. K., Takahashi, A., Ebana, Y., Ozaki, K., Christophersen, I. E., Ellinor, P. T., et al. (2017). Identification of six new genetic loci associated with atrial fibrillation in the Japanese population. *Nat. Genet.* 49, 953–958. doi: 10.1038/ng.3842
- Lu, Z., Scherlag, B. J., Lin, J., Yu, L., Guo, J. H., Niu, G., et al. (2009). Autonomic mechanism for initiation of rapid firing from atria and pulmonary veins: evidence by ablation of ganglionated plexi. *Cardiovasc. Res.* 84, 245–252. doi: 10.1093/cvr/cvp194
- Lubitz, S. A., Lunetta, K. L., Lin, H., Arking, D. E., Trompet, S., Li, G., et al. (2014). Novel genetic markers associate with atrial fibrillation risk in Europeans and Japanese. *J. Am. Coll. Cardiol.* 63, 1200–1210. doi: 10.1016/j.jacc.2013.12.015
- Lubitz, S. A., Yin, X., Fontes, J. D., Magnani, J. W., Rienstra, M., Pai, M., et al. (2010). Association between familial atrial fibrillation and risk of new-onset atrial fibrillation. *JAMA* 304, 2263–2269. doi: 10.1001/jama.2010.1690
- Mahida, S., Sacher, F., Derval, N., Berte, B., Yamashita, S., Hooks, D., et al. (2015). Science linking pulmonary veins and atrial fibrillation. *Arrhythmia Electrophysiol. Rev.* 4, 40–43. doi: 10.15420/aer.2015.4.1.40
- Malcolme-Lawes, L. C., Juli, C., Karim, R., Bai, W., Quest, R., Lim, P. B., et al. (2013). Automated analysis of atrial late gadolinium enhancement imaging that correlates with endocardial voltage and clinical outcomes: a 2-center study. *Heart Rhythm* 10, 1184–1191. doi: 10.1016/j.hrthm.2013.04.030
- Mandapati, R., Skanes, A., Chen, J., Berenfeld, O., and Jalife, J. (2000). Stable microreentrant sources as a mechanism of atrial fibrillation in the isolated sheep heart. *Circulation* 101, 194–199. doi: 10.1161/01.CIR.101.2.194
- Mansour, M., Mandapati, R., Berenfeld, O., Chen, J., Samie, F. H., and Jalife, J. (2001). Left-to-right gradient of atrial frequencies during acute atrial fibrillation in the isolated sheep heart. *Circulation* 103, 2631–2636. doi: 10.1161/01.CIR.103.21.2631

- Mansour, M., Ruskin, J., and Keane, D. (2002). Initiation of atrial fibrillation by ectopic beats originating from the ostium of the inferior vena cava. *J. Cardiovasc. Electrophysiol.* 13, 1292–1295. doi: 10.1046/j.1540-8167.2002.01292.x
- Marrouche, N. F., Brachmann, J., Andresen, D., Siebels, J., Boersma, L., Jordaens, L., et al. (2018). Catheter ablation for atrial fibrillation with heart failure. *N. Engl. J. Med.* 378, 417–427. doi: 10.1056/NEJMoa1707855
- Marrouche, N. F., Wilber, D., Hindricks, G., Jais, P., Akoum, N., Marchlinski, F., et al. (2014). Association of atrial tissue fibrosis identified by delayed enhancement MRI and atrial fibrillation catheter ablation: the DECAAF study. *JAMA* 311, 498–506. doi: 10.1001/jama.2014.3
- Medi, C., Kalman, J. M., Ling, L. H., Teh, A. W., Lee, G., Lee, G., et al. (2012). Atrial electrical and structural remodeling associated with longstanding pulmonary hypertension and right ventricular hypertrophy in humans. *J. Cardiovasc. Electrophysiol.* 23, 614–620. doi: 10.1111/j.1540-8167.2011.02255.x
- Medi, C., Kalman, J. M., Spence, S. J., Teh, A. W., Lee, G., Bader, I., et al. (2011). Atrial electrical and structural changes associated with longstanding hypertension in humans: implications for the substrate for atrial fibrillation. *J. Cardiovasc. Electrophysiol.* 22, 1317–1324. doi: 10.1111/j.1540-8167.2011.02125.x
- Metzner, A., Wissner, E., Tsyanov, A., Kalinin, V., Schluter, M., Lemes, C., et al. (2017). Noninvasive phase mapping of persistent atrial fibrillation in humans: Comparison with invasive catheter mapping. *Ann Noninvasive Electrocardiol.* 23:e12527. doi: 10.1111/anec.12527
- Mikhaylov, E., Kanidieva, A., Sviridova, N., Abramov, M., Gureev, S., Szili-Torok, T., et al. (2011). Outcome of anatomic ganglionated plexi ablation to treat paroxysmal atrial fibrillation: a 3-year follow-up study. *Europace* 13, 362–370. doi: 10.1093/europace/euq416
- Mitchell, A. R., Spurrell, P. A., and Sulke, N. (2003). Circadian variation of arrhythmia onset patterns in patients with persistent atrial fibrillation. *Am. Heart J.* 146, 902–907. doi: 10.1016/S0002-8703(03)00405-8
- Miyasaka, Y., Barnes, M. E., Bailey, K. R., Cha, S. S., Gersh, B. J., Seward, J. B., et al. (2007). Mortality trends in patients diagnosed with first atrial fibrillation: a 21-year community-based study. *J. Am. Coll. Cardiol.* 49, 986–992. doi: 10.1016/j.jacc.2006.10.062
- Moe, G. K., Rheinboldt, W. C., and Abildskov, J. A. (1964). A computer model of atrial fibrillation. *Am. Heart J.* 67, 200–220. doi: 10.1016/0002-8703(64)90371-0
- Morgan, R., Colman, M. A., Chubb, H., Seemann, G., and Aslanidi, O. V. (2016). Slow conduction in the border zones of patchy fibrosis stabilizes the drivers for atrial fibrillation: insights from multi-scale human atrial modeling. *Front. Physiol.* 7:474. doi: 10.3389/fphys.2016.00474
- Mun, H. S., Joung, B., Shim, J., Hwang, H. J., Kim, J. Y., Lee, M. H., et al. (2012). Does additional linear ablation after circumferential pulmonary vein isolation improve clinical outcome in patients with paroxysmal atrial fibrillation? Prospective randomised study. *Heart* 98, 480–484. doi: 10.1136/heartjnl-2011-301107
- Nademanee, K., Mckenzie, J., Kosar, E., Schwab, M., Sunsaneewitayakul, B., Vasavakul, T., et al. (2004). A new approach for catheter ablation of atrial fibrillation: mapping of the electrophysiologic substrate. *J. Am. Coll. Cardiol.* 43, 2044–2053. doi: 10.1016/j.jacc.2003.12.054
- Namino, F., Iriki, Y., Maenosono, R., Ichiki, H., Okui, H., Yoshimura, A., et al. (2015). The optimal setting of complex fractionated atrial electrogram software in substrate ablation for atrial fibrillation. *J. Arrhythm.* 31, 6–11. doi: 10.1016/j.joa.2014.04.006
- Narayan, S. M., Krummen, D. E., and Rappel, W. J. (2012a). Clinical mapping approach to diagnose electrical rotors and focal impulse sources for human atrial fibrillation. *J. Cardiovasc. Electrophysiol.* 23, 447–454. doi: 10.1111/j.1540-8167.2012.02332.x
- Narayan, S. M., Krummen, D. E., Shivkumar, K., Clopton, P., Rappel, W. J., and Miller, J. M. (2012b). Treatment of atrial fibrillation by the ablation of localized sources: CONFIRM (Conventional Ablation for Atrial Fibrillation With or Without Focal Impulse and Rotor Modulation) trial. *J. Am. Coll. Cardiol.* 60, 628–636. doi: 10.1016/j.jacc.2012.05.022
- Natale, A., Reddy, V. Y., Monir, G., Wilber, D. J., Lindsay, B. D., McElderry, H. T., et al. (2014). Paroxysmal AF catheter ablation with a contact force sensing catheter: results of the prospective, multicenter SMART-AF trial. *J. Am. Coll. Cardiol.* 64, 647–656. doi: 10.1016/j.jacc.2014.04.072
- Nattel, S. (2002). New ideas about atrial fibrillation 50 years on. *Nature* 415, 219–226. doi: 10.1038/415219a
- Nattel, S., and Dobrev, D. (2016). Electrophysiological and molecular mechanisms of paroxysmal atrial fibrillation. *Nat. Rev. Cardiol.* 13, 575–590. doi: 10.1038/nrccardio.2016.118
- Nattel, S., and Harada, M. (2014). Atrial remodeling and atrial fibrillation: recent advances and translational perspectives. *J. Am. Coll. Cardiol.* 63, 2335–2345. doi: 10.1016/j.jacc.2014.02.555
- Nattel, S., Xiong, F., and Aguilar, M. (2017). Demystifying rotors and their place in clinical translation of atrial fibrillation mechanisms. *Nat. Rev. Cardiol.* 14, 509–520. doi: 10.1038/nrccardio.2017.37
- Neumann, T., Wojcik, M., Berkowitsch, A., Erkacic, D., Zaltsberg, S., Greiss, H., et al. (2013). Cryoballoon ablation of paroxysmal atrial fibrillation: 5-year outcome after single procedure and predictors of success. *Europace* 15, 1143–1149. doi: 10.1093/europace/eut021
- Ng, J., Villanueva, R., Cokic, I., Schliamser, J. E., Gordon, D., Koduri, H., et al. (2011). Autonomic remodeling in the left atrium and pulmonary veins in heart failure – creation of a dynamic substrate for atrial fibrillation. *Circ. Arrhythm. Electrophysiol.* 4, 388–396. doi: 10.1161/CIRCEP.110.959650
- Nguyen, B. L., Fishbein, M. C., Chen, L. S., Chen, P.-S., and Masroor, S. (2009). Histopathological substrate for chronic atrial fibrillation in humans. *Heart Rhythm* 6, 454–460. doi: 10.1016/j.hrthm.2009.01.010
- Nguyen, B. L., Li, H., Fishbein, M. C., Lin, S. F., Gaudio, C., Chen, P. S., et al. (2012). Acute myocardial infarction induces bilateral stellate ganglia neural remodeling in rabbits. *Cardiovasc. Pathol.* 21, 143–148. doi: 10.1016/j.carpath.2011.08.001
- Nielsen, J. B., Fritsche, L. G., Zhou, W., Teslovich, T. M., Holmen, O. L., Gustafsson, S., et al. (2018a). Genome-wide study of atrial fibrillation identifies seven risk loci and highlights biological pathways and regulatory elements involved in cardiac development. *Am. J. Hum. Genet.* 102, 103–115. doi: 10.1016/j.ajhg.2017.12.003
- Nielsen, J. B., Thorolfsdottir, R. B., Fritsche, L. G., Zhou, W., Skov, M. W., Graham, S. E., et al. (2018b). Biobank-driven genomic discovery yields new insight into atrial fibrillation biology. *Nat. Genet.* 50, 1234–1239. doi: 10.1038/s41588-018-0171-3
- Oakes, R. S., Badger, T. J., Kholmovski, E. G., Akoum, N., Burgon, N. S., Fish, E. N., et al. (2009). Detection and quantification of left atrial structural remodeling using delayed enhancement MRI in patients with atrial fibrillation. *Circulation* 119, 1758–1767. doi: 10.1161/CIRCULATIONAHA.108.811877
- Oesterlein, T., Frisch, D., Loewe, A., Seemann, G., Schmitt, C., Dössel, O., et al. (2016). Basket-type catheters: diagnostic pitfalls caused by deformation and limited coverage. *Biomed Res. Int.* 2016:13. doi: 10.1155/2016/5340574
- Ogawa, M., Tan, A. Y., Song, J., Kobayashi, K., Fishbein, M. C., Lin, S. F., et al. (2009). Cryoablation of stellate ganglia and atrial arrhythmia in ambulatory dogs with pacing-induced heart failure. *Heart Rhythm* 6, 1772–1779. doi: 10.1016/j.hrthm.2009.08.011
- Oral, H., Chugh, A., Good, E., Wimmer, A., Dey, S., Gadeela, N., et al. (2007). Radiofrequency catheter ablation of chronic atrial fibrillation guided by complex electrograms. *Circulation* 115, 2606–2612. doi: 10.1161/CIRCULATIONAHA.107.691386
- Oral, H., Chugh, A., Yoshida, K., Sarrazin, J. F., Kuhne, M., Crawford, T., et al. (2009). A randomized assessment of the incremental role of ablation of complex fractionated atrial electrograms after antral pulmonary vein isolation for long-lasting persistent atrial fibrillation. *J. Am. Coll. Cardiol.* 53, 782–789. doi: 10.1016/j.jacc.2008.10.054
- Oster, H. S., Taccardi, B., Lux, R. L., Ershler, P. R., and Rudy, Y. (1997). Noninvasive electrocardiographic imaging. Reconstruction of epicardial potentials, electrograms, and isochrones and localization of single and multiple electrocardiac events. *Circulation* 96, 1012–1024.
- Oyen, N., Ranthe, M. F., Carstensen, L., Boyd, H. A., Olesen, M. S., Olesen, S. P., et al. (2012). Familial aggregation of lone atrial fibrillation in young persons. *J. Am. Coll. Cardiol.* 60, 917–921. doi: 10.1016/j.jacc.2012.03.046
- Pandey, A., Kim, S., Moore, C., Thomas, L., Gersh, B., Allen, L. A., et al. (2017). Predictors and prognostic implications of incident heart failure in patients with prevalent atrial fibrillation. *JACC Heart Fail.* 5, 44–52. doi: 10.1016/j.jchf.2016.09.016
- Pandit, S. V., and Jalife, J. (2013). Rotors and the dynamics of cardiac fibrillation. *Circ. Res.* 112, 849–862. doi: 10.1161/CIRCRESAHA.111.300158

- Panfilov, A. V., and Keener, J. P. (1993). Effects of high frequency stimulation on cardiac tissue with an inexcitable obstacle. *J. Theor. Biol.* 163, 439–448. doi: 10.1006/jtbi.1993.1129
- Pappone, C., Ciccone, G., Vicedomini, G., Mangual, J. O., Li, W., Conti, M., et al. (2018). Clinical outcome of electrophysiologically guided ablation for nonparoxysmal atrial fibrillation using a novel real-time 3-dimensional mapping technique: results from a prospective randomized trial. *Circ. Arrhythm. Electrophysiol.* 11:e005904. doi: 10.1161/CIRCEP.117.005904
- Pappone, C., Santinelli, V., Manguso, F., Vicedomini, G., Gugliotta, F., Augello, G., et al. (2004). Pulmonary vein denervation enhances long-term benefit after circumferential ablation for paroxysmal atrial fibrillation. *Circulation* 109, 327–334. doi: 10.1161/01.CIR.0000112641.16340.C7
- Parameswaran, R., Voskoboinik, A., Gorelik, A., Lee, G., Kistler, P. M., Sanders, P., et al. (2018). Clinical impact of rotor ablation in atrial fibrillation: a systematic review. *Europace Clinical impact of rotor ablation in atrial fibrillation: a systematic review.* 20, 1099–1106. doi: 10.1093/europace/eux370
- Parvez, B., Vaglio, J., Rowan, S., Muhammad, R., Kucera, G., Stubblefield, T., et al. (2012). Symptomatic response to antiarrhythmic drug therapy is modulated by a common single nucleotide polymorphism in atrial fibrillation. *J. Am. Coll. Cardiol.* 60, 539–545. doi: 10.1016/j.jacc.2012.01.070
- Pastor, A., Nunez, A., Magalhaes, A., Awamleh, P., and Garcia-Cosio, F. (2007). [The superior vena cava as a site of ectopic foci in atrial fibrillation]. *Rev. Esp. Cardiol.* 60, 68–71. doi: 10.1016/S0300-8932(07)74987-4
- Pathik, B., Kalman, J. M., Walters, T., Kuklik, P., Zhao, J., Madry, A., et al. (2018). Absence of rotational activity detected using 2-dimensional phase mapping in the corresponding 3-dimensional phase maps in human persistent atrial fibrillation. *Heart Rhythm* 15, 182–192. doi: 10.1016/j.hrthm.2017.09.010
- Patterson, E., Po, S. S., Scherlag, B. J., and Lazzara, R. (2005). Triggered firing in pulmonary veins initiated by *in vitro* autonomic nerve stimulation. *Heart Rhythm* 2, 624–631. doi: 10.1016/j.hrthm.2005.02.012
- Pedersen, O. D., Abildstrom, S. Z., Ottesen, M. M., Rask-Madsen, C., Bagger, H., Kober, L., et al. (2006). Increased risk of sudden and non-sudden cardiovascular death in patients with atrial fibrillation/flutter following acute myocardial infarction. *Eur. Heart J.* 27, 290–295. doi: 10.1093/eurheartj/ehi629
- Pertsov, A. M., Davidenko, J. M., Salomonsz, R., Baxter, W. T., and Jalife, J. (1993a). Spiral waves of excitation underlie reentrant activity in isolated cardiac muscle. *Circ. Res.* 72:631. doi: 10.1161/01.RES.72.3.631
- Pertsov, A. M., Davidenko, J. M., Salomonsz, R., Baxter, W. T., and Jalife, J. (1993b). Spiral waves of excitation underlie reentrant activity in isolated cardiac muscle. *Circ. Res.* 72, 631–650.
- Peters, D. C., Wylie, J. V., Hauser, T. H., Nezafat, R., Han, Y., Woo, J. J., et al. (2009). Recurrence of atrial fibrillation correlates with extent of post-procedural late gadolinium enhancement: a pilot study. *JACC Cardiovasc. Imaging* 2, 308–316. doi: 10.1016/j.jcmg.2008.10.016
- Pison, L., Gelsomino, S., Lucà, F., Parise, O., Maessen, J. G., Crijns, H. J. G. M., et al. (2014). Effectiveness and safety of simultaneous hybrid thoracoscopic and endocardial catheter ablation of lone atrial fibrillation. *Ann. Cardiothor. Surg.* 3, 38–44. doi: 10.3978/j.issn.2225-319X.2013.12.10
- Pison, L., La Meir, M., Van Opstal, J., Blaauw, Y., Maessen, J., and Crijns, H. J. (2012). Hybrid thoracoscopic surgical and transvenous catheter ablation of atrial fibrillation. *J. Am. Coll. Cardiol.* 60, 54–61. doi: 10.1016/j.jacc.2011.12.055
- Platonov, P. G., Mitrofanova, L. B., Orshanskaya, V., and Ho, S. Y. (2011). Structural abnormalities in atrial walls are associated with presence and persistency of atrial fibrillation but not with age. *J. Am. Coll. Cardiol.* 58, 2225–2232. doi: 10.1016/j.jacc.2011.05.061
- Po, S. S., Nakagawa, H., and Jackman, W. M. (2009). Localization of left atrial ganglionated plexi in patients with atrial fibrillation. *J. Cardiovasc. Electrophysiol.* 20, 1186–1189. doi: 10.1111/j.1540-8167.2009.01515.x
- Pokushalov, E., Romanov, A., Katritsis, D. G., Artyomenko, S., Shirokova, N., Karaskov, A., et al. (2013). Ganglionated plexus ablation vs. linear ablation in patients undergoing pulmonary vein isolation for persistent/long-standing persistent atrial fibrillation: a randomized comparison. *Heart Rhythm* 10, 1280–1286. doi: 10.1016/j.hrthm.2013.04.016
- Potpara, T. S., Polovina, M. M., Licina, M. M., Marinkovic, J. M., and Lip, G. Y. (2013). Predictors and prognostic implications of incident heart failure following the first diagnosis of atrial fibrillation in patients with structurally normal hearts: the belgrade atrial fibrillation study. *Eur. J. Heart Fail.* 15, 415–424. doi: 10.1093/eurjhf/hft004
- Prasad, S. M., Maniar, H. S., Camillo, C. J., Schuessler, R. B., Boineau, J. P., Sundt, T. M. III, et al. (2003). The Cox maze III procedure for atrial fibrillation: long-term efficacy in patients undergoing lone versus concomitant procedures. *J. Thorac. Cardiovasc. Surg.* 126, 1822–1828. doi: 10.1016/S0022-5223(03)01287-X
- Ramanathan, C., Ghanem, R. N., Jia, P., Ryu, K., and Rudy, Y. (2004). Noninvasive electrocardiographic imaging for cardiac electrophysiology and arrhythmia. *Nat. Med.* 10, 422–428. doi: 10.1038/nm1011
- Ramanathan, C., Jia, P., Ghanem, R., Calvetti, D., and Rudy, Y. (2003). Noninvasive electrocardiographic imaging (ECGI): application of the generalized minimal residual (GMRes) method. *Ann. Biomed. Eng.* 31, 981–994. doi: 10.1114/1.1588655
- Reddy, Y. N. V., Obokata, M., Gersh, B. J., and Borlaug, B. A. (2018). High prevalence of occult heart failure with preserved ejection fraction among patients with atrial fibrillation and dyspnea. *Circulation* 137, 534–535. doi: 10.1161/CIRCULATIONAHA.117.030093
- Redfearn, D. P., Skanes, A. C., Gula, L. J., Griffith, M. J., Marshall, H. J., Stafford, P. J., et al. (2007). Noninvasive assessment of atrial substrate change after wide area circumferential ablation: a comparison with segmental pulmonary vein isolation. *Ann. Noninvasive Electrocardiol.* 12, 329–337. doi: 10.1111/j.1542-474X.2007.00182.x
- Reumann, M., Bohnert, J., Osswald, B., Hagl, S., and Doessel, O. (2007). Multiple wavelets, rotors, and snakes in atrial fibrillation—a computer simulation study. *J. Electrocardiol.* 40, 328–334. doi: 10.1016/j.jelectrocard.2006.12.016
- Richer, L.-P., Vinet, A., Kus, T., Cardinal, R., Ardell, J. L., and Armour, J. A. (2008). α -Adrenoceptor blockade modifies neurally induced atrial arrhythmias. *Am. J. Physiol.* 295, R1175–R1180. doi: 10.1152/ajpregu.00840.2007
- Roberts, J. D., and Gollob, M. H. (2010). Impact of genetic discoveries on the classification of lone atrial fibrillation. *J. Am. Coll. Cardiol.* 55, 705–712. doi: 10.1016/j.jacc.2009.12.005
- Roberts, J. D., and Gollob, M. H. (2014). A contemporary review on the genetic basis of atrial fibrillation. *Method Debakey Cardiovasc. J.* 10, 18–24. doi: 10.14797/mdcj-10-1-18
- Roberts-Thomson, K. C., John, B., Worthley, S. G., Brooks, A. G., Stiles, M. K., Lau, D. H., et al. (2009). Left atrial remodeling in patients with atrial septal defects. *Heart Rhythm* 6, 1000–1006. doi: 10.1016/j.hrthm.2009.03.050
- Rocken, C., Peters, B., Juenemann, G., Saeger, W., Klein, H. U., Huth, C., et al. (2002). Atrial amyloidosis: an arrhythmogenic substrate for persistent atrial fibrillation. *Circulation* 106, 2091–2097. doi: 10.1161/01.CIR.0000034511.06350.DF
- Roney, C. H., Bayer, J. D., Zahid, S., Meo, M., Boyle, P. M., Trayanova, N. A., et al. (2016). Modelling methodology of atrial fibrosis affects rotor dynamics and electrograms. *Europace* 18, iv146–iv155. doi: 10.1093/europace/euw365
- Roney, C. H., Cantwell, C. D., Bayer, J. D., Qureshi, N. A., Lim, P. B., Tweedy, J. H., et al. (2017). Spatial resolution requirements for accurate identification of drivers of atrial fibrillation. *Circ. Arrhythm. Electrophysiol.* 10:e004899. doi: 10.1161/CIRCEP.116.004899
- Roselli, C., Chaffin, M. D., Weng, L. C., Aeschbacher, S., Ahlberg, G., Albert, C. M., et al. (2018). Multi-ethnic genome-wide association study for atrial fibrillation. *Nat. Genet.* 50, 1225–1233. doi: 10.1038/s41588-018-0133-9
- Rostamian, A., Narayan, S. M., Thomson, L., Fishbein, M., and Siegel, R. J. (2014). The incidence, diagnosis, and management of pulmonary vein stenosis as a complication of atrial fibrillation ablation. *J. Interv. Card. Electrophysiol.* 40, 63–74. doi: 10.1007/s10840-014-9885-z
- Rostock, T., Rotter, M., Sanders, P., Takahashi, Y., Jais, P., Hocini, M., et al. (2006). High-density activation mapping of fractionated electrograms in the atria of patients with paroxysmal atrial fibrillation. *Heart Rhythm* 3, 27–34. doi: 10.1016/j.hrthm.2005.09.019
- Rostock, T., Steven, D., Lutomsky, B., Servatius, H., Drewitz, I., Klemm, H., et al. (2008). Atrial fibrillation begets atrial fibrillation in the pulmonary veins. on the impact of atrial fibrillation on the electrophysiological properties of the pulmonary veins in humans. *J Am Coll Cardiol.* 51, 2153–2160. doi: 10.1016/j.jacc.2008.02.059
- Rudy, Y. (2013). Noninvasive electrocardiographic imaging of arrhythmogenic substrates in humans. *Circ. Res.* 112, 863–874. doi: 10.1161/CIRCRESAHA.112.279315
- Rudy, Y., and Messinger-Rapport, B. J. (1988). The inverse problem in electrocardiography: solutions in terms of epicardial potentials. *Crit. Rev. Biomed. Eng.* 16, 215–268.

- Rudy, Y., and Oster, H. S. (1992). The electrocardiographic inverse problem. *Crit. Rev. Biomed. Eng.* 20, 25–45.
- Ruigomez, A., Johansson, S., Wallander, M. A., Edvardsson, N., and Garcia Rodriguez, L. A. (2009). Risk of cardiovascular and cerebrovascular events after atrial fibrillation diagnosis. *Int. J. Cardiol.* 136, 186–192. doi: 10.1016/j.ijcard.2008.04.050
- Ruigomez, A., Johansson, S., Wallander, M. A., and Garcia Rodriguez, L. A. (2002). Risk of mortality in a cohort of patients newly diagnosed with chronic atrial fibrillation. *BMC Cardiovasc. Disord.* 2:5. doi: 10.1186/1471-2261-2-5
- Sampson, K. J., and Henriquez, C. S. (2002). Interplay of ionic and structural heterogeneity on functional action potential duration gradients: implications for arrhythmogenesis. *Chaos* 12, 819–828. doi: 10.1063/1.1497735
- Sanders, P., Morton, J. B., Davidson, N. C., Spence, S. J., Vohra, J. K., Sparks, P. B., et al. (2003). Electrical remodeling of the atria in congestive heart failure: electrophysiological and electroanatomic mapping in humans. *Circulation* 108, 1461–1468. doi: 10.1161/01.CIR.0000090688.49283.67
- Sanders, P., Morton, J. B., Deen, V. R., Davidson, N. C., Sparks, P. B., Vohra, J. K., et al. (2002). Immediate and long-term results of radiofrequency ablation of pulmonary vein ectopy for cure of paroxysmal atrial fibrillation using a focal approach. *Intern. Med. J.* 32, 202–207. doi: 10.1046/j.1445-5994.2002.00215.x
- Scanavacca, M., Pisani, C. F., Hachul, D., Lara, S., Hardy, C., Darrieux, F., et al. (2006). Selective atrial vagal denervation guided by evoked vagal reflex to treat patients with paroxysmal atrial fibrillation. *Circulation* 114, 876–885. doi: 10.1161/CIRCULATIONAHA.106.633560
- Scherr, D., Dalal, D., Cheema, A., Cheng, A., Henrikson, C. A., Spragg, D., et al. (2007). Automated detection and characterization of complex fractionated atrial electrograms in human left atrium during atrial fibrillation. *Heart Rhythm* 4, 1013–1020. doi: 10.1016/j.hrthm.2007.04.021
- Schotten, U., Verheule, S., Kirchhof, P., and Goette, A. (2011). Pathophysiological mechanisms of atrial fibrillation: a translational appraisal. *Physiol. Rev.* 91, 265–325. doi: 10.1152/physrev.00031.2009
- Schreiber, D., Rieger, A., Moser, F., and Kottkamp, H. (2017). Catheter ablation of atrial fibrillation with box isolation of fibrotic areas: lessons on fibrosis distribution and extent, clinical characteristics, and their impact on long-term outcome. *J. Cardiovasc. Electrophysiol.* 28, 971–983. doi: 10.1111/jce.13278
- Schuessler, R. B., Grayson, T. M., Bromberg, B. I., Cox, J. L., and Boineau, J. P. (1992). Cholinergically mediated tachyarrhythmias induced by a single extrastimulus in the isolated canine right atrium. *Circ. Res.* 71, 1254–1267. doi: 10.1161/01.RES.71.5.1254
- Seitz, J., Bars, C., Theodore, G., Beurheret, S., Lellouche, N., Bremondy, M., et al. (2017). AF ablation guided by spatiotemporal electrogram dispersion without pulmonary vein isolation: a wholly patient-tailored approach. *J. Am. Coll. Cardiol.* 69, 303–321. doi: 10.1016/j.jacc.2016.10.065
- Seitz, J., Horvilleur, J., Lacotte, J., Mouhoub, Y., Salerno, F., Moynagh, A., et al. (2013). Automated detection of complex fractionated atrial electrograms in substrate-based atrial fibrillation ablation: better discrimination with a new setting of CARTO(R) algorithm. *J. Atr. Fibrillation* 6:673. doi: 10.4022/jafib.673
- Shah, A. J., Hocini, M., Xhaet, O., Pascale, P., Roten, L., Wilton, S. B., et al. (2013). Validation of novel 3-dimensional electrocardiographic mapping of atrial tachycardias by invasive mapping and ablation: a multicenter study. *J. Am. Coll. Cardiol.* 62, 889–897. doi: 10.1016/j.jacc.2013.03.082
- Shah, D., Haissaguerre, M., Jais, P., and Hocini, M. (2003). Nonpulmonary vein foci: do they exist? *Pacing Clin. Electrophysiol.* 26, 1631–1635. doi: 10.1046/j.1460-9592.2003.t01-1-00243.x
- Shen, M. J., Shinohara, T., Park, H. W., Frick, K., Ice, D. S., Choi, E. K., et al. (2011). Continuous low-level vagus nerve stimulation reduces stellate ganglion nerve activity and paroxysmal atrial tachyarrhythmias in ambulatory canines. *Circulation* 123, 2204–2212. doi: 10.1161/CIRCULATIONAHA.111.018028
- Shi, Y., Li, D., Tardif, J. C., and Nattel, S. (2002). Enalapril effects on atrial remodeling and atrial fibrillation in experimental congestive heart failure. *Cardiovasc. Res.* 54, 456–461. doi: 10.1016/S0008-6363(02)00243-2
- Shinagawa, K., Shi, Y. F., Tardif, J. C., Leung, T. K., and Nattel, S. (2002). Dynamic nature of atrial fibrillation substrate during development and reversal of heart failure in dogs. *Circulation* 105, 2672–2678. doi: 10.1161/01.CIR.0000016826.62813.F5
- Silver, M. A., Pick, R., Brilla, C. G., Jalil, J. E., Janicki, J. S., and Weber, K. T. (1990). Reactive and reparative fibrillar collagen remodelling in the hypertrophied rat left ventricle: two experimental models of myocardial fibrosis. *Cardiovasc. Res.* 24, 741–747. doi: 10.1093/cvr/24.9.741
- Sinner, M. F., Tucker, N. R., Lunetta, K. L., Ozaki, K., Smith, J. G., Trompet, S., et al. (2014). Integrating genetic, transcriptional, and functional analyses to identify 5 novel genes for atrial fibrillation. *Circulation* 130, 1225–1235. doi: 10.1161/CIRCULATIONAHA.114.009892
- Spach, M. S., and Dolber, P. C. (1986). Relating extracellular potentials and their derivatives to anisotropic propagation at a microscopic level in human cardiac muscle. Evidence for electrical uncoupling of side-to-side fiber connections with increasing age. *Circ. Res.* 58, 356–371. doi: 10.1161/01.RES.58.3.356
- Spach, M. S., Dolber, P. C., and Heidlage, J. F. (1988). Influence of the passive anisotropic properties on directional differences in propagation following modification of the sodium conductance in human atrial muscle. A model of reentry based on anisotropic discontinuous propagation. *Circ. Res.* 62, 811–832. doi: 10.1161/01.RES.62.4.811
- Starobin, J. M., Zilberman, Y. I., Rusnak, E. M., and Starmer, C. F. (1996). Wavelet formation in excitable cardiac tissue: the role of wavefront-obstacle interactions in initiating high-frequency fibrillatory-like arrhythmias. *Biophys. J.* 70, 581–594. doi: 10.1016/S0006-3495(96)79624-8
- Stinnett-Donnelly, J. M., Thompson, N., Habel, N., Petrov-Kondratov, V., Correa De Sa, D. D., Bates, J. H., et al. (2012). Effects of electrode size and spacing on the resolution of intracardiac electrograms. *Coron. Artery Dis.* 23, 126–132. doi: 10.1097/MCA.0b013e3283507a9b
- Straube, F., Dorwarth, U., Ammar-Busch, S., Peter, T., Noelker, G., Massa, T., et al. (2016). First-line catheter ablation of paroxysmal atrial fibrillation: outcome of radiofrequency vs. cryoballoon pulmonary vein isolation. *Europace* 18, 368–375. doi: 10.1093/europace/euv271
- Sun, H., Gaspo, R., Leblanc, N., and Nattel, S. (1998). Cellular mechanisms of atrial contractile dysfunction caused by sustained atrial tachycardia. *Circulation* 98, 719–727. doi: 10.1161/01.CIR.98.7.719
- Tahir, K., Kiser, A., Caranasos, T., Mounsey, J. P., and Gehi, A. (2018). Hybrid epicardial-endocardial approach to atrial fibrillation ablation. *Curr. Treat. Options Cardiovasc. Med.* 20:25. doi: 10.1007/s11936-018-0613-3
- Takahara, A., Sugimoto, T., Kitamura, T., Takeda, K., Tsuneoka, Y., Namekata, I., et al. (2011). Electrophysiological and pharmacological characteristics of triggered activity elicited in guinea-pig pulmonary vein myocardium. *J. Pharmacol. Sci.* 115, 176–181. doi: 10.1254/jphs.10232FP
- Takarada, K., Overeinder, I., De Asmundis, C., Stroker, E., Mugnai, G., De Regibus, V., et al. (2017). Long-term outcome after second-generation cryoballoon ablation for paroxysmal atrial fibrillation - a 3-years follow-up. *J. Interv. Card. Electrophysiol.* 49, 93–100. doi: 10.1007/s10840-017-0237-7
- Takigawa, M., Kuwahara, T., Takahashi, A., Okubo, K., Takahashi, Y., Nakashima, E., et al. (2015a). Simultaneous isolation of superior and inferior pulmonary veins on both the left and right sides could yield better outcomes in patients with paroxysmal atrial fibrillation. *Europace* 17, 732–740. doi: 10.1093/europace/euu372
- Takigawa, M., Takahashi, A., Kuwahara, T., Okubo, K., Takahashi, Y., Nakashima, E., et al. (2015b). Impact of non-pulmonary vein foci on the outcome of the second session of catheter ablation for paroxysmal atrial fibrillation. *J. Cardiovasc. Electrophysiol.* 26, 739–746. doi: 10.1111/jce.12681
- Takigawa, M., Takahashi, A., Kuwahara, T., Okubo, K., Takahashi, Y., Watari, Y., et al. (2017). Long-term outcome after catheter ablation of paroxysmal atrial fibrillation: impact of different atrial fibrillation foci. *Int. J. Cardiol.* 227, 407–412. doi: 10.1016/j.ijcard.2016.11.028
- Tilz, R. R., Heeger, C. H., Wick, A., Saguner, A. M., Metzner, A., Rillig, A., et al. (2018). Ten-year clinical outcome after circumferential pulmonary vein isolation utilizing the hamburg approach in patients with symptomatic drug-refractory paroxysmal atrial fibrillation. *Circ. Arrhythm. Electrophysiol.* 11:e005250. doi: 10.1161/CIRCEP.117.005250
- Tusscher, K. H. W. J. T., and Panfilov, A. V. (2005). Wave propagation in excitable media with randomly distributed obstacles. *Multisc. Model. Simulat.* 3, 265–282. doi: 10.1137/030602654
- Umapathy, K., Nair, K., Masse, S., Krishnan, S., Rogers, J., Nash, M. P., et al. (2010). Phase mapping of cardiac fibrillation. *Circ. Arrhythm. Electrophysiol.* 3, 105–114. doi: 10.1161/CIRCEP.110.853804
- Vaquero, M., Calvo, D., and Jalife, J. (2008). Cardiac fibrillation: from ion channels to rotors in the human heart. *Heart Rhythm* 5, 872–879. doi: 10.1016/j.hrthm.2008.02.034

- Venteclef, N., Guglielmi, V., Balse, E., Gaborit, B., Cotillard, A., Atassi, F., et al. (2015). Human epicardial adipose tissue induces fibrosis of the atrial myocardium through the secretion of adipo-fibrokines. *Eur Heart J.* 36, 795–805a. doi: 10.1093/eurheartj/eht099
- Verheule, S., Tuyls, E., Gharaviri, A., Hulsmans, S., Van Hunnik, A., Kuiper, M., et al. (2013). Loss of continuity in the thin epicardial layer because of endomyocardial fibrosis increases the complexity of atrial fibrillatory conduction. *Circ. Arrhythm. Electrophysiol.* 6, 202–211. doi: 10.1161/CIRCEP.112.975144
- Verma, A., Jiang, C. Y., Betts, T. R., Chen, J., Deisenhofer, I., Mantovan, R., et al. (2015). Approaches to catheter ablation for persistent atrial fibrillation. *N. Engl. J. Med.* 372, 1812–1822. doi: 10.1056/NEJMoa1408288
- Verma, A., Novak, P., Macle, L., Whaley, B., Beardsall, M., Wulfhart, Z., et al. (2008). A prospective, multicenter evaluation of ablating complex fractionated electrograms (CFEs) during atrial fibrillation (AF) identified by an automated mapping algorithm: acute effects on AF and efficacy as an adjuvant strategy. *Heart Rhythm* 5, 198–205. doi: 10.1016/j.hrthm.2007.09.027
- Verma, A., Sanders, P., Champagne, J., Macle, L., Nair, G. M., Calkins, H., et al. (2014). Selective complex fractionated atrial electrograms targeting for atrial fibrillation study (SELECT AF): a multicenter, randomized trial. *Circ. Arrhythm. Electrophysiol.* 7, 55–62. doi: 10.1161/CIRCEP.113.000890
- Vigmond, E., Pashaei, A., Amraoui, S., Cochet, H., and Hassaguerre, M. (2016). Percolation as a mechanism to explain atrial fractionated electrograms and reentry in a fibrosis model based on imaging data. *Heart Rhythm* 13, 1536–1543. doi: 10.1016/j.hrthm.2016.03.019
- Vijayakumar, R., Vasireddi, S. K., Cuculich, P. S., Faddis, M. N., and Rudy, Y. (2016). Methodology considerations in phase mapping of human cardiac arrhythmias. *Circ. Arrhythm. Electrophysiol.* 9:e004409. doi: 10.1161/CIRCEP.116.004409
- Viskin, S., Golovner, M., Malov, N., Fish, R., Alroy, I., Vila, Y., et al. (1999). Circadian variation of symptomatic paroxysmal atrial fibrillation. Data from almost 10 000 episodes. *Eur Heart J.* 20, 1429–1434. doi: 10.1053/euhj.1999.1632
- Vlachos, K., Letsas, K. P., Korantzopoulos, P., Liu, T., Georgopoulos, S., Bakalakos, A., et al. (2016). Prediction of atrial fibrillation development and progression: current perspectives. *World J. Cardiol.* 8, 267–276. doi: 10.4330/wjc.v8.i3.267
- Vogler, J., Willems, S., Sultan, A., Schreiber, D., Luker, J., Servatius, H., et al. (2015). Pulmonary vein isolation versus defragmentation: the CHASE-AF clinical trial. *J. Am. Coll. Cardiol.* 66, 2743–2752. doi: 10.1016/j.jacc.2015.09.088
- Vogt, J., Heintze, J., Gutleben, K. J., Muntean, B., Horstkotte, D., and Nolker, G. (2013). Long-term outcomes after cryoballoon pulmonary vein isolation: results from a prospective study in 605 patients. *J. Am. Coll. Cardiol.* 61, 1707–1712. doi: 10.1016/j.jacc.2012.09.033
- Voskoboinik, A., Moskovitch, J. T., Harel, N., Sanders, P., Kistler, P. M., and Kalman, J. M. (2017). Revisiting pulmonary vein isolation alone for persistent atrial fibrillation: a systematic review and meta-analysis. *Heart Rhythm* 14, 661–667. doi: 10.1016/j.hrthm.2017.01.003
- Wakili, R., Voigt, N., Kaab, S., Dobrev, D., and Nattel, S. (2011). Recent advances in the molecular pathophysiology of atrial fibrillation. *J. Clin. Invest.* 121, 2955–2968. doi: 10.1172/JCI46315
- Wang, Y., Cuculich, P. S., Zhang, J., Desouza, K. A., Vijayakumar, R., Chen, J., et al. (2011). Noninvasive electroanatomic mapping of human ventricular arrhythmias with electrocardiographic imaging. *Sci. Transl. Med.* 3:98ra84. doi: 10.1126/scitranslmed.3002152
- Weimar, T., Schena, S., Bailey, M. S., Maniar, H. S., Schuessler, R. B., Cox, J. L., et al. (2012). The cox-maze procedure for lone atrial fibrillation: a single-center experience over 2 decades. *Circ. Arrhythm. Electrophysiol.* 5, 8–14. doi: 10.1161/CIRCEP.111.963819
- Wijffels, M. C., Kirchhof, C. J., Dorland, R., and Allessie, M. A. (1995). Atrial fibrillation begets atrial fibrillation. A study in awake chronically instrumented goats. *Circulation* 92, 1954–1968. doi: 10.1161/01.CIR.92.7.1954
- Winfree, A. T. (1973). Scroll-shaped waves of chemical activity in three dimensions. *Science* 181, 937–939. doi: 10.1126/science.181.4103.937
- Wu, T. J., Liang, K. W., and Ting, C. T. (2001). Relation between the rapid focal activation in the pulmonary vein and the maintenance of paroxysmal atrial fibrillation. *Pacing Clin. Electrophysiol.* 24, 902–905. doi: 10.1046/j.1460-9592.2001.00902.x
- Xu, J., Luc, J. G. Y., and Phan, K. (2016). Atrial fibrillation: review of current treatment strategies. *J. Thorac. Dis.* 8, E886–E900. doi: 10.21037/jtd.2016.09.13
- Yamada, T., Murakami, Y., Okada, T., and Murohara, T. (2006). Focal atrial fibrillation associated with multiple breakout sites at the crista terminalis. *Pacing Clin. Electrophysiol.* 29, 207–210. doi: 10.1111/j.1540-8159.2006.00320.x
- Yamaguchi, T., Tsuchiya, T., Miyamoto, K., Nagamoto, Y., and Takahashi, N. (2010). Characterization of non-pulmonary vein foci with an EnSite array in patients with paroxysmal atrial fibrillation. *Europace* 12, 1698–1706. doi: 10.1093/europace/euq326
- Yamaguchi, T., Tsuchiya, T., Nakahara, S., Fukui, A., Nagamoto, Y., Murotani, K., et al. (2016). Efficacy of left atrial voltage-based catheter ablation of persistent atrial fibrillation. *J. Cardiovasc. Electrophysiol.* 27, 1055–1063. doi: 10.1111/jce.13019
- Yang, B., Jiang, C., Lin, Y., Yang, G., Chu, H., Cai, H., et al. (2017). STABLE-SR (electrophysiological substrate ablation in the left atrium during sinus rhythm) for the treatment of nonparoxysmal atrial fibrillation: a prospective, multicenter randomized clinical trial. *Circ. Arrhythm. Electrophysiol.* 10:e005405. doi: 10.1161/CIRCEP.117.005405
- Yue, L., Xie, J., and Nattel, S. (2011). Molecular determinants of cardiac fibroblast electrical function and therapeutic implications for atrial fibrillation. *Cardiovasc. Res.* 89, 744–753. doi: 10.1093/cvr/cvq329
- Zhang, J., Desouza, K. A., Cuculich, P. S., Cooper, D. H., Chen, J., and Rudy, Y. (2013). Continuous ECGI mapping of spontaneous VT initiation, continuation, and termination with antitachycardia pacing. *Heart Rhythm* 10, 1244–1245. doi: 10.1016/j.hrthm.2012.01.001
- Zhao, J., Hansen, B. J., Csepe, T. A., Lim, P., Wang, Y., Williams, M., et al. (2015). Integration of high resolution optical mapping and 3D Micro-CT imaging to resolve the structural basis of atrial conduction in the human heart. *Circ. Arrhythm. Electrophysiol.* 8, 1514–1517. doi: 10.1161/CIRCEP.115.003064

Conflict of Interest Statement: The authors declare that the research was conducted in the absence of any commercial or financial relationships that could be construed as a potential conflict of interest.

Copyright © 2018 Cheniti, Vlachos, Pambrun, Hooks, Frontera, Takigawa, Bourier, Kitamura, Lam, Martin, Dumas-Pommier, Puyo, Pillois, Duchateau, Klotz, Denis, Derval, Jais, Cochet, Hocini, Haissaguerre and Sacher. This is an open-access article distributed under the terms of the Creative Commons Attribution License (CC BY). The use, distribution or reproduction in other forums is permitted, provided the original author(s) and the copyright owner(s) are credited and that the original publication in this journal is cited, in accordance with accepted academic practice. No use, distribution or reproduction is permitted which does not comply with these terms.



Modeling Left Atrial Flow, Energy, Blood Heating Distribution in Response to Catheter Ablation Therapy

Desmond Dillon-Murphy^{1*}, David Marlevi², Bram Ruijsink¹, Ahmed Qureshi¹, Henry Chubb³, Eric Kerfoot¹, Mark O'Neill¹, David Nordsletten¹, Oleg Aslanidi¹ and Adelaide de Vecchi^{1*}

¹ School of Biomedical Engineering and Imaging Sciences, King's College London, London, United Kingdom, ² School of Engineering Sciences in Chemistry, Biotechnology and Health, KTH Royal Institute of Technology, Stockholm, Sweden, ³ Department of Cardiothoracic Surgery, Stanford University, Palo Alto, CA, United States

OPEN ACCESS

Edited by:

Alexander Panfilov,
Ghent University, Belgium

Reviewed by:

Luca Dede',
Politecnico di Milano, Italy
Vijay Vedula,
Stanford University, United States

*Correspondence:

Desmond Dillon-Murphy
desmond.dillon-murphy@kcl.ac.uk
Adelaide de Vecchi
adelaide.de_vecchi@kcl.ac.uk

Specialty section:

This article was submitted to
Computational Physiology and
Medicine,
a section of the journal
Frontiers in Physiology

Received: 11 May 2018

Accepted: 20 November 2018

Published: 14 December 2018

Citation:

Dillon-Murphy D, Marlevi D, Ruijsink B, Qureshi A, Chubb H, Kerfoot E, O'Neill M, Nordsletten D, Aslanidi O and de Vecchi A (2018) Modeling Left Atrial Flow, Energy, Blood Heating Distribution in Response to Catheter Ablation Therapy. *Front. Physiol.* 9:1757. doi: 10.3389/fphys.2018.01757

Introduction: Atrial fibrillation (AF) is a widespread cardiac arrhythmia that commonly affects the left atrium (LA), causing it to quiver instead of contracting effectively. This behavior is triggered by abnormal electrical impulses at a specific site in the atrial wall. Catheter ablation (CA) treatment consists of isolating this driver site by burning the surrounding tissue to restore sinus rhythm (SR). However, evidence suggests that CA can concur to the formation of blood clots by promoting coagulation near the heat source and in regions with low flow velocity and blood stagnation.

Methods: A patient-specific modeling workflow was created and applied to simulate thermal-fluid dynamics in two patients pre- and post-CA. Each model was personalized based on pre- and post-CA imaging datasets. The wall motion and anatomy were derived from SSFP Cine MRI data, while the trans-valvular flow was based on Doppler ultrasound data. The temperature distribution in the blood was modeled using a modified Pennes bioheat equation implemented in a finite-element based Navier-Stokes solver. Blood particles were also classified based on their residence time in the LA using a particle-tracking algorithm.

Results: SR simulations showed multiple short-lived vortices with an average blood velocity of 0.2–0.22 m/s. In contrast, AF patients presented a slower vortex and stagnant flow in the LA appendage, with the average blood velocity reduced to 0.08–0.14 m/s. Restoration of SR also increased the blood kinetic energy and the viscous dissipation due to the presence of multiple vortices. Particle tracking showed a dramatic decrease in the percentage of blood remaining in the LA for longer than one cycle after CA (65.9 vs. 43.3% in patient A and 62.2 vs. 54.8% in patient B). Maximum temperatures of 76° and 58°C were observed when CA was performed near the appendage and in a pulmonary vein, respectively.

Conclusion: This computational study presents novel models to elucidate relations between catheter temperature, patient-specific atrial anatomy and blood velocity, and predict how they change from SR to AF. The models can quantify blood flow in critical regions, including residence times and temperature distribution for different catheter positions, providing a basis for quantifying stroke risks.

Keywords: left atrium, computational fluid dynamics, atrial fibrillation, thermal modeling, catheter ablation

1. BACKGROUND

Atrial Fibrillation (AF) is the most common cardiac arrhythmia, affecting over 30 million people worldwide (Kirchhof et al., 2016). It is characterized by irregular, rapid activations of the atria and carries a high risk of heart failure and stroke. This irregular electrical activity causes the atrium to quiver instead of contracting, thus compromising the atrial flow dynamics and the amount of blood pushed into the ventricle. In the case of the Left Atrium (LA), this can reduce cardiac output by up to 30% (Iwasaki et al., 2011). Catheter Ablation (CA) has proven to be an effective treatment for permanent termination of AF and is gradually supplanting antiarrhythmic drug therapy. This procedure involves the targeted application of Radio-Frequency (RF) energy to the myocardium to create transmural lesions that neutralize the abnormal electrical impulses by isolating the source of irregular activity (e.g., the pulmonary veins (PV), the mitral annulus and isthmus) from the surrounding tissue and restore the normal Sinus Rhythm (SR) (O'Neill et al., 2007).

The increased risk of heart failure and stroke in AF patients have been associated with higher residence times of blood in the fibrillating LA (Camm et al., 2012; Soor et al., 2016). In the healthy atria, blood forms high-speed vortices, while in AF these structures merge into a single slow-moving vortex, contributing to blood stasis and potential thromboembolism formation (Fyrenius, 2001; Fluckiger et al., 2013; Koizumi et al., 2015; Gülan et al., 2017). Such effects of AF on the atrial flow dynamics become even more important during CA. Thus, the risk of thrombus formation, which is high in regions with propensity to blood stasis such as the LA appendage, is exacerbated by both the low blood flow velocities that occur in AF and the localized heating of the blood surrounding the site where CA is performed (Cibis et al., 2017). Recent studies showed that the blood washout in the LA is considerably lower during fibrillation and the number of blood particles remaining in the LA appendage after three cycles almost doubles in AF compared to SR conditions, suggesting an increased likelihood of blood stasis and subsequent thrombus formation (Masci et al., 2017a,b). A 10% incidence of thrombus was reported during CA (Ren et al., 2004). A study in dogs showed a rate of thromboembolism 2.5 times higher after CA (mean temperature $66 \pm 5.5^\circ\text{C}$) than after cryoenergy ablation (mean temperature $-60 \pm 12.1^\circ\text{C}$) (Khairy et al., 2003). *In-vitro* evidence proved that plasma aggregation occurs in a few seconds at $50\text{--}80^\circ\text{C}$ in stationary blood (Demolin et al., 2002). In patients, an incidence of coagulum up to 8% was found for CA temperatures above 75°C (Calkins et al., 1994).

The interplay between atrial flow, catheter temperatures and thrombogenic events during AF is poorly understood, due to the difficulty in characterizing atrial flow dynamics and to the scarcity of data on blood residence times in the LA pre- and post-CA. As blood flow rates vary considerably inside the LA, the temperature distribution and heat dissipation are hard to predict. Although various models can successfully quantify atrial blood flow in AF, none of these includes the simulation of CA and temperature in the blood flow to address this issue (Mouret et al., 2004; Zhang and Gay, 2008; Chnafa et al., 2012, 2014; Koizumi et al., 2015; Vedula et al., 2015). Conversely, tissue temperature distribution during CA has been simulated in a variety of models that either do not include blood flow (Tungjitusolmun et al., 2001; Lai et al., 2004; Gallagher et al., 2013), or only simulate the cooling effect of blood flow on the ablated tissue rather than the effect of heat on the blood itself (Jain and Wolf, 2000a,b; Berjano, 2006; González-Suárez and Berjano, 2016).

Blood residence times in the atria, and their links with thrombi formation and movement, have also been poorly characterized. Particle tracking provides a well-known technique to classify blood flow components based on their residence time in the heart. This type of analysis relies on the existence of a time point, such as the onset of systole in the Left Ventricle (LV), where there is no inflow nor outflow from the chamber, and from which the particle tracking is performed (Bolger et al., 2007; Eriksson et al., 2010). This approach was used to understand disease progression in the LV of patients with dilated cardiomyopathy (Carlhäll and Bolger, 2010; Eriksson et al., 2011, 2012). More recently, a similar technique was proposed to investigate atrial flow dynamics through continuous particle seeding from the Pulmonary Vein (PV), since blood inflow in the LA occurs continuously throughout both systole and diastole, unlike in the LV, with preliminary results showing that approximately half of the blood volume entering the healthy LA in one cycle is ejected in the same cycle (Gaeta et al., 2018).

The goal of this study is to understand better how LA flow is affected first by AF, then by AF termination by CA. Personalized models are generated by combining information from imaging data (Cine MRI and Doppler echocardiography) and atrial wall motion tracking. Computational fluid dynamics (CFD) with heat modeling is then performed using the Finite Element (FE) based software package CHeart (Lee et al., 2016; Hessenthaler et al., 2017) to simulate the patient-specific fluid-thermal dynamics, with further application of the particle tracking techniques. This workflow is applied to two patients presenting with AF pre- and post-CA, to explore how the complex fluid-thermal dynamics and flow distribution change between AF (pre-CA) and SR (post-CA).

2. METHODS

2.1. Patient Data

SSFP Cine MRI data with a spatial resolution of $1.25 \times 1.25 \times 10 \text{ mm}^3$ and temporal resolution of 50 timesteps/cycle were acquired for the full heart from two patients (Chubb et al., 2018). Data for patient A were acquired 84 days prior to and 89 days post CA. Data for patient B were acquired 63 days prior to and 90 days post CA. This patient also presented with type 2 diabetes mellitus. Both patients exhibited persistent AF in initial scans, and SR in the follow up scan. Patient A's was 69 BPM in the initial scan and 70 BPM in the post treatment scan, while Patient B's heart rate was 82 BPM for both scans. This data is summarized in **Table 1**.

2.2. Segmentation Process and Mesh Generation

Segmentations of the LA and LV were performed with the image processing package MITK (Wolf et al., 2005) on each Cine MRI dataset at end-systole to create a patient-specific 3D atrial and ventricular mesh (**Figure 1**). Surface smoothing was applied via a 3D mathematical interpolation routine. Care was taken to insure the resulting interpolated segmentation conformed closely to the imaging data (Maleike et al., 2009). The atrial segmentation was processed using the software package Paraview (Ahrens et al., 2005) to identify the inflow planes for each of the PV and the outflow plane in the Mitral Valve (MV). A tetrahedral volume mesh of the LA was then generated from the smoothed surface mesh using the software package VMTK (Antiga et al., 2008) ($h_{\max} \approx 2.9 \text{ mm}$, $h_{\min} \approx 0.7 \text{ mm}$, and $h_{\text{mean}} \approx 1.5 \text{ mm}$) to perform FE flow simulations.

2.3. Motion Tracking

The visualization and analysis of the data was performed using the software package Eidolon (Kerfoot et al., 2016). Specifically, the motion of structures throughout the time-dependant image series was described via a motion tracking algorithm based on temporal sparse free-form deformations, where the deformation is reconstructed from an image sequence. A reference frame was chosen as source image for the other images in the sequence. This algorithm guarantees the periodicity of the deformation by enforcing cyclic motion. The algorithm was applied to the Cine MRI data to generate a transformation field for the entire image volume that represents the wall motion of the LA and LV.

This tracking field was then applied to the LA and LV surfaces meshes. The deforming mesh was visually checked in three different views (sagittal, axial and coronal) to ensure tracking was accurate throughout the cycle. This process resulted in a deformed surface mesh for each of the 50 steps/cardiac cycle for both the LA and LV. Specifically, the motion of structures throughout the time-dependant image series was described via a motion tracking algorithm based on temporal sparse free-form deformations, where the deformation is reconstructed from an image sequence (**Figure 2**).

2.4. Boundary Conditions

The nodal coordinates of the 50 surface meshes of the LA were then interpolated with cubic splines and a periodic end condition to artificially increase the temporal resolution to 1,000 steps/cycle. A wall velocity boundary condition for each step was calculated and was then applied at the LA-blood interface to deform the mesh tracking the LA structure in the image throughout the cardiac cycle. The same steps were applied to the LV.

Using the tracked LV mesh, the volume of each chamber was calculated throughout the cardiac cycle. Flow through the MV, Q_{MV} , was quantified by calculating the differential in positive volume change, dV/dt from maximum to minimum volume over the cycle and assuming perfect functioning of the aortic valve and MV, such that

$$Q_{\text{MV}} = 0, \text{ if } dV/dt \text{ is negative,}$$

$$Q_{\text{MV}} = \frac{dV}{dt}, \text{ if } dV/dt \text{ is positive.}$$

The resulting flow velocity waveforms were validated against velocities recorded at the MV using Doppler ultrasound. The MV was defined as an ellipse fitted to the MV annulus. Q_{MV} was interpolated across this elliptical valve with a paraboloid shape to create a time-dependant velocity field, which was applied as a Dirichlet boundary condition on the MV plane. The maximum velocities were defined in the centre of the MV in a direction normal to the MV face and zero velocity was prescribed at the edges of the ellipse.

At each of the PV faces backflow stabilization, zero pressure stabilizing Neumann conditions were applied to avoid an excessive flux of momentum into the domain, and hence prevent

TABLE 1 | Patient data.

	Age range (Years)	Vascular disease	AF duration (years)	LA fibrosis	LA max Vol (ml)	LV EDV (ml)
Patient A	55–60	Yes	2	Nil	113	114
Patient B	55–60	Nil	4	Nil	197	210
	HR pre CA BPM	HR post CA BPM	LV stroke Pre CA (ml)	LV stroke Post CA (ml)		
Patient A	69	70	56	80		
Patient B	82	82	101	149		

A summary of the relevant data for the patients used in this study.

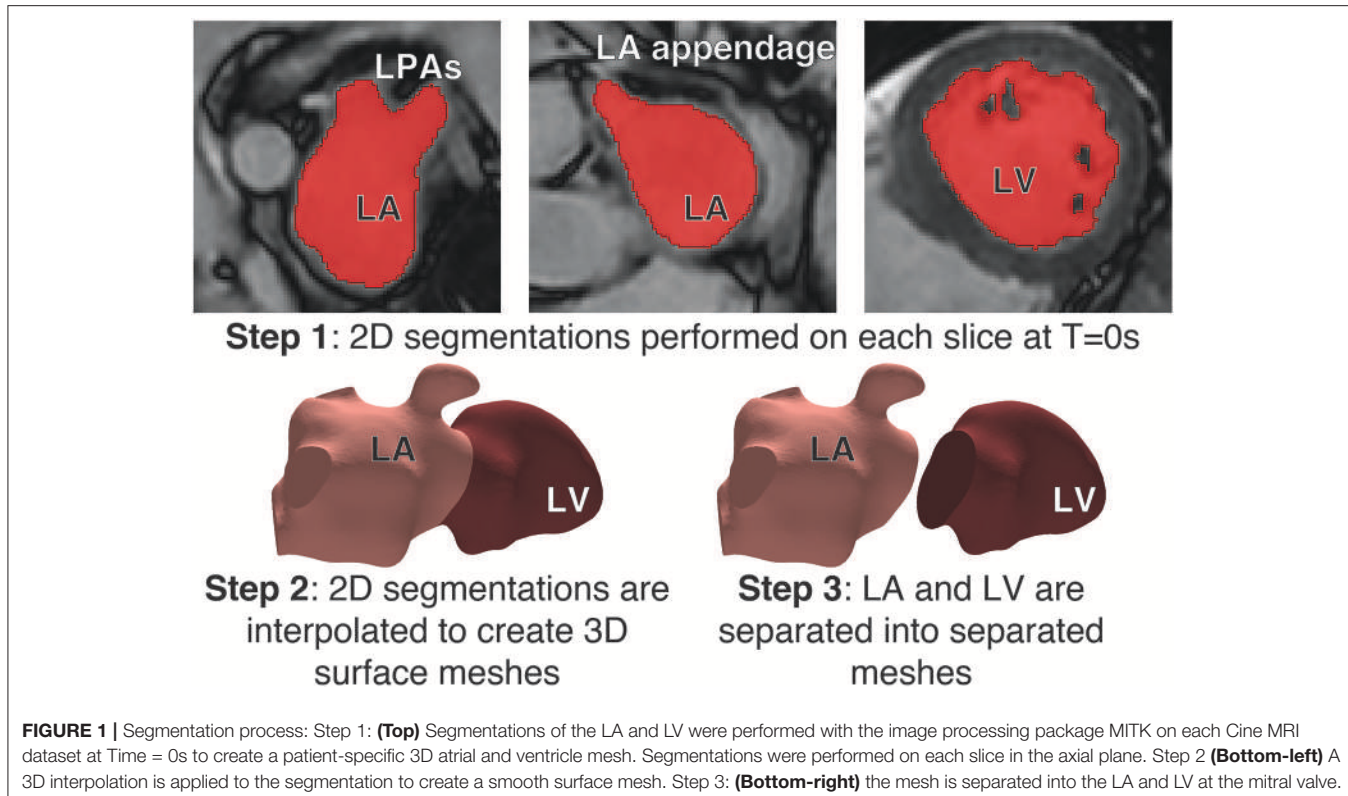


FIGURE 1 | Segmentation process: Step 1: **(Top)** Segmentations of the LA and LV were performed with the image processing package MITK on each Cine MRI dataset at Time = 0s to create a patient-specific 3D atrial and ventricle mesh. Segmentations were performed on each slice in the axial plane. Step 2 **(Bottom-left)** A 3D interpolation is applied to the segmentation to create a smooth surface mesh. Step 3: **(Bottom-right)** the mesh is separated into the LA and LV at the mitral valve.

instabilities, following a previously proposed approach (Esmaily Moghadam et al., 2011).

2.5. Computational Fluid Dynamics Simulations

CFD simulations of the patient-specific LA flow were then performed using the stabilized Streamline Upwind Petrov-Galerkin (SUPG) Arbitrary Lagrangian-Eulerian (ALE) Navier-Stokes solver for incompressible flows implemented in the software package CHeart (Lee et al., 2016). The temporal resolution was set to 0.73 ms, resulting in 1000 time steps per cycle. Up to 10 cardiac cycles were simulated using 98 cores of a 640 core SGI Altix-UV high performance computing (HPC) cluster with Nehalem-EX architecture at King's College London. Blood density ρ was defined as 1.06 kg/m^3 and viscosity μ as $3.5 \times 10^{-3} \text{ Pa s}$. The results were checked to ensure periodicity.

Flow energies were also computed to describe LA function. Kinetic Energy (KE) is directly related to flow velocities and is described mathematically as

$$KE = \frac{\rho}{2} \| v_{blood} \|^2$$

where v_{blood} is the blood velocity (m/s).

Viscous energy quantifies the energy dissipation that occurs due to the conversion of KE to thermal energy or to the presence of high-friction, vortical flow. The rate of viscous energy dissipation, (\dot{E}), can be described as

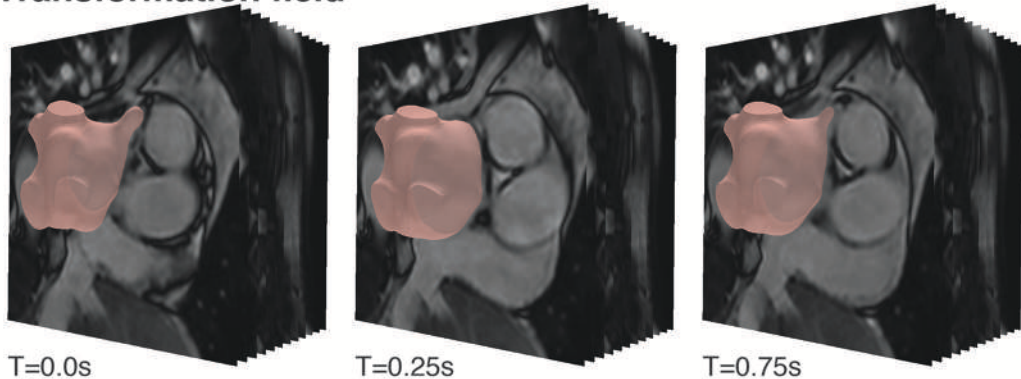
$$\dot{E} = \mu \frac{[\nabla v_{blood} + (\nabla v_{blood})^T]^2}{2}$$

To compare the changes in KE and \dot{E} between the AF and SR states, the data was integrated over the volume of the atrial cavity (Elbaz et al., 2017). Reduced vortical flows have been associated with patients in AF and are associated with an increased risk of thrombus formation and embolization (Fyrenius, 2001).

2.6. Particle Tracking

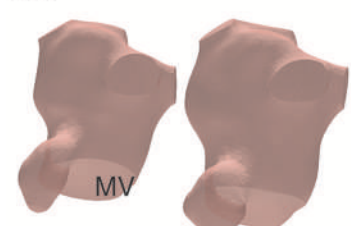
Following the CFD simulations particle tracking was applied to the generated LA velocity field for the final simulated cycle. The geometry was uniformly seeded with massless particles at the instant the MV opens. The seeding was performed at the onset of systole in all cases. A uniform grid was imposed on the entire LA cavity and the particles were seeded at each nodal position of the grid from this starting point (no reseeding was performed). The number of particle was approximately 10,000 with small variations between the two patient cases due to differences in the size of the cavity. The trajectory of each particle was computed using 4th order Runge-Kutta estimations based on the velocity field for a single full cardiac cycle and as such was unique. Hence, in order to cover the entire cycle, each particle was tracked backwards and forwards in time starting from a fixed seeding point at the onset of systole, so the forward tracing would cover systole and the backward tracing diastole.

Motion is mapped from image data to mesh using a Transformation field



Resulting deforming meshes

LA

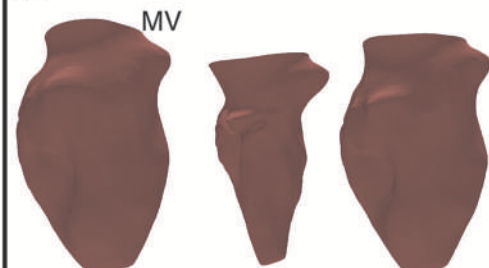


T=0s

T=0.25s

T=0.75s

LV



T=0s

T=0.25s

T=0.75s

FIGURE 2 | Cardiac Motion Tracking: **(Top)** Using the visualization and analysis package, Eidolon, an algorithm based on MIRTK which uses temporal-sparse free form deformations applied to the Cine MRI data to generate a transformation field for the entire image volume describing the motion of structures throughout the time-dependant image series, including the motion of the LA and LV. **(Bottom)** The tracking field was then applied to the LA and LV mesh and the deforming mesh was visually checked to ensure tracking was accurate throughout the cycle.

Particles were defined by their behavior during the cycle, in analogy with the spatial flow component analysis proposed in previous studies on left ventricular fluid dynamics (Bolger et al., 2007; Eriksson et al., 2010). Retained Inflow (RI) was defined as those particles that enter via the pulmonary veins (PV) during diastole and are not ejected at the end of the cycle analyzed. Delayed Ejection (DE) was defined as those particles present in the LA at the start of the cycle (diastole) and ejected during systole. Residual volume (RV) was defined as that flow that resides in the LA for at least two complete cycles. Finally diastolic Direct Flow (DF) was defined as the blood that enters the LA during diastole and is ejected in the following systole. Particles were also tagged based on which PV they emanated from to allow quantification of the contribution of each Pressure-Volume (PV).

Particle tracking convergence analysis was performed with respect to time tracking and particle density in a previous cardiac dataset (De Vecchi et al., 2018). These indicated that stabilized flow components (RI, DE, RV, DF) were achieved with $\sim 10,000$ uniformly seeded particles, traced forward and backward with 0.5 ms time stepping.

2.7. Thermal Simulations

Thermal processes during CA were modeled using a modified version of the Pennes bioheat equation (Soor et al., 2016):

$$\dot{T} + (v_{blood} - v_{wall}) \cdot \nabla T - \nabla \cdot D \nabla T - Q_{cath} + Q_{perf} - Q_{meta} = 0$$

The heat loss due to perfusion (Q_{perf}) and metabolic heat gain (Q_{meta}) were set to zero, since they have negligible physiological values. v_{wall} is wall velocity m/s calculated from the Computational Fluid Dynamics (CFD) simulation. The heat gain from the catheter (Q_{cath}) was defined in a sphere of radius 5 mm near the LA wall, which mimiced the catheter tip; the value of Q_{cath} was chosen to produce temperature of 90°C at the tip (Dillon-Murphy et al., 2017). T is the temperature of the blood in $^{\circ}\text{C}$. $D = k/\rho \cdot c$, k being the thermal conductivity of blood set to 0.57 W/m·K and c is the blood specific heat capacity, which was set to 3.9 J/kg·K. The initial conditions for blood temperature was 37°C everywhere except for the catheter tip. Zero-flux boundary conditions on temperature were applied at all boundaries.

The thermal problem was found to be dominated by advection, which was reflected in a high Peclet number ($\sim 10^7$).

Therefore, the simulation of the thermal diffusion on the CFD mesh resulted in numerical instabilities. To resolve this, the velocity field from the CFD analysis was interpolated and mapped to a denser LA mesh ($h_{max} \approx 1.75$ mm, $h_{min} \approx 0.38$ mm, and $h_{mean} \approx 0.92$ mm) (Figure 3). Simulations on such a fine mesh with about 2 million elements were less efficient computationally, but allowed us to avoid instabilities and generate the required proof-of-concept data.

3. RESULTS

3.1. Flow Velocity Analysis

Both simulations of SR patients showed flow velocities within a normal physiological range. Patient A ranged between 0 and 2.0 m/s, mean velocity 0.22 m/s, while patient B ranged between 0 and 2.3 m/s with a mean velocity of 0.2 m/s with blood forming several fast, short-lived vortices in both cases (see Supplementary Video 1 for patient A).

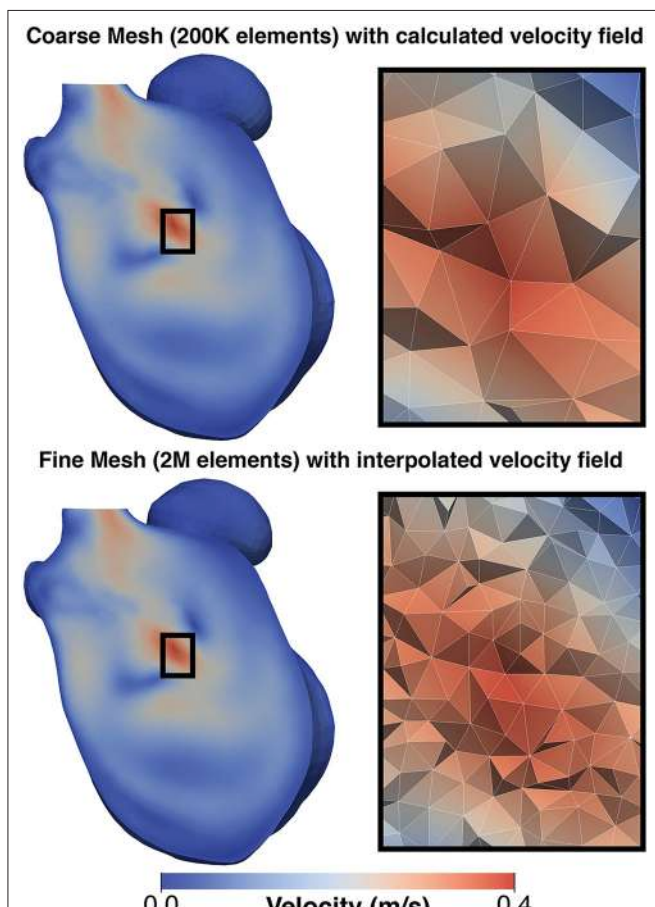


FIGURE 3 | Comparison of mesh for CFD simulation and thermal simulation: **(Top)** shows a velocity field generated on the CFD and **(Bottom)** shows the same field mapped to the finer mesh used for the thermal simulation. To the left of each image is a detailed view of the mesh structure in the center of the domain. This mapping was performed to avoid numerical issues due to the advection dominant behavior of heat in blood.

Simulations of AF patients tended to show larger slower vortices in the middle of the LA cavity (see Supplementary Video 2 for patient A) compared to those in SR, and there was a greater degree of stagnant flow in the LA appendage of both patients. When in AF patient A exhibited velocities in the range 0–1.2 m/s, mean velocity 0.08 m/s and patient B exhibited velocities in the range of 0–1.5 m/s with mean velocity of 0.14 m/s, a drop of 64 and 30% from SR, respectively. These simulation results are in good agreement with previous patient measurements based on the application of 4D flow MRI and phase-contrast MRI (Fluckiger et al., 2013).

After treatment, when the patients were in SR, both patients exhibited a relatively normal double-peaked MV flow waveform, with the first peak corresponding to the main outflow wave and the second to the atrial contraction in late diastole.

Before treatment, when the patients were in AF, the double-peaked MV flow was less evident. In patient A both outflow peak velocities were approximately 37 and 50% lower in AF than in SR (Figure 4). In patient B, while in AF, the two velocity peaks were fused into a single one that occurred later in systole and had a lower magnitude than the first main peak SR (25% reduction), as shown in Figure 5.

When comparing AF to SR conditions in the Left Atrial Appendage (LAA), the velocity went from a maximum value of 0.22 m/s and a mean value of 0.02 m/s when in AF to a maximum value of 0.75 m/s and a mean value of 0.05 m/s when in SR for patient A, and a maximum value of 0.35 m/s and a mean value of 0.05 m/s to a maximum value of 0.44 m/s and a mean value of 0.06 m/s for patient B.

3.2. Energy Analysis

Figure 6 shows the plot of the calculated kinetic energy for patient A and patient B for the cardiac cycle, which is proportional to $\| v_{blood} \|^2$. The dashed blue line shows the results for the AF case and the dashed orange shows the results for the SR case. Both patients showed a significant increase in the total kinetic energy in SR with the mean KE increasing 9-fold from 6.3 J/m^3 when in AF to 58.8 J/m^3 when in SR for patient A, and increasing over 2-fold from 15.9 J/m^3 to 34.8 J/m^3 for patient B.

This increase in overall KE is associated with an increase in the rate of viscous energy loss as shown in Figure 7. The mean \dot{E} for patient A increased 10-fold from 3.7 W/m^3 to 38.3 W/m^3 , and for patient B increased over 2-fold from 7.4 to 16 W/m^3 .

The energy peaks in Figures 6, 7 show a large difference in magnitude between AF and SR, especially in patient A, supporting our observation that restoration of SR by CA can improve dramatically the intra-cavity flow velocity.

3.3. Particle Tracking

Figures 8, 9 shows the particle tracking results for patient A and B respectively. Each figure shows the results pre and post CA treatment. The results are highlighted at three time points as described previously, the instant prior of the MV opening, the instant of peak MV flow, and the instant of LA systole associated with the booster pump function of the LA. The figure also contains a table of the percentage breakdown of each class of particles with a color key for each class. The relevant MV flow

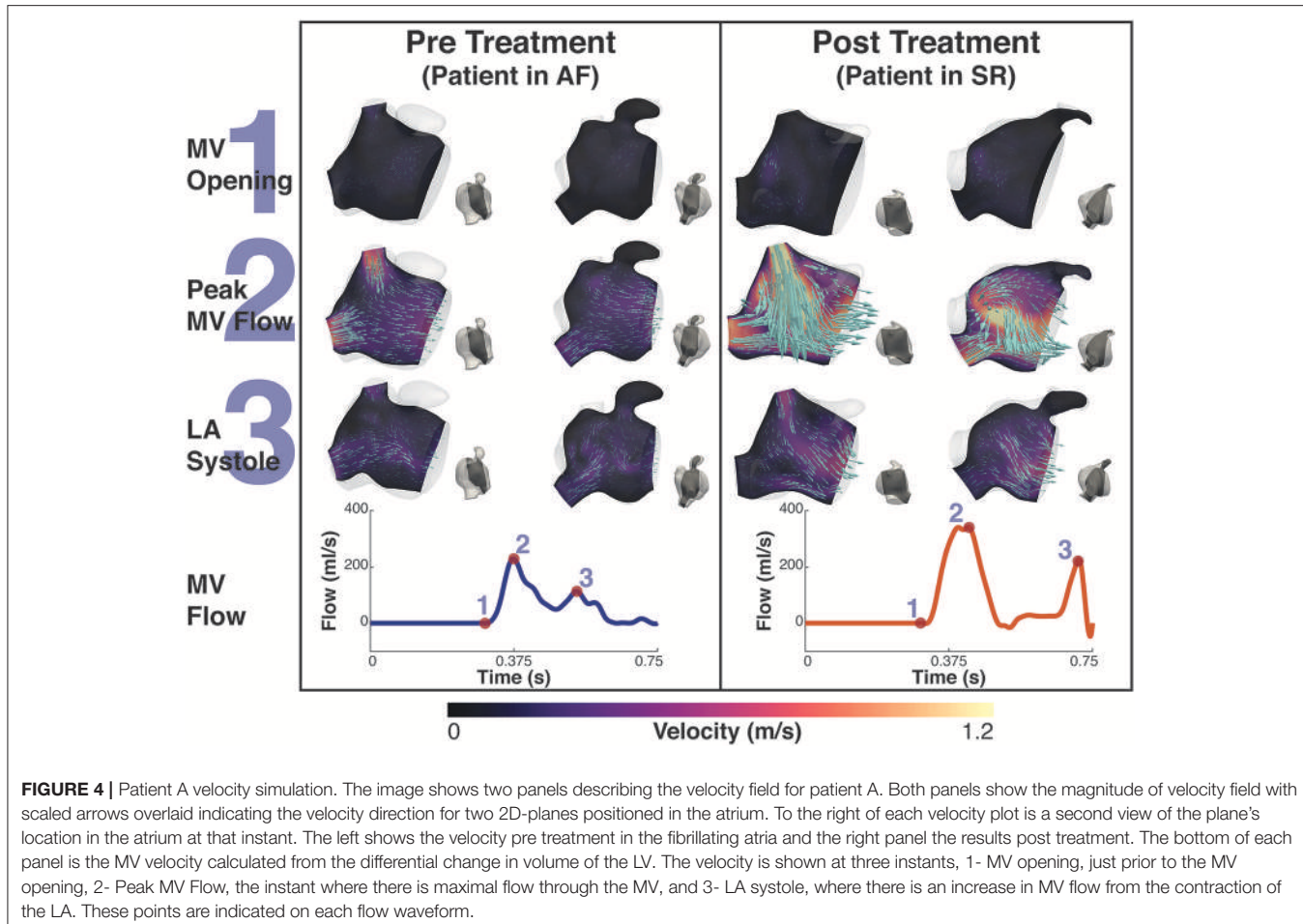


FIGURE 4 | Patient A velocity simulation. The image shows two panels describing the velocity field for patient A. Both panels show the magnitude of velocity field with scaled arrows overlaid indicating the velocity direction for two 2D-planes positioned in the atrium. To the right of each velocity plot is a second view of the plane's location in the atrium at that instant. The left shows the velocity pre treatment in the fibrillating atria and the right panel the results post treatment. The bottom of each panel is the MV velocity calculated from the differential change in volume of the LV. The velocity is shown at three instants, 1- MV opening, just prior to the MV opening, 2- Peak MV Flow, the instant where there is maximal flow through the MV, and 3- LA systole, where there is an increase in MV flow from the contraction of the LA. These points are indicated on each flow waveform.

waveform is also provided at the bottom right of each panel. **Table 2** provides a comprehensive quantitative breakdown of the proportion of particles attributable to each class, including a breakdown of which DF and RI particles are attributable to the superior and inferior Left Pulmonary Vein (LPV) and Right Pulmonary Vein (RPV). In both patients a decrease in RV was observed after CA (24.7 vs. 7.7% in patient A and 20.2 vs. 16.4% in patient B, pre- and post-CA respectively). This change was associated with a substantial increase in DF post-treatment (1.9 vs. 15.3% in patient A and 3.1 vs. 18.6% in patient B). The combined RV and RI pre-CA was 65.9 and 43.3% for patients A and B respectively, and 62.2 vs. 54.8% post-CA.

3.4. Thermal Analysis

Figure 10 shows the thermal simulation results for Patient A. The simulation was run with the catheter tip in two locations, Pos 1, with the catheter tip in the vicinity of the LAA, and Pos 2, with the catheter tip in the vicinity of the inferior RPV. The figure features a slice through the volume intersecting with the inferior RPV, the two tip locations, the LAA and the MV. For reference the figure also shows the velocity field overlaid on the thermal results. To the right of the thermal results is a volume representation of the slice orientation and tip locations. The figure also describes the

maximum temperatures and their locations at that instant in the cycle.

The temperature of the catheter tip was set to 90°C, although this temperature was never actually recorded in the blood as the heat was advected immediately away from the tip. At the time point prior to the MV opening, the maximum temperature at the catheter tip was approximately 83°C and the maximum blood temperature was 76°C for Pos 1 and 58°C for Pos 2. When the tip was in Pos 1, close to the LAA, the maximum temperature observed in the LAA was 47°C. When in Pos 2, the temperature in the LAA did not exceed 40°C.

4. DISCUSSION

This study performed thermal-fluid simulations in two patients who presented AF before treatment and were brought back in SR following CA. The results highlight significant differences in the LA fluid dynamics. In both cases flow velocities during AF were severely compromised and the vortex formation dynamics were also altered, in agreement with previous patient measurements based on the application of 4D flow MRI and phase-contrast MRI (Fluckiger et al., 2013; Masci et al., 2017a,b). The most noticeable difference between the two states was

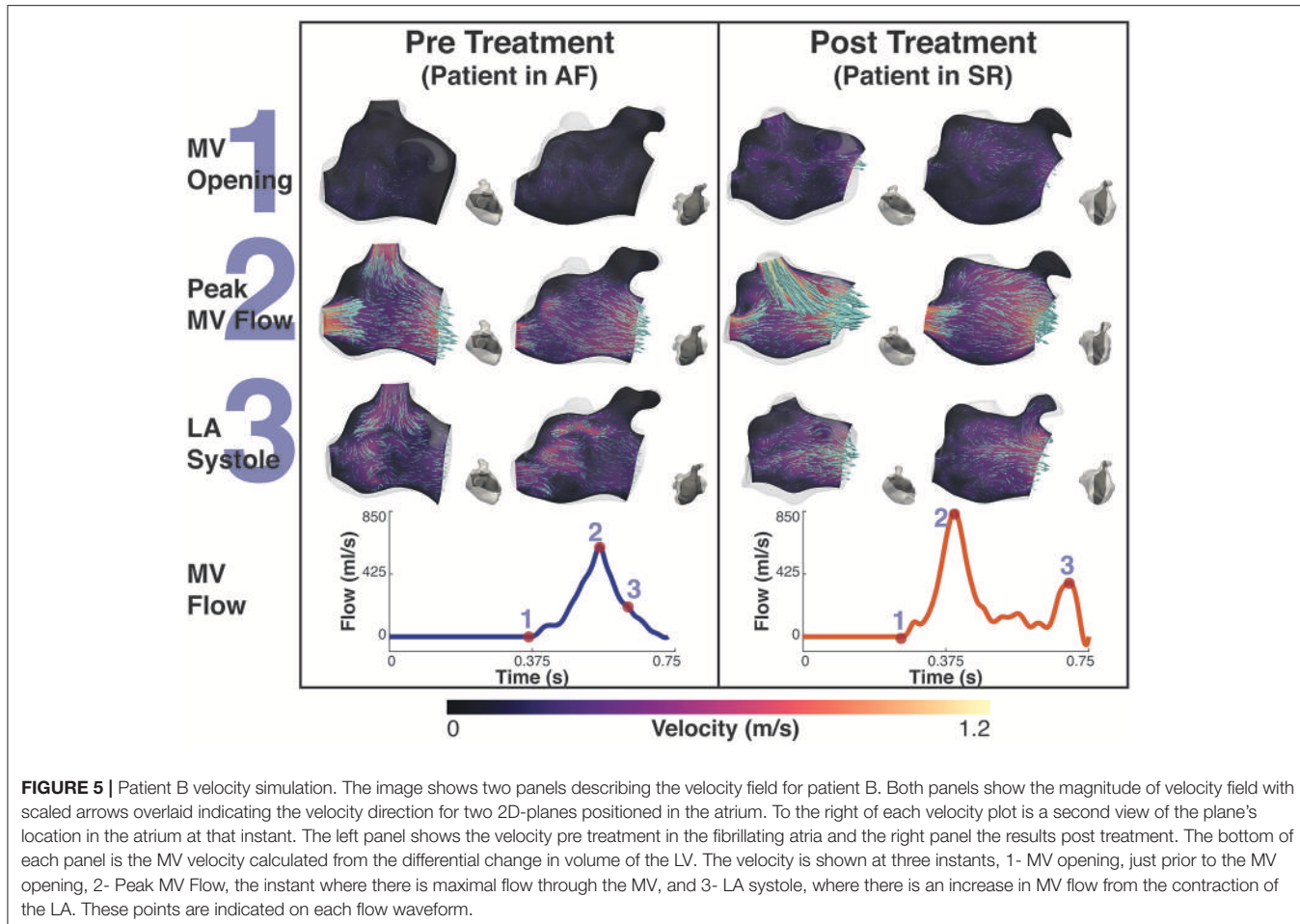


FIGURE 5 | Patient B velocity simulation. The image shows two panels describing the velocity field for patient B. Both panels show the magnitude of velocity field with scaled arrows overlaid indicating the velocity direction for two 2D-planes positioned in the atrium. To the right of each velocity plot is a second view of the plane's location in the atrium at that instant. The left panel shows the velocity pre treatment in the fibrillating atria and the right panel the results post treatment. The bottom of each panel is the MV velocity calculated from the differential change in volume of the LV. The velocity is shown at three instants, 1- MV opening, just prior to the MV opening, 2- Peak MV Flow, the instant where there is maximal flow through the MV, and 3- LA systole, where there is an increase in MV flow from the contraction of the LA. These points are indicated on each flow waveform.

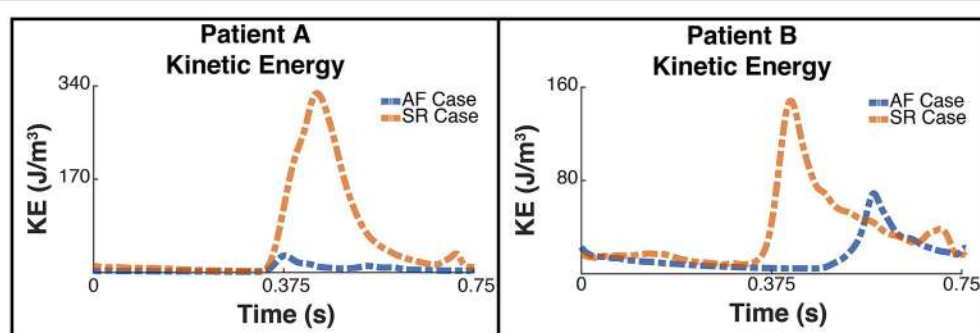


FIGURE 6 | Total Kinetic Energy. The image shows two panes of the total kinetic energy which is proportional to $\| v_{blood} \|^2$ for patient A (Left) and patient B (Right). The blue dashed line shows the total kinetic energy for each patient pre ablation, ie when the patient is in AF, and the orange line shows the post treatment SR case.

observed in the marked decrease during AF of the atrial booster pump function, which is responsible for the A-wave at the end of ventricular filling (atrial kick). This function was almost entirely absent in patient B, in analogy with previous findings that showed that suppression of atrial kick during AF can lead to a decrease in the total blood volume ejected into the LV by approximately 10% alone (Koizumi et al., 2015).

Lower blood velocities also corresponded to a decrease in the kinetic energy and viscous dissipation rate integrated over the total cavity volume. If this is to be expected given the direct proportionality with flow velocity, the results also showed that the peak kinetic energy and viscous energy dissipation during AF occurs earlier in patient A and later in patient B. This discrepancy is related to the fusion of the MV flow peak velocities into a single peak that occurs later in diastole

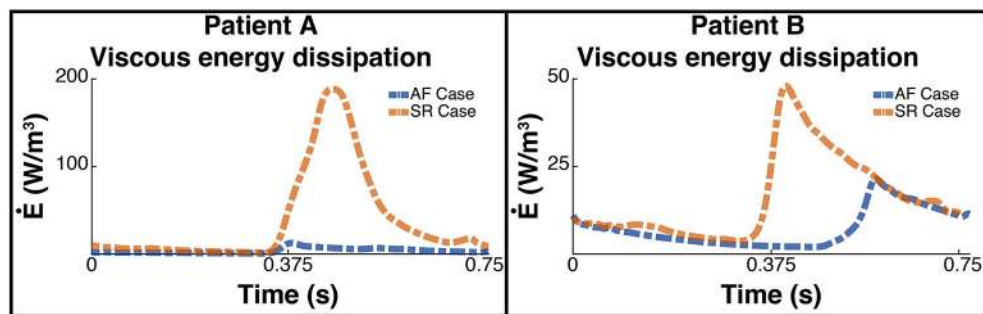


FIGURE 7 | Rate of viscous energy dissipation. The image shows two panes of the viscous energy loss waveforms for patient A (Left) and patient B (Right). The blue dashed line shows the instantaneous energy loss for each patient pre ablation, i.e., when the patient is in AF, and the orange line shows the post treatment SR case.

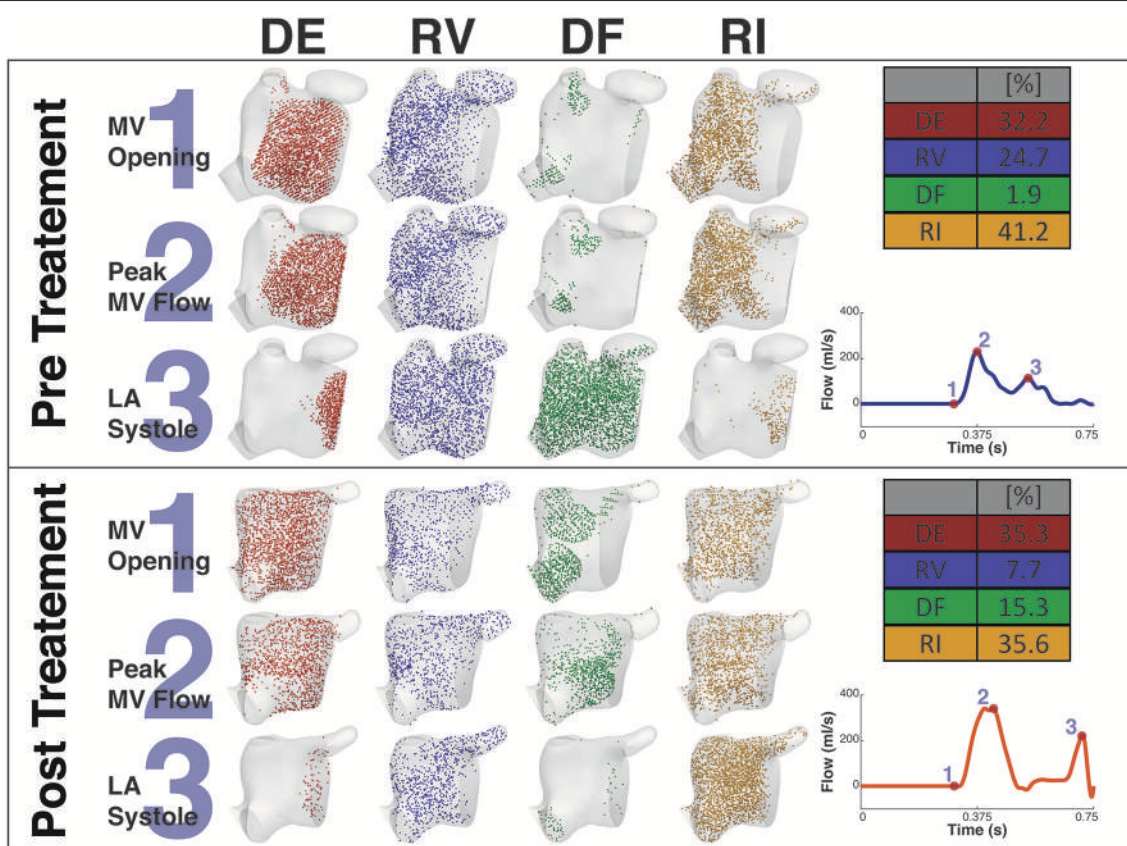


FIGURE 8 | Particle tracking results Patient A. The image shows the particle tracking results for patient A. The image consists of two panels. Each panel shows the visualization of the different classification of particles DE, RV, DF, and RI at three points in the cardiac cycle, just prior to MV Opening (1), Peak MV Flow (2), and LA Systole (3). Top-right of each panel shows the quantification of each classification of particle as a percentage, and Bottom-right shows the MV flow wave form with the instant of each timepoint under consideration. The top panel shows the Pre CA results when the patient exhibited AF while the bottom shows the post CA results when the patient was in SR.

for patient B, which does not occur in patient A, where the double-peaked flow is retained in AF (Figures 4, 5). This shows that the main contribution to the kinetic energy is during the mitral E-wave as expected from the mitral flow profile. However, in the fused peak case, the E-wave is delayed and the A-wave suppressed in the fusion, supporting the observation

that the atrial booster pump function is the most compromised in the fibrillating atrium. The fusion of the two flow peaks at the MV is also observed in cases of severely impaired LV relaxation, where a slow fall in the LV pressure leads to a longer isovolumic relaxation time and to a reduction in the E-wave.

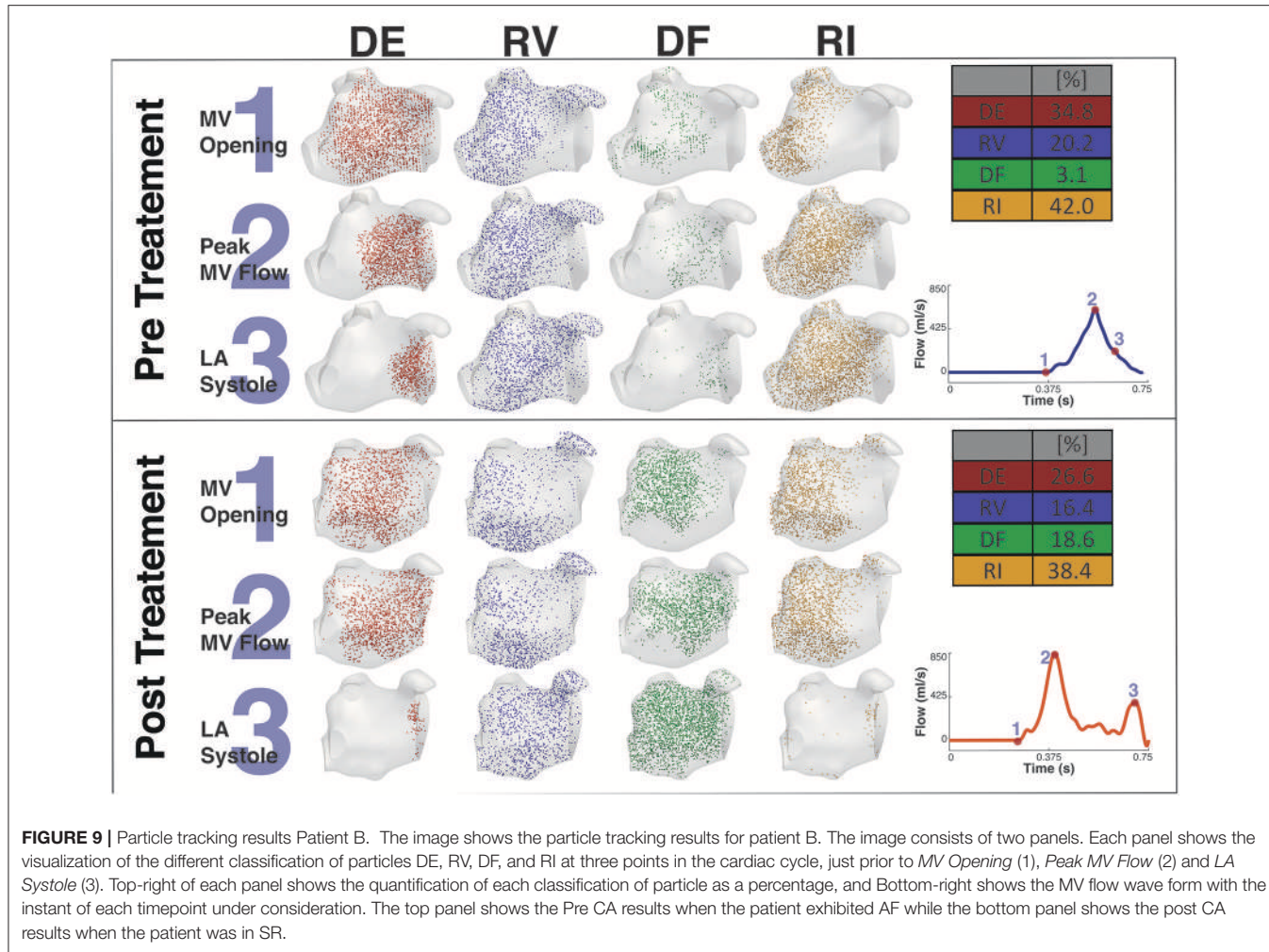


FIGURE 9 | Particle tracking results Patient B. The image shows the particle tracking results for patient B. The image consists of two panels. Each panel shows the visualization of the different classification of particles DE, RV, DF, and RI at three points in the cardiac cycle, just prior to MV Opening (1), Peak MV Flow (2) and LA Systole (3). Top-right of each panel shows the quantification of each classification of particle as a percentage, and Bottom-right shows the MV flow wave form with the instant of each timepoint under consideration. The top panel shows the Pre CA results when the patient exhibited AF while the bottom panel shows the post CA results when the patient was in SR.

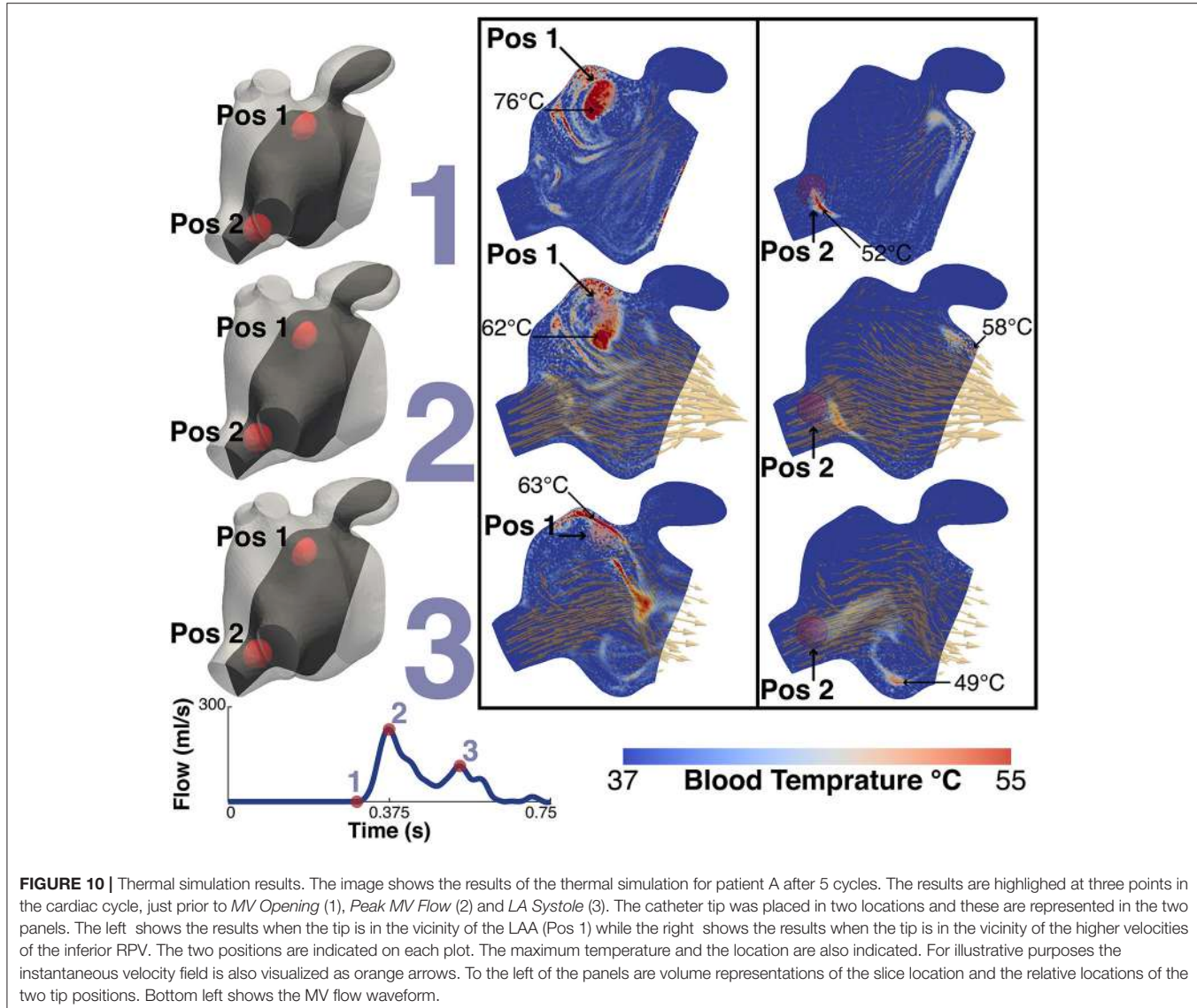
TABLE 2 | Comparative breakdown of proportion of particle classification.

Particle classification	Patient A Pre CA (%)	Patient A Post CA (%)	Patient B Pre CA (%)	Patient B Post CA (%)
Delayed Ejection (DE)	32.2	35.3	34.8	26.6
Residual Volume (RV)	24.7	7.7	20.2	16.4
Direct Flow (DF) superior LPV	0.9	2.0	0.1	4.3
Direct Flow (DF) inferior LPV	0.2	4.3	0.3	4.1
Direct Flow (DF) superior RPV	0.6	7.5	1.9	7.7
Direct Flow (DF) inferior RPV	0.2	1.6	0.8	2.4
Direct Flow (DF) Total	1.9	15.3	3.1	18.6
Retained Inflow (RI) superior LPV	3.7	6.0	1.9	5.4
Retained Inflow (RI) inferior LPV	21.3	12.2	11.7	4.9
Retained Inflow (RI) superior RPV	21.3	13.3	25.1	22.7
Retained Inflow (RI) inferior RPV	11.9	4.2	3.4	5.4
Retained Inflow (RI) Total	41.2	35.6	42.0	38.4

The table provides a comprehensive breakdown of the proportion of particles which can be attributed to each particle classification, including a breakdown of the proportion of DF and RI particles associated with the superior and inferior LPV and RPV.

The main consequence of this impaired atrial contraction is a sharp increase in the proportion of flow that resides in the LA for more than one cycle. During AF, the sum of the RV and RI flow

components is 65.9% in patient A and 64.2% in patient B, which is successfully reduced to 44.7 and 54.8% after restoration of SR, in line with the results obtained in a recent study of the healthy LA



(Gaeta et al., 2018). Note that the majority of these slow particles (RV+RI) are located in the LAA, which is a well-known site for thrombus formation in AF.

In both patients, restoration of SR leads to an increase in the diastolic DF that is particularly evident in the RPVs (in particular in the superior RPV). According to a PC-MRI based study, the right side of the pulmonary veins provides inflow that is conveyed along the atrial wall to the MV with minimal entrainment into the systolic vortex in the middle of the atrial cavity (Fyrenius, 2001). This increase in the diastolic DF from these veins post-treatment suggests therefore an improvement in conduit function. Supporting this conclusion, in patient A this increase in diastolic DF from the right side is also associated with a marked decrease in the RI component from the RPVs post-ablation.

Interestingly, while RI is mainly located near the PV side pre-treatment, LAA is predominantly occupied by RV flow, which has the highest residence time in the LA. This is particularly relevant

when localized heating during CA is delivered in a position close to the opening of the appendage, such as Position 1 in the simulations. This scenario sees an increase in the temperature of the RV flow in the appendage, which reaches 47°C. This value is in the range of the threshold of 50°–80°C for triggering plasma aggregation in stationary blood (Demolin et al., 2002). This critical value is however exceeded in the blood close to the tip of the catheter during the procedure. When ablation is performed at the level of the pulmonary vein the blood temperature does not rise as much, suggesting that the continuous inflow plays an important role in heat advection.

It is worth noticing that the DF flow component reported here represents the blood that enters the LA during diastole and leaves it in the following systole. Given that the PVs do not have valves, the inflow to the LA is continuous and occurs during both systole and diastole. Our current workflow does not take into account the flow that enters the LA during systole and therefore this additional contribution is not included in DF. This however

does not detract from the observation that CA has a substantial beneficial effect on the DF flow components, which increases after restoration of SR.

Albeit the recognized importance of blood hemodynamics in the left ventricle as a herald of structural adaptive mechanisms (Pedrizzetti et al., 2014, 2015; Mittal et al., 2016), the LA hemodynamics has received comparatively less attention. In this context, the present study aims to demonstrate the value of image-based blood flow modeling as a predictive tool that is not restricted to a single application, and can be applied to improve CA and provide insights into the mechanisms underlying AF pathophysiology and leading to life-threatening complications, such as subclinical thromboembolism.

5. CONCLUSIONS

This study presents novel patient-specific modeling workflow for characterizing the thermal-fluid dynamics in the atria of SR and AF patients, post- and pre-CA, respectively. The models enable simulation of atrial blood flow and its changes from SR to AF, including: (1) substantial decrease in the average flow velocity and kinetic energy, as well as increase in the percentage of blood remaining in the LA for longer than one cycle after CA, (2) the emergence of regions of blood stasis in the LAA and the resultant increase of blood temperature during CA in this region, which reaches values close to the threshold for coagulation. Decreased blood flow velocities during AF, region of blood stasis and the localized heating of the blood surrounding the CA sites all have been associated with increased risks of thrombus formation. Therefore, the novel workflow can be utilized for the improved quantification of the risks of thromboembolism and stroke, especially in challenging patient populations with low empirical CHADS2VaSc score.

REFERENCES

- Ahrens, J., Geveci, B., and Law, C. (2005). ParaView : an end-user tool for large data visualization. *Energy* 836, 717–732. doi: 10.1021/ol051115g
- Antiga, L., Piccinelli, M., Botti, L., Ene-Iordache, B., Remuzzi, A., and Steinman, D. A. (2008). An image-based modeling framework for patient-specific computational hemodynamics. *Med. Biol. Eng. Comput.* 46, 1097–1112. doi: 10.1007/s11517-008-0420-1
- Berjano, E. J. (2006). Theoretical modeling for radiofrequency ablation: state-of-the-art and challenges for the future. *BioMedical Eng. OnLine* 5:24. doi: 10.1186/1475-925X-5-24
- Bolger, A., Heiberg, E., Karlsson, M., Wigström, L., Engvall, J., Sigfridsson, A., et al. (2007). Transit of blood flow through the human left ventricle mapped by cardiovascular magnetic resonance. *J. Cardiovasc. Magn. Resonan.* 9, 741–747. doi: 10.1080/10976640701544530
- Calkins, H., Prystowsky, E., Carlson, M., Klein, L. S., Saul, J. P., and Gillette, P. (1994). Temperature monitoring during radiofrequency catheter ablation procedures using closed loop control. Atakr Multicenter Investigators Group. *Circulation* 90, 1279–1286.
- Camm, A. J., Lip, G. Y. H., De Caterina, R., Savelieva, I., Atar, D., Hohnloser, S. H., et al. (2012). 2012 focused update of the ESC Guidelines for the management of atrial fibrillation. *Eur. Heart J.* 33, 2719–2747. doi: 10.1093/eurheartj/ehs253
- Carlhäll, C. J., and Bolger, A. (2010). Passing strange: flow in the failing ventricle. *Circulat. Heart Fail.* 3, 326–331. doi: 10.1161/CIRCHEARTFAILURE.109.911867
- Chnafa, C., Mendez, S., and Nicoud, F. (2014). Image-based large-eddy simulation in a realistic left heart. *Comput. Fluids* 94, 173–187. doi: 10.1016/j.compfluid.2014.01.030
- Chnafa, C., Mendez, S., Nicoud, F., Moreno, R., Nottin, S., and Schuster, I. (2012). Image-based patient-specific simulation: a computational modelling of the human left heart haemodynamics. *Comput. Methods Biomed. Eng.* 15, 74–75. doi: 10.1080/10255842.2012.713673
- Chubb, H., Karim, R., Roujol, S., Nuñez-Garcia, M., Williams, S. E., Whitaker, J., et al. (2018). The reproducibility of late gadolinium enhancement cardiovascular magnetic resonance imaging of post-ablation atrial scar: a cross-over study. *J. Cardiovasc. Magn. Resonan.* 20:21. doi: 10.1186/s12968-018-0438-y
- Cibis, M., Lindahl, T. L., Ebbers, T., Karlsson, L. O., and Carlhäll, C.-J. (2017). Left atrial 4D blood flow dynamics and hemostasis following electrical cardioversion of atrial fibrillation. *Front. Physiol.* 8:1052. doi: 10.3389/fphys.2017.01052
- De Vecchi, A., Marlevi, D., Nordsletten, D. A., Ntalas, I., Leipsic, J., Bapat, V., et al. (2018). Left ventricular outflow obstruction predicts increase in systolic pressure gradients and blood residence time after transcatheter mitral valve replacement. *Sci. Reports* 8: 15540. doi: 10.1038/s41598-018-33836-7
- Demolin, J. M., Eick, O. J., Münch, K., Koullick, E., Nakagawa, H., and Wittkampf, F. H. M. (2002). Soft thrombus formation in radiofrequency catheter ablation. *Pacing Clin. Electrophysiol.* 25, 1219–1222. doi: 10.1046/j.1460-9592.2002.01219.x
- Dillon-Murphy, D., Nordsletten, D., Soor, N., Chubb, H., O'Neill, M., de Vecchi, A., et al. (2017). “Computational evaluation of radiofrequency catheter ablation settings for variable atrial tissue depth and blood flow conditions,” in *Computing in Cardiology*, Vol. 44, 1–4.
- Elbaz, M. S., van der Geest, R. J., Calkoen, E. E., de Roos, A., Lelieveldt, B. P., Roest, A. A., et al. (2017). Assessment of viscous energy loss and the association

AUTHOR CONTRIBUTIONS

DD-M: main contributor; DM, BR, AQ, HC, EK, and MO: support; DN, OA, and AdV: support contributions; MO, DN, OA, and AdV: senior authors.

ACKNOWLEDGMENTS

This work was supported by project grants from the EPSRC (EP/P013228/1) and the BHF (PG/15/8/31130), and by the Wellcome EPSRC Center for Medical Engineering at King's College London (WT 203148/Z/16/Z) and the NIHR Biomedical Research Center at Guy's and St. Thomas' NHS Foundation Trust and KCL. The views expressed are those of the authors and not necessarily those of the NHS, the NIHR, or the DoH. According to UK Research Councils' Common Principles on Data Policy, all data supporting this study will be openly available at <http://dx.doi.org/10.18742/RDM01-423>.

SUPPLEMENTARY MATERIAL

The Supplementary Material for this article can be found online at: <https://www.frontiersin.org/articles/10.3389/fphys.2018.01757/full#supplementary-material>

Supplementary Video 1 | Vortices in SR: The video shows the velocity magnitude field overlaid with red velocity vectors on a plane cut intersecting the MV, RPV, LPV and the LAA for patient A in SR. The video shows multiple fast moving, short-lived vortices created at peak systole, one is seen between the LPV and RPV (left) and another one near the LAA (top right). This is typical of patients in SR.

Supplementary Video 2 | Vortices in AF: The video shows the velocity magnitude field overlaid with red velocity vectors on a plane cut intersecting the MV, RPV, LPV and the LAA for patient A in AF. The video shows a single relatively slow vortex moving anti-clockwise in the middle of the LA cavity.

- with three-dimensional vortex ring formation in left ventricular inflow: *in vivo* evaluation using four-dimensional flow MRI. *Magn. Reson. Med.* 77, 794–805. doi: 10.1002/mrm.26129
- Eriksson, J., Bolger, A. F., Ebbers, T., and Carlhall, C.-J. (2012). Four-dimensional blood flow-specific markers of LV dysfunction in dilated cardiomyopathy. *Euro. Heart J. Cardiovasc. Imaging* 14, 417–424. doi: 10.1093/ehjci/jes159
- Eriksson, J., Carlhäll, C., Dyerfeldt, P., Engvall, J., Bolger, A. F., and Ebbers, T. (2010). Semi-automatic quantification of 4D left ventricular blood flow. *J. Cardiovasc. Magn. Reson.* 12:9. doi: 10.1186/1532-429X-12-9
- Eriksson, J., Dyerfeldt, P., Engvall, J., Bolger, A. F., Ebbers, T., and Carlhäll, C. J. (2011). Quantification of presystolic blood flow organization and energetics in the human left ventricle. *Am. J. Physiol. Heart Circulat. Physiol.* 300, H2135–H2141. doi: 10.1152/ajpheart.00993.2010
- Esmaily Moghadam, M., Bazilevs, Y., Hsia, T.-Y., Vignon-Clementel, I. E., and Marsden, A. L. (2011). A comparison of outlet boundary treatments for prevention of backflow divergence with relevance to blood flow simulations. *Comput. Mechan.* 48, 277–291. doi: 10.1007/s00466-011-0599-0
- Fluckiger, J. U., Goldberger, J. J., Lee, D. C., Ng, J., Lee, R., Goyal, A., et al. (2013). Left atrial flow velocity distribution and flow coherence using four-dimensional FLOW MRI: A pilot study investigating the impact of age and Pre- and Postintervention atrial fibrillation on atrial hemodynamics. *J. Magn. Reson. Imaging* 38, 580–587. doi: 10.1002/jmri.23994
- Fyrenius, A. (2001). Three dimensional flow in the human left atrium. *Heart* 86, 448–455. doi: 10.1136/heart.86.4.448
- Gaeta, S., Dyerfeldt, P., Eriksson, J., Carlhäll, C.-J., Ebbers, T., and Bolger, A. F. (2018). Fixed volume particle trace emission for the analysis of left atrial blood flow using 4D Flow MRI. *Magn. Reson. Imaging* 47, 83–88. doi: 10.1016/j.jmri.2017.12.008
- Gallagher, N., Fear, E. C., Byrd, I. A., and Vigmond, E. J. (2013). Contact geometry affects lesion formation in radio-frequency cardiac catheter ablation. *PLoS ONE* 8:e73242. doi: 10.1371/journal.pone.0073242
- González-Suárez, A., and Berjano, E. (2016). Comparative analysis of different methods of modeling the thermal effect of circulating blood flow during RF cardiac ablation. *IEEE Trans. Biomed. Eng.* 63, 250–259. doi: 10.1109/TBME.2015.2451178
- Gülan, U., Saguner, A., Akdis, D., Gotschy, A., Manka, R., Brunckhorst, C., et al. (2017). Investigation of atrial vortices using a novel right heart model and possible implications for atrial thrombus formation. *Sci. Reports* 7:16772. doi: 10.1038/s41598-017-17117-3
- Hessenthaler, A., Röhrl, O., and Nordsletten, D. (2017). Validation of a non-conforming monolithic fluid-structure interaction method using phase-contrast MRI. *Int. J. Num. Methods Biomed. Eng.* 33:e2845. doi: 10.1002/cnm.2845
- Iwasaki, Y.-k., Nishida, K., Kato, T., and Nattel, S. (2011). Atrial fibrillation pathophysiology: implications for management. *Circulation* 124, 2264–2274. doi: 10.1161/CIRCULATIONAHA.111.019893
- Jain, M. K., and Wolf, P. D. (2000a). A three-dimensional finite element model of radiofrequency ablation with blood flow and its experimental validation. *Ann. Biomed. Eng.* 28, 1075–1084. doi: 10.1114/1.1310219
- Jain, M. K., and Wolf, P. D. (2000b). *In vitro* temperature map of cardiac ablation demonstrates the effect of flow on lesion development. *Ann. Biomed. Eng.* 28, 1066–1074. doi: 10.1114/1.1310218
- Kerfoot, E., Fovargue, L., Rivolo, S., Shi, W., Rueckert, D., Nordsletten, D., et al. (2016). “Eidolon: visualization and computational framework for multi-modal biomedical data analysis,” in *Lecture Notes in Computer Science*, Vol. 9805 (Springer), 425–437.
- Khairy, P., Chauvet, P., Lehmann, J., Lambert, J., Macle, L., Tanguay, J. F., et al. (2003). Lower incidence of thrombus formation with cryoenergy versus radiofrequency catheter ablation. *Circulation* 107, 2045–2050. doi: 10.1161/01.CIR.0000058706.82623.A1
- Kirchhof, P., Breithardt, G., Bax, J., Benninger, G., Blomstrom-Lundqvist, C., Borliani, G., et al. (2016). A roadmap to improve the quality of atrial fibrillation management: proceedings from the fifth Atrial Fibrillation Network/European Heart Rhythm Association consensus conference. *Europace* 18, 37–50. doi: 10.1093/europace/euv304
- Koizumi, R., Funamoto, K., Hayase, T., Kanke, Y., Shibata, M., Shiraishi, Y., et al. (2015). Numerical analysis of hemodynamic changes in the left atrium due to atrial fibrillation. *J. Biomechan.* 48, 472–478. doi: 10.1016/j.jbiomech.2014.12.025
- Lai, Y.-C., Choy, Y., Haemmerich, D., Vorperian, V., and Webster, J. (2004). Lesion size estimator of cardiac radiofrequency ablation at different common locations with different tip temperatures. *IEEE Trans. Biomed. Eng.* 51, 1859–1864. doi: 10.1109/TBME.2004.831529
- Lee, J., Cookson, A., Roy, I., Kerfoot, E., Asner, L., Vigueras, G., et al. (2016). Multiphysics computational modeling in CHeart. *SIAM J. Sci. Comput.* 38, C150–C178. doi: 10.1137/15M1014097
- Maleike, D., Nolden, M., Meinzer, H.-P., and Wolf, I. (2009). Interactive segmentation framework of the Medical Imaging Interaction Toolkit. *Comput. Methods Progr. Biomed.* 96, 72–83. doi: 10.1016/j.cmpb.2009.04.004
- Masci, A., Alessandrini, M., Forti, D., Menghini, F., Dedé, L., Tommasi, C., et al. (2017a). “A patient-Specific computational fluid dynamics model of the left atrium in atrial fibrillation: development and initial evaluation,” (Springer), 392–400.
- Masci, A., Forti, D., Alessandrini, M., Menghini, F., Dede, L., Corsi, C., et al. (2017b). 590Development of a patient-specific computational fluid dynamics model of the LA in AF for stroke risk assessment. *EP Europace* 19(Suppl.3), iii120–iii121. doi: 10.1093/ehjci/eux143.002
- Mittal, R., Seo, J. H., Vedula, V., Choi, Y. J., Liu, H., Huang, H. H., et al. (2016). Computational modeling of cardiac hemodynamics: current status and future outlook. *J. Computat. Phys.* 305, 1065–1082. doi: 10.1016/j.jcp.2015.1
- Mouret, F., Garitey, V., Bertrand, E., Derivaux, F., Fuseri, J., and Rieu, R. (2004). *In vitro* atrial flow dynamics: normal conditions versus atrial fibrillation. *J. Biomech.* 37, 1749–1755. doi: 10.1016/j.jbiomech.2004.01.026
- O’Neill, M. D., Jais, P., Hocini, M., Sacher, F., Klein, G. J., Clementy, J., et al. (2007). Catheter ablation for atrial fibrillation. *Circulation* 116, 1515–1523. doi: 10.1161/CIRCULATIONAHA.106.655738
- Pedrizzetti, G., La Canna, G., Alfieri, O., and Tonti, G. (2014). The vortex—an early predictor of cardiovascular outcome? *Nat. Rev. Cardiol.* 11, 545–553. doi: 10.1038/nrccardio.2014.75
- Pedrizzetti, G., Martinello, A. R., Bianchi, V., D’Onofrio, A., Caso, P., and Tonti, G. (2015). Cardiac fluid dynamics anticipates heart adaptation. *J. Biomech.* 48, 388–391. doi: 10.1016/j.jbiomech.2014.11.049
- Ren, J.-F., Marchlinski, F. E., and Callans, D. J. (2004). Left atrial thrombus associated with ablation for atrial fibrillation: identification with intracardiac echocardiography. *J. Am. Coll. Cardiol.* 43, 1861–1867. doi: 10.1016/j.jacc.2004.01.031
- Soor, N., Morgan, R., Varela, M., and Aslanidi, O. V. (2016). “Towards patient-specific modelling of lesion formation during radiofrequency catheter ablation for atrial fibrillation,” in *2016 38th Annual International Conference of the IEEE Engineering in Medicine and Biology Society (EMBC)*, Vol. 44 (IEEE), 489–492.
- Tungkitkusolmun, S., Vorperian, V., Bhavaraju, N., Cao, H., Tsai, J.-Z., and Webster, J. (2001). Guidelines for predicting lesion size at common endocardial locations during radio-frequency ablation. *IEEE Trans. Biomed. Eng.* 48, 194–201. doi: 10.1109/10.909640
- Vedula, V., George, R., Younes, L., and Mittal, R. (2015). Hemodynamics in the left atrium and its effect on ventricular flow patterns. *J. Biomech. Eng.* 137, 1–8. doi: 10.1115/1.4031487
- Wolf, I., Vetter, M., Wegner, I., Böttger, T., Nolden, M., Schöbinger, M., et al. (2005). The medical imaging interaction toolkit. *Med. Image Anal.* 9, 594–604. doi: 10.1016/j.media.2005.04.005
- Zhang, L. T., and Gay, M. (2008). Characterizing left atrial appendage functions in sinus rhythm and atrial fibrillation using computational models. *J. Biomech.* 41, 2515–2523. doi: 10.1016/j.jbiomech.2008.05.012

Conflict of Interest Statement: The authors declare that the research was conducted in the absence of any commercial or financial relationships that could be construed as a potential conflict of interest.

Copyright © 2018 Dillon-Murphy, Marlevi, Ruijsink, Qureshi, Chubb, Kerfoot, O’Neill, Nordsletten, Aslanidi and de Vecchi. This is an open-access article distributed under the terms of the Creative Commons Attribution License (CC BY). The use, distribution or reproduction in other forums is permitted, provided the original author(s) and the copyright owner(s) are credited and that the original publication in this journal is cited, in accordance with accepted academic practice. No use, distribution or reproduction is permitted which does not comply with these terms.



OPEN ACCESS

Edited by:

Jichao Zhao,
The University of Auckland,
New Zealand

Reviewed by:

Arun V. Holden,
University of Leeds, United Kingdom
Kumari Sonal Choudhary,
University of California, San Diego,
United States

***Correspondence:**

Gary Tse
tseg@cuhk.edu.hk
Yunlong Xia
yunlong_xia@126.com

[†]These authors share first authorship

Specialty section:

This article was submitted to
Computational Physiology and
Medicine,
a section of the journal
Frontiers in Physiology

Received: 30 November 2017

Accepted: 11 December 2018

Published: 17 January 2019

Citation:

Chen C, Li D, Ho J, Liu T, Li X, Wang Z, Lin Y, Zou F, Tse G and Xia Y (2019) Clinical Implications of Unmasking Dormant Conduction After Circumferential Pulmonary Vein Isolation in Atrial Fibrillation Using Adenosine: A Systematic Review and Meta-Analysis. *Front. Physiol.* 9:1861. doi: 10.3389/fphys.2018.01861

Clinical Implications of Unmasking Dormant Conduction After Circumferential Pulmonary Vein Isolation in Atrial Fibrillation Using Adenosine: A Systematic Review and Meta-Analysis

Cheng Chen^{1†}, Daobo Li^{1†}, Jeffery Ho², Tong Liu³, Xintao Li¹, Zhao Wang¹, Yajuan Lin¹, Fuquan Zou¹, Gary Tse^{2,4*} and Yunlong Xia^{1*}

¹ Department of Cardiology, First Affiliated Hospital of Dalian Medical University, Dalian, China, ² Li Ka Shing Institute of Health Sciences, Faculty of Medicine, Chinese University of Hong Kong, Hong Kong, China, ³ Tianjin Key Laboratory of Ionic-Molecular Function of Cardiovascular Disease, Department of Cardiology, Tianjin Institute of Cardiology, Second Hospital of Tianjin Medical University, Tianjin, China, ⁴ Department of Medicine and Therapeutics, Faculty of Medicine, Chinese University of Hong Kong, Hong Kong, China

Purpose: Circumferential pulmonary vein isolation (CPVI) is a routine ablation strategy of atrial fibrillation (AF). The adenosine test can be used to unmask dormant conduction (DC) of pulmonary veins after CPVI, thereby demonstrating possible pulmonary vein re-connection and the need for further ablation. However, whether adenosine test could help improve the long term successful rate of CPVI is still controversial. This systemic review and meta-analysis was to determine the clinical utility of the adenosine test.

Methods: PubMed, EMBASE, Web of Science and Cochrane Library database were searched through July 2016 to identify relevant studies using the keywords “dormant pulmonary vein conduction,” “adenosine test,” “circumferential pulmonary vein isolation,” and “atrial fibrillation.” A random-effects model was used to compare pooled outcomes and tested for heterogeneity.

Results: A total of 17 studies including 5,169 participants were included in the final meta-analysis. Two groups of comparisons were classified: (1) Long-term successful rate in those AF patients underwent CPVI with and without adenosine test [Group A (+) and Group A (-)]; (2) Long-term successful rate in those patients who had adenosine test with and without dormant conduction [Group DC (+) and Group DC (-)]. The overall meta-analysis showed that no significant difference can be observed between Group A (+) and Group A (-) (RR 1.08; 95% CI 0.97–1.19; $P = 0.16$; $I^2 = 66\%$) and between Group DC (+) and Group DC (-) (RR 1.01; 95% CI 0.91–1.12; $P = 0.88$; $I^2 = 60\%$).

Conclusion: Pooled meta-analysis suggested adenosine test may not improve long-term successful rate in AF patients underwent CPVI. Furthermore, AF recurrence may not be decreased by eliminating DC provoked by adenosine, even though adenosine test was applied after CPVI.

Keywords: adenosine, dormant conduction, atrial fibrillation, circumferential pulmonary vein isolation, meta-analysis

INTRODUCTION

Atrial fibrillation (AF) is a common cardiac arrhythmia, placing a significant burden on healthcare systems worldwide. It has been estimated that 33.5 million people suffering from AF with an increasing prevalence partly attributable to an aging population (Thacker et al., 2013; Chugh et al., 2014). Because pulmonary veins (PVs) are often the triggering sites for initiating and maintaining AF, circumferential PV isolation (CPVI) has been cornerstone of catheter ablation strategy to restore sinus rhythm for AF (Haïssaguerre et al., 2000; Jaïs et al., 2008; Kirchhof et al., 2017). Although feasibility and visibility of the three-dimensional electroanatomic mapping system have been improved, AF recurrence remains a problem due to PV reconnection after CPVI ablation (Ouyang et al., 2005). A study suggested that 20% of AF patients required repeat procedures after a median follow-up of 13 months (Hocini et al., 2005). Previous studies have suggested that PV re-connection can be identified by unmasking dormant conductions (DCs) induced by adenosine (Arentz et al., 2004; Theis et al., 2015; Ghanbari et al., 2016). The adenosine test has been used extensively to identify DCs (Arentz et al., 2004). The mechanism is thought to involve hyperpolarization of the membrane potential of dormant PVs by activating the I_{KAdo} inward rectifier current, which would transiently establish PV reconnection (Datino et al., 2010).

A recent systematic review and meta-analysis has demonstrated a positive outcome on assessment and ablation of dormant conduction (McLellan et al., 2013). However, some of the enrolled studies were based on segmental ablation strategy. Moreover, many studies suggested that whether DCs are associated with high rate of AF recurrence or adenosine test can improve clinical outcome of PVI remains controversial (Elayi et al., 2013; Kobori et al., 2015; Theis et al., 2015; Ghanbari et al., 2016; Kim et al., 2016). Several investigators have attempted to use the appearance of DCs as indication of further ablation using adenosine test after PVI for AF ablation, while results were restricted by low number of participants (McLellan et al., 2013). Therefore, if adenosine test will help to improve ablation success rates after CPVI remains controversial. We conducted this systematic review and meta-analysis to determine the clinical significance of unmasking DCs after CPVI based on long-term follow up using adenosine test as the guidance of extra ablation for AF patients.

Abbreviations: AF, atrial fibrillation; CPVI, circumferential pulmonary vein isolation; PVI, pulmonary vein isolation; DC, dormant conduction; PVs, pulmonary veins

METHODS

Search Strategy

The databases Pubmed, EMBASE, Web of Science and Cochrane library were searched using searching terms and related items including keywords “dormant pulmonary vein conduction,” “adenosine test,” “circumferential pulmonary vein isolation,” and “atrial fibrillation.”

Inclusion and Exclusion Criteria

The inclusion criteria were limited to articles published in English, involving human subjects of adult age, and published between 2010 and 2016. The exclusion criteria were: (1) ablation for non-AF patients; (2) no adenosine test used; (3) studies including fewer than 90 participants; (4) follow-up period <12 months; (5) CPVI was not used for AF ablation; (6) articles that were case reports, reviews and meta-analyses.

Study Selection

Data from the different studies were entered in pre-specified spreadsheet in Microsoft Excel. All potentially relevant reports were retrieved as complete manuscripts and assessed for compliance with the inclusion criteria. Two reviewers (C.C. and D.L.) independently reviewed each included study and disagreements were resolved by adjudication with input from a third reviewer (Y.X.). Records matching searching goal were enrolled.

Data Analysis

The meta-analysis was performed using Review Manager (RevMan 5.3, Cochrane Collaboration, Oxford, UK). Relative risk (RR) values with 95% confidence intervals (CI) were calculated. Categorical variables were pooled using the Mantel-Hanseal method. The I^2 statistic from the standard chi-square test (χ^2), which describes the percentage of the variability in effect estimates resulting from heterogeneity. A fixed effect model was used if $I^2 \leq 0.25$, otherwise the random effect model was used (Higgins and Green, 2011). P -value < 0.05 (two-tailed) was considered statistical significant.

Quality Assessment

We used the modified Newcastle-Ottawa scale for quality assessment of non-randomized trials and the methodological quality of RCTs was assessed by the components recommended by the Cochrane Collaboration (Higgins and Green, 2011). The quality of each trial except RCTs was quantified by a score of 0–9.

RESULTS

Search Results and Study Characteristics

A flow diagram detailing the above search terms with inclusion and exclusion criteria is shown in **Figure 1**. A total of 4,669 records were identified from Pubmed, EMBASE, Web of Science and Cochrane Library databases. Of these, 17 studies met the inclusion criteria and were included in the final meta-analysis (Kumagai et al., 2010; Matsuo et al., 2010; Miyazaki et al., 2012; Van Belle et al., 2012; Cheung et al., 2013; Elayi et al., 2013; Kaitani et al., 2014; Zhang et al., 2014; Compier et al., 2015; Kobori et al., 2015; Kumar et al., 2015; Lin et al., 2015; Macle et al., 2015; Ghanbari et al., 2016; Kim et al., 2016; Tebbenjohanns et al., 2016). Twelve were prospective studies (Matsuo et al., 2010; Van Belle et al., 2012; Elayi et al., 2013; Kaitani et al., 2014; Compier et al., 2015; Kobori et al., 2015; Kumar et al., 2015; Lin et al., 2015; Macle et al., 2015; Theis et al., 2015; Ghanbari et al., 2016; Kim et al., 2016), four were retrospective studies (Kumagai et al., 2010; Matsuo et al., 2010; Miyazaki et al., 2012; Zhang et al., 2014) and four were randomized controlled trials (RCTs) (Kobori et al., 2015; Macle et al., 2015; Theis et al., 2015; Ghanbari et al., 2016). One study used prospective participants as a study group

and retrospective cohort as control group (Tebbenjohanns et al., 2016). A total of 5,169 participants were included.

These studies used selective venography or 3-dimensional Electroanatomical Mapping System (including CARTO, Ensite NavX) to identify the PV antrum and subsequently performed CPVI. In four studies, PVI was guided by cryoballoon (second generation cryoballoon, CB-2G) (Van Belle et al., 2012; Compier et al., 2015; Kumar et al., 2015; Tebbenjohanns et al., 2016). The endpoint of electrophysiological study was the presence of entrance block defined by the circular mapping catheter (Lasso, Biosense Webster) or the elimination of all PV potentials or establishment of a bidirectional conduction block between left atrium (LA) and PVs. All participants underwent further ablation if DCs was induced. Two studies described the additional use of superior vena cava isolation (Compier et al., 2015; Kumar et al., 2015).

In this meta-analysis, we supposed to determine: (1) if adenosine test would help to increase the success rate of PVI; and (2) furthermore, if DCs induced by adenosine play an important role in AF recurrence after CPVI. Hence, in the first part, Group A (+) and Group A (−) were divided according to whether adenosine was administrated or not. And in the second part, Group DC (+) and Group DC (−) were divided according to whether the DCs appeared or not after adenosine administration. All of DCs induced by adenosine test in Group A (+) and Group DC (+) patients were eliminated after CPVI. The baseline characteristics of these studies are listed in **Table 1**, and those of procedure parameter are shown in **Table 2**. Quality assessment of the included studies was made using the Newcastle–Ottawa Scale for non-randomized case–control studies and the Cochrane Collaboration’s tool for randomized trials (**Table 3**).

Long-term Success Rate of PVI Between Group A (+) and Group A (−)

The pooled meta-analysis demonstrated that there was no significant difference in freedom from recurrent AF between Group A (+) and Group A (−) (RR = 1.08, 95% CI: 0.97–1.19, $P = 0.16$, $I^2 = 66\%$; **Figure 2**). A funnel plot plotting standard errors against the logarithms of the RR are shown in **Figure 3**, demonstrating no significant publication bias.

Long-term Success Rate of PVI Between Group DC (+) and Group DC (−)

No significant difference was observed between Group DC (+) and Group DC (−) with a pooled RR of 1.01 (95% CI: 0.91–1.12; $P = 0.88$; $I^2 = 60\%$; **Figure 4**). A funnel plot plotting standard errors against the logarithms of the RR are shown in **Figure 5**, demonstrating no significant publication bias.

Subgroup Analyses

Additional subgroup analyses were performed for radiofrequency catheter ablation (RFCA) and CB-2G catheter ablation for PVI in Group A (+) and Group A (−). For RFCA, no difference in success rate was observed in Group A (+) and Group A (−) for patients with a RR of 1.02 (95% CI: 0.89–1.17; $P = 0.80$; **Figure 6**), which was accompanied by significant

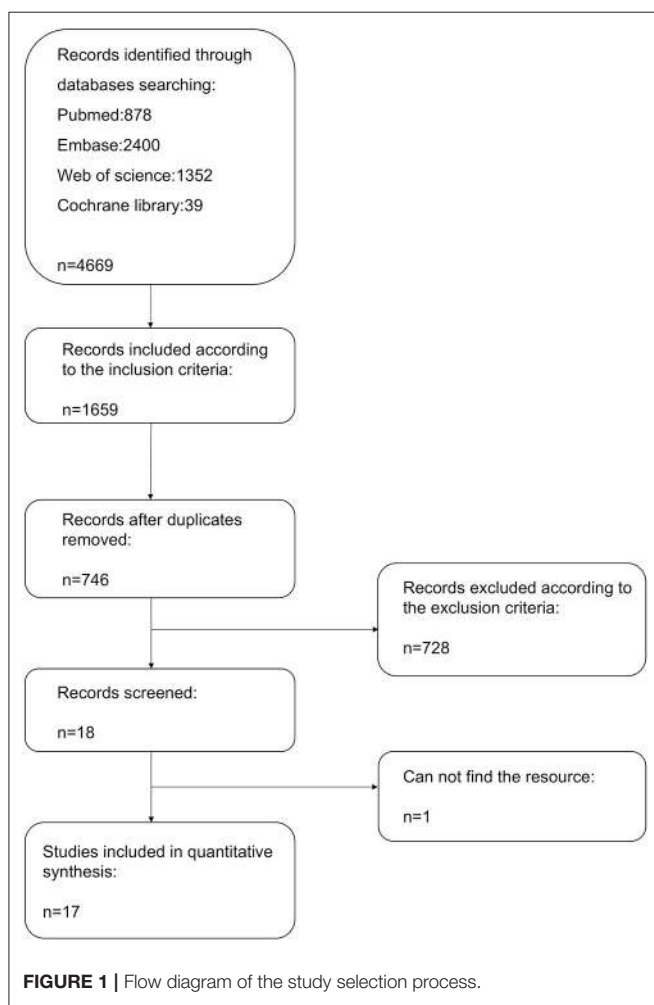


TABLE 1A | Basic information and operation details in Group A (+) and Group A (-).

Article	Comparator groups	Publish year	Center	Study type	Electroanatomic mapping system	Type of AF ablation*	Ablation endpoint	RF energy*	MPT (min)*	MFT (min)*
Kobori et al., 2015	ATP guided PVI Conventional PVI	2015	Multiple	Prospective RCT*	CARTO, Ensite NavX	CPVI*	Disappearance of DC in ATP-guided PVI group*	35 W* (limited to 20 W on the posterior wall)	195 192	58.4 58.0
Theis et al., 2015	Adenosine group Control group	2015	Single	Prospective RCT	Ensite NavX	Standardized PVI procedure*	Elimination of PV potentials recorded on circumferential PV catheter*	Maximum power 30 W	126 ± 45	23 ± 9
Elayi et al., 2013	Group 1 Group 1A Group 1B Group 1C Control Group 2	2013	Single	Prospective CT*	Lasso, Lasso 2515, Biosense-Webster	PVAl, SVC was also isolated by ablation of the sharp SVC potentials*	Electrical isolation of the PV antrum region*	30–35 W on the posterior wall; 40–45 W at other locations	–	60 ± 24 53 ± 17
Ghanbari et al., 2016	Adenosine No adenosine	2016	Single	Prospective RCT	CARTO, Biosense-Webster	Encircle PV ostia	–	25 W	216.8 ± 60.6 202.0 ± 62.5	33.6 ± 13.4 32.1 ± 13.2
Kumagai et al., 2010	ATP group Control group	2010	Single	Retrospective analysis	BeAT, Japan Lifeline Co., Ltd., Japan	Circumferential ablation	Creation of bidirectional conduction block	≤35 W and ≤30 W on sites near the esophagus	–	–
Compier et al., 2015	Adenosine + group Adenosine – group	2015	Single	Prospective CT	Lasso 2515 catheter	PVI guided by cryoballoon and circular mapping catheter	Entrance and exit was block	–	57 + 21 51 + 11	24 + 11 34 + 10
Kumar et al., 2015	Adenosine group Non-adenosine group	2015	Single	Prospective CT	–	Inner lumen endoluminal spiral catheter, CB-2G balloon guided PVI.	Twice 4 min applications of each PV and there was entrance and exit block after adenosine test	–	174 + 44 212 + 47	34 + 13 40 + 18
Van Belle et al., 2012	Adenosine group No adenosine group	2012	Single	Prospective CT	A circular mapping catheter	28 mm, 12 Fr cryoballoon catheter	–	–	202 ± 68	41 ± 24
Tebbenjohans et al., 2016	Study group Control group	2016	Single	Prospective retrospective	A spiral mapping catheter	CB* catheter	–	–	78 + 12 93 + 12	14 + 3 14 + 4
Article	Comparator groups			ATP (dose/period time)		Follow up(m)	Follow up(method)	Free form AF n (%)	P	Conclusion*
Kobori et al., 2015	ATP guided PVI Conventional PVI			0.4 mg/kg without waiting period	15	12-lead electrocardiogram, one-channel electrocardiogram, ambulatory electrogram recorder, 24 h Holter monitoring	79.2% 76.9%	Primary endpoint 0.09 secondary efficacy endpoint 0.07	–	(Continued)

TABLE 1A | Continued

Article	Comparator groups	ATP (dose/period time)	Follow up(m)	Follow up(method)	Free form AF n (%)	P	Conclusion*
Theis et al., 2015	Adenosine group Control group	≥10-mg adenosine, incremental values increased by 5-mg steps	24.8 ± 4.01 29.16 ± 4.87	48-h Holter-ECGs, ECG*	88% 92%	0.001 (overall follow-up)	+
Elayi et al., 2013	Group 1 Group 1A Group 1B Group 1C Control Group 2	Intravenous injection of 12 mg. ISP infusion was started: 5 mcg for 3 min, then 10 mcg for 3 min, 15 mcg for 3 min, 20 mcg for 3 min, and 30 mcg for 3 min	22 ± 8	48-h Holter monitors, event recorder	–	Groups 1A/1B and 1B/1C ($P < 0.001$) groups 1A and group 1C ($P = 1.0$) groups 1 and groups 2 ($P = 0.038$)	+
Ghanbari et al., 2016	Adenosine No adenosine	6–24mg adenosine ISP infused at rates of 5, 10, 15, and 20 μ g/min for 2 min at each infusion rate in each group as above	9.2 ± 7	Auto-triggered event recorder	24/61 [39.3%] 23/68	0.83	–
Kumagai et al., 2010	ATP group Control group	10mg ATP administered during an intravenous ISP infusion (5 μ g'/min)*	16 ± 5.2 16 ± 6.9	ECG, 24-h Holter monitoring	76.4% 62.3%	0.03	+
Compier et al., 2015	Adenosine + group Adenosine – group	Adenosine initiated at 6/12 mg, increased up to 30 mg until at least one atrial beat with AV-block was observed with 30-min waiting period	12 + 1 11 + 1	ECG, 24h Holter	64% 47%	0.02	+
Kumar et al., 2015	Adenosine group Non-adenosine group	Waiting time of 30 min, 12–15mg adenosine	13 + 1 12 + 2	–	84% 79%	0.06	–
Van Belle et al., 2012	Adenosine group No adenosine group	25mg adenosine	17 ± 5	ECG, 24-h Holter recording, a symptom questionnaire, Transtelephonic Holter monitoring	23 (68%) 29 (46%)	0.04	+
Tebbenjohans et al., 2016	Study group Control group	A bolus of adenosine with a short duration	15 ± 3.6	24-h Holter monitoring and external event recording	81% 79%	NS	–

Parts of values represent mean ± difference. Conclusion:(+) represents experiment group and controlled group have significant difference; (–) represents experiment group and controlled group have no significant difference. PV, pulmonary vein isolation; CPVT*, circumferential pulmonary vein isolation; PV*, pulmonary vein; RCT*, randomized controlled trial; DC*, dormant conduction; CT*, clinical trial; ISP*, isoproterenol; MPT*, mean fluoroscopic time; AF*, atrial fibrillation; RF*, radiofrequency; SVC*, superior vena cava; ECG*, electrocardiograph; CB-2G*, second-generation cryoballoon; CB, cryoballoon; W, watt.

TABLE 1B | Baseline information in Group A (+) and Group A (-).

Article	Comparator groups	Numbers of Sample	Numbers of group	Age	Male n (%)	PSAF* n (%)	AF history	LAD* (mm)	
Koborij et al., 2015	ATP guided PVI Conventional PVI	2120 1001	1112 723 (72.7)	58.6+8.6 68.5+8.8	856 (77.0) 683 (68.2)	737 (66.3) 683 (68.2)	23.3 26.4	38.9+6.3 39.2+6.2	
Theis et al., 2015	Adenosine group Control group	152 388	76 32 83 74	63 ± 10 64 ± 9.11 63.5 ± 10.5 63.6 ± 10.1 63.9 ± 10.4	45 (59) 33 (43) 20 (62%) 54 (65%) 58 (78%)	152 (100%) 3 (10%) 11 (13%) 12 (16%)	22.17 ± 5.18 cm ² 23.24 ± 4.81 cm ² 46.3 ± 4.3 46.0 ± 4.2 45.8 ± 4.2	46 (61) 53 (70) 15 (47%) 39 (47%) 32 (43%)	
Elayi et al., 2013	Group 1A Group 1B Group 1C Control Group 2 Adenosine No adenosine ATP group	129 61 68 212 106 36 62 45 45 34 65 53 139	196 61 68 106 106 36 62 45 45 34 65 53 61+11	63.6 ± 10.2 59.7 ± 8.7 58.9 ± 10.7 58 ± 11 59 ± 10 61 + 10 59 + 11 57.4 + 9.5 56.6 + 11.2 57 ± 12 57 ± 12 66 + 10 61 + 11	150 (76%) 37 (60.6%) 53 (77.9%) 70.0% 78.3% 78% 70% 27 34 24 46 27 39 34 65 27 75	30 (15%) 129 (100%)	4.7 ± 4.1 y —	46.3 ± 4.3 41.0 ± 5.3 41.2 ± 6.4 39.4 ± 5.4 5.0 ± 5.5 y 64 + 60 m 58 + 53 m 8 + 7.1 y 7 + 3.8 y 7 + 5 y 7 + 6 y 6 + 4 y 5 + 3 y	93 (48%) 33 (54.1%) 28 (45.9%) 21.7 20.0 50 52 14 (31%) 18 (40%)
Ghannabai et al., 2016	Kumagai et al., 2010	129 106 36 62 45 34 65 53 139	106 106 61 + 10 59 + 11 57.4 + 9.5 56.6 + 11.2 57 ± 12 57 ± 12 66 + 10 61 + 11	58 ± 11 59 ± 10 61 + 10 59 + 11 57.4 + 9.5 56.6 + 11.2 57 ± 12 57 ± 12 66 + 10 61 + 11	94.86 90% 90% 40 39 34 65 27 87 (63%)	4.5 ± 3.9 y — — — — — — — — —	39.7 ± 5.7 42 + 6.7 42 + 5.6 LA volume: 72 + 14 cc 77 + 18 cc 45 ± 7 42 ± 6 40 + 6 41 + 7	93 (48%) 33 (54.1%) 28 (45.9%) 21.7 20.0 50 52 14 (31%) 18 (40%)	
Compier et al., 2010	Kumar et al., 2015	129 106 36 62 45 34 65 53 139	106 106 61 + 10 59 + 11 57.4 + 9.5 56.6 + 11.2 57 ± 12 57 ± 12 66 + 10 61 + 11	58 ± 11 59 ± 10 61 + 10 59 + 11 57.4 + 9.5 56.6 + 11.2 57 ± 12 57 ± 12 66 + 10 61 + 11	94.86 90% 90% 40 39 34 65 27 87 (63%)	4.5 ± 3.9 y — — — — — — — — —	39.7 ± 5.7 42 + 6.7 42 + 5.6 LA volume: 72 + 14 cc 77 + 18 cc 45 ± 7 42 ± 6 40 + 6 41 + 7	93 (48%) 33 (54.1%) 28 (45.9%) 21.7 20.0 50 52 14 (31%) 18 (40%)	
Van Belle et al., 2012	Non-adenosine group Adenosine group No adenosine group Study group Control group	99 34 65 53 139	34 34 65 53 61+11	34 24 46 27 75	39 34 65 38 (72%) 87 (63%)	7 + 3.8 y 7 + 5 y 7 + 6 y 6 + 4 y 5 + 3 y	— — — — —	— — — — —	
Article	Comparator groups	Numbers of Sample	Numbers of group	Age	Male n (%)	Ischemic heart disease	Diabetes (n/%)	LVEF* (%)	
Koborij et al., 2015	ATP guided PVI Conventional PVI	17 (1.5%) 20 (2.0%)	17 (1.5%) 20 (2.0%)	17 (1.5%) 20 (2.0%)	141 (12.7%) 141 (14.1%)	141 (12.7%) 141 (14.1%)	64.2 + 7.9 64.6 + 7.3	64.2 + 7.9 64.6 + 7.3	
Theis et al., 2015	Adenosine group Control group	— <td>5 (15%) 13 (16%) 15 (20%) 40 (20%)</td> <td>—<td>4 (12%) 8 (10%) 11 (15%) 25 (13%)</td><td>—<td>54 ± 12 55 ± 9 57 ± 11 55 ± 9</td><td>54 ± 12 55 ± 9 57 ± 11 55 ± 9</td></td></td>	5 (15%) 13 (16%) 15 (20%) 40 (20%)	— <td>4 (12%) 8 (10%) 11 (15%) 25 (13%)</td> <td>—<td>54 ± 12 55 ± 9 57 ± 11 55 ± 9</td><td>54 ± 12 55 ± 9 57 ± 11 55 ± 9</td></td>	4 (12%) 8 (10%) 11 (15%) 25 (13%)	— <td>54 ± 12 55 ± 9 57 ± 11 55 ± 9</td> <td>54 ± 12 55 ± 9 57 ± 11 55 ± 9</td>	54 ± 12 55 ± 9 57 ± 11 55 ± 9	54 ± 12 55 ± 9 57 ± 11 55 ± 9	
Elayi et al., 2013	Group 1A Group 1B Group 1C Control Group 2 Adenosine No adenosine ATP group Control group Adenosine + group Adenosine – group	— <td>5 (15%) 13 (16%) 15 (20%) 40 (20%)</td> <td>—<td>4 (12%) 8 (10%) 11 (15%) 25 (13%)</td><td>—<td>54 ± 12 55 ± 9 57 ± 11 55 ± 9</td><td>54 ± 12 55 ± 9 57 ± 11 55 ± 9</td></td></td>	5 (15%) 13 (16%) 15 (20%) 40 (20%)	— <td>4 (12%) 8 (10%) 11 (15%) 25 (13%)</td> <td>—<td>54 ± 12 55 ± 9 57 ± 11 55 ± 9</td><td>54 ± 12 55 ± 9 57 ± 11 55 ± 9</td></td>	4 (12%) 8 (10%) 11 (15%) 25 (13%)	— <td>54 ± 12 55 ± 9 57 ± 11 55 ± 9</td> <td>54 ± 12 55 ± 9 57 ± 11 55 ± 9</td>	54 ± 12 55 ± 9 57 ± 11 55 ± 9	54 ± 12 55 ± 9 57 ± 11 55 ± 9	
Ghannabai et al., 2016	ATP guided PVI Conventional PVI	6 (0.8%) 8 (11.8%)	6 (0.8%) 8 (11.8%)	6 (0.8%) 8 (11.8%)	— <td>—<td>59.7 ± 5.4 59.3 ± 5.6</td><td>59.7 ± 5.4 59.3 ± 5.6</td></td>	— <td>59.7 ± 5.4 59.3 ± 5.6</td> <td>59.7 ± 5.4 59.3 ± 5.6</td>	59.7 ± 5.4 59.3 ± 5.6	59.7 ± 5.4 59.3 ± 5.6	
Kumagai et al., 2010	ATP group Control group	— <td>—</td> <td>—<td>—<td>—<td>65.1 ± 8.9</td><td>65.1 ± 8.9</td></td></td></td>	—	— <td>—<td>—<td>65.1 ± 8.9</td><td>65.1 ± 8.9</td></td></td>	— <td>—<td>65.1 ± 8.9</td><td>65.1 ± 8.9</td></td>	— <td>65.1 ± 8.9</td> <td>65.1 ± 8.9</td>	65.1 ± 8.9	65.1 ± 8.9	
Van Belle et al., 2012	Study group Control group	— <td>—</td> <td>—<td>—<td>—<td>63.8 ± 9.6</td><td>63.8 ± 9.6</td></td></td></td>	—	— <td>—<td>—<td>63.8 ± 9.6</td><td>63.8 ± 9.6</td></td></td>	— <td>—<td>63.8 ± 9.6</td><td>63.8 ± 9.6</td></td>	— <td>63.8 ± 9.6</td> <td>63.8 ± 9.6</td>	63.8 ± 9.6	63.8 ± 9.6	
Compier et al., 2015	Adenosine group Non-adenosine group Adenosine group No adenosine group Study group Control group	— <td>—<td>—<td>—<td>—<td>—<td>—</td></td></td></td></td></td>	— <td>—<td>—<td>—<td>—<td>—</td></td></td></td></td>	— <td>—<td>—<td>—<td>—</td></td></td></td>	— <td>—<td>—<td>—</td></td></td>	— <td>—<td>—</td></td>	— <td>—</td>	—	
Kumar et al., 2015	9 (20%) 8 (18%)	— <td>—<td>—<td>—<td>—<td>56 + 6 57 + 8</td><td>56 + 6 57 + 8</td></td></td></td></td>	— <td>—<td>—<td>—<td>56 + 6 57 + 8</td><td>56 + 6 57 + 8</td></td></td></td>	— <td>—<td>—<td>56 + 6 57 + 8</td><td>56 + 6 57 + 8</td></td></td>	— <td>—<td>56 + 6 57 + 8</td><td>56 + 6 57 + 8</td></td>	— <td>56 + 6 57 + 8</td> <td>56 + 6 57 + 8</td>	56 + 6 57 + 8	56 + 6 57 + 8	
Tebbenjohanns et al., 2016	— <td>—<td>—<td>—<td>—<td>—<td>—<td>—</td></td></td></td></td></td></td>	— <td>—<td>—<td>—<td>—<td>—<td>—</td></td></td></td></td></td>	— <td>—<td>—<td>—<td>—<td>—</td></td></td></td></td>	— <td>—<td>—<td>—<td>—</td></td></td></td>	— <td>—<td>—<td>—</td></td></td>	— <td>—<td>—</td></td>	— <td>—</td>	—	

*Abbreviations as per Table 1A. *PSAF*, paroxysmal atrial fibrillation; *LAD*, left atrial diameter; *HVE*, left ventricular ejection fraction.

TABLE 2A | Basic information and operation details in Group DC (+) and Group DC (−).

Article	Comparator groups	Publish year	Center	Study type	Electroanatomic mapping system	Type of AF ablation	Ablation end point	RF energy	MPT (min)	MFT (min)
Zhang et al., 2014	ATP (+) Group ATP (−) Group	2014	Single	Retrospective analysis	CARTO	Standard CPVI procedure by irrigated tip catheter	Entrance block	—	—	—
Kim et al., 2016	Dormant conduction No dormant conduction	2016	Single	Prospective CT	CARTO	4-mm open irrigated catheter, CPVI	No PV potentials recorded by the circular mapping catheter. Exit block was confirmed when PV to LA dissociation was observed during PV pacing ^a	25–35 W	194.0 ± 55.4	67.9 ± 51.9
Kaitani et al., 2014	DC – group DC+ group	2014	Multiple	Prospective observational study	CARTO XP, NavX	CPVI by irrigated-tip catheters	Entrance block as shown by t-elimination of the superior and inferior pulmonary vein potentials	20–40 W	—	—
Macle et al., 2015	Adenosine + No further ablation Adenosine + Ablation until adenosine – Adenosine – Registry group	2015	Multiple	Prospective RCT	—	Circumferential ablation at the PV ostia by the circular catheter	PV spikes are no longer recorded	—	—	—
Matsu et al., 2010	Group A: dormant PV conduction [+] Group B: dormant PV conduction [-]	2010	Single	Retrospective analysis	CARTO	Circular catheter venography was performed	Establishment of a bidirectional conduction block between LA and PV	25–35 W	220 ± 71	125 ± 43
Miyazaki et al., 2012	Group-1: no adenosine response Group-2: adenosine response	2012	Single	Retrospective analysis	CARTO	Circumferentially extensively ablated by circular mapping catheters	The elimination of all PV potentials	35 W	217 ± 65	132 ± 54
Cheung et al., 2013	Dormant conduction [+] group Dormant conduction [-] group	2013	Single	Prospective CT	CARTO or EnsiteNavX	Circumferential ablation (1) Entrance block or abolition of 45 W (<30 W on the posterior wall) (2) Exit block with absence of left atrial capture of the circular mapping catheter	(1) Entrance block or abolition of PV Potentials (2) Exit block with absence of left atrial capture of the circular mapping catheter	—	—	—
Lin et al., 2015	Dormant conduction group No Dormant conduction group	2015	Single	Prospective CT	CARTO or EnsiteNavX	Circumferential ablation (1) Entrance block or abolition of PV potentials (2) Exit block with absence of left atrial capture of the circular mapping catheter	15–50 W	—	—	—
Zhang et al., 2014	ATP (+) Group ATP (−) Group			ATP (40 mg during an intravenous ISP infusion (5 µg/min)	18.7 ± 6.4	—	30/39 (76.9%) 176/261 (67.3%)	ATP (+) vs. ATP (−) $p = 0.02$	+	(Continued)

TABLE 2A | Continued

Article	Comparator groups	ATP (dose/period time)	Follow up (m)	Follow up (method)	Free form AF n (%)	P	Conclusion
Kim et al., 2016	Dormant conduction No dormant conduction	20 mg If dormant conduction was observed, 12 and 6 mg adenosine were injected serially and dormant conduction was observed to identify the adequate adenosine dose	12	24-h Holter monitoring	74.8% 72.6%	0.9	–
Kaitani et al., 2014	DC – group DC+ group	A continuous isoproterenol infusion (0.5–2 mg/min) at begin. A waiting period of at least 15 min, 40 mg ATP	27.1 ± 15	ECG, Holter, an event recorder	66.7% 80.0%	0.12	–
Macle et al., 2015	Adenosine + No further ablation Adenosine + Ablation until adenosine – Adenosine – Registry group Adenosine – routine follow-up	12 mg ATP 20 min observation period	12.3	Holter	51 (37.2%) 88 (59.9%) 56 (48.7%) –	① vs. ② 0.0002 ① vs. ③ 0.0421 ② vs. ③	+
Matsu et al., 2010	Group A: dormant PV conduction [+] Group B: dormant PV conduction [-]	20 mg of ATP under ISPI infusions	30 ± 13	Electrocardiogram recordings 24-h ambulatory monitoring	125 (89.9%) 86 (91.5%)	0.0639	–
Miyazaki et al., 2012	Group-1: no adenosine response Group-2: adenosine response	40 mg during intravenous ISP infusion	12	ECG, Holter, event recorder	72.8% 51.3%	0.03	+
Cheung et al., 2013	Dormant conduction [+] Dormant conduction [-] group	12-mg adenosine was injected followed by 20 mL saline.	12.5	7–14 days continuous mobile telemetry monitors	64% 76%	0.062	–
Lin et al., 2015	Dormant conduction group No Dormant conduction group	A-12 mg adenosine was injected followed by 20 cc of saline with escalating doses of 18 mg and 24 mg if atrioventricular block was not observed.	20 ± 9	7–14 days continuous mobile telemetry monitors; telephone follow-up for symptoms	47% 61%	0.12	–

Abbreviations as per Table 1A. LA, left atrial.

TABLE 2B | Baseline information in Group DC (+) and Group DC (−).

Article	Comparator groups	Numbers of sample	Numbers of group	Age	Male <i>n</i> (%)	PSAF <i>n</i> (%)	AF history	LAD (mm)	HP (%)	Ischemic heart disease	Diabetes	LVEF (%)
Zhang et al., 2014	ATP (+) Group ATP (−) Group	300 261	39 54.7 ± 4.9 54.4 ± 6.7	19 125	300 (100%) —	3.2 ± 0.6 y 3.7 ± 0.4 y	37.4 ± 3.4 36.8 ± 4.2	—	—	—	—	61.4 ± 2.7 62.2 ± 3.6
Kim et al., 2016	Dormant conduction No dormant conduction	378 286	92 60.7 ± 11.3 60.2 ± 11.1	69 186	49 (53.3%) 151 (52.8%)	—	43.7 ± 12.6 43.1 ± 13.5	44 (47.8%) 146 (51.0%)	—	17 (8.5%) 43 (5.0%)	—	—
Kaitani et al., 2014	DC – group DC+ group	110 35	75 62.5 + 9.8 61.8 + 9.2	55 26	—	45.9 ± 40 m 59.3 ± 7 m	38.2 + 6 38.7 + 0.5	49 (65.3%) 22 (62.9%)	—	8 (10.7%) 4 (11.4%)	—	—
Macle et al., 2015	Adenosine + No further ablation Adenosine + Ablation until adenosine – Adenosine – Registry group	550 133	137 147 117	97 108 87	100% 60.2 58.9	3.4 y 4.0 y 3.0 y	39.6 40.1 40.1	50 (36.5%) 62 (42.2%) 54 (46.2%)	15 (10.9%) 16 (10.9%) 10 (8.5%)	6 (4.4%) 8 (5.4%) 11 (9.4%)	60.1 59.9 59.1	60.2
Matsu et al., 2010	Group A: dormant PV conduction [+] Group B: dormant PV conduction [−]	233 94	139 54.3 ± 9.6 54.2 ± 10.9	122 84	89 55	4.5 ± 4.0 y 4.3 ± 3.7 y	38.5 ± 5.5 39.7 ± 5.7	31 (22.3%) 27 (28.7%)	—	—	65.9 ± 6.6 65.8 ± 7.4	—
Miyazaki et al., 2012	Group-1: no adenosine response Group-2: adenosine response	109 39	70 61.4 ± 11.2 59.4 ± 10.3	58 33	109 (100%) 57.4 ± 43.9 m	60.7 ± 59.1 m 39.4 ± 5.5	38.1 ± 5.4 24 (34%)	—	—	—	65.8 ± 8.3 66.4 ± 9.0	—
Cheung et al., 2013	Dormant conduction [+] group Dormant conduction [−] group	152 108	44 62 ± 9 60 ± 11	34 86	29 (66%) 67 (62%)	29 (66) 67 (62)	4.0 ± 0.6 4.3 ± 0.7	23 (52%) 42 (39%)	—	7 (16%) 11 (10%)	60 ± 11 59 ± 11	—
Lin et al., 2015	Dormant conduction group No Dormant conduction group	152 107	45 61 ± 9 59 ± 11	35 85	30 (67%) 66 (62%)	30 (67) 66 (62)	—	23 (51%) 41 (38%)	—	7 (16%) 11 (10%)	60 ± 10 59 ± 11	—

*Abbreviations as per **Table 1A**.

TABLE 3A | Assessment of the quality of included studies in Group A (+) and Group A (-)*.

Study	Assessment	Classification (attributable stars)
Kobori et al., 2015	Unclear risk of selection bias (insufficient information about the sequence generation and allocation concealment); Unclear risk of performance bias (insufficient information about blinding of participants and personnel); Unclear risk of detection bias (insufficient information about blinding of outcome assessment); low risk of attrition bias (complete outcome for all the patients enrolled); Unclear risk of reporting bias (insufficient information about selective reporting); Unclear risk of other bias (insufficient information about other sources of bias).	—
Theis et al., 2015	Unclear risk of selection bias (insufficient information about the sequence generation and allocation concealment); Unclear risk of performance bias (insufficient information about blinding of participants and personnel); Unclear risk of detection bias (insufficient information about blinding of outcome assessment); low risk of attrition bias (complete outcome for all the patients enrolled); Unclear risk of reporting bias (insufficient information about selective reporting); Unclear risk of other bias (insufficient information about other sources of bias).	—
Elayi et al., 2013	Adequate case definition; consecutive series of cases; hospital controls; adequate information concerning the selection and definition of controls; groups controlled for all the baseline characteristics; ascertainment of outpatient exposure to adenosine test based on medical records for experiment groups; patients not blinded to case-control status.; same non-Response rate for both groups.	6
Ghanbari et al., 2016	Low risk of selection bias (treatment assignment was concealed in numbered, sealed envelopes, the research staff opened the envelope and revealed the randomization assignment in the electrophysiology laboratory and insufficient information about the sequence generation); Unclear risk of performance bias (insufficient information about blinding of participants and personnel); Unclear risk of detection bias (insufficient information about blinding of outcome assessment); low risk of attrition bias (complete outcome for all the patients enrolled); Unclear risk of reporting bias (insufficient information about selective reporting); Unclear risk of other bias (insufficient information about other sources of bias).	—
Kumagai et al., 2010	Adequate case definition; consecutive series of cases; hospital controls; adequate information concerning the selection and definition of controls; groups controlled for all the baseline characteristics; ascertainment of outpatient exposure to adenosine test based on medical records for experiment groups; patients not blinded to case-control status.; same non-Response rate for both groups.	6
Compier et al., 2015	Adequate case definition; consecutive series of cases; hospital controls; adequate information concerning the selection and definition of controls; groups controlled for all the baseline characteristics; ascertainment of outpatient exposure to adenosine test based on medical records for experiment groups; patients not blinded to case-control status.; same non-Response rate for both groups.	6
Kumar et al., 2015	Adequate case definition; consecutive series of cases; hospital controls; adequate information concerning the selection and definition of controls; groups controlled for all the baseline characteristics; ascertainment of outpatient exposure to adenosine test based on medical records for experiment groups; patients not blinded to case-control status.; same non-Response rate for both groups.	6
Van Belle et al., 2012	Adequate case definition; consecutive series of cases; hospital controls; adequate information concerning the selection and definition of controls; groups controlled for all the baseline characteristics except the LA* diameter; ascertainment of outpatient exposure to adenosine test based on medical records for experiment groups; patients not blinded to case-control status.; same non-Response rate for both groups.	5
Tebbenjohanns et al., 2016	Adequate case definition; consecutive series of cases; hospital controls; adequate information concerning the selection and definition of controls; groups controlled for all the baseline characteristics except the age and history with AF*; ascertainment of outpatient exposure to adenosine test based on medical records for experiment groups; patients not blinded to case-control status.; same non-Response rate for both groups.	5

*Assessment of the quality of included studies according to Newcastle–Ottawa Scale for nonrandomized case–controls studies and the Cochrane Collaboration’s tool for assessing risk of bias in randomized trials; *LA, left atrial; *AF, atrial fibrillation.

heterogeneity ($I^2 = 73\%$). Similarly, for CB-2G, success rates for those who underwent adenosine testing ($n = 134$) were not significantly different from those who did not have such a test ($n = 212$), with a pooled RR of 1.18 (95% CI = 0.99–1.42; $P = 0.07$; **Figure 7**) with significant heterogeneity ($I^2 = 62\%$).

Sensitivity Analysis

Sensitivity analysis included study design and adenosine test, and none of them showed significant interference with study outcomes. Results are shown in **Table 4**.

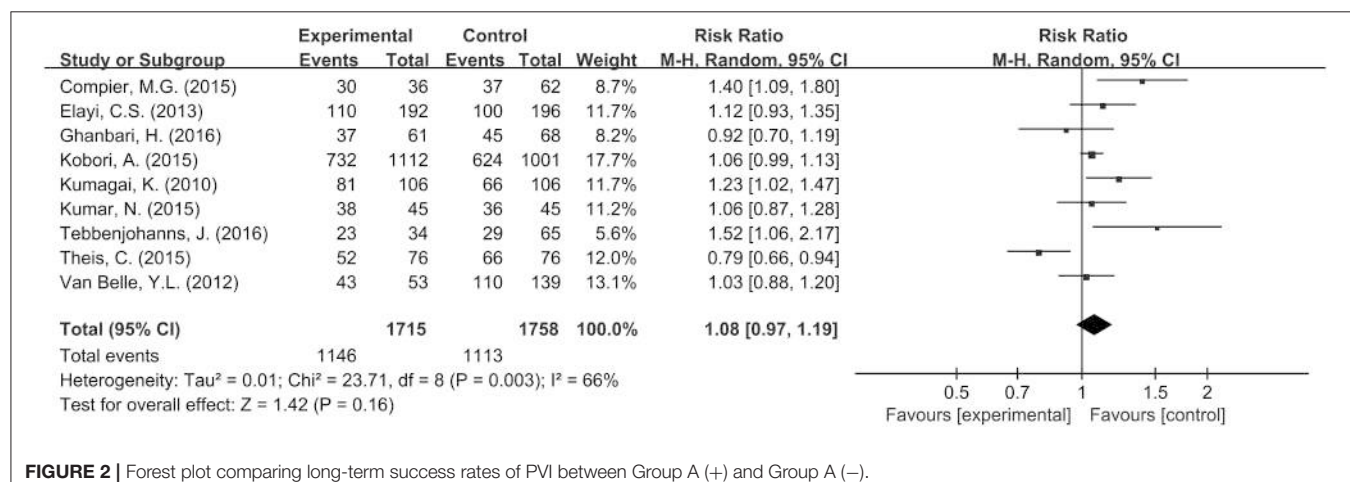
DISCUSSION

Adenosine testing after AF ablation procedures has been widely adopted for demonstrating DCs, which are further ablated to reduce AF recurrence rates (Hocini et al., 2005). However, in our study, the result of pooled meta-analysis suggested that adenosine test may not help to reduce the long-term AF recurrence after CPVI, and further subgroup analysis also confirmed the result. Some recent studies also suggested negative result of adenosine test based on CPVI (Theis et al., 2015; Ghanbari et al., 2016). The reason might be explained by the mechanism of PVI reconnection after CPVI ablation dose not totally attributed by DCs

TABLE 3B | Assessment of the quality of included studies in Group DC (+) and Group DC (-)*.

Study	Assessment	Classification (attributable stars)
Zhang et al., 2014	Adequate case definition; consecutive series of cases; hospital controls; adequate information concerning the selection and definition of controls; groups controlled for all the baseline characteristics; ascertainment of outpatient exposure to adenosine test based on medical records for experiment groups and controls; patients not blinded to case-control status.; same non-Response rate for both groups.	7
Kim et al., 2016	Adequate case definition; consecutive series of cases; hospital controls; adequate information concerning the selection and definition of controls; groups controlled for all the baseline characteristics; ascertainment of outpatient exposure to adenosine test based on medical records for experiment groups and controls; patients not blinded to case-control status.; same non-Response rate for both groups.	7
Kaitani et al., 2014	Adequate case definition; consecutive series of cases; hospital controls; adequate information concerning the selection and definition of controls; groups controlled for all the baseline characteristics; ascertainment of outpatient exposure to adenosine test based on medical records for experiment groups and controls; patients not blinded to case-control status.; same non-Response rate for both groups.	7
Macle et al., 2015	Low risk of selection bias (randomization was done with permuted blocks of eight and the allocation sequence was computer-generated by an independent organization); low risk of performance bias (Patients were enrolled by study personnel and masked to their randomization assignment for the duration of the trial and study staff doing catheter ablations could not be masked to treatment allocation); low risk of detection bias (All efficacy and adverse outcomes were assessed by an independent adjudicating committee masked to treatment allocation); low risk of attrition bias (complete outcome for all the patients enrolled); low risk of reporting bias (we can find the research plan with "Adenosine following pulmonary vein isolation to target dormant conduction elimination (ADVICE): methods and rationale" though Pubmed); Unclear risk of other bias (insufficient information about other sources of bias).	-
Matsuo et al., 2010	Adequate case definition; consecutive series of cases; hospital controls; adequate information concerning the selection and definition of controls; groups controlled for all the baseline characteristics; ascertainment of outpatient exposure to adenosine test based on medical records for experiment groups and controls; patients not blinded to case-control status.; same non-Response rate for both groups.	7
Miyazaki et al., 2012	Adequate case definition; consecutive series of cases; hospital controls; adequate information concerning the selection and definition of controls; groups controlled for all the baseline characteristics; ascertainment of outpatient exposure to adenosine test based on medical records for experiment groups and controls; patients not blinded to case-control status.; same non-Response rate for both groups.	7
Cheung et al., 2013	Adequate case definition; consecutive series of cases; hospital controls; adequate information concerning the selection and definition of controls; groups controlled for the baseline characteristics are not mentioned; ascertainment of outpatient exposure to adenosine test based on medical records for experiment groups and controls; patients not blinded to case-control status.; same non-Response rate for both groups.	5
Lin et al., 2015	Adequate case definition; consecutive series of cases; hospital controls; adequate information concerning the selection and definition of controls; groups controlled for all the baseline characteristics; ascertainment of outpatient exposure to adenosine test based on medical records for experiment groups and controls; patients not blinded to case-control status.; same non-Response rate for both groups.	7

*DC, dormant conduction; *Assessment of the quality of included studies according to Newcastle-Ottawa Scale for nonrandomized case-controls studies and the Cochrane Collaboration's tool for assessing risk of bias in randomized trials.



(Linz et al., 2018). Potential mechanisms of AF recurrence after CPVI may due to failure of trans-mural injury of PVAs (Rostock et al., 2006), heterogeneity of myocardial sleeves extending into the pulmonary veins (Ho et al., 2001) or so on. As a consequence, the necessity and applicability of adenosine test diminished in the context of CPVI adoption ablation strategy and Whether other techniques, such as pacing along the PVI line by the distal tip of the ablation catheter to identify viable myocardium or potential gaps (Schaeffer et al., 2015) improves PVI outcome should be investigated in the future.

However, a recent meta-analysis has shown that long-term success rates of PVI were improved by further eliminating DCs that have been identified by adenosine test for patients underwent segmental ablation for AF (McLellan et al., 2017). The discrepancy results with the results of the previous meta-analysis (McLellan et al., 2017) may due to improved ablation strategies (Ouyang et al., 2004). The 3-dimensional Electroanatomical Mapping System for RFA provides better visualization and reduce the need for excessive ablation (Ouyang et al., 2004). Ablation strategies based on CPVI ablation, instead of segmental ablation,

were comprehensively adopted for AF patients either paroxysmal AF or persistent AF, leading to better AF control in the long-term (Gepstein et al., 1997). Previous studies had shown that segmental ablation was inferior to long term treatment compared with CPVI, and leads to more complications, such as pulmonary stenosis (Oral et al., 2003). Additionally, cryo-application offers spherical contact with the PV autrum (PVA), guided by annular Achieve catheter and vasography, provided CPVI by the single-shot technique (Nakagawa et al., 2007). Consequently, modifying skills and appliances, meaningful of adenosine administration may have diminished the need for AF re-ablation.

Complications arising from ablating DCs could further contribute to the lack of efficacy. For example, excessive ablation creates scarring of the atrial myocardium, which can serve as substrates for re-entry (Pappone et al., 2004; Tse et al., 2016). Indeed, a previous study compared anatomically guided CPVI with wide atrial ablation, demonstrating that the latter approach significantly increased the likelihood of micro-reentry ablation by producing areas of conduction slowing and block (Hocini et al., 2005). Moreover, we found that fluoroscopic

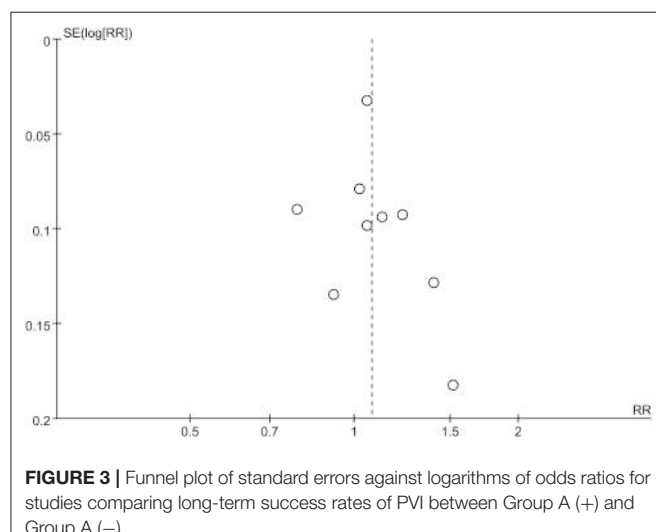


FIGURE 3 | Funnel plot of standard errors against logarithms of odds ratios for studies comparing long-term success rates of PVI between Group A (+) and Group A (-).

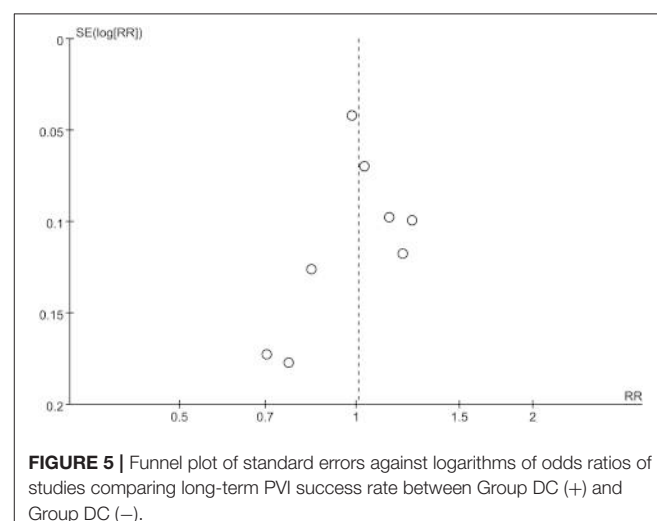


FIGURE 5 | Funnel plot of standard errors against logarithms of odds ratios of studies comparing long-term PVI success rate between Group DC (+) and Group DC (-).

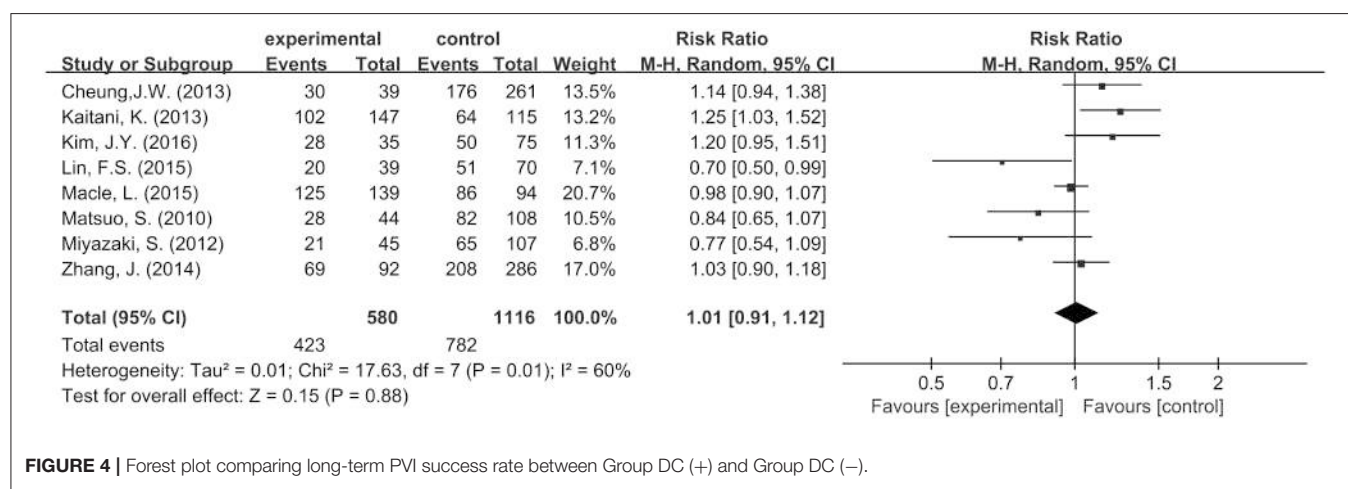


FIGURE 4 | Forest plot comparing long-term PVI success rate between Group DC (+) and Group DC (-).

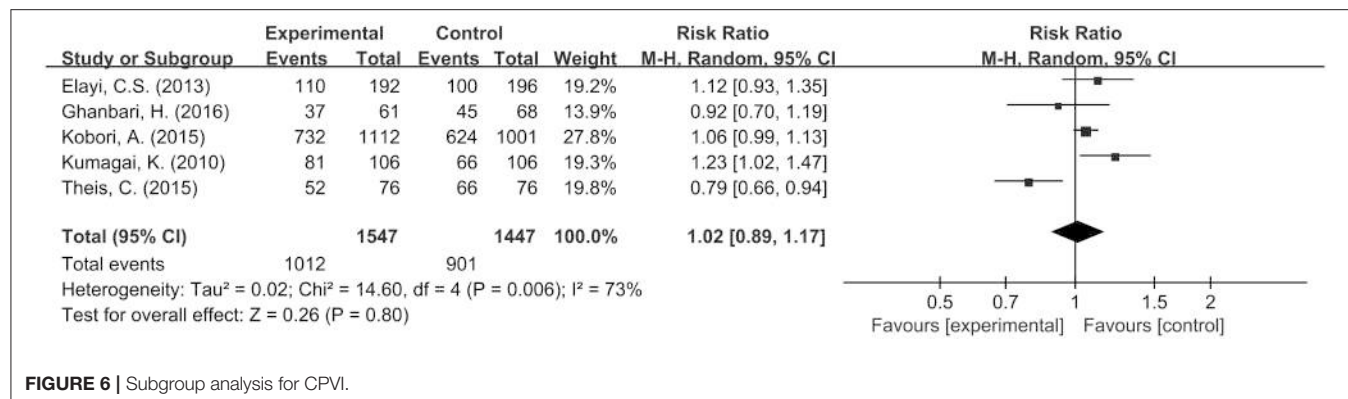


FIGURE 6 | Subgroup analysis for CPVI.

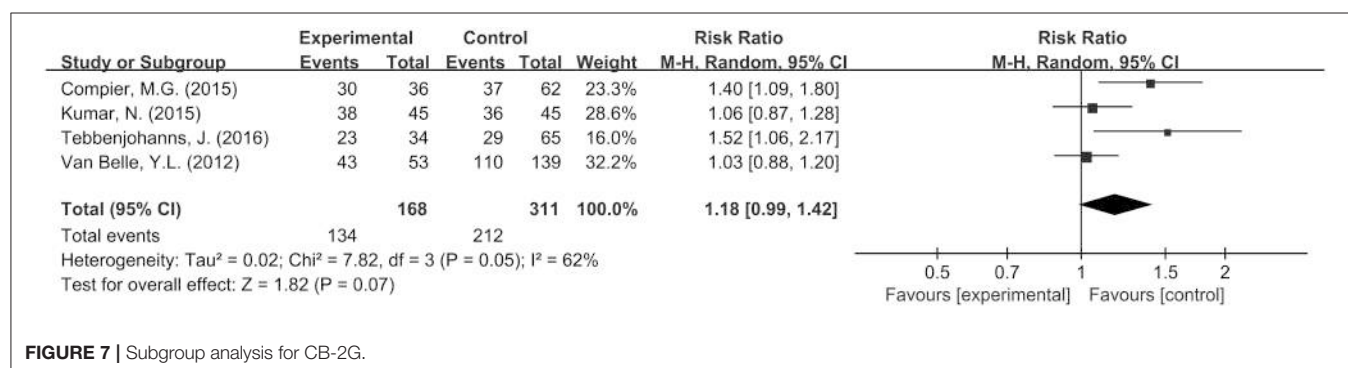


FIGURE 7 | Subgroup analysis for CB-2G.

Table 4 | Results of sensitivity analysis.

Studies	RR	95% CI	p-value*	Study heterogeneity				
				Chi ²	df	I ² , %	p-value*	
GROUP A (+) AND GROUP A (-)								
RCT	3	0.92	0.75–1.14	0.46	10.10	2	80	0.006*
AO*	6	1.07	0.93–1.23	0.33	19.43	5	74	0.002*
PSAF*	4	1.01	0.82–1.24	0.95	15.05	3	80	0.002*
GROUP DC (+) AND GROUP DC (-)								
AO*	4	1.02	0.87–1.19	0.83	8.53	3	65	0.04*
PSAF*	3	0.98	0.90–1.08	0.70	2.61	2	23	0.27

*Significance values; *AO, adenosine only; *PSAF, paroxysmal atrial fibrillation.

time and procedure time were prolonged due to adenosine administration.

LIMITATIONS

This systematic review and meta-analysis has several potential limitations. There was moderate heterogeneity across the included studies, which may be due to the following factors. Firstly, differences in study participants between each study especially the types of AF, and in detection criteria were observed. Secondly, several studies have used additional methods during adenosine testing for provoking DCs, such as isoproterenol administration during adenosine test. Thirdly, the dose of adenosine, administration method and procedure (such as waiting period after adenosine) used to unmask dormant conduction was not uniform, this may affect the clinical

outcomes. Fourthly, the successful rate of PVI may vary across medical centers due to variation in technical competencies, skills, and outcome measures. As such, the readers are advised to interpret the findings carefully. Nevertheless, funnel plot analysis revealed no significant publication bias. RCTs on CB-2G did not include a high number of participants and additional clinical trials are needed to confirm these findings.

CONCLUSIONS

In conclusion, regular adoption of adenosine test could not further improve PVI success rate basing on long-term observation and elimination of DCs provoked by adenosine after CPVI did not significantly reduce AF recurrence after catheter ablation.

AUTHOR CONTRIBUTIONS

YX conceived and designed the study. YX and GT guided the study. CC and DL searched and screened studies independently

and disagreements were resolved by adjudication with input from YX. XL, ZW, YL, and FZ helped finished the figures and tables. CC, DL, and GT finished the manuscript. JH and TL helped to refine the manuscript.

REFERENCES

- Arentz, T., Macle, L., Kalusche, D., Hocini, M., Jais, P., Shah, D., et al. (2004). "Dormant" pulmonary vein conduction revealed by adenosine after ostial radiofrequency catheter ablation. *J. Cardiovasc. Electrophysiol.* 15, 1041–1047. doi: 10.1046/j.1540-8167.2004.04031.x
- Cheung, J. W., Lin, F. S., Ip, J. E., Bender, S. R., Siddiqi, F. K., Liu, C. F., et al. (2013). Adenosine-induced pulmonary vein ectopy as a predictor of recurrent atrial fibrillation after pulmonary vein isolation. *Circ. Arrhythm. Electrophysiol.* 6, 1066–1073. doi: 10.1161/CIRCEP.113.000796
- Chugh, S. S., Havmoeller, R., Narayanan, K., Singh, D., Rienstra, M., Benjamin, E. J., et al. (2014). Worldwide epidemiology of atrial fibrillation: a global burden of disease 2010 study. *Circulation* 129, 837–847. doi: 10.1161/CIRCULATIONAHA.113.005119
- Compier, M. G., De Riva, M., Dyrda, K., Zeppenfeld, K., Schalij, M. J., and Trines, S. A. (2015). Incidence and predictors of dormant conduction after cryoballoon ablation incorporating a 30-min waiting period. *Europace* 17, 1383–1390. doi: 10.1093/europace/euu411
- Datino, T., Macle, L., Qi, X. Y., Maguy, A., Comtois, P., Chartier, D., et al. (2010). Mechanisms by which adenosine restores conduction in dormant canine pulmonary veins. *Circulation* 121, 963–972. doi: 10.1161/CIRCULATIONAHA.109.893107
- Elayi, C. S., Di Biase, L., Bai, R., Burkhardt, J. D., Mohanty, P., Santangeli, P., et al. (2013). Administration of isoproterenol and adenosine to guide supplemental ablation after pulmonary vein antrum isolation. *J. Cardiovasc. Electrophysiol.* 24, 1199–1206. doi: 10.1111/jce.12252
- Gepstein, L., Hayam, G., and Ben-Haim, S. A. (1997). A novel method for nonfluoroscopic catheter-based electroanatomical mapping of the heart. *In vitro and in vivo* accuracy results. *Circulation* 95, 1611–1622. doi: 10.1161/01.CIR.95.6.1611
- Ghanbari, H., Jani, R., Hussain-Amin, A., Al-Assad, W., Huether, E., Ansari, S., et al. (2016). Role of adenosine after antral pulmonary vein isolation of paroxysmal atrial fibrillation: a randomized controlled trial. *Heart Rhythm* 13, 407–415. doi: 10.1016/j.hrrthm.2015.10.016
- Haïssaguerre, M., Jaïs, P., Shah, D. C., Garrigue, S., Takahashi, A., Lavergne, T., et al. (2000). Electrophysiological end point for catheter ablation of atrial fibrillation initiated from multiple pulmonary venous foci. *Circulation* 101, 1409–1417. doi: 10.1161/01.CIR.101.12.1409
- Higgins, J., and Green, S. (2011). *Cochrane Handbook for Systematic Reviews of Interventions Version 5.1.0. The Cochrane Library*. Chichester: John Wiley & Sons.
- Ho, S. Y., Cabrera, J. A., Tran, V. H., Farré, J., Anderson, R. H., and Sánchez-Quintana, D. (2001). Architecture of the pulmonary veins: relevance to radiofrequency ablation. *Heart* 86, 265–270. doi: 10.1136/heart.86.3.265
- Hocini, M., Sanders, P., Jaïs, P., Hsu, L. F., Weerasoorya, R., Scavée, C., et al. (2005). Prevalence of pulmonary vein disconnection after anatomical ablation for atrial fibrillation: consequences of wide atrial encircling of the pulmonary veins. *Eur. Heart J.* 26, 696–704. doi: 10.1093/eurheartj/ehi096
- Jaïs, P., Cauchemez, B., Macle, L., Daoud, E., Khairy, P., Subbiah, R., et al. (2008). Catheter ablation versus antiarrhythmic drugs for atrial fibrillation: the A4 study. *Circulation* 118, 2498–2505. doi: 10.1161/CIRCULATIONAHA.108.772582
- Kaitani, K., Kurotobi, T., Kobori, A., Okajima, K., Yao, T., Nakazawa, Y., et al. (2014). Late re-conduction sites in the second session after pulmonary vein isolation using adenosine provocation for atrial fibrillation. *Europace* 16, 521–527. doi: 10.1093/europace/eut258
- Kim, J. Y., Kim, S. H., Song, I. G., Kim, Y. R., Kim, T. S., Kim, J. H., et al. (2016). Achievement of successful pulmonary vein isolation: methods of adenosine testing and incremental benefit of exit block. *J. Interv. Card. Electrophysiol.* 46, 315–324. doi: 10.1007/s10840-016-0122-9
- Kirchhof, P., Benussi, S., Kotecha, D., Ahlsson, A., Atar, D., Casadei, B., et al. (2017). 2016 ESC guidelines for the management of atrial fibrillation developed in collaboration with EACTS. *Eur. Heart J.* 70:50. doi: 10.1016/j.rec.2016.11.033
- Kobori, A., Shizuta, S., Inoue, K., Kaitani, K., Morimoto, T., Nakazawa, Y., et al. (2015). Adenosine triphosphate-guided pulmonary vein isolation for atrial fibrillation: the UNmasking dormant electrical reconnection by adenosine triphosphate (UNDER-ATP) trial. *Eur. Heart J.* 36, 3276–3287. doi: 10.1093/eurheartj/ehv457
- Kumagai, K., Naito, S., Nakamura, K., Hayashi, T., Fukazawa, R., Sato, C., et al. (2010). ATP-induced dormant pulmonary veins originating from the carina region after circumferential pulmonary vein isolation of atrial fibrillation. *J. Cardiovasc. Electrophysiol.* 21, 494–500. doi: 10.1111/j.1540-8167.2009.01667.x
- Kumar, N., Dinh, T., Phan, K., Timmermans, C., Philippens, S., Dassen, W., et al. (2015). Adenosine testing after second-generation cryoballoon ablation (ATSCA) study improves clinical success rate for atrial fibrillation. *Europace* 17, 871–876. doi: 10.1093/europace/euu352
- Lin, F. S., Ip, J. E., Markowitz, S. M., Liu, C. F., Thomas, G., Lerman, B. B., et al. (2015). Limitations of dormant conduction as a predictor of atrial fibrillation recurrence and pulmonary vein reconnection after catheter ablation. *Pacing Clin. Electrophysiol.* 38, 598–607. doi: 10.1111/pace.12596
- Linz, D., Kadhim, K., Lau, D., and Sanders, P. (2018). Recovery of adenosine-sensitive dormant conduction is but one mechanism of pulmonary vein reconnection. *Indian Pacing Electrophysiol. J.* 18, 201–202. doi: 10.1016/j.ipej.2018.10.003
- Macle, L., Khairy, P., Weerasoorya, R., Novak, P., Verma, A., Willem, S., et al. (2015). Adenosine-guided pulmonary vein isolation for the treatment of paroxysmal atrial fibrillation: an international, multicentre, randomised superiority trial. *Lancet* 386, 672–679. doi: 10.1016/S0140-6736(15)60026-5
- Matsuo, S., Yamane, T., Date, T., Hioki, M., Ito, K., Narui, R., et al. (2010). Comparison of the clinical outcome after pulmonary vein isolation based on the appearance of adenosine-induced dormant pulmonary vein conduction. *Am. Heart J.* 160, 337–345. doi: 10.1016/j.ahj.2010.05.025
- McLellan, A. J., Kumar, S., Smith, C., Morton, J. B., Kalman, J. M., and Kistler, P. M. (2013). The role of adenosine following pulmonary vein isolation in patients undergoing catheter ablation for atrial fibrillation: a systematic review. *J. Cardiovasc. Electrophysiol.* 24, 742–751. doi: 10.1111/jce.12121
- McLellan, A. J. A., Kumar, S., Smith, C., Ling, L. H., Prabhu, S., Kalman, J. M., et al. (2017). The role of adenosine challenge in catheter ablation for atrial fibrillation: a systematic review and meta-analysis. *Int J Cardiol.* 236, 253–261. doi: 10.1016/j.ijcard.2017.01.070
- Miyazaki, S., Kuwahara, T., Kobori, A., Takahashi, Y., Takei, A., Sato, A., et al. (2012). Impact of adenosine-provoked acute dormant pulmonary vein conduction on recurrence of atrial fibrillation. *J. Cardiovasc. Electrophysiol.* 23, 256–260. doi: 10.1111/j.1540-8167.2011.02195.x
- Nakagawa, H., Antz, M., Wong, T., Schmidt, B., Ernst, S., Ouyang, F., et al. (2007). Initial experience using a forward directed, high-intensity focused ultrasound balloon catheter for pulmonary vein antrum isolation in patients with atrial fibrillation. *J. Cardiovasc. Electrophysiol.* 18, 136–144. doi: 10.1111/j.1540-8167.2006.00715.x
- Oral, H., Scharf, C., Chugh, A., Hall, B., Cheung, P., Good, E., et al. (2003). Catheter ablation for paroxysmal atrial fibrillation: segmental pulmonary vein ostial ablation versus left atrial ablation. *Circulation* 108, 2355–2360. doi: 10.1161/01.CIR.0000095796.45180.88
- Ouyang, F., Antz, M., Ernst, S., Hachiya, H., Mavrakis, H., Deger, F. T., et al. (2005). Recovered pulmonary vein conduction as a dominant factor for recurrent atrial tachyarrhythmias after complete circular isolation of the pulmonary veins: lessons from double Lasso technique. *Circulation* 111, 127–135. doi: 10.1161/01.CIR.0000151289.73085.36
- Ouyang, F., Bänsch, D., Ernst, S., Schaumann, A., Hachiya, H., Chen, M., et al. (2004). Complete isolation of left atrium surrounding the pulmonary veins: new insights from the double-Lasso technique in paroxysmal atrial

- fibrillation. *Circulation* 110, 2090–2096. doi: 10.1161/01.CIR.0000144459.37455.EE
- Pappone, C., Manguso, F., Vicedomini, G., Gugliotta, F., Santinelli, O., Ferro, A., et al. (2004). Prevention of iatrogenic atrial tachycardia after ablation of atrial fibrillation: a prospective randomized study comparing circumferential pulmonary vein ablation with a modified approach. *Circulation* 110, 3036–3042. doi: 10.1161/01.CIR.0000147186.83715.95
- Rostock, T., O'Neill, M. D., Sanders, P., Rotter, M., Jaës, P., Hocini, M., et al. (2006). Characterization of conduction recovery across left atrial linear lesions in patients with paroxysmal and persistent atrial fibrillation. *J. Cardiovasc. Electrophysiol.* 17, 1106–1111. doi: 10.1111/j.1540-8167.2006.00585.x
- Schaeffer, B., Willems, S., Sultan, A., Hoffmann, B. A., Lüker, J., Schreiber, D., et al. (2015). Loss of pace capture on the ablation line during pulmonary vein isolation versus “dormant conduction”: is adenosine expendable? *J. Cardiovasc. Electrophysiol.* 26, 1075–1080. doi: 10.1111/jce.12759
- Tebbenjohanss, J., Hofer, C., Bergmann, L., Dedroogh, M., Gaudin, D., von Werder, A., et al. (2016). Shortening of freezing cycles provides equal outcome to standard ablation procedure using second-generation 28 mm cryoballoon after 15-month follow-up. *Europace* 18, 206–210. doi: 10.1093/europace/euv189
- Thacker, E. L., McKnight, B., Psaty, B. M., Longstreth, Jr., W. T., Dublin, S., et al. (2013). Association of body mass index, diabetes, hypertension, and blood pressure levels with risk of permanent atrial fibrillation. *J. Gen. Intern. Med.* 28, 247–253. doi: 10.1007/s11606-012-2220-4
- Theis, C., Konrad, T., Mollnau, H., Sonnenschein, S., Kämpfner, D., Potstawa, M., et al. (2015). Arrhythmia termination versus elimination of dormant pulmonary vein conduction as a procedural end point of catheter ablation for paroxysmal atrial fibrillation: a prospective randomized trial. *Circ. Arrhythm. Electrophysiol.* 8, 1080–1087. doi: 10.1161/CIRCEP.115.002786
- Tse, G., Lai, E. T., Yeo, J. M., Tse, V., and Wong, S. H. (2016). Mechanisms of electrical activation and conduction in the gastrointestinal system: lessons from cardiac electrophysiology. *Front. Physiol.* 7:182. doi: 10.3389/fphys.2016.00182
- Van Belle, Y. L., Janse, P. A., de Groot, N. M., Anné, W., Theuns, D. A., and Jordae, L. J. (2012). Adenosine testing after cryoballoon pulmonary vein isolation improves long-term clinical outcome. *Neth. Heart J.* 20, 447–455. doi: 10.1007/s12471-012-0319-1
- Zhang, J., Tang, C., Zhang, Y., and Su, X. I. (2014). Origin and ablation of the adenosine triphosphate induced atrial fibrillation after circumferential pulmonary vein isolation: effects on procedural success rate. *J. Cardiovasc. Electrophysiol.* 25, 364–370. doi: 10.1111/jce.12362

Conflict of Interest Statement: The authors declare that the research was conducted in the absence of any commercial or financial relationships that could be construed as a potential conflict of interest.

The handling editor is currently editing co-organizing a Research Topic with one of the authors GT, and confirms the absence of any other collaboration.

Copyright © 2019 Chen, Li, Ho, Liu, Li, Wang, Lin, Zou, Tse and Xia. This is an open-access article distributed under the terms of the Creative Commons Attribution License (CC BY). The use, distribution or reproduction in other forums is permitted, provided the original author(s) and the copyright owner(s) are credited and that the original publication in this journal is cited, in accordance with accepted academic practice. No use, distribution or reproduction is permitted which does not comply with these terms.



The Association Between Diabetes Mellitus and Atrial Fibrillation: Clinical and Mechanistic Insights

Loryn J. Bohne, Dustin Johnson, Robert A. Rose, Stephen B. Wilton and Anne M. Gillis*

Department of Cardiac Sciences and Department of Physiology and Pharmacology, University of Calgary and Libin Cardiovascular Institute of Alberta, Calgary, AB, Canada

OPEN ACCESS

Edited by:

Jichao Zhao,
The University of Auckland,
New Zealand

Reviewed by:

Martin Stiles,
The University of Auckland,
New Zealand

Ghassen Cheriti,

Centre Hospitalier Universitaire (CHU)
de Bordeaux, France

***Correspondence:**

Anne M. Gillis
amgillis@ucalgary.ca

Specialty section:

This article was submitted to
Computational Physiology and
Medicine,
a section of the journal
Frontiers in Physiology

Received: 30 April 2018

Accepted: 04 February 2019

Published: 26 February 2019

Citation:

Bohne LJ, Johnson D, Rose RA,
Wilton SB and Gillis AM (2019) The
Association Between Diabetes
Mellitus and Atrial Fibrillation: Clinical
and Mechanistic Insights.
Front. Physiol. 10:135.
doi: 10.3389/fphys.2019.00135

A number of clinical studies have reported that diabetes mellitus (DM) is an independent risk factor for Atrial fibrillation (AF). After adjustment for other known risk factors including age, sex, and cardiovascular risk factors, DM remains a significant if modest risk factor for development of AF. The mechanisms underlying the increased susceptibility to AF in DM are incompletely understood, but are thought to involve electrical, structural, and autonomic remodeling in the atria. Electrical remodeling in DM may involve alterations in gap junction function that affect atrial conduction velocity due to changes in expression or localization of connexins. Electrical remodeling can also occur due to changes in atrial action potential morphology in association with changes in ionic currents, such as sodium or potassium currents, that can affect conduction velocity or susceptibility to triggered activity. Structural remodeling in DM results in atrial fibrosis, which can alter conduction patterns and susceptibility to re-entry in the atria. In addition, increases in atrial adipose tissue, especially in Type II DM, can lead to disruptions in atrial conduction velocity or conduction patterns that may affect arrhythmogenesis. Whether the insulin resistance in type II DM activates unique intracellular signaling pathways independent of obesity requires further investigation. In addition, the relationship between incident AF and glycemic control requires further study.

Keywords: atrial fibrillation, diabetes mellitus, risk factors, mechanisms, atrial remodeling

INTRODUCTION

Atrial fibrillation (AF) is the most common sustained arrhythmia and is associated with substantial morbidity and mortality. Risk factors for atrial fibrillation include age, hypertension, obesity, valvular heart disease, heart failure, and obstructive sleep apnea (Benjamin et al., 1994; Staerk et al., 2017). Some but not all studies have reported that diabetes mellitus (DM) is an independent risk factor for AF (Benjamin et al., 1994; Krahn et al., 1995; Huxley et al., 2011). Here we will review the clinical data supporting the association between DM and AF and discuss the potential mechanism(s) by which DM may contribute to the electrophysiologic substrate for AF. We also suggest future potential research studies to advance our knowledge in this field.

ASSOCIATION BETWEEN DM AND AF: CLINICAL STUDIES

A potential association between DM and incidence of AF has long been postulated based on epidemiologic studies. The original Framingham Heart Study consisted of 5,209 patients (2,336 men, 2,873 women), age 30–62 years of age. This study initiated in 1948 represented a random sample of two thirds of the population of Framingham, Massachusetts and has conducted pivotal research defining cardiovascular risk factors (Tsao and Vasan, 2015). This study reported that hypertension, diabetes, congestive heart failure and valvular heart disease were independent risk factors for AF in both men and women (Benjamin et al., 1994). The odds ratio (OR) of risk of developing AF in the association with DM was 1.4 (95% CI 1.0–2.0) and 1.6 (95% CI 1.1–2.2) for men and women, respectively. However, in the absence of valvular heart disease, diabetes was no longer a significant risk predictor for the development of AF. The Framingham Heart Study did not include body mass index (BMI) or a history of obstructive sleep apnea in this initial analysis.

The Manitoba Follow-Up Study which also commenced in 1948 prospectively followed 3,983 healthy male air crew recruits for 44 years. The goal of this study was to examine the role that abnormalities on the resting electrocardiogram might play in the prediction of future cardiovascular disease. In this cohort, obesity [relative risk (RR) 1.28; 95% CI 1.02–1.62] but not DM was reported to be an independent risk factor for AF (Krahn et al., 1995).

In 2011, Huxley et al. reported the results of a systematic review and meta-analysis examining the association between DM and AF (Huxley et al., 2011). They identified seven prospective cohort studies and four case control studies that included 108,703 individuals with AF and 1,686,097 control subjects. Overall, DM was associated with a 39% increased risk of AF compared to controls (RR 1.39, 95% CI 1.10–1.75). However, only three of these studies reported multivariable adjusted risk estimates for AF (adjusting for age and some other risk factors). Perhaps, not surprisingly, after adjusting for these known factors the association between DM and AF was significantly attenuated and in two of these studies was no longer statistically significant. Thus, the association between DM and incident AF has likely been overestimated in this meta-analysis. Furthermore, these previous studies did not specifically distinguish between Type I or Type II DM, glycemic control or specific therapies.

Since this meta-analysis was published, several additional observational studies examining the association between DM and AF have been reported. The Atherosclerosis Risk in Communities study is comprised of 15,792 white and African American patients age 45–64 years pooled from 4 geographically distinct communities in the United States. A 2012 report from this cohort examined the associations between Type II DM, markers of glucose homeostasis and risk of AF (Huxley et al., 2012). After adjustment for a number of risk factors, DM was associated with a significant increased risk for AF [hazard ratio (HR) 1.35, 95% CI 1.14–1.60] (Figure 1). However, those with pre diabetes or undiagnosed diabetes were not at increased risk for AF.

The authors also reported a positive linear association between HbA1c and the risk of AF for both those with and without DM, though a similar positive relationship between fasting blood glucose and risk for AF was observed only in patients with previously diagnosed DM (Huxley et al., 2012).

In the Women's Health Study, Type II DM was a significant predictor of risk for AF (HR 1.37; 95% CI 1.03–1.83) after adjustment for cardiovascular risk factors including hypertension and BMI (Schoen et al., 2012). However, these investigators observed that the development of hypertension, obesity, and cardiovascular disease over time were stronger predictors of risk of incident AF compared to DM. In a subgroup analysis of the Women's Health Study, baseline HbA1c was not predictive of subsequent AF.

Risk factors for AF were evaluated in post-menopausal women in the Women's Health Initiative Observational Study (Perez et al., 2013). Consistent with earlier observational cohort studies, age, hypertension, obesity, diabetes, myocardial infarction, and congestive heart failure were all independently associated with incident AF. However, hypertension and overweight status/obesity contributed to 28.3 and 12.1% of the population attributable risk for AF whereas DM accounted for only 3.4% of this risk. A Korean National Health Insurance Service Database analysis confirmed that after adjustment for age, sex, BMI, and other covariates the population attributable risk of AF for hypertension, ischemic heart disease, heart failure and DM were 16, 8.2, 5.3, and 0.8%, respectively (Son et al., 2016). In this latter analysis, DM was not a significant risk predictor for AF.

A Danish Nation cohort study evaluated the risk of AF in individuals with DM compared to the background Danish population (Pallisgaard et al., 2016). After adjustment for multiple covariates, DM was associated with a relative 19% increased risk of incident AF. Interestingly, the incidence rate ratio was highest in the youngest age group 18–39 years (2.34, 95% CI 1.52–3.60) compared to older patients (1.20, 95% CI 1.18–1.23 age group 65–74). This analysis did not stratify relative risks for those with Type I vs. Type II DM or describe the duration of DM prior to AF diagnosis, so the apparent effect modification by age is not easily explained. The relative decrease in risk of AF in DM with increasing age may reflect the importance of other risk factors for AF that occur with advancing age.

A recent prospective, case control study examined the relationship between Type I diabetes and AF (Dahlqvist et al., 2017). Using a Swedish database, Dahlqvist compared 36 258 patients with Type I DM to 179,980 controls followed for a median of 9.7 years. The mean age of participants was 35 years. Type I DM was associated with a modest increase in the risk of AF in men (HR 1.13, 95% CI 1.01–1.25), but a 50% increase risk of AF in women (HR 1.5, 95% CI 1.3–1.72). The risk of AF was increased in those with worse glycemic control and renal complications (Figure 2).

In this issue of *Frontiers in Physiology* (Xiong et al., 2018), have summarized the current state of the literature in an updated systematic review and meta-analysis including

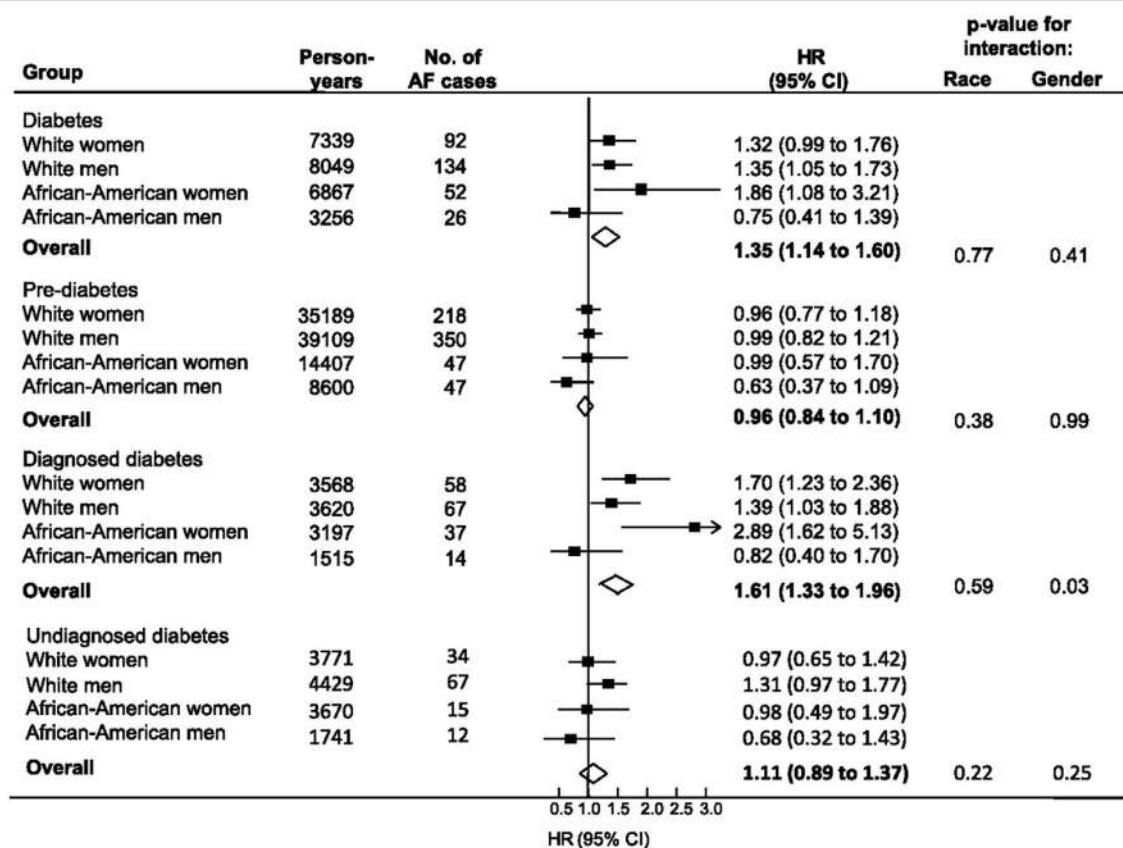


FIGURE 1 | Relationship between diabetes, pre-diabetes, and physician-diagnosed diabetes with incident atrial fibrillation from the ARIC study (1990–2007).

Individuals without diabetes comprised the reference group for each comparison. Diabetes included all individuals with FSG > 126 mg/dl or HbA1c > 6.5% or use of diabetic medication or history of physician-diagnosed diabetes. Undiagnosed diabetes defined as fasting serum glucose (FSG) > 126 mg/dl or HbA1c > 6.5% but no history of diabetic medication usage or physician diagnosed diabetes. Black boxes represent the estimate adjusted for age, education, income, prior history of cardiovascular disease, BMI, systolic blood pressure, use of hypertensive medications, and smoking. Horizontal lines represent 95% confidence intervals. Open diamonds represent the estimate of effect for the overall population. Note the strong correlation between DM and AF among African American women. Reproduced with permission from Huxley et al. (2012).

publications reported up to September 2017 that investigated the association between DM and AF. They used a novel machine learning approach to identify publications suitable for analysis. Twenty-nine studies (21 observational cohort or randomized trials and 8 case control studies) including 8,037,756 subjects were included in the analysis. Overall DM was associated with a pooled 49% increased risk of developing AF (RR 1.49, 95% CI 1.24–1.79). However, many studies did not adjust for known risk predictors including age, sex and cardiovascular risk factors. When restricted to studies reporting adjusted estimates, DM was associated with a weaker but still significant increased risk of new onset AF (RR 1.23, 95% CI 1.03–1.46). Furthermore, there was significant between-study heterogeneity in the observed associations that could not be explained by available differences in baseline covariates, type of DM, or study era. Interestingly, in this study the association between DM and incident AF was stronger in women than in men (RR 1.38, 95% CI 1.19–1.60 vs. 1.11, 95% CI 1.01–1.22). In addition, the association between DM and incident AF was stronger in more recent vs. older studies.

The clinical studies discussed are summarized in Table 1. These clinical studies examining the potential association between DM and AF incidence share important limitations. Most publications are secondary reports from large cohorts assembled for another purpose, without detailed characterization of the type, duration or severity of DM, nor standardized AF detection protocols. Furthermore, there has been variable adjustment for confounding by other risk factors such as obesity, obstructive sleep apnea, and heart failure. This may in part explain the contradictory results.

Notwithstanding these limitations, DM appears to be a significant if modest risk factor for development of AF. This association may be increasing in strength over time, as secular trends in other risk factors especially better control of hypertension and management of heart failure (Schnabel et al., 2015) and an increasing incidence of obesity and DM worldwide have been reported. These changes suggest that more attention to the diagnosis and management of DM as well as aggressive weight loss interventions for overweight/obese individuals may be important in curbing

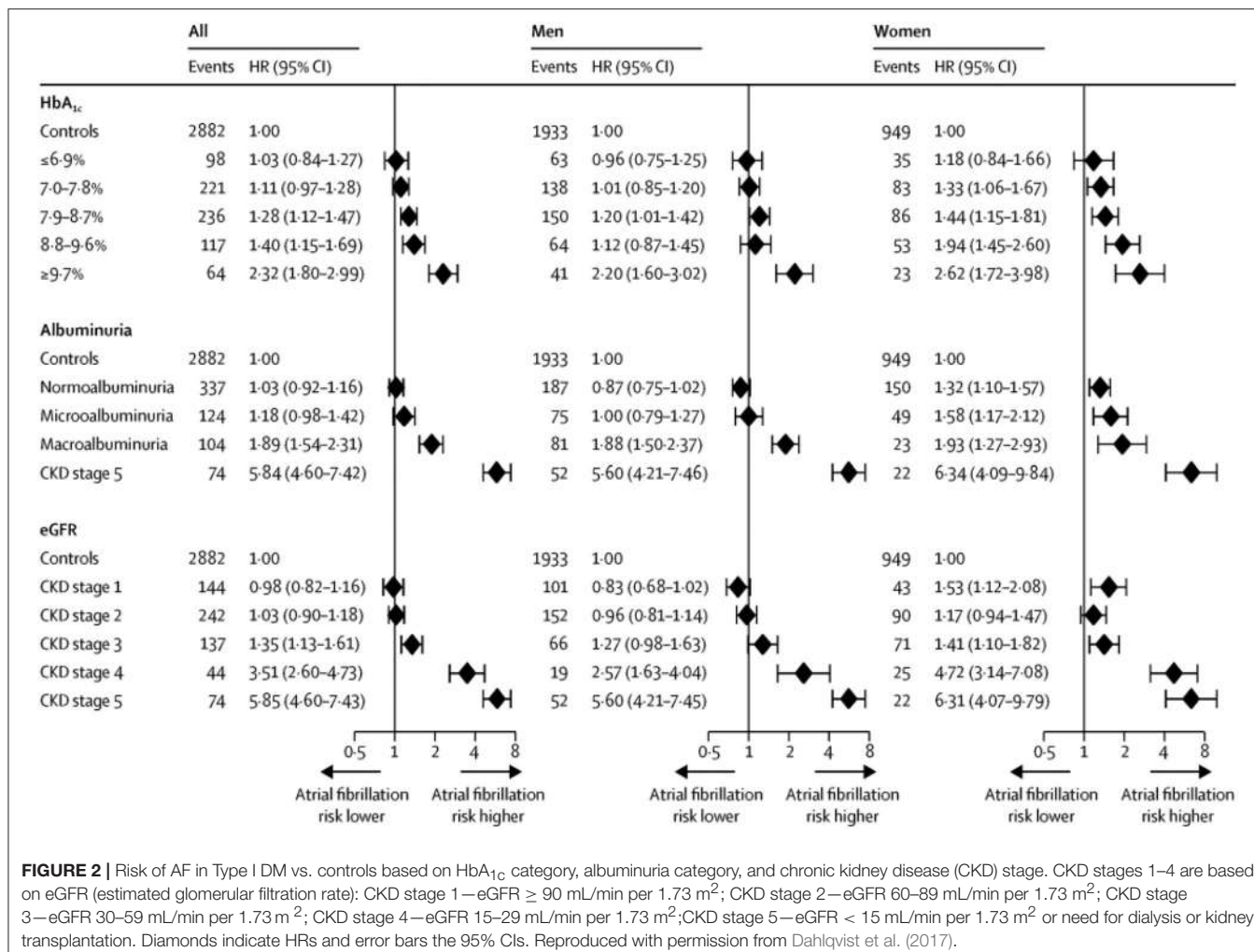


FIGURE 2 | Risk of AF in Type I DM vs. controls based on HbA_{1c} category, albuminuria category, and chronic kidney disease (CKD) stage. CKD stages 1–4 are based on eGFR (estimated glomerular filtration rate): CKD stage 1—eGFR \geq 90 mL/min per 1.73 m²; CKD stage 2—eGFR 60–89 mL/min per 1.73 m²; CKD stage 3—eGFR 30–59 mL/min per 1.73 m²; CKD stage 4—eGFR 15–29 mL/min per 1.73 m²; CKD stage 5—eGFR < 15 mL/min per 1.73 m² or need for dialysis or kidney transplantation. Diamonds indicate HRs and error bars the 95% CIs. Reproduced with permission from Dahlqvist et al. (2017).

the emerging epidemic of AF. The contradictory results from the available clinical data set also serves to highlight the importance of fundamental research to elucidate the mechanisms by which DM might promote AF, summarized in the next section.

MECHANISMS OF AF IN DM: INSIGHTS FROM EXPERIMENTAL STUDIES

Mechanisms of Atrial Fibrillation

While the mechanisms underlying AF are incompletely understood, research efforts have identified a substantial number of pathophysiological determinants, including at the cellular and molecular levels, that can lead to electrical and structural remodeling and thereby favor the occurrence of AF. These include a number of mechanisms that can lead to triggers for AF initiation as well as mechanisms that create a substrate for AF maintenance and progression (Heijman et al., 2014, 2018). Below, we focus our discussion on alterations that have been shown or proposed to lead to AF specifically in the setting of DM. These potential mechanism(s) are outlined in Figure 3.

Animal Models of Diabetes Mellitus and AF Research

A number of animal models of DM have been employed to study the atrial electrical and structural changes and the underlying molecular mechanism(s) that predispose to AF in this setting. These include models of Type I DM induced by chemical induction using streptozotocin or alloxan (King, 2012; Watanabe et al., 2012; Liu et al., 2014, 2017; Saito et al., 2014; Fu et al., 2015; Yi et al., 2015; Hayami et al., 2016), which have been successfully employed in rodents and rabbits. The Akita mouse model of Type 1 DM which arose due to a mutation in the insulin-2 gene replicates many of the complications of diabetes including retinopathy, neuropathy, nephropathy and increased oxidative stress (Hsueh et al., 2007). Most current animal models of type II DM are associated with obesity. These include monogenic models of leptin deficiency (mice) or deficiency in the leptin receptor (mice, Zucker fatty rats and diabetic fatty rats (King, 2012; Linz et al., 2016; Fukui et al., 2017). Type II DM induced by high fat feeding has been used in rabbits (Zarzoso et al., 2014). Models of metabolic syndrome characterized by central obesity, hyperlipidemia, glucose intolerance and hypertension have been

TABLE 1 | Characteristics of Clinical Studies Examining the Relationship Between Diabetes Mellitus and Atrial Fibrillation.

Authors	Study design	Findings	Limitations	Diabetes type
Benjamin et al., 1994	Prospective cohort 2,090 men 2,641 women Ages 55–94 years	HTN, DM, CHF, VHD independent risk factors for AF. DM risk: OR 1.4 men, 1.6 women	DM not a risk factor for AF after controlling for valvular heart disease. BMI and OSA not included in analysis	Not specified
Krahn et al., 1995	Prospective cohort 3,983 men	Abnormalities in resting ECG did not predict AF. Obesity but not DM a risk for AF		Not specified
Huxley et al., 2011	Systematic review and meta-analysis of 7 prospective cohort studies, 4 case control studies. 108,703 with AF 1,686,099 control subjects	39% increased risk of AF in DM compared to controls	Effect significantly attenuated after multivariable adjusted risk estimates	Type II DM
Huxley et al., 2012	Prospective cohort 13,025 subjects	35% increased risk of AF in DM after adjustment for known risk factors	Cases of AF ascertained through hospital discharge codes	Type II DM
Schoen et al., 2012	34,720 female health professionals	37% increased risk of for AF in DM. HTN, CVD, obesity stronger predictors of AF than DM	Possible under diagnosis of DM given lack of systemic screening	Type II DM
Perez et al., 2013	Observational cohort 81,892 post-menopausal women	Age, HTN, obesity, DM, MI, CHF risk factors for AF. DM risk: HR 1.55 in multivariable analysis	98% of incident AF based on hospital discharge codes	Not specified
Son et al., 2016	Korean National Health Insurance Data 206,013 subjects age >30 years	Diabetes not a risk factor for AF	Incident AF based on disease codes	Not specified
Pallisgaard et al., 2016	Danish National Registries 5,0081,087 subjects >18 years	19% increased risk of AF in DM IRR 2.34 age 18–39 IRR 1.20 age 65–74	Incident AF based on disease codes	Not specified
Xiong et al., 2018	Systemic review and meta-analysis 21 observational cohort or randomized trials and 8 case control studies 8,037,756 subjects	RR for AF in DM 1.38 (women) 1.11 (men)	Significant between study heterogeneity in observed associations	Majority Type II DM
Dahlqvist et al., 2017	Prospective case control study 36,258 patients Type I DM 179,980 control subjects	Modest 13% increased risk of AF in men Significant 50% increased risk of AF in women. Risk greater in those with poor glycemic control	No data on blood pressure or BMI	Type I DM

AF, atrial fibrillation; HTN, hypertension; CHF, congestive heart failure; IRR, incident risk ratio; CVD, cardiovascular disease; OR, odds ratio; DM, diabetes mellitus; RR, relative risk; HR, hazard ratio; VHD, valvular heart disease.

induced using a combination of high fat and high sucrose diets in rodents (Hohl et al., 2017) and rabbits (Arias-Mutis et al., 2017).

Atrial Structural Remodeling

Diabetes is known to exacerbate interstitial fibrosis in the atria. This is seen in both animal (Kato et al., 2008; Watanabe et al., 2012; Li et al., 2016) and human (Lamberts et al., 2014) studies. Atrial fibrosis has been demonstrated in studies of Type I DM (Kato et al., 2008) and Type II DM (Li et al., 2016). Obesity often leads to Type II DM and is associated with lipomatous metaplasia of the heart, a process that involves the transformation of fatty infiltrates into fibrotic tissue (Samanta et al., 2016). A sheep model of obesity induced by high caloric diet in the absence of DM induces significant atrial structural and electrical remodeling. The changes reported included left

atrial enlargement, biatrial conduction abnormalities, increased expression of profibrotic mediators, interstitial atrial fibrosis, and an increased propensity for inducible and spontaneous AF (Abed et al., 2013; Mahajan et al., 2015). Therefore, in the case of Type II DM, it is unclear whether the observed atrial interstitial fibrosis and associated atrial conduction abnormalities are the result of either chronic diabetes or excessive adiposity alone.

Fibrosis

Fibrosis can be a critical contributor to the establishment of a substrate for AF as increased collagen deposition in the atria can slow atrial conduction velocity and cause fragmentation of propagating wavefronts, which can result in re-entry (Schotten et al., 2016). Fibrosis is importantly determined by the function of cardiac fibroblasts, which play a central role in the deposition

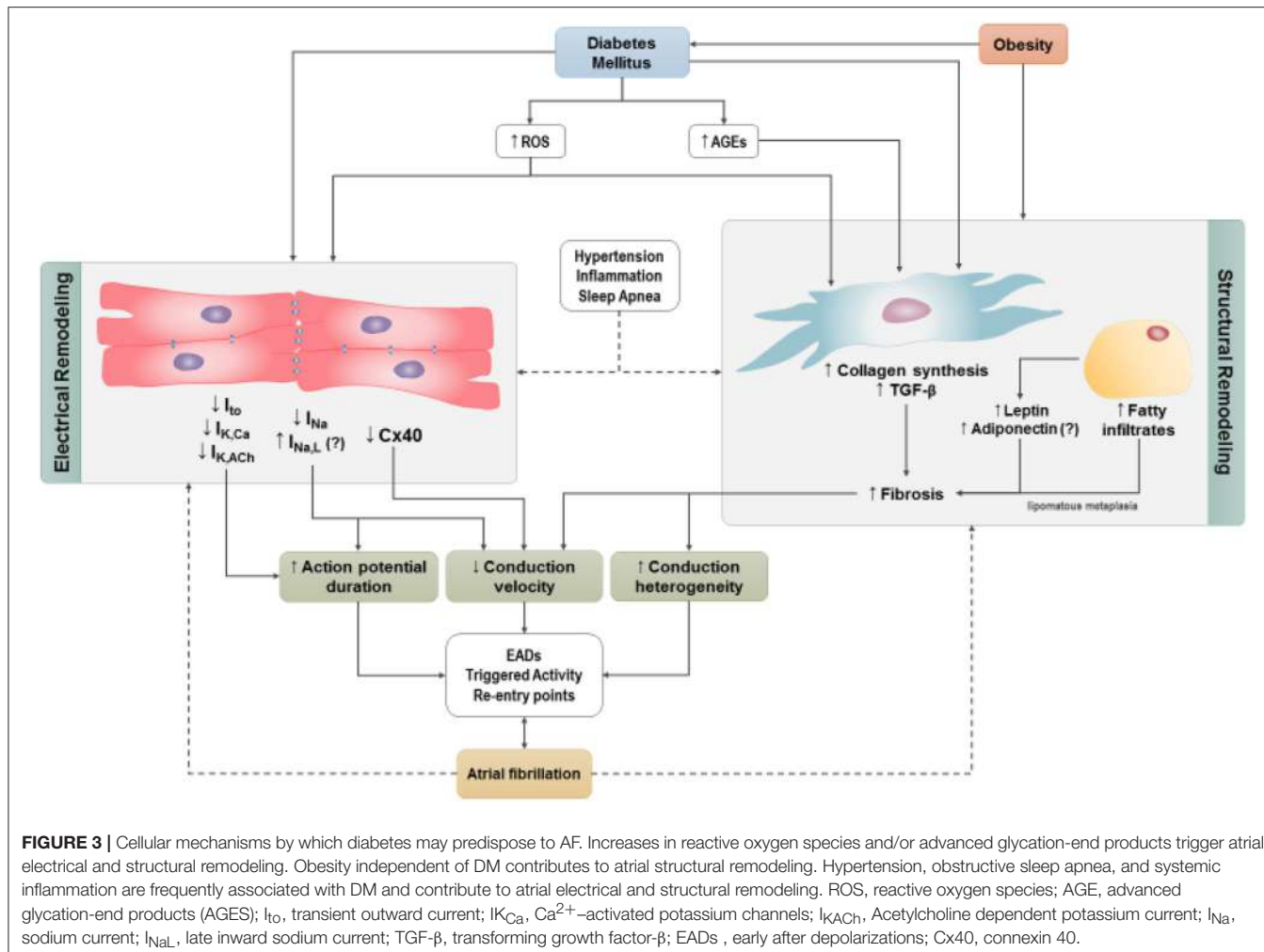


FIGURE 3 | Cellular mechanisms by which diabetes may predispose to AF. Increases in reactive oxygen species and/or advanced glycation-end products trigger atrial electrical and structural remodeling. Obesity independent of DM contributes to atrial structural remodeling. Hypertension, obstructive sleep apnea, and systemic inflammation are frequently associated with DM and contribute to atrial electrical and structural remodeling. ROS, reactive oxygen species; AGE, advanced glycation-end products (AGES); I_{to} , transient outward current; IK_{Ca} , Ca^{2+} -activated potassium channels; $I_{K,ACh}$, Acetylcholine dependent potassium current; I_{Na} , sodium current; I_{NaL} , late inward sodium current; $TGF-\beta$, transforming growth factor- β ; EADs, early after depolarizations; Cx40, connexin 40.

of the extracellular matrix. In a number of pathological conditions, fibroblasts are activated leading to inappropriate collagen production and deposition. Cardiac fibrosis has been clearly demonstrated in diabetic patients and, consistent with this, cardiac fibroblasts isolated from the atria of patients with Type II DM show enhanced levels of collagen synthesis, as indicated by increased expression of Type I collagen (Sedgwick et al., 2014). Similar results have been observed in db/db mice, in which cultured ventricular fibroblasts showed increased expression of Type I collagen and transforming growth factor β (TGF- β) (Hutchinson et al., 2013). Since this latter study was performed in ventricular fibroblasts it remains to be determined if similar changes occur in the atria of Type II diabetic mice. On the other hand, the notion of enhanced atrial fibrosis in association with increased expression of collagens is supported in studies of Type I diabetic Akita mice in which right and left atrial fibrosis was increased in association with enhanced atrial expression of Type I and Type III collagens (Krishnaswamy et al., 2015) (Figure 4). Interestingly, the increase in atrial fibrosis in Akita mice was preventable by chronic insulin treatment.

Hyperglycemia in Type I and Type II DM is associated with enhanced angiotensin II, TGF- β signaling, and increased reactive-oxygen species (ROS) production (Singh et al., 2008a,b; Patel et al., 2012; Fiaschi et al., 2014). These are all well-characterized pro-fibrotic signaling molecules that enhance collagen synthesis and secretion by cardiac fibroblasts suggesting that these factors may contribute to atrial fibrosis and enhanced susceptibility to AF in DM. Consistent with this, angiotensin-converting enzyme inhibitors have been shown to reduce collagen and TGF- β levels in both Type I DM (Singh et al., 2008b) and Type II DM (Toblli et al., 2005). Angiotensin II is well-known to induce cardiac fibrosis and the findings mentioned above are consistent with the hypothesis that Angiotensin II is an important mediator of atrial fibrosis in DM.

Additionally, elevations in blood glucose levels stimulate the production of advanced glycation-end products (AGEs), which can enhance interstitial fibrosis by forming crosslinks between collagen and laminin (Russo and Frangogiannis, 2016). AGEs function by activating their receptors (RAGEs) located on the surface of cardiac fibroblasts, thereby upregulating connective tissue growth factor and stimulating fibroblast proliferation (Kato

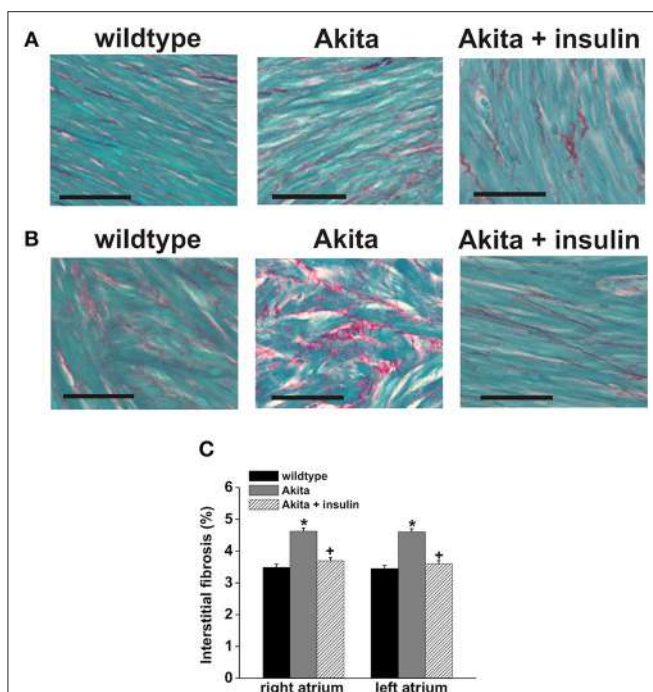


FIGURE 4 | Patterns of interstitial fibrosis in the right (A) and left atria (B) of wildtype Akita mice. The myocardium is stained in green and collagen deposition in red. Scale bars are 50 μ M. (C) The percent interstitial fibrosis is significantly increased both atria in the diabetic mice. Insulin treatment prevents the development of fibrosis in the diabetic mice, * p < 0.05. Reproduced with permission from Krishnaswamy et al. (2015).

et al., 2008). This is referred to as the AGE-RAGE system and is thought to be another important mediator of profibrotic signaling in the atria in DM.

Atrial fibrosis, and hence the substrate for AF, may also be affected by adipokines—important signaling molecules than can be produced in the epicardial fat layer on the surface of the heart and which can act in a paracrine manner. Adipokines such as leptin and adiponectin have been implicated in atrial fibrosis. Leptin levels are elevated in obesity and DM (Karmazyn et al., 2008) and it has been demonstrated that leptin plays an important role in the development of atrial fibrosis. Specifically, the development of atrial fibrosis and the increased susceptibility to AF in response to Angiotensin II treatment increased leptin and was attenuated in leptin deficient ob/ob mice. Angiotensin II was shown to increase leptin expression in wildtype atrial fibroblasts and the addition of leptin increased TGF- β signaling (Fukui et al., 2013). A subsequent study demonstrated that a high fat diet in wildtype mice resulted in hyperleptinemia as well as high susceptibility to AF in association with increased left atrial interstitial fibrosis and that these effects were attenuated in leptin deficient ob/ob mice (Fukui et al., 2017). The role of adiponectin in AF associated with diabetes is much less clear. Adiponectin has insulin sensitizing properties and anti-inflammatory properties and the levels of adiponectin decrease with increasing adiposity (Karmazyn et al., 2008). Interestingly, higher circulating levels of adiponectin have been associated with increased risk of AF

(Macheret et al., 2015). The basis for this observation is unclear and more work is needed to understand the role of adiponectin in cardiovascular diseases including diabetes and its links to AF.

Adipose Tissue

Type II DM presents a unique challenge in understanding the pathogenesis of AF because it typically coincides with obesity. Complications that arise from either condition are not mutually exclusive. Obesity is associated with increased thickness of epicardial adipose tissue (the fat that lies directly adjacent to the epicardium underneath the pericardium), which can have profound consequences on atrial electrophysiology and promote arrhythmogenesis (Abed et al., 2013; Mahajan et al., 2015; Evin et al., 2016). Indeed, increases in epicardial adipose tissue have been found to associate with adverse left atrial remodeling and increased incidence of AF, supporting the idea that epicardial adipose tissue could play an important role in the pathophysiology of AF (Sanghai et al., 2018). Coinciding with the increased epicardial adipose tissue volume, fatty infiltration of the atrial epicardium is also increased (Mahajan et al., 2015). Epicardial adipose tissue infiltration is associated with increased risk of AF due in part to pathological remodeling of epicardial adipose tissue itself whereby organized adipose tissue is replaced with fibro-fatty infiltrates (i.e., lipomatous metaplasia) leading to interstitial fibrosis. Indeed, an ovine model of induced AF revealed increased adipose tissue volume in the left and right atria as well as fibrosis of fatty infiltrates in comparison to their non-AF-induced counterparts (Haemers et al., 2017). Ultimately, this process impairs conduction velocity as well as homogeneity. Much like collagen fibers, fatty tissue is neither conductive nor contractile and can create physical barriers between cardiomyocytes, limiting both electro- and mechanotransduction. Additionally, the presence of these lipid deposits within the myocardium could potentially create re-entry points, further potentiating AF substrate development. It is not known if diabetes exacerbates this pathological process. Finally, epicardial adipose tissue is well-known to produce and release a number of compounds (including cytokines/adipokines, as discussed above) that could act in a paracrine fashion in the atria, thereby influencing atrial remodeling and arrhythmogenesis (Hatem and Sanders, 2014; Nagy et al., 2017). The role of paracrine effects of epicardial adipose tissue in the pathogenesis of AF is an important area for ongoing study.

Electrical Remodeling Ion Channels

Electrical remodeling in DM can also involve alterations in atrial action potential morphology due to changes in a number of ionic currents. Prolongation of the atrial action potential duration has been reported in rabbit and mouse models of Type I DM (Yi et al., 2015; Fu et al., 2016). Similar alterations have been described in the left atrium of Type II diabetic rats (Li et al., 2016). Although incompletely understood, alterations in atrial action potential morphology may involve Na^+ and K^+ channels, as well as Ca^{2+} homeostasis.

Evidence suggests that the Na^+ current (I_{Na}) is reduced in the atria of Type I diabetic rabbits (Liu et al., 2017). In contrast, a

study in Type II diabetic rats reported no differences in atrial I_{Na} (Li et al., 2016). Accordingly, more work is needed to determine how atrial I_{Na} is affected in type I and Type II DM. This is of importance as changes in I_{Na} amplitude affect atrial action potential upstroke velocity and hence conduction velocity. In this way, I_{Na} is an important determinant of the substrate for re-entry. Another aspect of I_{Na} that may be important is the late I_{Na} ($I_{Na,L}$) that can affect arrhythmogenesis by modulating action potential duration and the occurrence of EADs (Sicouri et al., 2013). $I_{Na,L}$ has been shown to be increased in ventricular myocytes in Akita and db/db mice (Lu et al., 2013); however, it is presently unknown if this is also the case in the atria.

K^+ currents play an essential role in action potential repolarization thereby controlling action potential duration and susceptibility to triggered activity (EADs). Several studies have identified changes in K^+ currents in the atria in DM. For example, Type I diabetic (Akita) mice have been shown to have a reduction in atrial acetylcholine-activated K^+ current (I_{KACH}) in association with reduced expression of GIRK1 and GIRK4 (Park et al., 2009; Zhang et al., 2014). These alterations in I_{KACH} and GIRK expression were associated with altered insulin signaling through glycogen synthase kinase 3 and altered transcriptional regulation by sterol regulatory element binding protein 1. A reduction in I_{KACH} could affect atrial action potential duration and arrhythmogenesis; however, the links between I_{KACH} and AF have not been explored in detail.

Separate studies have shown that expression of several other K^+ channels is altered in DM. Specifically, expression of Kv4.2/4.3, the channels that produce the transient outward K^+ current (I_{to}), is reduced in atrial myocytes in mouse models of diet induced obesity and Type II DM. The mechanism for this reduction is unclear, but may involve impaired insulin signaling as Kv4.2 expression has also been shown to be decreased in a cardiac specific insulin receptor knockout mouse (Lopez-Izquierdo et al., 2014).

Other investigations have demonstrated that Type I diabetic mice (STZ treatment) display reduced expression of small conductance Ca^{2+} -activated K^+ channels (SK), including SK2 and SK3 (Yi et al., 2015). These changes in the expression of SK channels occurred in association with increased oxidative stress. Consistent with these animal studies, expression of SK channels (SK1, 2, and 3) was found to be reduced in the atria of human patients with chronic AF (Yu et al., 2012; Skibsbye et al., 2014). Additional studies are needed to better understand the links between SK channel function, diabetes, and AF.

Gap Junctions

Gap junctions play an integral role in cell to cell communication and electrical conduction. These gap junctions are composed of connexin (Cx) proteins, with Cx40 and Cx43 being the predominant isoforms in the atrial myocardium. While data are limited, there is evidence of changes in Cx expression and function in the atria in DM. For example, it has been shown that Cx40 expression is reduced in the atria in a rat model of Type I DM. Consistent with this alteration in Cx40, optical mapping experiments showed that conduction velocity in the atria was reduced and conduction patterns lacked homogeneity (Figure 5)

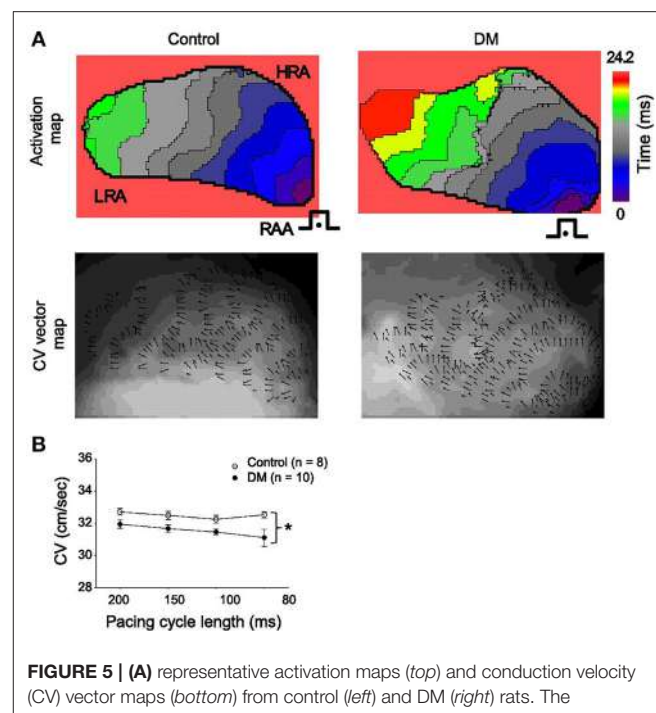


FIGURE 5 | (A) representative activation maps (top) and conduction velocity (CV) vector maps (bottom) from control (left) and DM (right) rats. The isochrones on the activation maps are drawn at 2.2 ms intervals. Pacing is (●) from the right atrial appendage (RAA) at a cycle length of 200 ms. The color scale bar ranged from 0 to 24.2 ms. Isochronal crowding is evident within right atrium (RA) of DM rats. The CV vector map and the direction and magnitude of focal CV vectors varies widely within RA from DM rats. **(B)** Mean CVs at different pacing cycle lengths in control ($n = 8$) and DM ($n = 10$) rats. $*P < 0.01$ vs. control. Reproduced with permission from Watanabe et al. (2012).

(Watanabe et al., 2012). These observations are in agreement with studies showing increased atrial arrhythmogenesis in Cx40 deficient mice (Hagendorff et al., 1999).

Cx43 expression in the atria does not appear to be changed in the setting of Type I or Type II DM. However, there is evidence that its subcellular distribution is altered. For example, in Type II diabetic rats, Cx43 expression was not changed, but these animals displayed increased lateralization of Cx43 in the left atrium (Li et al., 2016). Lateralization of connexins would increase conduction heterogeneity because fewer Cx43-comprised gap junctions would be localized to the intercalated disks. Consistent with this hypothesis, lateralization of Cx43 and altered conduction has also been demonstrated in the ventricles of rats with Type I DM (Nygren et al., 2007).

Translational Considerations: Glycemic Control and AF

A few clinical studies have attempted to elucidate association between markers of glycemic control and AF. An analysis of the Framingham Heart Study Offspring cohort followed for ≤ 10 years reported no association between insulin resistance and incident AF (Fontes et al., 2012). In contrast, in the Malmo Preventive Project, higher levels of fasting plasma insulin were associated with a lower risk of AF (Johnson et al., 2014). This relationship was significant only in the male cohort although the proportion of women

included in this study was lower (33%). Furthermore, the association was weaker in subjects with elevated fasting glucose. Spontaneous hypoglycemia has been reported to be significantly associated with the development of AF in Type II DM (Ko et al., 2018). However, the mechanism underlying this relationship is unknown. Our experimental data in Type I DM demonstrates that acute and chronic insulin therapy prevents the downregulation of the sodium current and reduces the inducibility of AF. This effect is mediated, in part, via phosphatidylinositol 3,4,5-triphosphate (Bohne et al., 2018). We have also shown that insulin treatment in this model also reduces the development of atrial fibrosis. Together these data suggest that insulin mitigates, at least in part, the development of the substrate for atrial reentry (Krishnaswamy et al., 2015).

A Danish nationwide cohort study investigated the role of thiazolidinediones compared to other second line diabetes therapy in 108,624 patients with DM and without prior AF who were treated with metformin or sulfonylurea as first line drug therapy (Pallisgaard et al., 2017). Thiazolidinediones compared to other second line diabetes therapy significantly reduced the risk of AF (HR 0.76, 95% CI 0.57–1.00). A subsequent meta-analysis was undertaken including three randomized clinical trials and four observational studies of 130,854 diabetic patients (Zhang et al., 2017). Overall, thiazolidinediones were associated with a 27% lower risk of developing AF compared to controls. Pioglitazone was reported to have a more beneficial effect for AF prevention compared to rosiglitazone. In an experimental model of Type II DM, rosiglitazone attenuated the atrial structural remodeling and vulnerability to AF (Liu et al., 2014). A more recent study, the Bypass Angioplasty Revascularization Investigation 2 Diabetes trial, randomized patients with Type II DM to insulin sensitization therapy vs. insulin provision therapy. The incidence of AF was similar in both patient groups (HR 0.91, 95% CI 0.60–1.38). Furthermore, the incidence rate of AF in those treated with thiazolidinediones was similar in those not treated with thiazolidinediones. Together these data suggest that glycemic control prevents adverse atrial remodeling and propensity to AF in DM. However, the current data do not support a unique drug specific effect for AF prevention.

Vascular Disease in DM

DM is associated with an accelerated development and increased risk of atherosclerosis. However, DM has been reported to be an independent risk factor for AF in most observational studies (Xiong et al., 2018). Nevertheless, coronary microvascular dysfunction characterized by reduced coronary flow reserve and endothelial dysfunction are associated with DM and precede the development of overt cardiac disease (Kibel et al., 2017). These abnormalities may develop as a consequence of metabolic, hormonal, hemodynamic, neural, and other factors associated with DM. Abnormalities of endothelial function may precede the development of AF (Shaikh et al., 2016). However, whether the presence of microvascular dysfunction directly influences the substrate for AF requires more experimental and clinical investigation.

Autonomic Dysfunction and AF

Abnormalities of the autonomic nervous system may play a role in the pathogenesis of AF. Autonomic neuropathy is a frequent complication associated with DM although data on the association of this complication with AF is limited. A strong relationship between autonomic dysfunction measured using heart rate variability as the marker of autonomic function and silent AF has been reported in patients with type 2 DM (Rizzo et al., 2015). Heart rate recovery, another index of autonomic function, has also been reported to be predictive of a risk for AF in type 2 DM independent of left atrial volume index and other clinical factors including hypertension and coronary artery disease suggesting a role for autonomic dysfunction in the pathogenesis of AF in DM (Negishi et al., 2013). The underlying cellular mechanisms have not been extensively studied and require further investigation.

Catheter Ablation and AF

Catheter ablation is an established therapy for symptomatic patients with AF. Some (Anselmino et al., 2015; Bunch et al., 2015; Akkaya et al., 2018; Budzianowski et al., 2018) but not all (Bogossian et al., 2016; Winkle et al., 2016) studies have suggested that recurrence rates in patients with DM undergoing catheter ablation are higher than in non-diabetic patients. However, in a meta-analysis of 15 studies including 1,464 patients with DM, long term maintenance of sinus rhythm following a redo procedure was similar to rates reported among the general population undergoing catheter ablation. In this meta-analysis, higher body mass index and higher glycated hemoglobin levels were associated with higher AF recurrence rates suggesting a role for the metabolic abnormalities in DM in promoting arrhythmogenesis (Anselmino et al., 2015).

Role of Computational Modeling

Computational biology and modeling can be powerful approaches for studying the mechanistic basis for cardiac arrhythmias, including in DM. Whenever possible, these approaches should be considered in order to complement clinical and basic science research as well as to generate new hypotheses that can then be tested in established models and in patients. Computational approaches have proven to be a valuable and important approach in assessing the links between DM and AF. In this regard, a recent study used a machine learning approach to automatically select studies for inclusion in an updated meta-analysis of the association between DM and new onset AF (Xiong et al., 2018). This study showed that machine learning could accurately and objectively select studies for inclusion in meta-analyses, which is important given that the exponential growth in numbers of publications makes manual selection increasingly challenging. This machine learning study demonstrates that DM is a strong, independent risk factor for AF (Xiong et al., 2018).

Computational modeling and simulations based on mechanistic insights into AF triggers and substrate derived from both experimental and clinical studies may also facilitate the development of safer and more effective therapeutic interventions (Boyle et al., 2016; Grandi and Malek, 2016).

In this regard, advanced analysis of the ECG and integration of detailed clinical data including cardiac imaging, biomarkers and genomics may facilitate the development of more precision directed medical therapy (Gillis et al., 2013; Boyle et al., 2016). Future studies are required to evaluate the role of personalized computational models for individualizing therapeutic strategies for the AF patient with DM.

Future Research Directions

Experimental data demonstrate that significant atrial electrical, structural and autonomic remodeling occur in both Type I and Type II DM and increase the vulnerability to AF. Whether the insulin resistance in type II DM activates unique intracellular signaling pathways independent of obesity requires further investigation. Future studies are also required to investigate the inter-relationships between obesity, hypertension, DM, obstructive sleep apnea, and other factors associated with the metabolic syndrome including systemic inflammation

and oxidative stress. The relationship between incident AF and glycemic control also requires further investigation. In addition, the role of computational models in directing more precision therapy for AF in this setting requires further study.

AUTHOR CONTRIBUTIONS

All authors listed have made a substantial, direct and intellectual contribution to the work, and approved it for publication.

FUNDING

This work was supported by operating grants from the Canadian Institutes of Health Research to RR (MOP 142486, 93718). RR holds a New Investigator Award from the Heart and Stroke Foundation of Canada. LB holds a Libin Cardiovascular Institute of Alberta Graduate Studentship.

REFERENCES

- Abed, H. S., Samuel, C. S., Lau, D. H., Kelly, D. J., Royce, S. G., Alasady, M., et al. (2013). Obesity results in progressive atrial structural and electrical remodeling: implications for atrial fibrillation. *Heart Rhythm* 10, 90–100. doi: 10.1016/j.hrthm.2012.08.043
- Akkaya, E., Berkowitsch, A., Zaltsberg, S., Greiss, H., Hamm, C. W., Sperzel, J., et al. (2018). Five-year outcome and predictors of success after second-generation cryoballoon ablation for treatment of symptomatic atrial fibrillation. *Int. J. Cardiol.* 266, 106–111. doi: 10.1016/j.ijcard.2018.03.069
- Anselmino, M., Matta, M., D'aszenzo, F., Pappone, C., Santinelli, V., Bunch, T. J., et al. (2015). Catheter ablation of atrial fibrillation in patients with diabetes mellitus: a systematic review and meta-analysis. *Europace* 17, 1518–1525. doi: 10.1093/europace/euv214
- Arias-Mutis, O. J., Marrachelli, V. G., Ruiz-Sauri, A., Alberola, A., Morales, J. M., Such-Miquel, L., et al. (2017). Development and characterization of an experimental model of diet-induced metabolic syndrome in rabbit. *PLoS ONE* 12:e0178315. doi: 10.1371/journal.pone.0178315
- Benjamin, E. J., Levy, D., Vaziri, S. M., D'agostino, R. B., Belanger, A. J., and Wolf, P. A. (1994). Independent risk factors for atrial fibrillation in a population-based cohort: The Framingham Heart Study. *JAMA* 271, 840–844. doi: 10.1001/jama.1994.03510350050036
- Bogossian, H., Frommeyer, G., Brachmann, J., Lewalter, T., Hoffmann, E., Kuck, K. H., et al. (2016). Catheter ablation of atrial fibrillation and atrial flutter in patients with diabetes mellitus: who benefits and who does not? Data from the German ablation registry. *Int. J. Cardiol.* 214, 25–30. doi: 10.1016/j.ijcard.2016.03.069
- Bohne, L. J., Polina, I., Jansen, H. J., Li, T., Krishnaswamy, P., Egom, E. E., et al. (2018). Distinct effects of acute and chronic insulin treatment on atrial electrophysiology and susceptibility to atrial fibrillation in type 1 diabetes mellitus. *Heart Rhythm* 15, Suppl. S7 (abstract).
- Boyle, P. M., Zahid, S., and Trayanova, N. A. (2016). Towards personalized computational modelling of the fibrotic substrate for atrial arrhythmia. *Europace* 18, iv136–iv145. doi: 10.1093/europace/euw358
- Budzianowski, J., Hiczkiewicz, J., Burchardt, P., Pieszko, K., Rzezniczak, J., Budzianowski, P., et al. (2018). Predictors of atrial fibrillation early recurrence following cryoballoon ablation of pulmonary veins using statistical assessment and machine learning algorithms. *Heart Vessels* 34, 352–359. doi: 10.1007/s00380-018-1244-z
- Bunch, T. J., May, H. T., Bair, T. L., Jacobs, V., Crandall, B. G., Cutler, M., et al. (2015). Five-year outcomes of catheter ablation in patients with atrial fibrillation and left ventricular systolic dysfunction. *J. Cardiovasc. Electrophysiol.* 26, 363–370. doi: 10.1111/jce.12602
- Dahlqvist, S., Rosengren, A., Gudbjornsdottir, S., Pivodic, A., Wedel, H., Kosiborod, M., et al. (2017). Risk of atrial fibrillation in people with type 1 diabetes compared with matched controls from the general population: a prospective case-control study. *Lancet Diabetes Endocrinol.* 5, 799–807. doi: 10.1016/S2213-8587(17)30262-0
- Evin, M., Broadhouse, K. M., Callaghan, F. M., McGrath, R. T., Glastras, S., Kozor, R., et al. (2016). Impact of obesity and epicardial fat on early left atrial dysfunction assessed by cardiac MRI strain analysis. *Cardiovasc. Diabetol.* 15:164. doi: 10.1186/s12933-016-0481-7
- Fiaschi, T., Magherini, F., Gamberi, T., Lucchese, G., Faggian, G., Modesti, A., et al. (2014). Hyperglycemia and angiotensin II cooperate to enhance collagen I deposition by cardiac fibroblasts through a ROS-STAT3-dependent mechanism. *Biochim. Biophys. Acta* 1843, 2603–2610. doi: 10.1016/j.bbamcr.2014.07.009
- Fontes, J. D., Lyass, A., Massaro, J. M., Rienstra, M., Dallmeier, D., Schnabel, R. B., et al. (2012). Insulin resistance and atrial fibrillation (from the Framingham Heart Study). *Am. J. Cardiol.* 109, 87–90. doi: 10.1016/j.amjcard.2011.08.008
- Fu, H., Li, G., Liu, C., Li, J., Cheng, L., Yang, W., et al. (2016). Probucol prevents atrial ion channel remodeling in an alloxan-induced diabetes rabbit model. *Oncotarget* 7, 83850–83858. doi: 10.18632/oncotarget.13339
- Fu, H., Li, G., Liu, C., Li, J., Wang, X., Cheng, L., et al. (2015). Probucol prevents atrial remodeling by inhibiting oxidative stress and TNF-alpha/NF-kappaB/TGF-beta signal transduction pathway in alloxan-induced diabetic rabbits. *J. Cardiovasc. Electrophysiol.* 26, 211–222. doi: 10.1111/jce.12540
- Fukui, A., Ikebe-Ebata, Y., Kondo, H., Saito, S., Aoki, K., Fukunaga, N., et al. (2017). Hyperleptinemia exacerbates high-fat diet-mediated atrial fibrosis and fibrillation. *J. Cardiovasc. Electrophysiol.* 28, 702–710. doi: 10.1111/jce.13200
- Fukui, A., Takahashi, N., Nakada, C., Masaki, T., Kume, O., Shinohara, T., et al. (2013). Role of leptin signaling in the pathogenesis of angiotensin II-mediated atrial fibrosis and fibrillation. *Circ. Arrhythm. Electrophysiol.* 6, 402–409. doi: 10.1161/CIRCEP.111.000104
- Gillis, A. M., Krah, A. D., Skanes, A. C., and Nattel, S. (2013). Management of atrial fibrillation in the year 2033: new concepts, tools, and applications leading to personalized medicine. *Can. J. Cardiol.* 29, 1141–1146. doi: 10.1016/j.cjca.2013.07.006
- Grandi, E., and Maleckar, M. M. (2016). Anti-arrhythmic strategies for atrial fibrillation: the role of computational modeling in discovery, development, and optimization. *Pharmacol. Ther.* 168, 126–142. doi: 10.1016/j.pharmthera.2016.09.012
- Haemers, P., Hamdi, H., Guedj, K., Suffee, N., Farahmand, P., Popovic, N., et al. (2017). Atrial fibrillation is associated with the fibrotic remodelling of adipose

- tissue in the subepicardium of human and sheep atria. *Eur. Heart J.* 38, 53–61. doi: 10.1093/eurheartj/ehv625
- Hagendorff, A., Schumacher, B., Kirchhoff, S., Luderitz, B., and Willecke, K. (1999). Conduction disturbances and increased atrial vulnerability in Connexin40-deficient mice analyzed by transesophageal stimulation. *Circulation* 99, 1508–1515. doi: 10.1161/01.CIR.99.11.1508
- Hatem, S. N., and Sanders, P. (2014). Epicardial adipose tissue and atrial fibrillation. *Cardiovasc. Res.* 102, 205–213. doi: 10.1093/cvr/cvu045
- Hayami, N., Sekiguchi, A., Iwasaki, Y. K., Murakawa, Y., and Yamashita, T. (2016). No additional effect of DPP-4 inhibitor on preventing atrial fibrosis in streptozotocin-induced diabetic rat as compared with sulfonylurea. *Int. Heart J.* 57, 336–340. doi: 10.1536/ihj.15-266
- Heijman, J., Guichard, J. B., Dobrev, D., and Nattel, S. (2018). Translational challenges in atrial fibrillation. *Circ. Res.* 122, 752–773. doi: 10.1161/CIRCRESAHA.117.311081
- Heijman, J., Voigt, N., Nattel, S., and Dobrev, D. (2014). Cellular and molecular electrophysiology of atrial fibrillation initiation, maintenance, and progression. *Circ. Res.* 114, 1483–1499. doi: 10.1161/CIRCRESAHA.114.302226
- Hohl, M., Lau, D. H., Muller, A., Elliott, A. D., Linz, B., Mahajan, R., et al. (2017). Concomitant obesity and metabolic syndrome add to the atrial arrhythmogenic phenotype in male hypertensive rats. *J. Am. Heart Assoc.* 6:e006717. doi: 10.1161/JAHA.117.006717
- Hsueh, W., Abel, E. D., Breslow, J. L., Maeda, N., Davis, R. C., Fisher, E. A., et al. (2007). Recipes for creating animal models of diabetic cardiovascular disease. *Circ. Res.* 100, 1415–1427. doi: 10.1161/01.RES.0000266449.37396.1f
- Hutchinson, K. R., Lord, C. K., West, T. A., and Stewart, J. A. Jr. (2013). Cardiac fibroblast-dependent extracellular matrix accumulation is associated with diastolic stiffness in type 2 diabetes. *PLoS ONE* 8:e72080. doi: 10.1371/journal.pone.0072080
- Huxley, R. R., Alonso, A., Lopez, F. L., Filion, K. B., Agarwal, S. K., Loehr, L. R., et al. (2012). Type 2 diabetes, glucose homeostasis and incident atrial fibrillation: the Atherosclerosis Risk in Communities study. *Heart* 98, 133–138. doi: 10.1136/heartjnl-2011-300503
- Huxley, R. R., Filion, K. B., Konety, S., and Alonso, A. (2011). Meta-analysis of cohort and case-control studies of type 2 diabetes mellitus and risk of atrial fibrillation. *Am. J. Cardiol.* 108, 56–62. doi: 10.1016/j.amjcard.2011.03.004
- Johnson, L. S., Juhlin, T., Engstrom, G., and Nilsson, P. M. (2014). Low fasting plasma insulin is associated atrial fibrillation in men from a cohort study—the Malmö preventive project. *BMC Cardiovasc. Disord.* 14:107. doi: 10.1186/1471-2261-14-107
- Karmazyn, M., Purdham, D. M., Rajapurohitam, V., and Zeidan, A. (2008). Signalling mechanisms underlying the metabolic and other effects of adipokines on the heart. *Cardiovasc. Res.* 79, 279–286. doi: 10.1093/cvr/cvn115
- Kato, T., Yamashita, T., Sekiguchi, A., Tsuneda, T., Sagara, K., Takamura, M., et al. (2008). AGEs-RAGE system mediates atrial structural remodeling in the diabetic rat. *J. Cardiovasc. Electrophysiol.* 19, 415–420. doi: 10.1111/j.1540-8167.2007.01037.x
- Kibel, A., Selhofer-Relatik, K., Drenjancevic, I., Bacun, T., Bosnjak, I., Kibel, D., et al. (2017). Coronary microvascular dysfunction in diabetes mellitus. *J. Int. Med. Res.* 45, 1901–1929. doi: 10.1177/0300060516675504
- King, A. J. (2012). The use of animal models in diabetes research. *Br. J. Pharmacol.* 166, 877–894. doi: 10.1111/j.1476-5381.2012.01911.x
- Ko, S. H., Park, Y. M., Yun, J. S., Cha, S. A., Choi, E. K., Han, K., et al. (2018). Severe hypoglycemia is a risk factor for atrial fibrillation in type 2 diabetes mellitus: nationwide population-based cohort study. *J. Diabetes Complicat.* 32, 157–163. doi: 10.1016/j.jdiacomp.2017.09.009
- Krahn, A. D., Manfreda, J., Tate, R. B., Mathewson, F. A., and Cuddy, T. E. (1995). The natural history of atrial fibrillation: incidence, risk factors, and prognosis in the Manitoba Follow-Up Study. *Am. J. Med.* 98, 476–484. doi: 10.1016/S0002-9343(99)80348-9
- Krishnaswamy, P. S., Egom, E. E., Moghadasie, M., Jansen, H. J., Azer, J., Bogachev, O., et al. (2015). Altered parasympathetic nervous system regulation of the sinoatrial node in Akita diabetic mice. *J. Mol. Cell. Cardiol.* 82, 125–135. doi: 10.1016/j.yjmcc.2015.02.024
- Lamberts, R. R., Lingam, S. J., Wang, H. Y., Bollen, I. A., Hughes, G., Galvin, I. F., et al. (2014). Impaired relaxation despite upregulated calcium-handling protein atrial myocardium from type 2 diabetic patients with preserved ejection fraction. *Cardiovasc. Diabetol.* 13:72. doi: 10.1186/1475-2840-13-72
- Li, B., Pan, Y., and Li, X. (2016). Type 2 diabetes induces prolonged P-wave duration without left atrial enlargement. *J. Korean Med. Sci.* 31, 525–534. doi: 10.3346/jkms.2016.31.4.525
- Linz, D., Hohl, M., Dhein, S., Ruf, S., Reil, J. C., Kabiri, M., et al. (2016). Cathepsin A mediates susceptibility to atrial tachyarrhythmia and impairment of atrial emptying function in Zucker diabetic fatty rats. *Cardiovasc. Res.* 110, 371–380. doi: 10.1093/cvr/cvw071
- Liu, C., Liu, R., Fu, H., Li, J., Wang, X., Cheng, L., et al. (2017). Pioglitazone attenuates atrial remodeling and vulnerability to atrial fibrillation in alloxan-induced diabetic rabbits. *Cardiovasc. Ther.* 35:e12284. doi: 10.1111/1755-5922.12284
- Liu, T., Zhao, H., Li, J., Korantzopoulos, P., and Li, G. (2014). Rosiglitazone attenuates atrial structural remodeling and atrial fibrillation promotion in alloxan-induced diabetic rabbits. *Cardiovasc. Ther.* 32, 178–183. doi: 10.1111/1755-5922.12079
- Lopez-Izquierdo, A., Pereira, R. O., Wende, A. R., Punske, B. B., Abel, E. D., and Tristani-Firouzi, M. (2014). The absence of insulin signaling in the heart induces changes in potassium channel expression and ventricular repolarization. *Am. J. Physiol. Heart Circ. Physiol.* 306, H747–H754. doi: 10.1152/ajpheart.00849.2013
- Lu, Z., Jiang, Y. P., Wu, C. Y., Ballou, L. M., Liu, S., Carpenter, E. S., et al. (2013). Increased persistent sodium current due to decreased PI3K signaling contributes to QT prolongation in the diabetic heart. *Diabetes* 62, 4257–4265. doi: 10.2337/db13-0420
- Macheret, F., Bartz, T. M., Djousse, L., Ix, J. H., Mukamal, K. J., Zieman, S. J., et al. (2015). Higher circulating adiponectin levels are associated with increased risk of atrial fibrillation in older adults. *Heart* 101, 1368–1374. doi: 10.1136/heartjnl-2014-307015
- Mahajan, R., Lau, D. H., Brooks, A. G., Shipp, N. J., Manavis, J., Wood, J. P., et al. (2015). Electrophysiological, electroanatomical, and structural remodeling of the atria as consequences of sustained obesity. *J. Am. Coll. Cardiol.* 66, 1–11. doi: 10.1016/j.jacc.2015.04.058
- Nagy, E., Jermendy, A. L., Merkely, B., and Maurovich-Horvat, P. (2017). Clinical importance of epicardial adipose tissue. *Arch. Med. Sci.* 13, 864–874. doi: 10.5114/aoms.2016.63259
- Negishi, K., Seicean, S., Negishi, T., Yingchoncharoen, T., Aljaroudi, W., and Marwick, T. H. (2013). Relation of heart-rate recovery to new onset heart failure and atrial fibrillation in patients with diabetes mellitus and preserved ejection fraction. *Am. J. Cardiol.* 111, 748–753. doi: 10.1016/j.amjcard.2012.11.028
- Nygren, A., Olson, M. L., Chen, K. Y., Emmett, T., Kargacin, G., and Shimoni, Y. (2007). Propagation of the cardiac impulse in the diabetic rat heart: reduced conduction reserve. *J. Physiol.* 580, 543–560. doi: 10.1113/jphysiol.2006.123729
- Pallisgaard, J. L., Lindhardt, T. B., Staerk, L., Olesen, J. B., Torp-Pedersen, C., Hansen, M. L., et al. (2017). Thiazolidinediones are associated with a decreased risk of atrial fibrillation compared with other antidiabetic treatment: a nationwide cohort study. *Eur. Heart J. Cardiovasc. Pharmacother.* 3, 140–146. doi: 10.1093/ehjcvp/pvw036
- Pallisgaard, J. L., Schjerning, A. M., Lindhardt, T. B., Procida, K., Hansen, M. L., Torp-Pedersen, C., et al. (2016). Risk of atrial fibrillation in diabetes mellitus: a nationwide cohort study. *Eur. J. Prev. Cardiol.* 23, 621–627. doi: 10.1177/2047487315599892
- Park, H. J., Zhang, Y., Du, C., Welzig, C. M., Madias, C., Aronovitz, M. J., et al. (2009). Role of SREBP-1 in the development of parasympathetic dysfunction in the hearts of type 1 diabetic Akita mice. *Circ. Res.* 105, 287–294. doi: 10.1161/CIRCRESAHA.109.193995
- Patel, V. B., Bodiga, S., Basu, R., Das, S. K., Wang, W., Wang, Z., et al. (2012). Loss of angiotensin-converting enzyme-2 exacerbates diabetic cardiovascular complications and leads to systolic and vascular dysfunction: a critical role of the angiotensin II/AT1 receptor axis. *Circ. Res.* 110, 1322–1335. doi: 10.1161/CIRCRESAHA.112.268029
- Perez, M. V., Wang, P. J., Larson, J. C., Soliman, E. Z., Limacher, M., Rodriguez, B., et al. (2013). Risk factors for atrial fibrillation and their population burden in postmenopausal women: the Women's Health Initiative Observational Study. *Heart* 99, 1173–1178. doi: 10.1136/heartjnl-2013-303798
- Rizzo, M. R., Sasso, F. C., Marfella, R., Siniscalchi, M., Paolisso, P., Carbonara, O., et al. (2015). Autonomic dysfunction is associated with brief episodes

- of atrial fibrillation in type 2 diabetes. *J. Diabetes Complicat.* 29, 88–92. doi: 10.1016/j.jdiacomp.2014.09.002
- Russo, I., and Frangogiannis, N. G. (2016). Diabetes-associated cardiac fibrosis: cellular effectors, molecular mechanisms and therapeutic opportunities. *J. Mol. Cell. Cardiol.* 90, 84–93. doi: 10.1016/j.yjmcc.2015.12.011
- Saito, S., Teshima, Y., Fukui, A., Kondo, H., Nishio, S., Nakagawa, M., et al. (2014). Glucose fluctuations increase the incidence of atrial fibrillation in diabetic rats. *Cardiovasc. Res.* 104, 5–14. doi: 10.1093/cvr/cvu176
- Samanta, R., Pouliopoulos, J., Thiagalingam, A., and Kovoov, P. (2016). Role of adipose tissue in the pathogenesis of cardiac arrhythmias. *Heart Rhythm* 13, 311–320. doi: 10.1016/j.hrthm.2015.08.016
- Sanghai, S. R., Sardana, M., Hansra, B., Lessard, D. M., Dahlberg, S. T., Aurigemma, G. P., et al. (2018). Indexed left atrial adipose tissue area is associated with severity of atrial fibrillation and atrial fibrillation recurrence among patients undergoing catheter ablation. *Front. Cardiovasc. Med.* 5:76. doi: 10.3389/fcvm.2018.00076
- Schnabel, R. B., Yin, X., Gona, P., Larson, M. G., Beiser, A. S., Mcmanus, D. D., et al. (2015). 50 year trends in atrial fibrillation prevalence, incidence, risk factors, and mortality in the Framingham Heart Study: a cohort study. *Lancet* 386, 154–162. doi: 10.1016/S0140-6736(14)61774-8
- Schoen, T., Pradhan, A. D., Albert, C. M., and Conen, D. (2012). Type 2 diabetes mellitus and risk of incident atrial fibrillation in women. *J. Am. Coll. Cardiol.* 60, 1421–1428. doi: 10.1016/j.jacc.2012.06.030
- Schotten, U., Dobrev, D., Platonov, P. G., Kottkamp, H., and Hindricks, G. (2016). Current controversies in determining the main mechanisms of atrial fibrillation. *J. Intern. Med.* 279, 428–438. doi: 10.1111/joim.12492
- Sedgwick, B., Riches, K., Baggeghni, S. A., O'regan, D. J., Porter, K. E., and Turner, N. A. (2014). Investigating inherent functional differences between human cardiac fibroblasts cultured from nondiabetic and Type 2 diabetic donors. *Cardiovasc. Pathol.* 23, 204–210. doi: 10.1016/j.carpath.2014.03.004
- Shaikh, A. Y., Wang, N., Yin, X., Larson, M. G., Vasan, R. S., Hamburg, N. M., et al. (2016). Relations of arterial stiffness and brachial flow-mediated dilation with new-onset atrial fibrillation: the Framingham Heart Study. *Hypertension* 68, 590–596. doi: 10.1161/HYPERTENSIONAHA.116.07650
- Sicouri, S., Belardinelli, L., and Antzelevitch, C. (2013). Antiarrhythmic effects of the highly selective late sodium channel current blocker GS-458967. *Heart Rhythm* 10, 1036–1043. doi: 10.1016/j.hrthm.2013.03.023
- Singh, V. P., Baker, K. M., and Kumar, R. (2008a). Activation of the intracellular renin-angiotensin system in cardiac fibroblasts by high glucose: role in extracellular matrix production. *Am. J. Physiol. Heart Circ. Physiol.* 294, H1675–H1684. doi: 10.1152/ajpheart.91493.2007
- Singh, V. P., Le, B., Khode, R., Baker, K. M., and Kumar, R. (2008b). Intracellular angiotensin II production in diabetic rats is correlated with cardiomyocyte apoptosis, oxidative stress, and cardiac fibrosis. *Diabetes* 57, 3297–3306. doi: 10.2337/db08-0805
- Skibsbye, L., Poulet, C., Diness, J. G., Bentzen, B. H., Yuan, L., Kappert, U., et al. (2014). Small-conductance calcium-activated potassium (SK) channels contribute to action potential repolarization in human atria. *Cardiovasc. Res.* 103, 156–167. doi: 10.1093/cvr/cvu121
- Son, M. K., Lim, N. K., Cho, M. C., and Park, H. Y. (2016). Incidence and risk factors for atrial fibrillation in Korea: the national health insurance service database (2002–2010). *Korean Circ. J.* 46, 515–521. doi: 10.4070/kcj.2016.46.4.515
- Staerk, L., Sherer, J. A., Ko, D., Benjamin, E. J., and Helm, R. H. (2017). Atrial fibrillation: epidemiology, pathophysiology, and clinical outcomes. *Circ. Res.* 120, 1501–1517. doi: 10.1161/CIRCRESAHA.117.309732
- Toblli, J. E., Cao, G., Derosa, G., and Forcada, P. (2005). Reduced cardiac expression of plasminogen activator inhibitor 1 and transforming growth factor beta1 in obese Zucker rats by perindopril. *Heart* 91, 80–86. doi: 10.1136/heart.2003.022707
- Tsao, C. W., and Vasan, R. S. (2015). The Framingham Heart Study: past, present and future. *Int. J. Epidemiol.* 44, 1763–1766. doi: 10.1093/ije/dyv336
- Watanabe, M., Yokoshiki, H., Mitsuyama, H., Mizukami, K., Ono, T., and Tsutsui, H. (2012). Conduction and refractory disorders in the diabetic atrium. *Am. J. Physiol. Heart Circ. Physiol.* 303, H86–H95. doi: 10.1152/ajpheart.00010.2012
- Winkle, R. A., Jarman, J. W., Mead, R. H., Engel, G., Kong, M. H., Fleming, W., et al. (2016). Predicting atrial fibrillation ablation outcome: the CAAP-AF score. *Heart Rhythm* 13, 2119–2125. doi: 10.1016/j.hrthm.2016.07.018
- Xiong, Z., Liu, T., Tse, G., Gong, M., Gladding, P. A., Smaill, B. H., et al. (2018). A machine learning aided systematic review and meta-analysis of the relative risk of atrial fibrillation in patients with diabetes mellitus. *Front. Physiol.* 9:835. doi: 10.3389/fphys.2018.00835
- Yi, F., Ling, T. Y., Lu, T., Wang, X. L., Li, J., Claycomb, W. C., et al. (2015). Down-regulation of the small conductance calcium-activated potassium channels in diabetic mouse atria. *J. Biol. Chem.* 290, 7016–7026. doi: 10.1074/jbc.M114.607952
- Yu, T., Deng, C., Wu, R., Guo, H., Zheng, S., Yu, X., et al. (2012). Decreased expression of small-conductance Ca^{2+} -activated K^{+} channels SK1 and SK2 in human chronic atrial fibrillation. *Life Sci.* 90, 219–227. doi: 10.1016/j.lfs.2011.11.008
- Zarzoso, M., Mironov, S., Guerrero-Serna, G., Willis, B. C., and Pandit, S. V. (2014). Ventricular remodelling in rabbits with sustained high-fat diet. *Acta Physiol.* 211, 36–47. doi: 10.1111/apha.12185
- Zhang, Y., Welzig, C. M., Picard, K. L., Du, C., Wang, B., Pan, J. Q., et al. (2014). Glycogen synthase kinase-3beta inhibition ameliorates cardiac parasympathetic dysfunction in type 1 diabetic Akita mice. *Diabetes* 63, 2097–2113. doi: 10.2337/db12-1459
- Zhang, Z., Zhang, X., Korantzopoulos, P., Letsas, K. P., Tse, G., Gong, M., et al. (2017). Thiazolidinedione use and atrial fibrillation in diabetic patients: a meta-analysis. *BMC Cardiovasc. Disord.* 17:96. doi: 10.1186/s12872-017-0531-4

Conflict of Interest Statement: SW–Consulting Arca Biopharma and <5,000. AG–Medtronic Inc research support.

The remaining authors declare that the research was conducted in the absence of any commercial or financial relationships that could be construed as a potential conflict of interest.

Copyright © 2019 Bohne, Johnson, Rose, Wilton and Gillis. This is an open-access article distributed under the terms of the Creative Commons Attribution License (CC BY). The use, distribution or reproduction in other forums is permitted, provided the original author(s) and the copyright owner(s) are credited and that the original publication in this journal is cited, in accordance with accepted academic practice. No use, distribution or reproduction is permitted which does not comply with these terms.



Understanding the Beat-to-Beat Variations of P-Waves Morphologies in AF Patients During Sinus Rhythm: A Scoping Review of the Atrial Simulation Studies

Dimitrios Filos^{1*}, **Dimitrios Tachmatzidis**², **Nicos Maglaveras**^{1,3}, **Vassilios Vassilikos**² and **Ioanna Chouvarda**¹

¹ Lab of Computing, Medical Informatics and Biomedical Imaging Technologies, School of Medicine, Aristotle University of Thessaloniki, Thessaloniki, Greece, ² 3rd Cardiology Department, Aristotle University of Thessaloniki, Thessaloniki, Greece,

³ Department of Industrial Engineering and Management Sciences, Northwestern University, Evanston, IL, United States

OPEN ACCESS

Edited by:

Edward Joseph Vigmond,
Université de Bordeaux, France

Reviewed by:

Mark Potse,
Inria Bordeaux – Sud-Ouest Research
Centre, France
Martin Bishop,
King's College London,
United Kingdom

*Correspondence:

Dimitrios Filos
dimfilos@auth.gr

Specialty section:

This article was submitted to
Computational Physiology
and Medicine,
a section of the journal
Frontiers in Physiology

Received: 15 May 2018

Accepted: 28 May 2019

Published: 18 June 2019

Citation:

Filos D, Tachmatzidis D, Maglaveras N, Vassilikos V and Chouvarda I (2019) Understanding the Beat-to-Beat Variations of P-Waves Morphologies in AF Patients During Sinus Rhythm: A Scoping Review of the Atrial Simulation Studies. *Front. Physiol.* 10:742. doi: 10.3389/fphys.2019.00742

The remarkable advances in high-performance computing and the resulting increase of the computational power have the potential to leverage computational cardiology toward improving our understanding of the pathophysiological mechanisms of arrhythmias, such as Atrial Fibrillation (AF). In AF, a complex interaction between various triggers and the atrial substrate is considered to be the leading cause of AF initiation and perpetuation. In electrocardiography (ECG), P-wave is supposed to reflect atrial depolarization. It has been found that even during sinus rhythm (SR), multiple P-wave morphologies are present in AF patients with a history of AF, suggesting a higher dispersion of the conduction route in this population. In this scoping review, we focused on the mechanisms which modify the electrical substrate of the atria in AF patients, while investigating the existence of computational models that simulate the propagation of the electrical signal through different routes. The adopted review methodology is based on a structured analytical framework which includes the extraction of the keywords based on an initial limited bibliographic search, the extensive literature search and finally the identification of relevant articles based on the reference list of the studies. The leading mechanisms identified were classified according to their scale, spanning from mechanisms in the cell, tissue or organ level, and the produced outputs. The computational modeling approaches for each of the factors that influence the initiation and the perpetuation of AF are presented here to provide a clear overview of the existing literature. Several levels of categorization were adopted while the studies which aim to translate their findings to ECG phenotyping are highlighted. The results denote the availability of multiple models, which are appropriate under specific conditions. However, the consideration of complex scenarios taking into account multiple spatiotemporal scales, personalization of electrophysiological and anatomical models and the reproducibility in terms of ECG phenotyping has only partially been tackled so far.

Keywords: atrial fibrillation, multiple P-wave morphologies, sinus rhythm, computational models, simulation, scoping review

INTRODUCTION

Over a century ago, Atrial Fibrillation (AF) had been recognized as the most common arrhythmia in adults (Nishida and Nattel, 2014). It is characterized by chaotic atrial activation leading to impaired atrial myocardial function. It is easily recognized on a surface electrocardiogram by lack of atrial depolarization represented by P-wave, quivering isoelectric line and irregular ventricular activation represented by QRS-complexes, which lead to contractile dysfunction (Pellman and Sheikh, 2015). In the case that AF converts to normal sinus rhythm (SR) within 7 days, it is classified as “paroxysmal,” while in the case of it lasting more than 7 days or more than a year it is classified as “persistent” or “long-standing persistent,” respectively (Camm et al., 2012a; Kirchhof et al., 2016).

Atrial fibrillation is associated with increased morbidity and mortality as it is widely recognized as a risk factor for embolic stroke and heart failure (HF) exacerbation (Camm et al., 2012b). On the other hand, numerous risk factors have been correlated with the development of AF. Aging doubles AF risk per decade, whereas gender influences the incidence of AF with males having 1.5 fold risk to develop AF (Andrade et al., 2014). Most cases of persistent and permanent AF are related to hypertensive, valvular, ischaemic or other types of structural heart disease, while lone AF represents only 15% of the cases (Markides and Schilling, 2003).

Initiation and maintenance of the abnormal rhythm in both lone AF and AF secondary to structural heart disease are supposed to require pathophysiological remodeling of the atria (Pellman and Sheikh, 2015). Remodeling can be grouped into three categories that include:

- (i) electrical remodeling, including modulation of L-type Ca^{2+} current, various K^{+} currents, and gap junction function,
- (ii) structural remodeling, including changes in tissues properties, size, and ultrastructure, and
- (iii) autonomic remodeling, including altered sympathovagal activity, and hyperinnervation (Pellman and Sheikh, 2015).

Electrical, structural, and autonomic remodeling all contribute to creating an AF-prone substrate which can produce AF-associated electrical phenomena including a rapidly firing focus, complex multiple reentrant circuits, or rotors (Nattel, 2002). Since the 1960s, the most popular theory has held that AF consists of multiple wavelets of functional re-entry (Moe et al., 1964). Conditions that increase the atrial size or decrease the wavelength (by decreasing the conduction velocity or refractory period or both) permit multiple wavelets and promote AF (Rensma et al., 1988).

Multiple factors have been found to relate and contribute to AF initiation or perpetuation mechanisms. Ionic currents and gap junction function are considered to be fundamental parts of electrical remodeling occurring in atrial cardiomyocytes, which leads to reduced action potential (AP) duration and refractoriness and affects conduction velocity and wavelength, both known determinants of AF initiation and

perpetuation (Gaspo et al., 1997; Pellman and Sheikh, 2015). Atrial enlargement has been associated with AF many decades ago (Henry et al., 1976). Moreover, scarring, fibrosis, and increased atrial size observed in HF patients, are related to conduction delay and refractory period prolongation (Sanders et al., 2003). The autonomic nervous system (ANS) exerts significant control over cardiac electrophysiology, while it has been proposed that patterns of baseline autonomic nerve activity are essential in the development of pacing-induced sustained AF (Shen et al., 2011). There is a suggestion that the increased sympathetic activity leads to heterogeneous changes in atrial refractoriness, which in turn favors reentrant waves that generally contribute to the maintenance of AF (Olgin et al., 1998). On the other hand, ablation of the ganglionated plexi can also improve long-term AF symptoms (Katritsis et al., 2013). Additionally, the muscular sleeves of the pulmonary veins (PVs) have been identified as a source of tachyarrhythmias and atrial premature beats that could trigger paroxysms of AF (Haïssaguerre et al., 1998). These findings lead to a unifying theory that focal tachycardias (mostly originating from the PVs) promote atrial remodeling and they are required to trigger and maintain a substrate capable of multiple wavelet reentry (Veenhuyzen et al., 2004). AF causes electrophysiological changes in the atrial myocardium itself, which might explain the progressive nature of the arrhythmia. In a landmark study, the perpetuation of AF was accompanied by a shortening of the atrial refractory period inducing electrophysiologic changes that promote further AF. These include electrical, contractile and structural modifications to the atria that have collectively become known as atrial remodeling and the authors concluded that “AF begets AF” (Wijffels et al., 1995). However, most of the findings are based on electrophysiological studies making the reproducibility of the experiments a challenging case.

The interplay of different factors contributing to AF and the inherent complexity of the biological systems, necessitates the development of computational models across different levels, from the cell, tissue, and patient level. Computational modeling can help study and shed light on the mechanisms of AF, and thus new therapeutic approaches can be developed and tested before applying them to patients (Jacquemet, 2016). The main advantage of computational modeling is that researchers have access to all levels of interest and thus they can perform experiments in controlled and repeatable conditions, which is a limitation of experimental and clinical research. The increased evidence on the importance and the effectiveness of computational modeling in several fields of science, including cardiac electrophysiology, in association with the advances in the computational speed (Virag et al., 2012) and the availability of such infrastructure, were the primary catalysts on the increased interest in the field of computational modeling during the recent years. Overall, computational modeling can link the phenomenological organ level findings, such as findings in the electrocardiography (ECG), and the actual mechanisms at smaller scales.

As regards the AF patients, the analysis of P-wave during SR is of clinical value, since P-wave morphology is affected by the site of origin of the SR beat and the atrial conduction routes (Platonov, 2012). The analysis of P-waves can reveal

information related to the prediction of AF initiation (Martínez et al., 2014a) or the success of the pulmonary vein isolation (Huo et al., 2015). Also, the analysis of the P-wave morphology variability, on a beat-to-beat basis, also revealed differences between healthy subjects and AF patients (Censi et al., 2016; Filos et al., 2017). However, the direct correlation of those ECG findings with the underlying substrate modifications is not well understood. The motivation behind this research was to find what mechanisms may explain the difference in the percentage of the primary/secondary P-wave morphologies observed in ECG signals of paroxysmal AF vs. normal subjects, and more importantly whether these mechanisms were studied, quantified and reproduced via simulation studies. To serve this need, we designed a scoping review, (a) to map the existing literature in the field of atrial models and their multifaceted properties/components related to AF, and (b) to synthesize this knowledge toward explaining the link between observable AF-related P-wave morphologies and computational atrial models of AF. Finally, this work attempts to identify the research gaps and to make recommendations for future research.

METHODOLOGY

We conducted a scoping review adopting the methodology proposed by Arksey and O’Malley (2005) and Peters et al. (2015). The aim of scoping reviews is to map existing literature in a particular field as well as to synthesize the knowledge. The definition proposed by Colquhoun et al. (2014) states that “A scoping review or scoping study is a form of knowledge synthesis that addresses an exploratory research question aimed at mapping key concepts, types of evidence, and gaps in research related to a defined area or field by systematically searching, selecting, and synthesizing existing knowledge.”

Objective

We focused on the identification of the mechanisms, either on cell, tissue or organ level, which can describe the variation of the P-wave morphologies in AF patients during SR while we tried to investigate the existence of computational models which can reproduce those mechanisms. The following research questions were posed:

- (1) How was AF modeled?
- (2) Which computational models were proposed for the description of patients prone to AF during SR?
- (3) How was the initiation of AF episodes modeled?
- (4) Were those models able to reproduce the multiple P-wave morphologies that appear in AF patients during SR?

The primary outcomes that are of interest in this scoping review are the characteristics of the AF substrate which describe atrial remodeling occurring as a result of AF. The comprehension of such mechanisms may lead to get more insights on the prediction of the AF onset and thus facilitate the management of patients in terms of the prevention and adaptation of the therapeutic approach.

Inclusion Criteria

We applied the PICO (Population, Intervention, Comparator, and Outcome) eligibility criteria. Regarding the population, we considered all AF studies without distinction between human and animal models. All types of AF were considered, including Asymptomatic, Paroxysmal, Persistent, or Permanent. As for the intervention, any level of computational models that enabled the simulation of the atrial activation was eligible for inclusion. Models focusing on the cell or tissue level, as well as on the organ level were examined.

Studies comparing simulated and real ECG phenotyping or comparison of different computational models were included in the literature review as well as studies without a comparator, such as theoretical models. Finally, any publication, such as articles, conference proceedings, editorials and chapters in textbooks, published after 1998 until 1 of March 2018, written in English was included in the review, whereas all review articles were excluded.

Search Strategy

A two steps search strategy was adopted to map the existing research on this topic. Two databases, which are extensively used in biomedical sciences, were searched (PubMed and Scopus). Initially, a limited search in both databases was undertaken followed by an analysis of the text words contained in the title and the abstract as well as on the indexed terms of the article. The second search step included the extensive literature search based on the keywords extracted in the first step and the manual inspection of the studies.

Regarding the text analysis made during the first step, review articles, published during the last 10 years, in which the words “cardiac” and “simulation” were included in their title or abstract were selected, as they are considered to cover the field of the current review. As a result, 115 and 163 articles were found in PubMed and Scopus, respectively. After removing the duplicates, 216 review papers were screened, whereas only 99 review articles were found to be relevant to our study. Subsequently, a text analysis of the titles and the abstract was conducted. A table of the most frequent words and phrases was produced, while equivalent words were identified (e.g., modeling and modeling). The word cloud depicted in **Figure 1** presents in a visual way the most frequent words. The most common phrases were found to be “computation model*,” “mathematical model*,” or “computer model*,” which describe the same process. On the other hand, the word “model*” and “simulat*” appeared in the same abstract, but not necessarily accompanied, to describe the same approach as the phrases above. The asterisk (*) following a word describes all of the words starting with the phrase before it [e.g., model(s), modeling are described as model*]. Based on these findings we formulated the first two blocks of **Figure 2**, which are connected to an OR logical gate. The terms “cardiac,” “atrial,” and “heart” were extracted as the most frequent words, that are related to the description of the model or the tissue of interest. Finally, the term “Atrial Fibrillation” was not extracted by the text analysis but it was used since each article was focused on AF.

These findings led to the creation of the search query that was used in the second step of the literature review

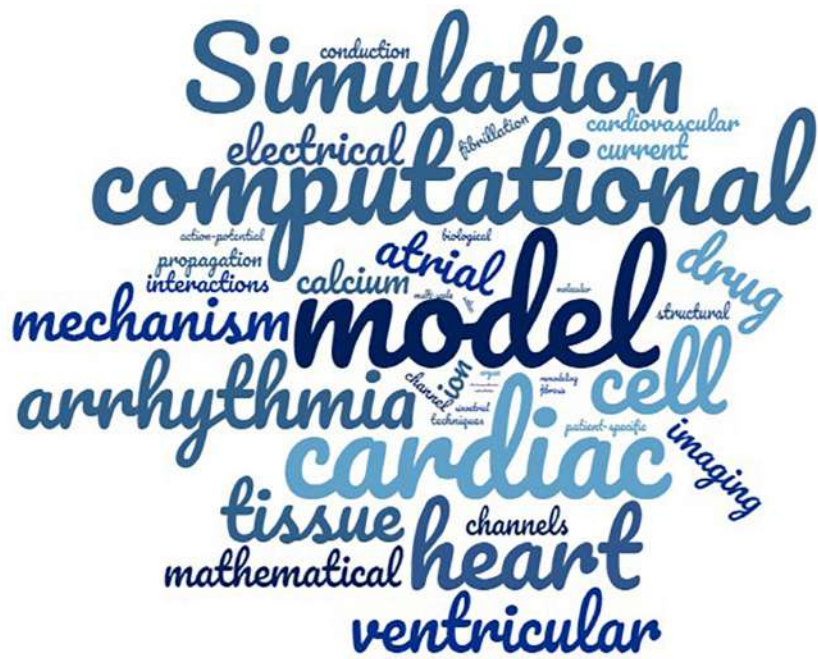


FIGURE 1 | Word cloud of the most frequent words, where the highest the font the higher the frequency. For the purposes of the visualization the terms model, models, modeling, and modeling were grouped under the term “model.” As depicted, the most used words are model, cardiac, computational, simulation, heart, and with frequencies 16.6, 11.16, 7.2, 6.5, and 5.7%, respectively.

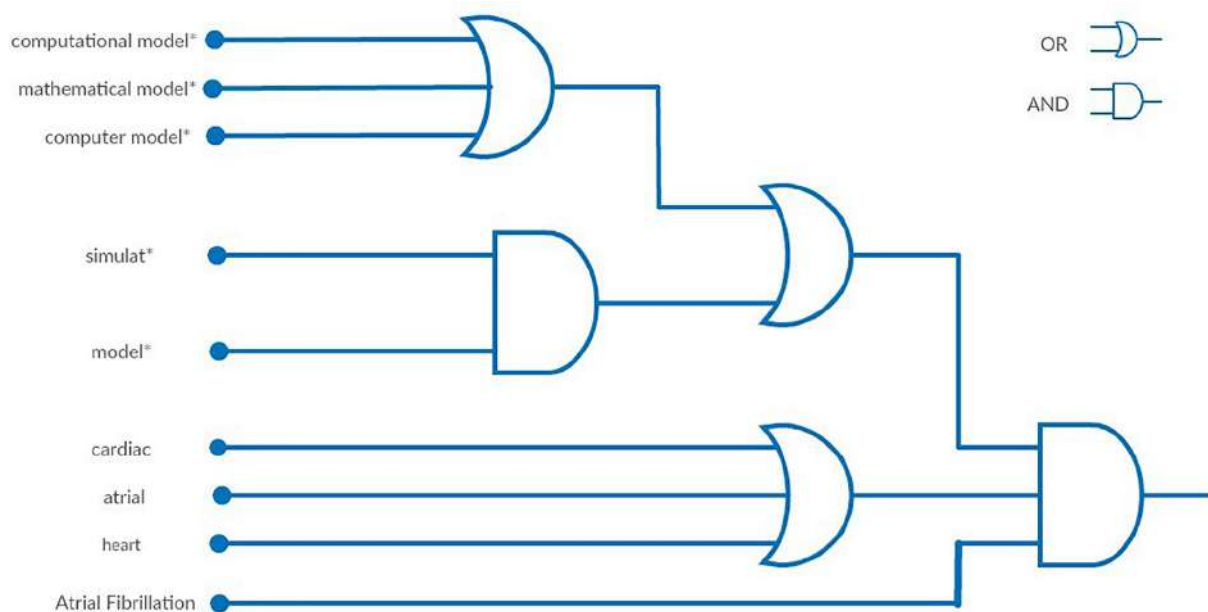


FIGURE 2 | Visual representation of the final query using logic gates. The final query is described as: (((“computational model*”[Title/Abstract] OR “mathematical model*”[Title/Abstract] OR “computer model*”[Title/Abstract]) OR (simulat*[Title/Abstract] AND model*[Title/Abstract])) AND (“cardiac”[Title/Abstract] OR “atrial”[Title/Abstract] OR “heart”[Title/Abstract])) AND “atrial fibrillation”[Text Word].

(Figure 2). In this step, the words and phrases identified were searched in the abstract, the title or the indexed keywords. The whole literature search, its evaluation, and categorization were

conducted independently by two reviewers (DF and DT). After the completion of the evaluation, in case of disagreement, the two reviewers worked together to reach a consensus.

RESULTS

A total number of 721 articles (excluding duplicates) was raised. Titles and abstracts were screened to check whether they are relevant to the research question or not. Approximately half of them (377) were eligible for full-text review. Seventy-six articles were excluded, resulting in a total of 301 articles which were finally included in the review (Figure 3). The observation of Figure 4 reveals a continuous increase in the number of articles published over time.

Modeling Components

The interplay of multiple factors can lead to the initiation and perpetuation of the arrhythmia (Kirchhof et al., 2016). In this section, the existing literature in the field of atrial models is presented while a categorization of the articles was made based on the factors that are addressed in each simulation study.

Model Experimental Context

Animal studies

While in the first years, the ratio between the studies focusing on humans or animals was approximately 1:1, during the last decade, an increased interest in human studies is observed (Figure 5). The animal studies can improve our understanding of

the pathophysiological properties of AF while their findings can be useful in human studies.

A detailed model of the canine atrial cell is presented by Ramirez et al. (2000) which is applicable in both normal and electrically remodeled cellular substrate. The following years, additional animal models were proposed able to describe the sheep (Goodman et al., 2005; Butters et al., 2013), rat (Majumder et al., 2016) or other animals' atrial myocardium (Aslanidi et al., 2009b). A novel computational model of the canine left atrium (LA) and PVs is proposed by Cherry et al. (2007) and Aslanidi et al. (2011a) through which an attempt was made to understand the arrhythmogenicity of PV and how re-entries and their geometry can promote their excitation. The differences between the right atrium (RA) and LA in terms of the electrophysiological properties in the animals are described in Aslanidi et al. (2009a) and in Xia et al. (2010).

Aslanidi et al. (2008) studied the effects of Ca^{2+} concentration in the cell of the RA in terms of AF initiation. According to the simulation performed in a cell and tissue level, no crucial effect of intracellular Ca^{2+} concentration on reentries has been observed as its results are reversible. Furthermore, Kneller et al. (2005) studied the influence of antiarrhythmic drugs in the canine atrium, and found that the inhibition of pure Na current during AF can terminate the arrhythmia.

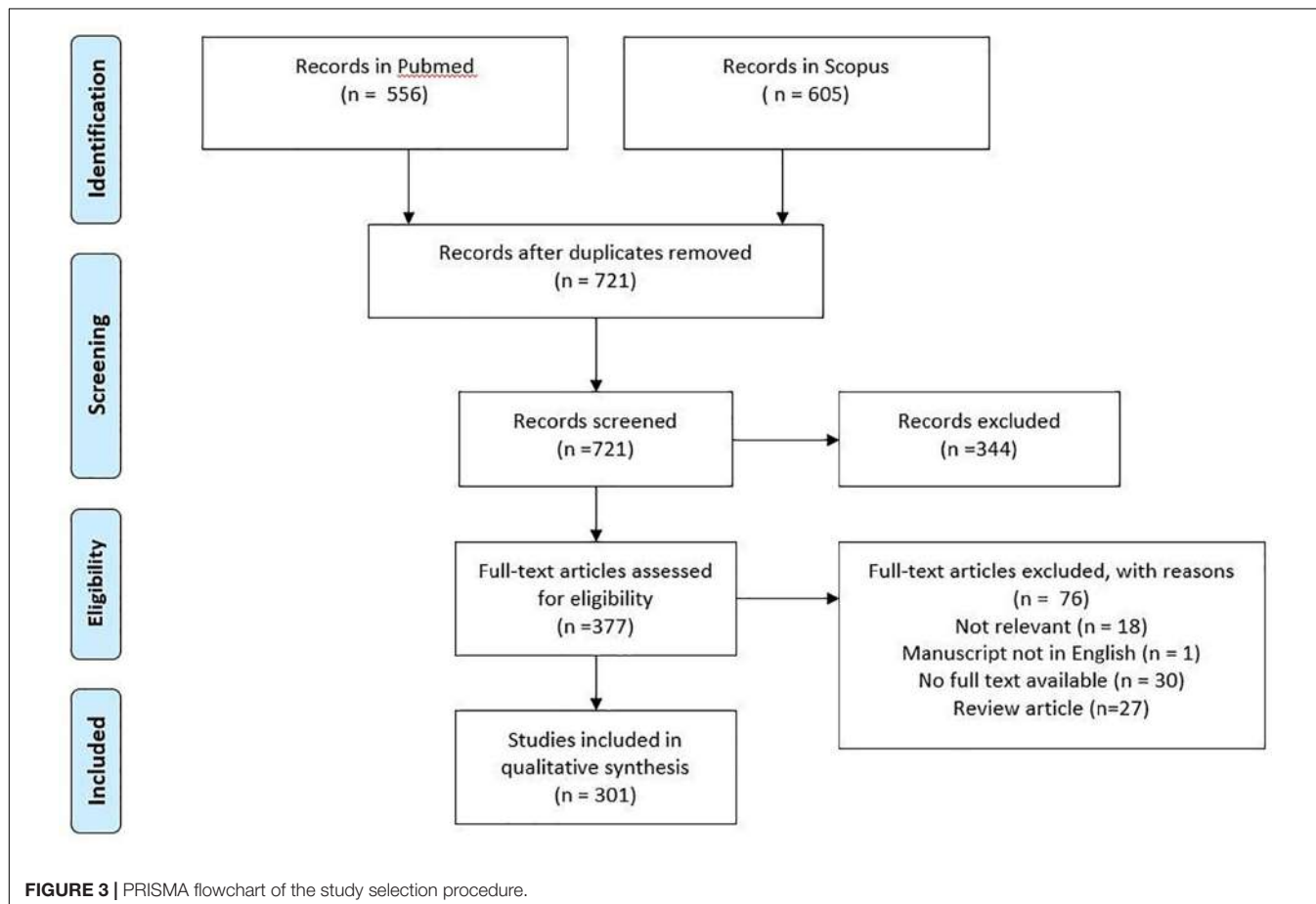


FIGURE 3 | PRISMA flowchart of the study selection procedure.

Evolution of the number of articles

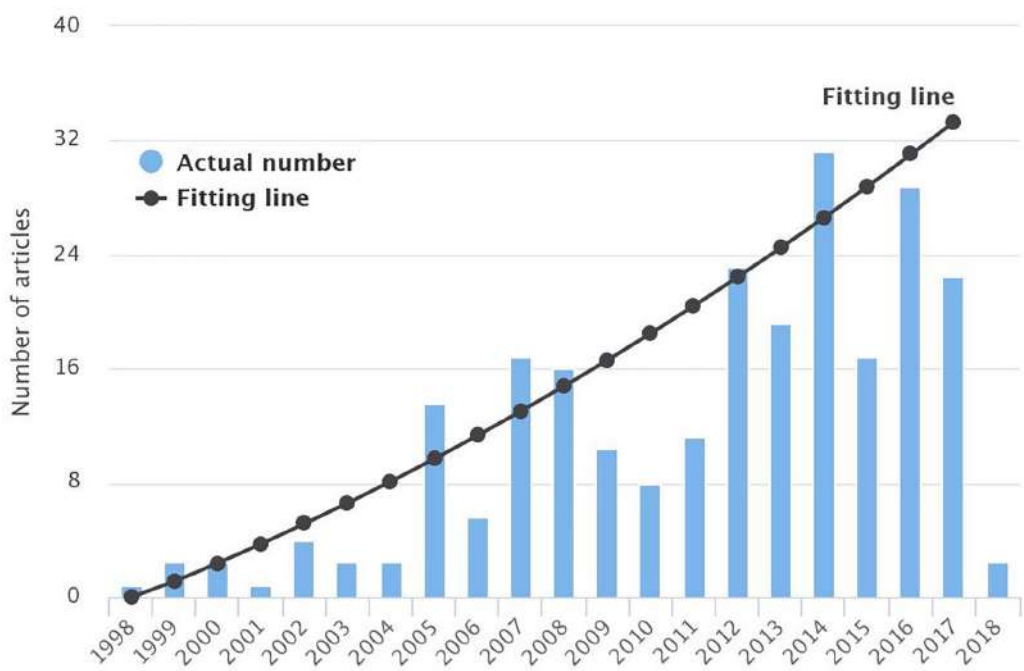


FIGURE 4 | Evolution of the number of publications in the field of AF modeling from 1998 till 1st March 2018. A parabolic line was found to fit better the data depicted in the bars ($R^2 = 0.7609$).

Human and animal studies

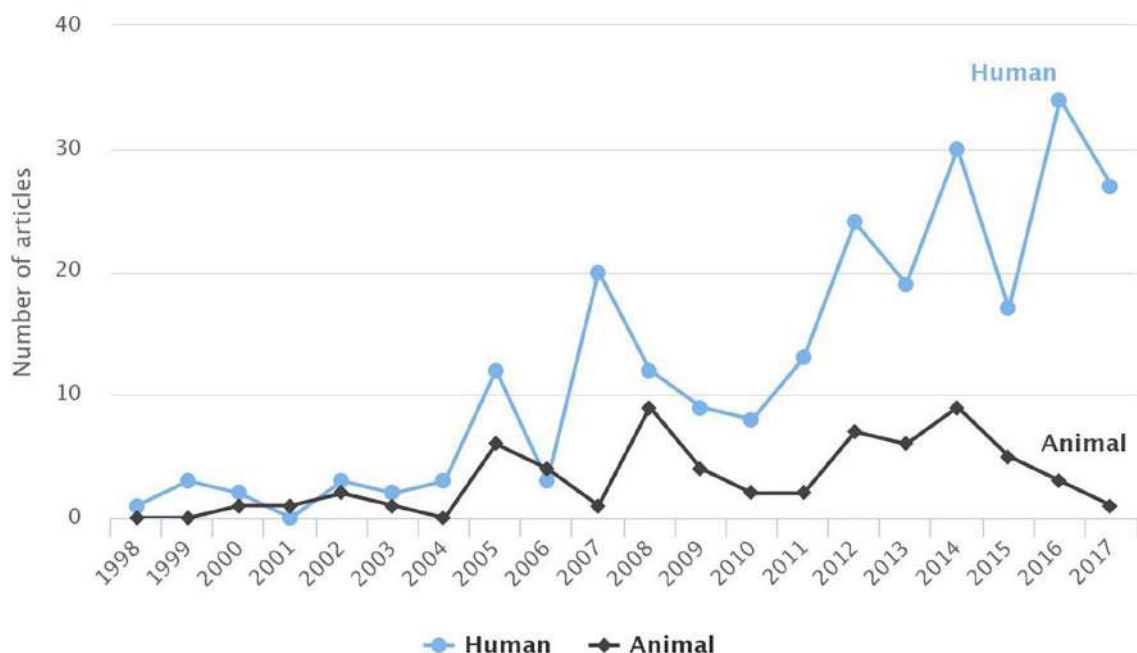


FIGURE 5 | Comparison of the studies based on human or animal models for AF for each year. For 2018, until 1st of March 2018, the studies targeting humans and animals were 3 and 0, respectively. To avoid any false perception those data have not been visualized.

Other mechanisms were also addressed in animal models before being incorporated in the human ones, such as the effect of ANS (Kneller et al., 2002) and of the antiarrhythmic drugs (Comtois et al., 2008; Almquist et al., 2010; Aguilar-Shardonofsky et al., 2012; Colman et al., 2014; Aguilar et al., 2015; Varela et al., 2016).

Vigmond et al. (2001) presented a morphologically realistic atrial model where all the major anatomical structures of the atrium, including fiber orientation, muscle structures such as crista terminalis and pectinate muscles and the orifices of the veins and valves, were considered and scaled to a canine atrium level. The resulting model did not consist of an exact representation of the atria. However, it reflected the interrelations between atrial anatomical structures. Zhao et al. (2012) proposed a detailed structural model of the sheep atria which was based on *ex vivo* analysis of the atrial chambers. The details of the fiber orientations and myofiber architecture were incorporated into an anatomical model. The simulation performed in normal and electrically remodeled conditions, confirm the unique roles of crista terminalis, pectinate muscles and Bachman's bundle on the activation time as well as the differences on the electrical propagation through the posterior LA.

In addition to animal models, many studies are taking into account findings from experiments performed on animals, to modify the human model. The goal of those studies extends from studying the effects of drug therapy (Gomez et al., 2005; Ehrlich et al., 2008) to impact of gene mutations (Hancox et al., 2014; Syeda et al., 2016).

Evaluation of model output

Computational modeling is by nature an approximation of reality and several approaches have been adopted to evaluate their output. However, most of the studies employed *in silico* experiments, rather than a direct evaluation of the simulation outputs with real recordings. On the other hand, some of the articles included a comparison between the *in silico* and the *in vivo* findings, based on electrophysiological findings (Courtemanche et al., 1998, 1999; Ramirez et al., 2000;

Wettwer et al., 2004; Kneller et al., 2005; Kuijpers et al., 2007; Comtois et al., 2008; Lombardo et al., 2016). Furthermore, the reproducibility of the simulated signals, electrograms or ECG, with the real recordings is discussed in the context of solving the forward (Ogawa et al., 2007; Burdumy et al., 2012) or inverse problem (Pedron-Torrecilla et al., 2016). Finally, the need for personalized anatomical and electrical models is highlighted toward the highest reproducibility of the results (Krueger et al., 2013c; Roney et al., 2016).

Model Electrophysiological Components at Different Scales

Electrophysiological cell models in humans

The core of each study is the electrophysiological model which describes the cellular ionic properties and transmembrane currents. A plethora of different approaches has been proposed to simulate electrical activity in human atria.

Initially, a common approach was the use of models describing the ventricular activity, such as those of Beeler and Reuter (1977) or Luo and Rudy (1991), to simulate atrial excitation (Virag et al., 2002). On the other hand, membrane kinetics describing the atrial myocardium in animals, such as in canines, have been applied in the human atrium (Ruchat et al., 2007b,c), hypothesizing similar ionic properties.

The CRN (Courtemanche et al., 1998) and Nygren et al. (1998) models are the first attempts to describe the ionic mechanism of the atrial myocytes in humans. The CRN model was based on adaptations made on a model describing ventricular myocytes. The Maleckar et al. (2009) model refined the description of Nygren model's K^{2+} current, while the Koivumäki et al. (2011) extended the Nygren model in order to improve the description of the Ca^{2+} dynamics. The Grandi et al. (2011) model focuses on patients with chronic AF (cAF) and in SR. Figure 6 depicts the number of articles focusing on the human atria that were based on each of the most frequently used electrophysiological models. The most frequently used model is the one proposed by Courtemanche et al. (1998). Compared to the first decade (1998–2007), the number of articles for AF which

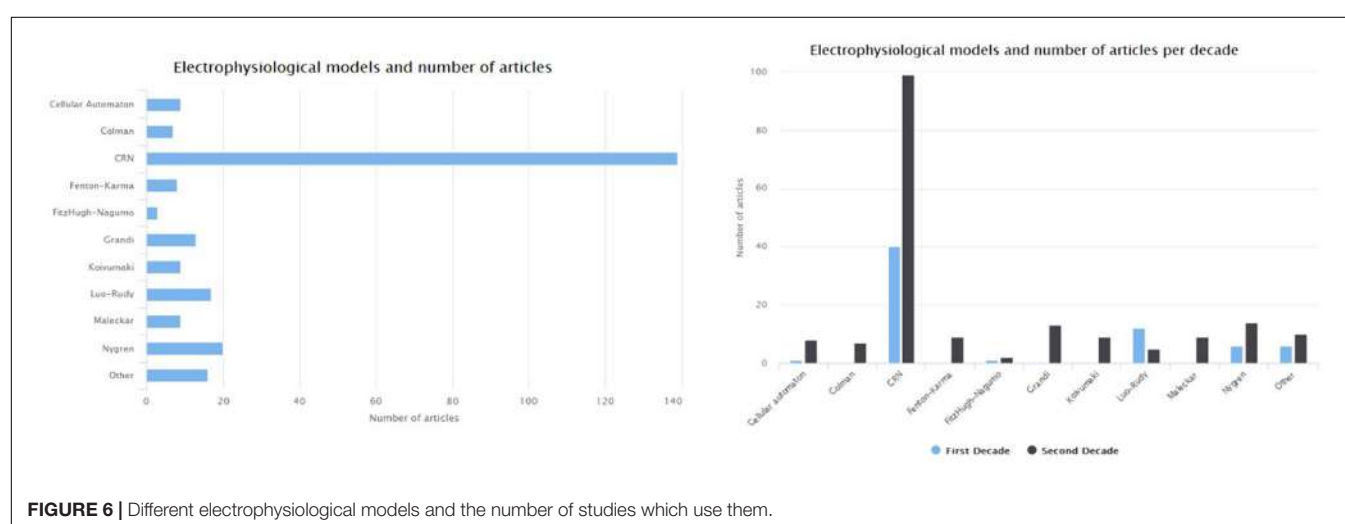


FIGURE 6 | Different electrophysiological models and the number of studies which use them.

adopt ventricular models [such as that of Luo and Rudy (1991)] decreased to half in the second decade (2008–2018). On the other side, the newly proposed models by Koivumäki et al. (2011), Grandi et al. (2011), and Colman et al. (2016) seem to gain the research community's acceptance.

Cherry and Evans (2008), as well as Krueger et al. (2013a) focused on the comparison of electrophysiological models. In particular, Krueger et al. (2013a) performed a comparison between CRN, Nygren, and Maleckar electrophysiological models adjusted to describe 13 different atrial regions heterogeneities, including electrical remodeling. A detailed and personalized MRI-based anatomical model, including fiber orientation detail and thorax model, was estimated for each of the eight patients to reproduce P and Ta-wave accurately. According to the results, the CRN model simulates better action potential duration (APD) in each of the atrial regions compared with the remaining two models. Furthermore, the simulated P-waves and Ta-waves morphology calculated using the CRN models fitted well with the experimental recordings in both physiological and AF-remodeled conditions. Wilhelms et al. (2013) compared the five most frequently used electrophysiological models of human atria and presented the main strengths and weaknesses of each of the models. Lombardo et al. (2016) performed a comparison between two electrophysiological models, a detailed and a simpler one. The results showed that both models reproduce the clinical recordings and the spiral waves dynamics were similar and thus, in the case that computationa cost is crucial, simple models could be used to model arrhythmias in spatially extended domains.

On the other hand, some articles (Ciaccio et al., 2017; Lin et al., 2017) adopted the use of a cellular automaton model (CA) like the one proposed by Moe et al. (1964), which was the first CA model for AF. In general, CA models describe the depolarization and repolarization of a cell based on rules of its present state as well as on its neighbors while more detailed CA models have been proposed recently (Manani et al., 2016). The main property of a CA model is that it is suitable for observation of macroscopic properties of the electrical propagation since it is a simplified model of cardiac electrophysiology and the required computational load is low.

Genes and mutations

Several studies reveal the occurrence of AF on a family basis which implies a genetic cause of this arrhythmia. Genetic mutations have been found to lead to modification of ionic channel functionality. The first study identified is the one of Seemann et al. (2004) where a 2D model of the RA was used to investigate the effect of a mutation in the KCNQ1 gene on the initiation of AF. In the following years, the effect of additional gene mutations or gene expressions on the initiation of AF was studied (Table 1). In all these studies, the parameters of the atrial models have been modified accordingly, to reproduce the findings from the electrophysiological studies. Most of the studies addressed the effect on the slow delayed outward rectifier potassium channel (I_{Ks}) (Seemann et al., 2004; Ehrlich et al., 2005; Kharche et al., 2012a) as well as on other potassium (Seemann et al., 2009) or sodium channels (Ziyadeh-Isleem et al., 2014).

TABLE 1 | Genes identified and modeled.

Gene	Articles
KCNQ1	Seemann et al., 2004; Hong et al., 2005; Sampson et al., 2008; Kharche et al., 2012a; Mann et al., 2012; Ki et al., 2014; Hancox et al., 2014
KCNE1	Ehrlich et al., 2005; Sampson et al., 2008; Mann et al., 2012
KCNH2	Carrillo et al., 2008; Seemann et al., 2009; Mann et al., 2012
KCNJ2	Kharche et al., 2008; Aslanidi et al., 2012a; Mann et al., 2012; Whittaker et al., 2017
KCNA5	Mann et al., 2012; Ni et al., 2014, 2017a
SCN5A	Ziyadeh-Isleem et al., 2014
ANK2	Wolf et al., 2013
PITX2	Syeda et al., 2016
hERG	Loewe et al., 2014; Lutz et al., 2014
KCND3, KCNIP2, KCNH2, KCNE3, KCNE4, KCNE5, KCNJ4, and KCNJ14	Mann et al., 2012

While most articles focus on the effects of gene expression on a cell or 2D tissue model, Whittaker et al. (2017) studied the stability of the re-entrant waves using a realistic atrial model. Finally, Ni et al. (2017a) examined six observed mutations of KCNA5 regarding their role in the electromechanical function of the atrium. Half of those mutations lead to gain-of-function resulting in a worsening of the contractile function of the atrium while the rest lead to loss-of-function of that mediated the positive inotropic effects.

Modeling drug effect on atrial cells and AF

Several types of antiarrhythmic drugs have been analyzed *in silico* regarding their performance on the termination of AF (Ehrlich et al., 2008; Sanchez et al., 2017), under SR and AF (Aslanidi et al., 2012a). Table 2 summarizes the studies focusing on each anti-arrhythmic drug category (class I to v).

The first study identified in this context, Namba et al. (1999) investigated the effects of a specific sodium channel blocker drug on the stability versus meandering of spiral waves in a canine atrial model.

One of the major challenges of antiarrhythmic drug therapy is the minimization of side effects, like QT prolongation and ventricular pro-arrhythmic conditions (Aguilar-Shardonofsky et al., 2012; Aguilar et al., 2015). A key concept to address these challenges is the design of drugs with atrial selectivity. Since ultrarapid delayed rectifying potassium current (I_{Kur}) is present in atrial and absent from ventricular myocardium, it is a justified target for AF antiarrhythmic therapy (Almquist et al., 2010). However, the effect of such a (I_{Kur}) blocker may be pro-arrhythmic during sinus rhythm and anti-arrhythmic during AF (Law et al., 2010). Moreover, the effect of selective (fast and slow onset) blockers of I_{Kur} depends on the level of electrical remodeling (Wettwer et al., 2004; Tsujimae et al., 2008). Although I_{Kur} is diminished in cAF, the I_{Kur} blockers show

TABLE 2 | Studies focusing on each anti-arrhythmic drug category.

Article	Drug category	Details
Namba et al., 1999; Comtois et al., 2008; Colman et al., 2014; Aguilar et al., 2015; Syeda et al., 2016	Class I (Ia, Ib, Ic)	Na channel blockers
Marshall et al., 2012; Colman et al., 2014; Kharche et al., 2014b	class II	β -blockers
Wettwer et al., 2004; Syed et al., 2005; Ehrlich et al., 2008; Tsujimae et al., 2008; Almquist et al., 2010; Law et al., 2010; Aslanidi et al., 2012a; Duarte et al., 2013; Colman et al., 2014; Tobón et al., 2014a, 2017; Aguilar et al., 2015; Cacciani and Zaniboni, 2015; Majumder et al., 2016; Syeda et al., 2016; Varela et al., 2016; Ni et al., 2017b, 2016	class III	K channel blockers
Colman et al., 2014; Cacciani and Zaniboni, 2015	class IV	Ca blockers
Krummen et al., 2012	class V	adenosine

prominent significance in cAF treatment, as investigated *in silico* in a number of theoretical drugs in both SR and cAF conditions (Ellinwood et al., 2017a,b).

Along this line, Ni et al. (2017b) studied *in silico* the effects of the multi-channel blockers on atrial and ventricular activation, and found that the synergistic use of a specific and potentially selective I_{Kur} potassium channel blocker (acacitin) and a I_{NA} blocker seems to have no significant impact on QT prolongation or on ventricular activation. As suggested, the synergistic antiarrhythmic treatment leads to more effective termination of atrial reentries (Aguilar et al., 2015; Ni et al., 2016), while ventricular side effects in the ventricles are limited. Furthermore, the relationship between drug concentration and AF termination is also considered in other studies (Duarte et al., 2013; Tobón et al., 2014a, 2017).

Colman et al. (2014) and Varela et al. (2016) studied the effectiveness of the antiarrhythmic therapy on termination of the wave breaks near the PVs. The latter study discusses the effect of the multi-channel class III antiarrhythmic drugs in combination with atrial heterogeneities on the termination of AF, using detailed 3D anatomical models of human atria. Additionally, the role of the antiarrhythmic drugs in the prevention of AF initiation due to bradycardia (Cacciani and Zaniboni, 2015) or how isoproterenol can induce AF (Krummen et al., 2012) were also studied.

A fundamental approach to AF treatment is β -blockers usage to control ventricular response. The chronic use of such treatment can lead to drug-induced remodeling. Marshall et al. (2012) studied these pharmacological remodeling effects of β -blockers on specific potassium currents in the human atrium. Kharche et al. (2014b) discussed this pharmaceutical remodeling and observed that chronic use of β -blockers suppresses AF by APD and effective refractory period (ERP) prolongation, with potential anti-arrhythmic consequences.

Autonomic nervous system and the role of ganglia

The effect of vagal tone on atrial arrhythmogenesis has been reported in several studies (Vigmond et al., 2004). Modifying the ion channel conductance, Ashihara et al. (2002) simulated the two branches of the ANS and used the Luo-Rudy-1 model to examine why vagally mediated AF lasts more than sympathetic mediated AF. Interestingly, it was found that sympathetic tone promotes spiral waves and restrains their breakup. In contrast, vagal tone promotes spiral wave breakup. A significant limitation of this study is that the modifications on the ion channels were speculative as there was insufficient information from clinical data.

A significant number of studies incorporates, in the electrophysiological models, the effect of Acetylcholine to model the vagal activation and study its effect on AF (Comtois and Nattel, 2011; Voigt et al., 2013). Acetylcholine (Ach) is a neurotransmitter used in vagal action studying, while its concentration affects the APD (Vigmond et al., 2004). Experimental findings reveal increased vagal activity during hemodialysis (HD) sessions suggesting that enhanced acetylcholine concentration can lead to ERP shortening and depolarization prolongation (Vincenti et al., 2014). Kneller et al. (2002) used the RNC canine atrial model, and the Ach effect was incorporated based on a novel description of the Ach-induced current ($I_{K,ACH}$) that is included in all the studies which consider the vagal influence on AF. Hwang et al. (2016) considered three different approaches for the distribution of the ACh concentration on the atrium: (1) random distribution, (2) ACh concentration within the four ganglionated plexi (GP) areas, and (3) using the octopus hypothesis where eight nerves with gradient ACh concentration originate from the GPs and spread through the atrium. The octopus hypothesis was adopted in order to examine the effect of both branches of ANS (sympathetic and parasympathetic nervous system) (Hwang et al., 2017). The parasympathetic system was modeled as an increase of the I_{KACH} in the ganglionated plexi and their nerves in the LA 3D model while the sympathetic system was modeled as an increase of the L-type calcium current. ANS stimulation can induce triggering activity and PV automaticity, leading to local re-entries in the LA-PV junction.

AF Remodeling

Atrial fibrillation is a progressive disease, where at the first stages the episodes are short and infrequent (paroxysmal AF), and later on, they are more frequent and more prolonged (persistent or permanent AF). As AF progresses to more stable types, different parameters of the electrophysiological models are modified to reflect the AF-induced electrical remodeling. These changes on ion currents and conductance are based on findings from experimental studies (Courtemanche et al., 1999; Zhang et al., 2005). The majority of the 301 studies included in this review focused on more stable types of AF while only about 10% of them directly referred to Paroxysmal AF (Ashihara et al., 2002; Gong et al., 2007; Severi et al., 2010; Duarte et al., 2013; Calvo et al., 2014; Vincenti et al., 2014; Voigt et al., 2014; Berenfeld, 2016).

The electrically remodeled substrate favors the initiation and the perpetuation of AF. APD shortening and decreased

conduction velocity lead to reduced wavelength. However, the mechanisms for AF initiation and perpetuation may differ (Chang and Trayanova, 2016) which is the subject of several studies (Krogh-Madsen et al., 2012; Colman et al., 2013; Koivumäki et al., 2014; Lee et al., 2016). Furthermore, studies included the extent of the electrical remodeling in each atrium (Luca et al., 2015), concerning its influence on the duration of AF episodes. Among the articles included in this review, 44 articles were found to study AF initiation and 25 AF termination, while the majority of the articles examine the AF perpetuation mechanisms. Finally, 37 articles investigate atrial activation under SR (Weber et al., 2009a,b; Krueger et al., 2013c,d; Voigt et al., 2013).

Apart from electrical remodeling, structural remodeling has also been found to influence the susceptibility to AF. It can be the result of structural heart disease or other conditions such as hypertension, while AF itself can also modify the atrial substrate. As AF progresses, apart from the electrical remodeling, structural remodeling is also present (Wijffels et al., 1995) and interestingly larger atrial size favors reentrant circuits, possibly due to more area available for rotor formation (Zou et al., 2005). The structural remodeling is modeled by considering fibrosis (including collagenous septa, remodeled gap junctions and proliferation of myofibroblast) (McDowell et al., 2013), scars as a result of previous ablation procedures (Gonzales et al., 2014), endo/epicardium dissociation (Gharaviri et al., 2017) and absence of t-tubules (Li et al., 2012). The role of structural remodeling in AF initiation and perpetuation has been thoroughly examined. Zhao et al. (2013b) confirmed that structural remodeling facilitates reentries and multiple wavelets, increasing AF susceptibility. Zahid et al. (2016) described the effect of atrial fibrosis on the appearance of reentrant drivers in patients with persistent AF, and by the use of patient-specific models of the atria, demonstrated that the reentrant activity in fibrotic zones perpetuates AF. The role of the fibroblasts, which can serve both as triggers and substrate to cardiac arrhythmias is described by Koivumäki et al. (2014).

Furthermore, Aguilar et al. (2014) investigated fibroblasts involvement in the maintenance of AF, in HF patients, where they are usually activated. Based on electrophysiological studies in dogs, it was found that a novel fibroblast K^+ current must be taken into account in the mathematical models to describe the effects of such type of structural remodeling. Finally, Jacquemet and Henriquez (2009) described the impact of microfibrosis progression on electrograms' fractionation as structural remodeling increases. However, fibrosis distribution can remarkably alter the activation pathways, so there is a great need for accurate atrial substrate mapping using advanced mapping techniques, such as Late Gadolinium (Zahid et al., 2016) and contrast-enhanced mapping (Zhao et al., 2017).

Integrating With Structure, Geometry, and Anatomy

Detailed anatomical structures

Atrial tissue presents a complex morphology both in terms of structural and electrical heterogeneities. Fiber orientation constitutes a key aspect of atrial anatomy while electrical heterogeneities (such as the fast conduction systems of Bachman

bundle, Pectinate muscles, and Crista Terminalis) alter active potential propagation and the way this can influence the initiation and maintenance of AF (Jacquemet and Henriquez, 2009). Vigmond et al. (2001) presented a simple geometrical representation of atrial anatomy toward assessing of the role of the various anatomical structures on the initiation of reentries. In that study, all major anatomical structures of the atrium were considered, including fiber orientation, muscle structures such as crista terminalis and pectinate muscles as well as the orifices of the veins and valves. The outcome model did not constitute an exact representation of the atria, although it reflected the interrelations between the anatomical structures of the atria.

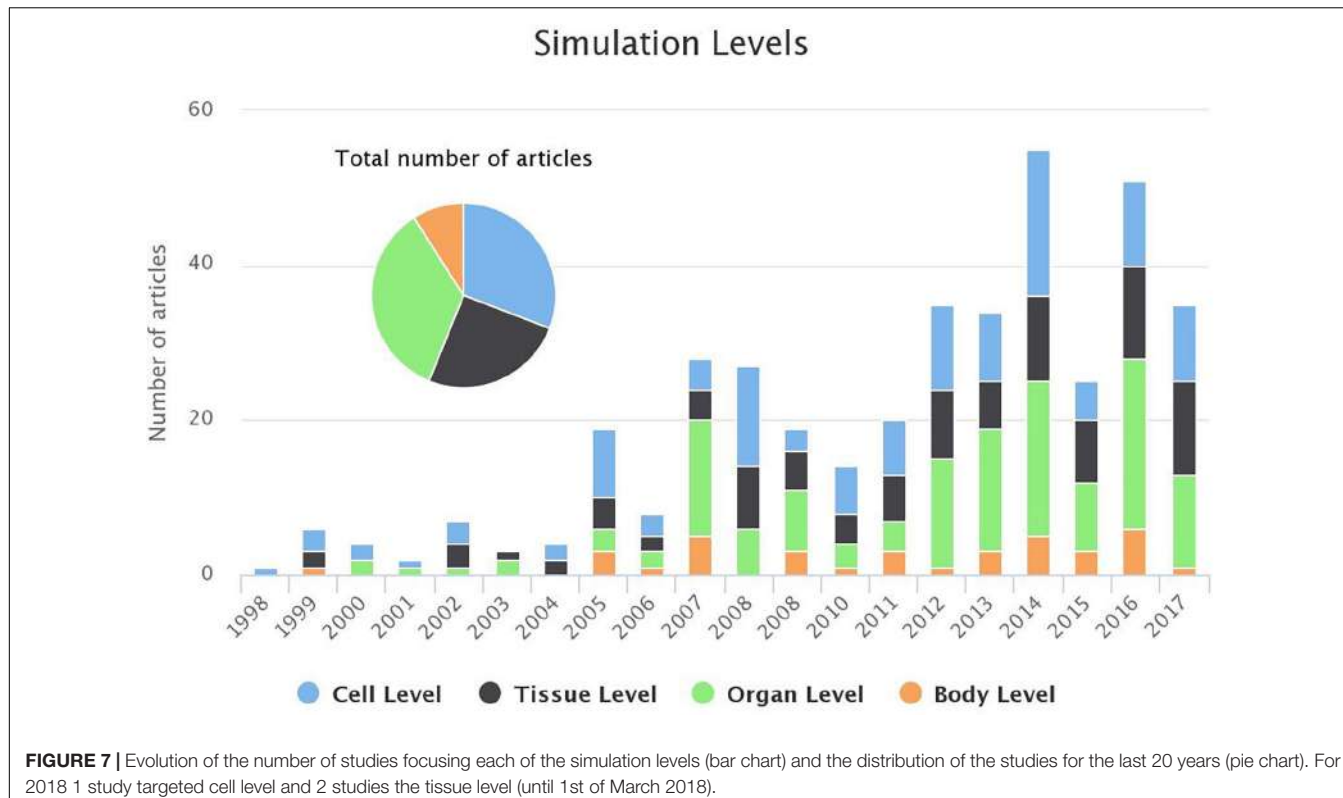
In most studies, fiber orientation was linear whereas, in another study, a sigmoid representation of fiber orientation was adopted (Ashihara et al., 2002). However, in 3D atrial models, fiber orientation is extracted based on imaging data and *ex vivo* tissue analysis (Zhao et al., 2012). Based on successive images from sheep atria, the myofiber orientation was determined by the purpose-development structure tensor analysis whereas the role of the fiber architecture on AF initiation has been studied (Zhao et al., 2013a). Kharche et al. (2014a) constructed a detailed model of rabbit atria from micro-CT images and found that fiber orientation anisotropy serves as a regulator of atrial activation while any modification of myofiber architecture may be pro-arrhythmic.

To develop realistic anatomical models of the atria, Zhao et al. (2008) suggested a methodology, based on *ex vivo* samples from pigs. During the following years, several models were designed to describe a realistic human or animal atrial anatomy (Deng and Xia, 2010; Aslanidi et al., 2011b; Tobón et al., 2013; Li et al., 2014; Ferrer et al., 2015; Zhao et al., 2017), whereas Zhao et al. (2017) proposed a novel 3D computational and structural model of human atria. This model is the output of a systematic analysis. It includes wall thickness, fiber orientation, and transmural fibrosis, and it is the most complete model of the human atrial structure.

Gharaviri et al. (2012a) introduced the novel approach of a dual-layer model for the study of AF. This model has been identified in 11 articles in the current review. Its basic hypothesis is that structural remodeling does not only lead to dissociation within the epicardial layer but also dissociation between the epicardial and endocardial layer promoting AF. AF induces this type of structural remodeling, based on experimental findings from goats (Eckstein et al., 2011), while it was revealed that this dissociation increases AF stability (Gharaviri et al., 2012b, 2017; Verheule et al., 2013). A methodology for the creation of a bilayer model of human atria, using CT images, is proposed by Vigmond et al. (2013), where the difference between RA and LA thickness, as well as the main anatomical structures and fiber orientation, is taken into account. The dual layer approach has also been adopted to examine the effectiveness of different radiofrequency ablation strategies (Bayer et al., 2016).

Simulation levels

Electrical activation of each cell results in modification of the electrophysiological properties spanning from the cell to the tissue, organ and body level. According to the scope of each study different observational outcomes were considered, such as AP,



activation map, electrogram or ECG. In the cell level simulations, a single cell is considered. In the tissue level studies, the atrial excitation is simulated in a 2D level including several anatomical structures (Seemann et al., 2005; Carrillo et al., 2008). In the organ level studies, 3D models of the atria are considered. 3D structures, like icosahedron (Ellis et al., 2000), or simple atrial representations (Vigmond et al., 2001) have been proposed, while realistic geometrical models of human atria were constructed using MRI (Virag et al., 2002; Aslanidi et al., 2011b; Colman et al., 2013) or CT images (Burdumy et al., 2012). Furthermore, advanced imaging techniques, like late gadolinium-enhanced magnetic resonance imaging (LGE-MRI) allow the construction of patient-specific atrial substrate with fibrosis (McDowell et al., 2012). In body level articles, a realistic model of a human torso is adopted to simulate body surface potentials and the produced ECG. One of the first works in this field is the one of Jacquemet et al. (2006) where an ECG signal representing atrial activation is created, using a geometrical model atrial and torso model, based on MR images. Finally, Krueger et al. (2013a) proposed torso models to simulate surface ECG recordings.

Studying the electrophysiological changes on AP and ion kinetics (Jones et al., 2012; Sanchez et al., 2012; Voigt et al., 2013, 2014) is the main subject of cell level simulations. 2D level studies target at identifying AF drivers, such as rotors and spiral waves (Becerra et al., 2014; Ganesan et al., 2016; Salmin et al., 2016; Duarte-Salazar et al., 2017; Aronis and Ashikaga, 2018) or the effect of spatial resolution on AF drivers detection (Rappel and Narayan, 2013; Roney et al., 2017). The use of patient-specific 3D models can give more insight into the mechanism of AF

(Zahid et al., 2016). Those simulations are used for the analysis of the mechanisms for AF initiation (Virag et al., 2002; Chang and Trayanova, 2016; Alcaine et al., 2017), AF stability (Rottmann et al., 2015) or the rotor drifting toward PVs (Calvo et al., 2014) and their anchoring in obstacles, such as fibrotic regions (Morgan et al., 2016; Nguyen et al., 2016; Deng et al., 2017). The detection of rotors is also studied using 3D simulations of human atria (Ugarte et al., 2014; Berenfeld, 2016; Martinez et al., 2016) to investigate the effectiveness of an ablation procedure (Dang et al., 2005; Hwang et al., 2014).

Apart from activation patterns analysis, signals can also be simulated (such as electrograms and ECG recordings). In the 2D or 3D case, the simulated electrograms can serve as a tool for AF drivers identification (Benson et al., 2014; Hummel et al., 2017; Sahli Costabal et al., 2018), atrial activation analysis and complex fractionated atrial electrogram (CFAE) regions detection (Jacquemet et al., 2003; Jacquemet and Henriquez, 2009; Ugarte et al., 2013, 2015; Roney et al., 2016). Jacquemet et al. (2005, 2009) constructed synthetic ECG signals to evaluate ventricular activity cancellation techniques. 3D simulations have been conducted to analyze the ECG characteristics, such as P-wave morphology (van Oosterom and Jacquemet, 2005; Ogawa et al., 2007; Krueger et al., 2013a,c). On the other hand, the inverse problem solutions and body surface recordings were employed for the detection of AF drivers (Pedrón-Torrecilla et al., 2014; Figuera et al., 2016b; Guillem et al., 2016; Pedrón-Torrecilla et al., 2016). Finally, an adaptation of the standard ECG systems for the optimization of the atrial signal recording was proposed by Ihara et al. (2007) and van Oosterom et al. (2007).

As shown in **Figure 7**, only a small minority of the studies adopt the body level simulations, whereas, more and more studies adopt a 3D realistic model of human atria to study the electrical activation during AF (organ level). Furthermore, the interest in the cell level analysis is persistent, as this constitutes the basis for any simulation protocol.

Electromechanics focus on the estimation of the electrical activation of the atria under the consideration of their mechanical function. Eight articles were found to include the electromechanical function in the simulations. In general, atrial contractility is associated with tissue depolarization as well as with the structural remodeling co-existence. Kuijpers et al. (2007) published the first model that integrates cardiac electromechanics with physiological details. According to this model, stretching of an atrial fiber influences the stretch-activated current (I_{SAC}). The model complies with experimental observations of conduction slowing and blocking as a result of an acutely dilated atria. This model was integrated into a 3D geometrical model of the atria in order to investigate the role of stretch-activated current on the onset and termination of AF episodes (Kuijpers et al., 2009). The role of acutely dilated atria on AF initiation was later reported (Kuijpers et al., 2011). Ni et al. (2014) used an electromechanical model of the ventricles (Adeniran et al., 2013) to study the effect of KCNA5 mutation on the electromechanical function of the human atrial cell while Adeniran et al. (2015) studied the effect of AF-induced electrical remodeling on the electromechanical function of the heart. Finally, a more recent study focused on the analysis of spiral waves when the atrial mechanoelectrical function is considered (Brocklehurst et al., 2017). In this study, one electrophysiological model of human atria (Colman et al., 2013) was modified to include the stretch-activated current, while combined with a mechanical model (Rice et al., 2008) which describes the active force generated in cellular level in response to the electrical signal. This study highlights the effect of mechanoelectrical feedback on AF.

Modeling Disease Context and Purpose

Rhythm status (SR or AF)

In a healthy heart, the electrical pulse originates from the sinus node and spreads through the atrium (Platonov, 2012), while during an AF episode chaotic activation of atrial myocardium occurs (Yamazaki and Jalife, 2012). In the majority of the papers included in this review, AF was induced and the analysis focused on the identification of AF drivers (Ashihara et al., 2004; Martínez et al., 2014b; Tobón et al., 2014b; Ugarte et al., 2014, 2015; Felix et al., 2015; Martinez et al., 2016; Salmin et al., 2016; Roney et al., 2017; Duarte-Salazar et al., 2017) or on the study of the electrical activation during AF in general. However, analysis of the electrical activation of the remodeled atria during SR was the subject of 52 studies, as this can also improve our understanding of the pathology.

The main property of Sinoatrial Node (SAN) models is their auto-oscillatory behavior (Fink et al., 2011). In most cases, they are used under normal conditions instead of a remodeled substrate. The effect of SAN dysfunction on AF initiation is addressed in several studies. Kharche et al. (2017) developed a 3D electro-anatomical model of the SAN, based on the

Fenton-Karma model. The model was based on histological studies, and the role of the SAN exit pathways was examined in terms of arrhythmias initiation. Glynn et al. (2014) adapted a detailed murine SAN model to confirm the restitution hypothesis, which states that the APD is associated with the duration of the previous diastolic intervals. They concluded that cycle length restitution analysis can enhance our understanding on SAN dysfunction and the initiation of arrhythmias. The simulations performed denote that the restitution curve can be useful for the analysis of cell dynamics and dysfunction in SAN. Lin et al. (2017) used a simplified spherical model of LA to investigate the mechanism of SR to AF transition. It was found that during SR, in healthy subjects, SAN to AV node conduction occurs through the interatrial septum via the fast pathway, while during AF, SAN long refractory period protects it from overdrive and the AV node filters the APs which would reach the ventricles (Li et al., 2014).

A common reason of SR usage is to test the reproducibility of the computational models, in both AF and normal SR (Goodman et al., 2005; van Oosterom and Jacquemet, 2005; Cherry and Evans, 2008; Grandi et al., 2011; Burdumy et al., 2012; Krueger et al., 2013a,d; Colman et al., 2016) or to examine differences in activation patterns with or without electrical remodeling (Zhao et al., 2012; Voigt et al., 2014). Simulation under SR, using patient-specific models, including fibrosis, can accurately reproduce local activation (Krueger et al., 2014). The reconstruction of the ECG signals by solving the forward problem of electrophysiology, to understand the genesis of the P-waves, was also found to be very accurate when the patient is in SR (Ferrer et al., 2015; Jacquemet, 2015; Figuera et al., 2016b). Finally, Zhao et al. (2012, 2013a) highlighted that the structurally remodeled substrate and the anatomical heterogeneities can increase the vulnerability to rhythm disturbances.

In addition, considering patients during SR, the effect of antiarrhythmic drugs, such as potassium or sodium channel blockers, on the APD or ionic current characteristics, has been studied (Wettwer et al., 2004; Ehrlich et al., 2008; Law et al., 2010; Aslanidi et al., 2012a; Marshall et al., 2012; Voigt et al., 2013; Ni et al., 2016; Skibsbye et al., 2016; Ellinwood et al., 2017b; Tobón et al., 2017). Ablation success, applied during SR, has been presented (Tobón et al., 2015; Bayer et al., 2016) and the changes occurring in the P-waves after the PV isolation procedure have also been examined (Saha et al., 2016).

AF initiation

The conditions, under which AF can be induced, were extensively studied and several approaches have been proposed. In general, a triggering factor, in the presence of an arrhythmogenic substrate, can favor the initiation of PAF. PVs have been reported to present pacemaking automaticity and triggering activity, and thus their role on arrhythmogenicity has been examined (Reumann et al., 2006; Cherry et al., 2007), whereas mathematical models have also been implemented to describe PVs in both animals (Lo et al., 2006; Seol et al., 2008) and humans. Jones et al. (2012) modeled the PVs under the experimental evidence that two types of cells exist in PVs, pacemaking, and non-pacemaking.

Abramovich-Sivan and Akselrod (1999) initiated a new approach, where a model of the atrial cells, able to describe the transition from normal rhythm to AF, is proposed. According to this study, the atrial cells are considered as “pacemaker-like” cells with different cycle length and different type of intercellular connection, where, the effect of the junctions between the different types of cell are taken into account to investigate how the initiation of atrial rhythm disturbances occurs and maintains.

The role of the coupling between anatomical heterogeneous regions, such as CT (Ellis et al., 2000; Reumann et al., 2007; Dorn et al., 2012; Butters et al., 2013; Zhao et al., 2013a), or between the PV and the LA (Aslanidi et al., 2012b, 2013) on the initiation of AF is discussed, whereas atrial contraction and electromechanics are proposed as a mechanism of arrhythmogenesis (Kuijpers et al., 2009). Fibrosis (McDowell et al., 2012; Zhao et al., 2013b; O’Connell et al., 2015) or other anatomical obstacles (Ciaccio et al., 2017), as well as the imperfect ablation lines (Dang et al., 2005) have also been proposed to facilitate AF initiation.

The effect of specific ion currents and electrolyte concentration on arrhythmogeneity was studied (Kuijpers et al., 2006; Aslanidi et al., 2008; Law et al., 2009; Varela et al., 2014; Voigt et al., 2014; Onal et al., 2017) whereas electrical remodeling, induced by AF, and its role on episodes induction is discussed by Colman et al. (2013) and Lee et al. (2016). Furthermore, Morgan et al. (2014) reported that co-existence of structural and electrical remodeling can promote AF initiation.

AF initiation by specific diseases, such as ankyrin-B syndrome (Wolf et al., 2013) and end-stage renal disease, was also examined. In particular, HD effect on AF is highlighted in several studies (Severi et al., 2008, 2010; Krueger et al., 2011) suggesting that HD sessions may be a triggering factor for the onset of the arrhythmia (Vincenti et al., 2014).

Atrial ectopies and heart rate (HR) variations have reported to induce AF. Virag et al. (2002) used three different stimulation protocols. The first one is the S1-S2 protocol, where the SA node stimulation is followed by an ectopic beat located in the RA. The second one is the S1-S2-S3 protocol where an additional ectopic beat is applied in the same areas as the previous one, while the third protocol is a burst pacing protocol of 20 Hz applied in the SA node for several seconds. These protocols, applied in both normal and electrically remodeled substrate, simulate both self-terminated AF episodes as well as more sustained types of AF. It is worth mentioning that most of the studies, analyzing AF drivers, use the S1-S2 protocol for AF initiation (Ramirez et al., 2000; Liu et al., 2007; Tobón et al., 2014b; Ugarte et al., 2015). Shusterman et al. (2003) mentioned that abrupt short-term variations in cycle length, such as atrial ectopic activity and HR variations, lead to spatial irregularities of the wavefront propagation and thus initiate reentries in a simple two-dimensional tissue model. The role of alternans as a proarrhythmic state has also been discussed (Chang et al., 2014; Chang and Trayanova, 2016). Gong et al. (2007) proposed that ectopies originating from the PVs facilitate reentry induction by prolonging the vulnerability window. Hwang et al. (2016) and Hwang et al. (2017) examined the effect of the ANS on arrhythmogenesis where the role of ganglia on the initiation of AF is highlighted. The concept of early warning

that can forecast a change of system’s stability is applied in AF electrophysiology (Garcia-Gudino et al., 2017). In this study, a cellular automaton is used to describe atrial conduction on the tissue. Applying different pacing approaches, along with real RR interval data derived from Fantasia database (Iyengar et al., 1996), it was shown that even when complex pacing is introduced, this approach can serve as a predictor of transition from normal rhythm to AF.

Finally, genetic background and gene mutations represent an additional field of research on AF initiation (Carrillo et al., 2008; Seemann et al., 2009; Kharche et al., 2012a; Whittaker et al., 2017).

Modeling the interventions for AF termination

Atrial fibrillation termination approaches include pharmacological treatment, ablation procedure, and electrical cardioversion. The first study identified on defibrillation usage for AF termination is the one by Boegli et al. (2000) where different defibrillation techniques were tested for their effectiveness. Kharche et al. (2012b), using a 3D realistic model of human atria, observed that low energy cardioversion efficacy depends on atrial anatomy. It has also been mentioned that in patients with no electrical remodeling lower cardioversion energy and shorter duration must be applied (Kharche et al., 2013). Rusu et al. (2014) proposed that pacing therapy must be patient-specific, due to its influence by the presence of heterogeneities in vagal activation and repolarization. On the other hand, it has been suggested patient-specific management of defibrillation (Kharche et al., 2015; Luca et al., 2016).

Dang et al. (2005) evaluated the outcome of the radiofrequency ablation and studied the effect of imperfect lines. In this study, the significance of the biophysical models’ application on the development of new ablation approaches is highlighted. The simulation results were confirmed with clinical data. The identification of the optimal ablation line is the subject of several studies which point out the need for tailored ablation lines for each patient (Rotter et al., 2007; Ruchat et al., 2007a,b,c; Reumann et al., 2008; Kwon et al., 2013; Hwang et al., 2014; Zhu et al., 2014; Rappel et al., 2015; Bayer et al., 2016). During the ablation procedure, in most cases, the PVs are isolated. However, fibrotic region ablation is also proposed (Ashihara et al., 2012) whereas other studies suggest other approaches which can guide the ablation procedure (Benson et al., 2014; Tobón et al., 2014b; Carrick et al., 2016; Kuklik et al., 2016; Li et al., 2016). In a 3D model of LA, the ablation of ganglia seems to terminate AF (Hwang et al., 2017). Interestingly, the effect of the poor contact of the electrodes with the tissue on AF drivers identification is discussed, and a methodology for signals reconstruction is proposed by Green et al. (2017).

Apart from the approaches mentioned above, drug treatment is also followed for AF termination. Most of the antiarrhythmic drugs, acting on atrial myocardium, may also have an effect on ventricular ion channels. State-dependent Na^+ -channel blockers (class I antiarrhythmic drugs) maximize their effect on the atrium while at the same time the influence on the ventricles is minimal. AF-selectivity of such drugs is the topic of Aguilar-Shardonofsky et al. (2012). According to this study, increased ventricular proarrhythmia correlates with drug effectiveness close

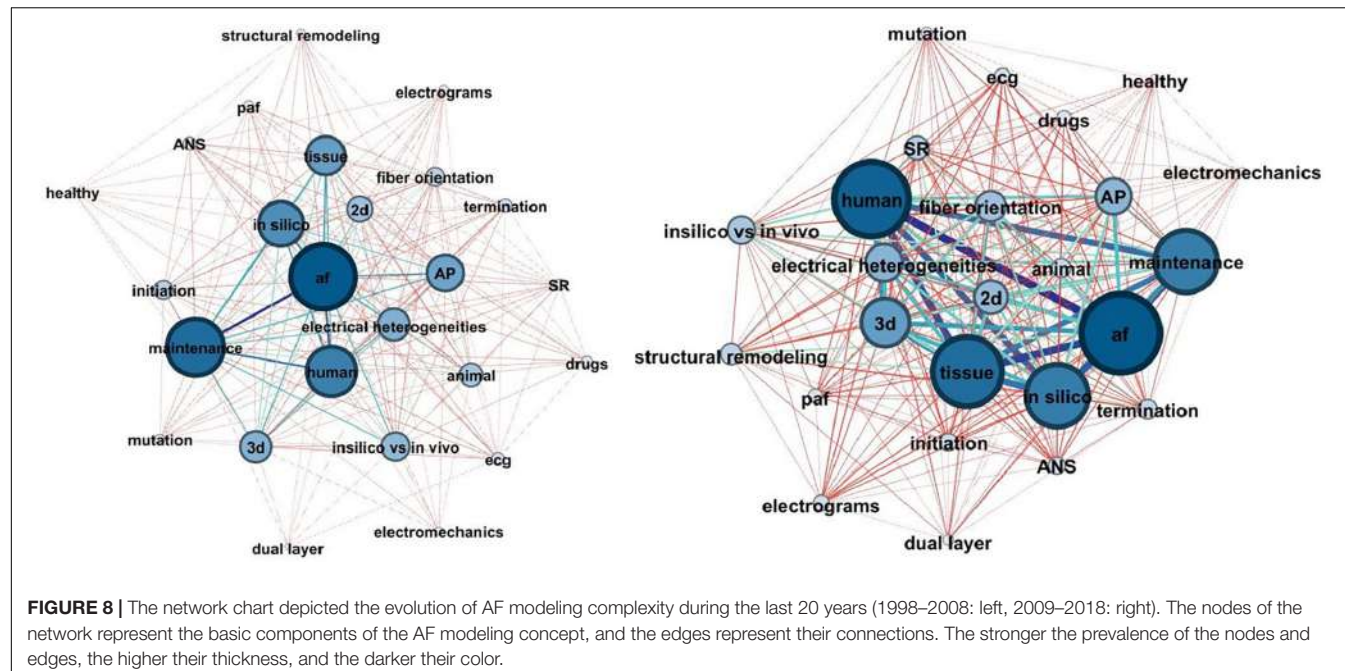


FIGURE 8 | The network chart depicted the evolution of AF modeling complexity during the last 20 years (1998–2008: left, 2009–2018: right). The nodes of the network represent the basic components of the AF modeling concept, and the edges represent their connections. The stronger the prevalence of the nodes and edges, the higher their thickness, and the darker their color.

to 100%, while in case of minimum ventricular proarrhythmia, AF termination rates were low. Furthermore, several potassium channel blockers were also analyzed, in terms of computer models, in order to examine their effect on AF termination (Scholz et al., 2013; Tobón et al., 2014a; Aguilar et al., 2017; Ellinwood et al., 2017a). Ni et al. (2017b) compared the effects on atrial and ventricular activation of these two types of blockers combination to single channel blockers usage. The human heart simulation results showed that synergistic antiarrhythmic treatment leads to more effective termination of reentries, compared to single channels block, while the side effects in the ventricles are limited. Moreover, analyzing inter-subject variability on AP, distinguishes drug responders from non-responders (Liberos et al., 2016).

The self-terminating nature of the arrhythmia has also been studied (Uldry et al., 2012), however, its transient nature is the main barrier while an analysis framework has been proposed (Lin et al., 2017). It was found that in low complexity AF, the spontaneous termination process lasted 3.2 s and was initially started in the LA, while the last fibrillatory signal was detected in the RA. On the other hand, in complex AF, the termination process is less predictable. Additionally, the role of electro-mechanical feedback on AF self-termination is discussed by Kuijpers et al. (2009).

Evolution of Models

Computational modeling evolution can be studied by network theory. The components, involved in AF modeling, are considered as nodes of a network, whereas, the connections between them represent the studies they are reported in. Two distinct periods (1998–2007 and 2007–2018) were considered, and two metrics, describing the network complexity were extracted. The first metric is the average degree (AD) of the

graph, which is defined as the average connections between the nodes, while the second one is the network density, defined as $D = \frac{2E}{N(N-1)}$, where E is the number of edges and N the number of nodes.

According to the analysis AD was 16.96 during the first decade its value increased to 21.52 during the second decade, demonstrating an increase in network complexity as more factors were involved in the computational modeling. D was also increased during the second decade, from 0.707 to 0.897. These results suggest that the simulation experiments are getting more and more complex, taking into account additional factors which influence AF.

As seen in Figure 8, the study of subjects such as the dual layer, the electromechanics and the involvement of ANS, gained the attention of the research community during the second decade. Additionally, 3D model simulations also doubled their frequency which can be attributed to the improvement of imaging techniques and the creation of detailed anatomical models of the atria. Finally, it is observed that more studies focus on atrial activation analysis during SR and not only while on AF.

On the other hand, the proportion of studies, conducting an AP model analysis seems to be the same between the two decades, implying a stable trend in the analysis of APs.

AF Models: What Do We Learn About ECG and P-Wave Morphology

One of the great challenges in the field of computational modeling is to translate the output of the simulation studies into clinical practice (Trayanova and Chang, 2016). ECG recordings constitute an accurate non-invasive tool for heart activity assessment which is extensively useful in daily practice. ECG signals extraction from computational studies and vice versa

would improve AF pathophysiology understanding and thus optimize clinical decision and treatment strategy. In the present review, several approaches for ECG signal reconstruction have been identified.

An attempt to extract a pseudoelectrocardiogram (pECG) was made by Namba et al. (1999) where a point in a realistic distance of the excitable tissue was considered and the pECG was calculated as the integration of all the membrane potentials, assuming a homogeneous and zero resistance area. In this work, it was found that the spiral wave results on a low Atrial Fibrillation Interval (FF) while under sodium channel blockers the FF intervals increase. Aslanidi et al. (2011b) described the development of the 3D virtual human atria which is a multi-scale detailed computational model. The anatomical model of the atria was based on MR images where the main anatomical structures, with different electrical characteristics, and fiber orientation were included. The 3D virtual atria model was adjusted in a torso model, enabling several activation patterns simulation and ECG extraction. A detailed anatomical model of human atria and torso, based on histological data and MR images, is also described by Ferrer et al. (2015). The concept of this work was to create a multi-scale framework used to explain, from an electrophysiological point of view, findings that are detectable in P-waves and body surface potential maps. P-wave morphology and duration were observed to be highly influenced by the conductivity properties of the torso and the fiber orientation in the atria.

Kuijpers et al. (2011) tested the effect of mechanical function on AF initiation and its effect on the extracted ECG was estimated. In another work from Krueger et al. (2013d) the personalized anatomical model in terms of the location of the interatrial bridges is studied. MRI images were used to create a personalized anatomical model while local activation time (LAT) maps were recorded using electroanatomical mapping systems [Ensite NavX (St. Jude Medical, St. Paul, MN, United States) or Carto (Biosense Webster, Haifa, Israel)] before the ablation procedure. Those LAT maps were used to localize the interatrial bridges in each patient. The simulation results, during SR, denote personalized interatrial bridges consideration can improve simulated and real body surface potentials concordance.

In an ECG signal atrial activity, especially atrial repolarization is hidden by the much higher amplitude of the ventricular electrical activity. In this respect, the cancelation of the ventricular wave is of great importance. Validation of ventricular activity cancelation algorithms is feasible employing computational modeling and ECG signal reconstruction. Jacquemet et al. (2009) created a realistic 3D model of human atria and torso, based on MR images, and the signal, reflecting atrial activity, was reconstructed in the points that a standard ECG lead is measured. That signal has later been summed with QRST complexes recorded during SR, adapting the RR intervals accordingly. This work does not focus on the analysis of the F-waves, but it provides the methodological framework for the evaluation of QRST cancelation techniques.

The standard ECG-lead systems, such as the 12-lead ECG, were designed in such a way to capture the ventricular activity effectively. Thus, these lead systems may be sub-optimal in

terms of atrial activity detection. A few studies have been conducted (Ihara et al., 2005, 2007) proposing the modification of these systems toward the effective capturing of atrial activity. Additionally, van Oosterom et al. (2007) suggested a modification of electrodes' placing vectorcardiographic (VCG) signals acquisition in AF patients, as, according to the authors, the Frank lead system seems suboptimal for atrial activity monitoring during AF. These studies are based on 3D models of atria and torso, where the ECG on the body surface is calculated using simulations.

Electrocardiography and vectorcardiographic recordings have been analyzed to identify AF drivers as well as to characterize atrial activation complexity. An interesting visual representation of the atrial activation, using the time course of the VCG dipole components, is based on a sphere where the main vessel and vein orifices were included. The trajectory of the atrial activation demonstrates the differences between SR and different types of AF (Jacquemet et al., 2006) while the extracted spatial characteristics can localize stable AF drivers in the atria (Lemay et al., 2007b, 2009). Lemay et al. (2007a) proposed that the existence of multiple AF drivers in the atrium can be revealed through the analysis of the full spectrum of the ECG signal instead of the analysis of the dominant frequency only. Duchêne et al. (2009) used a multiple frequency tracking algorithm to examine whether ECG signals analysis can provide information related to AF drivers complexity. Furthermore, rotor activity detection using spherical atrial and torso model and surface phase maps extraction is proposed in Rodrigo et al. (2014a,b). Finally, Ni et al. (2017b) examined the effect of antiarrhythmic drugs on the power spectrum of the simulated ECG.

In the surface ECG, atrial depolarization is mainly represented by P-wave. While AF is characterized by the absence of P-waves in the ECG signals, during SR, this complex can provide information related to the underline substrate. It is known that the first part reflects the activation of the RA and the second part the activation of the LA (Michelucci et al., 2002). According to Platonov (2012), the origin of the sinus rhythm, the shape and the size of the atria can affect the morphological characteristics of the P-waves. Solving of the forward or the inverse problem of the electrophysiology helps to translate the P-wave characteristics on tissue level phenomena. However, it is worth mentioning that both the inverse and forward approaches require a detailed representation of the torso as this affects the precision of the results (Bear et al., 2015).

Forward Problem – P-Wave Estimation

The estimation of the body surface potentials based on the epicardial ones, define the forward problem of electrophysiology. The key work from van Oosterom and Jacquemet (2005) used the Equivalent Double Layer (EDL) source model to simulate the atrial activity of the human body. The proposed approach was applied both during SR and AF. During SR, the application of the EDL model presented high correlation with the actual recorded signal, primarily related to the P-wave morphology. Furthermore, during AF, simulated signals were also highly correlated with the signals that are typically recorded in AF patients.

Krueger et al. (2013c) presented a framework for the generation and validation of multiscale cardiac modeling. This study describes how *a priori* knowledge, such as fiber orientation and electrophysiological models, can be enhanced by information derived from ECG characteristics like P-wave duration or HR, electrolytes concentrations and information from cardiac and thoracic MRI. The availability of LATs and ECG recordings can be used for models evaluation. As highlighted, HR must be considered during the simulation process as it has a significant impact on atrial repolarization. Additionally, P-wave morphology was properly reproduced only in specific leads, while P-wave duration is accurately computed in any lead. Krueger et al. (2013a) simulated P-wave as well as T-wave, based on the patient-specific detailed anatomical model. The simulated P-waves and T-waves morphology fitted well with the experimental recordings in both physiological and AF-remodeled conditions.

A typical example of macroscopic phenomena translation is to predict AF recurrences by analyzing the P-wave shortening observed in patients undergoing PVs isolation. P-wave duration reflects the interatrial conduction time while in AF patients the heterogeneous atrial propagation results in prolonged P-waves. Ogawa et al. (2007) used signal-averaged P-wave duration, P-wave dispersion and root-mean-square voltage of the terminal 20 ms (RMS20) of the averaged P-wave, to predict AF recurrences after successful PV ablation. Comparing real data from patient underwent cardiac ablation with P-wave generated by mathematical simulation of realistic human atria, it was found that the elimination of PV sleeve results on shortening of the P-wave duration and modification of its morphology. Jacquemet (2015) discussed LA and RA substrate contribution on P-wave morphology confirming that P-wave reflects any structural modification of the atrial substrate.

An effort to interpret the atrial substrate mechanisms, which lead to changes in P-wave duration after the ablation procedure, was performed by Saha et al. (2016). Using mathematical models of human atria and torso, VCG and 16-lead ECG were reconstructed before and after PVs isolation. According to the results, P-wave shortening is detected in leads V3 and V4 whereas these changes were more apparent when larger PV areas were isolated. Furthermore, the P-wave area was increased in V1, while decreased in V6. Additionally, possible reconnections in the PVs could be identified, and thus the 16-lead ECG can be used as a tool for PVs reconnections detection in patients undergone ablation.

P-wave terminal force in lead V1 (PTF-V1) has been proposed as an AF risk marker. PTF-V1 is the product of the duration and the amplitude of the terminal negative part of the P-wave (Morris et al., 1964). Loewe et al. (2016) studied the effect of the Early Activation Sites (EAS), as well as, their proximity to inter-atrial connections (IACs) on the PTF-V1. The term EAS is defined as the area where the sinus node excitation is captured by the myocardium. An inter-personal variability, as well as, a variation over time on the same individual has been observed. Based on experimental findings from dogs, this variation over time is suggested to reflect the vagal activation. On the other hand, the location and the conductive properties of the IACs are known to vary among subjects. Several anatomical models and multiple EAS consideration have shown that these two factors affect PTF-V1.

Alday et al. (2014, 2015) examined the effect of ectopic foci on P-wave morphology. In the latter study, the P-wave morphology is examined in terms of polarity (positive, negative, and biphasic). Under the assumption that a negative deflection on an ECG depicts a wavefront traveling away from the location where the electrodes are placed, the torso and the atria were separated into four quadrants. The analysis of the P-wave polarity in each of the quadrant can reveal the area from which the ectopic foci originates, while the implemented algorithm demonstrated high success rates on the localization of the ectopic source.

As mentioned, alternations on the ionic currents during HD sessions can induce PAF episodes. Observational studies have shown P-waves prolongation during HD sessions implying intra-atrial conduction slowing. A computer model describing the ionic concentrations of a patient during HD has been used to explain this macroscopic phenomenon (Severi et al., 2010). K^+ alternations (hypokalemia) result in conduction velocity reduction and ERP shortening. Krueger et al. (2011) confirmed these findings, where simulated ECGs were extracted, using realistic models of human atria and torso.

Finally, Zhu et al. (2014) examined P-wave morphology to check the effectiveness of 4 ablation protocols, on cAF treatment. Without providing any details on the evaluation of P-wave morphology, it is mentioned that simulated P-waves were similar after the application of different ablation protocols. The authors concluded that the Maze III approach is effective, and the transmural ablation has the same effectiveness as the non-transmural one. Table 3 summarizes the features mentioned above for the analysis of the P-wave using computational modeling approaches.

Inverse Problem

Estimation of bioelectric source potentials using remote electric field measurements is known as the inverse problem of electrophysiology, and it has been applied in both SR and AF scenarios (Pedrón-Torrecilla et al., 2014). The accuracy of the extracted results is a crucial topic and several studies focused on the implementation of algorithms able to reconstruct activation patterns matching with the observed ones (Pedrón-Torrecilla et al., 2016). Zemzemi et al. (2012) proposed one such approach based in machine learning techniques where the simulated ECGs, computed by the consideration of atria and torso model, were used for the training of the algorithms while the results were examined in terms of reproducibility. One of the application areas of this field is the identification of AF drivers in the atria (Guillem et al., 2016). On the other hand, different methods of estimating epicardial potentials, dominant frequency, phase maps, and singularity points locations, were examined for their accuracy (Figuera et al., 2016a,b).

DISCUSSION

Computational modeling is an emerging area of research useful to understand the mechanisms involved with pathophysiology, diagnosis, and treatment of human diseases (Bers and Grandi, 2011). This article presents the results of systematic scoping review related to multi-scale computational modeling of AF. In

TABLE 3 | Features used toward the analysis of the P-wave, during SR, using computational modeling approach.

Article	Intervention	Feature	Goal
Ogawa et al., 2007	ablation	PWD RMS20 P-wave dispersion	Prediction of AF recurrences
Krueger et al., 2011	HD	P-wave duration	HD-induced changes
Krueger et al., 2013a	–	PWD Ta-wave duration Ta-wave amplitude	Study atrial repolarization
Krueger et al., 2013c	–	PWD	Framework for personalized models
Alday et al., 2014	–	P-wave morphology (polarity)	Localize ectopic foci
Alday et al., 2015	–	P-wave morphology (polarity)	Localize ectopic foci
Ferrer et al., 2015	–	P-wave morphology duration amplitude	Multi-scale framework
Saha et al., 2016	ablation	PWD P-wave area duration of the positive part of P-wave	Changes after ablation on P-wave
Loewe et al., 2016	–	P-wave terminal force in lead V1 (PTF-V1)	Inter and intra-individual variation of the P-wave morphology

the context of this review, two databases were searched and 301 articles, published during the last 20 years, were identified as relevant for our purposes.

Atrial fibrillation is a complex arrhythmia, and the electrophysiological mechanisms for its initiation and maintenance are not clearly understood. In general, a triggering factor, as well as an arrhythmogenic substrate, must coexist for AF initiation. The complicated nature of AF is reflected in the significant number of studies included in the current review and the numerous factors to be considered on simulation protocols designing. The advances in imaging technologies led to the creation of detailed anatomical models, depicting the structural and electrical heterogeneities of the atria whereas, several mechanisms involved in arrhythmogenesis have been modeled related to electrical and structural remodeling. The computational approaches move toward more detailed models, incorporating multiple factors, such ANS effect, atrial electromechanical, the endo and epicardium layer dissociation, fibrosis and the genetic substrate. This progress will lead to patient-specific models creation (Krueger et al., 2013b) which can be useful in real-life cases analysis.

The observation of the number of articles published over time reveals an increased interest in the field of computational modeling of AF while this interest is projected to continue. Furthermore, the number of papers focusing on *in silico* AF models is increasing, and multiple scales are being analyzed, ranging from cell to tissue and organ level. In time to come, the advances of mapping and imaging techniques as well as high-performance computing engineering, will force computational models to adopt new elements to improve the repeatability and consistency with clinical observations (Trayanova and Chang, 2016). The main challenge is to transform the experimental knowledge into clinical practice in order to serve as a tool for physicians to perform for clinical interventions (Trayanova and McDowell, 2018). The importance of Physiome project (Hunter and Borg, 2003) and the Virtual Physiological Human (VPH) initiative (Viceconti and Hunter, 2016) and the positive effect they had on the increased interest on computational modeling must be highlighted.

Apart from atrial substrate analysis during AF, some articles focus on atrial excitation during SR. Computer simulations can help interpret the findings from ECG and P-wave analysis. As Dössel et al. (2017) mentioned, merging of biosignal analysis with computer modeling can enhance our understanding of AF.

Atrial geometry (Ihara et al., 2007) as well as the modification of anatomical IACs have also shown the ability to change the morphology of the P-waves (Loewe et al., 2016) while the effect of structural remodeling on the P-wave (Jacquemet, 2015) such as its shortening after the PV isolation procedure (Saha et al., 2016), has also been reported. Furthermore, P-wave is supposed to be reformed by ectopic foci (Alday et al., 2015), suggesting that any deflection from the SA node excitation can alter the conduction routes. P-wave morphology depends on (1) the origin of the SR as well as (2) the conduction route (Platonov, 2012). However, many studies have revealed the existence of a distinct secondary P-wave morphology in PAF patients (Filos et al., 2017), while the percentage of beats matching the main or the secondary P-wave morphology predict the outcome of PV isolation (Huo et al., 2015) or the chance for AF initiation (Martínez et al., 2012). Monfredi et al. (2010) investigated whether the variability in the P-wave morphology can be attributed either on a transient switch from one group of SAN pacemaker cells to another or on multiple activation routes. Studies in dogs revealed that ANS, and in particular the different branches shifted the EAS in different regions (Platonov, 2012). Apart from the effect of the ANS, additional factors which alter on different time scales, such as electromechanics and subcellular phenomena like metabolism, must also be included in the analysis of the P-wave morphology variability. However, there is a need to consider longer simulations times and analysis of more beats to capture the transient modification of the P-wave morphology.

However, atria must not be regarded as being isolated from the rest of the heart. The effect of AV node on AF, as well as the role of accessory pathways in conditions, such as Wolff–Parkinson–White Syndrome, must also be considered. Recently, the predictive value of corrected QT interval (QTc) prolongation, a metric of ventricular repolarization, on the AF incidence was highlighted (Zhang et al., 2018). However, this metric can be considered as a surrogate marker. Future simulation protocols should also incorporate the role of other anatomical structures of the heart to investigate the distributed conduction in the atrial substrate which is implied by the variable P-wave morphologies.

Any effort made in the field of computational modeling must seriously consider how the outcome can be used in clinical practice (Grandi and Maleckar, 2016). Guided ablation is one of the main topics influenced by the advances in cardiac

simulations (Zhao et al., 2015; Jacquemet, 2016). Computer models can identify AF drivers effectively when the effect of multiple factors on AF, such as structural heterogeneities and electrical remodeling, is considered. In the future, the analysis will be based on personalized atrial models since the evaluation of theoretical ablation procedures in such models showed their effectiveness on AF treatment. Upon application of these techniques in real patients, computational modeling is expected to optimize ablation procedures (Boyle et al., 2017). Furthermore, the development of more effective drugs with substantial atrial selectivity is foreseen (Grandi and Malek, 2016).

Limitations

Studies were limited to the AF while other pro-arrhythmic states were not included in the review. Furthermore, since one of the inclusion criteria was that the term “AF” needed to be indexed as a keyword, we recognize that some pioneering works on the field of computational modeling may be excluded. A typical example is the work from Vigmond et al. (2004), which was excluded because it was not indexed with the term “AF” as a keyword neither in PubMed nor in Scopus libraries, despite the fact its focus is on atrial arrhythmogenesis, and AF can be considered as a part of it. However, the fact that all the remaining inclusion criteria are met denotes the effectiveness of the query for the description of the field of computational modeling. Finally, the modeling of the AV node, which serves as a filter for the atrial AP to prevent the arrhythmia to be diffused into the ventricles, was not considered here, and thus its effect on the initiation and maintenance of AF was not studied.

REFERENCES

- Abramovich-Sivan, S., and Akselrod, S. (1999). Simulation of atrial activity by a phase response curve based model of a two-dimensional pacemaker cells array: the transition from a normal activation pattern to atrial fibrillation. *Biol. Cybern.* 80, 141–153. doi: 10.1007/s004220050512
- Adeniran, I., Hancox, J. C., and Zhang, H. (2013). In silico investigation of the short QT syndrome, using human ventricle models incorporating electromechanical coupling. *Front. Physiol.* 4:166. doi: 10.3389/fphys.2013.00166
- Adeniran, I., Maciver, D. H., Garratt, C. J., Ye, J., Hancox, J. C., and Zhang, H. (2015). Effects of persistent atrial fibrillation- induced electrical remodeling on atrial electro-mechanics - insights from a 3D model of the human atria. *PLoS One* 10:e0142397. doi: 10.1371/journal.pone.0142397
- Aguilar, M., Feng, J., Vigmond, E., Comtois, P., and Nattel, S. (2017). Rate-dependent role of *ikur* in human atrial repolarization and atrial fibrillation maintenance. *Biophys. J.* 112, 1997–2010. doi: 10.1016/j.bpj.2017.03.022
- Aguilar, M., Qi, X. Y., Huang, H., and Nattel, S. (2014). Fibroblast electrical remodeling in heart failure and potential effects on atrial fibrillation. *Biophys. J.* 107, 2444–2455. doi: 10.1016/j.bpj.2014.10.014
- Aguilar, M., Xiong, F., Qi, X. Y., Comtois, P., and Nattel, S. (2015). Potassium channel blockade enhances atrial fibrillation-selective antiarrhythmic effects of optimized state-dependent sodium channel blockade. *Circulation* 132, 2203–2211. doi: 10.1161/CIRCULATIONAHA.115.018016
- Aguilar-Shardonofsky, M., Vigmond, E. J., Nattel, S., and Comtois, P. (2012). In silico optimization of atrial fibrillation-selective sodium channel blocker pharmacodynamics. *Biophys. J.* 102, 951–960. doi: 10.1016/j.bpj.2012.01.032
- Alcaine, A., Masè, M., Cristoforetti, A., Ravelli, F., Nollo, G., Laguna, P., et al. (2017). A multi-variate predictability framework to assess invasive cardiac activity and interactions during atrial fibrillation. *IEEE Trans. Biomed. Eng.* 64, 1157–1168. doi: 10.1109/TBME.2016.2592953
- Alday, E. A. P., Colman, M. A., Langley, P., Butters, T. D., Higham, J., Workman, A. J., et al. (2015). A new algorithm to diagnose atrial ectopic origin from multi lead ecg systems - insights from 3d virtual human atria and torso. *PLoS Comput. Biol.* 11:e1004026. doi: 10.1371/journal.pcbi.1004026
- Alday, E. A. P., Colman, M. A., Langley, P., and Zhang, H. (2014). “Spatial refinement of a new algorithm to identify focus of atrial ectopic activity from 64-lead ECGs,” in *Computing in Cardiology*, (Washington, D.C: IEEE Computer Society), 501–504.
- Almquist, J., Wallman, M., Jacobson, I., and Jirstrand, M. (2010). Modeling the effect of Kv1.5 block on the canine action potential. *Biophys. J.* 99, 2726–2736. doi: 10.1016/j.bpj.2010.08.062
- Andrade, J., Khairy, P., Dobrev, D., and Nattel, S. (2014). The clinical profile and pathophysiology of atrial fibrillation: relationships among clinical features, epidemiology, and mechanisms. *Circ. Res.* 114, 1453–1468. doi: 10.1161/CIRCRESAHA.114.303211
- Arksey, H., and O’Malley, L. (2005). Scoping studies: towards a methodological framework. *Int. J. Soc. Res. Methodol. Theory Pract.* 8, 19–32. doi: 10.1080/1364557032000119616
- Aronis, K. N., and Ashikaga, H. (2018). Impact of number of co-existing rotors and inter-electrode distance on accuracy of rotor localization. *J. Electrocardiol.* 51, 82–91. doi: 10.1016/j.jelectrocard.2017.08.032
- Ashihara, T., Haraguchi, R., Nakazawa, K., Namba, T., Ikeda, T., Nakazawa, Y., et al. (2012). The role of fibroblasts in complex fractionated electrograms during persistent/permanent atrial fibrillation: implications for electrogram-based catheter ablation. *Circ. Res.* 110, 275–284. doi: 10.1161/CIRCRESAHA.111.255026

CONCLUSION

Computer models become more and more complex as they include an increasing number of parameters. The evolution of the complexity, depicted in **Figure 8**, clearly reflects this pattern. The consideration of ANS branches, in terms of ganglia modeling, and the development of detailed representations of the anatomical heterogeneities, using MRI techniques, improved the reproducibility of the simulations compared to clinical observations. The advances on genomics is also an aspect which is under consideration. The advances on high-performance computing can overcome the computation load and the barriers introduced and thus it can allow the observation of more macroscopic events, such as the transition of the conduction routes which are reflected in the existence of multiple P-wave morphologies in AF patients during SR. Eventually, electrophysiological models of the heart will be used to optimize AF treatment and improve the quality of life in this group of patients.

AUTHOR CONTRIBUTIONS

The study was initiated by the previous works of all the authors. DF and IC defined the inclusion/exclusion rules. DF, IC, and DT initiated the design, development, and synthesis of the studies and received feedback from NM and VV. DF and IC coordinated the writing of all drafts of the manuscript and all other authors contributed to the submitted versions of the manuscript. All authors have read and agreed to the manuscript being submitted as it is.

- Ashihara, T., Namba, T., Ikeda, T., Ito, M., Nakazawa, K., and Trayanova, N. (2004). Mechanisms of Myocardial Capture and Temporal Excitable Gap during Spiral Wave Reentry in a Bidomain Model. *Circulation* 109, 920–925. doi: 10.1161/01.CIR.0000118331.13524.75
- Ashihara, T., Yao, T., Namba, T., Kawase, A., Ikeda, T., Nakazawa, K., et al. (2002). Differences in sympathetic and vagal effects on paroxysmal atrial fibrillation: a simulation study. *Biomed. Pharmacother.* 56, 359s–363s.
- Aslanidi, O. V., Al-Owais, M., Benson, A. P., Colman, M., Garratt, C. J., Gilbert, S. H., et al. (2012a). Virtual tissue engineering of the human atrium: modelling pharmacological actions on atrial arrhythmogenesis. *Eur. J. Pharm. Sci.* 46, 209–221. doi: 10.1016/j.ejps.2011.08.014
- Aslanidi, O. V., Colman, M. A., Zhao, J., Smaill, B. H., Gilbert, S. H., Hancox, J. C., et al. (2012b). Arrhythmogenic substrate for atrial fibrillation: insights from an integrative computational model of pulmonary veins. *Conf. Proc. IEEE Eng. Med. Biol. Soc.* 2012, 203–206. doi: 10.1109/EMBC.2012.6345906
- Aslanidi, O. V., Boyett, M. R., and Zhang, H. (2008). Effects of the intracellular Ca²⁺ dynamics on restitution properties and stability of reentry in rabbit atrial tissue model. *Comput. Cardiol.* 35, 295–297. doi: 10.1109/CIC.2008.4749036
- Aslanidi, O. V., Boyett, M. R., and Zhang, H. (2009a). Left to right atrial electrophysiological differences: substrate for a dominant reentrant source during atrial fibrillation. *Lect. Notes Comput. Sci.* 5528, 154–161. doi: 10.1007/978-3-642-01932-6_17
- Aslanidi, O. V., Robinson, R., Cheverton, D., Boyett, M. R., and Zhang, H. (2009b). Electrophysiological substrate for a dominant reentrant source during atrial fibrillation. *Conf. Proc. IEEE Eng. Med. Biol. Soc.* 2009, 2819–2822. doi: 10.1109/EMBS.2009.5333573
- Aslanidi, O. V., Butters, T. D., Ren, C. X., Ryecroft, G., and Zhang, H. (2011a). Electrophysiological models for the heterogeneous canine atria: computational platform for studying rapid atrial arrhythmias. *Conf. Proc. IEEE Eng. Med. Biol. Soc.* 2011, 1693–1696.
- Aslanidi, O. V., Colman, M. A., Stott, J., Dobrzynski, H., Boyett, M. R., Holden, A. V., et al. (2011b). 3D virtual human atria: a computational platform for studying clinical atrial fibrillation. *Prog. Biophys. Mol. Biol.* 107, 156–168. doi: 10.1016/j.pbiomolbio.2011.06.011
- Aslanidi, O. V., Colman, M. A., Varela, M., Zhao, J., Smaill, B. H., Hancox, J. C., et al. (2013). Heterogeneous and anisotropic integrative model of pulmonary veins: computational study of arrhythmogenic substrate for atrial fibrillation. *Inter. Focus* 3:20120069. doi: 10.1098/rsfs.2012.0069
- Bayer, J. D., Roney, C. H., Pashaei, A., Jais, P., and Vigmond, E. J. (2016). Novel radiofrequency ablation strategies for terminating atrial fibrillation in the left atrium: a simulation study. *Front. Physiol.* 7:108. doi: 10.3389/fphys.2016.00108
- Bear, L. R., Cheng, L. K., LeGrice, I. J., Sands, G. B., Lever, N. A., Paterson, D. J., et al. (2015). Forward problem of electrocardiography: is it solved? *Circ. Arrhythmia Electrophysiol.* 8, 677–684. doi: 10.1161/CIRCEP.114.001573
- Becerra, M. A., Murillo-Escobar, J., Palacio, L. C., and Zuluaga, C. T. (2014). “Noise and spatial-resolution effect of electrode array on rotor tip location during atrial fibrillation: A simulation study,” in *Computing in Cardiology*, (Washington, DC: IEEE Computer Society), 797–800.
- Beeler, G. W., and Reuter, H. (1977). Reconstruction of the action potential of ventricular myocardial fibres. *J. Physiol.* 268, 177–210. doi: 10.1113/jphysiol.1977.sp011853
- Benson, B. E., Carrick, R., Habel, N., Bates, O., Bates, J. H. T., Bielau, P., et al. (2014). Mapping multi-wavelet reentry without isochrones: an electrogram-guided approach to define substrate distribution. *Europace* 16, iv102–iv109. doi: 10.1093/europace/euu254
- Berenfeld, O. (2016). The major role of IK1 in mechanisms of rotor drift in the atria: a computational study. *Clin. Med. Insights Cardiol.* 10(Suppl. 1), 71–79. doi: 10.4137/CMC.S39773
- Bers, D. M., and Grandi, E. (2011). Human atrial fibrillation: insights from computational electrophysiological models. *Trends Cardiovasc. Med.* 21, 145–150. doi: 10.1016/j.tcm.2012.04.004
- Boegli, M., Blanc, O., Virag, N., Vesin, J.-M., and Kappenberger, L. (2000). Study of the defibrillation process in a computer model of human atria. *Annu. Int. Conf. IEEE Eng. Med. Biol. Proc.* 3, 1848–1849. doi: 10.1109/EMBS.2000.900446
- Boyle, P. M., Zahid, S., and Trayanova, N. A. (2017). Using personalized computer models to custom-tailor ablation procedures for atrial fibrillation patients: are we there yet? *Expert Rev. Cardiovasc. Ther.* 15, 339–341. doi: 10.1080/14779072.2017.1317593
- Brocklehurst, P., Ni, H., Zhang, H., and Ye, J. (2017). Electro-mechanical dynamics of spiral waves in a discrete 2D model of human atrial tissue. *PLoS One* 12:e0176607. doi: 10.1371/journal.pone.0176607
- Burdumy, M., Luik, A., Neher, P., Hanna, R., Krueger, M. W., Schilling, C., et al. (2012). Comparing measured and simulated wave directions in the left atrium a workflow for model personalization and validation. *Biomed. Tech.* 57, 79–87. doi: 10.1515/bmt-2011-0059
- Butters, T. D., Aslanidi, O., Zhao, J., Smaill, B., and Zhang, H. (2013). A novel computational sheep atria model for the study of atrial fibrillation. *Inter. focus* 3:20120067. doi: 10.1098/rsfs.2012.0067
- Cacciani, F., and Zaniboni, M. (2015). Chronotropic modulation of the source-sink relationship of sinoatrial-atrial impulse conduction and its significance to initiation of AF: a one-dimensional model study. *Biomed. Res. Int.* 2015:18. doi: 10.1155/2015/496418
- Calvo, C. J., Deo, M., Zlochiver, S., Millet, J., and Berenfeld, O. (2014). Attraction of rotors to the pulmonary veins in paroxysmal atrial fibrillation: a modeling study. *Biophys. J.* 106, 1811–1821. doi: 10.1016/j.bpj.2014.02.030
- Camm, A. J., Al-Khatib, S. M., Calkins, H., Halperin, J. L., Kirchhof, P., Lip, G. Y. H., et al. (2012a). A proposal for new clinical concepts in the management of atrial fibrillation. *Am. Heart J.* 164, 292.e–302.e. doi: 10.1016/j.ahj.2012.05.017
- Camm, A. J., Lip, G. Y. H., De Caterina, R., Savelieva, I., Atar, D., Hohnloser, S. H., et al. (2012b). 2012 focused update of the ESC Guidelines for the management of atrial fibrillation: An update of the 2010 ESC Guidelines for the management of atrial fibrillation * Developed with the special contribution of the European Heart Rhythm Association. *Europace* 14, 1385–1413. doi: 10.1093/europace/eus305
- Carrick, R. T., Benson, B. E., Bates, J. H. T., and Spector, P. S. (2016). Prospective, tissue-specific optimization of ablation for multiwavelet reentry: predicting the required amount, location, and configuration of lesions. *Circ. Arrhythmia Electrophysiol.* 9:e003555. doi: 10.1161/CIRCEP.115.003555
- Carrillo, P., Seemann, G., Scholz, E., Weiss, D. L., and Dössel, O. (2008). Impact of the hERG channel mutation N588K on the electrical properties of the human atrium. *IFMBE* 22, 2583–2586. doi: 10.1007/978-3-540-89208-3_620
- Censi, F., Corazza, I., Reggiani, E., Calcagnini, G., Mattei, E., Triventi, M., et al. (2016). P-wave variability and atrial fibrillation. *Sci. Rep.* 6:26799. doi: 10.1038/srep26799
- Chang, K. C., Bayer, J. D., and Trayanova, N. A. (2014). Disrupted calcium release as a mechanism for atrial alternans associated with human atrial fibrillation. *PLoS Comput. Biol.* 10:e1004011. doi: 10.1371/journal.pcbi.1004011
- Chang, K. C., and Trayanova, N. A. (2016). Mechanisms of arrhythmogenesis related to calcium-driven alternans in a model of human atrial fibrillation. *Sci. Rep.* 6:36395. doi: 10.1038/srep36395
- Cherry, E. M., Ehrlich, J. R., Nattel, S., and Fenton, F. H. (2007). Pulmonary vein reentry-properties and size matter: insights from a computational analysis. *Hear. Rhythm* 4, 1553–1562. doi: 10.1016/j.hrrthm.2007.08.017
- Cherry, E. M., and Evans, S. J. (2008). Properties of two human atrial cell models in tissue: Restitution, memory, propagation, and reentry. *J. Theor. Biol.* 254, 674–690. doi: 10.1016/j.jtbi.2008.06.030
- Ciaccio, E. J., Biviano, A. B., Wan, E. Y., Peters, N. S., and Garan, H. (2017). Development of an automaton model of rotational activity driving atrial fibrillation. *Comput. Biol. Med.* 83, 166–181. doi: 10.1016/j.combiomed.2017.02.008
- Colman, M. A., Aslanidi, O. V., Kharche, S., Boyett, M. R., Garratt, C., Hancox, J. C., et al. (2013). Pro-arrhythmogenic effects of atrial fibrillation-induced electrical remodelling: insights from the three-dimensional virtual human atria. *J. Physiol.* 591, 4249–4272. doi: 10.1113/jphysiol.2013.254987
- Colman, M. A., Sarathy, P. P., Macquaide, N., and Workman, A. J. (2016). “A new model of the human atrial myocyte with variable T-tubule organization for the study of atrial fibrillation,” in *Computing in Cardiology*, (Washington, DC: IEEE Computer Society), 221–224.
- Colman, M. A., Varela, M., Hancox, J. C., Zhang, H., and Aslanidi, O. V. (2014). Evolution and pharmacological modulation of the arrhythmogenic wave dynamics in canine pulmonary vein model. *Europace* 16, 416–423. doi: 10.1093/europace/eut349

- Colquhoun, H. L., Levac, D., O'Brien, K. K., Straus, S., Tricco, A. C., Perrier, L., et al. (2014). Scoping reviews: Time for clarity in definition, methods, and reporting. *J. Clin. Epidemiol.* 67, 1291–1294. doi: 10.1016/j.jclinepi.2014.03.013
- Comtois, P., and Nattel, S. (2011). Impact of tissue geometry on simulated cholinergic atrial fibrillation: a modeling study. *Chaos* 21:13108. doi: 10.1063/1.3544470
- Comtois, P., Sakabe, M., Vigmond, E. J., Munoz, M., Texier, A., Shiroshita-Takeshita, A., et al. (2008). Mechanisms of atrial fibrillation termination by rapidly unbinding Na^+ channel blockers: Insights from mathematical models and experimental correlates. *Am. J. Physiol. Hear. Circ. Physiol.* 295, H1489–H1504. doi: 10.1152/ajpheart.01054.2007
- Courtemanche, M., Ramirez, R. J., and Nattel, S. (1998). Ionic mechanisms underlying human atrial action potential properties: insights from a mathematical model. *Am. J. Physiol.* 275, H301–H321. doi: 10.1152/ajpheart.1998.275.1.H301
- Courtemanche, M., Ramirez, R. J., and Nattel, S. (1999). Ionic targets for drug therapy and atrial fibrillation-induced electrical remodeling: Insights from a mathematical model. *Cardiovasc. Res.* 42, 477–489. doi: 10.1016/S0008-6363(99)00034-36
- Dang, L., Virag, N., Ihara, Z., Jacquemet, V., Vesin, J.-M., Schlaepfer, J., et al. (2005). Evaluation of ablation patterns using a biophysical model of atrial fibrillation. *Ann. Biomed. Eng.* 33, 465–474. doi: 10.1007/s10439-005-2502-7
- Deng, D., Murphy, M. J., Hakim, J. B., Franceschi, W. H., Zahid, S., Pashakhanloo, F., et al. (2017). Sensitivity of reentrant driver localization to electrophysiological parameter variability in image-based computational models of persistent atrial fibrillation sustained by a fibrotic substrate. *Chaos* 27:9392. doi: 10.1063/1.5003340
- Deng, D., and Xia, L. (2010). “Study the effect of tissue heterogeneity and anisotropy in atrial fibrillation based on a human atrial model,” in *Proceedings of the Computing in Cardiology*, (Belfast: IEEE), 433–436.
- Dorn, A., Krueger, M. W., Seemann, G., and Doessel, O. (2012). Modelling of heterogeneous human atrial electrophysiology. *Biomed. Tech.* 57, 350–353. doi: 10.1515/bmt-2012-4215
- Dössel, O., Lenis, G., Loewe, A., Pollnow, S., Rottmann, M., Verma, B., et al. (2017). “Atrial Signals – Modeling Meets Biosignal Analysis,” in *IFMBE Proceedings*, eds H. Eskola and O. Vaisanen (Tampere: Springer), 723–726. doi: 10.1007/978-981-10-5122-7_181
- Duarte, M., Restrepo, A. L., Tobon, C., Cardona, K., and Saiz, J. (2013). “Chloroquine effect on human atrial action potential under normal conditions and during paroxysmal and chronic atrial fibrillation. A simulation study,” in *Proceedings of the Pan American Health Care Exchanges, PAHCE*, (Medellin: IEEE).
- Duarte-Salazar, C. A., Orozco-Duque, A., Tobón, C., Peluffo-Ordóñez, D. H., Luna, J. A. G., and Becerra, M. A. (2017). “Comparison Between Unipolar And Bipolar Electrograms For Detecting Rotor Tip From 2D Fibrillation Model Using Image Fusion. A Simulation Study,” in *2016 IEEE Latin American Conference on Computational Intelligence, LA-CCI 2016 - Proceedings*, ed. G. J. B. Rodriguez (New Jersey: Institute of Electrical and Electronics Engineers Inc.).
- Duchêne, C., Lemay, M., Vesin, J. M., and Van Oosterom, A. (2009). Adaptive multiple frequency tracking algorithm: detection of stable atrial fibrillation sources from standard 12-lead ECG. *Comput. Cardiol.* 36, 505–508.
- Eckstein, J., Maesen, B., Limz, D., Zeemering, S., Van Hunnik, A., Verheule, S., et al. (2011). Time course and mechanisms of endo-epicardial electrical dissociation during atrial fibrillation in the goat. *Cardiovasc. Res.* 89, 816–824. doi: 10.1093/cvr/cvq336
- Ehrlich, J. R., Ocholla, H., Ziemek, D., Rütten, H., Hohnloser, S. H., and Gögelein, H. (2008). Characterization of human cardiac Kv1.5 inhibition by the novel atrial-selective antiarrhythmic compound AVE1231. *J. Cardiovasc. Pharmacol.* 51, 380–387. doi: 10.1097/FJC.0b013e3181669030
- Ehrlich, J. R., Zicha, S., Couto, P., Hébert, T. E., and Nattel, S. (2005). Atrial fibrillation-associated minK38G/S polymorphism modulates delayed rectifier current and membrane localization. *Cardiovasc. Res.* 67, 520–528. doi: 10.1016/j.cardiores.2005.03.007
- Ellinwood, N., Dobrev, D., Morotti, S., and Grandi, E. (2017a). In silico assessment of efficacy and safety of Ikur inhibitors in chronic atrial fibrillation: role of kinetics and state-dependence of drug binding. *Front. Pharmacol.* 8:799. doi: 10.3389/fphar.2017.00799
- Ellinwood, N., Dobrev, D., Morotti, S., and Grandi, E. (2017b). Revealing kinetics and state-dependent binding properties of Ikur-targeting drugs that maximize atrial fibrillation selectivity. *Chaos* 27:93918. doi: 10.1063/1.5000226
- Ellis, W. S., Sippensgroenewegen, A., Auslander, D. M., and Lesh, M. D. (2000). The role of the crista terminalis in atrial flutter and fibrillation: a computer modeling study. *Ann. Biomed. Eng.* 28, 742–754. doi: 10.1114/1.1289456
- Felix, J., Jacquemet, V., Alcaraz, R., and Rieta, J. J. (2015). Study on the trustability of phase mapping methods to represent atrial potentials in atrial fibrillation. *Comput. Cardiol.* 42, 49–52. doi: 10.1109/CIC.2015.7408583
- Ferrer, A., Sebastián, R., Sánchez-Quintana, D., Rodríguez, J. F., Godoy, E. J., Martínez, L., et al. (2015). Detailed anatomical and electrophysiological models of human atria and torso for the simulation of atrial activation. *PLoS One* 10:e0141573. doi: 10.1371/journal.pone.0141573
- Figuera, C., Suárez-Gutiérrez, V., Barquero-Perez, O., Goya-Esteban, R., Rodrigo, M., Hernández, I., et al. (2016a). “Performance of inverse problem regularization methods for driver location during atrial fibrillation,” in *Computing in Cardiology*, (Vancouver, BC: IEEE Computer Society), 693–696.
- Figuera, C., Suárez-Gutiérrez, V., Hernández-Romero, I., Rodrigo, M., Liberos, A., Atienza, F., et al. (2016b). Regularization techniques for ECG imaging during atrial fibrillation: A computational study. *Front. Physiol.* 7:466. doi: 10.3389/fphys.2016.00466
- Filos, D., Chouvarda, I., Tachmatzidis, D., Vassilicos, V., and Maglaveras, N. (2017). Beat-to-beat P-wave morphology as a predictor of paroxysmal atrial fibrillation. *Comput. Methods Programs Biomed.* 151, 111–121. doi: 10.1016/j.cmpb.2017.08.016
- Fink, M., Niederer, S. A., Cherry, E. M., Fenton, F. H., Koivumäki, J. T., Seemann, G., et al. (2011). Cardiac cell modelling: observations from the heart of the cardiac physiome project. *Prog. Biophys. Mol. Biol.* 104, 2–21. doi: 10.1016/j.pbiomolbio.2010.03.002
- Ganesan, P., Salmin, A., Cherry, E. M., and Ghoraani, B. (2016). “Development of a novel probabilistic algorithm for localization of rotors during atrial fibrillation,” in *Proceedings of the Annual International Conference of the IEEE Engineering in Medicine and Biology Society, EMBS*, (New Jersey: Institute of Electrical and Electronics Engineers Inc.), 493–496.
- Garcia-Gudino, D., Landa, E., Mendoza-Temis, J., Albarado-Ibanez, A., Toledo-Roy, J. C., Morales, I. O., et al. (2017). Enhancement of early warning properties in the Kuramoto model and in an atrial fibrillation model due to an external perturbation of the system. *PLoS One* 12:e0181953. doi: 10.1371/journal.pone.0181953
- Gasper, R., Bosch, R. F., Talajic, M., and Nattel, S. (1997). Functional mechanisms underlying tachycardia-induced sustained atrial fibrillation in a chronic dog model. *Circulation* 96, 4027–4035. doi: 10.1161/01.CIR.96.11.4027
- Gharaviri, A., Verheule, S., Eckstein, J., Potse, M., Kuijpers, N. H. L., and Schotten, U. (2012a). A computer model of endo-epicardial electrical dissociation and transmural conduction during atrial fibrillation. *Europace* 14, 10–16. doi: 10.1093/europace/eus270
- Gharaviri, A., Verheule, S., Kuijpers, N., and Schotten, U. (2012b). “Mutual influence between dyssynchrony and transmural conduction maintains atrial fibrillation,” in *Proceedings of the Computing in Cardiology*, (Krakow: IEEE), 897–900.
- Gharaviri, A., Verheule, S., Eckstein, J., Potse, M., Kuklik, P., Kuijpers, N. H. L., et al. (2017). How disruption of endo-epicardial electrical connections enhances endo-epicardial conduction during atrial fibrillation. *Europace* 19, 308–318. doi: 10.1093/europace/euv445
- Glynn, P., Onal, B., and Hund, T. J. (2014). Cycle length restitution in sinoatrial node cells: a theory for understanding spontaneous action potential dynamics. *PLoS One* 9:e89049. doi: 10.1371/journal.pone.0089049
- Gomez, R., Nunez, L., Caballero, R., Vaquero, M., Tamargo, J., and Delpon, E. (2005). Spironolactone and its main metabolite canrenoic acid block hKv1.5. Kv4.3 and Kv7.1 + minK channels. *Br. J. Pharmacol.* 146, 146–161. doi: 10.1038/sj.bjp.0706302
- Gong, Y., Xie, F., Stein, K. M., Garfinkel, A., Culianu, C. A., Lerman, B. B., et al. (2007). Mechanism underlying initiation of paroxysmal atrial flutter/atrial fibrillation by ectopic foci: A simulation study. *Circulation* 115, 2094–2102. doi: 10.1161/CIRCULATIONAHA.106.656504
- Gonzales, M. J., Vincent, K. P., Rappel, W. J., Narayan, S. M., and McCulloch, A. D. (2014). Structural contributions to fibrillatory rotors in a patient-derived

- computational model of the atria. *Europace* 16(Suppl. 4), iv3–iv10. doi: 10.1093/europace/euu251
- Goodman, A. M., Oliver, R. A., Henriquez, C. S., and Wolf, P. D. (2005). A membrane model of electrically remodelled atrial myocardium derived from *in vivo* measurements. *Europace* 7, S135–S145. doi: 10.1016/j.eupc.2005.04.010
- Grandi, E., and Malek, M. M. (2016). Anti-arrhythmic strategies for atrial fibrillation: The role of computational modeling in discovery, development, and optimization. *Pharmacol. Ther.* 168, 126–142. doi: 10.1016/j.pharmthera.2016.09.012
- Grandi, E., Pandit, S. V., Voigt, N., Workman, A. J., Dobrev, D., Jalife, J., et al. (2011). Human atrial action potential and Ca^{2+} model: Sinus rhythm and chronic atrial fibrillation. *Circ. Res.* 109, 1055–1066. doi: 10.1161/CIRCRESAHA.111.253955
- Green, H. D., Thomas, G., and Terry, J. R. (2017). Signal reconstruction of pulmonary vein recordings using a phenomenological mathematical model: application to pulmonary vein isolation therapy. *Front. Physiol.* 8:496. doi: 10.3389/fphys.2017.00496
- Guillem, M. S., Climent, A. M., Rodrigo, M., Hernandez-Romero, I., Liberos, A., Fernandez-Aviles, F., et al. (2016). “Noninvasive identification of atrial fibrillation drivers: Simulation and patient data evaluation,” in *Computing in Cardiology*, (Vancouver, BC: IEEE Computer Society), 121–124.
- Haïssaguerre, M., Jais, P., Shah, D. C., Takahashi, A., Hocini, M., Quiniou, G., et al. (1998). Spontaneous initiation of atrial fibrillation by ectopic beats originating in the pulmonary veins. *N. Engl. J. Med.* 339, 659–666. doi: 10.1056/NEJM199809033391003
- Hancox, J. C., Kharche, S., El Harchi, A., Stott, J., Law, P., and Zhang, H. (2014). In silico investigation of a KCNQ1 mutation associated with familial atrial fibrillation. *J. Electrocardiol.* 47, 158–165. doi: 10.1016/j.jelectrocard.2013.12.004
- Henry, W. L., Morganroth, J., Pearlman, A. S., Clark, C. E., Redwood, D. R., Itscoitz, S. B., et al. (1976). Relation between echocardiographically determined left atrial size and atrial fibrillation. *Circulation* 53, 273–279. doi: 10.1161/01.CIR.53.2.273
- Hong, K., Piper, D. R., Diaz-Valdecantos, A., Brugada, J., Oliva, A., Burashnikov, E., et al. (2005). De novo KCNQ1 mutation responsible for atrial fibrillation and short QT syndrome in utero. *Cardiovasc. Res.* 68, 433–440. doi: 10.1016/j.cardiores.2005.06.023
- Hummel, J. P., Baher, A., Buck, B., Fanarjian, M., Webber, C. L. J., and Akar, J. G. (2017). A method for quantifying recurrent patterns of local waveform direction during atrial fibrillation. *Comput. Biol. Med.* 89, 497–504. doi: 10.1016/j.combiomed.2017.08.027
- Hunter, P., and Borg, T. (2003). Integration from proteins to organs: the Physiome Project. *Nature* 4, 237–243. doi: 10.1038/nrm1054
- Huo, Y., Holmqvist, F., Carlson, J., Gaspar, T., Hindricks, G., Piorkowski, C., et al. (2015). Variability of P-wave morphology predicts the outcome of circumferential pulmonary vein isolation in patients with recurrent atrial fibrillation. *J. Electrocardiol.* 48, 218–225. doi: 10.1016/j.jelectrocard.2014.11.011
- Hwang, M., Kwon, S.-S., Wi, J., Park, M., Lee, H.-S., Park, J.-S., et al. (2014). Virtual ablation for atrial fibrillation in personalized *in-silico* three-dimensional left atrial modeling: comparison with clinical catheter ablation. *Prog. Biophys. Mol. Biol.* 116, 40–47. doi: 10.1016/j.pbiomolbio.2014.09.006
- Hwang, M., Lee, H.-S., Pak, H.-N., and Shim, E. B. (2016). Inducibility of human atrial fibrillation in an *in silico* model reflecting local acetylcholine distribution and concentration. *Korean J. Physiol. Pharmacol.* 20, 111–117. doi: 10.4196/kjpp.2016.20.1.111
- Hwang, M., Lim, B., Song, J.-S. J. S., Yu, H. T., Ryu, A.-J. A. J., Lee, Y. S. Y.-S., et al. (2017). Ganglionated plexi stimulation induces pulmonary vein triggers and promotes atrial arrhythmogenicity: *in silico* modeling study. *PLoS One* 12:e0172931. doi: 10.1371/journal.pone.0172931
- Ikeda, Z., Jacquemet, V., Vesin, J.-M., and Van Oosterom, A. (2005). “Adaptation of the standard 12-lead EGG system focusing on atrial electrical activity,” in *Proceedings of the Computers in Cardiology*, (Lyon: IEEE), 203–205.
- Ikeda, Z., van Oosterom, A., Jacquemet, V., and Hoekema, R. (2007). Adaptation of the standard 12-lead electrocardiogram system dedicated to the analysis of atrial fibrillation. *J. Electrocardiol.* 40, e1–e68. doi: 10.1016/j.jelectrocard.2006.04.006
- Yengar, N., Peng, C. K., Morin, R., Goldberger, A. L., and Lipsitz, L. A. (1996). Age-related alterations in the fractal scaling of cardiac interbeat interval dynamics. *Am. J. Physiol.* 271, R1078–R1084. doi: 10.1152/ajpregu.1996.271.4.R1078
- Jacquemet, V. (2015). Modeling left and right atrial contributions to the ECG: A dipole-current source approach. *Comput. Biol. Med.* 65, 192–199. doi: 10.1016/j.combiomed.2015.06.007
- Jacquemet, V. (2016). Lessons from computer simulations of ablation of atrial fibrillation. *J. Physiol.* 594, 2417–2430. doi: 10.1113/jphysiol.2016.271660
- Jacquemet, V., and Henriquez, C. S. (2009). Genesis of complex fractionated atrial electrograms in zones of slow conduction: a computer model of microfibrosis. *Hear. Rhythm* 6, 803–810. doi: 10.1016/j.hrthm.2009.02.026
- Jacquemet, V., Lemay, M., Uldry, L., Duchêne, C., Van Oosterom, A., Kappenberger, L., et al. (2009). The role of atrial modeling in the development of ECG processing tools. *IFMBE* 25, 429–432. doi: 10.1007/978-3-642-03882-2-114
- Jacquemet, V., Lemay, M., Van Oosterom, A., and Kappenberger, L. (2006). The equivalent dipole used to characterize atrial fibrillation. *Comput. Cardiol.* 33, 149–152.
- Jacquemet, V., Lemay, M., Vesin, J. M., Van Oosterom, A., and Kappenberger, L. (2005). A biophysical model of ECG signals during atrial fibrillation used to evaluate the performance of QRST cancellation algorithms. *Comput. Cardiol.* 2005, 343–346. doi: 10.1109/CIC.2005.1588107
- Jacquemet, V., Virag, N., Ihara, Z., Dang, L., Blanc, O., Zozor, S., et al. (2003). Study of Unipolar Electrogram Morphology in a Computer Model of Atrial Fibrillation. *J. Cardiovasc. Electrophysiol.* 14, S172–S179.
- Jones, G., Spencer, B. D., Adeniran, I., and Zhang, H. (2012). Development of biophysically detailed electrophysiological models for pacemaking and non-pacemaking human pulmonary vein cardiomyocytes. *Conf. Proc. IEEE Eng. Med. Biol. Soc.* 2012, 199–202. doi: 10.1109/EMBC.2012.6345905
- Katritsis, D. G., Pokushalov, E., Romanov, A., Giazitzoglou, E., Siontis, G. C. M., Po, S. S., et al. (2013). Autonomic denervation added to pulmonary vein isolation for paroxysmal atrial fibrillation: A randomized clinical trial. *J. Am. Coll. Cardiol.* 62, 2318–2325. doi: 10.1016/j.jacc.2013.06.053
- Kharche, S., Adeniran, I., Stott, J., Law, P., Boyett, M. R., Hancox, J. C., et al. (2012a). Pro-arrhythmogenic effects of the S140G KCNQ1 mutation in human atrial fibrillation - insights from modelling. *J. Physiol.* 590, 4501–4514. doi: 10.1113/jphysiol.2012.229146
- Kharche, S., Biktasheva, I., Seemann, G., Zhang, H. G., and Biktashev, V. (2012b). Cardioversion using feedback stimuli in human atria. *Comput. Cardiol.* 39, 133–136.
- Kharche, S., Castro, S., Thomas, B., Colman, M., Jarvis, J., Smaill, B., et al. (2014a). “Role of fiber orientation in atrial arrhythmogenesis,” in *Computing in Cardiology*, (Washington, D.C: IEEE Computer Society), 1041–1044.
- Kharche, S. R., Stary, T., Colman, M. A., Biktasheva, I. V., Workman, A. J., Rankin, A. C., et al. (2014b). Effects of human atrial ionic remodelling by β -blocker therapy on mechanisms of atrial fibrillation: A computer simulation. *Europace* 16, 1524–1533. doi: 10.1093/europace/euu084
- Kharche, S., Garratt, C. J., Boyett, M. R., Inada, S., Holden, A. V., Hancox, J. C., et al. (2008). Atrial proarrhythmia due to increased inward rectifier current (IK1) arising from KCNJ2 mutation - A simulation study. *Prog. Biophys. Mol. Biol.* 98, 186–197. doi: 10.1016/j.pbiomolbio.2008.10.010
- Kharche, S. R., Biktasheva, I. V., Seemann, G., Zhang, H., Zhao, J., and Biktashev, V. N. (2015). Computational modelling of low voltage resonant drift of scroll waves in the realistic human atria. *Lect. Notes Comput. Sci.* 9126, 421–429. doi: 10.1007/978-3-319-20309-6_48
- Kharche, S. R., Biktasheva, I. V., Zhang, H., and Biktashev, V. N. (2013). Simulating the role of anisotropy in human atrial cardioversion. *Conf. IEEE Eng. Med. Biol. Soc.* 2013, 6838–6841. doi: 10.1109/EMBC.2013.6611128
- Kharche, S. R., Vigmond, E., Efimov, I. R., and Dobrzynski, H. (2017). Computational assessment of the functional role of sinoatrial node exit pathways in the human heart. *PLoS One* 12:e0183727. doi: 10.1371/journal.pone.0183727
- Ki, C.-S., Jung, C. L., Kim, H.-J., Baek, K.-H., Park, S. J., On, Y. K., et al. (2014). A KCNQ1 mutation causes age-dependant bradycardia and persistent atrial fibrillation. *Pflugers Arch. Eur. J. Physiol.* 466, 529–540. doi: 10.1007/s00424-013-1337-1336
- Kirchhof, P., Benussi, S., Koteka, D., Ahlsson, A., Atar, D., Casadei, B., et al. (2016). 2016 ESC Guidelines for the management of atrial fibrillation developed

- in collaboration with EACTS. *Eur. Heart J.* 37, 2893–2962. doi: 10.1093/eurheartj/ehw210
- Kneller, J., Kalifa, J., Zou, R., Zaitsev, A. V., Warren, M., Berenfeld, O., et al. (2005). Mechanisms of atrial fibrillation termination by pure sodium channel blockade in an ionically-realistic mathematical model. *Circ. Res.* 96, e35–e47.
- Kneller, J., Zou, R., Vigmond, E. J., Wang, Z., Leon, L. J., and Nattel, S. (2002). Cholinergic atrial fibrillation in a computer model of a two-dimensional sheet of canine atrial cells with realistic ionic properties. *Circ. Res.* 90, E73–E87.
- Koivumäki, J. T., Clark, R. B., Belke, D., Kondo, C., Fedak, P. W. M., Maleckar, M. M. C., et al. (2014). Na(+) current expression in human atrial myofibroblasts: identity and functional roles. *Front. Physiol.* 5:275. doi: 10.3389/fphys.2014.00275
- Koivumäki, J. T., Korhonen, T., and Tavi, P. (2011). Impact of sarcoplasmic reticulum calcium release on calcium dynamics and action potential morphology in human atrial myocytes: A computational study. *PLoS Comput. Biol.* 7:e1001067. doi: 10.1371/journal.pcbi.1001067
- Koivumäki, J. T., Seemann, G., Maleckar, M. M., and Tavi, P. (2014). In silico screening of the key cellular remodeling targets in chronic atrial fibrillation. *PLoS Comput. Biol.* 10:e1003620. doi: 10.1371/journal.pcbi.1003620
- Krogh-Madsen, T., Abbott, G. W., and Christini, D. J. (2012). Effects of electrical and structural remodeling on atrial fibrillation maintenance: a simulation study. *PLoS Comput. Biol.* 8:e1002390. doi: 10.1371/journal.pcbi.1002390
- Krueger, M. W., Dorn, A., Keller, D. U. J., Holmqvist, F., Carlson, J., Platonov, P. G., et al. (2013a). In-silico modeling of atrial repolarization in normal and atrial fibrillation remodeled state. *Med. Biol. Eng. Comput.* 51, 1105–1119. doi: 10.1007/s11517-013-1090-1
- Krueger, M. W., Schulze, W. H. W., Rhode, K. S., Razavi, R., Seemann, G., and Dössel, O. (2013b). Towards personalized clinical in-silico modeling of atrial anatomy and electrophysiology. *Med. Biol. Eng. Comput.* 51, 1251–1260. doi: 10.1007/s11517-012-0970-0
- Krueger, M. W., Seemann, G., Rhode, K., Keller, D. U. J., Schilling, C., Arujuna, A., et al. (2013c). Personalization of atrial anatomy and electrophysiology as a basis for clinical modeling of radio-frequency ablation of atrial fibrillation. *IEEE Trans. Med. Imaging* 32, 73–84. doi: 10.1109/TMI.2012.2201948
- Krueger, M. W., Seemann, G., Rhode, K. S., Weber, F. M., Linton, N., Williams, S., et al. (2013d). Fusion of local activation time maps and image data to personalize anatomical atrial models. *Lect. Notes Comput. Sci.* 7945, 1–10. doi: 10.1007/978-3-642-38899-6_1
- Krueger, M. W., Rhode, K. S., O'Neill, M. D., Rinaldi, C. A., Gill, J., Razavi, R., et al. (2014). Patient-specific modeling of atrial fibrosis increases the accuracy of sinus rhythm simulations and may explain maintenance of atrial fibrillation. *J. Electrocardiol.* 47, 324–328. doi: 10.1016/j.jelectrocard.2013.11.003
- Krueger, M. W., Severi, S., Rhode, K., Genovesi, S., Weber, F. M., Vincenti, A., et al. (2011). Alterations of atrial electrophysiology related to hemodialysis session: Insights from a multiscale computer model. *J. Electrocardiol.* 44, 176–183. doi: 10.1016/j.jelectrocard.2010.11.016
- Krummen, D. E., Bayer, J. D., Ho, J., Ho, G., Smetak, M. R., Clopton, P., et al. (2012). Mechanisms of human atrial fibrillation initiation clinical and computational studies of repolarization restitution and activation latency. *Circ. Arrhythmia Electrophysiol.* 5, 1149–1159. doi: 10.1161/CIRCEP.111.969022
- Kuijpers, N., Ten Eikelder, H., and Verheule, S. (2009). Atrial anatomy influences onset and termination of atrial fibrillation: a computer model study. *Lect. Notes Comput. Sci.* 5528, 285–294. doi: 10.1007/978-3-642-01932-6_31
- Kuijpers, N. H. L., Keldermann, R. H., Ten Eikelder, H. M. M., Arts, T., and Hilbers, P. A. J. (2006). The role of the hyperpolarization-activated inward current If in arrhythmogenesis: A computer model study. *IEEE Trans. Biomed. Eng.* 53, 1499–1511. doi: 10.1109/TBME.2006.877801
- Kuijpers, N. H. L., Potse, M., Van Dam, P. M., Ten Eikelder, H. M. M., Verheule, S., Prinzen, F. W., et al. (2011). Mechanoelectrical coupling enhances initiation and affects perpetuation of atrial fibrillation during acute atrial dilation. *Hear. Rhythm* 8, 429–436. doi: 10.1016/j.hrthm.2010.11.020
- Kuijpers, N. H. L., Ten Eikelder, H. M. M., Bovendeerd, P. H. M., Verheule, S., Arts, T., and Hilbers, P. A. J. (2007). Mechanoelectric feedback leads to conduction slowing and block in acutely dilated atria: A modeling study of cardiac electromechanics. *Am. J. Physiol. - Hear. Circ. Physiol.* 292, H2832–H2853. doi: 10.1152/ajpheart.00923.2006
- Kuklik, P., Schäffer, B., Hoffmann, B. A., Ganesan, A. N., Schreiber, D., Moser, J. M., et al. (2016). Local electrical dyssynchrony during atrial fibrillation: theoretical considerations and initial catheter ablation results. *PLoS One* 11:e0164236. doi: 10.1371/journal.pone.0164236
- Kwon, S.-S., Yun, Y. H., Hong, S.-B., Pak, H.-N., and Shim, E. B. (2013). A patient-specific model of virtual ablation for atrial fibrillation. *Conf. IEEE Eng. Med. Biol. Soc.* 2013, 1522–1525. doi: 10.1109/EMBC.2013.6609802
- Law, P., Kharche, S., Higham, J., and Zhang, H. (2010). Anti-arrhythmic effects of atrial specific ikur block: A simulation study. *Comput. Cardiol.* 37, 429–432.
- Law, P., Kharche, S., Stott, J., and Zhang, H. (2009). Effects of elevated homocysteine hormone on electrical activity in the human atrium: A simulation study. in proceedings of the 31st annual international conference of the IEEE engineering in medicine and biology society: engineering the future of biomedicine. *EMBC* 2009, 3936–3939. doi: 10.1109/IEMBS.2009.5333530
- Lee, Y.-S., Hwang, M., Song, J.-S., Li, C., Joung, B., Sobie, E. A., et al. (2016). The contribution of ionic currents to rate-dependent action potential duration and pattern of reentry in a mathematical model of human atrial fibrillation. *PLoS One* 11:e0150779. doi: 10.1371/journal.pone.0150779
- Lemay, M., Jacquemet, V., Duchêne, C., Van Oosterom, A., Abächerli, R., and Vesin, J. M. (2009). “Activity level of an atrial ectopic focus observed through the atrial vectorcardiogram: A biophysical model,” in *Proceedings of the 36th Annual Computers in Cardiology Conference (CinC)*, (Park City, UT: IEEE), 221–224.
- Lemay, M., Jacquemet, V., Jousset, F., Vesin, J. M., and Van Oosterom, A. (2007a). “The mean firing rate of atrial fibrillation as estimated from the ECG evaluation using a biophysical model,” in *Proceedings of the Computers in Cardiology*, (Durham, NC: IEEE), 37–40.
- Lemay, M., Vesin, J. M., Jacquemet, V., Forclaz, A., Kappenberger, L., and van Oosterom, A. (2007b). Spatial dynamics of atrial activity assessed by the vectorcardiogram: from sinus rhythm to atrial fibrillation. *Europace* 9(Suppl. 6), vi109–vi118. doi: 10.1093/europace/eum215
- Li, C., Lim, B., Hwang, M., Song, J.-S., Lee, Y.-S., Joung, B., et al. (2016). The spatiotemporal stability of dominant frequency sites in in-silico modeling of 3-dimensional left atrial mapping of atrial fibrillation. *PLoS One* 11:e0160017. doi: 10.1371/journal.pone.0160017
- Li, J., Inada, S., Schneider, J. E., Zhang, H., Dobrzynski, H., and Boyett, M. R. (2014). Three-dimensional computer model of the right atrium including the sinoatrial and atrioventricular nodes predicts classical nodal behaviours. *PLoS One* 9:e112547. doi: 10.1371/journal.pone.0112547
- Li, Q., O'Neill, S. C., Tao, T., Li, Y., Eisner, D., and Zhang, H. (2012). Mechanisms by which cytoplasmic calcium wave propagation and alternans are generated in cardiac atrial myocytes lacking T-tubules-insights from a simulation study. *Biophys. J.* 102, 1471–1482. doi: 10.1016/j.bpj.2012.03.007
- Liberos, A., Bueno-Orovio, A., Rodrigo, M., Ravens, U., Hernandez-Romero, I., Fernandez-Aviles, F., et al. (2016). Balance between sodium and calcium currents underlying chronic atrial fibrillation termination: an in silico intersubject variability study. *Hear. Rhythm* 13, 2358–2365. doi: 10.1016/j.hrthm.2016.08.028
- Lin, Y. T., Chang, E. T., Eatock, J., Galla, T., and Clayton, R. H. (2017). Mechanisms of stochastic onset and termination of atrial fibrillation studied with a cellular automaton model. *J. R. Soc. Inter.* 14:20160968. doi: 10.1098/rsif.2016.0968
- Liu, J., Holden, A. V., and Zhang, H. (2007). Actions of an external electrical shock on human atrial excitation - a computer model study. *Lect. Notes Comput. Sci.* 4561, 659–667. doi: 10.1007/978-3-540-73321-8_76
- Lo, C.-P., Horng, T.-L., Luk, H.-N., Tien, H.-C., Yuan, J.-M., and Lee, D. (2006). A computational model of the canine pulmonary veins sleeves. *J. Med. Biol. Eng.* 26, 125–130. doi: 10.1109/EMBC.2012.6345906
- Loewe, A., Krueger, M. W., Holmqvist, F., Dössel, O., Seemann, G., and Platonov, P. G. (2016). Influence of the earliest right atrial activation site and its proximity to interatrial connections on P-wave morphology. *Europace* 18, iv35–iv43. doi: 10.1093/europace/euw349
- Loewe, A., Wilhelm, M., Fischer, F., Scholz, E. P., Dössel, O., and Seemann, G. (2014). Arrhythmic potency of human ether-à-go-go-related gene mutations L532P and N588K in a computational model of human atrial myocytes. *Europace* 16, 435–443. doi: 10.1093/europace/eut375
- Lombardo, D. M., Fenton, F. H., Narayan, S. M., and Rappel, W. J. (2016). Comparison of detailed and simplified models of human atrial myocytes

- to recapitulate patient specific properties. *PLoS Comput. Biol.* 12:e1005060. doi: 10.1371/journal.pcbi.1005060
- Luca, A., Jacquemet, V., Virag, N., and Vesin, J.-M. (2015). "Influence of right and left atrial tissue heterogeneity on atrial fibrillation perpetuation," in *Computing in Cardiology*, (Washington, DC: IEEE Computer Society), 449–452.
- Luca, A., Kallmyer, T., and Virag, N. (2016). Atrial fibrillation septal pacing: translation of modelling results. *Europace* 18, iv53–iv59. doi: 10.1093/europace/euw360
- Luo, C. H., and Rudy, Y. (1991). A model of the ventricular cardiac action potential. *Circ. Res.* 68, 1501–1526. doi: 10.1161/01.RES.68.6.1501
- Lutz, Y., Loewe, A., Wilhelms, M., Dössel, O., and Seemann, G. (2014). Specific antiarrhythmic therapy for familial atrial fibrillation in a numerical model of human atrial electrophysiology. *Biomed. Tech.* 59, S933–S936. doi: 10.1515/bmt-2014-5012
- Majumder, R., Jangsanthong, W., Feola, I., Ypey, D. L., Pijnappels, D. A., and Panfilov, A. V. (2016). A mathematical model of neonatal rat atrial monolayers with constitutively active acetylcholine-mediated K⁺ current. *PLoS Comput. Biol.* 12:e1004946. doi: 10.1371/journal.pcbi.1004946
- Malekar, M. M., Greenstein, J. L., Giles, W. R., and Trayanova, N. A. (2009). K⁺ current changes account for the rate dependence of the action potential in the human atrial myocyte. *AJP Hear. Circ. Physiol.* 297, H1398–H1410. doi: 10.1152/ajpheart.00411.2009
- Manani, K. A., Christensen, K., and Peters, N. S. (2016). Myocardial architecture and patient variability in clinical patterns of atrial fibrillation. *Phys. Rev. E* 94, 1–7. doi: 10.1103/PhysRevE.94.042401
- Mann, S. A., Otway, R., Guo, G., Soka, M., Karlsdotter, L., Trivedi, G., et al. (2012). Epistatic effects of potassium channel variation on cardiac repolarization and atrial fibrillation risk. *J. Am. Coll. Cardiol.* 59, 1017–1025. doi: 10.1016/j.jacc.2011.11.039
- Markides, V., and Schilling, R. J. (2003). Atrial fibrillation: classification, pathophysiology, mechanisms and drug treatment. *Heart* 89, 939–943. doi: 10.1136/heart.89.8.939
- Marshall, G. E., Russell, J. A., Tellez, J. O., Jhund, P. S., Currie, S., Dempster, J., et al. (2012). Remodelling of human atrial K⁺ currents but not ion channel expression by chronic β-blockade. *Pflügers Arch. Eur. J. Physiol.* 463, 537–548. doi: 10.1007/s00424-011-1061-z
- Martínez, A., Alcaraz, R., and Rieta, J. J. (2012). Study on the P-wave feature time course as early predictors of paroxysmal atrial fibrillation. *Physiol. Meas.* 33, 1959–1974. doi: 10.1088/0967-3343/33/12/1959
- Martínez, A., Alcaraz, R., and Rieta, J. J. (2014a). Morphological variability of the P-wave for premature envision of paroxysmal atrial fibrillation events. *Physiol. Meas.* 35, 1–14. doi: 10.1088/0967-3343/35/1/1
- Martínez, L., Romero, L., Tobón, C., Ferrero, J. M., Jalife, J., Berenfeld, O., et al. (2014b). "Accurate characterization of rotor activity during atrial fibrillation depends on the properties of the multi-electrode grid," in *Proceedings of the Computing in Cardiology*, (Washington, DC: IEEE Computer Society), 757–760.
- Martínez, L., Romero, L., Ferrer, A., Jalife, J., Berenfeld, O., and Saiz, J. (2016). "Effect of multi-electrode configurations on accuracy of rotor detection in the atria," in *Proceedings of the Computing in Cardiology*, (Washington, DC: IEEE Computer Society), 1085–1088.
- McDowell, K. S., Vadakkumpadan, F., Blake, R., Blauer, J., Plank, G., MacLeod, R. S., et al. (2012). Methodology for patient-specific modeling of atrial fibrosis as a substrate for atrial fibrillation. *J. Electrocardiol.* 45, 640–645. doi: 10.1016/j.jelectrocard.2012.08.005
- McDowell, K. S., Vadakkumpadan, F., Blake, R., Blauer, J., Plank, G., Macleod, R. S., et al. (2013). Mechanistic inquiry into the role of tissue remodeling in fibrotic lesions in human atrial fibrillation. *Biophys. J.* 104, 2764–2773. doi: 10.1016/j.bpj.2013.05.025
- Michelucci, A., Bagliani, G., Colella, A., Pieragnoli, P., Porciani, M. C., Gensini, G., et al. (2002). P wave assessment: State of the art update. *Card. Electrophysiol. Rev.* 6, 215–220. doi: 10.1023/A:1016368723033
- Moe, G. K., Rheinboldt, W. C., and Abildskov, J. A. (1964). A computer model of atrial fibrillation. *Am. Heart J.* 67, 200–220. doi: 10.1016/0002-8703(64)90371-90370
- Monfredi, O., Dobrzynski, H., Mondal, T., Boyett, M. R., and Morris, G. M. (2010). The anatomy and physiology of the sinoatrial node-A contemporary review. *Pacing Clin. Electrophysiol.* 33, 1392–1406. doi: 10.1111/j.1540-8159.2010.02838.x
- Morgan, R., Colman, M., Kruger, M., Seemann, G., Rhode, K., and Aslanidi, O. (2014). "Evaluating effects of fibrosis in atrial arrhythmogenesis using 3D computational modelling," in *Computing in Cardiology*, (Washington, DC: IEEE Computer Society), 765–768.
- Morgan, R., Colman, M. A., Chubb, H., Seemann, G., and Aslanidi, O. V. (2016). Slow conduction in the border zones of patchy fibrosis stabilizes the drivers for atrial fibrillation: insights from multi-scale human atrial modeling. *Front. Physiol.* 7:474. doi: 10.3389/fphys.2016.00474
- Morris, J. J., Estes, E. J., Whalen, R., Thompson, H. J., and McIntosh, H. (1964). P-wave analysis in valvular heart disease. *Circulation* 29, 242–252. doi: 10.1161/01.CIR.29.2.242
- Namba, T., Ashihara, T., Nakazawa, K., and Ohe, T. (1999). Effect of pilsicainide, a pure sodium channel blocker, on spiral waves during atrial fibrillation: Theoretical analysis by numerical simulation. *J. Electrocardiol.* 32, 321–334. doi: 10.1016/S0022-0736(99)90003-90001
- Nattel, S. (2002). New ideas about atrial fibrillation 50 years on. *Nature* 415, 219–226. doi: 10.1038/415219a
- Nguyen, H. Q., Bailey, A., Coleman, K. J., Desai, S., Fan, V. S., Gould, M. K., et al. (2016). Patient-centered physical activity coaching in COPD (Walk On!): A study protocol for a pragmatic randomized controlled trial. *Contemp. Clin. Trials* 46, 18–29. doi: 10.1016/j.cct.2015.10.010
- Ni, H., Adeniran, I., and Zhang, H. (2017a). In-silico investigations of the functional impact of KCNA5 mutations on atrial mechanical dynamics. *J. Mol. Cell. Cardiol.* 111, 86–95. doi: 10.1016/j.yjmcc.2017.08.005
- Ni, H., Whittaker, D. G., Wang, W., Giles, W. R., Narayan, S. M., and Zhang, H. (2017b). Synergistic anti-arrhythmic effects in human atria with combined use of sodium blockers and acacetin. *Front. Physiol.* 8:946. doi: 10.3389/fphys.2017.00946
- Ni, H., Colman, M. A., and Zhang, H. (2014). "Modelling the functional impact of KCNA5 mutations on the electrical and mechanical activities of human atrial cells," in *Computing in Cardiology*, (Washington, DC: IEEE Computer Society), 57–60.
- Ni, H., Whittaker, D. G., Wang, W., and Zhang, H. (2016). "Synergistic anti-arrhythmic effects of combined blockade of sodium and ultra-rapid delayed rectifier potassium channels in human atria," in *Proceedings of the Computing in Cardiology*, (Washington, DC: IEEE Computer Society), 837–840.
- Nishida, K., and Nattel, S. (2014). Atrial fibrillation compendium: Historical context and detailed translational perspective on an important clinical problem. *Circ. Res.* 114, 1447–1452. doi: 10.1161/CIRCRESAHA.114.303466
- Nygren, A., Fiset, C., Firek, L., Clark, J. W., Lindblad, D. S., Clark, R. B., et al. (1998). Mathematical model of an adult human atrial cell: the role of K⁺ currents in repolarization. *Circ. Res.* 82, 63–81. doi: 10.1161/01.RES.82.1.63
- O'Connell, R. P., Musa, H., Gomez, M. S. M., Avula, U. M., Herron, T. J., Kalifa, J., et al. (2015). Free fatty acid effects on the atrial myocardium: membrane ionic currents are remodeled by the disruption of t-tubular architecture. *PLoS One* 10:e0133052. doi: 10.1371/journal.pone.0133052
- Ogawa, M., Kumagai, K., Vakulenko, M., Yasuda, T., Siegerman, C., Garfinkel, A., et al. (2007). Reduction of P-wave duration and successful pulmonary vein isolation in patients with atrial fibrillation. *J. Cardiovasc. Electrophysiol.* 18, 931–938. doi: 10.1111/j.1540-8167.2007.00890.x
- Ogin, J. E., Sih, H. J., Hanish, S., Jayachandran, J. V., Wu, J., Zheng, Q. H., et al. (1998). Heterogeneous atrial denervation creates substrate for sustained atrial fibrillation. *Circulation* 98, 2608–2614. doi: 10.1161/01.CIR.98.23.2608
- Onal, B., Gratz, D., and Hund, T. J. (2017). Ca(2+)/calmodulin-dependent kinase II-dependent regulation of atrial myocyte late Na(+) current, Ca(2+) cycling, and excitability: a mathematical modeling study. *Am. J. Physiol. Heart Circ. Physiol.* 313, H1227–H1239. doi: 10.1152/ajpheart.00185.2017
- Pedrón-Torrecilla, J., Climent, A. M., Liberos, A., Rodrigo, M., Pérez-David, E., Millet, J., et al. (2014). "Accuracy of inverse solution computation of dominant frequencies and phases during atrial fibrillation," in *Proceedings of the Computing in Cardiology*, (Washington, DC: IEEE Computer Society), 537–540.
- Pedrón-Torrecilla, J., Rodrigo, M., Climent, A. M., Liberos, A., Pérez-David, E., Bermejo, J., et al. (2016). Noninvasive estimation of epicardial dominant high-frequency regions during atrial fibrillation. *J. Cardiovasc. Electrophysiol.* 27, 435–442. doi: 10.1111/jce.12931

- Pellman, J., and Sheikh, F. (2015). Atrial fibrillation: mechanisms, therapeutics, and future directions. *Compr. Physiol.* 5, 649–665. doi: 10.1002/cphy.c140047
- Peters, M. D. J., Godfrey, C. M., Khalil, H., McInerney, P., Parker, D., and Soares, C. B. (2015). Guidance for conducting systematic scoping reviews. *Int. J. Evid. Based. Healthc.* 13, 141–146. doi: 10.1097/XEB.0000000000000050
- Platonov, P. G. (2012). P-wave morphology: underlying mechanisms and clinical implications. *Ann. Noninvasive Electrocardiol.* 17, 161–169. doi: 10.1111/j.1542-474X.2012.00534.x
- Ramirez, R. J., Nattel, S., and Courtemanche, M. (2000). Mathematical analysis of canine atrial action potentials: Rate, regional factors, and electrical remodeling. *Am. J. Physiol. - Hear. Circ. Physiol.* 279, H1767–H1785.
- Rappel, W., and Narayan, S. M. (2013). Theoretical considerations for mapping activation in human cardiac fibrillation. *Chaos* 23:023113. doi: 10.1063/1.4807098
- Rappel, W.-J., Zaman, J. A. B., and Narayan, S. M. (2015). Mechanisms for the termination of atrial fibrillation by localized ablation: computational and clinical studies. *Circ. Arrhythmia Electrophysiol.* 8, 1325–1333. doi: 10.1161/CIRCEP.115.002956
- Rensma, P. L., Allessie, M. A., Lammers, W. J. E. P., Bonke, F. I. M., and Schalij, M. J. (1988). Length of excitation wave and susceptibility to reentrant atrial arrhythmias in normal conscious dogs. *Circ. Res.* 62, 395–410. doi: 10.1161/01.RES.62.2.395
- Reumann, M., Bohnert, J., and Doessel, O. (2006). Simulating pulmonary vein activity leading to atrial fibrillation using a rule-based approach on realistic anatomical data. *Conf. Proc. IEEE Eng. Med. Biol. Soc.* 1, 3943–3946. doi: 10.1109/IEMBS.2006.260383
- Reumann, M., Bohnert, J., Osswald, B., Hagl, S., and Doessel, O. (2007). Multiple wavelets, rotors, and snakes in atrial fibrillation-a computer simulation study. *J. Electrocardiol.* 40, 328–334. doi: 10.1016/j.jelectrocard.2006.12.016
- Reumann, M., Bohnert, J., Seemann, G., Osswald, B., and Dössel, O. (2008). Preventive ablation strategies in a biophysical model of atrial fibrillation based on realistic anatomical data. *IEEE Trans. Biomed. Eng.* 55, 399–406. doi: 10.1109/TBME.2007.912672
- Rice, J. J., Wang, F., Bers, D. M., and De Tombe, P. P. (2008). Approximate model of cooperative activation and crossbridge cycling in cardiac muscle using ordinary differential equations. *Biophys. J.* 95, 2368–2390. doi: 10.1529/biophysj.107.119487
- Rodrigo, M., Clirnent, A. M., Liberos, A., Pedrón-Torrecilla, J., Millet, J., Fernández-Avilés, F., et al. (2014a). “Non-invasive detection of reentrant drivers during atrial fibrillation: A clinical-computational study,” in *Proceedings of the Computing in Cardiology*, (Washington, DC: IEEE Computer Society), 9–12.
- Rodrigo, M., Guillem, M. S., Climent, A. M., Pedrón-Torrecilla, J., Liberos, A., Millet, J., et al. (2014b). Body surface localization of left and right atrial high-frequency rotors in atrial fibrillation patients: a clinical-computational study. *Hear. Rhythm* 11, 1584–1591. doi: 10.1016/j.hrthm.2014.05.013
- Roney, C. H., Bayer, J. D., Zahid, S., Meo, M., Boyle, P. M. J., Trayanova, N. A., et al. (2016). Modelling methodology of atrial fibrosis affects rotor dynamics and electrograms. *Europace* 18, iv146–iv155. doi: 10.1093/europace/euw365
- Roney, C. H., Cantwell, C. D., Bayer, J. D., Qureshi, N. A., Lim, P. B., Tweedy, J. H., et al. (2017). Spatial resolution requirements for accurate identification of drivers of atrial fibrillation. *Circ. Arrhythm. Electrophysiol.* 10:e004899. doi: 10.1161/CIRCEP.116.004899
- Rotter, M., Dang, L., Jacquemet, V., Virag, N., Kappenberger, L., and Haïssaguerre, M. (2007). Impact of varying ablation patterns in a simulation model of persistent atrial fibrillation. *Pacing Clin. Electrophysiol.* 30, 314–321. doi: 10.1111/j.1540-8159.2007.00671.x
- Rottmann, M., Unger, L., Kaltenbacher, W., Seemann, G., Loewe, A., Krueger, M. W., et al. (2015). “Methods for analyzing signal characteristics of stable and unstable rotors in a realistic heart model,” in *Proceedings of the Computing in Cardiology*, (Washington, DC: IEEE Computer Society), 485–488.
- Ruchat, P., Dang, L., Schlaepfer, J., Virag, N., von Segesser, L. K., and Kappenberger, L. (2007a). Use of a biophysical model of atrial fibrillation in the interpretation of the outcome of surgical ablation procedures. *Eur. J. Cardio-thoracic Surg.* 32, 90–95. doi: 10.1016/j.ejcts.2007.02.031
- Ruchat, P., Dang, L., Virag, N., Schlaepfer, J., von Segesser, L. K., and Kappenberger, L. (2007b). A biophysical model of atrial fibrillation to define the appropriate ablation pattern in modified maze. *Eur. J. Cardio-thoracic Surg.* 31, 65–69. doi: 10.1016/j.ejcts.2006.10.015
- Ruchat, P., Virag, N., Dang, L., Schlaepfer, J., Pruvot, E., and Kappenberger, L. (2007c). A biophysical model of atrial fibrillation ablation: what can a surgeon learn from a computer model? *Europace* 9(Suppl. 6), vi71–vi76. doi: 10.1093/europace/eum209
- Rusu, A., Jacquemet, V., Vesin, J.-M., and Virag, N. (2014). Influence of atrial substrate on local capture induced by rapid pacing of atrial fibrillation. *Europace* 16, 766–773. doi: 10.1093/europace/euu003
- Saha, M., Conte, G., Caputo, M. L., Regoli, F., Krause, R., Auricchio, A., et al. (2016). Changes in P-wave morphology after pulmonary vein isolation: insights from computer simulations. *Europace* 18, iv23–iv34. doi: 10.1093/europace/euw348
- Sahli Costabal, F., Zaman, J. A. B., Kuhl, E., and Narayan, S. M. (2018). Interpreting activation mapping of atrial fibrillation: a hybrid computational/physiological study. *Ann. Biomed. Eng.* 46, 257–269. doi: 10.1007/s10439-017-1969-3
- Salmin, A. J., Ganesan, P., Shillieto, K. E., Cherry, E. M., Huang, D. T., Pertsov, A. M., et al. (2016). A novel catheter-guidance algorithm for localization of atrial fibrillation rotor and focal sources. *Conf. Proc. IEEE Eng. Med. Biol. Soc.* 2016, 501–504. doi: 10.1109/EMBC.2016.7590749
- Sampson, K. J., Terrenoire, C., Cervantes, D. O., Kaba, R. A., Peters, N. S., and Kass, R. S. (2008). Adrenergic regulation of a key cardiac potassium channel can contribute to atrial fibrillation: Evidence from an IKs transgenic mouse. *J. Physiol.* 586, 627–637. doi: 10.1113/jphysiol.2007.141333
- Sanchez, C., Bueno-Orovio, A., Pueyo, E., and Rodriguez, B. (2017). Atrial fibrillation dynamics and ionic block effects in six heterogeneous human 3d virtual atria with distinct repolarization dynamics. *Front. Bioeng. Biotechnol.* 5:29. doi: 10.3389/fbioe.2017.00029
- Sanchez, C., Corrias, A., Bueno-Orovio, A., Davies, M., Swinton, J., Jacobson, I., et al. (2012). The Na+/K+ pump is an important modulator of refractoriness and rotor dynamics in human atrial tissue. *Am. J. Physiol. Heart Circ. Physiol.* 302, H1146–H1159. doi: 10.1152/ajpheart.00668.2011
- Sanders, P., Morton, J. B., Davidson, N. C., Spence, S. J., Vohra, J. K., Sparks, P. B., et al. (2003). Electrical remodeling of the atria in congestive heart failure: Electrophysiological and electroanatomic mapping in humans. *Circulation* 108, 1461–1468. doi: 10.1161/01.CIR.0000090688.4928.3.67
- Scholz, E. P., Carrillo-Bustamante, P., Fischer, F., Wilhelms, M., Zitron, E., Dössel, O., et al. (2013). Rotor termination is critically dependent on kinetic properties of I Kur inhibitors in an In Silico model of chronic atrial fibrillation. *PLoS One* 8:e83179. doi: 10.1371/journal.pone.0083179
- Seemann, G., Carillo, P., Weiss, D. L., Krueger, M. W., Dössel, O., and Scholz, E. P. (2009). Investigating arrhythmogenic effects of the herg mutation n588k in virtual human atria. *Lect. Notes Comput. Sci.* 5528, 144–153. doi: 10.1007/978-3-642-01932-6_16
- Seemann, G., Weiß, D. L., Sachse, F. B., and Dössel, O. (2004). “Familial atrial fibrillation: Simulation of the mechanisms and effects of a slow rectifier potassium channel mutation in human atrial tissue,” in *Proceedings of the Computers in Cardiology*, (Chicago, IL: IEEE), 125–128.
- Seemann, G., Ying, H., Weiss, D. L., Sachse, F. B., and Dössel, O. (2005). “Effects of electrophysiological remodeling in human right atrium: A simulation study,” in *Proceedings of the Computers in Cardiology*, (Lyon: IEEE), 69–72. doi: 10.1109/CIC.2005.1588036
- Seol, C. A., Kim, J., Kim, W. T., Ha, J. M., Choe, H., Jang, Y. J., et al. (2008). Simulation of spontaneous action potentials of cardiomyocytes in pulmonary veins of rabbits. *Prog. Biophys. Mol. Biol.* 96, 132–151. doi: 10.1016/j.pbiomolbio.2007.07.013
- Severi, S., Fantini, G., Corsi, C., Vincenti, A., and Genovesi, S. (2008). Role of hemodialysis in atrial fibrillation onset: preliminary results from a combined computational and experimental analysis. *Comput. Cardiol.* 35, 877–879. doi: 10.1109/CIC.2008.4749182
- Severi, S., Pogliani, D., Fantini, G., Fabbrini, P., Vigàò, M. R., Galbiati, E., et al. (2010). Alterations of atrial electrophysiology induced by electrolyte variations: Combined computational and P-wave analysis. *Europace* 12, 842–849. doi: 10.1093/europace/euq042
- Shen, M. J., Choi, E. K., Tan, A. Y., Han, S., Shinohara, T., Maruyama, M., et al. (2011). Patterns of baseline autonomic nerve activity and the development of pacing-induced sustained atrial fibrillation. *Hear. Rhythm* 8, 583–589. doi: 10.1016/j.hrthm.2010.11.040

- Shusterman, V., Aysin, B., Ermentrout, G. B., London, B., and Schwartzman, D. (2003). Detecting instabilities of cardiac rhythm. *J. Electrocardiol.* 36(Suppl.), 219–226. doi: 10.1016/j.jelectrocard.2003.09.063
- Skibbsby, L., Jespersen, T., Christ, T., Maleckar, M. M., van den Brink, J., Tavi, P., et al. (2016). Refractoriness in human atria: time and voltage dependence of sodium channel availability. *J. Mol. Cell. Cardiol.* 101, 26–34. doi: 10.1016/j.yjmcc.2016.10.009
- Syed, Z. F., Vigmond, E., and Leon, L. J. (2005). Suitability of genetic algorithm generated models to simulate atrial fibrillation and K⁺ channel blockades. *Conf. Proc. IEEE Eng. Med. Biol. Soc.* 7, 7087–7090.
- Syeda, F., Holmes, A. P., Yu, T. Y., Tull, S., Kuhlmann, S. M., Pavlovic, D., et al. (2016). PITX2 modulates atrial membrane potential and the antiarrhythmic effects of sodium-channel blockers. *J. Am. Coll. Cardiol.* 68, 1881–1894. doi: 10.1016/j.jacc.2016.07.766
- Tobón, C., Cardona, E. A., Palacio, L. C., Duque, J. E., Ugarte, J. P., Orozco-Duque, A., et al. (2015). “Ablation pattern guided by approximate entropy maps to prevent chronic atrial fibrillation: A simulation study,” in *IFMBE Proceedings*, ed. H. A. Braidot (Berlin: Springer Verlag), 560–563. doi: 10.1007/978-3-319-13117-7_143
- Tobón, C., Duarte, M., Duque, J. E., Becerra, M. A., Arango, S. S., Cardona, K., et al. (2014a). “Chloroquine effect on rotor termination under paroxysmal and chronic atrial fibrillation. 2D simulation study,” in *Proceedings of the 2014 IEEE Central America and Panama Convention, CONCAPAN 2014*, (Panama: Institute of Electrical and Electronics Engineers Inc.).
- Tobón, C., Palacio, L. C., Duque, J. E., Cardona, E. A., Ugarte, J. P., Orozco-Duque, A., et al. (2014b). “Simple ablation guided by ApEn mapping in a 2D model during permanent atrial fibrillation,” in *Computing in Cardiology*, (Washington, DC: IEEE Computer Society), 1029–1032.
- Tobón, C., Pachajoa, D., Ugarte, J. P., Saiz, J., Pérez, S., Ugarte, J. P., et al. (2017). “Dofetilide effect on human atrial action potential under normal and atrial fibrillation conditions,” in *Silico Study. in IFMBE Proceedings*, eds T. I. Bustamante and J. Sierra (Berlin: Springer Verlag), 38–41. doi: 10.1007/978-981-10-4086-3_10
- Tobón, C., Ruiz-Villa, C. A., Heidenreich, E., Romero, L., Hornero, F., and Saiz, J. (2013). A three-dimensional human atrial model with fiber orientation. Electrograms and arrhythmic activation patterns relationship. *PLoS One* 8:e50883. doi: 10.1371/journal.pone.0050883
- Trayanova, N. A., and Chang, K. C. (2016). How computer simulations of the human heart can improve anti-arrhythmia therapy. *J. Physiol.* 594, 2483–2502. doi: 10.1113/JP270532
- Trayanova, N. A., and McDowell, K. S. (2018). *Personalized Computational Modeling of Atrial Fibrosis to Guide Catheter Ablation of Atrial Fibrillation*. Baltimore: The Johns Hopkins University.
- Tsujimae, K., Murakami, S., and Kurachi, Y. (2008). In silico study on the effects of IK_{ur} block kinetics on prolongation of human action potential after atrial fibrillation-induced electrical remodeling. *Am. J. Physiol. Hear. Circ. Physiol.* 294, H793–H800. doi: 10.1152/ajpheart.01229.2007
- Ugarte, J. P., Orozco-Duque, A., Tobón, C., Kremen, V., Novak, D., Saiz, J., et al. (2014). Dynamic approximate entropy electroanatomic maps detect rotors in a simulated atrial fibrillation model. *PLoS One* 9:e114577. doi: 10.1371/journal.pone.0114577
- Ugarte, J. P., Orozco-Duque, A., Tobon, C., Saiz, J., Morillo, C. A., and Bustamante, J. (2013). “Localization of complex fractionated atrial electrograms by approximate entropy in a 3D model of human atria,” in *Proceedings of the Pan American Health Care Exchanges, PAHCE*, (Medellin: IEEE).
- Ugarte, J. P., Tobón, C., Orozco-Duque, A., Becerra, M. A., and Bustamante, J. (2015). Effect of the electrograms density in detecting and ablating the tip of the rotor during chronic atrial fibrillation: An in silico study. *Europace* 17, ii97–ii104. doi: 10.1093/europace/euv244
- Uldry, L., Jacquemet, V., Virag, N., Kappenberger, L., and Vesin, J.-M. (2012). Estimating the time scale and anatomical location of atrial fibrillation spontaneous termination in a biophysical model. *Med. Biol. Eng. Comput.* 50, 155–163. doi: 10.1007/s11517-011-0859-3
- van Oosterom, A., Ihara, Z., Jacquemet, V., and Hoekema, R. (2007). Vectorcardiographic lead systems for the characterization of atrial fibrillation. *J. Electrocardiol.* 40, e1–e343. doi: 10.1016/j.jelectrocard.2006.08.002
- van Oosterom, A., and Jacquemet, V. (2005). Genesis of the P wave: Atrial signals as generated by the equivalent double layer source model. *Europace* 7, S21–S29. doi: 10.1016/j.eupc.2005.05.001
- Varela, M., Colman, M. A., Hancox, J. C., and Aslanidi, O. V. (2016). Atrial heterogeneity generates re-entrant substrate during atrial fibrillation and anti-arrhythmic drug action: mechanistic insights from canine atrial models. *PLoS Comput. Biol.* 12:e1005245. doi: 10.1371/journal.pcbi.1005245
- Varela, M., Morgan, R., Ghavami, N., James, S., and Aslanidi, O. (2014). “Ionic mechanisms of triggered activity in atrial cell models,” in *Computing in Cardiology*, (Washington, DC: IEEE Computer Society), 1021–1024.
- Veenhuzen, G. D., Simpson, C. S., and Abdollah, H. (2004). Atrial fibrillation. *CMAJ* 171, 755–760. doi: 10.1503/cmaj.1031364
- Verheule, S., Tuyls, E., Gharaviri, A., Hulsmans, S., Van Hunnik, A., Kuiper, M., et al. (2013). Loss of continuity in the thin epicardial layer because of endomyocardial fibrosis increases the complexity of atrial fibrillatory conduction. *Circ. Arrhythmia Electrophysiol.* 6, 202–211. doi: 10.1161/CIRCEP.112.975144
- Viceconti, M., and Hunter, P. (2016). The virtual physiological human: ten years after. *Annu. Rev. Biomed. Eng.* 18, 103–123. doi: 10.1146/annurev-bioeng-110915-114742
- Vigmond, E., Labarthe, S., Cochet, H., Coudiere, Y., Henry, J., and Jais, P. (2013). A bilayer representation of the human atria. *Conf. Proc. IEEE Eng. Med. Biol. Soc.* 2013, 1530–1533. doi: 10.1109/EMBC.2013.6609804
- Vigmond, E. J., Ruckdeschel, R., and Trayanova, N. (2001). Reentry in a morphologically realistic atrial model. *J. Cardiovasc. Electrophysiol.* 12, 1046–1054. doi: 10.1046/j.1540-8167.2001.01046.x
- Vigmond, E. J., Tsoi, V., Kuo, S., Arevalo, H., Kneller, J., Nattel, S., et al. (2004). The effect of vagally induced dispersion of action potential duration on atrial arrhythmogenesis. *Hear. Rhythm* 1, 334–344. doi: 10.1016/j.hrrthm.2004.03.077
- Vincenti, A., Passini, E., Fabbrini, P., Luise, M. C., Severi, S., and Genovesi, S. (2014). Recurrent intradialytic paroxysmal atrial fibrillation: hypotheses on onset mechanisms based on clinical data and computational analysis. *Europace* 16, 396–404. doi: 10.1093/europace/eut346
- Virag, N., Jacquemet, V., Henriquez, C. S., Zozor, S., Blanc, O., Vesin, J.-M., et al. (2002). Study of atrial arrhythmias in a computer model based on magnetic resonance images of human atria. *Chaos* 12, 754–763. doi: 10.1063/1.1483935
- Virag, N., Jacquemet, V., and Kappenberger, L. (2012). *Modeling of Atrial Fibrillation*. New Jersey: Wiley-Blackwell.
- Voigt, N., Heijman, J., Trausch, A., Mintert-Jancke, E., Pott, L., Ravens, U., et al. (2013). Impaired Na⁺-dependent regulation of acetylcholine-activated inward-rectifier K⁺ current modulates action potential rate dependence in patients with chronic atrial fibrillation. *J. Mol. Cell. Cardiol.* 61, 142–152. doi: 10.1016/j.yjmcc.2013.03.011
- Voigt, N., Heijman, J., Wang, Q., Chiang, D. Y., Li, N., Karck, M., et al. (2014). Cellular and molecular mechanisms of atrial arrhythmogenesis in patients with paroxysmal atrial fibrillation. *Circulation* 129, 145–156. doi: 10.1161/CIRCULATIONAHA.113.006641
- Weber, F. M., Schilling, C., Straub, D., Gurm, S., Seemann, G., Lorenz, C., et al. (2009a). Extracting clinically relevant circular mapping and coronary sinus catheter potentials from atrial simulations. *Lect. Notes Comput. Sci.* 5528, 30–38. doi: 10.1007/978-3-642-01932-6_4
- Weber, F. M., Schilling, C., Straub, D., Seemann, G., Lorenz, C., and Dössel, O. (2009b). Localizing ectopic foci in the pulmonary veins from intracardiac ECGs - A simulation study. *IFMBE* 25, 645–648. doi: 10.1007/978-3-642-03882-2_172
- Wettwer, E., Hála, O., Christ, T., Heubach, J. F., Dobrev, D., Knaut, M., et al. (2004). Role of IK_{ur} in controlling action potential shape and contractility in the human atrium: Influence of chronic atrial fibrillation. *Circulation* 110, 2299–2306. doi: 10.1161/01.CIR.0000145155.60288.71
- Whittaker, D. G., Ni, H., Harchi, A. E., Hancox, J. C., and Zhang, H. (2017). Atrial arrhythmogenicity of KCNJ2 mutations in short QT syndrome: Insights from virtual human atria. *PLoS Comput. Biol.* 13:e1005593. doi: 10.1371/journal.pcbi.1005593
- Wijffels, M. C., Kirchhof, C. J., Dorland, R., and Allessie, M. A. (1995). Atrial fibrillation begets atrial fibrillation?: a study in awake chronically instrumented goats. *Circulation* 92, 1954–1968. doi: 10.1161/01.CIR.92.7.1954
- Wilhelms, M., Hettmann, H., Maleckar, M. M., Koivumaki, J. T., Dossel, O., Seemann, G., et al. (2013). Benchmarking electrophysiological models of human atrial myocytes. *Front. Physiol.* 3:487. doi: 10.3389/fphys.2012.00487

- Wolf, R. M., Glynn, P., Hashemi, S., Zarei, K., Mitchell, C. C., Anderson, M. E., et al. (2013). Atrial fibrillation and sinus node dysfunction in human ankyrin-B syndrome: A computational analysis. *Am. J. Physiol. Hear. Circ. Physiol.* 304, H1253–H1266. doi: 10.1152/ajpheart.00734.2012
- Xia, L., Gong, Y.-L., Zhu, X.-W., Zhang, Y., Sun, Q., and Zhang, H.-G. (2010). Mathematical models of canine right and left atria cardiomyocytes. *J. Zhejiang Univ. Sci. B* 11, 402–416. doi: 10.1631/jzus.B0900346
- Yamazaki, M., and Jalife, J. (2012). Pathophysiology of atrial fibrillation: From initiation to maintenance. *J. Arrhythmia* 28, 129–139. doi: 10.1016/j.joa.2012.05.002
- Zahid, S., Cochet, H., Boyle, P. M., Schwarz, E. L., Whyte, K. N., Vigmond, E. J., et al. (2016). Patient-derived models link re-entrant driver localization in atrial fibrillation to fibrosis spatial pattern. *Cardiovasc. Res.* 110, 443–454. doi: 10.1093/cvr/cvw073
- Zemzemi, N., Labarthe, S., Dubois, R., and Coudiere, Y. (2012). “From body surface potential to activation maps on the atria: A machine learning technique,” in *Proceedings of the Computing in Cardiology*, (Krakow: IEEE), 125–128.
- Zhang, H., Garratt, C. J., Zhu, J., and Holden, A. V. (2005). Role of up-regulation of IK1 in action potential shortening associated with atrial fibrillation in humans. *Cardiovasc. Res.* 66, 493–502. doi: 10.1016/j.cardiores.2005.01.020
- Zhang, N., Gong, M., Tse, G., Zhang, Z., Meng, L., Yan, B. P., et al. (2018). Prolonged corrected QT interval in predicting atrial fibrillation: a systematic review and meta-analysis. *Pacing Clin. Electrophysiol.* 41, 321–327. doi: 10.1111/pace.13292
- Zhao, J., Amiri, A., Sands, G. B., Trew, M., LeGrice, I., Smaill, B. H., et al. (2008). Structure specific models of electrical function in the right atrial appendage. *Conf. Proc. IEEE Eng. Med. Biol. Soc.* 2008, 145–148. doi: 10.1109/IEMBS.2008.4649111
- Zhao, J., Butters, T. D., Zhang, H., Legrice, I. J., Sands, G. B., and Smaill, B. H. (2013a). Image-based model of atrial anatomy and electrical activation: A computational platform for investigating atrial arrhythmia. *IEEE Trans. Med. Imaging* 32, 18–27. doi: 10.1109/TMI.2012.2227776
- Zhao, J., Stephenson, R. S., Sands, G. B., LeGrice, I. J., Zhang, H., Jarvis, J. C., et al. (2013b). Atrial fibrosis and atrial fibrillation: a computer simulation in the posterior left atrium. *Lect. Notes Comput. Sci.* 7945, 400–408. doi: 10.1007/978-3-642-38899-6_47
- Zhao, J., Butters, T. D., Zhang, H., Pullan, A. J., LeGrice, I. J., Sands, G. B., et al. (2012). An image-based model of atrial muscular architecture effects of structural anisotropy on electrical activation. *Circ. Arrhythmia Electrophysiol.* 5, 361–370. doi: 10.1161/CIRCEP.111.967950
- Zhao, J., Hansen, B. J., Wang, Y., Csepe, T. A., Sul, L. V., Tang, A., et al. (2017). Three-dimensional integrated functional, structural, and computational mapping to define the structural “fingerprints” of heart-specific atrial fibrillation drivers in human heart ex vivo. *J. Am. Heart Assoc.* 6, e005922. doi: 10.1161/JAHA.117.005922
- Zhao, J., Kharche, S. R., Hansen, B. J., Csepe, T. A., Wang, Y., Stiles, M. K., et al. (2015). Optimization of catheter ablation of atrial fibrillation: Insights gained from clinically-derived computer models. *Int. J. Mol. Sci.* 16, 10834–10854. doi: 10.3390/ijms160510834
- Zhu, X., Yang, D., Lu, W., Chen, W., Wei, D., Fukuda, K., et al. (2014). “Computer simulation of cathode ablation for atrial fibrillation,” in *Proceedings - 2014 IEEE International Conference on Computer and Information Technology, CIT 2014*, (New Jersey: Institute of Electrical and Electronics Engineers Inc.), 721–725. doi: 10.1109/CIT.2014.37
- Ziyadeh-Isleem, A., Clatot, J., Duchatelet, S., Gandjbakhch, E., Denjoy, I., Hidden-Lucet, F., et al. (2014). A truncating SCN5A mutation combined with genetic variability causes sick sinus syndrome and early atrial fibrillation. *Hear. Rhythm* 11, 1015–1023. doi: 10.1016/j.hrthm.2014.02.021
- Zou, R., Kneller, J., Leon, L. J., and Nattel, S. (2005). Substrate size as a determinant of fibrillatory activity maintenance in a mathematical model of canine atrium. *Am. J. Physiol. Heart Circ. Physiol.* 289, H1002–H1012. doi: 10.1152/ajpheart.00252.2005

Conflict of Interest Statement: The authors declare that the research was conducted in the absence of any commercial or financial relationships that could be construed as a potential conflict of interest.

Copyright © 2019 Filos, Tachmatzidis, Maglaveras, Vassilikos and Chouvarda. This is an open-access article distributed under the terms of the Creative Commons Attribution License (CC BY). The use, distribution or reproduction in other forums is permitted, provided the original author(s) and the copyright owner(s) are credited and that the original publication in this journal is cited, in accordance with accepted academic practice. No use, distribution or reproduction is permitted which does not comply with these terms.

Advantages of publishing in Frontiers



OPEN ACCESS

Articles are free to read for greatest visibility and readership



FAST PUBLICATION

Around 90 days from submission to decision



HIGH QUALITY PEER-REVIEW

Rigorous, collaborative, and constructive peer-review



TRANSPARENT PEER-REVIEW

Editors and reviewers acknowledged by name on published articles



REPRODUCIBILITY OF RESEARCH

Support open data and methods to enhance research reproducibility



DIGITAL PUBLISHING

Articles designed for optimal readership across devices



FOLLOW US
@frontiersin



IMPACT METRICS
Advanced article metrics track visibility across digital media



EXTENSIVE PROMOTION
Marketing and promotion of impactful research



LOOP RESEARCH NETWORK
Our network increases your article's readership